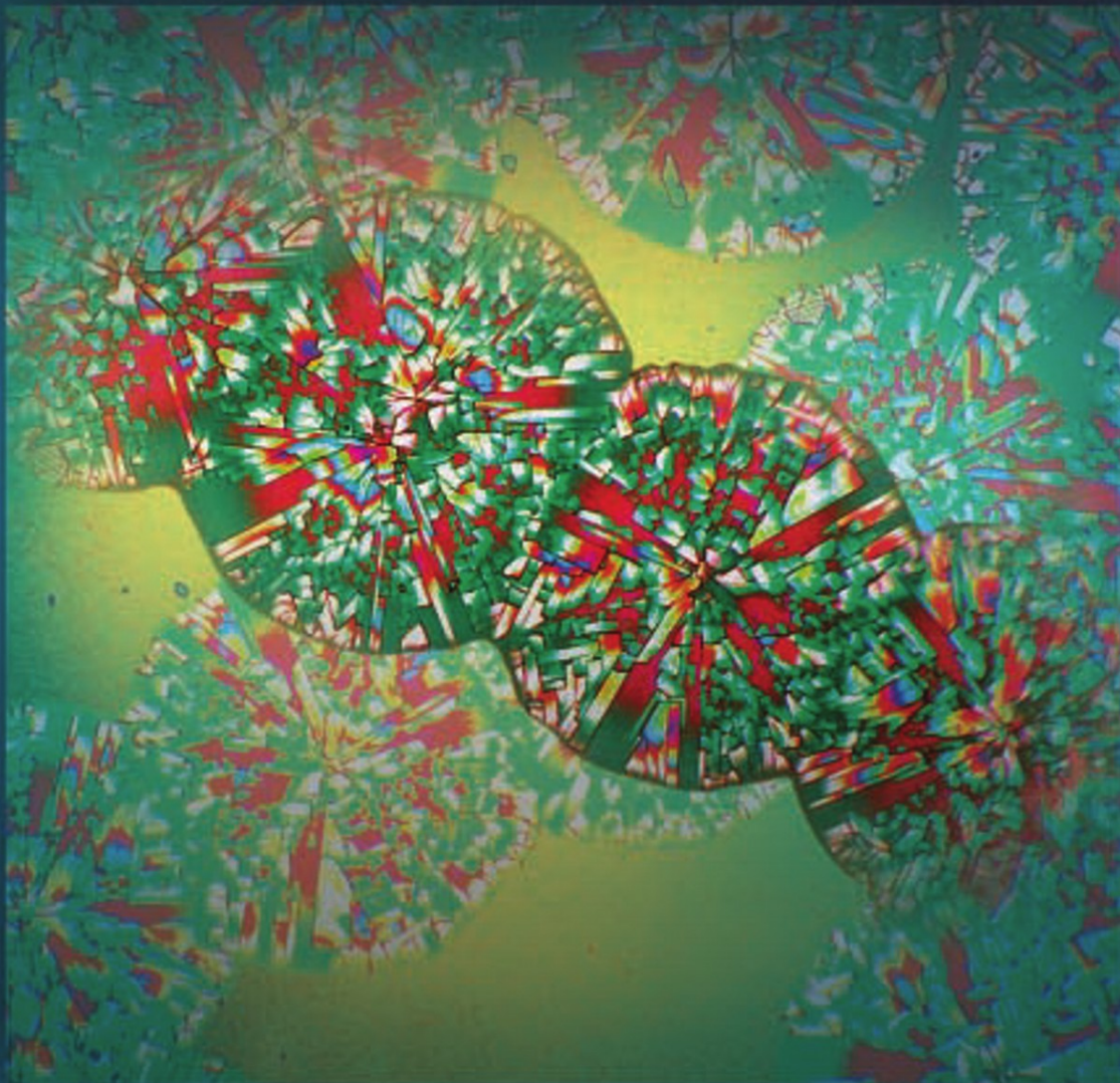


CERAMIC MATERIALS

Science and Engineering

C. BARRY CARTER • M. GRANT NORTON



Ceramic Materials

Ceramic Materials

Science and Engineering

C. Barry Carter
M. Grant Norton

 Springer

C. Barry Carter
Department of Chemical Engineering
and Materials Science
University of Minnesota
Minneapolis, MN 55455-0132

M. Grant Norton
School of Mechanical and Materials Engineering
Washington State University
Pullman, WA 99164-2920

Details for Figures and Tables are listed following the index

Library of Congress Control Number: 2006938045

ISBN-10: 0-387-46270-8 e-ISBN-10: 0-387-46271-6
ISBN-13: 978-0-387-46270-7 e-ISBN-13: 978-0-387-46271-4

Printed on acid-free paper.

© 2007 Springer Science+Business Media, LLC.

All rights reserved. This work may not be translated or copied in whole or in part without the written permission of the publisher (Springer Science+Business Media, LLC, 233 Spring Street, New York, NY 10013, USA), except for brief excerpts in connection with reviews or scholarly analysis. Use in connection with any form of information storage and retrieval, electronic adaptation, computer software, or by similar or dissimilar methodology now known or hereafter developed is forbidden.

The use in this publication of trade names, trademarks, service marks, and similar terms, even if they are not identified as such, is not to be taken as an expression of opinion as to whether or not they are subject to proprietary rights.

9 8 7 6 5 4 3 2 1

springer.com

*This text is dedicated to our wives
Bryony Carter and Christine Wall*

*Words cannot explain, describe, or say enough
Thanks to you both*

Preface

In today's materials science curriculum, there is often only time for one course on ceramic materials. Students will usually take courses on mechanical properties, thermodynamics and kinetics, and the structure of materials. Many will also have taken an introductory overview of materials science. In each of these courses, the students will have encountered ceramic materials. The present text assumes background knowledge at this introductory level but still provides a review of such critical topics as bonding, crystal structures, and lattice defects.

The text has been divided into seven parts and 37 chapters: we will explain the thinking behind these decisions. Part I examines the history and development of ceramic materials: how they have literally shaped civilization. We include this material in our introductory lectures and then make the two chapters assigned reading. Part II discusses the bonding, structure, and the relationship among phases. Students often find this part of the course to be the most difficult because structures are implicitly 3-dimensional. However, so many properties depend on the structure whether crystalline or amorphous. We have limited the number of structures to what we think the students can manage in one course, we give references to texts that the students can spend a lifetime studying and recommend our favorite software package. Part III consists of two chapters on our tools of the trade. Most ceramics are heated at some stage during processing. Unfortunately heat treatments are rarely exactly what we would like them to be; the heating rate is too slow, the furnace contaminates the sample, the environment is not what we want (or think it is), etc. Techniques for characterizing materials fill books and the students are familiar with many already from their studies on metals. So, the purpose of this chapter is, in part, to encourage the student to find out more about techniques that they might not have heard of or might not have thought of applying to ceramics; you could certainly skip Part III and make it assigned reading especially if the students are taking overlapping courses. Part IV discusses defects in ceramics and aims at providing a comprehensive overview while again not being a dedicated book on the subject. Part IV leads straight into Part V—a basic discussion of mechanical properties applied specifically to ceramics. The last two parts contain just over half the chapters. The two topics are Processing (Part VI) and Properties (Part VII) and are, of course, the reason we study ceramic materials. The warning is—these topics form the second half of the book because the student should understand the materials first, but it then becomes too easy to miss them in a one-semester course due to lack of time. We know, we have done this and the students miss the part that they would often appreciate most. Chapter 36 is probably the most fun for half the students and both the authors; Chapter 37 is the most important for all of us.

Many modern ceramists will acknowledge their debt to the late David Kingery. His pioneering 1960 text was one of the first to regard ceramics as a serious scientific subject. Both his book and his research papers have been referenced throughout the present text. Our definition of a ceramic material follows directly from Kingery's definition: a nonmetallic, inorganic solid. Nonmetallic refers to the bonding: in ceramics, it is predominantly covalent and/or ionic. Ceramics are always inorganic solids although they also may be major or minor components of composite materials.

Throughout the text we ask the question “what is special for ceramics?” The answer varies so much that it can be difficult to generalize but that is what we are attempting where possible. Having said that, ceramics are always providing surprises. Indium tin oxide is a transparent conductor of electricity. Yttrium barium copper oxide is a superconductor at 90 K. Doped gallium nitride is revolutionizing home lighting and is becoming a critical component for all traffic lights. Neodymium-doped garnet is the basis of many solid-state lasers.

A feature of this text is that we keep in mind that many of today’s high-tech ceramic materials and processing routes have their origin in the potter’s craft or in the jeweler’s art, and materials that are new to the materials scientist may be old friends to the mineralogist and geologist. Throughout the text we will make connections to these related fields. The history of ceramics is as old as civilization and our use of ceramics is a measure of the technological progress of a civilization.

The text covers ceramic materials from the fundamentals to industrial applications including a consideration of safety and their impact on the environment. We also include throughout the text links to economics and art. So many choices in ceramics have been determined by economics. We often think of ceramics as being inexpensive materials: bottles, bricks and tiles certainly are. Ceramics are also the most valuable materials we have: per gram, emerald still holds the record.

No modern materials text can be complete without considering materials at the nanoscale. Nanoceramics appear throughout this text but we decided not to create a special chapter on the topic. What we have done is to highlight some of these topics as they appear naturally in the text. It is worth noting that nanoscale ceramics have been used for centuries; it is just recently that we have had a name for them.

The figures generally contain much more information than is given in the text. We use this fact in some of the homework questions and hope that the extra detail will encourage the students to delve into the literature to learn more about the topic. One place to start this search is, of course, with the original citation if there is one. These citations are grouped together at the end of the text, in part for this purpose, but also to recognize the contributions of our colleagues.

On the Web site (<http://web.mac.com/ceramicsbook/iweb>), we are developing supplementary material including an extensive list of suggestions for filling any weak or missing areas in the student’s background and will update these suggestions periodically. We give annotated references to the original studies that have been quoted in the text. We also include further examples of images that supplement those in the text. The Web site will also house two sets of questions to complement those at the end of each chapter. One set consists of shorter questions that we use in pop quizzes but are also useful for students, especially those working alone, to assess their own progress. The second set includes questions, which we use for homework and take-home exams.

After reviewing some history, we consider bonding and structures (Chapters 3–8). Essentially, this set of chapters examines the science that underpins our definition of a ceramic material. The way atoms are connected together by covalent or ionic bonds is illustrated by considering simple and complex structures. We introduce glasses as a natural subsection of complex structures rather than as a separate branch of ceramics. Window glass is a ceramic material, just like lithium niobate, mica or silicon. The difference is that glasses are not crystalline: crystalline quartz has more in common with amorphous silica glass than it does with alumina. The final chapter in this sequence is important in most branches of materials science: which ceramics are compatible with other ceramics, which are not, and which of these materials react to form new compounds. We emphasize that these are equilibrium phase diagrams and that ceramics often need high temperatures and long times to attain equilibrium. (Geological times are needed in some cases.)

The next two topics (Chapters 9–10) examine two tools (in the broadest sense) that we will use: we need to prepare the ceramic material and this usually involves heating. Then we need to characterize it.

In Chapters 11 thru 15 we explore the whole topic of defects in ceramics, from point defects to voids, and elaborate on why they are important in the rest of the text. In Chapter 13 the combination of surfaces, nanoparticles and foams builds on the common theme of the surface as a defect but does not treat it in isolation from properties or real ceramic processing. The positioning of the next three chapters (Chapters 16–18) on mechanical properties was decided because of the authors' bias. This allows us to integrate mechanical behavior into processing, thin films, glass ceramics, and such in the immediately following chapters.

We begin the section on processing with a discussion of minerals and then consider the different forms and shapes of ceramic powders. The topic of glass is separated into Chapters 21 and 26 with the use of organic chemistry, the principles of shaping, and the processes that occur during shaping (sintering, grain growth and phase transformations) separating them. In this text we do not want to separate processing from the science; where we have separated them, this is only done to help the student absorb the concepts serially rather than in parallel! We discuss making films and growing crystals in Chapters 27–29. This group of chapters really gets to the heart of ceramic processing and mixes liquids (whether due to a solvent or to melting) in with the powders. We do not emphasize the mechanical aspects but make it clear that a full understanding requires that we think about them and not just for hot-pressing or for crystalline ceramics.

The remaining eight chapters cover the applications of ceramics with the emphasis on what property is being exploited, how we optimize it, and just how far we can still go with these materials; remember how the development of glass optical fibers has changed society forever in less than 40 years. Again our bias is clear. Ceramics are amazing materials and the underlying physics is fascinating but the subject of physics can easily obscure this excitement. Physicists are often not fully aware of the value of chemistry and all too often underestimate the *feel* a ceramist has for these materials. Before concluding the text with the most rapidly changing topic of industry and the environment in Chapter 37, we examine two groups of ceramics that affect us all even though we may not think about them—ceramics in biology/medicine and ceramics as gemstones. Whether as objects of beauty or symbols of something more lasting, polished natural single crystals of ceramics have inspired awe for centuries and challenged scientists for nearly as long.

We would like to thank our students and postdocs, past and present, who have helped us so much to appreciate and enjoy ceramic materials. The students include Katrien Ostyn, Karen Morrissey, Zvi Elgat, Bruno De Cooman, Yonn Rasmussen (formerly Simpson), David Susnitzky, Scott Summerfelt, Lisa Moore (formerly Tietz), Chris Scarfone, Ian Anderson, Mike Mallamaci, Paul Kotula, Sundar Ramamurthy, Jason Heffelfinger, Matt Johnson, Andrey Zagrebelny, Chris Blanford, Svetlana Yanina, Shelley Gilliss, Chris Perrey, Jeff Farrer, Arzu Altay, Jessica Riesterer, Jonathan Winterstein, Maxime Guinel, Dan Eakins, Joel LeBret, Aaron LaLonde, and Tyler Pounds. The postdocs include John Dodsworth, Monica Backhaus-Ricoult, Hermann Wendt, Werner Skrotski, Thomas Pfeiffer, Mike Bench, Carsten Korte, Joysurya Basu and Divakar Ramachandran and especially Ravi Ravishankar and Stuart McKernan. We thank Carolyn Swanson for carefully drawing so many diagrams for this text and Janet McKernan for her expert proofreading, continued patience, and rare commonsense. Janet generated the index, negotiated hyphens, and tried to remove all our errors and typos; those that remain that should not or are missing that should be present are solely the responsibility of the authors. We thank our many colleagues for providing figures and understanding on some of the special topics. In particular, we thank Richard Hughes, Rosette Gault, Peter Ilsley, Liz Huffman, and Fred Ward.

We thank our colleagues and collaborators. David Kohlstedt who introduced CBC to ceramics. Herman Schmalzried who is not only our guru on solid-state reactions but the model of a truly wonderful Professor and mentor. Gisela Schmalzried who provided meals and company during many visits to Hannover, Göttingen and Buntentock. Paul Hlava has been our guide and guru on everything to do with gems and

minerals: he is one of the world's natural teachers. MGN thanks Brian Cantor for hosting his sabbatic at Oxford University where parts of this text were written. Likewise, CBC thanks Eva Olssen at Chalmer's University, Yoshio Bando at NIMS, and Paul Midgley, Colin Humphreys and the Master and Fellows of Peterhouse at Cambridge University.

C. Barry Carter
M. Grant Norton

Contents

Preface	vii
PART I HISTORY AND INTRODUCTION	
1 Introduction	3
1.1 Definitions	3
1.2 General Properties	4
1.3 Types of Ceramic and their Applications	5
1.4 Market	6
1.5 Critical Issues for the Future	7
1.6 Relationship between Microstructure, Processing and Properties	8
1.7 Safety	9
1.8 Ceramics on the Internet	10
1.9 On Units	10
2 Some History	15
2.1 Earliest Ceramics: The Stone Age	15
2.2 Ceramics in Ancient Civilizations	17
2.3 Clay	19
2.4 Types of Pottery	19
2.5 Glazes	20
2.6 Development of a Ceramics Industry	21
2.7 Plaster and Cement	22
2.8 Brief History of Glass	24
2.9 Brief History of Refractories	25
2.10 Major Landmarks of the Twentieth Century	26
2.11 Museums	28
2.12 Societies	29
2.13 Ceramic Education	29
PART II MATERIALS	
3 Background You Need to Know	35
3.1 The Atom	35
3.2 Energy Levels	36
3.3 Electron Waves	37
3.4 Quantum Numbers	37
3.5 Assigning Quantum Numbers	39
3.6 Ions	42
3.7 Electronegativity	44
3.8 Thermodynamics: The Driving Force for Change	45
3.9 Kinetics: The Speed of Change	47

4	Bonds and Energy Bands	51
4.1	Types of Interatomic Bond	51
4.2	Young's Modulus	51
4.3	Ionic Bonding	53
4.4	Covalent Bonding	58
4.5	Metallic Bonding in Ceramics	63
4.6	Mixed Bonding	64
4.7	Secondary Bonding	64
4.8	Electron Energy Bands in Ceramics	66
5	Models, Crystals, and Chemistry	71
5.1	Terms and Definitions	71
5.2	Symmetry and Crystallography	74
5.3	Lattice Points, Directions, and Planes	75
5.4	The Importance of Crystallography	76
5.5	Pauling's Rules	76
5.6	Close-Packed Arrangements: Interstitial Sites	79
5.7	Notation for Crystal Structures	81
5.8	Structure, Composition, and Temperature	81
5.9	Crystals, Glass, Solids, and Liquid	82
5.10	Defects	83
5.11	Computer Modeling	83
6	Binary Compounds	87
6.1	Background	87
6.2	CsCl	88
6.3	NaCl (MgO, TiC, PbS)	88
6.4	GaAs (β -SiC)	89
6.5	AlN (BeO, ZnO)	90
6.6	CaF ₂	91
6.7	FeS ₂	92
6.8	Cu ₂ O	93
6.9	CuO	93
6.10	TiO ₂	93
6.11	Al ₂ O ₃	94
6.12	MoS ₂ and CdI ₂	95
6.13	Polymorphs, Polytypes, and Polytypoids	96
7	Complex Crystal and Glass Structures	100
7.1	Introduction	100
7.2	Spinel	101
7.3	Perovskite	102
7.4	The Silicates and Structures Based on SiO ₄	104
7.5	Silica	105
7.6	Olivine	106
7.7	Garnets	107
7.8	Ring Silicates	107
7.9	Micas and Other Layer Materials	108
7.10	Clay Minerals	109
7.11	Pyroxene	109
7.12	β -Aluminas and Related Materials	110
7.13	Calcium Aluminate and Related Materials	111
7.14	Mullite	111
7.15	Monazite	111

7.16	YBa ₂ Cu ₃ O ₇ and Related High-Temperature Superconductors (HTSCs)	112
7.17	Si ₃ N ₄ , SiAlONs, and Related Materials	113
7.18	Fullerenes and Nanotubes	113
7.19	Zeolites and Microporous Compounds	114
7.20	Zachariasen's Rules for the Structure of Glass	115
7.21	Revisiting Glass Structures	117
8	Equilibrium Phase Diagrams	120
8.1	What's Special about Ceramics?	120
8.2	Determining Phase Diagrams	121
8.3	Phase Diagrams for Ceramists: The Books	124
8.4	Gibbs Phase Rule	124
8.5	One Component ($C = 1$)	125
8.6	Two Components ($C = 2$)	126
8.7	Three and More Components	128
8.8	Composition with Variable Oxygen Partial Pressure	130
8.9	Quaternary Diagrams and Temperature	132
8.10	Congruent and Incongruent Melting	132
8.11	Miscibility Gaps in Glass	133
 PART III TOOLS		
9	Furnaces	139
9.1	The Need for High Temperatures	139
9.2	Types of Furnace	139
9.3	Combustion Furnaces	140
9.4	Electrically Heated Furnaces	141
9.5	Batch or Continuous Operation	141
9.6	Indirect Heating	143
9.7	Heating Elements	144
9.8	Refractories	146
9.9	Furniture, Tubes, and Crucibles	147
9.10	Firing Process	148
9.11	Heat Transfer	148
9.12	Measuring Temperature	149
9.13	Safety	151
10	Characterizing Structure, Defects, and Chemistry	154
10.1	Characterizing Ceramics	154
10.2	Imaging Using Visible-Light, IR, and UV	155
10.3	Imaging Using X-rays and CT Scans	157
10.4	Imaging in the SEM	158
10.5	Imaging in the TEM	159
10.6	Scanning-Probe Microscopy	161
10.7	Scattering and Diffraction Techniques	162
10.8	Photon Scattering	163
10.9	Raman and IR Spectroscopy	163
10.10	NMR Spectroscopy and Spectrometry	165
10.11	Mössbauer Spectroscopy and Spectrometry	166
10.12	Diffraction in the EM	168
10.13	Ion Scattering (RBS)	168
10.14	X-ray Diffraction and Databases	169
10.15	Neutron Scattering	171

10.16	Mass Spectrometry	172
10.17	Spectrometry in the EM	172
10.18	Electron Spectroscopy	174
10.19	Neutron Activation Analysis (NAA)	175
10.20	Thermal Analysis	175

PART IV DEFECTS

11	Point Defects, Charge, and Diffusion	181
11.1	Are Defects in Ceramics Different?	181
11.2	Types of Point Defects	182
11.3	What Is Special for Ceramics?	183
11.4	What Type of Defects Form?	184
11.5	Equilibrium Defect Concentrations	184
11.6	Writing Equations for Point Defects	186
11.7	Solid Solutions	187
11.8	Association of Point Defects	189
11.9	Color Centers	190
11.10	Creation of Point Defects in Ceramics	191
11.11	Experimental Studies of Point Defects	192
11.12	Diffusion	192
11.13	Diffusion in Impure, or Doped, Ceramics	193
11.14	Movement of Defects	197
11.15	Diffusion and Ionic Conductivity	197
11.16	Computing	199
12	Are Dislocations Unimportant?	201
12.1	A Quick Review of Dislocations	202
12.2	Summary of Dislocation Properties	206
12.3	Observation of Dislocations	206
12.4	Dislocations in Ceramics	208
12.5	Structure of the Core	208
12.6	Detailed Geometry	211
12.7	Defects on Dislocations	214
12.8	Dislocations and Diffusion	215
12.9	Movement of Dislocations	216
12.10	Multiplication of Dislocations	216
12.11	Dislocation Interactions	217
12.12	At the Surface	219
12.13	Indentation, Scratching, and Cracks	219
12.14	Dislocations with Different Cores	220
13	Surfaces, Nanoparticles, and Foams	224
13.1	Background to Surfaces	224
13.2	Ceramic Surfaces	225
13.3	Surface Energy	225
13.4	Surface Structure	227
13.5	Curved Surfaces and Pressure	230
13.6	Capillarity	230
13.7	Wetting and Dewetting	231
13.8	Foams	232
13.9	Epitaxy and Film Growth	233
13.10	Film Growth in 2D: Nucleation	233
13.11	Film Growth in 2D: Mechanisms	234
13.12	Characterizing Surfaces	235

13.13	Steps	239
13.14	<i>In Situ</i>	240
13.15	Surfaces and Nanoparticles	241
13.16	Computer Modeling	241
13.17	Introduction to Properties	242
14	Interfaces in Polycrystals	246
14.1	What Are Grain Boundaries?	246
14.2	For Ceramics	248
14.3	GB Energy	249
14.4	Low-Angle GBs	251
14.5	High-Angle GBs	254
14.6	Twin Boundaries	255
14.7	General Boundaries	258
14.8	GB Films	259
14.9	Triple Junctions and GB Grooves	262
14.10	Characterizing GBs	263
14.11	GBs in Thin Films	264
14.12	Space Charge and Charged Boundaries	265
14.13	Modeling	265
14.14	Some Properties	265
15	Phase Boundaries, Particles, and Pores	269
15.1	The Importance	269
15.2	Different Types	269
15.3	Compared to Other Materials	270
15.4	Energy	270
15.5	The Structure of PBs	271
15.6	Particles	272
15.7	Use of Particles	276
15.8	Nucleation and Growth of Particles	276
15.9	Pores	277
15.10	Measuring Porosity	278
15.11	Porous Ceramics	279
15.12	Glass/Crystal Phase Boundaries	280
15.13	Eutectics	281
15.14	Metal/Ceramic PBs	282
15.15	Forming PBs by Joining	283
 PART V MECHANICAL STRENGTH AND WEAKNESS		
16	Mechanical Testing	289
16.1	Philosophy	289
16.2	Types of Testing	291
16.3	Elastic Constants and Other “Constants”	292
16.4	Effect of Microstructure on Elastic Moduli	294
16.5	Test Temperature	295
16.6	Test Environment	296
16.7	Testing in Compression and Tension	296
16.8	Three- and Four-Point Bending	297
16.9	K_{Ic} from Bend Test	298
16.10	Indentation	299
16.11	Fracture Toughness from Indentation	300
16.12	Nanoindentation	301
16.13	Ultrasonic Testing	301

16.14	Design and Statistics	302
16.15	SPT Diagrams	305
17	Deforming: Plasticity	309
17.1	Plastic Deformation	309
17.2	Dislocation Glide	310
17.3	Slip in Alumina	312
17.4	Plastic Deformation in Single Crystals	313
17.5	Plastic Deformation in Polycrystals	314
17.6	Dislocation Velocity and Pinning	315
17.7	Creep	317
17.8	Dislocation Creep	317
17.9	Diffusion-Controlled Creep	318
17.10	Grain-Boundary Sliding	318
17.11	Tertiary Creep and Cavitation	319
17.12	Creep Deformation Maps	321
17.13	Viscous Flow	321
17.14	Superplasticity	322
18	Fracturing: Brittleness	325
18.1	The Importance of Brittleness	325
18.2	Theoretical Strength: The Orowan Equation	326
18.3	The Effect of Flaws: The Griffith Equation	327
18.4	The Crack Tip: The Inglis Equation	329
18.5	Stress Intensity Factor	329
18.6	<i>R</i> Curves	330
18.7	Fatigue and Stress Corrosion Cracking	331
18.8	Failure and Fractography	332
18.9	Toughening and Ceramic Matrix Composites	335
18.10	Machinable Glass-Ceramics	338
18.11	Wear	338
18.12	Grinding and Polishing	339
 PART VI PROCESSING		
19	Raw Materials	345
19.1	Geology, Minerals, and Ores	345
19.2	Mineral Formation	345
19.3	Beneficiation	347
19.4	Weights and Measures	347
19.5	Silica	348
19.6	Silicates	348
19.7	Oxides	351
19.8	Nonoxides	354
20	Powders, Fibers, Platelets, and Composites	359
20.1	Making Powders	359
20.2	Types of Powders	360
20.3	Mechanical Milling	360
20.4	Spray Drying	362
20.5	Powders by Sol-Gel Processing	363
20.6	Powders by Precipitation	363
20.7	Chemical Routes to Nonoxide Powders	364
20.8	Platelets	365
20.9	Nanopowders by Vapor-Phase Reactions	365

20.10	Characterizing Powders	366
20.11	Characterizing Powders by Microscopy	366
20.12	Sieving	366
20.13	Sedimentation	367
20.14	The Coulter Counter	368
20.15	Characterizing Powders by Light Scattering	368
20.16	Characterizing Powders by X-ray Diffraction	369
20.17	Measuring Surface Area (the BET Method)	369
20.18	Determining Particle Composition and Purity	370
20.19	Making Fibers and Whiskers	370
20.20	Oxide Fibers	371
20.21	Whiskers	372
20.22	Glass Fibers	372
20.23	Coating Fibers	373
20.24	Making Ceramic–Matrix Composites	374
20.25	Ceramic–Matrix Composites from Powders and Slurries	374
20.26	Ceramic–Matrix Composites by Infiltration	375
20.27	<i>In Situ</i> Processes	375
21	Glass and Glass-Ceramics	379
21.1	Definitions	379
21.2	History	380
21.3	Viscosity, η	383
21.4	Glass: A Summary of Its Properties, or Not	385
21.5	Defects in Glass	386
21.6	Heterogeneous Glass	386
21.7	Yttrium–Aluminum Glass	386
21.8	Coloring Glass	386
21.9	Glass Laser	388
21.10	Precipitates in Glass	388
21.11	Crystallizing Glass	388
21.12	Glass as Glaze and Enamel	390
21.13	Corrosion of Glass and Glaze	392
21.14	Types of Ceramic Glasses	393
21.15	Natural Glass	394
21.16	The Physics of Glass	396
22	Sols, Gels, and Organic Chemistry	400
22.1	Sol-Gel Processing	400
22.2	Structure and Synthesis of Alkoxides	401
22.3	Properties of Alkoxides	402
22.4	The Sol-Gel Process Using Metal Alkoxides	403
22.5	Characterization of the Sol-Gel Process	406
22.6	Powders, Coatings, Fibers, Crystalline, or Glass	407
23	Shaping and Forming	412
23.1	The Words	412
23.2	Binders and Plasticizers	413
23.3	Slip and Slurry	413
23.4	Dry Pressing	414
23.5	Hot Pressing	414
23.6	Cold Isostatic Pressing	415
23.7	Hot Isostatic Pressing	416
23.8	Slip Casting	417
23.9	Extrusion	418

23.10	Injection Molding	419
23.11	Rapid Prototyping	420
23.12	Green Machining	420
23.13	Binder Burnout	421
23.14	Final Machining	421
23.15	Making Porous Ceramics	422
23.16	Shaping Pottery	422
23.17	Shaping Glass	423
24	Sintering and Grain Growth	427
24.1	The Sintering Process	427
24.2	The Terminology of Sintering	429
24.3	Capillary Forces and Surface Forces	429
24.4	Sintering Spheres and Wires	429
24.5	Grain Growth	431
24.6	Sintering and Diffusion	431
24.7	Liquid-Phase Sintering	433
24.8	Hot Pressing	433
24.9	Pinning Grain Boundaries	434
24.10	More Grain Growth	435
24.11	Grain Boundaries, Surfaces, and Sintering	436
24.12	Exaggerated Grain Growth	437
24.13	Fabricating Complex Shapes	438
24.14	Pottery	439
24.15	Pores and Porous Ceramics	439
24.16	Sintering with Two and Three Phases	440
24.17	Examples of Sintering in Action	441
24.18	Computer Modeling	441
25	Solid-State Phase Transformations and Reactions	444
25.1	Transformations and Reactions: The Link	444
25.2	The Terminology	445
25.3	Technology	445
25.4	Phase Transformations without Changing Chemistry	447
25.5	Phase Transformations Changing Chemistry	448
25.6	Methods for Studying Kinetics	449
25.7	Diffusion through a Layer: Slip Casting	450
25.8	Diffusion through a Layer: Solid-State Reactions	451
25.9	The Spinel-Forming Reaction	451
25.10	Inert Markers and Reaction Barriers	452
25.11	Simplified Darken Equation	453
25.12	The Incubation Period	454
25.13	Particle Growth and the Effect of Misfit	454
25.14	Thin-Film Reactions	455
25.15	Reactions in an Electric Field	457
25.16	Phase Transformations Involving Glass	458
25.17	Pottery	459
25.18	Cement	459
25.19	Reactions Involving a Gas Phase	460
25.20	Curved Interfaces	461
26	Processing Glass and Glass-Ceramics	463
26.1	The Market for Glass and Glass Products	463
26.2	Processing Bulk Glasses	463
26.3	Bubbles	467

26.4	Flat Glass	468
26.5	Float-Glass	469
26.6	Glassblowing	470
26.7	Coating Glass	472
26.8	Safety Glass	473
26.9	Foam Glass	473
26.10	Sealing Glass	473
26.11	Enamel	474
26.12	Photochromic Glass	474
26.13	Ceramming: Changing Glass to Glass-Ceramics	474
26.14	Glass for Art and Sculpture	476
26.15	Glass for Science and Engineering	478
27	Coatings and Thick Films	481
27.1	Defining Thick Film	481
27.2	Tape Casting	481
27.3	Dip Coating	484
27.4	Spin Coating	484
27.5	Spraying	485
27.6	Electrophoretic Deposition	486
27.7	Thick-Film Circuits	488
28	Thin Films and Vapor Deposition	494
28.1	The Difference between Thin Films and Thick Films	494
28.2	Acronyms, Adjectives, and Hyphens	494
28.3	Requirements for Thin Ceramic Films	495
28.4	Chemical Vapor Deposition	495
28.5	Thermodynamics of Chemical Vapor Deposition	497
28.6	Chemical Vapor Deposition of Ceramic Films for Semiconductor Devices	498
28.7	Types of Chemical Vapor Deposition	499
28.8	Chemical Vapor Deposition Safety	500
28.9	Evaporation	500
28.10	Sputtering	501
28.11	Molecular-Beam Epitaxy	502
28.12	Pulsed-Laser Deposition	503
28.13	Ion-Beam-Assisted Deposition	504
28.14	Substrates	504
29	Growing Single Crystals	507
29.1	Why Single Crystals?	507
29.2	A Brief History of Growing Ceramic Single Crystals	507
29.3	Methods for Growing Single Crystals of Ceramics	508
29.4	Melt Technique: Verneuil (Flame-Fusion)	509
29.5	Melt Technique: Arc-Image Growth	511
29.6	Melt Technique: Czochralski	511
29.7	Melt Technique: Skull Melting	514
29.8	Melt Technique: Bridgman–Stockbarger	515
29.9	Melt Technique: Heat-Exchange Method	516
29.10	Applying Phase Diagrams to Single-Crystal Growth	516
29.11	Solution Technique: Hydrothermal	517
29.12	Solution Technique: Hydrothermal Growth at Low Temperature	519
29.13	Solution Technique: Flux Growth	519
29.14	Solution Technique: Growing Diamonds	521

29.15	Vapor Technique: Vapor–Liquid–Solid	521
29.16	Vapor Technique: Sublimation	522
29.17	Preparing Substrates for Thin-Film Applications	522
29.18	Growing Nanowires and Nanotubes by Vapor–Liquid–Solid and Not	522

PART VII PROPERTIES AND APPLICATIONS

30	Conducting Charge or Not	529
30.1	Ceramics as Electrical Conductors	529
30.2	Conduction Mechanisms in Ceramics	531
30.3	Number of Conduction Electrons	532
30.4	Electron Mobility	533
30.5	Effect of Temperature	533
30.6	Ceramics with Metal-Like Conductivity	534
30.7	Applications for High- σ Ceramics	535
30.8	Semiconducting Ceramics	537
30.9	Examples of Extrinsic Semiconductors	539
30.10	Varistors	540
30.11	Thermistors	541
30.12	Wide-Band-Gap Semiconductors	542
30.13	Ion Conduction	543
30.14	Fast Ion Conductors	543
30.15	Batteries	544
30.16	Fuel Cells	544
30.17	Ceramic Insulators	546
30.18	Substrates and Packages for Integrated Circuits	548
30.19	Insulating Layers in Integrated Circuits	549
30.20	Superconductivity	550
30.21	Ceramic Superconductors	551
31	Locally Redistributing Charge	556
31.1	Background on Dielectrics	556
31.2	Ferroelectricity	560
31.3	BaTiO ₃ : The Prototypical Ferroelectric	562
31.4	Solid Solutions with BaTiO ₃	565
31.5	Other Ferroelectric Ceramics	565
31.6	Relaxor Dielectrics	565
31.7	Ceramic Capacitors	565
31.8	Ceramic Ferroelectrics for Memory Applications	568
31.9	Piezoelectricity	569
31.10	Lead Zirconate–Lead Titanate (PZT) Solid Solutions	570
31.11	Applications for Piezoelectric Ceramics	571
31.12	Piezoelectric Materials for Microelectromechanical Systems	572
31.13	Pyroelectricity	572
31.14	Applications for Pyroelectric Ceramics	573
32	Interacting with and Generating Light	575
32.1	Some Background for Optical Ceramics	575
32.2	Transparency	577
32.3	The Refractive Index	578
32.4	Reflection from Ceramic Surfaces	579
32.5	Color in Ceramics	580
32.6	Coloring Glass and Glazes	581
32.7	Ceramic Pigments and Stains	581

32.8	Translucent Ceramics	583
32.9	Lamp Envelopes	584
32.10	Fluorescence	585
32.11	The Basics of Optical Fibers	586
32.12	Phosphors and Emitters	588
32.13	Solid-State Lasers	589
32.14	Electrooptic Ceramics for Optical Devices	590
32.15	Reacting to Other Parts of the Spectrum	594
32.16	Optical Ceramics in Nature	595
33	Using Magnetic Fields and Storing Data	598
33.1	A Brief History of Magnetic Ceramics	598
33.2	Magnetic Dipoles	599
33.3	The Basic Equations, the Words, and the Units	600
33.4	The Five Classes of Magnetic Material	601
33.5	Diamagnetic Ceramics	601
33.6	Superconducting Magnets	602
33.7	Paramagnetic Ceramics	603
33.8	Measuring χ	604
33.9	Ferromagnetism	604
33.10	Antiferromagnetism and Colossal Magnetoresistance	605
33.11	Ferrimagnetism	606
33.12	Estimating the Magnetization of Ferrimagnets	609
33.13	Magnetic Domains and Bloch Walls	609
33.14	Imaging Magnetic Domains	610
33.15	Motion of Domain Walls and Hysteresis Loops	611
33.16	Hard and Soft Ferrites	612
33.17	Microwave Ferrites	614
33.18	Data Storage and Recording	614
33.19	Magnetic Nanoparticles	616
34	Responding to Temperature Changes	619
34.1	Summary of Terms and Units	619
34.2	Absorption and Heat Capacity	619
34.3	Melting Temperatures	621
34.4	Vaporization	623
34.5	Thermal Conductivity	624
34.6	Measuring Thermal Conductivity	626
34.7	Microstructure and Thermal Conductivity	626
34.8	Using High Thermal Conductivity	628
34.9	Thermal Expansion	628
34.10	Effect of Crystal Structure on α	630
34.11	Thermal Expansion Measurement	631
34.12	Importance of Matching α s	632
34.13	Applications for Low- α	632
34.14	Thermal Shock	633
35	Ceramics in Biology and Medicine	635
35.1	What Are Bioceramics?	635
35.2	Advantages and Disadvantages of Ceramics	636
35.3	Ceramic Implants and the Structure of Bone	638
35.4	Alumina and Zirconia	639
35.5	Bioactive Glasses	640
35.6	Bioactive Glass-Ceramics	641
35.7	Hydroxyapatite	642

35.8	Bioceramics in Composites	644
35.9	Bioceramic Coatings	645
35.10	Radiotherapy Glasses	646
35.11	Pyrolytic Carbon Heart Valves	646
35.12	Nanobioceramics	647
35.13	Dental Ceramics	648
35.14	Biomimetics	648
36	Minerals and Gems	652
36.1	Minerals	652
36.2	What Is a Gem?	653
36.3	In the Rough	653
36.4	Cutting and Polishing	654
36.5	Light and Optics in Gemology	656
36.6	Color in Gems and Minerals	660
36.7	Optical Effects	661
36.8	Identifying Minerals and Gems	663
36.9	Chemical Stability (Durability)	664
36.10	Diamonds, Sapphires, Rubies, and Emeralds	664
36.11	Opal	666
36.12	Other Gems	667
36.13	Minerals with Inclusions	669
36.14	Treatment of Gems	670
36.15	The Mineral and Gem Trade	670
37	Industry and the Environment	675
37.1	The Beginning of the Modern Ceramics Industry	675
37.2	Growth and Globalization	676
37.3	Types of Market	677
37.4	Case Studies	677
37.5	Emerging Areas	680
37.6	Mining	682
37.7	Recycling	683
37.8	In the Nuclear Industry	685
37.9	Producing and Storing Hydrogen	685
37.10	As Green Materials	687
Index		691
Details for Figures and Tables		701

Part I

History and Introduction

1

Introduction

CHAPTER PREVIEW

In materials science we often divide materials into distinct classes. The primary classes of solid materials are ceramics, metals, and polymers. This classification is based on the types of atoms involved and the bonding between them. The other widely recognized classes are semiconductors and composites. Composites are combinations of more than one material and often involve ceramics, such as fiberglass. Semiconductors are materials with electrical conductivities that are very sensitive to minute amounts of impurities. As we will see later, most materials that are semiconductors are actually ceramics, for example, gallium nitride, the blue–green laser diode material.

In this chapter we will define what we mean by a “ceramic” and will also describe some of the general properties of ceramics. The difficulty when drawing generalizations, particularly in this case, is that it is always possible to find an exception to the rule. It is because of the wide range of properties exhibited by ceramics that they find application in such a variety of areas. A general theme throughout this book is the interrelationship between the way in which a ceramic is processed, its microstructure, and its properties. We give some examples of these interrelationships in this chapter to illustrate their importance.

1.1 DEFINITIONS

If you look in any introductory materials science book you will find that one of the first sections describes the classification scheme. In classical materials science, materials are grouped into five categories: metals, polymers, ceramics, semiconductors, and composites. The first three are based primarily on the nature of the interatomic bonding, the fourth on the materials conductivity, and the last on the materials structure—not a very consistent start.

Metals, both pure and alloyed, consist of atoms held together by the delocalized electrons that overcome the mutual repulsion between the ion cores. Many main-group elements and all the transition and inner transition elements are metals. They also include alloys—combinations of metallic elements or metallic and nonmetallic elements (such as in steel, which is an alloy of primarily Fe and C). Some commercial steels, such as many tool steels, contain ceramics. These are the carbides (e.g., Fe_3C and W_6C) that produce the hardening and enhance wear resistance, but also make it more brittle. The delocalized electrons give metals many of their characteristic properties (e.g., good thermal and electrical conductivity). It is because of their bonding that many metals have close packed structures and deform plastically at room temperature.

Polymers are macromolecules formed by covalent bonding of many simpler molecular units called mers.

Most polymers are organic compounds based on carbon, hydrogen, and other nonmetals such as sulfur and chlorine. The bonding between the molecular chains determines many of their properties. Cross-linking of the chains is the key to the vulcanization process that turned rubber from an interesting but not very useful material into, for example, tires that made traveling by bicycle much more comfortable and were important in the production of the automobile. The terms “polymer” and “plastic” are often used interchangeably. However, many of the plastics with which we are familiar are actually combinations of polymers, and often include fillers and other additives to give the desired properties and appearance.

Ceramics are usually associated with “mixed” bonding—a combination of covalent, ionic, and sometimes metallic. They consist of arrays of interconnected atoms; there are no discrete molecules. This characteristic distinguishes ceramics from molecular solids such as iodine crystals (composed of discrete I_2 molecules) and paraffin wax (composed of long-chain alkane molecules). It also excludes ice, which is composed of discrete H_2O molecules and often behaves just like many ceramics. The majority of ceramics are compounds of metals or metalloids and nonmetals. Most frequently they are oxides, nitrides, and carbides. However, we also classify diamond and graphite as ceramics. These forms of carbon are inorganic in the most basic meaning of the term: they were

not prepared from the living organism. Richerson (2000) says “most solid materials that aren’t metal, plastic, or derived from plants or animals are ceramics.”

Semiconductors are the only class of material based on a property. They are usually defined as having electrical conductivity between that of a good conductor and an insulator. The conductivity is strongly dependent upon the presence of small amounts of impurities—the key to making integrated circuits. Semiconductors with wide band gaps (greater than about 3 eV) such as silicon carbide and boron nitride are becoming of increasing importance for high-temperature electronics, for example, SiC diodes are of interest for sensors in fuel cells. In the early days of semiconductor technology such materials would have been regarded as insulators. Gallium nitride (GaN), a blue–green laser diode material, is another ceramic that has a wide band gap.

Composites are combinations of more than one material or phase. Ceramics are used in many composites, often for reinforcement. For example, one of the reasons a B-2 stealth bomber is stealthy is that it contains over 22 tons of carbon/epoxy composite. In some composites the ceramic is acting as the matrix (ceramic matrix composites or CMCs). An early example of a CMC dating back over 9000 years is brick. These often consisted of a fired clay body reinforced with straw. Clay is an important ceramic and the backbone of the traditional ceramic industry. In concrete, both the matrix (cement) and the reinforcement (aggregate) are ceramics.

The most widely accepted definition of a ceramic is given by Kingery *et al.* (1976): “A ceramic is a nonmetallic, inorganic solid.” Thus all inorganic semiconductors are ceramics. By definition, a material ceases to be a ceramic when it is melted. At the opposite extreme, if we cool some ceramics enough they become superconductors. All the so-called high-temperature superconductors (HTSC) (ones that lose all electrical resistance at liquid-nitrogen temperatures) are ceramics. Trickier is glass such as used in windows and optical fibers. Glass fulfills the standard definition of a solid—it has its own fixed shape—but it is usually a supercooled liquid. This property becomes evident at high temperatures when it undergoes viscous deformation. Glasses are clearly special ceramics. We may crystallize certain glasses to make glass–ceramics such as those found in Corningware®. This process is referred to as “ceramming” the glass, i.e., making it into a ceramic. We stand by Kingery’s definition and have to live with some confusion. We thus define ceramics in terms of what they are not.

It is also not possible to define ceramics, or indeed any class of material, in terms of specific properties.

- We cannot say “ceramics are brittle” because some can be superplastically deformed and some metals can be more brittle: a rubber hose or banana at 77 K shatters under a hammer.

- We cannot say “ceramics are insulators” unless we put a value on the band gap (E_g) where a material is not a semiconductor.
- We cannot say “ceramics are poor conductors of heat” because diamond has the highest thermal conductivity of any known material.

Before we leave this section let us consider a little history. The word ceramic is derived from the Greek *keramos*, which means “potter’s clay” or “pottery.” Its origin is a Sanskrit term meaning “to burn.” So the early Greeks used “keramos” when describing products obtained by heating clay-containing materials. The term has long included all products made from fired clay, for example, bricks, fireclay refractories, sanitaryware, and tableware.

In 1822, silica refractories were first made. Although they contained no clay the traditional ceramic process of shaping, drying, and firing was used to make them. So the term “ceramic,” while retaining its original sense of a product made from clay, began to include other products made by the same manufacturing process. The field of ceramics (broader than the materials themselves) can be defined as the art and science of making and using solid articles that contain as their essential component a ceramic. This definition covers the purification of raw materials, the study and production of the chemical compounds concerned, their formation into components, and the study of structure, composition, and properties.

1.2 GENERAL PROPERTIES

Ceramics generally have specific properties associated with them although, as we just noted, this can be a misleading approach to defining a class of material. However, we will look at some properties and see how closely they match our expectations of what constitutes a ceramic.

Brittleness. This probably comes from personal experiences such as dropping a glass beaker or a dinner plate. The reason that the majority of ceramics are brittle is the mixed ionic–covalent bonding that holds the constituent atoms together. At high temperatures (above the glass transition temperature) glass no longer behaves in a brittle manner; it behaves as a viscous liquid. That is why it is easy to form glass into intricate shapes. So what we can say is that most ceramics are brittle at room temperature but not necessarily at elevated temperatures.

Poor electrical and thermal conduction. The valence electrons are tied up in bonds, and are not free as they are in metals. In metals it is the free electrons—the electron gas—that determines many of their electrical and thermal properties. Diamond, which we classified as a ceramic in Section 1.1, has the highest thermal conductivity of any known material. The conduction mechanism is due to phonons, not electrons, as we describe in Chapter 34.

Ceramics can also have high electrical conductivity: (1) the oxide ceramic, ReO_3 , has an electrical conductivity

at room temperature similar to that of Cu (2) the mixed oxide $\text{YBa}_2\text{Cu}_3\text{O}_7$ is an HTSC; it has zero resistivity below 92 K. These are two examples that contradict the conventional wisdom when it comes to ceramics.

Compressive strength. Ceramics are stronger in compression than in tension, whereas metals have comparable tensile and compressive strengths. This difference is important when we use ceramic components for load-bearing applications. It is necessary to consider the stress distributions in the ceramic to ensure that they are compressive. An important example is in the design of concrete bridges—the concrete, a CMC, must be kept in compression. Ceramics generally have low toughness, although combining them in composites can dramatically improve this property.

Chemical insensitivity. A large number of ceramics are stable in both harsh chemical and thermal environments. Pyrex glass is used widely in chemistry laboratories specifically because it is resistant to many corrosive chemicals, stable at high temperatures (it does not soften until 1100 K), and is resistant to thermal shock because of its low coefficient of thermal expansion ($33 \times 10^{-7} \text{K}^{-1}$). It is also widely used in bakeware.

Transparent. Many ceramics are transparent because they have a large E_g . Examples include sapphire watch

covers, precious stones, and optical fibers. Glass optical fibers have a percent transmission $>96\% \text{km}^{-1}$. Metals are transparent to visible light only when they are very thin, typically less than $0.1 \mu\text{m}$.

Although it is always possible to find at least one ceramic that shows atypical behavior, the properties we have mentioned here are in many cases different from those shown by metals and polymers.

1.3 TYPES OF CERAMIC AND THEIR APPLICATIONS

Using the definition given in Section 1.1 you can see that large numbers of materials are ceramics. The applications for these materials are diverse, from bricks and tiles to electronic and magnetic components. These applications use the wide range of properties exhibited by ceramics. Some of these properties are listed in Table 1.1 together with examples of specific ceramics and applications. Each of these areas will be covered in more detail later. The functions of ceramic products are dependent on their chemical composition and microstructure, which determines their properties. It is the interrelationship between

TABLE 1.1 Properties and Applications for Ceramics

Property	Example	Application
Electrical	$\text{Bi}_2\text{Ru}_2\text{O}_7$	Conductive component in thick-film resistors
	Doped ZrO_2	Electrolyte in solid-oxide fuel cells
	Indium tin oxide (ITO)	Transparent electrode
	SiC	Furnace elements for resistive heating
	YBaCuO_7	Superconducting quantum interference devices (SQUIDs)
	SnO_2	Electrodes for electric glass melting furnaces
Dielectric	$\alpha\text{-Al}_2\text{O}_3$	Spark plug insulator
	$\text{PbZr}_{0.5}\text{Ti}_{0.5}\text{O}_3$ (PZT)	Micropumps
	SiO_2	Furnace bricks
	(Ba,Sr)TiO ₃	Dynamic random access memories (DRAMs)
	Lead magnesium niobate (PMN)	Chip capacitors
Magnetic	$\gamma\text{-Fe}_2\text{O}_3$	Recording tapes
	$\text{Mn}_{0.4}\text{Zn}_{0.6}\text{Fe}_2\text{O}_4$	Transformer cores in touch tone telephones
	$\text{BaFe}_{12}\text{O}_{19}$	Permanent magnets in loudspeakers
	$\text{Y}_{2.66}\text{Gd}_{0.34}\text{Fe}_{4.22}\text{Al}_{0.68}\text{Mn}_{0.09}\text{O}_{12}$	Radar phase shifters
Optical	Doped SiO_2	Optical fibers
	$\alpha\text{-Al}_2\text{O}_3$	Transparent envelopes in street lamps
	Doped ZrSiO_4	Ceramic colors
	Doped (Zn,Cd)S	Fluorescent screens for electron microscopes
	$\text{Pb}_{1-x}\text{La}_x(\text{Zr}_z\text{Ti}_{1-z})_{1-x/4}\text{O}_3$ (PLZT)	Thin-film optical switches
	Nd doped $\text{Y}_3\text{Al}_5\text{O}_{12}$	Solid-state lasers
Mechanical	TiN	Wear-resistant coatings
	SiC	Abrasives for polishing
	Diamond	Cutting tools
	Si_3N_4	Engine components
	Al_2O_3	Hip implants
Thermal	SiO_2	Space shuttle insulation tiles
	Al_2O_3 and AlN	Packages for integrated circuits
	Lithium-aluminosilicate glass ceramics	Supports for telescope mirrors
	Pyrex glass	Laboratory glassware and cookware

structure and properties that is a key element of materials science and engineering.

You may find that in addition to dividing ceramics according to their properties and applications that it is common to class them as *traditional* or *advanced*.

Traditional ceramics include high-volume items such bricks and tiles, toilet bowls (whitewares), and pottery.

Advanced ceramics include newer materials such as laser host materials, piezoelectric ceramics, ceramics for dynamic random access memories (DRAMs), etc., often produced in small quantities with higher prices.

There are other characteristics that separate these categories.

Traditional ceramics are usually based on clay and silica. There is sometimes a tendency to equate traditional ceramics with low technology, however, advanced manufacturing techniques are often used. Competition among producers has caused processing to become more efficient and cost effective. Complex tooling and machinery is often used and may be coupled with computer-assisted process control.

Advanced ceramics are also referred to as “special,” “technical,” or “engineering” ceramics. They exhibit superior mechanical properties, corrosion/oxidation resistance, or electrical, optical, and/or magnetic properties. While traditional clay-based ceramics have been used for over 25,000 years, advanced ceramics have generally been developed within the last 100 years.

Figure 1.1 compares traditional and advanced ceramics in terms of the type of raw materials used, the forming

and shaping processes, and the methods used for characterization.

1.4 MARKET

Ceramics is a multibillion dollar industry. Worldwide sales are about \$100 billion ($\10^{11}) per year; the U.S. market alone is over \$35 billion ($\3.5×10^{10}) annually. As with all economic data there will be variations from year to year. The *Ceramic Industry* (CI) is one organization that provides regular updates of sales through its annual *Giants in Ceramics* survey.

The general distribution of industry sales is as follows:

- 55% Glass
- 17% Advanced ceramics
- 10% Whiteware
- 9% Porcelain enamel
- 7% Refractories
- 2% Structural clay

In the United States, sales of structural clay in the form of bricks is valued at \$160M per month. However, financially, the ceramics market is clearly dominated by glass. The major application for glass is windows. World demand for flat glass is about 40 billion square feet—worth over \$40 billion.

Overall market distribution in the United States is as follows:

- 32% Flat glass
- 18% Lighting
- 17% Containers
- 17% Fiber glass
- 9% TV tubes, CRTs
- 5% Consumer glassware
- 1% Technical/laboratory
- 1% Other

Advanced ceramics form the second largest sector of the industry. More than half of this sector is electrical and electronic ceramics and ceramic packages:

- 36% Capacitors/substrates/packages
- 23% Other electrical/electronic ceramics
- 13% Other
- 12% Electrical porcelain
- 8% Engineering ceramics
- 8% Optical fibers

High-temperature ceramic superconductors, which would fall into the category of advanced ceramics, are not presently a major market area. They constitute less than 1% of the advanced ceramics market. Significant growth has been predicted because of their increased use in microwave filters and resonators, with particular application in the area of cell phones.

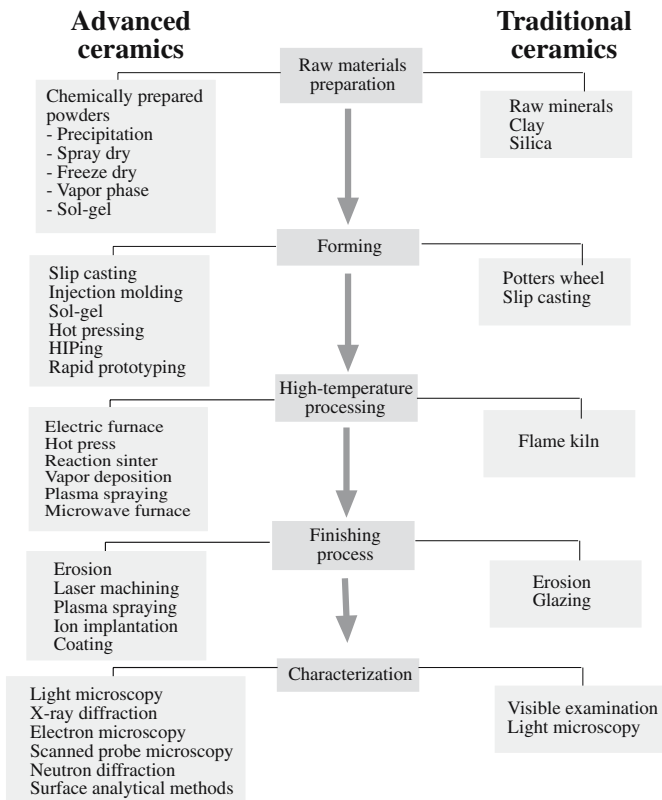


FIGURE 1.1 A comparison of different aspects of traditional and advanced ceramics.

Engineering ceramics, also called structural ceramics, include wear-resistant components such as dies, nozzles, and bearings. Bioceramics such as ceramic and glass-ceramic implants and dental crowns account for about 20% of this market. Dental crowns are made of porcelain and over 30 million are made in the United States each year.

Whiteware sales, which include sanitaryware (toilet bowls, basins, etc.) and dinnerware (plates, cups), account for about 10% of the total market for ceramics. The largest segment of the whiteware market, accounting for about 40%, is floor and wall tiles. In the United States we use about 2.5 billion (2.5×10^9) square feet of ceramic tiles per year. Annual sales of sanitaryware in the United States total more than 30 million pieces.

Porcelain enamel is the ceramic coating applied to many steel appliances such as kitchen stoves, washers, and dryers. Porcelain enamels have much wider applications as both interior and exterior paneling in buildings, for example, in subway stations. Because of these widespread applications it is perhaps not surprising that the porcelain enameling industry accounts for more than \$3 billion per year.

More than 50% of refractories are consumed by the steel industry. The major steelmaking countries are China, Japan, and the United States. Structural clay products include bricks, sewer pipes, and roofing tiles. These are high-volume low-unit-cost items. Each year about 8 billion bricks are produced in the United States with a market value of over \$1.5 billion.

1.5 CRITICAL ISSUES FOR THE FUTURE

Although glass dominates the global ceramics market, the most significant growth is in advanced ceramics. There are many key issues that need to be addressed to maintain this growth and expand the applications and uses of advanced ceramics. It is in these areas that there will be increasing employment opportunities for ceramic engineers and materials scientists.

Structural ceramics include silicon nitride (Si_3N_4), silicon carbide (SiC), zirconia (ZrO_2), boron carbide (B_4C), and alumina (Al_2O_3). They are used in applications such as cutting tools, wear components, heat exchangers, and engine parts. Their relevant properties are high hardness, low density, high-temperature mechanical strength, creep resistance, corrosion resistance, and chemical inertness. There are three key issues to solve in order to expand the use of structural ceramics:

- Reducing cost of the final product
- Improving reliability
- Improving reproducibility

Electronic ceramics include barium titanate (BaTiO_3), zinc oxide (ZnO), lead zirconate titanate [$\text{Pb}(\text{Zr}_x\text{Ti}_{1-x})\text{O}_3$], aluminum nitride (AlN), and HTSCs. They are used in applications as diverse as capacitor dielectrics, varistors,

microelectromechanical systems (MEMS), substrates, and packages for integrated circuits. There are many challenges for the future:

- Integrating with existing semiconductor technology
- Improving processing
- Enhancing compatibility with other materials

Bioceramics are used in the human body. The response of these materials varies from nearly inert to bioactive to resorbable. Nearly inert bioceramics include alumina (Al_2O_3) and zirconia (ZrO_2). Bioactive ceramics include hydroxyapatite and some special glass and glass-ceramic formulations. Tricalcium phosphate is an example of a resorbable bioceramic; it dissolves in the body. Three issues will determine future progress:

- Matching mechanical properties to human tissues
- Increasing reliability
- Improving processing methods

Coatings and films are generally used to modify the surface properties of a material, for example, a bioactive coating deposited onto the surface of a bioinert implant. They may also be used for economic reasons; we may want to apply a coating of an expensive material to a lower cost substrate rather than make the component entirely from the more expensive material. An example of this situation would be applying a diamond coating on a cutting tool. In some cases we use films or coatings simply because the material performs better in this form. An example is the transport properties of thin films of HTSCs, which are improved over those of the material in bulk form. Some issues need to be addressed:

- Understanding film deposition and growth
- Improving film/substrate adhesion
- Increasing reproducibility

Composites may use ceramics as the matrix phase and/or the reinforcing phase. The purpose of a composite is to display a combination of the preferred characteristics of each of the components. In CMCs one of the principal goals has been to increase fracture toughness through reinforcement with whiskers or fibers. When ceramics are the reinforcement phase in, for example, metal matrix composites the result is usually an increase in strength, enhanced creep resistance, and greater wear resistance. Three issues must be solved:

- Reducing processing costs
- Developing compatible combinations of materials (e.g., matching coefficients of thermal expansion)
- Understanding interfaces

Nanoceramics can be either well established or at an early stage in their development. They are widely used in cosmetic products such as sunscreens, and we know they

are critical in many applications of catalysis, but their use in fuel cells, coatings, and devices, for example, is often quite new. There are three main challenges:

- Making them
- Integrating them into devices
- Ensuring that they do not have a negative impact on society

1.6 RELATIONSHIP BETWEEN MICROSTRUCTURE, PROCESSING, AND APPLICATIONS

The field of materials science and engineering is often defined by the interrelationship between four topics—synthesis and processing, structure and composition, properties, and performance. To understand the behavior and properties of any material, it is essential to understand its structure. Structure can be considered on several levels, all of which influence final behavior. At the finest level is the electron configuration, which affects properties such as color, electrical conductivity, and magnetic behavior. The arrangement of electrons in an atom influences how it will bond to another atom and this, in turn, impacts the crystal structure.

The arrangement of the atoms or ions in the material also needs to be considered. Crystalline ceramics have a very regular atomic arrangement whereas in noncrystalline or amorphous ceramics (e.g., oxide glasses) there is no long-range order, although locally we may identify similar polyhedra. Such materials often behave differently relative to their crystalline counterparts. Not only perfect lattices and ideal structures have to be considered but also the presence of structural defects that are unavoidable in all materials, even the amorphous ones. Examples of such defects include impurity atoms and dislocations.

Polycrystalline ceramics have a structure consisting of many grains. The size, shape, and orientation of the grains play a key role in many of the macroscopic properties of these materials, for example, mechanical strength. In most ceramics, more than one phase is present, with each phase having its own structure, composition, and properties. Control of the type, size, distribution, and amount of these phases within the material provides a means to control properties. The microstructure of a ceramic is often a result of the way it was processed. For example, hot-pressed ceramics often have very few pores. This may not be the case in sintered materials.

The interrelationship between the structure, processing, and properties will be evident throughout this text but are illustrated here by five examples.

1. The strength of polycrystalline ceramics depends on the grain size through the Hall–Petch equation. Figure 1.2 shows strength as a function of grain size for MgO. As the grain size decreases the strength increases. The grain size is determined by the size of the initial powder

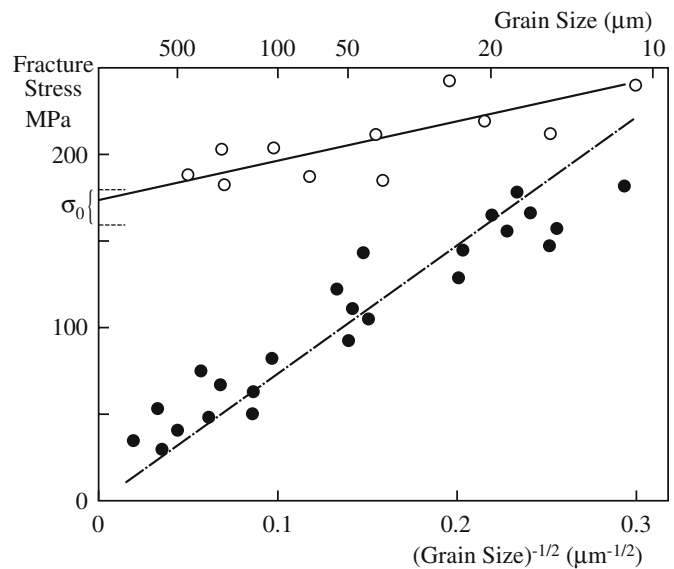


FIGURE 1.2 Dependence of fracture strength of MgO (at 20°C) on the grain size.

particles and the way in which they were consolidated. The grain boundaries in a polycrystalline ceramic are also important. The strength then depends on whether or not the material is pure, contains a second phase or pores, or just contains glass at the grain boundaries. The relationship is not always obvious for nanoceramics.

2. Transparent or translucent ceramics require that we limit the scattering of light by pores and second-phase particles. Reduction in porosity may be achieved by hot pressing to ensure a high-density product. This approach has been used to make transparent PLZT ceramics for electrooptical applications such as the flash-blindness goggles shown in Figure 1.3, developed during the 1970s



FIGURE 1.3 Pilot wearing the flash-blindness goggles (in the “off” position).

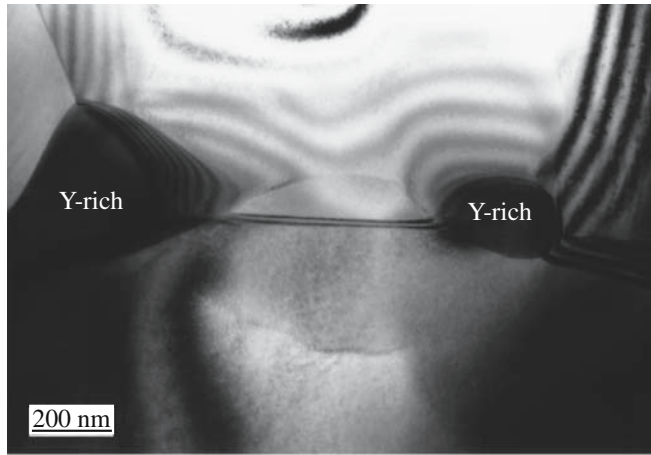


FIGURE 1.4 TEM image of grain boundaries in AlN showing yttria-rich second-phase particles at the triple junctions.

by Sandia National Laboratories in the United States for use by combat pilots.

3. Thermal conductivity of commercially available polycrystalline AlN is usually lower than that predicted by theory because of the presence of impurities, mainly oxygen, which scatter phonons. Adding rare earth or alkaline metal oxides (such as Y_2O_3 and CaO , respectively) can reduce the oxygen content by acting as a getter. These oxides are mixed in with the AlN powder before it is shaped. The second phase, formed between the oxide additive and the oxide coating on the AlN grains, segregates to triple points as shown in Figure 1.4.

4. Soft ferrites such as $Mn_{1-\delta}Zn_{\delta}Fe_2O_4$ are used in a range of different devices, for example, as the yoke that moves the electron beam in a television tube. The permeability of soft ferrites is a function of grain size as shown in Figure 1.5. Large defect-free grains are preferred because we need to have very mobile domain walls.

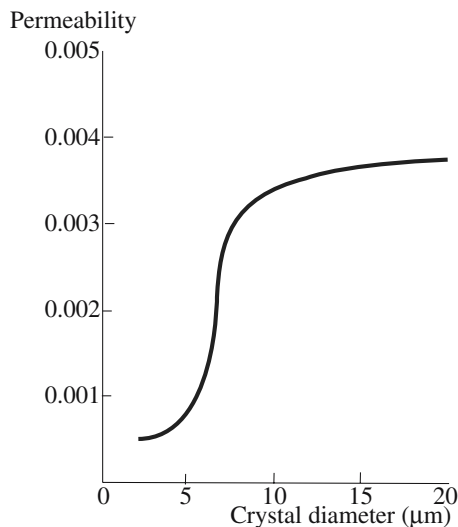


FIGURE 1.5 The variation of permeability with average grain diameter of a manganese-zinc ferrite with uncontrolled porosity.

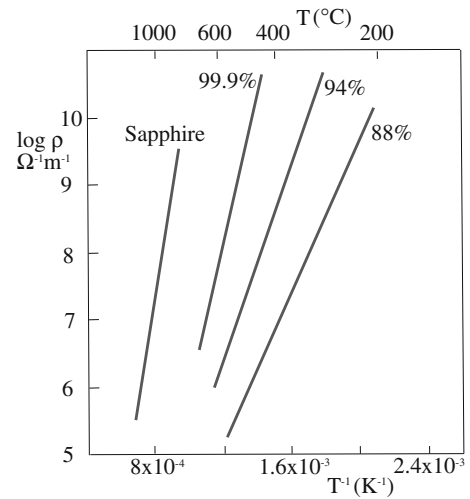


FIGURE 1.6 Dependence of resistivity on temperature for different compositions of alumina.

Defects and grain boundaries pin the domain walls and make it more difficult to achieve saturation magnetization.

5. Alumina ceramics are used as electrical insulators because of their high electrical resistivity and low dielectric constant. For most applications pure alumina is not used. Instead we blend the alumina with silicates to reduce the sintering temperature. These materials are known as debased aluminas and contain a glassy silicate phase between alumina grains. Debased aluminas are generally more conductive (lower resistivity) than pure aluminas as shown in Figure 1.6. Debased aluminas (containing 95% Al_2O_3) are used in spark plugs.

1.7 SAFETY

When working with any material, safety considerations should be uppermost. There are several important precautions to take when working with ceramics.

Toxicity of powders containing, for example, Pb or Cd or fluorides should be known. When shipping the material, the manufacturer supplies information on the hazards associated with their product. It is important to read this information and keep it accessible. Some standard resources that provide information about the toxicity of powders and the “acceptable” exposure levels are given in the References.

Small particles should not be inhaled. The effects have been well known, documented, and often ignored since the 1860s. Proper ventilation, improved cleanliness, and protective clothing have significantly reduced many of the industrial risks. Care should be taken when handling any powders (of both toxic and nontoxic materials). The most injurious response is believed to be when the particle size is $<1 \mu m$; larger particles either do not remain suspended in the air sufficiently long to be inhaled or, if inhaled, cannot negotiate the tortuous passage of the upper

TABLE 1.2 The Color Scale of Temperature

<i>Color</i>	<i>Corresponding T</i>
Barely visible red	525°C
Dark red	700°C
Cherry red just beginning to appear	800°C
Clear red	900°C
Bright red, beginning orange	1000°C
Orange	1100°C
Orange-white	1200°C
Dull white	1300°C
Bright white	1400°C

respiratory tract. The toxicity and environmental impact of nanopowders have not been clearly addressed, but are the subject of various studies such as a recent report by the Royal Society (2004).

High temperatures are used in much of ceramic processing. The effects of high temperatures on the human body are obvious. What is not so obvious is how hot something actually is. Table 1.2 gives the color scale for temperature. From this tabulation you can see that an alumina tube at 400°C will not show a change in color but it will still burn skin. Other safety issues involved with furnaces are given in Chapter 9.

Organics are used as solvents and binders during processing. Traditionally, organic materials played little role in ceramic processing. Now they are widely used in many forms of processing. Again, manufacturers will provide safety data sheets on any product they ship. This information is important and should always be read carefully.

As a rule, the material safety data sheets (MSDS) should be readily accessible for all the materials you are

using; many states require that they are kept in the laboratory.

1.8 CERAMICS ON THE INTERNET

There is a great deal of information about ceramics on the Internet. Here are some of the most useful web sites.

- www.FutureCeramics.com The web site for this text.
- www.acers.org The American Ceramic Society, membership information, meetings, books.
- www.acers.org/cic/propertiesdb.asp The Ceramic Properties Database. This database has links to many other sources of property information including the NIST and NASA materials databases.
- www.ceramics.com Links to many technical and industrial sites.
- www.ceramicforum.com A web site for the ceramics professional.
- www.ecers.org The European Ceramics Society.
- www.ceramicsindustry.com Source of industry data.
- www.porcelainenamel.com The Porcelain Enamel Institute.

1.9 ON UNITS

We have attempted to present all data using the Système International d'Unités (SI). The basic units in this system are listed in Table 1.3 together with derived quantities. The primary exceptions in which non-SI units are encountered is in the expression of small distances and wavelengths

TABLE 1.3 SI Units

SI Base Units		
<i>Base quantity</i>	<i>Name</i>	<i>Symbol</i>
Length	meter	m
Mass	kilogram	kg
Time	second	s
Electric current	ampere	A
Thermodynamic temperature	kelvin	K
Amount of substance	mole	mol
Luminous intensity	candela	cd
SI-Derived Units		
<i>Derived quantity</i>	<i>Name</i>	<i>Symbol</i>
Area	square meter	m ²
Volume	cubic meter	m ³
Speed, velocity	meter per second	m/s
Acceleration	meter per second squared	m/s ²
Wave number	reciprocal meter	m ⁻¹
Mass density	kilogram per cubic meter	kg/m ³
Specific volume	cubic meter per kilogram	m ³ /kg
Current density	ampere per meter	A/m ²
Magnetic field strength	ampere per meter	A/m
Amount-of-substance concentration	mole per cubic meter	mol/m ³
Luminance	candela per square meter	cd/m ²
Mass fraction	kilogram per kilogram	kg/kg = 1

TABLE 1.3 Continued

SI-Derived Units with Special Names and Symbols

Derived quantity	Name	Symbol	Expression in terms of other SI units	Expression in terms of SI base units
Plane angle	radian	rad	—	$m \cdot m^{-1} = 1$
Solid angle	steradian	sr	—	$m^2 \cdot m^{-2} = 1$
Frequency	hertz	Hz	—	s^{-1}
Force	Newton	N	—	$m \cdot kg \cdot s^{-2}$
Pressure, stress	pascal	Pa	N/m^2	$m^{-1} \cdot kg \cdot s^{-2}$
Energy, work, quantity of heat	joule	J	$N \cdot m$	$m^2 \cdot kg \cdot s^{-2}$
Power, radiant flux	watt	W	J/s	$m^2 \cdot kg \cdot s^{-3}$
Electric charge, quantity of electricity	coulomb	C	—	$s \cdot A$
Electric potential difference, electromotive force	volt	V	W/A	$m^2 \cdot kg \cdot s^{-3} \cdot A^{-1}$
Capacitance	farad	F	C/V	$m^{-2} \cdot kg^{-1} \cdot s^4 \cdot A^2$
Electric resistance	ohm	Ω	V/A	$m^2 \cdot kg \cdot s^{-3} \cdot A^{-2}$
Electric conductance	siemens	S	A/V	$m^{-2} \cdot kg^{-1} \cdot s^3 \cdot A^2$
Magnetic flux	weber	Wb	$V \cdot s$	$m^2 \cdot kg \cdot s^{-2} \cdot A^{-1}$
Magnetic flux density	tesla	T	Wb/m^2	$kg \cdot s^{-2} \cdot A^{-1}$
Inductance	henry	H	Wb/A	$m^2 \cdot kg \cdot s^{-2} \cdot A^{-2}$
Celsius temperature	degree Celsius	$^{\circ}C$	—	K
Luminous flux	lumen	lm	$cd \cdot sr$	$m^2 \cdot m^{-2} \cdot cd = cd$
Illuminance	lux	lx	lm/m^2	$m^2 \cdot m^{-4} \cdot cd = m^{-2} cd$
Activity (of a radionuclide)	becquerel	Bq	—	s^{-1}
Absorbed dose, specific energy (imparted), kerma	gray	Gy	J/kg	$m^2 \cdot s^{-2}$
Dose equivalent	sievert	Sv	J/kg	$m^2 \cdot s^{-2}$
Catalytic activity	katal	kat	—	$s^{-1} mol$

SI-Derived Units with Names and Symbols That Include Other SI-Derived Units

Derived quantity	Name	Symbol
Dynamic viscosity	pascal second	Pa·s
Moment of force	newton meter	N·m
Surface tension	newton per meter	N/m
Angular velocity	radian per second	rad/s
Angular acceleration	radian per second squared	rad/s ²
Heat flux density, irradiance	watt per square meter	W/m ²
Heat capacity, entropy	joule per kelvin	J/K
Specific heat capacity, specific entropy	joule per kilogram kelvin	J kg ⁻¹ K ⁻¹
Specific energy	joule per kilogram	J/kg
Thermal conductivity	watt per meter kelvin	W m ⁻¹ K ⁻¹
Energy density	joule per cubic meter	J/m ³
Electric field strength	volt per meter	V/m
Electric charge density	coulomb per cubic meter	C/m ³
Electric flux density	coulomb per square meter	C/m ²
Permittivity	farad per meter	F/m
Permeability	henry per meter	H/m
Molar energy	joule per mole	J/mol
Molar entropy, molar heat capacity	joule per mole Kelvin	J mol ⁻¹ K ⁻¹
Exposure (X and γ rays)	coulomb per kilogram	C/kg
Absorbed dose rate	gray per second	Gy/s
Radiant intensity	watt per steradian	W/sr
Radiance	watt per square meter steradian	W m ⁻² sr ⁻¹
Catalytic (activity) concentration	katal per cubic meter	kat/m ³

where the Å (angstrom) is used by electron microscopists and X-ray crystallographers and the eV (electron volt) is used as a unit of energy for band gaps and atomic binding energies. We have not used the former but do use the latter for convenience. In the ceramics industry customary U.S. units are commonly encountered. For example, tempera-

ture is often quoted in Fahrenheit ($^{\circ}F$) and pressure in pounds per square inch (psi). Conversions between SI units and some of the special British and U.S. units are provided in Table 1.4.

The SI base unit of temperature is the kelvin, K. We use both K and $^{\circ}C$ in this text. The degree Celsius is equal

TABLE 1.4 Conversion Factors between SI Base Units and SI-Derived Units and Other Systems

SI units	Related units	Special British and U.S. units
Length: 1 m	10^{10} Å	3.28 ft
Mass: 1 kg 1 t		2.205 lb 0.984 U.K. (long) ton 1.103 U.S. (short) ton
Time: 1 s		2.778×10^{-4} h, 1.667×10^{-2} min
Absolute temperature: yK	$y - 273.15^\circ\text{C}$	$32 + 1.8(y - 273.15)^\circ\text{F}$
Area: 1 m ²	10 ⁴ cm ²	10.76 ft ²
Volume: 1 m ³	10 ⁶ cm ³	35.3 ft ³
Density: 1 kg/m ³	10 ⁻³ g/cm ³	6.24×10^{-2} lb/ft ³
Force: 1 N 9.807 N	10 ⁵ dyn 1 kgf (kilogram force)	— 2.205 lbf
Pressure, stress: 10 ⁵ Pa	1 bar; 750 mmHg (torr)	14.5 psi 0.987 atm
Energy, work, quantity of heat 1 J 105.5 MJ 0.1602 aJ	10 ⁷ erg or 0.239 cal — 1 eV	— 10 ⁵ Btu —
Power: 1 W	0.86 kcal/h	1.341×10^{-3} hp
Dynamic viscosity: 1 dPa·s	1 P (poise) 10 ² cP	—
Surface tension, surface energy: 1 N/m	10 ³ dyn/cm 10 ³ erg/cm ²	—
Magnetic field strength: 1 A/m	$4\pi \times 10^{-3}$ oersted	—
Magnetic flux density: 1 T	10 ⁴ G (gauss)	—

in magnitude to the kelvin, which implies that the numerical value of a temperature difference or temperature interval whose value is expressed in °C is equal to the numerical value of the same temperature difference or interval when its value is expressed in K.

Several of the figures that we have used were obtained from sources in which the original data were not in SI units. In many cases we have converted the units into SI using conversions and rounding in accordance with ASTM Standard E 380. Any variations from this procedure are noted in the appropriate place.

The decade power notation is a convenient method of representing large and small values within the SI units. Examples that you will encounter in this book include nm (10⁻⁹ m) and pF (10⁻¹² F). The full decade power notation scheme is given in Table 1.5.

TABLE 1.5 Decade Power Notation^a

Factor	Prefix	Symbol	Factor	Prefix	Symbol
10 ²⁴	yotta	Y	10 ⁻¹	deci	d
10 ²¹	zetta	Z	10 ⁻²	centi	c
10 ¹⁸	exa	E	10 ⁻³	milli	m
10 ¹⁵	peta	P	10 ⁻⁶	micro	μ
10 ¹²	tera	T	10 ⁻⁹	nano	n
10 ⁹	giga	G	10 ⁻¹²	pico	p
10 ⁶	mega	M	10 ⁻¹⁵	femto	f
10 ³	kilo	k	10 ⁻¹⁸	atto	a
10 ²	hecto	h	10 ⁻²¹	zepto	z
10 ¹	deca	da	10 ⁻²⁴	yocto	y

^aFactors that are not powers of 1000 are discouraged.

CHAPTER SUMMARY

We adopted the definition of a ceramic as a *nonmetallic, inorganic solid*. This definition encompasses a wide range of materials, many of which you might find are described as semiconductors elsewhere. The definition of ceramics we adopted is not quite complete in that glass—which behaves at room temperature and below like a solid but has the structure of a liquid—is actually a very important ceramic. More than half the ceramic industry is devoted to producing glass. The second largest segment of the ceramics market is in advanced (also called special, engineering, or technical) ceramics. This area is exciting and includes many of the newer materials such as HTSCs, bioceramics, and nanoceramics. These areas are predicted to experience significant growth.

PEOPLE IN HISTORY

In most of the chapters we will include a short section relating to the history of the topic, usually one-line biographies of our heroes in the field—some of those who have defined the subject. If the section is a little short in some chapters, the names/events may be listed in another chapter. The purpose of this section is to remind you that although our subject is very old, it is also quite young and many of the innovators never thought of themselves as ceramists.

REFERENCES

In the reference sections throughout the book we will list general references on the overall theme of the chapter and specific references that are the source of information referenced in the chapter. If a general reference is referred to specifically in the chapter, we will not generally repeat it.

CERAMICS TEXTBOOKS

- Barsoum, M. (2003) *Fundamentals of Ceramics*, revised edition, CRC Press, Boca Raton, FL.
- Chiang, Y-M., Birnie, D., III, and Kingery, W.D. (1998) *Physical Ceramics: Principles for Ceramic Science and Engineering*, Wiley, New York.
- Kingery, W.D., Bowen, H.K., and Uhlmann, D.R. (1976) *Introduction to Ceramics*, 2nd edition, Wiley, New York. This has been the ceramics “bible” for 40 years since the publication of the first edition by David Kingery in 1960.
- Lee, W.E. and Rainforth, W.M. (1994) *Ceramic Microstructures: Property Control by Processing*, Chapman & Hall, London.
- Norton, F.H. (1974) *Elements of Ceramics*, 2nd edition, Addison-Wesley, Reading, MA.
- Richerson, D.W. (2005) *Modern Ceramic Engineering: Properties, Processing, and Use in Design*, 3rd edition, CRC Press, Boca Raton, FL.
- Van Vlack, L.H. (1964) *Physical Ceramics for Engineers*, Addison-Wesley, Reading, MA.

INTRODUCTION TO MATERIALS SCIENCE TEXTBOOKS

- Askeland, D.R. and Phulé, P.P. (2005) *The Science of Engineering Materials*, 5th edition, Thompson Engineering, Florence, KY.
- Callister, W.D. (2007) *Materials Science and Engineering: An Introduction*, 7th edition, Wiley, New York.
- Schaeffer, J.P., Saxena, A., Antolovich, S.D., Sanders, T.H., Jr., and Warner, S.B. (2000) *The Science and Design of Engineering Materials*, 2nd edition, McGraw-Hill, Boston.
- Shackelford, J.F. (2004) *Introduction to Materials Science for Engineers*, 6th edition, Prentice Hall, Upper Saddle River, NJ.
- Smith, W.F. and Hashemi, J. (2006) *Foundations of Materials Science and Engineering*, 4th edition, McGraw-Hill, Boston.

JOURNALS

- Bulletin of the American Ceramic Society*, published by the American Ceramic Society (ACerS). News, society information, industry updates, and positions. Free to society members.
- Ceramic Industry*, published by Business News Publishing Co., Troy, MI. Information on manufacturing. Designed mainly for the ceramist in industry.
- Ceramics International*
- Glass Technology*, published by The Society of Glass Technology, Sheffield, UK.
- Journal of the American Ceramic Society*, house journal of the ACerS contains peer-reviewed articles, published monthly.
- Journal of the European Ceramic Society*, house journal of the European Ceramic Society published by Elsevier.
- Journal of Non-Crystalline Solids*
- Physics and Chemistry of Glasses*
- Transactions of the British Ceramic Society*

CONFERENCE PROCEEDINGS

- American Ceramic Society Transactions*
- Ceramic Engineering and Science Proceedings*. Published by the American Ceramic Society; each issue is based on proceedings of a conference.

USEFUL SOURCES OF PROPERTIES DATA, TERMINOLOGY, AND CONSTANTS

- Engineered Materials Handbook*, Volume 4, *Ceramics and Glasses* (1991), volume chairman Samuel J. Schneider, Jr., ASM International, Washington, D.C.
- CRC Handbook of Chemistry and Physics*, 86th edition (2005), edited by D.R. Lide, CRC Press, Boca Raton, FL. The standard resource for property data. Updated and revised each year.

- CRC Handbook of Materials Science* (1974), edited by C.T. Lynch, CRC Press, Cleveland, OH. In four volumes.
- CRC Materials Science and Engineering Handbook*, 3rd edition (2000), edited by J.F. Shackelford and W. Alexander, CRC Press, Boca Raton, FL.
- Dictionary of Ceramic Science and Engineering*, 2nd edition (1994), edited by I.J. McColm, Plenum, New York.
- The Encyclopedia of Advanced Materials* (1994), edited by D. Bloor, R.J. Brook, M.C. Flemings, and S. Mahajan, Pergamon, Oxford. In four volumes, covers more than ceramics.
- Handbook of Advanced Ceramics* (2003), edited by S. Somiya, F. Aldinger, N. Claussen, R.M. Spriggs, K. Uchino, K. Koumoto, and M. Kaneno, Elsevier, Amsterdam. Volume I, Materials Science; Volume II, Processing and Their Applications.

SAFETY

- Chemical Properties Handbook* (1999), edited by C.L. Yaws, McGraw-Hill, New York. Gives exposure limits for many organic and inorganic compounds, pp. 603–615.
- Coyne, G.S. (1997) *The Laboratory Companion: A Practical Guide to Materials, Equipment, and Technique*, Wiley, New York. Useful guide to the proper use of laboratory equipment such as vacuum pumps and compressed gases. Also gives relevant safety information.
- CRC Handbook of Laboratory Safety*, 5th edition (2000), edited by A.K. Furr, CRC Press, Boca Raton, FL. Worthwhile handbook for any ceramics laboratory. Covers many of the possible hazards associated with the laboratory.
- Hazardous Chemicals Desk Reference*, 5th edition (2002), edited by R.J. Lewis, Sr., Van Nostrand Reinhold, New York. Shorter version of the next reference.
- Sax's Dangerous Properties of Industrial Materials*, 11th edition (2004), edited by R.J. Lewis, Sr., Wiley, New York. A comprehensive resource in several volumes available in most libraries.
- The Occupational Safety and Health Administration (OSHA) of the U.S. Department of Labor web site on the internet is a comprehensive resource on all safety issues, www.osha.gov.

SPECIFIC REFERENCES

- Nanoscience and Nanotechnologies: Opportunities and Uncertainties*, The Royal Society, London, published on 29 July 2004, available at www.nanotec.org.uk/finalReport.
- Richerson, D.W. (2000) *The Magic of Ceramics*, The American Ceramic Society, Westerville, OH. A coffee table book about ceramics illustrating their diverse applications and uses.

EXERCISES

- 1.1 Which of the following materials could be classified as a ceramic. Justify your answer. (a) Solid argon (Ar); (b) molybdenum disilicide (MoSi_2); (c) NaCl; (d) crystalline sulfur (S); (e) ice; (f) boron carbide (B_4C).
- 1.2 Is silicone rubber (widely used as a caulking material in bathrooms and kitchens) a ceramic or a polymer? Explain your reasoning.
- 1.3 There are several different phases in the Fe-C system. One phase is the γ -Fe (austenite), which can contain up to about 8 atomic % C. Another phase is cementite, which contains 25 atomic % C. Are either of these two phases a ceramic? Justify your answer.
- 1.4 The following definition has been proposed: "All ceramics are transparent to visible light." Is this a good way of defining a ceramic? Explain your reasoning.
- 1.5 In the distribution of industry sales of advanced ceramics (Section 1.4), 13% was listed as "Other." Suggest applications that might be included in this group.
- 1.6 Ceramic tile accounts for about 15% of the floor tile market. (a) What alternatives are available? (b) What advantages/disadvantages do ceramics have over the alternatives? (c) What factors do you think influence the total amount of ceramic floor tiles used?
- 1.7 Gerber, the baby food manufacturer, is replacing most of its glass baby food jars with plastic. Miller Brewing Co. now sells some of its popular beers in plastic containers. Compare glass and plastics in terms of their application for packaging food and beverages.
- 1.8 The steel industry is the major consumer of refractories. What other industries might be users of this ceramic product?
- 1.9 Pearls and garnets are both examples of gems. We classify garnet as a ceramic. Would you classify pearl as a ceramic? Briefly justify your answer.
- 1.10 Some nuclear reactors use MOX fuel. What is MOX and is it a ceramic?

2

Some History

CHAPTER PREVIEW

In this chapter we present a brief history of ceramics and glasses. Because of the length of time over which they have been important to human existence it would be possible, indeed it has been done, to fill entire volumes on this one topic. We do not have the luxury of spending so much time on any one topic but history is important. In ceramics, it helps if we understand why certain events/developments occurred and when and how they did. We are really interested in setting the scene for many of the subsequent chapters. The earliest ceramics that were used were flint and obsidian. These exhibit conchoidal fracture like many modern day ceramics, such as cubic zirconia and glasses. This property enabled very sharp edges to be formed, which were necessary for tools and weapons. During the latter period of the Stone Age (the Neolithic period) pottery became important. Clay is relatively abundant. When mixed with water, it can be shaped and then hardened by heating. We will describe the different types of pottery and how the ceramics industry developed in Europe. The Europeans were not responsible for many of the early inventions in pottery; they were mostly trying to copy Chinese and Near East ceramics. Europe's contribution was to industrialize the process. We are also going to describe some of the major innovations in ceramics that occurred during the twentieth century, such as the float glass process, bioceramics, and the discovery of high-temperature superconductivity. These developments are important in defining the present status of the field and also give some indications of areas in which future innovations may occur. We will conclude the chapter by giving information about museums that have major collections of ceramic materials as well as listing the relevant professional societies.

2.1 EARLIEST CERAMICS: THE STONE AGE

Certain ancient periods of history are named after the material that was predominantly utilized at that time. The Stone Age, which began about 2.5 million years ago, is the earliest of these periods. Stone, more specifically flint, clearly satisfies our definition of a ceramic given in Chapter 1.

Flint is a variety of chert, which is itself cryptocrystalline quartz. Cryptocrystalline quartz is simply quartz (a polymorph of SiO_2) that consists of microscopic crystals. It is formed from silica that has been removed from silicate minerals by chemical weathering and carried by water as ultrafine particles in suspension. Eventually, it settles out as amorphous silica gel containing a large amount of water. Over time, the water is lost and small crystals form, even at low temperatures. During settling, the chemical conditions are changing slowly. As they change, the color, rate of deposition, and texture of the precipitate can also change. As a result, cryptocrystalline quartz occurs in many varieties, which are named

based on their color, opacity, banding, and other visible features. Flint is a black variety of chert. Jasper is a red/brown variety.

Flint is easily chipped and the fracture of flint is conchoidal (shell-like), so that sharp edges are formed. The earliest stone tools are remarkably simple, almost unrecognizable unless they are found together in groups or with other objects. They were made by a process called percussion flaking, which results in a piece (a flake) being removed from the parent cobble (a core) by the blow from another stone (a hammer-stone) or hard object. Both the flake and the core have fresh surfaces with sharp edges and can be used for cutting. While pebble tools do have a cutting edge, they are extremely simple and unwieldy. These basic tools changed, evolved, and improved through time as early hominids began to remove more flakes from the core, completely reshaping it and creating longer, straighter cutting edges. When a core assumes a distinctive teardrop shape, it is known as a handaxe, the hallmark of *Homo erectus* and early *Homo sapiens* technology. Figure 2.1 shows an example of a stone tool made by percussion flaking that was found in Washington State.

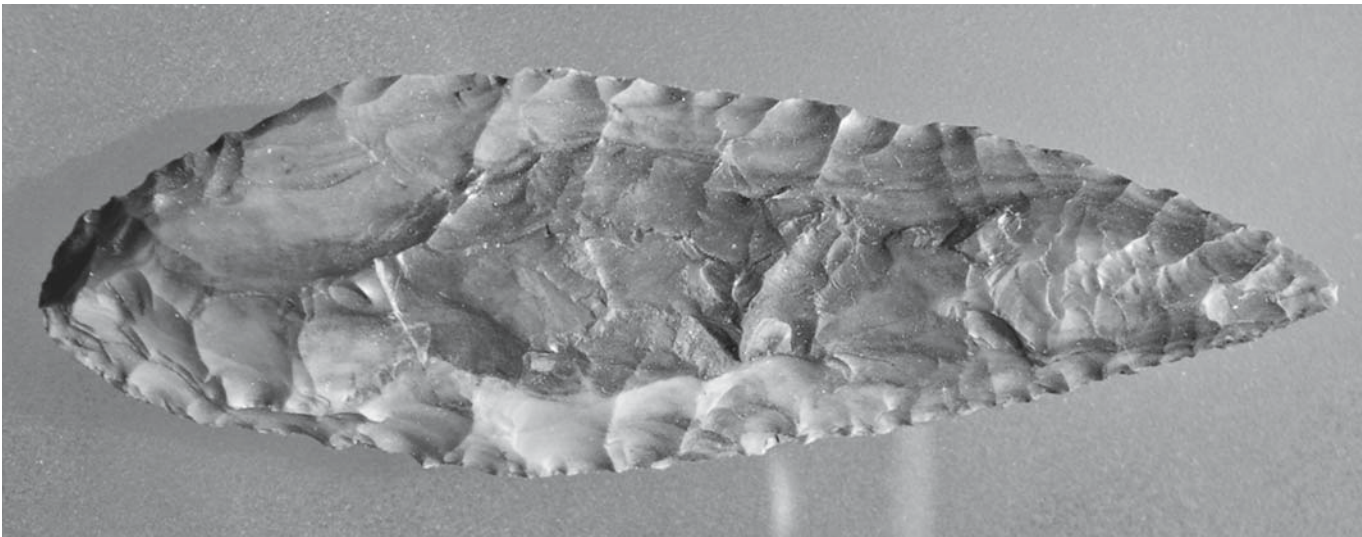


FIGURE 2.1 Example of a stone tool made by percussion flaking.

Period	Years Before Present	Stone Industry	Archaeological Sites	Hominid Species	Major Events
Neolithic	10,000	Blade tools	Lascaux Pincevent Dolni Vestonice Tabun Shanidar Klasies River Verteszöllös Kalambo Falls	<i>Homo sapiens sapiens</i> <i>Homo sapiens neanderthalensis</i>	Farming
Upper Paleolithic					Art
Middle Paleolithic					Mousterian flake tools
Lower Paleolithic	100,000	Clactonian chopping tools	Torraiba Terra Amata Olorgesailie Zhoukoudien Trinil	Archaic <i>Homo sapiens</i>	Burial of dead
	200,000				Oldest dwellings
	500,000				Use of fire
	1,000,000				Spread out of Africa
Basal Paleolithic		Acheulean handaxes		<i>Homo erectus</i>	Handaxes
	2,000,000	Oldowan pebble tools	Koobi Fora Olduvai Swartkrans	<i>Homo habilis</i>	Large brains First stone tools
	3,000,000		Hadar Laetoli	<i>Australopithecus</i>	
	6,000,000			<i>Ardipithecus</i>	Oldest hominid fossils

FIGURE 2.2 Chronology of the Stone Age.

Christian Thomsen first proposed the division of the ages of prehistory into the Stone Age, Bronze Age, and Iron Age for the organization of exhibits in the National Museum of Denmark in 1836. These basic divisions are still used in Europe, the United States, and in many other areas of the world. In 1865 English naturalist John Lubbock further divided the Stone Age. He coined the terms Paleolithic for the Old Stone Age and Neolithic the New Stone Age. Tools of flaked flint characterize the Paleolithic period, while the Neolithic period is represented by polished stone tools and pottery. Because of the age and complexity of the Paleolithic, further divisions were needed. In 1872, the French prehistorian Gabriel de Mortillet proposed subdividing the Paleolithic into Lower, Middle, and Upper. Since then, an even earlier subdivision of the Paleolithic has been designated with the discovery of the earliest stone artifacts in Africa. The Basal Paleolithic includes the period from around 2.5 million years ago until the appearance and spread of handaxes. These different periods are compared in Figure 2.2.

Stone tools that were characteristic of a particular period are often named after archeological sites that typified a particular technological stage.

- Oldowan pebble tools were found in the lowest and oldest levels of Olduvai Gorge.
- Acheulean handaxes are named after the Paleolithic site of St. Acheul in France, which was discovered in the nineteenth century.
- Clactonian chopping tools are named after the British site of Clacton-on-sea, where there is also the earliest definitive evidence for wood technology in the prehistoric record—the wood was shaped using flint tools.
- Mousterian flake tools are named after a site in France. The later blade tools are flakes that are at least twice as long as they are wide.

Another important ceramic during the Stone Age was obsidian, a dark gray natural glass precipitated from volcanic lava. Like other glasses it exhibits conchoidal fracture and was used for tools and weapons back into the Paleolithic period.

2.2 CERAMICS IN ANCIENT CIVILIZATIONS

The oldest samples of baked clay include more than 10,000 fragments of statuettes found in 1920 near Dolní Věstonice, Moravia, in the Czech Republic. They portray wolves, horses, foxes, birds, cats, bears, or women. One of these prehistoric female figures, shown in Figure 2.3,



FIGURE 2.3 A 25,000-year old baked clay Pavlovian figurine called the “Venus of Vestonice”; found in 1920 in Dolni Vestonice in the Czech Republic.

remained almost undamaged. It was named the “Venus of Vestonice” and is believed to have been a fertility charm. The absence of facial features on this and other “Venus” figures is causing many anthropologists to rethink the role these figures might have played in prehistoric society. The statuette stands about 10 cm tall and has been dated as far back as 23,000 BCE. One of the most recent archeological finds was made in the caves of Tuc d’Audoubert in France, where beautifully preserved clay bison have been found that are estimated to be 12,000 years old.

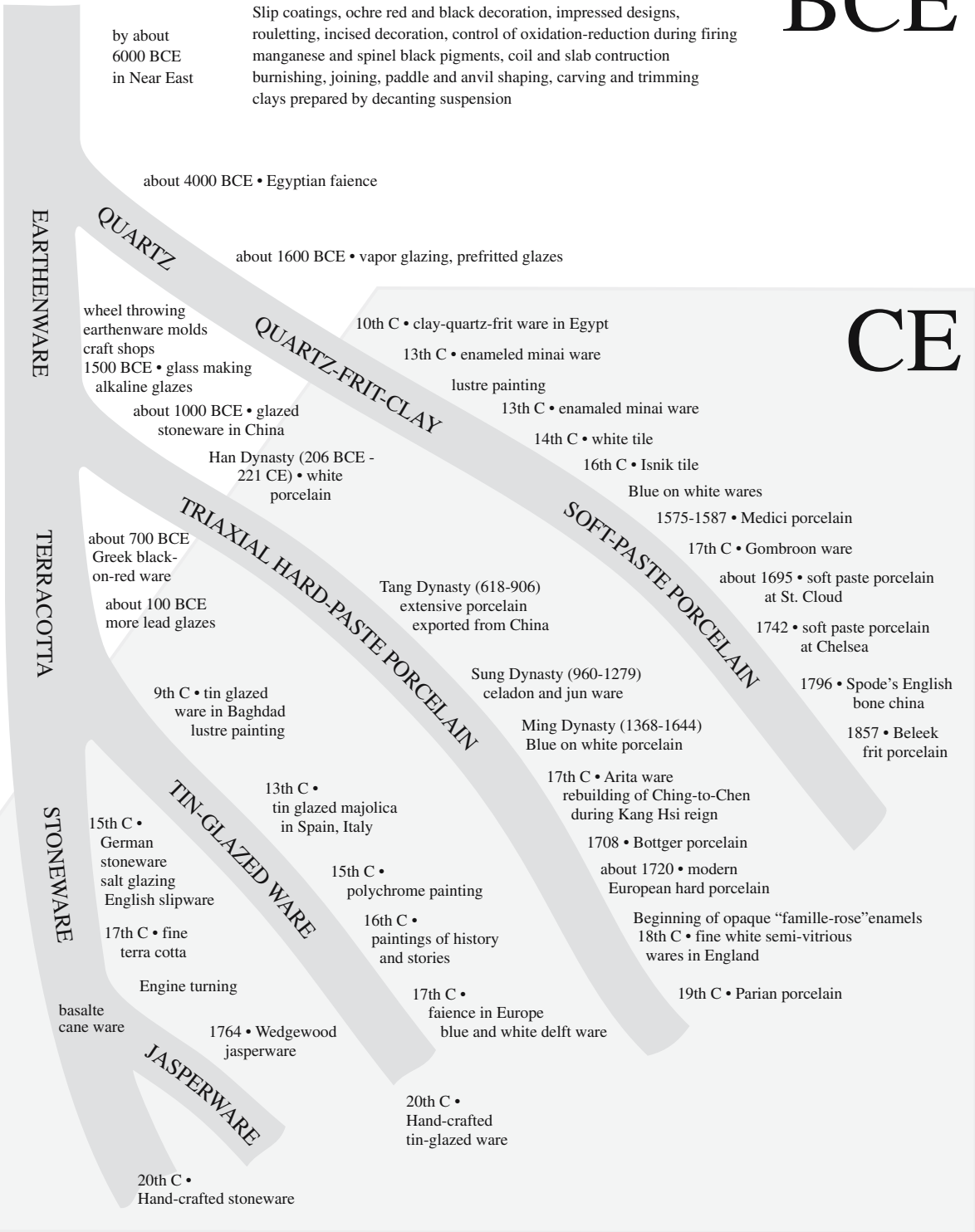
The earliest archeological evidence of pottery production dates back to about 10,000 BCE and the discovery of fragments from a cave dwelling near Nagasaki, Japan. This type of pottery is called Jomon pottery because of the characteristic surface patterns, which were made with a twisted cord. Jomon means “cord pattern.” The pottery also featured patterns made with sticks, bones, or fingernails. These vessels, like those produced in the Near East about 10,000 years ago, were fired at a low temperature compared to modern day pottery production.

By 6400 BCE, pottery making was a well-developed craft. Subsequent developments in the history of ceramics are shown in Figure 2.4. We will be describing some of these in a little more detail in later sections of this chapter.

about 22000 BCE • Earliest known fired clay figures

about 8000 BCE • Fired vessels in Near East

BCE



CE

FIGURE 2.4 The “flow” of ceramic history illustrates the mainstreams of earthenware, terra cotta, and stoneware, of “triaxial” hard-paste porcelain, of quartz-based bodies, and of tin-glazed ware. Some important shaping and decorative techniques are illustrated, but the diagram is far from complete.

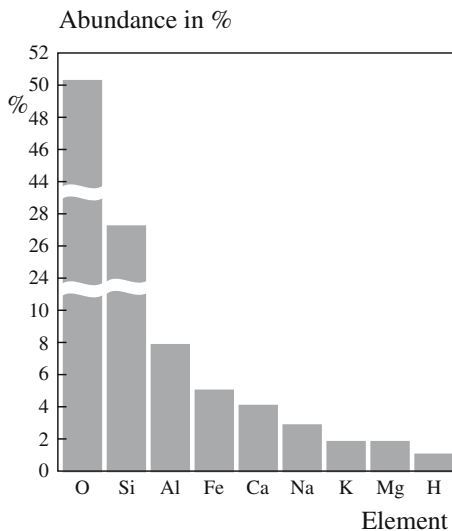


FIGURE 2.5 Abundance of common elements in the earth's crust.

2.3 CLAY

Silicate minerals make up the vast majority of the earth's crust, which is not surprising if we consider

- The abundance of Si and O (Figure 2.5)
- The high strength of the Si–O bond (Table 2.1)

Since silicate and aluminum silicate minerals are widely available, they are inexpensive and form the backbone of the traditional high-volume products of the ceramic industry. Their abundance also explains why earthenware products are found in nearly every part of the world. The situation is very different with regard to kaolinite, the essential ingredient, along with feldspar and quartz, needed to make porcelain, by far the finest and most highly prized form of ceramic. Kaolin deposits are more localized. There are excellent deposits, for example, in southwest England. In the United States most kaolin comes from the southeast between central Georgia and the Savannah River area of South Carolina.

Clay minerals remain the most widely used raw materials for producing traditional ceramic products. The total U.S. production of clays is about 40 million tons per year, valued at \$1.5 billion.

TABLE 2.1 Bond Strengths with Oxygen

Bond	Strength (kJ/mol)
Ti-O	674
Al-O	582
Si-O	464
Ca-O	423
Mn ^a -O	389
Fe ^a -O	389
Mg-O	377

^a2+ state.

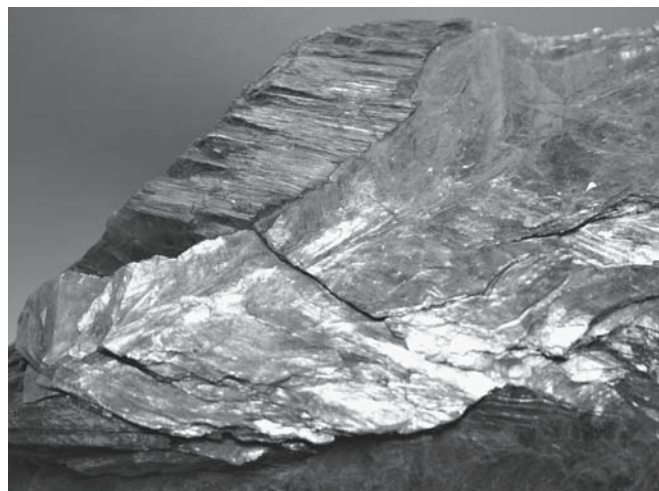


FIGURE 2.6 Large “grains” of mica clearly show the lamellar nature of the mineral. Two orientations are present in this one piece.

The clay minerals are layered or sheet silicates with a grain size <2 μm. Chemically they are aluminosilicates. In nature, mica (shown in Figure 2.6) is constructed by stacking layers together to form sheets. Kaolinite has a related structure but tends to have smaller “grains.” Rocks that contain a large amount of kaolinite are known as kaolin. When the sheets are separated by films of water, the platelets slide over one another to add plasticity to the mixture. This plasticity is the basis of the use of clay for pottery. Moreover, when the clay–water mixture is dried it becomes hard and brittle and retains its shape. On firing at temperatures about 950°C, the clay body becomes dense and strong. In Chapter 7 we describe the structures of some of the important clay minerals, including kaolin.

2.4 TYPES OF POTTERY

Pottery is broadly divided into

- Vitrified ware
- Nonvitrified ware

The classification depends upon whether the clay was melted during the firing process into a glassy (vitreous) substance or not. Within these divisions we have the following:

- *Earthenware* is made from red “earthenware clay” and is fired at fairly low temperatures, typically between 950 and 1050°C. It is porous when not glazed, relatively coarse, and red or buffcolored, even black after firing. The term “pottery” is often used to signify earthenware. The major earthenware products are bricks, tiles, and terra cotta vessels. Earthenware dating back to between 7000 and 8000 BCE has been found, for example, in Catal Hüyük in Anatolia (today’s Turkey).

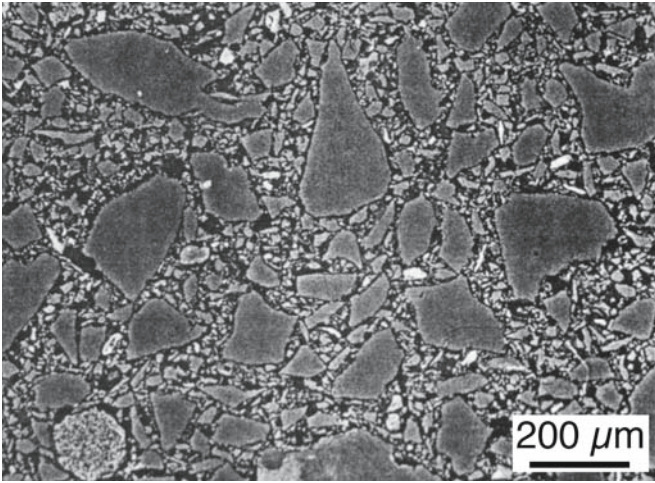


FIGURE 2.7 Microstructure of a “Masters of Tabriz” tile showing many large grains of crystalline SiO₂.

- *Stoneware* is similar to earthenware but is fired to a higher temperature (around 1200–1300°C). It is vitrified, or at least partially vitrified, and so it is nonporous and stronger. Traditional stoneware was gray or buff colored. But the color can vary from black via red, brown, and gray to white. Fine white stoneware was made in China as early as 1400 BCE (Shang dynasty). Johann Friedrich Böttger and E.W. von Tschirnhaus produced the first European stoneware in Germany in 1707. This was red stoneware. Later Josiah Wedgwood, an Englishman, produced black stoneware called basalte and white stoneware colored by metal oxides called jasper.
- *Porcelain* was invented by the Chinese and produced during the T'ang dynasty (618–907 CE). It is a white, thin, and translucent ceramic that possesses a metal-like ringing sound when tapped. Porcelain is made from kaolin (also known as china clay), quartz, and feldspar. Fired at 1250–1300°C it is an example of vitreous ware. The microstructure of porcelain is quite complicated. Figure 2.7 shows a backscattered electron image obtained using a scanning electron microscope (SEM) of the microstructure of a “Masters of Tabriz” tile (1436 CE) showing that it contains many large grains of quartz immersed in a continuous glass phase.
- *Soft-paste porcelain* is porcelain with low clay content that results in a low alumina (Al₂O₃) content. The most common form of soft-paste porcelain is formed of a paste of white clay and ground glass. This formulation allows a lower firing temperature, but provides a less

plastic body. Not being very tough, it is easily scratched and more rare than hard-paste porcelain.

- *Hard-paste porcelain* is porcelain with a relatively high alumina content derived from the clay and feldspar, which permits good plasticity and formability, but requires a high firing temperature (1300–1400°C). Böttger produced the first successful European hard-paste porcelain in 1707–1708 consisting of a mixture of clay and gypsum. This work laid the foundation for the Meissen porcelain manufacture in Saxony (Germany) in 1710.
- *Bone China* has a similar recipe to hard-paste porcelain, but with the addition of 50% animal bone ash (calcium phosphate). This formulation improves strength, translucency, and whiteness of the product and was perfected by Josiah Spode at the end of the eighteenth century. It was then known as “English China” or “Spode China.”

2.5 GLAZES

To hermetically seal the pores of goods made of earthenware an additional processing step called glazing was introduced around or probably even before 3000 BCE by the Egyptians. It involved the coating of the fired objects with an aqueous suspension consisting of finely ground quartz sand mixed with sodium salts (carbonate, bicarbonate, sulfate, chloride) or plant ash. The ware would then be refired, usually at a lower temperature, during which the particles would fuse into a glassy layer.

Two other types of glaze, which also date back several millennia, have been applied to earthenware. These are the transparent lead glaze and the opaque white tin glaze.

The Lead Glaze

The addition of lead reduces the melting or fusion point of the glaze mixture, which allows the second firing to be at an even lower temperature. The first lead-rich glazes were probably introduced during the Warring States period (475–221 BCE). The lead oxide (PbO) content was about 20%. During the Han dynasty (206 BCE–CE 200) higher lead oxide contents were typical, up to 50–60%. Lead glazing was subsequently widely used by many civilizations. However, lead from the glaze on tableware may be leached by food. Table 2.2 shows lead released from two glazes that were made to match those of two Eastern Han Dynasty lead glazes. The glaze formulations were remade

TABLE 2.2 Composition of Han Lead Glazes (wt%) and Lead Metal Release (ppm)

	PbO	SiO ₂	Al ₂ O ₃	Fe ₂ O ₃	TiO ₂	CaO	MgO	K ₂ O	Na ₂ O	BaO	CuO	SnO ₂	Cl	S	Pb release
Glaze 1	59.7	29.5	3.7	1.3	0.2	1.9	0.5	0.9	0.2	0.2	1.2	0.2	2.2	—	42
Glaze 2	43.5	33.4	3.9	2.0	0.6	2.0	0.7	0.5	0.4	7.7	3.0	1.2	—	0.6	120

and fired by CERAM (formerly the British Ceramic Research Association) in the UK. The amount of lead released in a standard leach test is determined by filling the glazed ceramic item with 4% acetic acid at 20°C for 24 hours; the acid is then analyzed for Pb by flame atomic absorption spectrometry. The present U.S. Food and Drug Administration limit for Pb release from small hollowware is 2 ppm.

Some historians believe that lead release from glazes on pitchers and other food and beverage containers and utensils poisoned a large number of Roman nobility and thus contributed (together with Pb from water pipes) to the fall of the Roman Empire (see, for example, Lindsay, 1968). Lead poisoning was responsible for the high mortality rates in the pottery industry even during the nineteenth century. Many countries have now outlawed lead glazing unless fritted (premelted and powdered) glazes are utilized that prevent the lead from being easily leached. The possibility of leaching a heavy metal from a glass is a concern today in the nuclear-waste storage industry.

The Tin Glaze

The Assyrians who lived in Mesopotamia (today's Northern Iraq) probably discovered tin glazing during the second millennium BCE. It was utilized for decorating bricks, but eventually fell into disuse. It was reinvented again in the ninth century CE and spread into Europe via the Spanish island of Majorca, after which it was later named (*Majolica*). Centers of majolica manufacture developed in Faenza in Italy (*Faience*) and in 1584 at the famous production center at Delft in the Netherlands (*Delftware*). Tin glazing became industrially important at the end of the nineteenth century with the growth of the ceramic sanitary ware industry.

2.6 DEVELOPMENT OF A CERAMICS INDUSTRY

Quantity production of ceramics began during the fourth millennium BCE in the Near East. Transition to a large-scale manufacturing industry occurred in Europe during the eighteenth century. At the beginning of the century, potteries were a craft institution. But this situation was transformed at several important sites:

- Vincennes and Sèvres in France
- Meissen in Germany
- Staffordshire in England

By the end of the eighteenth century, the impact of greater scientific understanding (such as chemical analysis of raw materials) had changed the field of ceramics. At the same time, the ceramic industry played an influential role in the industrial revolution and the development of factory systems in England and across Europe. Ceramics became

an important and growing export industry that attracted entrepreneurs and engineers to develop modern production and marketing methods. A leader in this revolution was Josiah Wedgwood.

In 1767 Wedgwood produced improved unglazed black stoneware, which he called "basalte." The famous Wedgwood "jasperware" began production in 1775 and consisted of

- One part flint
- Six parts barium sulfate
- Three parts potters' clay
- One-quarter part gypsum

Wedgwood was so excited by this new ceramic body that he wrote to his partner:

The only difficulty I have is the mode of procuring and conveying incog (*sic*) the raw material. . . . I must have some before I proceed, and I dare not have it in the nearest way nor undisguised.

Jasper is white but Wedgwood found that it could be colored an attractive blue by the addition of cobalt oxide. (The mechanism for color formation in transition metal oxides is described in Chapter 32.) The manufacturing process was soon changed (in part because of a sharp increase in the cost of the blue pigment) and the white jasper was coated with a layer of the colored jasper. Wedgwood jasper remains sought after and highly collectable. You can visit the Wedgwood factory in England and watch the production process.

Wedgwood also was instrumental in changing the way manufacturing was done. He divided the process into many separate parts, and allowed each worker to become expert in only one phase of production. This approach was revolutionary at the time and was designed to increase the performance of each worker in a particular area and reduce the requirement for overall skill. He was also concerned with trade secrets; each workshop at his factory had a separate entrance so workers would not be exposed to more than a limited number of valuable secrets.

In the increasingly competitive entrepreneurial economy of the eighteenth century, Wedgwood was one of the leading figures to have the foresight and the willingness to expend the necessary effort to promote the general interests of the ceramics industry. In the early days of the pottery industry in England, transport of raw materials in and product out was done with pack animals. It was clear that quantity production could not be achieved without better transportation. Wedgwood organized a potters' association to lobby for better roads and, more importantly, a canal system. The opening of the Trent-Mersey Canal in 1760 ensured that Staffordshire would remain the center of English pottery production.

As with many industries, the first stage of the industrial revolution did not result in a deterioration of working

conditions. A partly rural craft-based skill, such as pottery making, became an injurious occupation only as industrialization progressed, bringing into overcrowded town centers poor workers from the countryside. Occupational diseases were prevalent in the potteries. The main problem was diagnosed at an early date—lead poisoning. In 1949 British regulations forbade the use of raw lead in glaze compositions. Prior to this there were 400 cases of lead poisoning a year at the end of the nineteenth century. Although experiments with leadless glazes were recorded throughout the nineteenth century, lead was essential, and the safe solution adopted and approved early in the twentieth century was a lead glaze of low solubility, produced by making the glaze suspension out of fritted lead.

Another serious health risk for potters was pneumoconiosis: flint dust particles when inhaled caused gradual and often fatal damage to the lungs. It was a lingering disease, which took many decades to diagnose and control. Flint is still used as a component in the bodies of many traditional ceramic wares, but the risk of pneumoconiosis has been virtually eliminated through proper ventilation, the cleanliness of workshops, and the use of protective clothing.

In North America the origin of pottery production occurred in regions where there were deposits of earthenware clay and the wood needed for the kilns. The abundance of these raw materials were factors in the English settling in Jamestown, Virginia in 1607. And there is evidence that pottery production began in Jamestown around 1625 (see Guillard, 1971). Similar supplies were available in the Northeast for the English potters accompanying the small band of farmers and tradesmen who arrived in Plymouth in the 1620s. In New England and in Virginia potters used a lead glaze brushed onto the inside of the earthenware vessel to make the porous clay watertight. The important pottery centers in North America during the mid-nineteenth century were Bennington, VT, Trenton, NJ, and East Liverpool, OH. The geographical location of each center formed a right triangle located in the northeast. These locations had deposits of fine clay and river transportation, which provided easy access to markets. By 1840 there were more than 50 stoneware potteries in Ohio, earning Akron the tag “Stoneware City.”

In the past, ceramic production was largely empirical. To maintain uniformity, producers always obtained their raw materials from the same supplier and avoided changing any detail of their process. The reason was that they were dealing with very complex systems that they did not understand. Today, as a result of ~100 years of ceramics research, processing and manufacturing are optimized based on an understanding of basic scientific and engineering principles. Research in ceramics was spurred on by two main factors:

- Development of advanced characterization techniques such as X-ray diffraction and electron microscopy, which provided structural and chemical information
- Developments in ceramic processing technology

2.7 PLASTER AND CEMENT

A special ceramic is hydraulic (or water-cured) cement. World production of hydraulic cement is about 1.5 billion tons per year. The top three producers are China, Japan, and the United States. When mixed with sand and gravel, we obtain concrete—the most widely utilized construction material in the industrialized nations. In essence, concrete is a ceramic matrix composite (CMC) in which not just the matrix but also the reinforcing material is ceramic.

Ancient Romans and Greeks, 2000 years ago, pioneered the use of cement. Its unique chemical and physical properties produced a material so

lasting that it stands today in magnificent structures like the Pantheon in Rome. Roman cement consisted of a mixture of powdered lime (CaO) and volcanic ash (a mixture of mainly SiO₂, Al₂O₃, and iron oxide)—called *pozzolana*—from Mount Vesuvius, which buried the ancient city of Pompeii in 79 CE. This mixture hardens in the presence of water.

Contemporary hydraulic cement, for example, Portland cement (invented by Joseph Aspdin and named after a natural stone from the island of Portland in England, which it resembles), has a composition similar to pozzolanic cement. The chief ingredients of Portland cement are di- and tricalcium silicates and tricalcium aluminate. In the reduced nomenclature given in Table 2.3 these ingredients would be expressed as C₂S, C₃S, and C₃A, respectively. Portland cement is produced to have a specific surface area of ~300 m²/kg and grains between 20 and 30 μm. The average composition is given in Table 2.4. In Chapter 8 we will show you on a ternary phase diagram the composition range of Portland cements.

The setting reactions for Portland cement are similar to those for the ancient pozzolanic cement. The first reaction is the hydration of C₃A. This reaction is rapid, occurring within the first 4 hours, and causes the cement to set:

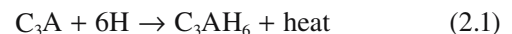


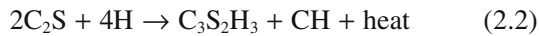
TABLE 2.3 Reduced Nomenclature for Cement Chemistry

Lime	CaO = C
Alumina	Al ₂ O ₃ = A
Silica	SiO ₂ = S
Water	H ₂ O = H

TABLE 2.4 Average Overall Composition of Portland Cement Clinker

By element	wt%	By Phase	Reduced nomenclature	Name	wt%
CaO	60–67	3CaO·SiO ₂	C ₃ S	Tricalcium silicate	45–70
SiO ₂	17–25	2CaO·SiO ₂	C ₂ S	Dicalcium silicate	25–30
Al ₂ O ₃	3–9	3CaO·Al ₂ O ₃	C ₃ A	Tricalcium aluminate	5–12
Fe ₂ O ₃	0.5–6	4CaO·Al ₂ O ₃ Fe ₂ O ₃	C ₄ AF	Tricalcium aluminoferrite	5–12
MgO	0.1–4	CaSO ₄ ·2H ₂ O	CSH ₂	Gypsum	3–5
Na ₂ O, K ₂ O	0.5–1.3				
SO ₃	1–3				

The C₃AH₆ phase or ettringite is in the form of rods and fibers that interlock. The second reaction, which causes the cement to harden, is slower. It starts after about 10 hours, and takes more than 100 days to complete. The product is tobermorite gel, a hydrated calcium silicate (Ca₃Si₂O₇·3H₂O), which bonds everything together.



Protuberances grow from the gel coating and form arrays of interpenetrating spines. Scanning electron microscopy (SEM) has been one tool that has been used to examine cement at various stages in the setting and hardening process. Figure 2.8 shows an SEM image recorded 8 days into the hardening process. The plate-like features are calcium hydroxide (CH); the cement (Ct) grains are already completely surrounded by the tobermorite gel (called CSH in Figure 2.8).

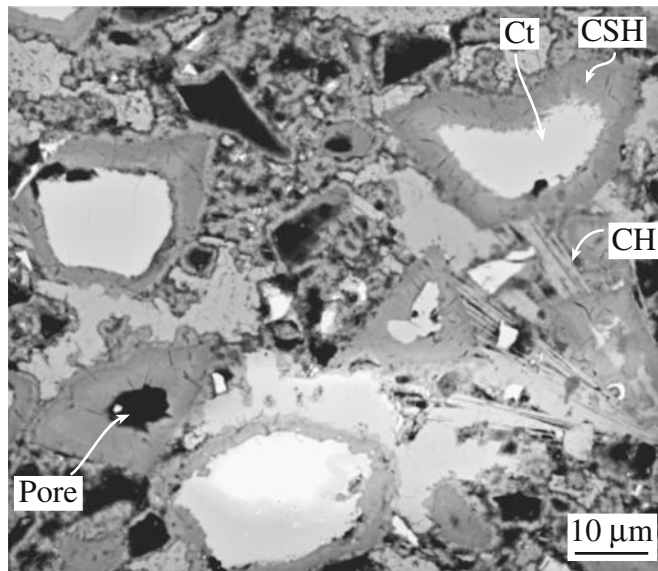


FIGURE 2.8 Reaction products in cement after 8 days hardening (SEM image).

The development of strength with time for Portland cement is shown in Figure 2.9. The reactions give off a lot of heat (Figure 2.10). In very large concrete structures, such as the Hoover Dam at the Nevada–Arizona border in the United States, heat is a potential problem. Cooling pipes must be embedded in the concrete to pump the heat out. These pipes are left in place as a sort of reinforcement. In the case of the Hoover Dam, the construction

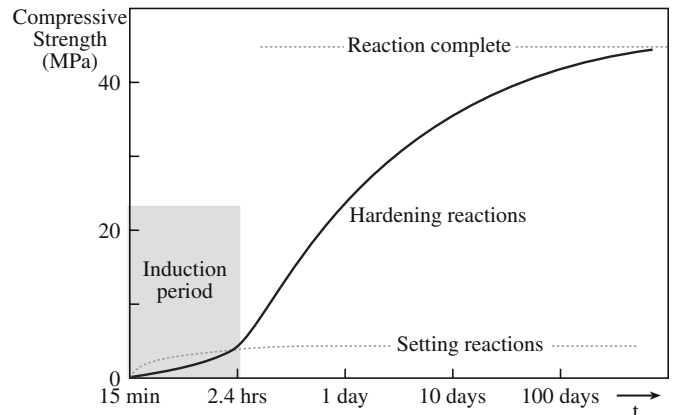


FIGURE 2.9 Increase in compressive strength of Portland cement with time.

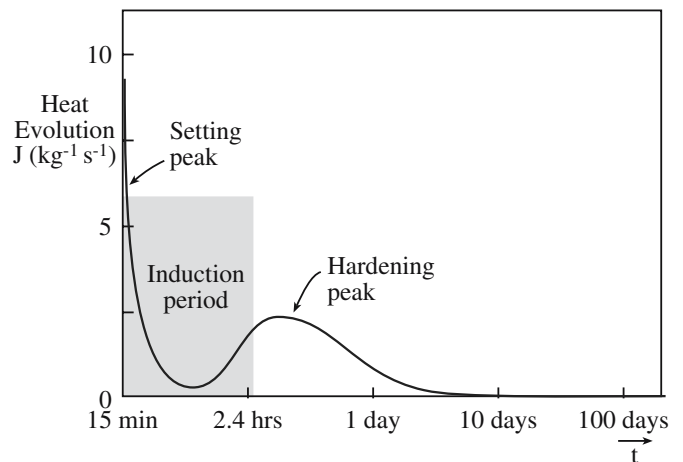
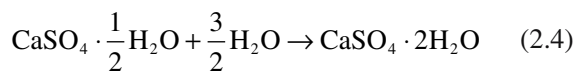


FIGURE 2.10 Heat evolution during the setting and hardening of Portland cement.

consisted of a series of individual concrete columns rather than a single block of concrete. It is estimated that if the dam were built in a single continuous pour, it would have taken 125 years to cool to ambient temperatures. The resulting stresses would have caused the dam to crack and possibly fail.

Plaster of Paris is a hydrated calcium sulfate ($2\text{CaSO}_4 \cdot \text{H}_2\text{O}$). It is made by heating naturally occurring gypsum ($\text{CaSO}_4 \cdot 2\text{H}_2\text{O}$) to drive off some of the water. When mixed with water, plaster of Paris sets within a few minutes by a cementation reaction involving the creation of interlocking crystals:



To increase the setting time a retarding agent (the protein keratin) is added. Plaster of Paris is named after the French city where it was made and where there are abundant gypsum deposits. Following the Great Fire of London in 1666 the walls of all wooden houses in the city of Paris were covered with plaster to provide fire protection. The earliest use of plaster coatings dates back 9000 years and was found in Anatolia and Syria. The Egyptians used plaster made from dehydrated gypsum powder mixed with water as a joining compound in the magnificent pyramids.

2.8 BRIEF HISTORY OF GLASS

The history of glass dates back as far as the history of ceramics itself. We mentioned in Section 2.1 the use of obsidian during the Paleolithic period. It is not known for certain when the first glass objects were made. Around 3000 BCE, Egyptian glassmakers systematically began making pieces of jewelry and small vessels from glass; pieces of glass jewelry have been found on excavated Egyptian mummies. By about 1500 BCE Egyptian glassmakers during the reign of Touthmosis III had developed a technique to make the first usable hollowware.

The glass was made from readily available raw materials. In the clay tablet library of the Assyrian King Ashurbanipal (669–626 BCE) cuneiform texts give glass formulas. The oldest one calls for 60 parts sand, 180 parts ashes of sea plants, and 5 parts chalk. This recipe produces an $\text{Na}_2\text{O}-\text{CaO}-\text{SiO}_2$ glass. The ingredients are essentially the same as those used today but the proportions are somewhat different. Pliny the Elder (23–79 CE) described the composition and manufacture of glass in *Naturalis Historia*. During Roman times glass was a much-prized status symbol. High-quality glassware was valued as much as precious metals.

Figure 2.11 shows a Flemish drawing from the early fifteenth century depicting glass workers in Bohemia, from the *Travels of Sir John Mandeville*. It shows the legendary pit of Mynon with its inexhaustible supply of sand.

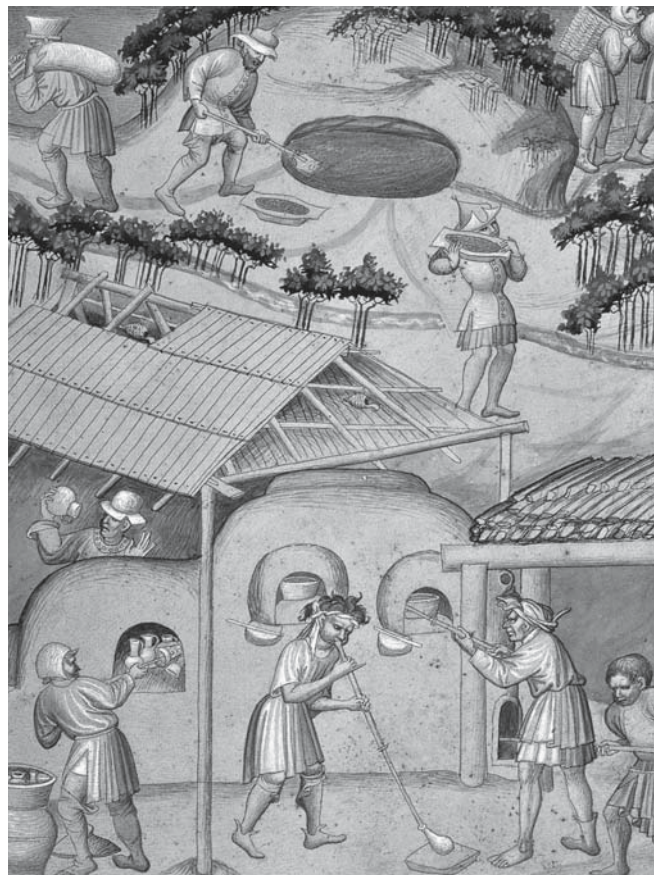


FIGURE 2.11 Glass workers in Bohemia, from the *Travels of Sir John Mandeville*, ink and tempera on parchment, Flemish, early fifteenth century.

And beside Acre runs a little river, called the Belyon [Abellin], and near there there is the Fosse of Mynon, all round, roughly a hundred cubits broad; and it is full of gravel. And however much be taken out in a day, on the morrow it is as full as ever it was, and that is a great marvel. And there is always a great wind in that pit, which stirs up all the gravel and makes it eddy about. And if any metal be put therein, immediately it turns to glass. This gravel is shiny, and men make good clear glass of it. The glass that is made of this gravel, if it be put back in the gravel, turns back into gravel, as it was at first. And some say it is an outlet of the Gravelly Sea. People come from far countries by sea with ships and by land with carts to get some of that gravel.

Sand is an important constituent of most oxide glasses. Early glassmakers would have made effective use of natural resources and set up their workshops near a source of raw materials. This practice was also adopted during the time of Josiah Wedgwood and was the reason that the ceramic industry developed in the north of England—not in London, the capital. The illustration also shows the entire cycle of producing a glass object from obtaining the raw materials to testing of the final product.

One of the most common methods used to form glass is glassblowing. Although this technique was developed

over 2000 years ago in Syria the glassblowing pipe has not changed much since then. The main developments are the automated processes used to produce glass containers and light bulbs in the thousands. In Chapter 21 we will summarize the important milestones in glass formation and production.

In this section we consider two specific aspects of the history of glass:

- Lead crystal glass
- Duty on glass

These events occurred between the very early experimentation with glass in Egyptian and other ancient civilizations and more modern developments in glass such as optical fibers and glass ceramics.

The Venetians used pyrolusite (a naturally occurring form of MnO_2) as a decolorizer to make a clear glass. This addition was essential because the presence of impurities, chiefly iron, in the raw materials caused the glass to have an undesirable greenish-brown color. The manganese oxidizes the iron, and is itself reduced. The reduced form of manganese is colorless but when oxidized it is purple (Mn in the +7 oxidation state). Manganese was used until quite recently as a decolorizer and some old windows may be seen, particularly in Belgium and the Netherlands, where a purple color has developed owing to long exposure to sunlight, which has oxidized the manganese back to the purple form.

Lead crystal glass is not crystalline. But the addition of large amounts of lead oxide to an aluminosilicate glass formulation produces a heavy glass with a high refractive index and excellent transparency. Suitable cutting, exploiting the relative ease with which lead glass can be cut and polished, enhances the brilliance. The lead content, in the form of PbO , in Ravenscroft's lead crystal glass has been determined to be about 15%. Now lead crystal glasses contain between 18 and 38% PbO . For tableware to be sold as "lead crystal" the PbO content must be about 25%.

Expansion of the British glass industry followed the success of lead crystal glass and during the eighteenth century it achieved a leading position that it held for a hundred years. The beautiful drinking glasses of this period are collector items. English production was hindered only by a steady increase of taxation between 1745 and 1787 to pay for the war against France. The tax was levied on glass by weight, and as the tendency had been to add more lead oxide, the production was checked. As a result, many glassmakers moved to Ireland where glass was free from duty and glassworks were set up in Dublin and Waterford.

During the eighteenth and nineteenth centuries the British government regarded the glass industry as an inexhaustible fund to draw on in times of war and shortage. A glass duty was first imposed by statute in 1695 and made perpetual the following year, but it was so high as to discourage manufacture and was soon reduced by half. The

duties were repealed in 1698 because of the reduction in the consumption of coal and the rise in unemployment. In 1746 duties were again levied, but they were also imposed on imported glassware. The Act of 1746 required a record to be kept of all furnaces, pots, pot chambers, and warehouses, and due notice to be given when pots were to be changed. In the same year the regulations were applied for the first time to Ireland, as a result of which many of the flourishing glassworks established there to avoid the excise duties began to decline. The duties seriously delayed technological innovation and in 1845 they were repealed. The industry immediately entered a new period of growth.

The Industrial Revolution started in England during the latter part of the eighteenth century, but this did not radically affect the glass industry in its early stages because mechanical power was not required in the glassworks. The impact of mechanization is shown best by its development in the American glass industry. American workers were scarce and wages were much higher than in Europe and so means were sought to increase productivity. One of the important developments at this time was a process for making pitchers by first pressing and then free-hand blowing, patented by Gillinder in 1865. This patent led to a period in which American container production changed from a craft industry to a mechanized manufacturing industry.

To the early glassmakers the nature of the structure of glass was a mystery. But they did know that the addition of certain components could modify properties. The most successful model used to describe the structure of oxide glasses is the random-network model devised by W.H. Zachariasen (1932). This model will be described in some detail in Chapter 21. Although the random-network model is over 60 years old it is still extensively used to explain the behavior and properties of oxide glasses and is widely used in industry in developing and modifying glass formulations.

2.9 BRIEF HISTORY OF REFRACTORIES

The development of refractories was important for many industries, most notably for iron and steel making and glass production. The iron and steel industry accounts for almost two-thirds of all refractories used. The discovery by Sidney Gilchrist Thomas and his cousin Percy Gilchrist in 1878 that phosphorus could be removed from steel melted in a dolomite-lined Bessemer converter (and subsequently on a dolomite hearth) was an important development. They solved a problem that had defeated the leading metallurgists of the day. And what is even more remarkable is that Thomas, who had originally wanted to be a doctor, was a magistrate's clerk at Thames police court in London. Out of interest he attended evening classes in chemistry, and later metallurgy, at Birkbeck Mechanics Institute (now Birkbeck College, University of London), where he became aware of the phosphorus problem. It took three attempts

(over a 1-year period) by Thomas and Gilchrist to report the successful outcome of their work to the Iron and Steel Institute. A lesson in perseverance! When their paper was finally presented (Thomas and Gilchrist, 1879) the success of their process had become widely known and they attracted an international audience.

Dolomite refractories are made from a calcined natural mineral of the composition $\text{CaCO}_3 \cdot \text{MgCO}_3$. The production of magnesite, a more slag-resistant refractory than dolomite, began in 1880. Magnesite refractories consist mainly of the mineral periclase (MgO); a typical composition will be in the range MgO 83–93% and Fe_2O_3 2–7%. Historically, natural magnesite (MgCO_3) that was calcined provided the raw material for this refractory. With increased demands for higher temperatures and fewer process impurities, higher purity magnesia from seawater and brine has been used. This extraction process is described in Chapter 19.

In 1931 it was discovered that the tensile strength of mixtures of magnesite and chrome ore was higher than that of either material alone, which led to the first chrome–magnesite bricks. Chrome refractories are made from naturally occurring chrome ore, which has a typical composition in the range Cr_2O_3 30–45% Al_2O_3 15–33%, SiO_2 11–17%, and FeO 3–6%. Chrome–magnesite refractories have a ratio of 70 : 30, chrome : magnesia. Such bricks have a higher resistance to thermal shock and are less liable to change size at high temperatures than magnesite, which they replaced in open-hearth furnaces. The new refractories also replaced silica in the furnace roof, which allowed higher operating temperatures with the benefits that these furnaces were faster and more economical than furnaces with silica roofs.

Finally, not the least important development in refractories was the introduction of carbon blocks to replace fireclay (compositions similar to kaolinite) refractories in the hearths of blast furnaces making pig iron. Early experience was so successful that the “all carbon blast furnace” seemed a possibility. These hopes were not realized because later experience showed that there was sufficient oxygen in the upper regions of the furnace to oxidize the carbon and hence preclude its use there.

As in the history of other ceramics, the great progress in refractories was partly due to developments in scientific understanding and the use of new characterization methods. Development of phase equilibrium diagrams and the use of X-ray diffraction and light microscopy increased the understanding of the action of slags and fluxes on refractories, and also of the effect of composition on the properties of the refractories.

2.10 MAJOR LANDMARKS OF THE TWENTIETH CENTURY

Uranium dioxide nuclear fuel. In 1954 and 1955 it was decided to abandon metallic fuels and to concentrate upon UO_2 (sometimes referred to as urania) as the fuel for

power-producing nuclear reactors. The water-cooled, water-moderated nuclear reactor would not have been possible without urania. The important properties are

1. Resistance to corrosion by hot water
2. Reasonable thermal conductivity, about 0.2–0.1 times that of metals
3. Fluorite crystal structure, which allows accommodation of fission products (see Section 6.5).

Reactor pellets are often cylinders, about 1 cm high and 1 cm in diameter, with a theoretical density of about 95%. Many pellets are loaded into a closely fitting zirconium alloy tube that is hermetically sealed before insertion into the reactor.

Following World War II (and the first use of nuclear weapons) there was a lot of research in the field of nuclear energy. Many of the people doing this research started with the wartime Manhattan project. Almost all worked in a few government-supported laboratories, such as those at Oak Ridge (in Tennessee) or Argonne (in Illinois) or at commercially operated laboratories that were fully government supported. In other countries most of the work was also carried out in government laboratories, for example, Chalk River in Canada and Harwell in England. The excitement in nuclear energy continued into the 1970s until the Three Mile Island incident. In the United States much of the interest and research in nuclear energy and nuclear materials have passed. Work continues in several countries including Japan, France, and Canada and will resume elsewhere as energy demands grow.

The float-glass process. Flat, distortion-free glass has long been valued for windows and mirrors. For centuries, the production of plate glass was a labor-intensive process involving casting, rolling, grinding, and polishing. The process required much handling of the glass and had high waste glass losses. As a result, plate glass was expensive and a premium product. Drawing processes were used extensively for window glass, but were not suitable for producing distortion-free sheets for the more demanding applications. In 1959 Alastair Pilkington introduced the float-glass process to make large unblemished glass sheets at a reasonable cost. It took 7 years and more than \$11 M (over \$150 M in 2006) to develop the process. We describe the technical details of the float-glass process in Chapter 21. Float-glass furnaces are among the largest glass-melting tank furnaces in use today and can produce 800–1000 tons of finished glass per day. A float-glass production line can be 700 feet long, with the tin path over 150 feet in length, and can produce a sheet with a width of 12 feet. The float-glass process dramatically decreased the cost of glass and led to a tremendous increase in the use of glass in modern architecture. Each year the float-glass process produces billions of dollars worth of glass.

Pore-free ceramics. During and following World War II new ceramics became important because of their special

properties. They were fabricated from single-phase powders by sintering. This process differed from the classical silicate ceramic processing in that no liquid phase was formed. In the early stages of their development all such ceramics were porous after firing and hence opaque. Robert Coble found that the addition of a small amount of MgO would inhibit discontinuous grain growth in Al_2O_3 and permit it to be sintered to a theoretical density to yield a translucent product. The first commercial product using this new property was called Lucalox (for transLUCent ALuminum OXide). It is used primarily to contain the Na vapor in high-pressure Na-vapor lamps, which give nighttime streets their golden hue. Operating at high temperature, Na-vapor lamps have a luminous efficiency $>100 \text{ lm W}^{-1}$, the highest of any light source (a 100-W tungsten-filament lamp has an efficiency of $\sim 18 \text{ lm W}^{-1}$). They have displaced almost all other light sources for outdoor lighting. Na-vapor lamps are produced at an estimated rate of 16 million per year. A new product, the ceramic-metal halide lamp, utilizes the same ceramic envelope. It has an intense white light and is just now being introduced. Lumex Ceramic utilizes much of the same understanding in its preparation. It is based on doped yttrium oxide and is used as a scintillation counter in the GE computed tomography X-ray scanner.

Nitrogen ceramics. Silicon nitride was first produced in 1857 (Deville and Wöhler, 1857), but remained merely a chemical curiosity. It wasn't until much later that it was considered for engineering applications. During the period 1948–1952 the Carborundum Company in Niagara Falls, New York, applied for several patents on the manufacture and application of silicon nitride. By 1958 Haynes (Union Carbide) silicon nitride was in commercial production for thermocouple tubes, rocket nozzles, and boats and crucibles for handling molten metal. British work in silicon nitride, which began in 1953, was directed toward the ceramic gas turbine. It was supposed that sea and land transport would require turbines with materials capabilities beyond those of the existing nickel-based superalloys. This work led to the development of reaction-bonded silicon nitride (RBSN) and hot-pressed silicon nitride (HPSN). In 1971 the Advanced Research Projects Agency (ARPA) of the U.S. Department of Defense placed a \$17 million contract with Ford and Westinghouse to produce two ceramic gas turbines, one a small truck engine and the other producing 30 MW of electrical power. The goal was to have ceramic engines in mass production by 1984. Despite considerable investment there is still no commercial ceramic gas turbine. The feasibility of designing complex engineering components using ceramics has been demonstrated and there has been increasing use of ceramics in engineering applications. Unfortunately there is no viable commercial process for manufacturing complex silicon nitride shapes with the combination of strength, oxidation resistance, and creep resistance required for the gas turbine, together with the necessary reliability, life prediction, and reproducibility.

Magnetic ferrites. The development of ceramic magnetic materials for commercial applications really started in the early 1930s. In 1932 two Japanese researchers Kato and Takei filed a patent describing commercial applications of copper and cobalt ferrites. J.L. Snoeck of N.V. Philips Gloeilampenfabrieken in Holland performed a systematic and detailed study of ferrites in 1948. This work launched the modern age of ceramic magnets. In the following year, Louis Néel, a French scientist, published his theory of ferrimagnetism. This was an important step in the history of magnetic ceramics because most of the ceramics that have useful magnetic properties are ferrimagnetic. About 1 million tons of ceramic magnets are produced each year.

Ferroelectric titanates. These materials are used as capacitors, transducers, and thermistors, accounting for about 50% of the sales of electroceramics. The historical roots leading to the discovery of ferroelectricity can be traced to the nineteenth century and the work of famous crystal physicists Weiss, Pasteur, Pockels, Hooke, Groth, Voigt, and the brothers Curie. Beginning with the work on Rochelle salt (1920–1930) and potassium dihydrogen phosphate (1930–1940), the study of ferroelectrics accelerated rapidly during World War II with the discovery of ferroelectricity in barium titanate. There then followed a period of rapid proliferation of ferroelectric materials including lead zirconate titanate (PZT), the most widely used piezoelectric transducer. Together with the discovery of new materials there was also an increase in the understanding of their structure and behavior, which led to new applications for ferroelectric ceramics, including microelectromechanical systems (MEMS).

Optical fibers. In 1964 Charles K. Kao and George A. Hockman, at the now defunct Standard Telecommunications Laboratory (STL) in the UK, suggested sending telecommunications signals along glass fibers. These early fibers had very high losses—the difference in the amount of light that went in versus the light that came out—compared to the fibers produced today. Robert Maurer, Donald Keck, and Peter Schultz at the Corning Glass Works in New York produced the first low-loss fibers in 1970. They were made by a chemical vapor deposition (CVD) process known as modified CVD (MCVD) and had losses $<20 \text{ dB/km}$. Today, losses typically are $0.2\text{--}2.0 \text{ dB/km}$. In 1988 the first transatlantic fiberoptic cable, TAT-8, began carrying telephone signals from America to Europe. The link is 6500 km long and can carry 40,000 conversations per fiber. Glass fibers are also critical in today's endoscopes.

Glass ceramics. S. Donald Stookey made the first true glass ceramic at Corning Glass Works in 1957. He accidentally overheated a piece of Fotoform glass—a photosensitive lithium silicate glass. The glass did not melt, instead it was converted to a white polycrystalline ceramic that had much higher strength than the original glass. The conversion from the glass to the crystalline ceramic was accomplished without distortion of the articles and with only minor changes in dimensions. Small silver crystals

in the glass acted as nucleation sites for crystallization. The development of this new Pyroceram composition launched Corning into the consumer products market. In 1958, Corningware® was launched. Stookey went on to develop a number of glass ceramics including one that was used as a smooth-top cooking surface for stoves. The invention of glass ceramics is a good example of serendipity. But Stookey had to be aware of the significance of what he had made. There are many other examples of the role of luck in the invention and development of new materials—Teflon, safety glass, and stainless steel.

Tough ceramics. Ceramics are inherently brittle with low toughness. In 1975 Garvie, Hannink, and Pascoe published a seminal article entitled “Ceramic Steel.” They were the first to realize the potential of zirconia (ZrO_2) for increasing the strength and toughness of ceramics by utilizing the tetragonal to monoclinic phase transformation induced by the presence of a stress field ahead of a crack.

A great deal of effort has been expended since to devise theories and develop mathematical frameworks to explain the phenomenon. It is generally recognized that apart from crack deflection, which can occur in two-phase ceramics, the $t \rightarrow m$ transformation can develop significantly improved properties via two different mechanisms: microcracking and stress-induced transformation toughening. We describe these mechanisms in Chapter 18. So far three classes of toughened ZrO_2 -containing ceramics have been made:

- Partially stabilized zirconia (PSZ)
- Tetragonal zirconia polycrystals (TZPs)
- Zirconia-toughened ceramics (ZTCs)

Bioceramics. The first suggestion of the application of alumina (Al_2O_3) ceramics in medicine came in 1932. But the field of bioceramics really did not develop until the 1970s with the first hip implants using alumina balls and cups. Studies showed that a ceramic ball was more biocompatible than metals and provided a harder, smoother surface that decreased wear. The Food and Drug Administration (FDA) in the United States in 1982 approved these for use. Each year about 135,000 hips are replaced in the United States; more than a million hip prosthesis operations using alumina components have been performed to date. Alumina is an example of a nearly inert bioceramic. Bioactive ceramics and glasses, materials that form a bond across the implant-tissue interface, were an important development. The first and most studied bioactive glass is known as Bioglass 45S5 and was developed by Larry Hench and co-workers at the University of Florida. The first successful use of this material was as a replacement for the ossicles (small bones) in the middle ear. A range of bioactive glass ceramics has also been developed.

Fuel cells. The British scientist Sir William Robert Grove (1839) discovered the principle on which fuel cells are based. Grove observed that after switching off the current that he had used to electrolyze water, a current

started to flow in the reverse direction. The current was produced by the reaction of the electrolysis products, hydrogen and oxygen, which had adsorbed onto the Pt electrodes. Grove’s first fuel cell was composed of two Pt electrodes both half immersed in dilute H_2SO_4 : one electrode was fed with O_2 and the other with H_2 . Grove realized that this arrangement was not a practical method for energy production. The first practical fuel cell was developed in the 1950s at Cambridge University in England. The cell used Ni electrodes (which are much cheaper than Pt) and an alkaline electrolyte. Pratt and Whitney further modified the alkaline fuel cell in the 1960s for NASA’s Apollo program. The cells were used to provide on-board electrical power and drinking water for the astronauts. The alkaline fuel cell was successful but too expensive for terrestrial applications and required pure hydrogen and oxygen. There are many different types of fuel cell, but the one most relevant to ceramics is the solid-oxide fuel cell (SOFC). The SOFC uses a solid zirconia electrolyte, which is an example of a fast-ion conductor. We will discuss later how fuel cells convert chemical energy into electrical energy.

High-temperature superconductivity. High-temperature superconductivity was discovered in 1986 by Bednorz and Müller at the IBM Research Laboratory in Zurich, Switzerland. Art Sleight had shown earlier that oxides could be superconductors, but the required temperature was still very low. The discovery that certain ceramics lose their resistance to the flow of electrical current at temperatures higher than metal alloys may be as important as the discovery of superconductivity itself. Because of the significance of their discovery Bednorz and Müller were awarded the Nobel Prize for Physics in 1987, only a year after their discovery! The impact of the discovery of high-temperature superconductivity launched an unprecedented research effort. The 2-year period after Bednorz and Müller’s discovery was a frenzied time with a host of new formulations being published. Paul Chu and colleagues at the University of Houston, Texas discovered the most significant of these new ceramics, $YBa_2Cu_3O_7$, in 1987. The YBCO or 123 superconductor, as it is known, is superconducting when cooled by relatively inexpensive liquid nitrogen. This opened up enormous possibilities and led to expansive speculations on a future based on these materials. The original promises have not been fulfilled. However, new applications are being developed and the field is still quite young. The current market is less than 1% of the advanced ceramics market. Predictions indicate that over the next 5 years annual growth rates up to 20% might be achieved.

2.11 MUSEUMS

There are many museums around the world that house collections of ceramics. The list that we give here is not exclusive, but it does include some of the major

collections as well as sites that have important historical significance.

- Ashmolean Museum, Oxford, UK. This is a museum of the University of Oxford. Founded in 1683, it is one of the oldest public museums in the world. Important collections include early Chinese ceramics and Japanese export porcelain. www.ashmol.ox.ac.uk.
- British Museum, London. This is one of the greatest museums in the world. It contains a large and outstanding collection of antiquities including numerous Stone Age artifacts. www.thebritishmuseum.ac.uk.
- Corning Museum of Glass in Corning, New York. This is one of the outstanding glass collections in the world. Containing more than 33,000 objects representing the entire history of glass and glassmaking. www.cmog.org.
- Metropolitan Museum of Art in New York City, New York. Ceramic collections include Medici porcelain and Böttger porcelain. The museum also has one of the finest glass collections in the world. www.metmuseum.org.
- Musée du Louvre, Paris. This is one of the greatest museums of the world. It contains extensive collections of antiquities, including many examples of ancient earthenware vessels, some dating from the Chalcolithic period. www.louvre.fr.
- Musée National de Céramique at Sèvres, France. The collection includes examples of early European porcelains including a Medici porcelain bottle made in 1581; the first success in European efforts to produce ware equivalent to Persian and Chinese porcelain. It also contains examples of French soft-paste porcelain as well as earlier ceramics. www.ceramique.com.
- Ross Coffin Purdy Museum of Ceramics at the American Ceramic Society headquarters in Westerville, Ohio. It houses a cross section of traditional and high-tech ceramics produced in the last 150 years. www.acers.org/acers/purdymuseum.
- Smithsonian Institution. The Freer Gallery of Art and the Arthur M. Sackler Gallery contain collections of ancient ceramics with important examples from China and the Near East. www.asia.si.edu
- Victoria and Albert Museum, London. This is the world's largest museum of the decorative arts. It contains the National Collections of glass and ceramics. The extensive ceramic collection includes Medici porcelain and early Chinese and Near East ceramics. www.vam.ac.uk.
- Wedgwood Museum and Visitors Center in Barlaston, Stoke-on-Trent, UK. It contains many rare and valuable exhibits tracing the history of the company. It is also possible to tour the Wedgwood factory. www.wedgwood.com.
- The World of Glass in St. Helens, UK. This is a new museum and visitor center in the hometown of Pilkington glass. Pilkington plc originated in 1826 as the

St. Helens Crown Glass Company. It contains the Pilkington glass collection. www.worldofglass.com.

2.12 SOCIETIES

There are several professional ceramics societies in the world. In the United States, the American Ceramic Society (ACerS) founded in 1899 is the principal society for ceramists. The society, which is based in Westerville, Ohio, is divided into 10 divisions: Art, Basic Science, Cements, Electronics, Engineering Ceramics, Glass & Optical Materials, Nuclear & Environmental Technology, Refractory Ceramics, Structural Clay Products, and Whitewares and Materials. The society organizes an annual meeting and publishes the *Journal of the American Ceramic Society*. The journal was created in 1918 and is one of the most important peer-reviewed journals in the field: www.acers.org.

Many other countries have professional societies for those working in the field of ceramics.

- Institute of Materials, Minerals and Mining (IoM³) www.iom3.org
- Deutsche Keramische Gesellschaft www.dkg.de.
- European Ceramic Society (ECerS) www.ecers.org
- Swedish Ceramic Society www.keram.se/sks
- Ceramic Society of Japan www.ceramic.or.jp
- Canadian Ceramics Society www.ceramics.ca
- Chinese Ceramic Society www.ceramsoc.com
- Society of Glass Technology www.sgt.org

2.13 CERAMIC EDUCATION

The first formal ceramics program (Clay-Working and Ceramics) in the United States was established in 1894 at the Ohio State University in Columbus, Ohio. This marked a change from on-the-job training that was prevalent in the traditional North American art potteries and family establishments of earlier years toward a formal university study. Ceramics was also taught at Alfred University in New York, and many other schools across the nation. One of the most remarkable ceramists of the time was Adelaide Robineau, who taught at Syracuse University in New York. Robineau was a studio ceramist who devised her own clay bodies, concocted her own glazes, threw the forms, and decorated, glazed, and then fired them herself. Few women at the time were involved in the technical aspects of ceramic production. It was considered proper for women to be decorators only, rather than be part of more technical pursuits, or to throw on the wheel, a physically demanding job regarded as better left to men.

From 1894 to 1930 a number of universities formed their own ceramic engineering programs:

- New York State School of Clay-Working and Ceramics at Alfred University: 1900
- Rutgers University: 1902
- University of Illinois: 1905
- Iowa State College: 1906
- University of Washington: 1919
- West Virginia University: 1921
- North Carolina State University: 1923
- Pennsylvania State College: 1923
- Georgia Institute of Technology: 1924
- Missouri School of Mines (now University of Missouri–Rolla): 1926
- University of Alabama: 1928
- Massachusetts Institute of Technology: 1930

In the 1960s the first Materials Science departments began to appear in universities. Many of these were based on existing Metallurgy departments. In some of the universities that had specific ceramics programs, these activities were also incorporated into the new materials departments. Now, ceramic science and engineering is mostly taught in Materials Science and Engineering (MS&E) programs in the United States.

CHAPTER SUMMARY

The history of ceramics is intertwined with human history. From the first use of flint and obsidian during the Stone Age, the formation of vessels from clay, the use of refractories in the iron and steel industry, to the fabrication of optical fibers for high-speed communication ceramics have impacted society and technology in many ways. We mentioned many of the more recent developments in the field of ceramics. The science behind these materials will be described in many of the later chapters.

PEOPLE IN HISTORY

Aspdin, Joseph was an English mason and invented Portland cement in 1824. It was so named because of its resemblance to white limestone from the island of Portland, England. The first Portland cement made in the United States was produced at Coploy, Pennsylvania in 1872.

Bednorz, Johannes Georg (born 1950) and Karl Alexander Müller (born 1927) were scientists at the IBM research laboratory in Zurich, Switzerland, where they discovered the phenomenon of high-temperature superconductivity. They were both awarded the Nobel Prize for Physics in 1987. They began working together in 1982.

Böttger, Johann Friedrich was born in 1682. The young Böttger was apprenticed as an apothecary in Berlin where he claimed to have transformed mercury into gold, a feat he apparently demonstrated very convincingly in 1701. When reports of this reached Frederick I, Böttger fled to Saxony, where, in addition to his metallurgical researches, he began his work in ceramics. He used von Tschirnhaus' mirrors and lenses to produce a dense red stoneware and a European equivalent to white Chinese porcelain. He died in 1719. An authoritative history of Böttger and Meissen has been written by Walcha (1981).

Kingery, W. David. Kingery played a key role in creating the field of ceramic science. He was the author of *Introduction to Ceramics*, first published in 1960, the “bible” for a generation of ceramists. He was well known for his work in the field of sintering. In his later years he worked extensively on the history of ceramics. He died in June 2000.

Orton, Edward, Jr. was born in 1863 in Chester, New York. He studied mining engineering at Ohio State University (OSU). He was the founder of the ceramic engineering program at OSU in 1894 and a founder of the American Ceramic Society. He died in 1932.

Pilkington, Sir Alastair was born in 1920. He served in the Second World War. In 1942 he was captured on the island of Crete and spent the rest of the war as a POW. After finishing his studies at Cambridge University he joined the Pilkington glass company in 1947. By 1959 the float glass process was a success and the production of flat glass was revolutionized. He died in 1995.

Ravenscroft, George developed lead crystal glass during the last quarter of the seventeenth century to rival the Venetian *crystallo* developed during the early sixteenth century. He was granted a patent in March 1674 for a “crystalline glass resembling rock-crystal.”

Seeger, Hermann A. was the world's pioneer scientific ceramist. The English translation of Seeger's work, *The Collected Writings of Hermann Seeger*, was published in 1913 by the American Ceramic Society.

Simpson, Edward, better known as “Flint Jack,” was an Englishman and one of the earliest experimental stone toolmakers. Using nothing more than a steel hammer he created replicas of ancient stone tools, which he sold in the late nineteenth century to museums and a Victorian public that was very interested in prehistoric times. He was able to make the tools appear old and worn by using chemicals and a lapidary tumbler. In 1867 he was sent to prison for theft.

von Tschirnhaus, Count Ehrenfried Walther was born in 1651. He was a physicist famous for his experiments with high temperatures and mineral fusions achieved by focusing sunlight in a solar furnace. He was made a foreign member of the French Royal Academy in 1683. He died in 1708.

Wedgwood, Josiah was born in 1730, the last child in a family of 12. He went into business for himself in 1759 in Staffordshire. One of the most remarkable innovators of the eighteenth century he revolutionized the process of manufacturing. He was a member of the Royal Academy and a member of the Lunar Society of Birmingham, which included in its members many of the great innovators of that period such as James Watt, the inventor of the steam engine. Mankowitz (1980) gives a detailed account of the life of Wedgwood and his pottery.

Zachariasen, William Houlder was born in 1906. He was a Norwegian-American physicist who spent most of his career working in X-ray crystallography. His description of the glass structure in the early 1930s became a standard. He died in 1979.

GENERAL REFERENCES

The American Ceramic Society, 100 Years (1998) The American Ceramic Society, Westerville, OH. A wonderfully illustrated history of the ACerS published to celebrate the societies centennial 1898–1998.

For the student with an interest in ceramic history the book by Kingery and Vandiver (1986) and the *Ceramics and Civilization* series edited by W.D. Kingery (1985, 1986), The American Ceramic Society, Westerville, OH are good resources. Volume I: *Ancient Technology to Modern Science* (1985). Volume II: *Technology and Style* (1986). Volume III: *High-Technology Ceramics—Past, Present, and Future* (1986).

Ceramics of the World: From 4000 B.C. to the Present (1991), edited by L. Camusso and S. Burton, Harry N. Abrams, Inc., New York. A beautifully illustrated history of ceramics with lots of historical details.

Douglas, R.W. and Frank, S. (1972) *A History of Glassmaking*, Fovels, Henley-on-Thames, Oxfordshire. The history of glassmaking is described and illustrated extensively. An excellent reference source.

Jelínek, J. (1975) *The Pictorial Encyclopedia of the Evolution of Man*, Hamlyn Pub Grp, Feltham, UK. Beautifully illustrated.

Kingery, W.D. and Vandiver, P.B. (1986) *Ceramic Masterpieces*, The Free Press, New York.

Lechtman, H.N. and Hobbs, L.W. (1986) "Roman Concrete and the Roman Architectural Revolution," in *Ceramics and Civilization III: High-Technology Ceramics—Past, Present, and Future*, edited by W.D. Kingery, The American Ceramics Society, Westerville, OH, pp. 81–128. This article gives a detailed historical perspective on this topic.

Levin, E. (1988) *The History of American Ceramics: 1607 to the Present*, Harry N. Abrams, Inc., New York. An illustrated history.

Schick, K.D. and Toth, N. (1993) *Making Silent Stones Speak: Human Evolution and the Dawn of Technology*, Simon & Shuster, New York.

SPECIFIC REFERENCES

Bednorz, J.G. and Müller, K.A. (1986) "Possible high T_c superconductivity in the Ba-La-Cu-O system," *Z. Phys. B—Condensed Matter* **64**, 189. The seminal paper describing "possible" high-temperature superconductivity in an oxide ceramic.

Deville, H. Ste.-C and Wöhler, F. (1857) "Erstmalige Erwähnung von Si_3N_4 ," *Liebigs Ann. Chem.* **104**, 256. Report of the first production of silicon nitride. Of historical interest only.

Garvie, R.C., Hannink, R.H., and Pascoe, R.T. (1975) "Ceramic steel?" *Nature* **258**, 703. The first description of the use of the tetragonal to monoclinic phase transformation for toughening ceramics.

Guillard, H.F. (1971) *Early American Folk Pottery*, Chilton Book Co., New York.

Kao, K.C. and Hockham, G.A. (1966) "Dielectric-fiber surface waveguides for optical frequencies," *Proc. IEE* **113**, 1151.

Lindsay, J. (1968) *The Ancient World: Manners and Morals*, Putnam, New York.

Mankowitz, W. (1980) *Wedgwood*, 3rd edition, Barrie and Jenkins, London. A standard biography of Josiah Wedgwood.

Moseley, C.W.R.D. (translated by) (1983) *The Travels of Sir John Mandeville*, Penguin Books, London, p. 57. Describes the Fosse of Mynon in Acre, a Syrian seaport on the Mediterranean.

Thomas, S.G. and Gilchrist, P.G. (1879) "Elimination of phosphorus in the Bessemer converter," *J. Iron Steel Inst.* **20**. A landmark paper that led to important changes in the steel making industry and also to the development of new types of refractory.

Walcha, O. (1981) *Meissen Porcelain*, translated by H. Reibig, G.P. Putnam's Sons, New York. A history of Böttger and Meissen based in large part on archival studies at Meissen.

Wood, N. (1999) *Chinese Glazes*, A&C Black, London. A beautifully illustrated book showing the early Chinese genius for ceramics.

Wu, M.K., Ashburn, J.R., Torng, C.J., Hor, P.H., Meng, R.L., Gao, L., Huang, Z.J., Wang, Y.Q., and Chu, C.W. (1987) "Superconductivity at 93 K in a new mixed-phase Y-Ba-Cu-O compound system at ambient pressure," *Phys. Rev. Lett.* **58**, 908. The first description of superconductivity at liquid-nitrogen temperature.

Zachariasen, W.H. (1932) "The atomic arrangement in glass," *J. Am. Chem. Soc.* **54**, 3841. Describes a model for the structure of oxide glasses that has become a standard for these materials.

EXERCISES

- 2.1 Gypsum, the raw material for Plaster of Paris, occurs in several varieties. The Greeks used a form of gypsum as windows for their temples. What particular property would be important for this application? What form of gypsum would be most suitable?
- 2.2 What do you think might be the role of CuO in the Han lead glaze (Table 2.2)?
- 2.3 Why do you think it was so important for the early ceramic industries to locate near the source of raw materials? Does a similar situation occur today?
- 2.4 The largest concrete construction project in the world is the Three Gorges Dam in China. How much concrete is used in this project?
- 2.5 Which company is the largest producer of glass optical fibers?
- 2.6 Corningware[®] is a glass ceramic product that was once widely used for cookware, but is rarely used now. What were some of the problems with Corningware[®] and would these problems be inherent to all glass ceramics?
- 2.7 Solid oxide fuel cells (SOFC) are not being used in transportation applications (such as automobiles and buses). What fuel cells are being used for these applications and what are their advantages over the ceramic-based SOFCs?
- 2.8 The transition temperature (T_c) for the YBCO superconductor is 95 K. Higher T_c s are found with other ceramic high-temperature superconductors, but these materials are not being used commercially. What are some of the other materials and what are some of the factors that are limiting their use?
- 2.9 The Hall of Mirrors (La Galerie des Glaces) at the Palace of Versailles in France was begun in 1678, well before the development of the float glass process. What technology was available in the seventeenth century for producing flat plates of glass?
- 2.10 Concrete is a mixture of gravel (called aggregate) and cement. The spectacular 142-foot internal diameter dome of the Pantheon in Rome is made of concrete. What material did the Romans use for aggregate in the construction of the Pantheon? Could the material they used be classified as a ceramic?

Part II

Materials

3

Background You Need to Know

CHAPTER PREVIEW

In this chapter we will summarize three concepts fundamental to all materials science: atomic structure, thermodynamics, and kinetics. You should be familiar with these topics from introductory chemistry, physics, and materials science classes so we give only a brief review here. Books are written on each of these topics. In ceramics, you can often avoid such books, but the details become more critical as you delve deeper into the subject.

The properties of a material are determined, to a large extent, by how the constituent atoms bond together. The nature of this bonding is determined by the electron configuration of the atoms. The electron configuration of an atom also determines the properties of the atom and materials that contain it. For example, the ceramic magnetite (Fe_3O_4) is magnetic due to the presence of unpaired electrons in the 3d level of Fe; you need to know what the 3, the d, and “unpaired” denote. To understand why Mn ions can exist with many different charge states but we invariably find only Al ions with a 3+ charge, you must know the electron configuration of the respective atoms.

Knowledge of both thermodynamics and kinetics is necessary to understand how ceramic materials behave and what happens when they are processed. Thermodynamics tells us what is possible while kinetics tells us how long we have to wait for the inevitable. Thus, thermodynamics tells us if a specific chemical or physical reaction can occur. In ceramics these changes are often brought about because samples are routinely heated and cooled. Ceramics may be processed at temperatures above 1800°C and then cooled to 25°C . Some processes may occur at 1800°C , but may continue or change as we cool the sample. Conversely, some ceramics change their properties at quite low temperatures: BaTiO_3 changes from the paraelectric cubic phase to the ferroelectric tetragonal phase at 120°C . Kinetics tells us how rapidly these reactions will proceed. Diamond is thermodynamically unstable at room temperature and atmospheric pressure, but the phase change occurs much too slowly to worry jewelers.

3.1 THE ATOM

The bases for understanding the structure of the atom are quantum theory and wave mechanics, which were developed in the early 1900s. The important conclusions of these studies, particularly as they relate to materials, are as follows:

- Electrons in atoms can move only in certain stable orbits, that is, only certain energy values are possible. We expand on this fact when we describe energy bands, which are used to explain electron conductivity.
- Transition between orbits involves the emission or absorption of energy. These transitions can be the source of color and we use them to analyze chemistry by spectroscopy.
- No two electrons in the same atom can have the same four quantum numbers. This requirement led to the

introduction of the spin quantum number. Atoms containing electrons with unpaired spins will have magnetic properties.

- It is impossible to know simultaneously the position and momentum of an electron with certainty. We use this property in tunnel diodes.
- Electrons have wavelike properties. This means that they can be diffracted. Electron diffraction, like X-ray diffraction, gives us the crystal structure.

In the following sections we summarize how these conclusions lead to our present view of the structure of the atom and, in particular, the nature and arrangement of the electrons in the atom. We are not attempting to summarize modern physics, but only the concepts that we use in this text. You need to understand the main aspects of the nature of the chemical bond in ceramic materials: what is an ionic bond, what is a covalent bond, and why do most

bonds show a mixture of the two. In spectroscopy and microscopy we will probe the electronic structure to determine the local chemistry of the ceramic.

3.2 ENERGY LEVELS

The quantization of energy is a key aspect in understanding atomic structure. Bohr's model involves electrons moving only in certain stable orbits. The angular momentum of the orbiting electrons is quantized so that only specific orbits are allowed and only certain energy values are possible.

These orbits are known as stationary states, and the one with the lowest energy is called the ground state.

The quantization of angular momentum is $nh/2\pi$, where n is the principal quantum number. As the principal quantum number increases

1. The radius, r , of the electron orbit increases, that is, the electron is further from the nucleus.
2. The energy, E , of that electron is also increased.

The first five Bohr orbits, that is, $n = 1$ through 5, are also referred to as shells; we define a shell as a group of states that have the same n . A letter is used to denote each shell:

Shell	K	L	M	N	O	...
n	1	2	3	4	5	...

Charles Barkla, an early X-ray spectroscopist, introduced this terminology for electron shells in 1911. We still use it today to designate characteristic X-rays in both X-ray diffraction and in chemical analysis using electron microscopy. Barkla named the two types of characteristic X-ray emissions he observed as the K-series and L-series. He later predicted that an M-series and a J-series might exist. An M-series was subsequently discovered, but no J-series. The K shell is hence the first shell.

The other aspect of Bohr's theory is that while an electron is in a stationary state, the atom does not radiate. Electrons can be excited into higher energy orbits if the atom is stimulated (thermally, electrically, or by the absorption of light). These orbits are the excited states and are more distant from the nucleus. The residence time of an electron in the excited state may be very short (~1 ns) before it spontaneously descends to a lower energy state and eventually the ground state. During each transition the

excess energy is emitted in the form of a photon. Any transition between orbits involves either the emission or absorption of energy. Understanding this concept is necessary in, for example, appreciating how a laser works. If

the energy emitted is in the visible part of the electromagnetic spectrum (Table 3.1), then we will be able to observe the emission. The emission from the ruby laser (ruby is a ceramic) is at 694 nm (in the red). A frequency doubled Nd-doped yttrium aluminum garnet (YAG) laser (YAG is another ceramic) operates in the green part of the spectrum at 530 nm.

Bohr's model was quite popular at the time because an electron circling the nucleus is conceptually similar to the earth circling the sun. The idea that orbiting electrons did not radiate was less easy to accept, Bohr simply insisted they did not and that was that! Most importantly, the model explained a number of physical phenomena. Bohr's assumption that electrons are particles with well-defined orbits was not consistent with the concept of "simultaneous indeterminacy" of position and momentum as propounded in the Heisenberg uncertainty principle.

What you should remember from this discussion is the origin of KLMNO and the terminology. We will use this again in Chapter 10.

Electron energy levels and the Bohr model are important for understanding the following:

- Atomic radii—as we fill shells going down a particular period the atoms get bigger (r increases).
- Ionization energy—as we fill shells going down a particular period it becomes progressively easier to remove the outer electron(s) (E increases with respect to the ground state).
- Covalent bond formation—ionization energies must be high (E large).

THE BOHR ATOM		
Quantization of angular momentum	$m_e v r = n \frac{h}{2\pi}$	Box 3.1
Radius of possible electron orbits	$r = \frac{\epsilon_0 n^2 h^2}{\pi m_e e^2}$	Box 3.2
Energy of the electron	$E = \frac{m_e e^4}{8\epsilon_0 n^2 h^2}$	Box 3.3

TABLE 3.1 The Visible Part of the Electromagnetic Spectrum

Energy, E (J)	Wavelength, λ (nm)	Color
2.84×10^{-19}	700	Red
3.20×10^{-19}	620	Orange
3.42×10^{-19}	580	Yellow
3.75×10^{-19}	530	Green
4.23×10^{-19}	470	Blue
4.73×10^{-19}	420	Violet

- Magnetic ceramics—we need to have an M shell.
- X-ray spectroscopy—we use the Barkla notation, the energy of the characteristic X-rays depends on the electron energy levels involved.

THE DE BROGLIE HYPOTHESIS

All matter possesses wave properties. Every moving particle can be associated with a wavelength, λ , given by

$$\lambda = \frac{h}{mv} = \frac{h}{p}$$

experiments that can be done on a system.” Thus, the Schrödinger wave equation includes information about the chemical behavior of all atoms and compounds and the answer to whether any proposed chemical reaction will take place or not.

3.3 ELECTRON WAVES

Demonstrating electron diffraction (a property associated with waves) was proof of their wave nature. In 1927 C.J. Davisson and L. Germer in the United States and, independently, G.P. Thomson and A. Reid in the United Kingdom showed that electrons could be diffracted in much the same way as X-rays. We care because we cannot explain the properties of electrons and X-rays without this understanding.

The wavelike nature of electrons enables electron diffraction studies of materials. Most electron diffraction patterns are obtained in a transmission electron microscope, which allows us to obtain structural information from very small regions. This is of particular importance in many new ceramics where we are often dealing with thin interface layers (such as at grain boundaries) and very small grains (nanopowders).

One of the most important consequences of the dual nature of electrons is Heisenberg’s uncertainty principle, which states that it is impossible to know simultaneously both the momentum and position of a particle with certainty. If we are describing the motion of an electron of known energy or momentum, we can speak only in terms of the probability of finding that electron at a particular position. This leads to the electron-density or electron-cloud representation of electron orbitals.

The Schrödinger equation, as central to quantum mechanics as Newton’s equations are to classical mechanics, relates the energy of an electron to its wave properties. The equation describes the likelihood that a single electron will be found in a specific region of space. The wave function, Ψ , depends on E and V , the total energy and the potential energy of the electron, respectively.

The importance of the wave function has been expressed by Atkins and de Paula (2002): “A wave function contains all there is to know about the outcome of

Mathematically, Ψ describes the motion of an electron in an orbital. The modulus of the wave function squared, $|\Psi(r)|^2$, is a direct measure of the probability of finding the electron at a particular location. The Schrödinger wave equation can be solved exactly for hydrogen. To apply it you must first transform it into polar coordinates (r, θ, ϕ) and then solve using the method of separation of variables (described in, e.g., Kreyszig, 1999).

The solution of these equations leads to three quantum numbers: n , l , and m_l .

The Schrödinger wave equation can be set for atoms with more than one electron, but it cannot be solved exactly in these cases. The second and subsequent electrons introduce the complicating feature of electron–electron repulsion. Nevertheless, the basic characteristics of the orbitals do not change and the results obtained for hydrogen are applied to many-electron atoms.

Methods are now becoming available that allow us to calculate the structure of some “bulk” materials. Generally, this is still done only rarely by starting with the Schrödinger equation. The calculations are just too difficult or too time-consuming. Actually, it is worse than it looks because we also have to deal with charge.

SCHRÖDINGER WAVE EQUATION

The time-independent form is

$$\nabla^2\Psi + 8\pi^2m/h^2 (E - V)\Psi = 0 \quad \text{Box 3.4}$$

∇^2 is the operator

$$\partial^2/\partial x^2 + \partial^2/\partial y^2 + \partial^2/\partial z^2 \quad \text{Box 3.5}$$

In polar coordinates Ψ has the form

$$\Psi(r, \theta, \phi) = R(r)\Theta(\theta)\Phi(\phi) \quad \text{Box 3.6}$$

$R(r)$, $\Theta(\theta)$, $\Phi(\phi)$ are each only functions of r , θ , and ϕ .

3.4 QUANTUM NUMBERS

Four quantum numbers are necessary to specify the state of any electron:

- n principal quantum number
- l orbital shape, or orbital angular momentum, quantum number
- m_l orbital orientation, or orbital magnetic, quantum number
- m_s spin, or spin magnetic, quantum number

A shell is a group of states that has the same n and corresponds to Bohr’s n . A subshell is a smaller group of

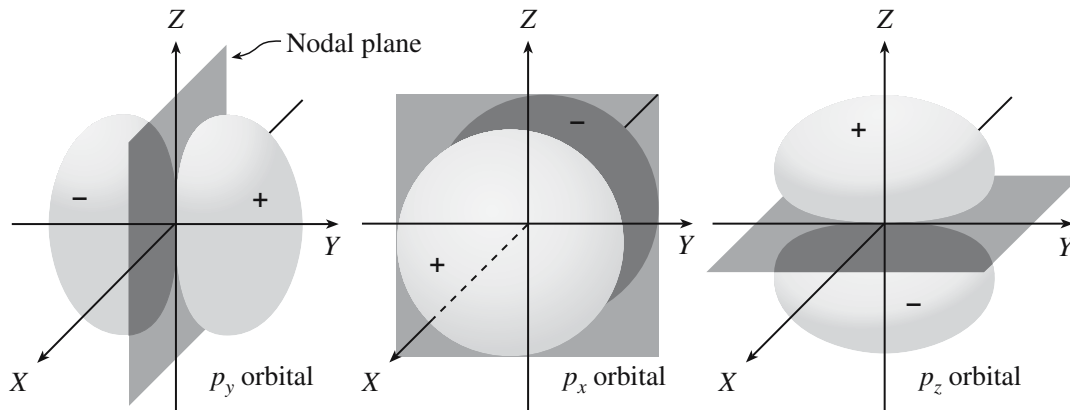


FIGURE 3.1 The $2p_x$, $2p_y$, and $2p_z$ orbitals. The nodal plane represents the area in which the probability of finding the electron is zero.

states having both the same value of n and l . An orbital is specified by n , l , and m_l , and can contain a maximum of two electrons with opposite spins.

- n has integer values, 1, 2, 3, . . . and determines the size
- l has integer values, 0, 1, 2, . . . , $n - 1$ (for any value of n) and determines shape
- m_l has integer values between $-l$ and $+l$ including 0 (for any value of l) and determines orientation
- m_s can have values of $\pm 1/2$ and specifies the direction of spin

The introduction of an external magnetic field provides the most convenient reference axis for m_l . The values of m_l are determined by the l quantum number. For each value of l there are $(2l + 1)$ values of m_l . For historical reasons the 0, 1, 2, and 3 values of the l quantum number are designated by the letters s, p, d, and f, respectively. (This choice is a relic of early spectroscopic studies when certain spectral series were designated “sharp,” “principal,” “diffuse,” or “fundamental.”)

The s orbitals are spherical and the three 2p orbitals have directional properties as shown in Figure 3.1. For example, the $2p_z$ orbital has regions of greatest concentration or probability along the z -axis and the probability of finding a $2p_z$ electron in the XY plane is zero. The shapes of the five 3d orbitals are more complicated (because there are more of them) (Figure 3.2) and we usually do not talk about f.

Are these numbers important for ceramics? The answer, of course, is yes.

- The color of a ceramic, such as ruby, derives directly from transitions between energy levels. The energy levels are the result of which orbitals are occupied and their relative energies.

QUANTUM NUMBERS

Li, Na, K and Cs have many common features because they all have a single electron in an outer s shell: 2s, 3s, 4s and 5s.

The main difference between MnO, FeO, CoO and NiO is due to the change in the d ($l = 3$) electrons on the transition-metal ion.

- We use transitions for chemical analysis of ceramics—certain transitions are allowed (quantum mechanical selection rules).

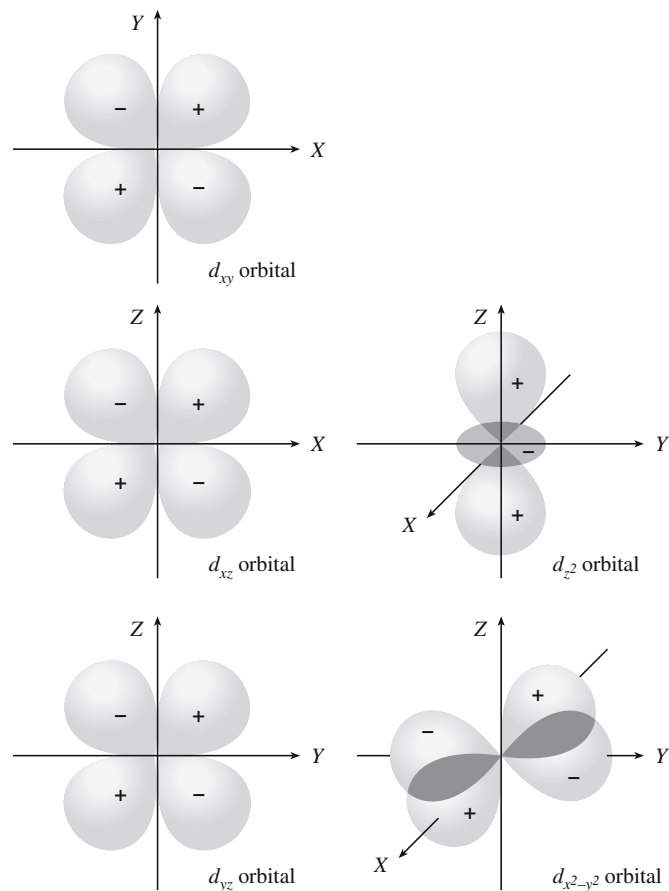


FIGURE 3.2 The 3d atomic orbitals. The 4d, 5d, and 6d orbitals are essentially identical to the 3d orbitals except they are bigger. The sign of the wavefunction changes from one lobe to the next in a given orbital and is important when we consider the formation of molecular orbitals.

- Magnetism relates directly to the spin of the electrons. If we have more spins up than down then we have magnetization.
- Atomic arrangements in covalently bonded ceramics can be understood by considering hybridization of atomic orbitals. It is the sp^3 hybridization of atomic orbitals in carbon that allows the tetrahedral arrangement of atoms in diamond. The s and the p in sp^3 refer to the atomic orbitals.

SUMMARY OF QUANTUM NUMBERS (QN)		
Name	Symbol	Value
Principal QN	n	1, 2, 3, . . .
Orbital-shape QN	l	0, 1, 2, . . . ($n - 1$)
Orbital-orientation QN	m_l	Integral values from $-l$ to $+l$ including zero
Spin QN	m_s	$\pm 1/2$

IONIZATION
 For ceramics, the important feature in all these models is which electrons we can move to make the ion and how easy it is going to be.

electron will go: For any set of orbitals of equal energy the electronic configuration with the maximum number of parallel spins results in the lowest electron–electron repulsion. Thus the ground state for atomic carbon is $1s^2 2s^2 2p_x^1 2p_y^1$.

We can build the ground-state electron configuration of atoms of all elements by filling the orbitals in order of increasing energy, making sure

that the Pauli exclusion principle and Hund’s rule are obeyed. (Hund’s rules are inviolate in predicting the correct ground state of an atom. There are occasional exceptions when the rules are used to discuss excited states that we encounter, e.g., in spectroscopy.) The total number of electrons that the orbitals can hold is given in Table 3.2.

There is no single ordering of orbital energies, but the following order is a useful guide:

$$1s < 2s < 2p < 3s < 3p < 4s < 3d < 4p < 5s < 4d < 5p < 6s < 4f \approx 5d < 6p < 7s < 5f \approx 6d$$

Figure 3.3 shows a mnemonic diagram that can be used for determining the filling order. You simply follow the arrows and numbers from one orbital to the next. Orbital energies depend on the atomic number and on the charge on the atom (ion).

In the sequence of orbital energies shown above the 4s orbitals have a lower energy than the 3d orbitals and so they will be filled first in keeping with the minimum energy principle. For example, the electron configuration of the outer 10 electrons of calcium (atomic number $Z = 20$) is $3s^2 3p^6 3d^0 4s^2$. In the filling of the electron orbitals for elements 21 to 29, there are two irregularities, one at 24 (chromium) and one at 29 (copper). Each of these elements contains one 4s electron instead of two. The reason

3.5 ASSIGNING QUANTUM NUMBERS

A shorthand notation that expresses the quantum numbers for each electron represents the electron configuration. The importance of this step is that it allows us, for example, to calculate the magnetic moment of magnetite and determine what happens if we replace the Fe^{2+} ions with Ni^{2+} .

The key to the building process for many-electron atoms is the Pauli exclusion principle: No two electrons in an atom can have the same set of four quantum numbers.

For example, the two electrons in the ground state of atomic He ($Z = 2$) must possess the following quantum numbers:

$$n = 1, \quad l = 0, \quad m_l = 0, \quad m_s = +1/2$$

$$n = 1, \quad l = 0, \quad m_l = 0, \quad m_s = -1/2$$

The two electrons in the He atom are placed in the 1s orbital with opposite spins, consistent with the Pauli’s principle. The electron configuration of He is abbreviated as $1s^2$. The next row in the periodic table is similar; we are just filling the next shell ($n = 2$ and so on).

Lithium ($Z = 3$) has the electron configuration $1s^2 2s^1$. We fill the 2s orbital before the 2p because of shielding effects that lower the energy of the 2s orbital with respect to the 2p orbital. Both the 2s and 2p orbitals in the Li atom are shielded from the +3 nuclear charge by the 1s electrons. However, the 2s orbital has a larger probability density close to the nucleus and is not shielded as strongly as the 2p orbital.

For a C atom ($Z = 6$) there are a number of possible configurations for the second electron in the set of three 2p orbitals. We use Hund’s rule to determine where the

TABLE 3.2 The s, p, d, and f Orbital Sets

Type of orbital	Orbital quantum numbers	Total orbitals in set	Total number of electrons that can be accommodated
s	$l = 0, m_l = 0$	1	2
p	$l = 1, m_l = 1, 0, -1$	3	6
d	$l = 2, m_l = 2, 1, 0, -1, -2$	5	10
f	$l = 3, m_l = 3, 2, 1, 0, -1, -2, -3$	7	14

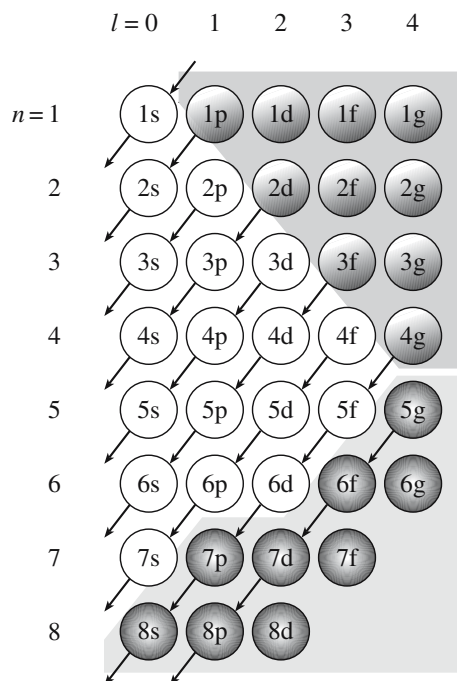


FIGURE 3.3 Mnemonic for predicting the filling order of the atomic orbitals. The upper gray block shows imaginary orbitals; orbitals in the lower gray block are not filled in the known elements.

for this apparent anomaly is that exactly filled and half-filled 3d orbitals are particularly stable (they have a lower energy) compared to the neighboring occupancies of four and nine, respectively. The electron configurations of the first row transition elements are given in Table 3.3. The electron configurations of the first row transition metals will be of importance when we discuss electrical conduc-

TABLE 3.3 Arrangement of Electrons for the First Row Transition Elements ($Z = 21\text{--}29$)

Z	Element	Electron configuration
21	Sc	$1s^2 2s^2 2p^6 3s^2 3p^6 3d^1 4s^2$
22	Ti	$1s^2 2s^2 2p^6 3s^2 3p^6 3d^2 4s^2$
23	V	$1s^2 2s^2 2p^6 3s^2 3p^6 3d^3 4s^2$
24	Cr	$1s^2 2s^2 2p^6 3s^2 3p^6 3d^5 4s^1$
25	Mn	$1s^2 2s^2 2p^6 3s^2 3p^6 3d^5 4s^2$
26	Fe	$1s^2 2s^2 2p^6 3s^2 3p^6 3d^6 4s^2$
27	Co	$1s^2 2s^2 2p^6 3s^2 3p^6 3d^7 4s^2$
28	Ni	$1s^2 2s^2 2p^6 3s^2 3p^6 3d^8 4s^2$
29	Cu	$1s^2 2s^2 2p^6 3s^2 3p^6 3d^{10} 4s^1$

tion and magnetic behavior of ceramics that contain these elements.

The electron configurations of all the elements in the periodic table are shown in Table 3.4 where we use the shorthand representation for the electron configurations (start with the nearest filled noble gas).

Examination of the electron configuration of the elements clearly shows the basis for their periodic behavior. Elements with atomic numbers 2, 10, and 18 are the noble gases. These elements are stable and chemically inert. Inertness is equated with completely filled shells of electrons. Elements with similar outer shell configurations possess many similar properties. Figure 3.4 shows the Periodic Table of Elements. It is clearly a good idea to know where the atoms lie in the periodic table since this is going to determine whether they lose or gain electrons more easily and, thus, how the ion is charged as we will now discuss.

TABLE 3.4 Electron Configurations of the Elements

Z	Element	Electron configuration	Z	Element	Electron configuration
1	H	$1s$	53	I	$[\text{Kr}]4d^{10}5s^25p^5$
2	He	$1s^2$	54	Xe	$[\text{Kr}]4d^{10}5s^25p^6$
3	Li	$[\text{He}]2s$	55	Cs	$[\text{Xe}]6s$
4	Be	$[\text{He}]2s^2$	56	Ba	$[\text{Xe}]6s^2$
5	B	$[\text{He}]2s^22p$	57	La	$[\text{Xe}]5d6s^2$
6	C	$[\text{He}]2s^22p^2$	58	Ce	$[\text{Xe}]4f5d6s^2$
7	N	$[\text{He}]2s^22p^3$	59	Pr	$[\text{Xe}]4f^36s^2$
8	O	$[\text{He}]2s^22p^4$	60	Nd	$[\text{Xe}]4f^46s^2$
9	F	$[\text{He}]2s^22p^5$	61	Pm	$[\text{Xe}]4f^56s^2$
10	Ne	$[\text{He}]2s^22p^6$	62	Sm	$[\text{Xe}]4f^66s^2$
11	Na	$[\text{Ne}]3s$	63	Eu	$[\text{Xe}]4f^76s^2$
12	Mg	$[\text{Ne}]3s^2$	64	Gd	$[\text{Xe}]4f^75d6s^2$
13	Al	$[\text{Ne}]3s^23p$	65	Tb	$[\text{Xe}]4f^96s^2$
14	Si	$[\text{Ne}]3s^23p^2$	66	Dy	$[\text{Xe}]4f^{10}6s^2$
15	P	$[\text{Ne}]3s^23p^3$	67	Ho	$[\text{Xe}]4f^{11}6s^2$
16	S	$[\text{Ne}]3s^23p^4$	68	Er	$[\text{Xe}]4f^{12}6s^2$
17	Cl	$[\text{Ne}]3s^23p^5$	69	Tm	$[\text{Xe}]4f^{13}6s^2$
18	Ar	$[\text{Ne}]3s^23p^6$	70	Yb	$[\text{Xe}]4f^{14}6s^2$
19	K	$[\text{Ar}]4s$	71	Lu	$[\text{Xe}]4f^{14}5d6s^2$
20	Ca	$[\text{Ar}]4s^2$	72	Hf	$[\text{Xe}]4f^{14}5d^26s^2$

TABLE 3.4 *Continued*

Z	Element	Electron configuration	Z	Element	Electron configuration
21	Sc	[Ar]3d4s ²	73	Ta	[Xe]4f ¹⁴ 5d ³ 6s ²
22	Ti	[Ar]3d ² 4s ²	74	W	[Xe]4f ¹⁴ 5d ⁴ 6s ²
23	V	[Ar]3d ³ 4s ²	75	Re	[Xe]4f ¹⁴ 5d ⁵ 6s ²
24	Cr	[Ar]3d ⁵ 4s	76	Os	[Xe]4f ¹⁴ 5d ⁶ 6s ²
25	Mn	[Ar]3d ⁵ 4s ²	77	Ir	[Xe]4f ¹⁴ 5d ⁷ 6s ²
26	Fe	[Ar]3d ⁶ 4s ²	78	Pt	[Xe]4f ¹⁴ 5d ⁹ 6s
27	Co	[Ar]3d ⁷ 4s ²	79	Au	[Xe]4f ¹⁴ 5d ¹⁰ 6s
28	Ni	[Ar]3d ⁸ 4s ²	80	Hg	[Xe]4f ¹⁴ 5d ¹⁰ 6s ²
29	Cu	[Ar]3d ¹⁰ 4s	81	Tl	[Xe]4f ¹⁴ 5d ¹⁰ 6s ² 6p
30	Zn	[Ar]3d ¹⁰ 4s ²	82	Pb	[Xe]4f ¹⁴ 5d ¹⁰ 6s ² 6p ²
31	Ga	[Ar]3d ¹⁰ 4s ² 4p	83	Bi	[Xe]4f ¹⁴ 5d ¹⁰ 6s ² 6p ³
32	Ge	[Ar]3d ¹⁰ 4s ² 4p ²	84	Po	[Xe]4f ¹⁴ 5d ¹⁰ 6s ² 6p ⁴
33	As	[Ar]3d ¹⁰ 4s ² 4p ³	85	At	[Xe]4f ¹⁴ 5d ¹⁰ 6s ² 6p ⁵
34	Se	[Ar]3d ¹⁰ 4s ² 4p ⁴	86	Rn	[Xe]4f ¹⁴ 5d ¹⁰ 6s ² 6p ⁶
35	Br	[Ar]3d ¹⁰ 4s ² 4p ⁵	87	Fr	[Rn]7s
36	Kr	[Ar]3d ¹⁰ 4s ² 4p ⁶	88	Ra	[Rn]7s ²
37	Rb	[Kr]5s	89	Ac	[Rn]6d7s ²
38	Sr	[Kr]5s ²	90	Th	[Rn]6d ² 7s ²
39	Y	[Kr]4d5s ²	91	Pa	[Rn]5f ² 6d7s ²
40	Zr	[Kr]4d ² 5s ²	92	U	[Rn]5f ³ 6d7s ²
41	Nb	[Kr]4d ⁴ 5s	93	Np	[Rn]5f ⁴ 6d7s ²
42	Mo	[Kr]4d ⁵ 5s	94	Pu	[Rn]5f ⁶ 7s ²
43	Tc	[Kr]4d ⁵ 5s ²	95	Am	[Rn]5f ⁷ 7s ²
44	Ru	[Kr]4d ⁷ 5s	96	Cm	[Rn]5f ⁷ 6d7s ²
45	Rh	[Kr]4d ⁸ 5s	97	Bk	[Rn]5f ⁹ 7s ²
46	Pd	[Kr]4d ¹⁰	98	Cf	[Rn]5f ¹⁰ 7s ²
47	Ag	[Kr]4d ¹⁰ 5s	99	Es	[Rn]5f ¹¹ 7s ²
48	Cd	[Kr]4d ¹⁰ 5s ²	100	Fm	[Rn]5f ¹² 7s ²
49	In	[Kr]4d ¹⁰ 5s ² 5p	101	Md	[Rn]5f ¹³ 7s ²
50	Sn	[Kr]4d ¹⁰ 5s ² 5p ²	102	No	[Rn]5f ¹⁴ 7s ²
51	Sb	[Kr]4d ¹⁰ 5s ² 5p ³	103	Lr	[Rn]5f ¹⁴ 6d7s ²
52	Te	[Kr]4d ¹⁰ 5s ² 5p ⁴			

H ¹																			He ²	
Li ³	Be ⁴											B ⁵	C ⁶	N ⁷	O ⁸	F ⁹	Ne ¹⁰			
1.0	1.5											2.0	2.5	3.0	3.5	4.0				
Na ¹¹	Mg ¹²											Al ¹³	Si ¹⁴	P ¹⁵	S ¹⁶	Cl ¹⁷	Ar ¹⁸			
0.9	1.2											1.5		2.1	2.5	3.0				
K ¹⁹	Ca ²⁰	Sc ²¹	Ti ²²	V ²³	Cr ²⁴	Mn ²⁵	Fe ²⁶	Co ²⁷	Ni ²⁸	Cu ²⁹	Zn ³⁰	Ga ³¹	Ge ³²	As ³³	Se ³⁴	Br ³⁵	Kr ³⁶			
0.8	1.0	1.3	1.5	1.6	1.6	1.5	1.8	1.8	1.8	1.9	1.6	1.6	1.8	2.0	2.4	2.8				
Rb ³⁷	Sr ³⁸	Y ³⁹	Zr ⁴⁰	Nb ⁴¹	Mo ⁴²	Tc ⁴³	Ru ⁴⁴	Rh ⁴⁵	Pd ⁴⁶	Ag ⁴⁷	Cd ⁴⁸	In ⁴⁹	Sn ⁵⁰	Sb ⁵¹	Te ⁵²	I ⁵³	Xe ⁵⁴			
0.8	1.0	1.2	1.4	1.8	1.8	1.9	2.2	2.2	2.2	1.9	1.7	1.7	1.8	1.9	2.1	2.5				
Cs ⁵⁵	Ba ⁵⁶	La ⁵⁷	Hf ⁷²	Ta ⁷³	W ⁷⁴	Re ⁷⁵	Os ⁷⁶	Ir ⁷⁷	Pt ⁷⁸	Au ⁷⁹	Hg ⁸⁰	Tl ⁸¹	Pb ⁸²	Bi ⁸³	Po ⁸⁴	At ⁸⁵	Rn ⁸⁶			
0.7	0.9	1.1	1.3	1.5	1.7	1.9	2.2	2.2	2.2	1.9	1.9	1.8	1.8	1.9	2.0	2.2				
Fr ⁸⁷	Ra ⁸⁸	Ac ⁸⁹	Th ⁹⁰	Pa ⁹¹	U ⁹²															
0.7	0.9	1.1	1.3	1.5	1.7															
			Ce ⁵⁸	Pr ⁵⁹	Nd ⁶⁰	Pm ⁶¹	Sm ⁶²	Eu ⁶³	Gd ⁶⁴	Tb ⁶⁵	Dy ⁶⁶	Ho ⁶⁷	Er ⁶⁸	Tm ⁶⁹	Yb ⁷⁰	Lu ⁷¹				

FIGURE 3.4 The Periodic Table of Elements as viewed by a ceramist showing atomic number and electronegativity. Different shadings show the groupings of some of the most important components of traditional and advanced ceramics. The lighter shading highlights elements used in traditional ceramics. The darker shading shows some of the elements found in advanced ceramics.

3.6 IONS

In ceramics we are usually dealing with materials that have a significant fraction of ionic character in their bonding. The requirements for ionic bonding are simple:

- One element must be able to lose 1, 2, or 3 electrons.
- The other element must be able to accept 1, 2, or 3 electrons.

In both cases the “3” is rare and it must not involve too much energy exchange. The ionization energy is the energy required to remove an electron from the gaseous atom. The first ionization energy (IE_1) is

IONIZATION ENERGY

$\text{Atom (g)} + IE_1 \rightarrow \text{Ion}^+ \text{(g)} + e^-$

This reaction is always endothermic ($IE_1 > 0$). The sign is a convention of thermodynamics; some fields use the opposite convention.

the energy required to remove one electron from the neutral gaseous atom to produce a gaseous ion with charge +1.

The noble gases have a complete shell of outer electrons and have very high ionization energies, whereas the elements in Group I, for example, Na and K, have an outer ns^1 orbital and have much lower ionization energies. Second ionization energies, the energy required to remove an electron from a gaseous ion with charge +1, are significantly higher than first ionization energies because when an electron is lost the effective nuclear charge, Z_{eff} ,

increases. As a result, the effective radius of an atom or ion decreases and the net attraction between the electrons and the nucleus increases (Table 3.5).

The electron affinity (EA) of an atom is the energy change

TABLE 3.5 Ionization Energies of the Elements (MJ/mol)

Z	Element	I	II	III	IV	V
1	H	1.3120				
2	He	2.3723	5.2504			
3	Li	0.5203	7.2981	11.8149		
4	Be	0.8995	1.7571	14.8487	21.0065	
5	B	0.8006	2.4270	3.6598	25.0257	32.8266
6	C	1.0864	2.3526	4.6205	6.2226	37.8304
7	N	1.4023	2.8561	4.5781	7.4751	9.4449
8	O	1.3140	3.3882	5.3004	7.4693	10.9895
9	F	1.6810	3.3742	6.0504	8.4077	11.0227
10	Ne	2.0807	3.9523	6.122	9.370	12.178
11	Na	0.4958	4.5624	6.912	9.544	13.353
12	Mg	0.7377	1.4507	7.7328	10.540	13.628
13	Al	0.5776	1.8167	2.7448	11.578	14.831
14	Si	0.7865	1.5771	3.2316	4.3555	16.091
15	P	1.0118	1.9032	2.912	4.957	6.2739
16	S	0.9996	2.251	3.361	4.564	7.013
17	Cl	1.2511	2.297	3.822	5.158	6.54
18	Ar	1.5205	2.6658	3.931	5.771	7.238
19	K	0.4189	3.0514	4.411	5.877	7.976
20	Ca	0.5898	1.1454	4.9120	6.474	8.144
21	Sc	0.631	1.235	2.389	7.089	8.844
22	Ti	0.658	1.310	2.6525	4.1746	9.573
23	V	0.650	1.414	2.8280	4.5066	6.294
24	Cr	0.6528	1.496	2.987	4.74	6.69
25	Mn	0.7174	1.5091	2.2484	4.94	6.99
26	Fe	0.7594	1.561	2.9574	5.29	7.24
27	Co	0.758	1.646	3.232	4.95	7.67
28	Ni	0.7367	1.7530	3.393	5.30	7.28
29	Cu	0.7455	1.9579	3.554	5.33	7.71
30	Zn	0.9064	1.7333	3.8327	5.73	7.97
31	Ga	0.5788	1.979	2.963	6.2	
32	Ge	0.7622	1.5374	3.302	4.410	9.02
33	As	0.947	1.7978	2.7355	4.837	6.043
34	Se	0.9409	2.045	2.9737	4.1435	6.59
35	Br	1.1399	2.10	3.5	4.56	5.76
36	Kr	1.3507	2.3503	3.565	5.07	6.24
37	Rb	0.4030	2.632	3.9	5.08	6.85
38	Sr	0.5495	1.0643	4.21	5.5	6.91

TABLE 3.5 *Continued*

<i>Z</i>	<i>Element</i>	<i>I</i>	<i>II</i>	<i>III</i>	<i>IV</i>	<i>V</i>
39	Y	0.616	1.181	1.980	5.96	7.43
40	Zn	0.660	1.267	2.218	3.313	7.86
41	Nb	0.664	1.382	2.416	3.69	4.877
42	Mo	0.6850	1.558	2.621	4.477	5.91
43	Tc	0.702	1.472	2.850		
44	Ru	0.711	1.617	2.747		
45	Rh	0.720	1.744	2.997		
46	Pd	0.805	1.875	3.177		
47	Ag	0.7310	2.074	3.361		
48	Cd	0.8677	1.6314	3.616		
49	In	0.5583	1.8206	2.705	5.2	
50	Sn	0.7086	1.4118	2.9431	3.9303	6.974
51	Sb	0.8337	1.595	2.44	4.26	5.4
52	Te	0.8693	1.79	2.698	3.610	5.669
53	I	1.0084	1.8459	3.2		
54	Xe	1.1704	2.046	3.10		
55	Cs	0.3757	2.23			
56	Ba	0.5029	0.96526			
57	La	0.5381	1.067	1.8501		
58	Ce	0.528	1.047	1.949	3.543	
59	Pr	0.523	1.018	2.086	3.758	5.543
60	Nd	0.530	1.034			
61	Pm	0.536	1.052			
62	Sm	0.543	1.068			
63	Eu	0.547	1.085			
64	Gd	0.591	1.17			
65	Tb	0.564	1.112			
66	Dy	0.572	1.126			
67	Ho	0.581	1.139			
68	Er	0.589	1.151			
69	Tm	0.596	1.163	2.288		
70	Yb	0.6034	1.174	2.43		
71	Lu	0.5235	1.34			
72	Hf	0.68	1.44	2.25	3.21	
73	Ta	0.761				
74	W	0.770				
75	Re	0.760				
76	Os	0.84				
77	Ir	0.88				
78	Pt	0.87	1.7911			
79	Au	0.8901	1.98			
80	Hg	1.0070	1.8097	3.30		
81	Tl	0.5893	1.9710	2.878		
82	Pb	0.7155	1.4504	2.0815	4.083	6.64
83	Bi	0.7033	1.610	2.466	4.37	5.40
84	Po	0.812				
85	At					
86	Rn	1.0370				
87	Fr					
88	Ra	0.5094	0.97906			
89	Ac	0.67	1.17			
90	Th		1.11	1.93	2.78	
91	Pa					
92	U					
93	Np					
94	Pu	0.56				
95	Am	0.58				

TABLE 3.6 Electron Affinities of the Elements (kJ/mol)

Element	Theory	Experimental	Element	Theory	Experimental
1. H	72.766	72.9	27. Co	90.3	
2. He		<0	28. Ni	123.1	
3. Li	59.8	58	29. Cu	173.8	
4. Be	-18 ^a	<0	30. Zn	-87 ^c	
5. B	29		31. Ga	17 ^c -48 ^d	
6. C	113	121	32. Ge	116 ^c -132 ^d	
7. N → N ⁻	-58 ^b	121	33. As	58 ^c -71 ^d	
N ⁻ → N ²⁻	-800 ^b		34. Se → Se ⁻	204 ^d -212 ^c	-420
N ²⁻ → N ³⁻	-1290 ^b		Se ⁻ → Se ²⁻		
8. O → O ⁻	120	142	35. Br		324.5
O ⁻ → O ²⁻		-780 ^b	36. Kr		<0
9. F	312-325	328-333	37. Rb		19-39
10. Ne	<0	<0	42. Mo		96
11. Na	52		48. Cd	-58 ^c	
12. Mg	-54 ^c	<0	49. In	19 ^c -69 ^d	
13. Al	48		50. Sn	142 ^d	
14. Si	134		51. Sb	59 ^d	
15. P	75		52. Te	220 ^c	
16. S → S ⁻	205	200	53. I		296
S ⁻ → S ²⁻		-590	54. Xe		<0
17. Cl	343	348	55. Cs		19-39
18. Ar		<0	74. W		48
19. K	45	34-72	75. Re		14
20. Ca		<0	81. Tl	117 ^d	
22. Ti	37.7		82. Pb	173 ^d	
23. V	90.4		83. Bi	-33 ^d	
24. Cr	94.6		84. Po	190 ^d	
26. Fe	56.2				

Source: Berry, R.S. (1969) *Chem. Rev.* **69**, 533, except ^aEdlen, B. (1960) *J. Chem. Phys.* **33**, 98; ^bBaughan, E.C. (1961) *Trans. Faraday Soc.* **57**, 1863; ^cGinsberg, A.P. and Miller, J.M. (1958) *J. Inorg. Nucl. Chem.* **7**, 351; ^dPolitzer, P. (1968) *Trans. Faraday Soc.* **64**, 2241.

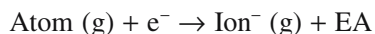
accompanying the addition of one electron to a neutral gaseous atom to produce a negative ion. Values of EA are shown in Table 3.6. A positive value indicates that the reaction

ELECTRON AFFINITY



Note: The sign convention used for EA is in contradiction to that usually found in thermodynamics, an unfortunate historical artifact.

and very reactive nonmetals. Two requisites are that the ionization energy to form the cation and the electron affinity to form the anion must be energetically favorable. The overall reaction will cost some, but not too much, energy.



Recap:

is exothermic.

The values of EA also show a periodic behavior that can be explained by examining the electron configurations of the elements. The electron affinity is high for elements in Group VII, for example, F and Cl. The addition of one electron to these atoms forms negative ions with a noble gas electron configuration—a stable arrangement. Atoms that already have full (e.g., He, Ne) or half-full orbitals (e.g., Be, N) often have negative electron affinities. Full and half-full orbitals are more stable.

As we will see in Chapter 4, ionic compounds generally form only between very reactive metallic elements

- Ionization energy, IE: the energy required to remove an electron from the neutral gaseous atom
- Electron affinity, AE: the change in energy when one electron is added to a neutral gaseous atom

3.7 ELECTRONEGATIVITY

Electronegativity is a measure of the strength with which an atom in a molecule attracts electrons. Like IE and EA, the dependence of electronegativity on *Z* can be explained

by examining electron configurations. Atoms with almost completely filled outer energy levels, like F and Cl, are strongly electronegative and readily accept electrons. However, atoms with nearly empty outer shells, such as Li and Na, readily give up electrons and are strongly electropositive. Higher Z elements also have a low electronegativity; because the outer electrons are at a greater distance from the positive nucleus, electrons are not as strongly attracted to the atom.

The electronegativity scale of the elements is included in Figure 3.4 using Pauling's classification: F is assigned the largest electronegativity, 4, and the other elements are then based on this value. The differences in the electronegativities of two atoms in a molecule can be used to estimate bond strengths and bond ionicities (i.e., the percentage of ionic character in the bond—the extent of “mixed” bonding; see Section 4.6 for numerical examples).

3.8 THERMODYNAMICS: THE DRIVING FORCE FOR CHANGE

Thermodynamic principles are important in all aspects of materials science. In this section we introduce some of the fundamentals, but thermodynamics will be used in several other chapters (e.g., point defects, Chapter 11, and surfaces, Chapter 13). The primary role of thermodynamics in ceramics is to indicate whether a system is stable and what conditions (usually changes in temperature or pressure) will cause it to change. Our system may be a crystal structure, a phase, a grain boundary, an aggregate of powder particles, or a concentration of defects. Table 3.7 lists some of the important thermodynamic parameters we meet in ceramics together with their units.

Thermodynamic Stability

The Gibbs free energy (G) is a property that provides a convenient measure of the driving force of a reaction and may be used to define thermodynamic stability. When we

GIBBS FREE ENERGY

The change in free energy is defined by

$$\Delta G = \Delta H - T\Delta S \quad \text{Box 3.7}$$

The change in enthalpy is given by

$$\Delta H = \Delta E + P\Delta V \quad \text{Box 3.8}$$

When the process involves no volume change, i.e., $P\Delta V = 0$, so $\Delta H = \Delta E$ we can write

$$\Delta G = \Delta E - T\Delta S \quad \text{Box 3.9}$$

CONVENIENT FORMS OF ΔG

Mixing A and B to form a solution (important in constructing phase diagrams)

$$\Delta G = RT(X_A \ln a_A + X_B \ln a_B)$$

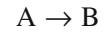
Oxidation of a metal to form a ceramic

$$\Delta G = RT \ln p_{O_2}$$

Electrochemical process (such as in a fuel cell)

$$\Delta G = -zFE \quad \Delta G = RT \ln p_{O_2}$$

want to know whether a process is energetically favorable, we have to determine the change in free energy (ΔG) associated with that process. For the change



which may be an oxidation reaction or a phase transformation, the change in free energy is

$$\Delta G = G_B - G_A$$

where G_B is the free energy of the final state and G_A is the free energy of the initial state.

- $\Delta G < 0$ for a favorable process. There is a natural tendency to move spontaneously from A to B.
- $\Delta G > 0$ for an unfavorable process. The reaction as written will not proceed spontaneously; the reverse reaction will be the spontaneous one.
- $\Delta G = 0$ for a process at equilibrium.

In many processes, particularly those that occur in ceramics, there is little if any volume change and so $P\Delta V = 0$. Because the sign of ΔG is dependent upon temperature and pressure, a particular system, such as a crystal structure, can be stable only within a certain range of P and T . By varying P and/or T , ΔG will eventually become negative relative to some other structure

TABLE 3.7 Important Thermodynamic Parameters

Parameter	Definition	Units
C_p	Heat capacity at constant pressure	J/K
c_p	Molar heat capacity at constant pressure	$\text{JK}^{-1} \text{mol}^{-1}$
C_v	Heat capacity at constant volume	J/K
c_v	Molar heat capacity at constant volume	$\text{JK}^{-1} \text{mol}^{-1}$
E	Energy	J
G	Gibbs free energy	J
H	Enthalpy	J
μ_i	Chemical potential	J
P	Pressure	Pa
S	Entropy	J/K
T	Temperature	K

and a phase transition will occur. This may be a transition from one crystal structure to another (e.g., the phase transformation in quartz), or it may be a transition from one aggregate state to another state (e.g., during sintering when we get grain growth and reduction in total grain boundary area), or it could be when we melt a solid to form a liquid.

The Gibbs free energy is a function of temperature, pressure, and the numbers of moles of all the species present in the system.

Effect of Temperature

Many of the processes of interest in ceramics occur at high temperature. At absolute zero, $T = 0$ K, the term containing the entropy change, $T\Delta S$, is zero and ΔG depends only on ΔE . However, as T increases the $T\Delta S$ term becomes increasingly important and at some temperature a process can occur spontaneously even though ΔE is positive. The values of ΔE and ΔS depend on temperature and we can rewrite Box 3.9:

$$\Delta G_T = \Delta E_T - T\Delta S_T \quad (3.1)$$

The subscript indicates that the values are given at a temperature, T . To obtain values of ΔE_T and ΔS_T we need to use the heat capacities of the material.

The molar heat capacities are

$$c_p = dH/dT \quad (3.2)$$

$$c_v = dE/dT \quad (3.3)$$

In many solids, particularly ceramics, with low coefficients of expansion $c_p \sim c_v$. It is easier to obtain values of c_p and the variation with temperature is normally fitted to an analytical expression of the form

$$c_p = a + bT + cT^{-2} \quad (3.4)$$

We use Eq. 3.4 in Chapter 34 (Eq. 34.3) to determine c_p for various ceramics.

Using c_p we can obtain expressions for ΔE_T and ΔS_T

$$\Delta H_T = \Delta H_{298} + \int_{298}^T \Delta c_p dT \quad (3.5)$$

$$S_T = S_0 + \int_0^T \frac{c_p}{T} dT \quad (3.6)$$

If the external work of expansion due to heating is zero, as it is when a material is heated at constant volume, or if it is negligible, as it is when solids are heated at atmospheric pressure, all the heat supplied goes into internal energy and we can approximate ΔH_T by ΔE_T . It is values of ΔH_{298} that you will find tabulated. The variation of ΔG with temperature is illustrated in Figure 3.5.

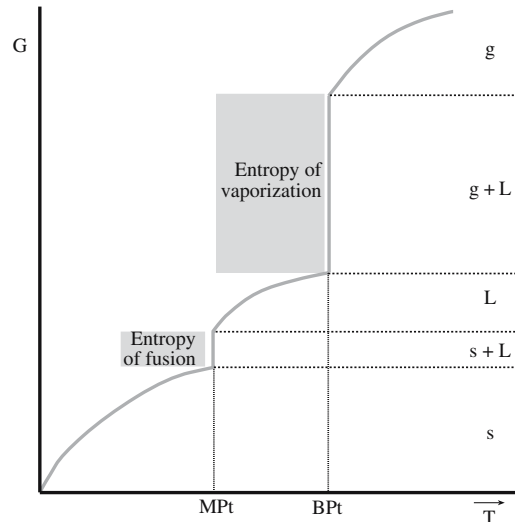


FIGURE 3.5 Variation in the Gibbs free energy as a function of temperature. The vertical segments are associated with phase transformations.

When the signs of ΔE_T and ΔS_T are the same, some reactions that are not favorable at one temperature become favorable at another, and vice versa. It is often useful to know the temperature at which a reaction becomes favorable. This is the temperature at which a positive ΔG_T switches to a negative ΔG_T due to the $-T\Delta S_T$ term. We find this crossover temperature by setting ΔG_T in Eq. 3.1 equal to 0 and solving for T

$$T = \frac{\Delta E_T}{\Delta S_T} \quad (3.7)$$

Figure 3.6 shows the effect of temperature on reaction favorability. The slopes of the two lines and the crossover temperature will depend on the specific system.

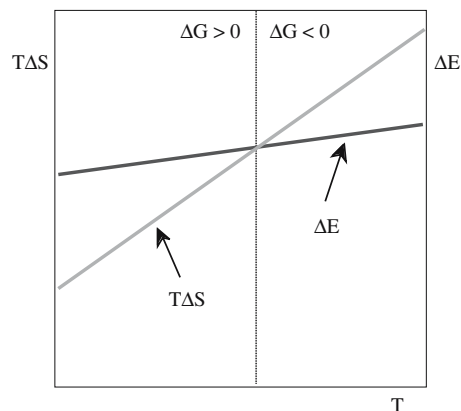


FIGURE 3.6 Effect of temperature on reaction spontaneity. The two lines cross when the energy contribution becomes less than the entropy contribution.

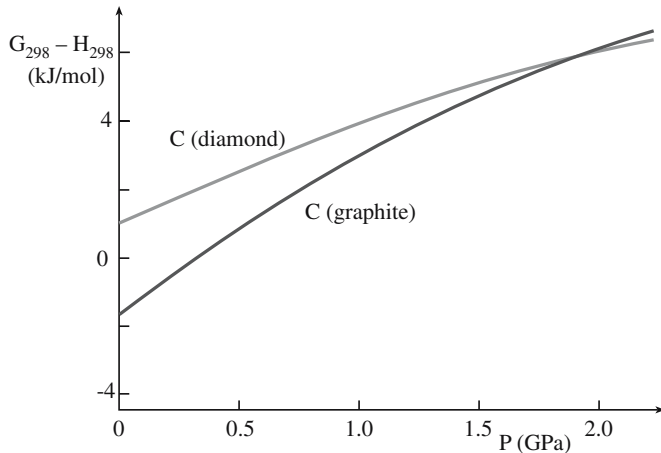


FIGURE 3.7 Pressure dependence of the Gibbs free energies of carbon in graphite and diamond. Diamond becomes more stable at high pressures.

Effect of Pressure

Higher pressures favor structures that have a higher density. Their formation involves a decrease in volume (negative ΔV). For instance, diamond ($\rho = 3.51 \text{ g cm}^{-3}$) is more stable than graphite ($\rho = 2.26 \text{ g cm}^{-3}$) at very high pressures. At room temperature graphite will transform to diamond at pressures greater than about 1.5 GPa (14,400 atm) as shown in Figure 3.7. Graphite is the stable phase at room temperature and pressure. The influence of pressure, at constant T , on the Gibbs free energies of two phases, α and β , is given by

$$(\partial G_{(\alpha \rightarrow \beta)} / \partial P)_T = \Delta V_{(\alpha \rightarrow \beta)} \quad (3.8)$$

Effect of Composition

In ceramics we are often dealing with multicomponent systems such as the ternary quartz, clay, and feldspar used in the formation of porcelains or the binary NiO , Al_2O_3 that react to form a spinel. Equilibrium, at constant T and P , is reached in these systems when the chemical potential, μ_i , of a component is the same in all of the phases in which it is present. The chemical potential, or the partial molar free energy of a component in a given phase, is defined as

$$\mu_i = (\partial G / \partial n_i)_{T,P,n_j} \quad (3.9)$$

where n_i is the number of moles of component i and n_j is the number of moles of component j .

Deduction of the phase rule (Chapter 8), which defines the conditions of equilibrium in terms of the number of phases and the components of a system, follows directly from the requirement that μ_i of each constituent i be the same in every phase at equilibrium. If μ_i is different then we will get a reaction, the rate of which will be determined by kinetics.

We can combine Eq. 3.9 with our definition of Gibbs free energy and produce a differential form of the Gibbs equation:

$$\partial G = V \partial P - S \partial T + \sum \mu_i \partial n_i \quad (3.10)$$

The importance of Eq. 3.10 is that it links the free energy of the system to our usual experimental variables (T and P) and the observable properties (V and concentration).

3.9 KINETICS: THE SPEED OF CHANGE

Thermodynamics tells us whether a process can happen. Kinetics tells us whether that process will happen at a reasonable, or measurable, rate. The rates of chemical reactions have been found to depend very strongly on the temperature. A useful rule of thumb is that the rate doubles for every 10 K increase in temperature. The rate, k , of many reactions follows the Arrhenius rate law

$$k = A \exp(-E_a/RT) \quad (3.11)$$

where R is the gas constant ($8.314 \text{ J K}^{-1} \text{ mol}^{-1}$), A is a temperature-independent preexponential constant, and E_a is the activation energy. A plot of k versus T gives a curve that increases exponentially. The activation energy represents the minimum energy required for a reaction to happen. The value of E_a may be determined from the logarithmic form of the Arrhenius equation:

$$\ln k = \frac{E_a}{RT} + \ln A \quad (3.12)$$

A plot of $\ln k$ against $1/T$ yields a straight line with slope $-E_a/R$, as shown in Figure 3.8. This type of plot is called an Arrhenius plot and a reaction giving such a straight line is said to show Arrhenius behavior.

Most reactions that proceed at a moderate rate, that is, occur appreciably in minutes or hours, have values of E_a between 50 and 100 kJ. For such reactions you can use Eq. 3.11 to verify the photographer's guide that reactions go two or three times as fast when the temperature increases by 10°C.

An important example of a process that exhibits Arrhenius behavior is diffusion. The diffusion coefficient D (units of cm^2/s) is a strong function of temperature.

$$D = D_0 \exp(-E_a/RT) \quad (3.13)$$

For ceramics the value of E_a varies over quite a wide range from about 50 kJ/mol to 800 kJ/mol ($\sim 0.5 \text{ eV}$ per atom to 8 eV per atom). The activation energy represents the energy necessary for an atom to jump from one atomic position to another.

The diffusion coefficient also depends on chemical potential and time. These changes are represented in Fick's laws, which we will describe in Chapter 11.

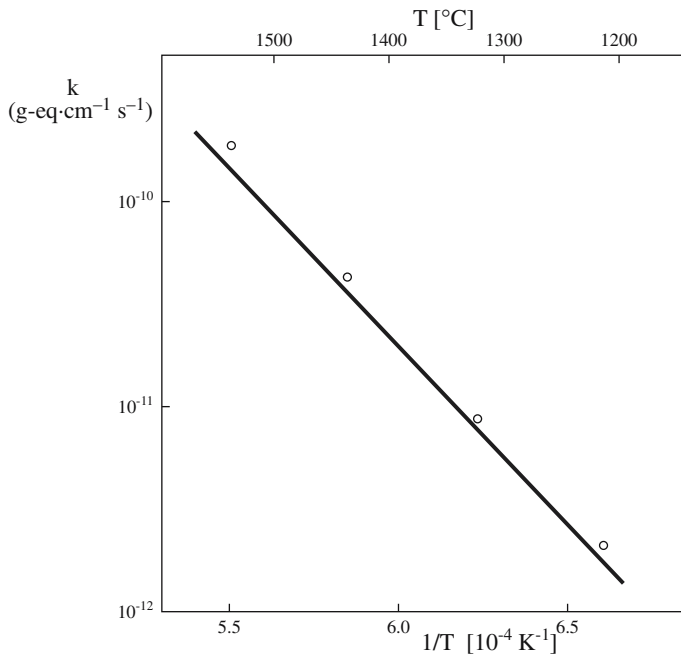


FIGURE 3.8 An Arrhenius plot. The slope of the line gives the activation energy for the process.

At sufficiently low temperatures any structure can be stabilized kinetically. Kinetic stability is not a well-defined term because the limit below which a conversion rate is considered to be negligible is arbitrary. There are many examples of kinetically stabilized materials. Two examples in ceramics are

- Glasses. At room temperature a glass is a kinetically stabilized material. Given enough time all glasses will transform to their crystalline counterpart.
- Tridymite (a high-temperature polymorph of SiO₂). Transformation of quartz at 867°C should lead to the formation of tridymite. However, the transformation is very slow (it involves a complete alteration of the crystal structure) and direct conversion by heating alone has not been proved. All natural tridymite contains other oxides, which it is believed stabilize the structure; pure tridymite cannot be obtained at room temperature.

Notice that we have not considered the environment of the combining atoms/ions, so we have not actually used the crystal/amorphous nature of the ceramic.

CHAPTER SUMMARY

We reviewed some of the fundamentals that underlie all aspects of materials science. Knowing the electron configuration of an atom allows us to understand some of the properties of materials that contain that atom. It also helps us to determine the type of bonding that occurs between different atoms. In ceramics the bonding is important because it is not straightforward. It often involves ionic and covalent contributions and sometimes also a metallic component.

Thermodynamics and kinetics enable us to explain why and how chemical reactions take place. This type of information is important in many areas of ceramics, but particularly in ceramic processing. Traditional processing of ceramic components is carried out at high temperatures because the kinetics would be too slow otherwise. Kinetics is often closely linked to economics. Processes that are slow are usually expensive.

PEOPLE IN HISTORY

Arrhenius, Svante August won the 1903 Nobel Prize in Chemistry for his work on the electrical conductivity of salt solutions (he was also nominated for the Physics Prize). He is often hailed as a pioneer of modern environmentalism for his work on the greenhouse effect. One of his predictions was that the United States might pump its last barrel of oil in 1935. Fortunately he was proved wrong, but his concern about the world's natural mineral resources and the need for alternative sources of energy was prescient. He died in 1927 at age 68.

Barkla, Charles Glover (1877–1944) was born in Widnes, Lancashire, England. After obtaining his master's degree in physics he went to work in the Cavendish Laboratory with J.J. Thomson. In 1913 he accepted the position of Chair in Natural Philosophy in the University of Edinburgh in Scotland and he remained there until he died. He was awarded the 1917 Nobel Prize in Physics for his discovery of the characteristic Röntgen radiation of the elements.

Bohr, Neils (Denmark) in 1913 proposed an atomic model where electrons could move only in certain stable orbits. He won the Nobel Prize in Physics in 1922 and died in 1962 at age 77.

Boltzmann, Ludwig Eduard was born in Vienna in 1844 and died at age 62. His constant is inscribed on his tomb in Vienna. Many argued strongly against his ideas and he committed suicide shortly before experiments justified them.

Davisson, Clinton Davis and Germer, Lester Halbert were working at Bell Labs at the time of their discovery of electron diffraction. Davisson died in 1958 at age 76 (born 1881) and Germer died in 1971 at age 75 (born 1896).

de Broglie, Louis in 1924 hypothesized that all matter possesses wave properties. A French Duke, he won the Nobel Prize in Physics in 1929. He died in 1987 at age 94.

Heisenberg, Werner (1901–1976) was born in Würzburg in Germany. He obtained his PhD in 1923 at the University of Munich. He published his theory of quantum mechanics when he was 23 and for this theory he was awarded the 1932 Nobel Prize in Physics. At the end of World War II he was taken prisoner by American troops and sent to England. He returned to Germany in 1946. He was Director of the famous Max Planck Institute for Physics and in 1953 became President of the Alexander von Humboldt Foundation. He died in 1976 at age 74.

Pauli, Wolfgang (1900–1958) was born in Vienna, Austria. He obtained his doctoral degree in 1921 from the University of Munich. After that he worked with Max Born and then with Neils Bohr. He held various appointments in the United States during World War II, including the Institute of Advanced Study in Princeton. After the war he returned to the Federal Institute of Technology in Zurich as Professor of Theoretical Physics. He won the 1945 Nobel Prize in Physics for developing the eponymous exclusion principle.

Pauling, Linus Carl won the Noble Prize for Chemistry in 1954 and in 1962 for Peace. He died in 1994 at age 93.

Schrödinger, Erwin was born in Vienna, Austria in 1887. His great discovery, Schrödinger’s wave equation, was made in 1926, and for that he won the Nobel Prize in Physics in 1933. When Hitler came to power in Germany (1933) Schrödinger moved to England. He then moved back to Austria but had to escape when his native country became annexed in 1938. He eventually moved to the Institute for Advanced Studies in Dublin where he remained until he retired. He died in 1961 at age 73.

Thomson, Joseph John and Thomson, George Paget were father and son. Rutherford was J.J. Thomson’s student at Cambridge. J.J. Thomson discovered the electron in 1897 and won the Nobel Prize in Physics in 1906. G.P. Thomson won the Nobel Prize in 1937 together with Davisson; he died in 1976 (born 1892). So, the father “proved” that electrons were particles and the son “proved” they were waves.

GENERAL REFERENCES

Atkins, P.W. and de Paula, J. (2002) *Atkins’ Physical Chemistry*, 7th edition, Oxford University Press, Oxford. A physical chemistry text often used at the sophomore/junior level.

DeHoff, R. (2006) *Thermodynamics in Materials Science*, 2nd edition, CRC, Boca Raton, FL. A standard thermodynamic text for materials science.

Gaskell, D.R. (2003) *Introduction to the Thermodynamics of Materials*, 4th edition, Taylor & Francis, New York. Thermodynamic text for undergraduate courses in materials science.

Huheey, J.E., Keiter, E.A., and Keiter, R.L. (1993) *Inorganic Chemistry: Principles of Structure and Reactivity*, 4th edition, Cummings, San Francisco. A standard inorganic chemistry textbook. Much of this should be background material.

Kreyszig, E. (1999) *Advanced Engineering Mathematics*, 8th edition, Wiley, New York. Senior level undergraduate/graduate-level engineering mathematics text that describes the method for transforming Cartesian coordinates into polar coordinates and the method of separation of variables.

Pauling, L. (1960) *The Nature of the Chemical Bond*, 3rd edition, Cornell University Press, Ithaca, NY. A classic, and one of the most frequently cited of all scientific texts. Gives a detailed description of his scale of electronegativity.

Planck, Max (1922) *Treatise on Thermodynamics*, Dover Publications. Winner of the 1918 Nobel Prize for Physics

SPECIFIC REFERENCES

Arrhenius, S. (1889) “Ober die Reaktionsgeschwindigkeit bei der Inversion von Rohrzucker durch Säuren,” *Z. Phys. Chem.* **4**, 226–248.

Bohr, N. (1913) “The constitution of atoms and molecules,” *Phil. Mag.* **26**, 1, 476.

Bohr, N. (1913) “Constitution of atoms and molecules III,” *Phil. Mag.* **26**, 1, 857.

Davisson, C. and Germer, L.H. (1927) “Diffraction of electrons by a nickel Crystal,” *Phys. Rev.* **30**, 705.

DeBroglie, L. (1925) “Recherches sur la théorie des quanta,” *Ann. Phys., Paris* **3**, 22.

Heisenberg, W. (1927) “The problem of several bodies and resonance in quantum mechanics. II,” *Z. Phys.* **41**, 239.

Hund, F (1925) “Interpretation of spectra,” *Z. Phys.* **33**, 345.

Thomson, G.P. and Reid, A. (1927) “Diffraction of cathode rays by a thin film,” *Nature* **119**, 890.

EXERCISES

- 3.1 Explain the trend in the first ionization energies of elements in the second row (Na to Cl) of the periodic table.

- 3.2 Explain the trend in ionization energies of singly charged ions of the halogens.
- 3.3 Explain the trend in electron affinities of elements in the second row (Na to Cl) of the periodic table.
- 3.4 What is the ionization energy of F^- ? Would you expect the process of ionization to be endothermic or exothermic?
- 3.5 Calculate the energy of the Na $3s^1$ electron. The value of the first ionization energy for Na is 0.50 MJ/mol. Explain the difference, if any, between these two numbers.
- 3.6 Explain the trend in Pauling electronegativities of elements in the second row (Na to Cl) of the periodic table.
- 3.7 An electron has the principal quantum number four. What are the possible values of l , m_l , and m_s for this electron?
- 3.8 Determine the activation energy for the reaction shown in Figure 3.8.
- 3.9 Even though glasses are not thermodynamically stable, we know they exist at room temperature. Explain this phenomenon and describe briefly how you could increase the rate at which a glass would crystallize.
- 3.10 Show that the volume change for the transformation graphite \rightarrow diamond is negative.

4

Bonds and Energy Bands

CHAPTER PREVIEW

Bonding in ceramic materials may be quite complicated. It will be primarily covalent and/or ionic, but it may also have a metallic component, a van der Waals component, etc. In this chapter we will review the basic types of primary and secondary bonds and see how they apply to ceramics. We will also review the concept of energy bands, which we use in discussing electrical properties later. The purpose of this chapter is to review the concepts that we will use throughout the text. If it is not a review for you, suggestions are given for suitable texts that will give you the details. Important topics include the type of bonding, the origin of hybridization, mixed bonding, and energy bands.

4.1 TYPES OF INTERATOMIC BOND

We can divide interatomic bonds into two categories:

- Primary (strong) bonds
- Secondary (weak) bonds

The types of primary and secondary bonds and their energy ranges are given in Table 4.1. In the next few sections we will briefly review the general characteristics of these bonds.

All interatomic forces are electrostatic in origin. The simplest expression for the bond energy is

$$E = -\frac{A}{r^n} + \frac{B}{r^m} \quad (4.1)$$

where r is the interatomic distance and A , B , n , and m are constants characteristic of the type of bonding. The first term is the attractive component the second is due to repulsion. Only when $m > n$ will a minimum (equilibrium) value of E be possible. Equation 4.1 indicates that attractive forces predominate when atoms are far apart and repulsive interactions predominate when the atoms are close together. The bond–energy curve can be plotted as shown in Figure 4.1a. When the energy is a minimum the atoms are at their equilibrium separation ($r = r_0$); the lowest energy state defines the equilibrium condition. In discussing ceramics, we usually think of the material in terms of ions; ions with the same sign always repel one another due to the Coulomb force.

If we differentiate Eq. 4.1 with respect to r , we obtain an equation that describes the resultant force F between a pair of atoms

$$F = \frac{dE}{dr} = \frac{nA}{r^{n+1}} - \frac{mB}{r^{m+1}} \quad (4.2)$$

The force will be zero at the equilibrium separation.

The sign conventions for force: In Figure 4.1a the force is attractive when F is positive. This is the usual convention in materials science (and in Newton’s law of universal gravitation). The force is attractive if $A > 0$ and negative if $A < 0$. Beware: in electrostatics, the convention is that a negative force is attractive.

4.2 YOUNG’S MODULUS

We can change the equilibrium spacing (r_0) of the atoms in a solid by applying a force. We can push the atoms closer together (compression), $r < r_0$, or pull them further apart (tension), $r > r_0$. Young’s modulus (\mathcal{E}) is a measure of the resistance to small changes in the separation of adjacent atoms (*modulus* is Latin for “a small measure”). It is the same for both tension and compression.

Young’s modulus is related to the interatomic bonding forces and, as you might expect, its magnitude depends on the slope of the force–distance curve at r_0 .

Close to r_0 the force–distance curve approximates a tangent; when the applied forces are small the displacement of the atoms is small and proportional to the force. We can define the stiffness of the bond, S_0 , as the slope of this line:

$$S_0 = \left(\frac{dF}{dr} \right)_{r=r_0} = \left(\frac{d^2E}{dr^2} \right)_{r=r_0} \quad (4.3)$$

TABLE 4.1 Typical Bond Strengths

Type of bond	Bond energy (kJ/mol)
Ionic	50–1000
Covalent	200–1000
Metallic	50–1000
van der Waals	0.1–10
Hydrogen	10–40

The stiffness is analogous to the spring constant or elastic force constant of a spring and is the physical origin of Hooke’s law. Close to r_0 we can assume that the force between two atoms that have been stretched apart a small distance r is

$$F = S_0(r - r_0) \tag{4.4}$$

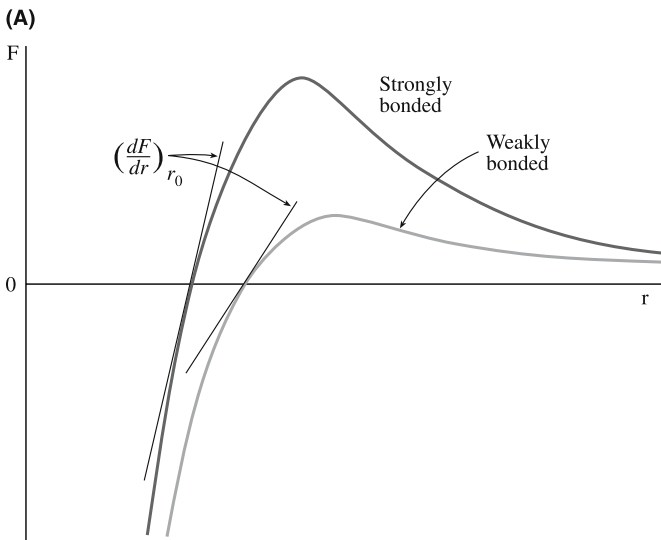
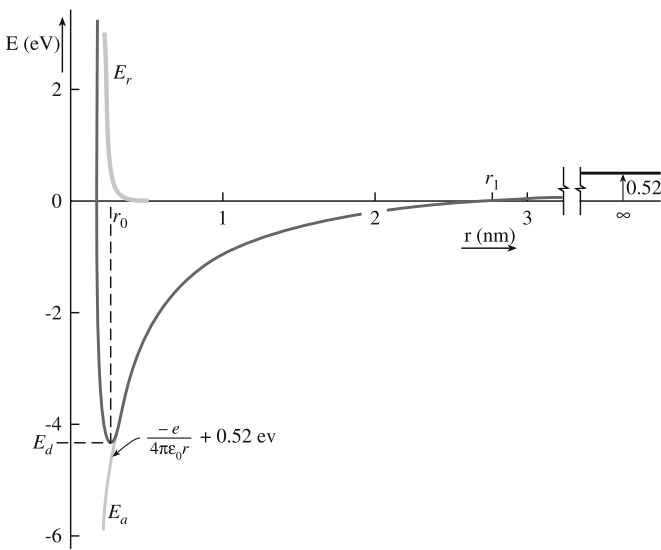


FIGURE 4.1 (a) Bond-energy curve for KCl. At infinite separation, the energy is that required to form K^+ and Cl^- from the corresponding atoms. (b) Force-distance curves for two materials: one where the bonding is strong and one where it is weak.

If we consider pulling two planes of atoms apart then the total force per unit area can be obtained by dividing F by r_0^2

$$\frac{F}{r_0^2} = \sigma = \frac{S_0(r - r_0)}{r_0^2} = \frac{S_0}{r_0} \left(\frac{r - r_0}{r_0} \right) = \mathcal{E} \epsilon \tag{4.5}$$

where σ and ϵ should be familiar to you already, they are stress and strain, respectively. Moduli obtained from this approach are approximate because they relate to two atoms only, ignoring the effects of neighboring atoms. (Although we only discussed Young’s modulus here the conclusions are applicable to the other elastic moduli we describe in Chapter 16.) As the interatomic spacing, and in some cases the bonding, varies with direction in a single crystal, Young’s modulus is dependent upon the direction of stress in relation to the crystal axes. Single crystals are elastically anisotropic.

Figure 4.1b shows force–distance plots for two materials; one having weakly bonded atoms and the other having strongly bonded atoms. With reference to bond–energy curves a material with a high modulus will have a narrow, steep potential energy well; a broad, shallow energy well would be characteristic of a low modulus. Table 4.2 lists values of Young’s moduli for different materials as a function of melting temperature. You can see the general trend: the higher the melting temperature, the higher the modulus. Melting temperatures are also indicative of bond strengths, which are determined mainly by the depth of the energy well. The modulus is determined by the curvature at the bottom of the well. It is this difference that accounts for deviations from the general trend.

As the temperature of a material is increased it is generally found that Young’s modulus slowly decreases as shown for single-crystal aluminum oxide (corundum) in

TABLE 4.2 Young’s Moduli as a Function of Melting Temperature

Compound	Average Young’s modulus (GPa)	Melting temperature, (°C)
Titanium carbide	310	3180
Tungsten	414	2996
Silicon carbide	345	Sublimes > 2800
Periclase (MgO)	207	2800
Beryllia (BeO)	310	2585
Spinel (MgAl ₂ O ₄)	241	2160
Corundum (Al ₂ O ₃)	366	2050
Iron	207	1539
Copper	110	1083
Halite (NaCl)	34	801
Aluminum	69	660
Magnesium	41	650
Polystyrene	2.8	<300
Nylon	2.8	<300
Rubber	0.07	<300

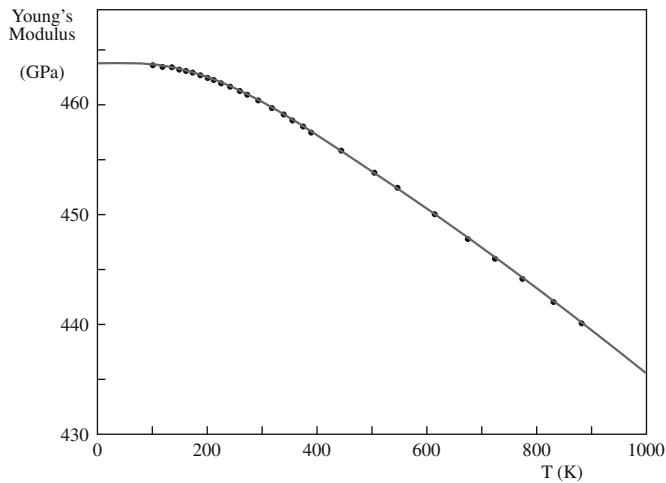


FIGURE 4.2 Temperature dependence of Young's modulus for corundum.

Figure 4.2. As we approach absolute zero, the slope of the curve approaches zero as required by the third law of thermodynamics. (The entropy of any pure substance in complete internal equilibrium is zero.) An empirical relationship that fits the data for several ceramics is

$$E = E_0 - bT \exp\left(\frac{-T_0}{T}\right) \quad (4.6)$$

E_0 is Young's modulus at absolute zero and b and T_0 are empirical constants; T_0 is about half the Debye temperature. (The Debye temperature is the temperature at which the elastic vibration frequency of the atoms in a solid is the maximum.) As the temperature is increased the separation between the atoms is increased and the force necessary for further increases is slightly decreased.

For polycrystalline ceramics there is an additional effect due to grain boundaries. At high temperatures there is a rapid decrease in the measured values of Young's moduli as shown in Figure 4.3. This has been attributed to nonelastic effects such as grain boundary sliding and grain boundary softening. So Young's modulus of a bulk ceramic is continuing to change as described by Eq. 4.6, but we are measuring changes due to the grain boundaries. The importance of grain boundaries in the mechanical behavior of ceramics will become very apparent in later chapters.

4.3 IONIC BONDING

In a pure ionic bond there is complete transfer of electrons from one atom to another. Pure ionic compounds do not exist. Although compounds such as NaCl and LiF are often thought of as being ionic, in general, all such "ionic" solids have a covalent component.

The requirement for ionic bonding is that the ionization energy to form the cation and the electron affinity to form the anion must both favor it energetically. The formation of isolated ions from isolated atoms requires energy and, thus, the formation of the pair of ions would not produce a stable situation. However, the pair of ions will have a strong mutual attraction that leads to a strong binding in the molecule. Because the Coulomb force is strong and long range, many ionic compounds have high melting and high boiling temperatures. Ionic bonds do not favor particular directions. This is very different from covalent bonding.

Energy of an Ion Pair

Before considering a lattice of ions, we will consider a single pair of oppositely charged ions separated by a distance r . The electrostatic attractive energy E is

$$E = -\frac{|Z_M||Z_X|e^2}{(4\pi\epsilon_0 r)} \quad (4.7)$$

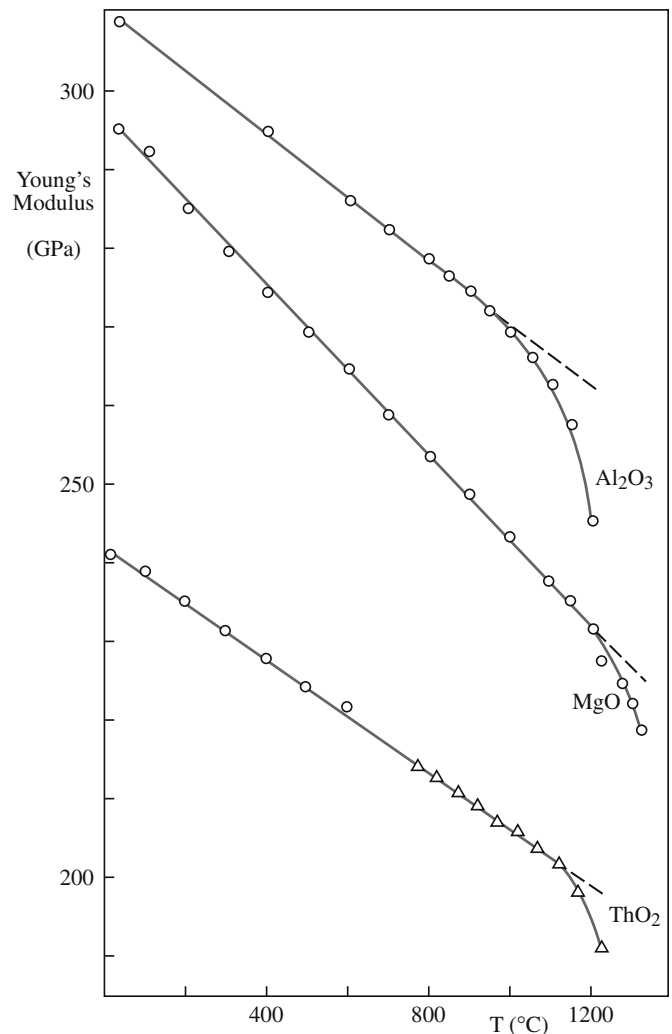


FIGURE 4.3 Temperature dependence of Young's modulus of several polycrystalline ceramics.

Z_M and Z_X are the charges on the cation and anion, respectively. The negative sign in Eq. 4.7 means that as r becomes smaller, the energy becomes increasingly more negative. To obtain equilibrium separation there must be repulsion to balance the attraction. Strong repulsive forces arise when the full electron orbitals of both ions overlap, because some electrons must then go into higher energy states in accordance with the Pauli exclusion principle. The repulsion energy rises rapidly with decreasing distance between the ions.

The repulsive energy is often given by an equation of the form

$$E_r = \frac{B}{r^n} \quad (4.8)$$

B is a constant and n is known as the Born exponent. Information about the Born exponent may be obtained from compressibility data since we are measuring the resistance of the ions to be closer together than r_0 . The Born exponent depends on the type of ion involved. Larger ions have higher electron densities and hence larger values of n (Table 4.3).

The total energy of the ion pair is given by summing Eqs. 4.7 and 4.8

$$E = -\frac{|Z_M||Z_X|e^2}{(4\pi\epsilon_0 r)} + \frac{B}{r^n} \quad (4.9)$$

The inset in Figure 4.1a shows how when r is large the bond energy is >0 , because of the net energy involved in forming the ion pair.

Madelung Constant

In a crystal lattice, all the ions will interact. The interaction between ions with opposite charge will be attractive, but will be repulsive between ions of like charge. The summation of all these

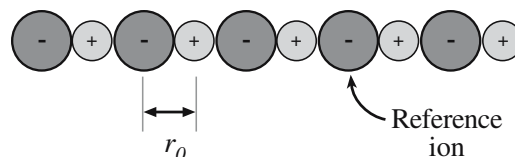


FIGURE 4.4 Linear array of ions of alternate sign separated by r_0 .

interactions is known as the Madelung constant, \mathcal{A} (Madelung, 1918). The energy per ion pair in the crystal is then

$$E = -\frac{\mathcal{A}|Z_M||Z_X|e^2}{(4\pi\epsilon_0 r_0)} \quad (4.10)$$

The Madelung constant is defined as the ratio of the Coulomb energy of an ion pair in a crystal to the Coulomb energy of an isolated ion pair at the same separation (the equilibrium separation of the ions in the crystal not in an isolated pair).

$$\mathcal{A} = \sum_i -\frac{Z_i Z_j}{|Z_i||Z_j|r_{ij}} \quad (4.11)$$

The distance r_{ij} is the separation between ions at equilibrium.

In three dimensions the series presents greater difficulty than the linear example. It is not possible to write down the successive terms by quick inspection. More importantly, the series converges slowly and keeps reversing

in sign so you have to consider the whole infinite crystal.

An approach we can use to obtain \mathcal{A} for a three-dimensional crystal structure is illustrated for NaCl (Figure 4.5). We want to consider the interactions between the central cation and all the other ions in the cell. Due to electroneutrality requirements in the unit cell, ions located on the cube faces count 1/2, those on the cell edges count 1/4, and the corner ions count 1/8. (This is the same

approach that you use when determining the number of atoms per cell.)

Using Eq. 4.11 we obtain

$$\mathcal{A} = -(6/2)(-1)/1 - (12/4)(1)/\sqrt{2} - (8/8)(-1)/\sqrt{3}$$

Hence

$$\mathcal{A} = 3 - 2.1212 + 0.5774 = 1.456$$

MADELUNG CONSTANT FOR LINEAR ARRAY

For the infinite linear array of ions shown in Figure 4.4 we obtain

$$\mathcal{A} = 2[1 - 1/2 + 1/3 - 1/4 + \dots]$$

The factor 2 occurs because there are two ions, one to the right and one to the left of our reference ion, at equal distances r_{ij} . We sum this series using the expansion

$$\ln(1+x) = x - x^2/2 + x^3/3 - x^4/4 + \dots$$

Thus the linear Madelung constant

$$\mathcal{A} = 2 \ln 2.$$

TABLE 4.3 Values of the Born Exponent, n

Ion configuration	n
He	5
Ne	7
Ar, Cu ⁺	9
Kr, Ag ⁺	10
Xe, Au ⁺	12

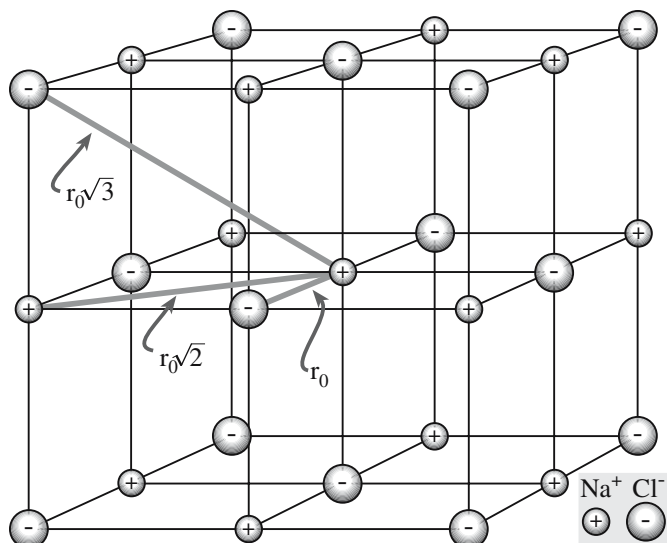


FIGURE 4.5 NaCl structure showing distances between ions in multiples of r_0 .

If we consider a larger cell size the value we obtain for the Madelung constant is closer to that determined for the NaCl structure using computer calculations. Doubling the length of the cell edge gives $\mathcal{A} = 1.75$. These simple calculations are a little misleading because the sum is really infinite. There are two important points:

- \mathcal{A} is well defined for a particular crystal structure, it is usually ~ 2 .
- \mathcal{A} is unique for a particular crystal structure and is the same for NaCl and MgO.

Table 4.4 lists Madelung constants for some common crystal structures. The value of the Madelung constant is determined only by the geometry of the lattice and is independent of the ionic radius and charge. Unfortunately, some tables incorporate ionic charge, so care is necessary when looking up and comparing values. For example, the Madelung constant for fluorite may be given as 5.038 and that of Al_2O_3 as 25.031; the constant for MgO may then be given as different from that for NaCl.

Table 4.4 confirms that the value of the Madelung constant for all these different crystal structures is greater

TABLE 4.4 Madelung Constants of Some Common Crystal Structures

Structure	Coordination number	Geometric factor, \mathcal{A}
Sodium chloride	6:6	1.74756
Cesium chloride	8:8	1.76267
Zinc blende	4:4	1.63806
Wurtzite	4:4	1.64132
Fluorite	8:4	2.51939
Rutile	6:3	2.408 ^a
Corundum	6:4	4.1719 ^a

than 1. The implication is that the crystal is more stable than an isolated ion pair. The fact that the Madelung constant for the NaCl structure, which has six nearest neighbors, is close to the Madelung constant of the CsCl structure, which has eight nearest neighbors, indicates that

- The number of neighbors does not significantly influence the lattice energy.
- The Coulomb energy does not depend on the type of crystal structure.

In Chapter 5 we will see that packing is the most important consideration in determining the structure adopted by predominantly ionically bonded crystals. The difference in \mathcal{A} between some crystal structures is very small. In such cases, for example, the zinc blende and wurtzite structures (named after the two crystalline forms of ZnS), the difference in the resulting electrostatic energy is small. For zinc blende and wurtzite it is $\sim 0.2\%$. When the energy difference between structure types of the same stoichiometry is small, we often encounter polymorphism: the compound can form with more than one structure. We will examine this useful complication in Chapter 7.

Lattice Energy

With knowledge of the Madelung constant we write the total energy for 1 mol of the crystal lattice containing an Avogadro's number (N) of ion pairs:

$$E = -\frac{\mathcal{A}N|Z_M||Z_X|e^2}{(4\pi\epsilon_0 r)} + \frac{NB}{r^n} \quad (4.12)$$

The minimum energy, E_0 , at r_0 is obtained by differentiating Eq. 4.12 with respect to r :

$$\frac{dE}{dr} = 0 = \frac{\mathcal{A}N|Z_M||Z_X|e^2}{(4\pi\epsilon_0 r_0^2)} - \frac{nBN}{r_0^{n+1}}$$

The constant B is then

$$B = \frac{\mathcal{A}N|Z_M||Z_X|e^2 r_0^{n-1}}{4\pi\epsilon_0}$$

Rewriting Eq. 4.12 gives the Born–Landé equation, which is quite successful in predicting accurate values of the lattice energy of an ionic compound:

$$E_0 = -\frac{\mathcal{A}N|Z_M||Z_X|e^2}{4\pi\epsilon_0 r_0} \left(1 - \frac{1}{n}\right) \quad (4.13)$$

It requires only knowledge of the crystal structure (in order to choose \mathcal{A} correctly) and r_0 . Both parameters are readily available from X-ray diffraction data.

As an example of using Eq. 4.13 we will calculate the value of E_0 for MgO. We need to substitute the following values:

$\mathcal{A} = 1.748$ (from Table 4.4)
 $n = 8$ (an average value based on Table 4.3)
 $r_0 = 210$ pm (from X-ray diffraction data)

This gives $E_0 = -4046.8$ kJ/mol.

The terms in Eq. 4.1 are modified in other models since it would be surprising for one value of n to fit all atoms when we have no physical justification for any particular number. For example, the repulsion term may be represented by

$$E_r = be^{-(r/\rho)} \quad (4.14)$$

Where b and ρ are constants determined from compressibility measurements. This gives the Born–Mayer equation (Born and Mayer, 1932) for lattice energy:

$$E_0 = -\frac{\mathcal{A}N|Z_M||Z_X|e^2}{4\pi\epsilon_0r_0}\left(1-\frac{\rho}{r_0}\right) \quad (4.15)$$

The Born–Mayer equation emphasizes the fact that Eq. 4.1 is designed only to match the observed phenomenon. It is not a fundamental “truth” like the Coulomb interaction.

The Born–Haber Cycle

The Born–Haber (Born, 1919; Haber, 1919) cycle shows the relationship between lattice energy and other thermodynamic quantities. It also allows the lattice energy to be calculated. The background of the Born–Haber cycle is Hess’s law, which states that the enthalpy of a reaction is the same whether the reaction proceeds in one or several steps. The Born–Haber cycle for the formation of an ionic compound is shown in Figure 4.6. It is a necessary condition that

$$\Delta H_f = \Delta H_{AM} + \Delta H_{AX} + \Delta H_{IE} + \Delta H_{EA} + E \quad (4.16)$$

or in terms of the lattice energy

$$E = \Delta H_f - \Delta H_{AM} - \Delta H_{AX} - \Delta H_{IE} - \Delta H_{EA} \quad (4.17)$$

ΔH_{AM} and ΔH_{AX} are the enthalpies of atomization of the metal and the nonmetal, respectively.

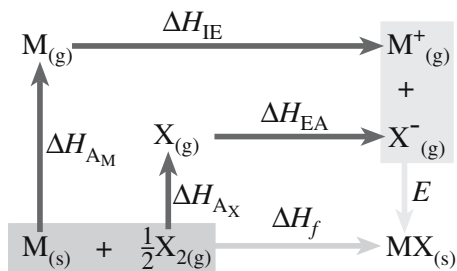


FIGURE 4.6 The Born–Haber cycle.

TABLE 4.5 Lattice Energies of Some Alkali and Alkaline Earth Metal Halides at 0K (kJ/mol)

Compound	Born–Haber cycle	Born–Landé equation
NaF	–910	–904
NaCl	–772	–757
NaBr	–736	–720
NaI	–701	–674
KCl	–704	–690
KI	–646	–623
CsF	–741	–724
CsCl	–652	–623
CsI	–611	–569
MgF ₂	–2922	–2883
CaF ₂	–2597	–2594

For gaseous diatomic molecules ΔH_A is the enthalpy of dissociation (bond energy plus RT) of the diatomic molecule. For metals that vaporize to form monatomic gases ΔH_A is identical to the enthalpy of sublimation. If a diatomic molecule M_2 sublimates, then the dissociation enthalpy of the reaction ($M_2 \rightarrow 2M$) must also be included. As defined earlier, E is the lattice energy of the crystal and represents the heat of formation per mole of a crystal MX from $M^+_{(g)}$ and $X^-_{(g)}$.

As an example of using the Born–Haber cycle we will calculate the lattice energy of MgO . The values of the various thermodynamic parameters can be found in Kubaschewski *et al.* (1993), Johnson (1982), and in the NIST-JANAF tables (Chase, 1998).

For MgO :

ΔH_f	–601.7 kJ/mol
ΔH_{AM}	147.7 kJ/mol
ΔH_{AX}	249 kJ/mol [the actual value for the dissociation enthalpy is 498 kJ/mol, but we need to take half this value because we are considering the reaction $\frac{1}{2}O_2(g) \rightarrow O(g)$]
ΔH_{IE}	2188 kJ/mol
ΔH_{EA}	–638 kJ/mol

By substitution into Eq. 4.17 we get $E = -2548.4$ kJ/mol.

If we compare this value with that calculated using the Born–Landé equation we see that they are quite different. The Born–Haber cycle gives a lattice energy about 60% higher than the Born–Landé value. The reason for this difference is that although we often regard MgO as essentially an ionic ceramic, it does have an appreciable covalent character. If similar calculations, using the Born–Landé equation and the Born–Haber cycle, are performed for $NaCl$ or one of the other alkali halides the values obtained using the two methods agree to within 1% or 2% as shown in Table 4.5. The differences in the above calculations are sometimes used as a means of defining an ionic compound—if the results are similar, it must be ionic. Although this definition is not too useful within the context of ceramics, it does serve as an illustration that the bonding in most ceramics is not simply ionic.

Ionic Radii

We know from quantum mechanics that atoms and ions do not have precisely defined radii. However, the concept of an ion as a hard sphere with a fixed radius is very useful when predicting crystal structures. Experimental evidence shows that such a model has some justification: the model often “works.” Nevertheless, always bear in mind that atoms and ions are not rigid spheres and their size will be affected by their local environment.

We cannot measure ionic radii directly. What we can measure rather easily, and with high accuracy using X-ray crystallography, in most crystals is r_0 .

$$r_0 = r_M + r_X \quad (4.18)$$

r_M is the radius of the cation (usually a metal) and r_X is the radius of the anion.

To obtain ionic radii it is necessary to fix the radius of one of the ions in Eq. 4.18. Historically, the radius of the F^- ion was fixed and the other radii calculated with respect to it (Landé, 1920). Later, Pauling (1960) produced a consistent set of ionic radii that has been used widely for many years.

Many mineralogists use Goldschmidt’s values. The most comprehensive set of ionic radii is that compiled by Shannon and Prewitt (1969) and revised by Shannon (1976). Table 4.6 lists Shannon’s ionic radii. Although there are several different tabulations they are, for the most part, internally consistent. So it is important to use radii from only one data set. Never mix values from different tabulations.

There are several important trends in the sizes of ions:

- The radii of ions within a group in the periodic table increase with increasing Z (this is for main group elements; the transition metals often behave differently).
- The radius of a cation is smaller than the corresponding atom.
- The radius of an anion is larger than the corresponding atom.
- In a particular row of the periodic table the anions are larger than the cations.

Using X-ray methods, it is possible to obtain accurate electron density maps for ionic crystals; NaCl and LiF are shown in Figure 4.7. It has been suggested that the

TABLE 4.6 Ionic Crystal Radii (in pm)

Coordination Number = 6												
Ag ⁺	Al ³⁺	As ⁵⁺	Au ⁺	B ³⁺	Ba ²⁺	Be ²⁺	Bj ³⁺	Bj ⁵⁺	Br ⁻	C ⁴⁺	Ca ²⁺	Cd ²⁺
115	54	46	137	27	135	45	103	76	196	16	100	95
Ce ⁴⁺	Cl ⁻	Co ²⁺	Co ³⁺	Cr ²⁺	Cr ³⁺	Cr ⁴⁺	Cs ⁺	Cu ⁺	Cu ²⁺	Cu ³⁺	Dy ³⁺	Er ³⁺
87	181	75	55	80	62	55	167	77	73	54	91	89
Eu ³⁺	F ⁻	Fe ²⁺	Fe ³⁺	Ga ³⁺	Gd ³⁺	Ge ⁴⁺	Hf ⁴⁺	Hg ²⁺	Ho ³⁺	I ⁻	In ³⁺	K ⁺
95	133	78	65	62	94	53	71	102	90	220	80	138
La ³⁺	Li ⁺	Mg ²⁺	Mn ²⁺	Mn ⁴⁺	Mo ³⁺	Mo ⁴⁺	Mo ⁶⁺	N ⁵⁺	Na ⁺	Nb ⁵⁺	Nd ³⁺	Ni ²⁺
103	76	72	83	53	69	65	59	13	102	64	98	69
Ni ³⁺	O ²⁻	OH ⁻	P ⁵⁺	Pb ²⁺	Pb ⁴⁺	Rb ⁺	Ru ⁴⁺	S ²⁻	S ⁶⁺	Sb ³⁺	Sb ⁵⁺	Sc ³⁺
56	140	137	38	119	78	152	62	184	29	76	60	75
Se ²⁻	Se ⁶⁺	Si ⁴⁺	Sm ³⁺	Sn ⁴⁺	Sr ²⁺	Ta ⁵⁺	Te ²⁻	Te ⁶⁺	Th ⁴⁺	Tj ²⁺	Tj ³⁺	Tj ⁴⁺
198	42	40	96	69	118	64	221	56	94	86	67	61
Tl ⁺	Tl ³⁺	U ⁴⁺	U ⁵⁺	U ⁶⁺	V ²⁺	V ⁵⁺	W ⁴⁺	W ⁶⁺	Y ³⁺	Yb ³⁺	Zn ²⁺	Zr ⁴⁺
150	89	89	76	73	79	54	66	60	90	87	74	72
Coordination Number = 4												
Ag ⁺	Al ³⁺	As ⁵⁺	B ³⁺	Be ²⁺	C ⁴⁺	Cd ²⁺	Co ²⁺	Cr ⁴⁺	Cu ⁺	Cu ²⁺	F ⁻	Fe ²⁺
100	39	34	11	27	15	78	58	41	60	57	131	63
Fe ³⁺	Ga ³⁺	Ge ⁴⁺	Hg ²⁺	In ³⁺	Li ⁺	Mg ²⁺	Mn ²⁺	Mn ⁴⁺	Na ⁺	Nb ⁵⁺	Ni ²⁺	O ²⁻
49	47	39	96	62	59	57	66	39	99	48	55	138
OH ⁻	P ⁵⁺	Pb ²⁺	S ⁶⁺	Se ⁶⁺	Sn ⁴⁺	Si ⁴⁺	Ti ⁴⁺	V ⁵⁺	W ⁶⁺	Zn ²⁺		
135	17	98	12	28	55	26	42	36	42	60		
Coordination Number = 8												
Bj ³⁺	Ce ⁴⁺	Ca ²⁺	Ba ²⁺	Dy ³⁺	Gd ³⁺	Hf ⁴⁺	Ho ³⁺	In ³⁺	Na ⁺	Nd ³⁺	O ²⁻	Pb ²⁺
117	97	112	142	103	105	83	102	92	118	111	142	129
Rb ⁺	Sr ²⁺	Th ⁴⁺	U ⁴⁺	Y ³⁺	Zr ⁴⁺							
161	126	105	100	102	84							
Coordination Number = 12												
Ba ²⁺	Ca ²⁺	La ³⁺	Pb ²⁺	Sr ²⁺								
161	134	136	149	144								

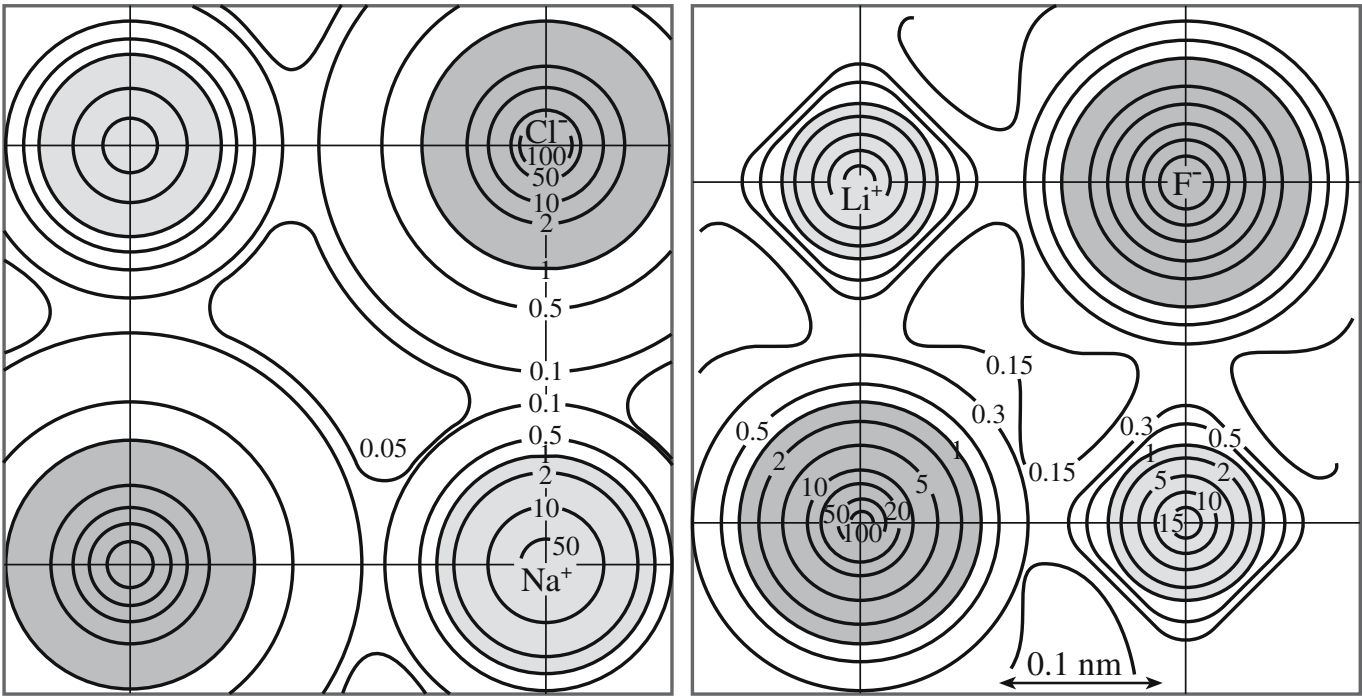


FIGURE 4.7 Electron density maps for (a) NaCl and (b) LiF.

minimum in the electron density contours between the nuclei could be taken as the radius position for each ion. The ionic radii values obtained by this method differ somewhat from those obtained by other methods and tend to make the anions smaller and the cations larger. Notice that the electron density does not go to zero in the region between nuclei even for “ionic” crystals.

4.4 COVALENT BONDING

A pure covalent bond forms when atoms that have the same electronegativity combine; the electrons are shared equally. Such a bond occurs only between identical atoms. Examples of pure covalent bonds are the C—C bond in diamond and the Si—Si bond in silicon. If the atoms have similar electronegativities, then a bond can form that has a large covalent component. The most important such bonds for ceramics are the Si—O bond found in silicates and the Al—O bond in alumina.

The bond-energy curve for a covalent bond has the same general shape as that shown in Figure 4.1a. The main difference is that we do not have the additional energy term associated with the formation of ions. The forces involved are still electrostatic:

- Attractive forces are forces between the electrons of one atom and the nucleus of the neighboring atom.
- Repulsive forces are forces between electrons on neighboring atoms.

Molecular Orbitals

One way to consider covalent bond formation is to look at what happens to the individual atomic orbitals (AOs) on adjacent atoms as they overlap at short distances to form molecular orbitals (MOs). The simplest case is that of two 1s orbitals. At relatively large separations (≥ 1 nm) the electron orbital on one atom is not influenced significantly by the presence of the other atom. As the two atoms approach each other the orbitals overlap and the electron density between the nuclei increases. At r_0 , the individual AOs become a single MO—called a bonding MO—with the electron density concentrated between the nuclei.

A bonding MO can be described as the sum of the wave functions of the contributing AOs:

$$\Psi_{\text{Bond}} = \Psi_A + \Psi_B \quad (4.19)$$

The probability of finding an electron at a given point in the MO is proportional to Ψ_{Bond}^2 :

$$(\Psi_{\text{Bond}})^2 = (\Psi_A + \Psi_B)^2 \quad (4.20)$$

Equation 4.20 is shown as a function of internuclear distance in Figure 4.8.

We can represent an MO pictorially in a manner similar to the way we do for AOs by outlining a shape that encloses most of the electron density and, consequently, is given by the molecular wave function. Figure 4.9 represents the bonding MO formed by the combination of two

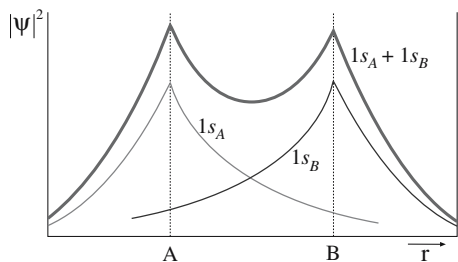


FIGURE 4.8 Distribution showing the probability of finding an electron at a given point in an MO as a function of distance.

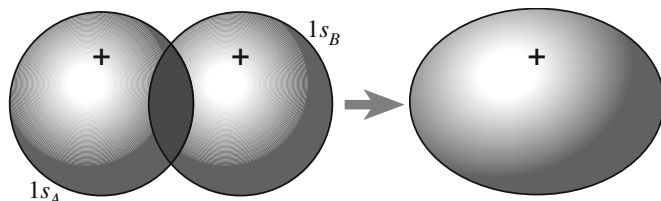


FIGURE 4.9 Pictorial representation of a bonding MO obtained by summing two AOs. In this case the example is H₂.

1s AOs. Because regions of high electron density lie between the atoms, covalent bonds are directional. The directional nature greatly influences the atomic arrangements in covalently bonded solids and their mechanical properties. Diamond, a purely covalently bonded ceramic, is the hardest known material.

We can also form an MO—called an antibonding MO—by subtracting the wave functions of the contributing orbitals:

$$\Psi_* = \Psi_A - \Psi_B \quad (4.21)$$

In the antibonding MO, illustrated in Figure 4.10, the electron density is greatly reduced in the overlap region and is zero midway between the nuclei. The antibonding MO is less stable than the isolated AOs from which it is derived and consequently is higher in energy.

MOs that are symmetrical when rotated around a line joining the nuclei are called sigma (σ) MOs. The bonding

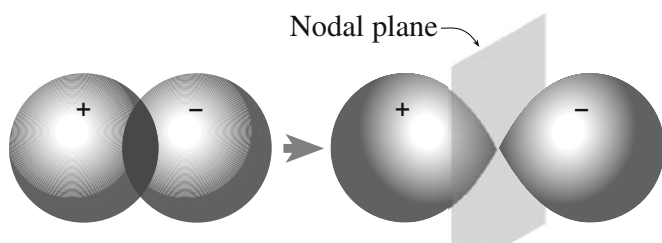


FIGURE 4.10 Pictorial representation of the formation of an antibonding MO. An appropriate example would again be H₂.

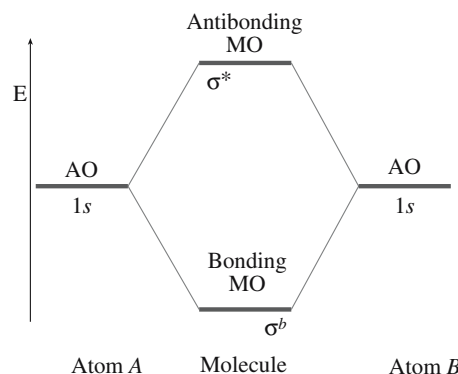


FIGURE 4.11 Energy level diagram for the H₂ MOs and the corresponding AOs.

and antibonding MOs are referred to as σ^b and σ^* , respectively. Figure 4.11 shows the relative energies of these MOs at r_0 . From two 1s AOs, which have the same energy, we can construct two MOs. The bonding MO is lower in energy than the AOs and the antibonding MO is higher in energy.

We can also form MOs from the overlap of p orbitals. There are three p orbitals that are equivalent in shape and volume but point along different coordinate axes. Figure 4.12 shows six different kinds of MO formed from overlap of the p_x , p_y , and p_z orbitals.

On the convention of assigning coordinate axes: The line that connects the nuclei in a diatomic molecule is designated the z-axis and is thus common to both nuclei. The two sets of corresponding x- and y-axes are parallel.

The overlap of the p_z orbitals is qualitatively similar to the overlap of s orbitals and the bonding MO is designated

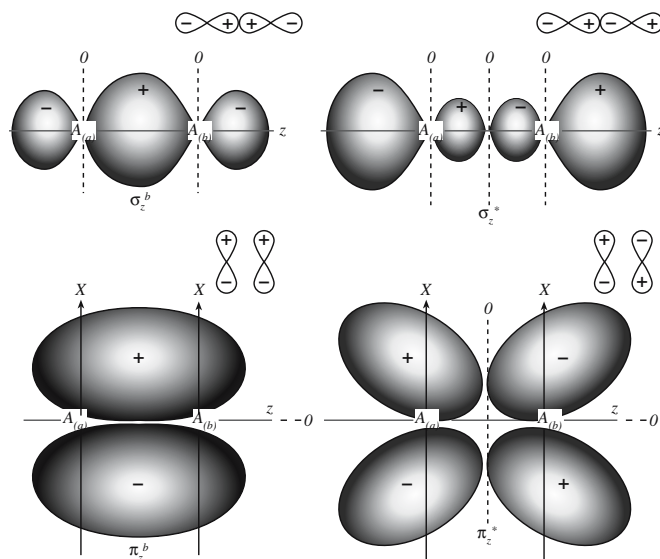


FIGURE 4.12 MOs formed from the p_z (top figure) and p_x (bottom figure) AOs. The original AOs are shown at the upper right of each MO.

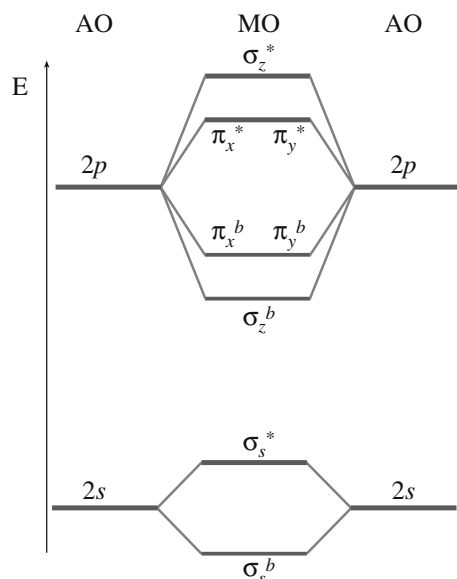


FIGURE 4.13 Energy level diagram for homonuclear diatomic molecule where there is negligible s-p hybridization.

σ_z^b . The two p_x orbitals and the two p_y orbitals do not overlap along the z -axis, rather they overlap above and below it. This type of MO is called a π orbital. The π MOs that concentrate electron density in the region between the two nuclei are known as π bonding MOs. The combination of p_x orbitals produces a bonding MO π_x^b , while the combination of p_y orbitals produces a bonding MO π_y^b . These two MOs have the same shape and energy, but are orthogonal.

Following the convention used for the antibonding σ MOs, the π antibonding MOs are denoted by π_x^* and π_y^* . Assuming no mixing of the s and p orbitals, the relative energies of the MOs are

$$\sigma_s^b < \sigma_s^* < \sigma_z^b < \pi_x^b = \pi_y^b < \pi_x^* = \pi_y^* < \sigma_z^*$$

A diagram of these energy levels is shown in Figure 4.13. It was constructed by allowing only those interactions between those orbitals on atom A and atom B, which have the same energy. Actually interactions can occur between AOs on the *same* atom provided that the energy between the orbitals is not too large. This new arrangement of the electrons is called hybridization.

Hybridization of Atomic Orbitals

In atoms containing AOs that are close in energy different orbitals can mix to give so-called hybrid orbitals. Mixing between $1s$ and $2s$ orbitals will not occur. For example, in Na the energy difference between these orbitals is 9 MJ/mol. The energy difference between the $2s$ and $2p$ orbitals is less and varies with Z . In F, the energy difference between the s and p orbitals is large enough that we

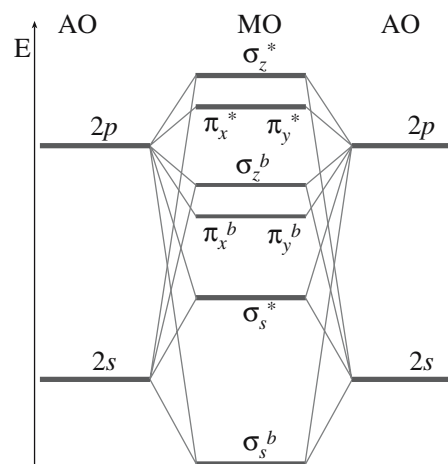


FIGURE 4.14 Energy level diagram for homonuclear diatomic molecule where s-p hybridization has occurred.

neglect mixing. However, in the case of elements to the left of F in the periodic table mixing between the $2s$ and $2p$ AOs is important and results in a change in the order of the levels as shown in Figure 4.14.

An sp hybrid orbital formed from one s orbital and a single p orbital is illustrated in Figure 4.15. A combination

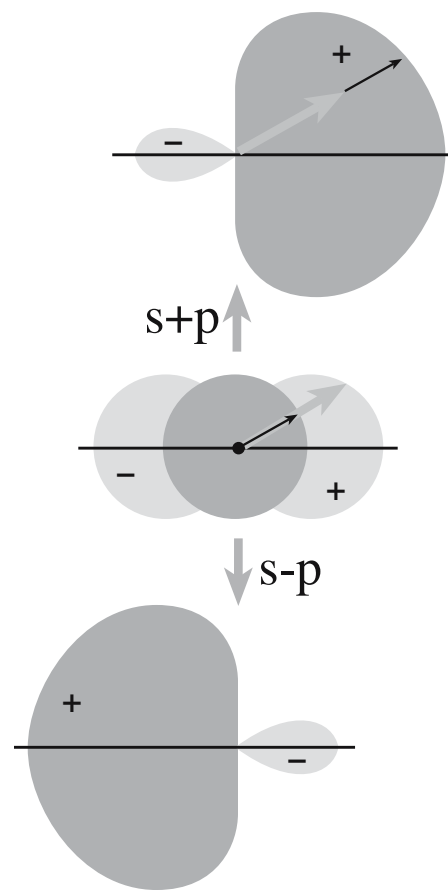


FIGURE 4.15 Two sp hybrid orbitals formed by adding and subtracting the corresponding wave functions.

of s and p orbitals causes reinforcement in the region in which the sign of the wave function is the same and cancellation where the signs are opposite.

We can represent these situations mathematically:

$$\Psi_{sp1} = \Psi_s + \Psi_p \quad (4.22)$$

$$\Psi_{sp2} = \Psi_s - \Psi_p \quad (4.23)$$

where Ψ_s and Ψ_p are the wave functions of an s and p orbital and Ψ_{sp1} and Ψ_{sp2} represent the new sp orbitals. This process is very similar to the formation of MOs. Keep in mind, however, that in the present case we are combining two or more orbitals on the same atom to form a new set of hybrid AOs.

Hybridized Orbitals in Ceramics

A very important example of hybridization occurs between one s orbital and three p orbitals to form sp^3 hybrid orbitals. In carbon, the ground state electron configuration is $1s^2 2s^2 2p_x^1 2p_y^1$; in this state carbon would be divalent because only the unpaired electrons in the p_x and p_y orbitals are available for bonding. To form four bonds, carbon must be raised to its valence state. This requires the promotion of one of the s electrons from the 2s orbital to the formerly empty $2p_z$ orbital. The electron configuration now becomes $1s^2 2s^1 2p_x^1 2p_y^1 2p_z^1$. This promotion costs 406 kJ/mol, but is more than compensated for by the formation of two extra C–C bonds. The C–C bond energy is 348 kJ/mol.

Hybridization between the 2s, $2p_x$, $2p_y$, and $2p_z$ orbitals occurs to form four equivalent sp^3 hybrid orbitals, as shown for carbon in Figure 4.16. Each sp^3 hybrid orbital has 25% s and 75% p character. The four sp^3 orbitals are directed toward the corners of a regular tetrahedron. Thus, in diamond each carbon atom has four localized tetrahedral sp^3 hybrid orbitals. A C–C MO is formed when orbitals from neighboring carbon atoms combine. The angle between three carbon bonds is $109^\circ 28'$. For covalently bonded materials that show tetrahedral coordination, sp^3 hybridization must occur.

Points to Note:

- Promotion of electrons to form an excited state can occur independently of hybridization.
- Hybridization prohibits certain configurations and allows others (C hybridizes sp^3 in diamond and sp^2 in graphite).
- The local atomic order depends upon mutual repulsion of the valence electrons and space requirements.
- The structure a material adopts is the one that has the lowest energy.

In diamond, for each tetrahedral group there are four sp^3 orbitals associated with the central carbon and one

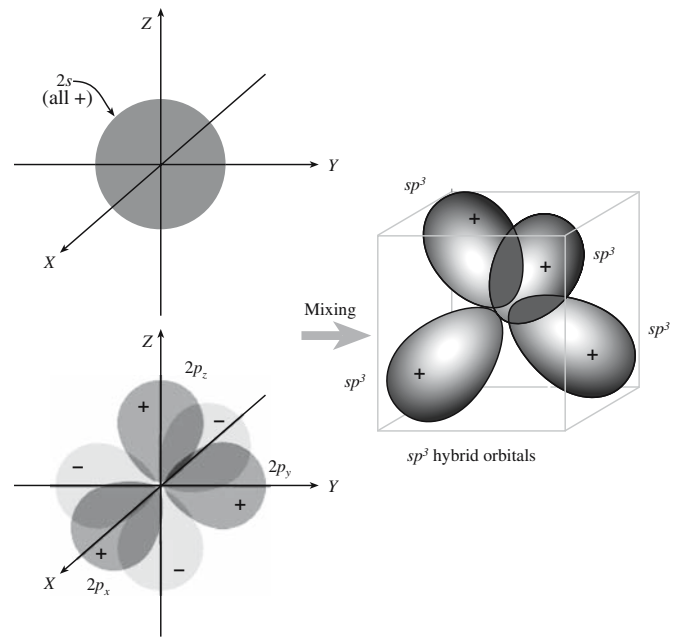


FIGURE 4.16 Formation of sp^3 hybrid orbitals.

from each neighboring carbon, forming four bonds. The four electrons from the central carbon and one from each neighboring carbon are just sufficient to fill the bonding MOs. The four antibonding orbitals are empty. In diamond, the bonding and antibonding MOs are separated by a large energy as shown in Figure 4.17. This energy gap is the reason diamond is an electrical insulator at room temperature. (We will discuss the energy gap again in Section 4.8 and Chapter 30.)

Several other important ceramic materials in which the bonding is predominantly covalent have tetrahedral

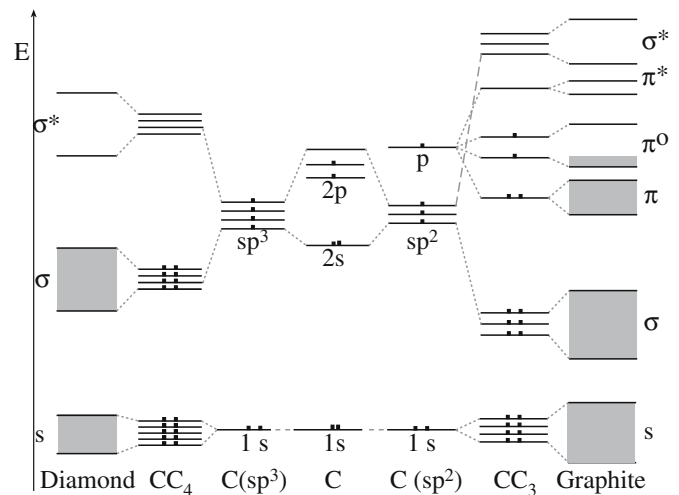


FIGURE 4.17 Energy level diagram for diamond and graphite.

coordination of nearest-neighbor atoms, for example, silicon carbide (SiC) and aluminum nitride (AlN). In these materials sp^3 hybridization has occurred but, because of the different electronegativities of the constituent atoms, the electron density will not be symmetrical in a plane drawn between the atoms. The crystal structure of these materials is described in Chapter 6.

In graphite, the carbon atoms are in a trigonal planar arrangement with each carbon bonded to three nearest neighbors. The carbon is sp^2 hybridized. Hybridization occurs between the C 2s orbital and the $2p_x$ and $2p_y$ orbitals producing three hybrid orbitals lying in a plane at 120° to each other. Overlap of the sp^2 hybrid orbitals to produce localized bonds between carbon atoms results in a hexagonal network.

The strong bonding between carbon atoms causes overlap of adjacent $2p_z$ orbitals, which are aligned perpendicular to the plane of the hybrid orbitals. This overlap is termed π -type overlap. Since the $2p_z$ orbital is half-filled the π band will only be half full as shown in Figure 4.17. This half-filled band is why graphite has a high electrical conductivity.

In hexagonal boron nitride (h-BN), which has a structure similar to graphite, the bonding between the B and N atoms is predominantly covalent and the trigonal planar structure in the layers is a result of sp^2 hybridization of the atomic orbitals of the B and N atoms. The ground state electronic configuration of B is $1s^2 2s^2 2p_x^1$; one 2s electron is promoted to the $2p_y$ orbital giving the electron configuration $1s^2 2s^1 2p_x^1 2p_y^1$. The unfilled 2s and 2p orbitals hybridize to form three equivalent sp^2 hybrid orbitals. Nitrogen has the electronic configuration $1s^2 2s^2 2p_x^1 2p_y^1 2p_z^1$. Promotion of one of the 2s electrons gives the following electron configuration to the atom $1s^2 2s^1 2p_x^1 2p_y^1 2p_z^1$. The three half-filled orbitals combine to give three sp^2 hybrids in the xy plane.

The spatial arrangement of atoms around each N atom is the same as that around each B atom. Structurally there are many similarities between h-BN and graphite and both can be converted under high temperature and pressure into a cubic form. The crystal structures of cubic boron nitride (c-BN) and diamond are similar. However, unlike graphite, h-BN is an electrical insulator. The reason for this difference is that the p_z orbitals in h-BN, which lie perpendicular to the plane of the network, are either empty in the case of B or filled in the case of N. Because the energies of the p orbitals on B and N are quite different, there is little interaction, with no delocalization as was the case in graphite.

- h-BN is a white or colorless insulator.
- Graphite is a shiny black or gray electrical conductor.

Hybridization can also involve d orbitals (for atoms with $Z > 21$). The shapes produced are more complicated than those for hybridization only between s and p orbitals. Table 4.7 lists some hybrid orbitals containing s, p, and d orbitals and these are illustrated in Figure 4.18. Hybridization involving s, p, and d orbitals occurs in MoS_2 . Mo ($Z = 42$) has the electron configuration [Kr] $4d^5 5s^1$. One of the 4d electrons is promoted into the empty p_x orbital to give the following electron configuration: [Kr] $4d^4 5s^1 5p_x^1$. Hybridization occurs to produce d^4sp hybrid orbitals on each Mo atom, resulting in trigonal prismatic coordination with each Mo being surrounded by six sulfur atoms.

For most ceramic materials we will not need to consider hybridization involving d orbitals. However, even when they are not involved in bonding the d orbitals can be extremely important in determining the properties of materials (particularly magnetism).

TABLE 4.7 Orbital Geometries for Hybridization

Number of bonds	Representation	Shape	Example
2	sp	Linear	$BeH_2, HgCl_2$
3	sp^2	Trigonal	$B_2O_3, BN, graphite$
4	$sp^3,$ dsp^2	Tetrahedral Square planar	$SiO_2, diamond$ $AuBr_4$
5	$dsp^3, d^3sp,$ d^2sp^2, d^4s	Trigonal bipyramid Square pyramid	PCl_5 IF_5
6	$d^2sp^3,$ d^4sp	Octahedral Trigonal prism	MoO_3 MoS_6 in MoS_2
8	$d^4sp^3,$ d^5p^3	Dodecahedral Square antiprism	— —

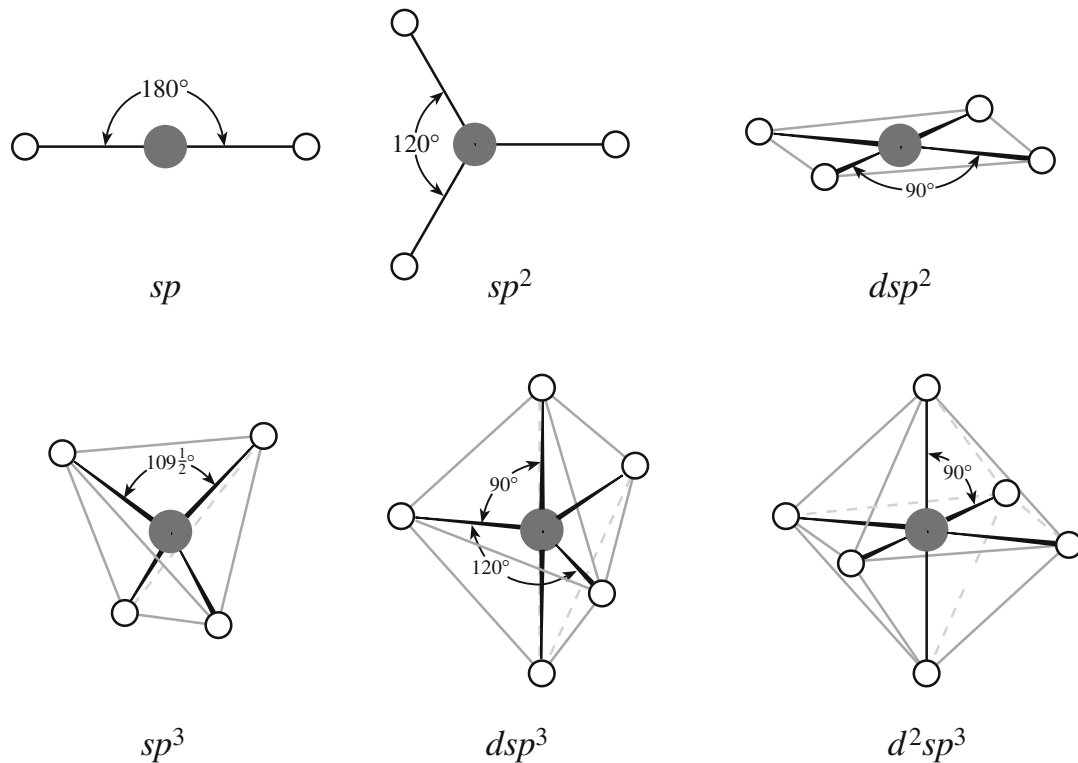


FIGURE 4.18 Geometric arrangements of some hybrid orbitals involving s, p, and d AOs.

4.5 METALLIC BONDING IN CERAMICS

Metallic bonding is the primary bond in metals and can be thought of as an electrostatic interaction between the delocalized valence electrons and the positively charged ion cores. It is the delocalized electron gas that gives rise to many of the characteristic properties of metals such as high electrical and high thermal conductivities. Metallic bonds do not require a balance of the electric charge between the elements; the electrostatic equilibrium is between the metal ions and the electron gas. For this reason different elements can mix in metallic alloys in arbitrary ratios.

Metallic bonding is traditionally neglected because of the definition of a ceramic. However, some compounds that are thought of as ceramics can, under certain conditions, show metallic behavior. Others can even be superconducting. (Superconductivity is a property associated with both metals and ceramics.) So it helps to keep a more open view of ceramics.

In addition to bonds showing mixed covalent and ionic character, the bonding in some ceramics shows partial metallic character. Transition metal carbides (e.g., TiC and Mo₂C) and nitrides (e.g., TiN and NbN) have properties that suggest both metallic and covalent bonding occurs in the crystal.

- TiN is gold in color and is an electrical conductor.
- TiN has a very high melting point (2949°C) and is brittle at 25°C.

The former suggests it is a metal; the latter properties are associated with ceramics. The bonding in transition metal carbides and nitrides is very complex. It consists of a combination of metal-to-metal and metal-to-nonmetal interactions and involves simultaneous contributions of metallic, covalent, and ionic bonding.

The exact details of the bonding mechanisms in these ceramics are still controversial, and several different approaches to explain the wide range of observed properties have been suggested. One common feature to all the proposed mechanisms is that of orbital hybridization. Hybridization of the s, p, and d orbitals of the transition metal as well as hybridization of the s and p orbitals of the nonmetal has been proposed.

The transition metal borides also show characteristics of covalent and metallic materials. The bonding in the borides is also complicated by the fact that there are interactions between the B atoms to form chains, layers, or three-dimensional networks. In the carbides and nitrides there are no C–C or N–N interactions. Despite these complexities we can still use some of the same approaches that we use for simple oxides (Chapter 6) to predict the crystal

structure of these ceramics. The point to remember is that the bonding in ceramics is usually mixed and is occasionally very complex. Many of the new ceramics are interesting because of their special properties and these often occur because the bonding is mixed.

4.6 MIXED BONDING

From the preceding sections it should be clear that in ceramics we do not usually have pure ionic bonds or pure covalent bonds but rather a mixture of two, or more, different types of bonding. Even so it is still often convenient and a frequent practice to call predominantly ionically bonded ceramics “ionic ceramics” and predominantly covalently bonded ceramics “covalent ceramics.”

From the series of electronegativity values we can form some general rules about bonding.

- Two atoms of similar electronegativity will form either a metallic bond or a covalent bond, according to whether they can release or accept electrons, respectively.
- When the electronegativities differ the bond is partially ionic.

The ionic character of a bond increases with the difference in electronegativity of the two atoms as shown by Eq. 4.24:

$$\text{Fraction of ionic character} = 1 - \exp[-0.25 (X_M - X_X)^2] \quad (4.24)$$

X_M and X_X represent the electronegativities of M and X (keeping the cation/anion labeling). Using Eq. 4.26 and electronegativity values in Table 3.6 we can see that B_4C , SiC, and BN are highly covalent (6%, 12%, and 22% ionic character, respectively). Oxides of the alkali metals and alkaline-earth metals are predominantly ionic. The metal–oxygen bond in MgO has 73% ionic character and 82% ionic character in BaO. Some important ceramics fall in between these limits, for example, GaN (38% ionic character), SiO_2 (51% ionic character), ZnO (59% ionic character), and Al_2O_3 (63% ionic character). In bonding that shows mixed ionic-covalent characteristics, the electrons are located closer to the electronegative atom (compare the electron densities around the Li^+ and F^- ions in Figure 4.19).

Since the covalent bond is directional, while the ionic bond is not, the degree of directionality changes with bond character. Such changes can have a marked influence on crystal structure. Both ionic and covalent bonds can be very strong, but since covalent bonds are directional, covalent materials respond differently to deformation. The fraction of covalent character can thus influence the mechanical properties of the ceramic.

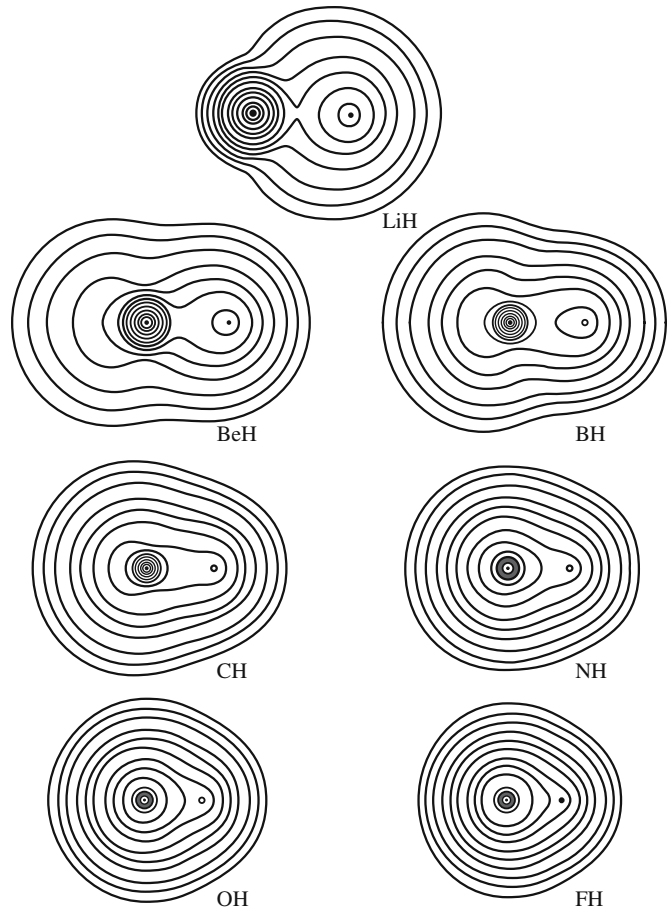


FIGURE 4.19 Contours of constant electron density in the first row hydrides.

4.7 SECONDARY BONDING

Secondary bonds are so called because the compound involved invariably also has ionic or covalent bonding. Secondary bonds are generally much weaker than primary bonds, although they can be critical in determining both the existence of a particular crystal structure and the properties of a material.

van der Waals Bonding

The origin of van der Waals bonding (known also as the London interaction) is weak electrostatic attraction between closely spaced neutral atoms and molecules. The explanation for this universally attractive force is that even a neutral atom has a charge distribution that fluctuates very rapidly. When two atoms are brought together the fluctuations in one can induce a field around the other and this coupling results in the attractive force. Although van der Waals bonding is present in all crystalline solids it is important only when not overwhelmed by strong bonding forces.

The energy of a crystal bound by van der Waals forces can be expressed by the Lennard–Jones potential with two constants, A_{LJ} and B_{LJ}

$$E = -\frac{A_{LJ}}{r^6} + \frac{B_{LJ}}{r^{12}} \quad (4.25)$$

Again, the potential is empirical: it provides a good fit to the experimental data. Both the repulsive and attractive terms decrease rapidly with increasing r . The attractive van der Waals forces are proportional to $1/r^7$ and are, therefore, of much shorter range than the ionic (Coulombic) forces, which are proportional to $1/r^2$.

In ceramics, van der Waals bonding is important in layered structures. In pyrophyllite, a layered silicate, van der Waals bonds between the oxygen ions in adjacent layers allow easy slip parallel to the layers. In the mineral talc, van der Waals bonds between the layers are even weaker than in pyrophyllite. You can cleave talc with your fingernail.

In graphite and hexagonal boron nitride there is strong covalent bonding within each layer. Between the layers the bonding is van der Waals. These materials show highly anisotropic properties, for example, in their mechanical strength. Little effort is required to separate the sheets, but much more effort is required to break them.

MoS₂ has a structure built of MoS₆ units where each Mo is surrounded by six S atoms. The layers are joined by van der Waals bonds between the S atoms and can slip

over one another easily so that MoS₂ has mechanical properties that are similar to those of graphite.

Hamaker Constant

van der Waals interactions are just as important at the macroscopic level, where they can influence behavior such as wetting and fracture, as they are at the atomic and molecular level. The interaction energies between different macroscopic geometries can be described in terms of the Hamaker constant, \mathcal{A} as shown in Figure 4.20.

$$\mathcal{A} = \pi^2 A_{LJ} \rho_1 \rho_2 \quad (4.26)$$

where A_{LJ} is the coefficient in Eq. 4.25 and ρ_1 and ρ_2 are the number of atoms per unit volume in the two bodies. Typical values for Hamaker constants are about 10^{-19} J for interactions

across vacuum (or air); values for some ceramics are listed in Table 4.8. We can use these values to estimate the strength of the van der Waals interactions between, for example, two spherical particles using the equations in Figure 4.20. Remember that the forces are obtained by differentiating the energies with respect to distance.

TYPICAL VALUES IN CALCULATING \mathcal{A}

$A_{LJ} \sim 10^{-77} \text{ J m}^6$
 $\rho \sim 3 \times 10^{28} \text{ m}^{-3}$ (for $r \sim 0.2 \text{ nm}$)

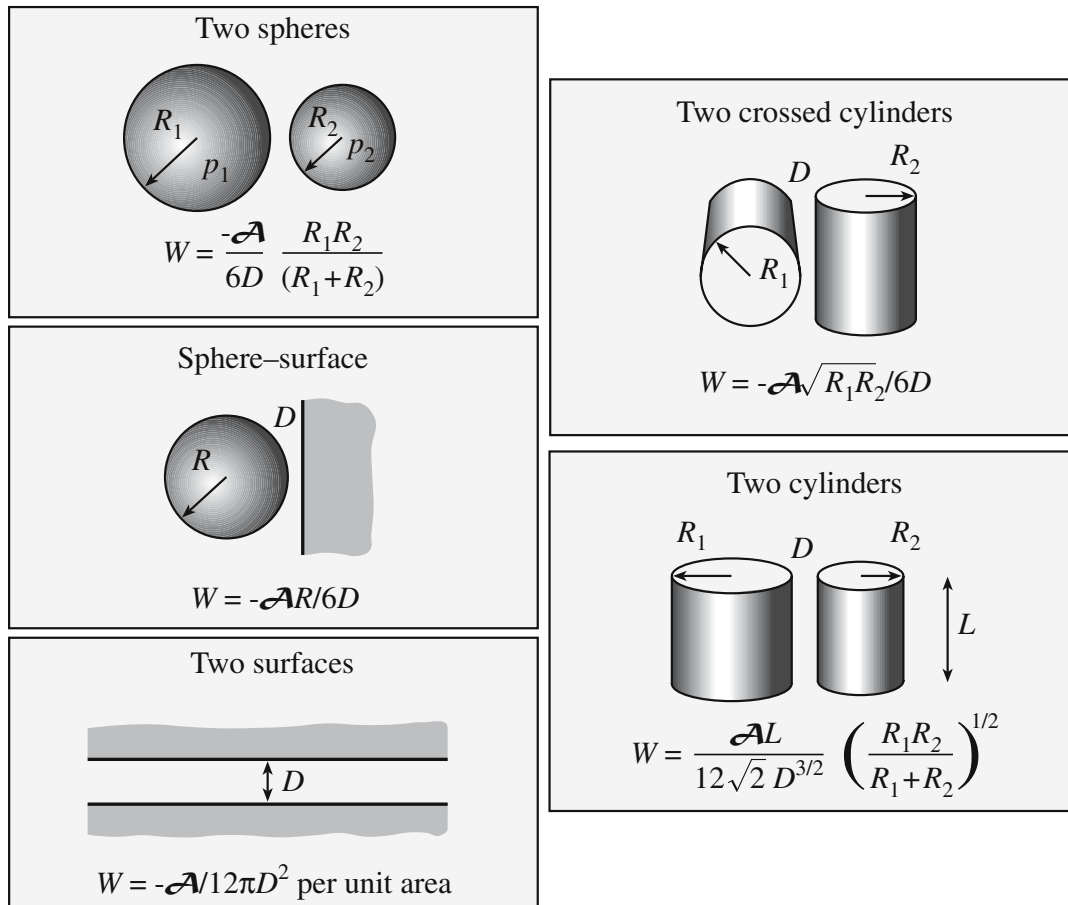


FIGURE 4.20 Interaction energies for macroscopic geometries. The key is the Hamaker constant, \mathcal{A} .

TABLE 4.8 Hamaker Constant

Material	\mathcal{A} (zJ)
Al ₂ O ₃	140
Fe ₃ O ₄	210
ZrO ₂	270
TiO ₂	430
SiC	440
Fused quartz	63
Mica	100
CaF ₂	70

TABLE 4.9 Hamaker Constants for Fused Quartz Interacting with Air across Another Medium

Medium	\mathcal{A} (zJ)
Water	-8.7
Octane	-7
Tetradecane	-4

Things, as you might expect, are actually a little more complicated than Eq. 4.26 implies. We need, as in the calculation of the Madelung constant, to consider the influence of neighboring atoms on the interaction between any pair of atoms. An alternative method developed by Lifshitz (1956) for determining \mathcal{A} uses bulk properties of a material such as dielectric constants and refractive indices. The values given in Table 4.8 were calculated using this approach. In general, materials with high dielectric constants and refractive indices have higher values of \mathcal{A} . If the interactions occur across a medium then the value and sign of \mathcal{A} may change as shown in Table 4.9.

Hydrogen Bonding

Hydrogen bonds are usually stronger than van der Waals bonds but still considerably weaker than primary bonds. Hydrogen bonds occur when a hydrogen atom that is in an ordinary covalent bond joins another, usually highly electronegative atom. The classic example in which such bonds are important is, of course, water. The H–O bonds in the H₂O molecule are fully saturated, yet the bonds between the molecules can be so strong that ice forms with a well-defined crystal lattice.

In kaolinite, hydrogen bonds can form between basal oxygen atoms of one plane and the upper hydroxyl groups of the next. The weak hydrogen bonding between each octahedral–tetrahedral double layer makes the materials very anisotropic. Layers easily slip over one another giving the material a greasy feel and making it excellent for molding, particularly when water is present.

4.8 ELECTRON ENERGY BANDS IN CERAMICS

The energy levels for electrons in a single isolated atom are highly discrete and given by Box 3.6 in Chapter 3. When a number of atoms are brought together to form a solid the Pauli exclusion principle does not allow any two electrons to have the same set of four quantum numbers. The energies that were identical in the isolated atoms shift relative to one another in the formation of a molecule and subsequently a solid. The sharply defined electronic energy levels broaden into an allowed band of energies when a large number of atoms are brought together to form a solid. We illustrated how this happens in diamond and graphite in Figure 4.17.

If we think of a solid as just a very large molecule then we can view the formation of electron energy bands as arising from a combination of a large number of MOs. As the molecule becomes larger, the number of MOs increases and they become more closely spaced in energy. In a solid the number of MOs is so large that we can regard them simply as a continuous band of energy levels.

If we consider the case of diamond, the highest occupied band, referred to by chemists as the highest occupied molecular orbital (HOMO), is σ^b . The lowest unoccupied band, referred to as the lowest unoccupied molecular orbital (LUMO), is the σ^* . Although the bands themselves are important, the most significant aspect of these diagrams is the energy gap between bands. Knowledge of the band gap energy, which is related to chemical bonding, will allow us to draw important conclusions about the electrical conductivity of a material.

The effect of distance on the formation of energy bands is illustrated in Figure 4.21. The closer the atoms are together the more marked is the shift in available energy states. The higher energy states broaden first. Broadening of the lower energy states, which are closer to the nucleus, is less marked.

In materials science we usually define the highest filled electron energy band when the material is in its ground state as the valence band. The lowest energy band containing unoccupied states when the material is in its ground state is the conduction band. At absolute zero the electrons occupy the lowest available energy states; the energy of the highest occupied state is the Fermi energy,

E_F . This energy level separates the occupied from the unoccupied electron levels only when the electron configuration is in its ground state (i.e., at 0 K).

A solid behaves as an insulator if the allowed energy bands are either filled or empty, for then no electrons can move in an

DENSITY OF STATES

$$N(E) = \frac{\pi}{4} \left(\frac{8m}{h^2} \right)^{\frac{3}{2}} E^{\frac{1}{2}}$$

Fermi–Dirac distribution:

$$P(E) = \frac{1}{\exp[(E - E_F)/kT] + 1}$$

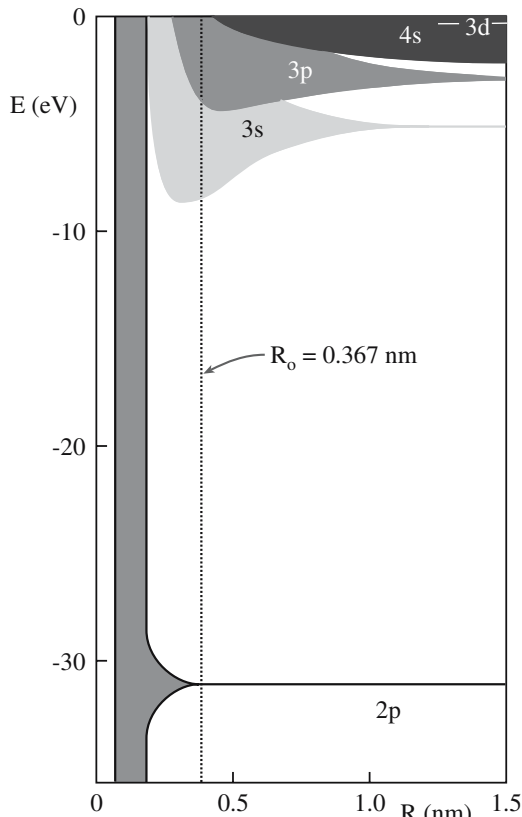


FIGURE 4.21 Formation of electron “bands” as the interatomic spacing is reduced.

electric field. Metals always have a partially filled valence band; the Fermi energy is in the middle of the band and this makes the metals electrical conductors. In semiconductors and insulators we always have completely filled or completely empty electron bands; the Fermi energy lies between the bands, and consequently they are not good electrical conductors at ambient temperatures.

Classically, the valence and conduction bands in ceramics are well separated, so they are insulators. In perfect insulators the gap between bands is so large that thermal excitation is insufficient to change the electron energy states, and at all temperatures the conduction band contains essentially zero electrons and the next lower band of energy is completely full, with no vacant states.

In models of electrons in solids we usually introduce two functions:

- Density of states, $N(E)$, defines the number of energy states available to electrons. There are no available energy states in the band gap and so $N(E)$ is zero in this region.
- Fermi function, $P(E)$, defines the probability of finding an electron at a particular energy state.

These functions are shown graphically in Figure 4.22 together with the electron distribution function $F(E)$:

$$F(E) = 2N(E)P(E) \quad (4.27)$$

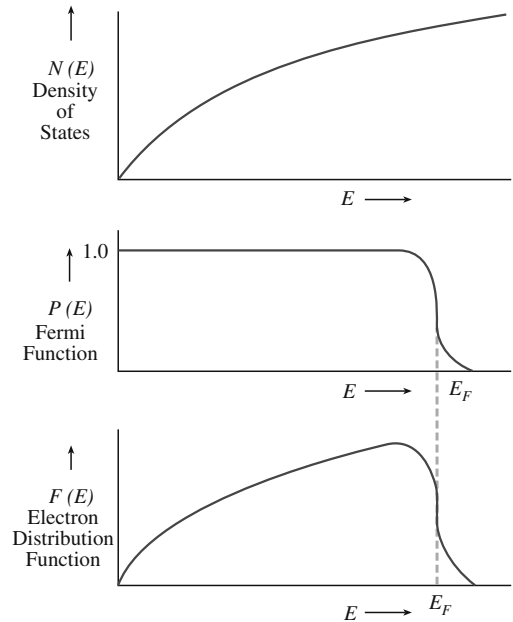


FIGURE 4.22 Electron distribution functions.

In this book we will primarily represent the energy levels of a solid as the familiar and simple block diagrams showing the band gaps. This approach is straightforward, but the question that is often asked is what are we plotting on the x -axis? A more satisfactory form is illustrated in Figure 4.23 where we plot the density of states versus energy. Either description allows the prediction of the electrical properties of a material based on the size of E_g . So we can determine whether a material will behave as a conductor or an insulator.

It is possible to convert an insulator to a metal under very high pressures as a result of the broadening of the energy bands that occurs when the atomic cores are moved closer together as shown in Figure 4.24. If we assume that the Fermi level does not change, then the material will undergo a transition from insulator to metal at the point at which the valence and conduction bands begin to overlap. Very high pressures are required to cause this type of transition. For example, germanium is usually a

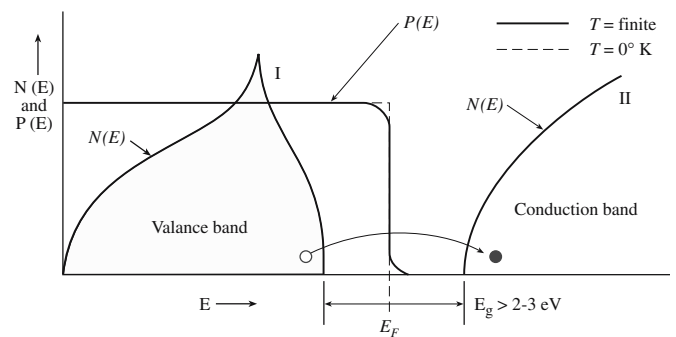


FIGURE 4.23 Plot of the density of states function and Fermi function versus energy.

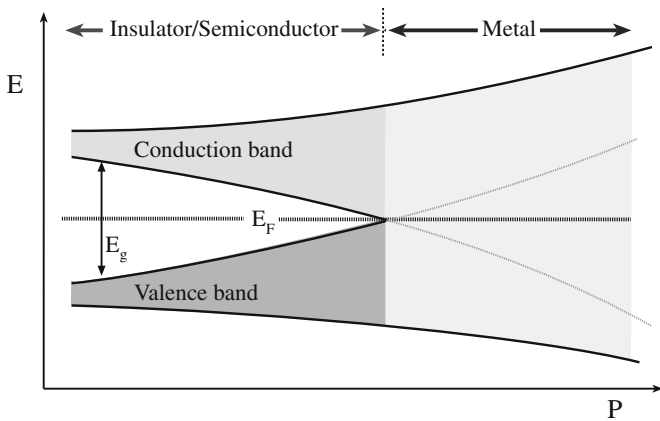


FIGURE 4.24 Plot of energy versus pressure illustrating how an insulator-to-metal transition can occur at high pressures.

TABLE 4.10 Critical Pressure for Metal–Insulator Transformation at 300K

Material	P (GPa)
C	168
BN	211
SiC	64
AlN	90
GaN	87

semiconductor with a band gap of 0.7 eV. It becomes a metal under a pressure of 12 GPa. Examples of critical pressures for insulator–metal transitions at 300 K in some ceramics are given in Table 4.10.

To understand some of the optical properties of ceramics and why certain materials may be favored for solar cell or laser applications, we need to know whether the band gap is direct or indirect. The two situations are illustrated in Figure 4.25. The electrons in a band have both energy and momentum (they are not bound) expressed as a wave vector, \mathbf{k} , with units of reciprocal length (usually cm^{-1}). Energy diagrams can be plotted for different wave vectors.

In direct band gap materials the top of the valence band and the bottom of the conduction band are located at the same point in \mathbf{k} space. This is not the case for an

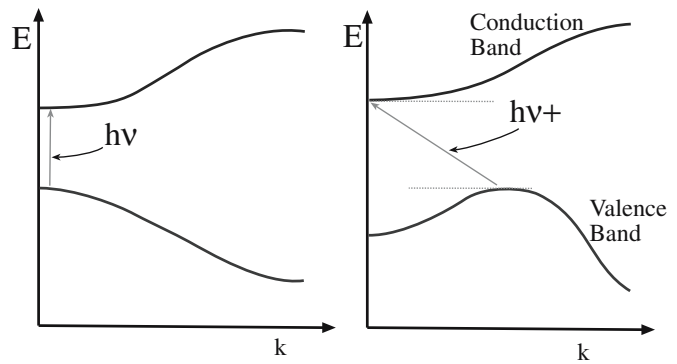


FIGURE 4.25 Illustration of direct and indirect band gap transitions. Energy is plotted versus wave vector.

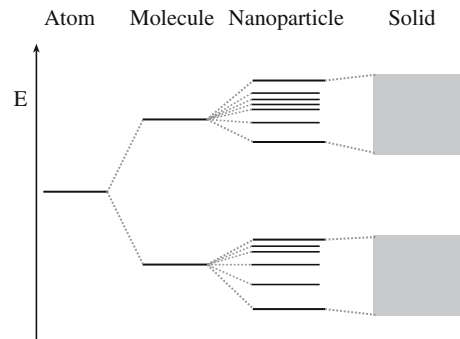


FIGURE 4.26 Illustration of how the energy band gap arises in a nanoparticle.

indirect band gap. It is direct band gap materials that are of most interest for optoelectronic applications.

The probability of electronic transitions across the band gap is higher in materials with a direct band gap and this results in higher efficiency in devices such as lasers and LEDs.

Before we leave this chapter a word must be given about nanomaterials. The value of E_g for nano-sized crystals is often significantly larger than for the bulk form of the material. This is associated with how the bands broaden as the number of atoms in the solid increases as illustrated in Figure 4.26.

As an example, bulk silicon has $E_g = 1.1$ eV. For nanocrystalline silicon E_g varies with the size of the crystals and for sizes less than 2 nm $E_g > 2$ eV.

CHAPTER SUMMARY

This chapter was a review of things that you already knew. There are three types of primary bonds that are used to hold atoms together. In introductory materials science classes we tend to think of each type of bond as being a distinct form, with materials adopting one type or another. At a qualitative level this approach might work, and in the cases of many metals, semiconductors, and polymers it is usually quite close to the actual situation we encounter. However, in ceramics almost every bond has a mixture of covalent, ionic, and, in some cases, metallic character. The type of interatomic bond affects the crystal structure that a material adopts. The influence of mixed bonding can mean that the type of structure predicted, based

on either purely ionic or purely covalent bonding, is incorrect. The role of hybridization, or mixing, of atomic orbitals is very important in ceramics, which are predominantly covalently bonded. For example, the tetrahedral coordination of carbon atoms in diamond requires the sp^3 hybridization.

We discussed the concept of energy bands here, both in terms of the broadening of electron energy states and also from the MO approach. Knowledge of electron energy band diagrams is essential in understanding the electrical properties of materials. The most important feature of the energy band diagram is the band gap. There are no available states in this region.

Secondary bonding is also important in many ceramics. The most familiar properties of graphite, hexagonal-BN, and clay minerals are determined by the presence of weak secondary bonds.

PEOPLE IN HISTORY

Born, Max was born in Breslau in 1882. He graduated from the University of Göttingen in 1907 where he worked on the stability of elastic wires and tapes. During the World War I he had to join the German Armed Forces where in a scientific office he worked on the theory of sound ranging. After the war he was appointed Professor at the University of Frankfurt-on-Main. In 1933 he was forced to emigrate from Germany and came first to Cambridge University in England, then to the Indian Institute of Science in Bangalore, and finally to the University of Edinburgh in Scotland, where he worked until his retirement in 1953. He won the 1954 Nobel Prize in Physics and died in 1970.

Haber, Fritz was born in Breslau, Germany in 1868. He completed his studies at the University of Heidelberg, the University of Berlin, and the Technical School at Charlottenberg. The Haber process for the synthesis of ammonia was patented in 1908 and by 1914 the process was into quantity production. Ammonia was important in Germany's war efforts as a source of nitric acid, which is essential for the manufacture of explosives. It is clear that this prolonged the war. Haber was given the 1918 Nobel Prize in Chemistry (actually awarded in 1919) for his work on nitrogen fixation. In 1933 Haber resigned from his post as Director of the Institute for Physical and Electrochemistry at Berlin-Dahlem. He died in exile in Switzerland in 1934.

Madelung, Erwin was born in 1881 in Bonn, Germany. From 1921 to 1949 he was Professor of Theoretical Physics at Frankfurt University. He died in 1972.

van der Waals, Johannes Diderik was a Dutch physicist, born in Leyde in 1837; he died in Amsterdam in 1923. He was awarded the Nobel Prize for physics in 1910 for his work on the equation of state for gases and liquids.

Young, Thomas was born in 1773. His accomplishments include his introduction of the Modulus of Elasticity. He is best known for his work in optics. He died in 1829.

GENERAL REFERENCES

Huheey, J.E. (1993) *Inorganic Chemistry: Principles of Structure and Reactivity*, 4th edition, Harper & Row, London. If the different interactions are not familiar to you from introductory chemistry or materials science classes, this text covers the material in some detail.

Kittel, C. (2004) *Introduction to Solid State Physics*, 8th edition, Wiley, New York. A more rigorous and mathematical treatment of energy bands than we give in this chapter.

Pauling, L. (1960) *The Nature of the Chemical Bond*, Cornell University Press, Ithaca, NY. Often referenced and well worth seeing.

SPECIFIC REFERENCES

Born, M. (1919) "A thermo-chemical application of the lattice theory," *Verhandl. Deut. Phys. Ges.* **21**, 13.

Born, M. and Mayer, J.E. (1932) "Lattice theory of ionic crystals," *Z. Phys.* **75**, 1.

Chase, M.W., Jr. (1998) *NIST-JANAF Thermochemical Tables*, 4th edition, American Chemical Society, Washington D.C.; American Institute of Physics for the National Institute of Standards and Technology, New York.

Haber, F. (1919) "Theory of the heat of reaction," *Verhandl. Deut. Phys. Ges.* **21**, 750.

Hamaker, H.C. (1937) "London-van der Waals attraction between spherical particles," *Physica* **4**, 1058. The original.

Johnson, D.A. (1982) *Some Thermodynamic Aspects of Inorganic Chemistry*, 2nd edition, Cambridge University Press, Cambridge, UK.

Kubaschewski, O., Alcock, C.B., and Spencer, P.J. (1993) *Materials Thermochemistry*, 6th edition, Elsevier, Oxford, UK.

Lande, A. (1920) "Size of atoms," *Z. Phys.* **1**, 191.

- Lifshitz, E.M. (1956) "The theory of molecular attractive forces between solids," *Soviet Phys. JETP-USSR* **2**, 73.
- Madelung, E. (1918) "The electric field in systems of regularly arranged point charges," *Phys. Z.* **19**, 524.
- Shannon, R.D. and Prewitt, C.T. (1969) "Effective ionic radii in oxides and fluorides," *Acta Crystallogr* **B25**, 925. Gives the alternatives to Pauling's radii.
- Shannon, R.D. (1976) "Revised effective ionic radii and systematic studies of interatomic distances in halides and chalcogenides," *Acta Crystallogr.* **A32**, 751.
- van Vechten, J.A. (1973) "Quantum dielectric theory of electronegativity in covalent systems. III. Pressure-temperature phase diagrams, heats of mixing, and distribution coefficients," *Phys. Rev.* **B7**, 1479.

WWW

http://www.lrsm.upenn.edu/~frenchrh/hamaker_software.htm. Roger French's site for calculating the Hamaker constant.

www.deconvolution.com/Overview/170.htm. More on Hamaker.

EXERCISES

- 4.1 By considering the hybridization of orbitals in diamond explain why it is (a) an electrical insulator at room temperature and (b) extremely hard.
- 4.2 Why are covalently bonded materials in general less dense than metallically or ionically bonded ones?
- 4.3 Calculate the force of attraction between a Na^+ and a Cl^- ion the centers of which are separated by 1.5 nm.
- 4.4 Calculate Born–Landé lattice energies of the following compounds: NaCl, KCl, and CsCl. Compare the values you obtain to those given in Table 4.5 and discuss any differences.
- 4.5 Sketch bond-energy curves for two ceramics, one with a high Young's modulus and one with a low Young's modulus.
- 4.6 Rank the following ceramics in terms of increasing fraction of ionic character in their bonds: SiC, AlN, Si_3N_4 , B_4C , GaN, Al_2O_3 , and SiO_2 .
- 4.7 Sketch a bond-energy curve for two atoms held together by van der Waals forces. Describe how this curve differs from the one shown in Figure 4.1, which is for ionic bonding.
- 4.8 What do we mean by the term "insulator–metal transition." Are there any practical applications for such a transition?
- 4.9 Estimate the force of adhesion between two spherical Al_2O_3 particles of radius 1 μm separated by a distance of 10 nm. How does the force change as the separation increases?
- 4.10 Estimate the surface energy of Al_2O_3 . Assume that for two surfaces in contact $D \sim 0.2$ nm.

5

Models, Crystals, and Chemistry

CHAPTER PREVIEW

Most ceramics are crystalline. The exception is glass, which we usually discuss separately. Not only do the properties of ceramic crystals depend on how the atoms or ions are arranged, but the type and nature of defects also depend on crystal structure. You probably first encountered crystallography when discussing metals. Sixty-five (almost 90%) of the metallic elements are either cubic or hexagonal. In ceramics, many of the most important materials are neither cubic nor hexagonal, so we need to be more familiar with the rest of the subject. It is recommended that you memorize the main structures described in Chapters 6 and 7. In this chapter we provide the means to make this study more systematic.

To understand why ceramics have particular structures and why certain defects form in these structures, it is really important to understand Pauling's rules. These rules require you to visualize a tetrahedron and an octahedron and to see how they fit together. To understand properties such as piezoelectricity or the mechanisms of phase transformations, you must be able to visualize the crystal structure of the material. This is particularly important when we want to predict the properties of single crystals. We summarize the features of crystallography that we use throughout the text and give references to more specialized resources for rigorous proof of theorems and more detailed discussion.

An important point to keep in mind is that the term "ceramic" generally refers to materials that have been processed in the laboratory or the factory plant but that often do exist in nature. Sometimes the natural minerals are rare such as moissanite, which is now being manufactured as a gemstone. There are far more materials and structures in nature than are used in technology. Understanding the basic principles and knowing where to learn more about minerals may help you find the next monazite or at least to know why it might be useful. A great source for further reading lies in the mineralogical literature.

5.1 TERMS AND DEFINITIONS

We will begin by defining the vocabulary of the subject. Most of this section should be familiar to you from other courses.

Crystal Lattice: A three-dimensional array of points related by translational symmetry. The translation can occur in three independent directions giving three independent base vectors. We can fully describe such a lattice by three vectors, **a**, **b**, **c**, and three angles, α , β , γ . The special property of a crystal lattice is that the lattice points are identical: if we have an atom at or near one point, there must be an identical atom at the same position relative to every other lattice point.

Unit Cell: The vectors **a**, **b**, **c** define a cell. There is, in principle, an infinite number of ways to define a unit cell in any crystal lattice. But, as in many areas of crystallography, there is a convention:

1. The unit cell should have the same symmetry as the crystal—the base vectors are parallel to symmetry axes or perpendicular to symmetry planes.
2. The origin of the unit cell is usually a center of symmetry.
3. The base vectors should be as short as possible and the cell volume should be as small as possible. The exceptions arise when choosing a longer vector and a larger cell makes the symmetry more obvious.
4. The angles between the axes should be as close as possible to 90° , or if not then $>90^\circ$.
5. A unit cell having the smallest possible volume is called a primitive cell.

Lattice Parameters: The vectors **a**, **b**, **c** and the angles α , β , γ are called the lattice parameters of the unit cell. Tabulated lattice parameters are, unless otherwise stated, values at room temperature and pressure. They vary with changes in temperature or pressure.

Crystal System: There are seven unique shapes that can each be used to fill three-dimensional space.

These are the seven crystal systems into which all crystals are classified. They are listed in order of increasing symmetry in Table 5.1.

Bravais Lattices: There are 14 different ways to arrange lattice points. These are constructed as three separate types:

- Primitive (P) lattices—one lattice point per unit cell
- Body-centered (I) lattices—a lattice point at the corners and one in the center of the cell
- A-, B-, C-, or F-centered lattices—a lattice point at the corners and others at one (A, B, C) or all three (F) of the faces

The 14 Bravais lattices are shown in Figure 5.1. For reasons of symmetry (Rule 1 above) we do not always choose a primitive cell. The face-centered cubic cell may be referred to the rhombohedral cell (which is primitive), but the cubic cell reflects the higher symmetry of the lattice.

Lattice Points Per Cell: Primitive cells have only one lattice point per cell whereas nonprimitive cells have more than one. A lattice point in the interior of a cell (N_i) can be thought of as belonging entirely to that cell; one in a cell face (N_f) is shared by two cells and a corner one (N_c) is shared by eight. The number of lattice points (N) per cell is given by

CRYSTAL SYSTEMS
All crystals belong to one of the seven crystal systems.

$$N = N_i + \frac{N_f}{2} + \frac{N_c}{8} \quad (5.1)$$

Basis: Group of atoms associated with each and every lattice point. We can describe crystal structures in terms of a Bravais lattice and a Basis:

$$\text{Bravais Lattice} + \text{Basis} = \text{Crystal Structure} \quad (5.2)$$

This approach is often used by solid-state physicists and is particularly useful when we want to determine the structure factor of a crystal. Crystal structures are formed by placing a basis of atoms either on the points of a Bravais lattice or in some fixed relation to those points. There may be no atoms actually located on the lattice points.

Coordination Number (CN): Number of nearest neighbors.

Symmetry Elements: These symmetry elements are easy to understand because you can see them by handling real crystals or crystal shapes. For example, crystals of MgO are cubic and calcite (CaCO_3) is trigonal as shown in Figure 5.2. They apply to macroscopic shapes, but we limit our choice by ignoring those in which the shape could not correspond to the unit cell of a crystal.

- *Rotation Axis.* Clockwise rotation of $360^\circ/n$ about the axis. Crystals may have 2-fold (diad), 3-fold (triad), 4-fold (tetrad), or 6-fold (hexad) rotation axes; the 1-fold axis is always present. Any other rotation, such as a 5-fold axis, is not consistent with the requirement that a crystal lattice must have translational symmetry.
- *Mirror Plane.* When a plane can be chosen such that all features on one side of the plane appear, as if in a mirror, on the other side of the plane, then the crystal has a mirror plane (also known as a plane of symmetry). We call this an m plane.
- *Center of Symmetry.* If every feature in or on the object can be joined by an imaginary line through the center of the object to an identical feature, then we say the object has a center of symmetry.
- *Inversion Axis.* If when any point is rotated about an axis and then moved through the center of symmetry it arrives at an identical point, then the object has an inversion axis.

We refer to such axes as $\bar{1}$, $\bar{2}$, $\bar{3}$, $\bar{4}$, or $\bar{6}$ axes. Notice that the $\bar{1}$ axis is, in fact, describing a center of symmetry. The $\bar{2}$ axis is an alternative description of an m plane.

There are other symmetry elements such as screw axes that are meaningful for crystals but not for our macroscopic crystal shapes. Figure 5.3 illustrates some of the symmetry elements for a cube. The most important are the four 3-fold axes along the $\langle 111 \rangle$ diagonals.

TABLE 5.1 The Seven Crystal Systems

System	Relationship between lattice parameters	Example
Triclinic	$a \neq b \neq c$ $\alpha \neq \beta \neq \gamma \neq 90^\circ$	Turquoise Kyanite Albite feldspar
Monoclinic	$a \neq b \neq c$ $\alpha = \gamma = 90^\circ; \beta \neq 90^\circ$	Monazite Titanite Orthoclase
Orthorhombic	$a \neq b \neq c$ $\alpha = \beta = \gamma = 90^\circ$	Olivine Brookite Stibnite
Tetragonal	$a = b \neq c$ $\alpha = \beta = \gamma = 90^\circ$	Zircon Rutile Hausmannite
Hexagonal	$a = b \neq c$ $\alpha = \beta = 90^\circ; \gamma = 120^\circ$	High quartz Wurtzite Beryl
Rhombohedral (or Trigonal)	$a = b = c$ $\alpha = \beta = \gamma \neq 90^\circ$	Ilmenite Calcite Corundum
Cubic	$a = b = c$ $\alpha = \beta = \gamma = 90^\circ$	Halite Magnetite Garnet

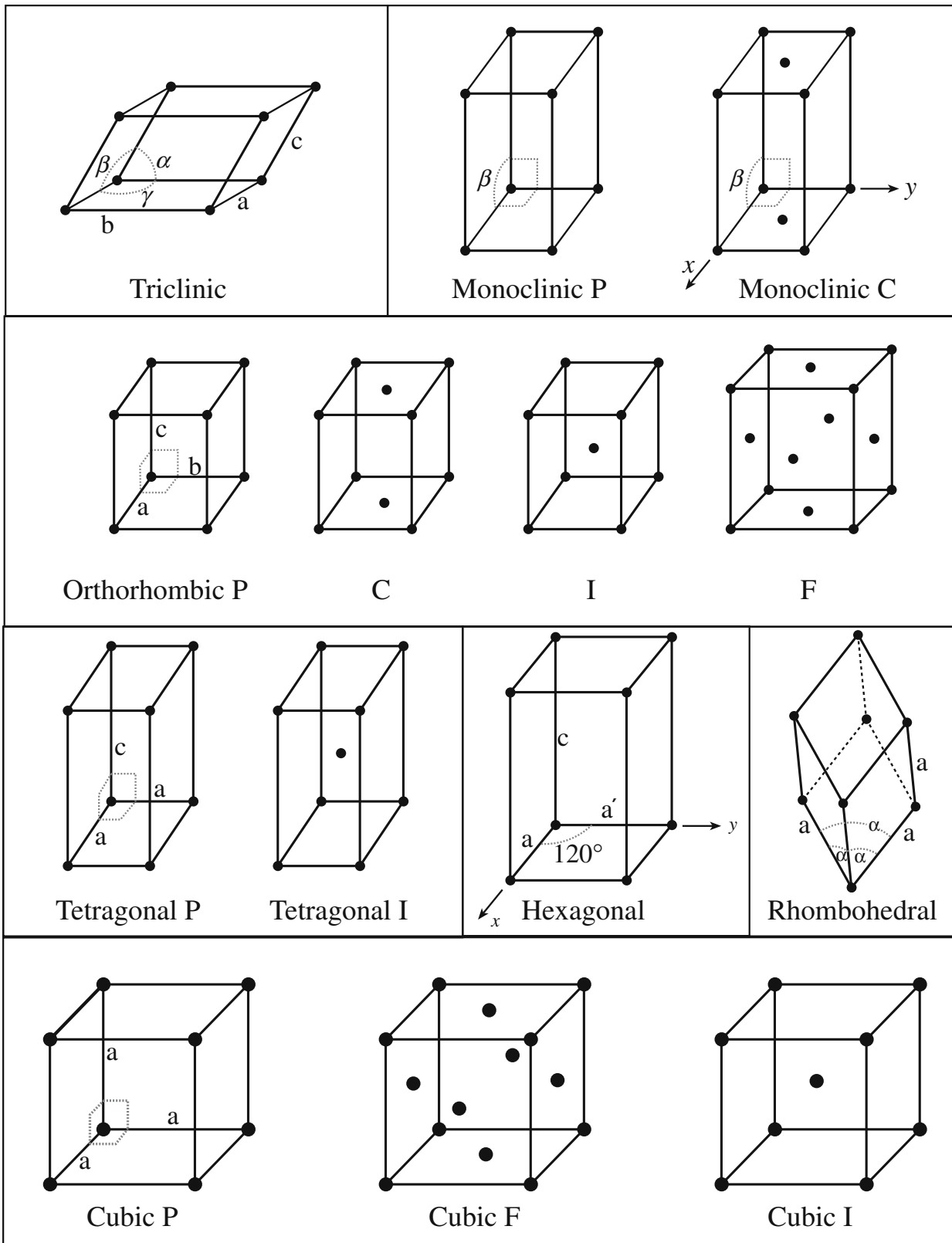
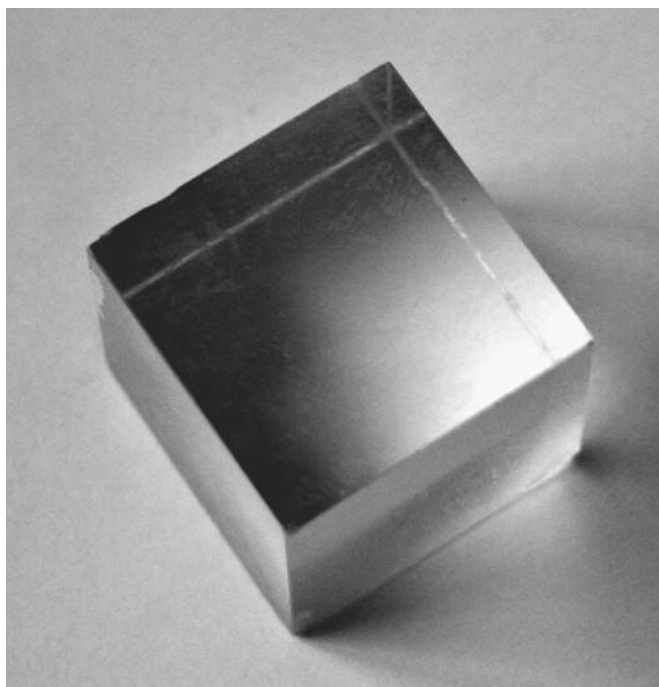


FIGURE 5.1 The fourteen Bravais lattices.



(A)



(B)

FIGURE 5.2 Crystals with faceted surfaces illustrating macroscopic symmetry elements; (a) MgO, (b) calcite.

5.2 SYMMETRY AND CRYSTALLOGRAPHY

Describing the symmetry of crystals is often more complicated than that of solid shapes such as the cube in Figure 5.3. For example, the crystal may have a cubic shape and belong to the cubic crystal system but not have the maximum internal symmetry.

Table 5.2 lists the Hermann–Mauguin notation for expressing the symmetry operators. Some combinations

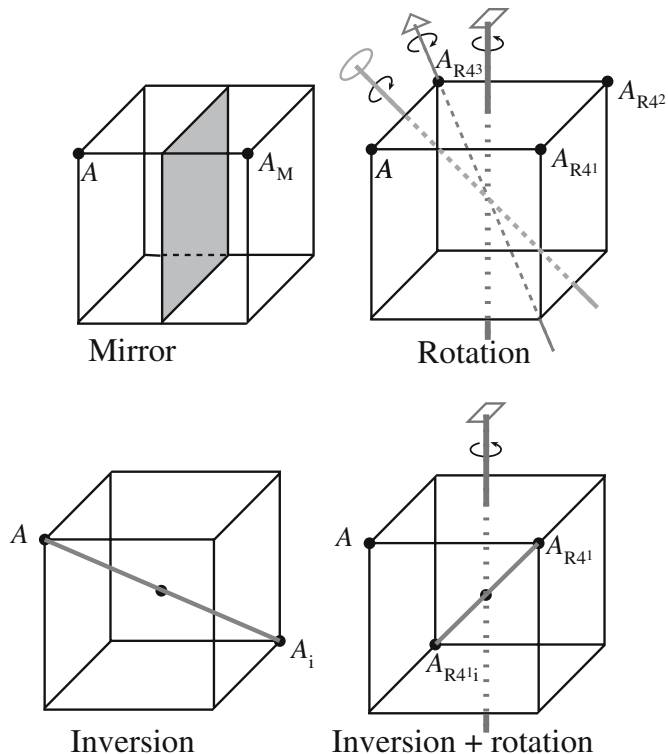


FIGURE 5.3 Symmetry elements for a simple cube.

of symmetry elements produce the same answer. For example, m is the same as $\bar{2}$ while $\bar{2}3$ and $2m3$ are both the same as $2/m3$, which is written as $m3$. So, as with any convention, the only way to get it right is to memorize it. Table 5.3 lists the symmetry operations associated with each of the seven crystal systems. The final column in Table 5.3 has the maximum possible symmetry and is called the holosymmetric point group. For example, NaCl is $m3m$ while FeS_2 is $m3$. Both crystals are cubic, but they have different symmetries; we will show the reasons for this in Chapter 6. The notation is not always the same as indicated at the top of the column. The symbols given here are known as the international convention. Actually we could write them out fully, but the reduced description contains the essentials; for example, $m3m$ is actually $\bar{4}/m3m$ and 43 is actually 432 .

TABLE 5.2 Symmetry Operators (Hermann–Mauguin Notation)^a

X	Rotation axis alone
\bar{X}	Inversion axis alone
X/m	Rotation axis with a symmetry plane <i>normal</i> to it
Xm	Rotation axis with a symmetry plane that is not normal to it (usually a vertical symmetry plane)
$\bar{X}m$	Inversion axis with a symmetry plane not normal to it
$X2$	Rotation axis with a diad normal to it
X/mn	Rotation axis with a symmetry plane normal to it and another not so

^aIn writing the symbol, the principal symmetry axis is placed first. For cubic, 3 is always second.

TABLE 5.3 The 7 Crystal Systems and the 32 Crystal Point Groups

Crystal system	Essential symmetry	X	\bar{X}	X/m	Xm	$\bar{X}m$	X2	X/mmm
Triclinic	1-fold axis	1	$\bar{1}$	—	—	—	—	—
Monoclinic	2-fold axis (parallel to y)	2	m	2/m	—	—	—	—
Orthorhombic	—	—	—	—	mm	—	222	mmm
Trigonal	3-fold axis (parallel to z)	3	$\bar{3}$	—	3m	$\bar{3}m$	32	—
Cubic	Four 3-fold axes	23	—	m3	—	$\bar{4}3m$	432	m3m
Tetragonal	4-fold axis (parallel to z)	4	$\bar{4}$	4/m	4mm	$\bar{4}32$	422	4/mmm
Hexagonal	6-fold axis (parallel to z)	6	$\bar{6}$	6/m	6mm	$\bar{6}m2$	622	6/mmm

You can find the full details of the international convention in the *International Tables for Crystallography* (1983). These symmetry operations or elements can be combined to provide 32 different crystal classes. The crystal classes are often called the crystal point groups. They are the point groups that are consistent with the translational symmetry of a crystal.

5.3 LATTICE POINTS, DIRECTIONS, AND PLANES

The notation used for identifying planes and faces of crystals is that of W.H. Miller and is referred to as the Miller indices of a plane. The lengths of the unit cell are *a*, *b*, and *c*. A family of planes cuts these axes at the origin and at $\frac{a}{h}$, $\frac{b}{k}$, $\frac{c}{l}$. The plane is then defined by the indices *h*, *k*, and *l*. If these indices are not all integers we multiply by the quotient to make them integers. Thus the intercepts $\frac{3}{2}a$, $4b$, and $1c$ give *h*, *k*, and *l* values of $\frac{2}{3}$, $\frac{1}{4}$, and 1 and this *hkl* is 8.3.12. We use periods to separate the numbers only if one of them is greater than 9. If the intercept is negative we write \bar{h} (bar *h*, sometimes read as *h* bar).

Figure 5.4 illustrates some of the low-index planes in the orthorhombic crystal system. Since there may be different combinations of *hkl* that give symmetry-equivalent planes we use (*hkl*) to denote a particular plane and {*hkl*} to denote an equivalent set of planes. The faces of the cube form the set of {100} planes.

Directions are easier to define. The vector $U\mathbf{a} + V\mathbf{b} + W\mathbf{c}$ is simply written as [UVW]. We can then write <UVW> to denote all the equivalent directions formed by permuting *U*, *V* and *W*. The vector $U\mathbf{a} - V\mathbf{b} + W\mathbf{c}$ is denoted by

[$U\bar{V}W$]. Some low-index directions in the orthorhombic system are illustrated in Figure 5.5.

**CONVERTING NOTATION:
MILLER AND MILLER-BRAVAIS**

$$U = u - t \quad u = (2U - V)/3$$

$$V = v - t \quad v = (2V - U)/3$$

$$W = w \quad t = -(u + v)$$

$$\quad \quad \quad = -(U + V)/3$$

$$\quad \quad \quad w = W$$

A special direction, known as the zone axis, is the one that is common to two planes $h_1k_1l_1$ and $h_2k_2l_2$. The directions [$h_1k_1l_1$] and [$h_2k_2l_2$] are the normals to the two planes and the zone axis [UVW] is then given by the vector cross-product. The zone axis has particular significance in electron

microscopy because it represents the direction of the incident electron beam with respect to the sample.

When discussing crystals with hexagonal symmetry, it is helpful to use Miller–Bravais indices because these clarify the symmetrically equivalent planes. In this scheme, a fourth index, *i*, is introduced such

MILLER INDICES

Low-index planes have small values of *h*, *k*, and *l* (and *i*). All are integers.

that $i = -(h + k)$. Figure 5.6 shows some planes and directions in the hexagonal system. The advantage of the four-index Miller–Bravais system, and the main reason for its use, is that similar planes have similar indices (as we saw in the case of the Miller system). For example, the planes (10 $\bar{1}$ 0), (01 $\bar{1}$ 0), ($\bar{1}$ 100), ($\bar{1}$ 010), (0 $\bar{1}$ 10), and (1 $\bar{1}$ 00) are the six sides (called prism planes) of the hexagonal lattice; these clearly are of similar type. In the Miller system, however, these will be (100), (010), ($\bar{1}$ 10), ($\bar{1}$ 00), (0 $\bar{1}$ 0), and (1 $\bar{1}$ 0), and they are definitely not of a similar type.

FINDING THE ZONE AXIS

$$[UVW] = [h_1k_1l_1] \times [h_2k_2l_2]$$

$$U = k_1l_2 - l_1k_2$$

$$V = l_1h_2 - h_1l_2$$

$$W = h_1k_2 - k_1h_2$$

To transform directions, it is helpful to remember from Figure 5.6 that the vector [1 1 1 0] is a null vector: it has no length!

Thus we can change the three-index direction [1 1 0] in Figure 5.6 to its four-index form as follows [1 1 0] → [1 1 0 0] → [1+*f* 1+*f* *f* 0]. So that our four-index notation for directions is the same as for planes (i.e., $U + V + W = 0$), we want $2 + 3*f*$ to be zero. Thus $f = -\frac{2}{3}$ and the direction is [$\frac{1}{3} \frac{1}{3} -\frac{2}{3} 0$] or [1 $\bar{2}$ 0].

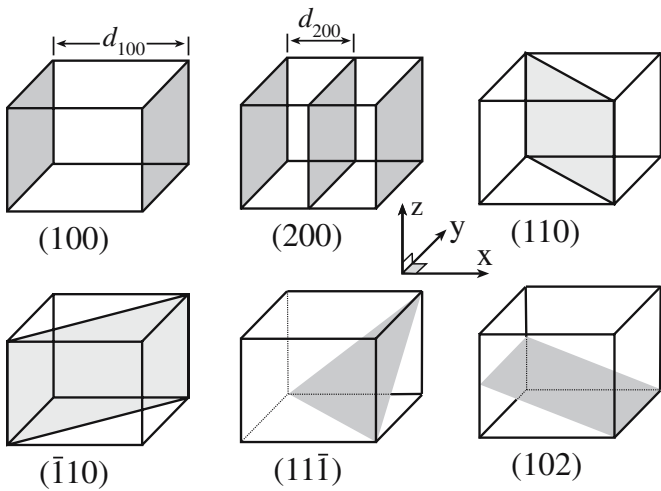


FIGURE 5.4 Miller indices of some lattice planes. The lattice-plane spacing is given by d_{hkl} .

The two notations are related and it is straightforward to convert between them. The Miller–Bravais system is widely used in ceramics because alumina (sapphire) often behaves as if it were hexagonal, although it is actually trigonal.

5.4 THE IMPORTANCE OF CRYSTALLOGRAPHY

Understanding the crystalline structure of ceramics is critical to understanding many of their properties.

- Diffusion. Often depends on the size and number of interstitial sites, both functions of the crystal structure.
- Deformation by slip or twinning. In ceramics there are both crystallographic and electrostatic considerations. The slip direction is usually along a close packed direction. The slip plane will usually be a closely packed plane or one that does not put like charges in

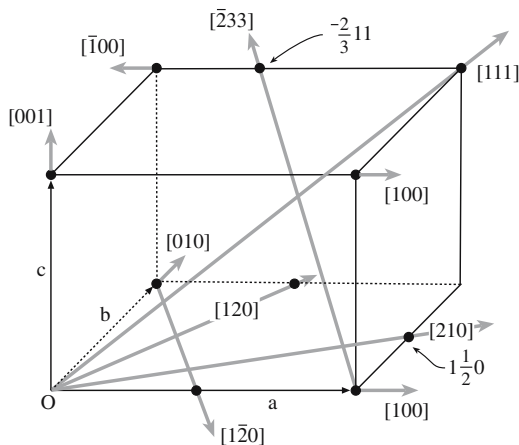


FIGURE 5.5 Indices of directions in an orthorhombic unit cell with examples of vectors included.

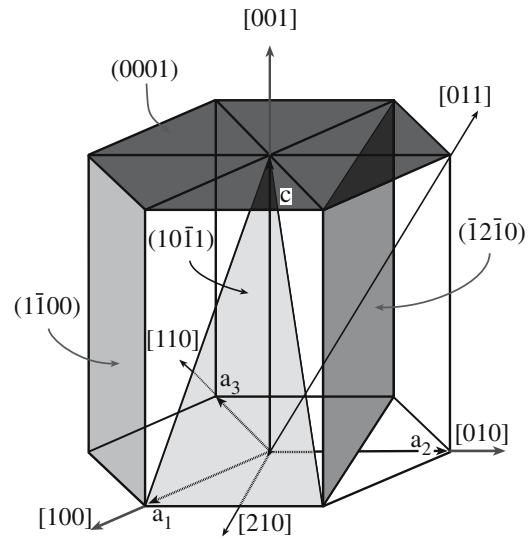


FIGURE 5.6 Indices of planes (using Miller–Bravais notation) and directions (using three-index Miller notation) in the hexagonal unit cell.

juxtaposition. Twin planes are usually special low-index planes.

- Piezoelectricity. Crystals must be noncentrosymmetric.
- Thermal conductivity. Phonon conductivity is most efficient in simple crystal structures formed by small atoms.
- Fracture. Often crystallographic, but not always (e.g., glass and cubic zirconia).
- Cleavage. Always crystallographic. Cleavage planes have high atomic density, but we also need to consider charge.
- Ferrimagnetism. In ferrimagnets the coordination number of the magnetic cation (usually an Fe ion) determines its behavior in an applied magnetic field.

To really appreciate the importance, and complexities, of the relationships between crystallography and properties, see Nye (1985).

5.5 PAULING'S RULES

Ceramic materials are often thought of as being ionically bonded and ions thought of as being charged spheres. Many important ceramics are oxides in which the oxygen anion is much larger than the cation. The crystal structure adopted by the material is based on a balance between the attractive and repulsive forces in the crystal. The electrostatic attractive force between ions of unlike charge implies that an ion with a high CN would be more stable than an ion with a low CN, that is, the electrostatic attraction is maximized. However, if too many ions of the same charge are clustered around an individual ion of the opposite charge, they begin to interfere with one another, that is, the electrostatic repulsion is maximized. There exists a

CN where the attraction is maximized and the repulsion is minimized. This number is determined by the ratio of the radii of the two ions. Questions then arise as to why certain oxides have the structure they do and how this affects mixing or doping of oxides.

Pauling proposed a set of rules to use when discussing such topics. These rules work so well that they are sometimes regarded as laws, which they are not. We will discuss the origin of the rules and then the rules themselves.

The idea is simply that ions of opposite sign pack together in such a way as to keep ions of like sign apart.

Rule 1: A coordinated polyhedron of anions is formed about each cation. The cation–anion distance is determined by the sum of the two radii and the CN is determined by the radius ratio.

Rule 2: In a stable structure, the total strength of the bonds that reach an anion in a coordination polyhedron from all neighboring cations should be equal to the charge of the anion.

Rule 3: The polyhedra in a structure tend not to share edges or faces. If the edges are shared, the shared edges are shortened. Shared faces are the least favorable.

Rule 4: Crystals containing different cations of high valence and small CN tend not to share polyhedron elements with each other.

Rule 5: The number of essentially different kinds of constituents in a crystal tends to be small.

When reading the discussion of these rules, keep in mind the following questions and remember that all rules have exceptions.

- Why do CsCl and NaCl have different structures?
- Why do Mg^{2+} ions tend to occupy tetrahedral sites while Al^{3+} ions occupy octahedral sites in spinel, when both ions occupy octahedral sites in MgO and Al_2O_3 ?
- Why do zinc blende and wurzite have different structures when both are ZnS? Why does GaAs have one structure and AlN have the other?
- What determines the structure of silicates? Are any other structures like this?
- Is the structure of BaTiO_3 important regarding its properties?

On Rule 1: A coordinated polyhedron of anions is formed about each cation. The cation–anion distance is determined by the sum of the two radii. CN is determined by the radius ratio:

A MNEMONIC
 Ca^{2+} is a cation.

$$\text{Radius ratio} = \frac{r_M}{r_X} \quad (5.3)$$

A given CN is stable only when the ratio of cation to anion radius is greater than some critical value. These limits are given in Table 5.4. The derivation of these limits is strictly geometric as shown in Figure 5.7.

MX
M is the cation and is often a metal.
X is the anion and is never a metal.
You will sometimes see CA or +- instead of MX.

Why are the radius ratio and CN related? Coulomb interactions mean that like signs should be as far apart as possible and opposite signs as close together as possible.

Crystal structures are thus at their most stable when the cations have the maximum CN allowed by r_X . In many well-known ceramics, the cation coordination polyhedron is the basic building block.

On Rule 2: In a stable structure, the total electrostatic strength of the bonds, S , reaching an anion in a coordination polyhedron from all neighboring cations should be equal to the charge of the anion

$$S = \frac{Z_M}{\text{CN}} \quad (5.4)$$

where CN is the coordination number and Z_M = charge on the cation. The fundamental idea is that the crystal must be electrically neutral.

We can illustrate this idea for the oxygen anion. Each O^{2-} might bond to a combination of cations:

- Si^{4+} ions, $S = 4/4 = 1$. Two bonds of strength 1 reach the shared oxygen ion from the surrounding silicon ions. This is the case in, for example, cristobalite (a polymorph of SiO_2). The Si^{4+} are surrounded by four O^{2-} ions in a tetrahedral arrangement.
- Al^{3+} ions, $S = 3/6 = 1/2$. Each O^{2-} ion is surrounded by four Al^{3+} , each with a bond strength of 1/2. The Al^{3+} is surrounded by six O^{2-} ions in an octahedral arrangement. This is the case in, for example, corundum.
- In the mineral kyanite, Al_2SiO_5 , we have one Si^{4+} plus two Al^{3+} ions surrounding each O^{2-} ion. There are six O^{2-} around each octahedral Al^{3+} ion.
- In forsterite, Mg_2SiO_4 , we have one Si^{4+} ion plus three octahedral Mg^{2+} ions ($S = 2/6$). We need three Mg^{2+} ions to balance the charge.

TABLE 5.4 Pauling's Critical Radius Ratios		
Polyhedron	CN	Minimum (= r_M/r_X)
Cube	8	0.732
Octahedron	6	0.414
Tetrahedron	4	0.225
Triangle	3	0.155

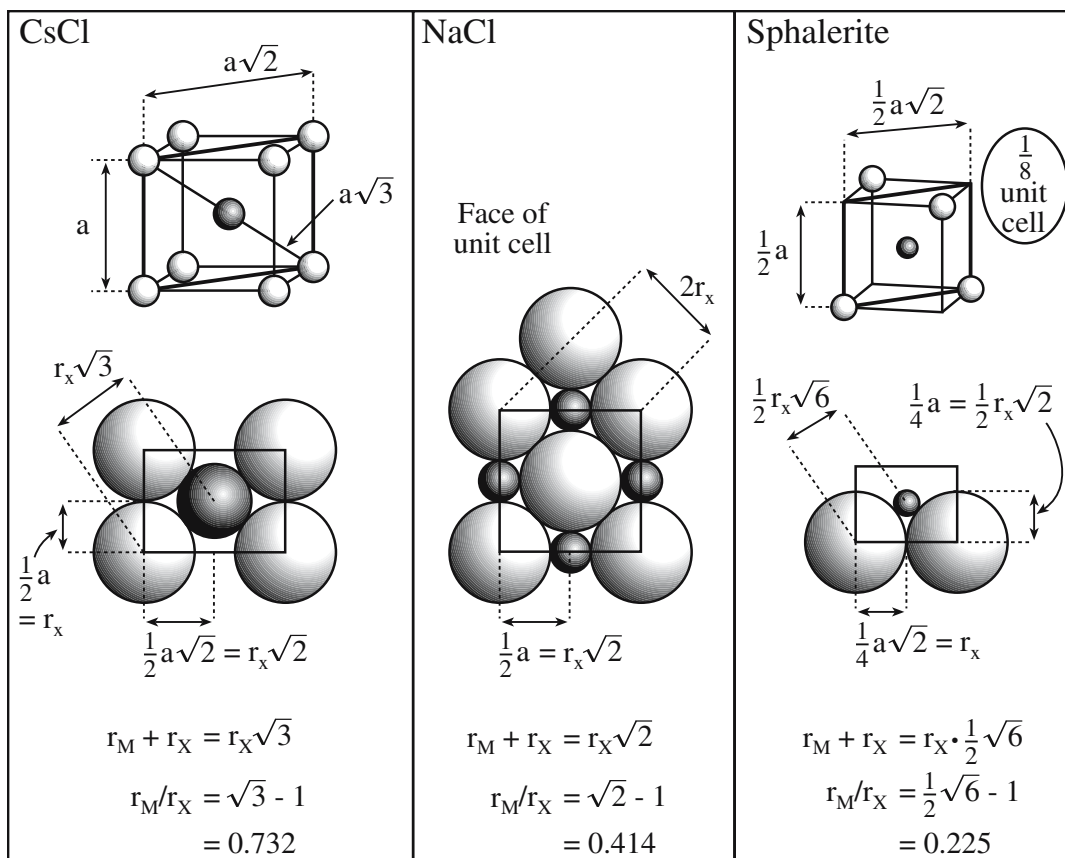


FIGURE 5.7 Geometric method for calculating limiting radius ratios.

In silicates, the Si atoms are each surrounded by four O^{2-} anions, so each O ion has an additional charge of -1 that must be used to bond to another ion. Thus, for an aluminosilicate, we need a large cation with a charge of $+1$ or $+2$ so it can be surrounded by eight or more oxygen ions. Calcium (with CN = 8) fits this requirement to give calcium aluminosilicate. Table 5.5 shows values of predicted CN and S for various cations.

On Rule 3: Polyhedra in a structure prefer not to share edges or faces. Clearly, if the faces are shared, then at least three edges are also shared.

This effect is large for cations with a high valence and small coordination number. In the first case, the charge on the cation is large increasing the Coulomb repulsion. It is especially large when the radius approaches the lower

limit of stability of the polyhedron. Thus, if two anion polyhedra have an edge or face in common, then the cations are being brought too close together. We can provide an alternative statement of the rule. The existence of edges, and particularly faces, common to two anion polyhedra in a coordinated structure decreases its stability.

Examples:

CsCl: the anions sit at the corners of cube and share faces.

NaCl: the anions sit at the corners of octahedra and share edges.

ZnS: The anions sit at the corners of tetrahedra and share vertices.

If polyhedra share edges, these edges tend to be shortened. We can think of this shortening as concentrating more “anion” between cations, which are too close together! The converse of the rule is that if you find an apparent violation it is likely that the bonding is not ionic. However, many materials with the ZnS structure, which does the best job of separating like ions, have predominantly covalent bonding. Determination of the fraction of ionic character in a bond can be made using Eq. 4.24.

Some examples:

TABLE 5.5 Predicted Coordination and Strength of the Bond

Ion	r_M/r_X	Predicted coordination	Strength of bond
Si^{4+}	0.29	4	1
Al^{3+}	0.39	4 or 6	$\frac{3}{4}$ or $\frac{1}{2}$ ($\frac{3}{4}$ or $\frac{3}{6}$)
Mg^{2+}	0.51	6	$\frac{1}{3}$ ($\frac{2}{6}$ $\frac{2}{6}$)
Ti^{4+}	0.44	6	$\frac{2}{3}$ ($\frac{4}{6}$)
K^+	0.99	8	$\frac{1}{8}$

- In FeS₂ (iron pyrites, fool's gold and a ceramic) the [FeS₆] octahedra are linked by shared edges that are longer than expected.
- Silicates contain [SiO₄]⁴⁻ tetrahedra; in all cases, they share corners due only to strong mutual repulsion between Si⁴⁺. Again there is actually a large covalent component to the bonding.
- It is thus a geometric rule again, but is, nonetheless, important. For example, the edges of the occupied octahedra in Al₂O₃ are 0.25 nm long, not 0.28 nm long.

On Rule 4: Crystals containing different cations of high valence and small CN tend not to share polyhedron elements with each other. Sharing parts of polyhedra decreases the stability of the structure, so this rule is really a corollary to rule 3.

As an example, in CaTiO₃, [CaO₁₂] polyhedra share edges and [TiO₆] polyhedra share corners. The Ti⁴⁺ cation is more highly charged than the Ca²⁺ cation, so the CN is smaller; the Coulombic repulsion between cations is proportional to the product of the charges.

On Rule 5: The number of essentially different kinds of constituents in a crystal tends to be small. As far as possible, the environment of chemically similar atoms will be similar (and Pauling's analysis assumes that the bonding is all ionic).

If all types of bonding are possible, it is difficult to predict what will happen, but if every oxygen has the same environment then there is only one possibility. The result is actually found in garnet. This rule only requires the ions to be SIMILARLY COORDINATED. Their actual geometric positions need *not* be equivalent. They are *not* structurally indistinguishable. The rule actually has limited value because in a majority of silicates, the oxygen ions do not have like environments.

5.6 CLOSE-PACKED ARRANGEMENTS: INTERSTITIAL SITES

A close-packed structure is one that has the maximum volume of the unit cell occupied by atoms. The occupied fraction of the unit cell can be determined by calculating the atomic packing factor (APF):

$$\text{APF} = \frac{\text{number of atoms per cell} \times \text{volume of one atom}}{\text{volume of unit cell}} \quad (5.5)$$

The *maximum* possible APF for packing of spheres all having the same size is 0.74. This arrangement is the one

seen in grocery stores in which oranges in adjacent layers sit off-center, resting within the pocket created by the oranges sitting side by side below. Materials scientists and crystallographers (as well as greengrocers) have known that this is the most efficient way to stack a bunch of round objects, but mathematicians took a long time to be convinced (see the interesting book on this topic and other mathematical riddles by Singh, 1997). A mathematical proof for what is known as the Kepler conjecture was announced in 1998 and the manuscript was published 7 years later (Hales, 2005).

Crystal structures having an APF of 0.74 are called close-packed structures. There are only two close-packed structures:

- Face-centered cubic (fcc)
- Hexagonal close-packed (hcp)

We will consider the fcc and hcp structures in some detail because they are so common. For the fcc structure all the points are actually lattice points. In the hcp structure this is not the case. Thus we should never say the "hcp lattice" but we do. The hcp structure describes a particular arrangement of similar atoms, but it is not a lattice of identical points.

The relationship between the fcc and hcp structures is illustrated in Figure 5.8a. The atoms on the (111) planes of the fcc structure are arranged in a hexagonal pattern just like the atoms on the (0002) planes of the hcp structure. The only difference between the two structures is the way in which these hexagonal sheets of atoms are arranged above one another. In the hcp structure, the atoms in the second layer are above the hollows in the first layer and the atoms in the third layer are above the atoms in the first layer, so the stacking sequence can be summarized as A B A B A B . . . The stacking in the hcp structure is illustrated in Figure 5.8b. The first two atom layers in the fcc structure are put down in the same way, but the atoms of the third layer are placed in the hollows of the second layer; not until the fourth layer does a position repeat. The stacking sequence for fcc is therefore A B C A B C A . . . This sequence is illustrated in Figure 5.8c.

In predominantly ionically bonded oxide ceramics, the O²⁻ ion approximates a sphere. So we can view these structures as based on a close-packed arrangement of spheres and then filling the remaining space. We must remember that the anions are not necessarily touching, but they are merely arranged in a way that is the same as that in the close-packed structures.

GARNET			
Ca ₃ Al ₂ Si ₃ O ₁₂ is not only a gemstone but also a ceramic. Other garnets such as yttrium aluminum garnet (YAG) and gallium gadolinium garnet (GGG) are technologically much more important materials.			
Ion:	Ca ²⁺	Al ³⁺	Si ⁴⁺
O ²⁻ coordination	8	6	4
O bond strength, <i>S</i>	$\frac{2}{8} = \frac{1}{4}$	$\frac{3}{6} = \frac{1}{2}$	$\frac{4}{4} = 1$

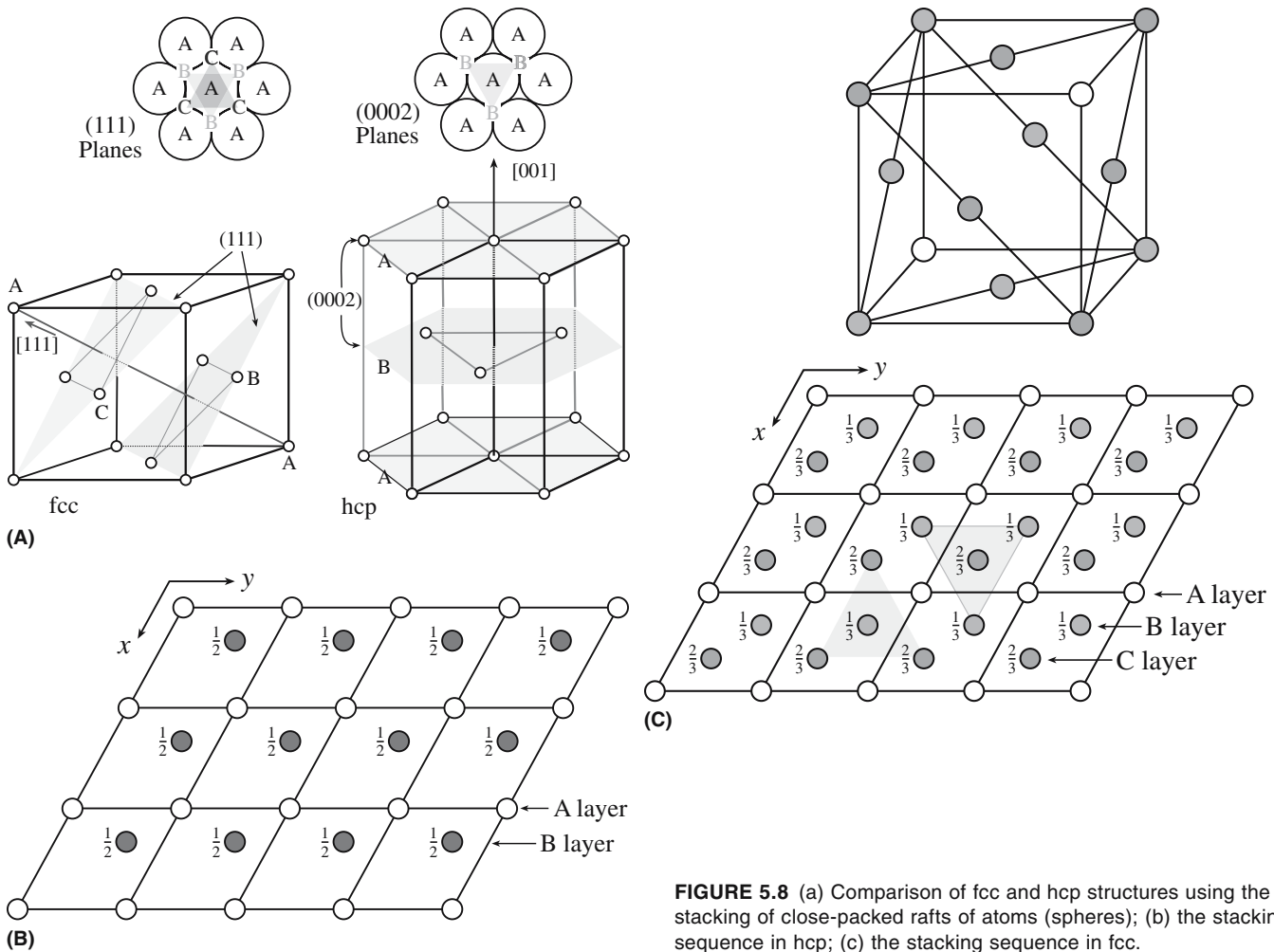


FIGURE 5.8 (a) Comparison of fcc and hcp structures using the stacking of close-packed rafts of atoms (spheres); (b) the stacking sequence in hcp; (c) the stacking sequence in fcc.

So we now need to answer the following questions:

- Where are the interstitial sites?
- What is their CN?
- How many sites are there?

The fcc and hcp arrangements offer both octahedral and tetrahedral interstices, making them good hosts for cations, since two size ranges can be incorporated. Both fcc and hcp arrangements can be stabilized by filling just the tet-

rahedral sites or just the octahedral sites. The fcc lattice can be stabilized by filling a combination of tetrahedral and octahedral sites. In the fcc arrangement there are eight tetrahedral sites and four octahedral sites per cell. The location of these sites is shown in Figure 5.9a. There are four tetrahedral sites and two octahedral sites per cell in the hcp arrangement. The location of these sites is shown in Figure 5.9b.

In ceramics the APF is always < 0.74 , even though we have increased the number of atoms per cell. As an

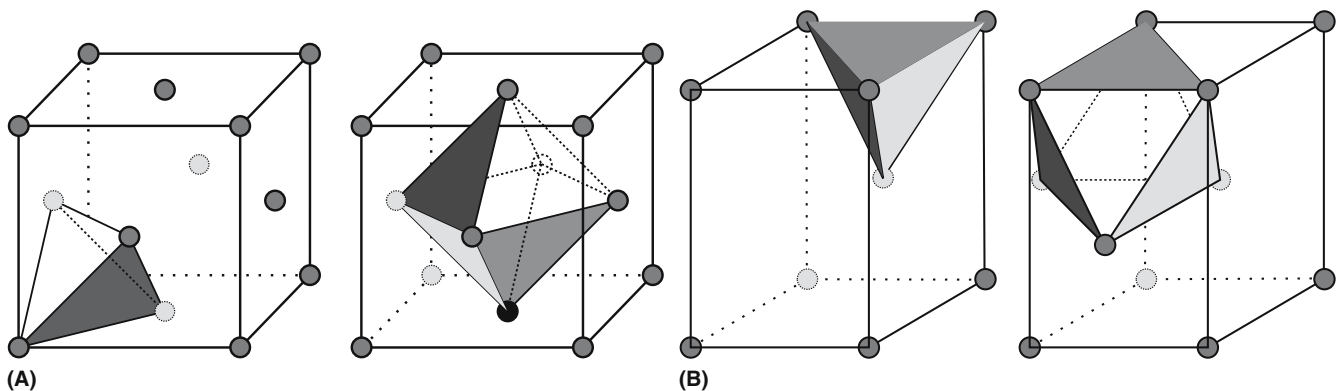


FIGURE 5.9 (a) Interstitial sites in the fcc structure; (b) interstitial sites in the hcp structure.

TABLE 5.6 The Strukturbericht Notation

Symbol	Definition	Symbol	Definition
A	Element	E-K	Complex
B	AB compounds	L	Alloys
C	AB ₂	O	Organic
D	A _m B _n	S	Silicates

example, if we fill all the octahedral sites in an fcc arrangement of O²⁻ with cations (e.g., Mg²⁺) as we'll see in Chapter 6, the APF is 0.69. In other words, 69% of the cell volume is occupied by ions.

5.7 NOTATION FOR CRYSTAL STRUCTURES

One of the things you will notice is that many crystal structures are named after particular materials (often a naturally occurring mineral) that exhibit the structure. There are no systematic names for crystal structures, as there are, for example, for organic compounds, which are named using a system recommended by the International Union of Pure and Applied Chemistry (IUPAC). This system provides us with a systematic way of naming many organic compounds on sight and the name indicates the structure of the compound. A similar system is not used for naming crystal structures. However, there are several different notations for specifying crystal structures that can be very useful.

- *Strukturbericht*. The symbol consists of a letter that characterizes the type of structure and a number designating a specific type within a letter category. The rules are given in Table 5.6.
- *Pearson*. The symbols give, successively, the crystal system, the Bravais lattice symbol, and the number of atoms per unit cell. The notation is summarized in

TABLE 5.7 Symbols Used in The Pearson Notation

Symbol	System	Lattice
aP	Triclinic (anorthic)	P
mP	Simple monoclinic	P
mC	Base-centered monoclinic	C
oP	Simple orthorhombic	P
oC	Base-centered orthorhombic	C
oF	Face-centered orthorhombic	F
oI	Body-centered orthorhombic	I
tP	Simple tetragonal	P
tI	Body-centered tetragonal	I
hP	Hexagonal	P
hR	Rhombohedral	R
cP	Simple cubic	P
cF	Face-centered cubic	F
cI	Body-centered cubic	I

TABLE 5.8 Notation for Different Crystal Structures

Strukturbericht	Prototype	Pearson	Space group
A1	Cu	cF4	Fm $\bar{3}$ m
A2	W	cI2	Im $\bar{3}$ m
A3	Mg	hP2	P6 ₃ /mmc
A9	Graphite	hP4	P6 ₃ /mmc
B _h	WC	hP2	P6m2
B _k	BN	hP4	P6 ₃ /mmc
B1	NaCl	cF8	Fm $\bar{3}$ m
B2	CsCl	cP2	Pm $\bar{3}$ m
B3	Sphalerite	cF8	F4 $\bar{3}$ m
B4	Wurtzite	hP4	P6 ₃ mc
B10	PbO	tP4	P4/nmm
B26	CuO	mC8	C2/c
C2	FeS ₂ (pyrite)	cP12	Pa $\bar{3}$
C3	Ag ₂ O	cP6	Pn $\bar{3}$ m
C4	TiO ₂ (rutile)	tP6	P4 ₂ /mnm
C6	CdI ₂	hP3	P $\bar{3}$ ml
C7	MoS ₂	hP6	P6 ₃ /mmc
C8	High quartz	hP9	P6 ₂ 22
C9	β Cristobalite	cF24	Fd $\bar{3}$ m
C10	β Tridymite	hP12	P6 ₃ /mmc
C18	FeS ₂ (marcasite)	oP6	Pnnm
C21	TiO ₂ (brookite)	oP24	Pbca
C43	ZrO ₂	mP12	P2 ₁ /c
D0 ₉	ReO ₃	cP4	Pm $\bar{3}$ m
D0 ₁₁	Fe ₃ C	oP16	Pnma
D5 ₁	α -Al ₂ O ₃	hR10	R $\bar{3}$ c
D5 ₂	La ₂ O ₃	hP5	P $\bar{3}$ c1
D5 ₃	Mn ₂ O ₃	cI80	Ia $\bar{3}$
E2 ₁	CaTiO ₃	cP5	Pm $\bar{3}$ m
H1 ₁	MgAl ₂ O ₄	cF56	Fd $\bar{3}$ m
L1 ₀	AuCu	tP2	P4/mmm
L1 ₁	CuPt	hR32	R $\bar{3}$ m
L1 ₂	AuCu ₃	cP4	Pm $\bar{3}$ m

Table 5.7. Even though you will be able to find out the crystal system, the Bravais lattice, and the number of atoms from this notation, you will not be able to differentiate among different structures with similar notations. For example, cF8 refers to sodium chloride, diamond cubic, and zinc blende structures, which are different from one another.

Examples of Strukturbericht and Pearson symbols are given in Table 5.8.

5.8 STRUCTURE, COMPOSITION, AND TEMPERATURE

Many ceramics exist in different structures at different temperatures. These structures are known as polymorphs and we will give some examples in Chapter 6. The most stable structure at any particular temperature is governed by its free energy, *G*. The polymorph with the lowest free energy is the most stable. Expressions for the free energy and internal energy were given in Chapter 3. Both the internal energy, *E*, and the entropy, *S*, depend on crystal structure.

The following rules can be given for the temperature and pressure dependence of thermodynamically stable structures:

- At $T = 0$, $G = E$, that is, the free energy is fixed by the internal energy.
- At $T > 0$, the TS term becomes increasingly important and structures with a low degree of order are favored.
- At a sufficiently high temperature a polymorph with a larger S may achieve a lower G in spite of its larger E , as illustrated in Figure 5.10. The increased values of E and S of the high-temperature forms correspond to more open structures (larger specific volumes) with higher symmetry.
- There are two components to entropy (both increase as T increases)—thermal entropy and configurational entropy.
- In the liquid state, the order is even lower and it is the lowest in the gaseous state. Raising the temperature will lead to melting and finally to evaporation.
- Higher pressures favor structures that occupy a lower volume, that is, that have a higher density.

The crystal structure of a ceramic also depends on composition. As an example, consider three oxides of iron:

1. Wüstite (FeO): Cubic rocksalt structure. Iron is in the 2+ oxidation state.
2. Hematite (Fe_2O_3): Rhombohedral corundum structure. Iron is in the 3+ oxidation state.
3. Magnetite (Fe_3O_4): Cubic spinel structure. Iron is in 3+ and 2+ oxidation states.

The reasons for these differences are explained by Pauling's rules.

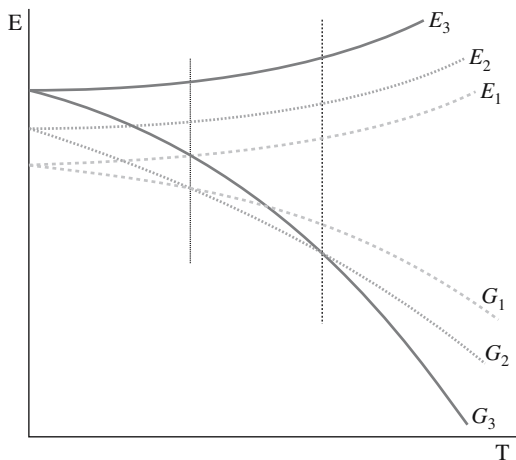


FIGURE 5.10 Schematic showing the relationship between internal energy E and free energy G of three polymorphic forms: $E_3 > E_2 > E_1$ and $S_3 > S_2 > S_1$. The form with the lowest G will be the one usually found at a specific temperature.

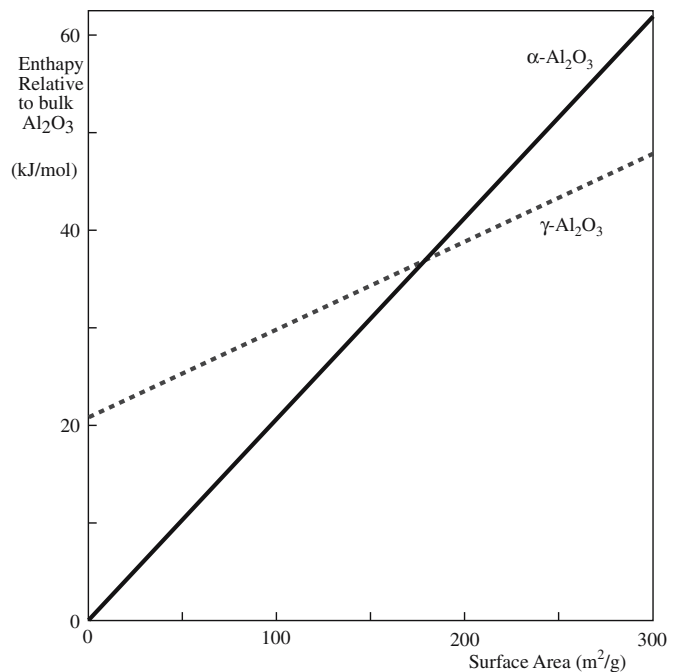


FIGURE 5.11 Calculated enthalpy of alumina (γ - and α -) polymorphs as it varies with the surface area. The calculation is an MD simulation using data for small surface areas. A large surface area per gm implies small particles.

There is another factor that can influence the equilibrium structure of a material and that is surface energy. The effect of surface energy has become of increasing importance with the interest in nano-sized particles of ceramics. When particle size becomes very small the fraction of atoms on the surface becomes very large. Surface energy effects can then dominate as illustrated in Figure 5.11, which shows that $\gamma\text{-Al}_2\text{O}_3$, rather than $\alpha\text{-Al}_2\text{O}_3$, can become the thermodynamically stable phase of aluminum oxide when the surface area exceeds $\sim 175 \text{ m}^2/\text{g}$. The key thing to remember is that nanomaterials do not always behave the same as the bulk material.

5.9 CRYSTALS, GLASS, SOLIDS, AND LIQUID

Classically, there are three distinct states of matter: gas, liquid, and solid. (The newer two, plasma and Bose-Einstein condensates, are not applicable to our discussion so we omit them.) In the previous section we noted how as temperature increases it is thermodynamically favorable for transitions to occur from a more ordered form to a less ordered one. The atoms or molecules that make up a gas are randomly arranged (E and S are high) and widely separated. A gas will fill all the available space inside a container. The atoms or molecules that make up a liquid are also randomly arranged, but they are closer together than those in a gas and they move relative to one another. The characteristic of a liquid is that it will fill a container

to the extent of its own volume. The third state of matter is solid, which can be defined as having a fixed shape. Solids can be classified as either *crystalline* or *noncrystalline*.

When we discuss crystals we are concerned with interatomic bonding, interatomic distances, the environment of the ions and long-range ordering. All of these concepts, except for long-range ordering, are relevant to noncrystalline materials such as glass. In fact, when we discuss silica-based glasses, the main point is how we do or do not link SiO₄ tetrahedra together. The concept of order that is important is separating the different classes of condensed matter. The basic differences are summarized below:

Crystal	Ordering on lattice—long-range order
Glass	Short-range order
Liquid	No order to short-range order

There are many amorphous ceramics (glasses). There are fewer amorphous semiconductors and some amorphous metal alloys. The main consideration, as you will see in Chapter 21, is the rate of cooling necessary to avoid crystallization. In many oxides the critical rate of cooling is very easy to achieve because the number of components is large and we have directional (covalent) bonding. The latter consideration also holds for the semiconductors, but for metal alloys we usually can rely only on frustrating crystallization using complex compositions and rapid quenching.

5.10 DEFECTS

One reason that we need to understand the structure of perfect crystals is so that we can begin to understand imperfect crystals. The topic is not just specific to ceramics. The interaction of defects is often most important to us. For ceramics, a special example of such interactions occurs in grain growth. Grain-boundary movement in ceramics usually involves the movement of point defects.

Understanding atomic bonding helps us understand the structures of crystals and glass. When we think of crystals, we think of atoms arranged in a perfect way. We traditionally think in terms of crystal defects, but we will also consider how these ideas apply to defects in glass.

One question to keep in mind is “how is this feature different from metals?” The answer is not always as obvious as it might seem at first, because we often compare ceramic materials to particularly simple (usually fcc) metals. Apart from carbon and the elemental semiconductors, Si and Ge, all ceramics contain two or more different atoms, so we should at least compare them with metal alloys not pure metals. The next question is “how do defects influence the properties of the ceramic?” For that we need to understand defects first.

We classify defects as having 0, 1, 2, or 3 dimensions, as shown in Table 5.9. Actually all of the defects we will

TABLE 5.9 Hierarchy of Crystal Lattice Defects

“Dimension”	Defect	Some topics
0	Point defects	Geometry, strain energy, charge
1	Line defects	Geometry, energy
2	Surfaces Grain boundaries Phase boundaries	Thermodynamics Structure, chemistry, wetting Phase distribution
3	Volume defects	Precipitates, particles, and voids

discuss are three-dimensional defects. Ceramics usually have mixed bonding, that is, a combination of ionic and covalent bonding. So, when we introduce defects, we usually change the local distribution of charge or break bonds, depending on which type of bond predominates. Any change in charge distribution can produce long-range effects. A broken covalent bond is known as a dangling (unpaired electron) bond that also behaves like a localized charge.

We have discussed the packing of ions in terms of coordination polyhedra. When we create defects in a crystal we can create new polyhedra that are not found in the perfect crystal. Pauling’s rules were developed for perfect crystals, but the principles still apply when we examine defects. One complication is that as we introduce grain boundaries, for example, new sites are produced that depend on the detailed nature of the grain boundary. Amorphous materials present a new challenge when describing point defects. Two amorphous materials can have different structures that depend on the processing history even if the chemistry is the same.

5.11 COMPUTER MODELING

Computer modeling of oxide structures and of defects in oxides is becoming more important, in part because the code is improving, but mainly because faster computers can make more realistic calculations. The problems for ceramic materials are those discussed in Chapters 3 and 4. If the bonding is ionic, then the ion–ion interactions are both strong and long-range. If there is a covalent component to the bonding, then the bonds have a directional character. (Glasses exist in a metastable state so their structure is, by definition, not the equilibrium one.) The problem is 2-fold. We need a computer code that can handle the long-range interactions. Even simple ceramics can have large unit cells, which means that the computer must be able to handle a large number of atoms.

We will summarize the approaches being used by different researchers to calculate properties of ceramics. This discussion is very brief and incomplete, but it should provide an idea of how the subject is developing. One

encouraging feature is that software packages that are suitable for the knowledgeable researcher who is not an expert programmer are becoming available commercially. These packages fall into two categories that can be linked. In one the atomic structure of a ceramic crystal can be displayed after inputting the appropriate crystal parameters. Such programs are simply using the rules of crystallography to generate the structures. The other, and far more complex, programs also use the interatomic potentials to deduce features of the structure and are performed using molecular dynamic (MD) approaches.

Terms Used in Modeling

We will begin by listing some of the terms you will encounter: *Pseudo-potential* is an expression that is being used to represent a real crystal potential. An equation like Eq. 4.1 is chosen and the parameters changed until a calculated value is obtained that agrees well with the known value of a physical parameter. This process will be carried out simultaneously for several parameters that are chosen to have some relevance to what you would like to calculate. *Electronic structure calculation*: Although ceramics are thought of as insulators, the electrons are important in understanding optical properties, for example.

Computer Modeling of Structures: The Need for Potentials

Most ceramics cannot be modeled from first principles simply because we do not know the potentials well enough. So the challenge with modeling crystals is that we have to use a model for the potential. These are available for Si and are quite good for Al_2O_3 and MgO .

We can summarize the problems for modeling ceramics as follows:

- Ceramics usually contain charged species. This means that the interionic forces extend over very large distances (remember the Madelung constant). To model such materials we need large unit cells. This problem becomes more difficult when we model defects.
- When the ceramic is covalent or has a large covalent component to the bonding, directions are important. Si is the classic example of a covalent material and can be modeled, but only because enormous effort could be justified by its commercial importance. Modeling silicates, which also have a large covalent component, is less developed.

Ceramics lag behind metals for two reasons. First, most ceramics contain more than one component so we need to have potentials for each ion. (FeO contains three ions for this purpose.) Second, the potentials have to be used to predict known quantities and these are not usually as well known as they are for metals.

A number of software packages are now available as shareware or commercially. One such program is GULP: the acronym stands for Generalized Utility Lattice Program. GULP can be used to perform different types of simulation on three-dimensional periodic solids and on isolated defects in such materials. GULP simulates structures of ionically bonded materials using a shell model and uses the crystal symmetry to accelerate the calculations and to simplify the input. These two factors can make it faster and more efficient than other programs. If you use GULP, for example, you will have access to at least 23 different potentials or models, including Buckingham, Morse, Coulomb, and Stilinger-Weber. Examples of the uses of GULP are modeling Al_2O_3 , defects in garnets, zeolites, and molecular sieves, and the structure of Al_2SiO_5 polymorphs. CeriusTM, another software package for simulating structures, also includes diffraction modules.

CHAPTER SUMMARY

This is the chapter in which we introduce crystallography. Some students object to having to learn this material. Our view is that you cannot understand point defects, piezoelectricity, grain boundaries, elasticity of noncubic crystalline materials, etc., unless you understand the differences between the different crystal structures, and for this you must understand the principles of crystallography. Pauling's rules for ionic ceramics give us a set of tools to allow us to predict the coordination of ions and even to guess the structure of a crystal that may be new to us. The exceptions to these rules often result from the presence of a covalent component to the bonding, which itself gives clues to the coordination. Once we know the crystal structure, we can predict what point defects might occur and even guess at the energies involved—just from counting broken bonds, for example. The best-known examples of such point defect sites are the octohedra and tetrahedral in the close packed (fcc or hcp) lattices, but we find these polyhedra in many different crystal structures, though they may be more difficult to recognize elsewhere. So just by considering Pauling's rules, we are introduced to one of the most useful concepts of solid-state chemistry—the concept of crystals being constructed by arranging polyhedra. The polyhedra are clusters of atoms that behave in quite systematic ways. As we will see in the following chapters, the most important of these polyhedra will be the tetrahedron formed by four oxygen ions with an Si ion at the center, but it is certainly not the only polyhedron of interest to us.

PEOPLE IN HISTORY

- Bravais, Auguste (1811–1863) presented his ideas on crystallography to the French Academy of Sciences in 1849. He was interested in a number of fields including botany, astronomy, and physics. It is for his work in crystallography that he is best remembered.
- Goldschmidt, Victor Moritz was born in Zurich, but spent his scientific career in Norway (1888–1947). Like Pauling, he derived rules for ionic radii.
- Haiüy, René-Just (1743–1822) published his essay in 1784 on a theory of the structure of crystals; the story is that his interest in crystals began when he examined a specimen of calcite that he had accidentally just dropped.
- Hooke, Robert (1635–1703) published *Micrographica* in 1665 showing images taken with his microscope. A genius.
- Miller, William Hallowes (1801–1880) was born in South Wales and was Professor of Mineralogy at Cambridge University from 1832 until he died. He wrote the book that explained the notation developed by William Whewell (who also coined the word scientist); he gave full credit to the pioneering work of his mentor, Whewell, but we still refer to Miller indices.
- Wulff, Georgii (Yurii) Viktorovich was a Russian crystallographer born in 1863. The initial G was used in translations of his papers rather than the Y. He died in 1925 in Moscow.
- Wyckoff, Ralph Walter Graystone was born in 1897 and died in 1994. He was the author of the classic book, *The Stucutre of Crystals*, 1931.

GENERAL REFERENCES

- A great source for further reading lies in the mineralogical literature. The books by Putnis (1992), Deer, Howie, and Zussman (1992), etc. provide great insight, as does the literature from solid-state chemistry such as the books of Wells (1970), Hyde and Anderson (1989), etc. These references are given in Chapters 6 and 7.
- Barrett, C.S. and Massalski, T.B. (1980) *Structure of Metals*, 3rd edition, Pergamon, New York. Together with Pearson (below) gives more on the Strukturbericht notation.
- Buerger, M. (1978) *Elementary Crystallography*, The MIT Press, Cambridge, MA. One of the best introductions to the subject. At the level of this text.
- Burdett, J.K. (1995) *Chemical Bonding in Solids*, Oxford University Press, Oxford.
- Crystal modeling on a Macintosh or using Windows XP is easy using CrystalMaker. <http://www.crystalmaker.co.uk>.
- Gale, J.D. (1996) Empirical potential derivation for ionic materials, *Phil. Mag. B*, **73**, 3.
- Giacovazzo, C. *et al.* *Fundamentals of Crystallography*, 2nd edition, IUCr/Oxford University Press, Oxford. Comprehensive.
- International Tables for Crystallography*, Vol. A, 5th edition (2002), edited by T. Hahn, D. Reidel, Boston.
- Molecular Simulations Inc. (MSI) produces CeriusTM. The corresponding structure modeling package is CASTEP. <http://www.msi.com/materials/cerius2/castep.html#info>.
- Nyberg, M., Nygren, M.A., Pettersson, L.G.M., Gay, D.H., and Rohl, A.L. (1996) “Hydrogen dissociation on reconstructed ZnO surfaces,” *J. Phys. Chem.* **100**, 9054.
- Phillips, F.C. (1972) *An Introduction to Crystallography*, 4th edition, Wiley, New York. Includes a clear description of the Herman–Mauguin notation and the 32 classes of crystal symmetry. First published in 1946.

SPECIFIC REFERENCES

- Gale, J.D. (1997) “GULP—a computer program for the symmetry adapted simulation of solids,” *JCS Faraday Trans.* **93**, 629.
- Hales, T.C. (2005) “A proof of the Kepler conjecture,” *Ann. Math.* **162**, 1065. The paper is 121 pages long! Twelve reviewers spent more than 4 years reviewing it.
- Nye, J.F. (1985) *Physical Properties of Crystals*, Clarendon Press, Oxford.
- Pearson, W.B. (1972) *The Crystal Chemistry and Physics of Metals and Alloys*, Wiley, New York. Gives many more details on crystal notation (see also Villars and Calvert below).
- Singh, S. (1997) *Fermat’s Last Theorem*, Fourth Estate, London.
- Villars, P. and Calvert, L.D. (1985) *Pearson’s Handbook of Crystallographic Data for Intermetallic Phases*, Vols. 1, 2, 3, ASM International, Metals Park, OH.

EXERCISES

- 5.1 Calculate the percentage of free space in an fcc stacking of spheres and a cubic stacking of spheres. Relate the result to two important different ceramic structures.
- 5.2 Based on Pauling’s radii, how do you expect the lattice parameters of Si and SiO₂ (high cristobalite) to compare? How does this fit with experiment? Discuss.

- 5.3 When the {111} planes of SiC stack with the sequence ABABAB, the SiC has hexagonal symmetry. When they stack with the sequence ABCABC, it has cubic symmetry. What symmetry does it have when it stacks ABCBABCBAABCBA? Explain your reasoning.
- 5.4 The face-centered cubic cell may be referred to the rhombohedral cell. Using a sketch show the relationship between the two cells.
- 5.5 Are there any interstices in hcp that are not present in fcc?
- 5.6 Why is there no Bravais lattice called orthorhombic A, monoclinic B, or tetragonal C?
- 5.7 If a sapphire crystal showed only one type of rhombohedral plane and the two basal planes, what would the shape of the crystal be?
- 5.8 FeS is a more complicated structure than FeO. Why would you not be surprised at this result?
- 5.9 In calcite (CaCO_3) the Ca^{2+} ion has a CN 6. Using the appropriate Pauling rule determine the ion environment around each O^{2-} ion.
- 5.10 From the ionic radii given, estimate the coordination numbers for the following oxides: (a) MgO, (b) Al_2O_3 , (c) Li_2O ; Li^+ 76 pm; O^{2-} 140 pm; Mg^{2+} 72 pm; Al^{3+} 54 pm.

6

Binary Compounds

CHAPTER PREVIEW

In this and the following chapter, we will describe the most important simple (binary) crystal structures found in ceramic materials. You need to know the structures we have chosen because many other important materials have the same structures and because much of our discussion of point defects, interfaces, and processing will use these materials as illustrations. Some, namely FeS_2 , TiO_2 , CuO , and Cu_2O , are themselves less important materials and you would not be the only ceramist not to know their structure. We include these oxides in this discussion because each one illustrates a special feature that we find in oxides. These structures are just the tip of the topic known as crystal chemistry (or solid-state chemistry); the mineralogist would have to learn these, those in Chapter 7, and many more by heart. In most examples we will mention some applications of the chosen material.

In traditional ceramic oxides, the anion is usually the larger ion, so we often think of a ceramic crystal structure as a three-dimensional (3D) array of anions with cations inserted in the interstices. Whether or not a particular structure is stable depends on Pauling's rules. We first review some of the important lattices, paying particular attention to the polyhedra that are formed by groups of anions. As the variety of ceramics being used in today's high-technology environment increases, some of the above assumptions cease to be valid. In certain oxides, the cation is larger than the anion and covalently bonded oxides and nonoxides cannot be treated as arrays of hard spheres. So we learn the rules and try to understand the exceptions. The concept of crystals being arrays of polyhedra will still work whether the bonding is ionic or covalent and whether the anion or the cation is larger.

In this and the following chapter, the xyz -axes in the schematics of cubic crystal structures lie along the cube edges; the length of the cube edge is the lattice parameter.

6.1 BACKGROUND

Using Pauling's rules, we can think of all crystal structures in terms of filling polyhedra. The polyhedra are those we discussed in Chapter 5. Particularly simple cases are the simple-cubic (sc), the hexagonal close-packed (hcp), and the face-centered cubic (fcc) lattices. In oxides like Al_2O_3 and MgO , the anion is the larger ion, which we consider to form a scaffold so that the cations fill the interstices between the anions. This thinking has a historical bias to it. It comes from the days when ceramics were light-element oxides. Such compounds automatically have smallish cations.

With the growing importance of ternary and tertiary oxides and the nonoxide ceramics, we have to be careful when making such assumptions. You must also remember that Pauling's rules apply to compounds in which the bonding is primarily ionic. In some compounds, the structure is the one predicted by Pauling's rules, but the reason may not be the one we gave when deriving the rules! In other words, if the bonding has a large covalent compo-

nent, beware. Similarly, if the cation is large (e.g., in UO_2), we should not (though we sometimes do) consider the structure as a close-packed stacking of anions even if they do appear to lie on an fcc lattice.

Although we will examine only a few materials here, each one has the same structure as other important materials; we will list a few of these isomorphous materials. The examples chosen are also important because other crystal structures can be related to them with only a small distortion added to change the symmetry.

The logic of this chapter is summarized as follows:

CsCl	sc lattice with a two-atom basis
NaCl, GaAs	fcc lattice with a two-atom basis
CaF_2 , FeS_2	fcc lattice with a three-atom basis
AlN	Hexagonal "close-packed" structure with a two-atom basis
Cu_2O	More complex but still cubic
TiO_2 , CuO	Much more complex
Al_2O_3 , CdI_2	"hcp" anions but not hcp structures
MoS_2	Layered material

6.2 CsCl

We start with the CsCl structure because it is the simplest possible, not because of its importance. The Bravais lattice of the CsCl structure is sc. We can view this structure in two ways:

- Two interpenetrating sc lattices, one of Cs^+ and one of Cl^- . The two sublattices are displaced by $\frac{1}{2}\langle 111 \rangle$
- One sc lattice with a two-atom basis (Cs^+ at 0,0,0 and Cl^- at $\frac{1}{2}, \frac{1}{2}, \frac{1}{2}$)

The concept of a sublattice is helpful when visualizing structures, but the phrase is sometimes used when the atoms do not really lie on a lattice. In this example, the lattice could be based on the positions of either the Cs^+ ions or the Cl^- ions.

We can check this structure against Pauling's rules. The ratio of the ionic radii (in pm) is

$$r_{\text{Cs}^+}/r_{\text{Cl}^-} = 170/181 = 0.94$$

As the ratio is >0.732 the Cs^+ should be 8-fold coordinated. It is clear from Figure 6.1 that the coordination number is indeed 8. This structure does not appear to occur for oxides since the (divalent) cation radius would need to be >102.5 pm (O^{2-} is 140 pm). It is not directional bonding that causes the structure to be adopted, just the packing requirements. This structure is the model B2 structure found in some important intermetallics like NiAl. It is also adopted by a number of halides having useful optical properties: as shown in Figure 6.2, CsBr, CsI, TlCl, and TlBr transmit in part of the ultraviolet (UV), all of the visible (the shaded region), and the near infrared (IR).

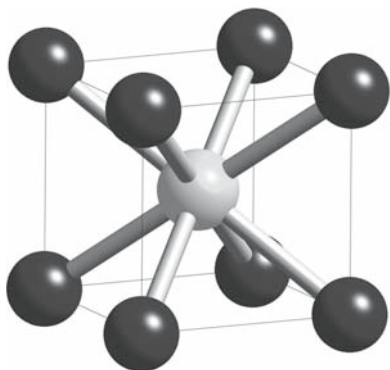


FIGURE 6.1 CsCl crystal structure. The polyhedron is the cube.

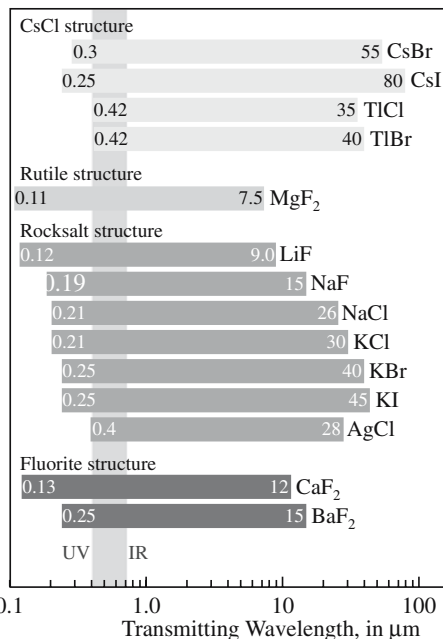


FIGURE 6.2 Range of transmittance for halide samples grouped by structure. (Each sample is 2mm thick; 10% cut off.) The vertical band shows the visible range.

6.3 NaCl (MgO, TiC, PbS)

The NaCl (rocksalt or halite) structure is quite simple and is found for sulfides and carbides and some oxides, including MgO, CaO, SrO, BaO, CdO, FeO, and NiO. The anions are in an fcc arrangement and all the octahedral interstices are occupied by cations, as shown by Figure 6.3. The CN is 6 for both anions and cations.

The NaCl structure can be represented as follows:

- Two interpenetrating fcc lattices: one of anions and the other of cations displaced by $\frac{1}{2}\langle 001 \rangle$ or by $\frac{1}{2}\langle 111 \rangle$
- An fcc lattice with a two-atom (Na-Cl) basis (Na^+ at 0,0,0 and Cl^- at $\frac{1}{2}, 0, 0$ or alternatively Na^+ at 0,0,0 and Cl^- at $\frac{1}{2}, \frac{1}{2}, \frac{1}{2}$)

Of course, this structure is actually not close packed even though we have an fcc arrangement of anions. In the fcc metals each atom has 12 nearest neighbors (CN is 12); in NaCl each ion has six nearest neighbors (CN is 6), so the packing of the anions must be less dense than fcc. (By Pauling's rules, the octahedral interstice between the Cl^- ions must be larger than the minimum or the structure will be unstable.)

For MgO (magnesia or periclase), $r_{\text{Mg}^{2+}}/r_{\text{O}^{2-}} = 0.6$ so that the Mg must be surrounded by oxygen ions in an octahedral configuration. The bond strength (valence/coordination), $S_{\text{Mg}} = +\frac{2}{6} = +\frac{1}{3}$ so each O^{2-} must also be surrounded by 6Mg ions. There is not a lot of choice on how to join them. Notice that $r_{\text{Na}^+}/r_{\text{Cl}^-} = 0.56$, which is also >0.414 but less than 0.732.

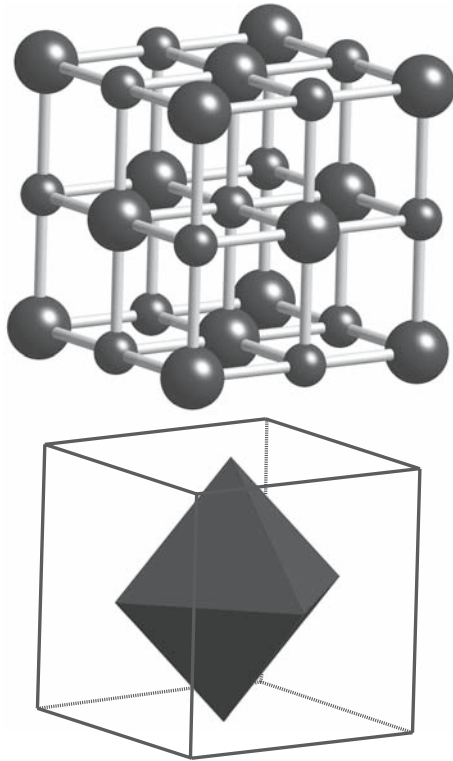


FIGURE 6.3 The NaCl crystal structure with Cl at 000. (Top) Ion positions; (bottom) an edge-sharing Cl octahedron.

FeO, CoO, MnO, and NiO are similar. NiO has the NaCl structure above its Néel temperature (523 K). Below this temperature magnetic ordering makes it rhombohedral. MnO and FeO behave similarly, but CoO undergoes a tetragonal distortion when the spins align; the Néel temperatures are 122, 198, and 293 K, respectively. Stoichiometric NiO is pale green. When heated in air it oxidizes and becomes a semiconductor.

Many of the oxides, carbides, and nitrides with the NaCl structure tend to be nonstoichiometric. Titanium monoxide exists over the range $Ti_{0.85}O$ to TiO , while FeO never occurs; it is always nonstoichiometric with a composition ranging from $Fe_{0.90}O$ to $Fe_{0.96}O$. As a consequence of these vacancies, the transition metal exists in two valence states, causing the oxide to exhibit semiconductor properties (as for NiO).

In the transition metal carbides and nitrides, think of the metal as being in the close-packed arrangement with the carbon or nitrogen atoms located in interstices. The coordination number can again be determined by the radius ratio, which in this case is given by r_x/r_m where r_x is the radius of the interstitial atom and r_m is the radius of the metal atom. Some values of atomic radius and radius ratios for transition metal carbides and nitrides are given in

TABLE 6.1 Atomic Radius and Radius Ratios for Some Carbides and Nitrides

Metal (<i>M</i>)	Ti	Zr
Atomic radius (nm)	0.147	0.160
C/M ratio	0.525	0.482
N/M ratio	0.511	0.470

Table 6.1. The radius-ratio values given in Table 6.1 are consistent with a CN of 6 based on the critical radius ratios given earlier in Table 5.4. The interstitial atoms are located either in an octahedral site or in the center of a trigonal prism. For the transition metals, the tetrahedral interstices in the close-packed structures are too small for C or N.

All the octahedral interstitial sites are occupied in the NaCl structure. In general, when the radius ratio is less than 0.59 the metal atoms form very simple structures. The interstitial atom and its nearest metal neighbors comprise a structural unit. We can consider the structure of these materials as a metal structure with occupied interstitial sites. In the carbides and nitrides there are no C–C or N–N interactions.

Some of the nitrides and carbides such as NbC, TaC, and ZrN, which adopt the NaCl structure, are low-temperature superconductors. Although there is no evidence that this property is a direct consequence of the crystal structure, the crystal structure may play an important role.

Carbides with the NaCl structure have high hardness, are chemically inert, and have high melting temperature. The best-known example is TiC. It melts at 3147°C, has a Knoop hardness of 2470 kg/mm², a Young’s modulus of 310 GPa, and is resistant to oxidation up to 1200°C (for more discussion of this see Chapters 16–18).

6.4 GaAs (β -SiC)

We can represent this structure as follows:

- Two interpenetrating fcc lattices one of anions and the other of cations displaced by $\frac{1}{4}\langle 111 \rangle$
- An fcc lattice with a two-atom basis (one atom at 0,0,0 and the other at $\frac{1}{4}, \frac{1}{4}, \frac{1}{4}$)

This structure is rather open: the atomic packing factor (APF) for GaAs is only 0.41. In the GaAs structure each atom has only four nearest neighbors; the coordination number (CN) for both Ga and As is 4. The structure is shown in Figure 6.4 in 3D. The (110) projection is important because it clearly shows the tunnels along the $\langle 110 \rangle$ direction

II–VI, III–V, AND IV–IV

The classical name for this structure is zinc blende or sphalerite (ZnS).

GaAs, InP, InSb, etc. are not minerals.

Cubic SiC is known as carborundum or moissanite.

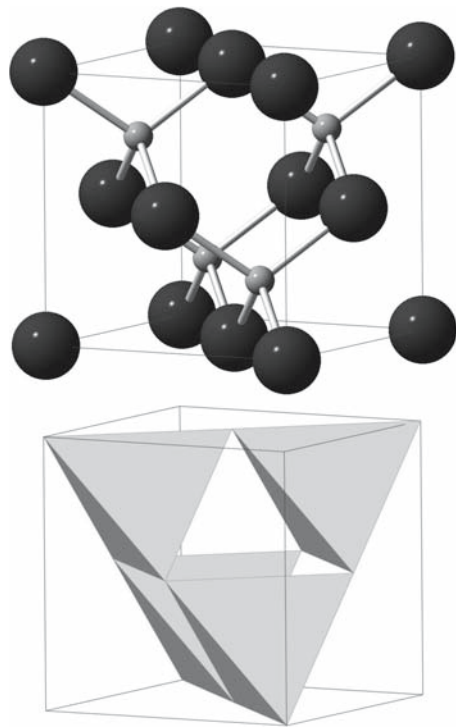


FIGURE 6.4 The zinc-blende crystal structure. (Top) Ion positions; (bottom) corner-sharing tetrahedra.

(remember that there are six equivalent $\langle 110 \rangle$ directions). You will see many high-resolution transmission electron microscope (TEM) images recorded with this sample orientation since it optimizes the detail seen in the image. An example is shown in Figure 6.5.

We can form the structure by stacking the anions in an fcc sequence and then filling half the tetrahedral interstices with cations.

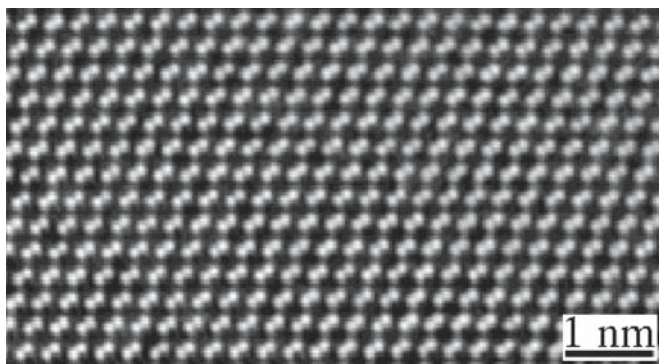


FIGURE 6.5 HRTEM image of GaAs showing the Ga-As 0.14-nm dumbbell.

TABLE 6.2 Relationship between Band Gap Energies and Bonding in III-V Semiconductors

Compound	E_g (eV)	Ionic character in bond (%)
AlP	3.0	9
GaP	2.35	6
AlAs	2.1	6
AlSb	1.55	4
GaAs	1.35	4
InP	1.30	4
GaSb	0.70	2
InAs	0.33	2
InSb	0.17	1

(% ionic character was calculated using Eq. 4.24)

We could have chosen to stack the cations and then fill the interstices with anions, but the anions are usually larger. Other isomorphous materials include InP, InSb, GaP (known collectively as the III-Vs), and cubic SiC.

Materials with a GaAs structure are usually semiconductors; this property is a direct consequence of the covalent bonding. In the III-Vs the band gap increases as the ionic component to the bonding increases, as shown in Table 6.2. If we replace all the Ga and all the As by C, Si, or Ge, we have the diamond-cubic (dc) structure of diamond, Si and Ge. Now the bonding is entirely covalent (and Pauling's rules would not work). We consider the GaAs structure again in comparison to AlN.

6.5 AlN (BeO, ZnO)

APPLY PAULING'S RULES

$$\text{BeO} \quad r_{\text{Be}^{2+}}/r_{\text{O}^{2-}} = 0.25$$

$$\text{ZnS} \quad r_{\text{Zn}^{2+}}/r_{\text{S}^{2-}} = 0.34$$

A second polymorph of ZnS is wurtzite (with a "t" in English but würzite in German). Many AB compounds such as AlN, GaN, BeO, and ZnO form in the

wurtzite and zinc-blende structures under different conditions. We can form the wurtzite structure by arranging the anions with hcp stacking and then filling half the tetrahedral interstices with cations. The structure is illustrated in Figure 6.6. The CN for both anions and cations is 4. The first nearest-neighbor environment in AlN is identical to that in GaAs but in GaAs there are four identical $\langle 111 \rangle$ directions whereas AlN only has one [0001] direction. Consider BeO: the bond strength is $S_{\text{Be}^{2+}} = +\frac{2}{4} = +\frac{1}{2}$. Each O^{2-} must be surrounded by four Be^{2+} . So the structure has to be created by stacking tetrahedra.

- For wurtzite we stack the tetrahedra ABABAB
- For zinc blende we stack the tetrahedra ABCABC

Although the theory clearly works beautifully, the catch is that the bonding between the Be^{2+} ions and the O^{2-} ions, or the Zn^{2+} ions and the S^{2-} ions, actually has a large

covalent component; sulfides in particular do tend to be covalently bonded. So it is not really correct to apply Pauling's rules that were developed for ionic materials!

Another material that can be grown in either the wurtzite or zinc blende forms is SiC. The bonding here is mainly covalent (~88%) since both Si and C are group IV elements. SiC is special in that it is very difficult to produce in a single structure. It always has the chemical composition SiC, but tends to be a mixture of the two stacking sequences. The two structures are two of the polytypes of SiC. The cubic form of SiC is being produced as a diamond simulant known as moissanite.

BeO and AlN have both been used for electronic packaging because of their high thermal conductivity. BeO has the higher thermal conductivity, but its powder is highly toxic.

ZnO is a semiconductor where the conductivity depends on an excess of zinc atoms; its use in varistors

PACKING IN ZnS

We have hcp packing of S^{2-} ions for wurtzite and fcc packing of S^{2-} for zinc blende. In both structures Zn^{2+} ions are located in half the tetrahedral interstices to maximize their separation.

relies on the properties of its grain boundaries as will be seen in Chapter 14. GaN is of great interest for manufacturing blue-green laser diodes and blue and green LEDs. In the future

it will be ubiquitous in solid-state white lighting for energy-efficient domestic use and is already the best material available for green traffic lights.

6.6 CaF₂

FLUORITE-STRUCTURE OXIDES

c-ZrO₂, CeO₂, UO₂

The mineral CaF₂ is known as fluorite, fluspar, and Blue John. The ionic radii are $r_{Ca^{2+}} = 100$ pm and $r_{F^-} = 130$ pm, so $r_{Ca^{2+}}/r_{F^-}$ is

~0.8. By Pauling's rules; the Ca^{2+} ions should have CN = 8 and the F^- ions should have CN = 4. Since the fluoride ions are larger, we should think of the structure as a simple cubic stacking of the F^- ions with the Ca^{2+} ions filling every other cube interstice. However, you may remember the structure better by arranging the Ca^{2+} ions on an fcc lattice and then placing the F^- anions on the $\frac{1}{4}, \frac{1}{4}, \frac{1}{4}$ sites. These are the sites occupied by the Ga in GaAs, but now we occupy all such sites not just half of them. There is a large unoccupied cube interstice in the middle of the cell at $\frac{1}{2}, \frac{1}{2}, \frac{1}{2}$ (the unoccupied site in the other description). The fluorite structure is shown in Figure 6.7.

Cubic zirconia (CZ) is stable only at high temperatures or when stabilized by the addition of a dopant. CZ is a well-known diamond simulant in jewelry. Ceria and urania are both stable in the fluorite structure. In UO₂, our alternate description of the structure is now clearly the better one: the U^{4+} ion is large. The unoccupied cube interstice

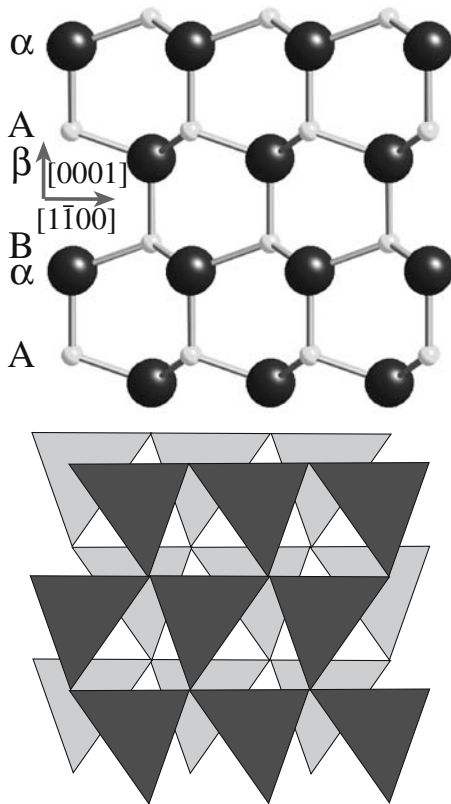


FIGURE 6.6 The wurtzite crystal structure viewed along [1120]. (Top) Ion positions showing the $A\alpha B\beta$ stacking; (bottom) two interpenetrating arrays of corner-sharing tetrahedra. (Only one set is needed to construct the crystal.)

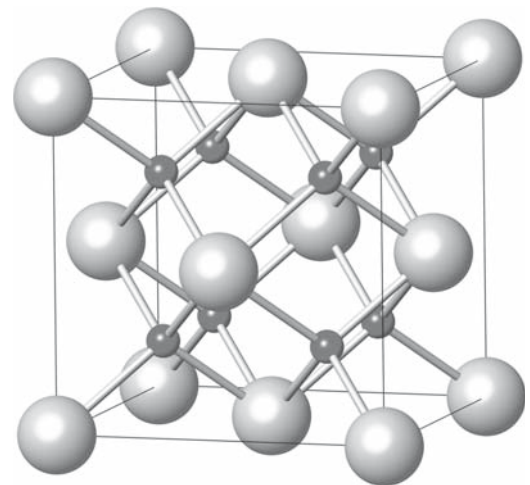


FIGURE 6.7 The fluorite crystal structure. The fluorine ions occupy the eight tetrahedral sites (or the Ca ions occupy half the cube sites with an empty one at the center of the unit cell).

at $\frac{1}{2}, \frac{1}{2}, \frac{1}{2}$ (in the center of the cell) in UO_2 is very important; it can accommodate nuclear fission products (like He) without straining the lattice. The oxides Li_2O , Na_2O , and K_2O are said to have an antifluorite structure because the location of the anions and cations is reversed relative to fluorite.

There is a great deal of interest in fluorides with the CaF_2 structure for optical applications. State-of-the-art production processes for semiconductor devices use deep-UV lasers to produce circuits with features as small as 130 nm. CaF_2 will then be the material of choice for semiconductor lithography. It is one of only a few materials that are transparent at the shorter wavelengths of deep-UV light (refer to Figure 6.2, CaF_2 is transparent down to 0.13 μm). The next major steps for lithography are expected to be systems using even shorter wavelength light, ultimately achieving feature sizes down to 70 nm when even CaF_2 will not suffice. You will also see top-of-the-line cameras using fluorite lenses so optical-quality CaF_2 will retain its value.

6.7 FeS_2

The structure of pyrite (fool's gold) is complicated but interesting. The Fe cations sit inside a sulfur octahedron. Three such octahedra then share a common vertex and there is no edge sharing. The S–S bond length within the octahedron is 0.307 nm or 0.332 nm, but the S–S bond that joins the octahedra together is only 0.218 nm long. The space group is $P\bar{a}3$ with $a = 0.542$ nm. It is instructive to compare pyrite and NaCl. The pyrite structure is shown in Figure 6.8. Both appear to have an fcc cell with the Cl being replaced by an S_2 dumbbell, but the dumbbells point

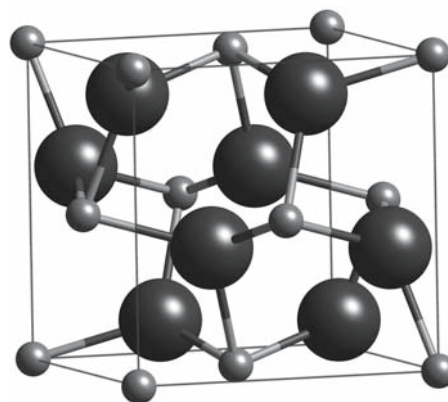


FIGURE 6.8 The FeS_2 crystal structure. The Fe ions occupy the fcc positions; the cubic cell also contains four S-S dumbbells.

along different directions for each of the edges. The result is that NaCl belongs to the $m3m$ class but pyrite belongs to the $m3$ class (still cubic but with a lower symmetry). Hence, NaCl has a 4-fold axis along $[001]$ while FeS_2 does not, but you can find large (>4 cm on the side) single-crystal cubes of pyrite. Many binary metal chalcogenides (compounds containing S, Se, or Te) have an FeS_2 structure, as do a few oxides (CdO_2 , $\alpha\text{-K}_2\text{O}$, $\beta\text{-Na}_2\text{O}$). Note that S is below O in the periodic table—so we might ask what is the charge on Fe in FeS_2 ?

Some relationships between the NaCl structure and materials with related structures such as pyrite are shown in Figure 6.9. This schematic is one illustration of how a simple structure can be systematically distorted to produce a host of new crystal structures.

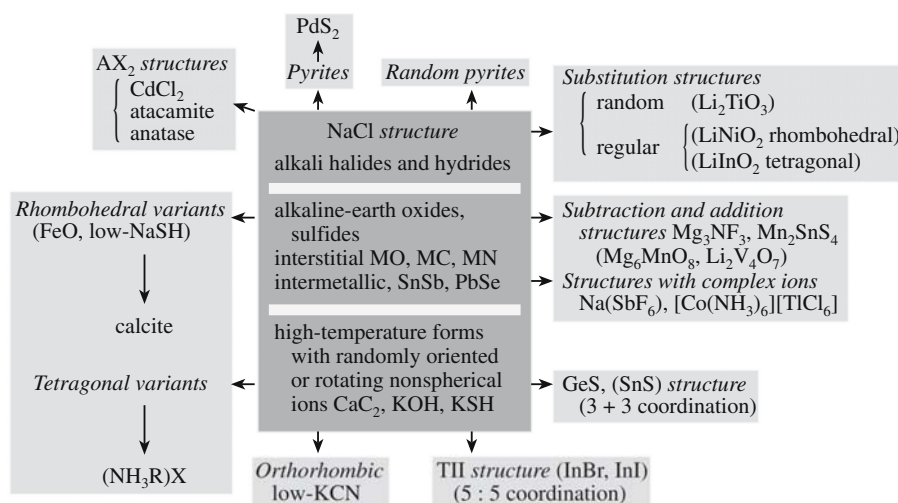


FIGURE 6.9 Schematic showing how two simple structures (NaCl and FeS_2) can be related to more complicated crystal structures.

6.8 Cu₂O

There are two main oxides of copper, Cu₂O and CuO. Cuprite, Cu₂O, is cubic with the $m\bar{3}m$ crystal group. It takes a little effort to imagine the structure. Start with the Si structure (dc) and replace all of the Si atoms with O²⁻ anions. Each anion is now surrounded by four other anions. Place a Cu⁺ cation between every pair of anions. Then, where there is no tetrahedron in the dc structure, insert a new filled tetrahedron. We could alternatively have just created the tetrahedra of anions with cations between each one, and then stacked the maximum number (without changing their rotation) into the cube. This structure is difficult to visualize!

A simpler way of remembering the structure is shown in Figure 6.10. Four Cu ions form an fcc unit cell and the two O ions occupy two of the tetrahedral sites. The O²⁻ ions are much larger than the Cu⁺ ions. (Remember how we think about the fluorite structure.)

This structure is particularly interesting because it consists of two linkages of tetrahedra that are rotated 90° to one another. The upper tetrahedron in Figure 6.10 is linked to another along the $[\bar{1}10]$ direction at the top and along the $[110]$ direction at the bottom (A connects to B). The second tetrahedron has the reverse arrangement.

Isomorphous oxides are Ag₂O and Pb₂O. Cu₂O and Ag₂O are p-type semiconductors because they contain excess oxygen atoms. The energy gap in Cu₂O is ~1.5 eV, and the impurity levels (acceptors) are about 0.3–0.6 eV above the valence band edge. Cuprite occurs naturally as a transparent red mineral.

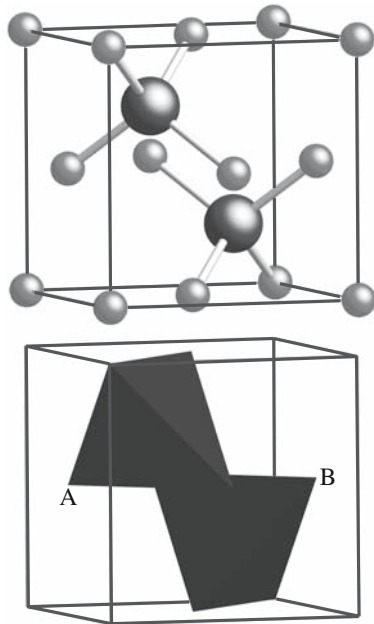


FIGURE 6.10 The Cu₂O crystal structure. (Top) Ion positions; (bottom) two “occupied” tetrahedra. The Cu ions sit at the fcc sites; two O ions “occupy” tetrahedral sites.

6.9 CuO

You might think CuO would have a simple structure (following CoO, NiO, and ZnO). Actually, tenorite (also known as melaconite) is monoclinic with the $2/m$ crystal class. The Cu atoms lie approximately in the middle of a square plane of four anions. Each anion is surrounded by four cations in what resembles a distorted tetrahedron. The square-plane coordination is the special feature of the cupric, Cu²⁺, ion. Knowing the complex structure of these oxides can help in understanding the oxidation mechanisms of Cu. The square-plane coordination seen in this binary oxide will be relevant when we later think about complex copper-based oxides, such as YBCO.

6.10 TiO₂

TiO₂ exists as rutile, anatase, and brookite. These structures are different and we cannot think in terms of simply packing oxygen anions and filling the interstices. Each of the TiO₂ structures consists of Ti⁴⁺ cations in the center of oxygen octahedra. In rutile, which has tetragonal symmetry, the structure is constructed by linking octahedra. An octahedron is placed at each of the eight corners such that two are actually sharing an apex (e.g., at T). The six points on these octahedra are then connected by one rotated octahedron sitting in the center of the unit cell. The edges of the octahedra thus link together to give chains along the z -axis, as shown in Figure 6.11. Each Ti⁴⁺ is thus surrounded by six O²⁻ ions and each O²⁻ anion is surrounded by three Ti⁴⁺ ions. The structure is primitive tetragonal with $a = 0.459$ nm, $c = 0.296$ nm, and two formula units per unit cell. The easiest projection is (001) where we are looking along the 4-fold axis.

In anatase, the arrangement of the anions and cations is similar and the crystal is again tetragonal, but now each octahedron is somewhat distorted and shares four of its edges with other octahedra. In brookite, the structure is even more complicated with octahedra sharing both edges and corners. So the trend rutile–anatase–brookite is to ever decreasing symmetry.

Rutile is the simplest compound of a family of titanates that has high dielectric constants ranging from $\kappa \sim 100$ for rutile to several thousand for BaTiO₃. Of the other oxides that share the rutile structure, CrO₂ is ferromagnetic with a Curie temperature of 389 K, and VO₂ and MnO₂ are antiferromagnetic with Néel temperatures of 343 K and 84 K, respectively. SnO₂ (cassiterite) and several binary fluorides such as MgF₂ are isomorphous. A lesser known isomorphous compound is stishovite, which is a high-pressure form of SiO₂.

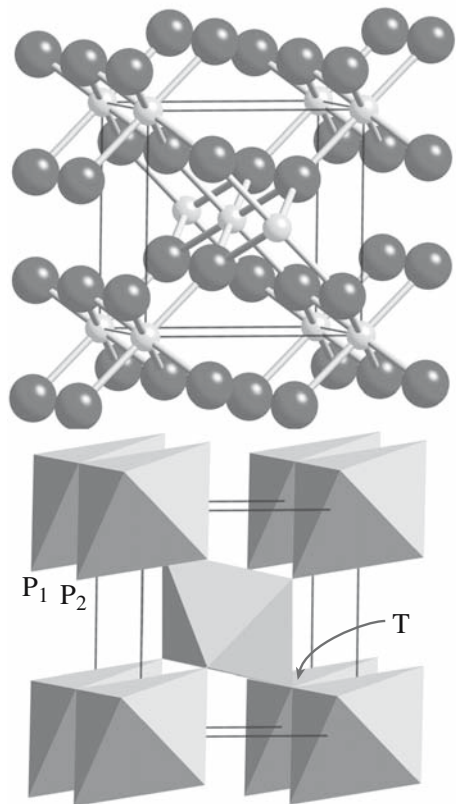


FIGURE 6.11 Rutile crystal structure viewed nearly parallel to the z -axis. Each of the pairs of overlapping octahedra (e.g., P_1/P_2) shares an edge. The two octahedra in the lower right thus have point T in common. The central octahedron touches each of the eight at the corners.

6.11 Al_2O_3

Alumina (the ceramic) or corundum (the mineral) refers to $\alpha\text{-Al}_2\text{O}_3$. When it is doped with Cr^{3+} the mineral is called ruby; when doped with Ti ions we call it sapphire. Natural sapphire actually contains a combination of Ti^{4+} and Fe^{2+} , which compensate the charge difference. Some of the Fe^{2+} can be replaced by Ti^{2+} so that the Fe:Ti ratio can vary. (We may also have Ti^{3+} present.) Hematite, Fe_2O_3 , is isomorphous with alumina; it actually has almost exactly the same c/a ratio. Ilmenite is closely related, but with Fe + Ti instead of Al + Al. Cr_2O_3 and Ga_2O_3 have a related structure. (In_2O_3 is completely different!)

The crystal structure of Al_2O_3 is trigonal with a $\bar{3}m$ crystal class, and has a pseudo-hexagonal oxygen sublattice (which is why we usually use a hexagonal cell and four-index Miller–Bravais notation) but the symmetry really is 3-fold, not 6-fold. In Al_2O_3 the oxygen ions have what can be thought of as hcp stacking with the Al^{3+} ions occupying two-thirds of the octahedral interstices (balancing the charge). The corundum structure is shown from two directions in Figure 6.12. Six parallel (0001) planes of oxygen ions are required to build the Al_2O_3 rhombohedral cell because the stacking is $A\alpha B\beta A\gamma B\alpha A\beta B\gamma$; the Al^{3+} ions always sit in the C positions (thinking of the ABC fcc

stacking), which is why we see the Al^{3+} ions when looking down the c -axis.

It is instructive to consider this structure in some detail. We can build it by stacking occupied octahedra (shown on the right). Each octahedron shares a face with the one above and the one below, but these are not regular octahedra. Pauling’s rules say that it is not favorable to share faces of polyhedra. To compensate, the Al^{3+} cations move away from each other and toward the unoccupied octahedron (e.g., P_1 and P_2) as can be seen in Figure 6.12; the oxygen anions move close together (e.g., the boxed group labeled S) to shield the nearby positive charges. The result is that the (0001) “plane” of Al^{3+} cations actually lies on two distinct (0001) planes. This also means that there are two different oxygen–oxygen ion distances in the octahedra. We saw a similar effect in Section 6.7.

Specific letters are used to designate several of the common crystallographic planes in corundum (Table 6.3). These different orientations are shown schematically in Figure 6.13. It is useful to know this convention, especially

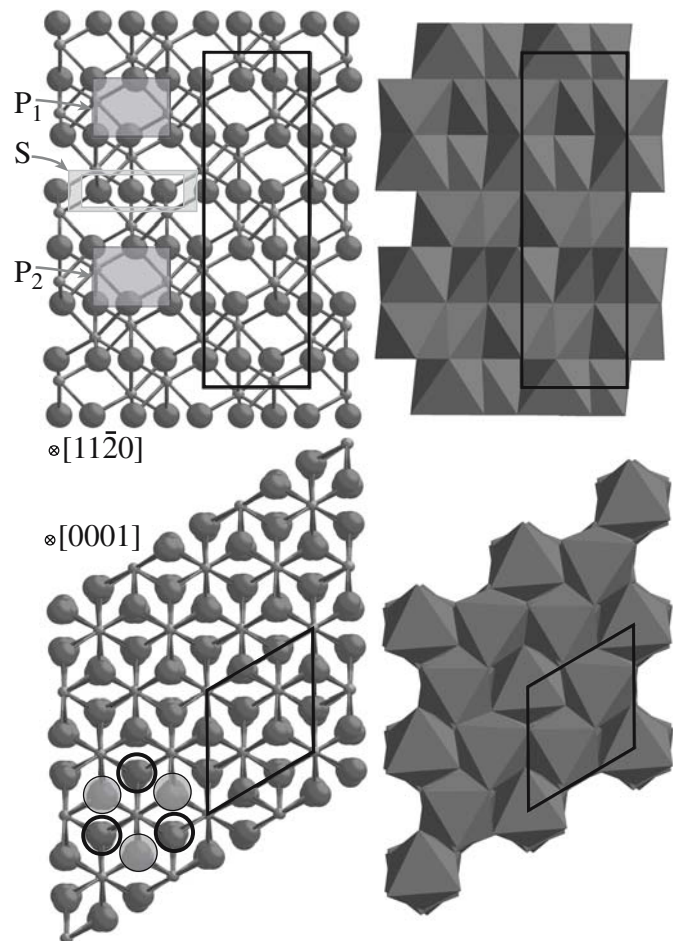


FIGURE 6.12 The sapphire crystal structure. (Top) $[11\bar{2}0]$ view; (bottom) $[0001]$ view; (left) atomic models; (right) stacking octahedra. P_1 and P_2 are two unoccupied octahedra. S is a triangle of more closely spaced O^{2-} ions. Open circles in the lower left show the AB stacking of the anions. The unit cell is outlined for both projections.

TABLE 6.3 Common Crystallographic Planes in Sapphire

Plane "name"	Miller-Bravais index	d spacing (nm)
a	(11 $\bar{2}$ 0)	0.2379
c or basal plane	(0001)	0.2165
m	(10 $\bar{1}$ 0)	0.1375
n	(11 $\bar{2}$ 3)	0.1147
r	(1 $\bar{1}$ 02)	0.1740

if you want to order or use single-crystal sapphire substrates.

Aluminum oxide is by far the most widely used compound with this structure. As a single crystal it is used in watch bearings and pressure-resistant windows. Hot-pressed powders are employed as electrical insulators, windows or radomes transparent to microwaves, envelopes for lamps, and electrical devices. In polycrystalline form it is also the basis of refractory bricks, crucibles, and spark-plug insulators.

6.12 MoS₂ AND CdI₂

MoS₂ and CdI₂ are based on the hcp structure. In molybdenite, the Mo atoms are located in the positions corresponding to the unit cell of the hcp structure. An S-S pair is centered along the *c*-direction directly opposite the Mo atoms, giving the structure shown in Figure 6.14. The stacking sequence can be written as AbA BaB, where the capital letters denote the S atoms and the lowercase letters the Mo atoms. The coordination number of the metal atom is 6, as it is in the TiO₂ and CdI₂ structures. Thus, we would

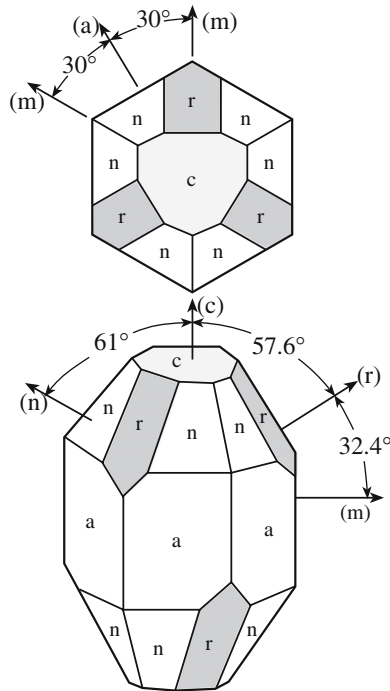


FIGURE 6.13 The location of important planes in sapphire.

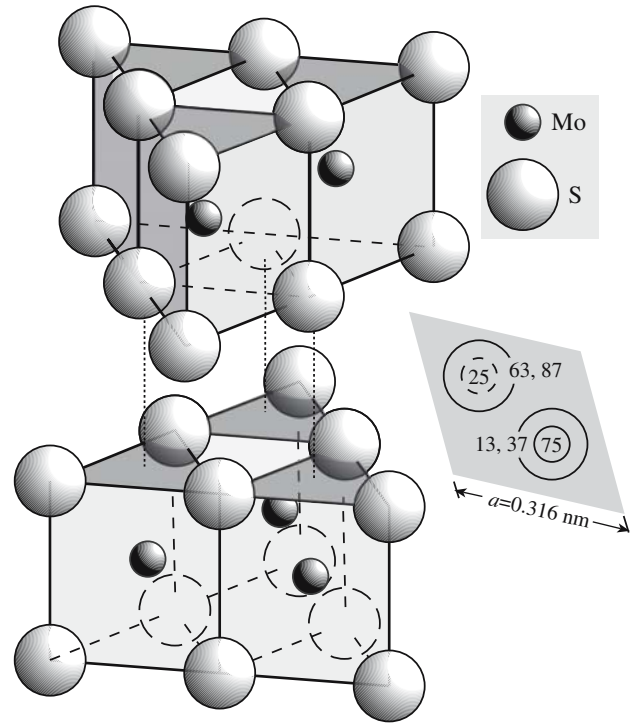


FIGURE 6.14 The crystal structure of molybdenite. The S ions stack AABB while the Mo ions occupy half the trigonal prisms in each S "sandwich".

expect that phases with r_M/r_X between 0.41 and 0.73 would form any of these structures. However, the more ionic compounds form the rutile structure, while the more covalent compounds have the CdI₂ structure. Those in which the bonding is intermediate adopt the MoS₂ structure.

Several of the Mo and W chalcogenides adopt the molybdenite structure, but MoS₂ is the most interesting phase and is an excellent (dry) lubricant. It is instructive to compare the MoS₂ structure to the structure of graphite, which is shown for comparison in Figure 6.15. The unit

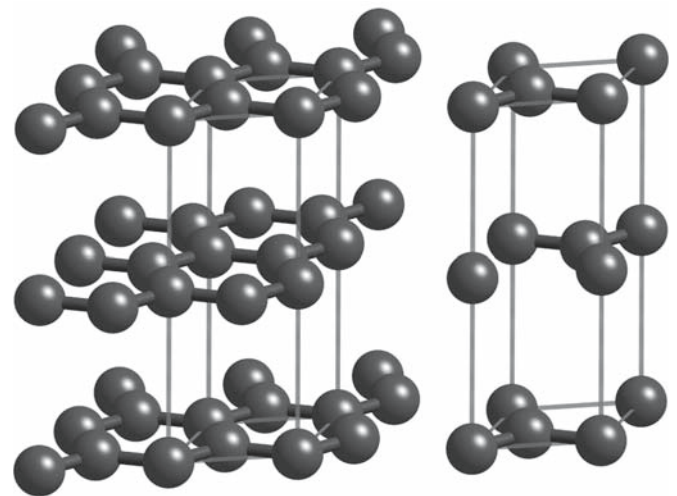


FIGURE 6.15 The crystal structure of graphite. The C atoms form hexagonal rings as seen on the left. A unit cell is outlined and is shown alone on the right.

cell of graphite is clearly hexagonal and has lattice parameters $a = 0.2456\text{ nm}$ and $c = 0.6696\text{ nm}$. The C–C bond length is 0.142 nm in the sheets and 0.335 nm between sheets. The six-membered rings are stacked to give an ABAB stacking sequence. It is the long bond distance in the c -direction that gives graphite similar properties as a solid lubricant. (Actually, it is the weak bonds between pairs of basal planes that cause the bonds to be long, which is the underlying reason.) As expected, graphite has highly anisotropic properties. The properties of graphite within the sheets are similar to those of a metal, whereas the properties perpendicular to the sheets are more like those of semiconductors.

Since in MoS_2 and graphite the interlayer, van der Waals, bonding is very weak, the structures can also exist in a rhombohedral form with a stacking sequence AbA BaB CcC; other layer materials naturally adopt this structure.

The crystal structure of BN is closely related to that of graphite except that the atoms in one layer lie directly above those in the next and the six-membered rings are made up of alternating B and N atoms.

This structure can also be derived from the hcp structure by replacing the metal atoms in the unit cell by I atoms and by adding Cd atoms at the corners of the unit cell. Thus, the I ions sit in an hcp arrangement with the Cd^{2+} ions between them. The more covalent AB_2 phases tend to form the CdI_2 structure. Thus, the larger polarizable iodides and bromides form this structure with highly polarizing cations, while the fluorides favor the rutile structure.

6.13 POLYMORPHS, POLYTYPES, AND POLYTYPOIDS

Polymorphs are materials that have the same chemical composition but different crystal structures. Many ceramic materials show this behavior, including SiO_2 , BN, BaTiO_3 , ZrO_2 , and BeO. Transitions between the different polymorphs may occur as a result of changes in temperature or pressure. The relationships between the polymorphic forms of silica are shown in Figure 6.16 with the corresponding transformation temperatures. These are not the only known phases of SiO_2 . At pressures around 2 GPa, quartz transforms into coesite. At even higher pressures, around 7.5 GPa, coesite transforms to stishovite. The high-pressure forms have been prepared experimentally and are also found at the famous Cañon Diablo Meteor site in Arizona. (We will examine these structures further in Chapter 7.)

When an element exists in different solid phases we refer to the phases as allotropes. Graphite and diamond are two allotropes of carbon.

Polytypism is a special—one-dimensional—type of polymorphism in which the different crystal structures

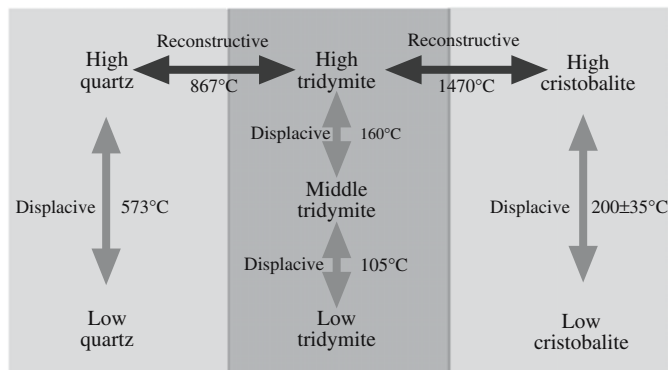


FIGURE 6.16 Schematic of how the polymeric forms of silica can be converted into one another by displacive or reconstructive structural transformations.

assumed by a compound differ only in the order in which a two-dimensional layer is stacked. The effect is common in layer structures (e.g., MoS_2 , graphite, and layer silicates). Silicon carbide (SiC), a ceramic material of considerable importance, displays the richest collection of polytypic forms. More than 200 SiC polytypes have been determined. Figure 6.17 shows the structural relationship between five of the different polytypes. Table 6.4 gives the stacking sequence and lattice parameters for the polytypes.

You will notice in Figure 6.17 that we have translated the usual cubic representation of the zinc blende cell into a rhombohedral one, which can be compared directly with the unit cells of the other SiC polytypes. A way of viewing the cubic (3C) cell as a rhombohedral cell is shown in Figure 6.18. The former cubic-cell diagonal has now become the c -axis of the corresponding rhombohedral cell. Of course, the arrangement of the atoms remains unchanged.

You will also notice that we introduced a new notation scheme in Table 6.4. The Ramsdell notation is frequently used when referring to different polytypic forms and describes the stacking sequence in these complex structures. The notation consists of a number and a letter. The number indicates the number of layers in the sequence. The letter indicates the structure type (C = cubic, H = hexagonal, R = rhombohedral). At one extreme we have the zinc blende SiC (3C) with pure cubic stacking in the [111] direction. At the other extreme we have wurtzite SiC (2H) with pure hexagonal stacking in the [0001] direction. The other polytypes have either H or R stacking sequences. For example, the carborundum III (B5) structure in Figure 6.17 has the Ramsdell symbol 4H—the sequence consists of four layers, then repeats, and the structure is hexagonal.

This chapter discusses the structure of a series of binary compounds that are also used as models for other compounds. All ceramics students must learn some of these structures by heart, but it is equally important to

TABLE 6.4 Relationship between Polytypes in Silicon Carbide

Structure	Strukturbericht	Stacking sequence	Lattice parameters		Ramsdell notation
			<i>a</i> (nm)	<i>c</i> (nm)	
Wurtzite	B4	AB	0.3076	0.5048	2H
Zinc blende	B3	ABC	0.308	0.755	3C
Carborundum III	B5	ABAC	0.3076	1.004	4H
Carborundum II	B6	ABCACB	0.3080	1.509	6H
Carborundum I	B7	ABACBCACBABCACB	0.3080	3.781	15R

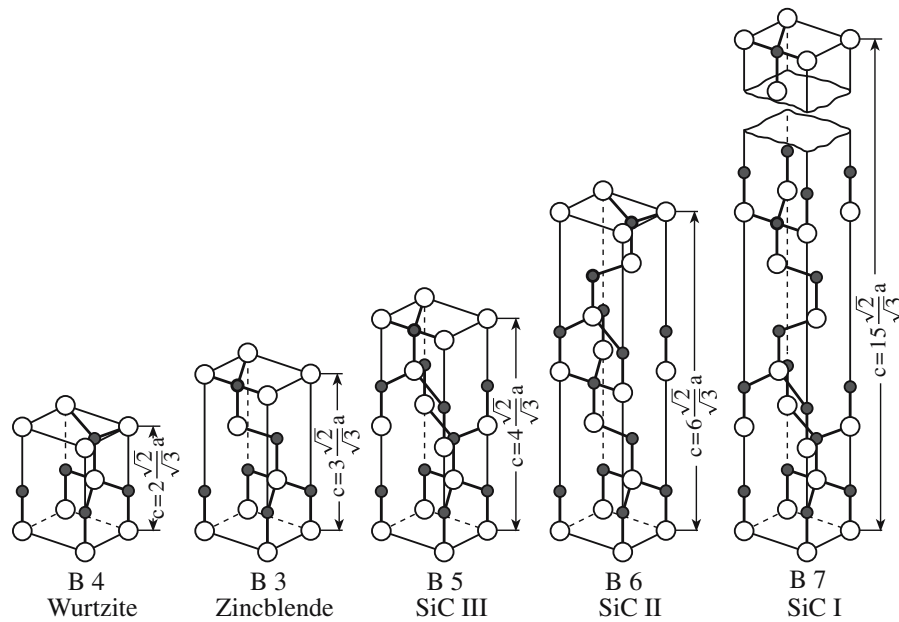


FIGURE 6.17 The stacking sequence for five SiC polytypes.

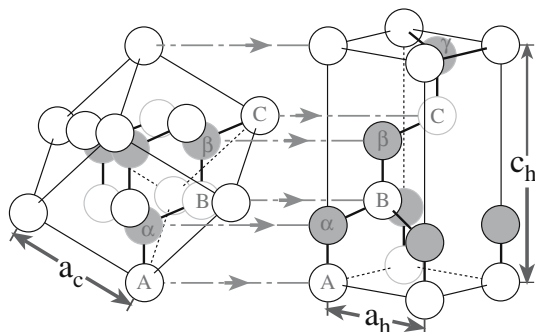


FIGURE 6.18 Relating the cubic and rhombohedral unit cells for zinc blende.

know the reason we chose these structures and how they relate to Pauling’s rule (Chapter 5). Also remember that Pauling’s rules were developed for ionic materials, so any covalent component may compromise the predictions. The polyhedra found in these simple structures reappear in much more complex structures as will be seen in Chapter 7. Each of the compounds has an application as illustrated here, but we concentrate more on those in later chapters. As an example, CaF₂ used to be known as an interesting structure and a semiprecious stone. That it would today be grown as 200-mm-diameter crystals for 135- μ m UV lithography would not have been imagined a few years ago. Although it is used for its optical properties, the orientation of the crystal must be controlled because the optical properties depend on the crystal orientation. The best large sapphire windows (with minimum birefringence) are cut from (0001) crystals. The crystal structure of crystalline materials controls most of the properties of these materials.

CHAPTER SUMMARY

To really understand ceramic materials, you must know their basic crystal structures. Then you can picture the polyhedra such as the tetrahedron and the octahedron and know what we mean when we talk about linking them, distorting them, substituting them, etc. Always keep in mind Pauling's rules. We have discussed the most important of the structures of the binary compounds: you must know CsCl, NaCl, GaAs, AlN, CaF₂, MoS₂, and Al₂O₃ by heart. We have also included FeS₂, Cu₂O, CuO, CdI₂, and TiO₂ in part because these materials are becoming more important in their own right, but also because they provide insight into many related binary compounds. Throughout this chapter and in Chapter 7 we have drawn many of the diagrams using CrystalMaker. This is an affordable program for the Mac and PC and should be available to every student taking any ceramics or mineralogy course. It is today's equivalent of the real (wooden) ball-and-(steel) stick models that used to be passed around the class but rarely were taken home to your dorm-room. It allows you to switch from ball-and-stick to polyhedra at the click of a mouse.

PEOPLE IN HISTORY

Bragg, W.H. and son W.L. Bragg did not discover X-ray diffraction, but they realized that it could be used to determine the structure of crystals. The first structure they solved was that of NaCl. They won the 1915 Nobel Prize in Physics "for their services in the analysis of crystal structure by means of X-rays." Aside from the Braggs, the other father and son tandem of Nobel laureates is the Thomsons (Sir Joseph Thomson, Physics 1906, and his son George Paget Thomson, Physics 1937) and the Siegbahns (Karl Manne Siegbahn, Physics 1924, and his son Kai Siegbahn, Physics 1981).

Coes, Loring, a high-pressure scientist, gave his name to the high-pressure form of quartz. He first synthesized coesite in 1953 in the Norton Laboratories.

Moissan, Ferdinand Frédéric-Henri began researching diamond synthesis in 1889. His idea was to produce diamonds by passing an electrical current through a sample of iron and sugar charcoal, then rapidly quenching it in cold water. However, after one experiment Moissan did isolate very small diamond octahedral crystals. After his death in 1907 it was revealed that one of Moissan's assistants had planted natural diamonds to make Moissan feel better. Moissan did actually make SiC, which was later given the name moissanite.

IUCr is the International Union of Crystallography. The Society publishes the journal *Acta Crystallographica*. IUCr recorded: "the very first specialized X-ray diffraction meeting with international representation was an informal one and was held at Ewald's mother's house on the Ammersee, Germany, in 1925. In addition to Ewald, the small group included W. L. Bragg, L. Brillouin, C. G. Darwin, P. J. W. Debye, R. W. James, M. von Laue, I. Waller and R. W. G. Wyckoff."

GENERAL REFERENCES

Bragg, W.L. and Claringbull, G.F. (1965) *Crystal Structure of Minerals*, Cornell University Press, Ithaca, Volume IV of the series *The Crystalline State*. If you have time to look at the original work, see this in your library.

CrystalMaker. www.crystallmaker.co.uk We repeat this information: you should try it.

Deer, W.A., Howie, R.A., and Zussman, J. (1996) *An Introduction to the Rock-Forming Minerals*. 2nd edition, Prentice-Hall, Englewood Cliffs, NJ. This is a classic for good reason.

Galasso, F.S. (1970) *Structure and Properties of Inorganic Solids*, Pergamon, Oxford. A useful reference that surveys a wide range of structures. Not as complete as Wells.

Hyde, B.G. and Anderson, S. (1989) *Inorganic Crystal Structures*, Wiley, New York. The structures of many crystals are beautifully described and related in this book.

Megaw, H. (1973) *Crystal Structures: A Working Approach*, W.B. Saunders Co., Philadelphia. This is such a nice text.

O'Keeffe, M. and Hyde, B.G. (1996) *Crystal Structures, I. Patterns and Symmetry*, Mineralogical Society of America, Washington, D.C. Another treasure.

Putnis, A. (1992) *Introduction to Mineral Sciences*, Cambridge University Press, Cambridge.

Wells, A.F. (1984) *Structural Inorganic Chemistry*, 5th edition, Oxford University Press, Oxford. This is the book that you go to first when you want to learn about a new structure. The price may mean that you consult it in the library rather than buying your own copy.

SPECIFIC REFERENCES

Ramsdell, R.S. (1947) "Studies on silicon carbide," *Am. Mineral.* **32**, 64. The original description of the notation.

Xu, X., Beckman, S.P., Specht, P., Weber, E.R., Chrzan, D.C., Erni, R.P., Arslan, I., Browning, N., Bleloch, A., and Kisielowski, C. (2005) "Distortion and segregation in a dislocation core region at atomic resolution," *Phys. Rev. Lett.* **95**, 145501.

EXERCISES

- 6.1 Draw and label (the ions and at least three directions) the [100], [111], and [110] projections for rocksalt, GaAs, CsCl, and fluorite.
- 6.2 Draw and label (the ions and at least three directions) the [0001], [1 $\bar{1}$ 00], and [11 $\bar{2}$ 0] projections for hematite.
- 6.3 Draw and label (the ions and at least three directions) the [0001], [1 $\bar{1}$ 00], and [11 $\bar{2}$ 0] projections for ZnO.
- 6.4 Estimate the radius of the cubic interstice in UO₂. Discuss this result using Pauling's rules.
- 6.5 You know the crystal class of FeS₂ and its space group. Explain the relationship.
- 6.6 Prove that the APF for GaAs is 0.41. The atomic radii for Ga and As are 0.135 and 0.125 nm, respectively. The lattice parameter is 0.565 nm.
- 6.7 The coordination number for silver and copper ions in Ag₂O and Cu₂O is four. This is quite unusual for these ions. What would you expect the coordination number to be based on the sizes of the ions and how might you explain the observed differences, if any. The ionic radii of the ions are given in Table 4.6.
- 6.8 Does rutile obey Pauling's rules?
- 6.9 How do the densities of high cristobalite and silica glass compare? You will need to dig for the data on this one—the library or the Internet.
- 6.10 NaCl, TiC, and PbS all have the same structure. Are they all good examples of Pauling's rules in action?

7

Complex Crystal and Glass Structures

CHAPTER PREVIEW

This chapter is separated from the previous one just to make it less overwhelming. We have demonstrated the principles in Chapter 5 and considered some of the simpler ceramic structures in Chapter 6. Now we are considering structures that have more than two chemically different atoms in the unit cell (like $\text{YBa}_2\text{Cu}_3\text{O}_7$), although some will still only have two components. We will include materials (like SiO_2) in which covalent bonds are particularly important and encounter materials involving secondary bonds such as van der Waals interactions (especially in the clay minerals).

It is a little difficult to learn these structures by heart but some, like cristobalite and perovskite, you should know. For others, you may survive by just knowing the basic ideas involved. This emphasizes the reason for this chapter (and Chapter 6)—if you understand the building blocks, you can better appreciate the properties of more complex structures that are composed of combinations of such building blocks. The logic behind the order in which these are discussed is first cubic, then the silicates (starting with silica), then the complicated ones, and finally some new materials that challenge our perception of what a ceramic is.

Glass has often been treated separately from ceramics, but today few programs in materials science have the time for a specialized course on glass. We include a discussion of glass structures in this chapter since they link so closely with the crystal structure of crystalline silicates and the general concept of coordination polyhedra. We will discuss the properties of glass later. Remember that the structure of glass is *not* random; it just lacks long-range order. We have point defects and other defects in glass just as we do in crystals; the challenge is to define the nondefective structure to which we can relate them. What makes a point defect in glass a defect and not just part of the glass?

A common mantra throughout this chapter is that diagrams are essential. A difficulty is that you generally need more than one diagram (view) to appreciate a three-dimensional (3D) structure. Computer programs can make the 3D aspects much more apparent.

In this and the previous chapter, the xyz -axes in the schematics of cubic crystal structures lie along the cube edges; the length of the cube edge is the lattice parameter.

7.1 INTRODUCTION

In most simple metal-oxide structures, $r_M \ll r_X$ and the structures can be built up by considering a nearly close-packed arrangement of oxygen ions with cations located in interstices. The ionic radius ratios given earlier are useful and provide a means of predicting the coordination number (CN) of a particular compound and often the predictions are in good agreement with observed values. In cases in which the observed CN differs greatly from the expected value, such as 12 for K^+ in mica, $\text{KAl}_3\text{Si}_3\text{O}_{10}(\text{OH})_2$, it is probable that the other ions present play the most important part in determining the arrangement.

The ions that are close to the transition values of the radius ratio can show variations in CN. An example is the

Al^{3+} ion ($r_{\text{Al}^{3+}}/r_{\text{O}^{2-}} = 0.38$), which sits inside oxygen tetrahedra in many aluminosilicates but inside octahedra in others (as is the case for Al_2O_3). The Al^{3+} ion has a CN of both 4 and 6 in sillimanite, both 5 and 6 in andalusite, but only 6 in kyanite, even though all three are stable minerals and all have the composition Al_2SiO_5 . Another example is the Zr^{4+} ion ($r_{\text{Zr}^{4+}}/r_{\text{O}^{2-}} = 0.51$), which is octahedrally coordinated in several crystals, e.g., CaZrO_3 (isomorphous with perovskite), but has a CN of 8 in zircon, ZrSiO_4 . As Pauling said, the size of the ion depends on the site that it occupies.

Table 7.1 lists some deviations from the CN predicted by radius ratios. Where the observed CN is larger than predicted there is a gain in electrostatic energy by increasing the number of nearest neighbors. This gain is larger than the energy expended in deforming the surrounding

TABLE 7.1 CN and Bond Strength, S, of Various Cations with Oxygen

Ion	r_M (pm)	CN_{theory}	CN_{obs}	S
B ³⁺	27	3	3, 4	1 or $\frac{3}{4}$
Li ⁺	76	6	4	$\frac{1}{4}$
Si ⁴⁺	40	4	4, 6	1
Al ³⁺	54	4 or 6	4, 5, 6	$\frac{3}{4}$ or $\frac{1}{2}$
Ge ⁴⁺	53	4	4, 6	1 or $\frac{2}{3}$
Na ⁺	102	6	4, 6, 8	$\frac{1}{6}$
Zr ⁴⁺	72	6	6, 8	$\frac{2}{3}$ or $\frac{1}{2}$
Ca ²⁺	100	6, 8	6, 7, 8, 9	$\frac{1}{4}$
Ce ⁴⁺	87	6	8	$\frac{1}{2}$
K ⁺	138	8, 12	6, 7, 8, 9, 10, 12	$\frac{1}{9}$

ions. Remember that the ions are not rigid spheres. Where the observed CN is smaller than predicted there is often an appreciable amount of covalent character to the bonding. Covalent bonds are strongly directional.

Why so much about silicates? Effort is devoted to silicates not just because they are the main constituents of the earth's upper mantle (and therefore the geological materials we most readily see), but because they are really ubiquitous (even when you do not at first realize it) and therefore provide many of our raw materials. We suspect that silicates also have an enormous range of unexplored applications. Silicates also link in with the second unusual topic for such a chapter, namely glass: many glasses are silicates that lack long-range order.

7.2 SPINEL

The mineral spinel is MgAl₂O₄. Spinel has the general formula AB₂O₄ although later we will also write it as AO · nB₂O₃, where n describes the nonequimolarity. Bragg and Nishikawa actually solved the spinel structure independently in 1915. The spinel structure is so important because the magnetic ferrites are spinels. For the ferrites we express the chemical formula as MO · Fe₂O₃, where M is a divalent metal ion like Mn, Ni, Fe, or Co (or a mixture of such ions).

Although structurally quite simple, spinel has a large number of atoms or ions associated with each lattice point in its Bravais lattice. The Bravais lattice is face-centered cubic (fcc), and the unit cell contains a total of 56 ions (32 oxygen ions). There are four lattice points per fcc unit cell and thus 14 ions associated (two formula units) with each lattice point.

In spinel we often think of the O²⁻ ions as sitting on the fcc lattice sites. Actually, they are generally slightly displaced from these exact positions. Considering the cations and thinking of MgAl₂O₄, the Al³⁺ ions now occupy some of the octahedral sites with the Mg²⁺ ions being located on tetrahedral sites. This arrangement is the “normal” as opposed to “inverse” spinel structure; most spinels are not exactly normal! Note that the arrangement of the oxygen ions is essentially the same as in MgO, but now some of the octahedral and some of the tetrahedral interstices are occupied instead of only the octahedral ones.

- Normal spinel: the A²⁺ ions occupy only tetrahedral sites and the B³⁺ ions occupy only octahedral sites.
- Inverse spinel: all the A²⁺ ions and half the B³⁺ ions sit on the octahedral sites; the tetrahedral sites are occupied now by the other half of the B³⁺ ions.

SOME IMPORTANT SPINELS	
γ -Fe ₂ O ₃	Maghemite
MgAl ₂ O ₄	“Real” spinel
NiFe ₂ O ₄	A classic ferrite
Fe ₃ O ₄	Magnetite

The arrangement of the cations is such that the lattice parameter of the spinel MgAl₂O₄ is close to twice that of the corresponding MgO. If we think

of the spinel cubic unit cell as divided into eight cubes, these smaller cubes would be almost exactly the size of the MgO unit cell. This means that six parallel {111} planes of oxygen ions are required to construct the rhombohedral cell rather than three.

Looking at some ionic radii, we can understand why the same structure can be formed with Ni or Co substituting for Mg. Similarly Fe or Cr can substitute for Al.

O²⁻, 140 pm; Mg²⁺, 72 pm; Ni²⁺, 69 pm; Co²⁺, 75 pm
O²⁻, 140 pm; Al³⁺, 54 pm; Fe³⁺, 65 pm; Cr³⁺, 62 pm

If we look at this structure along a [110] direction (Figure 7.1a and b), we can see the tetrahedra and octahedra. Remember that the anions are in an fcc stacking sequence, so this is a close-packed direction for the O ions. Spinel thus shows particularly clearly how a structure can be built up by systematically filling some of the octahedral (O) sites and some of the tetrahedral (T) sites. The apparently touching tetrahedra are actually at different heights in this projection, so they do not share an edge. The lines P₁ and P₂ remind you where the edge-on {111} planes lie. If we rotate the structure through 90° about the horizontal [110] axis, we reach the [001] projection shown in Figure 7.1c.

We can look at the structure in several ways. In Figure 7.1b, the cell has been divided into eight distinct layers of ions. This sequence is PqRsTuVw, where the upper case refers to mixed O²⁻ plus octahedral cation layers and the lower case refers to the tetrahedral cations. This method of building the structure emphasizes that there are only two different “planes” of ions to stack! The row of

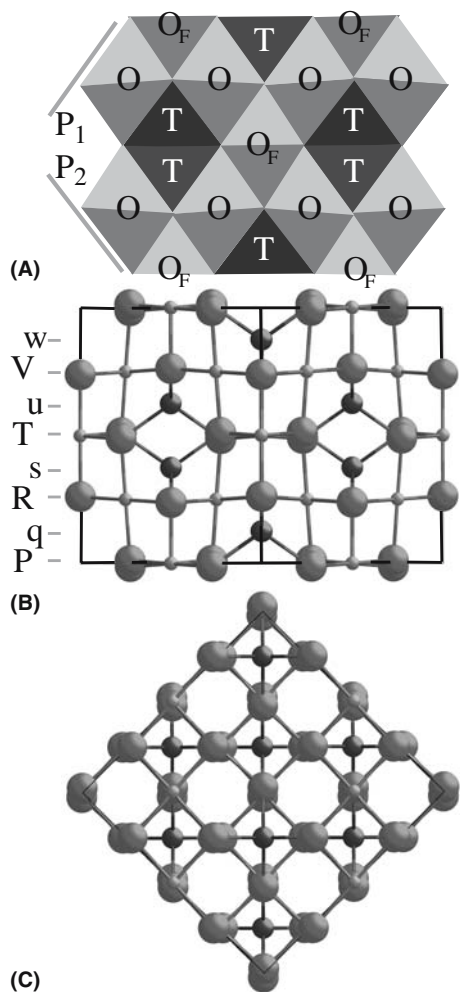


FIGURE 7.1 (a–c) The spinel crystal structure. The 32 anions in the unit cell form eight slightly distorted fcc oxygen lattices. The cations are then distributed with one tetrahedron occupied in each “subcell” (rather like Cu_2O). The 16 octahedral sites are then distributed in rows along one $\langle 110 \rangle$ direction or the orthogonal one depending on the layer [V,R or T,P in (b)].

octahedral sites actually rotates 90° every $1/4$ cell (i.e., every two layers). Hence layers P and T are shifted relative to one another, but are rotated 90° relative to R and V. The structure is effectively shifted by $1/4$ $[1\bar{1}0]$ every four layers (half way up the cell). (We will return to this stacking in Chapter 14.)

How did Bragg determine the spinel structure and how can you distinguish normal and inverse? X-ray diffraction measures the distribution of electrons and, hence, allows us to deduce atom position by measuring the structure factor. The positions x_n , y_n , and z_n are fractional coordi-

nates of atoms in the unit cell. Since the structure factor, F , depends on x_n , y_n , and z_n , the value of $F_{\text{normal}} \neq F_{\text{inverse}}$.

In $\gamma\text{-Fe}_2\text{O}_3$, the other cation is a “vacancy”; maghemite is known as a defect spinel and is related to the other important defect spinel $\gamma\text{-Al}_2\text{O}_3$ (although there may be other complications involving H^+ ions in this case). The Fe ions in magnetite occupy both tetrahedral and octahedral sites so it is FeFe_2O_4 , but we have not specified which ion (Fe^{2+} or Fe^{3+}) sits where. Spinel is notorious for being nonequimolar ($n \neq 1$, which does not mean the same as nonstoichiometric). When the formula is written as $\text{AO} \cdot n\text{B}_2\text{O}_3$, the value of n can vary from 1 to 3.5 depending on A, B, and T (temperature).

7.3 PEROVSKITE

With a general formula ABO_3 , the A cation and the anions effectively form an fcc array with a large octahedron in the center of the cell but no available tetrahedra (because of the charge). The ideal perovskite structure is simple cubic, and this is what we generally imply when we refer to the perovskite structure. The mineral perovskite is CaTiO_3 and is actually orthorhombic at room temperature, becoming cubic only at temperatures above 900°C . Other ceramics with the perovskite structure include BaTiO_3 , SrTiO_3 , and KNbO_3 , each being written in the general form ABO_3 . Do not confuse the structure with that of ilmenite, FeTiO_3 , which is related to the alumina structure.

The perovskite structure is shown in Figure 7.2a. Looking at the ionic radii, we can see a trend. The O^{2-} anion and the larger cation (A^{2+}) have similar radii, so that the structure is not just determined by O^{2-} . The larger cation and the anion combine to form a “close-packed” arrangement with the smaller cation, B^{4+} , sitting in the oxygen octahedral interstices. The octahedra then link together by sharing corners as shown in Figure 7.2b.

The bond strength is given as

$$\text{Ti}-\text{O} = +\frac{4}{6} = \frac{2}{3}; \quad \text{Ca}-\text{O} = +\frac{2}{12} = \frac{1}{6}$$

Each O^{2-} anion coordinates with two Ti^{4+} and four Ca^{2+} cations so that the total bond strength is

$$2 \times \frac{2}{3} + 4 \times \frac{1}{6} = +2$$

Barium titanate (BaTiO_3) is the prototype ferroelectric material. It has the ideal perovskite structure above 120°C . At temperatures below 120°C the small cation (Ti^{4+}) shifts

BaTiO ₃ AND KNbO ₃		
A	B	O
$r_{\text{Ba}^{2+}} = 135 \text{ pm}$	$r_{\text{Ti}^{4+}} = 61$	$r_{\text{O}^{2-}} = 140 \text{ pm}$
$r_{\text{K}^+} = 138 \text{ pm}$	$r_{\text{Nb}^{5+}} = 64$	$r_{\text{O}^{2-}} = 140 \text{ pm}$

CaCO ₃ AND CaTiO ₃
The carbonate is an inorganic salt. The anion is CO_3^{2-} , which is quite like a sphere, although it actually has 3-fold symmetry and is shown as a triangle in Figure 7.3. This anion and the Ca^{2+} are arranged in a similar way to NaCl but with a 3-fold distortion.

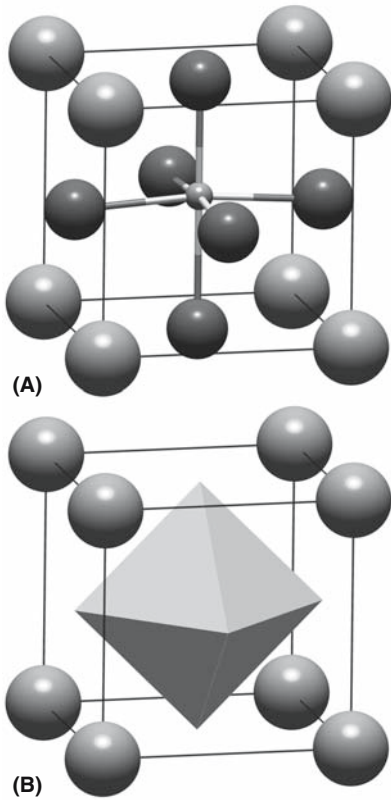


FIGURE 7.2 The perovskite crystal structure. The lattice is simple cubic with several cations able to occupy the central octahedron. (a) Atomic model; (b) the polyhedron.

off its ideal symmetric position at the center of each octahedral interstice. This shift creates an electric dipole; it polarizes the structure electrically, which in turn causes the material to become noncubic; this changes the cell dimensions. Spontaneous electrical polarization in the absence of an applied electric field is termed *ferroelectricity*. The link between electric field and mechanical deformation of the unit cell is known as the *piezoelectric effect*: it allows us to convert an electrical signal to a mechanical one and vice versa. This shift actually has the same origin as the flexibility of this structure: many ions can fit in the central octahedron.

The perovskite structure is particularly important for several reasons:

- Many perovskites are ferroelectric
- Many perovskites are piezoelectric
- Many perovskites have a high dielectric constant

The perovskite structure is also of interest to mineralogists. A mineral with the perovskite structure of composition close to MgSiO_3 is believed to be the predominant mineral in the lower mantle (depths of about 600 km) of the earth. The perovskite structure of MgSiO_3 is stable only at very high pressures.

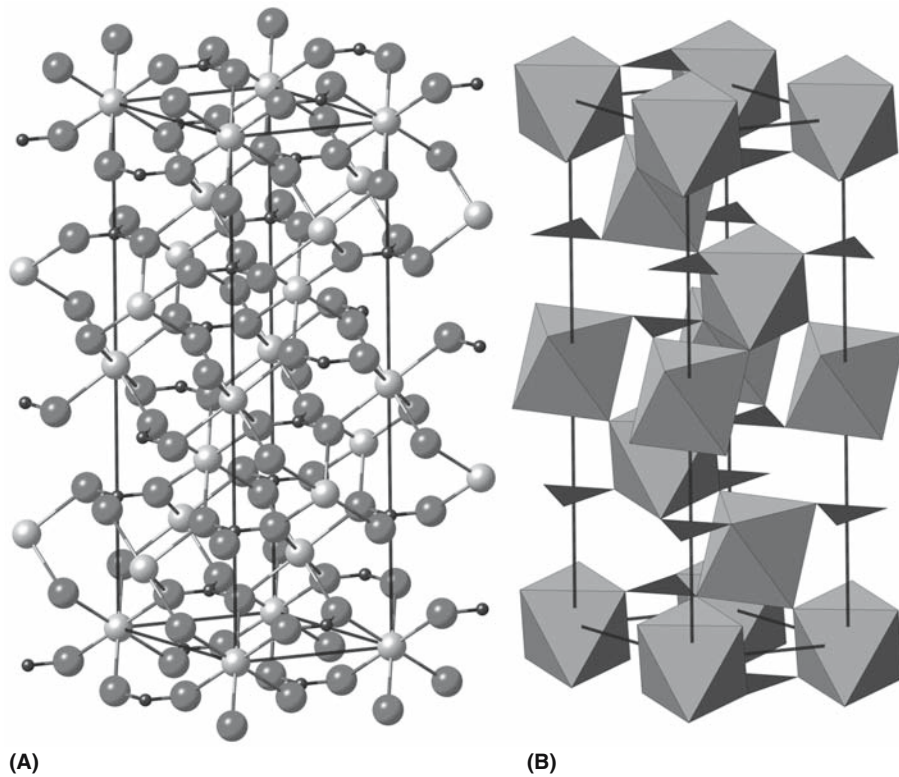


FIGURE 7.3 The crystal structure of calcite. The Ca^{2+} cations sit in an octahedral site; the CO_3^{2-} ions are represented as a triangle that each links six octahedra. The octahedra have one of two orientations each and “stack” in an ApBqCr sequence giving the 3 symmetry producing the c lattice parameter of 1.71 nm (a is 0.50 nm).

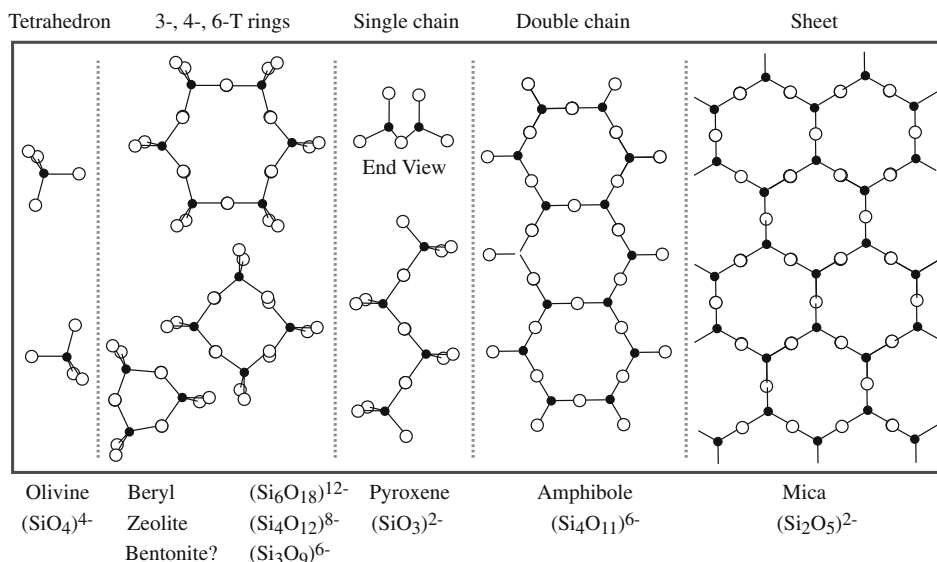


FIGURE 7.4 Arranging SiO_4 tetrahedra in different silicates. The exception is the sheet that extends indefinitely in all directions in the plane. These are the best known ways of combining (or not) the SiO_4 tetrahedra.

Perovskites have also received much attention since 1986 because the superconducting oxide YBCO contains perovskite structural elements. The importance of this structure was again realized in 1993 when the phenomenon of colossal magnetoresistance (CMR) was discovered in a range of manganate ceramics with a layered perovskite structure similar to that found in YBCO and other high-temperature superconductors.

7.4 THE SILICATES AND STRUCTURES BASED ON SiO_4

We can start by considering ionic radii and Pauling's rules.

$$r_{\text{Si}^{4+}}/r_{\text{O}^{2-}} = 0.40/1.40 = 0.29 < 0.41$$

Thus, tetrahedral coordination is expected and the bond strength, S , is $+1 (= +\frac{4}{4})$. The $(\text{SiO}_4)^{4-}$ units are the building blocks for all silicates; each O^{2-} ion is coordinated with two Si^{4+} ions, so the tetrahedra join at corners. Actually there is a very large covalent component too so that the Si–O bond is very strong (it is only ~40% ionic); therefore Pauling's rules do not really apply and we just talk about the SiO_4 unit and take account of the charge separately.

Some possible linkages of SiO_4 tetrahedra are illustrated in Figure 7.4. This is a key idea in understanding silicates. We can either keep the SiO_4 tetrahedra separate or link them to one another. If we link them, then we can form chains or rings. Then we can join rings to make sheets or join chains to make double chains. Units formed by these combinations are listed in Table 7.2.

To give you an idea of the variety of structures that are then possible, a discussion of just the structures (not properties—just structures) of rock-forming minerals consisting of isolated SiO_4 tetrahedra is the subject of a 900-page text. Table 7.3 lists some examples of the classes of silicates with special structures; Table 7.4 gives an idea of the complex crystallography involved. Clearly, we cannot go through all the ideas of silicates since this is an enormous field. You should know the general principles, the bonding, etc., and the language!

A special feature of the silicates is that it is often quite easy to replace the cations that are outside the SiO_4 tetrahedra. This leads to the idea of isomorphous replacement. We can even replace the Si^{4+} in the SiO_4 tetrahedron with other similar sized ions such as Al^{3+} having the same oxygen coordination. The idea is that $r_{\text{Al}^{3+}}/r_{\text{O}^{2-}} = 0.39$, which is close to 0.41. Al^{3+} can have six or four coordination. To balance the charge we also need to replace some

TABLE 7.2 Linking SiO_4 Tetrahedra to Make Silicates

Number of shared vertices	Structure unit	Structure formula
0	$[\text{SiO}_4]^{4-}$	Orthosilicates
1	$[\text{Si}_2\text{O}_7]_n^{6-}$	Pyrosilicates
2	$[\text{SiO}_3]_n^{2n-}$	Pyroxene chain
2.5	$[\text{Si}_4\text{O}_{11}]_n^{6n-}$	Amphibole
		Note the difference between this and infinite-sheet clays (Si_2O_5)
3	$[\text{Si}_2\text{O}_5]_n^{2n-}$	
4	$[\text{SiO}_2]_n^0$	3D network

TABLE 7.3 Examples of Silicate Structures

Orthosilicates	Forsterite Fayalite Monticellite Grossular	Olivine and garnet refer to groups containing many well-known minerals
Ring silicates	Beryl Cordierite	Rings of SiO ₄ tetrahedra connected at a corner
Chain silicates	Enstatite Diopside	Pyroxenes are single-chain compounds
Sheet silicates	Muscovite Biotite Talc	Mica and kaolinite refer to groups of sheet silicates
Framework silicates	Anorthite	Groups include the quartz minerals, feldspars, and zeolites

Na⁺ (say) by Ca²⁺. The following are two well-known examples:

- Forsterite and fayalite are structurally almost identical and thus form a continuous solid solution with Mg²⁺ gradually being replaced by Fe²⁺ across the series (as we go to fayalite).
- The feldspar minerals fall into two main series, the alkali (K–Na) feldspars, where we gradually replace Na⁺ by K⁺ across the series, and the plagioclase (Ca–Na) feldspars, where there is a continuous variation in composition by substituting Ca²⁺ + Al³⁺ for Na⁺ + Si⁴⁺.

7.5 SILICA

Silica has many different polymorphic forms (see Section 6.13). We will discuss three forms of SiO₂, namely quartz, tridymite, and cristobalite (note the spelling). For each form, at low temperatures (the α phase) we find a structure that is a distortion of the high-temperature form (the β phase). In each case, changing from the α to β structure

TABLE 7.5 Some Densities

Oxide	a (nm)	c (nm)	Density (g/cm ³)
High quartz	0.501	0.547	2.65
High tridymite	0.503	0.822	2.26
High cristobalite	0.713		2.32
MgO			3.59
Al ₂ O ₃			3.96

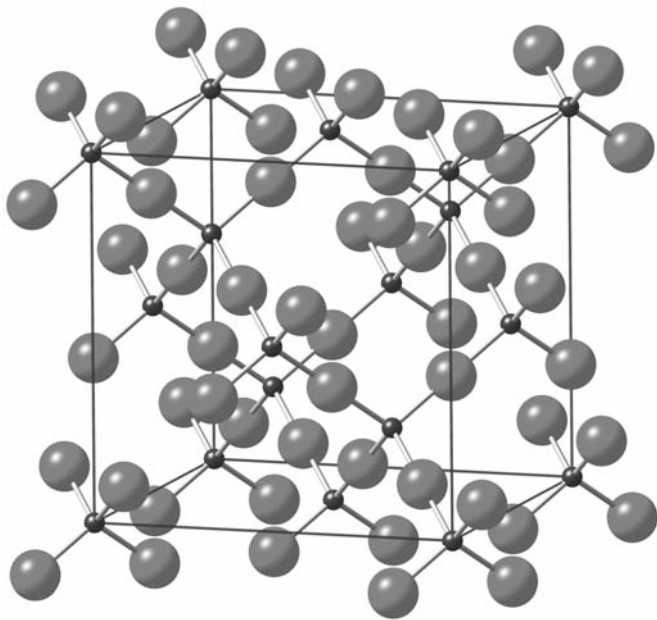
involves a displacive phase transformation; the atoms need to move only slightly relative to one another. However, to change from one form to another requires breaking bonds. This process is much more difficult and is known as a reconstructive phase transformation.

The Si–O–Si arrangement of ions does not always lie exactly on a straight line, especially for the low-temperature forms. If the bonding were purely ionic, the line would be straight and the O²⁻ should lie exactly in the middle: the reason in each case is that we want to maximize the electrostatic attractive forces and minimize the electrostatic repulsion. However, the Si–O bond is ~60% covalent, so there is a strong tendency toward directional bonding. The different forms of silica have different densities, each being much less dense than the more ionic oxides as shown in Table 7.5.

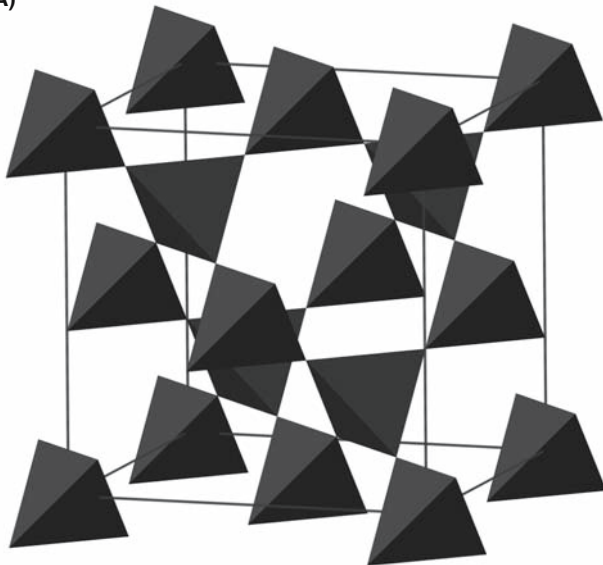
The structure of high cristobalite, showing the highest symmetry, is illustrated in Figure 7.5 as arrangements of atoms and as a stacking of tetrahedra. The Si⁴⁺ cations sit in the same positions as the Si atoms in the diamond-cubic (dc) Si structure. An O²⁻ anion is located between each pair of Si⁴⁺ cations! In high tridymite the Si⁴⁺ cations sit on wurtzite sites instead of zinc blende and the O²⁻ anion again sits between the cations! You can appreciate the movement that is needed to transform tridymite to cristobalite. When tridymite is found, it always contains small amounts of impurities. It is possible that these impurities are necessary to stabilize the structure.

TABLE 7.4 Some Silicates

Olivine	P mmm	Orthorhombic	Island silicate
Zircon	I 4/mmm	Tetragonal	Island silicate
Beryl	C 6/mmm	Hexagonal	Island silicate
Cordierite	C mmm	Orthorhombic	Ring silicate
Tourmaline	R 3m	Trigonal	Ring silicate
Enstatite	P mmm	Orthorhombic	Chain silicate
Talc	C 2/m	Monoclinic	Layer silicate
Mica	C 2/m	Monoclinic	Layer silicate
Cristobalite	F m3m	Cubic	Framework silicate
Albite	C -1	Triclinic	Framework silicate
Anorthite	P -1	Triclinic	Framework silicate



(A)



(B)

FIGURE 7.5 The crystal structure of cristobalite. The most symmetric of SiO_2 having cubic symmetry ($m\bar{3}m$) and a lattice parameter of 0.72 nm.

7.6 OLIVINE

The olivine minerals are orthosilicates: the SiO_4 tetrahedra are isolated from one another, meaning that the tetrahedra do not share oxygen ions. The structure is seen from two directions in Figure 7.6, which shows that the structure can be envisioned in a way that relates it to spinel and alumina. The hexagonal ABAB stacking of the anions seen in Figure 7.6a is just like alumina as is the view from normal to these close-packed layers shown in Figure 7.6b. Unlike alumina, some of the cations are in tetrahedral sites while others are in octahedral sites, like spinel; but unlike spinel, the two types of site are present between every close-packed layer of anions. Like spinel, the pairs

of tetrahedra are not actually sharing edges, as appears to be the case in Figure 7.6a. The result of this distribution of cations is that the crystal structure is orthorhombic with the b lattice parameter by far the longest at 1.02 nm; the a and c lattice parameters are 0.48 nm and 0.60 nm, respectively. The O^{2-} anions at the corners of the tetrahedra are linked by O–A–O bonds (A being Mg or similar); some tetrahedra point up and others point down. In forsterite, this Mg^{2+} ion is located at the center of an octahedron just as it is in MgO .

The best-known composition of olivine, the light green gemstone peridot, is $(\text{Mg}_{0.9}\text{Fe}_{0.1})_2\text{SiO}_4$. The olivines are a group of minerals showing isomorphous replacement.

- Forsterite, Mg_2SiO_4 : up to 10% Fe replaces Mg.
- Fayalite, Fe_2SiO_4 : up to 10% Mg replaces Fe.
- Monticellite, $\text{Ca}(\text{Mg},\text{Fe})\text{SiO}_4$: the Ca and Mg/Fe give an ordered stacking.
- Tephroite, Mn_2SiO_4 : this is a rare mineral that may contain Zn, Fe, or Mg substituting for Mn.

Olivine is one of the most important materials in the earth sciences.

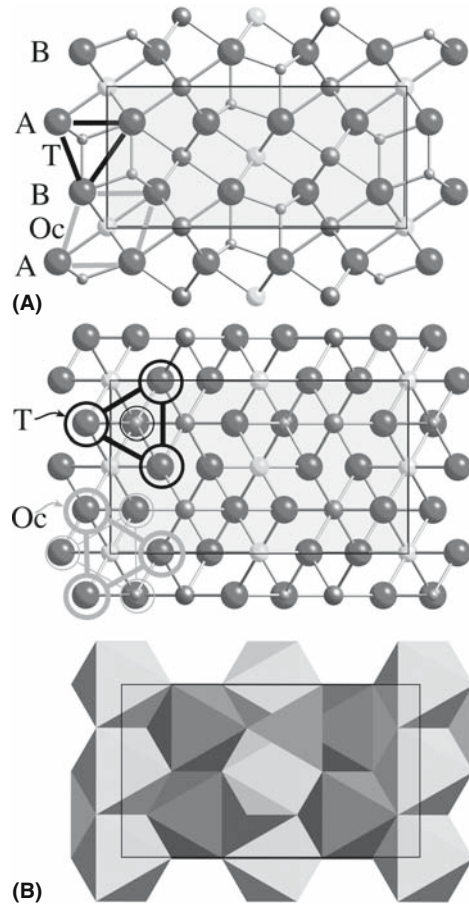


FIGURE 7.6 The crystal structure of olivine, an orthosilicate. (a) View along $[001]$; (b) view along $[100]$. Examples of octahedra and tetrahedra are outlined in both figures. Typified by forsterite, Mg_2SiO_4 .

TABLE 7.6 Examples of Garnets			
Garnet	Formula	Alternate	a (nm)
Pyrope	Mg ₃ Al ₂ Si ₃ O ₁₂	Mg ₃ Al ₂ (SiO ₄) ₃	1.146
Almandine	Fe(II) ₃ Al ₂ Si ₃ O ₁₂	Fe(II) ₃ Al ₂ (SiO ₄) ₃	1.153
Spessartine	Mn ₃ Al ₂ Si ₃ O ₁₂	Mn ₃ Al ₂ (SiO ₄) ₃	1.162
Grossular	Ca ₃ Al ₂ Si ₃ O ₁₂	Ca ₃ Al ₂ (SiO ₄) ₃	1.185
Andradite	Ca ₃ (Fe(II),Ti) ₂ Si ₃ O ₁₂	Ca ₃ Fe(III) ₂ (SiO ₄) ₃	1.205
Uvarovite	Ca ₃ Cr ₂ Si ₃ O ₁₂	Ca ₃ Cr ₂ (SiO ₄) ₃	1.202
Hydrogrossular	Ca ₃ Al ₂ Si ₂ O ₈ (SiO ₄) _{1-m} (OH) _{4m}		
YAG	Al ₃ Al ₂ Y ₃ O ₁₂	Al ₅ Y ₃ O ₁₂	
YIG (I: iron)	Fe ₃ Fe ₂ Y ₃ O ₁₂	Fe ₅ Y ₃ O ₁₂	
GGG	Ga ₃ Ga ₂ Gd ₃ O ₁₂	Ga ₅ Gd ₃ O ₁₂	

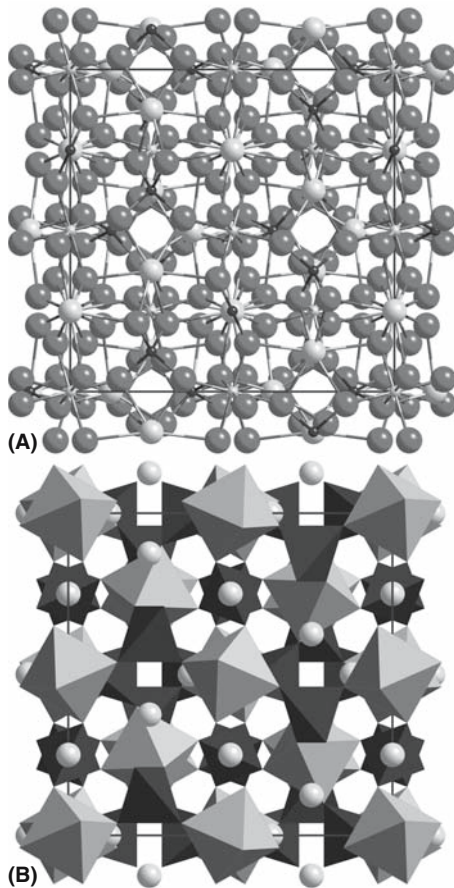


FIGURE 7.7 The crystal structure of garnet. The general formula is $A_3B_3(CO_4)_3$ where C is Si for the silicates. The B cation sits in an octahedral site while the largest cation A is located in a dodecahedron. The bcc unit cell has a lattice parameter of ~ 1.1 nm. With 20 atoms in the chemical formula there are 160 atoms in the unit cell.

7.7 GARNETS

Garnet refers to both the garnet group of silicates and the garnet structure, which is also adopted by nonsilicates. Some names and chemical composi-

RING SILICATES	
Beryl	Be ₃ Al ₂ Si ₆ O ₁₈
Cordierite	Al ₃ Mg ₂ (Si ₅ Al)O ₁₈
Tourmaline	XY ₃ Z ₆ B ₃ Si ₆ (O,OH) ₃₀ (OH,F)

tions of garnets are summarized in Table 7.6. The garnets have the general formula $A_3B_2(DO_4)_3$, where A and B refer to divalent and trivalent cations; D is Si in the case of silicates. In the nonsilicates, the structure is interesting because the same trivalent ion can sit in two very different sites, the A site and the B site. Important nonsilicate garnets include YAG (a laser host material) and YIG (a magnetic garnet)

It may help to remember the composition of YAG, say, by remembering that it is $4(X_2O_3)$, where X is a combination of trivalent cations. The structure is formed by combining DO_4 tetrahedra and BO_6 octahedra (at the corners). The 3D framework thus formed contains cavities that can be viewed as distorted cubes of a triangular dodecahedron as shown in Figure 7.7. The A cation sits in the large dodecahedral site (CN = 8). This is a very flexible crystal structure that has certainly not been fully exploited due to its complexity. However, many new garnets are now being produced such as the erbium-doped yttrium scandium gallium garnet [(Y,Er)₃Sc₂Ga₃O₁₂, or Er:YSGG] single crystals. These materials are being used for diode-pumped solid-state lasers that radiate in the 3- μ m range.

7.8 RING SILICATES

The ring silicates are also known as the metasilicates. Well-known ring silicates are beryl, tourmaline, and cordierite. The first two are mainly thought of as gemstones; all have interesting properties and cordierite has already found a special application. Its low coefficient of thermal expansion means that it does not fracture easily during rapid heating or cooling and thus finds use in refractories. In fact, it is the material used to form the honeycomb structure of catalytic converters.

The structures of beryl and cordierite are closely related: to change from one to the other replace $3Be^{2+} + 2Al^{3+}$ (= 12+) by $3Al^{3+} + 2Mg^{2+}$ (= 13+).

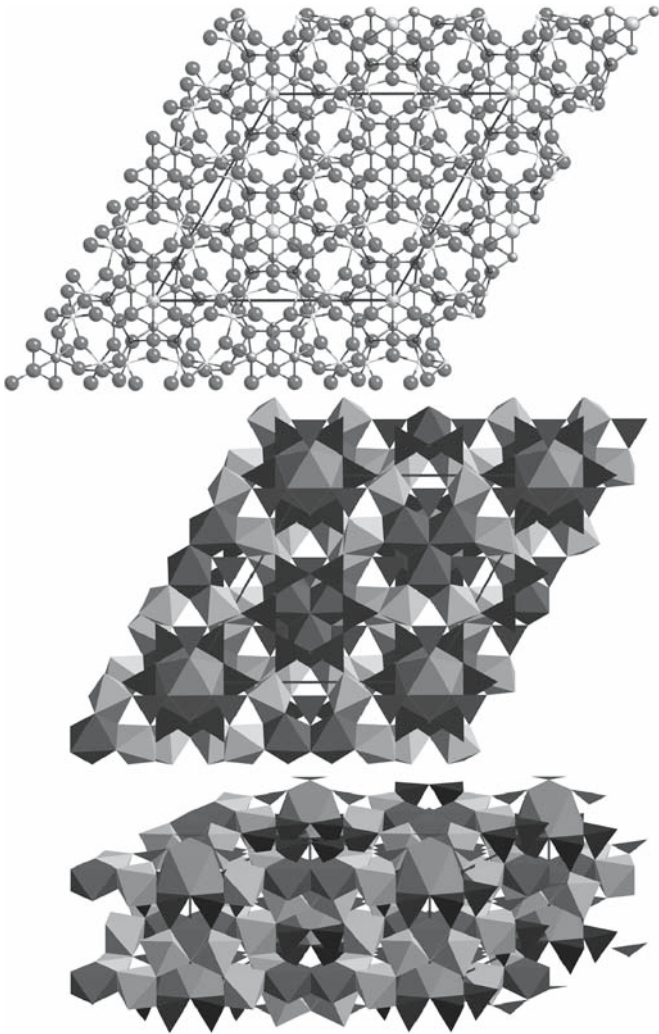


FIGURE 7.8 The crystal structure of tourmaline. The 3-fold axis can be seen. The lattice parameters are $a = 1.58$ and $c = 0.71$ nm. Most of the nominal 140 atoms in the cell sit in tetrahedral or octahedral sites, but the important boron ion sits at the center of three planar anions.

Then maintain overall neutrality by replacing one Si^{4+} ion by an Al^{3+} ion.

Tourmaline is quite complex, with one end member having the formula $\text{NaAl}_3\text{Al}_6\text{B}_3\text{Si}_6\text{O}_{30}(\text{OH})$. The structure shown in Figure 7.8 is interesting because it exhibits trigonal not hexagonal symmetry. Since it is piezoelectric, tourmaline was used in the 1940s as a pressure-sensing component in the A-bomb. It is now used by some to “attract inspiration and to promote understanding.”

7.9 MICAS AND OTHER LAYER MATERIALS

Micas have very special properties: they are very rigid, but cleave very easily along one plane. The crystal structure is well defined; the bonds within the layers are very

strong, but those between the layers are weak; hence they are known as layer materials. Before window glass was available, mica sheets were used as window material. We can easily cleave the sheets to produce a thin transparent ceramic.

Figure 7.9 shows the structure of mica. The van der Waals bonding between the sheets is not usually shown since it is so weak. Mica comes in several forms including muscovite, biotite, and the lesser-known phlogopite variety. Micas are used to provide easy paths for crack propagation in some commercial machinable ceramics.

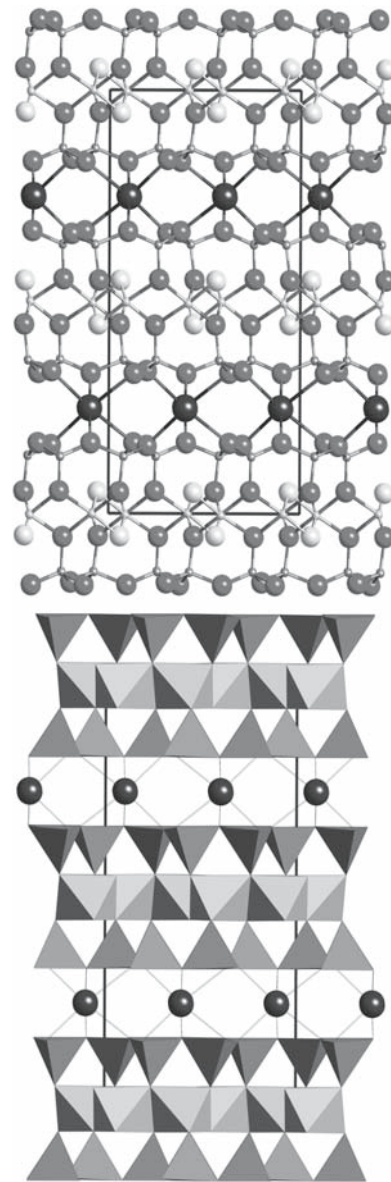


FIGURE 7.9 The crystal structure of mica showing the large K^+ ions forming a sheet of octahedral sites. The c lattice parameter normal to this sheet is 2.0 nm with a and b being much smaller, 0.52 and 0.90, respectively. The polyhedron model emphasizes the layer nature of the structure.

7.10 CLAY MINERALS

CLAY MINERAL GROUP Kaolinites Smectites Illites Vermiculites

Clay minerals are among the most important materials we know or have ever known since they form the basis of pottery and building bricks. The properties of clays are determined by the fact that they are layer materials. They are a subgroup of the layer silicates. In general, the clay minerals are hydrated aluminum silicates based on $(\text{Si}_2\text{O}_5)_n$ sheets.

Kaolinite $[\text{Al}_2\text{Si}_2\text{O}_5(\text{OH})_4]$ is the most common clay mineral; it is a 1:1 layer silicate, meaning that the structure consists of alternating layers of $[\text{SiO}_4]^{4-}$ tetrahedra combined with octahedrally coordinated aluminum ions as shown schematically in Figure 7.10.

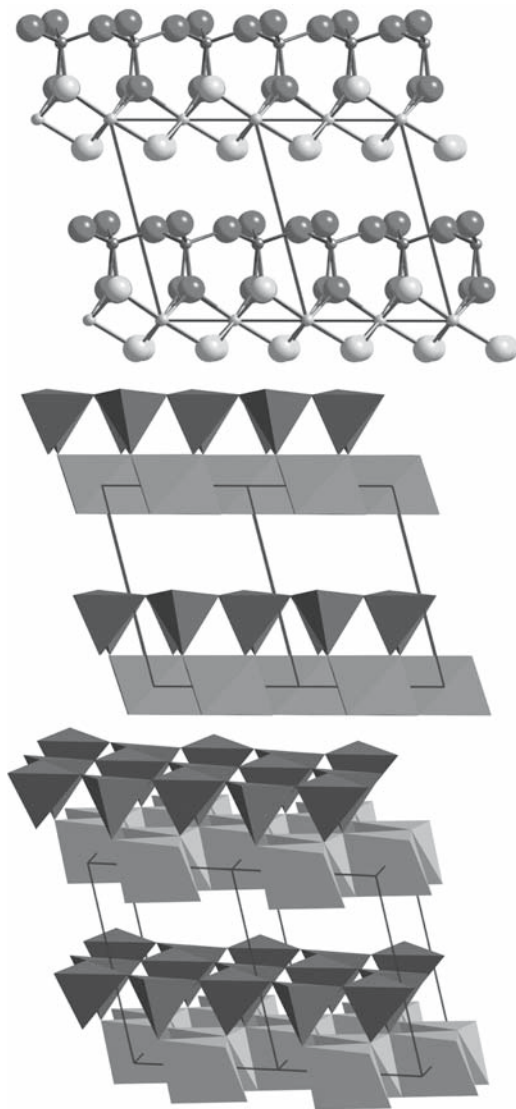


FIGURE 7.10 In the crystal structure of kaolinite, the SiO_4 tetrahedra form one side of the sheet while the octahedra contain OH^- on the outer layer attached to the Al^{3+} ions. The sheets are held together only by van der Waals bonds.

- In the tetrahedral sheet each $[\text{SiO}_4]^{4-}$ tetrahedron shares three corners, forming a continuous sheet with the general formula $(\text{Si}_2\text{O}_5)^{2n-}$.
- The nonbonded tetrahedral apices of the sheet all point in the same direction.
- These apices connect the tetrahedral sheet to the octahedral sheet.
- The O atoms at the apex of each tetrahedron are shared with an octahedral sheet.
- The octahedral sheet is made up of an array of edge-sharing octahedra with either (OH) groups or O atoms at the corners.

Because the charge must be balanced, Al^{3+} ions occupy only two-thirds of the octahedral sites in kaolinite. The linkage between the tetrahedral and the octahedral sheets imposes restrictions on their relative sizes. If the fit between the sheets is not ideal then the resultant misfit leads to the formation of small crystals, as the strain imposed by any misfit will increase with the area of the layer.

There is strong primary (covalent/ionic) bonding within each of the layers. However, the bonding between the layers is the weaker van der Waals type. Because the bonding is weak between the sheets, these silicates exhibit perfect one-directional cleavage.

Another member of the illite group is hydrous mica, in which the principal interlayer cation is K. A smectite you might encounter is montmorillonite; smectites can expand by incorporating water or organics between the structural layers. Vermiculite is derived from the Latin *vermiculare*, which means to breed worms, and describes what appears to happen when the material is heated rapidly. Otherwise it is very similar to phlogopite mica. As you would guess, most of these minerals have complex chemical compositions.

7.11 PYROXENE

The pyroxene group of minerals contains ferromagnesium silicates that occur in almost all types of igneous rock, so they are very important in mineralogy. Names you might encounter include enstatite, diopside, augite, jadeite, and spodumene; there are 20 accepted names of minerals in the group. The Si–O tetrahedra are linked at two corners and form an infinite chain parallel to the z -axis. The base of each tetrahedron is nearly parallel to the (001) plane. The chains are then linked laterally by layers of octahedra that contain six- or eight-coordinated cations such as Ca, Mg, Fe, or Na. The octahedra share edges and thus form continuous sheets on the (100) plane. A projection of the pyroxene structure is given in Figure 7.11.

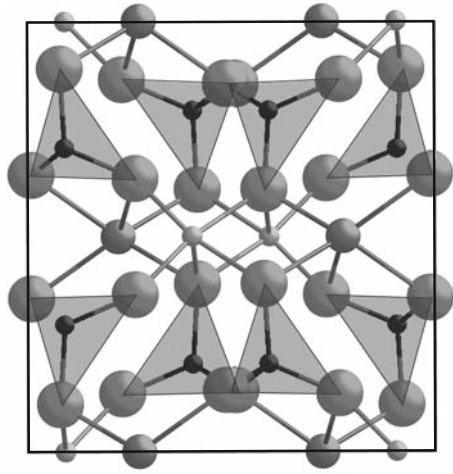


FIGURE 7.11 The crystal structure of a pyroxene (spodumene) shows layers of Li^+ (larger) and Al^{3+} (smaller) ions in octahedra alternating with layers of Si^{4+} in tetrahedra giving a nominal formula of $\text{LiAlSi}_2\text{O}_6$.

Diopside	monoclinic	$\text{Ca}(\text{Mg,Fe})\text{Si}_2\text{O}_6$ ($a = 0.975 \text{ nm}$, $b = 0.892 \text{ nm}$, $c = 0.525 \text{ nm}$, $\beta = 105.83^\circ$)
Enstatite	orthorhombic	$(\text{Mg,Fe})_2\text{Si}_2\text{O}_6$ ($a = 1.822 \text{ nm}$, $b = 0.881 \text{ nm}$, $c = 0.517 \text{ nm}$)
Jadeite	monoclinic	$\text{NaAlSi}_2\text{O}_6$
Spodumene	monoclinic	$\text{LiAlSi}_2\text{O}_6$

You can guess the complexity of the structure from the lattice parameters! While these materials are extremely important in mineralogy, they are not yet exploited much in ceramics.

7.12 β -ALUMINAS AND RELATED MATERIALS

The β -aluminas are a family of nonstoichiometric aluminates of which the most important have the approximate formulas $\text{Na}_2\text{O} \cdot 11\text{Al}_2\text{O}_3$ (β -alumina), $\text{Na}_2\text{O} \cdot 8\text{Al}_2\text{O}_3$ (β' -alumina), and $\text{Na}_2\text{O} \cdot 5\text{Al}_2\text{O}_3$ (β'' -alumina).

There are actually quite a few important ceramics that can be thought of as being constructed with layers of spinel separated by less dense arrays of cations. These include not only the β -aluminas, but also the magnetoplumbites and $\text{CaAl}_{12}\text{O}_{19}$ (CA_6 ; see Section 7.13). A model of the β -alumina structure is shown in Figure 7.12. We can think of this structure as being two twin-related blocks of spinel separated by a plane containing the large Na^+ ions. The result is that this “twin” plane is an open struc-

ture and that the c lattice parameter is large (2.12 nm for CA_6): it is a very anisotropic structure.

The Na^+ ions can move quite freely within the “twin” plane between the spinel layers; as a result the cation conductivity is high within these planes but negligible in the perpendicular direction. The high ion conductivity makes these ceramics of interest for battery applications, and this has been exploited in the Na–S cell. This cell was developed around 1965 by Ford Motor Co., but has not been used in production. The main difficulty is that the cell must be kept at an operating temperature of 350°C to keep the electrode molten.

The mineral barium magnetoplumbite has the chemical formula $\text{BaFe}_{12}\text{O}_{19}$ or $\text{BaO} \cdot 6\text{Fe}_2\text{O}_3$ and is perhaps the most important of the hexagonal ferrite since it is a hard magnet with the spins all aligned along the c -axis. This oxide is used in the magnetic stripe on credit cards.

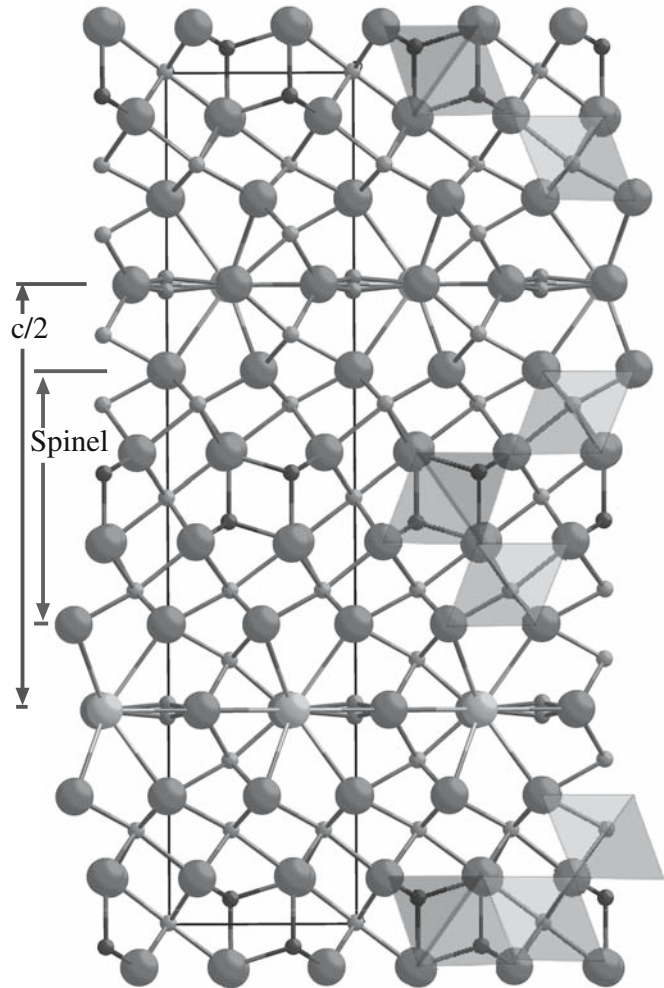


FIGURE 7.12 The crystal structure of β -alumina. The main features are the large value of c , the twinned spinel blocks, and the mirror plane containing the Na^+ (or K^+ or Ca^+) ion.

7.13 CALCIUM ALUMINATE AND RELATED MATERIALS

In Chapter 2 we mentioned cement and the reactions that occur during the setting and hardening of this material. There is a class of cements known as calcium aluminate cements (CACs) or high-alumina cements (HACs). These ceramics are not used as widely as Portland cement, but their attraction is the rapid hardening reactions. In 1 day CAC achieves the same strength as Portland cement achieves in a month.

The principal component present in CAC is calcium monoaluminate (CA in cement chemistry nomenclature, see Table 2.3). Its structure resembles that of β -tridymite, one of the polymorphs of SiO_2 . Rather than having $[\text{SiO}_4]^{4-}$ tetrahedral sharing corners in CA we have $[\text{AlO}_4]^{5-}$ tetrahedra. The large Ca^{2+} ion distorts the tridymite network and the structure is monoclinic.

The $[\text{AlO}_4]^{5-}$ tetrahedron is about the same size as the $[\text{SiO}_4]^{4-}$ tetrahedron and can form rings, chains, two-dimensional sheets, or three-dimensional networks in the same way by sharing oxygen corners. Other related calcium aluminates are also important in the chemistry of high alumina cements. The common feature of the structures of grossite (CA_2) and mayenite (C_{12}A_7) is that they too contain corner-sharing AlO_4 tetrahedra.

- Grossite, calcium dialuminate, is monoclinic. It is less reactive than CA.
- Mayenite, dodecacalcium heptaaluminate is cubic. It is the most reactive species in HACs.
- Hibonite, CA_6 , is found in Ca-rich aluminas and has a magnetplumbite structure (see Section 7.12).

7.14 MULLITE

Mullite is thought by some to be the most important ceramic, although (like spinel) the name now refers to a group of ceramic materials. It is an orthorhombic silicate made up of chains of AlO_6 octahedra running parallel to the z -axis and cross-linked by tetrahedra containing Si and Al. In Figure 7.13 these chains of octahedra (Oc) are seen at the corners and center of the unit cell and run into the paper; the two parallel chains are rotated relative to one another. The polyhedron labeled C is not a tetrahedron, although it looks like one in this projection; T is a tetrahedron though. Sometimes the structure is rather different (it is a derivative), but the material is still called mullite (or a mullite). Mullite, the mineral was originally from the Isle of Mull in Scotland, is $3\text{Al}_2\text{O}_3 \cdot 2\text{SiO}_2$ or simply $3/2$ -mullite. The composition actually varies over a wide range corresponding to $\text{Al}_2[\text{Al}_{2+2x}\text{Si}_{2-2x}]\text{O}_{10-x}$, quite a solid-solution range. The crystal structure can be related to that of sillimanite (Al_2SiO_5 , i.e., $x = 0$ in the general formula or $\text{Al}_2\text{O}_3 \cdot \text{SiO}_2$), but is much more complicated!

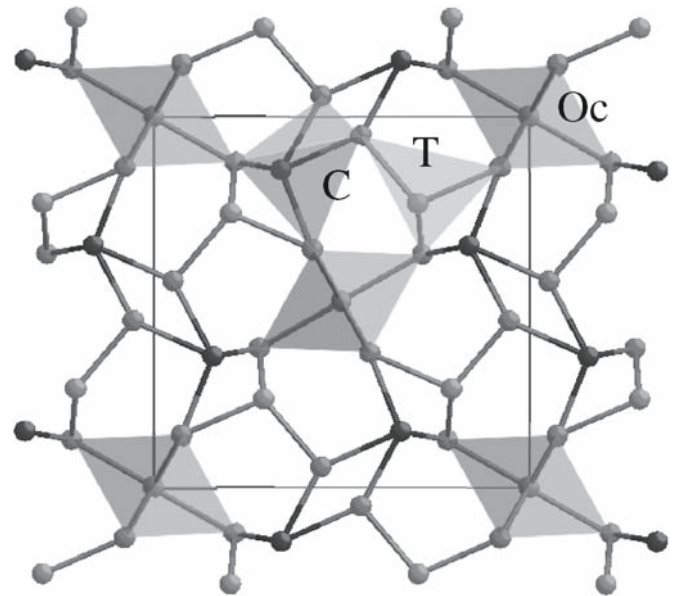


FIGURE 7.13 The crystal structure of mullite viewed along the short z -axis ($a = 0.76$ nm, $b = 0.77$ nm, $c = 0.29$ nm). The sites Oc and T are never fully occupied so this is an idealized schematic of this orthorhombic orthosilicate. The chains of octahedra at the corners and center lie along z .

This causes problems when determining Burgers vectors of dislocations—the details of the crystal structure can be different in different mullites. $2\text{Al}_2\text{O}_3 \cdot 2\text{SiO}_2$ has been produced synthetically. Fe^{3+} and Ti^{3+} can replace Al^{3+} ; it is a very accommodating structure.

Mullite has many important high-tech applications. We use mullite for coatings and for fibers. One use of mullite is in ceramic–matrix composites or CMCs; it has useful mechanical strength and has promise as the matrix for oxide-reinforcing fibers. Above all, when we heat a clay containing Al_2O_3 and SiO_2 we form mullite. Hence the claim that mullite is the most important ceramic and certainly the most important silicate for the ceramist.

7.15 MONAZITE

The mineral monazite has the composition LnPO_4 ; the anion is effectively $(\text{PO}_4)^{3-}$. In nature, the mineral actually consists of a mixture of several slightly different minerals since Ln (representing a lanthanide) can easily be replaced by one or more rare earths, such as Ce, La, Nd, etc., and usually also contains thorium. There is some disagreement on the lattice parameters for monazite in the literature, which may, in part, depend on its purity. There are also two unit cells in use:

1. Monoclinic, $P2_1/n$, with $a = 0.6782$ nm, $b = 0.7057$ nm, $c = 0.6482$ nm, and $\beta = 103.21^\circ$
2. Monoclinic, $P2_1/c$, with $a =$ same, $b =$ same, but $c = 0.6269$ nm ($a + c$ of “1”), and $\beta = 126.53^\circ$

The latter is correct by today's crystallographic conventions, but the former is found to be useful in describing defects such as twin boundaries, so you may encounter both. Monazite is the primary ore for Th, Ce, and La; the first of these means that it is often radioactive. Mineral engineers have long known that it is a principal source of Ce, but even then it often contains significant concentrations of ThO_2 . Until the mid-1990s, few ceramists had heard of it. Then it was found to be a potential coating material for fibers to be used in ceramic composites. In this application, the composition is usually chosen to be LaPO_4 .

7.16 $\text{YBa}_2\text{Cu}_3\text{O}_7$ AND RELATED HIGH-TEMPERATURE SUPERCONDUCTORS (HTSCs)

$\text{YBa}_2\text{Cu}_3\text{O}_7$ (YBCO) has an orthorhombic layered-perovskite structure, with $c \sim 3a$ and $a \sim b$, as shown in Figure 7.14a. The Cu and O ions are arranged as chains along the b direction between the Ba–O layers and as planes between the Ba–O and Y layers. Figure 7.14b shows how the YBCO structure is related to the perovskite struc-

ture. The structure consists of a sequence of oxide layers perpendicular to the c -axis as follows:

1. A Cu–O layer has two oxygen vacancies as compared with the “fully oxidized” YBCO perovskite. The Cu(1) site in this oxygen layer has CN = 4 and is surrounded by four oxygen ions in a square arrangement (as found in CuO). In $\text{YBa}_2\text{Cu}_3\text{O}_7$ this is the plane made by the CuO “chains.”
2. A Ba–O layer.
3. A Cu–O layer in which the Cu(2) has a CN = 5 and is surrounded by five oxygen ions that form a square-based pyramid. This is the plane we call CuO₂ plane.
4. A Y layer that has four oxygen vacancies as compared with the fully oxidized perovskite.

You will see in the literature that the chemical formula of YBCO is alternatively written as $\text{YBa}_2\text{Cu}_3\text{O}_{6+x}$ or $\text{YBa}_2\text{Cu}_3\text{O}_{7-\delta}$. The reason is that the material is almost always oxygen deficient. So which form is correct? $\text{YBa}_2\text{Cu}_3\text{O}_6$ is an insulator. It has to be doped to gradually become a metallic-like conductor and a superconductor below T_c . The doping is achieved by adding additional

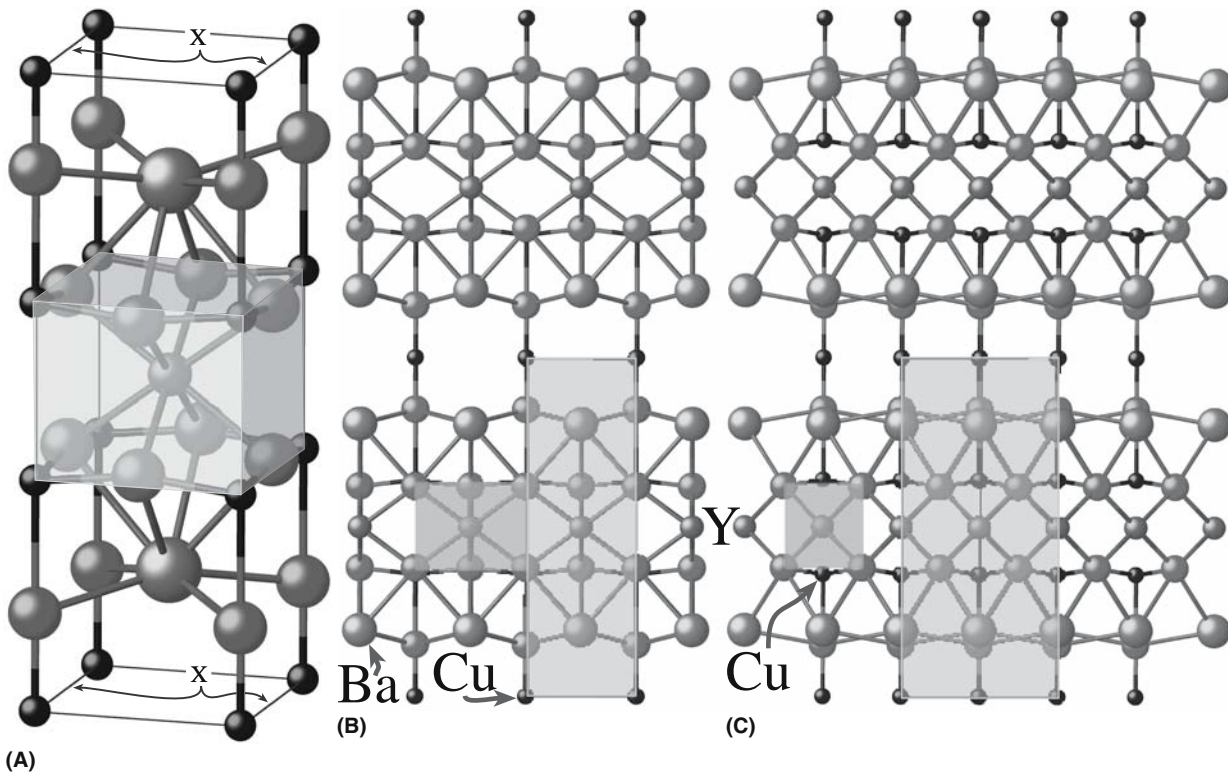


FIGURE 7.14 Models for YBCO. (a) The unit cell; the shaded region shows the perovskite unit with Y in the center and Cu at the corners, X points to the location of oxygen ions in the fully oxygenated orthorhombic ($a \neq b$) compound (with . . . O₇). The structure is more readily appreciated from (b) [100] and (c) [110] views, each showing six unit cells. Note how the perovskite “unit cell” is rotated 45° relative to the unit cell of the YBCO.

oxygen-forming CuO “chains.” These oxygen ions attract electrons from the CuO₂ planes that then become metallic. So the “correct” formula for YBCO is YBa₂Cu₃O_{6+x} where *x* corresponds to partial oxygen content:

For 0.0 < *x* < 0.4, YBa₂Cu₃O_{6+x} is an insulator.
 For ~0.4 < *x* < 1.0, YBa₂Cu₃O_{6+x} is a superconductor.

The oxygen content can be changed reversibly from 6.0 to 7.0 simply by pumping oxygen in and out of the parallel chains of CuO running along the *b*-axis. Careful studies indicate that the maximum *T_c* is reached for *x* ~ 0.93 (*T_c* = 94 K) and that for *x* = 1.0 *T_c* = 92 K. (The important point is that liquid N₂ boils at 77 K.)

It is thought that superconductivity essentially takes place within the quasi-two-dimensional CuO₂ planes. The Cu–O chains can be considered as a “charge-reservoir” that is needed to transfer charge into the CuO₂ planes. This means we can consider this HTSC as CuO₂ planes separated by a charge reservoir. Charge carriers are added by doping: adding oxygen to YBa₂Cu₃O₆, which enters the compound as O²⁻ and forms CuO chains. To maintain charge balance, electrons are removed from the copper oxide planes and the remaining holes are mobile (hence conduction). The properties are anisotropic (i.e., different along different directions). Therefore, the orientation of the individual grains is essential in the fabrication of polycrystals or epitaxial thin films.

The other high-temperature superconductors—bismuthates and thallates—are all layered structures with Cu–O planes present. The different phases are formed by stacking the same building-block layers in different sequences as shown in Figure 7.15 producing, e.g., Bi₂Sr₂CaCu₂O₈ (known as the Bi 2212 phase).

•	•	•	•	•	•
•	•	•	•	•	•
•	•	•	•	•	•
CaO	Ca	Ca	•	Ca	Ca
CuO ₂	CuO ₂	CuO ₂	•	CuO ₂	CuO ₂
SrO	SrO	SrO	BaO	BaO	BaO
Bi ₂ O ₂	Bi ₂ O ₂	Bi ₂ O ₂	Tl ₂ O ₂	CuO ₂	CuO ₂
CaO	Ca	Ca	BaO	Ca	Ca
CuO ₂					
SrO	SrO	SrO	BaO	BaO	BaO
Bi ₂ O ₂	Bi ₂ O ₂	Bi ₂ O ₂	Tl ₂ O ₂	Tl ₂ O ₂	Tl ₂ O ₂
CaO	SrO	SrO	BaO	BaO	BaO
CuO ₂					
•	•	•	•	•	•
•	•	•	•	•	•
2111	2122	2223	2021	2122	2223

FIGURE 7.15 Schematic of the different building-block layers that produce the biphasic oxide superconductors.

7.17 Si₃N₄, SiAlONs, AND RELATED MATERIALS

Most of the materials discussed so far in this chapter have been oxides, and, in general, ceramists have neglected nonoxides. Part of the reason is that materials are often processed, in a partial pressure of O₂. In what follows we will briefly introduce some of the exceptions that have not been mentioned previously.

Silicon nitride, Si₃N₄, exists in two forms designated as α and β. The structures and lattice parameters of these forms were determined by X-ray diffraction data.

α-Si₃N₄; hexagonal: *a* = 0.7748 nm; *c* = 0.5617 nm. Space group *P6₃/m*.

β-Si₃N₄; hexagonal: *a* = 0.7608 nm; *c* = 0.29107 nm. Space group *P31c*.

Each Si is at the center of a slightly irregular tetrahedron of nitrogen atoms. The SiN₄ units then share corners; each N is common to three tetrahedra. The structures differ in the arrangement of the tetrahedral units. Planes of atoms in the β form are linked along the [001] direction in a sequence ABAB . . . , whereas in the α form the sequence is ABCDABCD. . . .

The SiN₄ and SiO₄ tetrahedra are similar, except that whereas each oxygen atom in SiO₄ is common to two tetrahedra, each nitrogen atom in SiN₄ is common to three tetrahedra.

By substituting O²⁻ for N³⁻ and Al³⁺ for Si⁴⁺ we can form a family of compounds known as “SiAlONs.” These can be produced by high-temperature reactions between, for example, Si₃N₄ and Al₂O₃. The general formula for the SiAlONs is (Si,Al)₃(O,N)₄. Other metal atoms can be incorporated into the structure giving (Si,M)(O,N)₄; possibilities for M include Mg+Al, Li+Al, and Y.

The interest in β-C₃N₄ is that it is predicted to have a bulk elastic modulus comparable to diamond. Several attempts have been made, with varying degrees of success, to produce it in bulk and as a thin film. The structure of β-C₃N₄ is related to the β-Si₃N₄ structure. The CN₄ tetrahedra link by sharing N atoms. Each C atom has four nearest neighbors forming an almost regular tetrahedron, whereas each N atom has three nearest-neighbor C atoms forming 120° bond angles.

7.18 FULLERENES AND NANOTUBES

In Chapter 6, we discussed the structure of diamond and graphite—allotropes of carbon. The discovery of the C₆₀ molecule in 1985 introduced a new, third, ordered form of carbon—the fullerenes. The special new feature of C₆₀ (shown in Figure 7.16a) is the regular incorporation of five-sided rings of C atoms that allows the formation of curved sheets of carbon atoms. C₆₀ has 12 pentagonal (five-sided) and 20 hexagonal (six-sided) faces

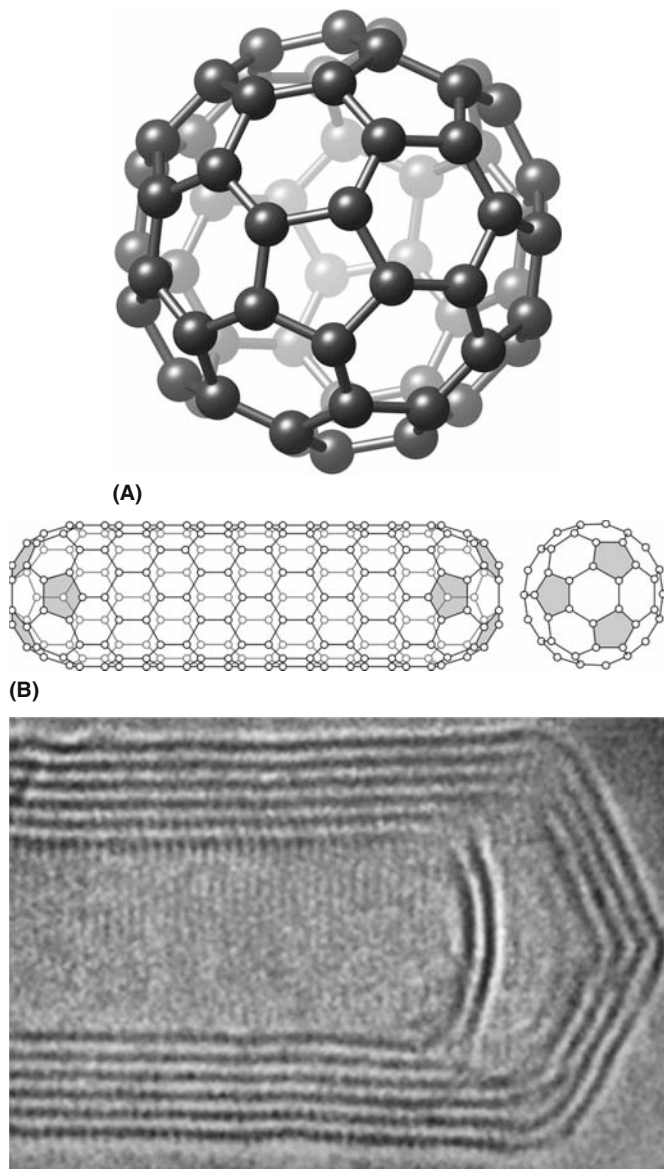


FIGURE 7.16 The structure of (a) C_{60} and (b) carbon nanotubes. (c) Image of the end of a six-layer carbon nanotube.

symmetrically arrayed to form a molecular ball; in fact, a soccer ball uses the same geometric configuration as fullerene.

In the solid state, the C_{60} molecules bind with each other through weak van der Waals forces and can self-assemble to form an fcc arrangement. At room temperature the size of the cubic unit cell is 1.4 nm, and the nearest-neighbor C_{60} - C_{60} distance is 1.0 nm. At lower temperatures the arrangement of the fullerenes may become simple cubic with a larger unit cell. In the fcc arrangements there are, of course, interstices with either an octahedral or tetrahedral character. Alkali metal atoms such as K or Rb can be incorporated into the interstitial sites to give a molecular formula of K_3C_{60} or Rb_3C_{60} . The interest in these doped fullerenes is that they are superconductors. The highest T_c in the series of alkali metal-doped C_{60} is 33 K for Cs_2RbC_{60} .

A wide variety of fullerene structures have been produced with the general formula C_n , where n can take on small (70) or very large values (240 and 540). In each case, the structure consists of 12 uniformly distributed pentagons connecting an array of hexagons.

Although pentagons are necessary to give an approximately spherical shape, by simply rolling a hexagonal graphite sheet we can produce carbon nanotubes. These objects can be considered as a new source of mesoporous ceramics. They are dimensionally confined in two directions. If the ends are closed, as shown in Figure 7.16b, we again need to incorporate the pentagon. Just as graphite grows as sheets, the single-walled nanotube (SWNT) can grow as a multiwalled nanotube as can be seen in Figure 7.16c. The “layer” spacing of the walls is usually what we expect from graphite except at the closed ends. It is an interesting exercise to take a single sheet of graphite (drawn on paper), roll it, and rejoin the bonds; you immediately realize that you can introduce a shear or chirality (like a screw dislocation along the tube). The chirality determines the electrical conduction along the nanotube.

Many variations on the C nanotube can be produced using other layer materials, such as MoS_2 . Tubes built from other oxides that are not layer materials might sometimes be better described as pipes.

7.19 ZEOLITES AND MICROPOROUS COMPOUNDS

Zeolites are aluminosilicates that have a framework structure with large cavities built in. The general formula of the zeolites is $(Na_2, K_2, Ca, Ba)[(Al, Si)O_2]_n \cdot xH_2O$, which means that they are chemically related to the feldspars. They are found in nature as crystals with large mineral specimens coming from Pune (near Mumbai in India). They are becoming much more important as synthetic minerals when they are used as molecular sieves or catalyst supports. The atlas of zeolite types lists 98 tetrahedral frameworks that are structurally distinct and are known as the TO4 frameworks where T (at the center of the O tetrahedron) is usually either Si or Al, but could be P, Ga, B, or other components. The International Zeolite Association (IZA) has compiled a list of the different structural types and has given each one a three-letter code, which is called, the Structural Type Code. The 3D frameworks are then assembled using secondary building units (SBUs) that consist of four, five, and six rings. This can be illustrated by examining the example shown in Figure 7.17. This figure represents sodalite, which is actually cubic with a lattice parameter of 0.887 nm.

Microporous ceramics are being designed to extend the concept of zeolites by building structures that do not necessarily have the well-defined walls of a zeolite crystal but still have the large cavities; an ordered alignment of the cavities can make it appear that the material is crystalline. The IUPAC definition is that a microporous material

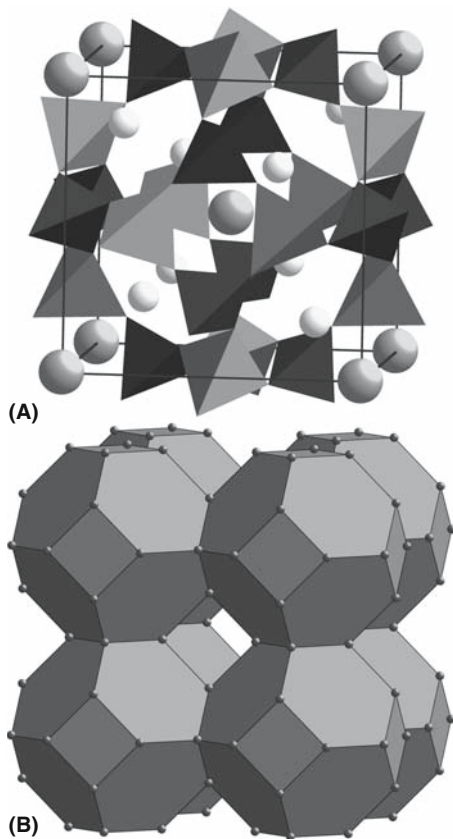


FIGURE 7.17 The structure of sodalite, a zeolite. The tetrahedra shown in (a) link together to form large “cages”; the most important features are the channels between the cages, which are seen in (b). In (a) the corner and body-centering ions are Cl⁻; the others are Na⁺ ions. The tetrahedra contain either Si⁴⁺ or Al³⁺.

contains micropores (free diameter < 2 nm); mesoporous materials contain mesopores (free diameter 2–50 nm).

7.20 ZACHARIASEN'S RULES FOR THE STRUCTURE OF GLASS

Many compounds can form glasses. Silicate glasses are what we usually think of as “glass.” However, the topic actually includes many other materials that are thought of as amorphous, although even that terminology can be misleading. In this section, we will discuss the aspects of structure only as they relate to the theme of polyhedra. We leave the question of “what is a glass?” to Chapter 21.

In 1932 W.H. Zachariasen proposed a set of rules that is usually satisfied when an oxide forms a glass. His analysis was based on the following considerations:

The interatomic bonding forces in glasses and crystals must be similar given the similar elastic modulus of the two types of solids.

Like crystals, glasses consist of an extended three-dimensional network, but the network does not have translational periodicity.

Studying the structure of glass is difficult because of the lack of translational symmetry. X-ray diffraction spectra from glasses show diffuse maxima not sharp spots or even sharp rings. These diffuse rings can be interpreted in terms of a radial distribution function [RDF; the quantity is $\rho(\mathbf{r})$].

$$\rho(\mathbf{r}) = \text{atom density in a spherical shell of radius } r \text{ from the center of any selected atom.}$$

An illustration of such a function is shown in Figure 7.18. The peaks in this figure correspond to the broad bands seen in the diffraction pattern. The corresponding plot for the crystalline material is also shown. The function is equally applicable for a crystal, but the peaks are then delta functions. What is less clear is whether a particular (or any) glass is truly amorphous or if “crystallites” at the nanometer scale are present.

The structure of an oxide glass can be modeled in terms of coordination polyhedra of cations surrounded by a variable number of oxygen ions. In crystalline oxides, the polyhedra cannot share only corners but must also share edges and/or faces; in glasses the polyhedra can share only corners. Silica glass is then pictured as a disordered version of the crystal with all oxygen ions bridging tetrahedra as shown in Figure 7.19.

Zachariasen summarized his findings as four rules and emphasized how the structure of SiO₂ glass differs from the crystalline form shown here as the (111) plane of cristobalite.

1. An oxygen ion will link to two or fewer glass-forming atoms.
2. CN of the glass-forming atoms is small (usually it is 4).
3. Oxygen polyhedra share only corners.
4. The polyhedra form a 3D network.

These rules have been used since the 1930s and have become almost folklore. Remember that they were

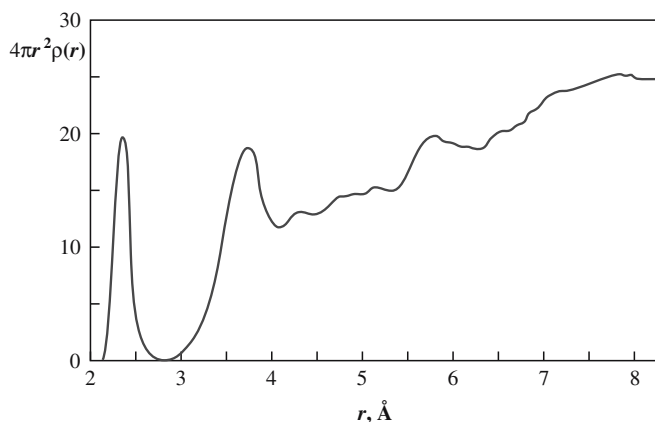


FIGURE 7.18 RDF of a glass showing a sharp first-neighbor peak, a broader second-neighbor peak, and then a gradual increase with increasing r .

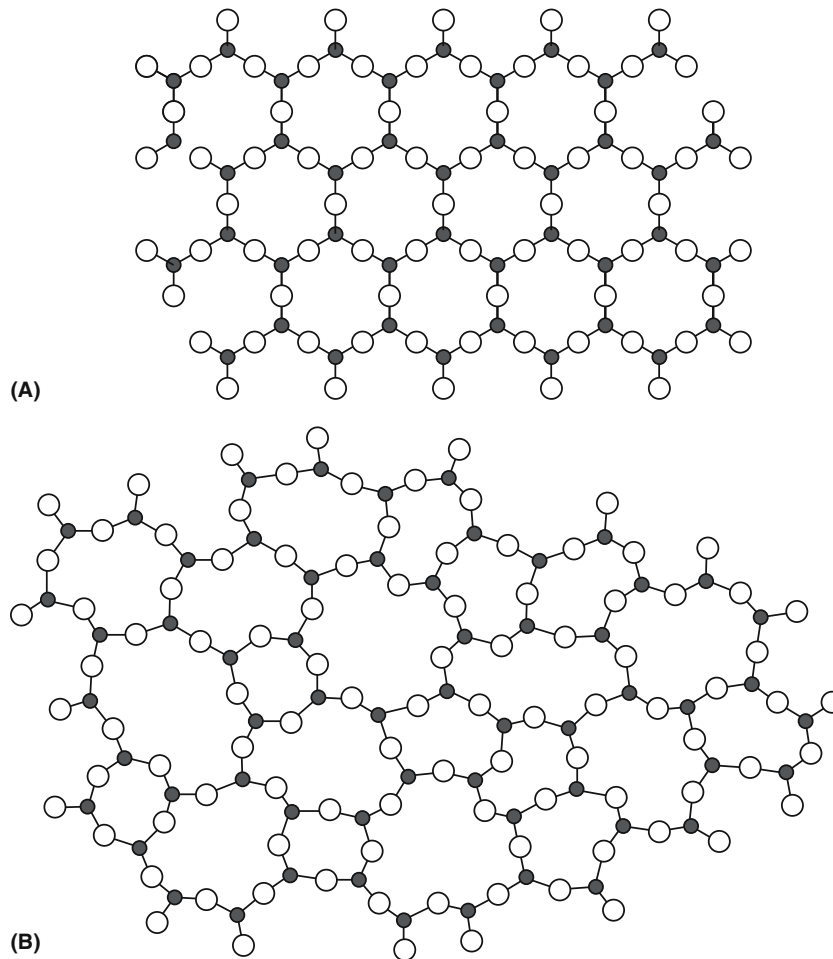


FIGURE 7.19 Comparing the structure of (a) crystalline silica and (b) glass.

proposed when the main glasses studied were silicates, although borate and phosphate glasses were known.

Further tendencies for glass formers have been listed:

1. The valence of the cation is 3 or greater.
2. As the size of the cation decreases so does its glass-forming tendency.
3. The cation's electronegativity is between 1.5 and 2.5.

In a general way, the role of the cations depends on the valence, CN, and the related values of the single-bond strength. Cations of higher valence and lower coordination than the alkalis and alkaline earth oxides may also contribute, in part, to the network structure. We can list the cations in three groups. The different types of ion present in oxide glasses are summarized in Table 7.7.

1. Network formers are cations that form coordination polyhedra in glass (like Si).
2. Network modifiers are oxides that do not participate directly in the network (like Na).
3. Intermediate ions can sometimes act in either role (like Al).

TABLE 7.7 CN for Formers, Modifiers, and Intermediates

<i>Formers</i>		<i>Intermediates</i>		<i>Modifiers</i>	
<i>Dopant</i>	<i>CN</i>	<i>Dopant</i>	<i>CN</i>	<i>Dopant</i>	<i>CN</i>
Si	4			Li	1
Ge	4			Na	1
B	3			K	1
Al	3	Al	3	Cs	1
P	5			Rb	1
V	5	Be	2	Be	2
As	5			Mg	2
Sb	5			Ca	2
Zr	4	Zr	4	Ba	2
				Sr	2
		Zn	2	Zn	2
		Cd	2	Cd	2
				Hg	2
				Ga	3
				Sn	4
		Pb	2	Pb	4

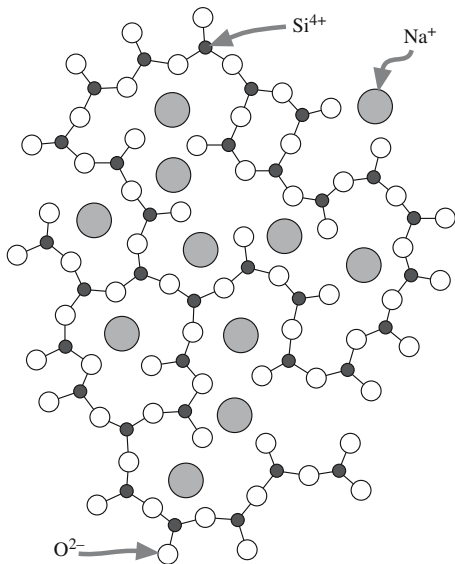


FIGURE 7.20 Schematic of how network modifiers in glass cause nonbridging O ions.

In practice, in oxide glasses, the polyhedra are triangles and tetrahedra. When a network modifier such as Na_2O is added to silica glass (SiO_2), a specific number of Si–O bonds is broken. This process is represented schematically in Figure 7.20. Si–O bonds are broken and the added oxygen saturates the unsatisfied bond of one Si and two Si–O[−] bonds are formed. The excess negative charge on the oxygen is compensated by the nearby Na^+ cations (adding an ionic character to the glass). The Si–O–Si

bridge-rupture mechanism leads to a loosened network structure with two types of oxygens:

Bridging oxygens are bonded to two Si.
 Nonbridging oxygens (NBOs) are bonded to one Si.

To summarize, Zachariasen’s model has dominated glass science for several decades and is still extremely useful. However, diffraction methods do not actually provide definite proof for such a model; they can only confirm that the results do not contradict this hypothesis. Remember also that the model was developed specifically for oxide glasses and is not necessarily applicable to other types of glasses.

7.21 REVISITING GLASS STRUCTURES

The Zachariasen model began to be reexamined in the 1990s. The important point is that silicate glass is, in many ways, just like the other silicates that *do* have long-range order. In particular, they are all 3D solids. Figure 7.21 shows the same information as Figure 7.19b but redrawn to show different ways of looking at this structure. A crystal composed of corner-sharing SiO_4 tetrahedra has orientational and translational symmetry. We can then call such a network “topologically ordered.” A silica glass is then topologically disordered—we cannot describe it by symmetry operations but it looks very similar to the crystalline form otherwise. The tetrahedron is an example of a rigid structuring element called a

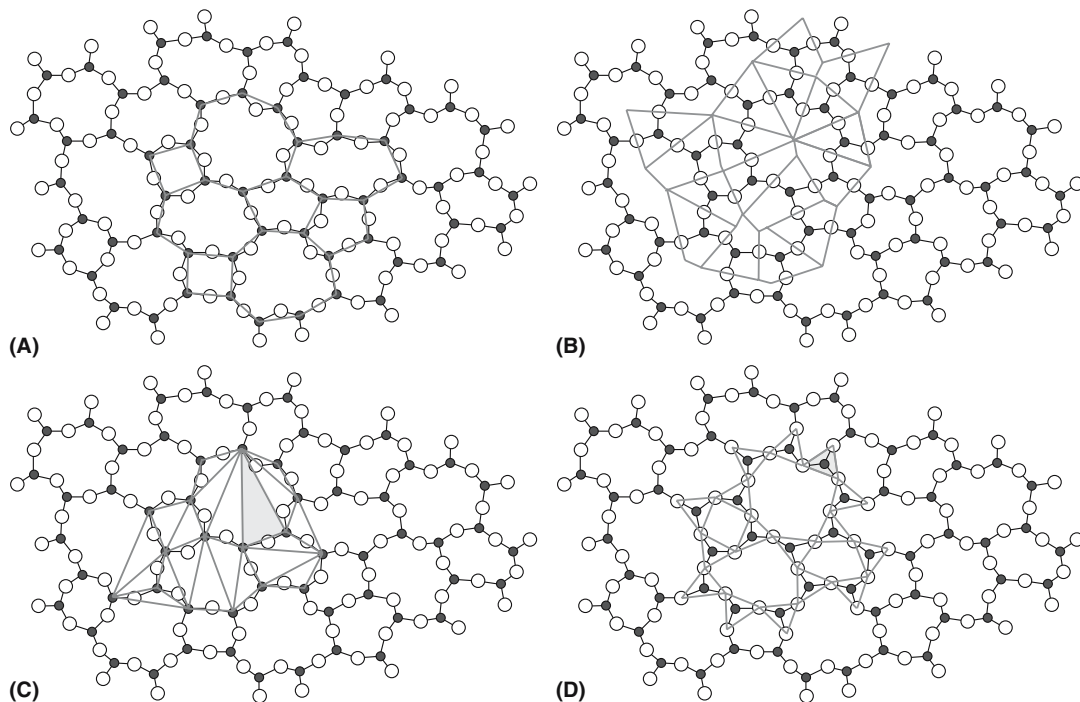


FIGURE 7.21 Different ways (a–d) of representing the same array of ions in a silica glass.

polytope (i.e., our polyhedra). The connectivity of a 3D structure can be described by the parameter $\{V,C\}$, where V is the number of vertices per polytope and C is the number of polytopes sharing a vertex. Incidentally, the polytope for the glass former B_2O_3 is the BO_3 triangle, so the tetrahedron is not the essential polytope. A network of triangles on a plane joined at the vertices is a $\{3,2\}$ arrangement.

For our (SiO_4) tetrahedron V is 4 but the diagram shown in Figure 7.19b is actually a 2D continuous random network of triangular polytopes with $V = 3$ and $C = 2$ (so

it is $\{3,2\}$). The Si atoms define a point (which can be called a node) in each triangle. If we join these nodes, as in Figure 7.21a, we have an array of primitive rings; now this network of nodes is a $\{2,3\}$ set because we are just joining lines and three join at each junction. This new network is said to tile or tessellate the 2D space. The set of tetrahedra associated with this ring is then called a local cluster and can be compared to the unit cell in a crystal. Alternative tiling schemes are shown in Figure 7.21b and c. The challenge is to describe the 3D structure. Our usual way of looking at it is shown in Figure 7.21d.

CHAPTER SUMMARY

This chapter examined some crystal structures that students must learn, including spinel and perovskite. Students should also know the different arrangements of the SiO_4 tetrahedra. Most of the other structures are looked up as needed, but the idea of how to build micas and clays really should be known. The structures of materials like the β -aluminas, YBCO, the SiAlONs, and the fullerenes all use concepts that we examined in Chapter 6, but in a more complicated form. The special feature in the fullerenes is the five-sided ring; in Chapters 12 and 14 we will see five-sided rings in dislocation cores and grain boundaries in Si and Ge where they have been known since before 1960. These structural features were well known years before they were discovered. You can look up the complex structures, but you should be able to recognize the special features of each one and how they are constructed from simple atomic groupings. Zeolites are endlessly fascinating and are like enormous 3D crossword puzzles. These materials are often left to inorganic chemists to synthesize or chemical engineers to use, which is unfortunate since their applications in materials science and engineering are far reaching. Three pages on glass is not an adequate treatment, but hopefully will indicate some of the potential for discovery in these noncrystalline solids.

PEOPLE IN HISTORY

Curl, Robert F. Jr. (1933–), Richard E. Smalley (1943–2005), and Sir Harold W. Kroto (1939–) shared the 1996 Nobel Prize in Chemistry for their discovery of fullerenes. In 1999, buckyballs were found to exist naturally in a meteor.

Fuller, Richard Buckminster (1895–1983) is the architect and inventor of the geodesic dome, which resembles the structure of C_{60} shown in Figure 7.16a. C_{60} is often referred to as the buckyball.

Megaw, Helen Dick died in 2002 aged 94. She reported the crystal structure of $BaTiO_3$ in *Nature* **155**, 484 (1945). She spent most of her academic career in Cambridge.

Zachariasen, William Houlder (1906–1979). The Norwegian-American physicist spent most of his career working in X-ray crystallography. But he is best remembered for his description of the glass structure in the early 1930s. He wrote only one paper on glass and was surprised to see it become the work that he is remembered for (information courtesy of J.C. Phillips).

GENERAL REFERENCES

In addition to the references given in Chapter 6, the following are recommended.

Baerlocher, Ch., Meier W.M. and Olson, D.H. (2001) *Atlas of Zeolite Framework Types*, 5th edition, Elsevier, Amsterdam. This requires a good understanding of crystallography but includes lots of sources for future exploration. You can download the atlas from the site for the International Zeolite Association: <http://www.iza-structure.org/databases>.

Deer, W.A., Howie, R.A., and Zussman, J. (1992) *An Introduction to the Rock-Forming Minerals*, 2nd edition, Longman, London. This book (680+ pages) contains a wealth of data on the subject. Olivines, garnets, and pyroxenes abound.

Doremus, R.H. (1994) *Glass Science*, 2nd edition, John Wiley & Sons, New York. This is the first book to go to when you continue your study of glass.

Griffen, Dana T. (1992) *Silicate Crystal Chemistry*, Oxford University Press, Oxford. Clear diagrams but does not include mullite.

Hobbs, L.W. (1995) "The role of topology and geometry in the irradiation-induced amorphization of network structures," *J. Non-Cryst. Solids* **182**, 27. Polyhedra as polytopes and much, much more.

- Hobbs, L.W., Jesurum, C.E., Pulim, V., and Berger, B. (1998) "Local topology of silica networks," *Phil. Mag.* **A78**, 679.
- Liebau, F. (1985) *Structural Chemistry of Silicates*, Springer, Berlin. Great reading but not easy.
- Melody, J.G. (1995) *Love Is in the Earth: A Kaleidoscope of Crystals*, Earth-Love Publishing, Wheat Ridge, CO. If you are interested in an entirely different assessment of ceramics.
- Parthé, E. (1964) *Crystal Chemistry of Tetrahedral Structures*, Gordon and Breach, New York, Chapter IV and Appendix A.
- Schneider, H. and Komarneni, S., Eds. (2005) *Mullite*, Wiley-VCH, Weinheim, Germany. The definitive text on this important though structurally complex group, of materials.
- Sosman, R.B. (1965) *The Phases of Silica*, Rutgers University Press, New Brunswick, NJ. The classic, though now a little neglected, text on silica.
- Stanworth, J.E. (1971) "Oxide glass formation from the melt," *J. Am. Ceram. Soc.* **54**, 61.
- Wells, A.F. (1984) *Structural Inorganic Chemistry*, 5th edition, Oxford University Press, Oxford. Repeated here because this book is so important.
- Wenk, H.-R. and Bilakh, A. (2004) *Minerals Their Constitution and Origin*, Cambridge University Press, Cambridge. Concentrates on the materials—a super resource.

SPECIFIC REFERENCES

- Fenner, C.N. (1913) "The stability relations of the silica minerals" *Am. J. Sci.* **36**, 331. Gave the original version of the silica phase diagram.
- Hardie, D. and Jack, K.H. (1957) "Crystal structures of silicon nitride", *Nature* **180**, 332. Initial report of the structures of Si_3N_4 .
- Hay, R.S. and Marshall, D.B. (2003) "Deformation twinning in monazite," *Acta Mater.* **51**, 5235. [And Hahn T. ed. (1985) *Space Group Symmetry*, International Tables for Crystallography, Brief Teaching Edition, D. Reidel Publishing Co., Dordrecht.]
- Jack, K.H. (1976) "SiAlONs and related nitrogen ceramics," *J. Mater. Sci.* **11**, 1135. A review article by the pioneer in the field. The most cited article in *Journal of Materials Science*.
- Liu, A.Y. and Cohen, M.L. (1989) "Predication of new low compressibility solids," *Science* **245**, 841. Proposes a compound, $\beta\text{-C}_3\text{N}_4$, which should have outstanding mechanical properties but is not widely available (it is rare). This paper has over 1200 citations.
- Zachariasen, W.H. (1932) "The atomic arrangement in glass," *J. Am. Chem. Soc.* **54**, 3841. The random network model for glass structure has been the dominant factor in developing glass formulations for 70 years. This is the classic reference for that model.

EXERCISES

- 7.1 Compare the ionic sizes in CaZrO_4 and CaSiO_4 and discuss how well they fit Pauling's rules and if they should.
- 7.2 Discuss for Mg_2TiO_4 and Mn-Zn ferrite, which is preferred, normal or inverse spinel, on the basis of Pauling's rules.
- 7.3 In spinel, other than $\langle 110 \rangle$, is there a low-index direction where only like cations project on one another?
- 7.4 How many ions do you expect to find in a unit cell of grossular?
- 7.5 Discuss whether we should write the formula for superconducting YBCO as $\text{YBa}_2\text{Cu}_3\text{O}_{7-\delta}$ or $\text{YBa}_2\text{Cu}_3\text{O}_{6+x}$.
- 7.6 We often say that the structure of YBCO is related to the perovskite structure. Draw diagrams of the two crystal structures and then explain this relationship.
- 7.7 By delving into the literature, explain which three materials you think are the next (after those discussed in the chapter) most important in each of these categories: silicates, oxides, nonoxides. Then summarize how they are processed.
- 7.8 In silicon oxynitride, $\text{Si}_2\text{N}_2\text{O}$, we have $\text{Si}_3\text{N}_3\text{O}$ tetrahedra. Sketch the possible structure of this ceramic.
- 7.9 Consider the fcc arrangement of doped solid C_{60} that we described in Section 7.18. Explain why we get only Cs_1C_{60} when we dope with Cs and why for sodium doping we can get Na_6C_{60} and $\text{Na}_{10}\text{C}_{60}$.
- 7.10 By examining the literature, discuss how niobates and titanates can be combined and how the perovskite structure facilitates this.

Equilibrium Phase Diagrams

CHAPTER PREVIEW

Most ceramics are multicomponent materials and the most stable phase at any temperature will be the one with the lowest free energy, G . One use of phase diagrams is to represent the phase or phases we might expect to be present as a function of temperature. There are a large number of books just concerned with this one topic. Much work was carried out in the 1950s and 1960s, but many systems have remained almost completely unexplored and it is not a well-funded area in the United States now. The lack of effort is in spite of the demonstration that new complex ceramics, such as the high-temperature superconductors YBCO and BiSCCO and the magnetic manganates, possess extraordinary, and potentially very useful, properties.

Much of the classical work on phase equilibria has actually been concerned with processing metals. Thus the Fe–O phase diagram is perhaps the most thoroughly characterized because of its importance to the iron and steel industry.

A word to keep in mind throughout our discussion is equilibrium: we are talking about equilibrium phase diagrams. Often we use a phase diagram as a guide to processing. If the process is in progress then it is not in equilibrium. And, by definition, a chemical reaction is not an equilibrium process. If a reaction is exothermic then a rise in temperature favors the reactants. Although most of the phase diagrams we use in ceramics are for a pressure of 1 atmosphere, in one-component systems such as carbon, pressure is a very important variable. It tells us what pressure we need for direct synthesis of diamond. In metal–oxygen diagrams the partial pressure of oxygen determines what is the stable form of the oxide.

8.1 WHAT'S SPECIAL ABOUT CERAMICS?

Since many ceramics are oxides, the oxygen partial pressure, pO_2 , is an important variable. There is a lot of information about many metal–oxygen systems. In part, this is due to interest in how to obtain metals by direct reduction from their oxides. A frequent way of representing free energies of formation of oxides as a function of pO_2 and T is the Ellingham diagram (Ellingham, 1944) that was popularized by Richardson and Jeffes (1948) for iron and steel production. Much less is known about nitrides and oxynitrides or even carbides.

Many ceramics are multicomponent materials and, hence, many of the important phase diagrams involve three or more components. Here are some

examples of where phase diagrams have very practical applications in the use of ceramics:

Refractory silica brick: This was used for the roof of the open-hearth furnace, which was once an important method for steel production. Now silica refractories are used in coke ovens and as roofs in glass tanks. Typical operating temperatures are 1625–1650°C. The phase diagram tells us that the SiO_2 needs to be quite pure (only 0.2–1.0 wt% Al_2O_3) or it will melt.

Fire-clay brick: This is a classic clay product with composition close to kaolinite. Although it is used at temperatures below 1587°C, the phase diagram tells us that some liquid will often be present since these ceramics contain 22–33 wt% Al_2O_3 . This material is so important because it performs the task very well and is cheap to produce.

DALTON'S LAW OF PARTIAL PRESSURES

$$P_A = X_A P$$

P_A is the partial pressure of A.
 X_A is the mole fraction of A.
 P is the total pressure of the gas mixture.

Barium titanate: Pure cubic BaTiO₃ single crystals cannot be grown from a melt of that composition because the hexagonal phase is in equilibrium with the liquid at the solidification temperature (1618°C). Although the hexagonal phase is transformed to the cubic phase at 1460°C, the phase change is sluggish and thus the hexagonal phase can exist at room temperature. The hexagonal form of BaTiO₃ is not ferroelectric, which is the property in which we are most often interested. In Chapter 29 we describe how single crystals of cubic BaTiO₃ can be grown.

Adhesion of metals in integrated circuits: Aluminum has been used for over 30 years as interconnect and top-level metallization in integrated circuits. One of the reasons Al is so good is that it reduces SiO₂ to form interfacial metal–oxide bonds that promote adhesion and stability. One of the problems with copper metallizations is that SiO₂ is more stable than Cu₂O. Despite this difficulty, Cu has several significant advantages over Al and is now used in many commercial devices such as IBM’s processor for the Apple G5, Intel’s Pentium IV, and AMD’s Athlon. The relative oxidizing powers of metals are represented frequently on Ellingham diagrams. In Chapter 15 we will show how these diagrams can be useful in developing brazes for ceramics.

8.2 DETERMINING PHASE DIAGRAMS

We refer you to basic thermodynamics texts for the details on the origin of phase diagrams and the phase equilibria book by Bergeron and Risbud. In this section we will just summarize some key points. First, some thermodynamic background to phase diagrams is presented.

- The phase with the lowest free energy, G , is thermodynamically stable.
- The chemical potential, μ_i , of a component is the same in all of the phases in which it is present. This requirement is used in the derivation of Gibbs Phase Rule.
- At equilibrium the temperatures and pressures of all phases are equal.

Determining a phase diagram requires measuring which phases are in equilibrium under well-defined conditions. An especially critical factor for ceramics is being sure that we have equilibrium. In ceramics we have two challenges:

- We need to make measurements at high temperature where direct determination of phases is difficult.
- The valence of the cations may change as the temperature or pressure changes. If the cation is polyvalent, then the valence depends on the oxygen activity, which, as we will see later, depends on the partial pressure of oxygen, pO_2 .

To ensure we have equilibrium, the two bulk phases should really be in intimate contact separated by a flat (planar) interphase boundary.

The number of techniques we can use for direct determination of phase diagrams of ceramic systems is quite limited because of the requirements for high temperatures.

- High-temperature X-ray diffraction. The maximum operating temperatures are up to 2500°C in high vacuum, 2400°C in inert atmospheres, and 1700°C in air.
- TEM with hot-stage. The maximum temperature is usually 1300°C, working in vacuum, typically $\sim 10^{-4}$ Pa, so there is no control of pO_2 .

Most techniques that are used to determine phase diagrams experimentally use an indirect approach. Note that often we are not trying to determine an entire diagram, but rather the specific parts that may be of interest, such as the solvus lines, the liquidus, or the eutectic temperature. Figure 8.1 shows an example of using cooling curves to determine the liquidus and eutectic temperature for a binary system. Heating curves produce similar results and are often easier to achieve experimentally. Phase changes produce the deviations in the time–temperature curves. These measurements would be made using differential

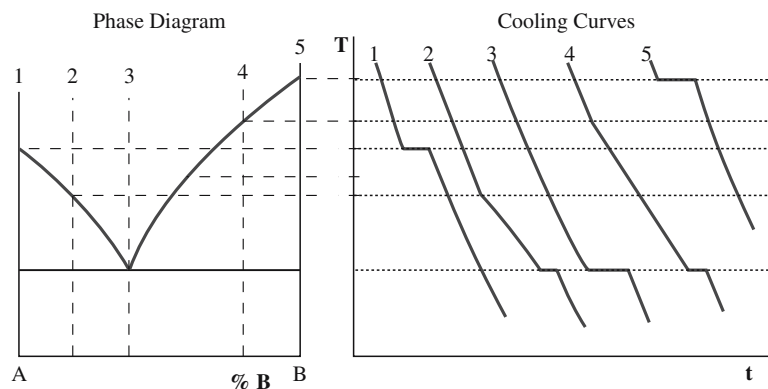


FIGURE 8.1 Illustration of the use of cooling curves to determine the liquidus and eutectic in a binary phase diagram.

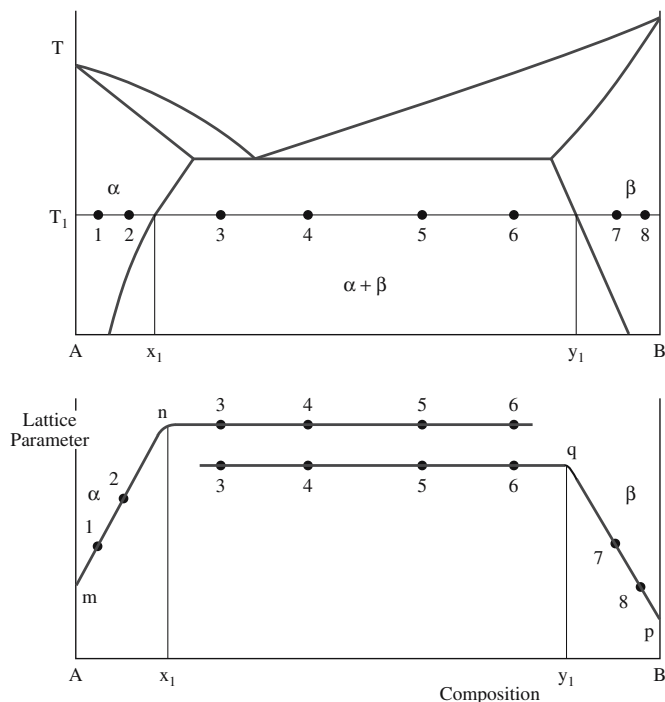


FIGURE 8.2 Parametric method for determination of the solvus lines in a binary phase diagram.

thermal analysis (DTA) or differential scanning calorimetry (DSC). Maximum temperatures for these instruments are about 1700°C. At this temperature many of the important ceramics such as Al₂O₃ (melts at 2054°C), SiO₂ (melts at 1710°C), and ZrO₂ (melts at 2677°C) are still solid. Another problem with ceramic melts, especially those containing SiO₂, is their high viscosity. Most oxide glasses are silicates. Crystallization from these melts is often difficult and reaching equilibrium can take a very long time (years!).

A frequently used method for studying phase equilibria in ceramics is X-ray diffraction on samples that have been equilibrated at high temperature then quenched. This technique is particularly useful for the solid-state portions of the phase diagram, such as determining the position of the solvus lines. In each single solid-solution region of a binary phase diagram there is a change in lattice parameter with composition. In the phase field where both solid solutions exist the lattice parameter of each solid solution remains constant with composition as shown in Figure 8.2. The position of the solvus line,

CLAUSIUS–CLAPEYRON EQUATION

Change in vapor pressure (*P*) of a solid with a change in *T*

$$\frac{dP}{dT} = \frac{\Delta H_s}{T(V_v - V_s)}$$

ΔH_s = enthalpy of sublimation of solid
 V_v = molar volume of vapor
 V_s = molar volume of solid

SOME USEFUL DATA

NiO $T_M = 2257$ K; $\Delta H_f = 50.6$ kJ/mol
MgO $T_M = 3073$ K; $\Delta H_f = 77.4$ kJ/mol
BeO $T_M = 2830$ K; $\Delta H_f = 71.1$ kJ/mol
UO₂ $T_M = 3150$ K; $\Delta H_f = 54.0$ kJ/mol

at a particular temperature, corresponds to the change in slope. It is important that the conditions are sufficient for the system to reach equilibrium and that high-purity powders are used.

We can calculate phase diagrams using the requirement that the lowest free energy state is the equilibrium one. If calculations are performed for a range of temperatures then the phase boundaries can be determined. Because we often do not know the absolute values for thermodynamic quantities, but changes in these, we use the following expression:

$$\Delta G = \Delta H - T\Delta S \quad (8.1)$$

ΔH and ΔS can be determined at any temperature using the heat capacity, c_p :

$$\Delta H_{T_2} - \Delta H_{T_1} = \int_{T_1}^{T_2} \Delta c_p dT \quad (8.2)$$

and

$$\Delta S_{T_2} - \Delta S_{T_1} = \int_{T_1}^{T_2} \frac{\Delta c_p}{T} dT \quad (8.3)$$

The problem is that heat capacities are not known for many compounds. As a result, we often make assumptions that allow us to determine the part of the phase diagram that is important to us.

Estimation of Liquidus and Eutectic Temperature

for a Binary System

We can estimate the position of the liquidus assuming that our mixture forms an ideal solution, hence it obeys Raoult's law. From the Clausius–Clapeyron equation with some integration and algebraic manipulation we can obtain

$$\ln X_A = -\frac{\Delta H_f}{R} \left(\frac{T_M - T}{T_M T} \right) \quad (8.4)$$

where X_A is the mole fraction of component A and ΔH_f is the enthalpy of fusion. Values of T are plotted against composition. At the intersection of these lines is the eutectic point. This approach works well for many alkali halide systems (such as the NaF–KF) but

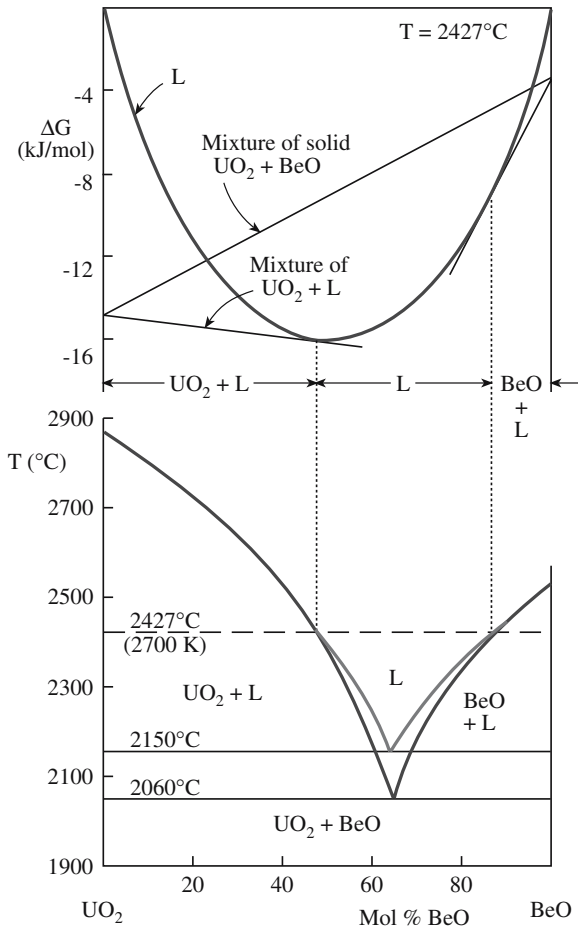


FIGURE 8.3 The UO_2 - BeO phase diagram determined using free energy calculations.

not so well for many oxides. For example, the PbO - B_2O_3 system shows dissociation on melting.

An alternative method to calculate the liquidus is to calculate differences in free energy of the solid (G_s) and liquid (G_l) phases as a function of temperature:

$$G_s - G_l = -\Delta H_f \ln \frac{T_M}{T} \quad (8.5)$$

We need to know the enthalpy of fusion, ΔH_f , and the melting temperature, T_M .

Figure 8.3 shows how this method has been used to construct the phase diagram for the UO_2 - BeO system. The agreement with the published diagram is quite good.

Estimation of Liquidus and Solidus for Systems with Complete Solid Solubility

Figure 8.4 shows free energy versus composition plots at 2700°C for the NiO - MgO system and the corresponding

phase diagram. This system is one in which the components are mutually soluble in both the solid and liquid states. Determination of the free energy curves uses Eq. 8.5 and the free energy change associated with mixing liquid NiO and liquid MgO , which can be calculated using

$$\Delta G = RT[X \ln X + (1 - X) \ln(1 - X)] \quad (8.6)$$

The use of computer methods for calculating phase diagrams is becoming increasingly important. The results of many of these studies are available in CALPHAD: Computer Coupling of Phase Diagrams and Thermochemistry (Saunders, 1998 and on-line). Figure 8.5 illustrates such computed phase diagrams.

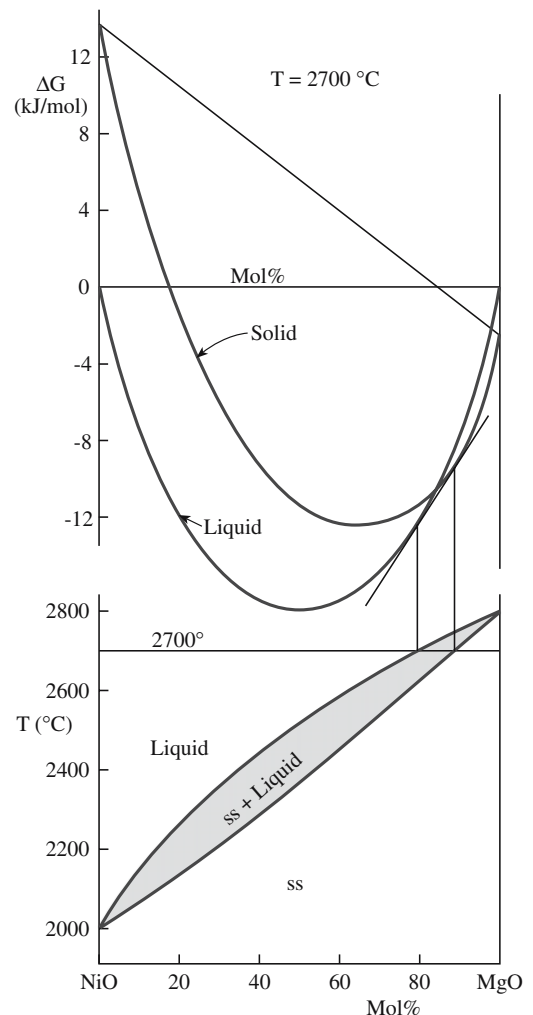
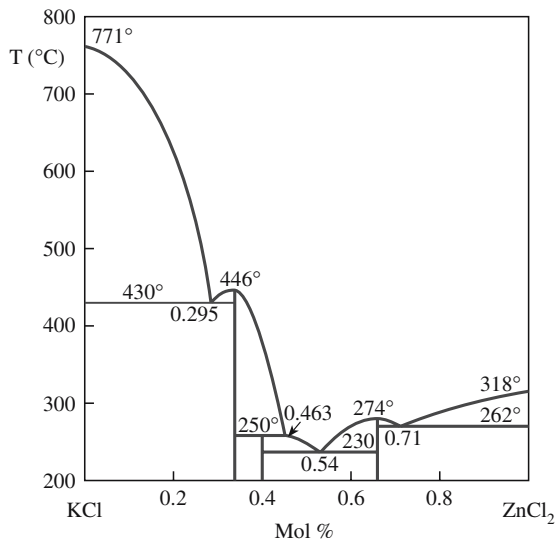
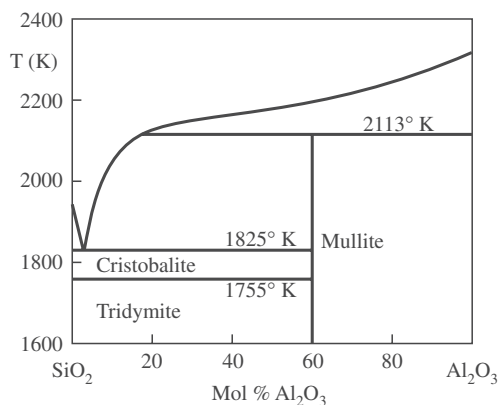


FIGURE 8.4 The NiO - MgO phase diagram and free energy curves at $T = 2700^\circ\text{C}$.



(A)



(B)

FIGURE 8.5 (a) CALPHAD phase diagram for KCl–ZnCl₂. (b) CALPHAD phase diagram for SiO₂–Al₂O₃.

8.3 PHASE DIAGRAMS FOR CERAMISTS: THE BOOKS

Because the books are really important for ceramics we will emphasize them here rather than just at the end of the chapter: all ceramicists must be familiar with “the books.” The first volume of the series, *Phase Diagrams for Ceramists*, was published in 1964 and is in daily use. The series currently contains 12 volumes. The companion volume by Bergeron and Risbud is entitled *Introduction to Phase Equilibria in Ceramics* and should always sit on the same shelf. The books are unique in that the later volumes contain both new and

GIBBS C, F, AND X

C is for component
F is for freedom
X is for phase

updated diagrams, but the old diagrams found in the earlier volumes are still often quoted. Many of these diagrams resulted from research in the 1950s and 1960s, but there are many going back to 1915. The first diagram in the book (Fig. 1), produced in 1951, is for the system Al–Al₂O₃ and shows the gaseous species over liquid Al₂O₃ as a function of *T* and *P*. One of the earliest is for the AgNO₃–NaNO₃ system that was devised in 1900 (Fig. 1040). Unfortunately, this field is not currently well supported. In our brief discussion in this chapter, we take the approach of “learn by example.”

A warning on units is necessary. Since many of the data were collected before the establishment of SI units, the plots contain combinations of weight percent, mole fraction, and mole percent, kbars and atm for pressure, but fortunately only °C (not °F for temperature).

8.4 GIBBS PHASE RULE

We derive the Gibbs Phase Rule in three steps.

Step 1. Consider the situation in which we have *C* components that exist in *X* phases. If Fe and O are the components, Fe and FeO would be examples of phases. So there are *XC* composition variables. Adding the two important external variables in ceramics, *P* (pressure) and *T*, gives *XC* + 2 variables.

Start with *XC* + 2

Step 2. If we described the composition of a phase in terms of the mole fraction of its components, then when we have described all but one of the mole fractions, the last one must be known because together the mole fractions all add up to unity. This happens for each of the *X* phases, so *X* of the variables are actually fixed.

Deduct *X*

Step 3. In equilibrium, the chemical potential of a component must be the same in all the phases (otherwise it will not be equilibrium). If the concentration is fixed in one phase then the chemical potential is fixed in that phase. The chemical potential must then be fixed in all the phases since it is the same in all phases. Thus, if the concentration is known in one phase, then *X* – 1 variables (the concentrations in the other phases) are automatically fixed (even though they are not necessarily the same—their chemical potential is the same). Since this is true for all *C* of the components, (*X* – 1)*C* variables are fixed (they are not independent variables).

Deduct $(X - 1)C$

Hence the number of independent variables is given by

$$F = (XC + 2) - X - (X - 1)C$$

Rearranging gives us Gibbs Phase Rule

$$F + X = C + 2 \quad (8.7)$$

Note that many texts use P for the number of phases and V for the degree of freedom. We use F for (degrees of) freedom, P , an important variable, for pressure, V for volume, and X for the number of phases.

Most of the time we just examine different systems with up to three components ($C = 1, 2, \text{ or } 3$). The difficulty sometimes is in counting the components. There are also four- and five-component diagrams in ceramics. We always have to be aware that the sample might contain nonequilibrium phases.

8.5 ONE COMPONENT ($C = 1$)

In each of these examples, we have one component, meaning that the chemical composition of the material does not vary. From the phase rule we have P and T as two variables, which is what we plot in each case. Using $F + X = C + 2$, for a one-phase region we can vary both P and T . For a two-phase region (the line), if we vary P then T is determined. For a three-phase region in a one-component system there are no variables.

Example 1: Water: One component (Figure 8.6). X takes its maximum value of 3 when $F = 0$. The three coexisting phases are then solid, liquid, and gas at point A, or the liquid and two solid phases at point B. Points A and B occur at unique combinations of temperature and pressure. Lines correspond to locations where two

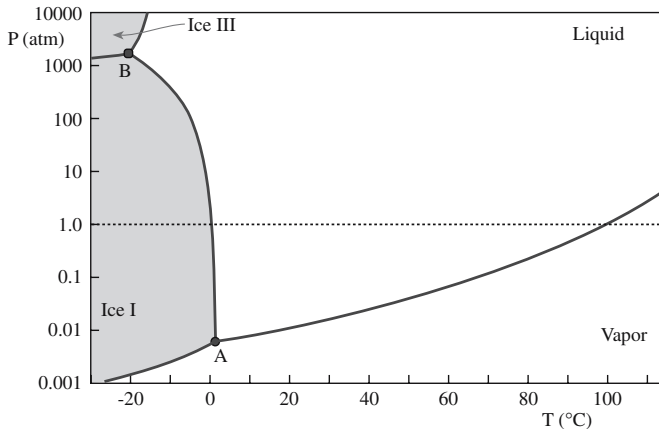


FIGURE 8.6 The H_2O phase diagram. (1000 atm is ~ 100 MPa.)

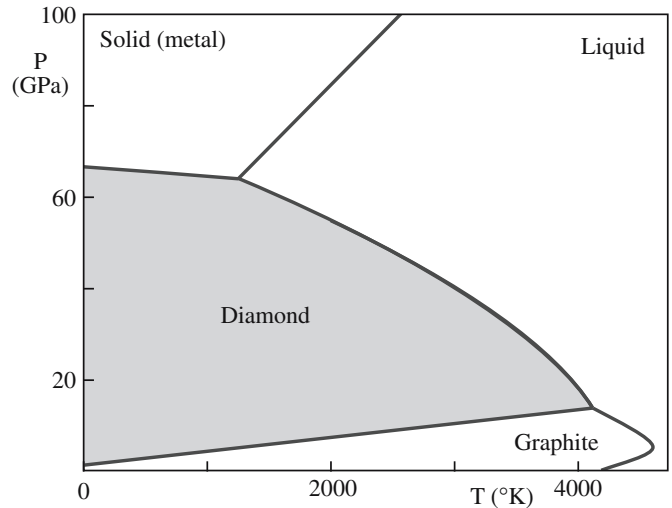


FIGURE 8.7 The C phase diagram.

phases are in equilibrium ($X = 2$ and $F = 1$). If we vary T , then P must vary so that we stay on the line. This diagram is a simplification of what we know now since there are many (11 or 12) other known crystalline forms of ice. The form that occurs in nature is called ice Ih (a hexagonal form) and has a density of 0.931 g/cm^3 (water is 1.00 g/cm^3 ; hence the iceberg phenomenon). The other forms exist at either lower values of T or higher values of P than shown in Figure 8.6. (We have kept this pressure in atm because the most important equilibrium occurs at 1 atm.)

Example 2: Carbon: One component (Figure 8.7). This is a classic example of an element with three solid phases. We often remind owners that diamonds are only metastable, but fortunately the kinetics of the phase transformation are very slow. Notice where we live—in a dot at the bottom left corner.

Example 3: SiO_2 : One component (Figure 8.8). Silica is not only one of the most important ceramics, but its

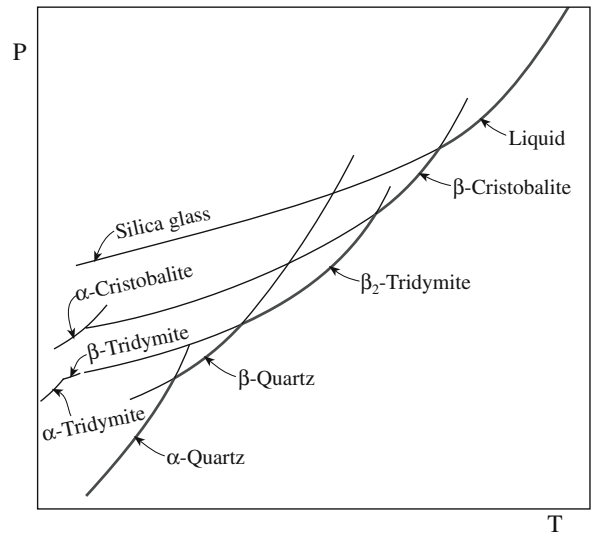


FIGURE 8.8 The SiO_2 phase diagram.

phase diagram is also very interesting. Remember, the composition is constant. This schematic diagram emphasizes both the relationship between the glass and the liquid and the fact that the glass is the high-pressure phase; the glass is denser than any of the crystalline forms (similar to ice). The phase rules always apply.

8.6 TWO COMPONENTS ($C = 2$)

Binary phase diagrams are very important for ceramics. The two most important cases for ceramics are the combination of a metal plus oxygen and the combination of two oxides. A model two-component system is shown in Figure 8.9 where we are now using the third dimension to display the data.

If there is one phase ($X = 1$) as at B, then the three variables are pressure, temperature, and one other, for example, the composition (x/y ratio).

If there are two phases present ($X = 2$) such as the liquid and one solid phase at A, then $F = 2$. If, for example, we fix P , we are free to vary T and move along the liquid/solid phase boundary (a surface).

The special feature is that we have introduced surfaces into the phase diagram. In ceramic materials, the gas phase may be very important. This is where ceramics are particularly different from metals: oxygen (or nitrogen or water vapor and

HUME-ROTHERY RULES FOR COMPLETE SOLID SOLUBILITY

- Same crystal structure
- Equal valence
- Ionic radius within $\pm 15\%$
- No chemical reactivity

If we have two oxides we need consider only the sizes and valences of the cations.

hence hydrogen) may be a component of the system. The gas phase is not important if the valence of the cations is fixed and the total pressure, P , is fixed at 1 atm. We will consider materials with variable valence in Section 8.8.

Example 1: NiO/CoO: Two components and P fixed (Figure 8.10). The special feature about this diagram is that both oxides have a rocksalt structure. Pauling's rules tell us not to be surprised that they are fully interchangeable. However, it is reported that there is a two-phase region at low temperatures. Notice three points:

- At the high temperatures, the diagram contains only dashed lines—intelligent guesses.
- The two-phase region occurs where kinetics are quite slow.
- The composition is given as a mole fraction.

This is a case in which you start with “the book” and then go back to the original reference to learn how the pO_2 was controlled, how the two phases were identified, etc.

Example 2: MgO/CaO:

Two components and P fixed (Figure 8.11). This diagram is a classic eutectic even though CaO and MgO both adopt the rocksalt structure. Because the sizes of the two cations differ by more than 15%, solid solubility is limited.

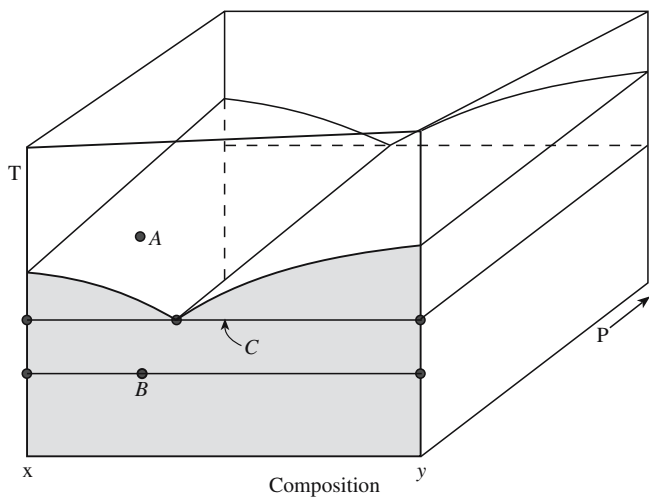


FIGURE 8.9 A model binary phase diagram showing T , P , and composition as variables.

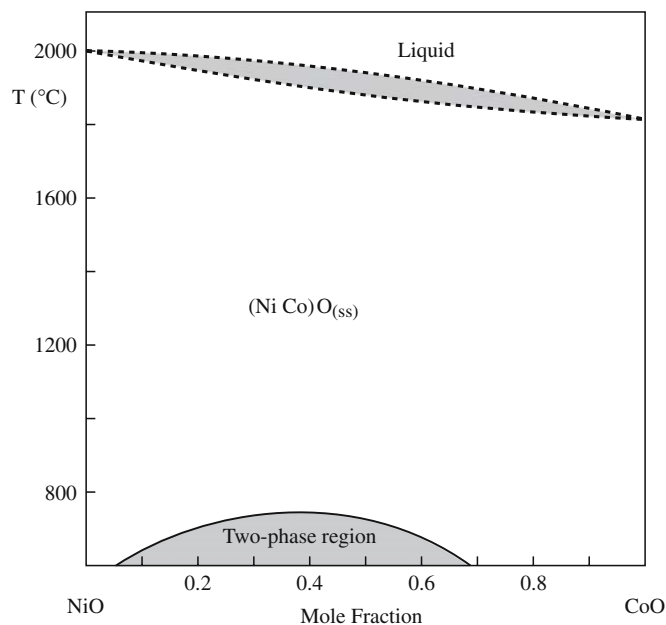


FIGURE 8.10 The NiO–CoO phase diagram.

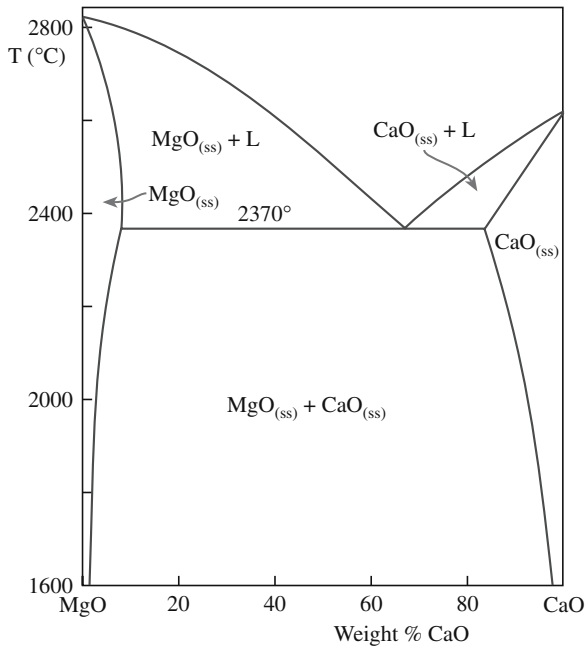


FIGURE 8.11 The MgO–CaO phase diagram.

Example 3: MgO/MgAl₂O₄/Al₂O₃: Two components and *P* fixed (Figure 8.12). This is a particularly important, but relatively simple, system in ceramics. It involves three widely used materials, which are also archetypical structures. We can choose the two components to be MgO and Al₂O₃. Then in the one-phase region we have one variable in addition to *P* and *T*. In the two-phase region we can vary *T* or the MgO:Al₂O₃ ratio, but not independently. Notice that the composition is given in weight percent, which is not too bad for this system but really distorts the related MgO/Cr₂O₃ and NiO/Al₂O₃ systems. The spinel phase field is already quite wide at 1600°C and becomes wider at high temperatures, especially toward the Al₂O₃-rich

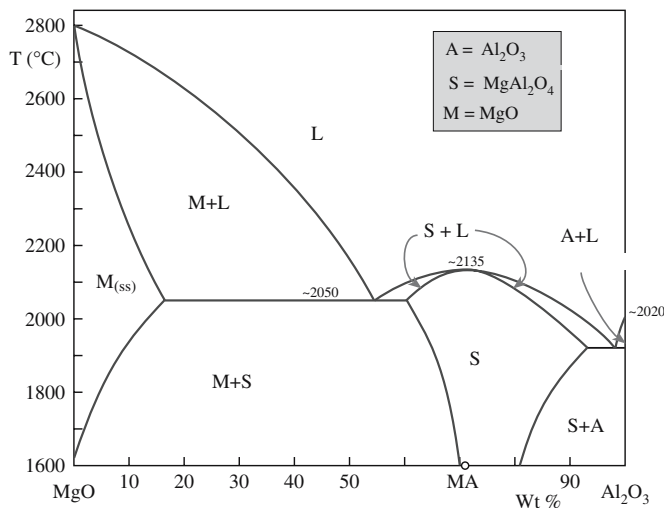


FIGURE 8.12 The MgO–Al₂O₃ phase diagram.

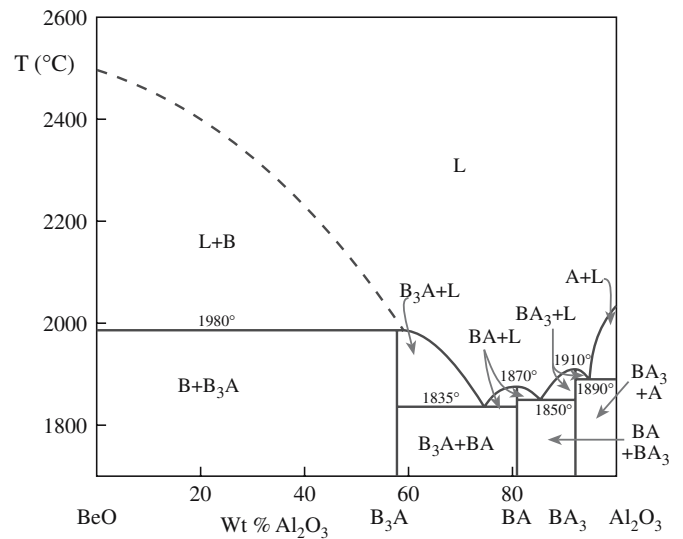


FIGURE 8.13 The BeO–Al₂O₃ phase diagram.

side. We can grow two eutectic structures; one essentially contains pure Al₂O₃.

Example 4: BeO/Al₂O₃: Two components and *P* fixed (Figure 8.13). Notice that all the phases can be regarded as combinations of BeO and Al₂O₃, so we can denote them as B₃A, BA, and BA₃. From a chemical point of view, the system looks quite similar to MgO/Al₂O₃, but clearly it is very different; three separate eutectics are shown; none of the compounds has the spinel structure. BeAl₂O₄ is the mineral chrysoberyl and has a structure similar to olivine, which is not unrelated to spinel.

Example 5: MgO/TiO₂: Two components and *P* fixed (Figure 8.14). This system is interesting because of the

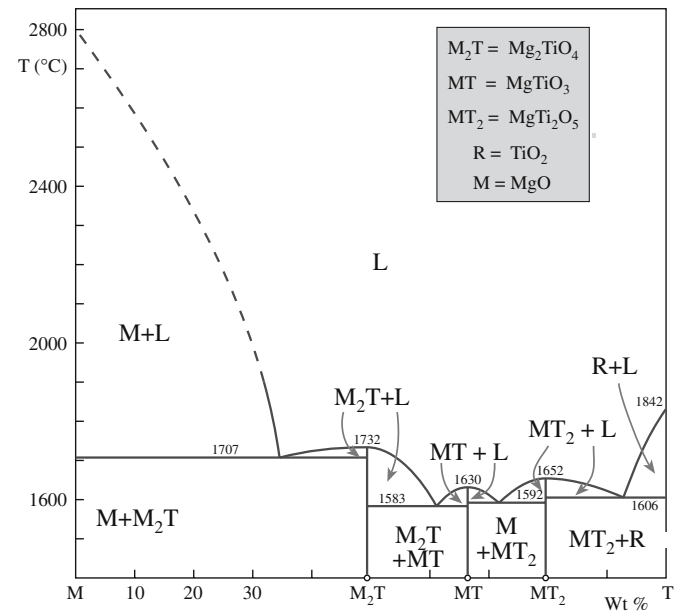
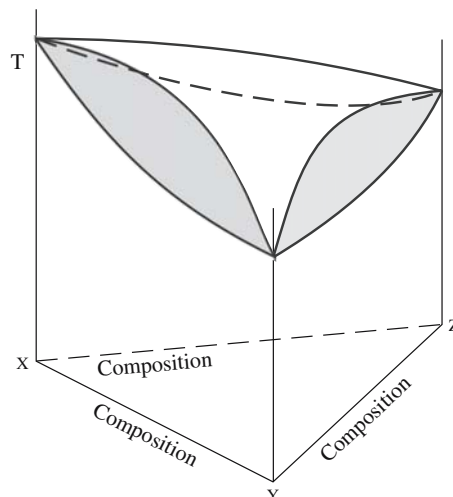
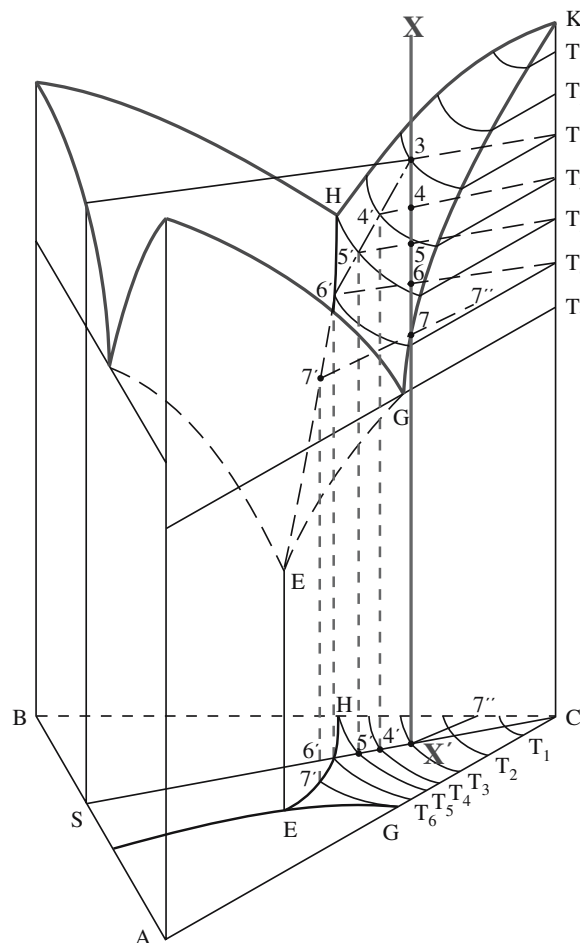


FIGURE 8.14 The MgO–TiO₂ phase diagram.

occurrence of four different eutectics. Such eutectics in this and other systems have been used to prepare some interesting two-phase materials. For example, when a liquid with composition in the MgO-rich region is cooled from the eutectic temperature at 1707°C it will produce a material that consists of alternating lamellae of nearly pure MgO and Mg₂TiO₄. Other systems show different structures, which are determined in part by the interfacial energies. Of course, interfacial energies are usually not considered in the analysis of phase diagrams.



(A)



(B)

FIGURE 8.15 (a) A model ternary phase diagram for a system showing three solid solutions. (b) A model ternary phase diagram for a system showing three eutectics.

8.7 THREE AND MORE COMPONENTS

When three components (ternary systems; $C = 3$) are present the phase diagrams become more difficult to draw because we then have $F + X = 5$. If the pressure is fixed then we have four variables. We need one axis for each component and one for the temperature, say, so we draw the compositions on a triangle and plot T as the vertical coordinate as shown in Figure 8.15a. The base triangle is called the Gibbs triangle. The example shown in Figure 8.15a corresponds to the case in which three oxides form solid solutions (extending the NiO/CoO example). The example shown in Figure 8.15b is the case of three simple binaries each with a single eutectic (extending the MgO/CaO example). Figure 8.15b is worth some effort to understand. The lines of constant temperature at the solid/liquid phase boundary are projected onto the base of the Gibbs triangle. The location of each of the three eutectics is also projected and will correspond to an abrupt change in the curvature of the constant-temperature contour. The three eutectics then meet at a “grand eutectic” at E. For sufficiently slow cooling, E will correspond to the ultimate eutectic temperature—below T_E the sample is solid.

In the materials that are often most important, the diagrams are more complicated. The phase diagram books then often show them as projected triangles as in Figures 8.16–8.18.

Example 1: MgO/Al₂O₃/SiO₂: Three components and P fixed (Figure 8.16). Notice that there are perhaps three locations for E. This diagram contains several really important ceramics. We have already examined one of the binary diagrams included here (MgO/Al₂O₃) and will examine another below (MgO/SiO₂). Diagrams like this have difficulty in showing what is happening at temperatures other than the liquidus.

Example 2: CaO/Al₂O₃/SiO₂: Three components and P fixed (Figure 8.17). Figure 8.17 illustrates the extension of the use of abbreviations to three components. It also illustrates how the eutectics can be combined with a set of tie lines. The CA_{*n*} ceramics are found in high-alumina cements. The phases are all shown as

being crystalline. Notice that CS is close to the midpoint, but that AS and CA are closer to Al₂O₃.

Example 3: Na₂O/CaO/SiO₂: Three components and P fixed (Figure 8.18). This system is particularly interesting because of its relevance to soda-lime glass

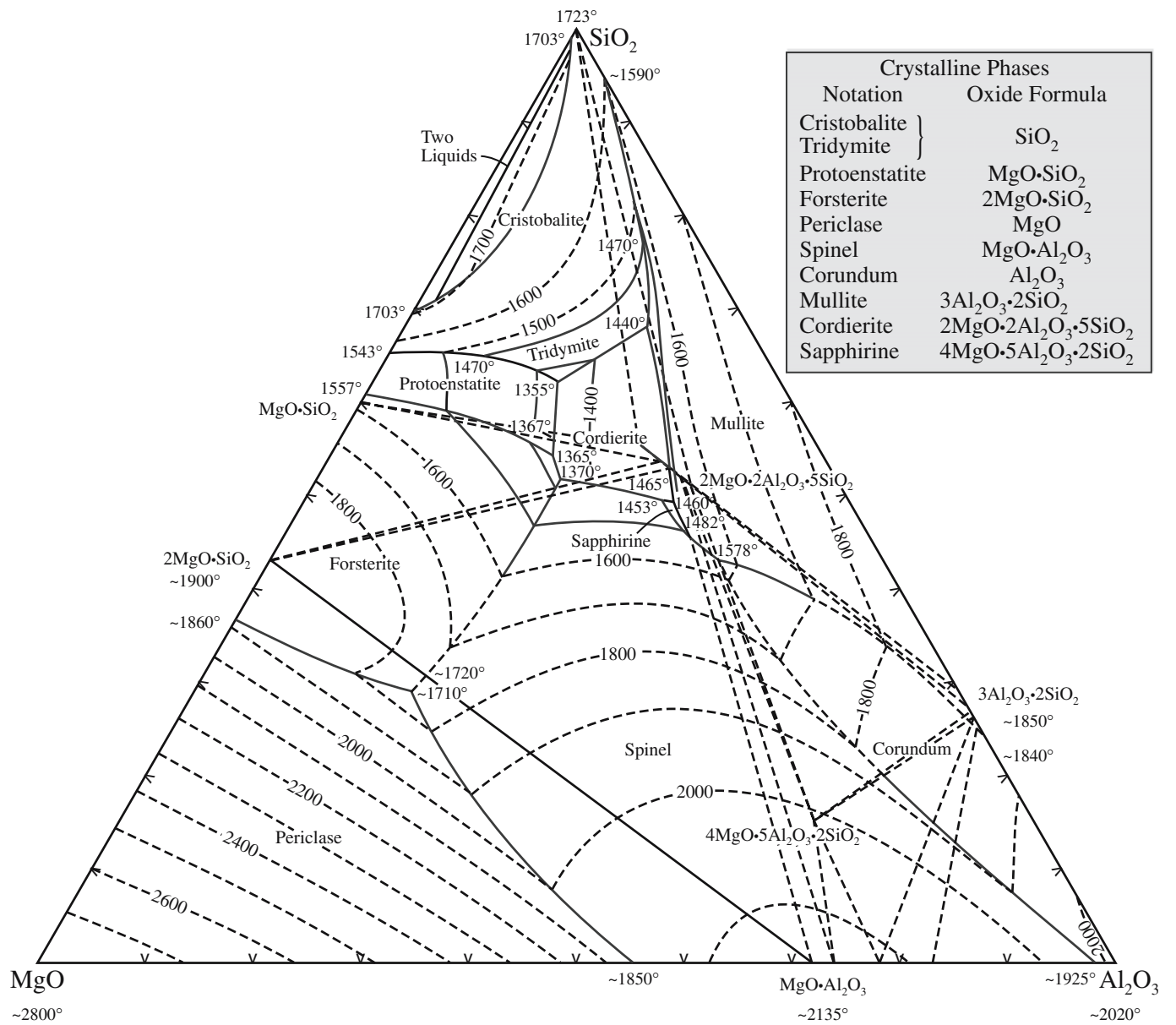


FIGURE 8.16 The MgO–Al₂O₃–SiO₂ phase diagram.

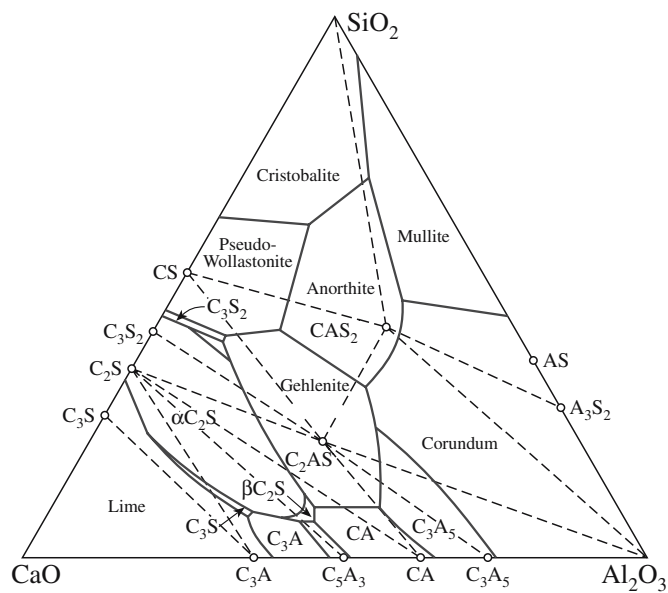


FIGURE 8.17 The CaO–SiO₂–Al₂O₃ phase diagram.

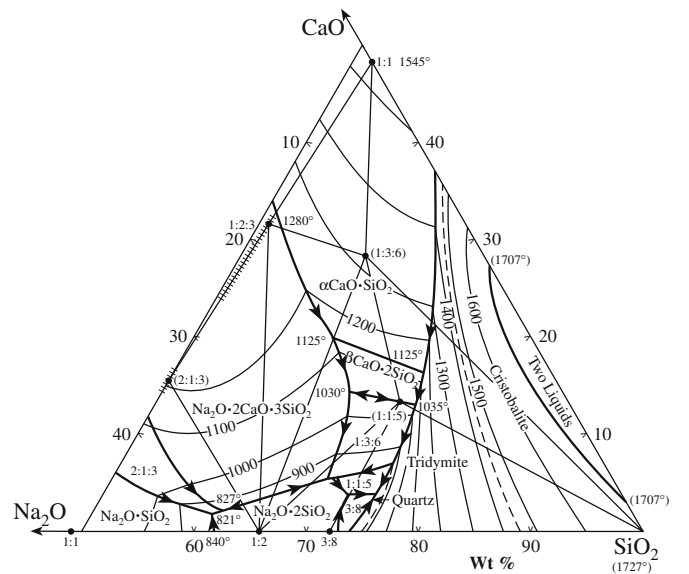


FIGURE 8.18 The Na₂O–CaO–SiO₂ phase diagram.

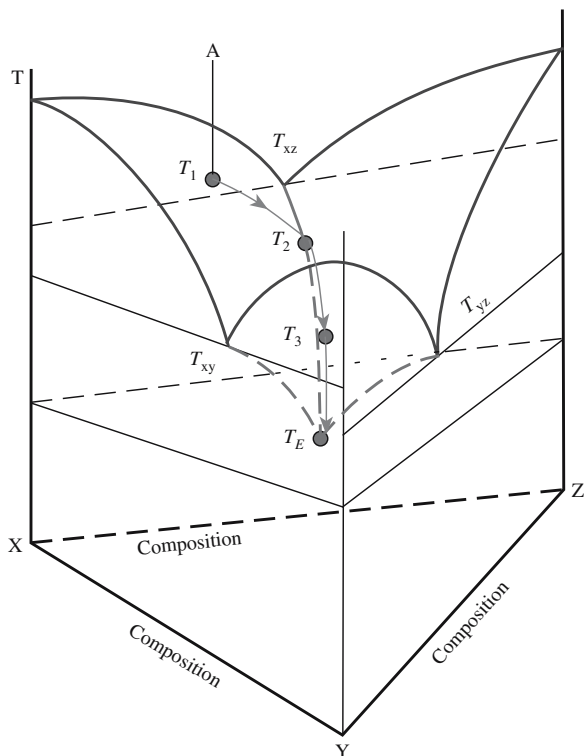


FIGURE 8.19 Illustration of a cooling path in a ternary system.

formation. Because of this interest, the diagram has been limited to the silica-rich corner of the Gibbs triangle.

Each of these diagrams shows the contours of the solid/liquid boundary. It is now a little more difficult to envision what occurs as we lower the temperature of the liquid phase. The basic ideas are the same as for the two-component systems as shown in Figure 8.19. The cooling path follows the steepest descent on the liquidus until, in this case, it reaches T_E , at which point the whole sample is solid and kinetics become the controlling factor.

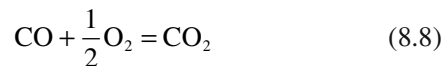
8.8 COMPOSITION WITH VARIABLE OXYGEN PARTIAL PRESSURE

The gas phase, particularly the oxygen partial pressure, pO_2 , is important when the valence of the cation can change.

In ceramics, we usually run experiments at 1 atm, but geologists are interested in much higher pressures, and hot pressing is an established commercial method for processing ceramics.

There are two ways to control the pO_2 . Usually, we do not try to change or control the total pressure—we avoid vacuum systems whenever possible because they greatly

increase the expense. The approach used is to fix the pO_2 using one of the following reactions:



If there is no solid present then we just have one phase, namely, the gas, and $X + F = C + 2$ gives $F = 3$. So we can vary T , P_{total} , and the composition (CO_2/CO ratio or H_2/H_2O ratio).

If there is a solid present (e.g., graphite or Ni) then we have just two variables (since we have two phases, $X = 2$), which will fix the system. If Ni is present, for example, then essentially the Ni/NiO equilibrium sets the pO_2 . The same occurs if Fe is present.

We will spend some time discussing the Fe–O diagram shown in Figure 8.20; here gas is important. In the Fe–O phase diagram, we have two components. We can call them Fe and O or FeO and Fe_2O_3 as we wish. The special feature in Figure 8.20 is the fact that usually the lines of constant pO_2 are horizontal whereas in two-phase fields they are inclined to the horizontal. They are inclined when the phase field contains a single phase (wüstite or magnetite).

In the two condensed phases region (region W + M: wüstite plus magnetite) there are two condensed phases plus the gas (O_2), so $X = 3$. There are two components ($C = 2$; Fe and O), so we have only one degree of freedom: we can vary T or pO_2 . So the oxygen isobars (lines of constant pO_2) on the phase diagram must be horizontal.

In the wüstite phase (region W) there is one condensed phase plus the gas (O_2), so $X = 2$. There are two components ($C = 2$; Fe and O), so we have two degrees of freedom ($F = 2$). The reason the isobars have the particular slope is that they must connect the appropriate isobars at each side of their phase field.

This is the special feature for ceramics, especially when processing ceramics with a variable-valence cation in air: pO_2 is important.

The diagram in Figure 8.20b shows the Fe–O diagram as a function of oxygen activity, which is essentially the pO_2 . This diagram shows what condensed phase is stable at

each combination of temperature and pO_2 . Although this diagram does not show as much information as Figure 8.20a (because it does not show the composition of the condensed phase), it does emphasize one special feature: if we increase the temperature while keeping the pO_2 constant, the oxidation state of the Fe ion decreases. In Figure 8.20b, the areas show situations in which only one phase is

PRESSURE CONVERSION

- 1 Pa = 1 N m⁻² = 1 m⁻¹·kg s⁻²
- 1 N = 1 m·kg s⁻²
- 1 bar = 0.1 MPa
- 1 kbar = 100 MPa
- 1 atm = 1.013 Pa
- 1 mm Hg = 1 torr = 0.1333 MPa

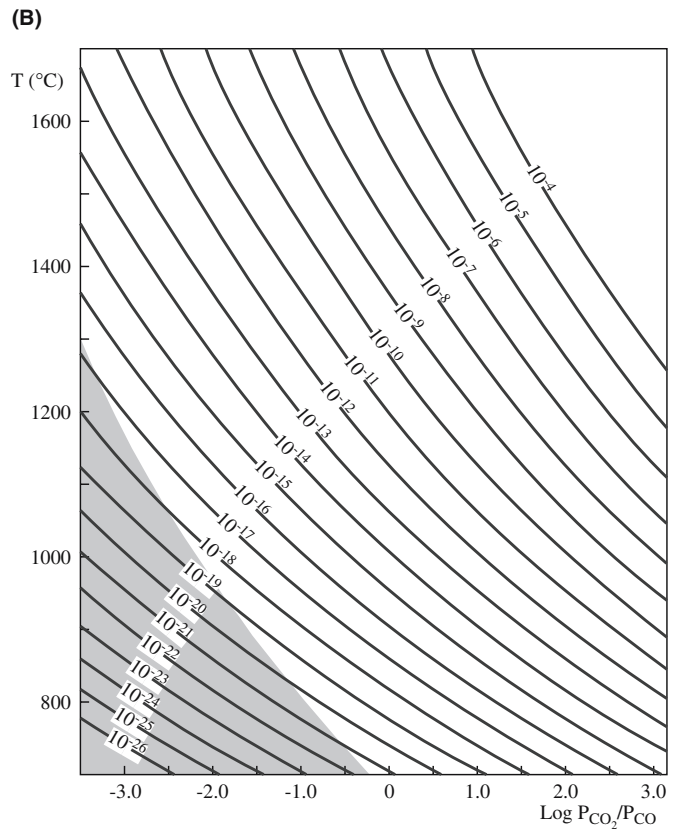
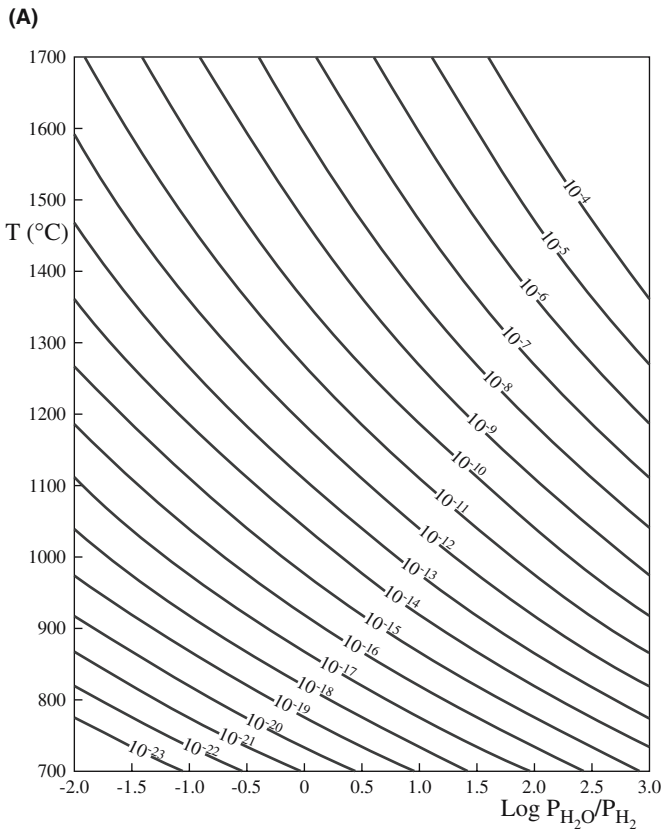
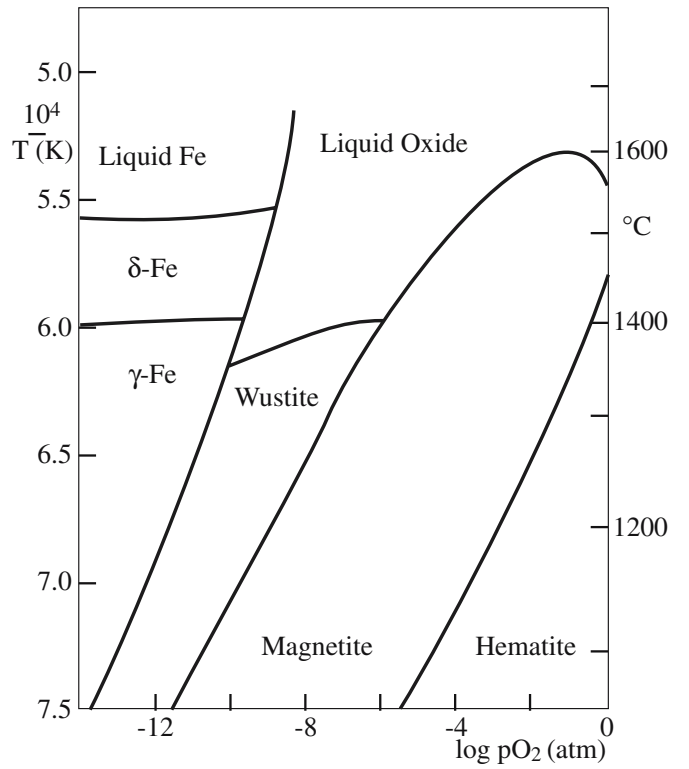
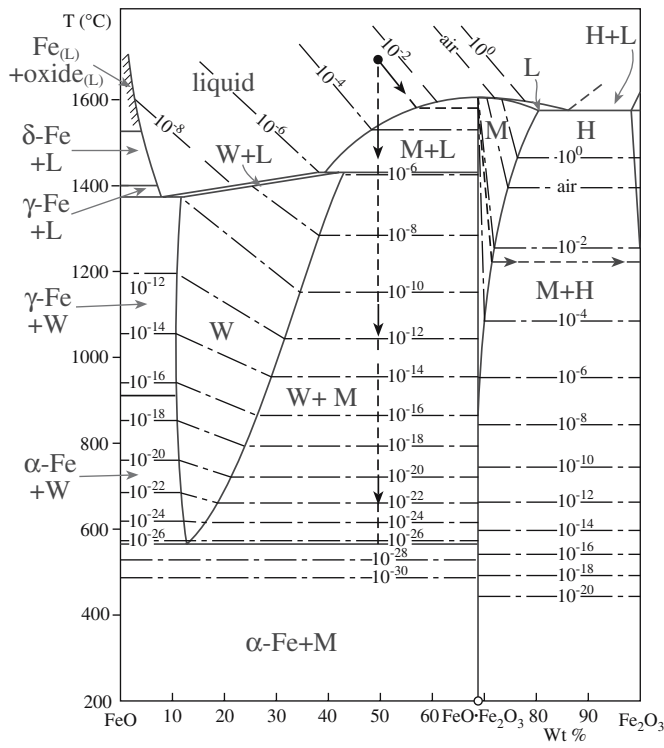


FIGURE 8.20 (a, b) The FeO–Fe₂O₃ phase diagram; (c) the H–O system; (d) the C–O system.

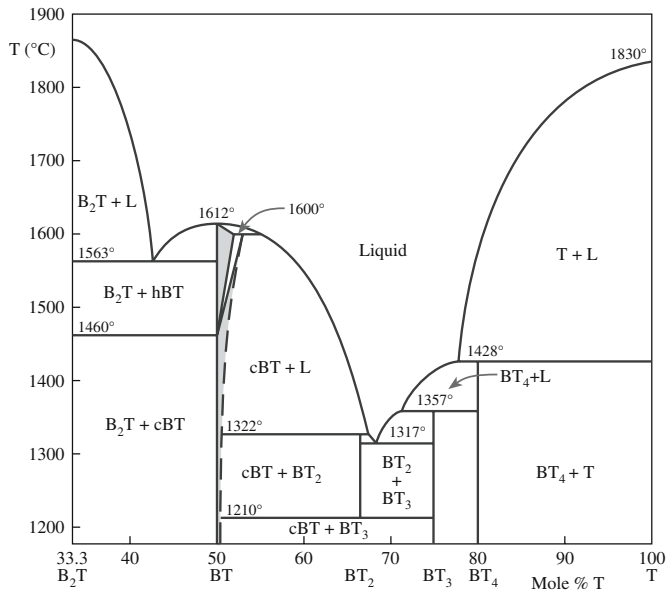


FIGURE 8.23 The BaTiO₃ phase diagram.

system (Figure 8.23). This diagram illustrates the concept of incongruent melting: there are actually three incongruently melting compounds. The diagram also shows that we cannot produce pure cubic BaTiO₃ by solidifying a liquid of that composition, which will be important when we discuss crystal growth later. Notice that all the compounds on this phase diagram are BT_n (BT, BT₄, etc.)

8.11 MISCIBILITY GAPS IN GLASS

Can glass be described by equilibrium phase diagrams? The question refers to the fact that glass is not itself in equilibrium. We can, however, describe some aspects of the glass microstructure in terms of phase diagrams, especially that of liquid immiscibility, which leads to the phenomenon of phase separation as illustrated in Figure 8.24.

The random-network model considers glasses as homogeneous. However, microscopic features on the scale of 3 nm to hundreds of nanometers can exist. These small features exist in a range of glasses and can result from a process of phase separation, in which a liquid that is homogeneous at high temperatures separates into two or more liquid phases on cooling.

Figure 8.25 shows the phase diagram for the BaO–SiO₂ system, which exhibits phase separation. The dome, shown by dashed lines because the system is metastable, is the key feature in a phase diagram in which phase separation occurs (a similar dome occurs for Al₂O₃/Cr₂O₃, so this dome is not peculiar to glass).

The microstructure of glasses in the system BaO–SiO₂ can be determined using transmission electron microscopy (TEM). We find the following:

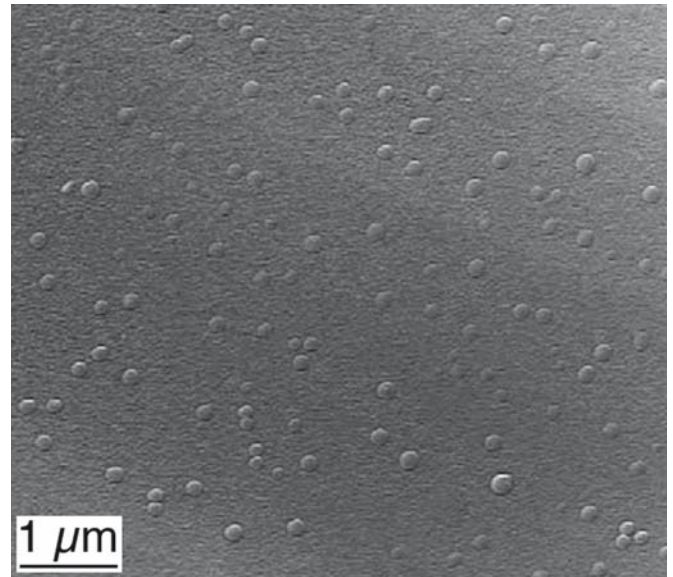


FIGURE 8.24 Image of small droplets of glass in a glass matrix. The composition of the glass is 16wt% CaO, 10wt% MgO, 14wt% Al₂O₃, and 60wt% SiO₂.

- At the silica rich side of the miscibility gap there are discrete spherical particles of a BaO-rich phase embedded in a continuous matrix of an SiO₂-rich phase.
- Near the center of the miscibility gap there is a three-dimensionally interconnected mixture of BaO and SiO₂ phases.

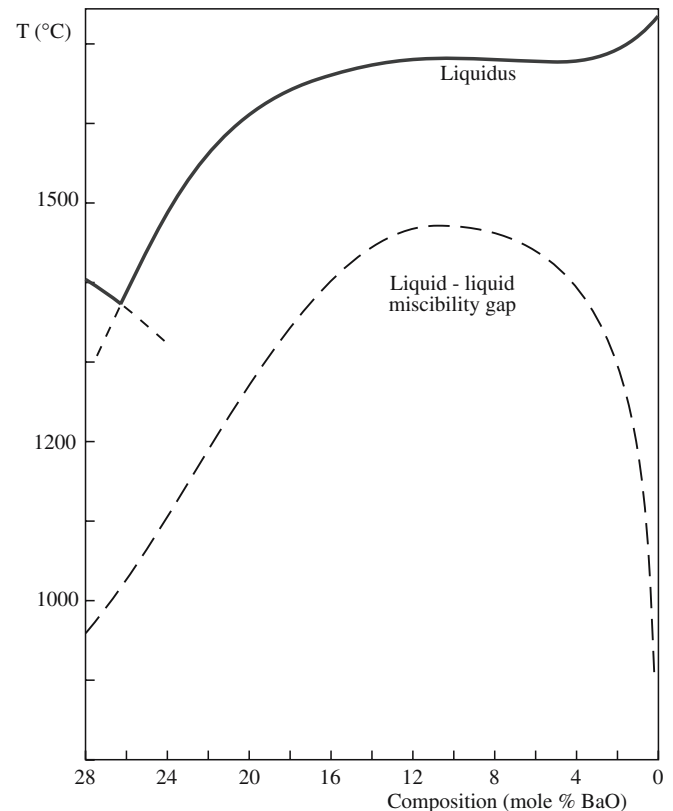


FIGURE 8.25 The silica-rich end of the BaO–SiO₂ phase diagram.

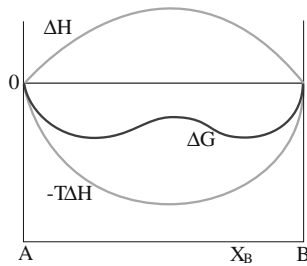


FIGURE 8.26 Energy diagram for a hypothetical system in which unmixing occurs.

- At the BaO-rich side of the miscibility gap there are discrete spherical particles of an SiO₂-rich phase embedded in a continuous matrix of a BaO-rich phase.

GIBBS FREE ENERGY OF MIXING

For an ideal solution ΔG_M is

$$\Delta G_M = RT(X_A \ln X_A + X_B \ln X_B)$$

and $\Delta H_M = 0$.

For nonideal solutions, $\Delta H_M \neq 0$.

The B₂O₃–PbO system is another glass-forming system that shows a miscibility gap and phase separation.

The reason for phase separation of a liquid into two phases may be found by consideration of the thermodynamics of mixing. Figure 8.26 shows the three thermodynamic functions, ΔG , ΔH , and ΔS , plotted at temperature T as a function of composition.

The common tangent to the minima in the free-energy curve determines the composition of the two phases in the glass and the proportions of each are determined by the lever rule.

Phase separation is important for some commercial glass formulations.

Vycor Process: Glass containing 75 wt% SiO₂, 20 wt% B₂O₃, and 5 wt% Na₂O melts at relatively low temperatures due to the high B₂O₃ content. It can then be formed into desired shapes and heat treated in the range of 500–600°C so that the glass separates into two distinct phases, one consisting of almost pure SiO₂ and another rich in Na₂O and B₂O₃. If this product is exposed to a suitable solvent at modest temperature, the sodium borate phase is leached out, leaving an SiO₂-rich framework with a network of pores that are ~4–15 nm in diameter.

This porous glass can be subsequently compacted at ~1000°C to yield a transparent glass containing about 96 wt% SiO₂. The advantage of this process is that we can form this silica-rich glass at relatively low temperature.

It would not be feasible to shape 96% silica glass by conventional methods because of the very high temperatures required to decrease the viscosity of a high-silica glass.

Pyrex: Pyrex glass also belongs to the Na₂O–B₂O₃–SiO₂-system. It exhibits phase separation on a very fine scale, typically less than 5 nm. By controlling the cooling process, we develop a glass with a special microstructure and very useful properties. It is the inclusion of a soluble phase within an insoluble one that explains the chemical durability of Pyrex.

CHAPTER SUMMARY

Phase diagrams are the key to understanding many aspects of ceramic processing. Whether we are interested in forming a material by a solid-state reaction or growing a single crystal by solidification of a melt, the first approach is to look up the appropriate phase diagram. Knowing where to find these diagrams (in the “books”) is almost as important as being able to interpret them. The basic principles are the same for ceramics as they are for metals. So our approach was to highlight some important aspects of phase diagrams as they relate to ceramics.

PEOPLE IN HISTORY

Gibbs, Josiah Willard (1839–1903) was born in New Haven, Connecticut. He was educated at Yale University and was awarded his doctorate in 1863—the first doctorate of engineering to be conferred in the United States. He was appointed professor of mathematical physics in 1871 prior to having any publications. He published the first part of his very famous work *On the Equilibrium of Heterogeneous Substances* in 1876 and the second part in 1878. He published many other important papers in thermodynamics as well as other areas of physical science.

Hume-Rothery, William (1899–1968) founded the Department of Metallurgy (now the Department of Materials) at Oxford University in the mid-1950s. HR, as he was known at Oxford, was the author of many books on metallurgy. One of his books, *Electrons, Atoms, Metals, and Alloys*, is a dialogue between an older metallurgist and a younger scientist.

Le Chatelier, Henry (1850–1936) is known for his principle and for inventing the optical pyrometer in 1892.

GENERAL REFERENCES

Bergeron, C.G. and Risbud, S.H. (1984) *Introduction to Phase Equilibria in Ceramics*, The American Ceramic Society, Westerville, OH. This should be available in every ceramics laboratory.
DeHoff, R.T. (2006) *Thermodynamics in Materials Science*, 2nd edition, CRC, Boca Raton, FL.
Gaskell, D.R. (2003) *Introduction to the Thermodynamics of Materials*, 4th edition, Taylor & Francis, New York.

Hummel F.A. (1984) *Phase Equilibria in Ceramic Systems*, Marcel Dekker, New York.

McHale, A.E. (1998) *Phase Diagrams and Ceramic Processes*, Chapman & Hall, New York.

Muan, A. and Osborn, E.F. (1965) *Phase Equilibria among Oxides in Steelmaking*, Addison-Wesley Publishing Co., Reading, MA. Reference for experimental determination of phase diagrams in ceramics. Inspirational with very helpful commentary; a “must see” text.

Phase Diagrams for Ceramists, Vols. I–VIII, The American Ceramic Society, Columbus, OH:

I (1964) edited by E.M. Levin, C.R. Robbins, and H.F. McMurdie

II (1969) edited by E.M. Levin, C.R. Robbins, and H.F. McMurdie

III (1973) edited by E.M. Levin and H.F. McMurdie

IV (1981) edited by R.S. Roth, T. Negas, and L.P. Cook

V (1983) edited by R.S. Roth, T. Negas, and L.P. Cook

VI (1987) edited by R.S. Roth, J.R. Dennis, and H.F. McMurdie

Volumes I–VI include mostly oxide and metal + oxide systems.

VII (1989) edited by L.P. Cook and H.F. McMurdie (halide systems, many calculated diagrams with methods discussed)

VIII (1990) edited by B.O. Mysen (geological, high pressure, and hydrothermal systems)

Under a new series title, but continuous numbering, *Phase Equilibria Diagrams, Vols. IX–XII*:

IX (1992) “Semiconductors and Chalcogenides,” edited by G.B. Stringfellow

X (1994) “Borides, Carbides, and Nitrides,” edited by A.E. McHale

XI (1995) “Oxides,” edited by R.S. Roth

XII (1996) “Oxides,” edited by A.E. McHale and R.S. Roth

The books are available on CD-ROM from www.esm-software.com/pd-ceramists but are too costly for most individuals.

Also a part of this series are *Phase Equilibrium Diagrams, Annuals '91, '92, and '93*, edited by A.E. McHale (these annuals contain a number of complex oxide systems), and *Phase Diagrams for High T_c Superconductors*, edited by J.D. Whittler and R.S. Roth (1991).

Ragone, D.V. (1995) *Thermodynamics of Materials*, Volume I, Wiley, New York.

Swalin, R.A. (1972) *Thermodynamics of Solids*, 2nd edition, Wiley, New York.

WWW

<http://thayer.dartmouth.edu/%7Eicelab/> The site of the ice laboratory at Dartmouth.

<http://www.ceramics.nist.gov/webbook/glossary/ped/glossary.htm> NIST’s site for phase equilibria of ceramics.

SPECIFIC REFERENCES

CALPHAD [computer file], Elsevier, New York. Available in many university libraries on line.

Ellingham, H.J.T. (1944) “Reducibility of oxides and sulfides in metallurgical processes,” *J. Soc. Chem. Ind. (London)* **63**, 125.

Hazen, R.M. (1999) *The Diamond Makers*, Cambridge University Press, Cambridge. Attaining the high pressures.

Richardson, F.D. and Jeffes, J.H.E. (1948) “The thermodynamics of substances of interest in iron and steel making from 0°C to 2400°C,” *J. Iron Steel Inst. (London)* **160**, 261.

Saunders, N. and Miodownik, A.P. (1988) *CALPHAD (Calculation of Phase Diagrams): A Comprehensive Guide*, Pergamon, Oxford.

Torres, F.C. and Alarcón, J. (2004) “Mechanism of crystallization of pyroxene-based glass-ceramic glazes,” *J. Non-Cryst. Sol.* **347**, 45.

EXERCISES

- 8.1. The iron–iron carbide phase diagram is probably the most important of all binary phase diagrams. Why is the diagram not a true equilibrium diagram? Does it matter?
- 8.2. Explain what we mean by the set of equations $\mu_1^a = \mu_1^b = \dots = \mu_1^c$. What is the significance of this expression?

- 8.3 The maximum operating temperature of high-temperature X-ray diffraction is 2500°C in vacuum but only 1700°C in air. Why the big difference? What, if any, effect would the lower operating temperature in air have on the determination of phase diagrams?
- 8.4 The $\text{UO}_2\text{-BeO}$ system shown in Figure 8.3 does not show any solid solution formation. Would you expect it to?
- 8.5 With reference to the phase diagram for water (Figure 8.6), explain (a) how the boiling point of water would change if you were to climb to the top of a mountain and (b) why ice-skating is possible.
- 8.6 Using Figure 8.7 determine the necessary conditions for direct conversion of graphite to diamond.
- 8.7 Using Figure 8.8 indicate all the triple points in the SiO_2 system.
- 8.9 Describe fully what happens when you cool down a melt of 40 mol% NiO -60 mol% MgO . Give the compositions of the phases and their relative amounts for at least three temperatures in the two-phase field.
- 8.10 Describe the phases that you expect to form as a liquid of composition BaTiO_3 is cooled down to room temperature. Given the statement we make in Section 8.10 about the growth of single crystals of cubic BaTiO_3 , what factors besides thermodynamics determine our ability to grow single crystals?

Part III

Tools

9

Furnaces

CHAPTER PREVIEW

Furnaces are the essential equipment in any ceramics laboratory. They can range in size from small electrically heated box furnaces, often called muffle furnaces, which can fit on a bench, to the enormous gas-fired furnaces used to melt glass. In between these extremes there are furnaces of many shapes and sizes, designed to run at a range of temperatures and in a range of atmospheres. In addition to obtaining a high temperature, it is necessary to have furnace components that can withstand these temperatures without degradation. These materials are known as refractories. Much of our knowledge of refractory ceramics has come from early developments in the iron and steel industries. Whenever temperatures are high, vapor pressures may also be high, so be aware that the furnace material may contaminate the material you are processing. We will also describe methods for measuring high temperatures and some of the important safety considerations that you must know when using furnaces and working at high temperatures.

9.1 THE NEED FOR HIGH TEMPERATURES

There are many areas in ceramics where we need high temperatures:

- Sintering: Most bulk ceramic components are made by sintering a powder compact. We need to use high temperatures ($>1200^{\circ}\text{C}$) because of the low self-diffusion coefficients in the solid state. Even for liquid phase sintering, temperatures are still often $>1200^{\circ}\text{C}$.
- Reactions: Forming mixed metal oxides such as BaTiO_3 and NiAl_2O_4 by solid-state reaction of the component oxides requires the use of elevated temperatures.
- Phase Transformations: An important phase transformation involves crystallization of a glass to form a glass-ceramic. Although the temperatures involved are not as high as those needed for glass melting, the phase transformation is typically carried out at around 800°C . Control of temperature is often necessary to ensure that the desired crystalline phase is formed and in the optimum particle size.
- Glass Melting: Glass products form the largest single segment of the ceramics industry. Glass production frequently requires melting of a batch consisting of a mixture of powdered metal oxides and metal carbonates. The temperature necessary to form a homogeneous liquid melt varies with batch composition, but is typically in the range $1300\text{--}1600^{\circ}\text{C}$. The melt is also

very corrosive, which provides additional considerations in the choice of refractories.

- Crystal Growth: Most of the methods used to form single crystals, whether in the laboratory or in industry, require the use of high temperatures. Many single crystals are produced from the melt or by using suitable fluxes, and particular attention has to be paid to avoiding contamination of the melt and controlling the temperature during growth.

9.2 TYPES OF FURNACE

We can categorize the furnaces used to fire and sinter ceramic components in several ways. One way is based on the type of heat source used:

- Combustion
- Resistive
- Microwave, radiofrequency (RF), or infrared (IR)/visible light

Alternatively we could group them as

- Periodic or batch furnaces
- Continuous furnaces

Electrical furnaces can produce direct (resistive) or indirect (induction or microwave) heating. We will look at

the characteristics of each group of furnaces, keeping in mind that there is overlap. For example, we can have continuous gas-fired furnaces or continuous electrically fired furnaces. Historically, continuous furnaces and gas-fired furnaces are usually found in industry. Batch and electrically fired furnaces are used widely in university laboratories and in many small- to medium-sized industrial applications. The current trend toward more environmental controls and demand for higher quality will continue to expand the applications for electrically powered furnaces. Electric furnaces account for about 60% of the total industrial heating equipment market (about \$3 billion in total). There is still growth in the use of combustion furnaces, in particular, for applications in the metal and cement industries.

This chapter is called furnaces, but it could have been called kilns or ovens, as all these terms are used to describe many of the same types of equipment. “Kiln” is widely used in the traditional ceramics industry and the pronunciation is sometimes “kil.” In the Potteries in England, for example, you may encounter the alternative pronunciation. “Furnace” is used interchangeably with kiln. “Oven” is more often used for either equipment used for drying ceramics (typically using lower temperatures) or for small furnaces.

9.3 COMBUSTION FURNACES

The most common combustion furnaces used in ceramic processing are gas fired and use gaseous hydrocarbons as fuel. The large amount of energy produced heats the furnace and the parts inside. Gas-fired furnaces are used mainly in large industrial applications such as glass melting, the production of ceramic colors, and firing of traditional ceramic articles, for example, tiles and white-ware. Figure 9.1 shows an example of a commercial glass-melting furnace.

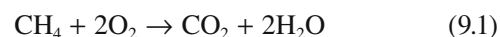


FIGURE 9.1 Gas-fired batch furnace used in a commercial glass blowing operation.

TABLE 9.1 Standard Molar Enthalpies of Combustion, ΔH_c° (kJ/mol)

CH ₄ (g)	890
C ₂ H ₂ (g)	1300
C ₂ H ₄ (g)	1411
C ₂ H ₆ (g)	1560
C ₄ H ₁₀ (g)	2877
C ₆ H ₁₂ (l)	3920
C ₆ H ₁₄ (l)	4163
C ₆ H ₆ (l)	3268
C ₁₀ H ₈ (s)	5157
CH ₃ OH (l)	726
CH ₃ CHO (g)	1193
CH ₃ CH ₂ OH (l)	1368
CH ₃ COOH (l)	874
CH ₃ COOC ₂ H ₅ (l)	2231
C ₆ H ₅ OH (s)	3054

Combustion is an oxidative process; for the case in which methane is the fuel:



The standard molar enthalpy, or heat, of combustion (ΔH_c°) may be calculated using Eq. 9.2:

$$\Delta H_c^\circ = \sum \Delta H_f^\circ(\text{products}) - \sum \Delta H_f^\circ(\text{reactants}) \quad (9.2)$$

For the reaction given in Eq. 9.1 we can write

$$\Delta H_c^\circ = \Delta H_f^\circ(\text{CO}_2) + \Delta H_f^\circ(2\text{H}_2\text{O}) - [\Delta H_f^\circ(\text{CH}_4) + \Delta H_f^\circ(2\text{O}_2)]$$

ΔH_f° refers to the enthalpy of formation, and these values are tabulated for many substances. One source is the thermochemical tables (e.g., Barin, 1989). Making the appropriate substitutions we get

$$\begin{aligned} \Delta H_c^\circ &= -393.51 + 2(-285.83) - (-74.81) \\ &= -890.36 \text{ kJ/mol} \end{aligned}$$

(Note that ΔH_f° for a material in its standard state is zero.)

The simple idea is that the amount of energy released during combustion depends on the strength of the bond in the gas. Fuels with many weak (less stable) bonds such as C–C and C–H yield more energy than fuels with fewer such bonds or fuels that contain large numbers of strong bonds, e.g., C–O and O–H. Table 9.1 lists the standard molar enthalpies of combustion for a range of hydrocarbons.

For many combustion reactions the standard enthalpy changes are listed as a function of temperature. If this information is not available then it is necessary to calculate the enthalpy change at the temperature of interest, $\Delta H_c^\circ(T)$ using Eq. 9.3.

$$\Delta H_c^\circ(T) = \Delta H_c^\circ(298) + \int_{298}^T \Delta c_p dT \quad (9.3)$$

TABLE 9.2 Temperature Dependence of Heat Capacities, $c_{p,m}$

Gases (298–2000 K)			
	a ($\text{JK}^{-1}\text{mol}^{-1}$)	b ($10^{-3}\text{JK}^{-2}\text{mol}^{-1}$)	c (10^5JKmol^{-1})
H ₂	27.28	3.26	0.50
O ₂	29.96	4.18	-1.67
CO ₂	44.23	8.79	-8.62
H ₂ O	30.54	10.29	0
CH ₄	23.64	47.86	-1.92

where c_p is the molar heat capacity at constant pressure, which can be expressed in the form

$$c_p(T) = a + bT + cT^{-2} \quad (9.4)$$

The temperature-independent coefficients a , b , and c are listed for several species in Table 9.2. It is important to remember that a , b , and c are valid only over certain temperature ranges.

Thermodynamics determines the maximum amount of energy that can be produced by a combustion reaction. This can be quantified by what is known as the adiabatic flame temperature, which is shown for several possible gas mixtures in Table 9.3. These values, and those for other gas mixtures, can be calculated by solving the enthalpy balance (Kirchhoff's law)

$$\Delta H_c^\circ(298\text{ K}) + \int_{298\text{ K}}^T \sum c_p dT = 0 \quad (9.5)$$

The maximum temperature that can be achieved in a gas-fired furnace is well below the adiabatic flame temperature because of heat loss caused by incomplete combustion and dissociation of the combustion gases (an endothermic process) at high temperature. Heat is also lost by conduction through the refractories and imperfect insulation.

9.4 ELECTRICALLY HEATED FURNACES

Most electrically heated furnaces use the principle of Joule, or resistance, heating where current flowing through a resistor produces heat. The starting point is Ohm's law:

$$V = IR \quad (9.6)$$

TABLE 9.3 Adiabatic Flame Temperatures of Various Gas Mixtures

Gas	Fuels with air		Fuels with O ₂	
	K	°C	K	°C
H ₂	2450	2177	3395	3122
CH ₄	2276	2003	3849	3576
C ₂ H ₂	2657	2384	3737	3464

relating the current, I , through a resistance, R , to the applied potential, V . As current flows power (P) is dissipated:

$$P = VI = I^2R \quad (9.7)$$

What we are often most interested in is the amount of energy converted into heat, Q , which is obtained simply by multiplying P by time, t :

$$Q = RI^2t = \rho \frac{l}{A} I^2t \quad (9.8)$$

The units of Q are joules, but are often given as kWh (the kilowatt hour), the familiar unit used by power utility companies to determine electricity usage.

The heat source in the earliest electric furnaces was dc arcs formed between carbon electrodes, so the heating element really was an element. Carbon (in the form of graphite) is still used as a heating element, but most heating elements are now made from compounds. There are several different types of heating element and we will describe some of the important ones in Section 9.7. The choice of heating element depends on the maximum temperature that is required and the environment to which the element will be exposed.

There are several advantages to electric heating:

- It is easy to measure power input
- It is easy to control heating rates and temperature
- The furnace can operate in an atmosphere independent of the heating source

The main disadvantage of electric heating is that it usually costs more per energy unit than gas heating. However, the total energy usage for electric furnaces may often be lower than for gas-fired furnaces. The cost issue is not normally a problem in a university laboratory, but it can be a major concern for industrial applications. Two other types of furnace that use electricity are induction furnaces and microwave furnaces.

9.5 BATCH OR CONTINUOUS OPERATION

Figure 9.2 shows an example of a small electrically heated batch furnace. These types of furnace are used for temperatures up to 1800°C and are designed to be used in air. Figure 9.3 shows another example of a batch furnace. This particular furnace is known as a tube furnace. By flowing gases along a tube placed inside the furnace the heating environment can be controlled. The usual operation of a batch furnace involves inserting the ceramic parts into the furnace at room temperature, heating to the desired temperature, then cooling back to room temperature. In some cases the parts may be inserted and removed while the furnace is at high temperature. For powders this approach



FIGURE 9.2 A small electrically heated box furnace.

does not usually produce any problems, but for large consolidated parts the problem of cracking due to thermal shock is an important consideration. Batch furnaces are mainly used for small-scale heating experiments and for process development and evaluation. But they can also be



FIGURE 9.3 An electrically heated tube furnace.

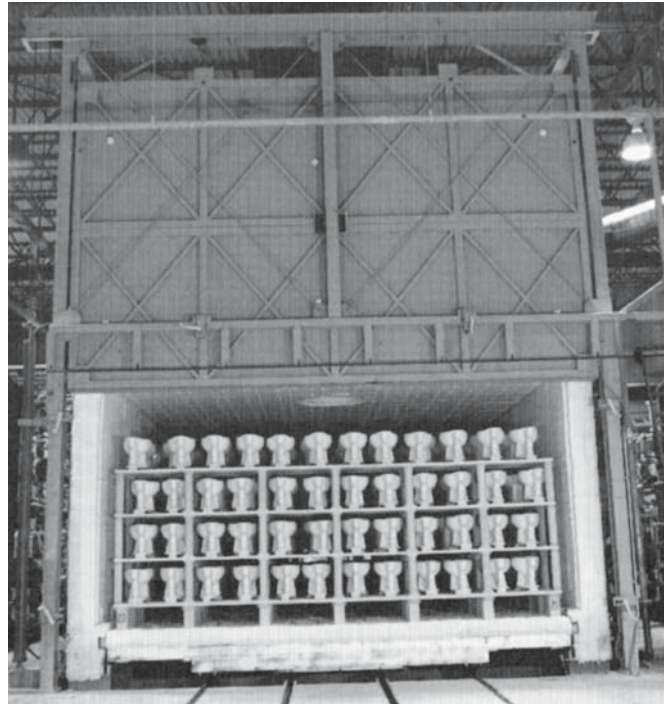


FIGURE 9.4 A large batch furnace used in the production of traditional ceramic products.

found in large industrial applications as shown in Figure 9.4. The advantages of batch furnaces are that they are simple to operate and flexible.

Figure 9.5 shows an example of a large industrial continuous furnace. The classic use is for firing bricks, pottery, tiles, and whitewares. Similar furnaces are used in the production of advanced ceramics such as multilayer ceramic chip capacitors.

In a continuous furnace, the temperature at each location in the furnace is constant with time. The parts are moved through the furnace at a velocity giving the desired time-temperature profile. Continuous furnaces are best

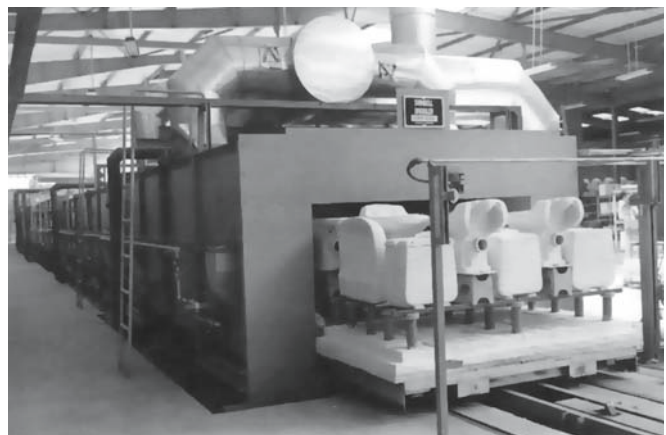


FIGURE 9.5 A large continuous furnace used in industry to produce traditional ceramic products and advanced ceramics such as multilayer chip capacitors.

for mass production where large quantities of material are subjected to the same conditions. The disadvantages of continuous furnaces are that the furnace temperature must be maintained throughout the process and their lack of flexibility.

9.6 INDIRECT HEATING

Induction furnaces. Induction heating provides a means for precise heating of electrically conducting objects. The object is immersed in an alternating magnetic field, which is usually produced by an external coil energized by an ac source. The magnetic field induces voltages in the conductive material, and these voltages produce circulating currents (called eddy currents). The magnitude of the induced voltage and the impedance of the material determine the size of the induced currents. It is the flow of induced currents that produces Joule heating of the material. A piece of metal may be introduced to begin the heating process—we must be able to couple the applied field to the ceramic. If the material we want to heat is an insulator we can place it inside a conductive crucible, such as graphite. A typical induction furnace is shown in Figure 9.6.

Induction heating gives many advantages:

- It is clean and fast
- The process is easily reproducible
- It can be automated
- Localized heating is possible (actually, it is essential)

Induction furnaces operate at frequencies from 60 to 1000 Hz and are thus often referred to as RF furnaces. They can be used to obtain temperatures up to 3000°C. Since the coil currents may be as high as 15 kA, the Cu coil conductors are usually hollow to permit water circulation for cooling.

Induction furnaces are generally used for melting and surface hardening. They are sometimes used in sintering in conjunction with hot pressing. These are the furnaces used in the skull-melting process, which is used to produce cubic zirconia.

Microwave furnaces. Microwave heating is an application of induction heating using higher frequencies. In many ways microwave furnaces are just expensive microwave ovens.

Heat is generated in nonconducting materials when microwave radiation excites the molecules in the material. The high-frequency radiation causes molecular polarization and the ability of the molecules to follow the rapid reversal of the electric field results in the conversion of electromagnetic energy into heat within the irradiated material. The two predominant frequencies are 915 and 2450 MHz (the microwave region extends from about 1 GHz up to about 300 GHz). Household microwave ovens operate typically at 2450 MHz. The main difference between the microwave oven you use at home and those used in industrial applications is the power. The maximum power of a domestic appliance is about 700 W; industrial versions have powers up to 5 kW.

Microwave furnaces currently are used for research and small-scale production because the available power sources are limited in size. Microwave processing is an area in which considerable research is being performed. The main direction for this research, and the possibility for future commercial applications, is in the reduction of production times and lowering the amount of energy consumption required for part processing.

The term “microwave safe” is used for various ceramic, glass, and plastic food and beverage containers. All glass and glass-ceramic cookware is microwave safe because it can withstand the high temperatures that can occur when cooking foods that are high in fat or sugar. Many plastics do not satisfy this requirement.

Arc-image furnaces. This is comparable to heating with electric light bulbs. The light is focused onto the sample using ellipsoidal mirrors. The heat is clean and the sample can be held in an inert or oxidizing atmosphere. An important application of arc-image furnaces is in the growth of single crystals of ceramics with high melting temperatures (Chapter 29).

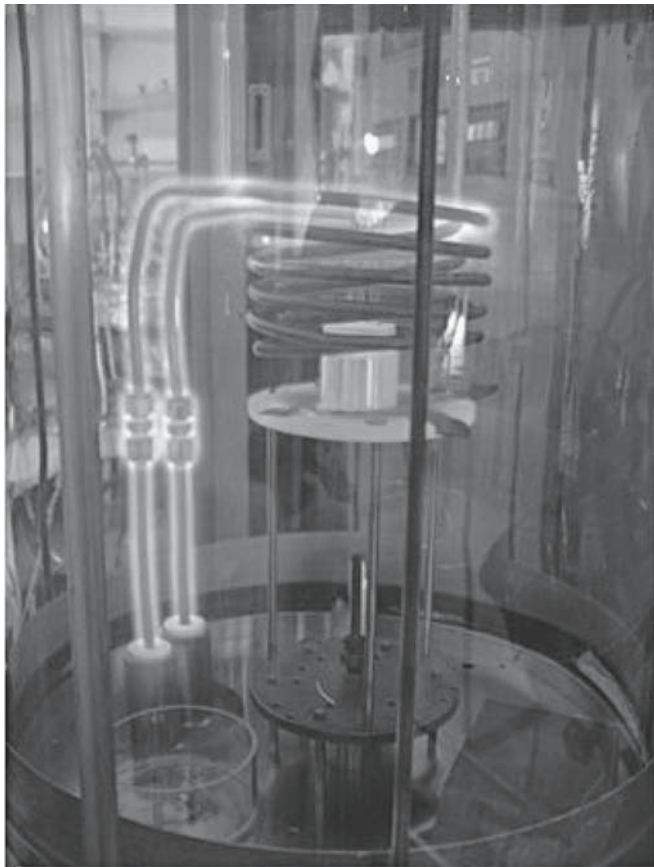


FIGURE 9.6 An induction furnace. The sample is mounted within the coils, which are usually water-cooled copper.

Lasers and electron beams. These can be used to provide local heating or to heat small quantities. The temperature control is not great, but these techniques are very versatile. Electron beams are used to vaporize silicon for thin-film deposition using molecular-beam epitaxy. A focused laser beam is the basis of the pulsed-laser deposition (PLD) thin-film growth technique (Chapter 28).

9.7 HEATING ELEMENTS

Never use a furnace like a black box. The heating elements will go to certain temperatures, but even then you may not want that type of material close to your sample to minimize contamination. Table 9.4 lists the materials used for electrical resistance heating.

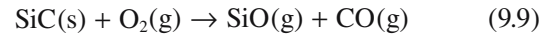
- Furnaces operating in air at temperatures up to 1300°C usually use wire-wound Cr alloys.
- For higher temperatures in air either precious metals or SiC rods are used.
- For very high temperatures requiring an oxidizing environment ceramic elements, most commonly ZrO₂, are used.
- In cases in which reducing atmospheres can be tolerated, graphite or refractory metals such as Mo and W can be used.

We will now look, in a little more detail, at some of the ceramic materials that are used as heating elements in furnaces. We will also mention one other type of resistance element, SnO₂, which is used in electrically heated glass-melting furnaces.

Silicon Carbide

Silicon carbide is the most widely used nonoxide ceramic for heating elements for high-temperature furnaces. SiC

heating elements can be used up to 1500°C in air because of the formation of a protective oxide layer. At temperatures in the range 1500–1600°C SiC decomposes:



There are three main methods used to produce SiC heating elements:

- *In situ* reaction
- Reaction bonding
- Sintering

In the first method a carbon tube is heated to about 1900°C in a bed of sand (SiO₂) and coke (C). The tube may be directly resistance heated or heated indirectly by a sacrificial tube of smaller diameter. Silicon monoxide is generated from Reaction 9.9 and infiltrates the carbon tube transforming it to SiC. The SiC tube is then removed and the residual carbon is burnt out. The tube has a porosity of about 30% and a large internal surface area. To prevent internal oxidation during use, the outer surfaces of the tube are coated with a thin layer of a calcium aluminosilicate glass and are then fired at about 1450°C. In this form the tubes have a uniform resistance along their length. A higher-resistance heating section is made by diamond sawing a spiral through the tube wall as shown in Figure 9.7. Adjusting the pitch of the cut varies the resistance.

In the second method a mix of SiC and carbon powders and a polymer binder is extruded to a rod. The “green” form is then brought in contact with molten silicon. The liquid penetrates the pores reacting with the carbon to form silicon carbide and bonding the grains together. The resulting ceramic has low porosity and, consequently, a long service life. The resistance of the hot section of the rod is adjusted to the required value by spiraling, which is easier to do when the ceramic is in the “green” state.

TABLE 9.4 Electrical Resistance Heating Element Materials

<i>Material</i>	<i>Maximum useful temperature (°C)</i>	<i>Usable atmosphere^a</i>
Chromium alloys		
Chromel C, Nichrome, Kanthal DT	1100	ONR
Kanthal A, Chromel A	1300	ONR
Metals		
Pt	1400	ONR
Pt–Rh alloys	1500–1700	ONR
Mo	1800	NR
W	2800	NR
Ceramics		
SiC	1500	ON
MoS ₂	1700	ON
Lanthanum chromite	1800	O
Thoria, stabilized	2000	ONR, shock
Zirconia, stabilized	2800	ONR, shock
Graphite	3000	NR

^aO, oxidizing; N, neutral; R, reducing. Shock, particularly poor resistance to thermal shock.



FIGURE 9.7 Examples of SiC furnace elements.

In the third method, SiC powder is mixed with a polymer binder and extruded. The rod is then sintered in a carbon furnace at approximately 2300°C. To give the rod low-resistance terminations the ends are dipped into molten silicon, which is allowed to infiltrate along a pre-determined length. In all cases the ends of the elements are coated with aluminum to make electrical contacts.

The main disadvantage of silicon carbide heating elements is that they are extremely brittle and must be handled carefully, especially when being installed and wired.

Molybdenum Disilicide

Many metals form conductive silicides that, like SiC, are resistant to oxidation through the formation of stable layers of silicates or silica on their surfaces at high temperatures. Molybdenum disilicide (MoSi_2) has been developed as a heating element for use in air at temperatures $>1500^\circ\text{C}$. The resistivity of MoSi_2 behaves in the same way as for a metal—it increases with increasing temperature. The room-temperature resistivity of MoSi_2 is $2.5 \times 10^{-7} \Omega\text{-m}$; it increases to about $4 \times 10^{-6} \Omega\text{-m}$ at 1800°C .

A commercial MoSi_2 heating element, known as Kanthal Super, is composed of a mixture of MoSi_2 particles bonded together with an aluminosilicate glass phase, which forms 20% of the total volume. The elements are fabricated by extruding a mixture of fine MoSi_2 powder with clay. The rods are dried, sintered, and cut to various lengths. The heating zones are bent to the required shape at high temperature and are then welded to the larger-diameter terminal sections. The best grade of MoSi_2 element is capable of operating at temperatures up to 1800°C .

Zirconia

Cubic stabilized zirconia (ZrO_2) is used as a furnace element allowing temperatures $>2000^\circ\text{C}$ to be achieved. Because of the low conductivity of ZrO_2 at room temperature, it requires preheating by gas or conventional resistance elements to reduce the resistance to a level at which

Joule heating is effective. At temperatures above 1000°C the ceramic becomes sufficiently conductive to be self-heating. Zirconia can also be used as a susceptor for induction heating.

Tin Oxide

SnO_2 is frequently used as electrodes in glass melting furnaces, particularly those used for making glasses for optical components and lead “crystal” tableware. The requirements for the electrode material are very specific:

- Electrical conductivity must be high at glass-melting temperatures.
- Resistance to corrosion by the molten glass must be high.
- It should not discolor the glass.

The electrodes are formed by mixing SnO_2 powder with small amounts of sintering aids such as ZnO and CuO and additives such as Sb and As , which make the material semiconducting. Typical electrode compositions contain more than 98 wt% SnO_2 . The oxide powders, together with binders, are pressed or slip cast into cylinders and fired in oxidizing conditions at temperatures of approximately 1400°C . The largest electrodes made in this way are in the form of cylinders 600 mm long and 150 mm in diameter weighing about 60 kg. Cooling from the sintering temperature is carried out, in part, in a nitrogen atmosphere with the object of creating oxygen vacancies and so increasing the room-temperature conductivity, which is typically about 0.1 S/m. A high conductivity minimizes Joule heating in the electrode region outside the molten glass.

In electrically heated glass-melting furnaces the batch is preheated, using oil or gas, to about 1000°C , at which time it has sufficient conductivity to be directly heated to the “glass-finishing” temperature ($1300\text{--}1600^\circ\text{C}$) by power dissipated internally. By supplying the heat from within the body of the glass melt rather than from the outside, the free surface temperature is kept relatively low and loss of volatile elements, particularly lead, is avoided. The process is economic since the heat is generated where it is required, i.e., in the glass. The elements are resistant to attack by glass and last about 2 years before being replaced.

Graphite

Graphite is a good choice as a heating element for resistive heating because it has a high melting temperature and a very low vapor pressure even at temperatures above 3000°C . These characteristics led to the use of graphite filaments in early incandescent lamps. (They were eventually replaced by tungsten, which came into general use as a filament for incandescent lamps in 1911.) The major disadvantages of using graphite furnace elements are

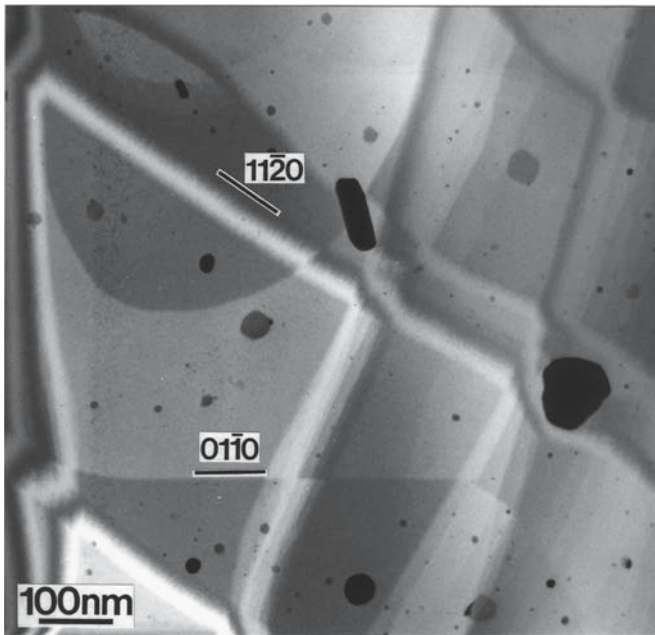


FIGURE 9.8 A TEM image showing small particles of tungsten contamination formed on SiC.

- Reactivity with oxide ceramics
- Susceptibility to oxidation

All metal oxides are reduced when in direct contact with graphite at high temperatures. Even the most refractory oxides will be reduced if the temperature is high enough.

Molybdenum and Tungsten

Both of these refractory metals are used as heating elements. Molybdenum reacts with oxygen above 700°C to form molybdenum trioxide (MoO₃). For applications above this temperature it is necessary to have a reducing environment or vacuum. The maximum usable temperature for molybdenum heating elements is about 1500°C. Above this temperature creep is a problem. Tungsten can be used for temperature up to 3000°C in inert atmospheres.

Figure 9.8 illustrates a problem that can occur with any furnace element—sample contamination. The sample is α-SiC, which was heated in a tungsten furnace for 12 hours at 1300°C. The dark features are tungsten particles evaporated onto the surface during heat treatment.

9.8 REFRACTORIES

Refractories are materials capable of withstanding high temperatures and not degrading in a furnace environment when in contact with corrosive liquids and gases. Refractory insulators are used in high-temperature applications to reduce heat losses and to save fuel. Table 9.5 lists some of the important furnace insulation materials together with their maximum usable temperature and thermal con-

TABLE 9.5 Refractories for Thermal Insulators

Material	T_{max} (°C)	k ($Wm^{-1}K^{-1}$)
Glass, fiber	600	0.05
SiO ₂ , fiber	1000	0.17
Firebrick, insulating	1200–1500	0.52
Fiberfrax	1650	0.12
Al ₂ O ₃ , bubble	1800	1.04
MgO, powder	2200	0.52
MgO, solid	2300	2.94
Carbon or graphite, powder	3000	0.09
Radiation shields, Mo	2100	0.69

ductivity, k . The lower the value of k , the better the thermal insulating effect for equal thickness.

Figure 9.9 shows the arrangement of refractory bricks in a typical glass-melting furnace. Approximately 70% of all refractories used by industry are in the form of preformed bricks that come in a variety of shapes. There are several different types of refractory brick and the choice depends mainly on the maximum operating temperature of the furnace and on the size of the furnace.

- Silica brick is made from naturally occurring sources of silica and is bonded by adding 3–3.5% CaO to promote liquid phase sintering.
- Semisilica brick is a silica brick containing between 18 and 25% Al₂O₃.
- Fireclay brick is made from kaolinite (Al₂O₃ · SiO₂ · 2H₂O) with between 25 and 45% Al₂O₃.
- High-alumina brick has an alumina content in the range 45–100 wt%.
- Dolomite brick is made from dolomite (CaCO₃ · MgCO₃).
- Magnesia brick contains mainly MgO (typically >90% MgO).
- Chrome brick is made from naturally occurring chrome ore. It contains 34% Al₂O₃ and 30% Cr₂O₃. Often MgO is added to produce chrome-magnesia brick.
- Zircon is ZrO₂ · SiO₂. Zircon refractory bricks may contain 4% CaO.

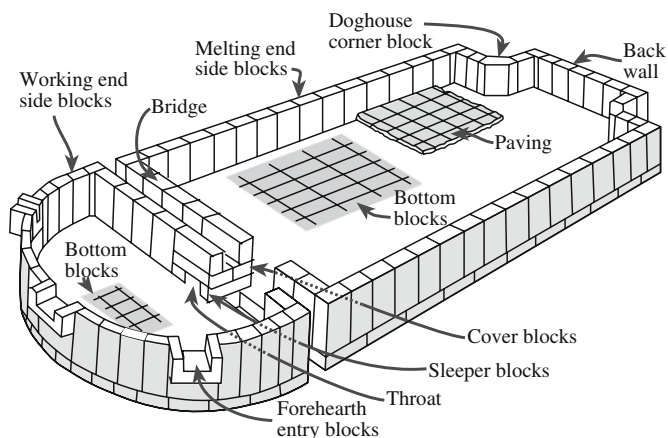


FIGURE 9.9 The layout of refractories in an industrial glass melting furnace.

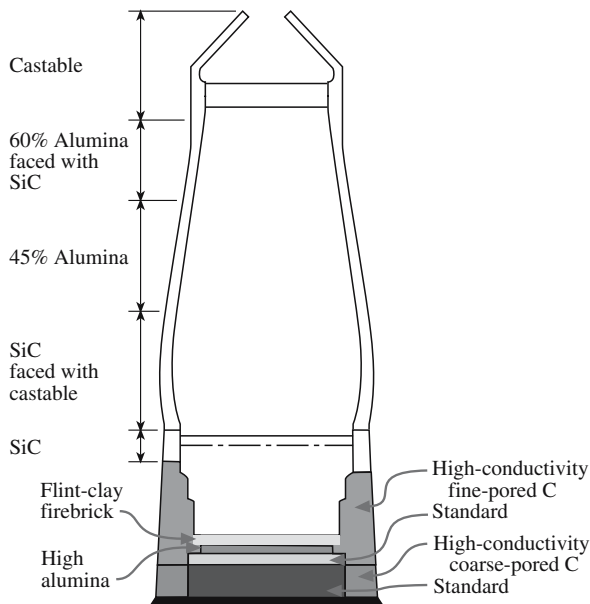


FIGURE 9.10 Diagram of a blast furnace indicating the type of refractories used in each region.

The schematic diagram of a blast furnace in Figure 9.10 shows how different types of refractories are used within the furnace. The maximum temperature ($>1700^{\circ}\text{C}$) is reached toward the base of the furnace where the air “blast” comes in and where the slag is formed. Slag is a glassy waste product made up of limestone and silica (impurities in the iron ore), ash, and oxides. It is lighter than the molten iron and so forms a layer above it.

Refractories are one example where a high-density ceramic product is not desirable—the space-shuttle tiles being the extreme example. The thermal conductivity, k_p , of air is only $0.026\text{ W m}^{-1}\text{ K}^{-1}$, significantly less than that of most crystalline ceramics. The thermal conductivity of a porous ceramic can be calculated using Eq. 9.10.

$$k_m = k_c \left(\frac{1 + \{2V_p[1 - (k_c/k_p)]/[2k_c/k_p + 1]\}}{1 - \{V_p[1 - (k_c/k_p)]/[k_c/k_p + 1]\}} \right) \quad (9.10)$$

k_c is the thermal conductivity of the ceramic, k_p is the thermal conductivity of air, and V_p is the volume fraction of porosity.

When $k_c > k_p$, the resultant thermal conductivity is

$$k_m \sim k_c[(1 - V_p)/(1 + V_p)] \quad (9.11)$$

As an illustration we can use Eq. 9.11 to estimate the thermal conductivity of a silica firebrick containing 30 vol% porosity, i.e., $V_p = 0.3$. The values of k_c and k_p are 1.4 and $0.026\text{ W m}^{-1}\text{ K}^{-1}$, respectively. This gives a value of $k_m = 0.75\text{ W m}^{-1}\text{ K}^{-1}$.

Consequently, ceramics containing a high volume fraction of porosity have low values of k . The ceramic provides the high strength and high melting point require-

ments of the insulating material and the porous microstructure ensures a very low k . We will discuss other factors that affect thermal conductivity in Chapter 34.

In addition to their use in furnaces for ceramics processing, refractories are also a very important sector of the ceramics industry because they are widely used in most high-temperature manufacturing processes:

- Iron and steel making (accounting for almost two-thirds of all refractories used)
- Copper and aluminum smelting
- Cement and ore processing
- Petroleum refining
- Petrochemical manufacturing

9.9 FURNITURE, TUBES, AND CRUCIBLES

Table 9.6 lists some of the important crucible materials. Crucibles and other furnace equipment such as boats and setter plates must meet the same requirements as refractory materials used for furnace insulation, i.e., they must be able to withstand high temperatures and also contact with any corrosive liquids or gases used. Items such as crucibles and boats should also possess good thermal

TABLE 9.6 Crucible and Furnace Materials

Material	T_{max} ($^{\circ}\text{C}$) (useful)	Usable atmosphere
Glasses		
Pyrex	500	ONR
Vycor	1100	ONR
Silica glass (fused quartz)	1200	ON(R)
Oxides		
Porcelain	1100–1300	ONR
Steatite, talc	1250	ONR
Firebrick, fireclay	1200–1500	ONR
Firebrick, high alumina	1600	ON(R)
Mullite ($3\text{Al}_2\text{O}_3 \cdot 2\text{SiO}_2$)	1700	ON(R)
Sillimanite ($\text{Al}_2\text{O}_3 \cdot \text{SiO}_2$)	1700	ON(R)
Zircon ($\text{ZrO}_2 \cdot \text{SiO}_2$)	1750	ON(R)
Spinel ($\text{MgO} \cdot \text{Al}_2\text{O}_3$)	1800–1900	ONR, shock
Alumina (Al_2O_3)	1850–1950	ONR
Magnesia (MgO)	2300	O, shock
Zirconia, stabilized	2300	ON(R), shock
Thoria, stabilized	2700	ON, shock
Metals		
Iron, nickel	1100	(O)NR
Platinum	1500	ONR
Rhodium	1800	ONR
Tantalum	2000	NR
Iridium	2100	ONR
Molybdenum	2100	NR
Tungsten	3000	NR
Other		
Silicon carbide	1500	ON
Silicon nitride	2900	ON
Carbon, graphite	3000	NR

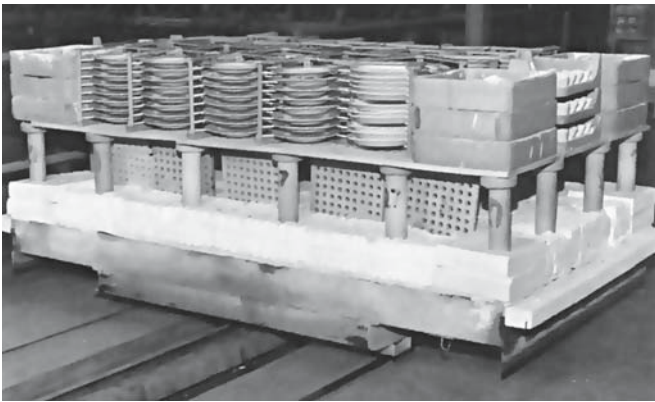


FIGURE 9.11 Kiln furniture used in the production of dinnerware.

shock resistance as they may be heated and cooled rapidly. Figure 9.11 shows an example of kiln furniture used for the production of dinnerware. Any component in contact with a crucible or other piece of furnace equipment at high temperature can be contaminated. SiO_2 is a major contaminant unless you are very careful.

9.10 FIRING PROCESS

A furnace is fired up in three stages.

- The heating-up stage
- The soaking period
- The cooling stage

The variations in the heating-up rate are chosen so that the changes of state to which the product is subject and the stresses that arise from the thermal expansion of the product and the combustion of binders do not cause damage (e.g., cracks and pores). A common phase transformation that occurs during firing of silica-containing ceramics (such as whitewares) is that between α and β quartz at 537°C .

Furnace design and the heating mechanism determine the maximum heating rate of a furnace. It is important to always check the operating manual that came with a furnace before setting the controller.

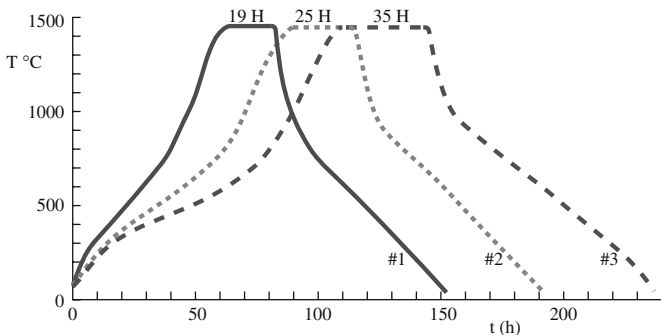


FIGURE 9.12 Firing curves for clay-bearing ceramic compositions. The soaking periods are in hours.

The degree of sintering is a function of time and temperature. Different processes use different soaking periods (the time at the desired firing temperature). For example, in the firing of thick-film inks the typical soaking period is relatively short, only 6–10 minutes. Figure 9.12 shows examples of much longer soaking periods used in the firing of clay-bearing ceramics.

Crystallization and other phase transformations that may occur in a product as well as thermal contraction must be taken into account in the cooling stage. At the beginning of the cooling process the material is generally still rather plastic. It can be cooled fairly quickly at this stage, because the thermal contraction does not cause the stresses to increase very much. Below a certain temperature the plastic characteristics disappear. For many clay-based ceramics this is between 800°C and 600°C . In this range, a higher cooling rate accompanied by a steep temperature gradient can cause stresses to form in the product. In temperature ranges in which phase transformations accompanied by volume changes take place, too high a cooling rate can produce cracks. Especially when using raw materials rich in quartz, the specification of the cooling rate requires special care. One of the goals in processing both traditional and advanced ceramics is to decrease the product throughput time. Fast firing seeks to reduce total costs because of lower energy consumption and improved efficiency.

9.11 HEAT TRANSFER

The liberation of heat energy is only the first stage of the heating operation. This energy has to be transferred to the material to be heated. There are three fundamental types of heat transfer: conduction, convection, and radiation. All modes of heat transfer

- Require the existence of a temperature difference
- Are from the high-temperature medium to a lower-temperature one

A detailed study of heat transfer is best left to a specific course on this topic or you can consult one of the standard texts, for example, Chapman (1984). Below we give a very brief description of each mode.

- Conduction is the transfer of heat from one part of a body to another part of the same body, or from one body to another that is in physical contact with it.
- Convection is the transfer of heat from one point to another within a fluid, gas, or liquid, by mixing of one portion of the fluid with another. In natural convection, the motion of the fluid is entirely the result of differences in density resulting from temperature.
- Radiation is the transfer of heat from one body to another, not in contact with it, by means of wave motion through space.

Any, or all, of these mechanisms may be important in a particular heating application. Usually they operate simultaneously, but often one predominates. At very high temperatures such as those encountered in ceramic sintering, radiation is often the most important. At lower temperatures convection is most likely to predominate.

9.12 MEASURING TEMPERATURE

In this section we will describe some of the approaches used to determine the high temperatures employed in the processing of ceramics. More detailed information on temperature measurement can be found in McGee (1988).

Thermocouples

The most common and convenient means of measuring temperature is to use a thermocouple. The principle behind the operation of a thermocouple is the Seebeck effect discovered in 1821 by Thomas Seebeck. If two wires of different metallic composition are connected at their ends forming a closed circuit, an electric current flows if one of the connections is heated. Measuring the potential (emf) causing this current allows the determination of temperature. In Seebeck's original research the two metals were bismuth and copper.

There are many different types of thermocouples available to cover temperatures ranging from -273°C to 2000°C ; the most important ones are given in Table 9.7. The type of thermocouple you would use depends mainly on the temperature range over which you will be requiring information and the desired accuracy of the temperature reading. The most commonly used thermocouples for

ceramic applications are types K, R, and C. These are used for temperatures up to 1250°C , 1450°C , and 2300°C , respectively. At lower temperatures it is preferable to use a base metal combination such as chromel-alumel, which gives greater accuracy.

In furnaces, the leads of the thermocouple are usually isolated from each other and other parts of the furnace by placing them either in thin alumina sheaths or by threading alumina beads along their length. The thermocouple should ideally be placed directly into the furnace cavity close to the object being heated. The external circuitry that measures temperature and, through an associated electrical circuit, controls the power to the heating elements is kept outside the furnace.

A thermocouple is a very accurate means of measuring temperature. But you should always bear in mind that the temperature being measured is that at the thermocouple tip. Unless the thermocouple is in intimate contact with the ceramic parts being heated, they may actually be at a different temperature than that measured by the thermocouple. A good illustration of this point is that thermocouples are often used to give substrate temperatures during thin film growth. The thermocouple is frequently attached to be substrate support but is not in direct contact with the substrate itself. In controlled tests it has been found that the measured thermocouple temperature and the actual surface temperature of the substrate can be off by as much as 100°C or in some cases even more.

Pyrometers

At any temperature, above 0K, all objects emit electromagnetic radiation in accordance with the Stefan-Boltzmann law:

TABLE 9.7 Characteristics of Thermocouples

Type	Combination of metals or alloys	Output ^a at 900°C (mV)	Temperature limit $^{\circ}\text{C}$	Applications
T	Copper-constantan	20.9 ^b	400	Mild oxidizing, reducing, vacuum, or inert. Good where moisture is present. Low temperature and cryogenic applications.
J	Iron-constantan	21.9 ^b	760	Reducing, vacuum, inert. Limited use in oxidizing at high temperatures. Not recommended for low temperatures.
E	Chromel-constantan	68.8	900	Oxidizing or inert. Limited use in vacuum or reducing. Highest EMF change per degree.
K	Chromel-alumel	37.3	1250	Clean, oxidizing, and inert. Limited use in vacuum or reducing. Wide temperature range. Most popular calibration.
S	Pt-Pt 10% Rh	8.4	1450	Alternative to Type K. More stable at high temperatures. Oxidizing or inert. Do not insert into metal tubes. Beware of contamination. High temperature.
R	Pt-Pt 13% Rh	9.2	1450	Same as Type S.
B	Pt 6% Rh-Pt 30% Rh	4.0	1700	Oxidizing or inert. Do not insert into metal tubes. Beware of contamination. High temperature. Common use in glass industry.
G (W)	W-W 26% Re	12.3	2300	Vacuum, inert, hydrogen. Beware of embrittlement. Not practical below 750°C . Not for oxidizing atmosphere.
C (W5)	W 5% Re-W 26% Re	16.4	2300	Same as Type G. Nonoxidizing atmosphere only
D (W3)	W 3% Re-W 25% Re	15.1	2300	Same as Type G. Nonoxidizing atmosphere only

^aThe higher the output voltage, the simpler the associated circuitry and/or the more accurate the temperature reading.

^bOutput at 400°C .

$$E = \sigma T^4 \quad (9.12)$$

σ is the Stefan–Boltzmann constant, which has a value of $5.6718 \times 10^{-8} \text{ JK}^{-4} \text{ m}^{-2} \text{ s}^{-1}$. The total energy (E) emitted at all wavelengths is proportional to T^4 . It is possible to estimate the temperature of a hot object by its color. In 1557 in his work on Renaissance pottery, Cipriano Piccolpasso described how the furnace operator was able to use color variations to judge furnace temperatures. As the temperature of an object increases the range of wavelengths that it emits increases and shifts to shorter values. At temperatures above about 500°C there will be a red coloration that will become increasingly orange as the temperature increases beyond 1000°C . At 1400°C the object will appear bright white. Be careful when looking at hot objects and remember that an object can still be too hot to handle even if it is not glowing red.

Optical pyrometers allow direct measurement of the temperature of an object. The disappearing filament optical pyrometer works by matching the intensity of radiant energy coming from an incandescent source to the intensity of a calibrated filament when both the source and the filament are viewed through a red filter. When the filament and the source intensities are the same, the image of the filament disappears as it is superimposed on the image of the source. An obvious requirement of this technique is that it can be used only to measure temperatures that produce visible incandescence, above about 750°C .

The advantages of the disappearing filament pyrometer are as follows:

- The distance from the target to the source is not important (it is only necessary to have a clear image to compare with the filament image).
- Various places on a target can be examined for temperature distribution.
- Very high temperatures can be measured.
- The visible image ensures that the instrument is measuring the temperature of the desired portion of the target.
- Reasonable accuracy (at best $\pm 0.2^\circ\text{C}$ at 775°C reduced to $\pm 1^\circ\text{C}$ at 1225°C) can be obtained.

The disadvantages are as follows:

- The instrument either must be sighted under blackbody conditions or the reading corrected for emittance.
- Absorption by dust, windows, flame, and other optical interference can produce errors.
- The disappearing filament optical pyrometer is slow and manual. However, other pyrometers such as the photoelectric optical pyrometer can be automated.

Pyrometric Cones

Pyrometric cones are small triangular ceramic prisms that when set at a slight angle (known as self-supporting cones)

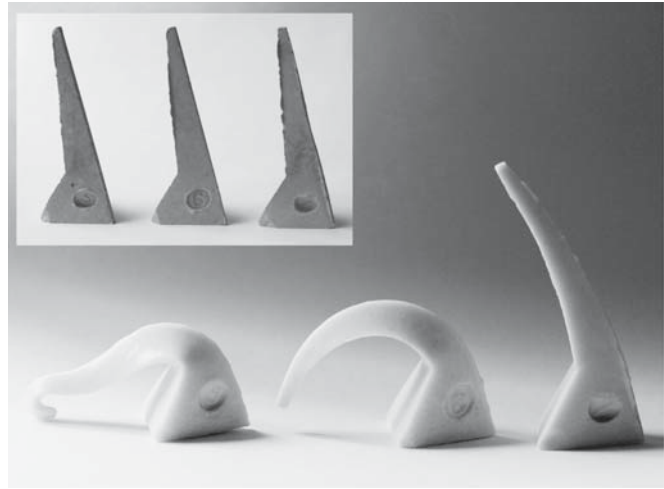


FIGURE 9.13 Orton cones: the self-supporting type. The cones shown are 6 cm tall in their initial state.

bend over in an arc so that the tip reaches the level of the base at a particular temperature if heated at a particular rate, as shown in Figure 9.13. The bending of the cones is caused by the formation of a viscous liquid within the cone body, so that the cone bends as a result of viscous flow. The endpoint temperature when the tip of the cone touches the supporting plate is calibrated for each cone composition when heated at a standard rate. Values of endpoint temperatures for Orton cones (the U.S. name) are listed in Table 9.8 for the higher temperatures; the series actually runs from Cone 022 at 600°C , through Cone 06 at 999°C , to Cone 42 at the top of the scale. Since pyrometric cones are sensitive to both time and temperature, the actual temperatures associated with each cone can vary, but this is also one of the reasons why they are very useful for ceramic processing. Sintering, for example, depends on both time and temperature.

TABLE 9.8 End Points of Orton Pyrometric Cones

Cone number	End point ($^\circ\text{C}$)	Cone number	End point ($^\circ\text{C}$)
12	1337	31	1679
13	1349	31½	1699
14	1398	32	1717
15	1430	32½	1730
16	1491	33	1741
17	1512	34	1759
18	1522	35	1784
19	1541	36	1796
20	1564	37	1830
23	1590	38	1850
26	1605	39	1865
27	1627	40	1885
28	1638	41	1970
29	1645	42	2015
30	1654		

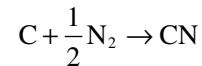
9.13 SAFETY

The safety issues associated with the use of furnaces can be divided into three categories.

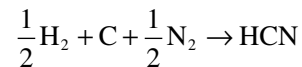
- *High-temperature hazards.* Working with high temperatures is the obvious safety hazard when using furnaces. Protective goggles or safety glasses should be used in all situations. As the temperature increases, the intensity of the emitted light rises and the maximum shifts to shorter frequencies. This is apparent to an observer. At 1000°C the color of a furnace enclosure is a pleasing red. At 1600°C it is a brilliant painful white and goggles or glasses with green lenses should be used. Handling objects that have come from a furnace should be done using specially designed tongs and furnace tools and hands should be protected with insulating gloves. Even if an object is not glowing red it can still be at a temperature of >500°C.
- *Electrical hazards.* Electrical dangers should never be underestimated. All electrical equipment operating at mains voltages can be lethal. A current >100 mA (ac or dc) would almost invariably be fatal if passed through the body. Most electrical accidents are caused by worn-out equipment or faulty wiring, both of which can be avoided. All potentials in excess of a few tens of volts must be properly insulated and physically isolated before maintenance. A typical laboratory box furnace uses 240 or 208 V single phase at 50 or 60 Hz to generate 10 kW of power. This requires a current of about 40 A. All electrical equipment not fully insulated must be properly earthed in the interests of safety.
- *Chemical hazards.* Some of the chemicals used in ceramic processing are toxic. One important example is lead and its oxides, which are widely used in the production of certain types of glasses and pigments. Care should be taken to read safety data sheets that accompany any chemicals and to take the necessary preventative action. Other safety issues can arise from unwanted reactions that occur within the furnace.

Carbon monoxide (CO) is a deadly gas that can form from a reaction between trapped moisture (for example, in the furnace insulation) and carbon. The source of carbon may be the graphite used in some furnaces for heating elements or in graphite-felt insulation. Problems can be avoided by ensuring that the furnace is kept dry. Domestic CO alarms can be installed in the laboratory area as an added precaution.

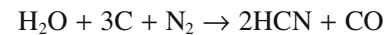
The importance of nitrogen ceramics, such as silicon nitride, means that furnaces are often operated using nitrogen gas. At high temperatures it is possible to form cyanide complexes such as cyanogen (CN) and hydrogen cyanide (HCN). In graphite furnaces the following reaction can occur:



Above temperatures of 2200°C the CN concentration exceeds the lethal concentration guidelines. Fortunately the gas is unstable and can be destroyed by passing it through an oxidizing flame. Hydrogen cyanide can form in graphite furnaces that contain mixtures of H₂/N₂ (called forming gas).



Forming gas is used in metal sintering furnaces and in some metallization processes to avoid oxidation of the metal. HCN can also form when water vapor, graphite, and nitrogen react:



It is essential to maintain dry conditions in these furnaces, as the reaction is thermodynamically favored at all temperatures. In cases that can involve the build-up of deadly gases it is essential that the laboratory is well ventilated and the discharge is vented away from the immediate work area.

CHAPTER SUMMARY

Furnaces are ubiquitous in all aspects of ceramics research, development, and production. High temperatures may be obtained through harnessing the heat generated by combustion reactions, but more usually resistance heating is used. Ceramic materials, most notably SiC, are widely used as resistive elements in electrically heated furnaces. They are also used to provide thermal insulation in all types of furnace. These materials are known by the collective term refractories because of their stability at high temperatures and their resistance to corrosive environments. Refractories are a major sector of the ceramics industry with the largest consumers being the iron and steel companies.

PEOPLE IN HISTORY

Joule, James Prescott (1818–1889), the English physicist born in Salford near Manchester, showed that heat is produced by motion and thus helped end the caloric theory.

Kirchhoff, Gustav Robert (1824–1887) was born in Prussia (now part of Russia) and died in Berlin. He introduced the term black-body radiation, the laws of electrical networks, and much more.

- Morse, Samuel patented the disappearing filament optical pyrometer in 1899.
- Norton, Frederick Harwood formed the Ceramics Division at MIT and wrote two classic texts on Ceramics.
- Orton, Edward J. Jr. established the first ceramic engineering program at The Ohio State University in 1894 and founded the American Ceramic Society in 1899. He created the Standard Pyrometric Cone Company, to make pyrometric cones, in a basement at Ohio State University; these cones became the standards for monitoring firings and are known as Orton cones. <http://www.ortonceramic.com>. Similar cones may have been used in China in the Northern Song Period—before 1127 CE, although Josiah Wedgwood used pyrometric beads instead. Outside the United States similar cones may be called Seger cones (after Hermann Seger) or Staffordshire Cones in the UK.
- Seebeck, Thomas Johann (1770–1831) was born in Estonia. He showed that a current flowed when you join two metals that are at different temperatures (the thermoelectric effect); this led to the invention of the thermocouple.

GENERAL REFERENCES

- Barin, I. (1989) *Thermochemical Data for Pure Substances*, VCH Verlagsgesellschaft GmbH, Weinheim, Germany. Gives tables and compilations of thermodynamic data.
- Chapman, A.J. (1984) *Heat Transfer*, 4th edition, Macmillan, New York. A standard heat transfer text.
- Chesters, J.H. (1973) *Refractories: Production and Properties*, The Iron and Steel Institute, London. Gives comprehensive information about the composition and properties of the different types of refractory brick.
- Finn, C.W.P. (1991) “Furnaces and related equipment,” in *Engineered Materials Handbook Volume 4 Ceramics and Glasses*, ASM International, pp. 244–254. A review of furnaces and related equipment.
- Gilchrist, J.D. (1963) *Furnaces*, Pergamon Press, Oxford. Although more than 40 years old this is a useful (and concise) monograph with a great deal of useful information. It goes into much more detail concerning thermodynamics and the theory of heating and heat transfer than we do.
- McGee, T.D. (1988) *Principles and Methods of Temperature Measurement*, Wiley, New York.
- Nassau, Kurt (1984) *Gemstone Enhancement: Heat, Irradiation, Impregnation, Dyeing and Other Treatments Which Alter the Appearance of Gemstones, and the Detection of Such Treatments*, Butterworth Heinemann, London. Appendix A is a brief and clearly written description of the different types of furnaces often encountered in ceramics laboratories.
- Norton, F.H. (1968) *Refractories*, 4th edition, McGraw-Hill, New York. This also covers furnace construction and the use of refractories in the metallurgical industries.
- Piccolpasso, C. (1557) *The Three Books of the Potter's Art*; translated by R. Lightbown and A. Caiger-Smith, Scholar Press, London (1980).
- Remmey, G.B. (1994) *Firing Ceramics*, World Scientific, Singapore.

WWW

<http://intarch.ac.uk/journal/issue1/peacey/toc.html> is an excellent introduction to furnaces in archeology. It gives the definition of a muffle from Searle, A.B. (1930) *The Encyclopedia of the Ceramic Industries*, London as “A chamber, case or box of refractory material, which is built in a furnace, and used to heat articles out of direct contact with flames or other products of combustion. It serves a purpose similar to a saggar, but being larger, is more suitable for some purposes.” The muffle is actually the enclosed section that protects the material from the combustion products of the furnace. The heat is conducted to the sample through the walls of the muffle. www.claygirl.com/glossary.html gives other definitions for the potter.

EXERCISES

- 9.1 Table 9.4 lists materials used as furnace elements for ceramic processing. Find the costs of each type of element.
- 9.2 Small electrically heated box furnaces are probably the most widely used furnaces in university ceramics laboratories. What are the characteristics of these furnaces that make them so useful?
- 9.3 Why is a muffle furnace so named?
- 9.4 (a) Explain briefly why the standard molar enthalpy of combustion for ethane (C_2H_6) is greater than that for methane. (b) Which is more useful as a fuel, methane or methanol? Briefly explain how you arrived at your answer. (c) Calculate the standard molar enthalpy of combustion of methane at 1000 K.
- 9.5 Explain why most refractory materials such as firebricks and fiber board insulation have high volume fractions of porosity.
- 9.6 Is a high thermal expansion coefficient an advantageous or deleterious property of a refractory brick? Explain briefly the reasoning behind your answer.

- 9.7 Briefly explain how a thermocouple works.
- 9.8 The most widely used thermocouples for ceramic processing are types K, R, and C. Explain what alloys are used for each type and under what conditions each would be most appropriate.
- 9.9 Pyrometric cones are widely used in industry for temperature measurement, yet they are rarely used in university ceramics laboratories. Why does this discrepancy exist?
- 9.10 Pyrex and Vycor are both glasses that are used as crucibles. Why is the maximum useful temperature of Pyrex less than half that of Vycor?

Characterizing Structure, Defects, and Chemistry

CHAPTER PREVIEW

In this chapter we will discuss techniques that can produce useful information about the structure, chemistry, and bonding in ceramics. There are so many characterization methods available that books are written on each one. Since we cannot cover all the details or even all the techniques, we will give examples and aim at making you aware of the key ones and their applications.

We can group the techniques into six categories:

- Imaging using visible (or nearly visible) light
- Imaging using electrons [mainly scanning electron microscopy (SEM) and transmission electron microscopy (TEM)]
- Imaging using sensing [atomic force microscopy (AFM) and other scanned probes that “sense” a force or field]
- Scattering and diffraction (using X-rays, neutrons, α -particles, electrons)
- Spectroscopy and spectrometry [using X-rays for energy dispersive spectrometry (EDS) and wavelength dispersive spectroscopy (WDS), Raman, infrared (IR), etc.]
- Thermal analysis (measuring changes, e.g., enthalpy, as a function of temperature)

Most of the techniques we describe can be used to study other classes of materials, but our examples will all be related to ceramics.

The suitability of a characterization technique depends on the type of information we hope to obtain and may also be dictated by the size of our sample, what part of the sample is important, and whether we can destroy the sample. There are some limitations:

- Reflection techniques examine only surfaces.
- Techniques using electrons require the sample to be in a vacuum.
- Techniques using transmitted electrons generally require the sample to be thin.
- For nanomaterials we need high resolution.

We always ask two questions:

- How much material is required for the analysis?
- Is it destructive or nondestructive?

For example, TEM is invariably destructive, but you need a very small amount of material for the analysis.

10.1 CHARACTERIZING CERAMICS

In characterizing a ceramic, whether it is a single crystal, polycrystalline, or a glass, there are certain types of information that we are interested in obtaining:

- Chemistry. What is the composition, how does it vary within the sample, etc.?
- Structure. Is the ceramic crystalline or glass or a mixture of the two? What polymorph is present?
- Microstructure. Is the structure the same throughout the sample? Polycrystalline ceramics cannot be uniform. Even glass can be structurally inhomogeneous.
- Surface. Whether the sample is crystalline or not, the nature of the surface is often particularly important. If the sample is crystalline then surface orientation may

TABLE 10.1 Summary of Tools for Ceramics Using Chemical and Physical Characteristics

<i>Chemical characteristic</i>	<i>Characterization tool</i>
Composition	X-ray diffraction (XRD) X-ray fluorescence (XRF) Neutron activation analysis (NAA) Mass spectrometry (Mass Spec)
Elemental distribution/local chemistry	Scanning electron microscope (SEM) with X-ray energy-dispersive spectroscopy (XEDS) Electron probe microanalysis (EPMA) Transmission electron microscopy (TEM) with XEDS TEM with electron energy-loss spectroscopy (EELS)
Surface/interface chemistry	X-ray photoelectron spectroscopy (XPS, ESCA) Auger electron spectroscopy (AES) Secondary ion mass spectroscopy (SIMS) Rutherford backscattering spectrometry (RBS) Ultraviolet photoelectron spectroscopy (UPS) Infrared (IR) spectroscopy Raman spectroscopy
Phase changes (e.g., decomposition and dehydration)	Thermomechanical analysis (TMA) Thermogravimetric analysis (TGA) Differential thermal analysis (DTA) Differential scanning calorimetry (DSC) Mass Spec (MS) <i>In situ</i> XRD
Surface area/porosity (see Chapter 20)	Small-angle neutron scattering (SANS) Small-angle X-ray scattering (SAXS) Mercury porosimetry
Density homogeneity	VLM SEM X-ray radiography/CT scan Ultrasound Die penetration
Particle/grain size, distribution, morphology, and texture	VLM and quantitative stereology SEM and quantitative stereology Electron backscattering spectroscopy (EBSD) TEM XRD
Phase identification/molecular structure	XRD EBSD FTIR Raman spectroscopy EXAFS Neutron diffraction Mössbauer spectroscopy Nuclear magnetic resonance
(NMR)	
Phase transitions: e.g., structural transformations	DTA DSC TMA <i>In situ</i> XRD

be critical. Even the surface of a glass will be different chemically and structurally from the bulk. In nanomaterials the surface is the most important feature, since most of the atoms are there.

- Defects. In crystals we often want to determine dislocation density. In both crystals and glass we may be interested in the nature, concentration, and distribution of point defects. Techniques for characterizing defects are dealt with mainly in their respective chapters.

What we want to know determines which technique we should use. In the following sections our approach is to illustrate the type of information that can be obtained. Most of these methods are applicable not only to ceramics but to other classes of material. However, there are certain special features associated with ceramics:

- Techniques using electrons can be complicated because many ceramics charge locally, thus deflecting an electron beam.
- We are often interested in what happens while ceramics are being processed. Because of the environment or the high temperatures involved, such *in situ* studies may not be possible with the desired resolution.
- Ceramics are often multicomponent systems; knowing the average composition may not be too useful. So we may need local compositional analysis on a scale that may be in the nanometer range.
- Many ceramics contain light elements (e.g., B, C, N, O), which can be difficult to quantify.
- If we are interested in interfaces, for example, the interface may facet over short (<100 nm) distances and it may contain steps that are only nanometers high. In studying such interfaces, it is essential that both grains be observed, so that techniques requiring the sample to be broken along the interface would not be ideal (though they may be necessary).

Table 10.1 lists some of the techniques that you might consider to obtain specific information about your material. In most cases the use of a particular technique depends in part on its availability, and often a combination of techniques is necessary to get the complete picture.

10.2 IMAGING USING VISIBLE-LIGHT, IR, AND UV

Light interacts with the specimen in many ways; we then study the resulting image contrast. Contrast is produced by reflection, absorption, refraction, polarization, fluorescence, or diffraction. This contrast can be modified by physically changing the optical components and illumination mode of the microscope. The final image can also be processed, now mainly using computer techniques.

Visible-light microscopy (VLM) is used routinely for all ceramics. It is often referred to as optical microscopy, but essentially all microscopy is optical. The magnification of a VLM can range from 10× (a magnifying glass) to 50k× using a liquid between the specimen and the lens. Modern VLMs are equipped with digital cameras (video or still) and feed straight into the computer. Ceramics are often transparent, especially (but not necessarily) if they are glass, so we can then use reflected or transmitted light. The sample can be viewed supported on a table or inverted. The inverted microscope has some advantages, in particular, you can attach contacts to, indent into, or support liquids on the free surface. You also have more flexibility with the lighting.

The lateral resolution using VLM is about 250 nm and the depth of field has a similar value. Because of the poor depth of field of the VLM we often examine polished surfaces (as in metallography). Vertical resolution can be less than 1 nm using interference contrast, and this is bettered only by the scanned probe techniques.

Visible-light microscopy is usually available in every laboratory. While a conventional VLM may cost only \$2000, the best metallographic microscopes can cost >\$100k. There are numerous imaging methods used in VLM so we list only a few here:

Dark-field. The image is formed using only scattered light (if there is no specimen present then the image is dark). It is widely used in mineralogy where multiphase materials are common.

Polarized light. Polarized VLM distinguishes between isotropic and anisotropic materials and provides information on absorption color and boundaries between minerals of differing refractive indices. The technique provides local information on the structure and composition of materials as shown in Figure 10.1, which is an image of a neodymium-doped yttrium orthovanadate laser crystal. Individual grains, separated by low-angle grain boundaries, are clearly revealed by polarized VLM.

Nomarski (differential interference contrast). The idea here is that we use interference. Contrast is generated by phase differences between two rays (a sample ray and a reference ray). In the Nomarski microscope the two rays are created after the light has passed through the sample, where path differences occur because of regions having different refractive indices. The ray is split by a prism (called a Wollaston prism) and after passing through a polarizing filter it is recombined using a second prism at the image plane. By using a rotating stage the image contrast can be varied. Using this technique it is possible to create very

attractive images, because of the enhanced contrast. Nomarski microscopes are more expensive than conventional VLMs because of the cost of the Wollaston prisms.

NSOM (near-field scanning optical microscopy, also known as SNOM). This is a broad and growing topic.

The idea is that the resolution in VLM is limited by λ . If the light source is a fiber with an aperture in the end and we detect the reflected/scattered light with the same fiber, then the spatial resolution is determined by the diameter of the fiber. The limitation is that since the aperture diameter is smaller than λ (Figure 10.2), the emerging wave is evanescent so the signal strength is small. The use of a laser provides the necessary intensity and defines λ . The usefulness of the technique relies on the ceramics sample having suitable features to scatter the light. The technique can be used for other wavelengths and other signals (e.g., Raman). The latter technique is still being developed.

IR and UV. Because semiconductors are transparent to IR radiation, defects in these materials can be examined with IR microscopy. A detector sensitive to IR is required. With IR and ultraviolet (UV) light, a con-

NSOM PARAMETERS
Aperture size: 25–10 nm
Tip/sample gap 5–50 nm

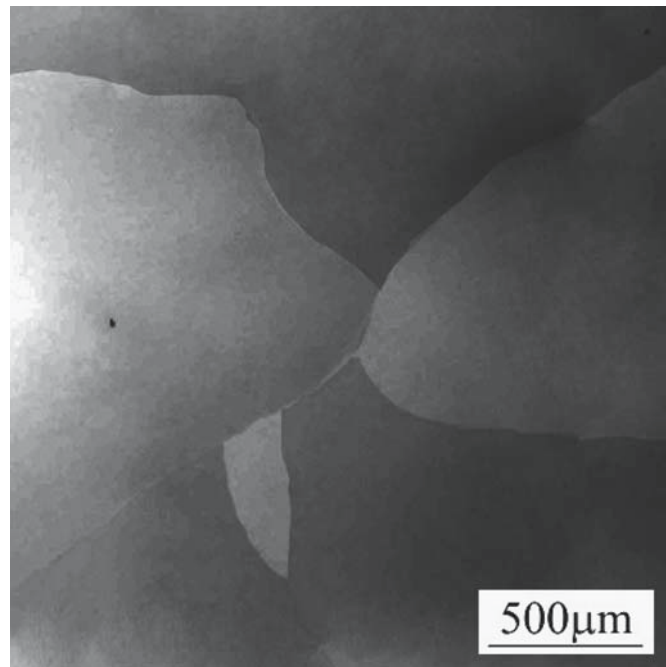


FIGURE 10.1 Slightly misoriented grains in a laser element imaged using polarized VLM. The crystal is yttrium orthovanadate with 0.27% Nd.

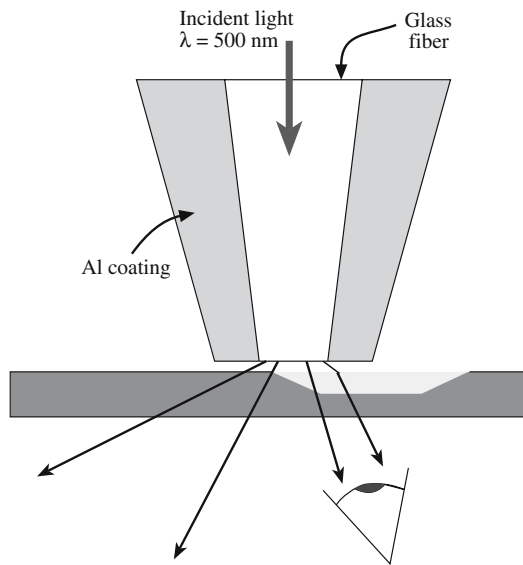


FIGURE 10.2 Schematic of the end of the fiber and the sample in NSOM.

verter or detector is also required. An advantage of UV microscopy is that because the wavelength of UV light is smaller than visible light the resolution of these microscopes is higher than VLMs. UV microscopy is widely used in the biological sciences to study sub-cellular structures. Using intense vacuum UV sources (available at national laboratories) it is possible to obtain results on, for example, electronic states.

10.3 IMAGING USING X-RAYS AND CT SCANS

X-ray topography can be used to obtain images of individual lattice defects in single crystals. This technique has been widely used to study crystal growth and, in particular, silicon. It can be used in

- Reflection (Berg–Barrett method)
- Transmission (Lang method or Borrmann method)

In either method it is the variation in intensity within the diffraction spot that is recorded. It is not usually the defects themselves that are imaged but rather the strain fields around them. These strains cause variations in plane spacing from their equilibrium value, thereby modifying the X-ray scattering process. Figure 10.3 shows a Lang topographic image of dislocations in potassium dihydrogen phosphate (KDP; KH_2PO_4). KDP has a relatively large electrooptic effect and can be grown as large strain-free crystals. X-ray topography has several advantages for characterizing defects in single crystals. It is nondestructive, does not require ultrathin samples (as is required in

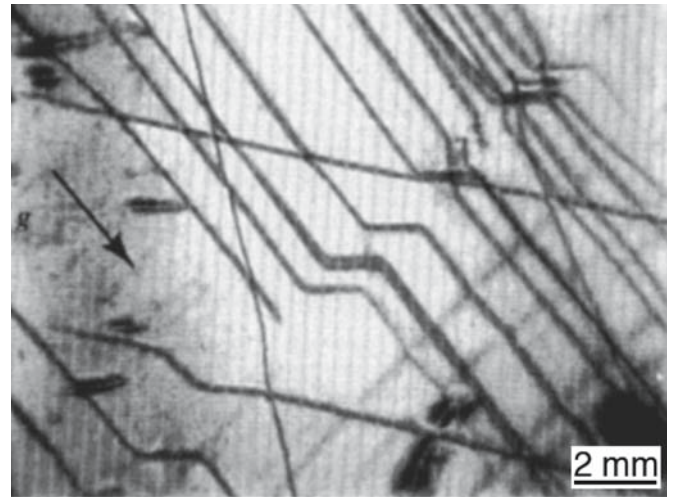


FIGURE 10.3 X-ray topography image showing dislocations in KDP imaged using a 022 reflection.

TEM), and can be used to observe very low dislocation densities (limit in TEM $>10^4 \text{mm}^{-2}$).

Computed tomography (CT) is used to determine inhomogeneities arising from local differences in density. It is applicable to a range of ceramics and minerals and is particularly useful for identifying defects in single crystals. The sample is placed on an automated stage that rotates as a series of X-ray images (radiographs) is captured (much like a medical CAT scan except that details as small as a few tens of micrometers can be resolved even in dense samples). A computer then processes the X-ray images and creates a three-dimensional (3D) reconstruction of the sample. Areas of lower density such as cracks and voids appear as darker contrast against a lighter background. Figure 10.4 shows density variations in the core of an Nd-doped YVO_4 sample.

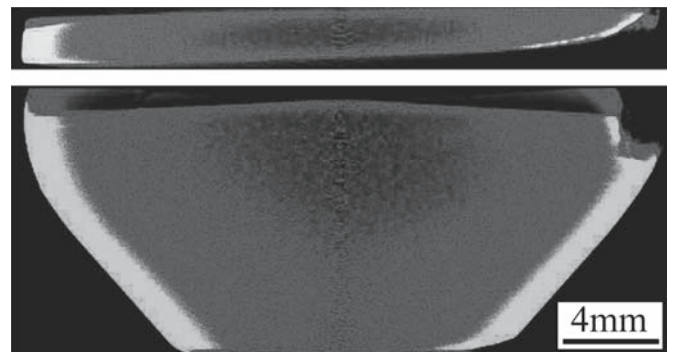


FIGURE 10.4 High-resolution X-ray CT images from the top and side of the same sample.

10.4 IMAGING IN THE SEM

The basic layout of the SEM is shown in Figure 10.5. The SEM can have two imaging detectors, one for secondary electrons (SEs) and one for higher-energy backscattered electrons (BSEs). The SEM typically has a resolution in SE mode of 0.7 nm (at 25 kV) and 2.5 nm in BSE mode at 5 kV. In addition to the excellent spatial resolution, the other great advantage of the SEM is that it has a much greater depth of field than the VLM (the depth of field is several millimeters). So the images appear more three-dimensional. The physical reason for this is that the electron beam is very narrow.

SEs are low-energy electrons so they are very sensitive to surface topology. Figure 10.6 shows an example of an SE image illustrating the excellent depth of field. BSEs are higher-energy electrons and are sensitive to the atomic number of the scattering atom. Hence the intensity of the BSE signal depends on a combination of the average atomic number and density of the ceramic. As the kilovolts are reduced, the scattering volume becomes more localized close to the surface of the sample. (The BSE electrons penetrate further into the sample and have further to come out after being scattered.) Hence the BSE image can give excellent mass discrimination even at low voltages. In

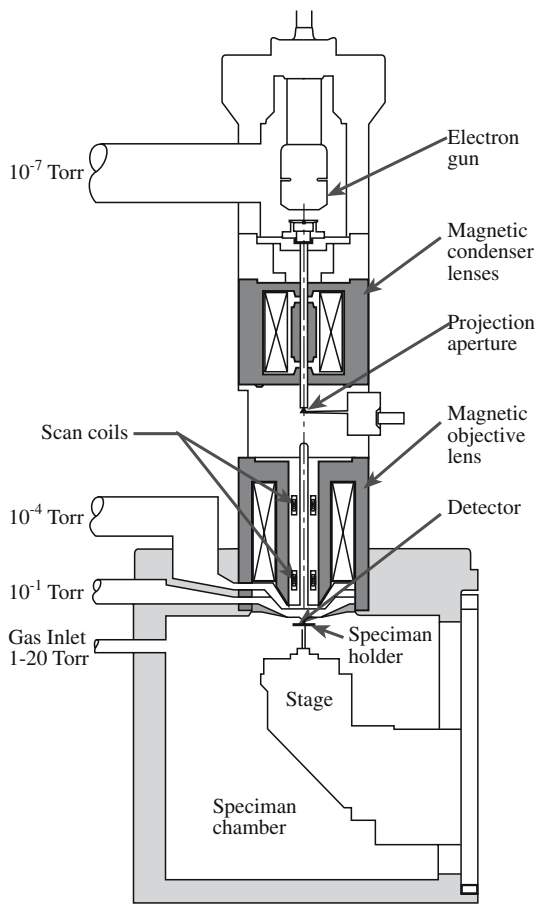


FIGURE 10.5 Schematic of an SEM showing examples of pressures used.

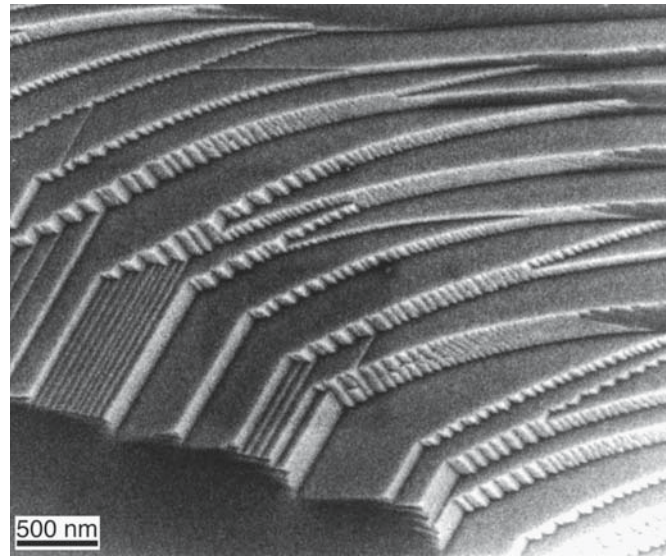


FIGURE 10.6 SE image showing steps on an alumina surface.

Figure 10.7 the three regions correspond to three different layers in a reaction couple. The MgO substrate is darkest, the In_2O_3 is lightest, and the spinel, MgIn_2O_4 , is intermediate. The very bright regions are Pt nanoparticles.

Charging in the SEM is usually avoided by coating the specimen (e.g., with a 1-nm layer of Pt). Working at lower accelerating voltages can also reduce charging effects, but then the resolution is compromised; electron lenses work better at higher resolutions. In low-voltage SEM imaging, you are trying to balance the electrons emitted as the specimen is irradiated with the charge building up on the specimen. Another way to avoid applying a conductive coating is to use an environmental or low-vacuum SEM. Then, the charging of the specimen is essentially grounded by the gas in the chamber. Variations in the SEM are summarized in Table 10.2.

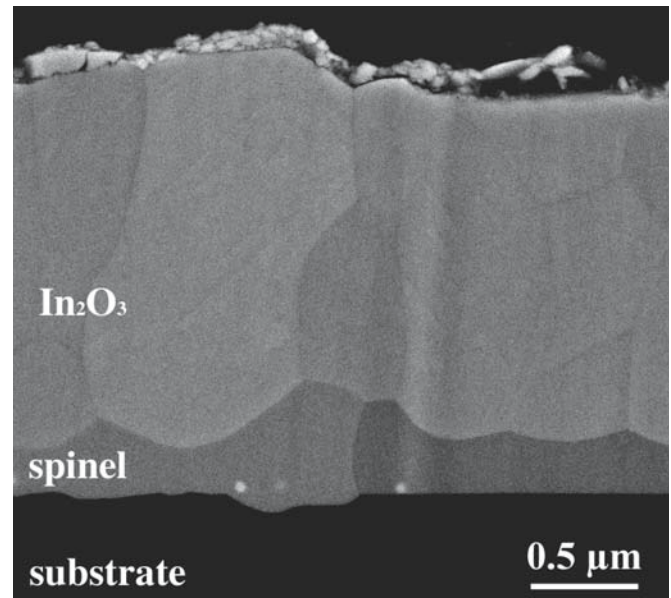


FIGURE 10.7 BSE image showing different contrast from different materials in an $\text{MgO}/\text{In}_2\text{O}_3$ reaction couple.

Signal	Energy	Source	Use
Secondary electrons	~5 eV	Loosely bound electrons scattered from surface	Main signal for image formation
Backscattered electrons	Energies up to incident beam energy	Beam electrons scattered back after collision	Atomic number contrast, channeling patterns, magnetic contrast
Characteristic X-rays	Discrete values for each element	Interband transitions usually involving K and L	Chemical analysis
Light (cathodoluminescence)	UV, visible, IR	Interband transitions between higher energy levels	Imaging dislocations in semiconductors

Environmental SEMs allow operation at pressures of several torr (0.1–20 torr) in the sample chamber and at temperatures >1000°C. In addition to being able to examine insulators it is also possible to follow dynamic processes such as drying of cement and crystallization.

10.5 IMAGING IN THE TEM

Figure 10.8 shows a state-of-the-art TEM with a field emission source. The key requirement for using TEM

RESOLUTION

The higher the resolution the smaller the features we can resolve.

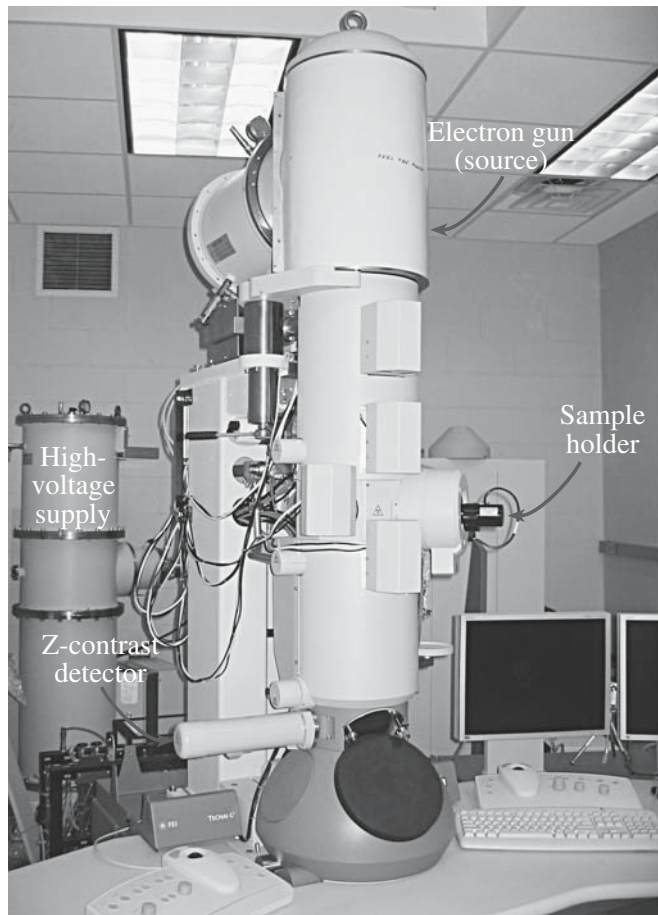


FIGURE 10.8 A TEM with key features labeled.

is that we require the sample to be very thin (usually ≤ 200 nm). So the technique is destructive and specimen preparation can be time consuming. The benefits, however, are significant. Because of the large range of signals generated by the incident electron beam (Figure 10.9), a TEM allows full characterization of a sample at high resolution. The conventional imaging modes in a TEM are bright-field (BF) imaging and dark-field (DF) imaging. In BF

imaging the image is formed using only the direct beam. An aperture (the objective aperture) is used to exclude all the diffracted electrons from contributing to the image. In DF imaging the image is formed from one of the elastically scattered beams and the objective aperture blocks the direct beam and all the other scattered electrons. The BF image in Figure 10.10a shows a thick particle of NiO sitting on a thin film of Al₂O₃; the different gray levels in the films correspond to different thicknesses in the Al₂O₃ film. The DF image in Figure 10.10b shows the same region after reacting the two oxides at high temperature; by using a reflection that is excited only by the spinel product, we can see exactly where the spinel has formed.

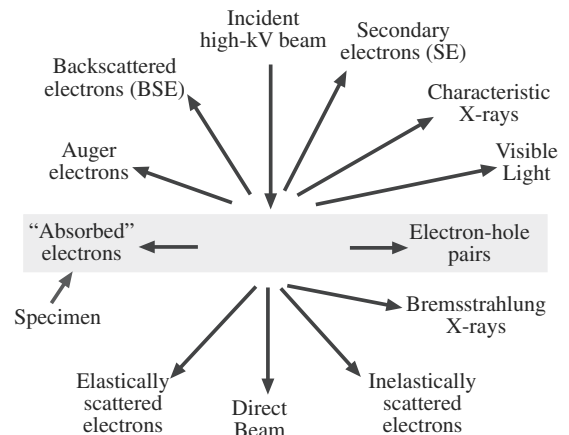


FIGURE 10.9 Signals produced in a TEM.

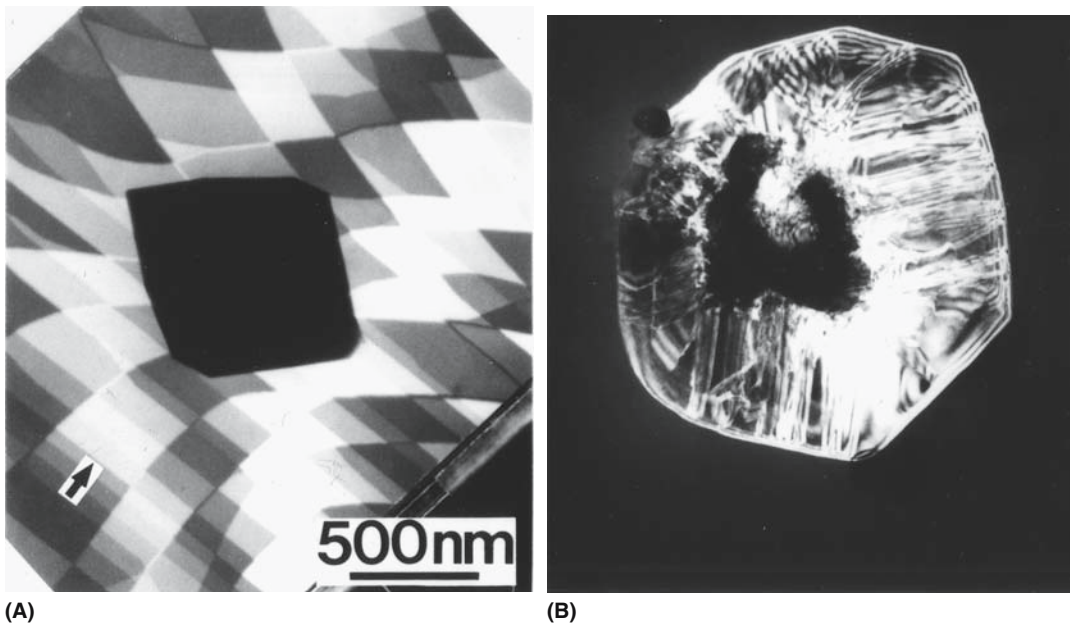


FIGURE 10.10 (a) BF and (b) DF image (using a spinel reflection) of a particle of NiO on a film of Al₂O₃ before and after reaction.

The resolution of a TEM is determined by the energy of the electrons (controlled by the accelerating voltage), the thickness of the specimen (we want to avoid multiple scattering within the sample), the distance between the sample and the objective lens, and the inherent quality of the lens (defined by its spherical aberration coefficient). Figure 10.11 shows an image of SrTiO₃ showing variations in the oxygen occupancy. At present, the best high-resolution TEM (HRTEM) has a resolution of ~0.08 nm (sub-Å!), but 0.05 nm should be achievable. For nanotechnology an HRTEM is an essential tool. An example is its use in studying crystals of KCl grown in a carbon nanotube as shown in Figure 10.12.

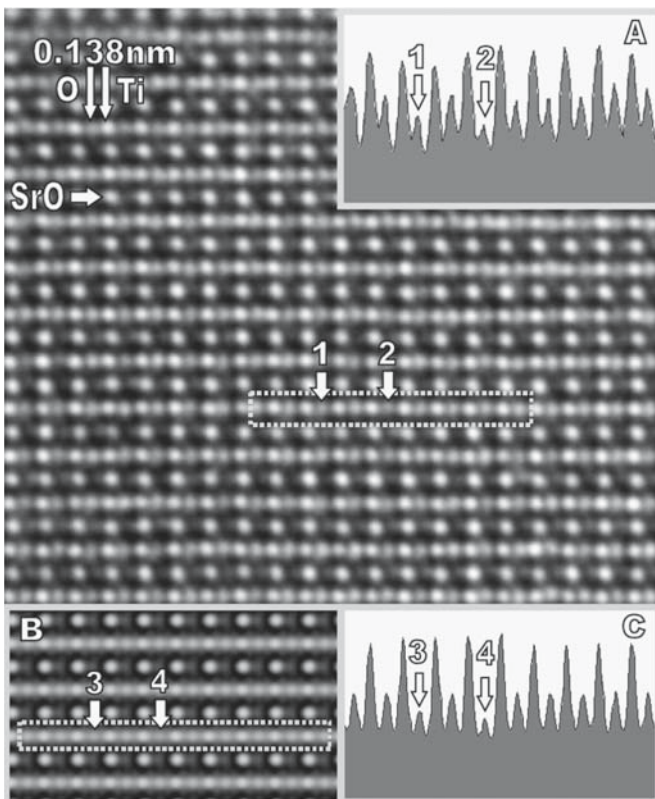


FIGURE 10.11 HRTEM image of the structure of SrTiO₃.

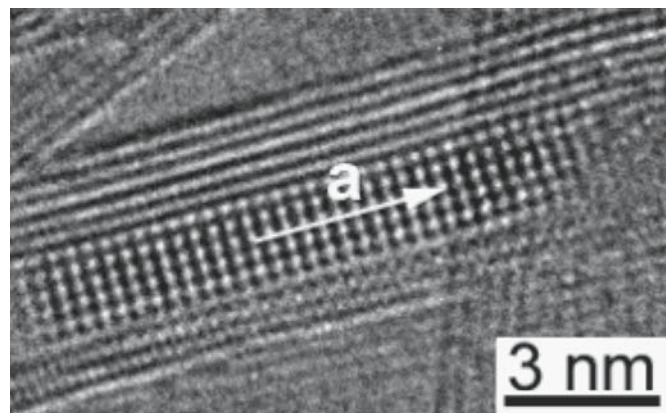


FIGURE 10.12 HRTEM image of a C nanotube partly loaded with a crystal of KCl.

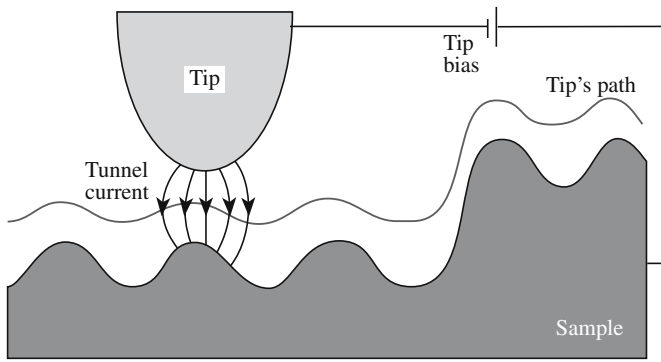


FIGURE 10.13 Schematic of the tip/sample interaction in STM; the tip does not make physical contact with the sample.

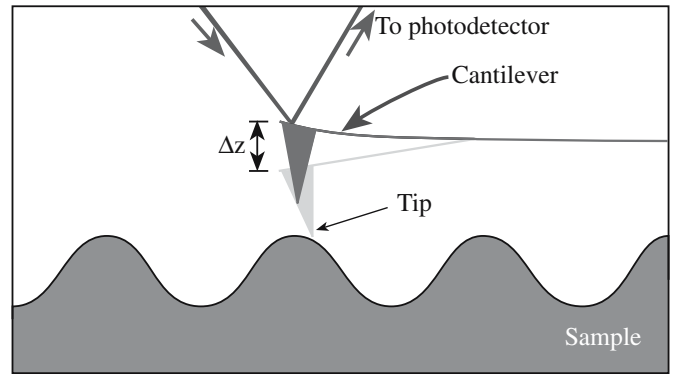


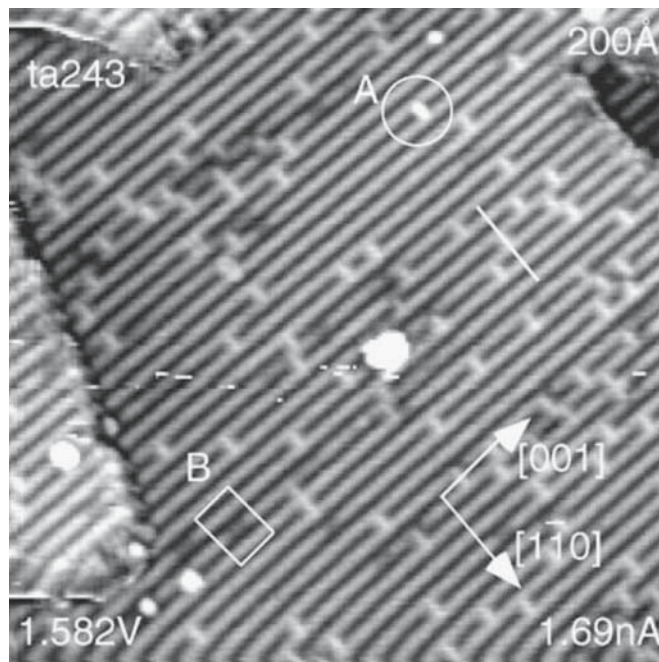
FIGURE 10.15 Schematic of the tip/sample interaction in AFM using a cantilever system.

10.6 SCANNING-PROBE MICROSCOPY

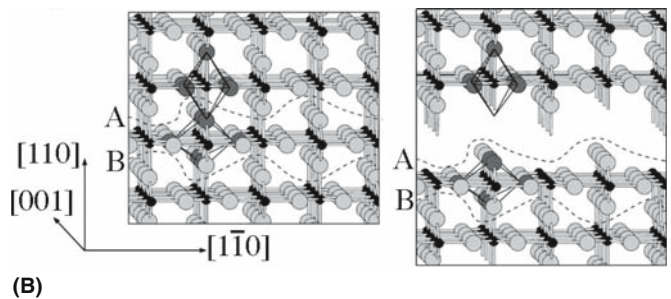
The topic of scanned probe microscopy includes several different techniques, which grew out of the development of scanning tunneling microscopy (STM) (for which Binnig and Rohrer shared the Nobel Prize in 1986). The basic principle is that the tip of the probe determines the resolution of the image as shown in Figure 10.13. Scanning tunneling microscopy has been used to study the atomic structure of ceramic surfaces. Figure 10.14 shows the reconstructed (110) surface of TiO_2 . In addition to STM there are now several other types of scanned

AFM AND STM “IMAGE” ATOMS
Both AFM and STM provide atomic resolution, meaning we can resolve individual atoms.

probe microscopy. The most widely used is atomic-force microscopy (AFM), which is illustrated in Figure 10.15. Atomic-force microscopy is extensively used to study the surfaces of nonconducting oxides. A pair of AFM images at low and high magnification is shown in Figure 10.16. The lines are straight single steps (0.4 nm high) on the surface of (111) spinel; the high-magnification image shows the origin of the steps as a pair of dislocations emerging at the surface. A nanoscale indenter can be attached to the AFM making it into an indenter with integrated imaging. Table 10.3 summarizes the common operating modes of the AFM.



(A)



(B)

FIGURE 10.14 STM image of the (110) surface of TiO_2 . The features labeled 'A' have been assigned as oxygen vacancies; the features labeled 'B' have not been identified. The schematics show the TiO_2 structure (compare to Fig. 6.11) and a model showing the proposed surface reconstructon.

10.7 SCATTERING AND DIFFRACTION TECHNIQUES

The fundamental idea is that we scatter particles or waves from the constituent atoms in the sample. If the waves interfere constructively, we have diffraction, which implies that the sample is at least partly crystalline. If the sample is not crystalline, we may still learn about the distribution of the atoms from the radial distribution function (rdf). The process of scattering generally implies particles; diffraction generally suggests Bragg diffraction or constructive interference of waves.

We can summarize some techniques in diffraction and scattering (of photons, electrons, neutrons, etc.).

Photon scattering	Raman and Fourier transform infrared (FTIR) are well-known techniques for the chemist and are increasingly important in ceramics
Electron diffraction	Selected-area diffraction (SAD) in the TEM Convergent-beam electron diffraction (CBED) in the TEM Electron-beam backscattering diffraction (EBSD) in the SEM Reflection high-energy electron diffraction (RHEED) in UHV for surfaces
Ion scattering	Rutherford backscattering spectrometry (RBS)
X-ray diffraction	Powder diffraction for statistical determination of lattice spacings Laue back-reflection for orienting single crystals
Neutron scattering	Small-angle scattering in a range of environments

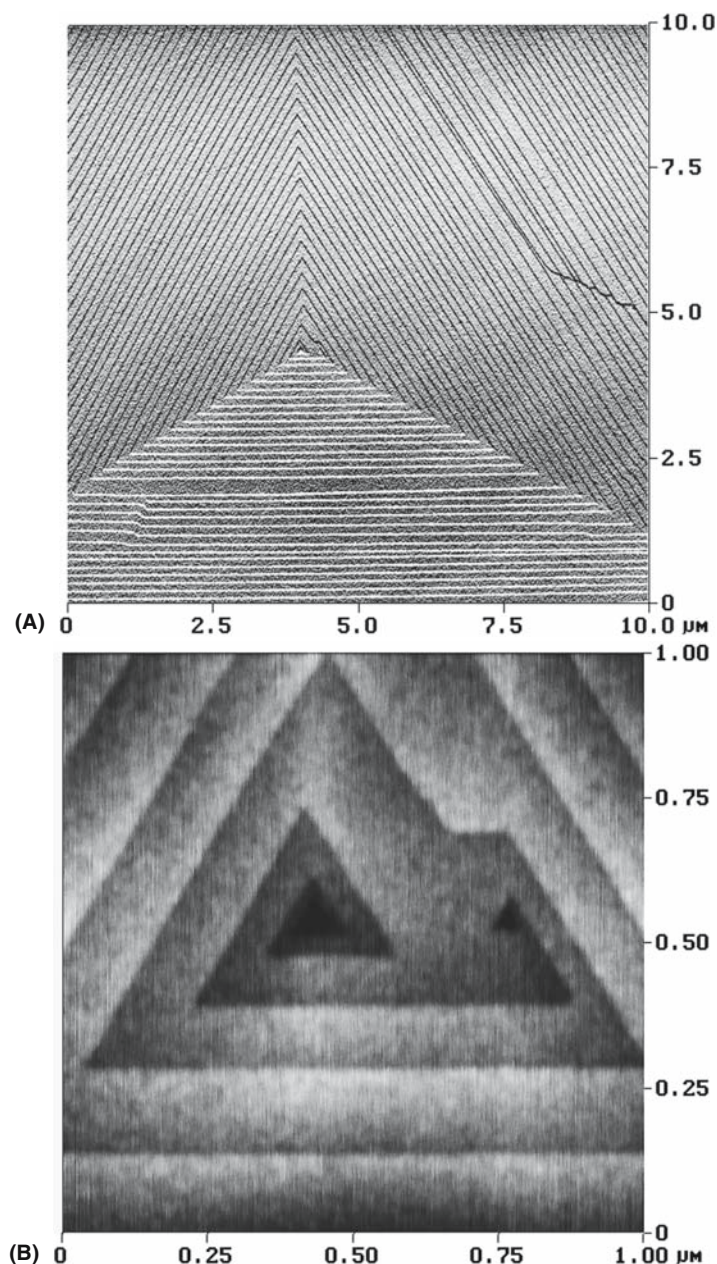


FIGURE 10.16 AFM image showing long (up to 10 μm) straight steps on the surface of an Mg–Al spinel. The steps are 0.4 nm high. The lower image shows the central region at higher magnification.

TABLE 10.3 Modes of Operating the Atomic-Force Microscope

Mode of operation	Force of interaction
Contact mode	Strong (repulsive); constant force or constant distance
Noncontact mode	Weak (attractive)-vibrating probe
Intermittent contact mode	Strong (repulsive)-vibrating probe
Lateral force mode	Frictional forces exert a torque on the scanning cantilever
Magnetic force	Magnetic field of the surface is imaged
Thermal scanning	Variation in thermal conductivity is imaged

Electrons interact most strongly with the sample, so for transmission the specimen must be thin and in a vacuum. Neutrons are at the other extreme, but can be used only in dedicated (usually national) facilities because they require radioactive sources.

We will use diffraction in the TEM to study the crystallography of the interfaces and characterize other crystal defects. Bragg made the first direct determination of a crystal structure using X-ray diffraction (XRD), which is still generally the most accurate method for characterizing crystal symmetry, providing the sample is large enough and can be isolated. However, XRD does not provide a high spatial resolution because the beam diameter is typically 1 mm, although with a rotating anode generator it may be 0.1 mm and with a synchrotron 1 μm or less is possible.

TABLE 10.4 Electromagnetic Spectroscopy

E (eV)	10^{-7}	10^{-5}	10^{-2}	10^{-1}	10^1	10^3	$>10^3$
T (K)	1.16×10^{-3}	1.16×10^{-1}	1.16×10^2	1.16×10^3	1.16×10^5	1.16×10^7	$>10^7$
ν (Hz)	2.4×10^{-7}	2.4×10^9	2.4×10^{12}	2.4×10^{13}	2.4×10^{15}	2.4×10^{17}	$>10^{17}$
λ (cm)	1.24×10^3	1.24×10^1	1.24×10^{-2}	1.24×10^{-3}	1.24×10^{-5}	1.24×10^{-7}	$>10^{-7}$
Radiation	Radio	Micro	IR	VIS	UV	X	γ
Atomic subsystem transitions	Nuclear spins	Electron spins	Rotation vibration	Outer shell electrons	Inner shell electrons	Nuclei	
Primary quantity measured	Local interactions (magnetic, electric field gradient)		Atomic molecular potentials	Energy levels	Energy levels	Energy levels	Energy levels
Kinetic parameter detected	Diffusional atomic motions		Vibrational frequencies	Macroscopic, real time kinetic coefficients, point defect concentrations			
Effects on reactivity			Transport activation by heat	Photochemistry	Radiation chemistry		
Characteristic sample dimension (cm)	10^{-1} – 10^0	10^{-2} – 10^{-1}	ca. 10^0	10^{-4} – 10^0		10^{-2} (A1, 10^4 eV)	10^{-3} [Fe(MS)] 10^{-1} [In(PAC)]
Examples of methods	NMR	ESR	Raman	Absorption spectroscopy	XAS		Mössbauer, PAC

10.8 PHOTON SCATTERING

Electromagnetic spectroscopy involves the interaction of electromagnetic waves and matter. We can use all regions of the electromagnetic spectrum and each will give specific information about a material. Table 10.4 provides a summary and succeeding sections deal with each of the methods in a little more detail with specific application to ceramics. Once again, to really understand each of the methods you need to read a specialist text.

10.9 RAMAN AND IR SPECTROSCOPY

Raman and IR spectroscopy both involve the scattering of light. In IR spectroscopy, the light is polychromatic and couples to vibrational modes in the solid through dipole moments, which are associated with the vibration. These vibrational modes cause a dip in the transmission spectra or a peak in the absorption spectra. The IR range is from 0.78 to $1000\mu\text{m}$ ($12,820$ to 10cm^{-1}). The region where most fundamental vibrational modes occur, which is the most useful for materials characterization, is between 2.5 and $25\mu\text{m}$ (4000 – 400cm^{-1}). This is sometimes called the mid-IR region. The light source is a heated ceramic (usually a conducting ceramic or a wire heater coated with ceramic) that emits a range of frequencies.

- Spectroscopy: the art of using a spectroscope
- Spectrometry: the act of using a spectroscope

An important variant is the FTIR spectrometer. The main advantages of FTIR are that it is much quicker because it measures all the frequencies simultaneously and it is more sensitive than dispersive IR spectrometers.

Cryo-cooled HgCdTe detectors are used for weak signals or high resolution. The key component of an FTIR is the interferometer, which can be understood by considering the Michelson interferometer shown in Figure 10.17. A parallel beam directed from the source is split at B_s so that 50% of the light is transmitted and reflected back by mirror M_F , while the rest is reflected at B_s and then again at M_M . The beams recombine at B_s . The recombined beam will show constructive or destructive interference depending on the difference in the path lengths B_s to M_F and B_s to M_M . As M_M is moved smoothly toward or away from B_s the detector sees a signal that alters in intensity. If the recombined beam from B_s is passed through a sample before reaching the detector sample absorptions will show up as gaps in the frequency distribution. The complex intensity distribution received by the detector is Fourier transformed by a computer to produce an absorption spectrum.

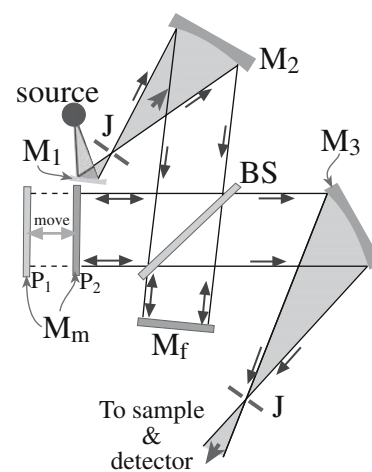


FIGURE 10.17 Schematic of the arrangement of mirrors and ray paths in FTIR.

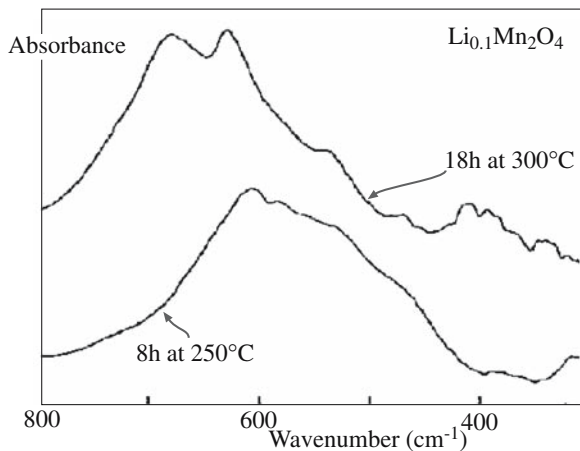


FIGURE 10.18 FTIR absorption spectra from $\text{Li}_x\text{Mn}_2\text{O}_4$ insertion electrodes after different heat treatments.

IR spectra are output in the form of plots of intensity (percent transmittance, % T , or absorbance, A) versus either energy (in J), frequency (in Hz), wavelength (in μm), or wavenumber (in cm^{-1}). The use of wavenumber is preferred, but some of the standard reference sources of IR spectra use wavelength. FTIR can be used to determine the oxygen content in silicon. The Si–O stretching band occurs at 1105 cm^{-1} and from the peak intensity the oxygen concentration can be determined using ASTM standard F 121. The FTIR absorption spectra in Figure 10.18 is from $\text{Li}_{0.1}\text{Mn}_2\text{O}_4$ after heating for 8 hours at 250°C and 18 hours at 300°C . These FTIR readily distinguishes them from the binary oxide MnO_2 .

In Raman spectroscopy, the light is nearly monochromatic and is usually in the visible range. The light source is a laser, e.g., a 50-mW 785-nm diode laser. Raman spectroscopy has become a routine tool for exploring the structure and chemical properties of materials. It can provide more information than IR spectroscopy. There are three types of signal in a typical Raman experiment as illustrated in Figure 10.19.

The scattering process can be anti-Stokes, Rayleigh, or Stokes. We are then interested in measuring the intensity and the Raman shift.

In *Rayleigh scattering*, a molecule is excited by the incident photon to a virtual energy level. This energy level is caused by a distortion of the electron distribution of a covalent bond. The molecule returns to the vibrational ground state by emitting the same energy, E_0 ($E_0 = h\nu_0$). Rayleigh scattering is an elastic process.

Vibrational excitations can be created, which causes a decrease in the frequency (i.e., in energy) of the scattered light, or they can be annihilated, which causes an increase. The decrease in frequency is called *Stokes scattering* and the increase is *anti-Stokes scattering*. Stokes scattering is the normal Raman effect and Raman spectroscopy generally uses Stokes radiation.

Figure 10.20 shows a typical Raman spectrum. It is a plot of scattered light intensity as a function of frequency

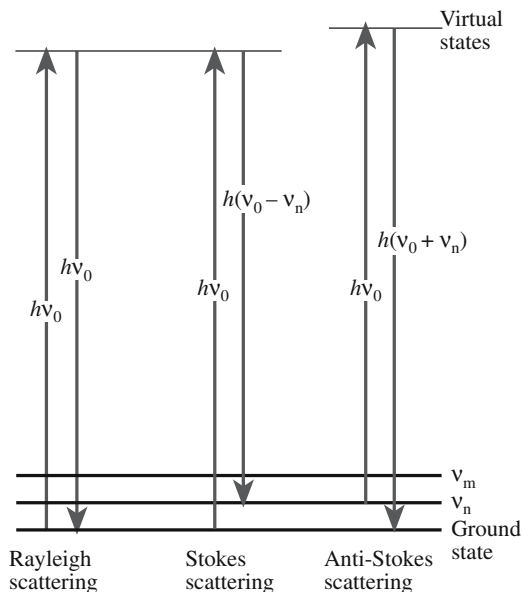


FIGURE 10.19 Schematic of transitions occurring in Raman spectroscopy.

shift (Raman shift in cm^{-1}) in which the shift is calculated relative to the laser line frequency that is assigned as zero. The material is TiO_2 films prepared by the sol-gel technique that have been annealed at temperatures between 400°C and 800°C . The features in the spectra correspond only to anatase until the film reaches 800°C . At this temperature, a mixed anatase–rutile phase is seen, while the pure rutile phase is obtained only at 900°C .

There are increasing applications for Raman spectroscopy. One application is its use in the identification of different pigments in the characterization of historical artifacts. Table 10.5 lists blue pigments used on or before about 1850 that have been identified by Raman spectroscopy.

Variations in Raman spectroscopy include the following:

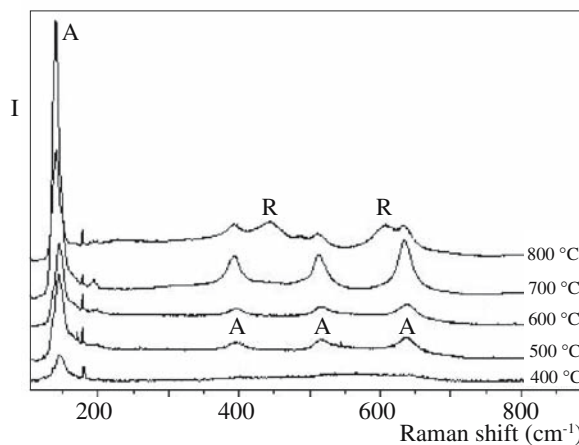


FIGURE 10.20 Example of Raman spectra from TiO_2 films heated to different temperatures. R, rutile; A, anatase.

TABLE 10.5 Blue Pigments Identified by Raman Spectroscopy

Name	Composition	Band wavenumbers, cm^{-1} and relative intensities	Excitation λ and power	Notes and date
Azurite	Basic copper(II) Carbonate $2\text{CuCO}_3 \cdot \text{Cu}(\text{OH})_2$	145w; 180w; 250m; 284w; 335w; 403vs; 545w; 746w(sh); 767m; 839m; 940w; 1098m; 1432m; 1459w; 1580m; 1623vw	514.5 nm 2 mW	Mineral
Cerulean blue	Cobalt(II) stannate $\text{CoO} \cdot n\text{SnO}_2$	495m(sh); 532s; 674vs	514.5 nm 4 mW	1821
Cobalt blue	Cobalt(II)-doped alumina Glass, $\text{CoO} \cdot \text{Al}_2\text{O}_3$	203vs; 512vs	514.5 nm 4 mW	1775
Egyptian blue	Calcium copper(II) Silicate, $\text{CaCuSi}_4\text{O}_{10}$	114m; 137m; 200w; 230w; 358m; 377m; 430vs; 475m(sh); 571w; 597vw; 762w; 789w; 992w; 1012w; 1040w; 1086s	514.5 nm 4 mW	3000 BC; also known as cuprorivaite
Lazurite	S3- and S2- in a sodium aluminosilicate matrix $\text{Na}_8[\text{Al}_6\text{Si}_6\text{O}_{24}]\text{Sn}$	258w; 548vs; 822w; 1096m	514.5 nm 4 mW	Mineral (lapis lazuli) Synthetic c.1828 = ultramarine
Posnjakite	Basic copper(II) sulfate $\text{CuSO}_4 \cdot 3\text{Cu}(\text{OH})_2 \cdot \text{H}_2\text{O}$	135vw; 208vw; 278vw; 327vw; 467w; 612w; 983vs; 1092vw; 1139vw	632.8 nm 3 mW	Mineral
Prussian blue	Iron(III) hexacyanoferrate(II) $\text{Fe}_4[\text{Fe}(\text{CN})_6]_3 \cdot 14\text{-}16\text{H}_2\text{O}$	282vw; 538vw; 2102m; 2154vs	514.5 nm 2 mW	1704; earliest synthetic modern
Smalt	Cobalt(II) silicate $\text{CoO} \cdot n\text{SiO}_2$	462vs; 917m	514.5 nm 2 mW	~1500

Laser Raman Microprobe: This allows information to be collected from small samples via the use of a VLM, which allows the region to be selected from which the Raman spectrum will be obtained. **Surface-Enhanced Raman Scattering (SERS):** This is used to examine surfaces, oxidation, catalysis, and thin films.

Residual Stress Measurement: Scattering depends on local stress, which can be probed in regions as small as $0.7 \mu\text{m}$ in diameter by Raman spectroscopy.

Fortunately, there are many isotopes, such as ^{29}Si , ^{27}Al , and ^{11}B , that are important for ceramics that are suitable. Notice that we have to use ^{29}Si ($I = 1/2$) not the more abundant ^{28}Si .

When a nucleus that has a nonzero P_I is subjected to a magnetic field of strength H , the energy levels are split into $2I + 1$ different values. The energy separation of the different levels is

$$\Delta E = \gamma H h / 2\pi \tag{10.2}$$

10.10 NMR SPECTROSCOPY AND SPECTROMETRY

Just as each electron has a spin of $\pm 1/2$, each neutron and proton in the nucleus also has a spin, I , of $1/2$. These spins combine so that each atom has a total nuclear spin of 0, $1/2$, or 1, and an angular momentum P_I , given by

$$P_I = (h/2\pi)\sqrt{I(I+1)} \tag{10.1}$$

The principle of nuclear magnetic resonance (NMR) is that the probing beam is tuned until it couples with the natural angular momentum of the nucleus, which then resonates and emits energy that is measured. The specific quantities depend on the atom that is resonating. The precise value of the energy involved changes slightly if the electron distribution around the resonating nucleus changes, as is the case when the atom is bonded to other atoms; we use NMR to examine this chemical shift. Nuclear magnetic resonance thus probes the bonding of individual atoms. Clearly for the technique to be applicable, the nucleus must have a nonzero total nuclear spin.

γ is called the gyromagnetic ratio of the nucleus. If we then subject this nucleus to electromagnetic radiation and adjust the frequency, ν , to be ν_0 , so that it has the same energy ΔE (now $h\nu_0$), the quanta of radiation can be absorbed as transitions between the different nuclear spin energy levels occur. We then detect the NMR absorption in the spectrum as a single peak corresponding to ν_0 , which is broadened because the atoms interact differently depending on their neighbors.

There are two particularly important interactions to consider:

- The dipole interaction is the interaction between adjacent nuclei and the one you are probing (such as an interaction between magnetic dipoles).
- The electrons surrounding the nucleus will also move because of the applied magnetic field; this is the chemical shift—electrons determine chemistry.

The technique can be carried out using either a continuous wave (CW) or a pulsed spectrometer. The RF energy is used to excite the nuclear magnetization. The measurement is the response of the spin system to this excitation. In CW the nuclear magnetization is irradiated at a

constant level; the frequency of the irradiation or the magnetic field is then swept across the resonance.

Nuclear magnetic resonance systems are available in most research universities with a basic system costing from \$200,000 up to more than \$1,000,000, depending mostly on the desired field strength (1–14 T).

The following examples are selected to illustrate why NMR is so valuable for the ceramist. The x -axis is in units of ppm, which is the chemical shift as a fraction of the applied field or frequency. In Figure 10.21, three NMR powder patterns are shown for silicon in three different chemical environments, but where the Si is tetrahedrally coordinated in each case. The differences between the spectra are due to the number of nonbridging oxygen ions that are attached to the Si nucleus being probed: a chemical-shift effect. The value of NMR for studies of silicate glass is obvious.

Figure 10.22 shows a series of NMR spectra from Si–Al glasses. The field used was 11.7 T. The NMR spectra show that not only is the Al present in 4-fold, 5-fold, and 6-fold coordination, but there is also undissolved Al_2O_3 present in the glass (denoted “Cor” in the spectra). The chemical shift has been determined using a standard of octahedral ^{27}Al in AlCl_3 solution.

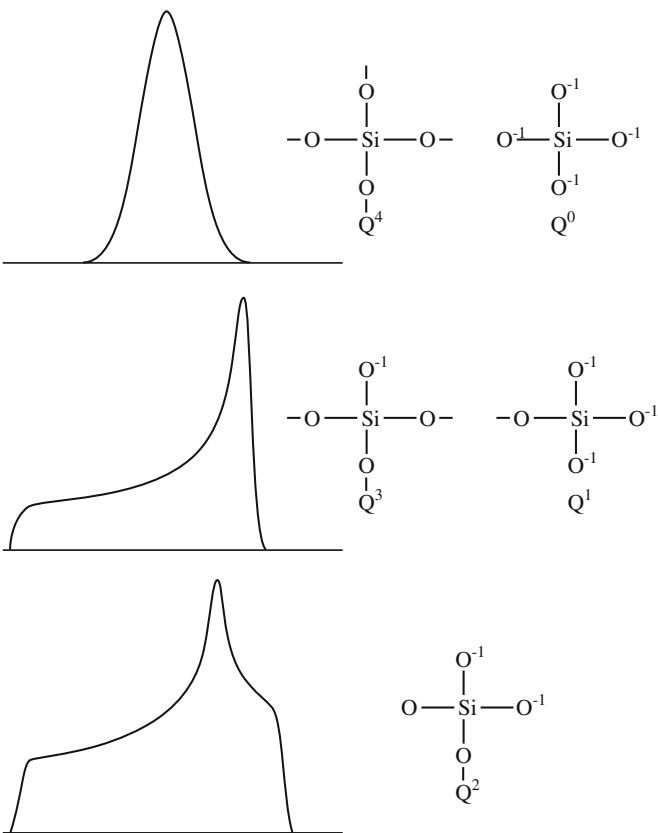


FIGURE 10.21 NMR signals from Si.

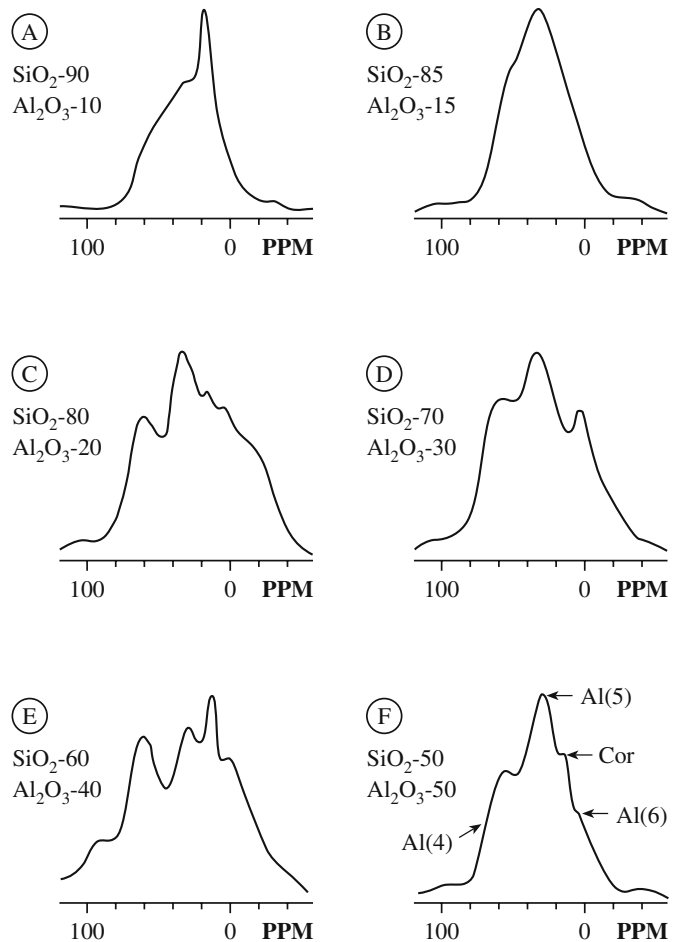


FIGURE 10.22 NMR signals from an Al–Si glass.

10.11 MÖSSBAUER SPECTROSCOPY AND SPECTROMETRY

Mössbauer spectroscopy is specialized, but it can be invaluable when it is available. The technique relies on the recoil-free emission and resonant absorption of γ -rays by nuclei that are bound in the solid state. (If it is not in a solid, the free nucleus recoils and no resonance is detected.) To see this resonance, we have to match the energy of the γ -ray emitter to the energy of the absorber (the sample), which means that only a small number of elements can be studied. Two that can be studied are tin and iron. The technique gives information on the bonding and coordination, and on the valence (oxidation) state. Since the technique relies on Z , it works for particular isotopes, ^{57}Fe for iron with ^{57}Co as the radioactive source of γ -rays. (Natural Fe contains ~ 2.19 wt% ^{57}Fe .)

Figure 10.23 shows a schematic of a Mössbauer spectrometer. The radioactive ^{57}Co source is embedded in a nonmagnetic matrix, which is chosen so as not to affect the sample or to absorb the γ -rays too strongly. The system can be calibrated using Fe metal; the six peaks seen in Figure 10.24 correspond to the six transitions expected for ^{57}Fe . The ^{57}Co source has an emission peak at 14.4 keV;

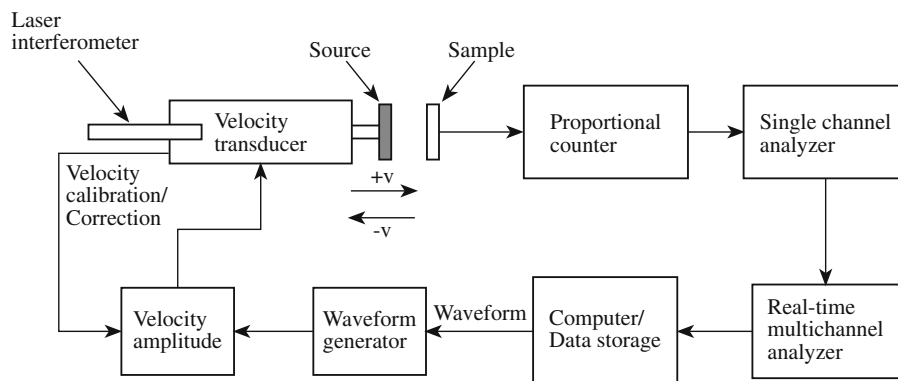


FIGURE 10.23 Schematic of the set-up for Mössbauer spectroscopy.

the source is moved through a range of velocities using a velocity transducer.

Mössbauer spectra from a series of glasses containing Fe in different oxidation states are shown in Figure 10.25. The differences in the curves are clear, but the analysis needed to determine the percentage of Fe in the 2+ state requires extensive calibration of the system. (Notice that peak locations are shown in units of velocity.) The value of the technique is its sensitivity to determining both the

oxidation state and the coordination of the Fe ion. Nuclei in different chemical surroundings from the source do not absorb at the same frequency; this is known as the chemical (or isomer) shift and is the key feature of Mössbauer spectroscopy.

Other isotopes that have been studied are ^{119}Sn (source: metastable ^{119}Sn), ^{121}Sb (source: metastable ^{121}Sb), and ^{151}Eu (source: ^{151}Sm). Table 10.6 lists chemical shifts for tin. It is then quite straightforward to determine the valence state of an unknown tin-compound from its Mössbauer spectrum. This type of analysis has been used in studying tin glazes and tin-containing ceramic pigments. It requires quite small amounts of material, typically 50 mg of powder. Bulk materials can also be examined.

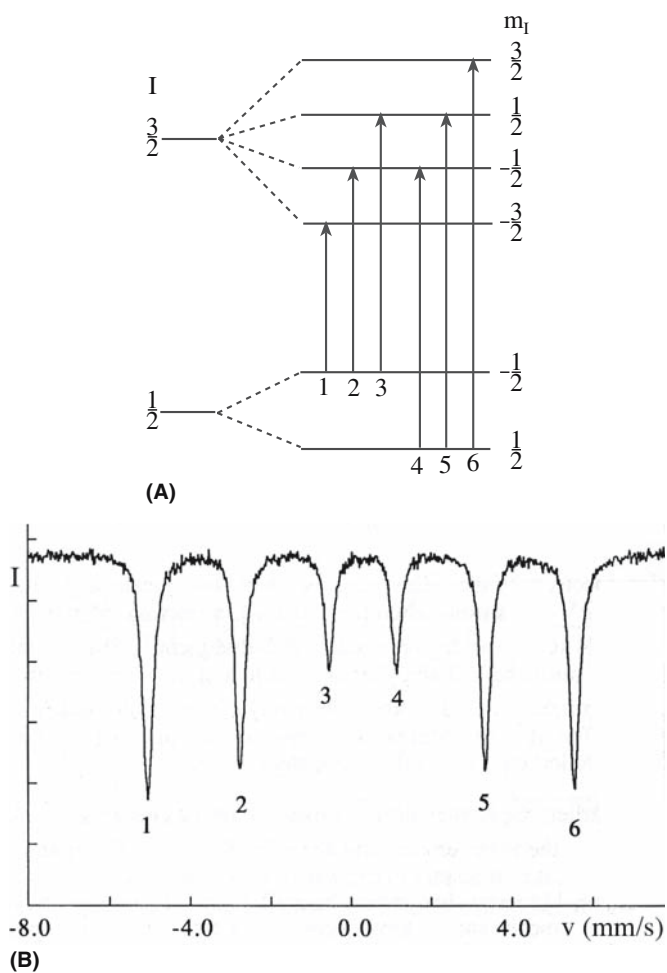


FIGURE 10.24 Transitions in Fe and the resulting Mössbauer spectrum.

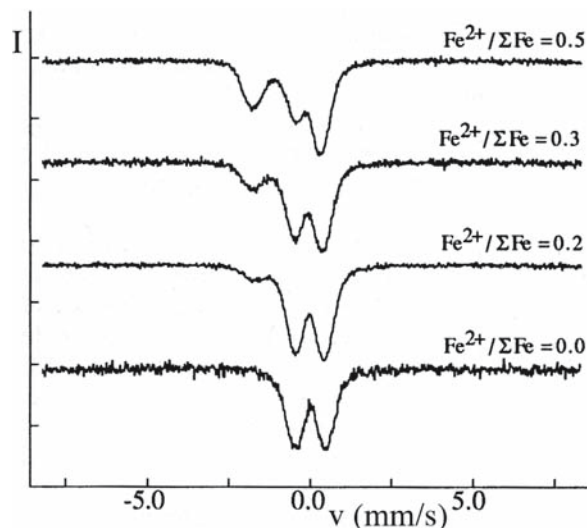


FIGURE 10.25 Mössbauer spectra from glasses containing different concentrations of Fe^{2+} .

TABLE 10.6 Chemical Shift of Some ^{119}Sn Compounds

Valence state	Electron configuration	Chemical shift (mm/s)
Sn^{4+}	$5s^05p^0$	0
Sn (4-covalent)	$5(sp^3)$	2.1
Sn^{2+}	$5s^25p^0$	3.7

10.12 DIFFRACTION IN THE EM

The techniques are

- SAD in the TEM
- CBED in the TEM
- EBSD in the SEM

Selected-area diffraction involves selecting an area on the sample (actually an image of the area) with an aperture and then looking at the diffracting pattern from that area. The diameter of the area can be as small as 100 nm with a modern machine. In CBED, the diffracting area is selected by focusing the electron beam onto a small area of the sample. The diameter of the area can actually be smaller than the unit cell. Figure 10.26 compares SAD and CBED patterns. From the positions of the spots (in SAD) and the discs (in CBED) we can obtain information about the structure and orientation of our sample. CBED patterns often contain an additional fine structure, which allows determination of symmetry such as the point group. The value of CBED lies in its ability to provide information on lattice parameters, sample thickness, and local crystallography on a scale of 10 nm or better. We can use the technique to characterize polarity change across antiphase boundaries (APBs) in GaN and AlN, to determine the site occupancy in nickel-titanate spinel, and to determine the thickness of a specimen. The latter parameter is used in analyzing the height of steps on surfaces and in quantifying X-ray energy dispersive spectrometry (XEDS) data.

Diffraction in the SEM can take several forms, but EBSD is now becoming a routine addition to the SEM. The beam penetrates into the sample and is backscattered; we can use these electrons to form a BSE image or we can record the actual diffraction pattern. A schematic of the

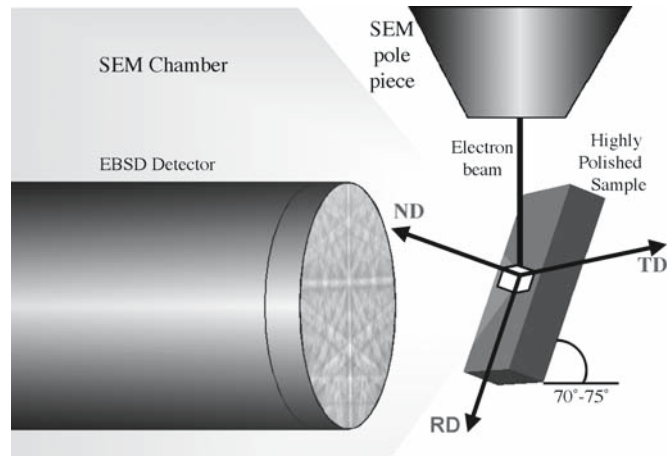


FIGURE 10.27 Schematic of the formation of an EBSD pattern.

system is shown in Figure 10.27 together with an example of an EBSD pattern.

10.13 ION SCATTERING (RBS)

Rutherford backscattering spectrometry again uses ions (a high-energy He beam) to produce the signal, but is more akin to electron energy loss spectroscopy (EELS). We analyze the energy of the backscattered ions and thus determine what atoms they interacted with and where those atoms were located in the sample relative to the surface. Rutherford backscattering spectrometry uses ions (typically 2 MeV helium ions, $^4\text{He}^+$) as the scattered particle. We can picture the interaction mechanism as being a collision resembling that between two billiard balls; the incoming ion transfers energy (and momentum) to the ion in the sample, it is detected as it recoils, and its energy is

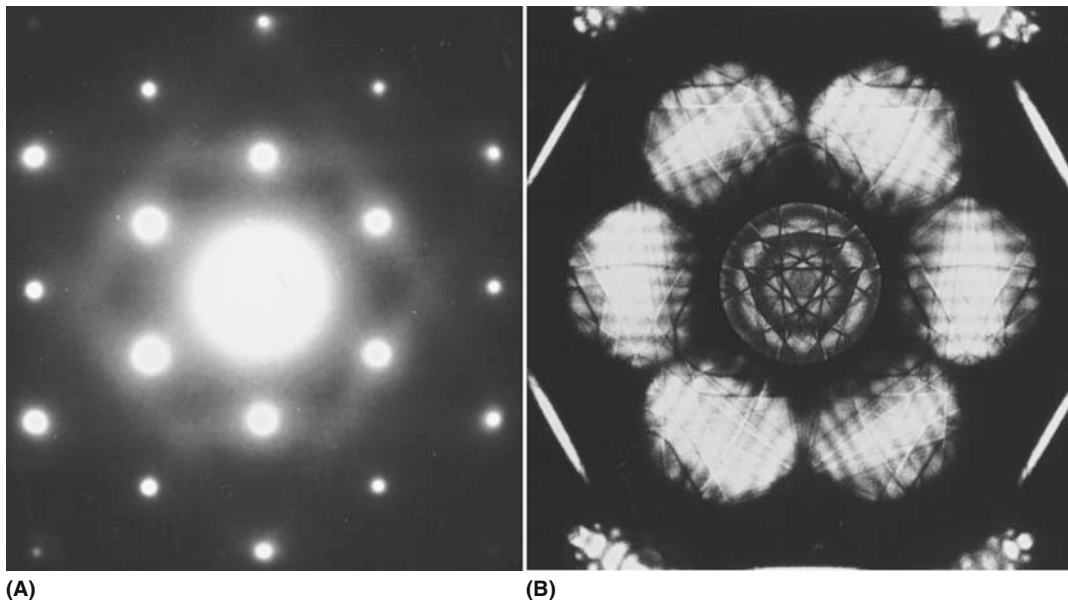


FIGURE 10.26 Diffraction patterns obtained using (a) SAD (TEM) and (b) CBED (TEM).

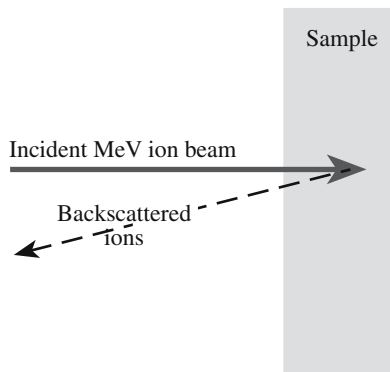


FIGURE 10.28 The backscattering process for RBS; the sample can be tilted to the beam to increase depth resolution.

determined (Figure 10.28). The data are provided in the form of a plot of backscattering yield versus energy and typical spectra are shown in Figure 10.29. Computer analysis of the spectrum gives us the types of atoms in a sample, their concentration, and their depth. The depth resolution is about 20 nm and RBS has been widely used in studies of ceramic thin films deposited onto ceramic substrates such as BaTiO₃ on MgO.

Rutherford backscattering spectrometry has a poor sensitivity to light elements such as oxygen and nitrogen, which are both important in many ceramics. However, an enhanced oxygen signal can be obtained at an incident energy of 3.045 MeV. It is also used to determine the composition of bulk ceramics and impurity profiles in semiconductors, e.g., As distribution in Si.

When the ion beam interacts with the sample, it produces particle-induced X-ray emission (PIXE), which is directly analogous to the production of X-rays in the SEM. Particle-induced X-ray emission has some special advantages over EDS in the SEM in that the background emission is lower, the depth penetration is large, and the sensitivity is high.

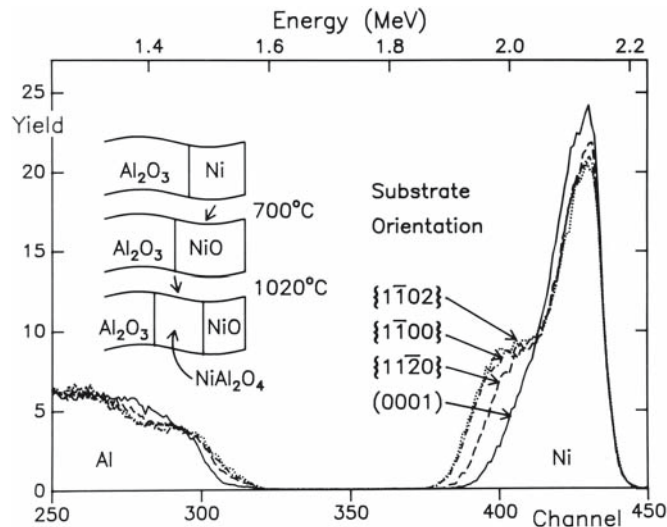


FIGURE 10.29 RBS data sets obtained using a 2.8-MeV beam of He²⁺ ions with the samples tilted 45°. Each sample has been annealed at 700°C for 2 hours followed by 1020°C for 5 hours; the Ni peak shows that the extent of the reaction varies with the surface orientation.

10.14 X-RAY DIFFRACTION AND DATABASES

X-ray diffraction is used in several forms depending on the equipment, the sample, and what you want to know. The great advantage of the technique is that a vacuum is not required and that the X-rays can travel through a container before and after interacting with the specimen. For example, the specimen can be heated inside a quartz tube to 1600°C and examined at that temperature. Using a synchrotron, the beam size and, hence, the spatial resolution can be reduced to ~1 μm. A monochromatic beam can be produced such that changes in energy due to absorption can be accurately measured. Table 10.7 lists types of analysis that can be undertaken using X-rays and the specific technique.

TABLE 10.7 X-Ray Diffraction Analysis		
Type of analysis	Method	Sample
Crystal geometry	Moving crystal-spot pattern	Single crystal
	Computer positioned diffractometer	Single crystal
	Solution of <i>d</i> -spacing equations	Powder
Arrangement of atoms	Analysis of diffracted intensities	Single crystal
	Refinement of whole pattern	Powder
Symmetry	Moving crystal-spot pattern	Single crystal
	Stationary crystal-spot pattern	Single crystal
Identification of compound	Identification of cell parameters	Single crystal
	Matching of <i>d</i> - <i>l</i> set	Powder
	Single-crystal back reflection	Large single crystal
Crystal orientation	Texture analysis	Powder compact
Size of crystal	Line broadening	Powder
Magnitude of strain	Line shifts	Powder compact
Amount of phase	Quantitative analysis	Powder
Change of state	Special atmosphere chambers	Single crystal or powder
Crystal perfection	Direct imaging	Single crystal
	Line shape analysis	Powder

One of the most useful sources of information for crystal structure data is the Powder Diffraction File (PDF). The PDF is a collection of single-phase X-ray powder diffraction patterns in the form of tables of interplanar spacings (d) and corresponding relative peak intensities. There are more than 80,000 patterns in the PDF. In the early days the patterns were printed as 3" × 5" index cards and even though everything is now on computer the files are still referred to as "cards."

Powder XRD is one of the most widely used techniques to characterize ceramics. The material is in the form of a powder so that the grains will be present in all possible orientations so that all d spacings, or θ values, will appear in one pattern. The classical powder pattern was recorded on photographic film. Now the data are in the form of a plot (known as a diffractogram) of counts or intensity versus scattering angle (2θ) as shown in Figure 10.30. A computer that contains the entire PDF is usually used for peak identification. In many examples you will see in the literature phase identification is the extent to which powder XRD is used. This ability alone makes it a powerful and indispensable tool for the ceramist. In a multiphase material the relative amounts of each phase can be determined from the peak areas.

Powder XRD can be used to estimate the sizes of particles. The Scherrer formula states that

$$\Delta\theta \cdot \Delta x = 2\pi \quad (10.3)$$

where $\Delta\theta$ is the peak width (scattering angle half-width) and Δx is the average particle diameter. The resolution of

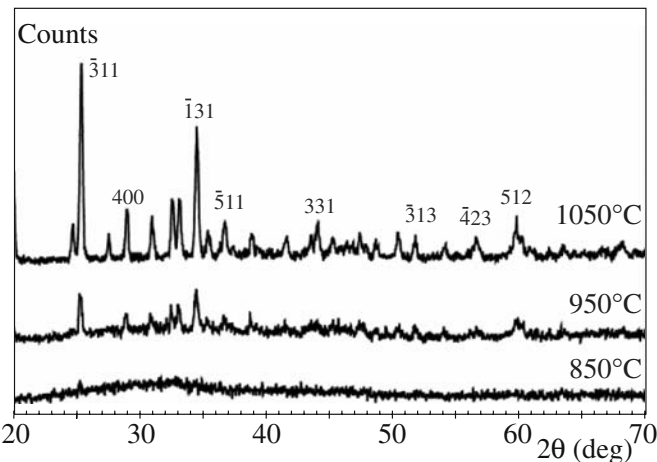


FIGURE 10.30 XRD patterns from a mixture of Ca oxide and alumina recorded while heating the sample at different temperatures.

PDF CARD NUMBERS

21–1272 Anatase
29–1360 Brookite

the diffractometer corresponds to an integral width of 0.32 nm.

Figure 10.31 shows the main components of an X-ray diffractometer. The important features include the following:

- X-ray source. Often Cu $K\alpha$ $\lambda = 0.154184$ nm because of its high intensity.
- Sample. Usually a powder, but it can be pressed or sintered. Only a few milligrams is needed.
- Detector. There are two main types: proportional detectors use photoelectrons generated in Xe; semiconductor detectors use electron-hole pairs created in p-i-n junctions formed in silicon.

In the $\theta/2\theta$ X-ray diffractometer, the sample and detector rotate relative to the X-ray source; when one moves through θ , the other moves through 2θ . Alternatively, the sample can be held fixed and the detector and source rotated in opposite directions. The conventional XRD geometry is often referred to as the Bragg–Brentano geometry. Several different geometries and modifications are used for studying ceramics.

Thin-film diffractometer. A glancing angle geometry is used with the sample surface at an angle of 5–10° to the X-ray beam. The basic idea is that the penetration depth of the X-rays is reduced so they are analyzing the surface. Longer wavelength X-rays can be used, which also reduces penetration (switch to a Cr $K\alpha$

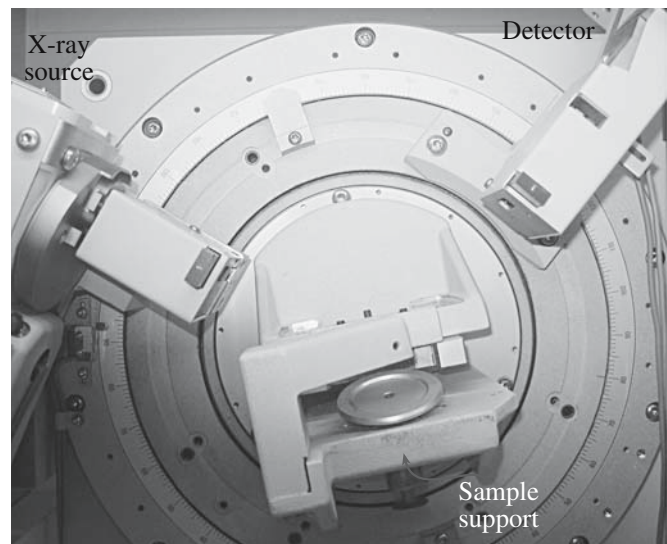


FIGURE 10.31 XRD apparatus showing the location of the source, sample, and detector (Siemens D5005).

source $\lambda = 0.229100\text{ nm}$). Polycrystalline thin films down to a few tens of nanometers thick can be examined.

Microdiffractometer. Collimators as small as $10\mu\text{m}$ are used to produce a small X-ray spot size. The geometry of the detection system is also different from a conventional diffractometer in that it uses an annular detector that allows sampling of the entire cone of diffracted radiation.

Hot-stage XRD. The sample is placed inside a quartz furnace tube that can be heated to temperatures up to 1600°C often in a range of different atmospheres. The main uses are to study phase changes and structural transformations as a function of temperature.

Pole figure. This uses a Eulerian goniometer cradle attached to the diffractometer to determine preferred crystal orientations.

Single-crystal XRD. A single-crystal diffractometer allows the orientation of the crystal to be controlled in such a way that every set of planes can be moved into a diffraction condition. The X-rays are usually detected by scintillation. The technique is not as routine as powder XRD and determination of a crystal structure can take many days or even turn into a thesis.

Laue technique. The diffracted beams produce a pattern consisting of an array of spots. It is used to orient single crystals (with an accuracy in a range of 0.3° to 1°) prior to cutting and polishing.

10.15 NEUTRON SCATTERING

The initial obvious statement is that, overall, neutrons interact with matter even less strongly than do X-rays. Table 10.8 summarizes the differences between the two probes. For both neutrons and X-rays, it is not as easy to direct the beam as it is with electrons or ions. In both cases, the experimental method involves measuring the intensity of the scattered beam as a function of scattering angle.

TABLE 10.8 Properties of X-rays and Neutrons

Property	X-ray	Neutron
Wavelength	0.05–0.25 nm	0.01–2 nm
Energy	12.4 keV	80 MeV
Velocity	$3 \times 10^8\text{ m/s}$	$4 \times 10^3\text{ m/s}$
Production	X-ray tube Synchrotron	Nuclear reactor Electron linear accelerator pulsed source Proton spallation pulsed source
Detection	Photographic film Proportional counter Scintillation counter	$^{10}\text{BF}_3$ or ^3He proportional counter ^6Li scintillation counter

The obvious question is: Why use them when other particles do interact strongly? Neutrons offer distinct advantages over X-rays and other probes. They have a magnetic moment so they can detect magnetic ordering. Because they do not interact strongly they can be used to obtain bulk information. A major application is residual stress measurement in materials as a function of depth.

Neutrons have been used to study glasses and show a first sharp diffraction peak at low angles. This implies that there is some ordering in the glass. Intentional patterns of voids in glasses give rise to such peaks. Table 10.9 provides a comparison of the parameters for XRD and neutron diffraction.

Neutrons are produced in several ways, but each way requires a reactor. Thus neutron diffraction facilities are generally national facilities. In the United States there are seven centers for neutron scattering and there are about 30 in the world. A schematic of a neutron diffractometer is shown in Figure 10.32.

TABLE 10.9 Scattering of X-rays and Neutrons

Dependence	X-ray	Neutron
Nonmagnetic atom	Electrons scatter	Nucleus scatters
θ dependence	Depends on θ through $f(\theta)$	Depends on isotropic scattering length \bar{b}
Variation with Z	$F(0) = Z$	\bar{b} varies with Z
Phase change on scattering	π	Not always π
Isotope dependence	None	\bar{b} depends on isotope
Anomalous dispersion	Near an absorption edge	Near an absorption resonance
Magnetic atom	Nothing extra	Additional scattering (depends on θ)
Absorption coefficient	Absorption large	Absorption usually small

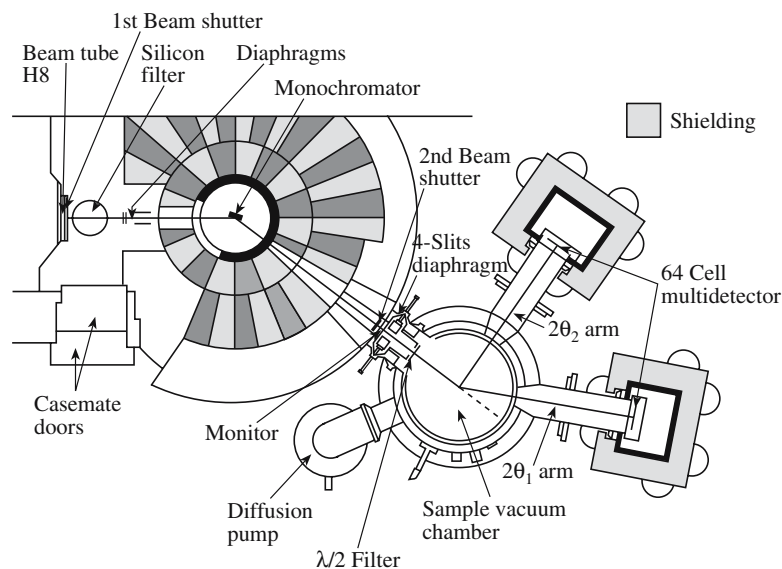


FIGURE 10.32 Schematic of a neutron scattering workstation. The width of the view is 10s of meters.

10.16 MASS SPECTROMETRY

Mass spectrometry is used to provide qualitative and quantitative chemical analysis. For ceramics we are mainly interested in analyzing solids, so a method for ionizing the material is necessary. In spark source mass spectrometry (SSMS) we use a high-voltage spark in a vacuum. The positive ions that are produced are analyzed by the spectrometer based on their mass. For insulating ceramics the material must be mixed with a conducting powder such as graphite or silver. Other methods can be used to ionize the sample:

1. Laser ionization MS uses an Nd:YAG laser and is ideal for insulators, but is qualitative more than quantitative because of the absence of standards.

2. Glow discharge ion source uses a gas discharge between two electrodes, so the sample must be conductive and formed into the cathode.

3. In secondary ion mass spectroscopy (SIMS) an incident ion beam with energy in the range of 4–15 keV is used to create secondary ions from the sample. This provides high-resolution depth profiles with a detection limit down to 1 ppb.

Secondary ion mass spectroscopy is like SEM, but it uses (usually Ga^+) ions instead of electrons. Since the ions have more energy, they eject near-surface atoms out of the sample; these are collected and the chemistry of the near-surface area is thus determined. By scanning the ion beam we can generate a chemical image of the surface and by repeating this process (each time ejecting the surface atoms) we can generate a 3D profile of the sample.

10.17 SPECTROMETRY IN THE EM

The chemistry of interfaces can be probed using both XEDS and parallel recording of electron energy-loss spectra (PEELS).

In the earliest studies of solid-state reactions between ceramic oxides, the width of the reaction product produced by bulk diffusion couples was determined by VLM. Using an SEM with a field-emission gun a much more precise EDS profile analysis can be performed providing chemical analysis at a spatial resolution of $\sim 2\text{ nm}$. Figure 10.33 shows a typical XEDS spectrum: a plot of counts versus X-ray energy. The X-rays are produced as a result of electron transitions within the atoms in the sample. The transitions and, hence, the peaks are characteristic of specific atoms. A doped silicon crystal is used to detect the X-rays, where they cause the formation of electron-hole pairs. New methods for detecting the X-rays are being developed that use the change in temperature caused by the X-ray and are known as calorimeters.

The electron microprobe or WDS can provide accurate chemical analysis or a chemical profile across the interface. The wavelength of the X-rays emitted when the electron beam interacts with the sample is measured. Wavelength dispersive spectroscopy is more accurate than XEDS, but is a serial acquisition, so it is slower. Table 10.10 compares WDS and XEDS.

Electron energy-loss spectroscopy (EELS) counts the number of electrons that have lost particular quantities of energy when the incident electron beam passed through the TEM specimen. The energy loss can occur by interactions with different components of the structure (phonons and plasmons) or by the beam exciting core electrons to a different energy state. The EELS spectrum thus contains

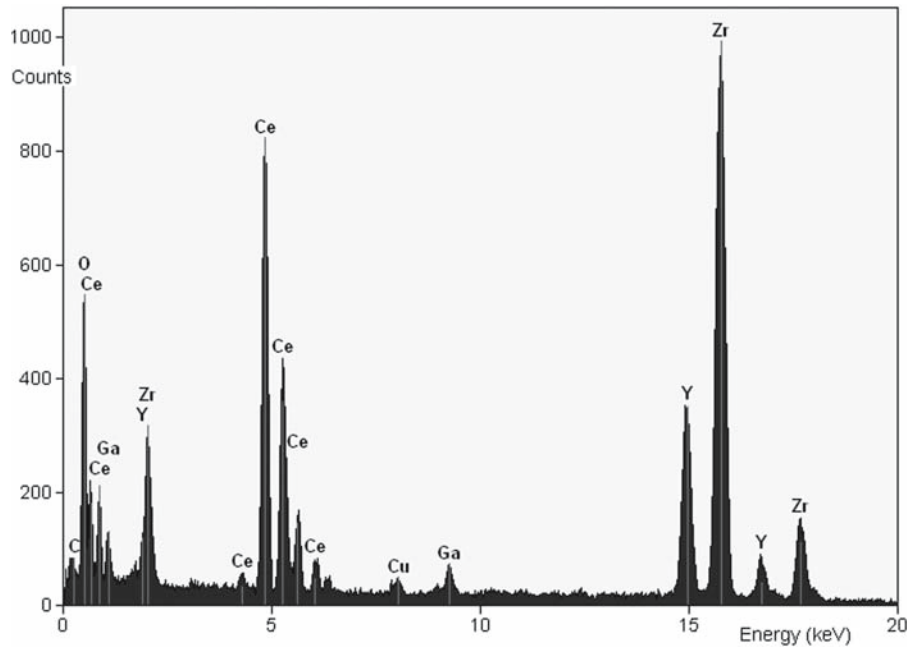


FIGURE 10.33 Example of an XEDS from a sample containing CeO₂ and YSZ in the range up to 20 keV.

information on the bonding and chemistry of the specimen. Since the beam in the TEM can now be as narrow as 0.1 nm, EELS can give highly localized information; it is particularly important in ceramics where low-Z elements tend to be particularly important. Figure 10.34 shows part of an EELS spectrum from two commercial ceria abrasives.

The fine structure of the EELS can be compared to the fine structure in X-ray scattering. It can be used in purpose-built chambers or, more recently, in the TEM. In the TEM you have the great advantage of knowing where you are getting the spectrum from—it is site specific. The difficulty with TEM, as usual, is that there are usually two surfaces to consider (you can try REELS—see REM). This technique will be used more in the future with the wider availability of TEM guns with a smaller spread in

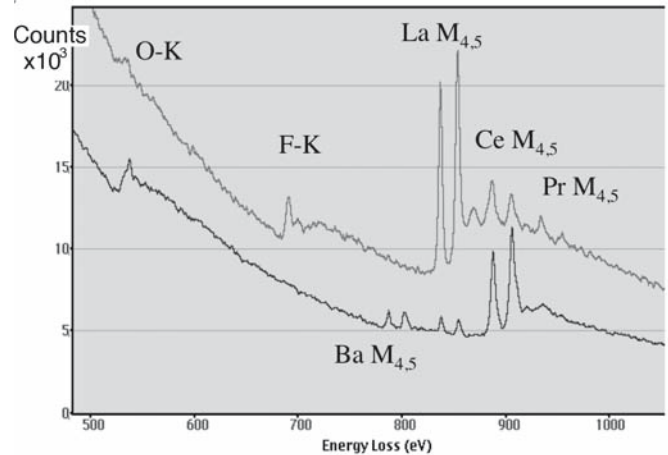


FIGURE 10.34 Example of EELS from two commercial ceria powders.

TABLE 10.10 Comparison of WDS and XEDS

Factor	WDS	XEDS	Reason for difference
Time for complete spectrum (minutes)	25–100	0.5–5	Collection efficiency XEDS measures whole spectrum simultaneously
Count rate on one peak (cps/nA)	1,000	10,000	Collection efficiency
Peak/background ratio	1,000	50	XEDS collects spurious X-rays and has high inherent noise
Maximum count rate (cps)	100,000	30,000	XEDS counts all channels simultaneously, and saturates
Resolution, 0.1–10 keV (eV)	5–10	150–200 80–100	Currently possible Theoretical limit; WDS inferior to XEDS above 25 keV (suitable crystals not available)
Detector limits (weight ppm)	50–1,000	2,000–5,000	WDS used at higher beam current, fewer overlapping peaks XEDS better if current is restricted, e.g., to avoid beam damage
Accuracy of analysis (%)	±1–2	±6	Experimentally determined
Light element analysis (min. atomic number)	4	4	Both have ability for light element detection providing windowless or polymer window used
Rough surface work	Bad	Good	XEDS insensitive to source position

energy. A major application for EELS, which we have only recently begun to use, is the direct measurement of bonding.

AUGER NOTATION

KVV refers to the series of electron transitions responsible for the Auger electron. V refers to electrons coming from the valence band of a solid.

10.18 ELECTRON SPECTROSCOPY

In the group of techniques known as photoelectron spectroscopy (PES) electrons are emitted from their filled electronic states in the solid by the absorption of single photons. Traditionally the energy of the photons corresponds to the UV or X-ray wavelengths and the techniques are known as ultraviolet photoelectron spectroscopy (UPS) or X-ray photoelectron spectroscopy (XPS). X-ray photoelectron spectroscopy used to be called electron spectroscopy for chemical analysis or ESCA and is still the most used surface-sensitive technique. The difficulty for ceramics is the usual one—as we remove electrons from the sample, the sample becomes charged and attracts the same electrons, which can distort the results. In principle you could use a flood gun to resupply the electrons, but the challenge is getting the balance right. The techniques do explore the surface region, not just the surface, so the surface effect must be separated from the larger bulk effect. Variations of the technique include angle-resolved photoemission spectroscopy (ARPES).

These techniques are mainly used for quantitative chemical analysis of surfaces by detecting electrons emitted from the surface. They can be differentiated by how the electrons are produced. In Auger electron spectroscopy (AES) the incident species are electrons. In XPS and UPS the incident species are photons. In XPS we illuminate the sample with X-rays and measure the energy of electrons that are then emitted. If the electrons come from regions close to the surface, we can obtain data on the chemistry and bonding close to the surface. The X-rays can be generated in a synchrotron and this will have both high spatial resolution and high intensity.

Auger electrons are created when an incident electron beam ionizes an atom by removing an inner-shell electron. An electron from a higher energy level will fill the hole and the resulting kinetic energy will be transferred to a loosely bound electron, which is detected. These Auger electrons have relatively low kinetic energy and, consequently, a short mean free path. They come from the top 0.5–3 nm of the surface. Their energy is characteristic of the atomic energy levels of the atom from which they came. Therefore, they are sensitive surface probes of chemical composition. Auger electron spectroscopy has been used extensively to study oxide surfaces. The problem is that the surface must be very clean and examined in UHV.

Figure 10.35 shows examples of carbon KVV Auger electron spectra generated from the surface of two different carbides, diamond and graphite. The

spectra are in the form of derivative electron yield versus electron energy and show the chemical shift effect and how this could be used for “fingerprinting” an unknown sample. Auger electron spectroscopy is the spectroscopist’s variation of low-energy electron diffraction (LEED). Its main use is to provide information on the chemistry, rather than bonding, and more specifically to determine if the sample is clean enough for LEED. The beam can be scanned across the sample to produce an image, hence scanning Auger microscopy (SAM).

In XPS electrons with binding energy (E_b) are ejected from core levels by an incident X-ray photon with energy E_0 . The ejected photoelectron has energy ($E_0 - E_b$). Output electron energies are typically >10 eV. X-ray photon spectroscopy, like AES, has excellent depth resolution and is sensitive to the near surface region of a material. The spectrum has the form of intensity versus binding energy.

By sputtering the surface in between acquisition of either an AES or XPS spectrum it is possible to obtain depth profiles. Sputtering must be conducted in the same system as the spectrometer to avoid contamination of the

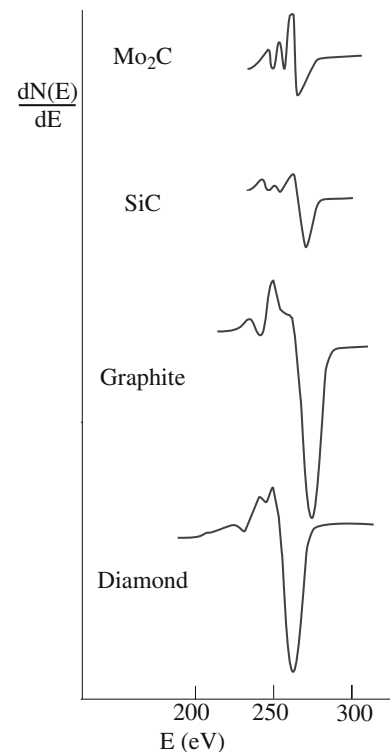


FIGURE 10.35 Derivative C KVV Auger electron spectra from two carbides, graphite, and diamond.

surface. Ultraviolet photoelectron spectroscopy uses UV light to produce electrons. Using these lower photon energies (typically ~ 21 eV) only the valence levels are accessible. A major application of UPS is in determining the band structure of solid surfaces.

10.19 NEUTRON ACTIVATION ANALYSIS (NAA)

The basis of neutron activation analysis is that if a material containing certain rare earth elements is exposed to a beam of neutrons it can become highly radioactive. If the induced radioactivity is then measured, it is possible to identify the elements that are present in the samples and quantify the amount present. The neutron interacts with the target nucleus and forms an excited nucleus, i.e., the neutron loses energy. The excited nucleus then quickly relaxes back to a more stable state by emitting a characteristic γ -ray (this is an n,γ nuclear reaction). The new nucleus may be radioactive, in which case it will then begin to decay by emitting additional characteristic γ -rays, but the rate of emission will be slower due to the longer half-life of the decaying nucleus. Figure 10.36 gives a schematic of the NAA process.

The quick emission of the γ -ray produces the PGNAA (prompt γ -ray NAA) technique and the slower emission produces the more usual DGNAA (delayed GNAA but often just called NAA) technique. Of the three principal different types of neutron sources (reactors, accelerators, and radioisotope neutron emitters), nuclear reactors generating neutrons by U fission give particularly high fluxes of neutrons. Thermal neutrons have energies <0.5 eV; if the neutrons are in thermal equilibrium with the moderator of the reactor, they have a mean energy of 25 meV, which means they have a velocity of 2.2 km s^{-1} . A 1-MW reactor will have a peak flux of thermal neutrons of $\sim 10^{13} \text{ cm}^{-2} \text{ s}^{-1}$. Table 10.11 shows how sensitive NAA is for detecting elements in a sample.

As an example of an analysis, crush a sample to a fine powder and put 150 mg in a plastic vial and 200 mg in a high-purity quartz capsule. Reference samples of known composition are also prepared. The plastic vial is given a

TABLE 10.11 The Sensitivity for Detecting Elements by NAA

(Sensitivity ng)	Elements
0.1	Dy, Eu
0.1–1	In, Lu, Mn
1–10	Au, Ho, Ir, Re, Sm, W
10–100	Ag, Ar, As, Br, Cl, Co, Cs, Cu, Er, Ga, Hf, I, La, Sb, Sc, Se, Ta, Tb, Th, Tm, U, V, Yb
100–1,000	Al, Ba, Cd, Ce, Cr, Hg, Kr, Gd, Ge, Mo, Na, Nd, Ni, Os, Pd, Rb, Rh, Ru, Sr, Te, Zn, Zr
1,000–10,000	Bi, Ca, K, Mg, P, Pt, Si, Sn, Ti, Tl, Xe, Y
10,000–100,000	F, Fe, Nb, Ne
1000,000	Pb, S

5-second irradiation with a flux of 8×10^{13} neutrons $\text{cm}^{-2} \text{ s}^{-1}$. The γ -rays are then counted for 720 seconds, which gives a γ -spectrum (PGNAA) for short-lived elements (Al, Ba, Ca, Dy, K, Mn, Na, Ti, V). The samples in quartz are irradiated for 24 hours with a flux of 5×10^{13} neutrons $\text{cm}^{-2} \text{ s}^{-1}$. After leaving the sample for 7 days, the γ -rays are counted for 2000 seconds. This middle count gives medium half-life elements As, La, Lu, Ne, Sm, U, and Y. After a further 4 weeks, the final count (9000 seconds) give a measure of the long half-life elements Ce, Co, Cr, Cs, Eu, Fe, Hf, Ni, Rub, Sb, Sc, Sr, Ta, Tb, Th, Zn, and Zr. The results are then compared to those from the known material. The accuracy can be better than parts per billion.

Applications have included identifying the origin of archeological ceramics: obsidian can be fingerprinted and the trade patterns of the Olmec civilization can be followed by identifying the area from which the clay they used in their pots originated and the source of contamination in semiconductors can be traced at the 1 ppb level.

10.20 THERMAL ANALYSIS

The term “thermal analysis” actually covers many different techniques that measure a change in a material as a function of temperature. Thermal analysis is particularly useful in characterizing decomposition and crystallization during ceramic powder processing. It is then possible to

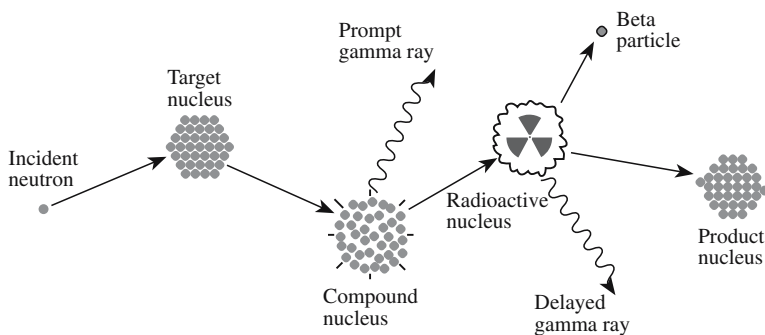


FIGURE 10.36 Schematic of the NAA process.

TABLE 10.12 Common Thermoanalytical Techniques

Method	Common abbreviation	Property measured
Thermogravimetry	TG (TGA)	Mass
Differential thermal analysis	DTA	ΔT between sample and reference
Differential scanning calorimetry	DSC	Heat absorbed or evolved by sample
Evolved gas analysis	EGA	Nature and amount of evolved gas species
Thermodilatometry	TD	Dimension
Thermomechanical analysis	TMA	Deformation/nonoscillatory load
Dynamic thermomechanometry	DMA	Deformation/oscillatory load
Thermomagnetometry	TM	Relative magnetic susceptibility

determine optimum calcination temperatures. A list of the main thermal analysis techniques is given in Table 10.12. The two most common are

- Thermogravimetric analysis (TGA), which measures weight loss during heating
- Differential thermal analysis (DTA), which measures relative changes in sample temperature during heating

DTA and TGA can be performed separately or simultaneously. Figure 10.37 shows examples of DTA and TGA analysis on an initially amorphous CA_2 powder as it crystallizes. The TGA plot shows that as temperature is

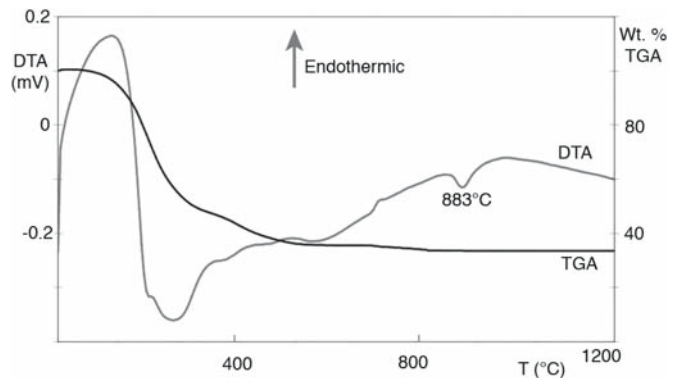


FIGURE 10.37 DTA and TGA measurements showing the reaction as CA_2 crystallizes.

increased the sample loses weight and by about 600°C weight loss is complete. The DTA plot shows that the CA_2 crystallization is exothermic.

Thermal analysis techniques are widely used to study ceramic processing. In addition to determining decomposition and crystallization processes it is also possible to monitor the burnout of organic binders, which are commonly added to powders prior to shaping, and shrinkage during drying. One of the earliest uses for DTA was in studying clay minerals. In montmorillonite the position of certain cations can have an influence on the dehydration behavior. Analysis of DTA curves from samples of montmorillonite containing Li, Na, or K shows that the presence of Li stabilizes the water of hydration and higher temperatures are required for dehydration.

CHAPTER SUMMARY

There are many different techniques for studying ceramics. The choice of which one to use depends on the type of information that we want to obtain and how valuable our material is. Transmission electron microscopy is destructive, but so are many other methods if we have to produce a fine powder. Whereas some of the techniques we described, such as VLM and SEM, are universal, there are many techniques that are available in only a few sites. Those requiring nuclear reactors or very high flux photon beams are usually found at National User Facilities.

A full understanding of a material or a process may require the use of several complementary techniques. For example, electron diffraction in the TEM combined with FTIR and Raman spectroscopies can unequivocally determine what polymorph of SiO_2 is present in a sample. For example, AES can give us the composition of the surface of a sample, AFM can give us the surface morphology, and RHEED can give us the surface crystallography.

The technological importance of nanomaterials means that we need high-resolution techniques. It is the need to understand the structure of nanomaterials and processes that happen on atomic and molecular levels that leads to the development of new instrumentation for characterizing materials.

PEOPLE IN HISTORY

Binnig, Gerd (1947–) and Heinrich Rohrer (1933–) of the IBM Research Laboratory in Switzerland won the Nobel Prize in Physics in 1986 for their invention of the STM.

Mössbauer, Rudolf (1929–) received the Nobel Prize in Physics in 1961 for the discovery of the Mössbauer effect.

Raman, Sir Chandrasekhara Venkata (1888–1970), the Indian scientist, discovered the phenomenon in 1928 while studying CCl_4 ; he was awarded the Nobel Prize in Physics in 1930.

Rutherford, Ernest (1871–1937) demonstrated ion scattering and its utility for chemical analysis. He won the 1908 Nobel Prize in Chemistry.

Stokes, George Gabriel, born 13 August 1819, died 1 February 1903, was Professor of Mathematics in Cambridge when Rayleigh was an undergraduate.

Strutt, John William (Lord Rayleigh) was born 12 November 1842 and died 30 June 1919. He won the Nobel Prize in Physics in 1904 for discovering Ar and succeeded James Clerk Maxwell as the Cavendish Professor in Cambridge.

GENERAL REFERENCES

Cahn, R.W. (2005) *Concise Encyclopedia of Materials Characterization*, 2nd edition, Elsevier, Amsterdam, The Netherlands. A good place to check out any technique.

Chu, W.K., Mayer, J.W. and Nicolet, M-A. (1978) *Backscattering Spectrometry*, Academic Press, New York. Detailed information about RBS.

Hartshorne, N.H. and Stuart, A. (1970) *Crystals and the Polarizing Microscope*, 4th edition, Arnold, London.

Hollas, J.M. (2004) *Modern Spectroscopy*, 4th edition, Wiley, Chichester, England. Covers a wide range of topics at the level you will need if you use the techniques.

Loehman, R.E. (Ed.) (1993) *Characterization of Ceramics*, Butterworth-Heinemann, Boston. Provides “case studies” in which various techniques are used.

Wachtman, J.B. (1993) *Characterization of Materials*, Butterworth-Heinemann, Boston. Overview and comparison of the different characterization techniques.

SPECIFIC REFERENCES

Binnig, G., Rohrer, H., Gerber, Ch., and Weibel, E. (1982) “Tunneling through a controllable vacuum gap,” *Appl. Phys. Lett.* **40**, 178. Paper describing the STM.

Blanpain, B., Revesz, P., Doolittle, L.R., Purser, K.H., and Mayer, J.W. (1988) “The use of the 3.05 MeV oxygen resonance for He-4 backscattering near-surface analysis of oxygen-containing high Z compounds,” *Nucl. Instrum. Methods* **B34**, 459. Describes the RBS method used to obtain the enhanced oxygen signal.

Philp, E., Sloan, J., Kirkland, A.I., Meyer, R.R., Friedrichs, S., Hutchison, J.L., and Green, M.L.H. (2003) “An encapsulated helical one-dimensional cobalt iodide nanostructure,” *Nature Materials* **2**, 788.

Raman, C.V. and Krishnan, K.S. (1928) “A new type of secondary radiation,” *Nature* **121**, 501. The original description of the “Raman effect.”

“Standard Test Method for Interstitial Atomic Oxygen Content of Silicon by Infrared Absorption,” F 121 *Annual Book of ASTM Standards*, Vol. 10.05, ASTM, Philadelphia, pp. 240–242.

EXERCISES

- 10.1 Construct a chart summarizing the principal scattering techniques used to characterize the structure, chemistry, and bonding in ceramics emphasizing which of the three features is most directly addressed by each technique.
- 10.2 In Figure 10.1 the grains boundaries are described as low-angle grain boundaries. Could this information be obtained directly from VLM? If not, what other methods might have been used to make this determination?
- 10.3 In Figure 10.6, why does the image have a 3D appearance?
- 10.4 In Figure 10.7 the image distinguishes the regions with different chemistry directly and with high spatial resolution. Explain the physical process underlying this observation?
- 10.5 During the processing of ceramics containing crystalline quartz a phase transformation occurs on cooling/heating between the α form and the β form. The phase transformation produces an appreciable change in volume that can lead to cracking. How would you determine from a fragment of a ceramic plate whether you had the α or β phase present in the sample?
- 10.6 How would you determine whether water vapor has chemisorbed onto the surface of particles of silica gel?
- 10.7 If we are examining steps of atomic dimensions in figure 10.14, redraw the schematic to scale and thus explain the factors that determine vertical and lateral resolution in AFM.
- 10.8 Compare the value of NMR and Mössbauer analysis for ceramic materials.
- 10.9 Referring to Figure 10.33, explain why we see multiple peaks for Y and Zn occur at different energies, and why we see Cu.
- 10.10 Examine the DTA/TGA plots in Figure 10.37. What can you say about the curves as the temperature is increased from 25°C to 1200°C?

Part IV

Defects

Point Defects, Charge, and Diffusion

CHAPTER PREVIEW

Point defects are particularly important in ceramics because of the role they can play in determining the properties of a material. The entire semiconductor industry is possible because of minute concentrations of point defects that are added to Si: the dopants determine if the Si is n-type, p-type, or semi-insulating: they determine the electrical properties. Solid-oxide fuel cells work because of the large concentrations of oxygen vacancies present: the vacancies provide fast ion conduction pathways. CZ is cubic because of the presence of point defects that stabilize the cubic structure.

We will address three principal questions in this chapter and leave the properties associated with point defects to later chapters where we will discuss conduction, light, and color, for example.

- What point defects are possible?
- How many point defects are present?
- How easily can they move?

To determine what defects are possible in a crystal we need to know its structure. Point defects also exist in glass, but there is the extra problem of how to define what is being “defective.” (What is the perfect structure of the glass?) To estimate the concentration of point defects, we should know (1) what types of defects are present and (2) how they form, which, in turn, determines (3) how many of each kind there will be. Answering the third question will give us many of the properties of the materials containing these defects. In some cases we want them to move quickly and in other cases we actually would rather they were immobile. To really understand this subject thoroughly you will need a good knowledge of thermodynamics and kinetics. These topics are so large that there are many texts devoted entirely to them.

11.1 ARE DEFECTS IN CERAMICS DIFFERENT?

Until now we have considered the ideal structures of crystals only when each atom or ion is on a regular site in the crystal. Real crystals contain a variety of imperfections or defects. In crystalline ceramics and glasses, the structure and chemistry of the material will be determined by the kinetics of defect movement. For example, the kinetics of the glass-to-crystal transformation are slow if the temperature is low (typically less than 1000°C) because the transformation occurs by atoms moving—in ceramics, this usually occurs by point defects moving. If point defects move too slowly, the structure with the lowest energy (the equilibrium structure) may never actually be achieved. How fast they move is determined by their structure.

The really special feature of ceramics is that they can contain charged defects; metals cannot. There are some definite differences when we compare defects in ceramics to similar ones in face-centered cubic (fcc) metal crystals such as Cu.

- The concentration of impurities in ceramics is usually much greater than that of intrinsic defects.
- Dislocations are usually much less important for deformation mechanisms than they are in metals.
- Surfaces and interfaces are even more important for ceramics.
- Pores and voids are often very much more important for ceramics.

THE OTHER DEFECT CHAPTERS

Dislocations—Chapter 12

Surfaces—Chapter 13

Grain boundaries—Chapter 14

Phase boundaries, particles, and voids—Chapter 15

The importance of pores and voids is a good illustration of how time changes our view of materials. In the past,

TABLE 11.1 Defect Hierarchy

Dimension	Name	Example
Zero	Point defect	Vacancy
One	Line defect	Dislocation
Two	Planar defect	Grain boundary
Three	Volume defect	Pore

processing ceramics often meant trying to remove pores and voids during sintering because they weakened the final material. While they still generally do so, we are now also very interested in highly porous ceramics because such materials can have a very large surface area, which may be critical in their application as catalysts, catalyst supports, or filters. In this chapter we concentrate on point defects, but remember that they do relate to all other defects in ceramics and their importance is that they determine many important properties.

11.2 TYPES OF POINT DEFECTS

Defects are often classified in terms of a dimensionality. This is known as the defect hierarchy. The classifications are given in Table 11.1. In spite of this table, remember that all these defects are three-dimensional. We will first summarize the different types of point defect that can occur in crystalline materials. To provide some idea of the importance of point defects, we will consider some specific examples.

Vacancies: If an atom is not present on the site that it should occupy in a perfect crystal then a vacancy is located at that site. A Schottky defect is a set of vacancies created by removing one atom for each atom in the chemical formula. Thus, in a stoichiometric crystal such as MgO, we get a pair of vacancies, one on the Mg sublattice and one on the O sublattice, as shown in Figure 11.1. In spinel, a Schottky defect consists of seven vacancies.

Interstitials: If an atom is present on any site that would be unoccupied in a perfect crystal then that atom is an interstitial. A Frenkel defect is a vacancy + interstitial pair formed by removing an atom from its site in the crystal structure and putting it into an interstice as illustrated in Figure 11.2. Frenkel defects formed in iodine-containing AgBr are essential to the photographic process.

Misplaced atoms: If an atom is present on a crystal site that should be occupied by a different atom, that atom is a misplaced atom and may be called an antisite defect. Antisite defects usually form in covalent ceramics such as AlN and SiC, but can also occur in complex oxides that have several different types of cation, for example, spinels and garnets. (We do not expect to see cations on anion sites and vice versa.)

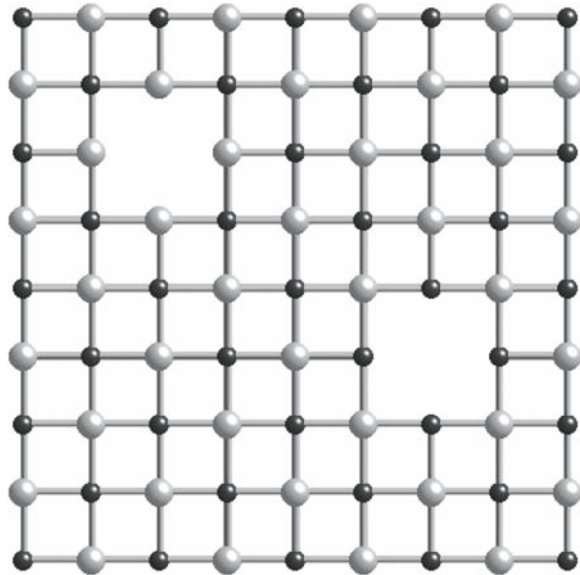


FIGURE 11.1 Schematic of a Schottky defect drawn in 2D.

Associated centers: When two point defects interact so that they can be considered as a single defect they are called an associated center or, if more atoms are involved, a defect cluster or a defect complex. Exposing a material to ionizing radiation such as X-rays and γ -rays can create large numbers of defect clusters.

Solute (substitutional) atoms: In Cu alloys, we can add up to 30 at% Zn before the structure is changed. All the Zn atoms sit on Cu sites so they substitute for the Cu and the crystal is said to be a solid solution of Zn in Cu. The effect is to add electrons to the *d* band of the alloy and it is this change in the electronic structure that determines the solubility limit. We can similarly substitute Ge in Si, but the solubility is limited due to the difference in atomic size. In GaAs we can replace the Ga atom by Al on the group III sublattice

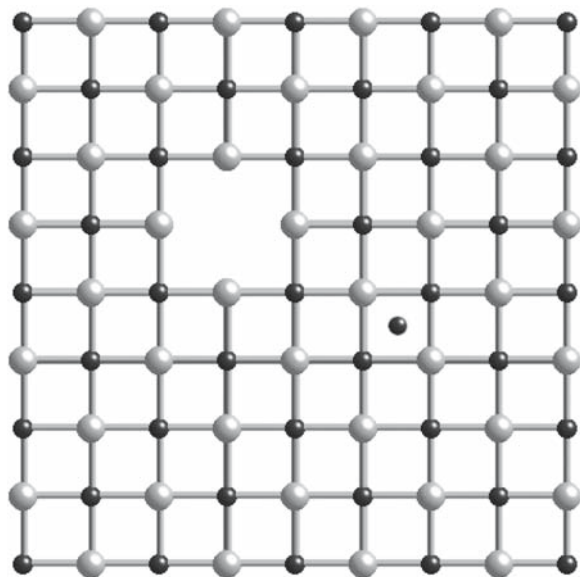


FIGURE 11.2 Schematic of a Frenkel defect drawn in 2D.

TABLE 11.2 The Kröger–Vink Notation for the Binary MX

Defect	Notation	Comments
Vacancy	V_x	V is also the chemical symbol for the element vanadium; if there is a possibility for confusion, such as expressing a vacancy on a vanadium site, then use “Va” for the vacancy
Interstitial	M_i and X_i	No “site”
Antisite atom	M_x and X_M	Usually in covalent solids
Associated defect	(M_iX_M)	Larger associations called “clusters”
Solute	S_x	Impurity substitution
Electron and hole	e' and h	
Schottky	(V_MV_X)	Special associated defects
Frenkel	(V_MM_i)	

giving a complete solid solution, $Ga_xAl_{1-x}As$, with x running from 0 to 1. GaAs and AlAs have the same structure and similar lattice parameters. We can replace As by P on the group V sublattice to give another continuous solid solution. This type of substitution occurs in both covalent and ionic ceramics as well as in metals.

Electronic defects: Electrons and holes can both exist in ceramics. They may be associated with particular ions, in which case they are simply charged point defects. This leads to the topic of color centers, which color alkali halide crystals, amethyst, diamond, etc.

We use the Kröger–Vink notation to identify these different point defects, which is summarized in Table 11.2. This notation is completely general in that it can apply to any crystalline compound or even to pure crystals. In this notation, structural elements are denoted as S_p^c .

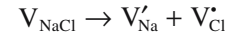
We will make use of Kröger–Vink notation in many sections in this chapter. We can write simple equations to describe the formation of point defects or their interactions. For example, if we remove a molecule, NaCl, from a crystal of rock salt,

NOTATION SUMMARY FOR S_p^c

S: Species
P: Position in the crystal
c: Charge relative to the perfect crystal

Charge notation:
 Negative: dash, $'$
 Positive: point, \cdot
 Neutral: x

we form a vacancy on both anion and cation sublattices, so we have to have a method for distinguishing these defects. The Kröger–Vink notation for the reaction we have just described is



We need such a notation because of one of the most special features about ceramics—the charge. Other notations are sometimes used, but the Kröger–Vink notation is the most widely accepted. (You may see variations in this notation so be careful in translating from one text to another.) The topic of point defects should not be completely new to you. Some of the fields in which you may have encountered point defects before are listed in Table 11.3.

11.3 WHAT IS SPECIAL FOR CERAMICS?

Point defects are special in ceramics when they involve either charge (ionic materials) or dangling bonds (covalent materials).

- Vacancies, interstitials, and substitutional defects can all be charged. The special point defect in ceramics is the charged vacancy. Frenkel and Schottky defects are overall neutral.
- Association of defects is particularly important for ceramics because Coulombic interactions are both strong and long-range.
- Electronic structure is increasingly important. In the past, the electronic structure was important only because the materials have a large band gap. Ionic materials are insulators. This is no longer the case—many old “insulators” (like SiC) are now also wide-band-gap semiconductors!
- Nonstoichiometry is so important because the concentration of point defects can be very large. In ionic materials, point defects are usually charged and they are often numerous.

TABLE 11.3 Examples of Commonly Encountered Point Defects in Materials

Type of point defect	Application	Comments
Solute atoms	Doping silicon for ICs	Concentration of dopant atoms very small, ~0.0001% can cause a 100 times increase in conductivity
Solute atoms	Solid solution strengthening of metals	A 50 Cu–50 Ni alloy has twice the tensile strength of pure copper
Interstitial	Carburizing of iron and steel	Surface hardening by heating metal in a hydrocarbon gas
Vacancies	Kirkendall effect	Failure mechanism in Au–Al bonds, e.g., Au wire bonds on Al metallizations in ICs
Vacancies and interstitials	Cold working of metals	At $T < 0.4 T_m$ solid-state diffusion is slow

Some special rules for ceramics:

- The number of sites is constant. This is the same as in metals, but we often have very different sites available in ceramics.
- The total charge is still zero.
- Intrinsic defect concentrations are often very much lower than impurity concentrations.

11.4 WHAT TYPE OF DEFECTS FORM?

Crystals with open lattice structures will tend to favor Frenkel defects. These crystals have structures with low coordination numbers and large interstitial sites, for example, the würtzite structure has CN = 4. If there is a large difference in size between the cations and anions, Frenkel defects are usually formed by displacing the smaller ion. In Al₂O₃, for example, the cation is smaller and we would expect to form cation Frenkel defects. However, anion Frenkel defects will form in UO₂, CeO₂, and ThO₂, which all have large cations. In contrast, we would expect to find Schottky defects in crystals with high coordination numbers such as MgO.

Vacancies may be present on different sites for the same type of ion. For example, NiFe₂O₄ is an inverse spinel [Fe(NiFe)O₄]; Fe³⁺ ions sit in both tetrahedral and octahedral sites. Thus, we can have Fe³⁺ vacancies on the tetrahedral or octahedral sites, but these two types of vacancy are not the same. You can imagine how complex the situation becomes for more complex crystals. We usually ignore such complications because they are too difficult to handle, but be aware that we are making this simplification.

11.5 EQUILIBRIUM DEFECT CONCENTRATIONS

We need to know how many point defects are present in thermal equilibrium. One of the simplest point defects that can occur in a crystal is a vacancy. In a binary compound, e.g., MgO, where only vacancies exist, we must have an equal number of each type of vacancy to maintain the stoichiometric formula.

At a given temperature there is an equilibrium concentration of point defects in a crystal. The implication of this statement is that a crystal containing point defects must have a lower free energy, G , than a corresponding crystal without any defects. From Chapter 3 we know that the change in free energy accompanying a process, such as the creation of vacancies, is given by

$$\Delta G = \Delta E - T\Delta S \quad (11.1)$$

We can use ΔH or ΔE in Eq. 11.1. ΔH would refer specifically to the enthalpy to form a point defect. ΔE is the change in the internal energy on forming the defect. The internal energy of the disordered crystal is the energy of the perfect crystal plus nE .

E is strongly affected by the nearest neighbors and the interatomic bonding. It costs energy to produce point defects; we have to break bonds. The internal energy increases when the number of point defects increases. At the same time the entropy (randomness of the structure) increases, and the product $T\Delta S$ also increases. The change in entropy is complex and consists of terms due to the vibration of the atoms around the defects and terms due to the arrangement of defects in the crystal. This configurational entropy relies on statistics (how many) and mechanics (how it is moving); the subject is statistical mechanics. So even though it requires energy to create vacancies, overall G may decrease because of

SCHOTTKY DEFECTS: THE CALCULATION

Show that the number of Schottky defects is

$$n_s \approx N \exp(-\Delta E_s/2kT) \quad \text{Box 11.1}$$

The units of ΔE_s are J/defect. Then determine entropy using probability theory.

$$S = k \ln W \quad \text{Box 11.2}$$

$$W = N! / [(N - n)! n!] \quad \text{Box 11.3}$$

$$W_A = N! / [(N - n_s)! n_s!] \quad \text{Box 11.4}$$

$$W_B = N! / [(N - n_s)! n_s!] \quad \text{Box 11.5}$$

$$W_A = W_B \quad \text{Box 11.6}$$

$$W_T = W_A W_B \quad \text{Box 11.7}$$

$$\Delta S = k \ln W_T = k \ln \{N! / [(N - n_s)! n_s!]^2\} \quad \text{Box 11.8}$$

$$\Delta S = 2k \ln \{N! / [(N - n_s)! n_s!]\} \quad \text{Box 11.9}$$

Next use math:

$$\ln N! \approx N \ln N - N \quad \text{Box 11.10}$$

$$\Delta S = 2k \{N \ln N - (N - n_s) \ln(N - n_s) - n_s \ln n_s\} \quad \text{Box 11.11}$$

Finally do the substitutions:

$$\Delta G = n_s \Delta E_s - 2kT \{N \ln N - (N - n_s) \ln(N - n_s) - n_s \ln n_s\} \quad \text{Box 11.12}$$

$$(\partial \Delta G / \partial n_s)_{T,P} = 0 \quad \text{Box 11.13}$$

$$\Delta E_s = 2kT \ln[(N - n_s) / n_s] \quad \text{Box 11.14}$$

$$n_s = (N - n_s) \exp(-\Delta E_s / 2kT) \quad \text{Box 11.15}$$

$$n_s \approx N \exp(-\Delta E_s / 2kT) \quad \text{Box 11.16}$$

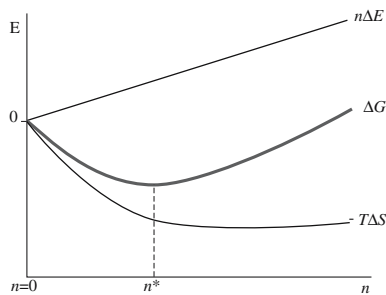


FIGURE 11.3 Schematic showing how the free energy decreases to a minimum as the number of vacancies increases.

the entropy contribution. The challenge is that to know ΔG , we have to know S , the entropy.

Figure 11.3 is a plot of $n\Delta E$, ΔS , and ΔG . From this plot you can see that introducing vacancies lowers the free energy of the crystal until an equilibrium concentration is reached; adding too many vacancies increases G again. At higher temperatures the equilibrium number of vacancies increases. The implications are important. In pure crystals we expect to find point defects at all temperatures above 0K. Since these defects are in thermodynamic equilibrium, annealing or other thermal treatments cannot remove them.

Usually the concentration of point defects is controlled by impurities.

Dopant-induced defects will also be in thermodynamic equilibrium so that the overall equilibrium is controlled by the dopants.

Schottky defects do not change the composition of the material. The concentration of Schottky defects in a crystal is deduced using standard statistical mechanics that appears in most thermodynamics textbooks (because it is such a clear application of basic thermodynamics). For most ceramics, we just need the result from the calculation. Notice that charge is not mentioned and the derivation assumes a pure simple binary compound, like MgO or NiAl.

ΔE_s is the energy to form a Schottky defect, and k , the Boltzmann constant, is in $J/^\circ C$. If ΔE_s is given in J/mol , then the number of Schottky defects in a unit volume is the same with R replacing k .

We will review how n_s is derived for a stoichiometric crystal AB. The derivation shows the importance of disorder. In this discussion, we have separated the equations from the text and mainly comment on the logic of the derivation.

If n_s is the number of Schottky defects per cubic centimeter in the crystal at T K, then we have n_s vacant cation sites and n_s vacant anion sites. In addition, in a crystal of this type there are N possible cation sites and N possible anion sites per cubic centimeter. We can determine the entropy change, ΔS , in a system of occupied and unoccupied sites by using the Boltzmann equation (Eq. Box 11.2).

(Note that we are neglecting thermal entropy effects.) W is the number of ways of distributing n defects over N sites at random.

The number of ways we can distribute the n_s cation vacancies over the available sites in the crystal will be given by Eq. Box 11.4; we can write a similar expression for the anion vacancies as shown in Eq. Box 11.5.

Because AB is a stoichiometric compound we can write Eq. Box 11.6. The total number of ways, W_T , of distributing these defects is given by the product of W_A and W_B , so we have Eq. Box 11.7, and therefore the change in entropy caused by introducing Schottky defects is given by Eq. Box 11.8, which we can rewrite as Eq. Box 11.9.

Now we use a standard trick for large N : Stirling's approximation (Eq. Box 11.10) eliminates the factorials, which leaves us with an expression for the entropy change associated with the formation of Schottky defects (Eq. Box 11.11).

Substituting Eq. Box 11.11 into Eq. 11.1 gives the overall change in Gibbs free energy for forming n_s pairs (Eq. Box 11.12). At equilibrium, the free energy change is a minimum with respect to the number of defects and is given by Eq. Box 11.13. We can thus differentiate Eq. Box 11.12 and set the result equal to zero so that after a little rearrangement we arrive at Eq. Box 11.14; in terms of the number of defects we write Eq. Box 11.15. The final step is another approximation: N is usually very much greater than n_s . So we arrive at Eq. Box 11.16 (i.e., Eq. Box 11.1).

We give some experimental values for the enthalpy of formation of Schottky defects in Table 11.4. We can use these numbers to calculate equilibrium defect concentrations as we have for NaCl in Table 11.5. The population of point defects is very low, but it is clear from Eq. Box 11.1 that vacancies are stable in the crystal at any temperature above absolute zero. Because energies for point defect formation in stoichiometric oxides such as

TABLE 11.4 The Formation Enthalpy of Schottky Defects in Some Compounds of Formula MX

Compound	ΔE_s (10^{-19} J)	ΔE_s (eV)
MgO	10.574	6.60
CaO	9.773	6.10
SrO	11.346	7.08
BaO	9.613	6.00
LiF	3.749	2.34
LiCl	3.397	2.12
LiBr	2.884	1.80
LiI	2.083	1.30
NaCl	3.685	2.30
NaBr	2.692	1.68
KCl	3.621	2.26
KBr	3.797	2.37
KI	2.563	1.60
CsBr	3.204	2.00
CsI	3.044	1.90

TABLE 11.5 Schottky Defect Concentrations in NaCl

Temperature (°C)	Temperature (K)	n_s/N	n_s (cm ⁻³)
27	300	4.79×10^{-20}	2.14×10^3
127	500	2.56×10^{-12}	1.14×10^{11}
427	700	5.25×10^{-9}	2.34×10^{14}
627	900	3.63×10^{-7}	1.62×10^{16}

MgO and CaO are so high, the concentration of intrinsic defects is going to be very much less than impurity concentrations (usually ~100 ppm or greater). Even close to the melting temperature we find that only one or two sites in one billion are vacant due to intrinsic effects.

To give you an idea of what these numbers mean calculate the equilibrium number of vacancies that would be in a single crystal of MgO the size of the earth ($r_{\text{earth}} \sim 6400$ km) at room temperature; it is still a pretty small number.

Intrinsic vacancies are much more numerous in metals. For example, in a 1-cm³ crystal of aluminum at room temperature there are about 9 billion vacancies. In a crystal of silicon in equilibrium at room temperature there are only about 1×10^{-18} intrinsic vacancies per cubic centimeter. This is considerably less than typical concentrations of extrinsic point defects (dopants) in silicon—about 0.0001%: another fortunate fact.

Vacancies are important for dislocation motion at high temperatures: the dislocations then move by climb—they absorb vacancies, which are more numerous at higher temperatures (the vacancies also move more easily at elevated temperatures).

Frenkel defects, like Schottky defects, also involve vacancies in the crystal structure. In this case, though, the vacancies exist on only one sublattice and the atom that should occupy the vacant positions is placed in an interstitial site in the crystal. The interstitial is a very special defect: it can exist on one or more non-equivalent sites, which are not normally crystal sites, so the Frenkel defect is not unique either.

The calculation of the number of Frenkel defects (n_f) in a crystal proceeds along lines that are similar to those for Schottky defects where we consider the number of ways of distributing N vacancies over N^* available interstitial positions.

The values for ΔE_f are usually quoted in J/mol and we therefore use the following equation:

$$n_f \approx (NN^*)^{1/2} \exp(-\Delta H_f/2RT) \quad (11.2)$$

Experimental values of the energy of formation of Frenkel defects in some oxide compounds are given in Table 11.6.

TABLE 11.6 Formation Enthalpy of Frenkel Defects in Some Compounds of Formula MX and MX₂

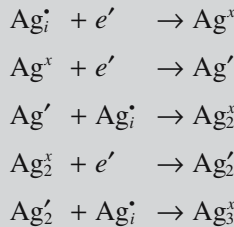
Material	ΔE_f (10 ⁻¹⁹ J)	ΔE_f (eV)
UO ₂	5.448	3.40
ZrO ₂	6.569	4.10
CaF ₂	4.486	2.80
SrF ₂	1.122	0.70
AgCl	2.564	1.60
AgBr	1.923	1.20
β-AgI	1.122	0.70

The actual type of defect found in the crystal will depend on the energy of formation. There may be either more Frenkel defects or more Schottky defects depending on which has the smaller energy of formation. As we have already mentioned, Frenkel defects are more likely to be important in crystals with open structures that can accommodate the interstitials without much lattice distortion.

Frenkel defects are the key to the photographic process. Photographic film contains crystals (called grains) of AgBr or I-doped AgBr. These are dispersed in gelatin, often along with various other chemicals known as sensitizers, on a thin plastic film (it used to be on glass). AgBr has a rocksalt structure, but rather than containing mainly Schottky defects (as we find in NaCl) it contains mostly cation Frenkel defects.

During irradiation with light, electrons are excited from the valence band to the conduction band. The band-gap energy is 2.7 eV, which corresponds to a wavelength of 460 nm (blue light). An electron will neutralize one of the silver interstitial ions. To produce what is known as a *latent image* it is necessary for silver atoms to form clusters of at least four atoms on the surface of the grains. The silver interstitials are mobile and can diffuse to the surface. The exact mechanism for cluster formation is not well understood, but this set of equations shows a possible sequence of reactions. The clusters act as catalysts that lead to the reduction of the AgBr grains in the presence of a suitable developer.

SILVER POINT DEFECTS



necessary for silver atoms to form clusters of at least four atoms on the surface of the grains. The silver interstitials are mobile and can diffuse to the surface. The exact mechanism for cluster formation is not well understood, but this set of equations shows a possible sequence of reactions. The clusters act as catalysts that lead to the reduction of the AgBr grains in the presence of a suitable developer.

11.6 WRITING EQUATIONS FOR POINT DEFECTS

In many instances we have to consider reactions that cannot be expressed within the normal chemical nomenclature. For example, if a dopant is incorporated into a crystal it can have profound effects upon the physical and chemical properties of the substance because of the defects that are necessarily introduced. However, defects

do not occur in the balance of reactants expressed in the traditional equations, and so these important effects are lost to the chemical accounting system that the equations represent. Using the Kröger–Vink notation we can build up a *defect chemistry*, provided the normal rules for balancing chemical equations are preserved. In writing equations for point defect reactions we must obey the following rules:

- Maintain the ratio of the number of sites, e.g., in M_aX_b , the ratio a/b is constant.
- V_M and M_x require sites; M_i does not require a new site.
- Maintain electrical neutrality overall.
- Surface sites are treated as if they are bulk sites (but could be treated separately).

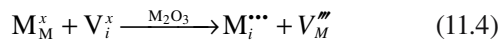
Example: Point Defects in the Model Oxide M_2O_3

We will illustrate how to formulate the Schottky and cation Frenkel defect reactions using Kröger–Vink notation for the model oxide M_2O_3 . For the Schottky defect reaction



We imagine that the molecule of M_2O_3 condenses at the surface of the material or at another interface. In writing Eq. 11.3, we maintain the ratio of M-to-O sites and balance the charge.

For the cation Frenkel defect reaction



The vacancy on an interstitial site is simply that there is no interstitial initially. Notice that Eq. 11.4 can be written for a single cation. We do not need to consider the number of sites, etc. The anion Frenkel defect reaction would be similar, but is unlikely to occur in a material such as Al_2O_3 .

11.7 SOLID SOLUTIONS

We consider solid solutions here because we can think of them as being formed by distributing a large number of point defects in a host crystal. As always, we must balance charge and be sure that the size of the “impurity” (guest) ion is appropriate to fit into the available site. If the impurity ions are incorporated in regular crystal sites the resulting phase is a substitutional solid solution. In an interstitial solid solution the impurity atoms occupy interstices in the crystal structure. The rules for substitutional solid solutions (the Hume–Rothery rules) can be summarized as follows. Note that the last two requirements are really very closely tied to the first two.

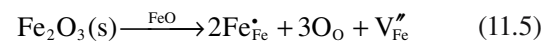
Rule	Example	Comments
Size factor (the “<15% rule”)	CdS–CdSe $r_s = 0.106\text{ nm}$ $r_{se} = 0.116\text{ nm}$	If the size difference is outside this range then substitution will be limited or may not occur
Valence factor	Ni^{2+} in MgO	This is not the same in metals where we do not have to consider charge
Chemical affinity	Al^{3+} in MgO $MgAl_2O_4$	The possibility of a new phase can limit solid solubility
Structure type	MgO and NiO (same) SiO_2 and TiO_2 (similar)	The more similar the structures, the greater the solubility

We can summarize the comparison to metals:

- In metals, we have the same rule for the formation of alloys regarding size; the new factor in ceramics is the charge.
- In elemental semiconductors, the rules are approximately the same; these are ceramics with a large covalent component to the bonding. The valence difference is important in forming p-type and n-type semiconductors.
- We will see that the silica-based glasses are somewhere between elemental semiconductors and ionic materials, but introduce other challenges.

Solid-Solution Example 1: FeO_{1-x}

We saw in our discussion of phase diagrams that FeO never exists. Consider wüstite with composition $Fe_{0.95}O$. To compensate the charge of V_{Fe}'' (i.e., for electrical neutrality), we need to replace $3Fe^{2+}$ ions by $2Fe^{3+}$ ions. This is the important point: the Fe ions change their valence from 2 to 3. This point defect reaction happens automatically. You can imagine it occurring by dissolving $Fe_2O_3(s)$ in $FeO(s)$.



To exhibit nonstoichiometry, the cation must be able to exist in two different valence states (so this is not the same as nonequimolarity that we saw for spinel). The ions Fe, Co, and, to a lesser extent, Ni can do this; Mg cannot. An alternative way of writing this point defect reaction is to bring oxygen from the gas state into FeO .

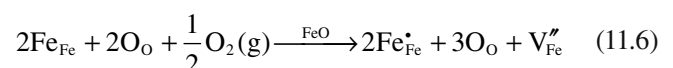


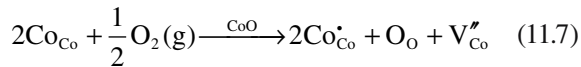
TABLE 11.7 Composition and Structure of Wüstite

Composition	Atom % Fe	Edge of unit cell (nm)	Density (g/cm ³)
Fe _{0.91} O	47.68	0.4290	5.613
Fe _{0.92} O	47.85	0.4293	5.624
Fe _{0.93} O	48.23	0.4301	5.658
Fe _{0.945} O	48.65	0.4310	5.728

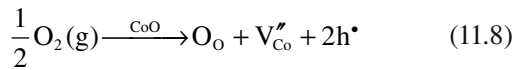
What we are doing is oxidizing an oxide. Oxides in which the cation can change its valence state, in general, show a variation of composition with oxygen partial pressure. This dependence can even cause a change in the dimensions of the crystal lattice as shown in Table 11.7.

Solid-Solution Example 2: Co_{1-x}O

The nonstoichiometry of CoO is similar to that of wüstite but not so pronounced.



We can write this in an alternate form.



We can apply equilibrium thermodynamics to Eq. 11.8 and write the equilibrium constant, *K*, for the reaction

$$K = \frac{[\text{O}_\text{O}][\text{V}_{\text{Co}}''][\text{h}^\bullet]^2}{(p\text{O}_2)^{1/2}} \quad (11.9)$$

The concentration of anions on anion sites, [O_O], is essentially unity. For each vacancy on the Co sublattice, there are two electron holes; i.e., the concentration of vacancies on cation sites is twice the concentration of holes.

$$2[\text{V}_{\text{Co}}''] = [\text{h}^\bullet] \quad (11.10)$$

$$K = \frac{[\text{V}_{\text{Co}}'']4[\text{V}_{\text{Co}}'']^2}{(p\text{O}_2)^{1/2}} \quad (11.11)$$

Thus, there is a direct relationship between the oxygen partial pressure, *p*O₂, and the extent of the nonstoichiometry.

$$(p\text{O}_2)^{1/6} \propto [\text{V}_{\text{Co}}''] \quad (11.12)$$

We can confirm this relationship by measuring the concentration of cation

vacancies as a function of *p*O₂. Brouwer diagrams (also known as Kröger–Vink diagrams) are used to represent defect concentrations as a function of *p*O₂. The complete diagram for an oxide of the type MO is shown in Figure 11.4. There are three distinct ranges (I to III) that correspond to different values of the oxygen partial pressure.

It is important to keep in mind that these Brouwer diagrams, while useful, can provide an indication only of what might happen; the equilibrium constants needed for accurate calculations are not widely available. Similar diagrams can be drawn for nonoxide systems.

Solid-Solution Example 3: Zn_{1+x}O

The point defect chemistry of ZnO is different partly because there are two charge states of Zn, namely 2+ (as in ZnO) and 1+. When we heat ZnO in Zn vapor, we form a Zn-rich oxide, Zn_{1+x}O. Experimentally it is found that the excess Zn sits on interstitial sites (as you would expect from the crystal structure). We can write the basic defect equation for the singly charged interstitial as



We then write the equilibrium constant for the reaction in the usual way

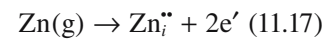
$$K = \frac{[\text{Zn}_i^\bullet][e']}{(P_{\text{Zn}})} \quad (11.14)$$

From the reaction equation we know that there is one electron for every Zn interstitial.

$$[\text{Zn}_i^\bullet] = [e'] \quad (11.15)$$

$$(P_{\text{Zn}})^{1/2} \propto [\text{Zn}_i^\bullet] \quad (11.16)$$

The excess zinc could be incorporated as a divalent interstitial, which means that there is a second reaction possibility:



$$(P_{\text{Zn}})^{1/3} \propto [\text{Zn}_i''] \quad (11.18)$$

Experimentally, we can measure the electrical conductivity as a function of the partial pressure of Zn, plot the results, and then look at the exponent. We find that $(P_{\text{Zn}})^{1/2} \propto [\text{Zn}_i^\bullet]$, which indicates that the Zn interstitial has a charge of +1. When you heat ZnO to high temperatures and control the oxygen partial

POINT DEFECTS AND VARIATION IN *p*O₂

Range I—Low *p*O₂

- The number of O vacancies increases.
- The oxide is reduced.
- $n = 2V_{\text{O}}''$

Range II—Intermediate *p*O₂

- Schottky defects dominate.

Range III—High *p*O₂

- Increase in cation vacancies.
- The oxide is oxidized.

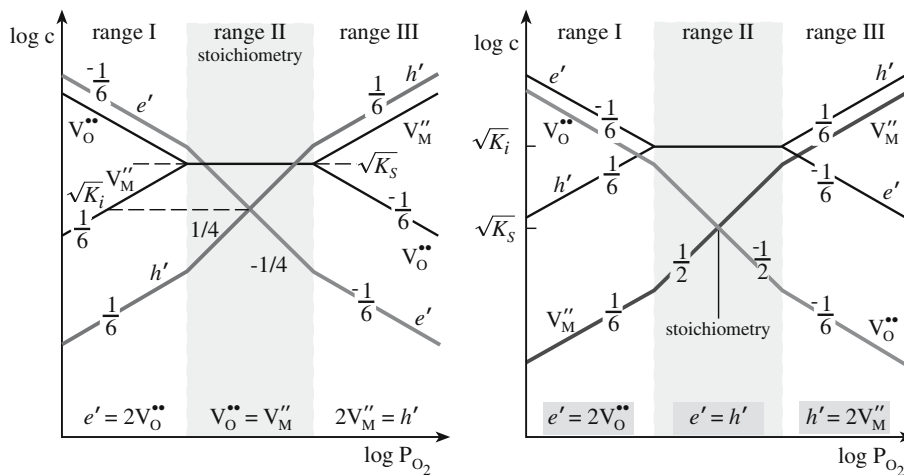


FIGURE 11.4 Examples of Brouwer diagrams in an oxide MO.

pressure the composition of the oxide will change. The equilibrium condition depends on pZn or pO_2 .

ZnO is a particularly important ceramic semiconductor: its conductivity decreases with increasing pO_2 . A major application for ZnO that makes use of its electrical properties is the varistor (*variable resistor*).

Solid-Solution Example 4: ZrO₂ Doped with CaO

Doping ZrO₂ with Ca is a special example of a ZrO₂ solid solution. We can incorporate ~15% CaO in the structure to form Ca-stabilized cubic zirconia (CSZ). (CZ is the general abbreviation for cubic zirconia.) The special feature here is that the cubic (fluorite structure) phase is not stable at room temperature unless the ZrO₂ is heavily doped. However, we write the point defect equations as if it were always stable. The Ca²⁺ cation substitutes for the Zr⁴⁺ cation as shown in Figure 11.5. Since the charges are different, we must compensate with other point defects.

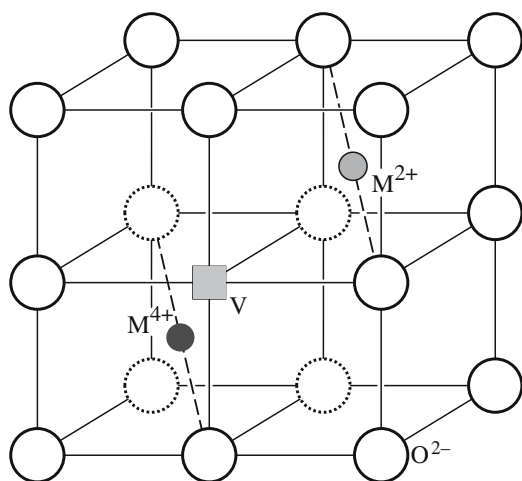
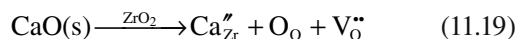


FIGURE 11.5 Accommodation of Ca²⁺ in ZrO₂. Note: this is just half of the unit cell.



The cubic structure can also be stabilized using MgO (with essentially the same equation) or with Y₂O₃ (to form YSZ) when the equation is a little different. Later we will see other rare earths partly substituting for Y to give CZ a wide range of colors. The large number of oxygen vacancies makes CZ a material of choice for solid-oxide fuel cells. The material is an electrical insulator but an ionic conductor: oxygen moves quite rapidly through CZ.

11.8 ASSOCIATION OF POINT DEFECTS

This phenomenon often occurs when defect concentrations reach more than about 1 mol%. Then the defects are very close together and defect interactions may result in lowering the overall energy for defect formation and in defect clustering. Clustering is especially important in nonstoichiometric oxides such as Fe_{1-x}O and UO_{2+x}.

This idea is special for ceramics because the effect is greatly enhanced due to the fact that the point defects are charged. In particular, since vacancies behave as if they are charged point defects, cation and anion vacancies can be strongly attracted to one another to form a defect complex denoted in the following equation by the parentheses.



We can write a law of mass action equation relating the fractional molar concentration of the vacancy pairs. At equilibrium

$$\frac{[(\text{V}'_{\text{Na}}, \text{V}'_{\text{Cl}})]}{[\text{V}'_{\text{Na}}][\text{V}'_{\text{Cl}}]} = K \quad (11.21)$$

We can then relate the equilibrium concentration of the vacancy pair to their free energy of formation, ΔG_{vp} , using

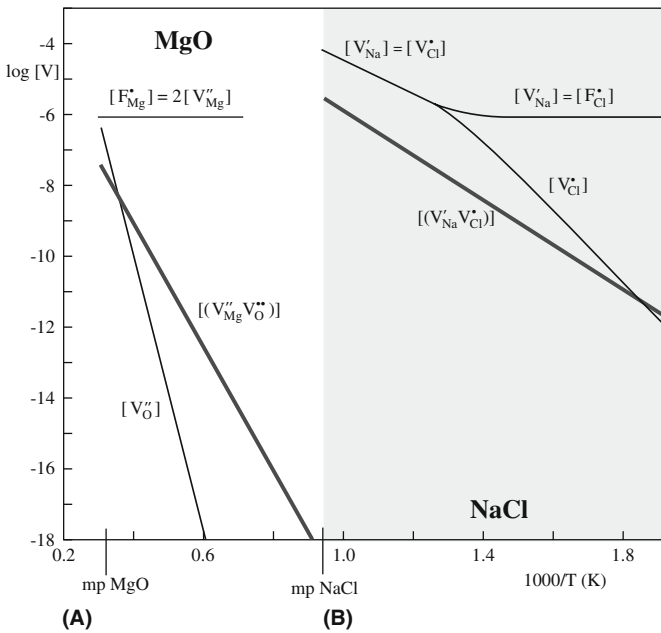


FIGURE 11.6 Plots of the vacancy concentrations varying with T^{-1} : (a) MgO; (b) NaCl.

$$\Delta G = -RT \ln K \quad (11.22)$$

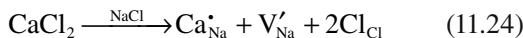
Hence

$$\frac{[(V'_{Na}, V\dot{C}l)]}{[V'_{Na}][V\dot{C}l]} = Z \exp\left(\frac{-\Delta G_{vp}}{kT}\right) \quad (11.23)$$

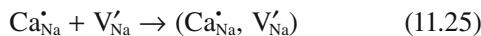
In Eq. 11.23, Z is the number of distinct orientations of the defect complex; it accounts for the configurational entropy. For example, if the vacancies sit on adjacent sites in NaCl, Z would be 12. Figure 11.6 shows calculated concentrations of Schottky defects and vacancy pairs in NaCl and MgO.

Association of Point Defects due to Doping

Dissolving CaCl_2 in NaCl increases the number of vacancies on the Na sublattice.



If the Ca^{2+} cations form a defect complex with such a vacancy (not now on adjacent sites), we can express this combination as

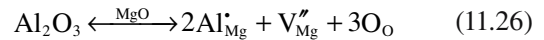


A Second Example of Doping

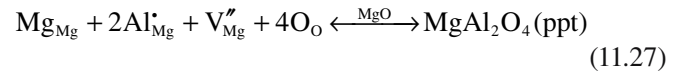
Consider what happens when we dissolve a small amount of Al_2O_3 in MgO.

COLOR OF F CENTERS

The crystal and color:
 NaCl—orange-brown/blue
 KCl—violet/green
 KBr—blue green/orange



The Al^{3+} sits on Mg sites requiring that vacancies be created on the Mg sublattice. Notice that the reaction can lead to precipitation of spinel, but then we are creating a new structure and, thus, new sites.



This equation emphasizes that four sites are required on each sublattice. We can write the law of mass action equation for the precipitation reaction

$$[\text{Mg}_{\text{Mg}}][\text{Al}'_{\text{Mg}}]^2 \propto \exp\left(+\frac{\Delta H_{\text{ppt}}}{kT}\right) \quad (11.28)$$

ΔH_{ppt} is the enthalpy of formation.

$$[\text{Al}'_{\text{Mg}}] \propto 2[V''_{\text{Mg}}] \quad (11.29)$$

$$[V''_{\text{Mg}}] \propto \left(\frac{1}{4}\right)^{1/3} \exp\left(+\frac{\Delta H_{\text{ppt}}}{3kT}\right) \quad (11.30)$$

In summary, we ask again what is special for ceramics—why don't we do this for metals? The special feature is the formation of defect associates as a result of the strong attraction between oppositely charged point defects. Of course, defect associates and precipitates are related, and both are clearly volume defects.

11.9 COLOR CENTERS

The term color center is now applied to any defect, including an impurity, that produces color in an insulator. The original observation was made in Germany using X-rays to color alkali halides by producing F centers ("F" is for Farben: German for color). The color is the complement of what is absorbed by the color center. Colors are produced in most of the alkali halides following irradiation with ionizing radiation and are characteristic of the crystal not the radiation source used. These F centers are due to an electron or hole trapped at an anion vacancy site. Other types of color center can give other colors.

Several different types of color center have been identified and some of the common ones are illustrated in Figure 11.7 for the alkali halides. V centers are is cation vacancies with trapped holes. Color centers can also form in oxides such as MgO. When a single electron is trapped at an anion vacancy in MgO, the defect is positively charged and is

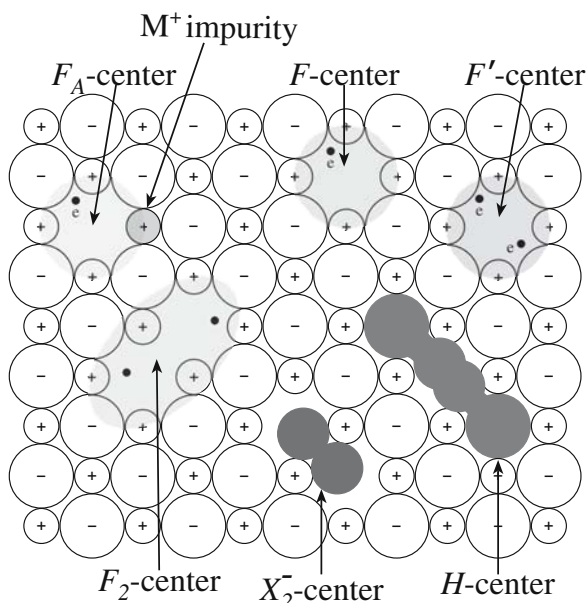


FIGURE 11.7 Schematics of color centers in alkali halides.

referred to as the F^+ center. An F center in MgO is a vacancy with two electrons.

Smoky quartz and amethyst are two natural examples of color centers. In smoky quartz a small amount of Al impurity atoms can substitute for Si . Because of the different valence of the two cations, electron neutrality is maintained by hydrogen ions. Ionizing radiation releases an electron from the $[AlO_4]^{5-}$ group, which is then trapped by the hydrogen ion:



The color center is the $[AlO_4]^{4-}$ group, which is electron deficient, and we can think of it as having a trapped hole. In amethyst the color center is $[FeO_4]^{4-}$, which is due to Fe^{3+} impurities substituting for Si .

We will discuss more examples of how impurities give rise to color in Chapter 32, but it is interesting to note that $NaCl$ crystals, doped to modify the color and increase the density of point defects, can be used for the $NaCl$ color-center laser.

11.10 CREATION OF POINT DEFECTS IN CERAMICS

There are several ways that we can create point defects in ceramics. We have seen already that point defects can be produced in nonstoichiometric oxides, such as ZnO ,

by heating in either high or low pO_2 . In Nd -doped yttrium aluminum garnet (YAG)—the most widely used solid-state laser crystal—the Nd is incorporated into the YAG structure (it substitutes for Y^{3+} in small amounts) when Nd_2O_3 is added to the YAG melt. A single crystal, which contains the Nd ions in solid solution, is pulled from the melt using the Czochralski method (see Chapter 29).

If a crystal is annealed at a sufficiently high temperature and for long enough, then the equilibrium concentration of vacancies will increase. Abrupt quenching of the material can “freeze in” unusually high concentrations of point defects.

Vacancies, usually Schottky defects or Frenkel pairs, can be produced as a result of ion bombardment in a process known as ion implantation. For example, many defects are formed in single crystal MgO when it is bombarded with high-energy Xe^+ ions. Figure 11.8 is a TEM image of MgO following implantation with $10^{14} Xe^+ cm^{-2}$ ions at 200 keV in a particle accelerator. The dark regions are typical of numerous point defect clusters. A large amount of work on ion implantation was performed to simulate what happens to materials inside a nuclear reactor

when they are bombarded with fast neutrons (energies $> 0.1 MeV$). Now the topic is again important as ceramics are used to contain radioactive waste and we start to plan for fusion (rather than fission) reactors. Ion implantation is also the technique that is

IONIZING RADIATION CAUSING POINT DEFECTS	
Ultraviolet light	$E \sim 10 eV$
X-rays	$E = 10-100 keV$
γ -rays	$E = 1.25 MeV$
High- E electrons	$E = 100 keV-0 MeV$
High- E protons	$E = 2.20 MeV$
Fast neutrons	$E > 0.2 keV$

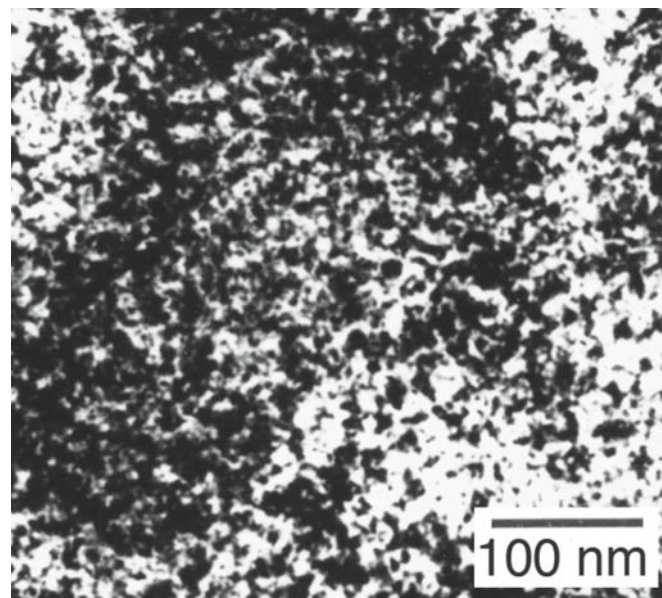


FIGURE 11.8 TEM image of defect clusters formed by ion implantation into MgO .

used to introduce dopant atoms to defined depths during the formation of semiconductor devices or to harden the surface of metals and ceramics.

Any form of ionizing radiation can be used to produce point defects in materials. The term ionizing radiation is used to describe radiation sources that generate electron or holes when interacting with matter.

THE DRIVING FORCE
If there is no bias (gradient in the chemical potential), then there is no driving force.

11.11 EXPERIMENTAL STUDIES OF POINT DEFECTS

It is very difficult to see individual point defects in a material. It is not that they are too small [transmission electron microscopy (TEM) has the resolution], but they have to be surrounded by atoms so we tend to see the surrounding atoms instead! Because point defects (especially substitutional atoms) are so important in determining the electrical properties of semiconductors, a great deal of work has been done to understand these defects. Figure 11.9 is a high-resolution scanning transmission electron microscopy (STEM) image showing columns of silicon atoms in a sample of Sb-doped Si. The brightest columns contain one Sb atom.

In Table 11.7 we showed how the lattice parameter of iron oxide changes as a function of the oxygen-to-iron ratio. The lattice parameter can be determined to a high precision using X-ray diffraction and the precise lattice-parameter method. It can then be correlated with the oxygen/iron ratio determined by chemical analysis.

We can also correlate point defect concentrations with a property measurement such as electrical conductivity, σ , or density, ρ . The density will show whether the dopant enters interstitially or is a replacement for the host ion.

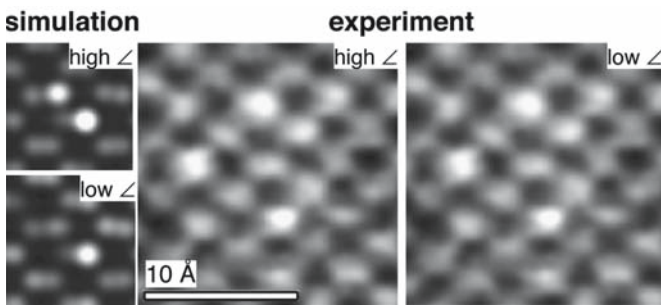


FIGURE 11.9 Atoms of Sb in Si; the Z-contrast image does not show where the atom sits in the column.

- An interstitial atom increases density.
- If a substitutional atom replaces a heavier atom the density may be reduced.

11.12 DIFFUSION

Diffusion occurs by atomic defects moving through the crystal; it is not a continuum process. We thus analyze diffusion as a statistical process. This is the kinetics part of the story. Diffusion of point defects is the key to understanding their properties. There are four basic mechanisms that can, in principle, occur; these are illustrated in Figure 11.10.

Diffusion is a thermally activated process so we plot the free energy versus distance. The region of high energy in this plot corresponds to an “activated complex.” It occurs because there is an activation energy barrier to diffusion. We can use reaction rate theory to understand diffusion behavior. First we consider two features of the process.

- Direct exchange (difficult and not energetically probable)
- Ring mechanism (cooperative motion: possible but not demonstrated)
- Vacancy mechanism (most common, dominant in metals)
- Movement of interstitials (occurs when you can put interstitials in); an example is Zn in ZnO.

NOTATION FOR DIFFUSION ACTIVATION	
AB^*	The activated complex
K^*	K for the activated complex
ν	The Debye atomic jump frequency, 10^{13} Hz
χ	The potential gradient per atom
N	Avogadro’s number

- Each step in a difficult process is relatively simple; if it appears more difficult, we break it into smaller steps.

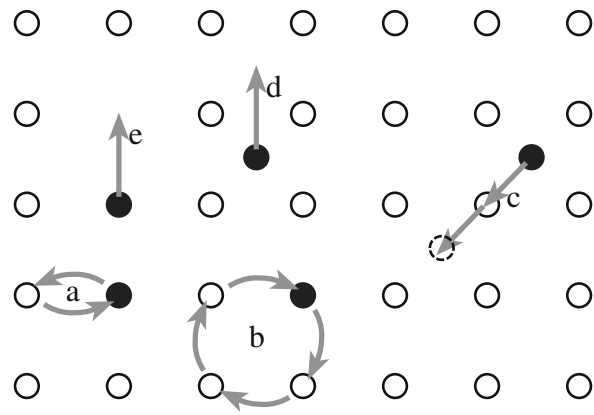


FIGURE 11.10 Possible mechanisms occurring during diffusion. (a) Exchange, (b) ring, (c) vacancy, (d) interstitial, (e) knock-on.

- The reaction path of each step, such as an individual atom jump, involves an activated complex, which gives an energy maximum.

For the chemical reaction (the route of transition of the activated complex, AB^* , into the product)



The concentrations are related by the equilibrium constant K^* .

$$\frac{[AB^*]}{[A][B]} = K^* \text{ and } \Delta G^* = -RT \ln K^* \quad (11.33)$$

The reaction rate, k , is $v[AB^*]$, which can be written as $vK^*[A][B]$. So the reaction rate for unit concentration is just vK^* . If there is no net flow to the right or left, because each time a point defect jumps to the right one also jumps to the left, we need to add a driving force, i.e., a potential gradient, to produce a flux. Now the flux of atoms is the rate in the forward direction minus the rate in the backward direction. ΔG forward is $\Delta G^* - \frac{1}{2}\chi\lambda$ for unit concentration forward. The analysis makes two assumptions:

1. The activity coefficient is unity.
2. D does not vary with the composition.

The diffusion coefficient does have a strong dependence on temperature.

$$D = D_0 \exp\left(\frac{-Q}{RT}\right) \quad (11.34)$$

The diffusion equations are summarized by Fick's laws. One assumption that is explicit in the derivation of these equations is that there is a well-defined value of D . We will see later that because of the high concentrations of defects in ceramic materials, there will be many important situations in which this assumption is not valid; i.e., D often does depend on the composition.

11.13 DIFFUSION IN IMPURE, OR DOPED, CERAMICS

Now you can compare diffusion in stoichiometric oxides with diffusion in nonstoichiometric oxides. The first question concerns the diffusing species when two species are present. For many ceramics ΔE_s is large. For MgO , Al_2O_3 , and B_2O_3 , ΔH_s is $\sim 600 \text{ kJ/mol}$ ($\sim 6 \text{ eV/formula unit}$). Thus

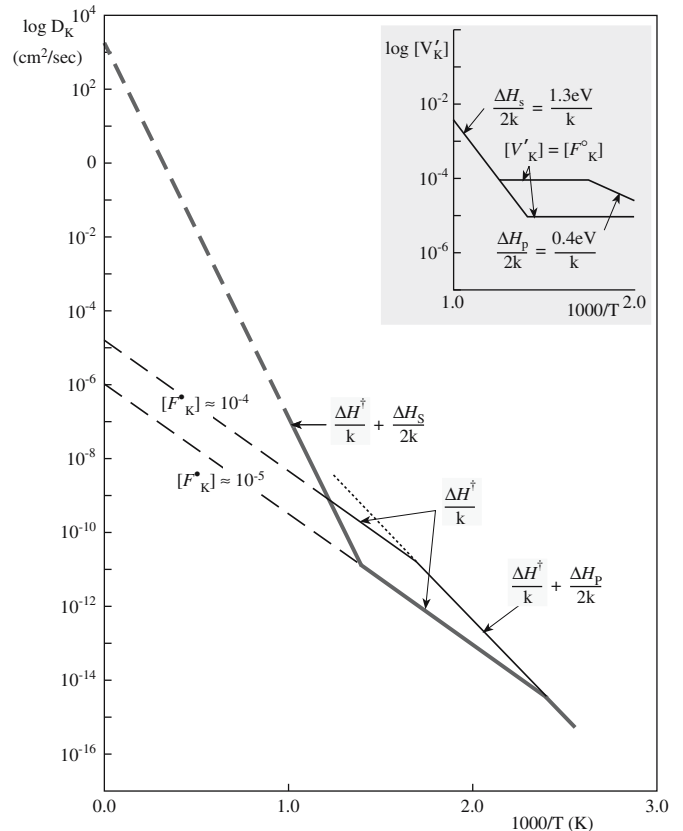


FIGURE 11.11 Diffusion coefficients in the intrinsic and extrinsic ranges. KCl with 10^{-4} and 10^{-5} atomic fraction divalent cation impurities.

the intrinsic concentration of vacancies, $[V]$, is $\sim 10^{-4}$ at 2000°C . As we lower the temperature, T , the equilibrium concentration of vacancies, $[V]$, decreases too.

Figure 11.11 shows a plot of intrinsic and extrinsic diffusion coefficients. The first part of this plot is almost never observed: most ceramics are never this pure (the exceptions are the semiconductors, Si and Ge, and a few others).

This means that an impurity concentration of between 1 part in 10^5 (10 ppm) and 1 part in 10^6 (1 ppm) is sufficient to dominate the vacancy concentration. There is always an attraction between oppositely charged point defects so that they will associate with one another, which will in turn affect their effective concentrations. (Consider how far apart point defects can be if the concentration is 1 in 10^6 — $\sim 20 \text{ nm}$, maximum.)

We will now consider examples that illustrate special features of diffusion in ceramics.

CaCl_2 in KCl shows the effect of changing the charge on the cation.

FICK'S LAWS

Fick's first law	$J = -D \left(\frac{\partial c}{\partial x} \right)$
Fick's second law	$\frac{\partial c}{\partial t} = D \frac{\partial^2 c}{\partial x^2}$

ZrO₂ doped with CaO is special because the structure of CSZ requires the Ca to be present and CZ is a fast conductor of oxygen.

Zn_{1+x}O is special because interstitials dominate and can have different charges.

FeO_{1-x} and CoO_{1-x} are special because neither oxide is ever stoichiometric because the cation is always present in two charge states.

CuO_{1-x} is special because it is oxygen deficient but behaves differently from Zn_{1+x}O; it shows the importance of crystal structure.

In each case, we clearly have to understand the defects before we can understand their behavior.

Diffusion Example 1: CaCl₂ in KCl

When we dope KCl with CaCl₂ diffusion of K⁺ cations occurs by an interchange between K⁺ cations and cation vacancies. The concentration of cation vacancies is given by

$$[V'_k] = \exp\left(\frac{\Delta G_s}{2kT}\right) \quad (11.35)$$

ΔG_s is the Schottky formation energy. The diffusion coefficient can then be written as

$$D'_k = [V'_k] \gamma \lambda^2 \nu \exp\left(-\frac{\Delta G}{kT}\right) \quad (11.36)$$

Here, γ is an orientation factor. The Gibbs free energy can then be rewritten as usual:

$$\Delta G = \Delta H - T\Delta S$$

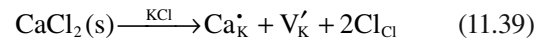
So the diffusion coefficient is

$$D'_k = \gamma \lambda^2 \nu \exp\left(\frac{(\Delta S_s/2) + \Delta S^*}{k}\right) \exp\left(\frac{(-\Delta H_s/2) - \Delta H^*}{kT}\right) \quad (11.37)$$

In this equation, $-\Delta H^*$ is the enthalpy of motion of an atom while ΔH_s is the enthalpy of formation of a Schottky defect. The constants are all well known: λ is ~ 0.2 nm, γ is ~ 0.1 , and the Debye frequency, ν , is 10^{13} s⁻¹. $\Delta S_s/2k$ and $\Delta S^*/2k$ are small positive numbers. Hence we can estimate that

$$\gamma \lambda^2 \nu \exp\left(\frac{(\Delta S_s/2) + \Delta S^*}{k}\right) \cong 10^2 \quad \text{or} \quad 10^3 \quad (11.38)$$

Why is diffusion controlled by a small amount of impurity in KCl? We can write an equation describing what happens when we dissolve CaCl₂ in KCl.



Once CaCl₂ is dissolved and you change T , nothing much will change because you have fixed the concentration of vacancies.

$$[V'_k] = [\text{Ca}_k^{\bullet}] = \text{fixed} \quad (11.40)$$

At high T we have a high intrinsic vacancy concentration; at low T we have a low intrinsic vacancy concentration. At low T the diffusion coefficient is controlled by the starred (dopant) quantities.

$$D'_k = \gamma \lambda^2 \nu [\text{Ca}_k^{\bullet}] \exp\left(\frac{\Delta S^*}{k}\right) \exp\left(\frac{-\Delta H^*}{kT}\right) \quad (11.41)$$

The slope is determined only by $\Delta H/kT$. If we increase $[\text{Ca}]$ to 10^{-4} , the curve will move up.

In general, even at high T , $[V'_k]$ due to thermal equilibrium is less than $[V'_k]$ due to $[\text{Ca}_k^{\bullet}]$. This is the case for most ceramics.

- Intrinsic diffusion is controlled by defects that are present at thermal equilibrium.
- Extrinsic diffusion is controlled by dopants (impurities) that are present.

The intrinsic part is not usually observed because an impurity concentration of between 1 in 10^5 and 1 in 10^6 is sufficient to control the vacancy concentration. There is another complication we should consider: as we saw in Section 11.8, there is attraction between $[\text{Ca}_k^{\bullet}]$ and $[V'_k]$ that results in defect complexes. The concentration of these complexes depends on the strength of this attraction; formation of these complexes will probably reduce the mobility of the point defects and thus decrease diffusion rates.

Diffusion Example 2: ZrO₂ Doped with CaO

We noted above that if ZrO₂ is doped with 15 at% CaO we can stabilize the cubic phase. The resulting material can be described as Zr_{0.85}Ca_{0.15}O_{1.85}. Experimentally we find that D_o decreases as the concentration of oxygen vacancies increases. Hence we know that oxygen diffuses by a vacancy mechanism.

In UO₂, which has the same fluorite structure, oxygen diffuses by an interstitial mechanism. (Look back to the discussion of the structure of fluorite to see why this might be so.) D_o increases as the concentration of oxygen vacancies increases. In such an interstitial mechanism, the interstitial moves onto a regular site and *bumps* the ion occupying that site onto an interstitial site. If you study diffusion using tracer atoms, the tracer atom has now temporarily stopped moving, but the interstitial ion may repeat the process and move on through the crystal. The

process is thus rather complicated. A typical activation energy for this process might be ~120 kJ/mol.

Notice that the crystals in these two examples both have the fluorite structure, but the diffusion mechanism that operates is very different because the point defects involved are different. Experimental data for diffusion in several oxides are plotted in Figure 11.12.

Diffusion Example 3: Zn_{1+x}O

In our discussion of point defects in nonstoichiometric ZnO, we noted that excess zinc is present as interstitials; the oxide is metal rich.

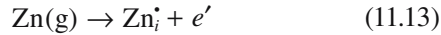


Figure 11.13 shows a plot for D_{Zn} : the steeper the slope, the larger the activation energy. Varying the partial pressure of Zn, P_{Zn} , has a large effect on D_{Zn} in ZnO because, as we saw above, P_{Zn} is proportional to the interstitial concentration. Thus, as P_{Zn} increases, the density of interstitials increases and the diffusion of Zn through the structure increases. This result again emphasizes the difference between a metal and its oxide: in metallic Zn, we do not

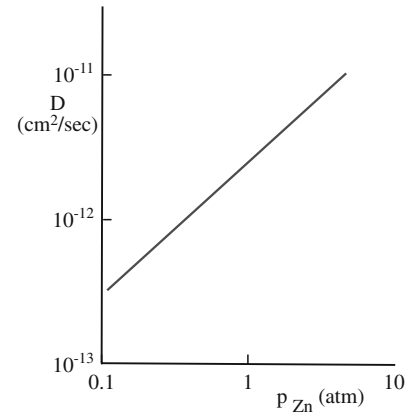
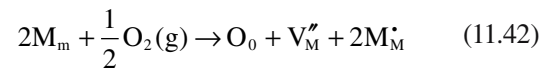


FIGURE 11.13 Plot for D_{Zn} as it varies with T^{-1} .

care about the partial pressure of the Zn; the Zn atoms diffuse by a vacancy mechanism, but the concentration of vacancies does not depend on P_{Zn} .

Diffusion Example 4: FeO_{1-x} and CoO_{1-x}

As we noted above, the group of binary oxides, FeO, NiO, CoO, and MnO (all have rocksalt structure), is metal deficient. The most important of these is Fe_{1-x}O. FeO does not exist (i.e., it is not stable) and can contain as many as 15 at% vacancies due to the equilibrium concentration of Fe³⁺ cations; we saw earlier that this equilibrium occurs by the cation changing its valence: Fe²⁺ changes to Fe³⁺. We can write an equation to dissolve excess oxygen in Fe_{1-x}O. We can generalize the equation we wrote for FeO and CoO as



Here M is the metal and M_M^{\bullet} represents an Fe³⁺ cation sitting on an Fe²⁺ site. The rest of the analysis follows from our discussion of CoO. The important point is that diffusion depends on pO_2 as illustrated for several oxides in Figure 11.14. There is an energy associated with the reaction and an energy associated with the motion of defects, but point defects are always present in FeO.

Good experimental observations are available for CoO. We can show that the diffusion coefficient for Co can be expressed as

$$D_{\text{Co}} = \gamma \lambda^2 \left(\frac{1}{4} \right)^{1/3} pO_2^{1/6} \exp \left(\frac{\Delta S_0}{3k} \right) \exp \left(\frac{\Delta S^*}{k} \right) \exp \left(- \frac{\Delta H_0^*}{3kT} - \frac{\Delta H^*}{kT} \right) \quad (11.43)$$

Experimentally, we find that D_{Co} is proportional to $pO_2^{1/n}$ with the value of n depending on T .

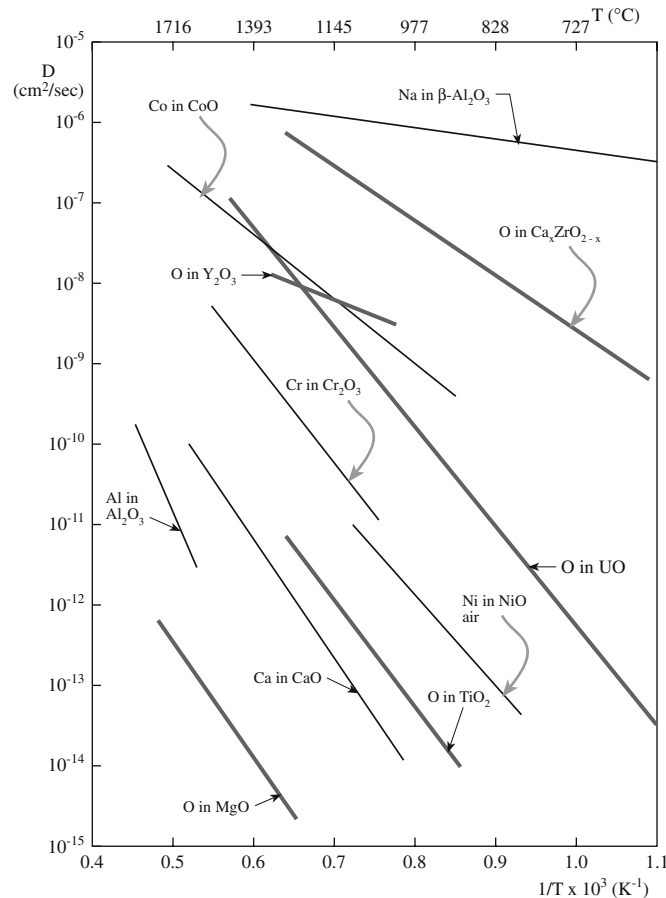


FIGURE 11.12 Arrhenius plots for different oxides: diffusion coefficients varying with T^{-1} .

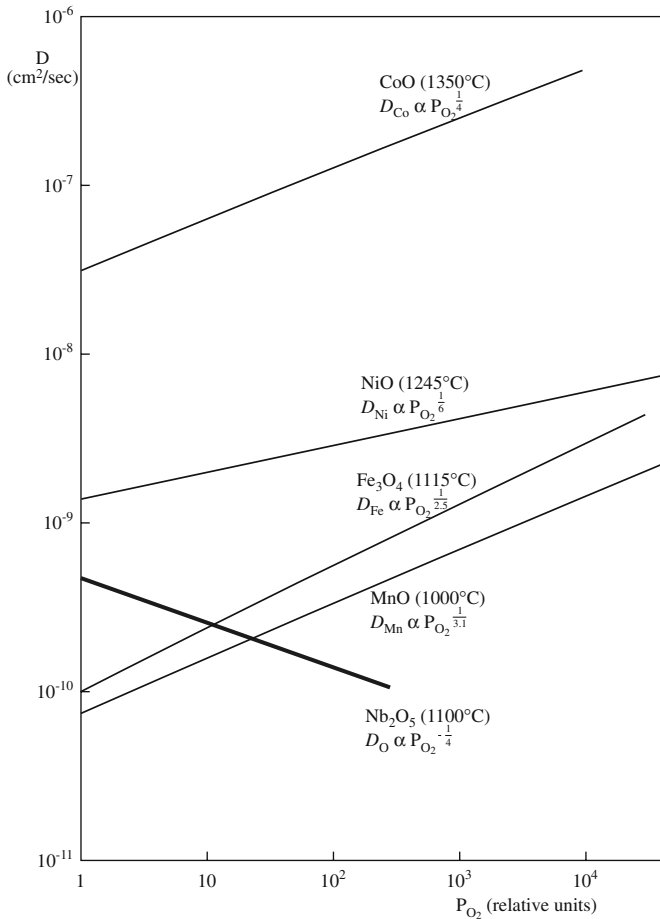


FIGURE 11.14 Diffusion coefficients varying with pO_2 .

- $n = 3.1$ at 1000°C
- $n = 3.3$ at 1200°C
- $n = 3.6$ at 1350°C

We expected D_{Co} to be proportional to $pO_2^{1/6}$. This means that as we increase pO_2 , the value of D_{Co} increases faster with vacancy concentration than we had predicted. The reason is that the defects are charged and that there is an association of defects (see the discussion of KCl above). We must consider two possibilities. A single cation vacancy might form a complex with one hole or with two holes. In the first case we write

$$\frac{1}{2}O_2^* = [h^*] + [(V_{Co}''h^*)] + O_0 \quad (11.44)$$

$$\frac{[h^*][V_{Co}''h^*]}{pO_2^{1/2}} = K_1 \quad (11.45)$$

$$[h^*] = [(V_{Co}''h^*)] \quad (11.46)$$

so that $[(V_{Co}''h^*)]$ is proportional to $pO_2^{1/4}$ and n is 4.

If two holes are involved in the complex, then

$$[(h^*V_{Co}''h^*)] \propto pO_2^{1/2} \quad (11.47)$$

Now, $D_{Co} \propto pO_2^{1/2}$ and n is 2. Experimentally we find n is ~ 3 so we can thus conclude that the vacancy must be associated with between one and two electron holes. It is not obvious that we actually make another assumption in this treatment. We perform a diffusion experiment, measure D_{Co} , and then assume that a vacancy in a complex moves at the same velocity as the free vacancy. So we should say that if the association of a vacancy and holes does not affect the movement of vacancies, then each vacancy must have between one and two electron holes associated with it.

Finally, we comment on the mobility (B_V) of the vacancy; B_V is proportional to Γ_V , the jump frequency. Similarly, for holes B_h is proportional to Γ_h . In CoO all the electrical current is carried by the electron holes (i.e., it is a p -type semiconductor) so that the mobility of holes is much greater than the mobility of the vacancies. In CoO we can say that

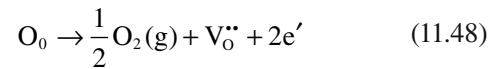
$$B_h \gg B_V$$

$$\Gamma_h \gg \Gamma_V$$

So when a vacancy jumps, holes follow. Thus a hole/vacancy pair will move at a rate determined by the jump frequency of the vacancy, the slower moving defect.

Diffusion Example 5: CuO_{1-x}

CuO is an example of a group of oxygen-deficient oxides, MO_{1-x} , where the nonstoichiometry is accommodated by oxygen vacancies. We write the equilibrium equation in the usual way.



We can determine the equilibrium constant and relate this to the Gibbs free energy ΔG .

$$[V_O''] \cong \left(\frac{1}{4}\right)^{1/3} (pO_2)^{-1/6} \exp\left(-\frac{\Delta G_O}{3kT}\right) \quad (11.49)$$

$$D_O = \gamma \lambda^2 \nu [V_O''] \exp\left(-\frac{\Delta G^*}{kT}\right) \quad (11.50)$$

$$D_O = \gamma \lambda^2 \nu \left(\frac{1}{4}\right)^{1/3} (pO_2)^{-1/6} \exp\left(-\frac{\Delta G_O}{3kT}\right) \exp\left(-\frac{\Delta G^*}{kT}\right) \quad (11.51)$$

If you increase the pO_2 , then the diffusion coefficient will decrease. This is found for a very wide temperature range and implies that diffusion is a complex process. It is interesting to compare this case to that of ZnO . Both cations exist in the 2+ or 1+ charge state, but the crystal structures and point defect chemistry are very different.

11.14 MOVEMENT OF DEFECTS

We often think that only cations move in ionic materials because so much work has been carried out on oxides or halides where the anion is much larger than the cation, for example, MgO, Al₂O₃, and NaCl. Ceramics that are being used for electronic applications often contain heavier (hence larger) cations so that the assumption is not necessarily valid. In solid-oxide fuel cells, it is the oxygen ion that diffuses.

Most perfect ceramic crystals have more unoccupied volume than there is in metals, so they tend to be less dense. There is thus more open volume through which point defects can move.

Covalent bonds are directional in character and must be “broken” as defects move. We will see that dislocations in Si do not move easily at room temperature so the material does not easily deform plastically and is brittle at this temperature. This simple fact has many consequences for the electronics industry. Where would silicon technology be if dislocations moved readily under an applied stress? The same consideration applies to point defects except that interstitials in Si do not need to break bonds!

The charge can affect the concentration of point defects. FeO contains at least 5% vacancies on the cation sublattice so the formula should be written as Fe_{1-δ}O [or better Fe(II)_{1-2δ}Fe(III)_δO]. The superconductor YBCO must be off stoichiometric to optimize its superconducting properties (YBa₂Cu₃O_{7-δ} or YBa₂Cu₃O_{6+x}).

The movement of grain boundaries is very important in ceramics because of the method of processing and their high-temperature applications. However, the properties of grain boundaries are very different from the bulk material and they may contain a second phase. Grain boundaries in ceramics are not as dense as in metals because the bonding is different (remember the open space in Si and Al₂O₃) so diffusion of point defects along, and across,

these interfaces is much faster than in the bulk. There may also be an excess charge of one sign at the grain boundary plane, which must be compensated in the bulk (the space-charge region) and will again affect the diffusion of charged point defects.

11.15 DIFFUSION AND IONIC CONDUCTIVITY

Some ceramics are important because they are ionic conductors. The band gap energy, E_g , of these materials is large (typically > 5 eV) and the only mechanism for conduction of charge is by the movement of ions. In some cases the rate of movement of the ions is very rapid and large conductivities are possible. In this section we will mention one application of ionic conductivity; we will consider more examples and details in Chapter 30. The ionic conductivity, σ , is

$$\sigma = \sum_i q_i N \mu_i \quad (11.52)$$

Here, q_i is the effective ionic charge, μ_i is the mobility, and N is the number of mobile defects.

Mobile defects contributing to ionic conductivity include Schottky defects. Figure 11.15 shows the example of Na⁺ motion in NaCl. Two different routes are shown for how the Na⁺ ion might reach the vacant site. The direct route,

although shorter, is unlikely because the two Cl⁻ ions will be very close together (“touching”) creating a large energy barrier for the migrating Na⁺ ion to overcome. Route 2 is more likely. The Na⁺ ion first passes through the face of the octahedron, then into the vacant tetrahedral site between the octahedra, then through the face of the opposite octahedron and into the vacant site. We cannot prove that this is what happens, but we expect the ion to follow the lowest energy pathway, which looks like route 2.

CORROSION

Diffusion of oxygen in oxidation scales occurs along grain boundaries. Corrosion of metals is controlled by formation and diffusion of point defects in the ceramic. Corrosion of polycrystalline ceramics also occurs most quickly along grain boundaries.

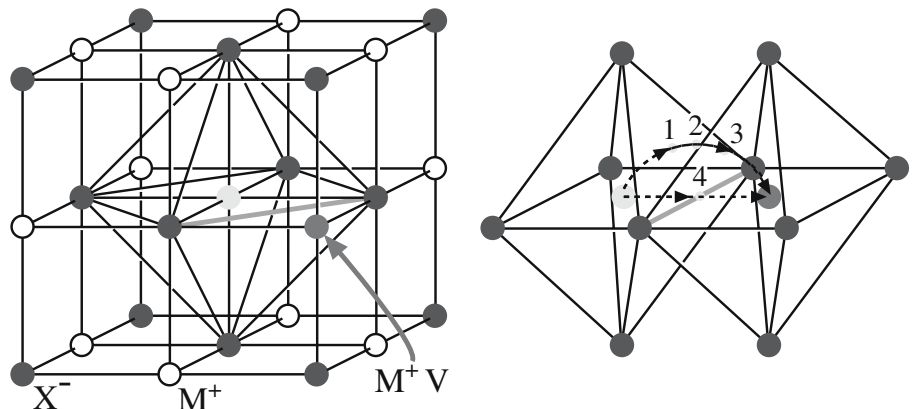


FIGURE 11.15 A probable diffusion mechanism in NaCl.

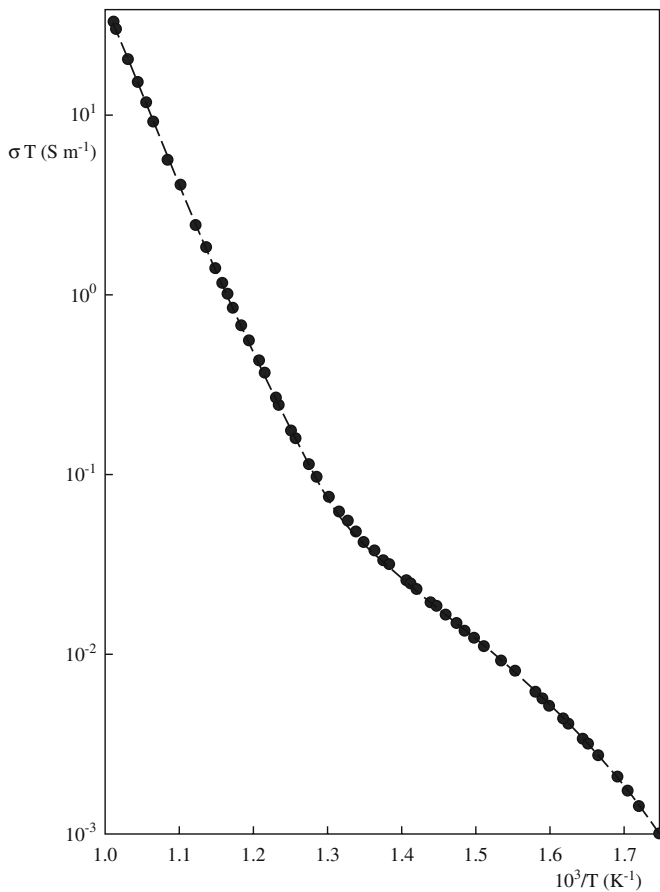


FIGURE 11.16 Ionic conductivity of NaCl varying with T^{-1} .

If ionic conductivity and diffusion occur by the same mechanism then μ and σ are related to D by the Nernst–Einstein equations

$$\mu = \left(\frac{q}{kT}\right)D \quad \sigma = \left(\frac{Nq^2}{kT}\right)D \quad (11.53)$$

In using Eq. 11.53 we have to be aware of the following points:

- Some defects may contribute to D but not to σ (paired cation and anion vacancies in the alkali halides, for example).

- Diffusion may occur along grain boundaries and dislocations (these are more rapid paths than bulk diffusion).
- Electronic contributions to σ are low (this is the case in wide band gap materials at low T).

For a simple vacancy transport mechanism both σT and D would obey Arrhenius relationships

$$\sigma T = A \exp(-Q/kT) \quad (11.54)$$

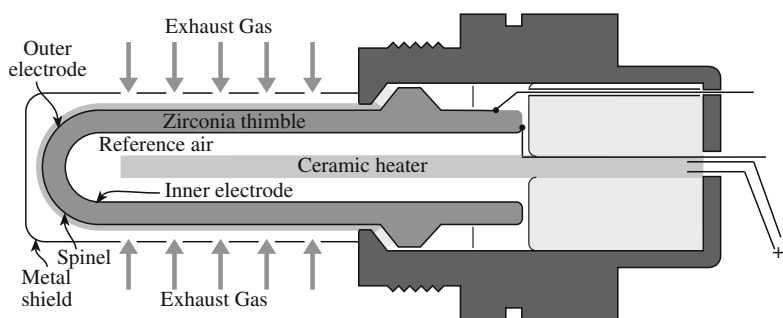
$$D = D_0 \exp(-Q/kT) \quad (11.55)$$

A and D_0 are temperature-independent constants and Q is the activation energy.

Figure 11.16 shows the variation in σT with T for a relatively pure sample of NaCl. As you can see, the relationship is complicated. The activation energy Q consists of two components, one due to the creation of the defect and one due to its motion, and these may have different temperature behaviors. For NaCl at temperatures above 550°C there is good correlation between D and σ . Below 550°C the trend is similar, i.e., there is the same change in slope, but the D values are greater than σ because of the presence of impurities. We can summarize some important characteristics of the plot.

- Stage I'—Anion disorder
- Stage I—Intrinsic conductivity; cation migration dominates
- Knee region—where the slope changes: separates the intrinsic dominated region from the impurity region
- Stage II—Extrinsic conductivity dominated by cation vacancies
- Stage III—Vacancy-impurity association

An application that makes use of ionic conductivity is the ZrO_2 oxygen sensor illustrated in Figure 11.17. These sensors are used, for example, to measure the pO_2 in automobile exhaust gases or in the gases present in the carburizing process used to harden steel components. Polycrystalline CZ (stabilized with either Ca^{2+} or Y^{3+} substituting for Zr^{4+}) is the electrolyte. At the operating temperature of the sensor ($\sim 900^\circ C$), CZ is a good oxygen ion conductor. The substitution for Zr^{4+} results in the



(B)

FIGURE 11.17 Schematic of a ZrO_2 -based oxygen sensor and an actual sensor unit.

formation of oxygen vacancies and these lead to high ion mobilities on the oxygen sublattice. Solid-oxide fuel cells use the same electrolyte or another with the same structure and work on a similar principle.

11.16 COMPUTING

Computer modeling is becoming a more widespread method of studying point defects because computers are now capable of addressing large numbers of atoms. In ceramics, although the structural aspects of point defects may be short-range, interactions tend to be long-range because of Coulombic forces. Atomistic simulation calculations usually require several steps, and the actual energy may depend on how the structure is able to relax around the defect.

- Choice of a modeling approach
- Choice of an interatomic potential describing the atoms or ions
- A starting model for the point defect or defect cluster

TABLE 11.8 Comparison of Calculated and Observed Defect Formation Energies in Ionic Crystals

<i>Compound</i>	<i>Defect</i>	<i>Calculated energy (eV)</i>	<i>Experimental energy (eV)</i>
NaCl	Schottky pair	2.32	2.30
CaF ₂	Frenkel pair	2.75	2.7
MgO	Schottky pair	7.5	5.7
ZnO	Cation Frenkel pair	2.51	—
AgCl	Cation Frenkel pair	1.4	1.45

This modeling approach is discussed in more detail later. The size of the modeled crystal must be considered and its other physical properties modeled. Modeling the potential is already much more difficult when the material is a compound rather than an elemental solid and we add charge. The choice of the starting model is important since calculations may suggest structures that are metastable but are not the lowest-energy configuration. Table 11.8 compares calculated values and experimental values of defect formation energies for which the agreement is good.

CHAPTER SUMMARY

This chapter is one of the most basic in ceramics and for the student, the easiest to learn. You need to know the different types of point defects and their names, the thermodynamic principles leading to the calculation of point defect concentrations, and how point defects make diffusion possible. The next level of complexity concerns how point defects interact with one another. We touch on much of this in the examples of real materials where we bring in the fact that the point defects are often (usually) charged. The importance of the topic is that point defects not only *affect* the properties of materials but, in many cases, *determine* and *control* the properties that interest us. An interesting question is how does this discussion change for nanoceramics—are point defects in nanoceramics important? The initial answer is that the surface (a two-dimensional defect) dominates everything when the particle is small, but one point defect in a nanoparticle can be a very high concentration!

PEOPLE IN HISTORY

Boltzmann, Ludwig (1844–1906) lived in Vienna and eventually committed suicide supposedly because his theory was ridiculed by some colleagues. He died before his theories were experimentally proven correct.

Fick, Adolf Eugen (1829–1901) is best known for his laws, which he first applied in 1855. He was actually also a physiologist and developed a technique for measuring cardiac output, but also was one of the first to experiment with contact lenses in 1887.

Frenkel, Jacov Il'ich was born 10 February 1894 in Rostov-on-Don, Russia and died 23 January 1952 in Leningrad, Russia. He worked on dislocations, twinning, and much more.

Kröger, Ferdinand Anna born Amsterdam (1915–2006) was the lead author on the paper that gave the Kröger–Vink notation. He retired as Professor from USC in ~1990.

Schottky, Walter was born July 23, 1886 in Zürich and died March 4, 1976 in Pretzfeld, Germany. He worked under Max Planck in Berlin. He discovered both the electron hole and the Schottky defect.

Wedgwood, Thomas (son of the famous potter) and Davy, Sir Humphrey, in 1802, reported in a communication to the Royal Institution in London a photographic process using AgCl to record an image.

GENERAL REFERENCES

Hayes, W. and Stoneham, A.M. (1985) *Defects and Defect Processes in Nonmetallic Solids*, John Wiley & Sons, New York. Chapter 3 (pp.106–168). Very nice but more advanced than our treatment.

- Kröger, F.A. (1964) *The Chemistry of Imperfect Crystals*, North-Holland, Amsterdam.
- Kröger, F.A. and Vink, H.J. (1956) "Relations between the concentrations of imperfections in crystalline solids," *Solid State Phys.* **3**, 307. The original proposal of the notation that is now universally used to describe charged point defects. This is an invaluable paper when you have time to study it. The official notation is given in the IUPAC *Red Book on the Nomenclature of Inorganic Chemistry*, Chapter I-6.
- Smyth, D.M. *The Defect Chemistry of Metal Oxides*, Oxford University Press, Oxford 2000. Clear and at the right level.
- Swalin, R.A. (1972) *Thermodynamics of Solids*, 2nd edition, John Wiley & Sons, New York. Chapter 11.
- Tilley, R.J.D. (1987) *Defect Crystal Chemistry and Its Applications*, Blackie, Glasgow. Chapter 1. A very readable text.
- Wagner, C. and Schottky, W. (1929) *Thermodynamik*, Springer, Berlin. The book by the masters—not often read.
- Wagner, C. and Schottky, W. (1930) "Theory of regular mixed phases," *Z. Phys. Chem.* **B11**, 163. An original paper.

WWW

MARVIN was originally authored by David H. Gay and Andrew L. Rohl. The program is "an advanced computer code for performing static and dynamic modeling of surfaces and interfaces." http://www.ri.ac.uk/DFRL/research_pages/resources/MARVIN_data/main.html

EXERCISES

- 11.1 What, if any, is the difference between a Schottky defect in Mg and a Schottky defect in MgO?
- 11.2 Would you expect Frenkel defects to be more likely in Al or Al₂O₃? What factors do we need to consider in answering this question?
- 11.3 How might you expect Si to diffuse in an alumina furnace tube at high temperatures? Would the mechanism be different if the alumina were in the form of a single crystal?
- 11.4 We form a Schottky defect in KCl. What is the difference in energy of the system if the two vacancies are $5.5a$ apart or $3.5a$ apart (a being the lattice parameter). Why do we choose 3.5 rather than 3, etc.? Discuss.
- 11.5 We dissolve (add) 100 ppm of Al₂O₃ to a cube of MgO (1 mm on the side). How many vacancies are formed and how much bigger is the cube?
- 11.6 Construct a table of defects and discuss the different types of point defects in Fe₂O₃. Compare this table with the table you produce for Fe₃O₄.
- 11.7 Write down a point defect reaction for ZnO in which you produce twice as many singly charged defects as doubly charged ones.
- 11.8 Write a balanced defect reaction equation using Kröger–Vink notation for substitution of Ca²⁺ in CaF₂ by Y³⁺.
- 11.9 During the movement of the Na⁺ ion in Figure 11.15, how does the CN of the Na⁺ ion change as it moves through route 2.
- 11.10 Express using Kröger–Vink notation the formation of Frenkel defects in AgBr and explain why you think these are more numerous than Schottky defects. How might you increase the concentration of Schottky defects in AgBr?

Are Dislocations Unimportant?

CHAPTER PREVIEW

We will begin our discussion with a reminder of the basic properties of single dislocations and conclude by considering combinations of dislocations, which will lead nicely into the next three chapters, which consider different types of interfaces.

Most students understand dislocations best by thinking about schematic diagrams and high-resolution transmission electron microscopy (TEM) images. Dislocations are line defects, but like all crystal defects, they are actually volume defects; i.e., we should think of them as tubes, or pipes, whose properties change across the tube radius and that generally do not have cylindrical symmetry.

We are not trying to cover everything about dislocations here; rather we will review the basic features of dislocations and then introduce the complexities of ceramics. Remember the important experimental observation that led to the “invention” of dislocations: the stress required to deform a metal single crystal is at least 10^3 times smaller than the theoretical value.

Two vectors define the fundamental properties of any dislocation:

- The line direction
- The Burgers vector

The glide plane of the dislocation is the plane that contains both vectors. To summarize:

Geometry	Burgers vector and line direction define the glide plane.
Displacement	When a dislocation is present, atoms are displaced from their positions in the perfect crystal; the material is strained so there must be a stress.
Movement	Dislocations move and interact (they even intersect).
Reacting	We generate dislocations, they multiply and combine (by intersecting).

Why consider dislocations in ceramics? Conventional wisdom says that dislocations are not nearly as important in the mechanical deformation of ceramics as they are for metals. The reason is that dislocations in ceramics do not move as easily as those in metals and they are usually not as numerous. So we should be asking why the last sentence is true. Dislocations in ceramics are extremely important because of what they do not do: they do not glide easily. Si devices would not work for long and ceramics, in general, would not be brittle if dislocations could glide easily. Understanding dislocations also helps us understand other more complex defects, how they interact with point defects, and how they can cause planar defects. Dislocations become very important when we use thin crystalline ceramic films, particularly when grown on crystalline substrates.

What is special about dislocations in ceramics?

- Complex and large unit cells are the norm rather than the exception.
- Charge—if you insert an extra half plane to make an edge dislocation, you must consider the charge.
- Directional bonds—if you break a bond, does it reform?

For the student, dislocations are a great test of whether the structure of a crystal is understood. They give a fine *probe* of what is happening in the material. Be aware though that much of

our understanding of dislocations comes from metallurgy, particularly from studies on Cu alloys. We often compare our dislocations to these, since those in metals are quite well understood, but ceramics do introduce new complications. A detailed understanding of dislocations and planar defects in ceramics is not as advanced as that of point defects.

12.1 A QUICK REVIEW OF DISLOCATIONS

Line defects in a crystalline material are known as dislocations (unless they are disclinations, which will be ignored because they are much more difficult and not nearly as important in ceramics). In contrast to point defects, dislocations never exist in thermodynamic equilibrium because they have formation energies of ~ 1 eV (or more) per atom along the line and there is no significant balancing entropy contribution as there is for point defects. They are almost always present in crystals because of how the crystal grew or because it was deformed. Therefore dislocations usually form due to nonequilibrium conditions, such as thermal and mechanical processing, or for thin films and single crystals, during growth. There are two special types of dislocation.

- Edge dislocations
- Screw dislocations

All other dislocations are referred to as “mixed.”

Defining the Burgers Vector and the Glide Plane

The Burgers vector is defined by constructing a closed circuit around the dislocation line. We first draw a circuit around the dislocation in a clockwise (right-handed screw) direction from the start (S) to the finish (F) as shown in Figure 12.1a. We then transfer this circuit to a perfect crystal as shown in Figure 12.1b. If there is a dislocation, this second loop will not close on itself. We then define the vector FS, which is required to close the loop in the perfect crystal, as the Burgers vector. This method of defining the Burgers vector, \mathbf{b} , is known as the FS/RH perfect-crystal convention. (The vector is named after J.M. Burgers so there is no apostrophe.) The Burgers vector is then defined with respect to the perfect crystal; you would not want to define it in the imperfect crystal!

It is important that you are consistent in using this convention. Some other texts, and even some of the classic papers, use a convention that produces the opposite sign for the Burgers vector. For example, they might use an anticlockwise circuit, set $\mathbf{b} = \mathbf{SF}$, or draw the circuit in the perfect crystal first. You must use a convention consistently.

- Edge dislocation: An extra half-plane of atoms is inserted above the glide plane as illustrated in Figure

12.1a. The Burgers vector is perpendicular to the dislocation line, \mathbf{u} . The Burgers vector will be opposite if the extra half plane is below the glide plane.

- Screw dislocation: Successive atomic planes are connected to form the surface of a helix (or screw) around the dislocation line as shown in Figure 12.2 where the dislocation is perpendicular to the planes: like the core of a spiral, parking ramp. The Burgers vector is parallel to the dislocation line and can point up or down for a left- or right-handed screw.
- Glide plane: This is the plane containing both the dislocation line and the Burgers vector.

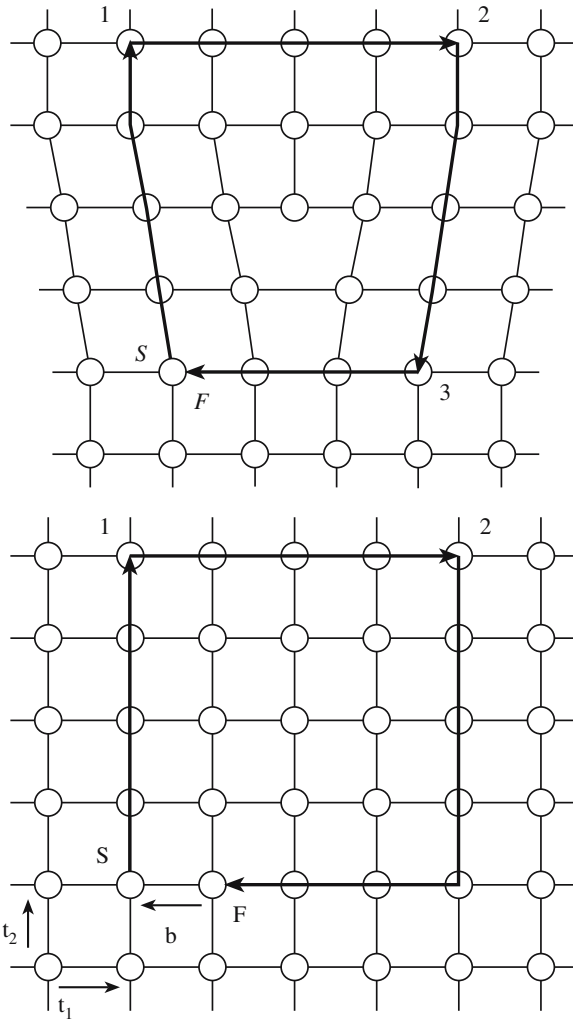


FIGURE 12.1 The Burgers circuit in the imperfect and perfect lattices for an edge dislocation in a simple-cubic crystal.

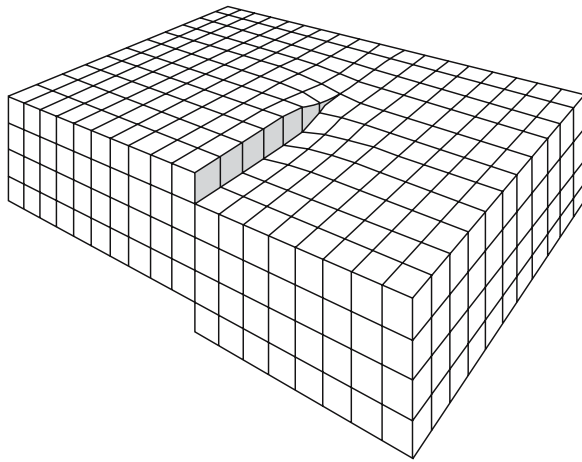


FIGURE 12.2 Schematic of a screw dislocation.

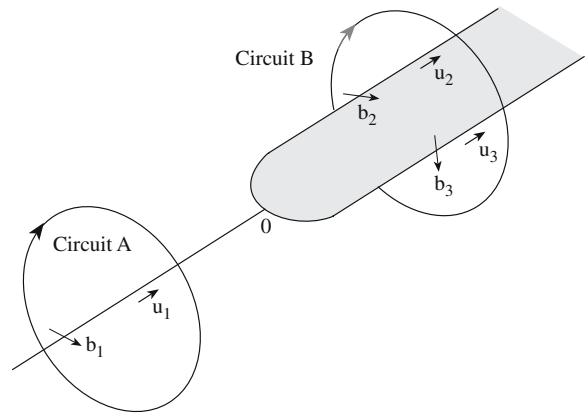


FIGURE 12.3 Diagram used for proving Frank's rule for conservation of \mathbf{b} .

The glide plane is not usually an actual plane of atoms, rather it is a plane between two planes of atoms. (Where actually is the dislocation line?) Dislocations are often more complicated than suggested by the two simple examples above, but they can always be resolved into a combination of edge and screw components.

Dislocation lines can end at the surface of a crystal and at grain boundaries, but never inside a crystal lattice. Thus, dislocations must either form closed loops or branch into other dislocations. The meeting of three or more dislocations at a point, or node, is a necessary condition indicating that the Burgers vector is conserved. Consider the dislocation \mathbf{b}_1 in Figure 12.3, which branches into two dislocations with Burgers vectors \mathbf{b}_2 and \mathbf{b}_3 . A Burgers circuit has been drawn around each dislocation according to the line sense, \mathbf{u} , indicated, and it follows from the diagram that \mathbf{b} is conserved.

$$\mathbf{b}_1 = \mathbf{b}_2 + \mathbf{b}_3 \quad (12.1)$$

The large circuit on the right-hand side of Figure 12.3 encloses two dislocations, but since it passes through the same good material as the \mathbf{b}_1 circuit on the left-hand side the Burgers vector must be the

SIGN OF \mathbf{b}

The sign of the dislocation is important: it determines the direction of motion when you apply a stress.

- Edge: \mathbf{b} points to the left or right: this determines whether the extra half-plane is above or below the glide plane.
- Screw: \mathbf{b} is parallel or antiparallel to \mathbf{u} : this determines whether the spiral goes up or down (clockwise or anticlockwise).

same, i.e., \mathbf{b}_1 . It is more usual to define the Burgers circuits by making a clockwise circuit around each dislocation line looking outward from the nodal point. This reverses the line sense (and hence the Burgers vector of dislocation 1 becomes $-\mathbf{b}_1$) on the left-hand side, and then Eq. 12.1 becomes

$$\sum \mathbf{b}_i = -\mathbf{b}_1 + \mathbf{b}_2 + \mathbf{b}_3 = 0 \quad (12.2)$$

Elasticity

We usually assume that elasticity (how stress is related to strain) is linear. The assumption is that strains are small so that stresses are linearly related to strains (Hooke's law). We then think of the crystal as a continuum (a structureless "sponge") with two independent elastic constants (for example, μ , the shear modulus, and ν Poisson's ratio). At the core of the dislocation, the strains are too large for this assumption to be valid so we exclude this region from our calculation and replace it by a fudge factor involving r_0 , the core radius (not ideal because it assumes nothing varies across the core and we do not know what r_0 is). One consequence of linear elasticity is that when

R FOR A SCREW DISLOCATION

The displacement of any point on this surface from its "perfect-crystal position" is given by

$$\mathbf{R} = \frac{\mathbf{b}\phi}{2\pi}$$

(ϕ is a fraction of 2π). The strain in the complete unwrapped surface is then

$$\gamma = \frac{b}{2\pi r}$$

The shear stress due to the screw dislocation is then

$$\tau = \mu\gamma$$

Burgers vectors are separated into screw and edge components, the stresses due to these separate components can be treated individually and then added to give the total stress.

We do not usually think of ceramics as being elastic but do not confuse local stresses with macroscopic behavior. Macroscopically the ceramic may be brittle, but if the atoms move slightly off their perfect-crystal sites because of an applied force, that is an elastic deformation. We can also have anisotropic elasticity (which becomes important for noncubic ceramics) and nonlinear elasticity, but usually approximate to the simple case.

Displacement Fields

We usually derive the displacement field of a screw dislocation because it is much easier than deriving the edge dislocation.

The screw dislocation is formed from a cylinder of crystal by making a cut along the cylinder and displacing one side relative to the other by a vector \mathbf{b} where \mathbf{b} is the same value everywhere on the cut and is parallel to the axis of the cylinder; we first have to cut out a cylinder at the core so as to make this process physically possible. We take the screw dislocation in Figure 12.4 and “unwrap” the surface at a distance r away from the dislocation core; remember that \mathbf{b} is parallel to the dislocation line so it does not matter where we start the unwrapping process. We then calculate the strain, γ , in the unwrapped surface and then calculate the shear stress due to the screw dislocation. As you move away from the center of the cylinder, the strain decreases as r^{-1} and, as noted earlier, when r becomes very small ($\sim r_0$), the assumptions of elasticity break down, so this relationship does not hold in the core region.

Remember μ depends on the interatomic bonding and \mathbf{b} depends on the crystal lattice.

For the edge dislocation, we will just quote the result for the stress field (Eqs. Box 12.1–12.4). This stress field

STRESSES FOR AN EDGE DISLOCATION

The stresses are referred to xyz coordinates for a dislocation parallel to z . This dislocation does not have cylindrical symmetry.

$$\sigma_{11} = -\frac{\mu b}{2\pi(1-\nu)} \frac{x_2(3x_1^2 + x_2^2)}{(x_1^2 + x_2^2)^2} \quad \text{Box 12.1}$$

$$\sigma_{22} = \frac{\mu b}{2\pi(1-\nu)} \frac{x_2(x_1^2 - x_2^2)}{(x_1^2 + x_2^2)^2} \quad \text{Box 12.2}$$

$$\sigma_{33} = \nu(\sigma_{11} + \sigma_{22}) \quad \text{Box 12.3}$$

$$\sigma_{12} = \frac{\mu b}{2\pi(1-\nu)} \frac{x_1(x_1^2 - x_2^2)}{(x_1^2 + x_2^2)^2} \quad \text{Box 12.4}$$

THE STRAIN ENERGY

For a screw dislocation

$$dE = \frac{1}{2} \mu \left(\frac{b}{2\pi r} \right)^2 l 2\pi r dr$$

$$dE = \frac{\mu b^2}{4\pi} l \frac{dr}{r}$$

$$E = \int_{r_0}^R dE = \frac{\mu b^2}{4\pi} l \ln \frac{R}{r_0}$$

For an edge dislocation this equation becomes

$$E = \int_{r_0}^R dE = \frac{\mu b^2}{4\pi(1-\nu)} l \ln \frac{R}{r_0}$$

will exert a force on any other neighboring dislocation. The force is given by

$$F = \sigma b \quad (12.3)$$

If we were being rigorous we would express the force as $\mathbf{b}\sigma$ since \mathbf{b} is a vector and σ is a tensor.

$$F = (\mathbf{b} \cdot \boldsymbol{\sigma}) \times \mathbf{u} \quad (12.4)$$

- The term $\mathbf{b} \cdot \boldsymbol{\sigma}$ represents a force per unit length, F , which acts in a direction that is normal to \mathbf{b} .

An important result of applying Eq. 12.4 is that the force acting on dislocation 1 due to the stress field of dislocation 2 depends on $\mathbf{b}_1 \cdot \mathbf{b}_2$: if $\mathbf{b}_1 \cdot \mathbf{b}_2$ is positive, then the dislocations repel one another; if it is negative, then the interaction is attractive (but be careful about the line direction).

Dislocation Strain Energy

Since a dislocation creates a strain field, which in turn creates a stress field, each

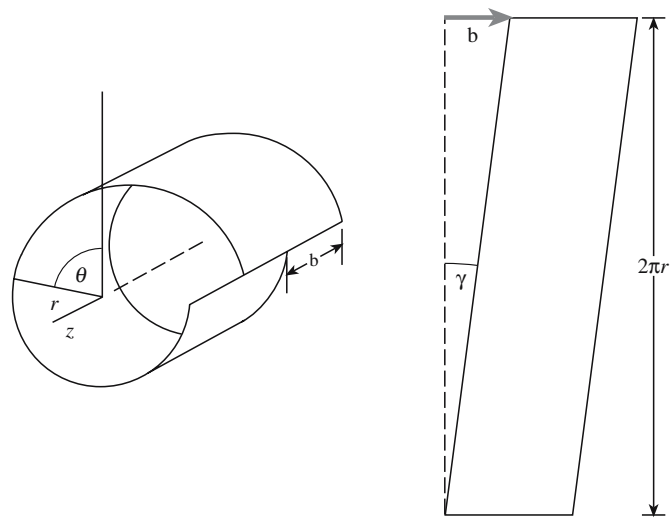


FIGURE 12.4 Deducing strain by “unwrapping” a screw dislocation.

dislocation will have an associated strain energy. This strain energy is termed the self-energy of the dislocation. We can then determine the strain energy per unit volume by integrating over the volume affected by the strain field (i.e., by determining the area under the triangle in the stress versus strain plot shown in Figure 12.5). For the screw dislocation, $l2\pi r dr$ is an element of volume at radius r around a length l of the dislocation.

At the center of a dislocation the crystal is highly strained with atoms displaced from their normal sites and we cannot use linear elasticity so we again exclude this region from the calculation by making the inner limit r_0 . There must be a contribution to the self-energy of the dislocation from this core, but we need atomistic modeling to estimate the value; it is usually assumed to be about 10% of the total strain energy of the dislocation. As before, we just quote the result for the edge dislocation. The only difference compared to the screw dislocation is the $1 - \nu$ factor. We can express the energy of a mixed dislocation as

$$E = \frac{\mu b^2}{4\pi} \left(\frac{\sin^2\theta}{1-\nu} + \cos^2\theta \right) \ln \frac{R}{r_0} \quad (12.5)$$

The important result is that the strain energy of a dislocation is proportional to the square of the Burgers vector \mathbf{b} and the shear modulus of the material.

$$E = \alpha\mu b^2 \quad (12.6)$$

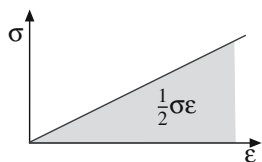


FIGURE 12.5 Elastic energy of a screw dislocation from a plot of stress versus strain.

FREE ENERGY OF A DISLOCATION

In Chapter 11 we showed how ΔG could be determined for the formation of point defects in a crystal using

$$\Delta G = \Delta E - T\Delta S$$

ΔS was obtained using statistical mechanics methods. What are the contributions to the entropy of a dislocation? There are three.

- Positional entropy—similar to the configurational entropy we described for point defects.
- Entropy due to vibration of the dislocation line about its equilibrium position.
- Changes in the vibrational entropy of the surrounding lattice because of the large strains near the dislocation core.

The total entropy contribution is only ~ 0.5 eV/atom. Less than E , but not negligible.

DISSOCIATION

$$b \rightarrow b_1 + b_2 + b_3 + \dots + b_{10}$$

$$b^2 \rightarrow b_1^2 + b_2^2 + b_3^2 + \dots + b_{10}^2$$

For dissociation into two Shockley partial dislocations

$$\mathbf{b} = \frac{a}{2}[110] \rightarrow \frac{a}{6}[121] + \frac{a}{6}[21\bar{1}] = \mathbf{b}_{p_1} + \mathbf{b}_{p_2}$$

We normally just take the constant α to be between 0.5 and 1.0. This result provides a criterion for what dislocations can be formed in a given crystal. Those with the smallest allowed Burgers vector have the lowest strain energy and, consequently, are the most likely to form. (This will be very important for a ceramic with a large unit cell; e.g., YAG.)

The crystal determines the actual value of \mathbf{b} . If \mathbf{b} is a perfect lattice vector, then the structure of the crystal will not be changed by the passage of a dislocation. If \mathbf{b} is not a lattice vector, then a planar defect (a stacking fault) will be present on one side of the dislocation and a second so-called partial (or imperfect) dislocation will be required to remove the stacking fault.

The important point is that the elastic energy depends on three factors:

- An elastic constant, μ , because the energy of the dislocation depends on the stress and strain that it causes in the lattice, and ν if there is an edge component.
- The radii, R and r (and r_0), because the total energy of the dislocation depends on the volume of crystal it effects.
- The Burgers vector, \mathbf{b} , because this determines the magnitude of the strain.

We will assume linear isotropic elasticity throughout this discussion.

Compact Core versus Spread Core

If a dislocation dissociates into partial dislocations, the self-energy will be reduced providing the angle between the Burgers vectors is acute (they are parallel not antiparallel). As a simple demonstration, consider the possibility that 10 partial dislocations each with Burgers vector $\mathbf{b}/10$ are formed. The strain energy is reduced by a factor of 10! Once formed, these dislocations will repel one another since they have parallel Burgers vectors. However, since the Burgers vectors of these partial dislocations are not

lattice vectors, a planar defect is created between each pair of partial dislocations. If the energy required to form these planar defects is greater than the reduction in the strain energy, then the dissociation will not occur. The best-known example of dislocation dissociation is found in face-centered cubic (fcc) metals. The dissociation produces two so-called Shockley partial dislocations, which do not have parallel Burgers vectors.

In an fcc crystal, the special feature of this dislocation dissociation is that the planar defect formed between the two partial dislocations can be regarded as a mistake in the stacking of the *close-packed* layers as shown in Figure 12.6. The term stacking fault is then applied to all such planar defects and the energy per unit area is the stacking-fault energy (SFE or γ , but do not confuse this γ with strain). Of course, for the general concept, the planes do not need to be close-packed planes; you can stack any planes incorrectly!

When calculating the SFE, we do not equate the SFE to the energy required to create the fault; instead we con-

sider the force balance. The two partial dislocations will try to repel each other ($\mathbf{b}_{P_1} \cdot \mathbf{b}_{P_2} > 0$), but they cannot separate too much because of the SF. Although we have deduced this dissociation for fcc metals using an energy argument, it is also important for the *behavior* of the dislocations. In fcc metals, these partial dislocations allow the atoms to move over “valleys” instead of over “hills” as the dislocation glides, and they restrict glide to the plane of the stacking fault. In Cu and Si, dislocations are widely ($\Delta \sim 4$ nm) dissociated, but the same dislocation in Al has a rather narrow core.

If the dislocation changes its line direction for a short segment, this segment is called a kink if it lies in the glide plane or a jog if it causes the dislocation to step out of its glide plane.

In general, a dislocation will itself contain many such defects along its length.

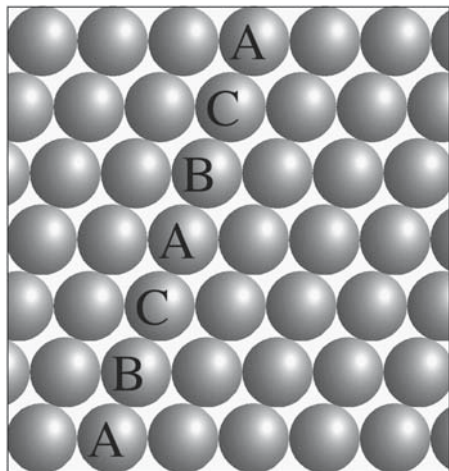
12.2 SUMMARY OF DISLOCATION PROPERTIES

We have not reviewed all the properties of dislocations, but have concentrated on those you should know when considering dislocations in ceramics.

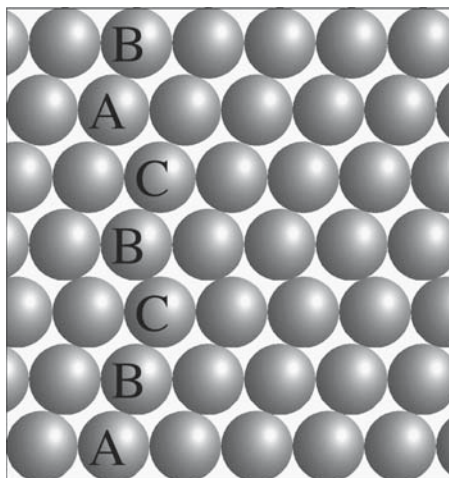
- Dislocations cannot end inside the crystal lattice.
- We almost always assume that strains are so small that linear elasticity is a good approximation; so, Hooke’s law holds.
- The displacement field for any dislocation falls off as r^{-1} as we move away from the dislocation.
- The strain energy (or self energy) of a dislocation actually depends on the character of the dislocation, but setting $E = \alpha Gb^2$ is a good estimate, where α is ~ 0.5 .
- Parallel dislocations repel one another if the angle between their Burgers vector is less than 90° . (Be careful with \mathbf{u} .)
- A dislocation can always lower its strain energy by spreading its core or dissociating. Whether this will lower the total energy depends on the energy required to form the distorted region between the “partial dislocations.” If dissociation occurs (forming identifiable partial dislocations) then this region is called a stacking fault.
- Dislocations glide by the movement of kinks and climb by the movement of jogs. Since climb requires changing the number of defects (reacting or absorbing them), we call it nonconservative motion.

12.3 OBSERVATION OF DISLOCATIONS

We can divide the techniques used to “see” dislocations into two categories:



(A)



(B)

FIGURE 12.6 The intrinsic stacking fault in an fcc crystal.

1. Direct
2. Indirect

Direct techniques allow us to see the arrangement of atoms around the dislocation. The most useful direct technique is high-resolution transmission electron microscopy (HRTEM). The resolution of commercial instruments allows direct observation of columns of atoms and edge dislocations can be identified as terminating planes of atoms as shown in Figure 12.7. These images look very much like the schematics we draw to illustrate edge dislocations, and the Burgers vectors can be determined directly from the image using the Burgers circuit construction (unless there is a screw component present).

Indirect techniques rely on the fact that dislocations create a strain field and are regions of high energy. The most widely used of the indirect methods is again TEM. We will show you several examples of TEM images of dislocations in ceramics in later parts of this chapter. Figure 12.8 shows how planes near a dislocation may be bent into an orientation where they are strongly diffracting even when the rest of the crystal is not. The intensity of the direct beam will be reduced (and that of the diffracted beam increased) and the dislocation will appear as a dark line in the bright-field image. Images of dislocations are often quite difficult to interpret and the position of the dislocation in the TEM image will generally not correspond exactly to its actual position in the crystal. However, this approach is extremely useful in answering many of

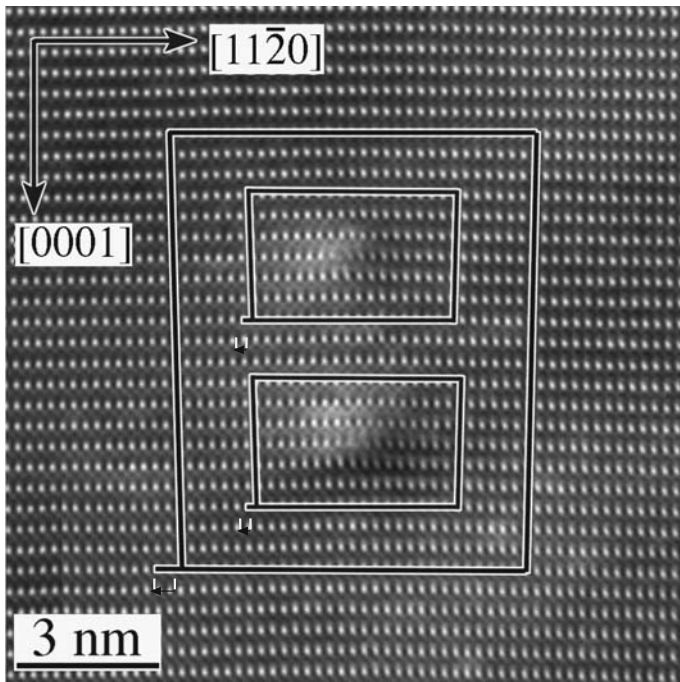


FIGURE 12.7 HRTEM of the core of a dislocation in Al_2O_3 .



FIGURE 12.8 Diffraction contrast from dislocations in Al_2O_3 .

the questions that arise about the nature of dislocations in a material.

- Is the dislocation interacting with other dislocations, or with other lattice defects?
- Is the dislocation jogged, kinked, or straight?
- What is the density of dislocations in the sample?
- Has the dislocation adopted some special configuration, such as a helix?

By tilting our specimen in the TEM to a condition in which the dislocations are invisible (or at least appear faint in the image), if we know the diffracting conditions (specifically the diffraction vector \mathbf{g}), then we can obtain \mathbf{b} using the invisibility criterion (generally needing three independent \mathbf{g} vectors).

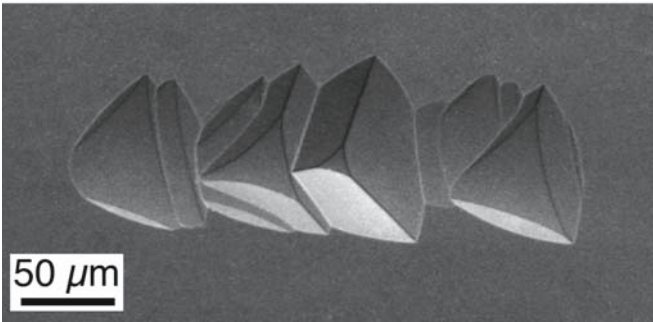
$$\mathbf{g} \cdot \mathbf{b} = 0 \quad (12.7)$$

Another indirect (but lower resolution) approach is the etch-pit method. In this technique the surface of the sample is polished and immersed in a suitable chemical etchant. The rate of removal of material around the dislocation (where the crystal is strained) is usually more rapid than in the surrounding crystal and pits are formed where the dislocation line intersects the surface. The clearest demonstration that etch pits are associated with dislocations is shown for Si in Figure 12.9a where the dislocations can be seen in cross section due to absorption of IR illumination by the Cu decorating the dislocation; today, this task might be more easily accomplished using a focused ion-beam (FIB) instrument. Figure 12.9b shows a plan-view image of etch pits in a single crystal of Nd-doped YAG. The etch pits were revealed by immersing the polished crystal in concentrated phosphoric acid at 250°C for 8 minutes.

The etch pit method is usually best when dislocation densities are low ($<10^4 \text{ mm}^{-2}$). If the dislocation densities are too high the etch pits overlap each other and it is very difficult to resolve their shape and count densities.



(A)



(B)

FIGURE 12.9 Etch pits at dislocations emerging at a surface in Si. (a) The cross-sectional view in Si; (b) the plan view in YAG.

12.4 DISLOCATIONS IN CERAMICS

In discussing dislocations in ceramic materials, the principle is always the same. We deduce the possible Burgers vectors first, then the glide planes. We will begin by asking if there is anything special about dislocations in ceramics; we can preempt the answer by saying yes, as usual, the bonding and charge can add their own effects. The second best-known special feature of dislocations in ceramics is actually that the unit cell of such materials is usually larger than for the simple metals, so we will see similarities to other materials such as the intermetallics that also have large unit cells.

The structure of the dislocation core in ceramics depends on three factors

1. Charge of the ions
2. Size of ions
3. Presence of directional bonds

Perhaps the more important question is: why learn about dislocations in ceramics when ceramics do not deform plastically as easily as metals? This question then leads us to question why this statement is true. Is it always true? Can we change anything? Modern materials often involve interfaces. Interfaces are directly related to dislocations. The growth of thin films often involves dislocations. Dislocations also play an important role in radiation damage of ceramics. So there are many reasons for understanding dislocations in ceramics.

12.5 STRUCTURE OF THE CORE

Not much is really known about the core of dislocations in ceramics. For the examples we will show, you should remember that we have usually chosen one Burgers vector (usually the most important one), one line direction, and thus one glide plane. Furthermore, we usually draw the edge dislocation because it is easiest to draw, not because it is the most important. In this section, we will assume that the dislocation core is compact. The examples are chosen to illustrate particular features.

- NaCl: it is relatively simple and illustrates the effect of charge.
- Si: it illustrates the effect of directional (covalent) bonding.
- Al_2O_3 and olivine: they are noncubic materials.

Although NaCl and MgO structures are both based on the cubic-F Bravais lattice, like Cu, there is no evidence for any dislocation dissociation. There are detailed atomistic calculations that confirm that the compact core is preferred. A schematic diagram of such a dislocation viewed along the [001] direction is shown in Figure 12.10. All the ions seen here lie in the same (001) plane. If we remove this plane of atoms the structure looks the same, but all the ions are reversed in sign. So charge is balanced as long as there are no jogs or kinks on the dislocation.

The glide plane for dislocations in NaCl and MgO is {110} rather than the {111} you might expect for fcc. You may read that the glide plane is {110} because this plane is electrically neutral and motion on this plane avoids charged layers gliding over one another. However, ErAs, an exotic semimetal (no ionic charge), with the NaCl structure, has the same glide system. PbS, a semiconductor with this structure, shows glide occurring on {001} planes and in TiC dislocations glide occurs on {111} planes. The real reason for the {110} glide plane is still being studied. The suspicion is that the core actually does spread on different planes, but that still does not tell us why the spreading depends on the material.

The simplest covalently bonded ceramics are Si and Ge. The covalent bond formed by two atoms sharing electrons is a localized and directional bond. Cubic ZnS has the same structure, but the Si-Si basis is replaced by Zn-

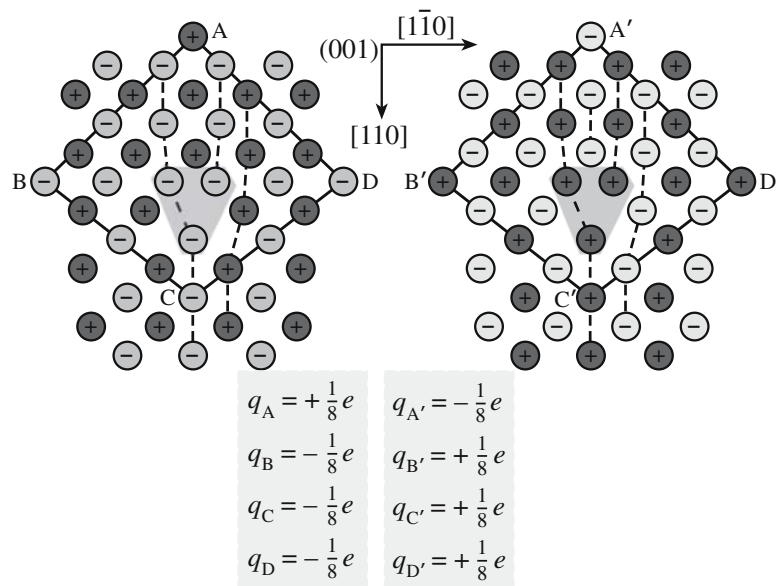


FIGURE 12.10 The core of a dislocation in NaCl.

S, although the bond still has a large covalent component. This feature is important in determining the characteristics of dislocations in covalent materials. Dislocations in these materials tend to be immobile at low temperatures. Extensive slip occurs only at elevated temperatures.

Of the many covalent crystals, the diamond-cubic and *c*-ZnS structures are among the simplest and most widely studied. Since the crystal lattice is fcc, perfect dislocations have the fcc Burgers vector $\frac{1}{2}\langle 110 \rangle$ (b^2 always wins). Like dislocations in fcc metals, dislocations in Si, Ge, and *c*-ZnS glide on $\{111\}$ planes. Figure 12.11a shows a $(\bar{1}\bar{1}0)$ projection of *c*-ZnS; you can recognize the $\{111\}$ planes (also shown by the projected tetrahedron). We make a dislocation by cutting out half a plane, as shown by the box labeled 1564. Then we merge the atom at P and Q; since these are on different levels (one is a large circle and the other is small), the dislocation will have a component of \mathbf{b} into the page: it is a 60° perfect dislocation. However, we could have removed the slice of material 1234 and joined atoms R and S to make exactly the same \mathbf{b} . Therefore, there are two possible $\{111\}$ slip planes, type I and type II, and two possible dislocation cores. [These slip planes are usually called the glide (I) and shuffle (II) planes, which can be confusing since the dislocation can glide on both!] The 60° dislocation is shown with its extra plane ending at a type II plane. Imagine removing material 1234: there is then one unpaired bond per atom along the dislocation core as shown in Figure 12.11b. This defect is called a *dangling bond*. This type of dislocation does exist as illustrated in Figure 12.11c. Here, the dislocation alternates between the compact core and a dissociated structure. The explanation for this change is that the dislocation

steps from a type I plane to a type II plane: it dissociates on one but not on the other because the SFE is different on the two planes. The step from the shuffle plane to the glide plane is a special jog. The dangling bonds can then reconstruct; now the bonds are distorted but not dangling! However, this dislocation cannot move without rebreaking the reconstructed bonds so the dislocation is *sessile*.

If we left the half-plane 1234 where it is but removed the other half, we would create a dislocation with the opposite \mathbf{b} , but instead of the last atom being R(S) it would be T(U): Zn instead of S! The core of the dislocation is fundamentally different: it is still a shuffle dislocation. These two dislocations are fundamentally different because the zinc blende structure does not have a center of symmetry. Similar considerations will hold for materials such as AlN and GaN, which also lack a center of symmetry but have the wurtzite structure crystal structure. The stacking fault in the diamond-cubic structure is described as AbBbCcBbCcAaBb: the pair of planes Aa behaves just as if it were one fcc plane in this case. Two possible SFs are shown in Figure 12.11d.

The thoroughly studied metals are either cubic or they have the closely related hcp structure. Many ceramic materials are neither cubic nor hcp. Olivine and sapphire both have oxygen sublattices that can be thought of as distorted hexagonal close packed (hcp), but the distribution of cations makes them very different.

Olivine. In the olivine group of minerals (important orthorhombic silicates), the energies of the $[100]$, $[010]$, and $[001]$ dislocations are all different. In fact, the energy of the $[010]$ dislocation will be much greater since it has a much larger Burgers vector.

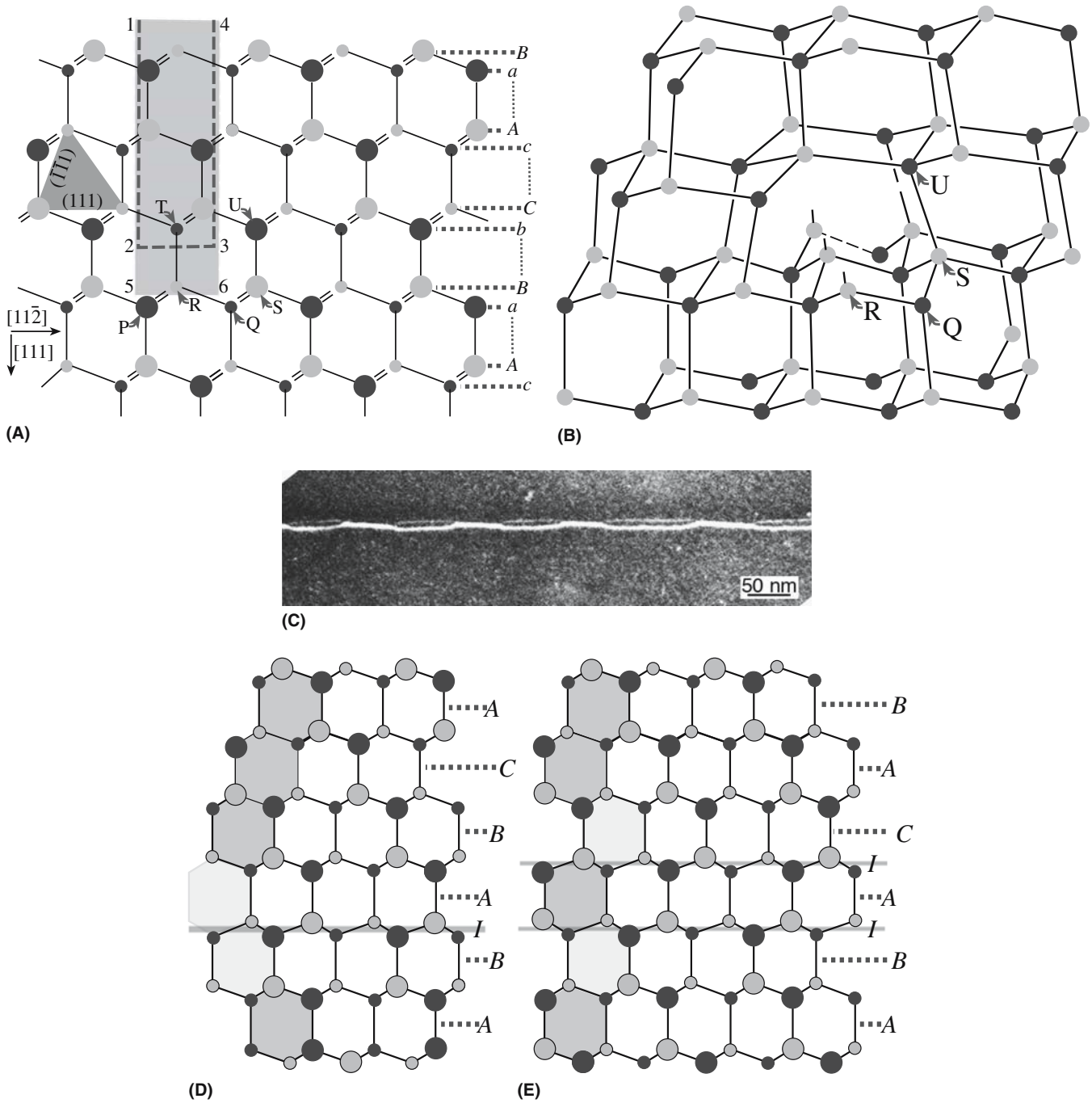


FIGURE 12.11 Models for forming dislocations and stacking faults in sphalerite. (a) Two cuts in which to make an edge dislocation; (b) dislocation made by removing 1234; (c) two structures for a dislocation with Burgers vector \mathbf{b} in Si; (d and e) intrinsic and extrinsic in Si.

For forsterite (Mg_2SiO_4): $a = 0.475 \text{ nm}$, $b = 1.020 \text{ nm}$, and $c = 0.598 \text{ nm}$.

For fayalite (Fe_2SiO_4): $a = 0.482 \text{ nm}$, $b = 1.048 \text{ nm}$, and $c = 0.609 \text{ nm}$.

For monticellite (CaMgSiO_4): $a = 0.4815 \text{ nm}$, $b = 1.108 \text{ nm}$, and $c = 0.637 \text{ nm}$.

The added complication is that olivine is not an isotropic material so using μ and ν (which automatically implies elastic isotropy) would be a simplification.

Sapphire. Al_2O_3 is also very anisotropic although we can use pseudoisotropic values of μ and ν when dislocations are confined to lie on the basal plane. The most common perfect dislocations do have the shortest Burgers vector $\frac{1}{3}\langle 11\bar{2}0 \rangle$ as seen in Figure 12.12, but other perfect dislocations have been reported including $[0001]$. Even when they have the shortest \mathbf{b} , they may glide (if they do at all) on other planes such as $\{1\bar{1}00\}$. Examples of dislocations in Al_2O_3 are shown in Figure 12.13.

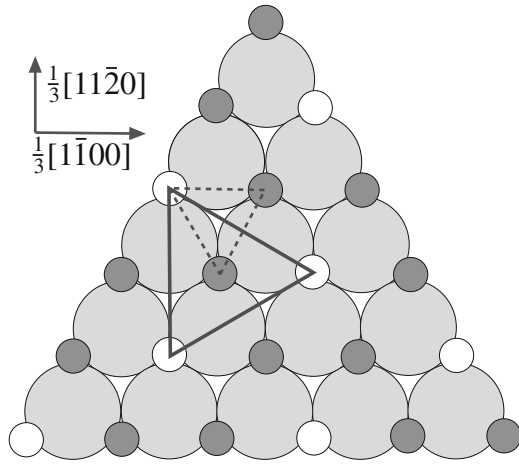


FIGURE 12.12 Schematic used to show **b** of perfect dislocations in Al_2O_3 .

12.6 DETAILED GEOMETRY

As we saw in Section 12.1, dislocations would always like to dissociate since this reduces the strain energy. Whether a particular dislocation will dissociate or not thus depends on the magnitude of the energy associated with the stacking fault. If the dislocation core spreads on the glide plane, it is glide dissociation; otherwise it is at least partly climb dissociation.

The glide dissociation seen in fcc metals does occur in ceramics. It is seen in III–V compounds, MoS_2 , graphite, and talc. (The last two are shown in Figure 12.14; more on this below.) In ceramics, since **b** is generally large, the energy ($\propto b^2$) can be very large. Crystals with the garnet structure are body-centered cubic (bcc) and the lattice parameter is ~ 1 nm. We can expect core spreading to occur, but there are very few observations available. Climb dissociation need not require adding or removing point defects to the dislocation as a whole because we can move point defects from one partial dislocation to the other, as

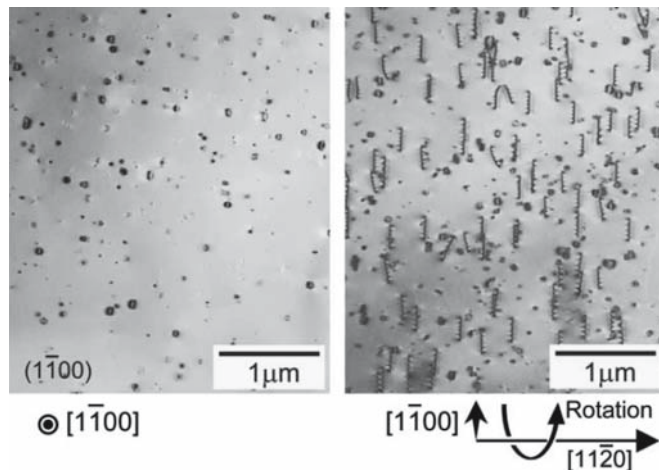


FIGURE 12.13 Images of dislocations in Al_2O_3 from two directions.

is illustrated schematically and experimentally for spinel in Figure 12.15 (more on this below). The result of this transfer is that one dislocation undergoes positive climb while the other undergoes negative climb.

Details on Glide Dissociation

Glide dissociation occurs when one of the partial dislocations moves on its glide plane. The classic example is Si, which, as we saw in Figure 12.11, can dissociate on a $\{111\}$ just like the fcc metals. Compounds such as ZnS, SiC, and GaAs, which have a zinc blende or sphalerite structure, behave in the same way. The illustration in Figure 12.14a–c is instructive. This 60° dislocation in graphite lies on the (0001) plane and we are looking onto this plane. The partial dislocation on the left is pure edge while that on the right is 30° . Notice that there are no broken bonds within the layers in this structure. The only broken bonds occur between the layers and these are the very weak van der Waals bonds. For the same reason the SFE is very small, so such partial dislocations may be widely separated as shown; graphite is sometimes seen to stack in the ABCABC sequence instead of ABAB. The SFE is small in talc and MoS_2 for similar reasons. Talc provides an interesting example in which more than one type of partial dislocation is formed, as we can see in Figure 12.14d and e.

Details on Climb Dissociation

Climb dissociation occurs when the stacking fault does not lie parallel to the glide plane of the partial dislocations. The phenomenon has not been seen in pure fcc metals, but it can occur in intermetallics. It is found in both covalent and ionic ceramics. We can make two comments here:

- Climb dissociation is always possible, but it may be more common in ceramics.
- Climb dissociation does not necessarily refer to how the configuration was achieved.

Climb dissociation may be more important in a ceramic than in an fcc metal because in fcc metals the glide plane is also the plane with by far the lowest SFE. A point to remember is that the word “dissociation” refers to the final configuration; it does not tell you that the perfect dislocation ever had a compact (undissociated) core.

An example involves a complex oxide, spinel. The smallest Burgers vector for a perfect dislocation in spinel is $\frac{1}{2}\langle 110 \rangle$, which is ~ 0.7 nm long. Such a dislocation can dissociate according to the reaction

$$\frac{1}{2}[110] \rightarrow \frac{1}{4}[110] + \frac{1}{4}[\bar{1}\bar{1}0] \quad (12.8)$$

This reaction reduces the total self-energy by 50%. Since $\frac{1}{4}[110]$ is a perfect lattice vector of the oxygen sublattice,

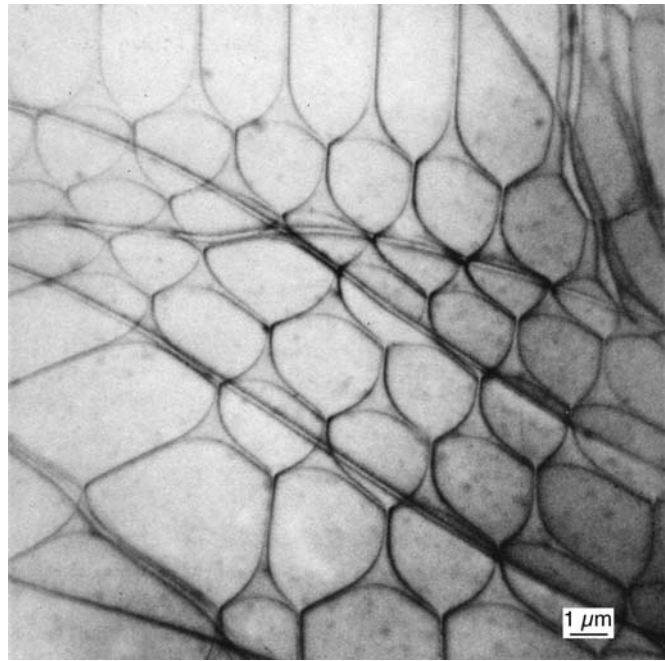
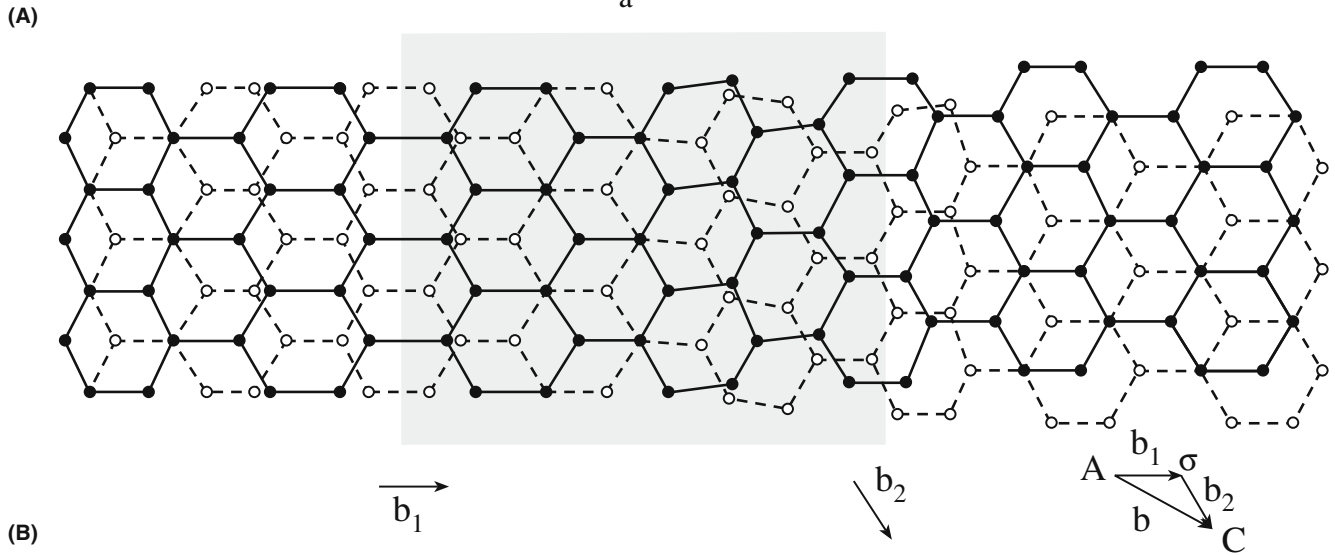
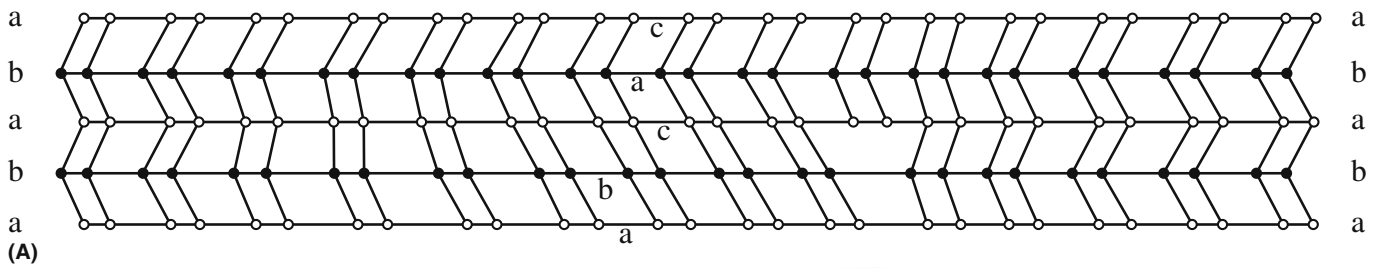


FIGURE 12.14 Dislocations in ceramics with low SFE. (a–c) Dissociation in graphite; (d and e) dissociation in talc.

this dissociation creates a stacking fault that exists only in the cation sublattice, so it has a low SFE. We know that in spinel stacking faults can form on $\{001\}$, $\{110\}$, and $\{111\}$ planes. In the example shown in Figure 12.15, the dislocation is dissociated on a $\{110\}$ plane. The

“stacking” situation is actually quite complex since we are stacking different layers and even when the layers are the same they may be rotated 90° , which is important if the layer (as is the case here) does not have 4-fold symmetry.

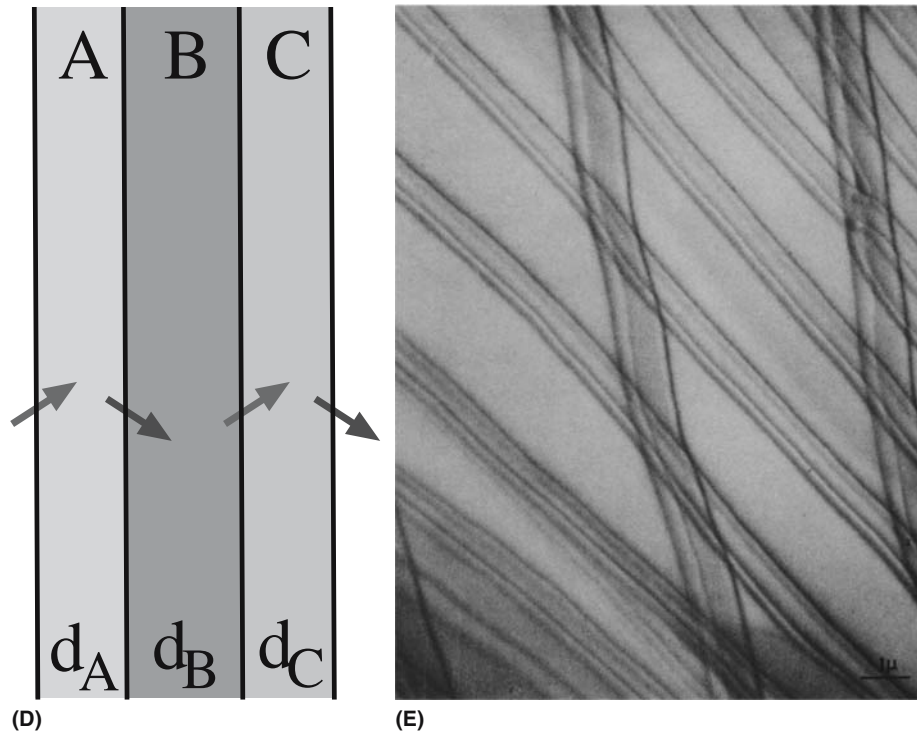


FIGURE 12.14 Continued

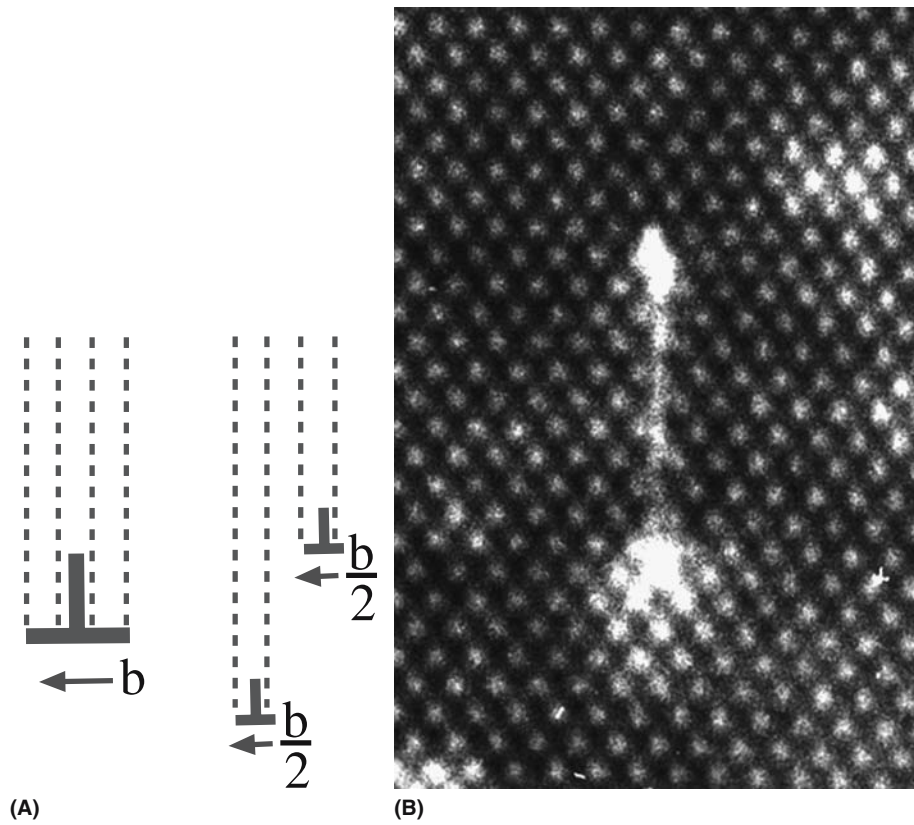


FIGURE 12.15 Climb dissociation of a dislocation in spinel: (a) schematic; (b) HRTEM image.

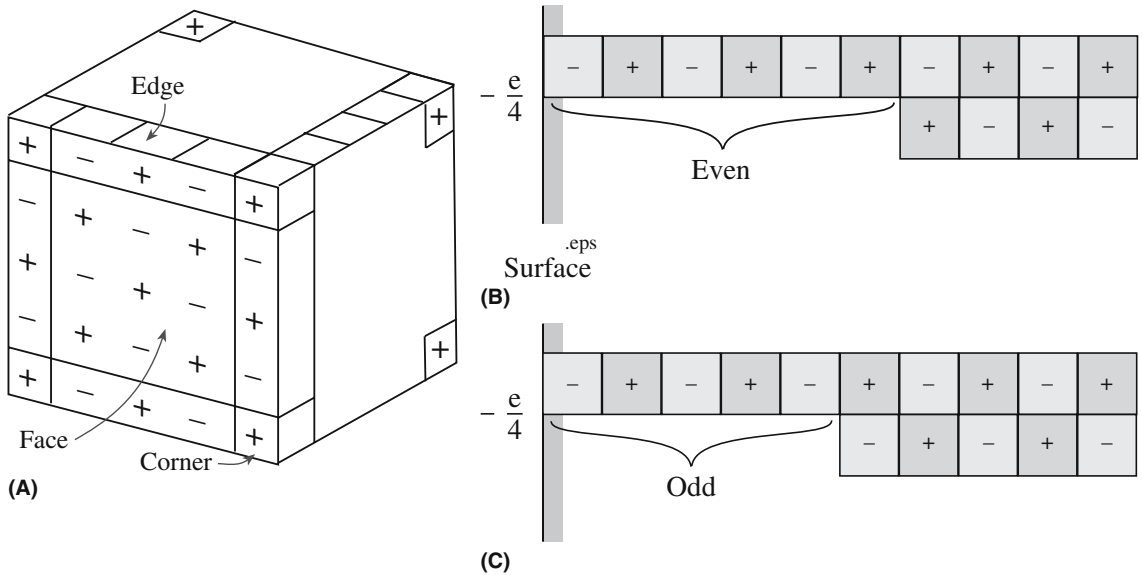


FIGURE 12.16 Schematic showing local charge on defects in rocksalt. (a) A corner is always charged; (b) and (c) possibilities for jog on an edge dislocation.

12.7 DEFECTS ON DISLOCATIONS

Even less is known experimentally about this subject for ceramic materials than for metals. However, the theory has been developed quite extensively and shows that this is one area in which ceramics are fundamentally very different from metals.

Consider a cube of NaCl cut so that every corner is occupied by a Na^+ ion (Figure 12.16a). The overall extra charge of the cube is $+e$. So, each corner has an effective charge of $+e/8$. We can extend this argument to show that there can be a charge at a jog. Consider a jog on a perfect edge dislocation in NaCl as shown in Figure 12.16b and c. Assume that there is a charge $+q$ on the jog. Now we can add a negative ion to the jog to produce the same configuration, but with the charge on the terminating ion reversed. The charge is now $-q$. Thus, we can identify q .

$$+q + (-e) = -q \quad (12.9)$$

The charge associated with the original jog was $q = +e/2$. Notice that you could not add a charge $+e$ because the jog is already positively charged. If a jogged dislocation in NaCl glides it can transfer a charge (carry a current). The transfer of current by deformation of NaCl has been measured experimentally. You can convince yourself of some properties of dislocations in NaCl.

- Straight dislocations are not charged.
- Dislocation kinks may be neutral or charged.
- The point at which an edge dislocation meets a surface carries a charge equal to $\pm e/4$.

Figure 12.17 shows two examples of a kink on a screw dislocation. In one case, the kink is charged while in the other it is neutral.

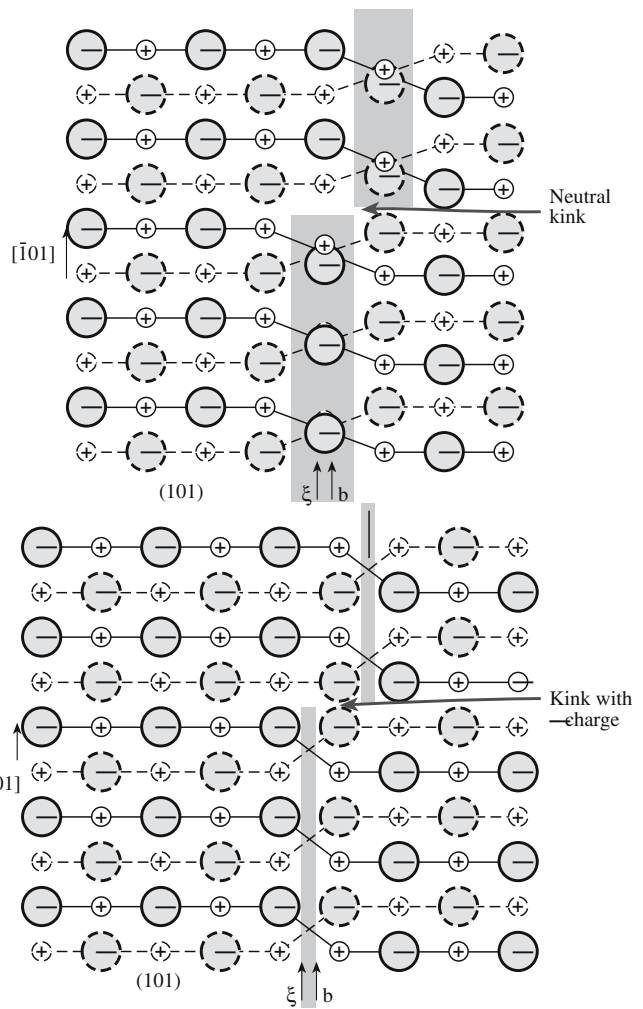


FIGURE 12.17 Schematic of kinks on a screw dislocation showing they may or may not be charged.

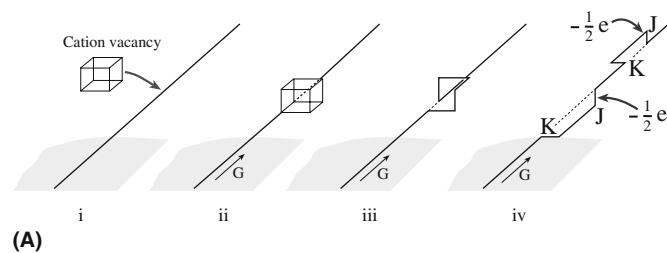
12.8 DISLOCATIONS AND DIFFUSION

Since point defects exert a strain on the surrounding lattice, they will interact with dislocations. It is simplest to consider Figure 12.2a. Large impurity atoms or interstitials will preferentially move toward the dilated part of the core at the edge dislocation while smaller impurity atoms or vacancies will move to the compressive side of the core. Screw dislocations will show no size preference since the strain field is produced by pure shear. However, point defects also produce a local change in the elastic constants (since they change the local bonding), which does cause an interaction with screw dislocations. We might say that some point defects are “hard” while others are “soft.”

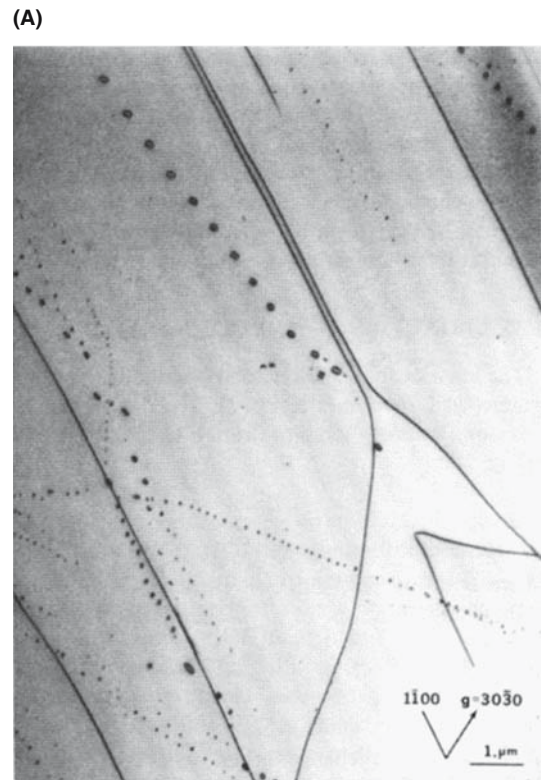
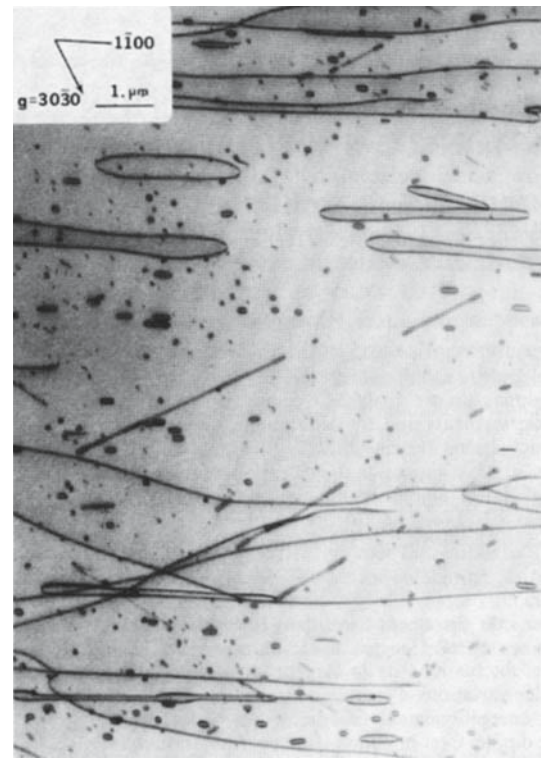
The dislocation core is always a more open region of the crystal. The number of bonds will be lower or there will be preexisting broken bonds. Thus, vacancies, interstitials, and other point defects can move more easily in the dislocation core. This leads to the concept of dislocation pipe diffusion.

Taking the NaCl structure again, if we condense a cation vacancy V'_{Na} on a screw dislocation we can form a pair of kinks and a pair of jogs. Notice that all of these “steps” can glide along the screw dislocation. These steps can then move apart as shown in Figure 12.18a. On this screw dislocation, kinks are neutral but the jogs each carry a charge of $-e/2$ (giving a total charge of $-e$), so this separation is encouraged by the repulsion of like charges. This process is the nucleation of the transformation of a screw dislocation into a dislocation helix; examples of such helices are shown in Figure 12.18b. Such a dislocation will be difficult to move. (What is the glide plane?)

Dislocation pipe diffusion may be quite important in ceramics because there are generally many more point



(B)
FIGURE 12.18 Forming a pair of kinks and a pair of jogs and how this leads to helical dislocations in MgO.



(B)
FIGURE 12.19 Dislocation loops in sapphire.

defects present than found in metals. Although we have very little information on this phenomenon, loop shrinking has been studied in Al_2O_3 . Rows of dislocation loops formed by the break-up of a long loop (dipole) are shown in Figure 12.19.

Movement of neutral atoms can also be enhanced along dislocation cores. For example, if there is a gradient in the oxygen potential, oxygen might move much more rapidly along the dislocation core than through the lattice. Such a process would not require charge balance since the diffusing species is neutral; the point defect is simply using the enhanced distortion at the dislocation core to move more easily: bonds are already broken so they are easier to distort a little more, if necessary.

12.9 MOVEMENT OF DISLOCATIONS

A dislocation can move in its glide plane or on another plane. In the first case the motion is glide; in the second case climb must be involved. We nucleate kinks and jogs in pairs, except at a surface, where we can create them one by one. Pairs of kinks and jogs are shown in Figure 12.20. The dislocations move as the kinks or jogs move apart. The dislocation is usually drawn as a straight line because dislocations in fcc metals should lie along close-packed directions (the Peierls valleys). The kinks step the dislocation line from one valley to the next.

Glide of an edge dislocation occurs when a half-plane of atoms is moved over the atoms below the glide plane. The movement occurs by the nucleation and movement of kinks. Remember that the reason that dislocations are so important in plasticity is because it is easier to move one block of material over another (shear the crystal) one half-plane of atoms at a time. Similarly, it is easier to move a dislocation by moving a kink along it one atom at a time. In fcc metals, the Peierls valleys are not deep, so the energy required to form a kink is small and dislocations bend (create kinks) quite easily.

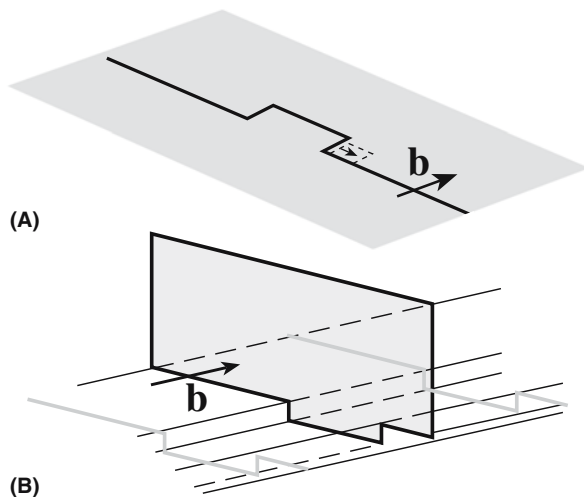


FIGURE 12.20 Schematics of (a) a pair of kinks and (b) a pair of jogs.

Climb is nonconservative motion because vacancies and/or interstitials must be absorbed or emitted (their number is not conserved). When a jog moves, it can either glide or climb. The special point to remember is that the glide plane of a jog is not the same as the glide plane of the dislocation on which it sits. If we force a dislocation jog to move on a plane, which is not its glide plane, it must adsorb or emit point defects, but it can glide. Since it is charged, it carries a current when it glides.

We know that as a general rule, it is more difficult to move dislocations in ceramics than in most metals. In fact, at low temperatures it is often easier to fracture the sample than it is to propagate dislocations. We must then ask the following questions :

- Why do dislocations not move more readily?
- When they move, what is the chosen glide plane?
- Why do they move more readily as T increases?

We know that dislocations in Ge move on $\{111\}$ planes, but they too can also move on $\{001\}$ and $\{011\}$ planes. Is the choice of glide plane due to the Peierls barrier or is it determined by the need to break bonds?

12.10 MULTIPLICATION OF DISLOCATIONS

The concentration of dislocations is conventionally defined as the number of dislocation lines that intersects a unit area. Carefully prepared crystals may contain 10^2 dislocation lines per square centimeter, and some bulk crystals and crystal whiskers have been prepared free, or nearly free, of all dislocations; after plastic deformation the concentration of dislocations increases tremendously, being as high as 10^{10} to 10^{11} dislocations per square centimeter for some heavily deformed metals. (We should not use cm^{-2} units so beware.)

Dislocation multiplication occurs when the dislocations are made to move during deformation. One possible multiplication mechanism is the Frank–Read source. Suppose that a dislocation is pinned at two points, which are a distance l apart, as shown in Figure 12.21a. Under the action of an applied stress the dislocation will bow out. The radius of curvature R is related to the applied shear stress, τ_0 .

$$\tau_0 = \frac{\mu b}{R} \quad (12.10)$$

Increasing the stress further causes the bowing to increase, i.e., R decreases. A minimum value of R is reached that is equal to $l/2$ (a segment of a circle in the isotropic case). As the stress is inversely proportional to R , this minimum

R configuration must correspond to the maximum stress. Consequently, once the dislocation has passed the critical configuration, the half-loop will continue to expand until the two segments, X and Y, meet and annihilate each other forming a complete loop and reforming the pinned dislocation. The complete loop continues to expand and moves away from the source. The pinned dislocation then repeats the process. Figure 12.21b is an experimental observation of such a source in Si; Figure 12.9a showed a related situation in Si in which half-loops had been punched into the sample.

Notice that as a screw dislocation bows, it adds small increments of edge character. The converse is true for bowing edge dislocations. The ease with which either type of dislocation moves depends on the relative energies of the screw and edge components. As you can see from the equations for these energies, the screw dislocation always has the lower energy in an isotropic material, so bowing a screw dislocation is harder than bowing

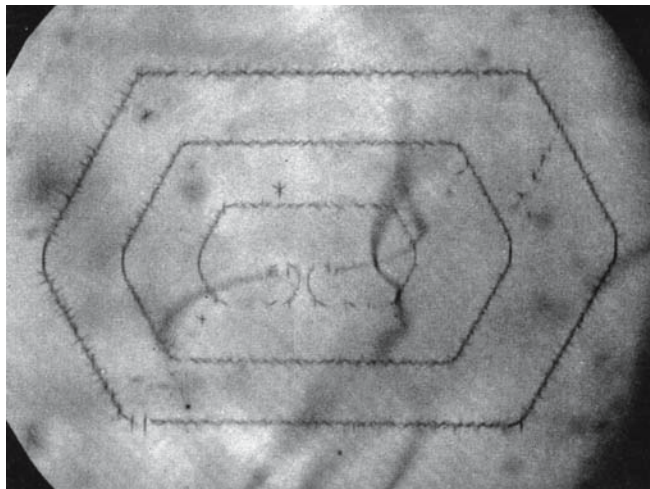
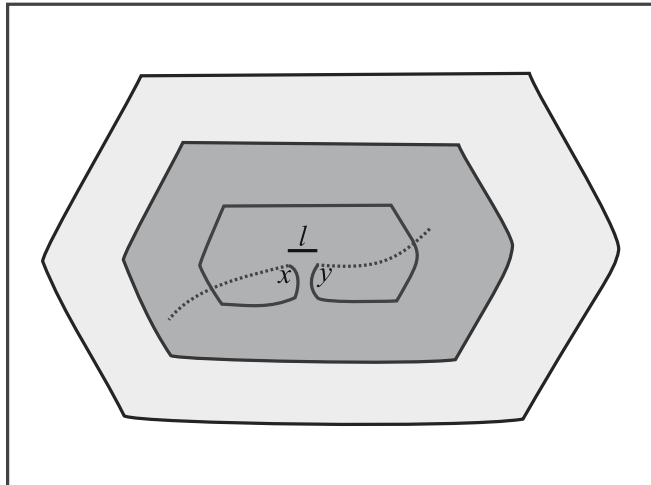
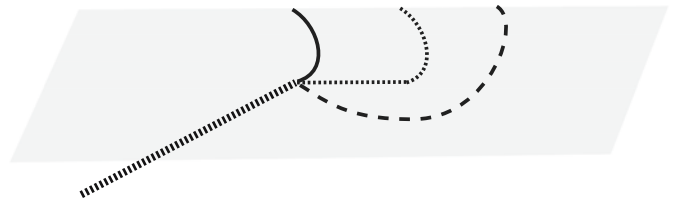
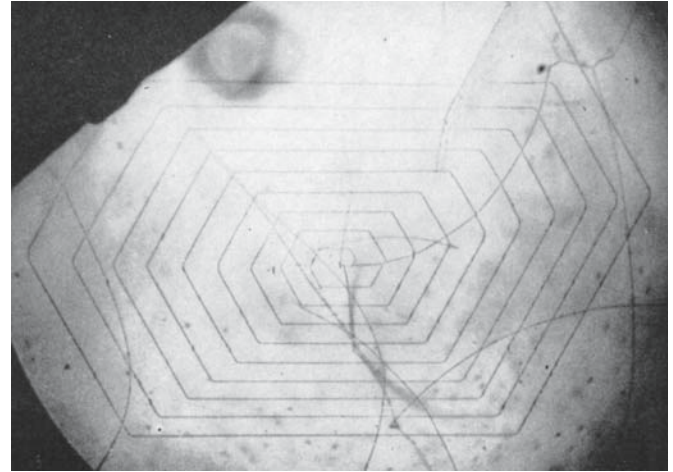


FIGURE 12.21 Schematic and IR image of a Frank–Read dislocation source in Si.



(A)



(B)

FIGURE 12.22 Schematic and IR image of a single-ended Frank–Read source in Si.

an edge dislocation. Dash illustrated the Frank–Read source in Si. Low-temperature deformation of Si causes straight dislocations because they lie along the Peierls valley. Another glide source that has been observed is the single-ended dislocation source. You can visualize this “mill” by removing half the Frank–Read source as shown schematically in Figure 12.22. In crystal growth, dislocations are often generated at the neck of the growing crystal; this is a highly stressed region and dislocations glide more easily at high temperatures used for growth. So the dislocation source will be close to the surface.

The Nabarro–Herring source is very similar to the Frank–Read source, but the dislocations move by climb instead of glide.

12.11 DISLOCATION INTERACTIONS

Interactions and Motion

When dislocations moving on inclined glide planes intersect one another they form nodes and locks. After the intersection is complete they will have created jogs or kinks in the other dislocation. The intersection process can instead result in the two dislocations knitting together to form part of a dislocation tangle; the

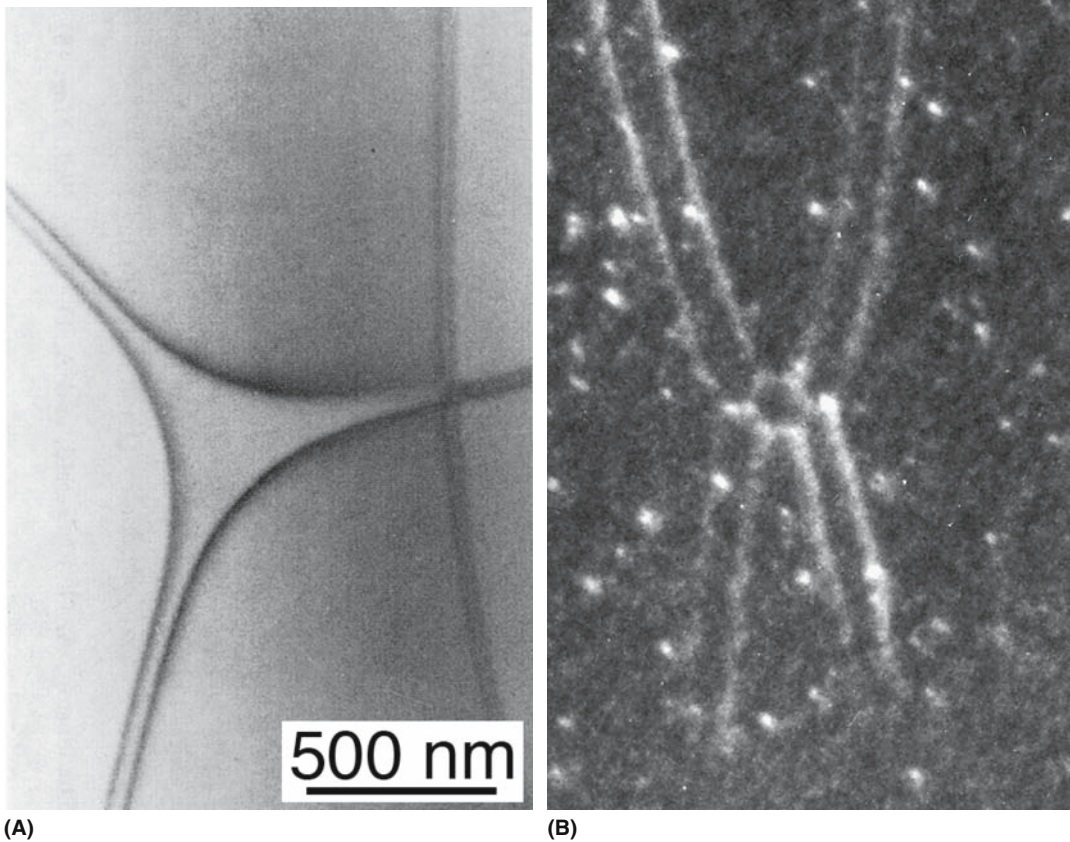


FIGURE 12.23 Dislocation nodes in (a) AlN; (b) spinel.

product dislocation may have a glide plane that is not a favored glide plane for that structure. The Lomer-Cottrell dislocation in fcc metals is an example of such a less mobile dislocation. It is referred to as a lock or barrier because it stops the interacting dislocations from moving and impedes the movement of other gliding dislocations.

Dipoles

Dipoles are commonly seen in MgO and Al₂O₃. They may form by dislocations trapping one another or they may be pulled out by a moving dislocation that is pinned somewhere along its length. If the temperature is high enough, they anneal out as they form. We can learn a little about local diffusion by carefully annealing samples containing dipoles (Figure 12.19). Consider how a dipole is annihilated and how this process is different in metals. To annihilate a dipole in MgO, we must add or remove ions on both sublattices. In metal alloys these different atoms can sit on the other lattice giving an antisite defect. This exchange is unlikely in ceramics because of the charge. It can, however, occur in compound semiconductors, which we sometimes think of as ordered covalently bonded alloys.

Nodes

Dislocation nodes occur when any three dislocations meet, when one dislocation divides into two, or when two dislocations join to form one. Nodes are quite common. The example in Figure 12.23 shows a node in AlN; Figure 12.14 showed nodes in graphite. Observations of such defects can give a measure of the stacking-fault energy so that we can, in principle, learn something about bonding in such materials. The catch is that the stacking-fault energy may be significantly lowered by segregation of impurities because the structure of the material is different at the SF. More interesting in ceramics are nodes where climb-dissociated dislocations meet. Consider the node in spinel shown in Figure 12.23b: this is a special defect because it is also the junction of three noncoplanar SFs.

Walls and Networks

We will discuss walls and networks in more detail when we talk about interfaces. We can arrange an array of dislocations to form a wall or grain boundary. Arrays of dislocations are essentially two-dimensional defects, i.e., the dislocations knit together to form a network. The dislocation array in Figure 12.14 is actually a network.

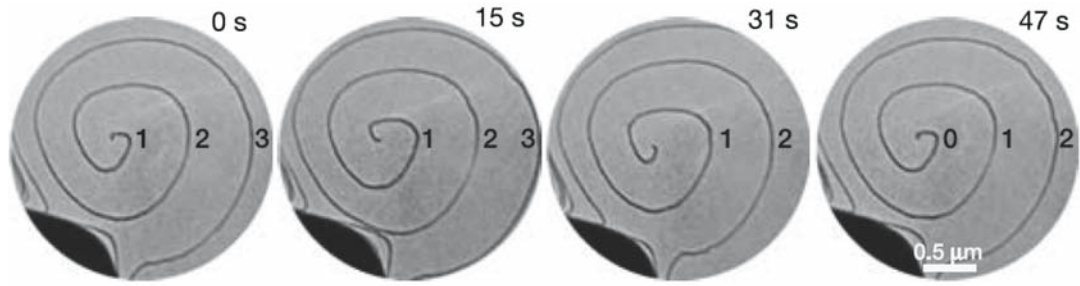


FIGURE 12.24 Dislocation in TiN intersecting the surface causing a spiraling step.

12.12 AT THE SURFACE

Dislocations cannot end inside the crystal, but they can end at a surface as we saw in Figure 12.9 where they were revealed by chemical etching. They can also be revealed by thermal etching, which is particularly important since it can provide insight into how the reverse process, namely crystal growth, occurs. Figure 12.24 shows a dislocation emerging at the surface of a TiN crystal. Notice two points: (1) if this interpretation is correct, then if you bonded an atomically flat surface to the surface imaged here, you would form a single-ended Frank–Read source; (2) we cannot be sure about the Burgers vector because such atomic force microscopy (AFM) images do not tell us about the component of \mathbf{b} parallel to the surface. Note that dislocations producing spirals such as shown here are not necessarily screw in character even though you will often see them referred to as such (even in some of the classic papers). All that is needed is that a component of the dislocation’s Burgers vector is inclined to the surface you are examining; you have to know where the disloca-

tion line is relative to its Burgers vector to be able to say that it has screw character; it could be a pure edge dislocation!

12.13 INDENTATION, SCRATCHING, AND CRACKS

Crack tips are line defects, but may resemble disclinations more than dislocations if the sides of the crack are inclined to one another rather than parallel. The differences are significant: deformation at the crack tip may be very large leading to the generation of dislocations in the plastically deformed region even in brittle ceramics. If this plastic deformation is large, it actually blunts the crack tip and toughens the ceramic.

Dislocations also form when we indent ceramics and are particularly important for nanoindentation studies (Figure 12.25). The reason cracking during indentation is different is that the sample is much more constrained. Cracks also form under the indenter tip itself and may dominate as the process continues, but to see the crack you usually remove the load, which allows it to heal. We can actually use indentation techniques to study the nucleation of dislocations. Again, in the nanoregime we have the additional advantage that computer modeling can be used for samples of similar dimensions. Scratching is essentially a moving indentation test, but is not as well controlled; in ceramics, it is the basis of the Mohs test. As shown in Figure 12.26, dislocations are emitted from the

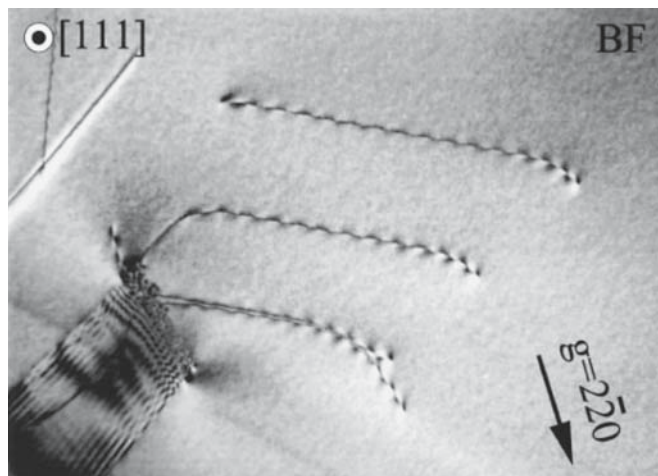


FIGURE 12.25 Dislocations being emitted at a crack tip in Si.

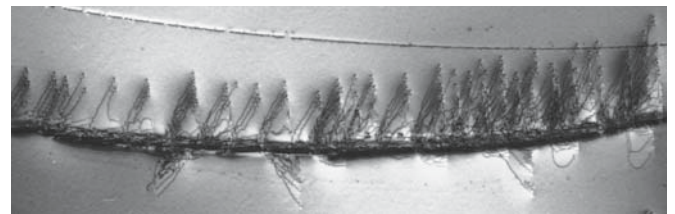


FIGURE 12.26 Dislocations produced by scratching Al_2O_3 .

region under the indenter and for low temperature tests will tend to move out on glide planes (since there are no mobile point defects). This deformation thus provides a method for studying the movement of dislocations in ceramics at room temperature.

12.14 DISLOCATIONS WITH DIFFERENT CORES

Frank predicted the existence of coreless dislocations long before they were unambiguously observed. The idea is that the surface energy associated with a hollow tube may be less than the strain energy associated with a large Burgers vector. Of course, you have to form this large- b dislocation first. Observations of coreless dislocations have been

reported in SiC and GaN; an example is shown in Figure 12.27. In each case, the dislocation is a growth defect, not a deformation defect. Coreless dislocations can, in principle, also occur in materials that are not ceramics, but observations of dislocations in metals tend to concentrate on deformation where such cores are unlikely to occur.

Dislocations can also act as sites for local amorphization of a ceramic because the bonds are already distorted at the core. This is a case of a phase transformation being initiated at a dislocation. An example of this occurring in quartz during electron irradiation is shown in Figure 12.28. The dislocation appears to become much broader, but it actually becomes a tube of amorphous material (not unrelated to the coreless dislocation). It would be very difficult for such a dislocation to move since the core would need to recrystallize.

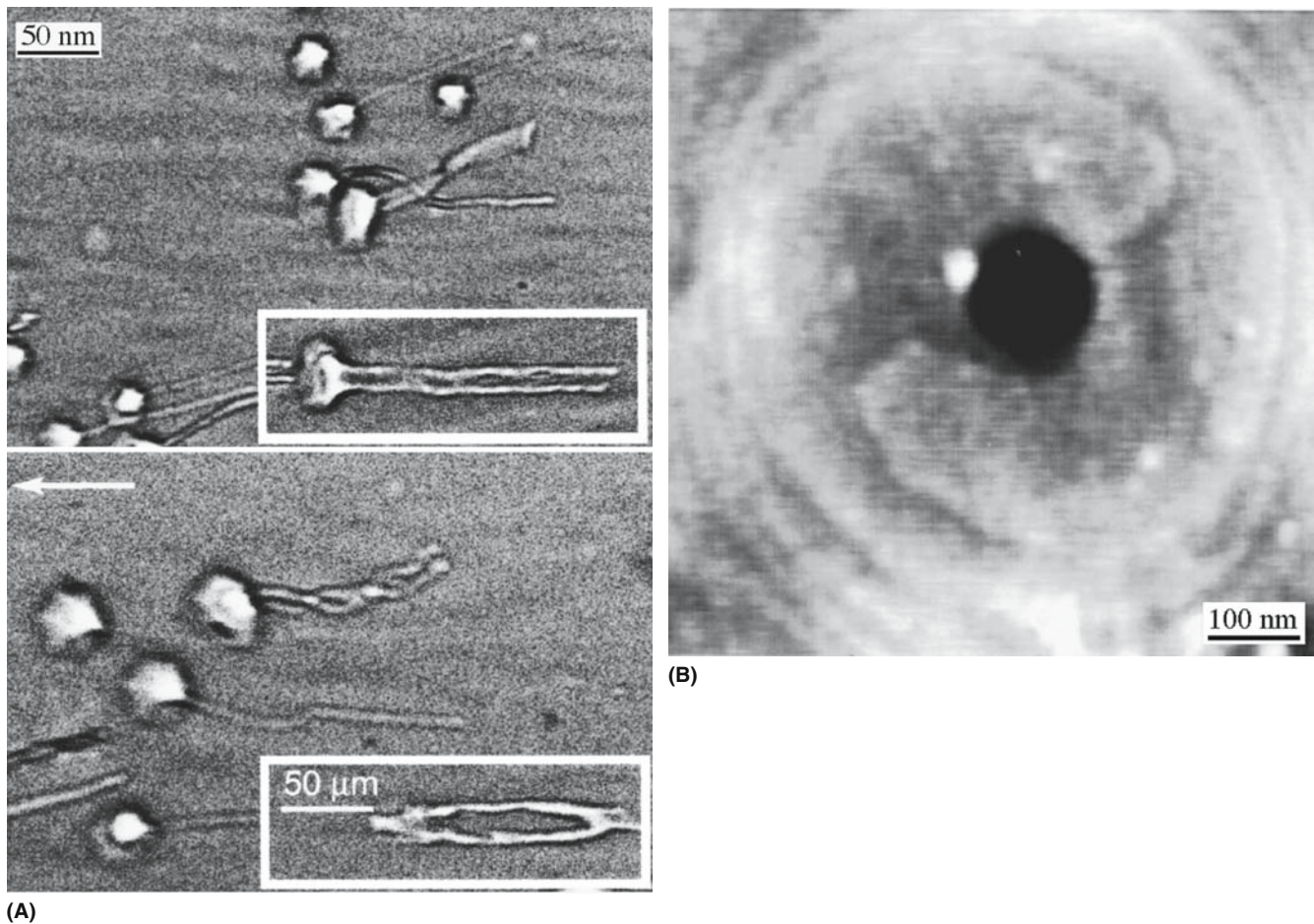


FIGURE 12.27 Coreless dislocations in (a) SiC (side view) and (b) GaN (end-on view).

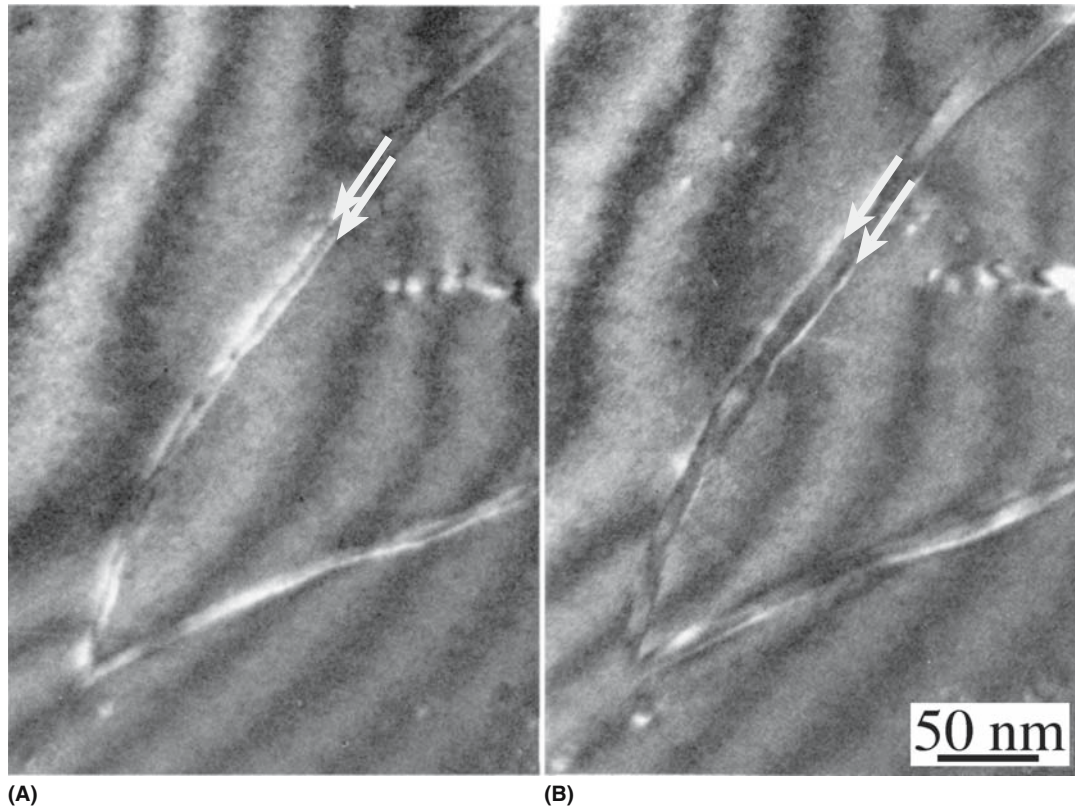


FIGURE 12.28 Amorphization of a dislocation core in quartz during observation in the TEM.

CHAPTER SUMMARY

Dislocations are often most important in ceramic materials for what they do not do: they do not usually move very easily unless the temperature is very high. Dislocations can be used as local probes, for example, when we look at loop annealing to learn about pipe diffusion versus bulk diffusion. It is important to understand dislocations if we want to understand structured interfaces, whether grain boundaries or phase boundaries, since these often consist of arrays of dislocations (or even dislocated arrays of dislocations). When materials are used for electronic applications, dislocations become quite common because these materials are often produced by epilayer growth. The discovery of the light-emitting properties of GaN suddenly made all the work on dislocations and interfaces in AlN relevant again.

The most important points to remember is that there are two key parameters: the Burgers vector and the line direction. After this you need the crystal elasticity parameters and the lattice parameters. The rest follows, with the only complications being charge and directional bonding.

PEOPLE IN HISTORY

Burgers, Johannes (Jan) Martinus (1895–1981), the brother of crystallographer W.G. Burgers, introduced the Burgers vector in 1939; his work was mainly on fluid dynamics.

Frank, Sir Charles (1911–1998) was born in Durban, South Africa (knighted 1977). He obtained his degrees from the University of Oxford. During World War II he worked for the Chemical Warfare Establishment at Porton Down and then for the scientific intelligence group at the Air Ministry. He moved to work on physics at the University of Bristol in 1946; he retired from Bristol in 1976, but remained active and shared a partitioned office with CBC in 1985/1986. In addition to dislocations, his interests included crystal growth, liquid crystals, nuclear physics, and even polymers.

Hooke, Robert (b. 1635 Isle of Wight; d.1703 London) proposed the elasticity theory. He also coined the term *cell* in his book *Micrographia* (1665) and much more; he feuded with Newton.

Peierls, Sir Rudolf Ernst (1907–1995) helped a colleague (Orowan) solve some “simple” math. The result is the Peierls valley and the Peierls–Nabarro force. Peierls was also part of the British contingent of the Manhattan Project.

Volterra, Vito (1860–1940) was born in Ancona, Papal States (now Italy). He began working in mathematics at age 11, obtained a Doctor of Physics degree in 1882, and was then Professor of Mechanics and then Chair of Mathematical Physics. During World War I Volterra was in the Air Force and returned to Rome after the war. He denounced fascism and left Italy to live mainly in Paris. Some say his most famous work was on integral equations.

GENERAL REFERENCES

Amelinckx, S. (1964) “The direct observation of dislocations,” *Solid State Phys.* Suppl. 6. One of the best “papers” ever written on the subject.

Hirth, J.P. and Lothe, J. (1982) *Theory of Dislocations*, 2nd edition, Wiley, New York. One of the two standard works on the subject. Inspirational. Professor Hirth retired from Washington State University in 2003.

Hull, D. and Bacon, D.J. (1984) *Introduction to Dislocations*, 3rd edition, Pergamon Press, Oxford. Bedtime reading for the materials scientist.

Nabarro, F.R.N. (1987) *Theory of Crystal Dislocations*, Dover Publications, New York. This was first published by the Clarendon Press (Oxford University Press) in 1967. The other standard work by one of the founders of dislocation theory. Professor Nabarro also edited the series Dislocations.

Weertman, J. and Weertman, J.R. (1992) *Elementary Dislocation Theory*, Oxford University Press, New York. Similar to H&B but with more equations and no micrographs.

SPECIFIC REFERENCES

Amelinckx, S., Bontinck, W., and Dekeyser, W. (1957) “Helical dislocations and spiral etch-pits,” *Philos. Mag.* **2**, 1264.

Carter, C.B. and Kohlstedt, D.L. (1981) “Electron irradiation damage in natural quartz grains,” *Phys. Chem. Minerals* **7**, 110.

Hornstra, J. (1960) “Dislocations, stacking faults and twins in the spinel structure,” *J. Phys. Chem. Sol.* **15**, 311.

Kodambaka, S., Khare, S.V., Swiech, W., Ohmori, K., Petrov, I., and Greene, J.E. (2004) “Dislocation-driven surface dynamics on solids,” *Nature* **429**, 49.

Kronberg M.L. (1957) “Plastic deformation of single crystals of sapphire—basal slip and twinning,” *Acta Metal.* **5**, 507.

Lee, W.E. and Lagerlof, K.P.D. (1985) “Structural and electron-diffraction data for sapphire ($\alpha\text{-Al}_2\text{O}_3$),” *J. Electron. Microsc. Techn.* **2**, 247.

Narayan, J. (1972) “Self-climb of dislocation loops in magnesium-oxide,” *Philos. Mag.* **26**, 1179.

Rabier, J. and Puls, M.P. (1989) “On the core structures of edge dislocations in NaCl and MgO. Consequences for the core configurations of dislocation dipoles,” *Philos. Mag. A* **59**(4), 821.

Ray, I.L.F. and Cockayne, D.J.H. (1971) “The dissociation of dislocations in silicon,” *Proc. R. Soc. Lond. A* **325**, 543.

Washburn, J., Kelly, A., and Williamson, G.K. (1960) “Direct observations of dislocations in magnesium oxide,” *Philos. Mag.* **5**, 192.

Weertman, J. (1957) “Helical dislocations,” *Phys. Rev.* **107**(5), 1259.

EXERCISES

- 12.1 What is the shortest perfect-dislocation Burgers vectors in the following materials: (i) CsCl, (ii) NiO, (iii) fluorite, (iv) BaTiO₃, (v) CZ, (vi) YAG, (vii) β -cristobalite, and (viii) GaAs.
- 12.2 What are the two shortest (crystallographically different) perfect-dislocation Burgers vectors in the following materials: (i) alumina, (ii) graphite, and (iii) MoS₂.
- 12.3 What are the three shortest (crystallographically different) perfect-dislocation Burgers vectors in the following materials: (i) olivine, (ii) wurzite, and (iii) YBCO.
- 12.4 Draw an end-on diagram for a perfect edge dislocation in PbS having a (001) glide plane. Label b and show its direction with an arrow.
- 12.5 Draw an end-on diagram for a perfect edge dislocation in NaCl having a (110) glide plane. Label b and show its direction with an arrow.
- 12.6 Consider a climb-dissociated $\frac{1}{2}[110]$ edge dislocation in spinel. Draw a model for the atomistic structure.
- 12.7 How can 1 cm² of MgO have a dislocation density of 10⁶ yet only contain one dislocation.

- 12.8 If 1 cm^2 of NiO contains one screw dislocation that is 2 cm long, how many distinct planes does the crystal contain?
- 12.9 A jogged edge dislocation in LiF lies parallel to the (110) surface, which is perpendicular to its Burgers vector. The dislocation contains a series of unit jogs, each with the same sign, spaced every 50 nm along its length. A stress is applied that makes the dislocation glide from the center side of a 1-mm cube until it exits the crystal. Assuming that the dislocation initially always lies parallel to the initial surface, estimate the current that flows across the sample.
- 12.10 Examine Figure 12.21. Estimate the stress required to make this mill operate. Explain all the assumptions and deductions you make—there will be many.

Surfaces, Nanoparticles, and Foams

CHAPTER PREVIEW

This chapter is the first of a three-part series on interfaces. We are dividing the discussion only to make it manageable. An interface is a planar region separating two domains or materials. Hence we have the definition of a surface as the region that separates a solid or liquid from a gas or vacuum. The word “region” is used to make it clear from the beginning that the surface has a thickness; it is not the mathematical definition. Powder processing is the traditional route for forming ceramics; in powders the ratio of surface area to volume is large. With nanoparticle powders, the ratio can be huge.

We will first discuss two important questions concerning surfaces.

- What do we mean by the word surface?
- Why are surfaces so important for ceramics?

We will then consider, from several viewpoints, the two most important properties of surfaces.

- The energy associated with a curved surface is greater than for a flat surface.
- We add material to the bulk solid by attaching it to the surface.

As always, we keep in mind the following question: what is special about ceramics?

13.1 BACKGROUND TO SURFACES

A surface is just the interface between a solid (or liquid) and a gas or vacuum. In general, the surface of a material, or any interface between materials, is a region of excess energy relative to the bulk or matrix. To maintain the lowest total energy for the system, the configuration of the surface adapts itself to minimize this excess energy. Impurities or dopants that lower the surface energy tend to concentrate in the surface. Similarly, such *defects* will move to the interface if by segregating there they lower the overall energy of the system even if it raises the interfacial energy. The surface will tend to orient parallel to certain crystallographic planes that have a lower energy.

The surface energy can be intentionally lowered using a wetting agent or a (liquid or solid) surfactant. For example, the interfacial energy of liquid Ni in contact with Al_2O_3 can be changed by the presence of Ti at the surface. The Ti is strongly attracted to the oxide interface because of its high chemical reactivity with oxygen. This type of interaction is so common that a major problem in studying ceramic surfaces is to know if the surface is clean. During

all ceramic processing we can assume that the surface is not perfectly clean.

Throughout our discussion of ceramic surfaces, we are concerned with four interrelated concepts; these are energy, formation, movement, and charge. As usual, only the final one, charge, is particular to ceramics.

- The energy of any surface depends on many factors, including the material and structure (crystalline or not), and if crystalline, the crystallography and plane. We will discuss how to measure this parameter.
- Formation will occur only if energetically favorable. We need to discuss the relevance of Wulff plots to understand surfaces.
- Movement can occur if this does not increase the total energy or if it minimizes this increase.
- Charge distribution, and thus the bonding, will be different at a surface. Charge must influence the value of the surface energy, but it is almost an unknown factor.

Many features of surfaces, and interfaces in general, are similar in all materials.

- A pressure difference is always present across a curved surface (thermodynamics).
- The structure of surfaces can relax from the bulk-terminated configuration (physics).
- Surfaces can be wetted by a thin layer of impurity or a second phase (energetics).
- The ionicity or covalency and crystallography can affect surfaces (chemistry).

SURFACES OF MINERALS

Interactions of minerals with the environment are important in decreasing contamination and waste management. This is sometimes referred to as the field of environmental mineralogy. Topics include microbial interactions with minerals, anthropogenic influences, contaminated land, and waste management.

So to answer what is special we need to summarize the features that are common to all materials first. Then we can ask: what is different in comparison to metals? Ionic materials and covalent materials (e.g., Si, Ge,

GaAs) both have local charge variations. The directional bonding of the covalent materials means that they can have “unsatisfied” bonds; these are known as dangling bonds. We have encountered these before in discussing dislocations.

Surfaces and their interaction with impurities and particles are being extensively modeled using the computer. Some researchers might say that computer modeling might be the only method for studying clean surfaces.

13.2 CERAMIC SURFACES

The surface is particularly important for ceramics because we are often using powders at some stage of processing: the surface area-to-volume ratio is larger for powders than bulk materials. Many uses of ceramics rely on their inertness or reactivity, but nanoparticles of “inert” ceramics can be very reactive, partly because of this enhanced ratio. Failure of a ceramic usually occurs first at the surface. Catalysis is enabled at the surface. Sintering, perhaps the most important processing route for ceramic materials, is the process of joining two surfaces together. Remember during this discussion that in the thermodynamic analysis of surfaces, surface energy and surface tension are properties of the continuum. Surface tension is usually assumed to be synonymous with surface energy, but this is not necessarily so. We must consider how to relate these continuum parameters to the atomic structure.

- Surface steps: when we need to consider the atomistics. Special surface sites influence the energy of surfaces.
- Composition: is the surface clean? If it is clean, does it have the bulk-terminated structure or has it relaxed?

So what is special about surfaces of ceramics? We have to think about surface structure otherwise we will not appreciate what is special.

- The charge and covalent bonds: charge cannot necessarily be redistributed.
- Surface energy tends to be much more dependent on the plane in ceramics.
- These two points are probably not independent.

Because the properties of interfaces vary so much, the morphology of interfaces in real ceramics may be unusual.

13.3 SURFACE ENERGY

Surface energy is clearly a very important quantity. It is almost never well known if it is *known* at all. There are two important questions that we need to answer about surface energy:

- How do we define the energy of a surface?
- What factors determine the surface energy?

The easiest way to define surface energy is to start with a liquid (it could, for example, be a molten ceramic) and imagine that it is suspended in a wire frame. One bar of the frame is movable and allows us to increase the surface area by an amount dA . The force that we have to apply must be sufficient to overcome the opposing surface tension, γ . The work done, dw , in increasing the surface area is

$$dw = -\gamma dA \quad (13.1)$$

The term “tension” is a little confusing when we consider solids because it implies that there is an associated stress. With our example of a liquid in a metal frame we are actually stretching the surface and the atoms in the liquid are moving from the bulk to the surface to increase the surface area. We could not imagine doing the same thing with a solid except perhaps close to the melting temperature. In solids we regard γ as the energy required to form the surface. It is important to note that the surface energy is not usually equal to the surface stress, the work required to deform the surface, though we often assume it is. For a liquid they are equal.

From the combined statement of the first and second laws of thermodynamics we can write that the change in internal energy, dE , is

$$dE = TdS - PdV + \gamma dA + \sum \mu_i dn_i \quad (13.2)$$

We can then define the surface energy as

TABLE 13.1 Surface Energies of Various Materials in Vacuum or Inert Atmospheres

Material	Temperature (°C)	Energy (mJ/m ²)
Water	Liquid	26
Cu	Liquid	1120
Ag	Liquid	1000
Alumina	Liquid	2080
Cu	Solid	1080
Ag	Solid	750
Alumina	Solid	1850
(100) NaCl	Solid	25
MgO	Solid	25

$$\gamma = \left(\frac{\partial E}{\partial A} \right)_{S,V,n_i} \quad (13.3)$$

A similar expression involving the Gibbs free energy can be written:

$$dG = -SdT + VdP + \gamma dA + \sum \mu_i dn_i \quad (13.4a)$$

And the surface energy is written as

$$\gamma = \left(\frac{\partial G}{\partial A} \right)_{P,T,n_i} \quad (13.4b)$$

Some examples of surface energies are given in Table 13.1. The range of values is quite large. Even if we compare only the values for solids you can see that for NaCl $\gamma = 300 \text{ mJ/m}^2$; it is three times greater for MgO (think about the charge). As a general rule, the surface energy decreases as the temperature increases (Eötvös rule). The surface energy of a liquid is lower than that of the corresponding solid. For example, we can compare values for Al₂O₃:

- Al₂O₃(solid) $\gamma = 905 \text{ mJ/m}^2$
- Al₂O₃(liquid) $\gamma = 700 \text{ mJ/m}^2$

In general, you should be very wary when given precise values for surface energies.

Approximation of Surface Energies

The surface energy of a solid depends on its crystal structure and orientation and can be estimated by a simple calculation. First we assume that the binding energy of an atom is the result of bonds to its nearest neighbors. The energy, ϵ , of one bond is then

$$\epsilon = \frac{\Delta H_s}{0.5ZN_A} \quad (13.5)$$

ΔH_s is the molar enthalpy of sublimation (the energy to break all the bonds), Z is the coordination number, and N_A is the Avogadro number.

The work, w , required to form a surface, for example, if we cleave a crystal, is going to depend on the number of bonds, x , per atom that we break (so x depends on the cleavage plane).

$$w = \frac{x}{2} \epsilon = \frac{x\Delta H_s}{ZN_A} \quad (13.6)$$

The surface energy, γ , is then

$$\gamma = \frac{x\Delta H_s}{ZN_A} \left(\frac{N}{A} \right) \quad (13.7)$$

The term (N/A) is the number of atoms per unit surface area. You can see from Table 13.1 that this approach gives only a very approximate (but not unreasonable) result, although it looks very precise. The reason is that second-nearest neighbors are not considered in the calculation (these are, of course, extremely important in ionic crystals) and it is also assumed that the strengths of the remaining surface bonds are the same as the bulk values. The calculation also does not consider charge—an important consideration for ionic ceramics! Estimated values for metals compare much more closely to the experimental values. (The calculation for Cu is given, for example, by Ragone, 1995.) What calculations using Eq. 13.7 do show us is that γ varies with the crystal structure and surface orientation. The practical application of these differences is evident when we try to etch materials using acids. Different planes etch at different rates. The chemical etch rates for Ge on the (100), (110), and (111) planes are 1.00, 0.89, and 0.62, respectively.

The implication is that the (100) plane of Ge has a higher energy than either the (110) or (111) planes. The importance is that often when we try to etch a semiconductor we want to produce a smooth surface rather than a faceted one—unless we want to make V-MOS devices.

CALCULATING A SURFACE ENERGY

We can estimate the value of γ for the (100) face of NaCl. Take $x = 1$. $\Delta H_s = 235,000 \text{ J/mol}$ (value for NaCl from Kubaschewski and Alcock, 1979). For NaCl, $Z = 6$.

$$N_A = 6.022 \times 10^{23} \text{ mol}^{-1}$$

$$(N/A) = 1.26 \times 10^{19} \text{ m}^{-2}$$

$$(a_{\text{NaCl}} = 0.5640 \text{ nm})$$

This gives $\gamma = 0.82 \text{ J/m}^2$

Effect of Structure and Orientation

The surface energy, γ , depends on the structure, which depends on the orientation. We have developed two approaches for considering this orientation dependence: the Wulff plot and the inverse Wulff plot.

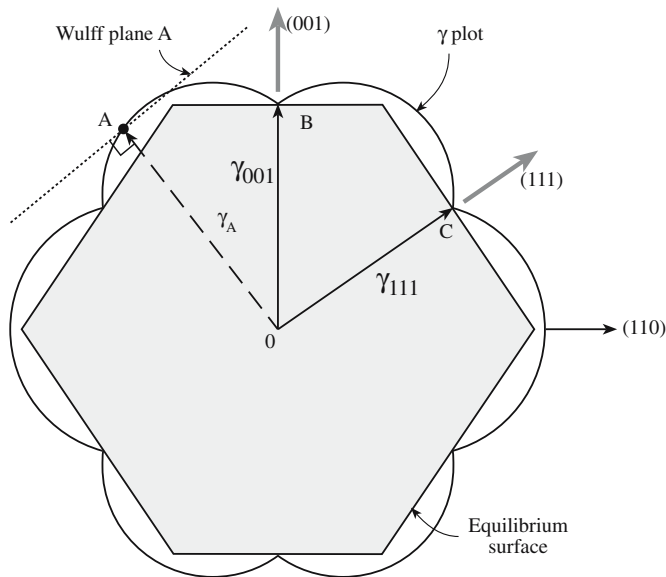


FIGURE 13.1 Wulff plot looking along the $[1\bar{1}0]$ direction for an fcc crystal.

- The Wulff plot draws a graph of γ versus θ . This construction was developed to allow the equilibrium shape of crystals to be determined when the surface energy depends on crystallography.
- The inverse Wulff plot shows $1/\gamma$ as a function of θ .

The Wulff plot is the conventional plot for surfaces; an example of such a plot is shown in Figure 13.1. The most important point is that you have cusps in γ versus θ . In ceramics, this certainly occurs; if the energy were isotropic, the Wulff plot would be a circle. What is not certain is how many cusps you have. It is instructive to compare surfaces with grain boundaries (section 14.3). In the latter case it is necessary to define the orientation of the grain-boundary plane, i.e., having fixed θ , you must still fix \mathbf{n} , the normal to both grains.

Experimentally we can determine the equilibrium shapes of crystals by annealing small single crystal particles at high temperature in an inert atmosphere or by annealing small voids (inverse particles) in a crystal.

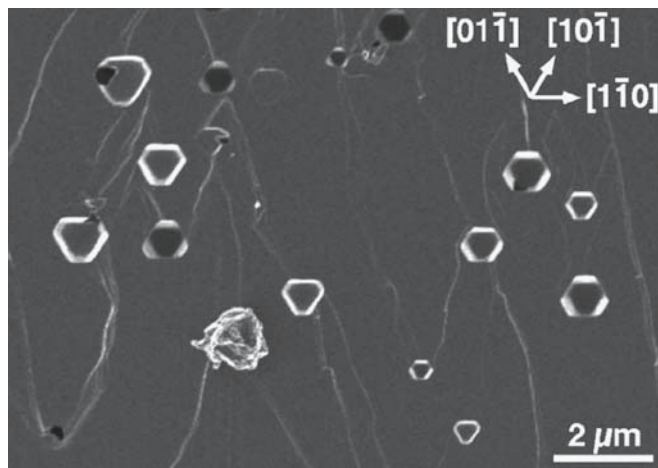


FIGURE 13.2 Faceting of small voids in UO_2 .

Figure 13.2 shows an example of a bulk UO_2 sample that has been heat treated so that the pores achieved a near equilibrium shape. The length of the facets in the small void can be used to determine the relative energies of (100) and (110) planes.

13.4 SURFACE STRUCTURE

We will illustrate some special surfaces using a series of figures. In continuum models of surfaces the surface is a smooth curve; at the atomic level, it is always faceted. A terminology for the different surfaces is summarized in Figure 13.3. The surface can form large flat facets (F) that are really facets on two planes separated by a ridge (S) and surfaces that are not atomically smooth at all (K). Beware of the bias that carries over from metals, such as the picture that crystals are built by stacking cubes or that all ions are hard sphere. Ions can relax into the surface (relative to their bulk positions) and this relaxation depends on the crystallography of the surface. The relaxations will also be different at steps on the surface.

Flat surfaces. The surface of a spinel crystal with an emerging dislocation is shown in Figure 13.4. The reason for choosing Figure 13.4 is that it shows a ceramic surface that is atomically flat parallel to the step in this figure for a distance over $10\ \mu\text{m}$. Step heights can be multiples of a unit value. When the unit cell is large, the definition of an atomically flat surface is less clear. For example, the surface of a zeolite is important in processing, but the surface and near-surface pores are connected: the surface area is much greater than the geometric area of the surface. (Remember the idea of the Möbius strip!)

Rumpled surfaces. The term *rumpled* refers to the local undulations on the surface. The rumpled surface is *crystallographically* flat, but local displacement of the ions means that it is not *geometrically* flat. The difference between relaxation and rumpling is that the term relax-

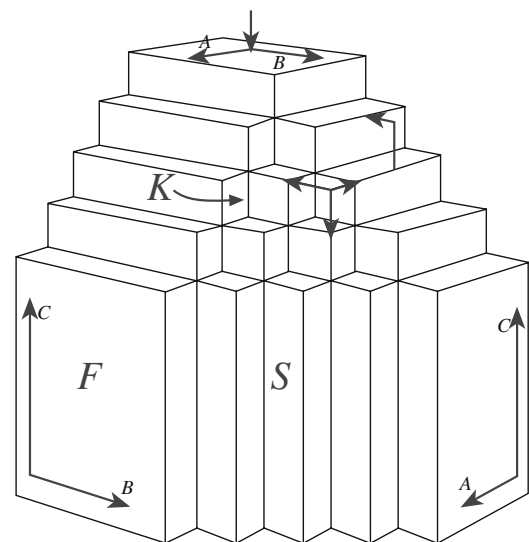
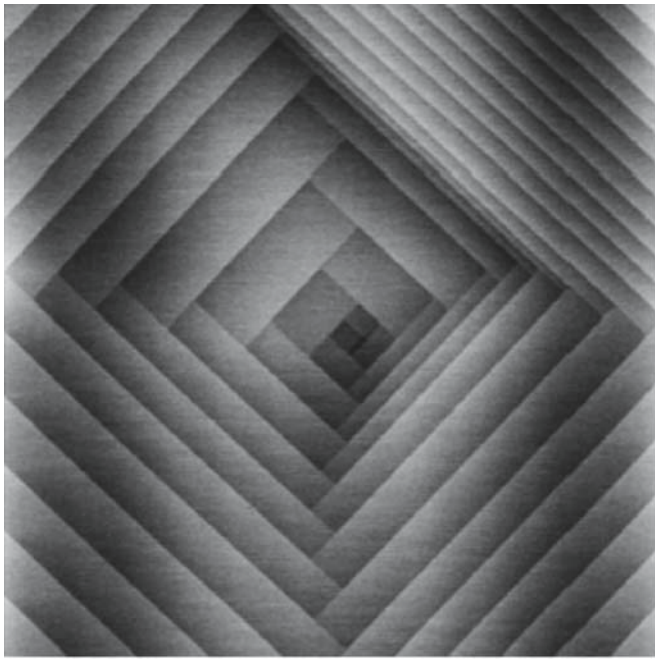
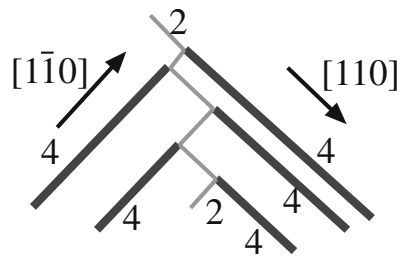


FIGURE 13.3 Terminology for facets, steps, and kinks on surfaces.



(A)



(B)

FIGURE 13.4 A faceted shallow thermal etch pit on the (001) surface of spinel. 2 and 4 refer to the height of the steps (0.2 nm and 0.4 nm).

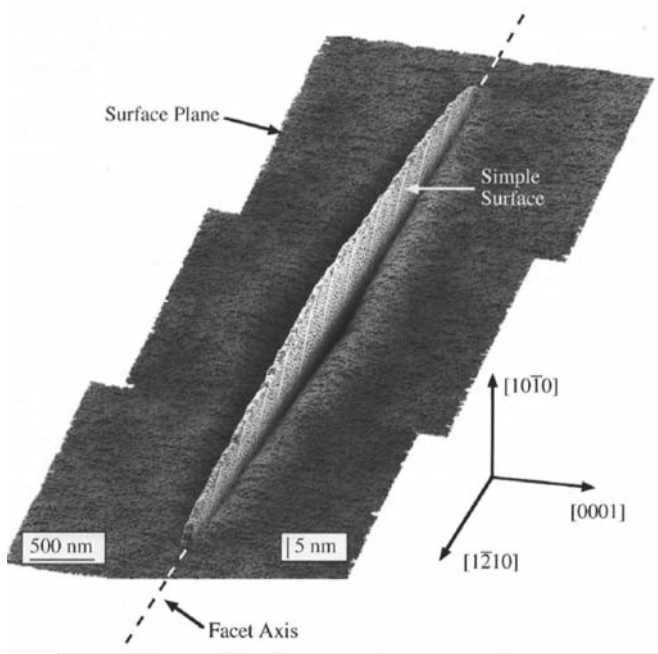
ation refers to the average change in the spacing of the plane nearest to the surface and the second plane when compared to the bulk value; rumpling, on the other hand, refers to the displacement of the cation layer relative to the anion layer in a direction normal to the surface.

If an initially flat surface is not in its lowest-energy configuration, then it will **facet** when heated to a high enough temperature. You can envision how this process can occur by considering Figure 13.5. The surface is initially flat; if no extra material is added then a trench must

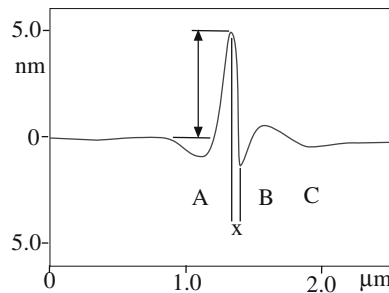
form if a ridge forms. Facet growth thus involves surface diffusion normal to the *geometric* surface.

We might say that the surfaces of **nanoparticles** are their most important feature since this determines all their properties. As is clear from Figure 13.6, the facet junctions on nanoparticles are also much more prominent.

The **chemistry** of surfaces can be very different from the bulk material. Clearly the bonding is different on the surface. On oxides, in particular, OH groups may be present even if you think the environment is dry. Detect-

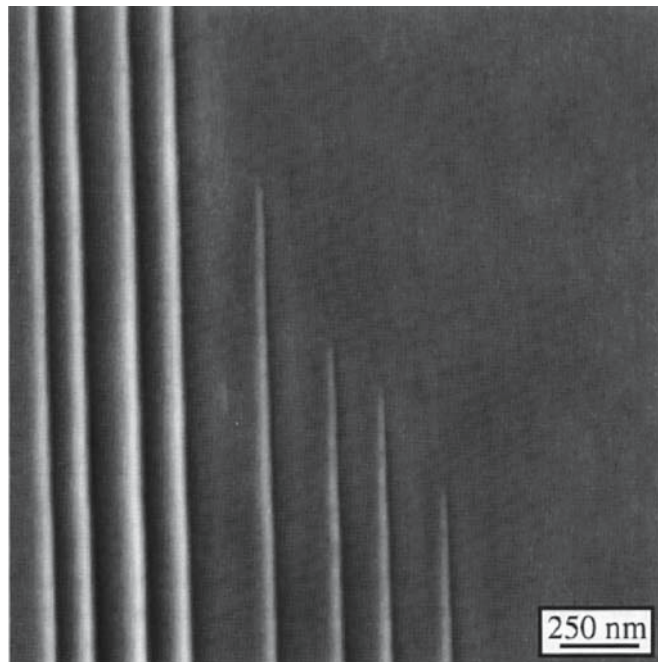


(A)

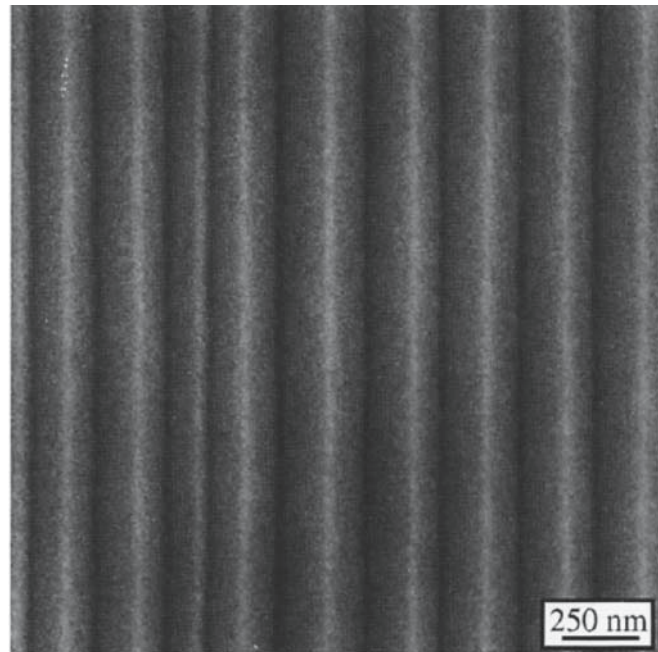


(B)

FIGURE 13.5 The initiation of faceting on the m plane of sapphire.



(C)

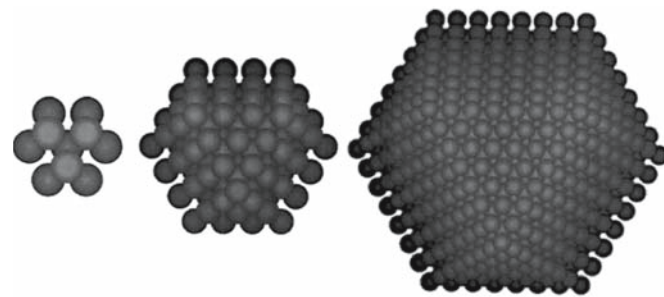


(D)

FIGURE 13.5 Continued

ing hydrogen in or on a material is tricky. Such hydrated surfaces behave differently and the surface energy can differ from that of the dry surface.

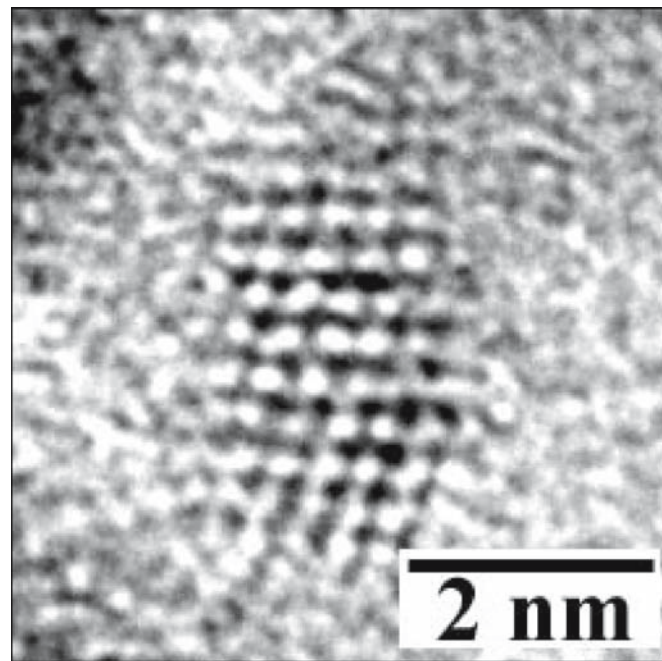
One special feature of ceramic surfaces is the result of covalent and ionic bonding. Ceramics have charges and charge dipoles; these charges are often uncompensated at the surface, at least on the short range as illustrated in Figure 13.7.



(A)

(B)

(C)



(D)

FIGURE 13.6 Illustrating the fraction of atoms sitting at the surface of a nanoparticle. (a) Ten atoms, all on the surface; (b) 92 atoms with 74 on surfaces (80%); (c) 792 atoms with 394 on surfaces (50%). (d) An HRTEM image of a faceted nanoparticle of CdSe.

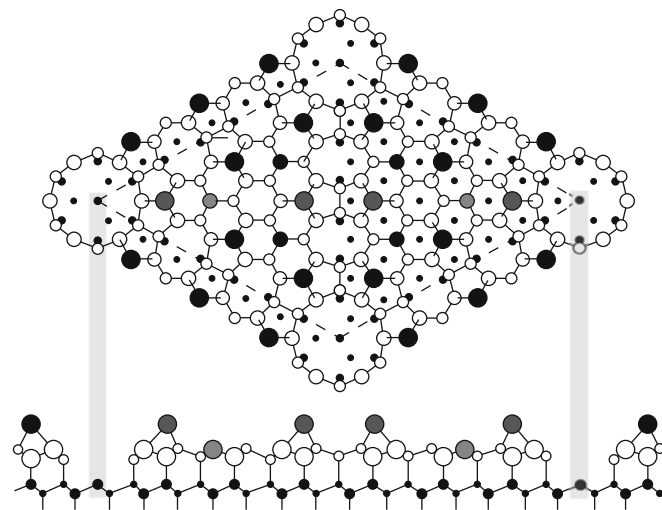


FIGURE 13.7 Relating dangling bonds to the 7×7 reconstruction of the {111} Si surface.

13.5 CURVED SURFACES AND PRESSURE

The idea is the same as discussed for the bowed dislocation, but we have added a dimension. If we reduce the area of the surface, we lower the energy. Hence, if a surface is curved, we can imagine that there is a force that wants to reduce the area of the surface: the force acts on an area of the surface and force divided by area is pressure. Picture how you can take a small ring, fill it with a soap film, and blow a bubble. The pressure is provided by the air: if you stop blowing, the surface becomes flat again. The analogy is quite close, except that the surface energy of the soap film is isotropic (and there are actually two surfaces).

There will actually also be a torque term in the surface tension, just as there is for curved dislocations, but this term is usually ignored. To make this force more physical to us, we will regard this surface energy as a surface tension. The pressure difference across a curved interface is real and occurs in all materials. In small gas-filled voids created by implanting Xe into MgO (or Si or Al), the Xe will be crystalline if the void is small enough because the internal pressure is so high; the Xe can interact with other defects just like any small crystal inside a crystalline matrix, unless the defect is a crack! A simple example is calculated in Table 13.2.

The concept of pressure due to surface curvature is very important in ceramics because we often encounter very curved surfaces, e.g., at small grains, voids, or particles, which are present because we start processing with powders. Thus we can have a large pressure difference that

A VERY IMPORTANT BUT SIMPLE CALCULATION

The pressure in the void must do work to change the surface area. The equilibrium condition is then given by the energy balance.

$$\Delta P dv + \gamma dA = 0$$

For simplicity, assume that the void is a sphere (in using one value for γ , we have already assumed that the energy is isotropic). We know dv and dA terms of r .

$$dv = 4\pi r^2 dr$$

$$dA = 8\pi r dr$$

Combining these three equations gives

$$\Delta P = \gamma \frac{8\pi r}{4\pi r^2} \left(\frac{dr}{dr} \right) = \gamma \frac{2}{r} = \frac{2\gamma}{r}$$

A surface will have two principal curvatures, r_1 and r_2 (which can either be positive or negative); we write

$$\Delta P = \gamma \left(\frac{1}{r_1} + \frac{1}{r_2} \right)$$

provides a large driving force. If r is ∞ , then r^{-1} and ΔP are zero. The result is that we can think of the pressure above a curved surface as being different from that above a flat surface.

13.6 CAPILLARITY

We will discuss wetting shortly, but you are already familiar with the capillarity effect from the traditional mercury-based or spirit-based thermometer. From Figure 13.8 we can obtain the following expression:

$$\Delta P = \frac{2\gamma}{r} = \gamma \frac{2\cos\theta}{r} = \rho gh \tag{13.8}$$

$$\gamma = \frac{r\rho gh}{2\cos\theta} \tag{13.9}$$

The equation $\Delta P = 2\gamma/r$ is very important because it says if $r \neq \infty$, then $\Delta P \neq 0$. The vapor pressure above a curved surface is not the same as the pressure above a flat surface due to ΔP .

$$V\Delta P = RT \ln \frac{P}{P_0} = V\gamma \left(\frac{1}{r_1} + \frac{1}{r_2} \right) \tag{13.10}$$

Here V = molar volume, P = vapor pressure, P_0 = vapor pressure over a flat surface, and R = the gas constant.

$$\ln \frac{P}{P_0} = \frac{V\gamma}{RT} \left(\frac{1}{r_1} + \frac{1}{r_2} \right) = \frac{M\gamma}{\rho RT} \left(\frac{1}{r_1} + \frac{1}{r_2} \right) \tag{13.11}$$

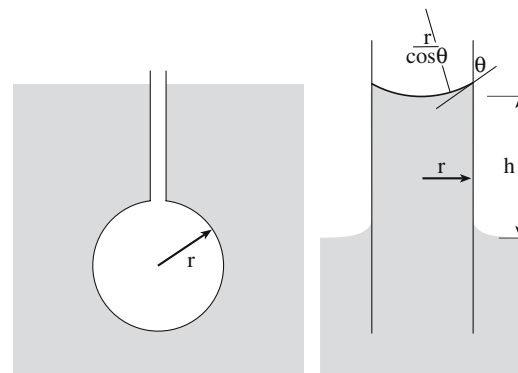


FIGURE 13.8 The geometry used to calculate the capillarity equation.

TABLE 13.2 Pressure due to Surface Curvature for Silica Glass (1700°C; $\gamma = 300 \text{ mJ/m}^2$)

Sphere diameter (μm)	ΔP (MPa)	$\frac{P}{P_0}$
0.1	12	1.02
1.0	1.20	1.002
10.0	0.12	1.0002

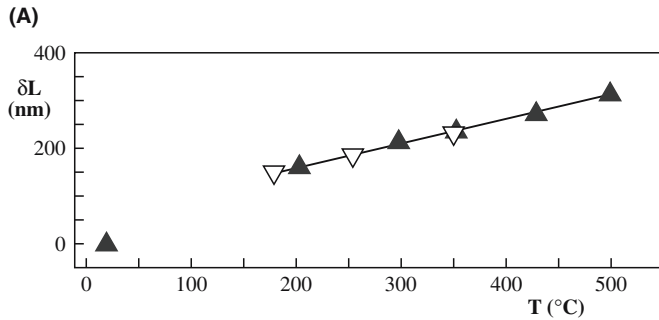
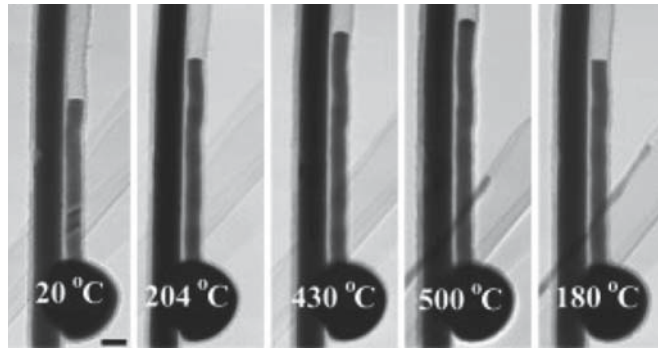


FIGURE 13.9 Capillarity effect in a silica nanothermometer.

Now, M = molecular weight and ρ = density. When $r_1 = r_2$, Eq. 13.11 becomes

$$\ln \frac{P}{P_0} = \frac{V\gamma}{RT r} \quad (13.12)$$

From Eq. 13.12 we can see that:

- The vapor pressure of a spherical particle is a function of its radius.
- The vapor pressure at the surface of a particle is higher if r is small.

We can also show that

- Small particles or small voids have large surface energies.
- At high temperatures small particles will tend to dissolve while large particles will grow (Ostwald ripening).
- Small particles have lower melting temperatures than large particles.

The thermometer shown in Figure 13.9 was made by filling a silica nanotube with Ga instead of Hg.

13.7 WETTING AND DEWETTING

The concepts of wetting and capillarity were first explained in ~1800; again, history is important in understanding the terminology. If you place a drop of water onto a really

clean glass slide, it remains as a drop on the surface even though it develops a glass/liquid interface. If you add soap to the water, it spreads over the surface; the liquid wets the glass and the interfacial (contact) area increases. The soap is a surfactant and lowers the energy of the glass/liquid interface. We will see later that we can use surfactants to treat ceramics and liquids other than water. An example of this being used commercially for glass surfaces is the development of new coatings for automobile windshields.

As usual ceramics tend to be more complicated; at the higher temperatures encountered when processing ceramics, vaporization can also occur. At these higher temperatures, the solid might not be inert, so it may react with the liquid; this is known as reactive wetting. When we talk about wetting or dewetting, one of the materials need not be liquid (both, or neither, could be), but we do need mobility (surface diffusion) for the wetting/dewetting layer to be able to move across the surface.

The relationship between surface and interfacial energies determines, to a large extent, the wetting behavior of a liquid on a solid surface. Later we will see that it also determines the phase morphology of mixtures of two or more phases. There are several interfacial tensions, γ , to contend with, and these are identified by the subscripts f, s, and v, which represent film, substrate, and vapor, respectively.

If we consider the stable configuration of a liquid placed on a solid surface, the equilibrium shape conforms to the minimum total interfacial energy for all the phase boundaries present. If the solid–liquid interfacial energy (γ_{sl}) is high, the liquid tends to form a ball having a minimum interfacial area as shown in Figure 13.10 (Hg on a glass slide will do this). If the liquid–vapor interfacial energy (γ_{sv}) is very small, the spreading of the liquid will depend entirely on the interfacial energy (γ_{sl}), but note the converse.

Young’s equation relates the angle between the solid surface and the tangent to the liquid surface at the contact point. (It is a force balance in the horizontal direction because we assume the surface is not free to move in the vertical direction.) This contact angle, θ , may vary between 0 and 180°. This angle specifies the conditions for minimum energy according to the relation

$$\gamma_{lv} \cos \theta = \gamma_{sv} - \gamma_{sl} \quad (13.13)$$

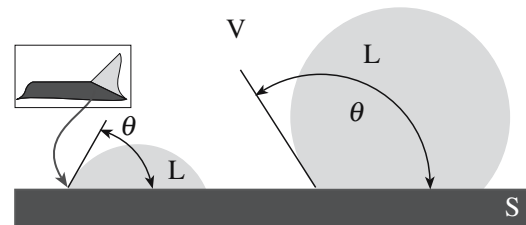


FIGURE 13.10 Drops on a solid surface showing wetting, nonwetting, and a real equilibrium (inset)

Therefore, the contact angle θ depends only on the surface properties of the materials involved. The importance of this equation is that it provides a method for comparing interfacial energies. Thomas Young first derived Eq. 13.13 in 1805 (Young, 1805), but often it is also referred to as the Young–Dupré equation (Dupré, 1869). Contact angles can be measured experimentally by the sessile drop technique. To study the wetting of glass on a ceramic or metal surface a small particle of the glass would be placed on the solid surface inside a tube furnace, one end of which is clear, allowing observation of the droplet, using a telemicroscope, and the contact angle, as a function of temperature. Experimentally it can be difficult to obtain reproducible values for θ . One of the problems is that of macroscopic surface roughness, which can be expressed as

$$\cos \phi = r \cos \theta \quad (13.14)$$

where r is the roughness, ϕ is the observed contact angle, and θ is the true contact angle. The other problem is that of hysteresis—the measured angle θ depends on whether the liquid is advancing or receding.

Table 13.3 shows measured contact angles for several metals and for a basic slag (think of the slag as liquid silicate glass) on MgO single-crystal surfaces (MgO is used as a furnace lining). As noted earlier, the surface energy of solids is dependent on the crystallographic orientation, which is demonstrated by the variation in wetting angle with crystallographic planes for MgO.

Layers of glass can be deposited on polycrystalline substrates and heat treated. The resulting faceting of the surface can be monitored while varying the annealing temperature, quench rate, etc. The glass/ Al_2O_3 interfacial energy is not isotropic. An important feature of this demonstration is that the glass does affect the faceting behavior of the surface. This wetting of single surfaces by a glass is more complex than the wetting of most solids by a liquid

TABLE 13.3 Measured Contact Angles of Liquids on Single-Crystal MgO

Liquid	Test temperature			
	(°C)	(100)	(110)	(111)
Cu	1300	106	159	149
Ag	1300	136	141	147
Co	1600	114	153	144
Fe	1600	59	110	90
Basic slag ^a	1400	9	17	32

^aComposition: 40% SiO_2 , 20% Al_2O_3 , 40% CaO .

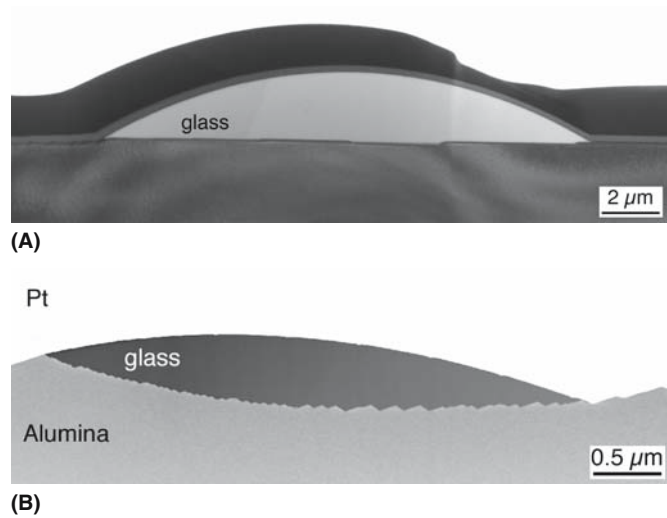


FIGURE 13.11 Experimental observations of glass droplets on the surface of Al_2O_3 : (a) c plane, (b) m plane.

CONVENTION

The contact angle, θ , is measured “through” the liquid.

LOTUS LEAF

Water “rolls off” the leaf because the surface is rough.

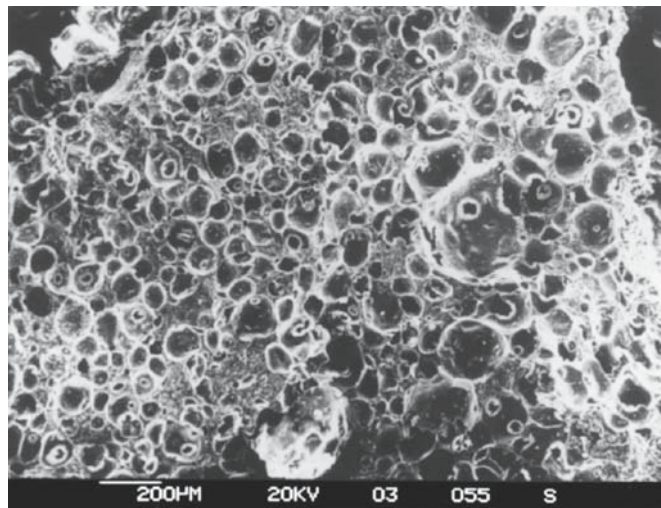
since the glass can be very reactive at the high temperatures where the wetting actually takes place. For example, at 1600°C a silicate glass can dissolve alumina. The situation is shown experimentally in Figure 13.11 for the (0001)

and $\{10\bar{1}0\}$ surfaces: the glass/ Al_2O_3 surface energy is different for different surfaces. How the glass actually dewets the surface depends on the crystal orientation of that surface.

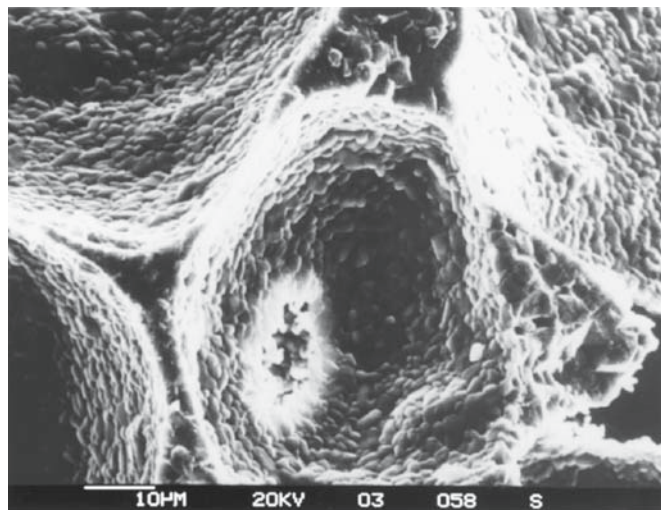
Wetting/dewetting is also a concern for nonoxides (especially when you want to join them to other materials) and for metal/ceramic interfaces such as the metal/Si, metal/ SiO_2 , and metal/ Si_3N_4 interfaces in the electronics industry and systems such as $\text{Al}/\text{Al}_2\text{O}_3$, which is important in protecting metals against corrosion.

13.8 FOAMS

Foams, which have been known forever, have been studied for over a century. They are hot topics in coffee shops and cosmology, but are not as well known in ceramics. When they are discussed in ceramics, they are not necessarily recognized as such, as is the case with pumice. (More about this is given in Chapter 21.) These cellular ceramics are also referred to as microporous or macroporous ceramics depending on the size of the cells. The common feature of these materials is that they consist of thin membranes of ceramic that enclose pores of various sizes. Thus they have a large surface and they are lightweight, but they still retain many of the properties of the ceramic. They are rigid, can be used to relatively high temperatures, and can be quite inert to chemical reactions.



(A)



(B)

FIGURE 13.12 The surface of foam.

Many cellular ceramics, as shown in Figure 13.12, are made by using natural materials such as wood, itself a cellular material, as a template: they are biomimetic ceramics—they mimic the biological materials. (More about this is given in Chapter 35.) Rattan cylinders have been infiltrated with Si liquid and zeolites to make a mixed microporous/macroporous ceramic. The rattan stems were first pyrolyzed, then infiltrated with liquid Si to give the Si/SiC matrix, and finally the internal surfaces were functionalized with a zeolite. The resulting materials was tested as a catalyst for *n*-hexane cracking.

The honeycomb of the catalytic converter provides a large surface area to support the catalyst particles and ensures that the gases pass close to these particles. When used as filters the pore (channel) diameter is engineered to suit the purpose. The synthetic bone needs the pores to encourage the intergrowth of regrowing natural bone, but if the pores are too large then the ceramic is weakened. One technique used to provide the porous structure and

the strength is to use tape casting (more about this is given in Chapter 27) to provide layers of material of different pore size, thus producing a graded porous structure.

We will see these foam geometries again when we discuss glass films in grain boundaries.

13.9 EPITAXY AND FILM GROWTH

We have two immediate questions:

- What is epitaxy?
- Why discuss it here?

The reason for discussing it here is that it essentially involves depositing one material onto the surface of another. If the thin layer coating the substrate is stable, then it is wetting the substrate. If the thin layer is aligned crystallographically with respect to the substrate such that directions in the films are aligned with those in the substrate, we say the film is epitaxial. In this case it is likely to wet the substrate—the interfacial energy is relatively low. Most thin films are not epitaxial.

Two ancient Greek words $\epsilon\pi\iota$ (epi—placed or resting upon) and $\tau\alpha\chi\iota\sigma$ (taxis—arrangement) give the root of the modern word *epitaxy*, which describes an important phenomenon exhibited by thin films. Epitaxy refers to the formation of an oriented (single crystal) film on top of a crystalline substrate. Most people say epitaxial, which is grammatically incorrect, but is now in dictionaries. Epitaxial or epitaxial would be the correct adjectives.

We will discuss details (matching, chemistry, bonding, lattice matching, and misfit dislocations) of such interfaces in Chapter 15 as well as what it means for them to be incommensurate. We will also discuss the different techniques for analyzing them there. For now, we want to consider how the atomistic topography of the substrate surface influences the behavior of the film. So we are concerned with surface steps and how they influence graphoepitaxy (an alignment of the film induced by surface topography). To complicate matters further, in ceramics, the film and the substrate may be amorphous, polycrystalline, or monocrystalline.

13.10 FILM GROWTH IN 2D: NUCLEATION

During film growth, atoms or molecules in the vapor phase arrive at the substrate, creating aggregates that will either grow in size or disintegrate into smaller entities through dissociation processes.

Nucleate the New Phase on the Substrate

When an atom from the vapor strikes a solid surface the collision decreases the energy of the atom so that it becomes partially bound to the crystal surface. Thus any

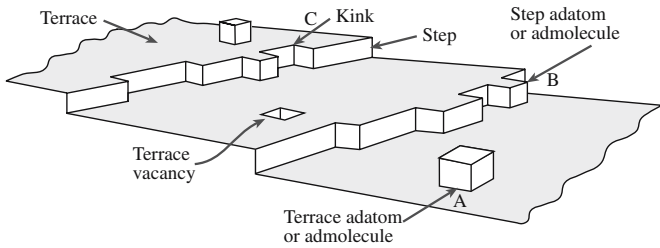


FIGURE 13.13 Surface attachment sites and the nucleation of thin films in 2D.

further motion of the atom is restricted to the surface of the substrate. Isolated nuclei are then formed from groups of such atoms coming together by chance through their thermal motion. A mobile “new” atom is most easily built into the crystal structure at a ledge corner, since this atom will interact strongly with three neighboring atoms and the local surface energy of the surface due to unsaturated surface bonds will not increase. Another convenient position will be sites such as steps, shown in Figure 13.13; in this way a continual supply of atoms will lead to the completion of the entire crystal plane.

Stabilize the Nucleus

Continuation of the growth process will rely on the formation of a new stable nucleus, shown schematically as a thin cylinder. This new nucleus involves an increase in free energy due to the atoms at the edge and a decrease of free energy as the atoms are incorporated in the interior. Thus the stability of the nucleus will depend upon the ratio of volume energy to surface energy, and there will be a critical radius of the nucleus, r_c , such that if $r > r_c$ the nucleus is stable and can grow.

Grow the Nuclei

If the lateral growth mechanism is relatively rapid, the rate of formation of the new nuclei on the completed planes will be the decisive factor in controlling the overall growth rate.

The free energy change accompanying the formation of an aggregate of mean dimension r is given by

$$\Delta G = a_3 r^3 \Delta G_v + a_1 r^2 \gamma_{vf} + a_2 r^2 \gamma_{fs} - a_2 r^2 \gamma_{sv} \quad (13.15)$$

In Chapter 15 we will consider homogeneous nucleation of a solid in a liquid. Here (using a simple qualitative

model) we consider the heterogeneous nucleation of a solid film on a planar substrate.

13.11 FILM GROWTH IN 2D: MECHANISMS

The many observations of film formation have pointed to three basic growth modes that can be distinguished on the basis of Eq. 13.13; these are illustrated schematically in Figure 13.14. Each mode is named after two scientists who did not necessarily work together.

- Island growth (Volmer–Weber) occurs when the smallest stable clusters nucleate on the substrate surface and then grow in three dimensions to form islands. This happens when atoms or molecules in the deposit are more strongly bound to each other than to the substrate.
- Layer-by-layer growth (Frank–van der Merwe) involves the extension of the smallest stable nucleus, which

occurs overwhelmingly in two dimensions, resulting in the formation of planar sheets. In this growth mode the atoms are more strongly bound to the substrate than to each other. The first complete monolayer is then covered with a somewhat less tightly bound second layer. Providing the decrease in bonding energy is continuous toward the bulk crystal value, the layer growth mode is sustained.

CONTACT ANGLE AND THE MODELS

Island growth: $\theta > 0$

$$\gamma_{sv} < \gamma_{fs} + \gamma_{vf}$$

Layer-by-layer growth: $\theta = 0$. The deposit “wets” the substrate.

$$\gamma_{sv} = \gamma_{fs} + \gamma_{vf}$$

Layer-by-layer growth:

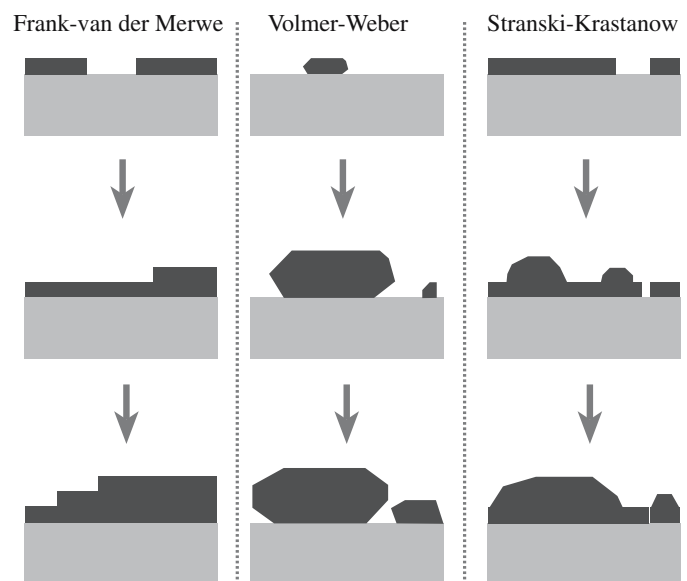
$$\gamma_{sv} > \gamma_{fs} + \gamma_{vf}$$


FIGURE 13.14 The three modes of thin-film growth.

- Layer-plus-island (Stranski–Krastanow) growth is a mechanism involving an intermediate combination of these two modes. In this case, after forming one or more monolayers, subsequent layer growth becomes unfavorable and islands form. The transition from two- to three-dimensional growth is not completely understood, but any factor that disturbs the monotonic decrease in binding energy characteristic of layer growth may be the cause.

Growth ledges: Experimentally we know that the growth of crystals from the vapor phase often occurs at measurable rates, even at low values of supersaturation. This has been associated with growth taking place at steps provided by dislocations intersecting the interface. Such dislocations can provide a self-perpetuating source of steps as molecules are added to the crystal. The emergence point of the dislocation acquires a higher curvature until a steady state is reached in which the form of the spiral remains constant and the whole spiral rotates uniformly around the dislocation. This process was illustrated in Figure 12.24.

Experiment: Start with well-defined facets so you have regions of planar surfaces. Then consider two cases.

- Large entropy change produces smooth surfaces and faceted interfaces. Examples are growth of silicates from the melt and the growth from vapor or dilute solutions.
- Small entropy change is isotropic with many growth sites. An example is the growth of a metal from the melt.

We can consider sites on the growing phase and in a simple model (shown in Figure 13.13) of counting the nearest neighbors, assign a binding energy to each of these sites. Let E_1 be the energy of attachment at the first nearest neighbor and E_2 at the second nearest neighbor. We can then draw up a table for each site. The growth rate per unit

area of interface (U), taking ν to be the usual frequency factor and a_0 the distance that the interface moves when an atom is added, can then be determined.

13.12 CHARACTERIZING SURFACES

The techniques for characterizing surfaces are applications or extensions of those discussed in Chapter 10. They basically fall into two groups: the direct and indirect

(D and I) techniques, which are summarized for surfaces in Table 13.4. Here we emphasize the application of techniques that are particularly important for ceramic surfaces. Each approach provides different information

and none answers all the questions we have. A major difficulty in studying ceramic surfaces is that many do not conduct electricity well. Thus techniques using electron beams can have limited application. To study surfaces in the transmission electron micrograph (TEM) or scanning electron micrograph (SEM) we may need to coat the sample with C or even Pt to prevent charge building up on the surface and thus deflecting the electron beam. In doing so, we hope we have not changed the surface, but of course we have.

Rather than just describing each technique, we will go through a set of examples to show just what is possible for the different techniques. In each e-beam technique, coating may be necessary—the rule is try it first then gradually increase the thickness of the coating. In SEM, for example, lowering the kV may allow you to avoid coating altogether. Sometimes, single-crystal sapphire can be studied in the TEM without coating. This possibility may depend on how clean your TEM is. You can also flash the sample with an electron beam to induce conduction for the short time that you make the observation/measurement.

Scanned probe microscopy is the method of choice for studying surfaces because it gives a direct picture of the surface, can give superb resolution, and can even give

ENERGY OF SITES IN FIGURE 13.13

Site	Energy Gain
A	$E_1 + 4E_2$
B	$2E_1 + 6E_2$
C	$3E_1 + 6E_2$

TABLE 13.4 Surface Characterization Techniques

Technique	Example	Special information	Limitations
AFM	D	Al ₂ O ₃	How smooth?
SEM	D	Fracture	Self selective
TEM	D	MgO, Al ₂ O ₃	Faceting; plan view
TEM	D	CeO ₂	Faceting; profile
TEM	D	REM	Plan view
LEED	I	Al ₂ O ₃	Average; vacuum
RHEED	I	Al ₂ O ₃	Average; vacuum
STM	D	Fe ₃ O ₄	Steps
STM	D	Si 7 × 7	Reconstruction
Auger	D	La ₂ O ₃ , Y ₂ O ₃	Chemistry

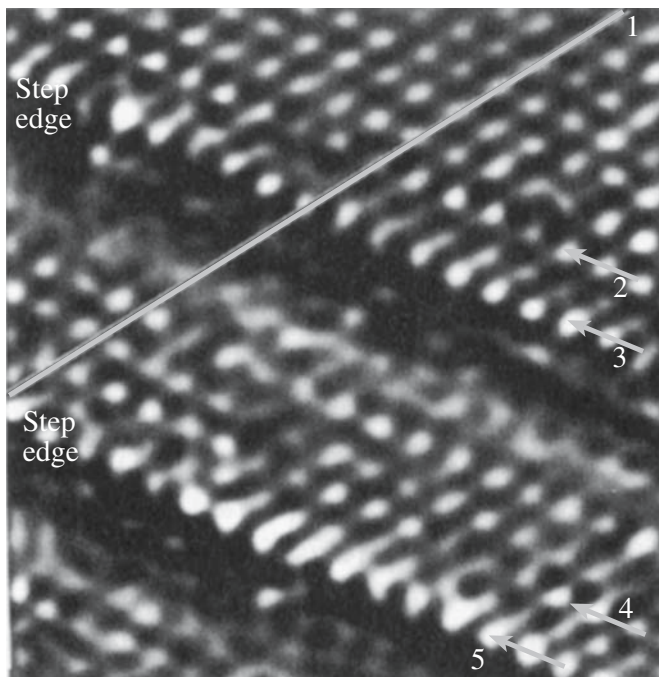


FIGURE 13.15 STM of a surface of Fe₂O₃. 1–5 indicate different rows of atoms.

spectroscopic information. It is also much quicker, easier, and cheaper than TEM.

Figure 13.15. Not only the well-known semiconducting ceramics (Si, Ge, GaAs, etc.), but also the less well known, but adequately conducting oxides, Fe₂O₃ and NiO, have been successfully imaged by scanning tunneling microscopy (STM). The main advantage of STM is that it gives better resolution normal to the plane than any other technique. Thus we can examine the out-of-plane relaxations and rumpling that are so important in determining surface energies.

Figure 13.16. When the ceramic is not conducting we can use atomic force microscopy (AFM) to examine the surface. The vertical resolution is not quite as good as STM, but the main loss is in the lateral resolution. This is because the geometry of the probe tip will influence the image as seen from the width of the lines in this figure. There are variations of AFM, as summarized in section 10.6, which can provide information on magnetic fields or even on the mechanical properties.

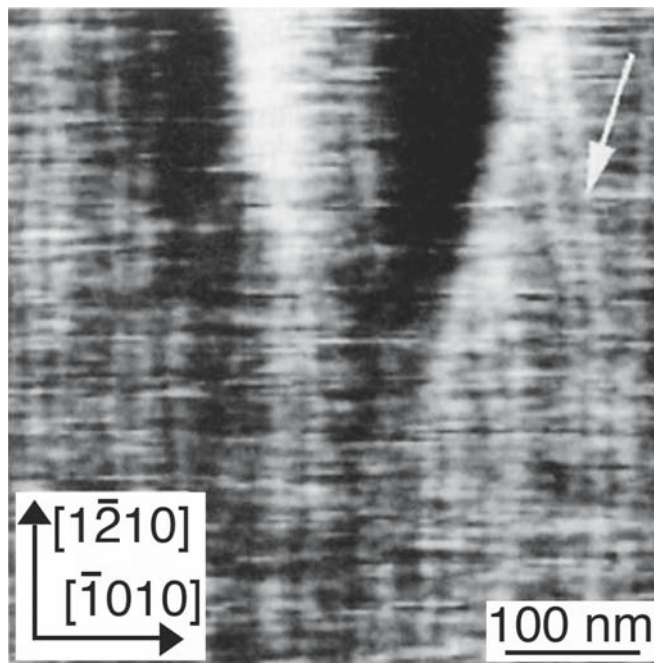
We can characterize the shape of the AFM tip using SEM and can even functionalize the tip by coating it as shown in Figure 13.17. In principle, using such a coating allows us to vary the chemistry of the tip/sample contact point.

Diffraction techniques are the classic approach and were widely used by surface scientists before the advent of scanned probes.

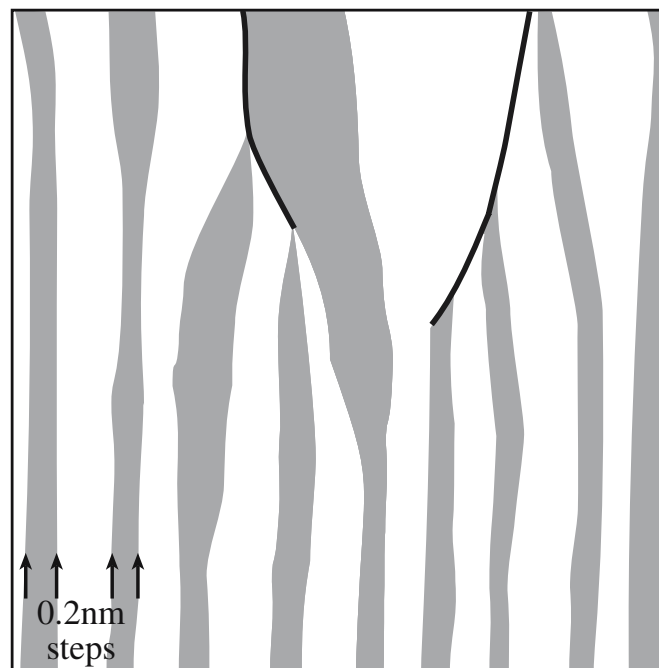
Figure 13.18. Low-energy electron diffraction (LEED), as its name implies, produces data in the form of a diffraction pattern, which must then be interpreted. Since

the energy of the electrons is low, the beam probes only the region closest to the surface. This is the strength of the technique, but it also means that the surface must be absolutely clean. Thus LEED experiments are carried out in UHV chambers under conditions that are never encountered in ceramics processing.

Figure 13.19. Reflection high-energy electron diffraction (RHEED) is the high-energy version of LEED. Because

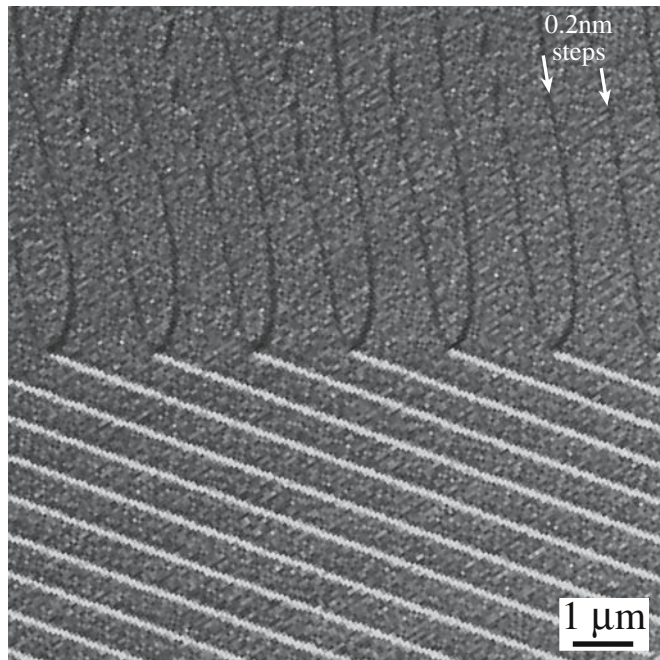


(A)



(B)

FIGURE 13.16 Sub-unit-cell surface steps on (a) sapphire and (b) spinel. The steps are 0.2nm high in each case.



(C)

FIGURE 13.16 Continued

the electron energy is higher, the beam now probes deeper into the sample, but this is partly compensated by the beam being incident on the surface at a glancing angle. RHEED is particularly valuable during thin-film growth in which the fact that it requires only a reasonably good vacuum may not be a disadvantage.

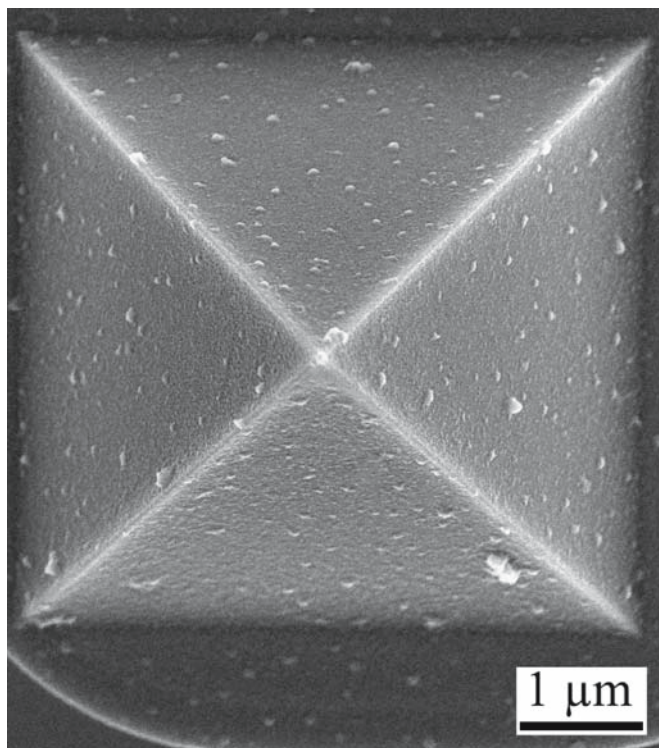
The TEM is used to study surfaces in many ways; here we will emphasize three imaging techniques, but note that combining diffraction with imaging at near atomic resolution in the TEM is its unique ability. We should dispel one bias immediately: TEMs can be UHV instruments. Usually they are not operated as such since they are required to be multiuser facilities, which is usually incompatible with UHV. So even though you may see surface steps, the TEM sample will usually have a layer (intentional or otherwise) of amorphous material on both surfaces. Another myth is that TEM samples are so thin that they do not represent the bulk. If you need a thick sample, you use a high-voltage machine where an Si TEM sample can be 5 μm thick (but you will not see atoms). Another myth is that the area viewed in the TEM is tiny. This is wrong: if the sample is prepared using a focused ion beam (FIB), the thin area can be greater than 25 μm square, have a uniform thickness, and be taken from a precisely located region of a bulk sample.

Figure 13.20. Plan-view (conventional) TEM (CTEM).

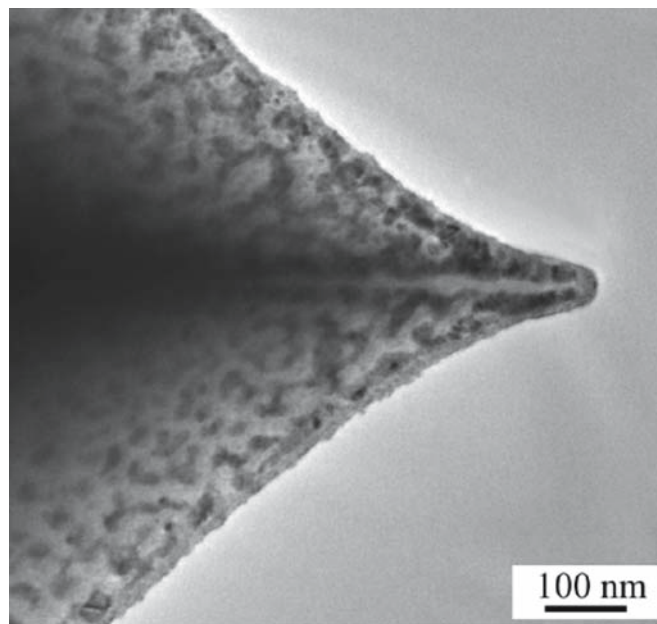
The electron beam is approximately normal to the plane of the thin TEM spinel and Al₂O₃ samples (although a sample may subsequently be tilted by as much as 70°).

Figure 13.21. Cross section TEM (XTEM).

The sample is usually prepared as a sandwich, and a thin section is cut to be normal to the median plane. This geometry allows us to see how features change as we move from



(A)



(B)

FIGURE 13.17 SEM image of AFM probe tips (a) end-on (SEM) and (b) side view (TEM); the latter has been coated to test the interaction with the sample.

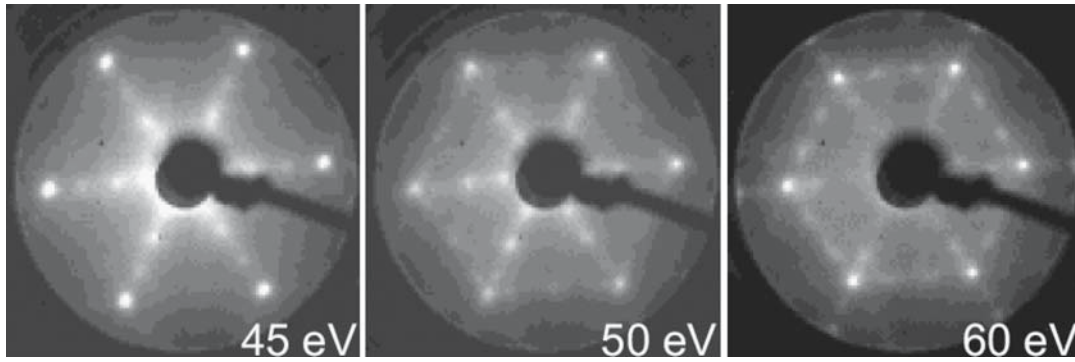


FIGURE 13.18 LEED patterns from GaN on Al_2O_3 as the accelerating voltage is changed.

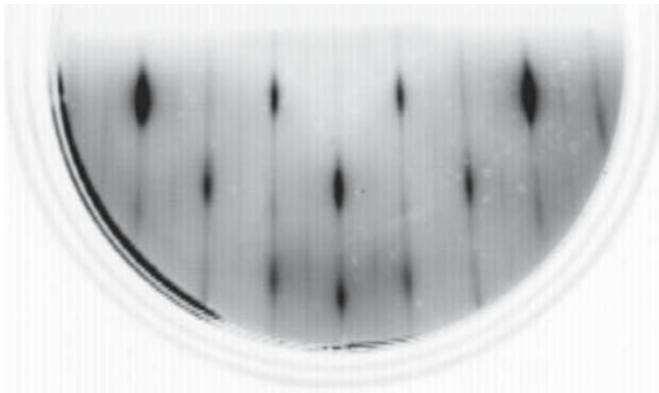


FIGURE 13.19 RHEED pattern from anatase film grown on LaAlO_3 .

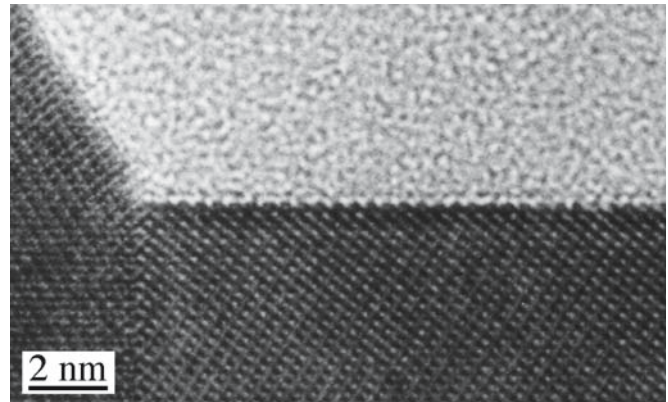
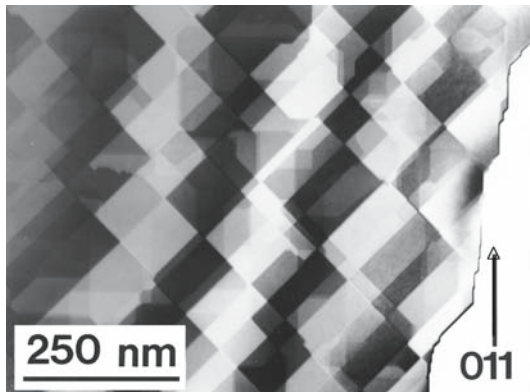


FIGURE 13.21 Cross section HRTEM image of a surface of Fe_2O_3 .



(A)



(B)

FIGURE 13.20 Plan view TEM images of steps on MgAl_2O_4 and Al_2O_3 ; the steps occur when the thickness of the TEM sample changes abruptly.

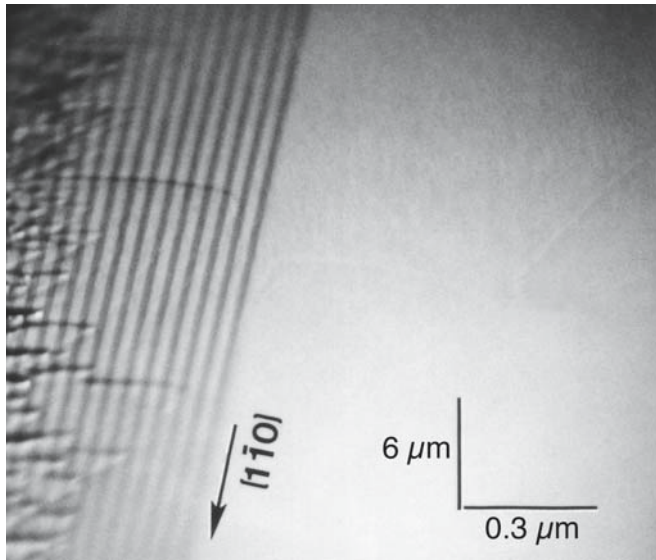


FIGURE 13.22 REM image from a GaAs substrate with a $\text{Al}_x\text{Ga}_{1-x}\text{As}/\text{GaAs}$ superlattice; the substrate has cleaved perfectly.

the bulk toward the surface; it is particularly useful in thin-film growth where we need to see the surface and how the layers developed.

Figure 13.22. Reflection electron microscopy (REM) is an old technique that was revived in the 1980s but is still not widely used. The sample is essentially bulk material with just one surface viewed. The electrons are diffracted off the surface as in RHEED (the diffraction pattern looks just like any other RHEED pattern), and are then imaged by the TEM in the usual way. The resolution is about 0.7 nm and chemical analysis can be considered as shown by the $\text{Al}_x\text{Ga}_{1-x}\text{As}/\text{GaAs}$ superlattice in this image; square millimeters of surface can be viewed just by scanning the sample. Notice the foreshortening.

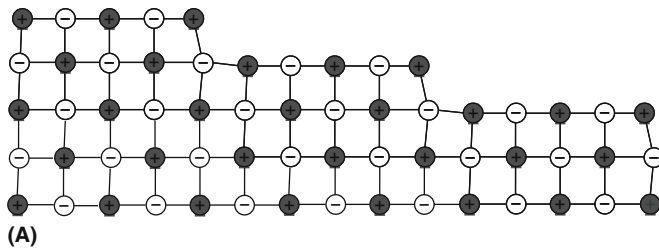


FIGURE 13.23 Different representations of surface steps: (a) (100) cross section of MgO; b) wurtzite; (c) (110) TiO_2 .

TEM is a superb tool for examining surfaces of ceramics; one problem is that you always probe two surfaces at once (except in REM).

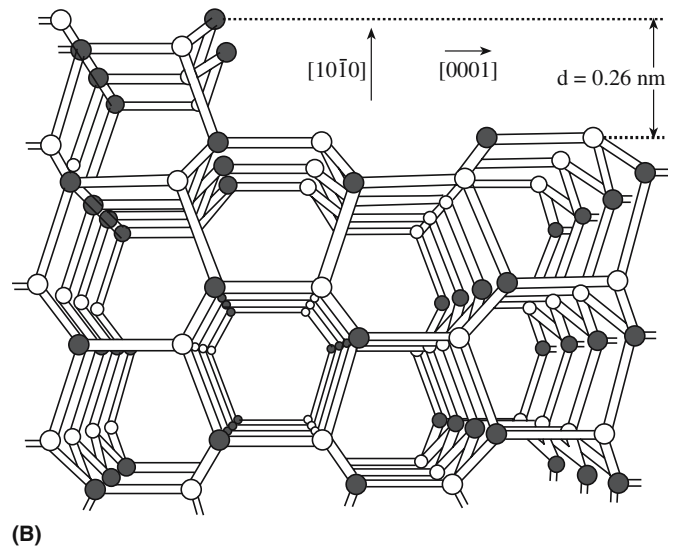
The SEM is used to study surfaces in many ways; as noted above, diffraction is also possible, and again SEMs can be UHV instruments. In fact, this is necessarily the case in the electronics industry.

13.13 STEPS

We saw in chapter 12 that dislocations move by the movement of jogs or kinks that are, themselves, defects on the dislocation. When we consider the movement of surfaces at an atomic scale, the surfaces (like dislocations) actually move by the translation of defects along them. The principal surface defects are line defects known as steps, or ledges if they are higher than a few lattice planes, and these, in turn, translate by kinks moving along them.

We usually assume that steps on ceramic surfaces will be quite straight, as shown for spinel in Figure 13.16b, but they can appear to be smoothly curved as seen in images of steps on the {001} surface of MgO. The lowest-energy plane for MgO is the {100} plane, which is also the cleavage plane. Some observations suggest that the {111} plane also has a low energy, but this surface may be stabilized by water. Steps are also usually multiples of unit cells in height, but those shown in Figure 13.16a are pairs of steps on the basal plane of Al_2O_3 that are only 0.2 nm high.

Steps on MgO, wurtzite, and rutile surfaces are shown in Figures 13.23. The steps on the MgO show theoretically predicted displacements at the step. [Since there is a periodic set of steps, this surface could be called the (501) surface.] The special feature of the steps on the wurtzite surface is the presence of the dangling bonds, which are localized at the step. The rutile surface shows that even when the surface is modeled using hard spheres, the structure of the steps depends on their orientation. [These two vicinal surfaces could be called (223) and (443).]



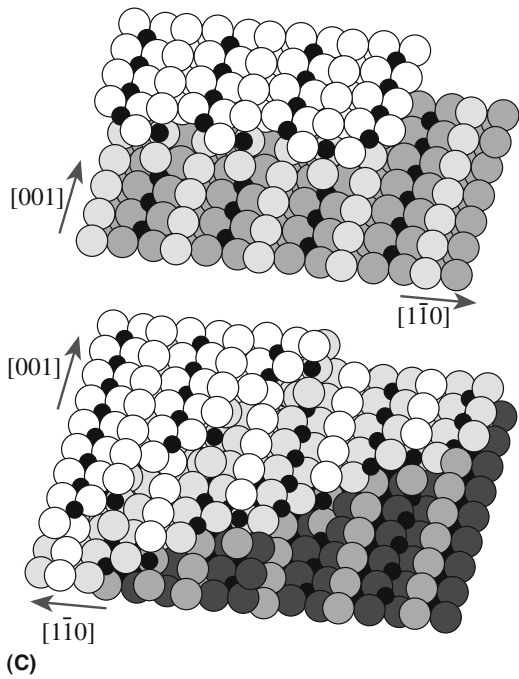


FIGURE 13.23 Continued

13.14 IN SITU

Many techniques can be adapted to study surfaces *in situ* at temperature, which is not the case for most other defects because they are not so accessible; the question is: can we learn anything new? The techniques we would most like to use are AFM and STM, neither of which is suitable because the high temperatures will quickly change the probe tip. The idea of *in situ* observation is simply that we do not need to cool the sample to room temperature before examining it, which is a terrific advantage when materials change as we cool them. The problem is that we often cannot control the conditions (such as the environment) as well as we would like when making such studies because controlling the environment is often incompatible with the

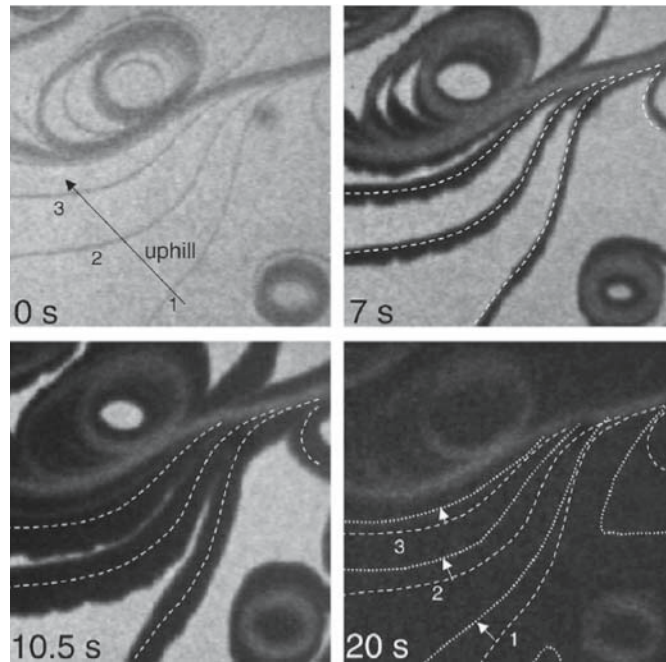


FIGURE 13.24 Studies of changes occurring at the surface of TiO_2 using LEEM. A total of 20 seconds separates the four images. The different contrast occurs because of the surface reconstruction.

technique we want to use to make the observation/measurement. EMs operate best in the highest vacuum, and a glass lens placed too close to an object at 1400°C will quickly degrade.

Although low-energy electron microscopy (LEEM) currently operates only to $\sim 900^\circ\text{C}$, it could in principle go higher. LEEM is particularly attractive since it is a direct imaging technique and gives excellent resolution on the height of steps. Use of LEEM to study the surface of TiO_2 is illustrated in Figure 13.24. REM should be able to provide similar data. The TEM can provide information on samples at temperatures up to 2000°C , but the detail tends to become less controllable as the temperature increases. In the image shown in Figure 13.25 a film of

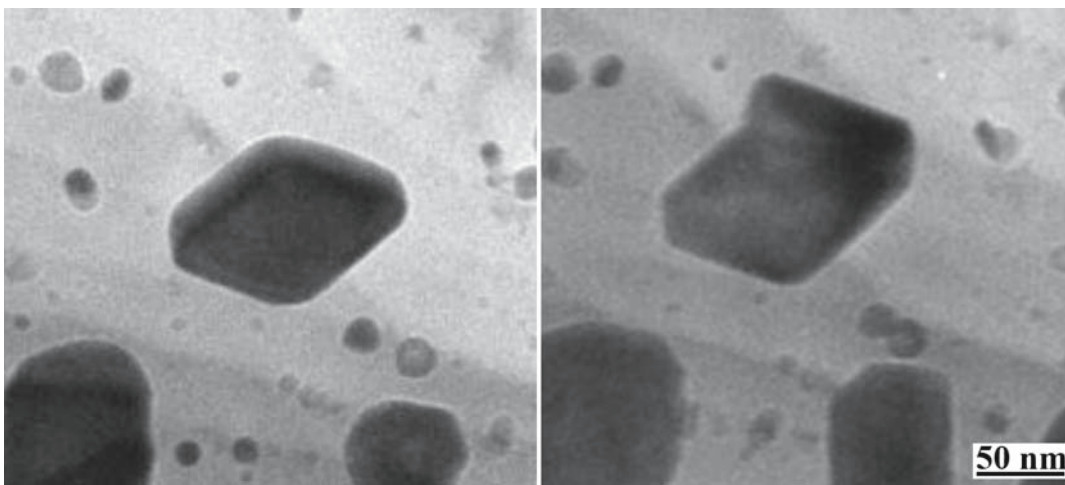


FIGURE 13.25 Changes occurring at a surface studied by *in situ* TEM. An NiO film has been reduced to Ni , which then dewets the sample and grows on the sapphire substrate.

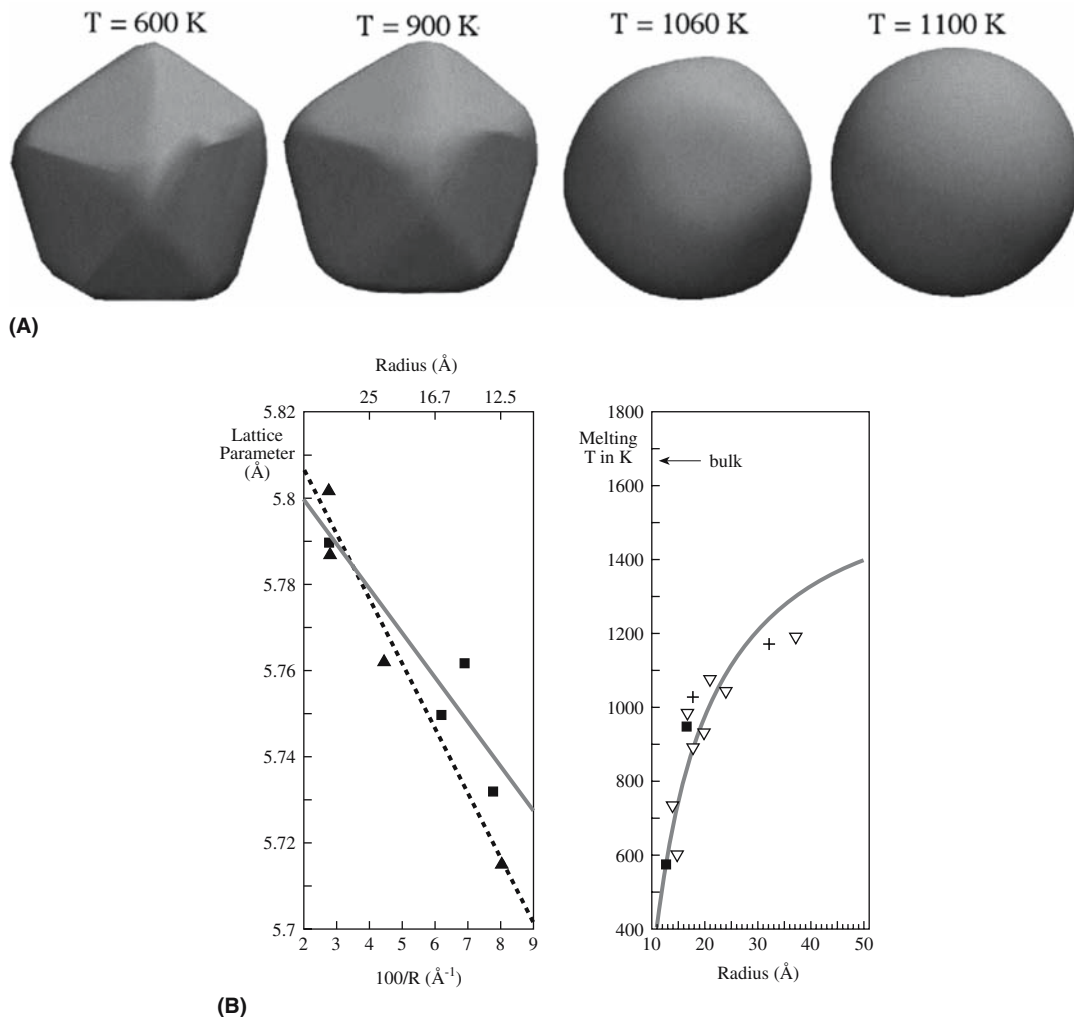


FIGURE 13.26 Nanoparticle melting: (a) computer modeling for Au; (b) showing the lattice parameter and melting temperature changes as the size of CdS nanoparticles decreases.

NiO has been reduced to Ni metal while heating in the TEM at 1000°C. New microscope holders and stages are becoming available so we will see much more use of *in situ* TEM in the future. Most of the work has been carried out using the SEM; environmental SEMs can heat the sample to ~1500°C, but again the challenge is in controlling the local pO_2 , etc.

13.15 SURFACES AND NANOPARTICLES

Surfaces are generally thought to melt before the bulk. Hence the melting temperature of small particles is lower than that of the bulk. Such measurements can be made only while the particles are at temperature, so we know this is very difficult experimentally. In comparison, for the computer it is quite straightforward as long as we can simulate physically meaningful situations. Computer modeling can be used to provide clues, as shown in Figure 13.26, which is a case where we are not taking account of the environment. Notice that the surface gradually

becomes more rounded starting at the edges. The shapes shown were calculated using a potential for Au; the graphs are experimental measurements for CdS.

There are examples in which the structure of a particular phase appears to be stabilized when in nanoparticle form just as some thin films can have their structure stabilized by being in contact with a substrate. Perhaps the best-known example is that $\gamma\text{-Al}_2\text{O}_3$ appears to be the stable structure at high T when in the form of nanoparticles.

13.16 COMPUTER MODELING

The use of computers to model surfaces and many other aspects of ceramics is a rapidly broadening field in which great caution is always needed. Commercial software packages are now available for PCs and supercomputers. However, if a computer analysis is relevant to your research, how can you know if the code was right, if the program has been applied correctly, if the input data were correctly typed, what potentials were used to describe the

ions, etc? Details like how the cell was constructed for the calculation are usually given, but it is very easy for these powerful black boxes to produce nonsensical results.

The Madelung problem for surfaces is, in one important way, more complicated than for bulk crystalline materials: a bulk sample must be neutral overall and the positions of the ions are well defined for each unit cell, At the surface, this is not necessarily the case. MARVIN (the acronym for Minimization And Relaxation of Vacancies and Interstitials for Neutral surfaces program) is one of the best-tested software packages. The essential part of using any software package is that for the material in question, it must be able to reproduce some experimentally determinable facts that were not used as input to the program! The value of computer modeling is illustrated by a nanoparticle of SrO growing on an MgO substrate in Figure 13.27; although the two oxides have the same structure, the SrO is slightly misoriented as it grows.

There are three distinctly different ways to terminate a (0001) surface in alumina: a single layer of Al^{3+} ions, a double layer of Al^{3+} ions, or only O^{2-} ions. This basal-plane surface of alumina has a lower energy than the rhombohedral-plane surface because the single outer layer of Al^{3+} ions can relax by moving in toward the bulk. We “know” this from computer modeling. It is very difficult to “observe” structure experimentally.

Surface Evolver is one of the most fascinating freeware packages available to materials scientists. The program (by Ken Brakker) uses finite-element analysis to compute the morphology of surfaces that are subjected to various forces, such as surface tension and interface stress. It runs on most computers, not just the Mac. If you are interested in modeling droplet geometries, for example, this is the program.

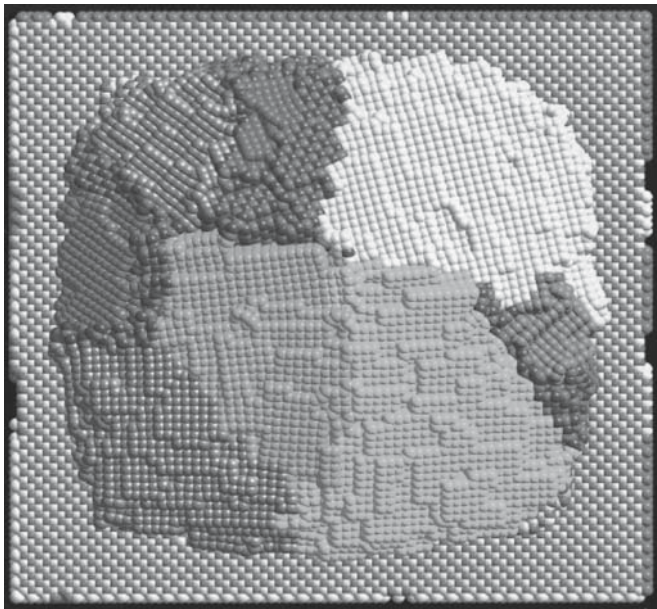


FIGURE 13.27 Computer modeling of oxide clusters on an oxide surface.

Wulffman (NIST) is a software package that allows you to model the Wulff shapes of crystals interactively. You can specify the crystal symmetry. The source for NIST's Wulffman program is available for you to use (www.ctcms.nist.gov/wulffman). There are commercial programs that address the same problem.

13.17 INTRODUCTION TO PROPERTIES

The properties of ceramic surfaces are so broad and far reaching (as we said in the beginning) that we will just provide a few examples, beginning with the general and becoming more specific, to emphasize this range of topics. The emphasis of this section is to introduce the fundamental ideas so that you can be aware of the possibilities and the pitfalls.

Growth. Thin films are invariably grown on surfaces.

Catalysis. A catalyst is either the surface itself or it is supported on a surface, with usually one or both of these components being a ceramic. Reactions occur at reactive sites, but the principle of catalysis is that the material facilitates, but is not chemically changed by, the process.

Joining. Materials are joined together by contacting two surfaces. In ceramics, the ionic and/or covalent nature of the bond tends to make this process more difficult than it is for metals or plastics.

Nanoparticles. The shape of a nanoparticle is determined in part by the surface energies, but the junctions between surfaces (double and triple junctions, i.e., edges and points) become more important as the size of the particle decreases; we know very little about these surface features.

Voids. We rarely encounter real voids in ceramics except in the computer (they all contain something). They have all the challenges of particles, including the junctions, and can have nanoparticle dimensions. Generally, they have not been extensively studied experimentally because they are difficult to see!

Superconductors. The high- T_c superconductors are being used by industry, but not to support high-speed trains as some had proposed in the early days. The applications often use thin films, for example, in SQUID devices produced by engineering the surfaces to produce particular grain boundaries.

Surface charge. The fact that ceramic surfaces can become charged means that it is possible to align nanoparticles, for example, using this charge. That this can be achieved is illustrated in Figure 13.28 for Pt particles on Al_2O_3 .

The concluding message is that we can clearly make enormous use of ceramics without understanding surfaces, but if we do understand them then we can start using ceramics to their full potential.

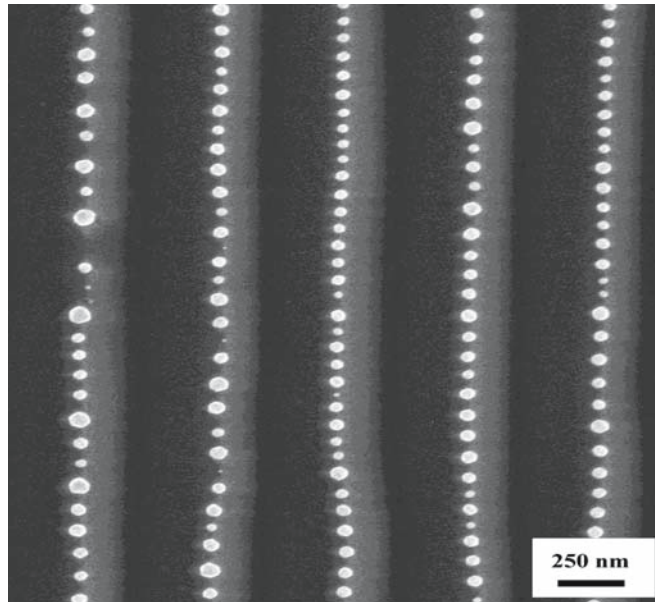


FIGURE 13.28 Self-assembly of Pt nanoparticles due to charging along a surface ridge in Al_2O_3 ; the particles sit on the ridge not the valley!

CHAPTER SUMMARY

The two key properties of any surface are that it has an associated energy and it is directly connected to the two media that it separates (e.g., a gas and a crystal). It is difficult to overemphasize the importance of surfaces especially in ceramics. We can summarize some of the most important results of this chapter quite briefly.

- The energy of crystal surfaces depends on the orientation of the surface.
- There is always a tendency for a curved surface to lower its energy by becoming flat.
- The surface is critical in the growth of thin films.
- Wetting and dewetting describe the addition or removal of material from a surface. The important consideration is why does one, or the other, occur and how can we make use of it.
- We can explore the surface structure and chemistry of surfaces at the atomic level because they are so accessible but the problem is keeping them clean. In ceramic processing, surfaces are rarely clean.

In nanotechnology surfaces become increasingly more important because a greater fraction of the atoms are at the surfaces. In the smallest nanoparticles, all the atoms may be at the surface of the particle. This property is quite closely related to a completely different group of materials, the foams. One difference between these two situations is the local curvature of the surface.

We will see in the following chapters that the surface is also critical when crystal grains join together (forming grain boundaries by sintering, etc.) or are separated (fracturing ceramics). We will also mention the role of surfaces in the polishing process.

PEOPLE IN HISTORY

Binnig, Gerd was born in Frankfurt, Germany in 1947. He joined the IBM research laboratory in Zürich in 1978. With Rohrer he developed the scanning tunneling microscope for which they shared the 1986 Nobel Prize in Physics.

Rohrer, Heinrich was born in St. Gallen, Switzerland in 1933. He did his PhD work at ETH (Swiss Federal Institute of Technology) on superconductivity and spent a 2-year postdoctoral at Rutgers University in New Jersey. In 1963 he joined the IBM research laboratory.

Young, Thomas was born in Milverton, Somerset (UK) in 1773. He was a physicist and physician who made contributions in many areas of science. He introduced the modulus of elasticity (known also as Young's

modulus) and the equation used to analyze the wetting of surfaces. His work in optics gave us Young's fringes and Young's slit. He was also an Egyptologist who helped decipher the Rosetta Stone. He died in London in 1829 and is buried in Westminster Abbey where his epitaph states that he was "a man alike eminent in almost every department of human learning."

Synge, E.H. (*Phil. Mag.* papers 1928–1932) proposed NSOM 50 years before it was discovered.

GENERAL REFERENCES

- Bailey, S.W., Frank-Kamenetskii, V.A., Goldsztaub, S., Kato, A., Pabst, A., Schulz, H., Taylor, H.F.W., Fleischer, M. and Wilson, A.J.C. (1977) *Acta. Cryst.* **A33**, 681. International Union of Crystallographers/Mineralogists report on Nomenclature (epitaxy). This report from a committee of eminent scientists defined the correct formation of adjectives for epitaxy and topotaxy. It was a lot of work and is generally ignored.
- Boys, C.V. (1959) *Soap Bubbles: Their Colors and the Forces which Mold Them*, Dover, New York. A series of lectures for "juvenile and popular audiences."
- Henrich, V.E. and Cox, P.A. (1996) *The Surface Science of Metal Oxides*, Cambridge University Press, Cambridge. Very useful.
- Herring, Conyers (1951) *Some Theorems on the Free Energies of Crystal Surfaces*, *Phys. Rev.* **82**(1), 87. This is a paper you can read.
- Israelachvili, Jacob (1991) *Intermolecular & Surface Forces*, Academic Press, London. The classic book on this topic.
- Kolasinski, Kurt W. (2002) *Surface Science*, Wiley, Chichester. An excellent introduction to the complexities of the surfaces of materials in general.
- Lagally, Max G., Ed. (1991) *Kinetics of Ordering and Growth at Surfaces*, Plenum, New York.
- Noguera, C. (1996) *Physics and Chemistry at Oxide Surfaces*, Cambridge University Press, Cambridge. Very useful.
- Perkowitz, S. (2000) *Universal Foam*, Walker & Co, New York. Puts foam into perspective. Should be required reading for materials science.
- Porter, D.A. and Easterling, K.E. (1981) *Phase Transformations in Metals and Alloys*, Van Nostrand Reinhold, New York. Chapter 3 gives a basic introduction to surface energy.
- Schwartz, A.J., Kumar, M., and Adams, B.L., Eds. (2000) *Electron Backscatter Diffraction in Materials Science*, Kluwer, New York.
- Young, Thomas (1805) *An Essay on the Cohesion of Fluids*. *Phil. Trans. R. Soc. Lond.* The paper was read on 20 December 1804. Worth reading yourself.
- Vaughan D.J. and Patrick, R.A.D., Eds. (1995) *Mineral Surfaces*, Mineralogical Society Series, Chapman & Hall, London. The source for information on this topic.

SPECIFIC REFERENCES

- Binnig, G., Rohrer, H., Gerber, C., and Weibel, E. (1982) "Surface studies by scanning tunneling microscopy," *Phys. Rev. Lett.* **49**, 57.
- Burton, W.K., Cabrera, N., and Frank, F.C. (1951) "The growth of crystals and the equilibrium structure of their surfaces," *Philos. Trans. R. Soc. London Ser. A* **243**, 299. Classic.
- Dupré, A. (1869) *Théorie Mécanique de la Chaleur*, Paris, p. 207.
- Frank, F.C. (1949) "The influence of dislocations on crystal growth," *Disc. Farad. Soc.* **5**, 48. (1952) "Crystal growth and dislocations," *Adv. Phys.* **1**, 91. Classics and easy to read.
- Goniakowski, J., Noguera, C., and Claudine, C. (1995) "Relaxation and rumpling mechanisms on oxide surfaces," *Surf. Sci.* **323**(1–2), 129.
- Kubaschewski, O. and Alcock, C.B. (1979) *Metallurgical Thermochemistry*, 5th edition, Pergamon, Oxford, Table D, p. 367. Values are given for many materials in kcal/mol; the conversion factor is 1 cal = 4.184 J.
- Lord, E.A. and Mackay, A.L. (2003) "Periodic minimal surfaces of cubic symmetry," *Current Sci.* **85**(3), 346. This paper on surfaces is an example of what you can do with Surface Evolver; not easy but fascinating.
- Ragone, D.V. (1995) *Thermodynamics of Materials*, Volume II, Wiley, New York, p. 100.
- Werner, J., Linner-Krcmar, B., Friess, W., and Greil, P. (2002) "Mechanical properties and in vitro cell compatibility of hydroxyapatite ceramics with graded pore structure," *Biomaterials* **23**, 4285.
- Wulff, G. (1901) "Zur Frage der Geschwindigkeit des Wachstums und der Auflösung der Kristallflächen," *Z. Kristallogr.* **34**, 449. The original paper on the Wulff construction.
- Young, T. (1805) "An essay on the cohesion of fluids," *Phil. Trans. R. Soc. London* **95**, 65.
- Zampieri, A., Kullmann, S., Selvam, T., Bauer, J., Schwieger, W., Sieber, H., Fey, T., and Greil, P. (2006) "Bioinspired rattan-derived SiSiC/zeolite monoliths: Preparation and Characterisation," *Microporous Mesoporous Mater.* **90**, 162.

WWW

www.intelligensys.co.uk/sim/metamorph.htm (050728) is the site for MetaMorph.

EXERCISES

- 13.1 A droplet of liquid silver is placed on an MgO substrate. The MgO(s)-Ag(l) interfacial energy is 850 mJ/m². (a) Calculate the contact angle of the Ag droplet. (b) Does the Ag wet the MgO? (c) If not, how might you lower the contact angle?
- 13.2 Repeat question 13.1 for the Al₂O₃(s)/Ag(l) system. The Al₂O₃(s)/Ag(l) system interfacial energy is 1770 mJ/m².
- 13.3 Determine the number of free bonds/m² on the (100), (110), and (111) planes of germanium. The lattice parameter of Ge is $a = 0.5658$ nm.
- 13.4 Using Eq. 13.7, compare the energy of the (110) and (001) surfaces in MgO.
- 13.5 Can you deduce any properties about the materials from the observations and graph in Figure 13.9?
- 13.6 Figure 13.6b indicates that there are 74 surface atoms. How is a surface atom defined in this context?
- 13.7 Estimate the number of atoms in the particle imaged in Figure 13.6.
- 13.8 Rank the following systems in terms of increasing interface energy: Al₂O₃(s)-silicate glaze(l), Al₂O₃(s)-Pb(l), SiO₂(glass)-sodium silicate(l), and SiO₂(glass)-Cu(l). Discuss how you arrived at your ranking system and state any assumptions that you make.
- 13.9 You are attempting to grow a copper thin film on MgO. What characterization technique (or techniques) might you use to determine which of the three growth modes shown in Figure 13.14 occur? What growth mechanism would you think would be most likely?
- 13.10 The most useful way to express surface area is in terms of m²/g. Using these units what is the surface area of Pt catalyst particles in Figure 13.28?

Interfaces in Polycrystals

CHAPTER PREVIEW

This chapter is part 2 of the three-part series on interfaces. Crystalline solids usually consist of a large number of randomly oriented grains separated by grain boundaries (GBs). Each grain is a single crystal and contains many of the defects already described.

A GB is defined as the surface between any two grains that have the same crystal structure and composition.

Many GBs, but not all, can be modeled as arrays of dislocations.

The dislocation model can be misleading; the GBs that may be most important in a ceramic may be the ones that do not appear to contain dislocations. So the warning is, we may sometimes concentrate on a particular type of GB just because we can understand that type of GB. Unless we fully understand GBs in ceramics, we will never have a full understanding of what happens during ceramic processing or why ceramics have certain mechanical properties, conductivity (thermal or electrical), etc. GBs become even more important as fine-grained nanostructured ceramics become more available. We also need to understand the junctions formed when three or four grains join: these are known as triple junctions (TJs) and quadruple junctions (QJs), which we might regard as new line and point defects, respectively. We conclude with a discussion of properties, not because they are unimportant (nor because of the bias of the authors). We want to understand GBs so as to explain some properties and to predict others.

14.1 WHAT ARE GRAIN BOUNDARIES?

Grain boundaries are internal interfaces and behave much like external surfaces, but now we have to be concerned with two crystal orientations, not one. Just as for surfaces, we have a pressure difference associated with the GB curvature and a driving force that tends to lead to an overall increase in grain size whenever possible. Grain morphology and GB topology are two aspects of the same topic. It is instructive to think of the model of soap foams: a soap film is flat when in equilibrium and it has a finite thickness. Three soap films meet along a line—a TJ. If you blow on a soap film (apply a pressure) it bows out until the “surface tension” balances the applied pressure.

Whenever we join two grains of the same composition and structure, we form a GB. The grains are related to one another by a

rotation axis and meet on a plane, which may be curved. The rotation axis is fixed only for a given boundary and is not unique, even for that boundary; there are different ways to form the same GB. We start by considering two identical grains. Fix one grain and rotate the other about any axis. Cut each crystal parallel to a particular flat plane (to keep it simple) in space and join the grains at this plane. This plane is the GB. Then allow the atoms to relax to a low-energy configuration (which may not be the minimum energy).

The conventional approach is to consider four types of GB based on the symmetry operation used to create them:

twist, tilt, mixed, and twin.

The first two (and hence the third) designations are really helpful only when the misorientation angle is small (low-angle GBs). This description is based on the location of the rotation axis.

TWIST, TILT, TWIN, LOW, HIGH, AND “GENERAL”

Twist	n normal to plane
Tilt	n parallel to plane
Twin boundary	Mirror across GB plane
Low-angle GB	$\theta < 10^\circ$ (low is small!)
High-angle GB	Structured, $\theta > 10^\circ$
General GB	Not a special GB!

- Tilt boundary. Rotation axis (\mathbf{n}) is in the boundary plane.
- Twist boundary. Rotation axis is normal to the boundary plane.

A symmetric twin boundary can also be described as a twist boundary or a tilt boundary—the difference depends on which aspect of the symmetry we think is most important. Not all twin boundaries are parallel to a mirror plane.

There are two well-known models of GBs that were developed primarily from studies of metals by considering the relative misorientation of the adjoining grains. These are the coincidence-site lattice (CSL) theory and the displacement-shift-complete lattice (DSCL). We first define two special quantities Σ and Γ . Imagine two infinite arrays of lattice points (one array for each crystal): they both run throughout space and have a common origin. For certain orientations, a fraction of the points in each lattice will be common to both lattices.

We call this fraction Σ^{-1} . (Then Σ is always an integer.) The lattice made up by these points is called the coincident-site lattice or CSL. The CSL is a lattice of common lattice sites, not common atoms.

If you translate one grain relative to the other, Σ is not changed.

The Idea of Σ

It is easiest to understand these concepts by looking at simple illustrations as shown in Figure 14.1 for both $\Sigma = 3$ (for Al_2O_3) and $\Sigma = 5$ (for MgO). (Look back to Chapter 6 for the crystal structures.) The $\Sigma = 3$ diagram shows two twin-related unit cells with the lattice sites identified. Overlapping these two cells produces the pattern in the shaded box and you can see that one in three lattice sites are common to the two grains (the ones at the corners of the box). The CSL for $\Sigma = 5$ (just the lattice sites are shown) is also identified in the shaded box. Note that we must take account of both ions in considering the actual structure (see later). Sometimes it appears that the most valuable feature of the CSL model is that it gives a shorthand notation for talking about GBs. Low-angle boundaries are all $\Sigma = 1$ GBs. Especially in ceramics, not all twin boundaries have $\Sigma = 3$. ($\Sigma = 3$ occurs in face-centered cubic (fcc) crystals because the stacking of close-packed planes is ABCABC, so one in three planes is coincident across the twin boundary.) For a particular GB, if we choose any plane, then a certain fraction of points will lie on this plane in both lattices. We call this fraction Γ^{-1} . Again, it is easiest to appreciate the meaning of these definitions by studying the examples in the following sections. Γ is not widely used but might be the most important factor and it reminds you that the different planes may be

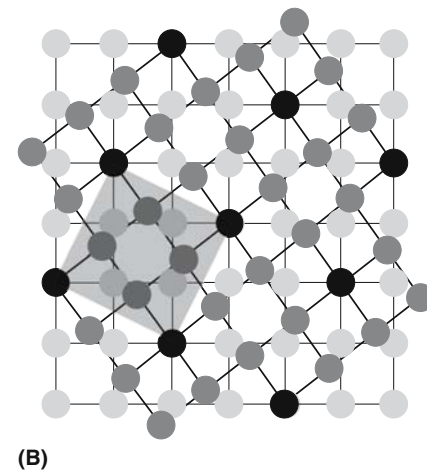
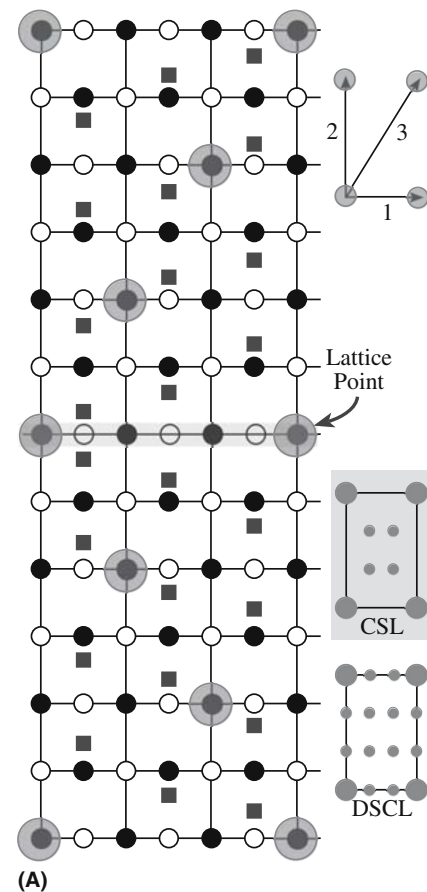


FIGURE 14.1 Schematics of two low- Σ GBs. (a) $\Sigma = 3$; (b) $\Sigma = 5$.

very different. Γ can equal 1 for the $\Sigma = 3$ GB, but could be 3, 9, or greater.

Throughout our discussion of GBs, you should keep in mind that there are many similarities to surfaces.

- There is a *pressure difference* across a curved GB just as there is across a surface.
- Charge affects the structure and chemistry of GBs.
- The structure of a GB determines its properties and behavior.
- GBs can be wet and dewet by GB films just as surfaces are by surface films.

Computer modeling of GBs can give considerable insights, but be careful when using older results in the literature. The complexity of ceramic structures and the Madelung problem cause difficulties and some older simulations may not be reliable, in part, because they used too little material in the calculation because of the capabilities of the computers.

We will discuss the properties of GBs later, but should keep in mind some features as we work through the chapter.

- The density of atoms in GBs is less than in the bulk crystal.
- The chemistry of a GB is not the same as the bulk (because the bonding must be different).
- Properties of GBs must differ from those of the bulk.

All GBs have a thickness (just like the soap films) and the GB is not uniform across that thickness; so GBs are actually volume defects again.

14.2 FOR CERAMICS

Ceramics are usually used in a polycrystalline form. GBs in ionic and covalent materials must be better understood to improve the science of processing of many modern ceramic materials; the properties of polycrystalline ceramics depend directly on the geometry and composition of GBs. The types of GBs commonly found in ceramic materials range from situations in which the distance between the grains is $\geq 0.1 \mu\text{m}$ and such grains are separated by a second phase (glass), to the basal twin boundary in Al_2O_3 , which is atomically abrupt and potentially very clean.

We need to understand how the presence of glass affects GBs in crystalline materials. This glass can be present on the surface of grains or within GBs as an intergranular film (IGF) in either single-phase materials or in materials with an intentionally high (or unavoidable) glass content.

The type of GB present in a sintered (or hot-pressed) compact may be significantly influenced by the surface characteristics of individual particles before and during sintering. Obviously if there is glass on the particle, there is likely to be glass in the GB. We need to understand the behavior of the surface at high temperatures under conditions appropriate to sintering (Chapter 24). Since GBs can be structured or can contain a thin noncrystalline layer, the chemistry of the region close to the GB is important.

We start by asking what is special about GBs in ceramics? This is the question we asked about surfaces and dislocations and the answer is basically the same.

- Ceramics have localized charge or covalent bonds. Dangling bonds exist at GBs.
- Since the bonding is ionic, covalent, or mixed ionic/covalent, there may be large local changes in density at the interface. Ceramic GBs have a space charge.

- Since the unit cells of all but the simplest binary compounds are large, it is likely that a GB with a fixed misorientation angle and interface plane will probably (rather than possibly) exist in more than one (meta)stable configuration. There will still only be one minimum energy.
- Energy is dependent on the GB plane, just as it is for surfaces. Accordingly, steps and facets (large steps) on these GBs will also be important. They are actually necessary for the GB to move.
- Many ceramics are processed in the presence of a second or third phase far away from conditions of thermodynamic equilibrium, and a remnant of this phase may remain at the GB even if it is not the lowest-energy configuration. Impurities segregate to GBs as illustrated by the XEDS and EELS plots in Figure 14.2.
- There is the problem of specimen preparation for analysis of interfaces in ceramics. In general, we cannot prepare a sample without altering the GB in some way.

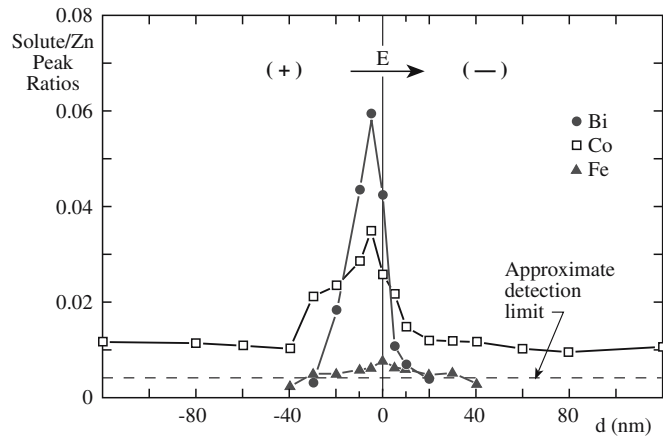
The extra difficulty is that we may never see a clean GB and, unlike surfaces, we have no way to clean one: ultrahigh vacuum (UHV) does not help us once the GB is there. What is different in comparison to metals? Metals try to make the density of atoms uniform due to the nature of the electron gas. GBs in ceramics may be much more open. The density of atoms in the GB can be very different from that in the bulk grains.

Is CSL theory important for ceramics? The CSL theory is relevant only when the adjoining grains are in direct contact. In ionic materials, we know that surfaces are almost never clean. Adsorption phenomena occur at internal interfaces as they do at surfaces. The driving force for segregation to GBs can be large. In fact, most GBs that have been studied have been “dirty.” Pure polycrystalline ceramic materials do not exist. The layer of glass that may be present at the GB is invariably associated with impurities. Such films are unusual in semiconductors (although they can exist) and would be exceptional in metals.

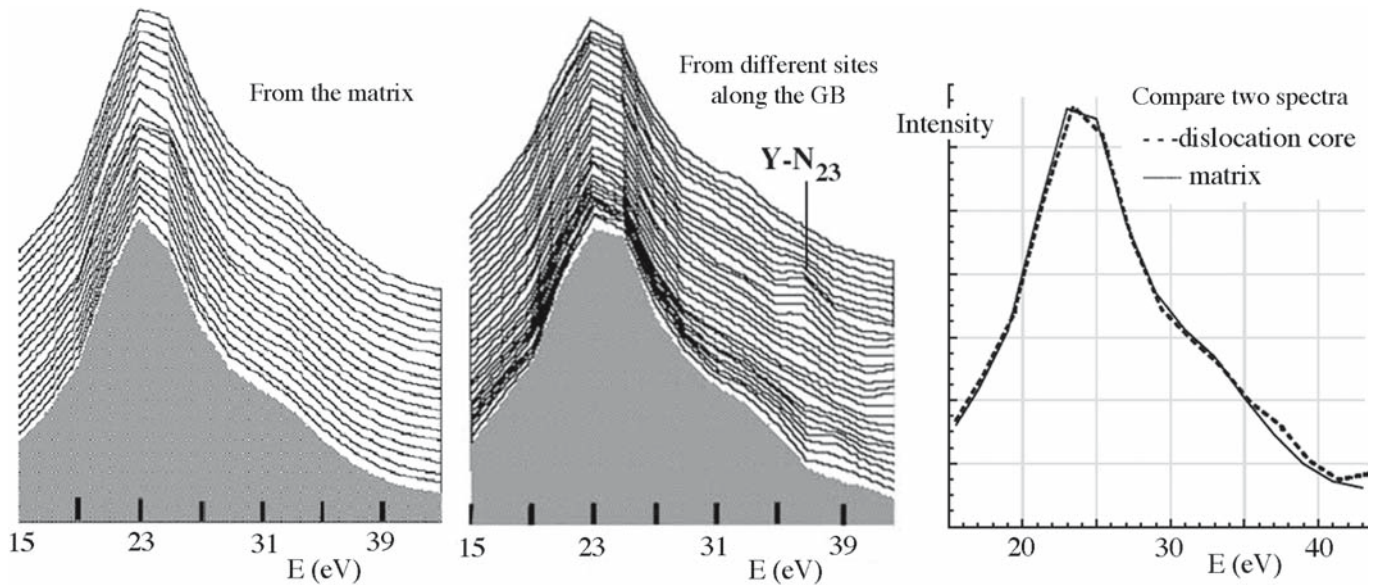
As with other materials, it is difficult to discuss so-called general GBs rather than special ones. Even special GBs in ceramics are not well understood. Both general and special boundaries are likely to be far less clean than models of such interfaces might assume. Methods for analyzing interfaces containing IGFs have been compared. It was concluded that the results can be ambiguous even when a combination of techniques is used. Unambiguous characterization will be achieved only when the structure, chemistry, and bonding are assessed simultaneously.

What *facts* are actually known about GBs in ceramics? We can make the following statements.

- *Structured GBs do exist in ceramic materials.* This conclusion applies to both high- and low-angle GBs.



(A)



(B)

FIGURE 14.2 Solute distribution at GBs. (a) Profiles using XEDS; (b) EELS spectra used to analyze a GB in sapphire. In (a) the integrated X-ray solute/Zn peak ratios are plotted against d , the distance from the GB.

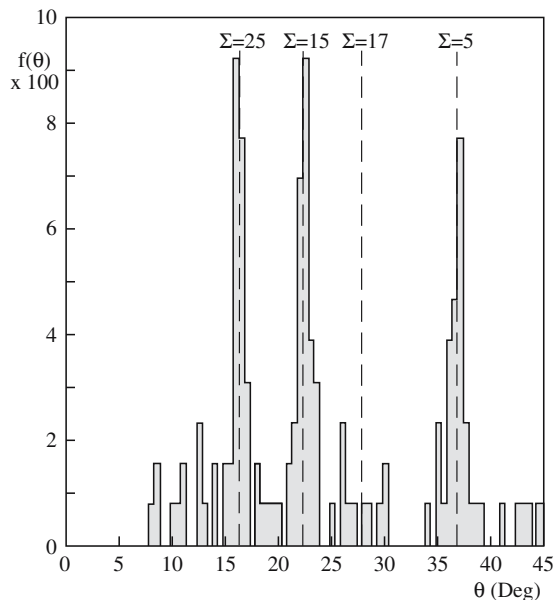
- GBs in ceramic materials do exist that are not “structured” but are, instead, wet over their entire area by an amorphous phase (an IGF).
- The structure of GBs in ceramic materials tends to be relatively more open (less dense) than is found for interfaces in metals that are otherwise crystallographically similar.
- The effects of several ions being present in the unit cell can be recognized. They can produce special interfaces in which only one sublattice is affected or can cause a modification of the interface structure itself.
- A particular interface may not have a unique structure because of the presence of two ions or because two or more structures are possible that do not have significantly different energies. It is also likely that the presence of impurities at the interface will modify the structure by favoring different polyhedral sites.

14.3 GB ENERGY

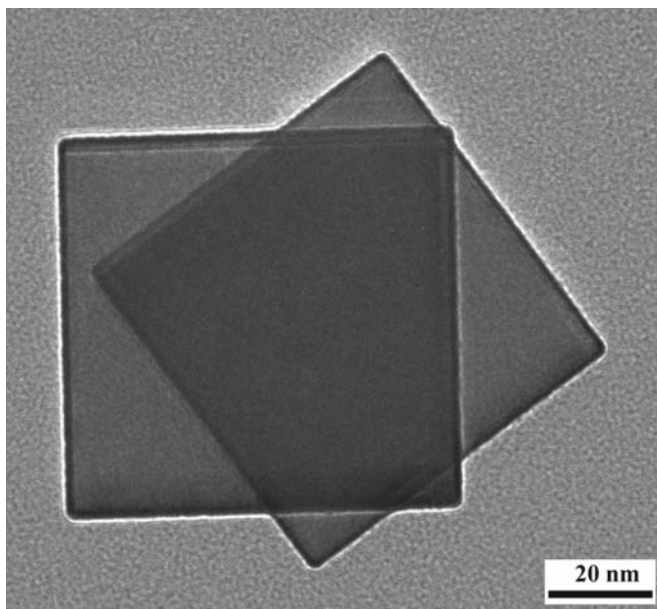
The energy of a GB is a very important quantity, but it is even less well known than for surfaces, and is usually determined in relation to surface energies. There are two key questions:

- How do we define the energy of a grain boundary?
- What factor causes a GB to have a low interfacial energy?

The GB energy, γ , depends on the misorientation of the two grains and on the orientation of the plane. We can again use the Wulff plot (γ versus θ where θ now means the misorientation) and the inverse Wulff plot (γ^{-1} versus θ). The challenge of γ versus θ plots is to define the orientation of the GB plane, i.e., having fixed θ , you must still fix \mathbf{n} , the GB normal for both grains. Keep in mind



(A)



(B)

FIGURE 14.3 Rotated MgO nanoparticles and their relation to Σ . The frequency of measuring a rotation θ is $f(\theta)$.

that we expect γ to decrease as the temperature increases as is found for surfaces (Eötvös rule); this dependence on temperature will be important in sintering. One approach to the problem is to plot the individual Wulff plots for the two separate grains and then to consider what happens when the two grains are joined along a particular plane.

MgO Smoke

One method used to examine the possibility of low-energy GBs is the classic MgO smoke experiment. Mg metal is burned in air and the resulting MgO smoke particles are caught on a grid. The relative orientations between cube

particles can be determined using TEM; the angles between different $\{001\}$ planes are measured much as Haüy originally did for single crystals. We now do this more accurately using diffraction patterns or high-resolution transmission electron microscopy (HRTEM) images. This experiment is special for ceramics because we are joining nanoparticles at high temperatures although we do not actually know when they joined so we do not know the sintering temperature. Figure 14.3 shows an example of such particles together with the frequency of occurrence, $f(\theta)$, of the misorientation angle. The oxide bicrystal particles form with a strong preference for certain orientations in which the two crystals have a fraction of their lattice sites in common: the coincidence boundaries. This experiment has long been one of the bases for believing that Σ is an important parameter in determining the energy of GBs. It does not measure γ but does suggest that γ is related to Σ . Unfortunately, results from computer modeling suggest that this is not necessarily the case, but it is such an attractive intuitive concept that it persists.

Energy of Low-Angle GBs

When θ is small, the energy of a low-angle GB is approximated as the total self-energy of the dislocations within a unit area of the boundary. However, as θ increases the stress fields of the dislocations progressively cancel out so that the energy increases at a decreasing rate and may peak before decreasing to a low value at a special orientation as shown in Figure 14.4. When the dislocation spacing is small, the dislocation cores overlap, so that when θ exceeds 10° (somewhere in the range of, say, $10\text{--}16^\circ$) it is not possible to identify the individual dislocations.

The Read–Shockley formula for the energy, E , of a low-angle GB considers the stress field and the core energy of the dislocations.

$$E = E_0\theta(A - \ln\theta) \quad (14.1)$$

E_0 is a constant that is a function of the elastic properties of the material (and hence of the stress field) and A is a

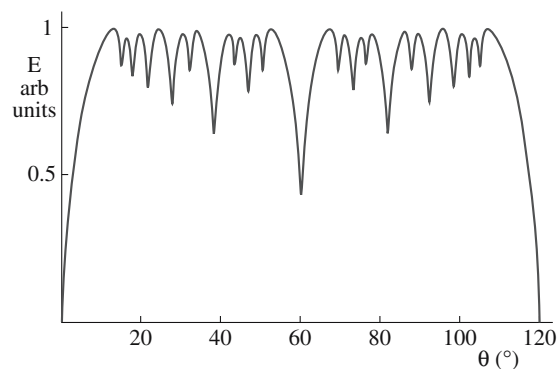


FIGURE 14.4 Cusp in a plot of GB energy versus misorientation angle, θ .

constant that depends on the core energy (remember our discussion of r_0 , the dislocation core radius).

We can also define the Gibbs adsorption isotherm for grain boundaries. We extend the analysis from surfaces to the internal interface.

$$\frac{\partial \gamma}{\partial \mu_i} = -\Gamma_i \quad (14.2)$$

where Γ_i is the excess moles of i per unit area of the GB. All the other variables (e.g., P and T) are held constant.

14.4 LOW-ANGLE GBs

Low-angle GBs contain arrays of dislocations. In its simplest form, the structure of the twist boundary consists of two sets of orthogonal screw dislocations as shown in Figure 14.5a and b; the schematics show the structure before and after relaxation to form the screw dislocations. Figure 14.5c shows how dislocations in a twist boundary might be seen emerging at the surface; you can see that part of the grain is physically twisted relative to the other because of the screw dislocations. The simplest tilt GBs consist of one set of edge dislocations as shown in Figure 14.6. Note that the statements both include the word “simplest.” Most tilt boundaries will have two different sets of edge dislocations, and twist boundaries in noncubic materials may be accommodated by only one set of dislocations! Figure 14.6b shows that we must use two sets of edge dislocations if the GB is not symmetric. (We sometimes have to, even if it is symmetric.)

Figure 14.7 is a TEM image of a twist boundary in Si; a tilt boundary in NiO is shown in Figure 14.8. The image of this tilt boundary is particularly interesting because it shows that the density is different at the GB.

The spacing of the dislocations, D , is related to the boundary misorientation angle, θ , and the Burgers vector of the dislocations, b .

$$D = \frac{b/2}{\sin \theta/2} \approx \frac{b}{\theta} \quad (14.3)$$

The latter relation holds only if θ is very small. In this case, we can either reveal the individual dislocations by decorating them or by etching the surface as shown in Figure 14.9. Equation 14.3 has been well tested for fcc metals and some simple ceramics.

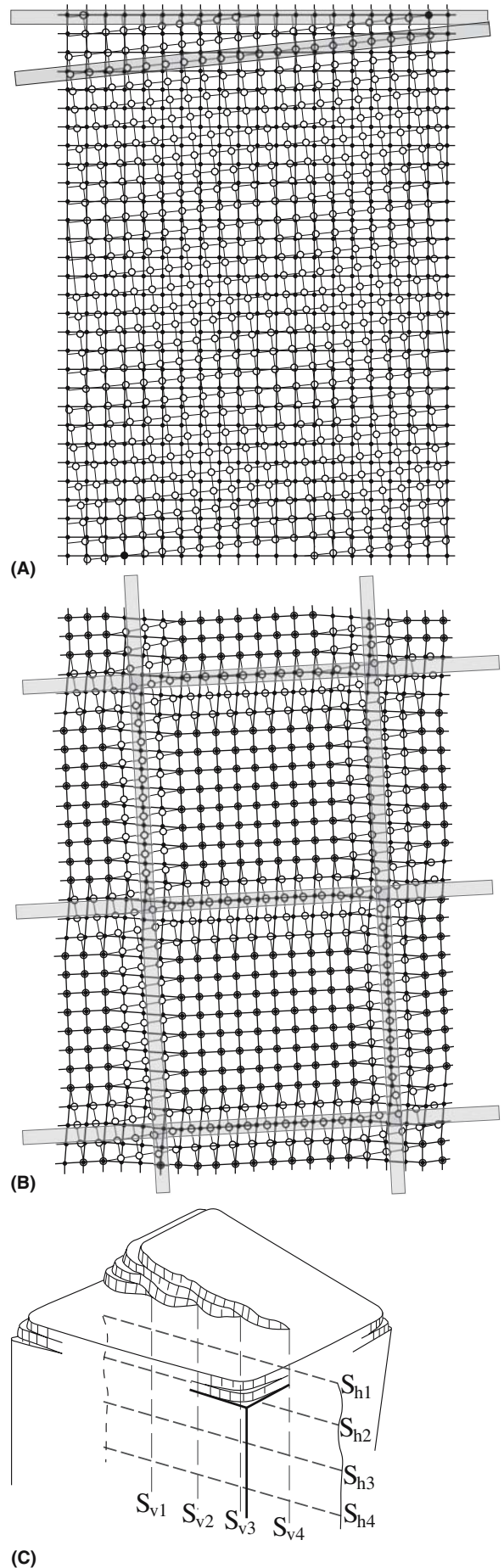
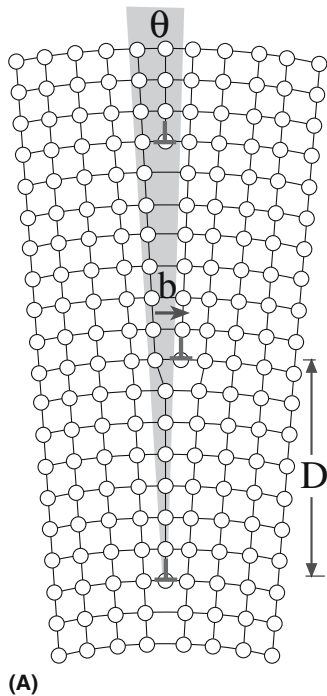
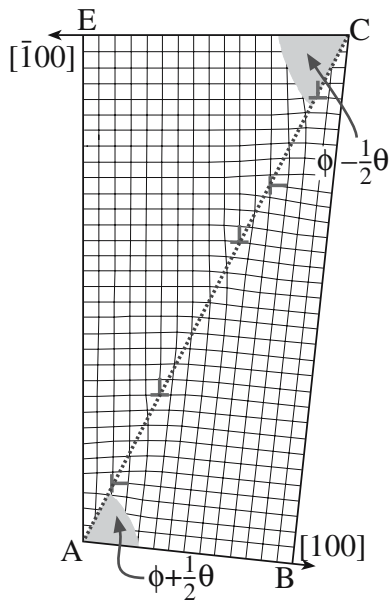


FIGURE 14.5 Schematics of a low-angle twist GB. (a) Before and (b) after local atomic relaxations. (c) The twist when the GB emerges at the surface.



(A)



(B)

FIGURE 14.6 Schematics of low-angle tilt GBs. (a) Symmetric; (b) asymmetric.

The structure of dislocations and interfaces in ionic and covalent materials has been the subject of much theoretical and experimental research, motivated in part by the realization that the extensive body of information and the concepts that have been accumulated for metallic systems cannot necessarily be directly transferred to these nonmetallic systems.

The structures of all defects in ceramic materials can be more complex than those of similar defects in the more thoroughly studied pure metals because of the presence of two or more ionic species on two sublattices. The implica-

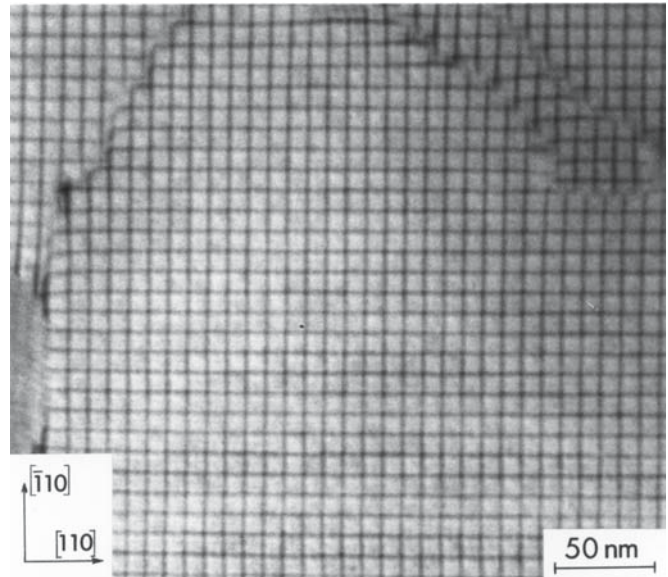


FIGURE 14.7 Two sets of orthogonal screw dislocations in a low-angle (001) twist GB in Si.

tion of the presence of two types of ions is well known in ceramics since it results in the phenomenon of dissociation by climb of dislocations in the lattice or in the GB. The phenomenon has been recorded for materials such as spinel, Al_2O_3 , and garnet. Actually, this phenomenon can also occur in more complex metallic, ordered alloys for precisely the same reason. In Al_2O_3 and MgAl_2O_4 the partial dislocations created by the dissociation process are “perfect” dislocations of the oxygen sublattice; the stacking fault thus formed is therefore only a fault on the cation sublattice.

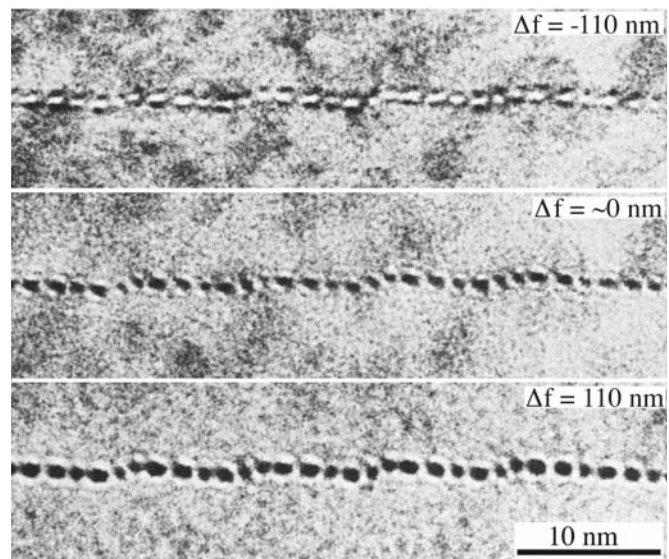
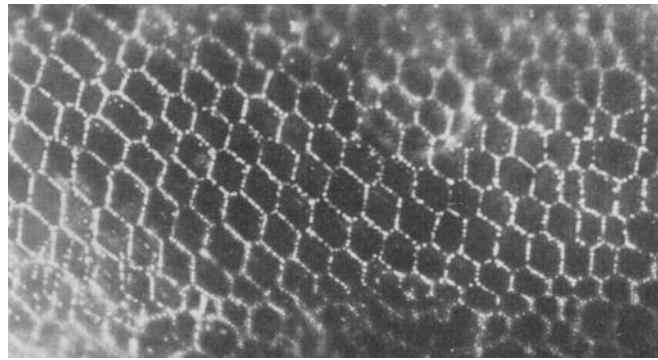
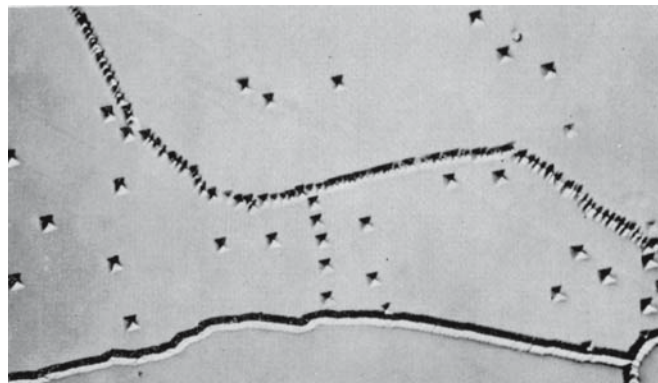


FIGURE 14.8 Dislocations in a low-angle tilt GB in NiO. The defocus (Δf) images show a change in density at the dislocation cores.



(A)



(B)

FIGURE 14.9 Seeing low-angle GBs by (a) decoration (silver particles on a GB in KCl) and (b) etch pits (LiF).

The effect of the large unit cell is well illustrated by the low-angle 111 twist boundary in MgAl_2O_4 . The (111) interface plane can be chosen as A or B in the schematic of the crystal

MULTIPLICITY

Low-angle and high-angle GBs and twin boundaries that appear to be macroscopically the same can exist with more than one different structure.

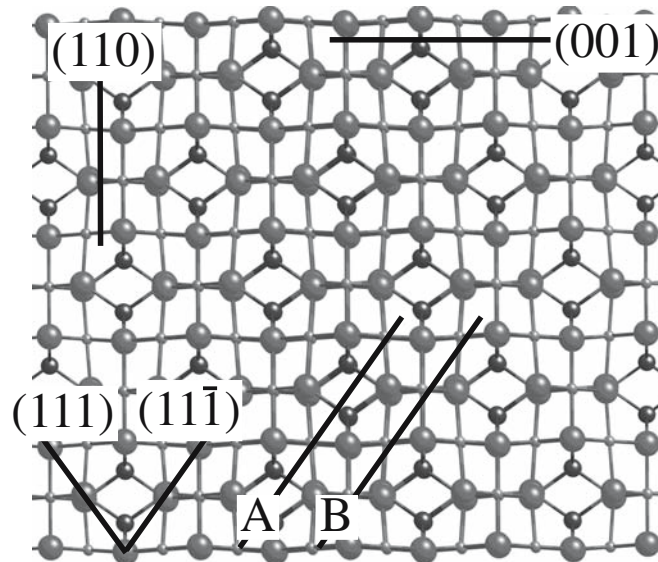


FIGURE 14.10 Spinel structure projected along $\langle 1\bar{1}0 \rangle$ summarizing the important crystallographic planes. A and B are parallel but structurally different (111) planes.

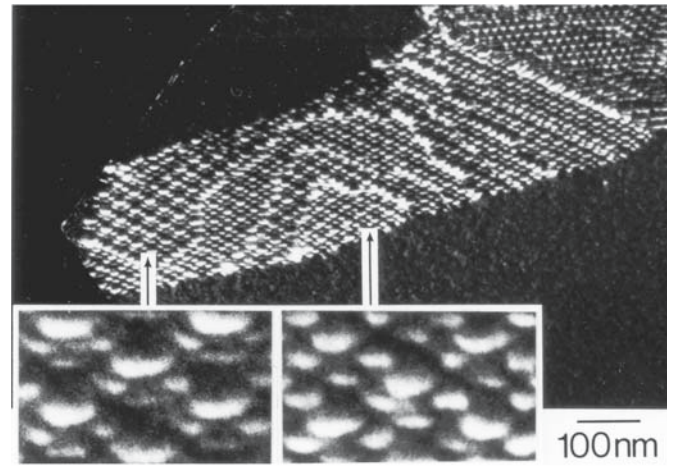


FIGURE 14.11 Low-angle {111} and {001} twist GBs in spinel showing two structures in each case.

structure shown in Figure 14.10. In the spinel (111) twist boundary, an $\frac{a}{2}[1\bar{1}0]$ screw dislocation can dissociate on the (111) plane into two parallel $\frac{a}{4}[1\bar{1}0]$ screw partial dislocations. (Because a is large and this dissociation produces dislocations that would have been perfect if we considered only the O ions.) Since the self-energy of a dislocation is proportional to b^2 , this dissociation halves the total dislocation self-energy. The partial dislocations are separated by a stacking fault (SF), but the energy of this fault depends on whether the glide plane of the plane of the stacking fault is A or B. Thus, there are two different SFs on a {111} plane and two different stacking fault energies (SFEs). The consequence of this multiplicity in the value of the SFE is illustrated in

Figure 14.11 where the width of the SF takes on two distinct values for both GBs.

Figure 14.12 shows the climb dissociation of edge dislocations in a spinel tilt boundary. (This is just an extension of Figure 12.15.) In Figure 14.13 we can see a so-called extrinsic dislocation (along [100]) interacting with the

width of the SF takes on two distinct values for both GBs.

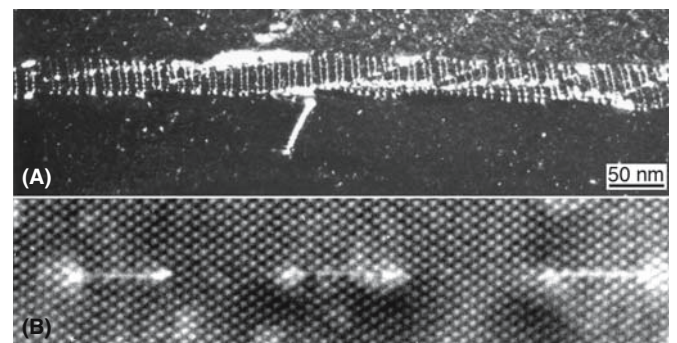


FIGURE 14.12 A low-angle tilt GB in spinel showing an array of climb-dissociated edge dislocations. (a) The GB viewed at an angle; (b) at higher magnification, the dislocations viewed end-on.

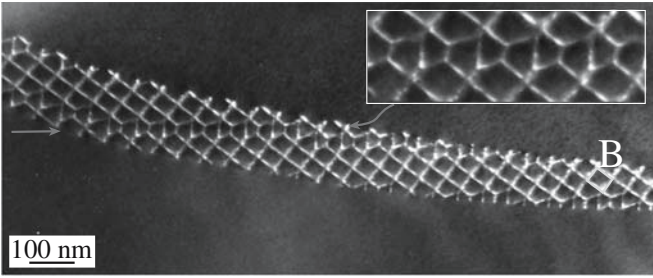


FIGURE 14.13 An extrinsic dislocation interacting with a low-angle {001} twist GB in spinel. Note how all the dislocations are changed by the interaction as seen in the enlarged inset.

screw dislocations that are already present in the interface (to accommodate the twist) in the (001) twist GB.

14.5 HIGH-ANGLE GBs

When θ is $>10^\circ$, the interface is referred to as a high-angle GB. Figures 14.14 and 14.15 show schematics of the $\Sigma = 5$ GB in NiO in the tilt and twist configuration, respectively, taking account of the presence of two ions. The situation is clearly complex: only the lower structure in Figure 14.14 could exist (the others have similarly charged ions too close together). The same considerations hold for the twist GB shown in Figure 14.15: when two ions of like charge are adjacent, one must be removed. As in the low-angle case, high-angle GBs can exist with more than one structure. Figure 14.16 shows images of two special GBs in ZnO; the difference between a symmetric high-angle GB

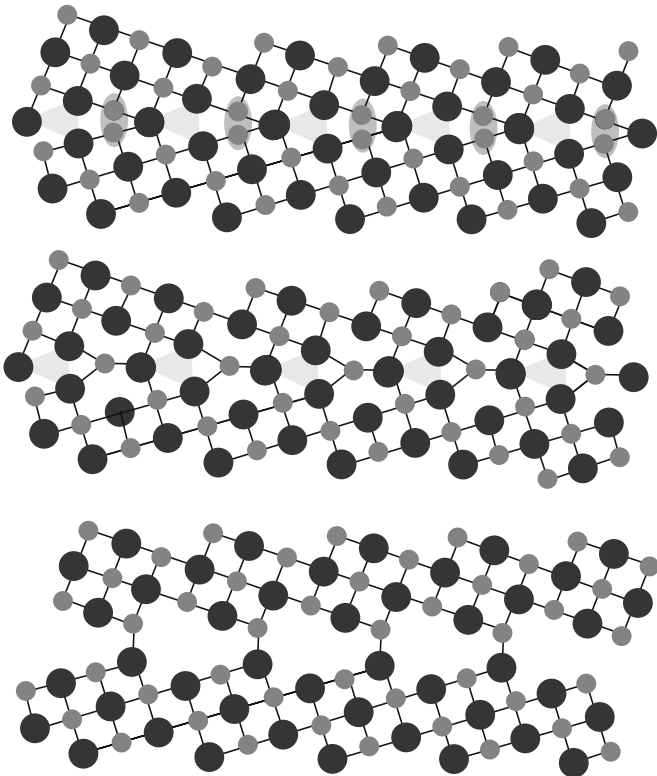


FIGURE 14.14 Schematics of the [001] $\Sigma = 5$ tilt GB in NiO; only the lower one is actually possible.

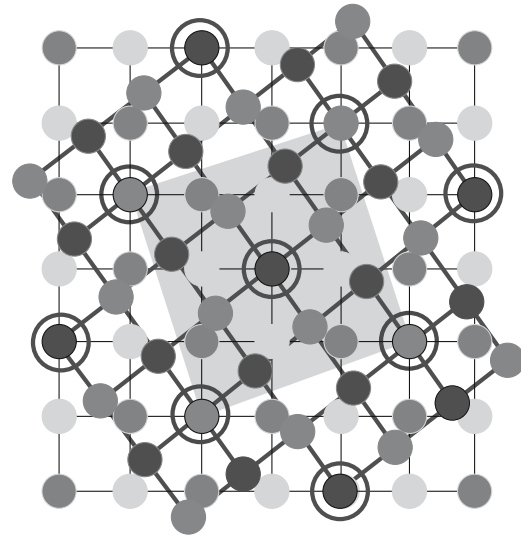


FIGURE 14.15 Schematic of the (001) $\Sigma = 5$ twist GB in NiO showing anions and cations. This structure cannot occur unless some ions are removed.

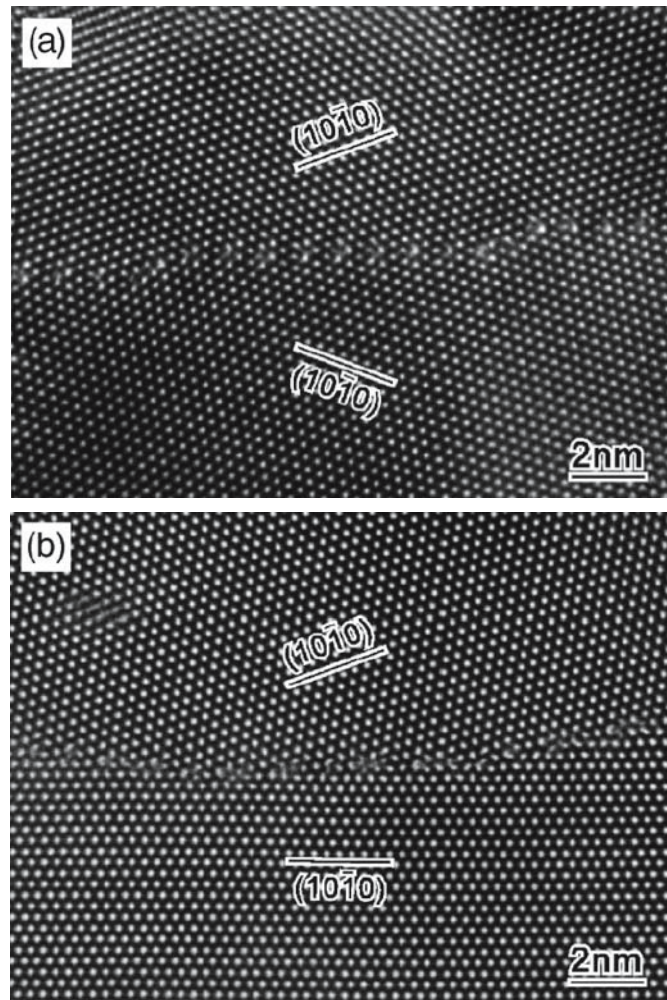


FIGURE 14.16 HRTEM images of two high-angle GBs in ZnO: (a) near-symmetric; (b) asymmetric.

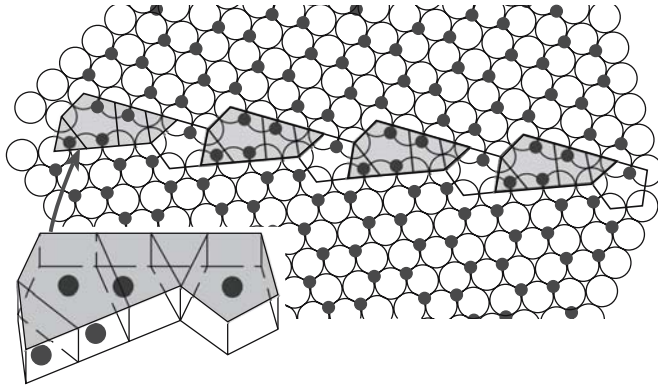


FIGURE 14.17 Schematic of a GB in Al_2O_3 showing the creation of new polyhedra in the GB. The inset shows a tilted view of the repeating group of polyhedra.

and the lower-angle asymmetric counterpart is striking; this type of asymmetric faceting often involves low-index planes as shown here. You can imagine why asymmetric units might be favored by examining Figure 14.17, which shows a schematic of a GB in Al_2O_3 . Polyhedra that were not present in the perfect crystal in Chapters 6 and 7 can be present at a high-angle GB, and these can accommodate larger impurity ions than can the bulk.

More complex high-angle GBs have been the subject of far fewer studies, in part because of the experimental difficulties in characterizing them. This lack of information is unfortunate since these interfaces are ubiquitous in sintered materials. High-angle GBs formed by hot-pressing together two single crystals of MgO appear to behave as would have been anticipated from studies on the corresponding interfaces in fcc metals and semiconduc-

tors and support the earlier interpretation of experiments on MgO “smoke.” However, such interfaces have been the subject of extensive computer-modeling studies that often give a contradictory view.

As these observations show, the plane adopted by a high-angle GB is a very important factor. Such GBs in ceramic materials show a particularly strong tendency to facet, so the plane must be important. These facet planes are almost invariably parallel to low-index planes in one or both grains. The basic argument is that low-index planes are the most widely separated planes and thus involve less energy when a “stacking error” is present in the crystal.

A particularly striking illustration that makes us question the importance of Σ as a measure of the energy of a GB is provided by observations of the $\Sigma = 99$ and $\Sigma = 41$ boundaries in spinel, where, by chance, the interface can facet parallel to several pairs of (different) low-index planes in both grains simultaneously. A similar situation exists for phase boundaries. It could be that the faceting onto low-index planes would lower the energy to below that of similar GBs having a lower Σ . There are no atomistic calculations for such GBs.

14.6 TWIN BOUNDARIES

As in metals, twin boundaries are common in many ceramic materials including MgO, spinel, Al_2O_3 , Fe_2O_3 , the rare earth oxides, quartz, Si, and, of course, the new high-Tc superconductors. Indeed, it seems certain that such interfaces will occur in all crystalline ceramic materials. Some special twin relationships observed in minerals are illustrated schematically in Figure 14.18. The

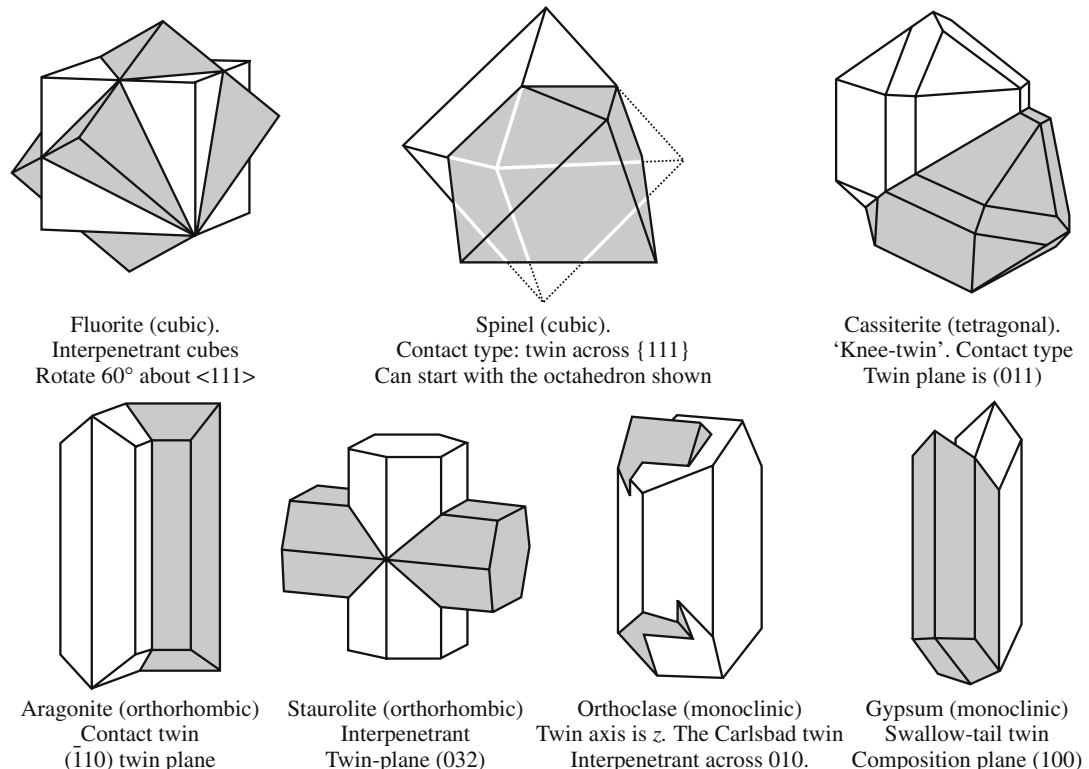


FIGURE 14.18 Examples of twinned grains found in different minerals.

observation of so many twin boundaries is interesting because they are found to facet parallel to low-index planes in at least one grain. We noted that such interfaces can accommodate impurity ions, and this can lead to the phenomenon of chemical twinning, wherein apparently different crystal structures can be related to one another by the periodic repetition of a pair of twin interfaces. This concept can be used to understand the actual mechanism of a phase transformation in a ceramic system.

Several different types of twin boundaries have been seen in Al_2O_3 ; the basal twin boundary is the $\Sigma = 3$ GB, which was discussed in Figure 14.1a. We can form a variety of twin boundaries in Al_2O_3 by mirroring the structure across low-index planes that are not mirror planes in the perfect crystal; hence the $(\bar{1}102)$ plane, the $(\bar{1}104)$ plane (illustrated in Figure 14.19), and the $(11\bar{2}3)$ plane all give twin boundaries [as does the (0001) plane, of course]. A rhombohedral twin boundary [the $(10\bar{1}2)$ twin boundary] is shown in Figure 14.20; notice that it is faceted.

All interfaces in spinel, even the $\Sigma = 3$, (111) twin boundary, can exist with at least two different structures. In a formal treatment of such interfaces the different structures considered here can, in principle, be described by choosing different rigid-body translation vectors. However, such translations are not the small relaxations familiar in, for example, the $\{112\}$ lateral twin boundary in Al, but are more closely related to stacking faults in fcc metals. The image illustrated in Figure 14.21 shows two parallel $\{111\}$ twin boundaries (separated by a microtwin). The translations at the two twin boundaries are different as you can see in the insets.

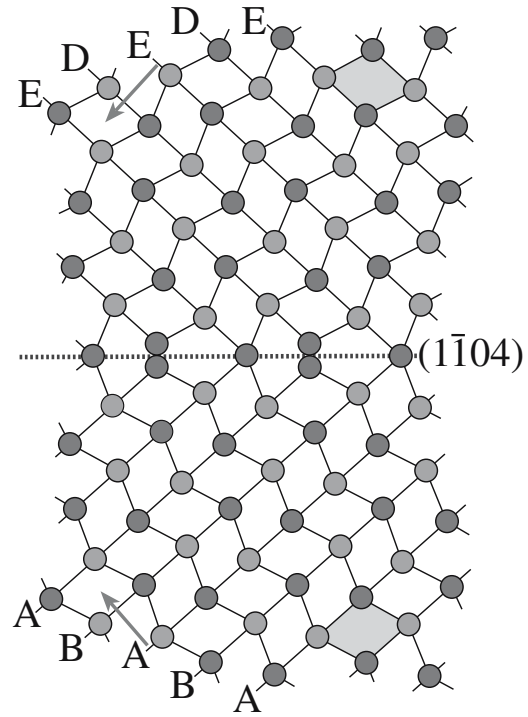


FIGURE 14.19 Schematic of a $(\bar{1}104)$ twin boundary in Al_2O_3 . The arrows show the $\langle 0001 \rangle$ directions; the letters show the hcp stacking of the anions. The cations are omitted but sit in the octahedral—shown by the shaded rhombi.

This translation, which is parallel to the $\{111\}$ plane, is seen because of the location of the cations. As far as the oxygen sublattice is concerned, the twin interface is actually a mirror plane: it is just like the $\{111\}$ twin boundary in fcc Cu.

THE TWINS

A twin is a grain; a twin boundary is a GB.

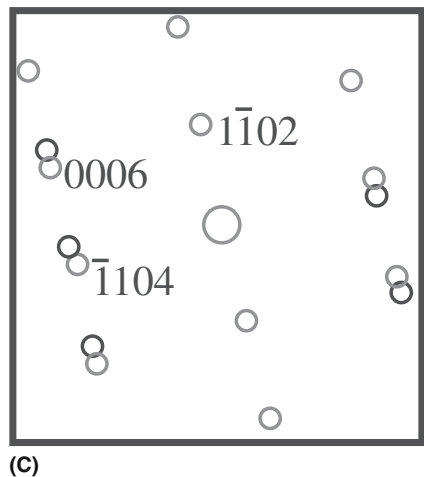
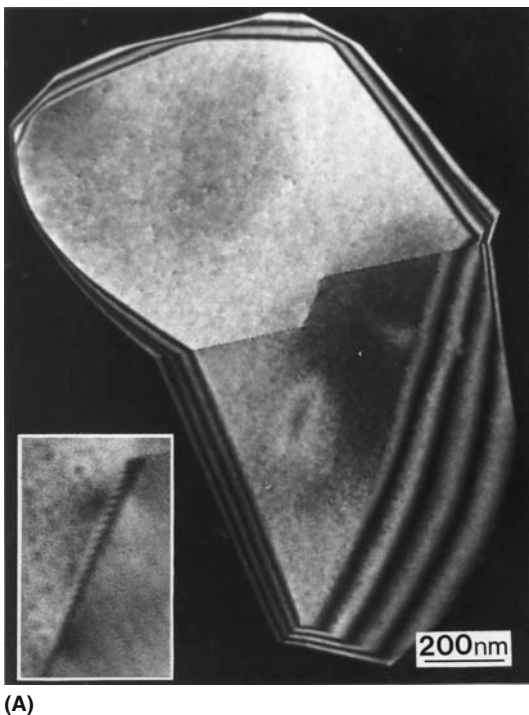


FIGURE 14.20 Rhombohedral twin boundary in Al_2O_3 and its diffraction pattern.

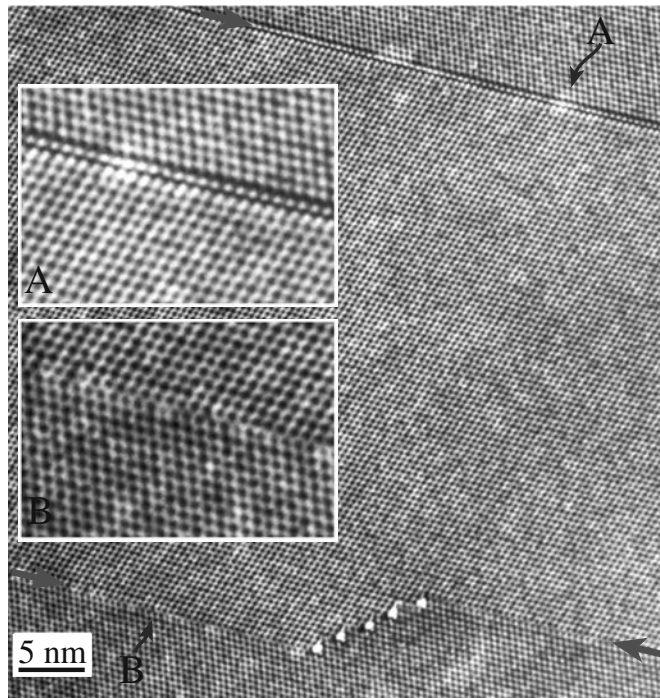


FIGURE 14.21 Two parallel $\{111\} \Sigma = 3$ twin boundaries in spinel having different structures (identified by the arrows). The insets show regions A and B at higher magnifications.

The lateral $\Sigma = 3$ twin boundary in spinel is also special. The structure of this interface can be entirely described in terms of $\{111\}$ segments (which may have different structures, as noted above) and triangular-prism channels, which lie along $\langle 110 \rangle$ directions and are observed as white spots in HRTEM images. The faceting consists entirely of ordered (aligned) arrays of these prism columns; the interface shown here is actually dislocation free, although the prisms can be modeled as an array of dislocation dipoles. There was no local strain contrast in the TEM image.

The image shown in Figure 14.22 is from a thin film of NiO and reminds us that GBs that correspond to a special twin orientation are not necessarily flat. In that case, they are probably more similar to other high-angle boundaries. The twin boundaries in the NiO film occur because NiO can grow on a basal-alumina substrate in two twin-related orientations. We see the twin boundaries because the density is lower at the GB.

An example of how twins can form in a more complex system is shown schematically in Figure 14.23 for aragonite. This figure shows the CO_3^{2-} anions as triangles (as we saw in calcite) while the closed circles represent Ca^{2+} ions. (The numbers give heights of ions in the cells and serve to emphasize the twin symmetry.)

A special group of closely related oxides is illustrated in Figure 14.24. These oxides consist of blocks of MO_6 octahedra (seen as squares along the cube direction), which can be shifted parallel to certain crystallographic planes (known as shear planes) to produce new structures.

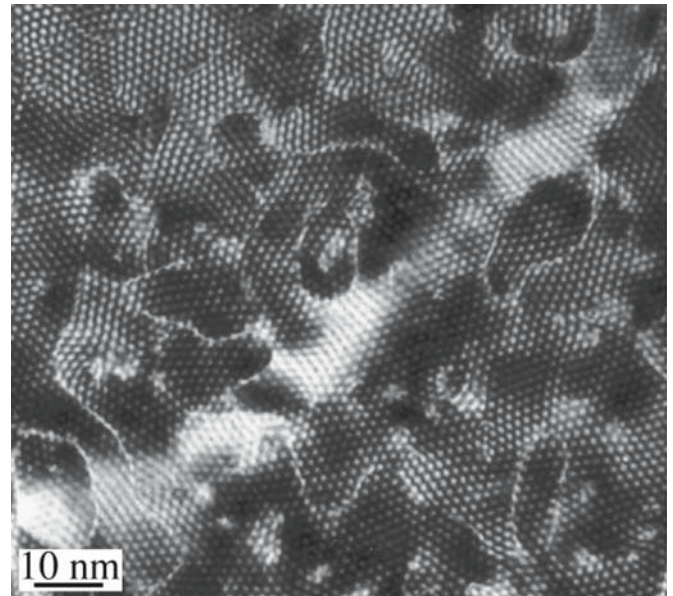


FIGURE 14.22 Curved twin boundaries in a thin film of NiO on an Al_2O_3 substrate. (The hexagonal pattern is a moiré interference effect.)

The circles are tetrahedral cations. Essentially, the shearing acts to change the chemistry along that plane. Crystallographic shear planes are thus like regular stacking faults, but the chemistry also changes—they are *chemical stacking faults*. An example of WO_{3-x} encapsulated in WS_2 is shown in Figure 14.25.

Twin boundaries, like other GBs, can accommodate new ions so that the chemistry changes along the twin

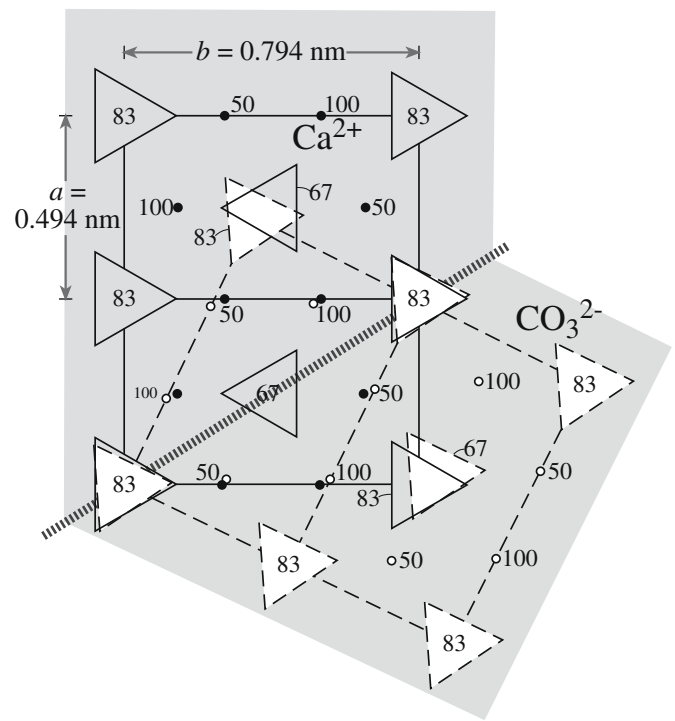


FIGURE 14.23 Mimetic twinning in aragonite. This gives rise to trilling twins when the operation is repeated.

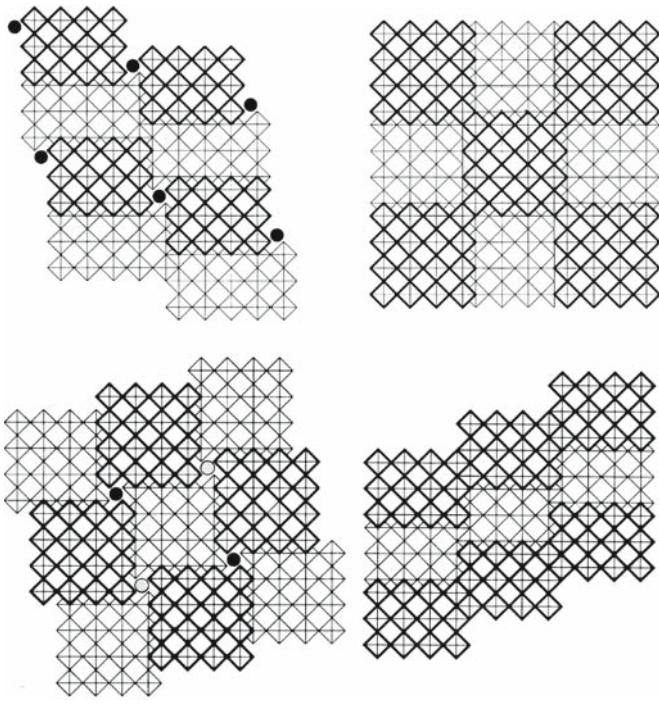


FIGURE 14.24 Shear planes in WO_3 . Dark and light lines are at heights 0 and 0.5.

plan. A periodic repetition of alternating twin planes, each of which accommodates ordered impurities, can then give rise to a new structure. This process is known as chemical twinning. The result for β''' -alumina is illustrated in Figure 14.26. Planar defects can readily be incorporated into this

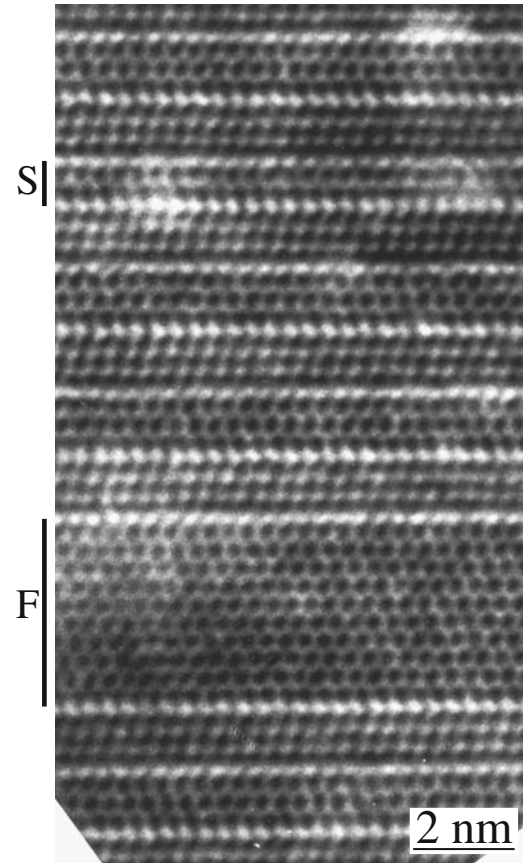


FIGURE 14.26 The structure of β''' -alumina as a repetition of chemical twin boundaries. S and F are a block of spinel and an SF, respectively.

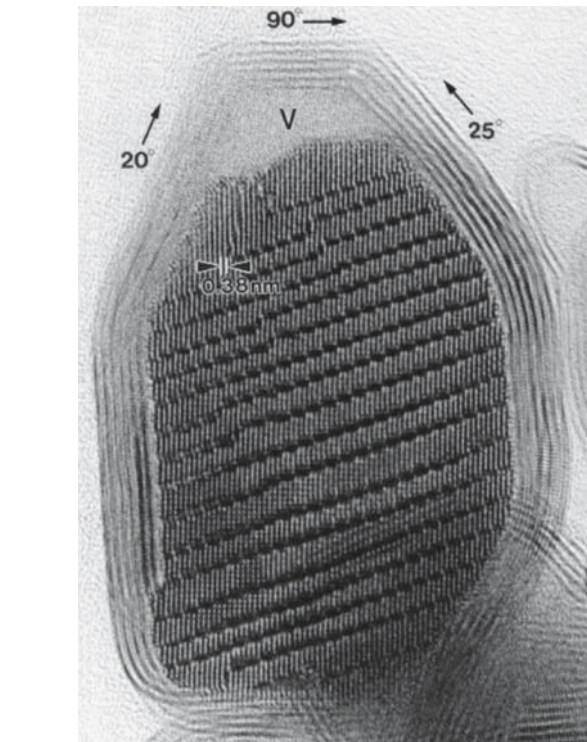


FIGURE 14.25 A defect W oxide encapsulated in a fullerene.

structure. This particle of β''' -alumina contains a sheet of spinel; the spinel is like a sheet of a second phase. As we have seen in Section 7.12, we can also think of the structure of the β''' - Al_2O_3 as being blocks of spinel that twin on every six $\{111\}$ oxygen planes. The attractive part of this description is that we can then understand the fault in the structure where the twin occurs after only four $\{111\}$ oxygen planes. Remember that the twin planes are not actually spinel twin planes because the chemistry is different on the twin plane.

14.7 GENERAL BOUNDARIES

General boundaries may be curved with no specific value of Σ . Can we determine if the GB is clean or what its structure is? We can know if it is not clean and put an upper limit on the impurity content, but we still will not know its structure.

The relationship between the physical parameters of any individual interface and the mechanical strength or properties of that interface has not been directly determined for any ceramic material. As with many

properties of ceramic materials, measurements on GBs are likely to be controlled by dopants or impurity phases; the latter may be present at the 10% level. Computer modeling is usually carried out for pure materials. Finite element modeling (used for fracture studies, crack initiation and propagation, etc.) generally makes assumptions regarding the elastic parameters, which may be very different at an impure interface in comparison to bulk material; the bonding at the interface is different, so the elastic properties must be different too.

14.8 GB FILMS

In Chapter 13 we discussed how a liquid behaves on a solid surface if the solid is not inert. We noted that the situation could change due to evaporation at high temperatures and that the wetting phase need not be a liquid to wet or dewet.

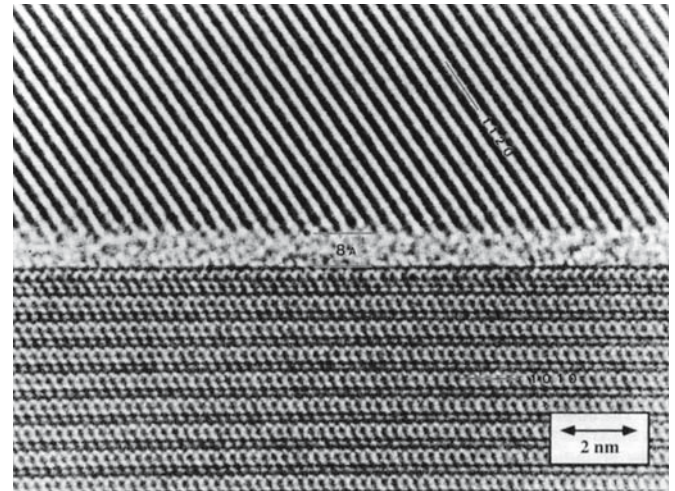
- GB films are directly analogous to films on surfaces or substrates.
- How thick must a film be before it is a new phase?
- Is a GB containing a film one interface or two?

The simple view of whether a glass film will be energetically favorable is that if $2\gamma_{sl} < \gamma_{GB}$, then the film is preferred. This statement is too simplistic, in part because GB films are unlikely to be uniform across their thickness. If γ_{sl} is $\sim\gamma_{GB}$ then we would expect the GB to be stable, but even in this case, the glass must go somewhere.

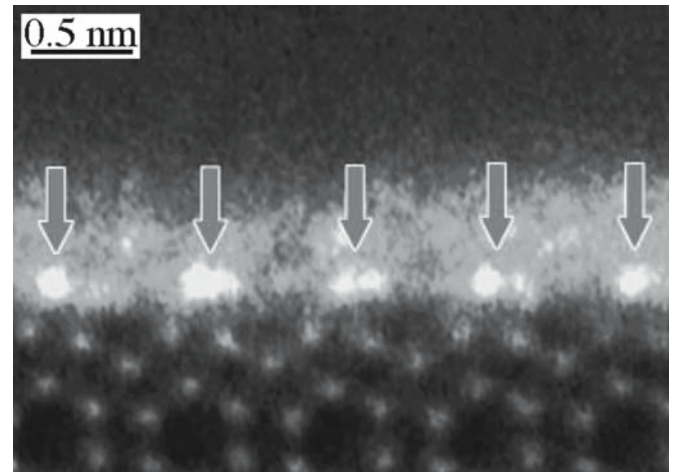
Any of the four types of GB could contain a GB film. How stable the film would be will clearly depend on the energy of the GB with the film versus without it and the availability of a mechanism for removing the film if this would lower the energy.

We know that liquid phases can be very important in polycrystalline ceramic materials. We also know that most interfaces in some ceramics (e.g., Si_3N_4) contain a very thin ($\sim 1\text{--}5\text{ nm}$) IGF as illustrated in Figure 14.27. Thin amorphous layers have been reported to be present in a wide range of ceramic materials (see Table 14.1). It is sometimes incorrectly assumed that all GBs (other than special twin boundaries) in Al_2O_3 contain such a thin amorphous film. In some materials the same interface may or may not contain an amorphous film, depending on how it was processed.

- Glass is very often present in ceramic materials whether intentionally included or not. In many oxides it is present because of impurities in the initial materials used to process the compact. In others it is intentionally



(A)



(B)

FIGURE 14.27 Examples of HRTEM image of IGFs in Si_3N_4 . (a) Phase-contrast image; (b) Z-contrast image showing ordering of rare-earth dopant at the glass/crystal interface.

added to lower the processing temperature via the process of liquid-phase sintering.

- The width of glassy GB films can vary from $\sim 1\text{ nm}$ to $>1\text{ }\mu\text{m}$.
- The TEM techniques used to identify these films do not always give unambiguous results.
- At high temperatures the mechanical properties of a ceramic may be drastically lowered if a glass is present. For example, the viscosity of the glass decreases significantly at a relatively low temperature leading to enhanced creep and related phenomena; remember that the viscosity of soda-lime-silica glass varies from $10^{15}\text{ dPa}\cdot\text{s}$ at 400°C to $10^2\text{ dPa}\cdot\text{s}$ at 1300°C . At the higher temperature glass cannot support a shear stress and allows

IGFs

A note on very thin films: if a film is $\sim 1\text{ nm}$ thick and the system is in equilibrium, then the film may be better described as an adsorbate layer. Experimentally, the challenge is knowing that the system is in equilibrium.

TABLE 14.1 Examples of Intergranular Phases

System	Property affected	Notes
Glass in Si_3N_4	Mechanical	Glass forms from components added as sintering aid and oxide on particle surface
Glass films in Al_2O_3	Mechanical	Impurities in the glass can affect its properties
Bismuth oxide in ZnO	Electrical	The IGF is the key to the operation of varistors
YAG in AlN	Thermal	Y_2O_3 added as sintering aid to allow lower cost production of substrates
Surface contamination	Chemical	Oxidation of SiC can passivate the surface
Clean GB in YBCO	Electrical	GB may not be superconducting; if very thin it can act as weak links

rapid deformation of the material. In other circumstances, the presence of the glass may be beneficial since it may assist in the branching and blunting of cracks by generally weakening grain boundaries.

- It is much easier to process ceramics in the presence of a liquid phase, in part for the same reason—the glass allows deformation at lower temperatures; diffusion is also faster through a glass. The glass thus allows the sample to be shaped and/or densified at lower temperatures.
- The composition of the IGF may vary across its width. In Figure 14.27, the rare-earth dopant has formed an La-rich monolayer at the glass/crystal interface.

It is well known that the presence of glass in GBs greatly enhances sintering, in part because transport of

matter along and across the intergranular regions is then even faster than when no glass is present. It is important to realize that the glass does not simply act as a catalyst, but also changes the character of the interfacial regions. The glass can dissolve the crystalline grain and reprecipitate it elsewhere. In particular, it tends to encourage faceting of the grains; the scale of this faceting may vary from nanometers to micrometers. After processing, the glass may remain as a thin layer in the interface during preparation of the polycrystalline compact as was initially demonstrated for Si_3N_4 . The glass may also crystallize to form an intergranular crystalline layer or it may withdraw from the planar interfaces into three-grain and four-grain junctions (the dewetting process). Even though great care may be taken to ensure that no glass is present during processing, the glass may subsequently enter the interfacial region during processing or service of the component. In either case, the properties of the ceramic may be greatly influenced by the presence of any glass in the grain boundary; a dramatic example is the effect on mechanical properties (e.g., for Si_3N_4 or Al_2O_3), which also aids sintering, although other properties (e.g., the thermal conductivity for AlN) may be just as strongly affected.

Figure 14.28 illustrates another feature associated with glass in crystalline ceramics. The pairs of grains joining at these two boundaries are similarly oriented. Both of the interfaces contain dislocations, i.e., they were glass free after processing. The topology of the two interfaces is, however, clearly different. In Figure 14.28a the interface is wavy, while in Figure 14.28b it is flat. The difference can be explained by the processing history; the bicrystal in Figure 14.28b initially contained a layer of glass, while that in Figure 14.28a was kept as clean as possible during processing. So the difference in the topography is ascribed to the effect of the glass while it was present in

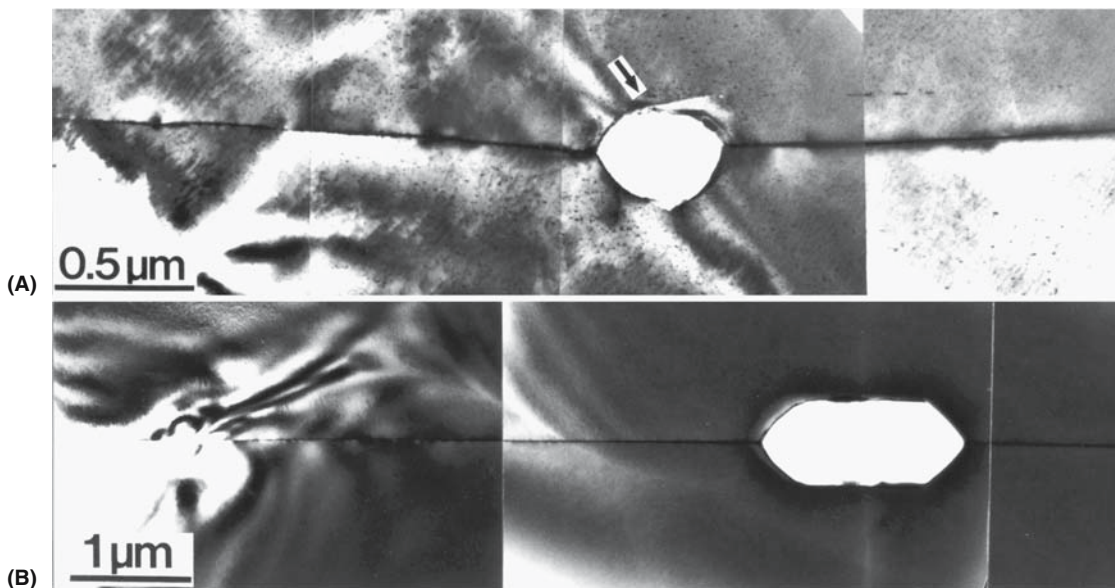


FIGURE 14.28 The same GB in Al_2O_3 processed with and without glass.

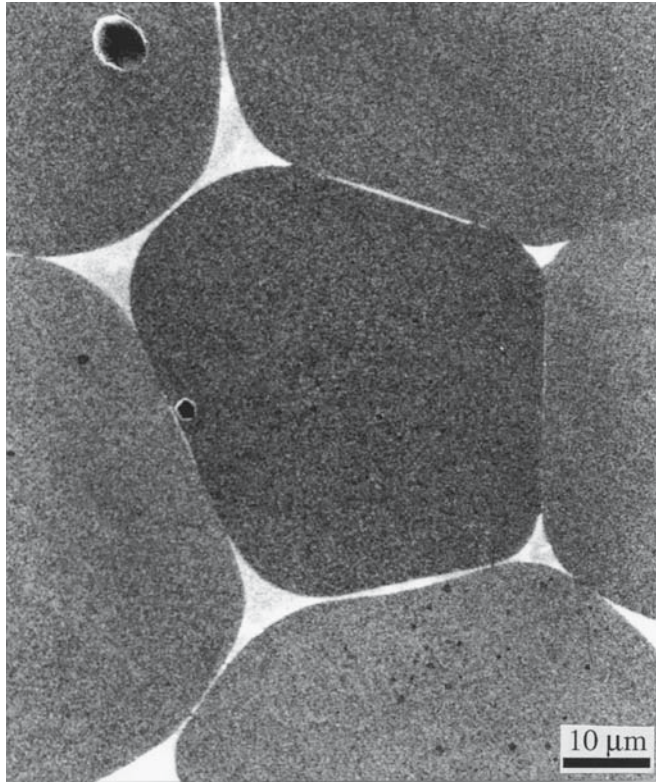


FIGURE 14.29 SEM image of glass-infiltrated MgO showing glass located at the GB and at TJs, but even in a GB it need not be a uniform layer.

the interface. Clearly this effect can potentially be very important in understanding such GBs, but it presents a major difficulty; the key component required to explain the structure of the GB had already disappeared before the processed compact could be examined.

Water in silicate GBs can significantly change the mechanical properties of the GB. The GBs really are wet in the everyday sense! The crystal structure of the grains causes ordering in the water and thus changes the viscosity of the water.

The behavior and effects of water in GBs are important topics in geology. There has been much discussion on the thickness of intergranular glass films. There may be an equilibrium thickness for such films, as has been reported for Si_3N_4 , but a more common situation is shown in Figure 14.29. This sample was a dense, small-grain, glass-free polycrystal that was intentionally infiltrated with monticellite glass. Here the width of the glass layer clearly varies from boundary to boundary and even along a particular boundary. Nearby boundaries can show a layer that is nearly uniformly $2\ \mu\text{m}$ wide or that is apparently glass free at this magnification. This image illustrates an important factor that is often overlooked: most of the glass is contained in TJs and QJs. These junctions serve as “pipes” for transporting the glass. Very little is known of the

characteristics of TJs (they are not TEM friendly) or their role in determining mechanical properties.

Figure 14.30 shows a $\Sigma = 13$ GB in alumina that was processed with an initial layer of anorthite glass that had a uniform thickness of $\sim 100\ \text{nm}$. The glass is still present in the interface after processing, but it varies in thickness along its length. Here the explanation for the thickness variations is clear: the two glass/crystal interfaces facet independently except in the regions where they appear to touch. The controlled preparation of such interfaces is not, in principle, limited to special boundaries, since any two such surfaces can be so joined and both the composition and the initial amount of glass can be predetermined and controlled.

Dewetting of GBs has been observed in Si where the glass was the native oxide, SiO_x ($x \sim 2$). Figure 14.31 shows TEM images of a $\Sigma = 1$ (low angle) $\langle 110 \rangle$ tilt boundary and a $\Sigma = 5$ (001) twist boundary. In both cases abrupt changes in contrast can be seen where the glass has dewetted the interface to accumulate in pockets. The pockets actually facet parallel to $\{001\}$ and $\{111\}$ planes due to the crystallography of the Si. Thus, even the $\Sigma = 5$ GB can achieve its low-energy structure, including the secondary dislocations, in the presence of a dewetting glass film.

Crystallizing intergranular glass layers after processing has been used to modify the mechanical properties of the resulting compact. The yttria-rich glass in polycrystalline Si_3N_4 and monticellite glass in MgO can be crystallized after liquid-phase sintering to change the properties of the polycrystal.

An important remaining question concerns how the presence of the second glass/crystal interface (in a GB) might affect the crystallization process. If topotactic crystallization nucleates at one glass/crystal interface, it is unlikely that the crystallizing glass will form a complex (high-energy) interface when it reaches the adjacent grain. Similarly, if crystallization nucleates at both glass/crystal interfaces, a complex grain boundary, possibly with residual glass, will form when the crystallized glass layers grow together.

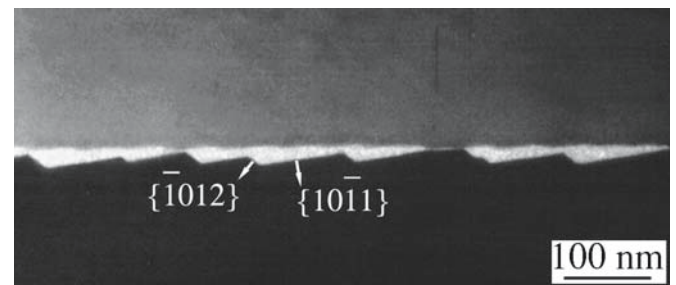
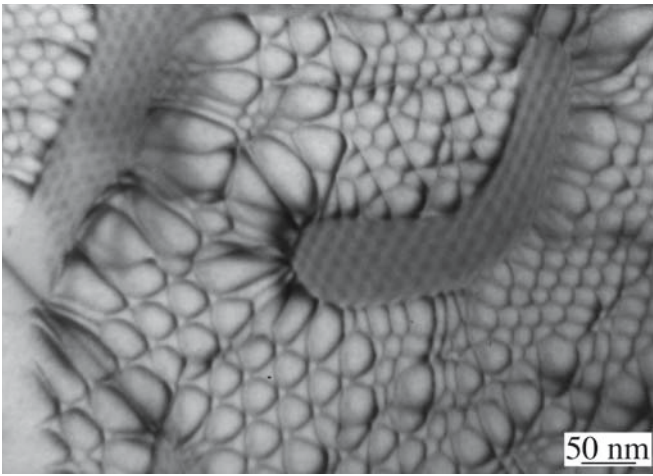
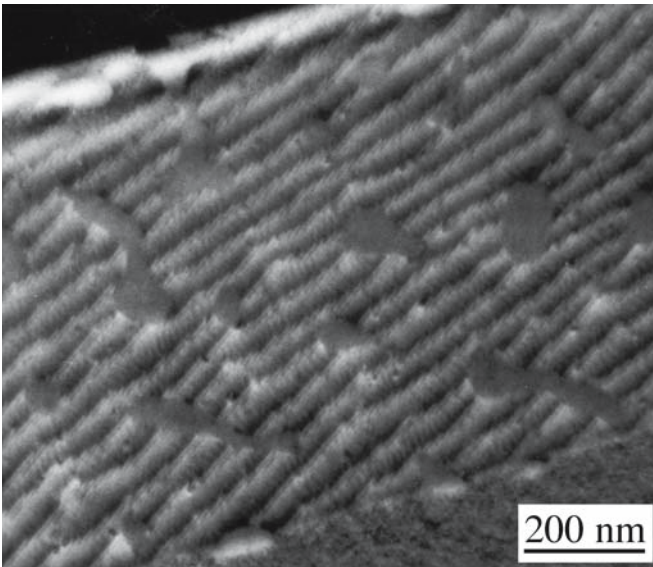


FIGURE 14.30 An IGF in Al_2O_3 that was initially uniformly thick varying in thickness after heat treatment.



(A)



(B)

FIGURE 14.31 Dewetting of IGFs in Si GBs: (a) $\Sigma = 1$ {111}; (b) $\Sigma = 5$ {001}.

14.9 TRIPLE JUNCTIONS AND GB GROOVES

We will not spend much time on TJs because not much is known about them. We can identify three different types of TJ.

1. One composition: Three-grain junctions
2. Two compositions: Two phase boundaries plus a GB
3. Three compositions: Three phase boundaries

Thus, for example, the groove formed when a GB emerges at a free surface is an example of a two-composition triple junction. Three TJs meet at a QJ. The pockets of second phase at TJs in Figure 14.32 could each be considered as sets of three two-composition TJs. Incidentally, looking at the surface will not give us an unambiguous picture of the dimensions.

A schematic diagram showing how GBs, TJs, and QJs change with changes in wetting behavior is shown in Figure 14.33. Wetting is clearly important when we process ceramics using a liquid phase. For the liquid phase to be effective in densification we want it to wet the grains, hence $\phi = 0$. But for optimum properties of the final ceramic we may not want the grains covered with a second phase. A good example is in AlN ceramics for electronic packaging. The second phase, which will almost always have a much lower thermal conductivity, should form isolated pockets at the TJs leaving a “clean” GB enabling maximum phonon transport.

A TJ can act like a capillary. The TJ in Figure 14.34 was covered with liquid glass at the processing temperature. When the sample was cooled, the liquid withdrew into the TJ like water escaping a bath (but the physics is different).

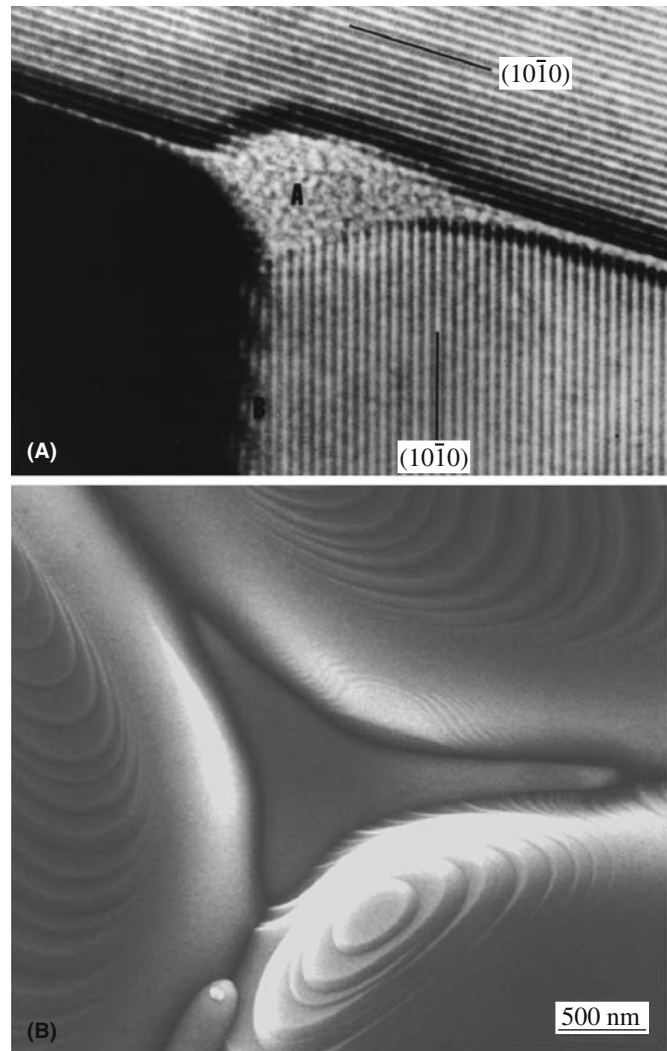


FIGURE 14.32 Examples of TJs: (a) Si_3N_4 using TEM; (b) MgO using SEM.

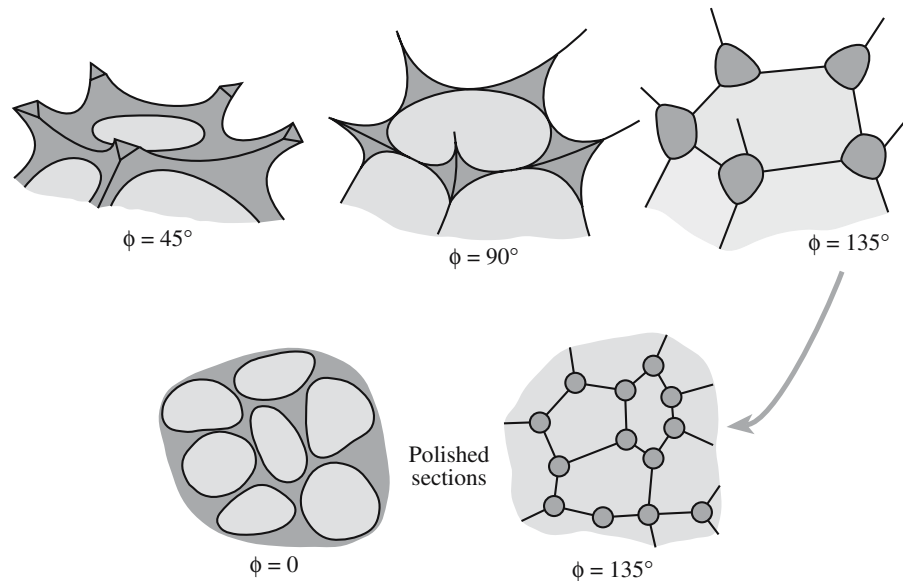


FIGURE 14.33 Schematics showing the relationship between IGFs, TJs, and QJs in 3D as the wetting angle is changed. Lower: a reminder that we usually see sections of these structures.

14.10 CHARACTERIZING GBs

When studying a GB, we want to know the structure, chemistry, and bonding. How do we characterize a GB? What are the parameters we need? Just to understand the structure, we have to know all the crystallographic parameters, then the chemistry, and then the bonding. No single technique gives us all this information. No ceramic GB has been fully characterized, although we are getting close with a few.

Plane of boundary—Is the GB flat?

Axis of misorientation—The GB is an internal interface, so we need the orientations of both grains.

Atomic structure of boundary—The GB must be flat for HRTEM.

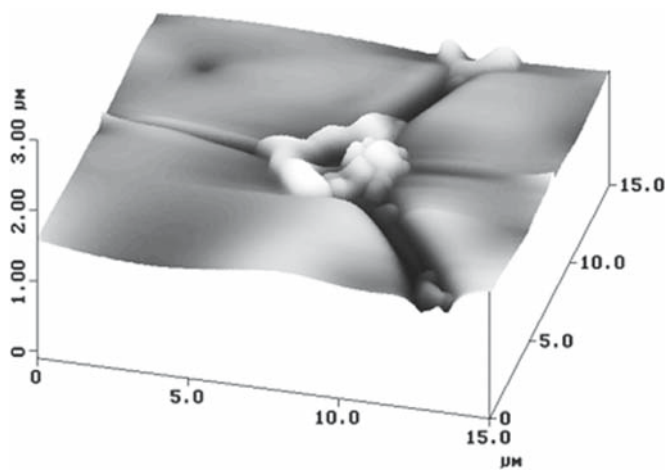


FIGURE 14.34 Direct evidence for the capillary effect at a TJ; the glass recedes into the TJ on cooling.

Internal interfaces are fundamentally different from surfaces because of their inaccessibility. The key tool for studying GBs is the TEM. This should be obvious from the number of TEM images in this chapter! Although the material must usually be thinned prior to examination in the TEM, the area of the GB we do examine is unchanged.

TEM can be used to observe a periodic array of edge dislocations; we use Burgers circuit to characterize the dislocations

We can probe a GB by STM only where it intersects the surface. Atomic force microscopy, however, (AFM) is a key tool for characterizing GB grooves

The specimen preparation problem for TEM: GBs in ceramics must be considered in terms of both their structure and chemistry (even in so-called pure materials). Just as the wetting behavior of a surface may be altered by the doping of the surface layer, so it is important to identify and characterize the segregation of impurities and additives to GBs in these materials. The problem here is 2-fold: the features of the GB (its misorientation and plane) must be identified and the distribution of “foreign” elements must then be accurately measured. The last part of this process is actually even more difficult than you might expect. The added complexity arises from the methods that are, at present, routinely used to prepare samples of ceramic materials for examination in the TEM.

The TEM specimen is usually thinned by ion-milling; crushing will fracture the sample along GBs. This thinning process has been shown to result in cross-contamination of the specimen and in the formation of a groove at the interface. The degree of contamination depends on a large number of factors:

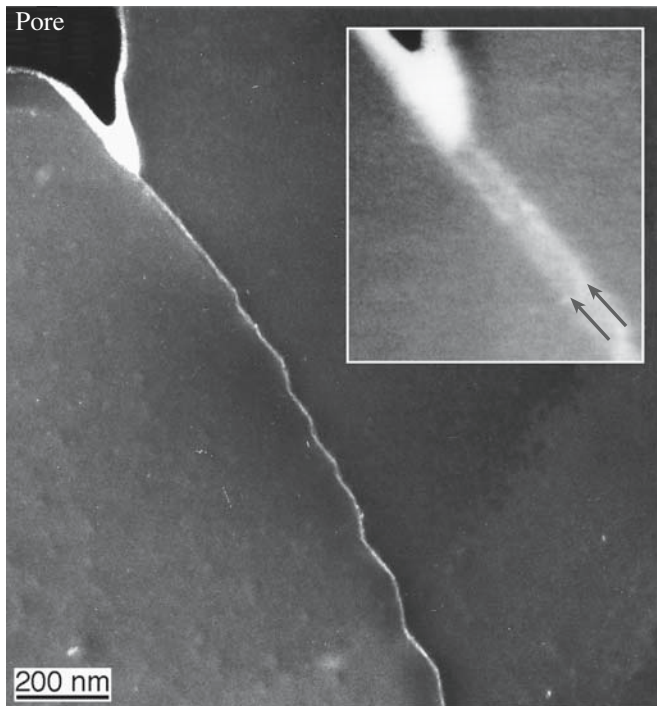


FIGURE 14.35 A cautionary tale: the “glass” in the faceted GB is actually material deposited in surface grooves during sample preparation.

- The type of oil used in the diffusion pump of the ion-miller (old ion-millers may use a silicone-based diffusion pump oil since it is less expensive and more resistant to cracking than are Si-free oils).
- The cleanliness of the system used to carbon coat the thinned TEM specimen.
- The ion-thinning process also preferentially removes the lighter atoms and may deposit what it removes somewhere else on the sample.
- Ion thinning can implant Ar into loose, or open, structures (like GBs).
- Ion thinning may thus both preferentially thin the GB (forming a groove) and then deposit material in that groove. (Figure 14.35 shows the problem.)

It is always best to use bicrystals for model experiments to relate the chemical profile of an interface to its structure since we can then know the initial composition of the GB, but these are not “real” materials.

The principal techniques are

- The Fresnel-fringe technique
- The diffuse-scattering technique
- Direct lattice-fringe imaging where the geometry of the interface is suitable

The diffuse scattering technique suggests amorphous-film thicknesses that are 50–100% larger than are found by high-resolution EM (HREM), i.e., at least part of the image obtained from diffusely scattered electrons must be

due to factors other than the presence of a thin amorphous film. It is important to use a combination of techniques to characterize, as fully as possible, any given interface. For example, diffuse scattering is very dependent on the specimen preparation techniques. The reasons for using these techniques can be appreciated by noting that the amorphous layer, which may be present at the interface, may be only 1 nm wide. The complexity of image interpretation when examining thin (1–>5 nm wide) GB films makes computer analysis and simulation necessary. We can use image simulation programs to simulate the formation of Fresnel fringes, taking into account the possibility of GB grooving at both surfaces.

14.11 GBs IN THIN FILMS

Why are we interested in this topic? Ceramic thin films are becoming increasingly important in the electronics industry for their novel magnetic and electrical properties. Often these films are neither amorphous nor single crystal, so GBs become relevant. There will be TJs in the film and at the substrate/film interface (even if the substrate is amorphous). The TJ can form a pit (a 3D groove) at the surface, but it will generally not groove at the substrate.

Figure 14.36 is a dark-field TEM image from recrystallized anorthite glass on sapphire. The substrate appears dark and the anorthite grains have faceted edges.

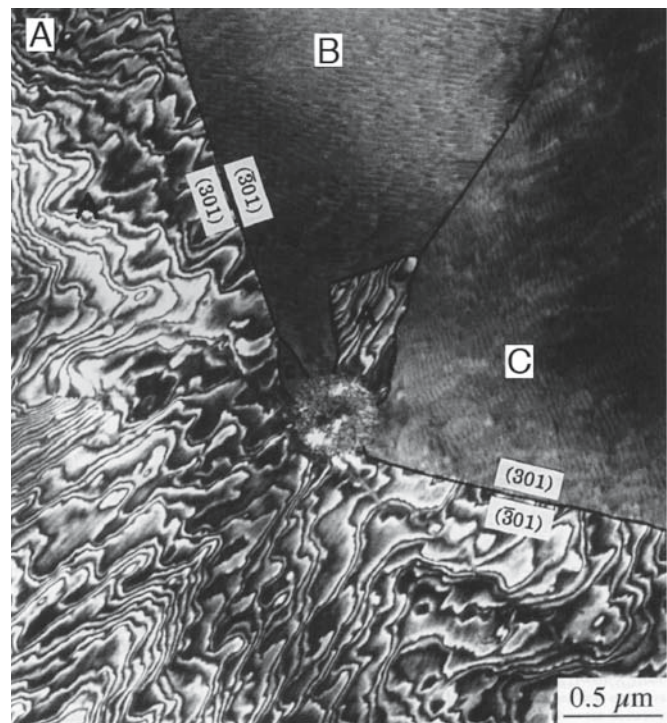


FIGURE 14.36 Example of GBs in thin films of anorthite on Al_2O_3 ; the three grains correspond to three epitaxial orientations, but only one shows the misfit dislocations in this TEM image.

The facets often meet at 60° or 120° angles. The three orientation variants are shown as A–C. Two TJs between all three variants can be seen in the image. Variant A contains irregular contrast associated with the interfacial dislocation network; variants B and C show moiré fringes.

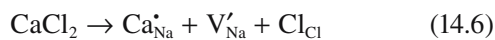
14.12 SPACE CHARGE AND CHARGED BOUNDARIES

We introduce this topic now because it shows the fundamental relationship between point defects and interfaces. The concept of a space charge is special for ceramics. Simply put, it is possible for an excess charge of one sign to be present at the interface. This excess charge must be balanced by a space charge further away from the boundary. There is not much experimental data, but the concept is widely accepted.

Consider NaCl: ions on either sublattice can, in principle, move to a new site on the GB leaving a vacancy in the lattice.



In general, the energy required to form these point defects at the GB is not the same as it is in the bulk and differs for the two ions. We therefore get more of one than the other at the grain boundary. Overall, the crystal is neutral, hence there must be a space charge in the bulk. Now add CaCl₂ to the NaCl crystal. The impurities (or dopants) give charged point defects.



We are adding the positively charged Ca²⁺ ion and are thus increasing the concentration of vacancies on the Na sites. We know that



So, adding CaCl₂ to the bulk decreases [V_{Cl}[•]] in the bulk (because it increases [V'_{Na}]). Since we have increased [V'_{Na}] in the bulk, [Na_{GB}[•]] must decrease in the GB, which implies that [Cl'_{GB}] increases in the GB. Hence the GB potential is negative. There is a complication: what about Ca_{Na}[•]? What if it all goes to the GB? The radii of the Ca²⁺ and Na⁺ ions are about the same (~0.1 nm). We do not know the radius of the Ca ion on the Na site. We have also not considered the possibility of forming a defect complex such as (Ca_{Na}[•], V'_{Na}); the binding energy is quite large, ~0.4 eV. The idea of the GB space charge is therefore important, but far from simple, and there is not much experimental data.

14.13 MODELING

The extensive analysis of the structure of GBs in ceramic oxides using computer modeling does not appear yet to explain the experimental observations. One limitation of the modeling approach is that the GB plane is fixed in the calculation. Furthermore, computer modeling of asymmetric interfaces is not routine—constructing the unit cell for asymmetric GBs is difficult. Most of this computer modeling has been directed at understanding the structure of GBs in materials with a rocksalt structure. In these materials (primarily NiO and MgO), the oxygen-ion sublattice is in an fcc arrangement whereas the cations are located at the octahedral sites. The situation is more complex for most other oxides when different interstices are occupied; as you know, in spinel two-thirds of the cations occupy octahedral interstices while one-third occupies tetrahedral interstices.

We cannot assume that all the ions have found their “ideal” sites in sintered material, e.g., some Al³⁺ ions in MgAl₂O₄ may be on tetrahedral sites. The structure predicted by computer modeling for the {112} lateral twin interface in NiO contains a rigid-body translation. Such a translation is not observed experimentally for the same type of interface in spinel, which has the same oxygen sublattice. It may be that the reason for this difference is that the translation-free configuration is what is present on a migrating GB and this becomes “frozen in” when the sample is cooled. The structure predicted by minimum energy calculations is a stationary structure.

The disagreement between experiment and modeling may be also due to the difficulty in preparing ideal clean interfaces in ceramic materials. For example, the Σ = 5 GB in NiO can be stabilized by adding Schottky defects to the interface, i.e., by decreasing the density at the GB while keeping it “pure.” Experimental observations do show that the density at interfaces is generally lower than that of the bulk material.

Most programs use a cell that repeats the structure of the GB and, hence, most calculations have been carried out for low-Σ GBs.

14.14 SOME PROPERTIES

GBs are everywhere in ceramics. The formation of GBs will be discussed in Chapter 24 since this is the initial product of the sintering process. The movement of GBs is the necessary process allowing grain growth to occur and will also be discussed there. GBs influence the behavior of polycrystalline ceramics—both bulk materials and thin films. We will discuss their properties extensively in later chapters. Here we just list a few examples so you can see their importance.

Example 1: GBs are probably the most important defect in ceramic superconductors. They can dramatically

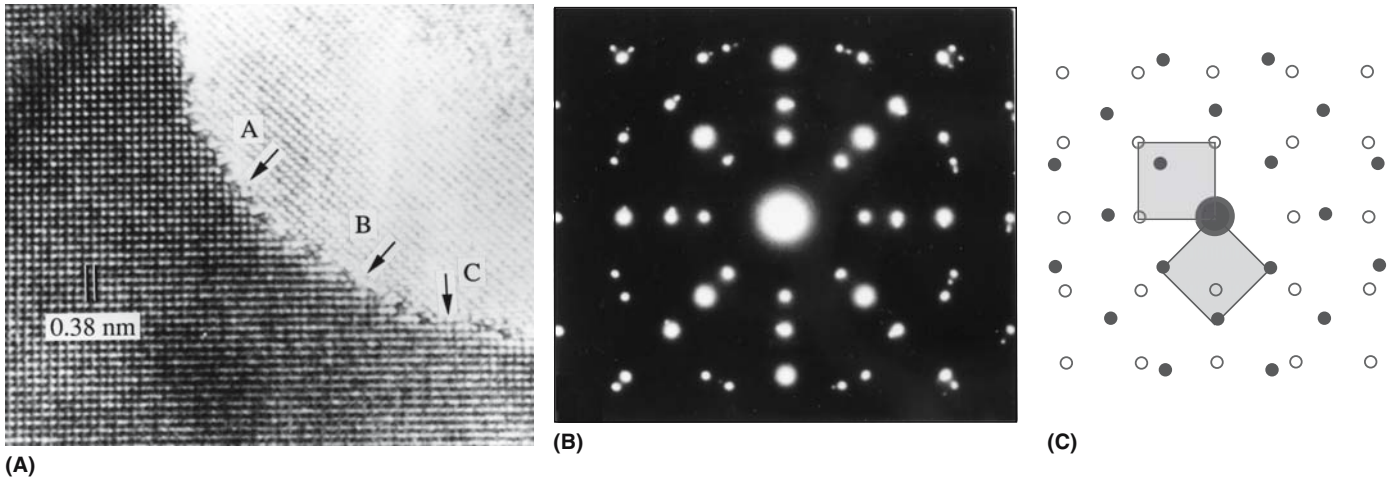


FIGURE 14.37 HRTEM image of the 45° GB in YBCO and the diffraction pattern.

reduce critical currents (J_c). The idea is that the GB acts as if it is a second phase. This sheet is not a superconductor—it may act like a sheet of insulator inside the superconductor. If the GB is very thin then it is possible to use its weak-link nature to fabricate a Josephson junction. Figure 14.37 is an HRTEM image of a near $\Sigma = 29$ GB in a YBCO thin film. The GB is narrow, abrupt, and faceted. We will revisit this topic in Chapter 30.

Example 2: GBs in AlN can reduce the thermal conductivity if they are not clean. Because AlN is difficult to sinter to high density without the use of a liquid phase (the bonding is mainly covalent), the GBs often contain a second phase, which always has a lower thermal conductivity (Chapter 34). Ytria may be added to react with oxide in the GBs to form YAG at the triple junctions: a GB-dewetting process.

Example 3: GBs in ZnO are processed intentionally to include a glass film. This film allows the ceramic to be used as a varistor (voltage-dependent resistor), a device that protects circuits from high-voltage spikes (Chapter 30). Figure 14.38 illustrates an IGF of varying thickness in ZnO and how this film controls the resistance.

Example 4: GBs in Si_3N_4 invariably contain glass films as shown earlier. At high temperatures they can lose their mechanical strength when the films soften (Chapter 18).

Example 5: GBs in magnetic ferrites affect the initial permeability, μ . The permeability of Mn-Zn ferrite increases from about 0.8×10^{-3} up to 3.5×10^{-3} when the grain size is increased from $5 \mu\text{m}$ to $15 \mu\text{m}$ (Chapter 33). Although porosity has a role, it has been determined that grain size is more important.

Example 6: GBs affect the scattering of light in transparent materials. Light scattering is greatest when the grain size is close to the wavelength. In addition, IGFs produce a change in refractive index as light passes through a material (Chapter 32).

In metals, GBs control mechanical properties when the grain size is small as seen from the Hall–Petch equation

$$\sigma_y = \sigma_0 + \frac{B}{d^{1/2}} \quad (14.8)$$

The yield strength (σ_y) is expressed in terms of the yield stress, σ_0 (σ_0 is related to the intrinsic stress, σ_i , resisting dislocation motion) and the grain size, d . When this relationship was deduced, it applied to a situation in which the grains were deformed by plastic deformation and the GBs acted as barriers to dislocation motion. This model is unlikely to be valid in general for ceramics since deformation by dislocation glide is not common. However, the relationship between d and σ_y does hold as we saw for polycrystalline MgO in Figure 1.2.

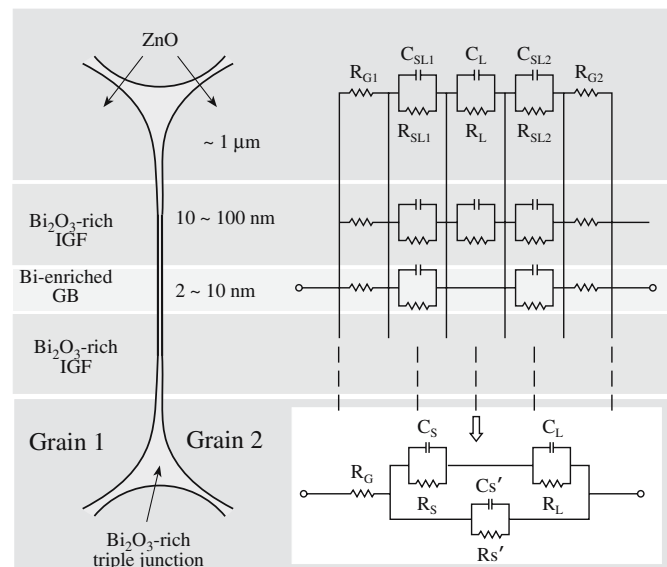


FIGURE 14.38 Modeling IGFs in ZnO varistor materials.

CHAPTER SUMMARY

GBs in ceramic materials are important in almost all applications of these materials since ceramics are usually polycrystalline. GBs have a thickness—we can think of them as thin films even if they are structured. This means that a polycrystalline material is really a composite one. An added difficulty is that essentially every GB “film” is different, but we can think of an *average* GB, which is especially good if there actually is an amorphous film (IGF) at the interface. The most important point to remember is the relationship between GB energy and GB (interface) tension, which includes the idea that there is a pressure difference across a curved GB just as there is across a curved surface. You should be able to define the words twist, tilt, mixed, and twin and to understand the concept of Σ (and Γ), how it relates to structure, and why it can be related to GB energy. Triple junctions and the space charge at GBs are very important, but we know little about them. There are two special features for ceramics: the space charge and IGFs. IGFs are special for ceramics because glass is easily formed and maintained, especially when the ceramic contains at least small concentrations of Si.

PEOPLE IN HISTORY

Bollmann, Walter was a pioneer in explaining the O-lattice concept.

Friedel, G. and Friedel J. were early contributors to the development of the CSL.

Matthews, John was best known for his work on misfit, epilayer growth, and MgO smoke.

Mullins, William W. explained and predicted observations on GB grooving. He died in 2002.

GENERAL REFERENCES

Grain boundaries have been extensively reviewed in several recent books. These texts cover all crystalline materials, but you will still need to go to the original papers to learn more about GBs in ceramics.

Bollman, W. (1970) *Crystal Defects and Crystalline Interfaces*, Springer-Verlag, New York. The original book giving the analysis of Σ , O lattice, etc.

Howe, J.M. (1997) *Interfaces in Materials: Atomic Structure, Thermodynamics and Kinetics of Solid/Vapor, Solid/Liquid and Solid/Solid Interfaces*, John Wiley & Sons, New York. A very readable book with a practical emphasis.

Hull, D. and Bacon, D.J. (2001) *Introduction to Dislocations*, 3rd edition, Butterworth-Heinemann, Philadelphia, A review of the basics.

Kelly, A., Groves, G.W., and Kidd, P. (2000) *Crystallography and Crystal Defects*, John Wiley & Sons, New York. Not broad or up-to-date but an excellent basic text.

Read, W.T. and Shockley, W. (1950) “Dislocation models of crystal grain boundaries,” *Phys. Rev.* **78**(3), 275. A classic readable paper with great diagrams.

Smith, D.A. and Pond, R.C. (1976) “Bollman’s O-lattice theory: a geometrical approach to interface structure,” *Inter. Met. Rev.* **205**, 61. Very readable discussion of the background to the GBs.

Stokes, R.J. and Evans, D.F. (1997) *Fundamentals of Interfacial Engineering*, John Wiley & Sons, New York. Bob Stokes retired from Honeywell and joined the University of Minnesota part time.

Sutton, A. and Balluffi, R. (1996) *Interfaces in Crystalline Materials*, Oxford University Press, Oxford, UK.

Wolf, D. and Yip, S. (Eds.) (1992) *Materials Interfaces: Atomic-Level Structure and Properties*, Chapman & Hall, London.

SPECIFIC REFERENCES

Amelinckx, S. (1958) “Dislocation patterns in potassium chloride,” *Acta Met.* **6**, 34. Seeing GBs in KCl by decoration.

Chaudhari, P. and Matthews, J.W. (1971) “Coincidence twist boundaries between crystalline smoke particles,” *J. Appl. Phys.* **42**, 3063. Original description of the MgO smoke experiment for GBs

Zhu, Y. and Granick, S. (2001) “Viscosity of interfacial water,” *Phys. Rev. Lett.* **87**(9), 096104. The idea is that the viscosity of water can be very different if it is constrained to be a film in a silicate grain boundary.

EXERCISES

- 14.1 Using the idea of capillarity and relating it to a triple junction, what happens as the temperature increases (so that viscosity decreases)?
- 14.2 Consider a 1-cm cube of a 100% dense ceramic that contains 5% glass that can wet the crystal grains. If the grain size changes from 100 nm to 10 mm due to heat treatment, how does the distribution of the glass change? Be careful to summarize your assumptions and list as many variables as you can.

- 14.3 Consider two small-angle (2°) tilt grain boundaries in MgO, both having a [001] tilt axis. For one the boundary plane is nearly (100) while for the other it is (110). Discuss the structure of these two grain boundaries.
- 14.4 The structure of the spinel, MgAl_2O_4 , projected onto the (110) plane is shown in Figure 7.1b. Spinel twins on {111} planes. Draw all the different allowed structures for the coherent (IT) plane and discuss which of them is most likely to occur giving clear reasons. Consider how your analysis might change if the spinel was not equimolar.
- 14.5 If the surface energy for (001) MgO is 1J/m^2 what is that in electron volts per oxygen ion on the surface. How does this number compare to the formation energy of the Schottky defect? How would this number be different if the material were NaCl instead of MgO?
- 14.6 Dislocations in a tilt boundary on the (011) plane in silicon lie 200nm apart. What is the misorientation of the two grains. Would the etch-pit method be a good way to examine this boundary? Explain your answer.
- 14.7 (a) For the TJ shown in Figure 14.34 derive a relationship between γ_{GB} , γ_{SL} , and the dihedral angle, ϕ , which is the angle subtended by the liquid. (b) Assuming that γ_{SL} is 700mJ/m^2 , determine γ_{GB} .
- 14.8 Construct a model for a $\Sigma = 7$ twin boundary in sapphire that is also a tilt boundary with a [0001] rotation axis.
- 14.9 Consider what might happen to the grain boundary charge when MgO is added to Al_2O_3 .
- 14.10 A tilt boundary in olivine lies on the (100) plane with a [001] rotation axis. The dislocations are all the same Burgers vector and are 100nm apart. What is the rotation angle?

Phase Boundaries, Particles, and Pores

CHAPTER PREVIEW

This chapter is both an extension of the chapters on surfaces and grain boundaries (GBs) and essential preparation for those on sintering and phase transformations. The theme of the chapter could be reworded as *interfaces between ceramics and different materials*; the material can be crystalline, amorphous (glassy), liquid, or gaseous (pore). Hence the topics include three critical areas for ceramics: phase boundaries (PBs), particles, and pores. Examples of PBs include ceramic/metal interfaces, crystal/crystal interfaces, and crystal/glass interfaces. Because we also include any interfaces that interact with pores it is a very large and important topic. By definition, PBs are the essential feature of composite materials. Solid-state reactions and reactions involving liquids and gases all occur by the movement of these interfaces, but the details of how this motion occurs are often even less well understood than the interfaces themselves.

15.1 THE IMPORTANCE

In ceramic materials, as in other materials systems, interfaces are the most important region of the material because that is where most of the action takes place. Phase boundaries are particularly important because they are the interfaces between dissimilar phases.

- Phase transformations take place by the movement of PBs.
- Growing one material on a different material generates a PB (a heterojunction).
- Bonding one material to another generates a PB.
- Most commercial and natural ceramics contain two or more phases and thus many PBs.

Forming PBs—Film Growth

Increasingly, we are growing thin films of ceramic materials on substrates, coating glass, coating metals, etc. A PB separates a ceramic film from the substrate. The behavior and properties of that PB will determine the usefulness of the thin film. This is not a new field—the electronics industry has been built on the ability to deposit layers of SiO_2 and Si_3N_4 on Si. The high- T_c superconductors in thin-film form are made this way. GaN is revolutionizing the lighting industry with thin films grown on Al_2O_3 and SiC.

Forming PBs—Processing

We usually process ceramic materials in the solid state (although small amounts of liquid may be present) either

to control the grain morphology or because going to the melting temperatures would be too expensive. Particles of different phases join together to form PBs.

Moving PBs

New phases form by a solid-state reaction when ceramic powders are reacted. The new phase grows at the expense of the starting phases: the reaction occurs by PBs moving. We will examine these reactions in Chapter 25; here we will concentrate on the interfaces themselves.

Properties of PBs

Whether the PBs separate thin films from a substrate or a bulk grain of one composition from one of another composition, the properties of the interface determine the usefulness of the material. There are innumerable examples of why PBs are important to ceramics: seals on Na-vapor lamps are the most likely source of failure; loss of adhesion of thermal barrier coatings (TBCs) leads to failure when the coating separates from the metal; GaAs on Si is not as widely used as was once hoped because the films do not align perfectly at the interface and they would be unlikely to remain perfect during cooling from the growth temperature.

15.2 DIFFERENT TYPES

Clearly there are many types of PB. We have already considered the solid/vapor and liquid/vapor PBs in Chapter 14; we also touched on the solid/liquid PB. Here we will

TABLE 15.1 Examples of PBs in Multiphase Ceramics

<i>PB</i>	<i>Material</i>
Glass/ceramic	Crystallization of a glass to form a glass-ceramic
Fiber composite	Ceramic fiber (e.g., SiC) with metal, ceramic, or polymer matrix
Geomaterial	Granite contains quartz along with other minerals such as orthoclase and microcline; there are multiple PBs
Cement	A ceramic matrix composite; cement is the matrix and aggregate (sand and small pebbles, or historically pumice) is the reinforcement
Porous ceramic	A very large developing topic, e.g., bioceramics, where we want controlled pore size for tissue ingrowth

discuss the solid/solid PB and use earlier concepts on the solid/gas PB.

We will examine two types of particles and the PBs between these and the matrix.

- Particles are a distinct second phase. Some could dissolve in the matrix if the temperature were high enough; some may never be able to dissolve until we exceed the melting temperature. They can be equiaxed, platelets, or needles. Note that in metals, the particles are often precipitates and the two words are used interchangeably. Particles in ceramic materials are less likely to have formed by precipitation.
- Pores are essentially negative particles, but there are some big differences: (1) there is a gas/solid PB, (2) there are no solid-state reactions at the interface, and (3) kinetics of point defect motion are fastest at the surface of the pore (the PB).

The idea of the pore as a particle may seem to be stretching the point at first. We will justify including this topic by showing that pores behave like particles and are a major component of many ceramic systems, including composites. Thin interfacial phases can also lie along PBs just as they do along GBs. When the intergranular films at a GB or triple junction become thicker than ~10nm, it is already a second phase and there are two PBs instead of one GB. We discussed intergranular films (IGFs) in Chapter 14 because the GB is essential to their existence (by definition).

Because PBs are everywhere in oxide minerals this is an enormously varied topic. We discuss this topic in more detail in Chapter 19, but for now a summary of some systems is given in Table 15.1. A point to keep in mind is that today's minerals are tomorrow's ceramics.

15.3 COMPARED TO OTHER MATERIALS

How are ceramics different from metals? Metals can be very clean. If particles are wanted they can often be precipitated by moderate heat treatments. In ceramics, particles are more likely to result from inclusion of insoluble impurities than from precipitation.

Impurities are common in all ceramics except in pure semiconductors.

Heat treatment may change the oxidation state of the constituent ions.

Alumina with 0.1 mol% impurities would be regarded as being a pure alumina; many commercial aluminas contain less than 98% alumina. In metals, we use precipitates to pin dislocations. In such materials, the aim is to optimize the number and spacing of the particles while controlling the total content. This is not usually done in ceramics—we do not need to pin the dislocations because they are not moving anyway. However, particles in ceramics have become more useful in preventing the movement of cracks—they help to toughen the ceramic. We can use ion implantation to harden ceramics (including glass). The process does produce particles, but again the defects that are impeded are cracks not dislocations. This technique is clearly restricted to the near-surface region.

Historical note. For many years, pores dominated the ceramics literature because of sintering—we wanted to remove them to make dense material. Now we may want to keep them or we may simply avoid them in the processing route. Intergranular phases are really special for ceramics and can be extremely useful, or disastrous, or both, but they are much more common than in metals. Particles are becoming more than just accidental inclusions present in impure materials as we start to use them in ways that are special for ceramics (e.g., in toughening). The mechanical strength of pores is not great(!) but pores can affect the mechanical properties in different ways. If the pore is small, it actually may be difficult to deform it.

15.4 ENERGY

In the same way that GBs have an associated energy, an interface between two different phases has a PB energy: the energy necessary to form a unit area of a new PB. (Two of these PBs were treated in Chapter 13 on surfaces.) If this interfacial energy is not less than the sum of the separate surface energies of the two phases the two phases will not join.

A low-energy geometry arises by minimizing the surface energy. In general, the interfacial energy between chemically similar phases is low compared with the sum of the surface energies. Thus, liquid metals or oxides on sapphire (or other solid oxides) generally have a small

interface energy. The interface energy is also low when there is a strong chemical attraction, i.e., when the two materials are likely to react readily.

Although new approaches have been developed for creating these interfaces, it has always been difficult to control the initial interface. In this example the structure is well known but the energy is usually still a mystery.

15.5 THE STRUCTURE OF PBs

Phase boundaries can be like GBs where the adjoining two grains may not only be rotated relative to one another but will also (or instead) be structurally and/or chemically different; of course, one or both phases may be a glass, which means the interface is not structured. As with heterojunctions, the word “hetero” is implied when we say “phase boundaries.” Semiconductor heterojunctions are examples of PBs; “heterojunction” usually indicates that we are talking about flat interfaces and a thin-film geometry. As is the case with GBs, almost all the detailed studies have been concerned with “special” PBs. We can summarize this idea and compare some PBs to GBs.

The “ $\Sigma = 1$ ” PB is particularly important since it is often associated with epitaxial growth.

NiO grows on MgO with both grains aligned so that corresponding planes and directions in the two crystals are nearly parallel. The difference in lattice parameter (Δa) will be accommodated by a square array of misfit dislocations.

When two phases have similar or related structures and are in close alignment, the mismatch due to differences in the lattice parameter may be accommodated by arrays of misfit dislocations. Such dislocations have been extensively studied in semiconductor systems and in some oxide systems. The image of Fe_2O_3 on Al_2O_3 in Figure 15.1 is complex because the $\Sigma = 1$ and the $\Sigma = 3$ interfaces exist side by side (the Fe_2O_3 films contain twin boundaries). In the $\Sigma = 1$ PB, Δa is accommodated by a hexagonal array of dislocations with Burgers vector $\frac{1}{3}\langle 11\bar{2}0 \rangle$; these are the displacement-shift-complete lattice (DSCL) vectors for this interface. In the $\Sigma = 3$ PB, the misfit dislocations are $\frac{1}{3}\langle 10\bar{1}0 \rangle$ (so they are closer together and more difficult to image).

The $\Sigma = 3$ PB often occurs in thin-film growth on $\{111\}$ or (0001) substrates: it is the PB version of the twin boundary.

If the corresponding planes [e.g., in the $(001)_{\text{NiO}}/(001)_{\text{MgO}}$ interface] are rotated about an axis that lies in the plane, then the interfacial dislocations must have a component that is normal to the plane of the interface. Again, this situation has been demonstrated for both semiconductors and oxides. The presence and distribution of

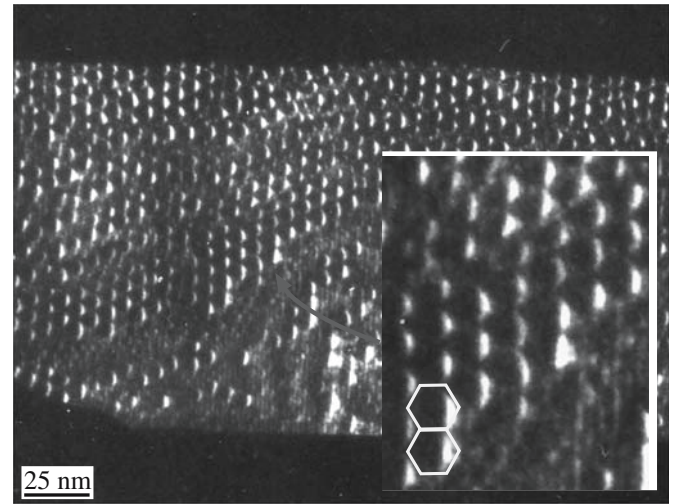


FIGURE 15.1 Image of an Fe_2O_3 film on an Al_2O_3 substrate showing both $\Sigma = 1$ and $\Sigma = 3$ PBs. The inset shows the hexagonal dislocation network.

these different dislocations have a direct relevance to the movement of any phase boundary and hence to the mechanisms of solid-state reactions because they are associated with steps in the PB. The latter point is not usually considered when discussing heterojunctions in semiconductor systems since the location of the interface is usually fixed before the growth of the epilayer.

Phase boundaries between ceramic oxides are particularly complex because the structure, the lattice misfit, and the different cations can each be influenced by external conditions, particularly the oxygen activity. The model system $\text{AO}/\text{AB}_2\text{O}_4/\text{B}_2\text{O}_3$ allows all of the above variables to be considered; A is a divalent cation and B is a trivalent cation. There is an extensive, although by no means complete, database for both the thermodynamic and kinetic aspects of such systems. The growth of spinel into alumina can take place by the movement of interfacial steps rather than dislocations as we will see in Chapter 25. Structurally different variations of the same “chemical” interface can exist as illustrated in Figure 15.2; new interfaces such as that in Figure 15.2b can be thought of as high-angle PBs. This particular PB can also be thought of as a plane-matching boundary, which has been recognized as a special form of GB (see Section 15.14).

At the interface between NiFe_2O_4 and NiO , which is shown in Figure 15.3, the oxygen sublattice is undisturbed by the presence of the interface. The distribution of the cations has changed in a way that is analogous to the stacking fault in spinel in that only the cations are shifted. Since there is actually a lattice-parameter difference, as this particle grows larger, dislocations must be nucleated at the interface. The resulting misfit dislocations are illustrated in Figure 15.3b.

Two notes: (1) PBs are more likely to be structured if the particles form by precipitation than if they form by inclusion during two-phase sintering. (2) Particles and

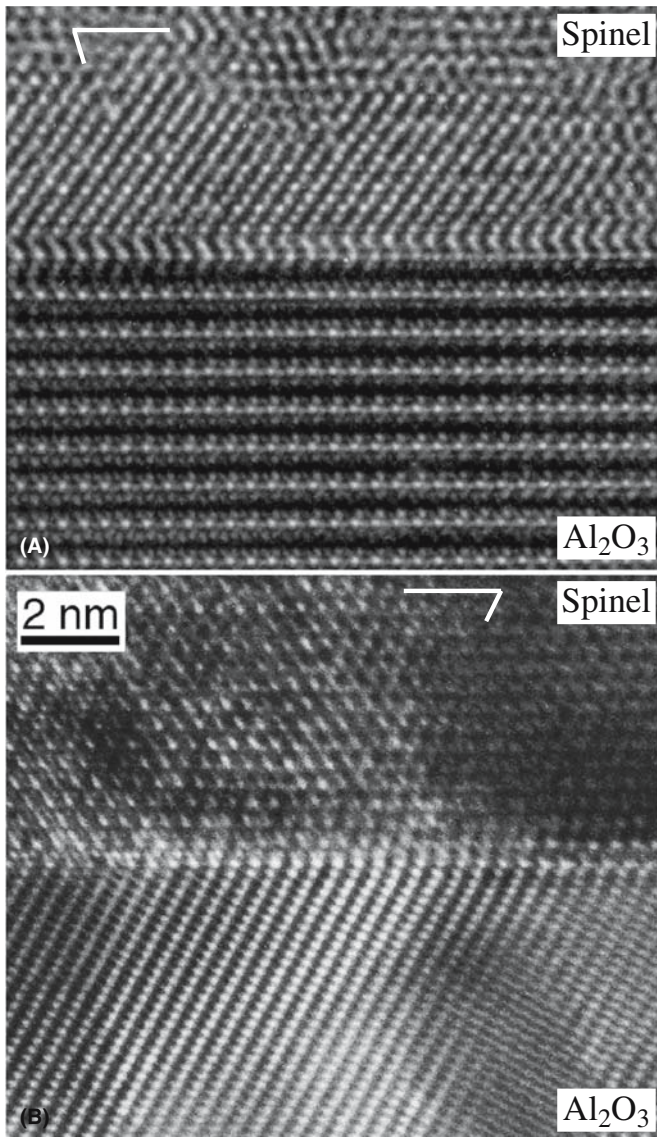


FIGURE 15.2 HRTEM images of crystallographically two different spinel/ Al_2O_3 PBs (a and b). White lines show the {111} planes in the spinel.

powders have a common feature—both are contained within another phase.

15.6 PARTICLES

Two particles that are located within the matrix can always lower the total surface energy by coalescing to form a single particle with the same volume but less surface; we ask the following questions: what is the driving force, how long will it take (thermodynamics and kinetics), and what is the influence of crystallinity?

For particles, we need to consider size, shape, and orientation.

The coalescence process, which is similar to the sintering of two particles that we discussed in Chapter 24, depends on the size of the particle. The phenomenon is known as Ostwald ripening—large particles grow while small particles shrink. The difficulty is that the initial joining of the particles must involve diffusion through the lattice unless there are defects connecting the particles. Particles of NiO that have grown in Ni titanate spinel are shown in Figure 15.4. The particles have grown following nucleation, but there is a thin layer of spinel separating the particles. This is similar to observations in Ni-based superalloys.

Shape: An example of spinel particles growing in an NiO matrix is given in Figure 15.5. The particles have an interesting shape consisting of six dendrites extending along $\langle 001 \rangle$ directions as they grow. This shape is determined by the soft elastic directions in the matrix and not by the gradients of the diffusing Fe^{3+} ; so the shape is determined by the orientation. When the same particle is

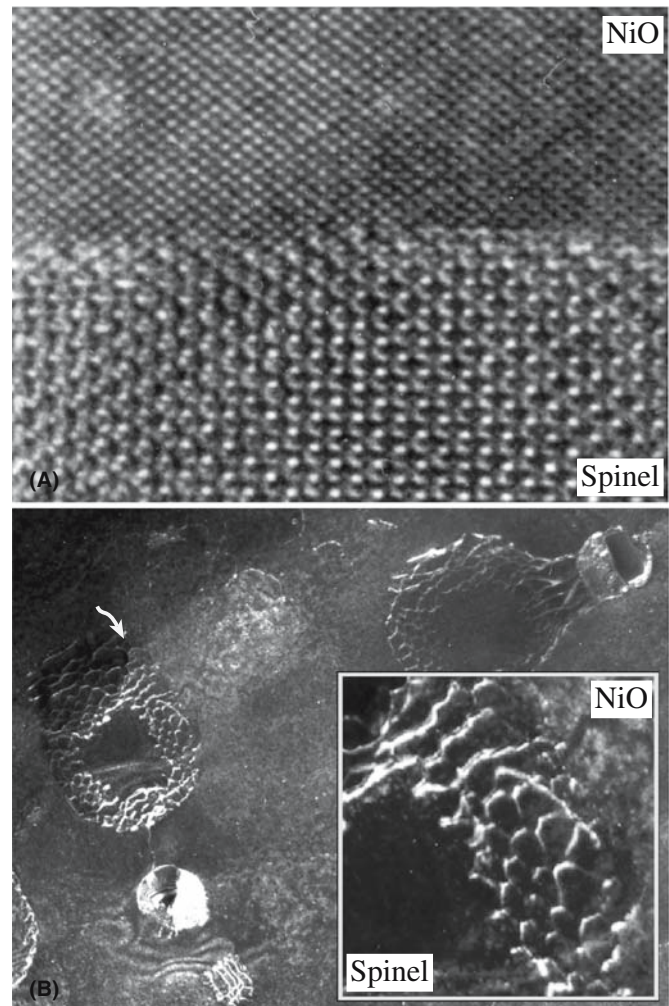


FIGURE 15.3 The spinel/NiO PB. (a) HRTEM image of lattice-matched PB; (b) dislocations are present at the interface after relaxation to accommodate lattice misfit. The inset is from the arrowed region.

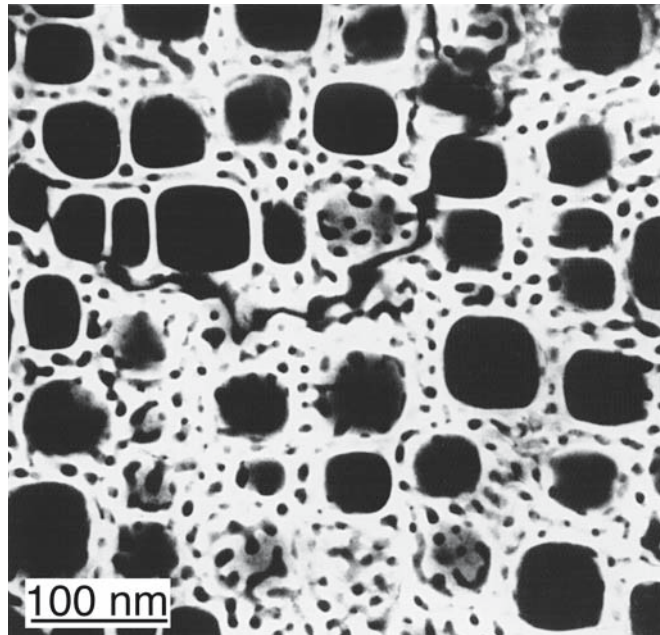


FIGURE 15.4 Lattice-matched particles of NiO in Ni-Ti spinel. Dark-field TEM image was formed by using a spinel reflection (that was not also an NiO reflection).

annealed after using all the available Fe^{3+} ions, the shape changes from kinetics controlled to energy controlled and becomes the octahedron enclosed by the low-energy $\{111\}$ planes. (More details on internal oxidation and reduction of ceramics are given in Chapter 25.)

These processes are similar to those affecting isolated powders. Nanoparticles of inert materials can be extremely reactive because of the driving force for reactions and growth caused by their high surface-to-volume energy ratio.

One low-energy PB: Some examples of particles formed by precipitation are summarized in Table 15.2. The particles of $\beta'''\text{-Al}_2\text{O}_3$, which can grow in a relatively pure (99.8%) α -alumina matrix, tend to grow parallel to the basal plane of the $\beta'''\text{-Al}_2\text{O}_3$ no matter what the orientation of the surrounding grain or grains as illustrated in Figure 15.6a. Figure 15.6b shows two types of precipitates in a garnet matrix. The large particles of ilmenite are randomly oriented, but the rutile needles are aligned with the matrix. The rutile particles gives us the star garnets (like star sapphire, but rarer), which we discuss in Chapter 36. The $\beta'''\text{-Al}_2\text{O}_3$ particles have grown as platelets because

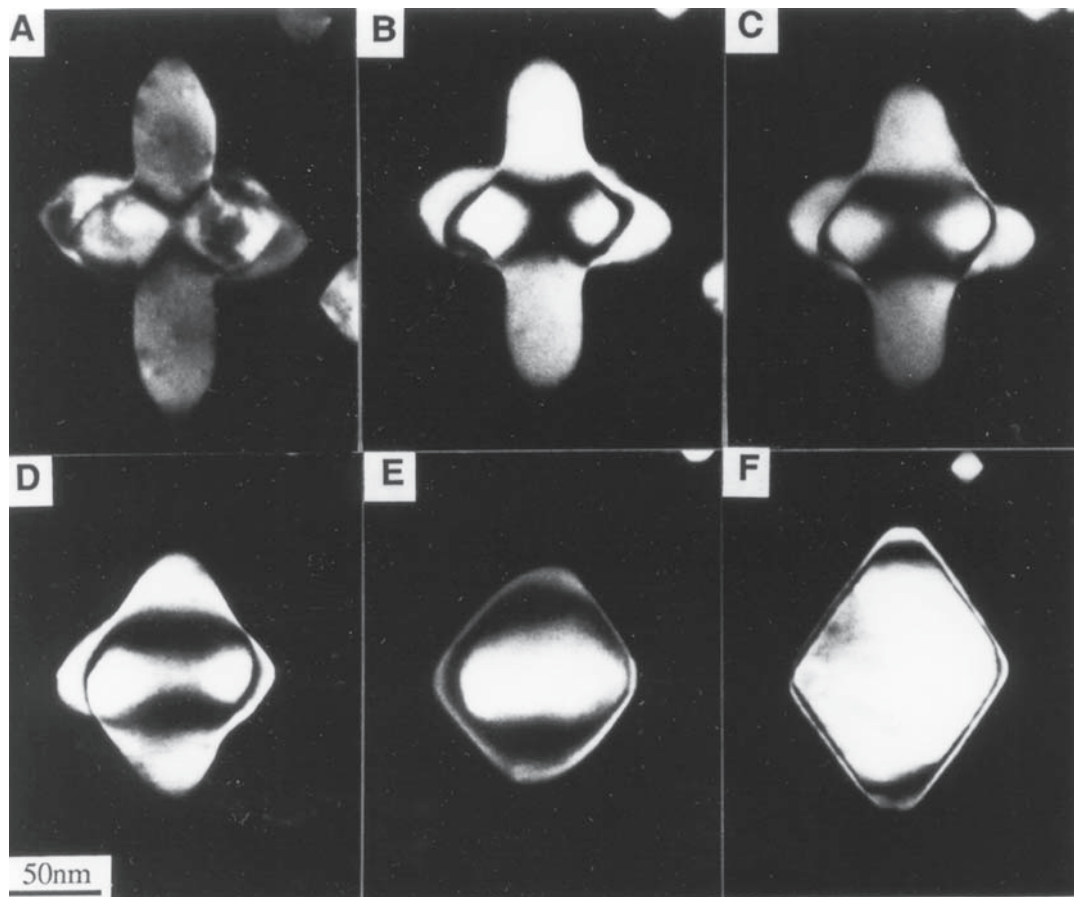
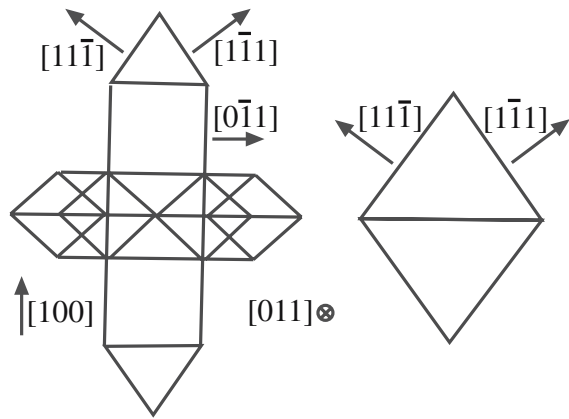
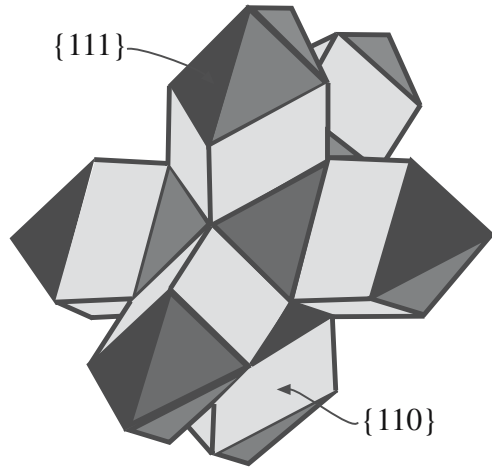


FIGURE 15.5 Spinel particles changing shape in NiO due to heat treatment. (The image is formed as for Figure 15.4.) (A) Looking along $[011]$: 30-minute heat treatment between images: (B) 800°C , (C) 825°C , (D) 850°C , (E) 875°C , (F) 900°C . The shape change is summarized in the schematics (G–I). The 3D figures shows the original shape.



(G)

(H)



(I)

FIGURE 15.5 Continued

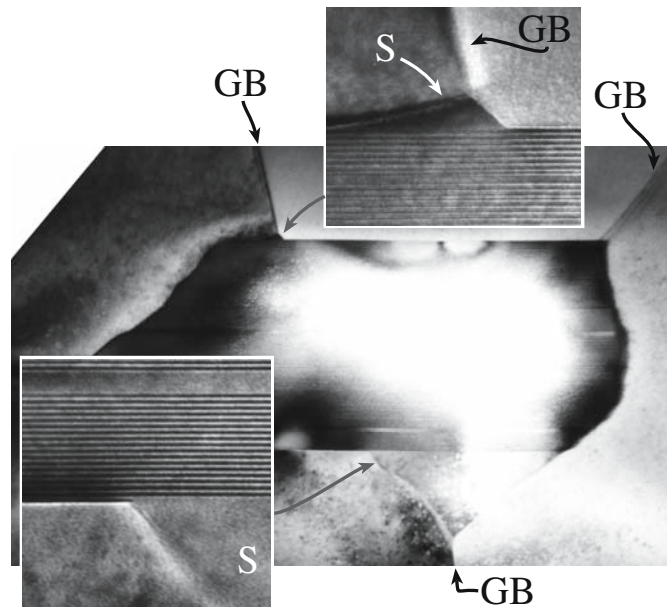
TABLE 15.2 Examples of Particles in Ceramics

Material	Situation
Spinel in NiO	Nucleation and growth
ZrO ₂ in Al ₂ O ₃	Toughening (ZTA)
TiO ₂ in Al ₂ O ₃	The gem stone, star sapphire
Y ₂ O ₃ in AlN	Sink for oxygen, forms garnet (YAG) at the triple junctions
Xe in MgO	Ion implantation; Xe is immiscible with MgO

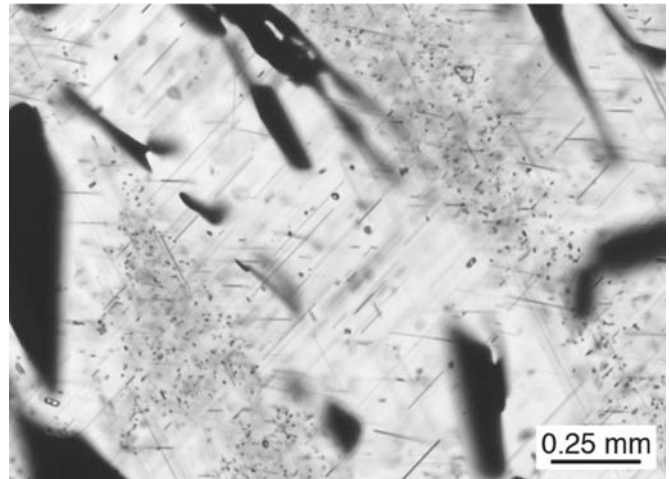
there is a good lattice match along one plane; the rutile particles are needles because the match is really good only along one direction.

Particles need not be crystalline as is illustrated in Figure 15.7 where a particle of glass has been grown in a thin-film matrix of α -Al₂O₃. The particle has a shape that is determined by the crystallography of the matrix.

Figure 15.8 shows two examples of precipitate-free zones (PFZ). Figure 15.8a is the classical PFZ at a GB. During cooling from the processing temperature, the Fe³⁺ ions in the doped NiO have segregated to the dislocations



(A)



(B)

FIGURE 15.6 Particle in a matrix. (a) TEM image of a second-phase β -Al₂O₃ growing along a GB in α -Al₂O₃. The insets show spinel (S) growing up the GBs. (b) VLM of rutile needles growing in a garnet grain.

in the low-angle GB. Figure 15.8b is a little complex. Here the Fe³⁺ ions have precipitated out onto large NiFe₂O₄ spinel particles that were present at high temperature. As the sample was cooled, the misfit dislocations around these large particles could not move because such movement requires defects on the oxygen sublattice. Hence the spinel particles grow out between the dislocations—the spinel grows into the NiO.

Finally, you can recognize several triple junctions (TJs) in the images shown in this chapter. For example, the spinel is forming at one TJ in Al₂O₃ in Figure 15.6 and

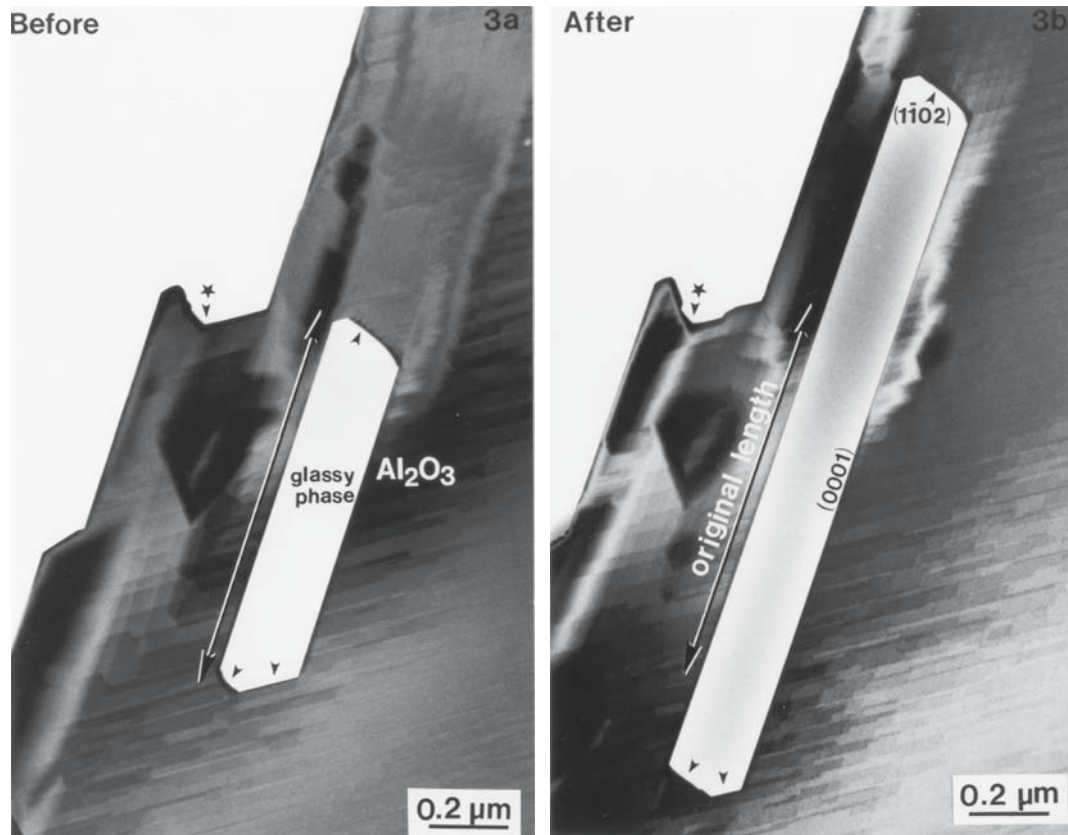


FIGURE 15.7 Glass “particles” in a thin film of α - Al_2O_3 before and after additional heat treatment.

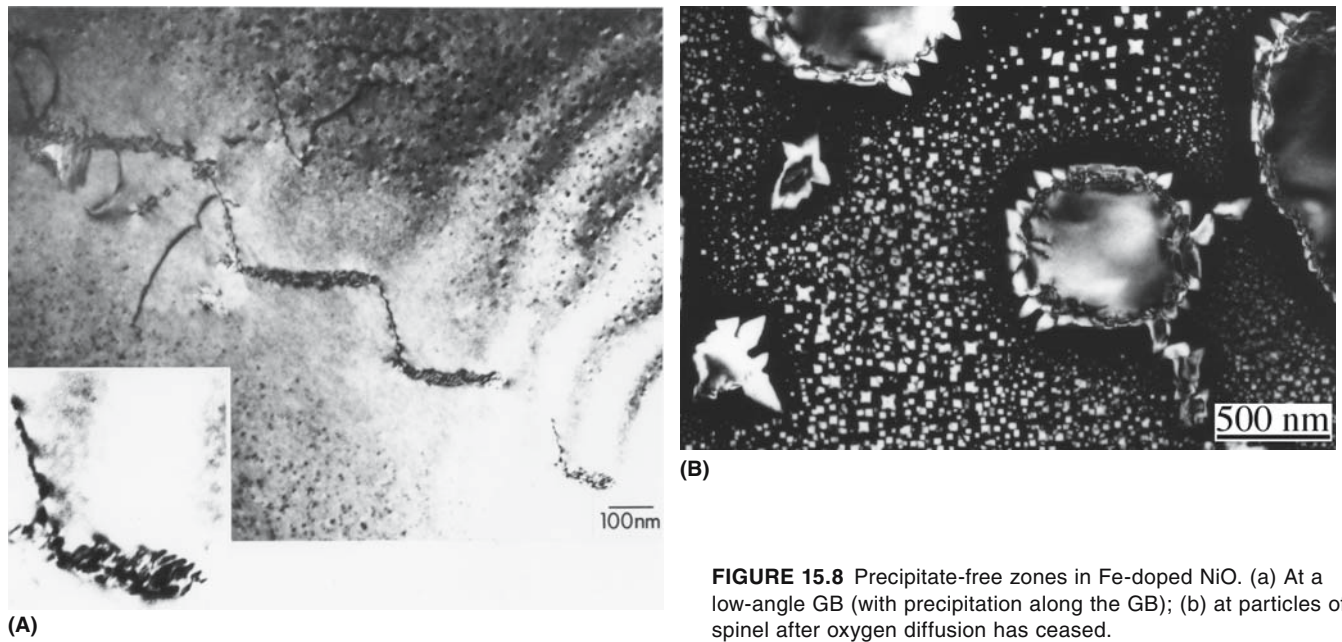


FIGURE 15.8 Precipitate-free zones in Fe-doped NiO. (a) At a low-angle GB (with precipitation along the GB); (b) at particles of spinel after oxygen diffusion has ceased.

β''' -Al₂O₃ is forming at the other two. Clearly the new phase is not wetting the Al₂O₃ GB.

If a polycrystalline sample of α -Al₂O₃ containing particles of ZrO₂ is heating during consolidation to a temperature at which the ZrO₂ is in the tetragonal phase, the matrix can stabilize the high-temperature phase as the sample is cooled. This is the concept used to toughen α -Al₂O₃ in Chapter 18.

15.7 USE OF PARTICLES

What are the properties of particles in ceramics and can we make use of them? Examples of the uses of ceramic particles in a matrix (rather than as a powder) include the use of glass beads for hardening rubber for tires and adding kaolin to paper to make it smoother and easier to print on. The properties depend not only on the particle but also on the PB that encloses it. Particles are used to seed crystallization and other phase transformations. Hematite particles can be used to seed the growth of α -Al₂O₃ at temperatures lower than the usual phase transformation so that the grain size can be kept small. This is now the basis of the widely used technique of crystal templating as illustrated in Figure 15.9. The principle involved is the use of particles for nucleating phase transformations so as to control the grain size during subsequent processing. In Chapter 26 we will use nanoparticles to seed crystallization in glass ceramics and in other specialty glasses such as Vycor.

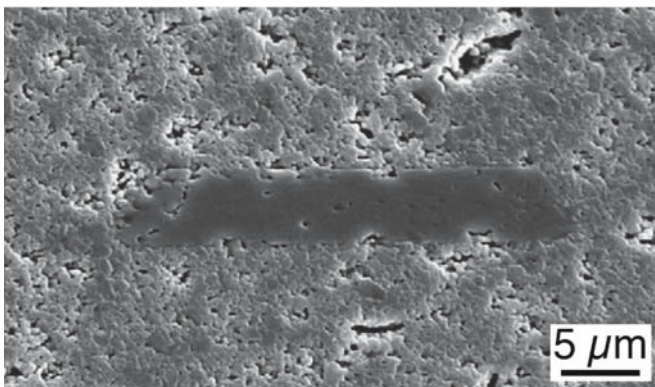


FIGURE 15.9 Templating grain growth. The seed is the elongated grain in the center.

PARTICLES IN RELATED FIELDS

You will find many of these processing techniques applied to particles in pharmaceuticals, cosmetics, pigments, paints, etc.

NUCLEATION OF A SPHERE

The free energy for a spherical particle depends on the surface area and the volume:

$$\Delta G_r = 4\pi r^2 \gamma_{sl} + \frac{4}{3} \pi r^3 \Delta G_v \quad \text{Box 15.1}$$

The two energy terms balance when

$$\frac{\partial(\Delta G_r)}{\partial r} = 0 \quad \text{Box 15.2}$$

The critical particle radius is

$$r^* = -2 \frac{\gamma_{sl}}{\Delta G_v} \quad \text{Box 15.3}$$

The critical value of ΔG^* is then

$$\Delta G^* = \frac{4}{3} \pi r^{*2} \gamma_{sl} = \frac{16}{3} \pi \frac{\gamma_{sl}^3}{\Delta G_v^2} \quad \text{Box 15.4}$$

15.8 NUCLEATION AND GROWTH OF PARTICLES

In metals we often form particles by precipitation from a solid solution as a result of heat treatment. The particles can adopt different shapes and set up different strain fields in the matrix during cooling. We can follow the same process in ceramics or we can add particles to the matrix during processing. We actually have an extra variable—we can change the oxygen activity and thus change the oxidation state of an ion. This process is illustrated in Figure 15.5.

Nucleation

The formation of nuclei requires the formation of an interface between the two phases (e.g., between a liquid and a solid). Thus, the formation of very small particles generally increases the total free energy of the system.

Growth

Once such particles reach a sufficiently large size, the interface energy increase is small compared with the volume energy decrease so that the total free energy begins to decrease as the particle size increases.

The classic example of precipitate nucleation in metals is the formation of GP zones in Al–Cu alloys. In ceramics, analogous examples include spinel in NiO, rutile in sapphire, or platelets of nitrogen in diamond. When particles are very small, the surface energy dominates. The calculation in Eqs. Box 15.1–Box 15.4 is instructive. Remember that the calculation is for a spherical nucleus and it ignores kinetics; kinetics are actually important as we saw in Figure 15.5.

Assuming a spherical nucleus, the total energy required for the formation of a nucleus of radius r is ΔG_r , which is a combination of two terms. The first term relates to the energy required to create the solid/liquid interface; γ_{sl} is

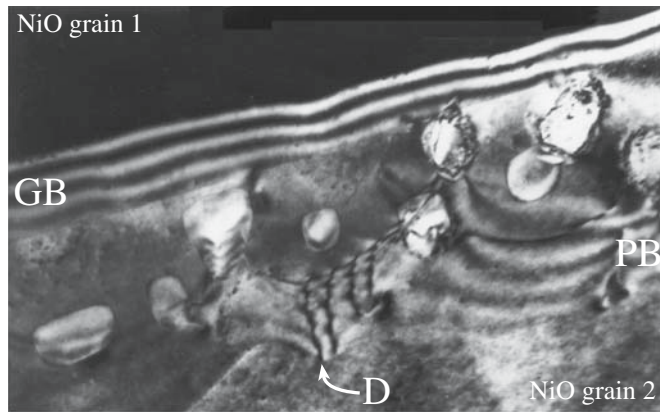


FIGURE 15.10 Growth of a particle along a GB. The particle is topotactically aligned with one NiO grain (along PB at grain 2) but not the other (grain 1). D shows a dislocation at the coherent interface.

the solid/liquid interfacial energy. This term dominates for small particles. The second term relates to the energy liberation associated with the volume change; ΔG_v is the free-energy change per unit volume for the new phase. The second term dominates when the particle size increases, so that once the particles reach some critical size further growth leads to an increasingly lower free energy and hence a more stable system.

We can deduce the size of the particle that has the maximum free energy, and that on further growth leads to a continuous decrease in free energy, by differentiating ΔG_r in Eq. Box 15.2. The critical value of r is given by Eq. Box 15.3 and implies there is a critical value of ΔG^* . When the particles have $r < r^*$ we call them clusters or embryos; nuclei are the stable particles with $r > r^*$.

Heterogeneous Nucleation

If particles nucleate at GBs or at surfaces they generally require less energy since an interface is already present. This is illustrated in Figures 15.8a and 15.10. The plate of spinel growing along the NiO GB has a topotactic alignment with one grain but not with the other since it is a high-angle GB. The presence of such particles in grain boundaries can change the properties of the material. For example, since $\beta'''\text{-Al}_2\text{O}_3$ is a fast ion conductor, such particles in polycrystalline Al_2O_3 provide short-circuit paths for rapid diffusion of Na, which can accelerate the degradation of Na-vapor lighting products.

15.9 PORES

Pores are very important in ceramics, in part because powder processing automatically creates them. The properties of pores are related to the surfaces that define them, but because the surfaces are usually curved they are not well understood. In ceramics, pores are everywhere and always contain some gas, although for simplicity we often think of them as surfaces enclosing a vacuum. Pores are

not so important in metals because they tend to collapse to form dislocation loops unless they contain a gas that cannot dissolve in the metal.

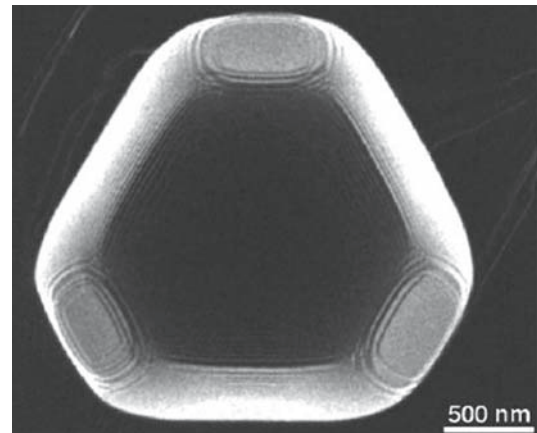
Pores or voids? We generally use the term *pore* since the term *void* suggests that the pore is empty. Most pores in ceramics are created during processing and most processing does not occur in a vacuum. Hence, in ceramics most pores contain at least some amount of gas.

These volume defects can have very important effects on the properties of crystalline solids and clearly relate closely to Chapter 13. Examples of these defects follow.

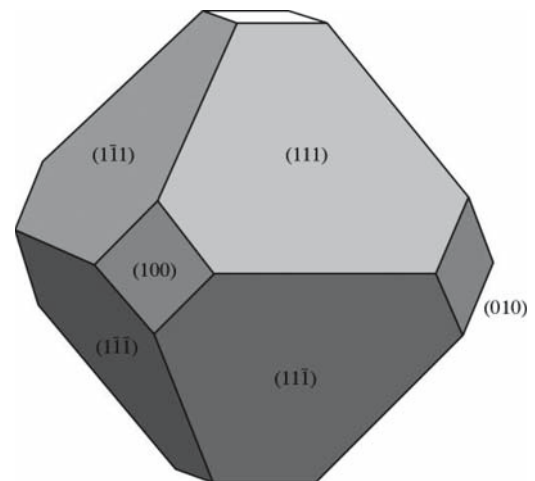
- Pores in the matrix: Isolated pores and surfaces
- Pores at grain boundaries and other grain junctions

We often start with very porous material so the “concentration of pores” may be large. We will extend this discussion in Chapter 24 (sintering). We may want a porous material (e.g., MCM-41). Pores interact with grain boundaries, phase boundaries, etc.

Does the pore have an equilibrium shape? The shape of the pores is determined by the surface energies. Faceted pores are shown in Figure 15.11. A technique has been developed to study systematically the annealing of pores



(A)



(B)

FIGURE 15.11 A faceted pore in UO_2 .

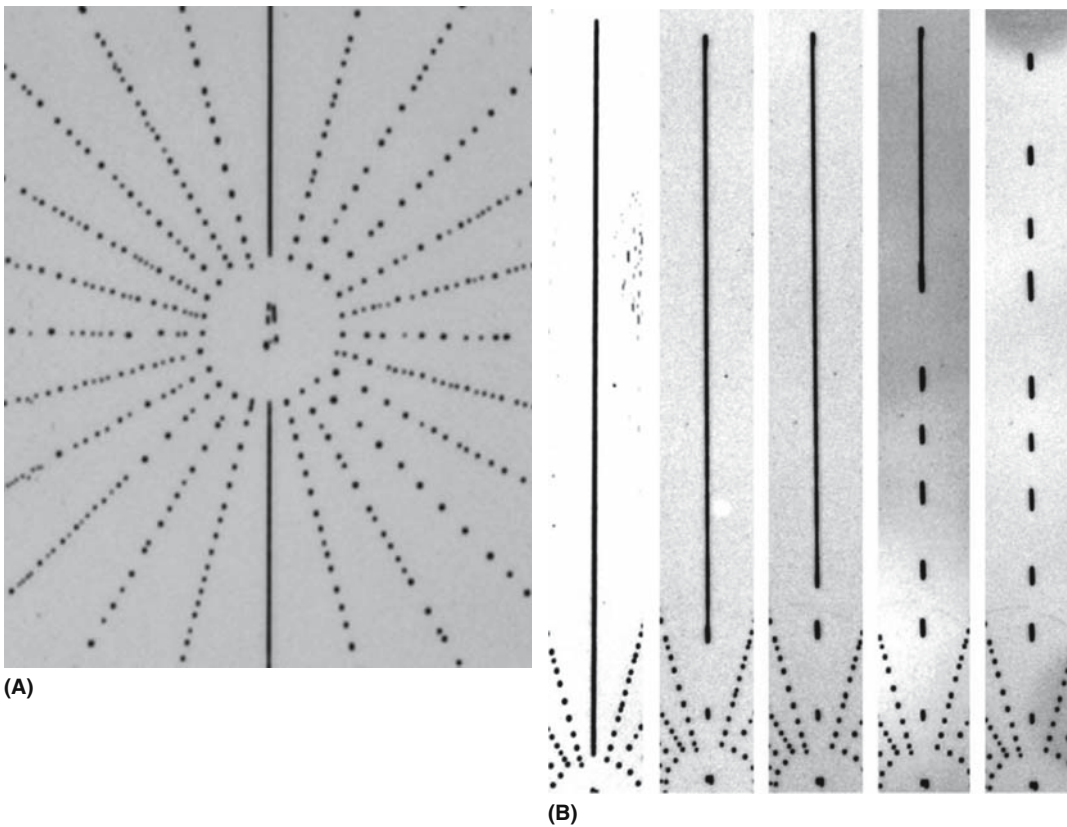


FIGURE 15.12 A method for systematically studying voids. (a) Grooves lying along different crystallographic directions break up to form pores at different rates. (b) The break up of one channel pore can be followed over time.

and the effect of dopants on this process. Channels or pores can be created in a $\Sigma = 1$ or high-angle GB by joining together two flat plates after patterning the surface of one grain using lithography as illustrated in Figure 15.12. The formation of such pores will occur when two nearly flat plates are joined, but will not be controlled. The technique has been extensively used to study pore annealing and the effect of dopants on this process in Al_2O_3 , but could easily be extended to other materials including glass. (See also the discussion of Figure 14.33.)

Pores can coalesce just as particles can. (Think of them as inverse particles.) The driving force is the same, namely, reduction of the total energy by reducing the area of the interface. The difference is that in order to shrink, the pore must nucleate a vacancy first. This vacancy must diffuse away through the lattice, along a dislocation or along an interface.

What is the effect of gas in pores? You can not remove the gas easily once the pore has separated from an interface because you then have to move a neutral atom through the lattice. Pores can move through the matrix as we will discuss in Section 24.15, but this process is likely to be slow and involves surface diffusion from one side of the pore to the other; as for a bubble rising in a liquid, we need a driving force.

Pores are also the principal defect in cement and concrete (see Section 2.7), which makes controlling porosity one of the main

tasks of the cement industry. Here, one way of minimizing porosity is to minimize the amount of water used in the cement. With suitable use of plasticizers and so-called microsilica, compressive strengths of $>100\text{N/mm}^2$ and tensile strengths of $\sim 15\text{N/mm}^2$ can be achieved. The plasticizers used for this are water soluble and mainly improve the packing density, thus decreasing pore content. Incidentally, cement can also be reinforced with up to 5% glass fiber and concrete may be reinforced with polypropylene fiber and of course steel “fibers.”

15.10 MEASURING POROSITY

We are interested in three quantities: (1) the size of the pores, (2) the distribution of the porosity, and (3) the total amount of porosity in the sample. Usually the actual shape of the pores is less important, although there may be situations in which the shape would be a critical factor. We can see pores in transmission electron microscopy (TEM), scanning electron microscopy (SEM), and atomic force microscopy (AFM). If they are large enough, we will also see them in visible light microscopy (VLM). None of these observations will give a statistical measurement of the amount of porosity.

The total amount of porosity can be estimated quite accurately if you know the phases present in the sample. You estimate

PORE PARAMETERS

Some closely related topics include pore size, particle size, total surface area, active surface area, and total material density.



FIGURE 15.13 A commercial porosimeter.

the theoretical density, deduce the actual density, and thus estimate the porosity. The other two quantities are much more difficult to determine. We can infiltrate a liquid and apply mercury-intrusion porosimetry. The principle is that the capillary pressure depends on the radius of the pore. If we vary the pressure on the Hg, it will fill pores down to a different size. If we then increase the pressure, more pores will be filled. The drawback to this approach is that we only measure the pores that are connected to the exterior. Commercially available equipment for measuring porosimetry is illustrated in Figure 15.13.

A related technique uses nuclear magnetic resonance (NMR) to measure the time taken by a liquid to fill the pores. It measures the relaxation times of the liquid filling the pores and relates this relaxation time to the thickness of the liquid and hence determines a surface-to-volume ratio for the pores. It is also possible to obtain information on the porosity using electron paramagnetic resonance (EPR), but neither EPR nor NMR is widely used for this purpose.

There are many other uses of porosity measurements; the oil exploration industry is a major example. There is clearly a strong link to powders: in some applications surface area may be more important than pore/particle size, but the two are not independent.

15.11 POROUS CERAMICS

We discussed the structure of zeolites in Chapter 7. The special feature of the crystal structure is the large void that is surrounded by a silicate cage but linked to other voids. A related void is that found in C_{60} and the other buckyballs.

This type of void is not what we mean by the term pore since these voids are an essential component of those crystalline structures. They may become filled with gas or liquid, but this is more closely analogous to an impurity occupying an interstice in other crystal structures as He can, for example, in the fluorite-structured UO_2 .

The new mesoporous materials have extremely high surface-to-volume ratios. An example of these materials is MCM41, which was invented by DuPont. A simple structure that can be manufactured in the laboratory is illustrated in Figure 15.14. The structure initially contained a periodic array of polymer spheres. When close packed, these spheres leave 26% of the volume empty. We can then infiltrate a liquid into these pores, burn out the spheres, and convert the liquid to a polycrystalline ceramic. Another synthesized porous ceramic is the cordierite honeycomb structure used to support the Pt catalyst in automobile catalytic converters. In this case the cylindrical pores are introduced mechanically in the extrusion process.

Pumice is a natural porous ceramic. It is produced by volcano eruptions and the gas is trapped inside the solid as it rapidly cools. The matrix is mainly glass, but it can contain small crystals. Synthetic ceramic foam is illustrated in Figure 15.15. Uses for ceramic foam are summarized in Table 15.3. One of the best-known applications for a porous ceramic is the space shuttle tile. An SEM image of such a tile is shown in Figure 15.16. Notice that in this case, the ceramic consists mainly of fiber (pressed not woven), so the principle is the same as for ceramic (glass) fiber for house insulation.

The structures shown in Figure 15.17 illustrate the result of computer modeling of foams. A thin membrane connects the structural ribs, as in a soap bubble in a wire frame. Since this film is amorphous, its surface energy is uniform and the film will be flat. The structure, of course,

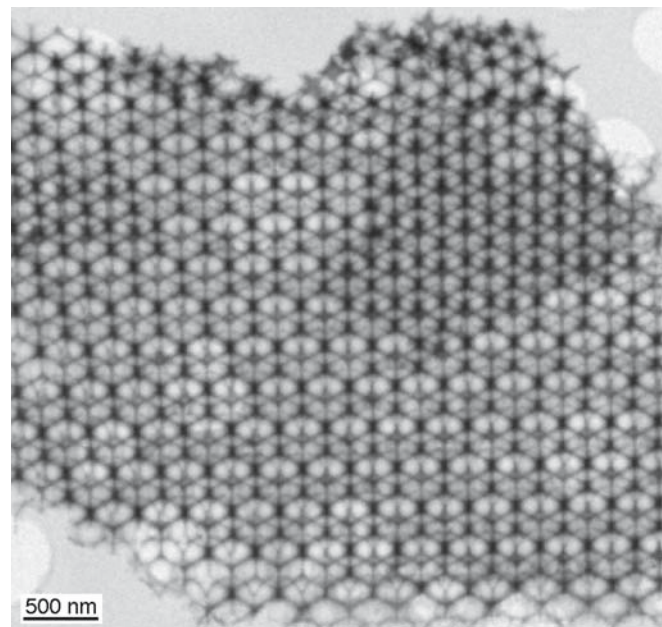


FIGURE 15.14 An ordered mesoporous material.

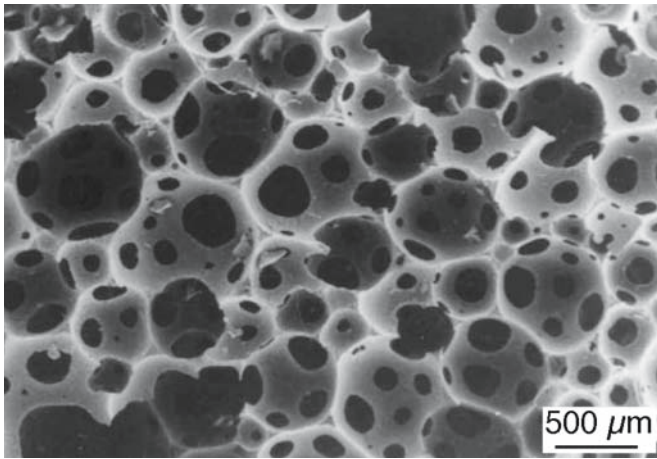


FIGURE 15.15 Sintered alumina foam made using a soap-nut slurry with a 40 volume % ceramic.

looks very similar to the glass films between grain boundaries, at triple junctions and at 4-fold junctions as discussed in Chapter 14, but all the “grain boundaries” are now flat (because the *grains* are pores).

15.12 GLASS/CRYSTAL PHASE BOUNDARIES

Crystals have been grown in glass matrices for hundreds of years. The luster glaze used on some medieval pottery owes its sparkle to nanoparticles of copper in the glass.

TABLE 15.3 Uses for Ceramic Foam	
Foam material	Application
Sieves	Molten metal filters
Sieves, microporous	Gas filters
Catalyst supports	Catalytic converter
Thermal insulators	Space shuttle tiles
Artificial opal	Optical

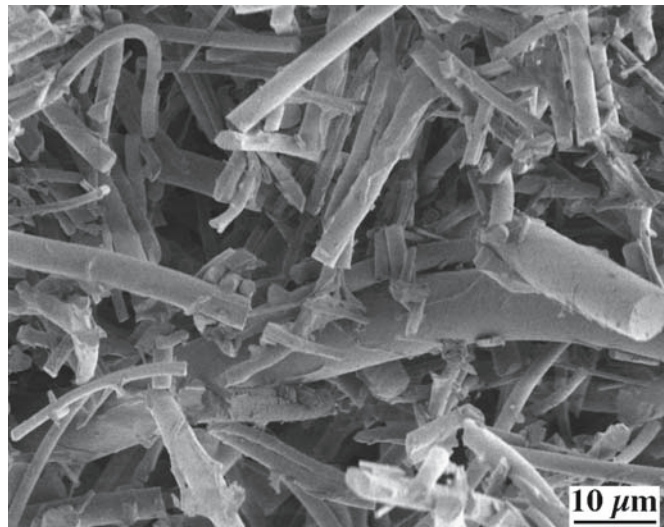


FIGURE 15.16 The porous material used to make insulating tiles for the space shuttle. The silica fibers are 2–4 μm in diameter.

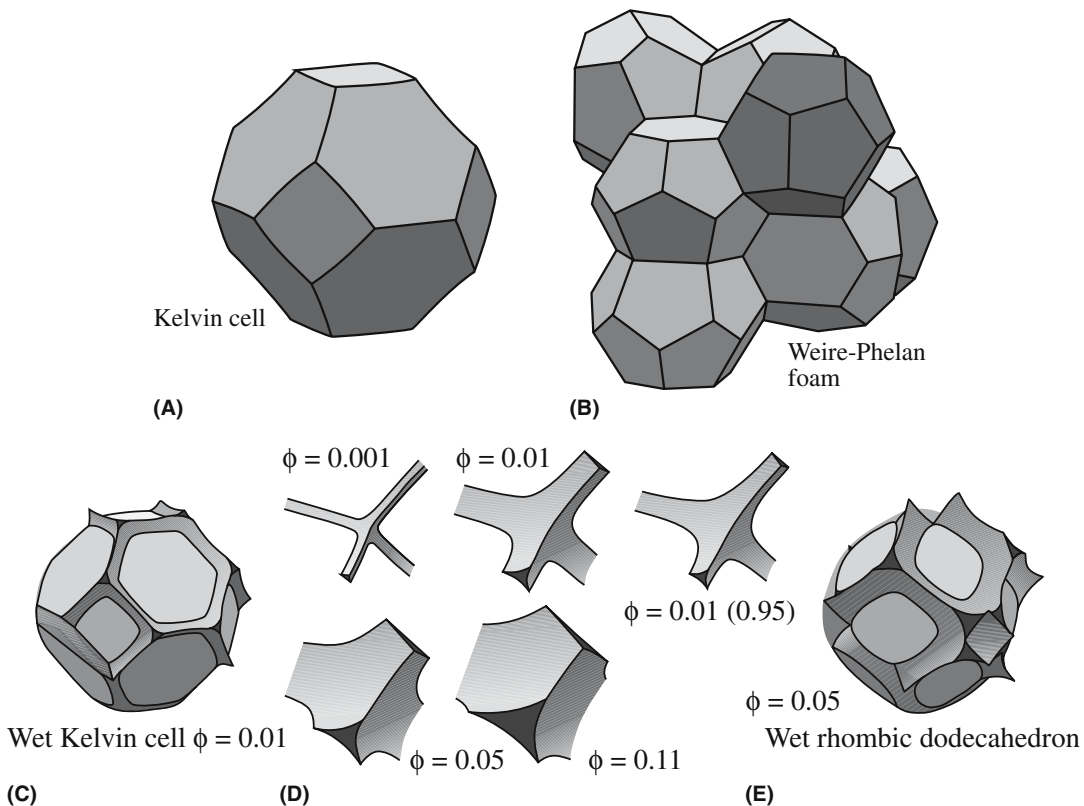


FIGURE 15.17 IGFs without grains. (a and b) Models of the Kelvin cell and a Weaire–Phelan foam used to describe soap bubbles; (c–e) how these relate to the structure of TJs and QJs.

TABLE 15.4 Observed Microstructures in Some Ceramic Eutectic Systems

System	T_{eut} (°C)	Growth Rate (cm/hour)	Comments
PbO–Pb ₂ Fe ₂ O ₄ (12.8wt% Fe ₂ O ₃)	730	0.5–2	Broken lamellar, two-phase matrix
PbO–Pb ₃ Nb ₂ O ₈ (6.85wt% Nb ₂ O ₅)	835	2	Lamellar
V ₂ O ₅ –Pb ₂ V ₂ O ₇ (5.7wt% V ₂ O ₅)	760	Cast	Lamellar
Pb ₄ GeO ₆ –Pb ₃ Ge ₂ O ₇ (15.0wt% GeO ₂)	707	1.45	Circular rod
WO ₃ –BaWO ₄ (18.5wt% BaO)	935	Cast	Water soluble
V ₂ O ₅ –BaV ₂ O ₆ (32.2wt% BaO)	550	Cast	Glassy
Bi ₄ Ge ₃ O ₁₂ –Bi ₁₄ GeO ₂₄ (10.3wt% GeO ₂)	880	Cast	Unbranched dendrites
V ₂ O ₅ –ZnV ₂ O ₆ (14.2wt% ZnO)	640	Cast	Coarse unbranched dendrites
V ₂ O ₅ –NiV ₂ O ₆ (9.2wt% NiO)	650	Cast	Coarse unbranched dendrites
V ₂ O ₅ –MnV ₂ O ₆ (9.10wt% MnCO ₃)	660	2	Coarse unbranched dendrites
PbO–Pb ₂ WO ₅ (17.6wt% WO ₃)	725	Cast	No fine two-phase areas seen
Bi ₂ O ₃ –Bi ₂₆ Zn ₂ O ₃₈ (1.24wt% ZnO)	750	2	Circular rod, spheroidized
BiFeO ₃ –Bi ₄₀ Fe ₂ O ₆₃ (1.14wt% Fe ₂ O ₃)	790	0.5–2.5	Circular rod, matrix may be faceted
Li ₂ WO ₄ –WO ₃ (19.1wt% WO ₃)	695	Cast	Porous, very soluble in water
V ₂ O ₅ –CuV ₂ O ₆ (12.7wt% CuO)	620	Cast	No fine two-phase areas seen
V ₂ O ₅ –CaV ₂ O ₆ (2.74wt% CaO)	618	Cast	No fine two-phase areas seen
Bi ₂ O ₃ –Bi ₂ Mn ₂ O ₉ (12.2wt% Mn ₂ O ₃)	790	Cast	Lamellar
Bi ₂ O ₃ –Bi ₈ TiO ₄ (0.53wt% TiO ₂)	835	Cast	Lamellar
WO ₃ –CaWO ₄ (7.46wt% CaO)	1135	Cast	Triangular rods
WO ₃ –SrWO ₄ (17.1wt% SrCO ₃)	1075	Cast	Triangular rods
WO ₃ –MgWO ₄ (12.6wt% MgCO ₃)	1120	2	Lamellar “Chinese script”
La ₂ O ₃ –LaFeO ₃ (28.5wt% La ₂ O ₃)	1430	~2	Triangular rods
Fe ₂ O ₃ –YFeO ₃ (15.9wt% Y ₂ O ₃)	1455	Coil	Lamellar/rod, matrix forms three-pronged webs
Gd ₂ O ₃ –GdFeO ₃ (15.0wt% Gd ₂ O ₃)	1500	Cast	Lamellar/rod, matrix forms three-pronged webs
BaTiO ₃ –BaTiSiO ₅ (9.9wt% SiO ₂ , 90.1wt% BaTiO ₂)	1260	2	Rodlike
BaTiO ₃ –BaTiO ₄ (41.9wt% TiO ₂)	1563	2	Lamellar and rod
Zn ₂ TiO ₄ –TiO ₂ (43.0wt% ZnO)	1418	2	Lamellar
Al ₂ O ₃ –ZrO ₂ (Y ₂ O ₃) (55wt% Al ₂ O ₃ , 38.3wt% ZnO ₂)	1890	0.5–10	Circular rod, matrix may be faceted

Household window glass will eventually form crystals of devitrite, an orthorhombic crystal with a formula like Na₂Ca₃Si₅O₁₆; these crystals usually form at the surface first. Crystalline glazes, which can make a pot look so spectacular, actually rely on spherulites consisting of many willemite (Zn₂SiO₄) crystals, with each acicular crystal growing in the [001] direction, to achieve the effect. (More on this topic is presented in Section 21.11.)

When two crystalline oxides are joined together to form a GB or PB, they are often thought of as being ionic materials even though the bonding may have a relatively large covalent component. Glass is usually viewed in the opposite way. Clearly we should take the nature of the bonding and the possibility of an interface space charge into account when we examine the glass/crystal interface. This point is particularly relevant to an understanding of glass-ceramic materials.

15.13 EUTECTICS

Is there anything special about ceramic eutectics? Not really (although they are very interesting), but it is sometimes a bit of a surprise that they can be formed just as

they can in metal systems. Eutectic structures are well known in metals, but have not been exploited in ceramics. One reason for this is that eutectics are associated with solidification of a liquid phase and we do not usually process ceramics using a liquid phase; this also means that processing temperatures are generally higher. In the examples listed in Table 15.4, one column gives the morphology of the respective phases. The minority phase can be sheets, rods, or particles; which of these actually occurs is determined in part by the energy of the PBs and the way in which the sample is cooled from the eutectic temperature. Directional solidification is generally required to optimize rods and platelets.

In the CoO/ZrO₂ eutectic solid, the two ceramics are both cubic, but they have very different structures. They grow in the cube-on-cube orientation, which means that all directions and planes in one material are parallel to the same directions and planes in the other material. As a possible application of such a material, oxygen diffuses rapidly in ZrO₂. It can then react with the CoO to produce a layer of Co₃O₄ at the interface between the two materials, resulting in the structure illustrated in Figure 15.18. Notice how uniform this spinel layer is: the growth is controlled by the reaction, not diffusion of O through the ZrO₂.



FIGURE 15.18 A CoO/ZrO₂ eutectic after solidification and subsequent oxidation. Z, ZrO₂; C, CoO; S, Co₃O₄ (spinel).

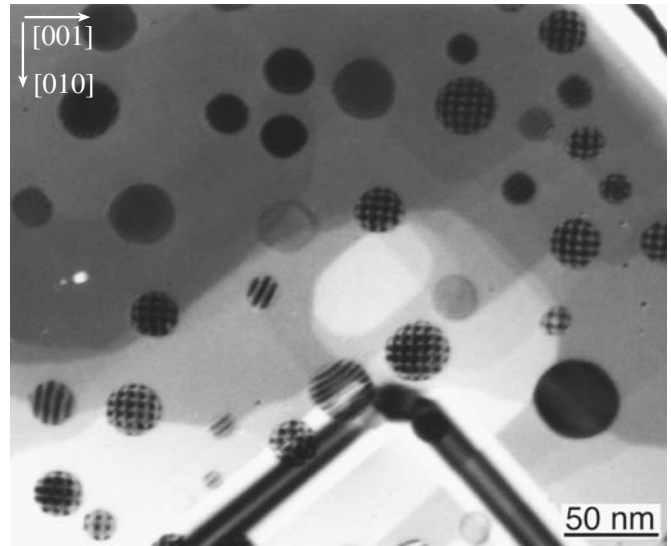


FIGURE 15.19 Particles of W on SiC. When crossed fringes are present (because of the lattice misfit), the alignment is excellent; otherwise, the islands are tilted relative to the substrate.

15.14 METAL/CERAMIC PBs

Metal/ceramic PBs are not only the most important feature in ceramic-reinforced metal-matrix composites, but they also occur when metals are oxidized or when oxides are reduced to the metal or when a metal film is grown on a ceramic substrate (or vice versa). In Figure 15.19 particles of W have grown on a single-crystal thin film of SiC. The

alignment and lattice mismatch of the two phases can be appreciated from the moiré fringes in the image.

High-resolution TEM (HRTEM) has now shown more details on such interfaces. The position of the misfit dislocation actually depends on the elasticity parameters of the two materials. The schematic diagram in Figure 15.20

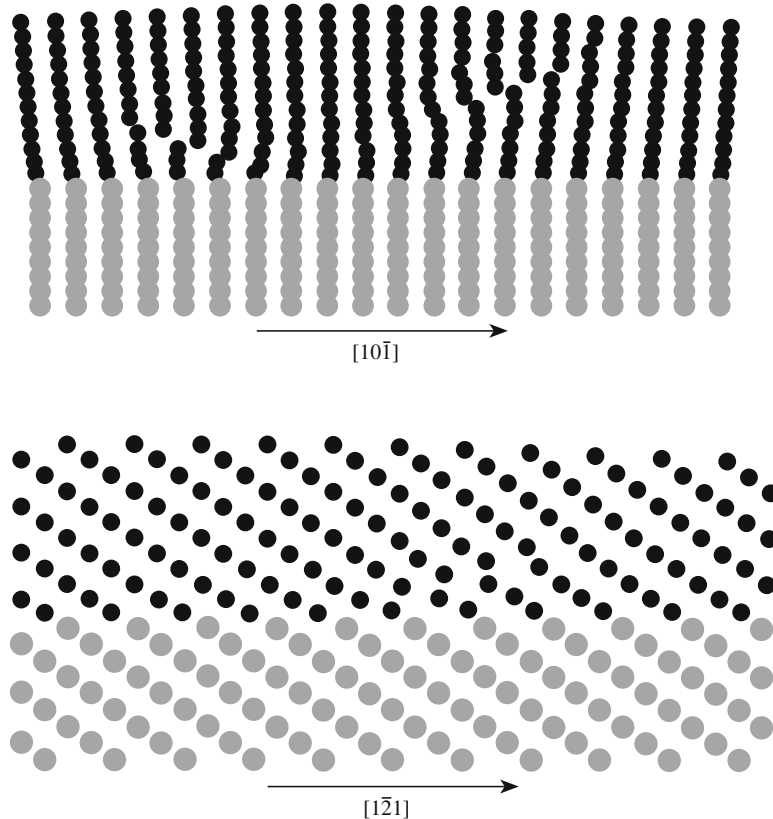


FIGURE 15.20 Schematic of stand-off dislocations accommodating lattice misfit between Nb and Al₂O₃.

TABLE 15.5 PBs in Applications

Bond	Material
Brazing	Join a ceramic to a metal
Metal–matrix composites	Make a two-phase material
Electronic interconnects	Bonding metal to a semiconductor
Oxidation of metal	Form an oxide from metal
Catalysis	Support catalyst particles

illustrates the dislocation stand-off, which is seen at the Nb/Al₂O₃ interface. The dislocations preferentially sit in the metal so as to lower the energy of the dislocation (remember, *E* depends on the elastic constants not just **b**) while still accommodating the misfit between the materials.

15.15 FORMING PBs BY JOINING

We form PBs whenever we join dissimilar materials.

Table 15.5 summarizes some applications of joining processes and the type of PB that is formed. Note that when

BRAZING AIN

Using an active metal such as Zr, we can get an idea about the possible reactions by using the Ellingham free-energy diagrams. Figure 15.21 is a plot of the free energy of formation of selected nitrides as a function of temperature. The lines represent the reaction

$$2 \text{Zr(s)} + \text{N}_2(\text{g}) = 2 \text{ZrN(s)}$$

Thus, when AlN is combined with Zr at high temperatures the reaction

$$\text{Zr} + \text{AlN} \rightarrow \text{ZrN} + \text{Al}$$

is favored. At 1123 K the free energy for this reaction is -83.3 kJ/mol .

bonding two materials together, we do not always want to produce strong bonds; some applications may prefer that the bond be weak (for example, in fiber composites). The formation of the bond has some requirements.

- Intimate contact between the two materials—the obvious requirement for a strong bond.
- Formation of a chemical bond—covalent bonding would be strong and van der Waals bonding would be weak.

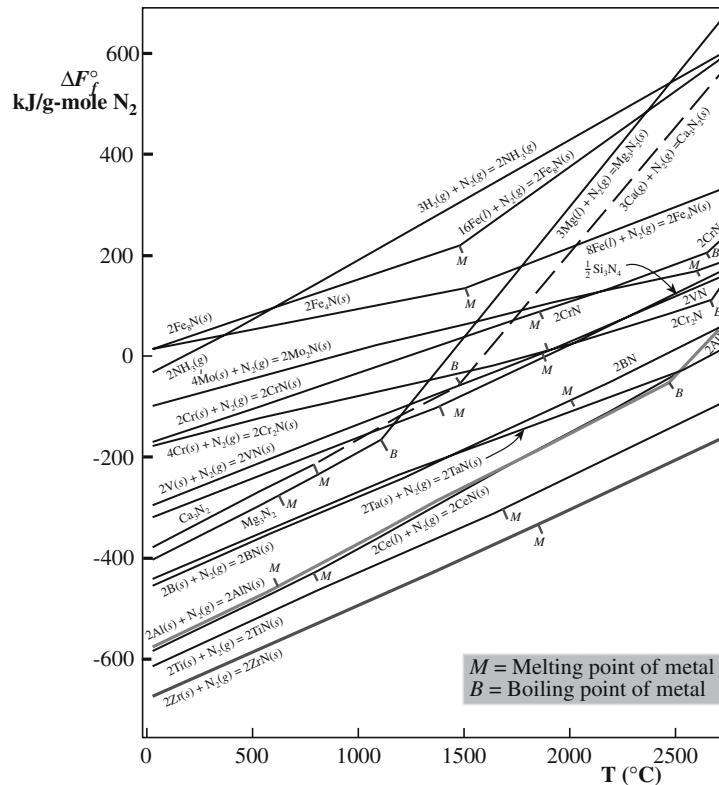


FIGURE 15.21 The Ellingham diagram. The lower line is used when brazing Zr.

- For a lasting bond, there must be a way to accommodate interfacial stresses.

The interfacial stresses may arise due to thermal expansion mismatch generated during cooling, or after fabrication, or because of temperature changes in operational conditions.

Brazing is joining a metal to a ceramic. The technique is well illustrated by considering metallization processes for AlN. There are several possible routes for forming the interfaces.

- Apply the metal in a liquid form
- Deposit either material from the vapor phase
- Use a solid-state reaction involving oxidation or reduction

Liquid metals have much higher surface energies than most ceramic oxides, and the PB energy is also high. The result is that liquid metals do not readily wet a ceramic and spread, unless special precautions are taken. Two approaches have been used for the development of metal brazes for oxides. In one method, active metals such as Ti or Zr are added to the metal; these effectively reduce the interfacial energy because the additives have a strong chemical attraction to the oxide and hence they enhance wetting behavior. The active metal is essentially acting as a surfactant! A braze must react with both the metal and ceramic components that you are joining and reach chemical equilibrium at the interfaces. Metal systems are generally compatible, resulting in wetting; the braze can then bond (by solution or diffusion) to the metal component.

Braze alloys for Al₂O₃-based ceramics might be Ag–Cu, Au–Ni, or Ag–Cu–Zn, but these alloys generally do not wet ceramics. The oxidation potentials of Cu and Ag are less than that of Al, so they do not react with the ceramic. If a small percentage of an active metal, e.g., Ti, is added, then the high oxidation potential of the Ti causes it to undergo a redox reaction with the ceramic (Al₂O₃). The result is the spreading of the braze because an oxide that is compatible with both phases forms at the interface; a chemical bond forms at the interface. Similar

approaches have been used to braze nonoxide ceramics. Zr may be a suitable candidate for an active metal for brazing of AlN ceramics.

In making electronic interconnects it is often necessary to metallize the surface of Al₂O₃ (in ceramic packaging for integrated circuit applications). We describe how metallization is accomplished using thick-film processing in Chapter 27. The development of an interlocking glass/ceramic and glass/metal structure is required for good adhesion because it provides mechanical interlocking in addition to chemical bonding between phases. To achieve the required microstructure at the conductor–substrate interface it is necessary for the glass to have the appropriate surface tension and viscosity during the firing process, and for it to wet the substrate.

In thin-film metallization by evaporation or sputtering of thin metal films onto a ceramic surface (Chapter 28), it has been demonstrated that a sequence of layers of different metals is required for optimum film properties. The first layer is usually a refractory metal such as Ti, Cr, or NiCr; this layer provides adhesion to the ceramic. These elements are reactive and bond through redox reactions with the substrate. The second layer acts as a diffusion barrier. The barrier material will usually be a noble metal, preferably Pt or Pd. The top layer will be the metal of choice for the particular application, for example, Au for wire-bonding applications and Ni or Ag–Pd for solderability.

A schematic for the process of anodic bonding is shown in Figure 15.22. The concept is that two materials are joined together by heating them while applying a voltage across the assembly (hence it is also known as field-assisted bonding). The temperature is typically between 300°C and 450°C while the applied voltage is ~80 V. Glass can be bonded to glass or to Si with this process. In principle, the limiting factor is being able to polish the abutting surfaces to a roughness of <100 nm. Glass works particularly well because the cations are quite mobile.

Some final examples of PBs are given. In catalysis, it is usually not possible to examine the interface between the support and the catalyst particle. An example of catalyst particles on a silica nanowire is shown in Figure 15.23. We will discuss composite materials in more detail later, but we note that the filler material (fiber or particle) and the matrix can be glass, crystalline ceramic, or another (see Chapter 20).

METALLIZING ALUMINA

A commercial process for metallizing debased alumina uses Mo or W; the alumina grains in the debased alumina are held together by a glassy phase binder. The Mo is applied to the surface as a powder, often mixed with manganese oxide, and fired in a reducing atmosphere with a controlled dew point so that the Mn is present as MnO and Mo as the metal. The MnO reacts with both the alumina grains and the liquid glassy phase. The glassy phase from the Al₂O₃ migrates into the metal powder under the influence of capillary forces and bonds the metal particles to each other and to the Al₂O₃ surface, producing a wettable surface layer. In the case of pure Al₂O₃ and oxides without binder phases, it is necessary to add glasses to the metallizing mixtures. The Mo coating is generally electroplated with Ni to provide a clean and continuous surface as well as one on which an applied braze would easily spread. A similar process is applied for W metallization.

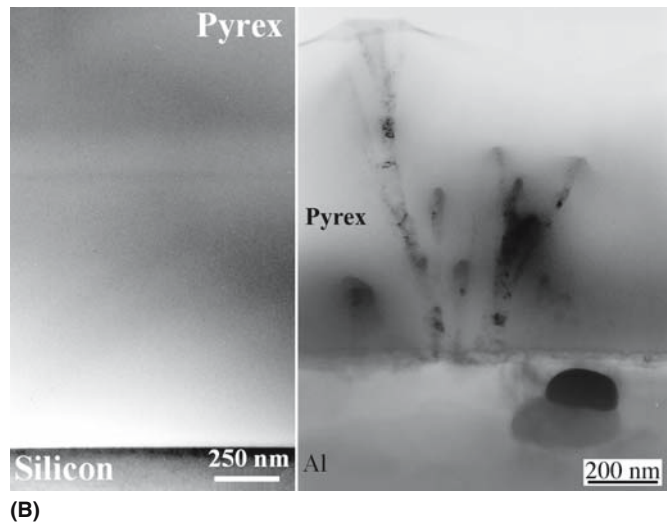
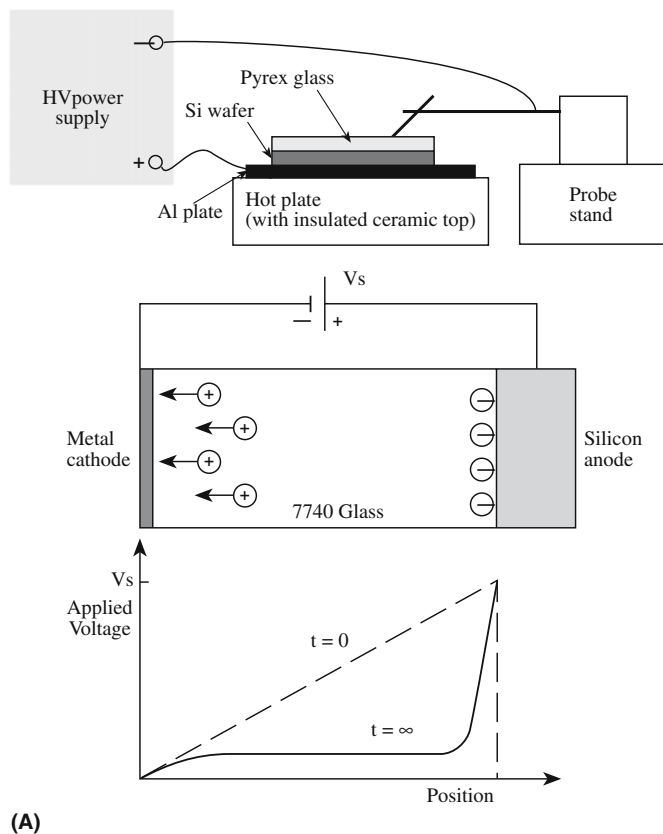


FIGURE 15.22 (a) Set-up for the anodic bonding of glass to Si and (b) an example of a glass/Si/glass sandwich produced using this process.

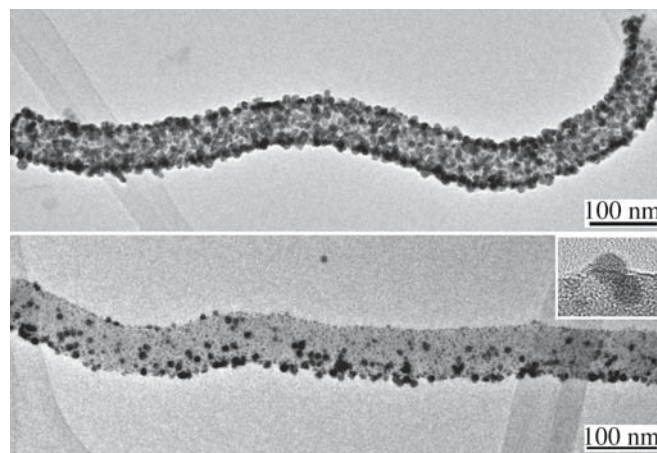


FIGURE 15.23 Au catalyst particles on a ceramic nanowire.

CHAPTER SUMMARY

There are several key ideas in this chapter. PBs are present wherever we have a second phase, particle, or precipitate in a matrix; we treat pores as a special particle. (The surface is actually a special PB.) Like GBs, PBs are everywhere in ceramics; we could develop a notation similar to the Σ for GBs but rarely use it. When a phase transformation occurs, the mechanism is the movement of a PB. Particles can be different in structure and/or composition in a ceramic matrix; precipitates are particles that have developed by a specific process. Pores are present in most ceramics and play important roles in determining properties. We have developed special methods for characterizing porosity and ceramics in which the pores are actually the major phase—porous ceram-

ics. We just touch on some special PBs, namely glass/crystal interfaces and metal/ceramic interfaces; we will see much more of the former in later chapters.

GENERAL REFERENCES

The details of nucleation and growth theory are given in many standard textbooks on kinetics and phase transformations: see the books on interfaces in Chapter 15 and on phase transformations in Chapter 25.

SPECIFIC REFERENCES

- Dhara, S., Pradhan, M., Ghosh, D., and Bhargava, P. (2005) "Nature inspired novel processing routes for ceramic foams," *Adv. Appl. Ceram.* **104**(1), 9.
- Formenti, Y. and Drittt, T.H. (2003) "Vesicle connectivity in pyroclasts and implications for the fluidisation of fountain-collapse pyroclastic flows in Montserrat (West Indies)," *Earth Plan. Sci. Lett.* **214**, 561.
- Gibson, L.J. and Ashby, M.F. (1999) *Cellular Solids: Structure and Properties*, 2nd edition, Cambridge University Press, Cambridge.
- Gibson, L.J., Ed. (2003) "Cellular solids," *MRS Bull.* **28**(4).
- Halperin, W.P., D'Orazio, F., Bhattacharja, S., and Tarczoz, J.C. (1989) "Magnetic resonance relaxation analysis of porous media," in *Molecular Dynamics in Restricted Geometries*, Wiley, New York, p. 311.
- Korda, G. and Kang, Y. (1991) "Three-dimensional electron paramagnetic resonance imaging technique for mapping porosity in ceramics," *J. Am. Ceram. Soc.* **74**, 709.
- Montanaro, L., Jorand, Y., Fantozzi, G., and Negro, A. (1998) "Ceramic foams by powder processing," *J. Eur. Ceram. Soc.* **18**, 1339.
- Penner, S., Rupprechter, G., Sauer, H., Su, D.S., Tessadri, R., Podlucky, R., Schlogl, R., and Hayek, K. (2003) "Pt/ceria thin film model catalysts after high-temperature reduction: a (HR)TEM study," *Vacuum* **71**(1–2), 71.
- Perkowitz, S. (2000) *Universal Foam*, Walker, New York. Pumice is on p. 128: this text puts it in perspective.
- Suvaci, E., Oh, K.-S., and Messing, G.L. (2001) "Kinetics of template growth in alumina during the process of templated grain growth (TGG)," *Acta Mater.* **49**, 2075.

EXERCISES

- 15.1 Given the information in the text, determine the orientation of the samples.
- 15.2 What is the crystallographic relationship between the two grains shown in Figure 15.2a? How does it differ from that of the interface shown in Figure 15.2b?
- 15.3 Using reasonable values of the solid/liquid interface energies and ΔG_v , estimate r^* for spinel in MgO versus Cu in Si.
- 15.4 Do you expect the conduction of Na^+ ions in an ionic conductor to depend on crystallography? If so, why, and what are the implications?
- 15.5 How would you propose characterizing nanoparticles in the glaze on a priceless pot? Breaking the pot, even a little bit, is not allowed.
- 15.6 In Section 15.14 we note that dislocations can be present at metal/ceramic interfaces. When is this most likely; when is it least likely? How will the interfacial energies and strengths differ?
- 15.7 What is the relationship between the methods used to form the images in Figures 15.4 and 15.8? Explain why this technique works.
- 15.8 Assuming the interfaces labeled in Figure 15.7 are all viewed edge on, what is the viewing direction (the direction defined with respect to the sapphire crystal)?
- 15.9 Suggest reasons for the shape of the particle shown in Figure 15.5. How does this explanation compare with that for the shape of the particle in Figure 15.11?
- 15.10 List the possible applications for zeolites and mesoporous ceramics.

Part V

Mechanical Strength and Weakness

Mechanical Testing

CHAPTER PREVIEW

The concepts of stress and strain and the elastic moduli should already be familiar. Where ceramics differ from most metals and polymers is that at room temperature most of them are brittle. Flaws play a major, often dominating, role in the mechanical behavior of ceramics. As a result, obtaining properties such as elastic moduli is often more difficult than it would be for metals: preparing the sample can lead to the introduction of flaws. Stress–strain curves for ceramics are usually obtained using a bending test rather than a tensile test. We need only to make our ceramic into a rectangular block. The brittle behavior of ceramics gives them low fracture toughness, a property that can most conveniently be obtained from indentation testing. A key point from this chapter is that when we use ceramics in load-bearing applications we need to understand the importance of flaws and how to incorporate them into our design approach.

16.1 PHILOSOPHY

The classical view of ceramic materials includes the following:

1. They are brittle.
2. Dislocations are not important because they do not move.
3. They are polycrystalline and fracture along grain boundaries.

Once again the classical view of ceramics and many of our preconceived ideas of how they behave are not always correct.

- We can bend a sheet of silicon into a tube.
- We can bend an alumina fiber into a circle.
- Dislocations move ahead of crack tips, are present at heterojunctions, and can be produced in large numbers during single-crystal growth.
- Single-crystal ceramics also fracture (Figure 16.1 shows an Nd-doped YAG single-crystal boule that fractured during growth).

The modern view of ceramics is therefore very different:

1. We may be using the ceramic as a thin film where stresses may be very high.
2. Deformation at high temperatures may be important.
3. In some special “new” ceramics, displacive transformations become important.

It will be important to keep these ideas in mind when you read older texts. We are not going to provide a treatise on mechanical properties of ceramics. There are many existing books that do and some of these are listed at the end of the chapter. What we will do is look at what is special for ceramics.

The general need is to understand the response of a material to an applied stress. The stress may be applied externally or induced by altering other parameters such as temperature (which can cause a phase transformation). The fundamental idea is the link to bonding. In Chapter 4 we described how the Young’s modulus is related directly to the bond-energy curve. In Chapter 12 we described the nature of dislocations in ceramics.

So the following three chapters have three special themes

- Mechanical testing—how to do it plus the fundamentals of elastic constants, etc.
- Plastic deformation and how it is accommodated
- Fracture and how to control it

The starting point for most discussions of mechanical properties of materials is a stress–strain (σ – ϵ) curve for a material in tension. Figure 16.2 shows σ – ϵ curves for three different materials at room temperature.

Material I: This has a high Young’s modulus, high failure stress, low ductility, low toughness, and fractures without significant plastic deformation. **This behavior is characteristic of many ceramics.**



FIGURE 16.1 Cracking in an Nd-doped YAG boule.

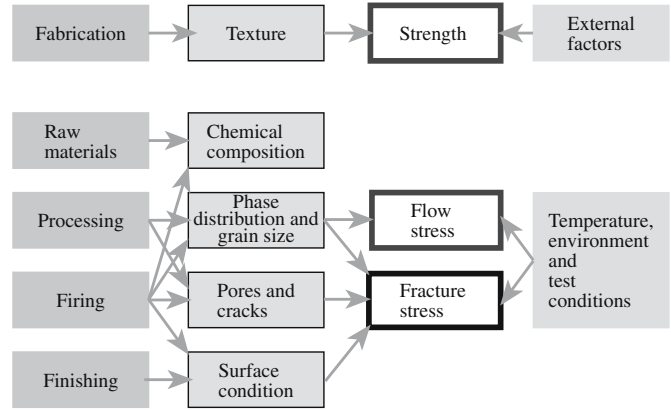


FIGURE 16.3 Factors affecting the mechanical properties of ceramics.

limited toughness. **This behavior is characteristic of many elastomers.**

The strength of ceramics is affected by many factors, and this complexity is illustrated in Figure 16.3. The composition and microstructure are particularly significant and mechanical properties depend strongly on these characteristics. Figure 16.4 shows two specific examples that

Material II: This has moderate strength, moderate ductility, deforms plastically prior to failure, and is the toughest of the three. **This behavior is characteristic of many metals.**

Material III: This has a low Young's modulus, is very ductile, and has low ultimate tensile strength and

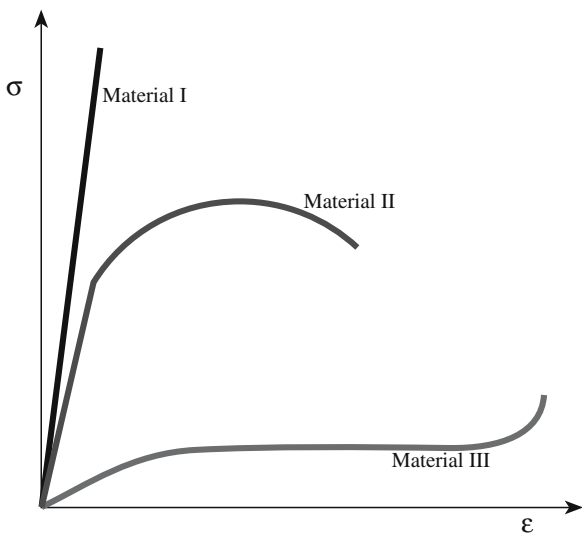
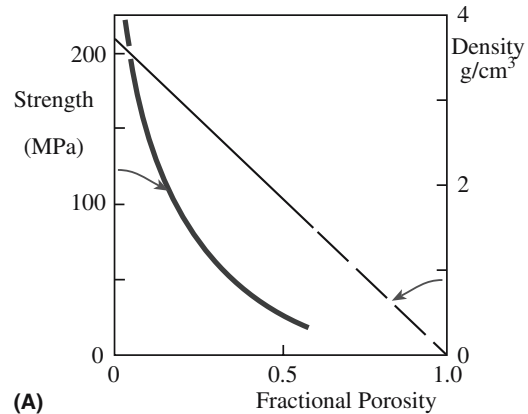
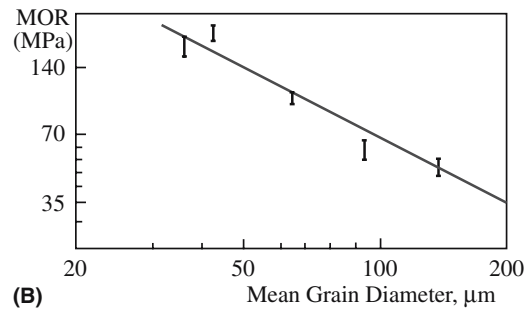


FIGURE 16.2 Idealized stress–strain curves for different materials classes.



(A)



(B)

FIGURE 16.4 (a) Effect of porosity on the strength of polycrystalline Al_2O_3 . (b) Effect of grain size on the strength of BeO .

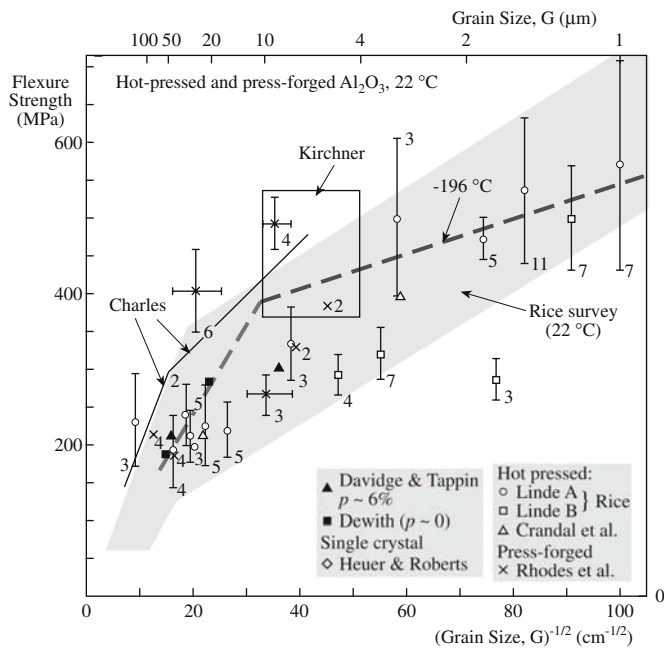


FIGURE 16.5 Compilation of strength data as a function of grain size for polycrystalline Al_2O_3 .

illustrate the role of microstructure on the strength of ceramics. In Figure 16.4a the strength of a porous polycrystalline alumina is shown to decrease much more rapidly than its density. The reason is that pores act to concentrate stress, which will not be uniform throughout the ceramic. The strength of nonporous ceramics decreases with increasing grain size as illustrated for the case of BeO in Figure 16.4b. Again, the observed behavior is due to flaws in the material that act as stress concentrators. In large grains there can be larger flaws. The effect of grain size is often more complicated than that shown in Figure 16.4b when we consider ceramics in which the grain size is just a few micrometers. Figure 16.5 is a compilation of flexural strength results for polycrystalline alumina at room temperature as a function of grain size. Despite the considerable scatter in the data, there are clearly two distinct regions. In both cases strength is proportional to the reciprocal square root of the grain size ($d^{-1/2}$) with different constants of proportionality. The reason for this behavior is that in addition to the preexisting flaws causing brittle fracture, there is a competing fracture mechanism that links dislocations and crack nucleation to subsequent failure.

It is therefore essential that when the mechanical properties of a ceramic material are listed, some details of the microstructure are also provided. As you can see from Figure 16.3 the measured value of a mechanical property may be affected by the test method. This is particularly true in the case of hardness.

High-performance structural ceramics combine the traditional advantages of ceramics (chemical inertness,

high-temperature capabilities, and hardness) with the ability to carry a significant tensile stress. The majority of the high-performance ceramics are based on silicon nitride, silicon carbide, zirconia, or alumina. Structural ceramics come in many forms—monoliths, composites, coatings, fibers, and whiskers.

16.2 TYPES OF TESTING

Ideally, before we use a ceramic in a load-bearing application we would like to have the following information about it:

- Young's modulus
- Average strength and Weibull modulus
- Toughness
- Crack propagation rate
- Cyclic fatigue resistance
- Creep curves
- Stress rupture data

We would also like to know these parameters as a function of temperature, in particular, over the temperature range at which our ceramic component is going to be used. Many different types of tests are used to obtain the mechanical properties of ceramics. There are major differences between how metals are tested compared to ceramics:

- It is often difficult to do tension tests on ceramics because of the possibility of introducing flaws.
- Ceramics are stronger in compression than they are in tension because of how cracks propagate.
- For ceramics, we need to be concerned with statistics because we do not know where the largest flaws are.

Because some mechanical properties depend on how the material was tested, it is important and necessary to establish specified test methods. Standard test methods have been adopted for ceramics. In the United States ASTM International (originally the American Society for Testing and Materials, ASTM) is the primary organization developing standards for materials testing. ASTM Committee C-28 on Advanced Ceramics has completed several standards and ones related to mechanical properties and testing are listed in Table 16.1. Specialized subcommittees work on specific areas within the field of advanced ceramics. Committee C28.01 is involved with standards related to mechanical properties and performance of monolithic ceramics. Committee C28.02 deals with reliability issues. The National Institute of Standards and Technology (NIST) has established several free databases that list mechanical properties of ceramics.

TABLE 16.1 ASTM Standards on Mechanical Properties and Testing of Ceramics

Mechanical properties and performance

C1161-02	Test Method for Flexural Strength of Advanced Ceramics at Ambient Temperature ^a
C1198-01	Test Method for Dynamic Young's Modulus, Shear Modulus, and Poisson's Ratio for Advanced Ceramics by Sonic Resonance
C1211-02	Test Method for Flexural Strength of Advanced Ceramics at Elevated Temperatures
C1259-01	Test Method for Dynamic Young's Modulus, Shear Modulus, and Poisson's Ratio for Advanced Ceramics by Impulse Excitation of Vibration
C1273-95	Test Method for Tensile Strength of Monolithic Advanced Ceramics at Ambient Temperature
C1291-95	Test Method for Elevated Temperature Tensile Creep Strain, Creep Strain Rate, and Creep Time-to-Failure for Advanced Monolithic Ceramics
C1326-99	Test Method for Knoop Indentation Hardness of Advanced Ceramics
C1327-97	Test Method for Vickers Indentation Hardness of Advanced Ceramics
C1361-01	Practice for Constant-Amplitude, Axial, Tension-Tension Cyclic Fatigue of Advanced Ceramics at Ambient Temperature
C1366-97	Test Method for Tensile Strength of Monolithic Advanced Ceramics at Elevated Temperatures
C1368-01	Test Method for Determination of Slow Crack Growth Parameters of Advanced Ceramics by Constant Stress-Rate Flexural Testing at Ambient Temperature
C1421-01	Test Method for the Determination of Fracture Toughness of Advanced Ceramics
C1424-99	Test Method for Compressive Strength of Monolithic Advanced Ceramics at Ambient Temperatures
C1465-00	Test Method for Determination of Slow Crack Growth Parameters of Advanced Ceramics by Constant Stress-Rate Flexural Testing at Elevated Temperature
C1499-02	Test Method for Monotonic Equi-biaxial Flexural Strength Testing of Advanced Ceramics at Ambient Temperature
C1525-02	Test Method for Determination of Thermal Shock Resistance for Advanced Ceramics by Water Quenching

Reliability

C1175-99	Guide to Test Methods for Nondestructive Testing of Advanced Ceramics
C1212-98	Practice of Fabricating Ceramic Reference Specimens Containing Seeded Voids
C1239-95	Practice for Reporting Uniaxial Strength Data and Estimating Weibull Distribution Parameters for Advanced Ceramics
C1322-02	Practice for Fractography and Characterization of Fracture Origins in Advanced Ceramics
C1336-96	Practice for Fabricating Non-Oxide Ceramic Reference Specimens Containing Seeded Inclusions
C1495-01	Test Method for Effect of Surface Grinding on Flexure Strength of Advanced Ceramics

^aStandards for both three-point and four-point bending; --**, year of current version of standard, e.g., -01 is 2001.

16.3 ELASTIC CONSTANTS AND OTHER "CONSTANTS"

In this section we will define some of the parameters that describe the mechanical behavior of materials. Some of these parameters are constants, like Young's modulus \mathcal{E} . Some, like hardness, are not. Hardness depends on how the material was tested.

Table 16.2 lists four elastic constants for different ceramics. These are the four that are most common.

1. \mathcal{E} (or Y , but be careful because Y is also used in our expression for stress intensity factor)—Young's modulus (also referred to as the elastic modulus) is a material constant defined by Eq. 16.1 for a linear elastic material under uniaxial tensile or compressive stress.

$$\sigma = \mathcal{E}\epsilon \tag{16.1}$$

It is therefore the slope of a σ - ϵ curve where only elastic deformation occurs.

2. ν —Poisson's ratio is the negative ratio of the transverse strain (ϵ_T) to longitudinal strain (ϵ_L).

$$\nu = -\epsilon_T/\epsilon_L \tag{16.2}$$

For many ceramics and glasses it is in the range 0.18–0.30.

3. μ —Shear modulus is the ratio of shear stress to shear strain.

$$\mu = \tau/\gamma \tag{16.3}$$

4. B —Bulk modulus is the ratio of stress to strain for hydrostatic compression.

$$B = -P(\Delta V/V) \tag{16.4}$$

Although these constants are related directly to bonding forces between atoms, in real ceramics they are affected by microstructure, e.g., porosity and the presence of second phases. Because strain is dimensionless, elastic moduli have the same dimensions as those of stress: force per unit area (N/m^2) or in the SI classification Pa.

Some texts use a pair of related elastic constants λ and μ . These are known as the Lamé constants. We already

TABLE 16.2 Elastic Constants of Selected Polycrystalline Ceramics (20°C)

Material	Crystal type	μ (GPa)	B (GPa)	ν	E (GPa)
<i>Carbides</i>					
C	Cubic	468	416	0.092	1022
SiC	Cubic	170	210	0.181	402
TaC	Cubic	118	217	0.270	300
TiC	Cubic	182	242	0.199	437
ZrC	Cubic	170	223	0.196	407
<i>Oxides</i>					
Al ₂ O ₃	Trigonal	163	251	0.233	402
Al ₂ O ₃ ·MgO	Cubic	107	195	0.268	271
BaO·TiO ₂	Tetragonal	67	177	0.332	178
BeO	Tetragonal	165	224	0.204	397
CoO	Cubic	70	185	0.332	186
FeO·Fe ₂ O ₃	Cubic	91	162	0.263	230
Fe ₂ O ₃	Trigonal	93	98	0.140	212
MgO	Cubic	128	154	0.175	300
2MgO·SiO ₂	Orthorhombic	81	128	0.239	201
MnO	Cubic	66	154	0.313	173
SrO	Cubic	59	82	0.210	143
SrO·TiO ₂	Cubic	266	183	0.010	538
TiO ₂	Tetragonal	113	206	0.268	287
UO ₂	Cubic	87	212	0.319	230
ZnO	Hexagonal	45	143	0.358	122
ZrO ₂ -12Y ₂ O ₃	Cubic	89	204	0.310	233
SiO ₂	Trigonal	44	38	0.082	95
<i>Chalcogenides</i>					
CdS	Hexagonal	15	59	0.38	42
PbS	Cubic	33	62	0.27	84
ZnS	Cubic	33	78	0.31	87
PbTe	Cubic	22	41	0.27	56
<i>Fluorides</i>					
BaF ₂	Cubic	25	57	0.31	65
CaF ₂	Cubic	42	88	0.29	108
SrF ₂	Cubic	35	70	0.29	90
LiF	Cubic	48	67	0.21	116
NaF	Cubic	31	49	0.24	77
<i>Other halides</i>					
CsBr	Cubic	8.8	16	0.26	23
CsCl	Cubic	10	18	0.27	25
CsI	Cubic	7.1	13	0.27	18
KCl	Cubic	10	18	0.27	25
NaBr	Cubic	11	19	0.26	28
NaCl	Cubic	15	25	0.25	38
NaI	Cubic	8.5	15	0.27	20
RbCl	Cubic	7.5	16	0.29	21

Note: All values were calculated from single-crystal data.

defined μ , so only λ is new. The expressions that relate elastic moduli are given in Table 16.3.

K_I —Stress intensity factor is a combination of flaw size, c , and applied stress, σ .

$$K_I = \sigma Y \sqrt{c} \quad (16.5)$$

Y in Eq. 16.5 is a dimensionless parameter that depends on the crack and loading geometries. For a simple interior crack of length $2c$ and tensile loading $Y = \sqrt{\pi}$ (this is the

original geometry considered by Griffith); for a surface crack under similar loading $Y = \sqrt{\pi/2}$). The units of K_I are $\text{MPa} \cdot \text{m}^{1/2}$.

The subscript refers to the type of loading geometry. There are three fundamental deformation modes that can be important for crack propagation. These modes are illustrated in Figure 16.6.

- Mode 1 opening. This is the most important for crack propagation in brittle solids. It can be achieved by an applied uniaxial tension.

TABLE 16.3 Expressions for Various Isotropic Elastic Moduli; Various Pairs of Moduli

Moduli	Independent pair of moduli			
	\mathcal{E}, μ	B, μ	B, ν	λ, μ
\mathcal{E}	\mathcal{E}	$9B\mu/(3B + \mu)$	$3B(1 - 2\nu)$	$\mu(3\lambda + 2\mu)/(\lambda + \mu)$
μ	μ	μ	$3B(1 - 2\nu)/2(1 + \nu)$	μ
B	$\mathcal{E}\mu/3(3\mu - \mathcal{E})$	B	B	$\lambda + (2\mu/3)$
ν	$(\mathcal{E}/2\mu) - 1$	$(3B - 2\mu)/(6B + 2\mu)$	ν	$\lambda/(2\lambda + \mu)$
λ	$(\mathcal{E} - 2\mu)\mu/(3\mu - \mathcal{E})$	$B - (2\mu/3)$	$3\nu B(1 + \nu)$	λ

- Mode 2 sliding
- Mode 3 tearing

K_{Ic} —Critical stress intensity factor or fracture toughness. Fracture of a material in tension occurs when $K_I \geq K_{Ic}$.

H —Hardness. There are different types of hardness. Why? Because the value of a material’s hardness depends on how it is tested. The hardness of a material is its resistance to the formation of a permanent surface impression by an indenter. You will also see it defined as resistance of a material to deformation, scratching, and erosion. So the geometry of the indenter tip and the crystal orientation (and therefore the microstructure) will affect the hardness. In ceramics, there tends to be wide variations in hardness because it involves plastic deformation and cracking. Table 16.4 lists hardness values on the Mohs’ hardness scale, a scratch test that can be used to compare hardness of different minerals. For example, quartz has a Mohs’ hardness of 7, which made flint (a cryptocrystalline quartz) particularly useful in prehistoric times for shaping bone (the mineral component is apatite with hardness 5) and shell (the mineral component is calcite with hardness 3). Mohs’ hardness scale was not the first scratch hardness technique. As long ago as 1690, Christian Huygens, the famous astronomer, had noticed anisotropy in scratch hardness.

Brittleness—Although not widely used, the brittleness index (BI) has been used to quantify the brittleness of a ceramic where $BI = H/K_{Ic}$.

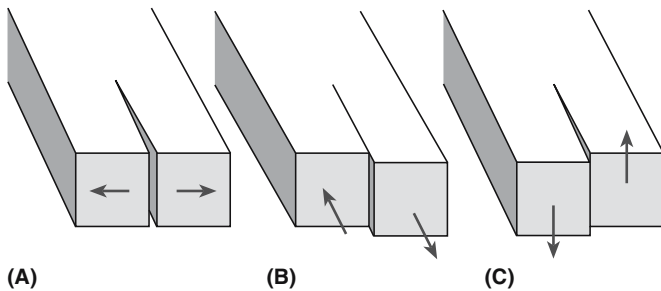


FIGURE 16.6 The three deformation modes for fracture: (a) Mode I opening. (b) Mode II sliding (in-plane shearing). (c) Mode III tearing (antiplane shearing).

16.4 EFFECT OF MICROSTRUCTURE ON ELASTIC MODULI

In Chapter 4 we showed that Young’s modulus is a property that is directly related to the bonding forces between atoms. We also showed that it varies as a function of temperature. In real ceramics we have to consider the fact that we often have more than one phase present. The overall modulus is then going to be a combination of the properties of each of the phases; it lies somewhere between the high- and low-modulus components.

Analytical expressions that represent the upper and lower bounds for Young’s modulus include the following.

Voiigt Model

Assumption: Strain in each constituent is the same. It represents the upper bound of Young’s modulus.

$$E = V_2 E_2 + (1 - V_2) E_1 \quad (16.6)$$

TABLE 16.4 Mohs’ Hardness

Hardness number	Mohs’ scale	Ridgeway’s extension of Mohs’ scale	Knoop hardness expanded scale
1	Talc	Talc	
2	Gypsum	Gypsum	32
3	Calcite	Calcite	135
4	Fluorite	Fluorite	163
5	Apatite	Apatite	430
6	Orthoclase	Orthoclase	560
7	Quartz	Vitreous silica	—
8	Topaz	Quartz or stellite	820
9	Corundum	Topaz	1340
10	Diamond	Garnet	1360
11		Fused zirconia	—
12		Fused alumina	2100
13		Silicon carbide	2480
14		Boron carbide	2750
15		Diamond	7000

TABLE 16.5 Relations between Porosity, P , and Young's Modulus, \mathcal{E}

$\mathcal{E} = \mathcal{E}_0(1 - aP)$	Linear decrease in Young's modulus with porosity when P is small, $a \sim 4$
$\mathcal{E} = \mathcal{E}_0(1 - aP + bP^2)$	For a low concentration of spherical pores ($a \sim 1.9$, $b \sim 0.9$)
$\mathcal{E} = \mathcal{E}_0(1 - aP)^b$	For solid foams with very high porosity $P > 0.7$ ($a = 1$, $b = 2$)
$\mathcal{E} = \mathcal{E}_0[(1 - P)^2/1 + (a - 1)P]$	a is a shape factor with values depending on porosity: $a = 2.5$ for interconnected porosity ($1/a = 0.4$) $a = 3.3\text{--}1.4$ for porosity that resembles ribbons ($1/a = 0.3\text{--}0.7$) $a = 0.6\text{--}1.0$ for isolated pores ($1/a = 0.6\text{--}1.0$) $(1/a$ is known as the Nielson shape factor)
$\mathcal{E} = \mathcal{E}_0 \exp(-aP)$	Empirical for oxides with porosity in the range 0–40% ($a \sim 4$)

Reuss Model

Assumption: Stress in each phase is the same. It represents the lower bound of Young's modulus.

$$\frac{1}{\mathcal{E}} = \frac{V_2}{\mathcal{E}_2} + \frac{(1 - V_2)}{\mathcal{E}_1} \tag{16.7}$$

Hashin and Shtrikman (HS) developed a narrower, more useful, set of bounds using basic elasticity energy theorems. The HS bounds have been shown to be best for the bulk modulus and are given by

$$\frac{B - B_1}{B_2 - B_1} = V_2 \left[\frac{V_1(B_2 - B_1)}{B_1 + H} \right]^{-1} \tag{16.8}$$

where $H = 4\mu_2/3$ or $H = 4\mu_1/3$. Young's moduli can be obtained from B if ν is known and reasonable fits with experimental data can be obtained as shown in Figure 16.7 for alumina-tetragonally stabilized zirconia ($\text{Al}_2\text{O}_3\text{--ZrO}_2$) composites.

If the second phase is porosity, as is often the case in polycrystalline ceramics, then intuitively we realize that there will be a decrease in the elastic modulus. A pore has zero stiffness. Several relationships have been developed

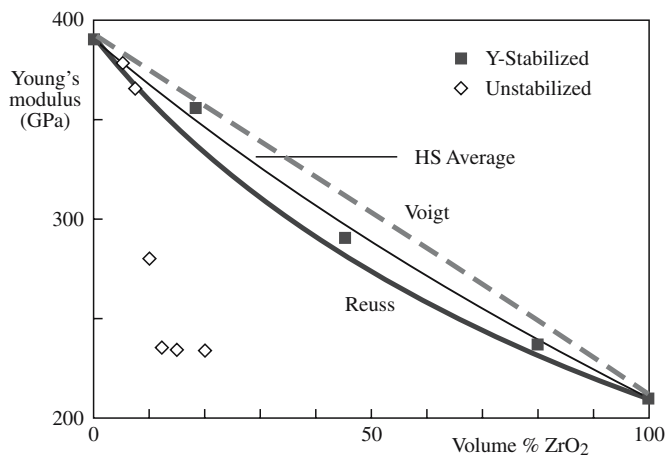


FIGURE 16.7 Comparison of predicted values of Young's modulus for an Al_2O_3 tetragonally stabilized ZrO_2 composite with experimental data.

to account for the change in Young's modulus with porosity, P . These are shown in Table 16.5 where the "constants" a and b are often empirically determined; \mathcal{E}_0 is the Young's modulus of the dense material.

16.5 TEST TEMPERATURE

Mechanical properties often show strong variations with temperature. We already considered in Chapter 4 how temperature affects Young's modulus. For some mechanical properties the change with temperature may be more abrupt than the gradual decrease in \mathcal{E} with increasing temperature. The ductile-to-brittle transition, which occurs with decreasing temperature, is an important topic in metals. The significance of this phenomenon really came to light during World War II when there were reports of serious fractures in some of the Liberty ships (mass-produced vessels of predominantly welded construction). One of the most striking instances of this type of fracture was the T2 tanker *S.S. Schenectady* built in Portland, Oregon, which suddenly broke into two sections at 10.30 PM on January 16, 1943. The reason was that the steel alloy used to construct the hull had undergone a ductile-to-brittle transition at a temperature of 4°C . This event gave particular impetus to the study of fracture in brittle materials.

Do ceramics experience a ductile-to-brittle (or the converse) transition and is it important? Ceramics can exhibit both types of behavior over different temperature ranges. Figure 16.8 illustrates the temperature dependence of strength for ceramics.

- Region A: the fracture is brittle and the fracture strain is $\sim 10^{-3}$. There is no significant plastic deformation prior to failure and the strength varies little with temperature.
- Region B: the fracture is again brittle but slight plastic deformation occurs prior to failure. The failure strain is usually in the region $10^{-3}\text{--}10^{-2}$ and strength falls with increasing temperature.
- Region C: Appreciable plastic flow occurs, with strains of the order of 10^{-1} prior to failure. This behavior is rarely observed in ceramics, even in ductile polycrystalline ceramics.

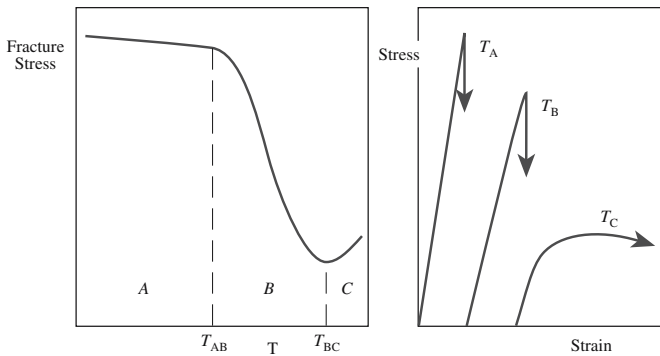


FIGURE 16.8 Illustration of the effect of temperature on fracture stress for a ceramic. The key temperatures are T_{AB} and T_{BC} .

The critical temperatures, T_{AB} and T_{BC} , vary greatly for different ceramics. For polycrystalline MgO the brittle-to-ductile transition occurs at $\sim 1700^\circ\text{C}$ ($0.6 T_m$). There is no plastic deformation in β -SiC below 2000°C . Talc, MoS₂, and graphite all deform at room temperature. MoS₂ and graphite are widely used as solid lubricants.

The transition can be important in structural ceramics (particularly nonoxides like silicon nitride) when they are used in high-temperature applications. Densification in these ceramics is often achieved using a second phase that forms a glass at grain boundaries and triple points. At temperatures near the glass softening temperature very extensive plastic flow occurs. Figure 16.9 shows σ - ϵ curves for silicon nitride at 1400°C containing different amounts of silica. For silica contents >20 wt% macroscopic plastic deformation occurs. At high silica contents it is believed that the glassy phase is no longer constrained at the triple points.

16.6 TEST ENVIRONMENT

In some cases the environment to which the ceramic is exposed is a very important consideration. For example, you will often see that mechanical tests on bioceramics are performed either *in vivo* or *in vitro*. Tests performed in the body are referred to as *in vivo*. Tests performed outside the body, often in conditions that seek to replicate or approximate the physiological environment, are referred to as *in vitro*. ISO Standard 6474 for alumina bioceramics specifies a bend strength >450 MPa after testing in Ringer's solution. Ringer's solution is a model liquid that resembles human body fluid.

RINGER'S SOLUTION (PARTS BY VOLUME)

NaCl solution 0.9%	94
KCl solution 1.15%	4
CaCl ₂ solution 1.22%	3
KH ₂ PO ₄ solution 2.11%	1
MgSO ₄ solution 3.82%	1
NaHCO ₃ solution 1.3%	14
NaHPO ₄ solution 1 M	13

RULE OF THUMB

Compressive fracture strength is 10–15 times greater than tensile fracture strength.

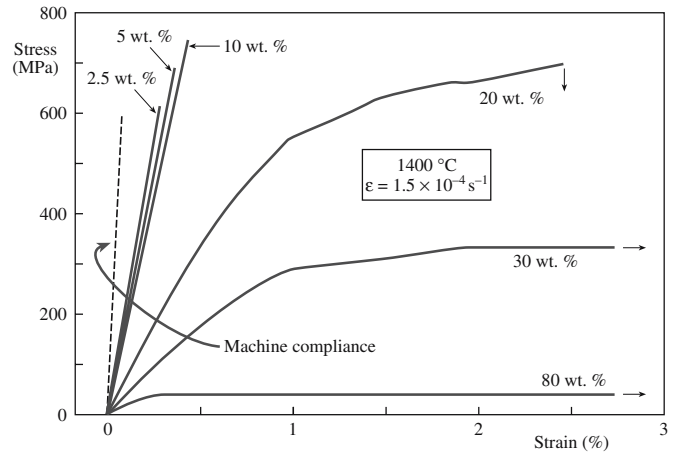


FIGURE 16.9 Stress–strain curve for Si₃N₄ at 1400°C for various amounts of silica. The machine compliance is the inherent displacement within the instrument.

16.7 TESTING IN COMPRESSION AND TENSION

The tensile test is the most frequently used procedure to determine the tensile strength of a metal. However, it is not used as widely for ceramics because of their inherent brittleness. It is difficult to make the typical “dog-bone”-shaped samples, where the cross-sectional area is reduced in the gage length. We could do this with a ceramic, but the machining needed to give this shape is likely to introduce surface flaws. In many tensile test instruments the sample under test is connected by means of a screw thread. This is often tricky to machine with a ceramic and it may also break in the grips. Finally, because ceramics fail after only about 0.1% strain, the specimens under test must be perfectly aligned or bending stresses will be introduced, which will complicate things.

In some practical situations we require ceramics to support a tensile load. Consider the growth of silicon single crystals by the Czochralski process, which involves pulling the crystal from the melt. The crystal is supported entirely by a narrow region called the neck, about 3 mm in diameter. It is possible to support a total crystal weight of about 200 kg. This requirement determines the maximum overall volume of a silicon boule. The diameter is controlled by our ability to produce dislocation-free crystals as described in Chapter 29. Steel-reinforced concrete and safety glass are two exam-

TABLE 16.6 Ratio of Compressive Strength σ_{cc} to Bending Strength, σ_c

Ceramic	Grain size (μm)	σ_{cc}/σ_c
TiB ₂	20–50	4–6
ZrB ₂	20–50	4–6
B ₄ C	1	7
WC	1–6	4–6
Al ₂ O ₃	1–100	4–30
MgAl ₂ O ₄	1	7
ThO ₂	4–60	13–17
UO ₂	20–50	5–18

ples in which a ceramic is prestressed in compression to increase its ability to support a tensile load.

Stress–strain curves for metals look very similar and provide similar results whether the testing is carried out in tension or compression. Ceramics are generally stronger in compression and can tolerate high compressive loads. Some examples are given in Table 16.6. However, reliable compressive strength data are limited for ceramics. Note that the Young’s modulus will be the same because the curves will have the same slope.

One ceramic that is widely tested in compression is concrete. Concrete is a ceramic-matrix composite consist-

ing of a mixture of stone and sand (called the aggregate) in a cement matrix. The aggregate provides the strength and the cement provides the workability. When concrete is used in construction it must always be loaded in compression. As shown in Figure 16.10 cracks behave differently in compression than they do in tension. In compression, cracks twist out of their original orientation and propagate stably along the compression axis. The result is that the sample will crush rather than fracture. Fracture is not caused by rapid unstable crack propagation as it is in tension.

In tension we are concerned with the largest crack, the “critical flaw,” particularly if it is on the surface. In compression we are concerned with the average flaw size, c_{av} . We can estimate the compressive stress to failure by substituting c_{av} into Eq. 16.5 and using a multiplier between 10 and 15. Teeth are ceramic composites: they survive for years even when many cracks are present.

16.8 THREE- AND FOUR-POINT BENDING

To avoid the high expense and difficulties of performing tensile tests on ceramics, tensile strength is often determined by the bend test. There are two geometries and these are illustrated in Figure 16.11. The main advantage of the bend test, other than its lower cost, is that we use simple sample geometries. The specimens have either a rectangular or cylindrical geometry. The four-point bend test is preferred because an extended region with constant bending moment exists between the inner rollers.

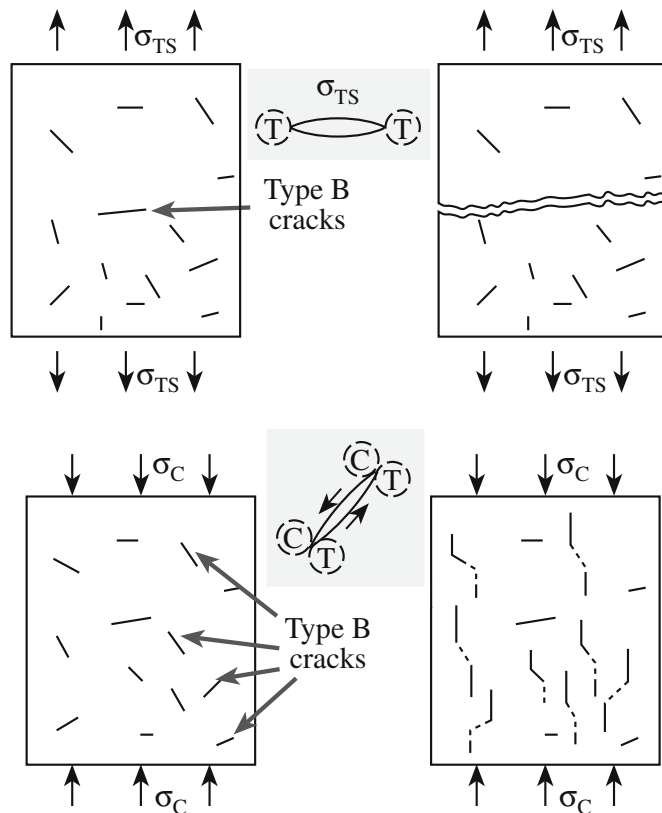


FIGURE 16.10 Illustration of unstable and stable crack propagation for a brittle material in tension (T) and compression (C), respectively. Stable crack propagation will lead to crushing.

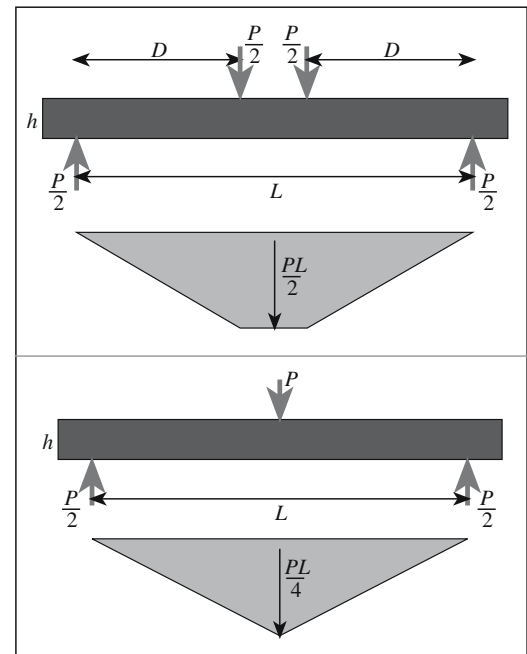


FIGURE 16.11 The geometries for three- and four-point bending.

The maximum tensile stress in the surface of the beam when it breaks is called the modulus of rupture (MOR), σ_r . For an elastic beam it is related to the maximum moment in the beam, M

$$\sigma_r = \frac{6M_r}{BW^2} \quad (16.9)$$

W is the height of the beam and B is its thickness. For the case of bend testing a ceramic this equation is applicable only when the distance between the inner rollers is much greater than the specimen height.

Other terms are also used including flexural strength, fracture strength, and bend strength. The bend test is also known as a flexure test and the resistance of a beam to bending is known as its flexural rigidity. The terminology can be a little confusing, but this test is important because it is widely used and probably the best studied strength test for ceramics.

Examples of data from such tests are shown in Figure 16.12 for polycrystalline alumina. The main comment that can be made is that there is a wide variation in the values! Grain

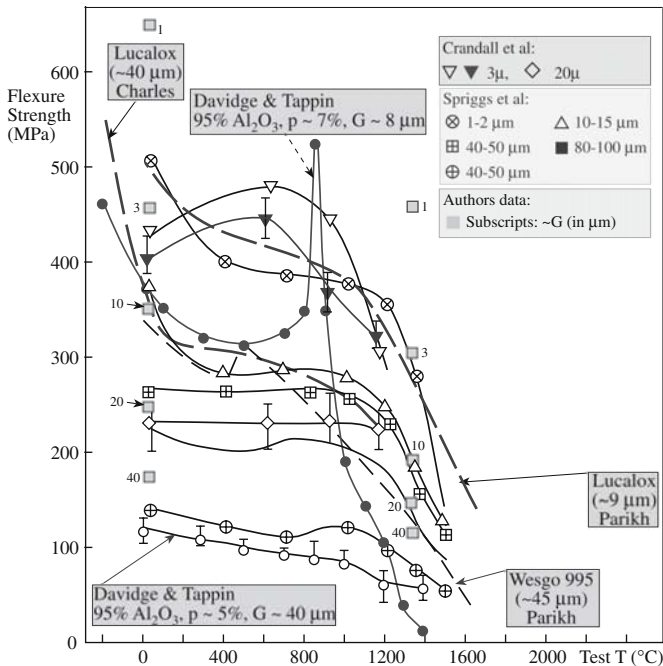


FIGURE 16.12 Flexural strength of polycrystalline Al_2O_3 as a function of test temperature.

MODULUS OF RUPTURE EQUATIONS

$$\text{Three-point bend: } \sigma_r = \frac{3PL}{2BW^2}$$

$$\text{Four-point bend: } \sigma_r = \frac{3PD}{BW^2}$$

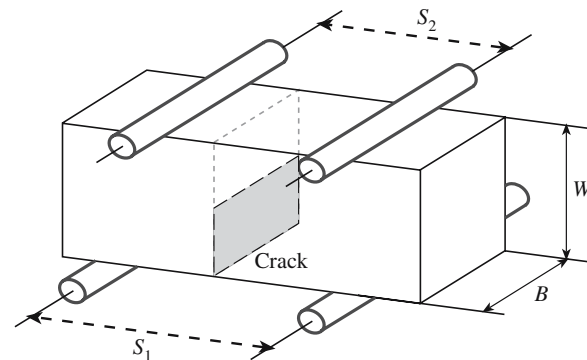
size differences between the samples are clearly one of the factors contributing to this variation.

The main disadvantage of the bend test is that the stress distributions can be complex and nonuniform.

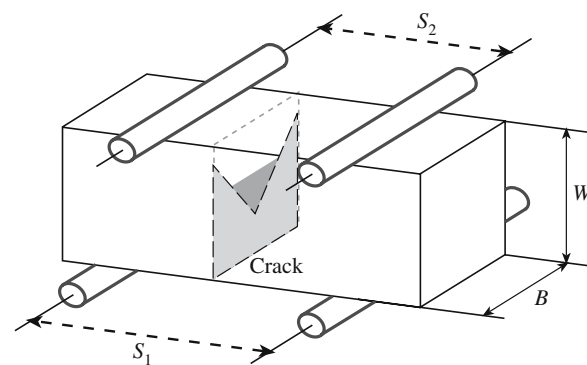
The consequence is that under certain conditions, particularly when the largest flaws in the sample are located in the interior of the specimen, the strength of the ceramic will be overestimated.

16.9 K_{Ic} FROM BEND TEST

There are several techniques to determine K_{Ic} for a ceramic. The two main approaches are to use indentation or bending. In the bend test a notch is introduced, usually using a diamond-tipped copper cutting wheel, into the tensile side of the specimen as shown in Figure 16.13. In Figure 16.13a the



(A)



(B)

FIGURE 16.13 Geometries for (a) SENB and (b) CN specimens used to determine K_{Ic} .

notch is flat (single-edged notched beam, SENB), whereas in Figure 16.13b it is chevron-shaped. The specimen is loaded, usually in four-point bend, until it fails at F_{Max} and K_{Ic} is calculated.

For the SENB

$$K_{Ic} = \frac{3\sqrt{c}(S_1 - S_2)\xi F_{Max}}{2BW^2} \quad (16.10)$$

c is the length of the initial crack that we introduced and ξ is a calibration factor. The advantage of the SENB test is that it is quite simple, although it tends to overestimate K_{Ic} because the crack is often not atomically sharp. For ceramics having very fine grain sizes the notch must be very narrow.

For the chevron notched (CN) specimen

$$K_{Ic} = \frac{(S_1 - S_2)\xi^* F_{Max}}{BW^{3/2}} \quad (16.11)$$

where ξ^* is a compliance function. Sometimes you will see Eq. 16.11 written in such a way that all the geometric terms are grouped together as a single geometric function Y^* . Then we have

$$K_{Ic} = \frac{F_{Max}}{B\sqrt{W}} Y^* \quad (16.12)$$

The value of Y^* is then necessary for different specimen geometries and different notch geometries. Two approaches can be used to obtain Y^* (see Specific References).

The advantage of the CN geometry is that we do not need to worry about introducing a sharp precrack. Our original notch is made by two saw cuts to produce a triangularly shaped cross section. A crack is easily initiated at the tip of the chevron, but the increasing cross section of the crack front causes crack growth to be stable prior to failure. Further crack extension requires an increase in the applied load and it is possible to create an atomically sharp crack before the specimen fails. Also you can see from Eq. 16.11 that we do not need to know the actual crack length. In fact, we do not need to know any of the materials properties.

16.10 INDENTATION

Measuring the hardness of a ceramic is important and this is usually done using an indentation test. The basic idea is that a permanent surface impression is formed in the material by an indenter. We then measure the actual or

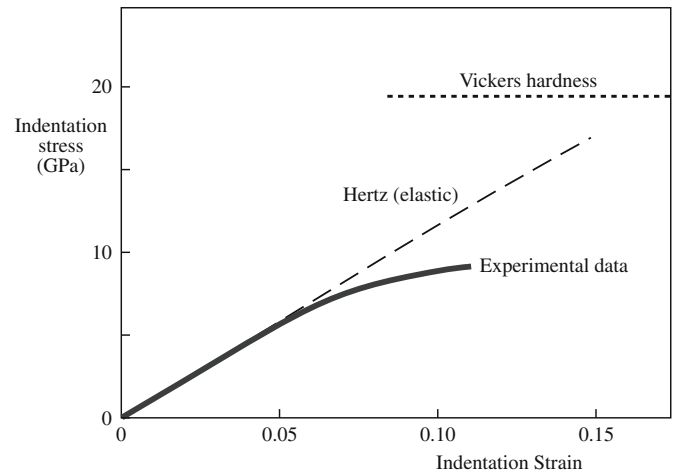


FIGURE 16.14 Indentation stress versus indentation strain.

projected area of the impression. The hardness is then determined by dividing the applied force, F , by this area. The processes that happen under the indenter tip can be quite complex. We often see a deviation from what is called “Hertzian” behavior where the indentation stress is proportional to the indentation strain (Figure 16.14). The deviation is due to plasticity beneath the indenter as illustrated in Figure 16.15. We discuss this more in Chapter 17. Cracking can also occur on indenting and this can be used as a means of determining fracture toughness.

There are many different hardness tests and each gives a different number. The common hardness tests are listed in Table 16.7 and the geometries of

the impression are shown in Figure 16.16. It is possible to convert between different hardness scales, but the conversion depends on both the material and its microstructure. The most reliable data are for steels because most of the work has been done on these alloys. Detailed conversion tables for metals and alloys are available in ASTM Standard E 140, “Standard Hardness Conversion Tables for Metals.” There are different regimes of hardness based on the load used as shown in Table 16.8. These divisions are somewhat arbitrary, but they are commonly accepted.

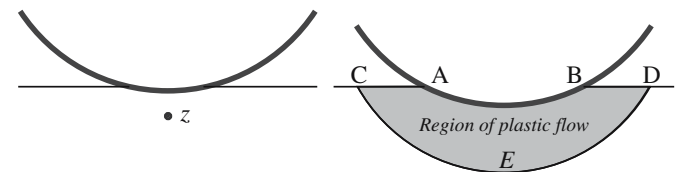


FIGURE 16.15 Plasticity under the indenter (the shaded area) causes the deviation from Hertzian behavior.

TABLE 16.7 Details of Common Hardness Tests

Test	Indenter	Description	Equation	Notes
Brinell	Hardened steel ball	Brinell hardness number (BHN) is applied force divided by surface area of indentation Meyer hardness number (MHN) uses projected area	$BHN = F/\pi Dt$ $MHN = 4F/\pi d^2$	Spherical indenters not used for ceramics
Vickers	Square pyramid	Vickers hardness number (VHN) using contact area VHN using projected area	$VHN = 1.854F/a^2$ $VHN = 2.000F/a^2$	The ceramics community uses mainly the number calculated using the projected area; need to be careful when comparing data from different sources
Knoop	Elongated pyramid	Knoop hardness number (KHN)	$KHN = 14.2F/L^2$	
Rockwell	Various indenter types/loads	Dimensionless number and various hardness scales		Widely used for metals but not often for ceramics except cemented carbides

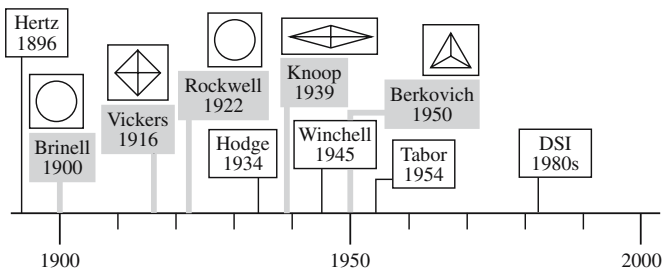


FIGURE 16.16 The evolution of common hardness tests and the corresponding indenter shapes.

TABLE 16.8 Hardness Regimes

Regime	Applied load (N)	Comments
Microhardness	0.0098–1.96	Hardness value decreases as load increases Possibility for very large variations in values depending on technique used and microstructure Surface effects may dominate
Low load hardness	1.96–98.1	
Standard hardness	>98.1	Hardness independent of applied load and microstructure.

16.11 FRACTURE TOUGHNESS FROM INDENTATION

We can obtain the fracture toughness from indentation tests. The basic idea is illustrated in Figure 16.17. We get an indent and radial cracks. The hardness is then

$$H = P/\alpha a^2 \quad (16.13)$$

α is a numerical factor that depends on the shape of the indenter. For a Vickers indenter $\alpha = 2$. P is the load in newtons.

The critical stress intensity factor is obtained by assuming that the applied stress intensity caused by the load is equal to the critical stress intensity for crack propagation.

$$K_{Ic} = \frac{\zeta(E/H)^{1/2} P}{c^{3/2}} \quad (16.14)$$

ζ is a dimensionless constant, which for ceramics has an average value of 0.016 ± 0.004 . The use of indentation techniques for determining K_{Ic} has been the subject of many studies since being introduced by Lawn and Wilshaw (1975). The most commonly used variant, termed the indirect method, uses indentation followed by determination of the strength after indentation using bend testing. The main concern is to ensure that the crack does not grow between indentation and bend testing. To minimize effects

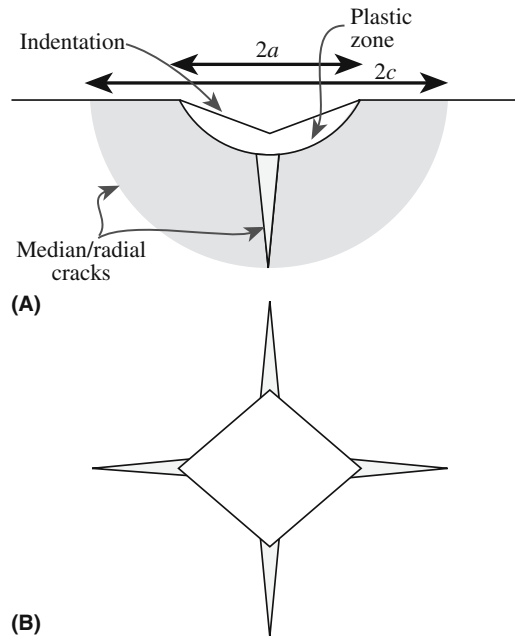
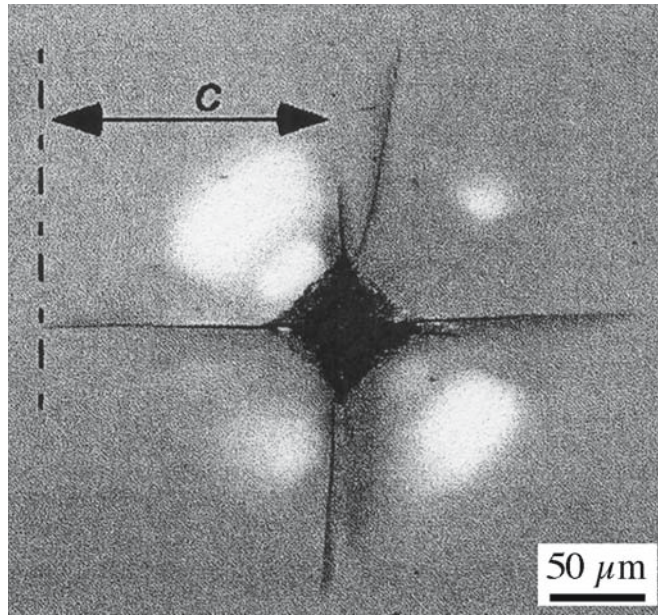


FIGURE 16.17 Cracks at an indent allow determination of K_{Ic} .



(C)

FIGURE 16.17 Continued

of reactive species such as water a drop of oil may be placed on the indent. Tests seem to give reproducible values for K_{Ic} .

16.12 NANOINDENTATION

The nanoindentation technique was developed in the 1980s because of the need to determine the mechanical properties of thin films and surfaces that had been modified, for example, by ion implantation. To avoid the influence of the substrate the penetration depth of the indenter must be less than 10% of the film thickness. Consequently penetration depths are on the order of nanometers rather than millimeters, which is common for conventional indentation tests.

Nanoindentation is also used to test small volumes of material. The low loads used mean that the extent of cracking is much smaller than in conventional indentation methods.

Two parameters are often of most interest in nanoindentation testing:

- Elastic modulus
- Hardness

Load (P) versus depth of penetration (h) curves, also called compliance curves, are the output from a nanoindentation test. The curves are obtained as load is applied to the indenter tip up to some maximum value and then back to zero. Figure 16.18 shows a general compliance curve for a material that undergoes both elastic and

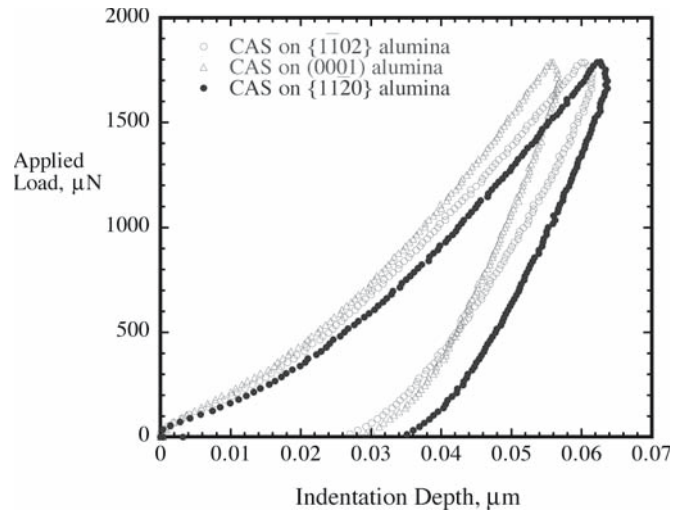


FIGURE 16.18 Load-displacement data on the 1.8 mN indentations of CAS films on three different alumina substrates.

plastic deformation. When the load applied to the indenter is released the material attempts to return to its original shape. The slope of the elastic unloading region (dP/dh) can be used to determine the modulus and hardness. There are several different equations depending on the tip geometry. If the material is plastically deformed it cannot return to its original shape and there is a residual impression, h_r . The magnitude of h_r will be greater for a metal such as steel than for a ceramic such as sapphire.

Nanoindentation is a powerful technique because the shape of the load-displacement curve can be used to identify effects such as phase transformations, cracking, and film delamination during indentation. It is also important in studying the mechanical properties of nanomaterials, such as carbon nanotubes. There is reference now to a picoindenter, which is a combination of a nanoindenter and an atomic force microscope (AFM).

16.13 ULTRASONIC TESTING

The basic principle of this method is that the velocity of an ultrasonic wave through a material is related to its density and elastic properties. This is one example of a dynamic method for determining elastic constants, such as Young's modulus and shear modulus. Dynamic methods are more accurate than static methods with uncertainties of $<0.5\%$ ($\pm 10\%$ would be more typical for static methods).

To determine the shear modulus and Poisson's ratio we need the velocity of the longitudinal and transverse waves, v_L and v_t . The equations are

TRANSVERSE WAVE VELOCITIES		
	Al_2O_3	Al
μ	163 GPa	25 GPa
ρ	3970 kg/m ³	2710 kg/m ³
v_t	6.4 km/s	3.0 km/s

$$\mu = \rho v_t^2 \quad (16.15)$$

$$v = \frac{1 - 2(v_t/v_L)^2}{2[1 - (v_t/v_L)^2]} \quad (16.16)$$

$$E = 2\mu(1 + v) \quad (16.17)$$

Conversely, if we know the elastic moduli we can determine the magnitude of the sound velocities. For ceramics with high moduli and low density the sound velocities will be much higher than many metals. The propagation of sound waves through ceramics is particularly important during earthquakes. The earth's crust is composed primarily of silica and aluminosilicates. Using Eqs. 16.15 and 16.16 we can show for SiO₂, the primary constituent of rocks such as granite, that the longitudinal waves are the first shocks to arrive after an earthquake, followed by the transverse waves; v_L = 6.04 km/s and v_t = 4.1 km/s for quartz. The surface waves are the last to arrive, having a velocity <4 km/s, but these often have the most devastating effect.

Ultrasonic testing is widely used in the concrete industry to determine the presence or absence of voids, cracks, and other imperfections and to measure deterioration that might have occurred due to age or through fire or frost damage.

16.14 DESIGN AND STATISTICS

When we measure the strength of a series of equivalent ceramic specimens we typically find considerable scatter in the results. The reason is due to the size distribution of flaws that are responsible for failure. This behavior is very different from that of metals. Consequently we have to adopt different design approaches when we use ceramics.

When we design components using metals we determine the maximum stress that will be present in the component and then select a metal that has a larger strength. A reasonable safety margin is often included. This approach is referred to as deterministic design. It does not work with ceramics because of the large scatter. Rather we have to use a probabilistic approach in which we represent this scatter in a quantitative way so that these materials can be used safely. The most popular method is to use Weibull statistics, which are based on the weakest link approach. The analogy is to consider a chain the strength of which is determined by the weakest link.

The Weibull distribution function is shown in Figure 16.19 and gives the probability of survival (P_S), or, alternatively, the probability of failure (P_F), of a stressed volume V .

$$P_S = 1 - P_F = \exp \left[- \int_V \left(\frac{\sigma - \sigma_{\min}}{\sigma_0} \right)^m dV \right] \quad (16.18)$$

The Weibull distribution function contains three parameters:

m = Weibull modulus, which indicates how rapidly the strength falls as we approach σ_0 .

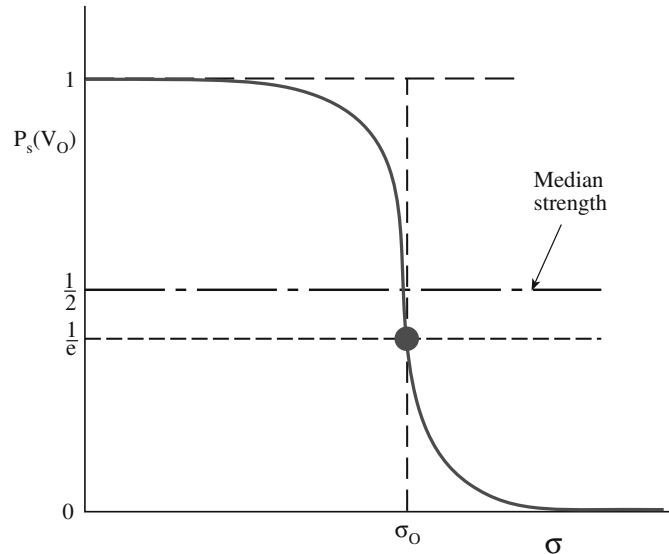


FIGURE 16.19 The Weibull distribution function.

σ_0 = the characteristic strength for which the survival probability is 0.37 ($1/e$).

σ_{\min} = the stress level below which the probability of failure is zero.

Because there is always a possibility, albeit slight, of our component having a very large flaw, we usually set $\sigma_{\min} = 0$. This leads to the two-parameter form that is used for ceramics.

$$P_S = \exp \left[- \int_V \left(\frac{\sigma}{\sigma_0} \right)^m dV \right] \quad (16.19)$$

If the full volume is under uniform uniaxial tension then we can write Eq. 16.19 as

$$P_S = \exp \left[- \left(\frac{\sigma}{\sigma_0} \right)^m \right] \quad (16.20)$$

For other geometries we need to include the loading factor L_F . This takes into account the stress distribution. For uniaxial tension $L_F = 1$; for other loading geometries see Table 16.9. The product ($L_F V$) is often termed the effective volume, V_{eff} , as it indicates how “effectively” the body is being stressed.

Taking the natural logarithm of both sides of Eq. 16.20 we get

$$\ln \left(\frac{1}{P_S} \right) = \left(\frac{\sigma}{\sigma_0} \right)^m$$

If we take natural logarithms again we get

TABLE 16.9 Examples of Loading Factors^a

Geometry	Loading factor, L_F
Uniaxial tension	1
Pure bending	$1/[2(m+1)]$
Three-point bending	$1/[2(m+1)^2]$
Four-point bending	$(mL_i + L_o)/[2L_o(m+1)^2]$

^a L_i , inner span; L_o , outer span.

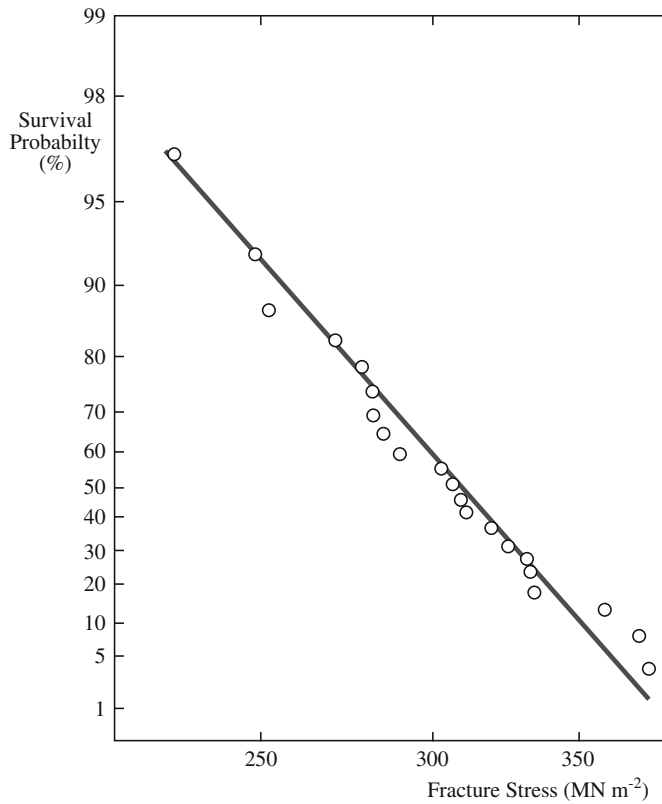


FIGURE 16.20 Weibull plot showing probability of failure as a function of fracture stress.

$$\ln \left[\ln \left(\frac{1}{P_s} \right) \right] = m \ln \left(\frac{\sigma}{\sigma_0} \right)^m = m \ln \sigma - m \ln \sigma_0$$

Now if we plot $-\ln \ln(1/P_s)$ versus $\ln \sigma$ we will get a straight line of slope $-m$ as shown in Figure 16.20. The higher the Weibull modulus the lower is the variability of strength. Values for ceramics are often in the range of 5–20 (compared, for example, to steels, which have values of about 100). Figure 16.21 shows how the Weibull modulus affects the survival probability.

The Weibull modulus, which is the parameter of most interest, is obtained experimentally by testing a batch of samples. We need a large number of specimens to get an accurate value of m . Usually a minimum of 30 samples is required, which will typically give m within 20%. Up to 100 samples is not uncommon, which will give m with a greater than 90% confidence.

The following sequence of steps is used to determine m from a set, N , of measured strengths:

1. Rank the specimens in order of increasing strength.
2. Determine P_s . For the j th specimen this is often given as the approximation $P_s(j) = 1 - j/(N + 1)$. A more accurate expression that may be used instead is $P_s = 1 - [(j - 0.3)/(N + 0.4)]$.

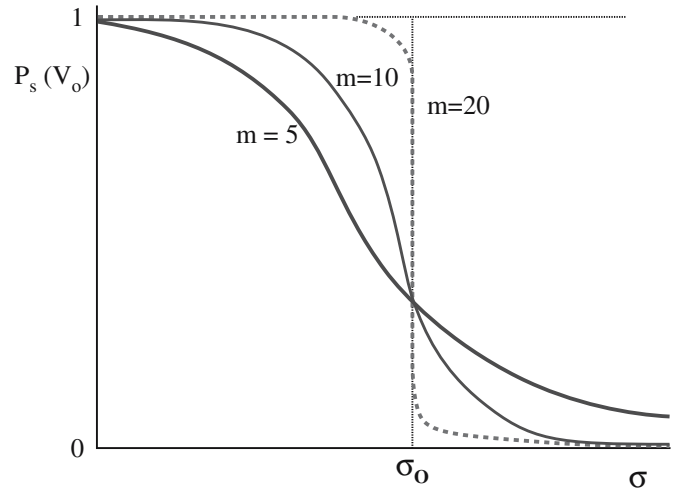


FIGURE 16.21 Illustration of the effect of m on survival probability. When m changes P_s changes.

3. A plot $-\ln \ln(1/P_s)$ versus $\ln \sigma$, the slope, which can be determined by a least-squares fit, gives m .

In ceramics there is a volume dependence of the strength. This can be illustrated quite easily using a stick of chalk. As the chalk becomes smaller it becomes stronger. The reason is again due to flaws. There is an increased probability of finding a larger flaw in a larger body as illustrated in Figure 16.22. This effect can be expressed mathematically as

$$P_s = \exp \left[- \left(\frac{V}{V_0} \right) \left(\frac{\sigma}{\sigma_0} \right)^m \right]$$

where $V = nV_0$. An example of the size effect is shown in Figure 16.23 for Si_3N_4 springs. The springs have different diameters of the wire and of the coil and different numbers of coils were measured.

STRENGTH AND VOLUME

The strength of metal samples does not depend on volume.

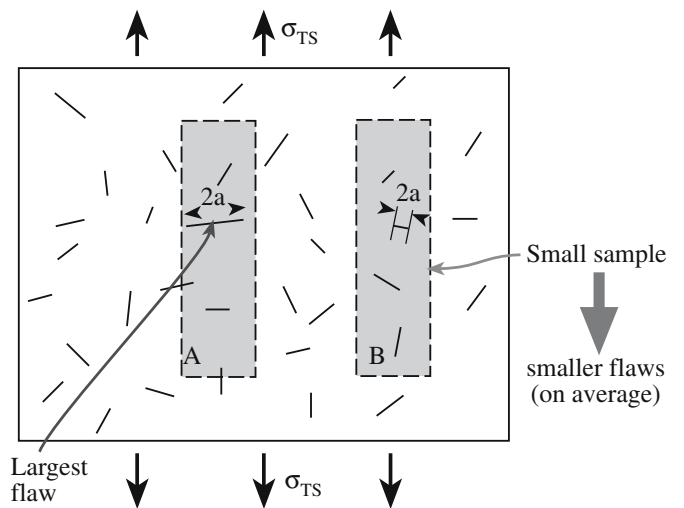


FIGURE 16.22 The largest flaw will be the weakest link and the source of failure. Smaller samples have smaller flaws.

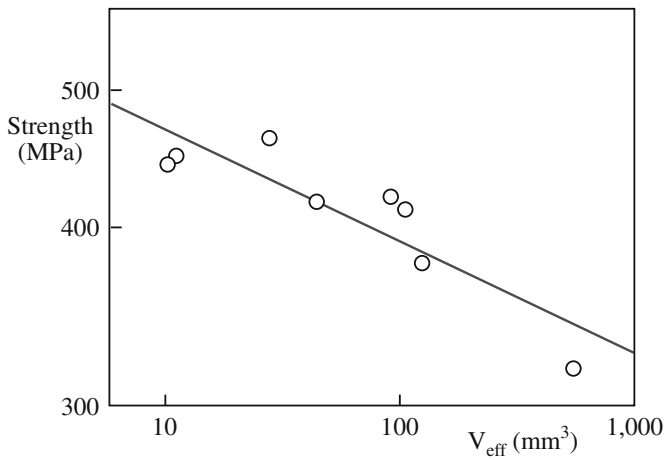


FIGURE 16.23 Fracture stress as a function of volume for Si_3N_4 springs.

Complications arise if we have different flaw populations, for example, we may have pores and inclusions introduced during sintering and surface flaws introduced during grinding. The different flaws may lead to different Weibull distributions and different Weibull moduli. Figure 16.24a illustrates the superposition of two flaw types and Figure 16.24b for a sample containing surface and volume flaws. And we have new equations.

For two different surface flaw types:

$$P_S = \exp \left[- \left(\frac{\sigma_c}{\sigma_1} \right)^{m_1} - \left(\frac{\sigma_c}{\sigma_2} \right)^{m_2} \right]$$

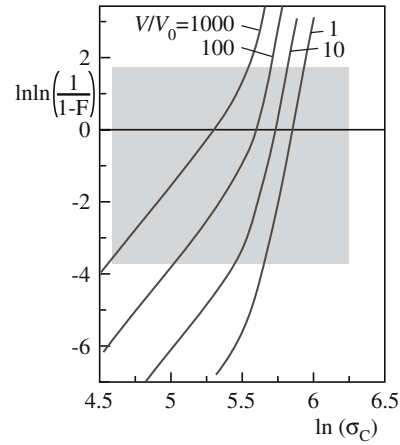
For flaw type 1 we have σ_1 and m_1 ; for flaw type 2 we have σ_2 and m_2 .

For two different types of volume flaws:

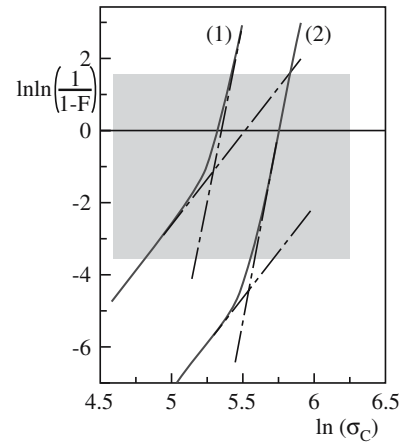
$$P_S = \exp \left[- \frac{V_{\text{eff1}}}{V_0} \left(\frac{\sigma_c}{\sigma_{v1}} \right)^{m_1} - \frac{V_{\text{eff2}}}{V_0} \left(\frac{\sigma_c}{\sigma_{v2}} \right)^{m_2} \right]$$

As you now realize it is impossible to design a ceramic where the probability of failure is zero. Table 16.10 gives some examples of what might be considered acceptable probabilities of failure.

Proof testing can be used to truncate the extreme tail of the Weibull distribution. Components are tested up to a certain proof-test stress, σ_{PT} (Figure 16.25), for a short period of time. The weakest ones obviously fail and can be weeded out. We then have increased confidence in the remaining components. We often have to proof test stresses close to the design stress. For a ceramic with $m = 10$, reducing the risk of rupture from 0.1 to 0.05 requires that the component be proof tested to 93% of the design stress. To reduce the probability of failure by an order of magnitude, down to 0.02, the part must be proof tested to 99% of the design stress (Figure 16.26). We have a good level



(A)



(B)

FIGURE 16.24 (a) Different flaws lead to different values of m . (b) Weibull plot for a sample having both surface and volume flaws.

of confidence in the remaining components withstanding any stress $< \sigma_{PT}$.

CARES (Ceramics Analysis and Reliability Evaluation of Structures) is a public-domain program from the National Aeronautic and Space Agency (NASA) that incorporates Weibull statistics. The program was formally known by the less friendly acronym SCARE (Structural Ceramics Analysis and Reliability Evaluation).

The NASA CARES program can be found at <http://www.grc.nasa.gov/WWW/LPB/cares/life/refs.html>.

The following considerations and assumptions apply to the use of Weibull statistics:

TABLE 16.10 Suggested Failure Probabilities

P_F	Possible consequences of failure	Example
0.3	Slight inconvenience	Sticks of chalk
10^{-2}	Inconvenience and small expense	Ceramic cutting tool
10^{-6}	Injury	Window on a vacuum system
10^{-8}	Loss of life and significant expense	Ceramic protective tile on space shuttle

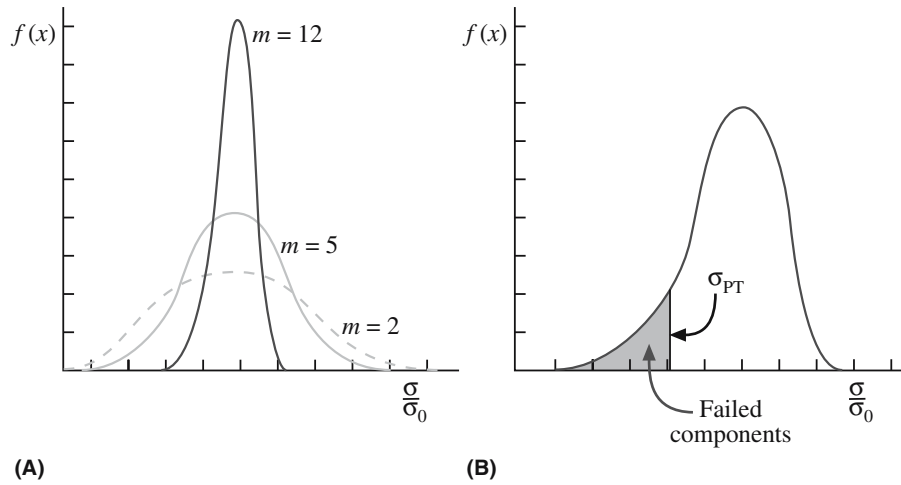


FIGURE 16.25 (a) Probability distributions for different values of m . (b) Proof testing up to σ_{PT} removes the weakest components from the distribution.

- There is a need to ensure that the conditions under which we are testing match those in service. For example, flaws in a component may appear during service as a result of oxidation or corrosion that might not be present in the test sample.
- There is a complex distribution of flaws.
- More than one type of flaw may be present.

16.15 SPT DIAGRAMS

Stress–probability–time (SPT) diagrams incorporate the time dependence of strength into failure statistics. They give lifetime predictions. An illustration of the use of SPT diagrams is in bioceramics.

An important requirement for any implant material is how long it will last. Because of the nature of failure of ceramic components it is not possible to provide a specific and definite lifetime for each individual implant. Rather we have to express failure in terms of probabilities. Figure 16.27 is an applied stress versus probability of time to failure (SPT) diagram for medical grade alumina. It shows that for a 30-year survival period with failure of no more than 1 in 100 components the maximum tensile stress that can be applied is limited to <200 MPa. If stresses of

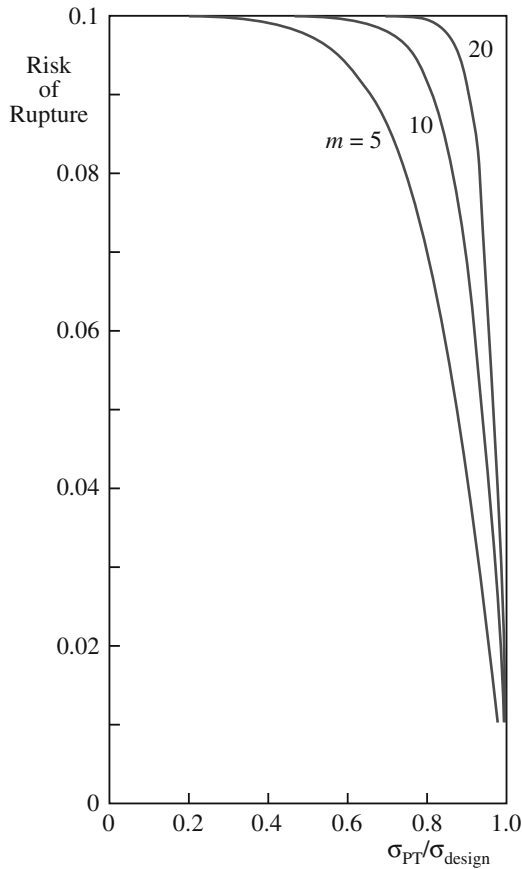


FIGURE 16.26 Plot showing the risk of rupture after proof testing to the ratio of proof-test stress to design stress.

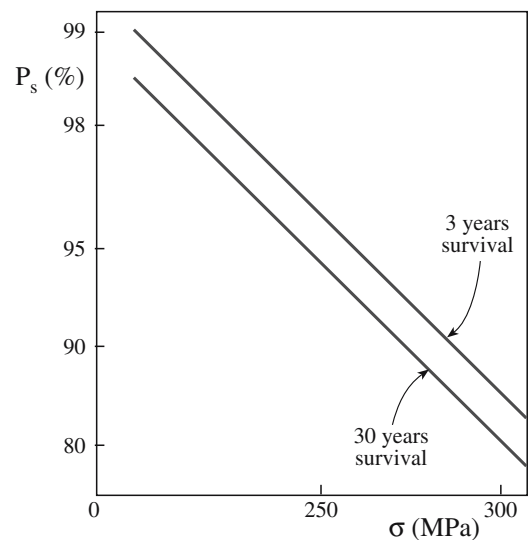


FIGURE 16.27 SPT diagram for medical grade Al_2O_3 . The survival probability decreases with increasing stress and longer times.

TABLE 16.11 Average Annual Wear Rates of Articulating Surfaces in Total Hip Prosthesis

Materials	Wear rate ($\mu\text{m}/\text{year}$)
Co–Cr–Mo alloy/UHMWPE	200
Alumina/UHMWPE	20–130
Alumina/alumina	2

250 MPa are applied to the ceramic component, within 3 years 4% of the implants is likely to fail and by 30 years 7% will probably fail. Use of SPT diagrams such as these, together with finite element analysis of local stress

distributions, makes it possible to design ceramic components that have very low probabilities of failure during the lifetime of the patient. Numerous clinical studies have been performed on patients receiving total hip replacement. One of the main problems that have been encountered is that of wear between the head (ball) and the socket. Although there is considerable variation in the data, it is generally found that the wear rate for systems with metal balls is much higher than the rate with alumina balls. And alumina balls in alumina sockets produce the least wear of any materials combination as indicated in Table 16.11.

CHAPTER SUMMARY

Flaws dominate the mechanical properties of ceramics. They determine how we test them and how we design components from them. Flaws are also the reason why ceramics are stronger in compression than tension. In this chapter we described the methods used to measure mechanical properties of ceramics. The important ones are bend testing, compression testing, and indentation. To determine the mechanical properties of small volumes we use nanoindentation. This technique is especially important for thin films, surfaces, and nanomaterials. An understanding of statistics is particularly important when using ceramics in load-bearing applications. The Weibull approach is the one most widely used for ceramics.

PEOPLE IN HISTORY

Mohs, Fredrich (1773–1839) was a German mineralogist. His original paper on the scratch test and the eponymous hardness scale was published in *Grundriss der Mineralogie* in 1822.

Poisson, Siméon Denis (1781–1840) was a French mathematician. He was more suited to mathematics than medicine because of his clumsiness. This was not an impediment for a mathematician! In 1837 he published a paper on probability, which described the Poisson distribution. During his career Poisson published more than 300 mathematical works and was reported to have said “Life is good for only two things, discovering mathematics and teaching mathematics.”

Ringer, Sidney (1835–1910) was a British physician and physiologist. His original salt solution was developed in 1882 and used to prolong the survival time of tissue taken from a frog’s heart. The solution used to test biomaterials differs in composition from that developed for amphibians.

Young, Thomas (1773–1829) was an English physician physicist. He could read fluently by age two and presented his first paper to the Royal Society at the young age of 20. By 1801 he was a professor at the Royal Institution in London. He was probably best known for his classic double slit experiment, which demonstrated the wave nature of light.

Weibull, E.H. Waloddi (1887–1979) was a Swedish engineer. The original paper describing his statistical analysis was published in 1939, “A Statistical Theory of the Strength of Materials,” *Ingeniörsvetenskapsakademiens Handlingar* **151**, 1–45. Weibull was a frequent visitor to Wright Patterson Air Force Base in Ohio and lectured at the Air Force Institute of Technology. In 1972 he was awarded the American Society of Mechanical Engineers gold medal for his achievements. King Carl Gustav XVI of Sweden presented Weibull with the Great Gold medal from the Royal Swedish Academy of Engineering Sciences in 1978.

GENERAL REFERENCES

Cook, R.F. and Pharr, G.M. (1994) “Mechanical properties of ceramics,” in *Materials Science and Technology*, edited by R.W. Cahn, P. Haasen, and E.J. Kramer, VCH, Weinheim, p. 339.

Davidge, R.W. (1979) *Mechanical Behavior of Ceramics*, Cambridge University Press, Cambridge, UK. A brief introduction.

Engineered Materials Handbook, Volume 4, *Ceramics and Glasses* (1991) ASM International (Materials Park, OH. A useful reference.

Fischer-Cripps, A.C. (2002) *Nanoindentation*, Springer, New York.

Gordon, J.E. (2002) *The New Science of Strong Materials, or Why You Don’t Fall Through the Floor*, 2nd edition, Penguin, London. An excellent introduction to mechanical properties of materials; the original was published in 1968.

- Green, D.J. (1998) *An Introduction to the Mechanical Properties of Ceramics*, Cambridge University Press, Cambridge, UK.
- Lawn, B. and Wilshaw, T.R. (1975) "Indentation fracture—principles and applications," *J. Mater. Sci.* **10**, 1049. The paper that showed how to derive K_{Ic} from indenter experiments.
- McColm, I.J. (1990) *Ceramic Hardness*, Plenum Press, New York.
- Munz, D. and Fett, T. (1999) *Ceramics: Mechanical Properties, Failure Behavior, Materials Selection*, Springer, Berlin.
- Richerson, D.W. (2006) *Modern Ceramic Engineering, Properties, Processing and Use in Design*, 3rd edition, Taylor & Francis, Boca Raton, FL. Chapter 18 describes design approaches for ceramics.
- Sines, G. and Adams, M. (1978) "Compression testing of ceramics," in *Fracture Mechanics of Ceramics*, Vol. 3, Plenum Press, New York, p. 403.
- Wachtman, J.B. (1996) *Mechanical Properties of Ceramics*, Wiley, New York.

SPECIFIC REFERENCES

- Blum, J.J. (1975) "Slice synthesis of three dimensional work-of-fracture specimens," *Eng. Fract. Mech.* **7**, 593. The slice model for determining Y^* , the geometric "constant" in K_{Ic} measurements (cf. Munz *et al.*).
- Hashin, Z. and Shtrikman, S. (1963) "A variational approach to the theory of the elastic behavior of multiphase materials," *J. Mech. Phys. Solids* **11**, 127.
- Lawn, B.R. and Marshall, D.B. (1979) "Hardness, toughness, and brittleness—indentation analysis," *J. Am. Ceram. Soc.* **62**, 347. Defines the brittleness index (BI).
- Munz, D.M., Shannon, J.L., and Bubsey, R.T. (1980) "Fracture-toughness calculation from maximum load in 4 point bend tests of chevron notch specimens," *Int. J. Fracture* **16**, R137. The straight-through crack assumption approach to determination of Y^* : the geometric "constant" in K_{Ic} measurements (cf. Blum *et al.*).
- Ridgeway, R.R., Ballard, A.H., and Bailey, B.L. (1933) *Trans Electrochem. Soc.* **63**, 267.
- Syed, S.A., Wahl, K.J., and Colton, R.J. (2000) "Quantitative study of nanoscale contact and pre-contact mechanics using force modulation," *Mat. Res. Soc. Symp. Proc.* **594**, 471. Developed the picoindenter—a combination of a nanoindenter and an AFM.
- Thoman, D.R., Bain, L.J., and Antle, C.E. (1969) "Inferences on the parameters of the Weibull distribution," *Technometrics* **11**, 445. Used numerical methods to determine m .
- Weibull, W. (1951) "A Statistical Distribution Function of Wide Applicability," *J. Appl. Mech.* **18**, 293.

WWW

- NIST Structural Ceramics Database
(<http://www.ceramics.nist.gov/srd/scd/scdquery.htm>)
- NIST Fracture Property Data Summaries: Oxide Glasses
(<http://www.ceramics.nist.gov/srd/summary/glsmain.htm>)
- NIST Fracture Toughness Data for Ceramics
(<http://www.ceramics.nist.gov/srd/summary/ftmain.htm>)
- NIST Property Data Summaries: Sintered Alumina
(<http://www.ceramics.nist.gov/srd/summary/scdaos.htm>)
- NIST Property Data Summaries: Silicon Carbide
(<http://www.ceramics.nist.gov/srd/summary/scdscs.htm>)

EXERCISES

- 16.1 In Figure 16.7 the experimental data for the unstabilized samples deviate from the predicted values for Young's modulus. (a) What do we mean by "unstabilized." (b) How can you account for the difference in the predicted values and experimental values?
- 16.2 Is Young's modulus affected more by the presence of an intergranular glass phase or an equal amount of porosity? Justify your answer with a suitable calculation.
- 16.3 Ten rectangular test specimens of MgO were tested in three-point bending. The bars were 1 cm wide and 0.5 cm high and were tested over a 5-cm span. The failure loads for each are given in ascending order: 140, 151, 154, 155, 158, 165, 167, 170, 173, and 180 kg. Calculate the MOR for each sample and the average MOR for this group of samples.
- 16.4 A commercially available polycrystalline alumina is tested using three different methods: three-point bend, four-point bend, and uniaxial tension. The resulting MOR values are 550, 410, and 175 MPa, respectively. What conclusions can you make about the material from these data?
- 16.5 The soda-lime silicate glass sample shown in Figure 16.17 was indented with a load of 20 N. Estimate (a) hardness and (b) fracture toughness. (c) How else might you obtain the fracture toughness?

- 16.6 For the data shown in Figure 16.20 determine the Weibull modulus.
- 16.7 The following data were obtained in a series of tensile strength tests on polycrystalline silicon carbide specimens (in MPa): 334, 289, 232, 294, 252, 337, 256, 339, 308, 365, 311, 341, 286, 314, 274, 285, 382, 379, 282, 324, 316. (a) Determine the Weibull modulus for these samples. (b) Would you expect the value of m for a set of steel specimens to be higher or lower than the value you calculated in part (a). Assuming that these SiC specimens were made by hot pressing, would you expect m for a series of SiC made by sintering to be higher or lower?
- 16.8 Calculate using the Voight and Reuss models the bounds for Young's modulus of MgO–Al₂O₃ composites as a function of volume fraction.
- 16.9 Explain briefly why there is a size dependence for the strength of ceramics but not for metals.
- 16.10 Sketch stress–strain plots for polycrystalline MgO at (a) 25°C, (b) 1000°C, (c) 1700°C, and (d) 2800°C.

Deforming: Plasticity

CHAPTER PREVIEW

In this chapter we are concerned with the deformation of ceramics leading to a permanent shape change. This is known as plastic deformation and is both nonrecoverable and irreversible. There are several mechanisms that are responsible for plastic deformation in crystalline materials: dislocation motion, vacancy motion, twinning, and phase transformation. In metals at room temperature dislocation motion is the most important of these mechanisms. In Chapter 12 we already noted that dislocations do not move easily in ceramics and this is the reason for their inherent brittleness. Nevertheless, dislocation motion is observed in ceramics under specific loading conditions. In general, plastic deformation of ceramics requires high temperatures and this is important because

- We often process ceramics at high temperature.
- Many potential applications for ceramics, such as in fuel cells and engines, require them to be stable at high temperature.

We know that glass flows and that we can produce complex shape changes in glass. There are no dislocations in glass so how does plastic deformation occur? And does the plastic deformation of glass always require a high temperature?

Selecting ceramics for use at high temperatures or under applied load requires consideration of their long-term stability. Time dependent deformation is known as creep, and creep resistance is a critical design parameter. Even if creep does not lead to failure, a change in shape or size may render a component useless. The mechanism responsible for creep depends on temperature, stress, and the microstructure of the ceramic.

17.1 PLASTIC DEFORMATION

The onset and extent of plastic deformation are often measured when the σ - ϵ behavior of a material is being determined. We showed some general σ - ϵ curves in Chapter 16. In Figure 17.1 σ - ϵ curves obtained for crystals of KBr and MgO tested in bending are shown. From these curves we can identify several parameters that may already be familiar to you from the discussion of the mechanical properties of metals.

The proportional limit P corresponds to departure from linearity and is defined as the onset of plastic deformation. If the transition from elastic to plastic deformation is gradual it may be difficult to determine precisely where P is and sometimes it is better avoided.

The yield strength σ_y is the stress determined by drawing a line parallel to the linear part of the σ - ϵ curve at some specified strain offset. We usually use a strain of 0.002. To compare the values of σ_y in Figure 17.1 you may

recall that for metals we see a wide range of values, e.g., for a low-strength aluminum alloy $\sigma_y = 35$ MPa and for a high-strength steel $\sigma_y > 1400$ MPa. We usually say yield strength rather than yield stress. Strength is a material property; stress is a measure of the applied load.

Fracture strength, σ_F , is the stress at a fracture. Because ceramics are often tested in bending we do not see any reduction in cross-sectional area during the test as we often see in a tensile test with a metal. As a result we would not expect to see a maximum in the σ - ϵ curve corresponding to the tensile strength or ultimate tensile strength.

Figure 17.2 shows a σ - ϵ curve for LiF that illustrates an abrupt elastic-plastic transition. Plastic deformation begins at the upper yield point and there is a decrease in stress. At the lower yield point deformation continues at lower stress levels. This type of behavior is similar to that of some low-carbon steels as well as aluminum oxide and magnesium oxide at high temperatures.

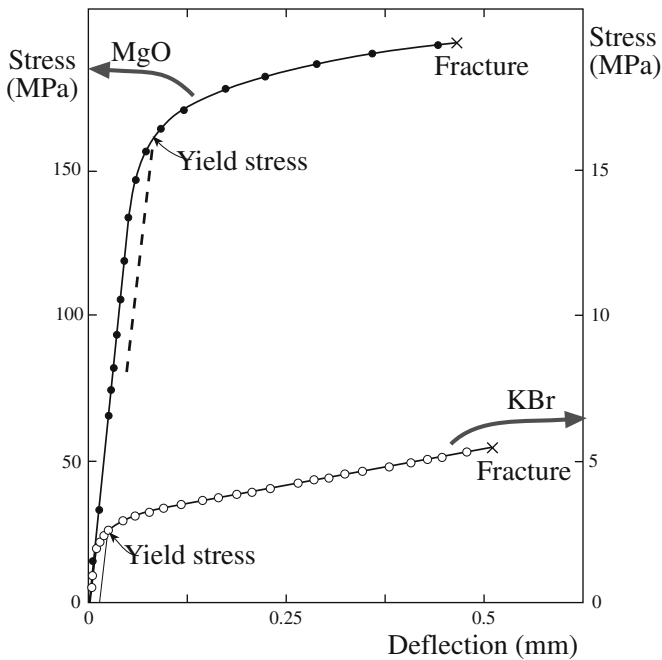


FIGURE 17.1 Stress–strain curves for KBr and MgO crystals tested in bending.

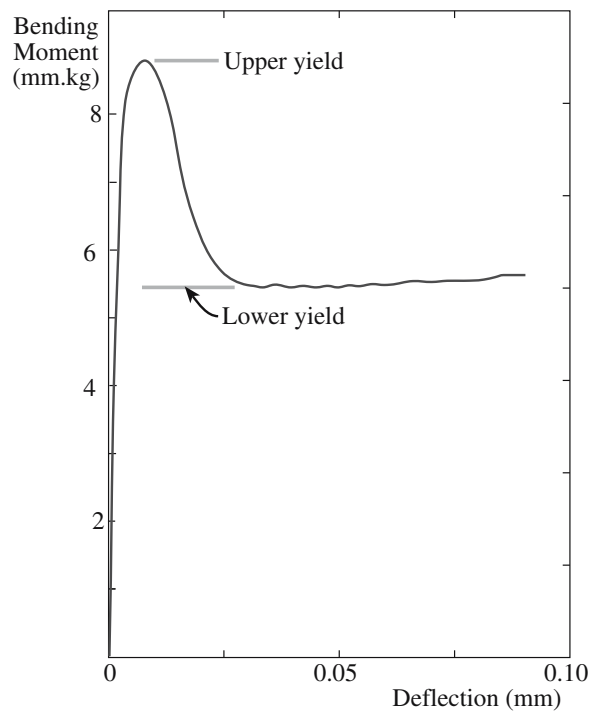


FIGURE 17.2 Stress–strain curve for a LiF single crystal.

17.2 DISLOCATION GLIDE

Dislocation glide (or slip) is a primary mechanism for plastic deformation in crystals. Slip takes place discontinuously in bands as illustrated in Figure 17.3. Although we often think of dislocations in ceramics as immobile, they can glide as shown in Figure 17.4a. In this case a crystal of LiF has been plastically bent and the dislocations revealed by etching. Figure 17.4b is a dark-field transmission electron microscopic (TEM) image that shows a glide band in spinel. The dislocations are visible in the dark-field image as bright lines against a dark background.

Both the direction of slip and usually the slip plane have a definite crystallographic orientation, which together are known

as a slip system. Slip systems for several ceramics are given in Table 17.1. Primary slip systems are those for which slip is easiest; it is more difficult on secondary slip systems and these are usually activated at higher temperature. What determines the slip system for ceramics?

The slip direction is usually the direction having the smallest spacing between atoms or ions of the same type (the highest linear density). In metals, the slip plane is often the closest packed plane (the highest planar density). In ceramics, we consider planar density, but there is often

SLIP SYSTEM

A slip system is a plane and a direction and is represented as $\{hkl\}\langle uvw\rangle$.

the additional consideration of electrostatic interaction between ions. We can illustrate these considerations by looking at the familiar rocksalt structure (structure of NaCl and MgO). This is an interesting example to choose to start with because the first studies of crystal plasticity, which were conducted by Reusch in 1867, were conducted using sodium chloride. He concluded that the slip system for NaCl is $\{110\}\langle 1\bar{1}0\rangle$.

The choice of slip plane has often been explained by considering the position of ions during slip. Figure 17.5 compares the ion positions during slip on $\{100\}$ and $\{110\}$. The key difference is that slip on $\{100\}$ would increase

the distance between opposite ions. However, during slip on $\{110\}$ oppositely charged ions are brought closer together. The overall effect is that slip on $\{110\}$

would lead to a decrease in the electrostatic interaction energy. Clearly this is not the complete story as we mentioned in Section 12.5. Not all crystals with a rocksalt structure share the same slip system as shown in Table 17.2. The primary glide plane depends on the atoms present. For PbS and PbTe the primary glide plane is $\{100\}$ not $\{110\}$. The explanation proposed back in 1930 by Buerger is based on the polarizability or “deformability” of the ions. As the sum of the polarizability of both ions increases there is increasing ease of slip on $\{100\}$ and increasing plasticity.

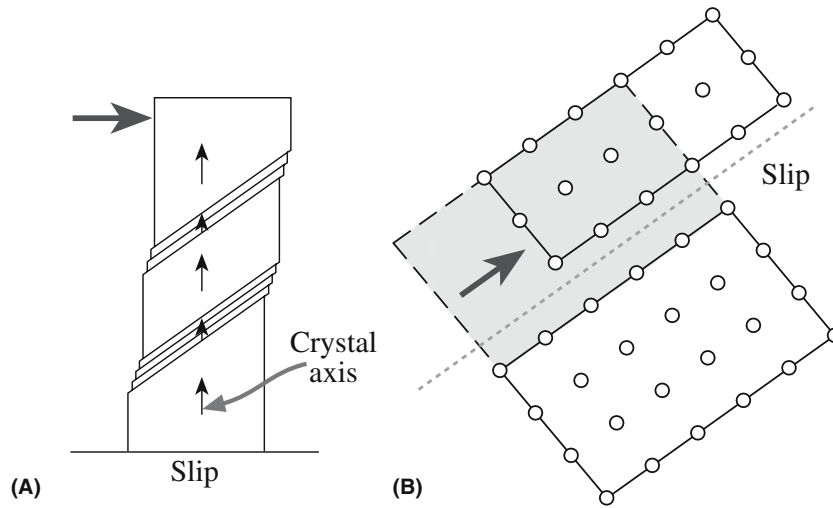
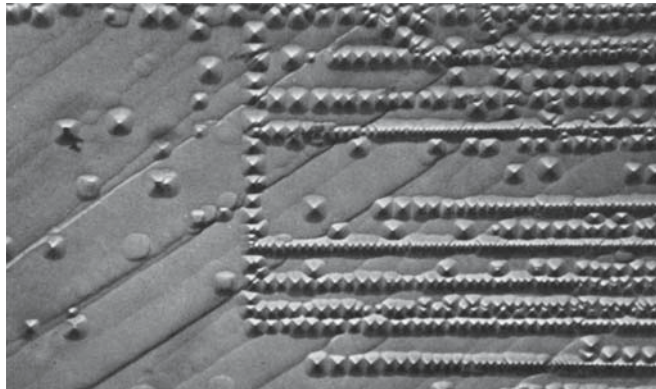
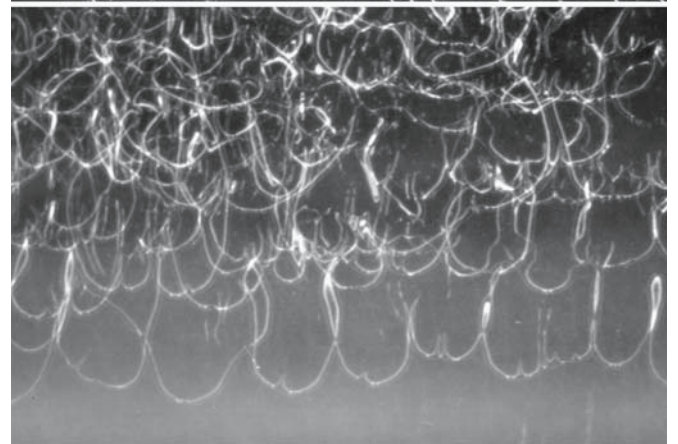
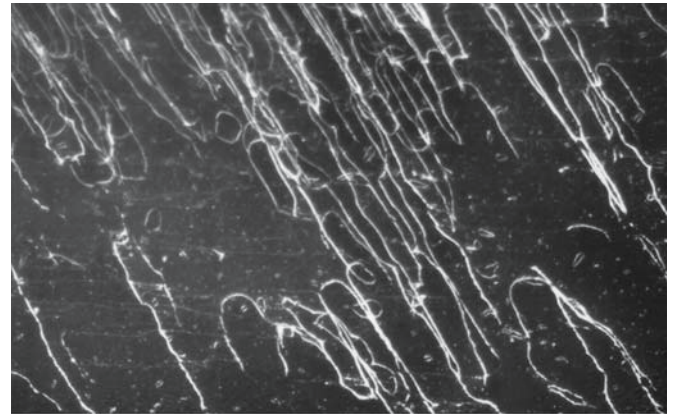


FIGURE 17.3 Illustration of slip bands: (a) macroscopic appearance; (b) showing atomic movements.



(A)



(B)

FIGURE 17.4 (a) Glide bands in LiF revealed by etching. (b) "Glide" bands in spinel: (top) 200°C; (bottom) 950°C.

TABLE 17.1 Slip Systems for Several Ceramics

Material	Crystal structure	Slip systems		Activation temperature (°C)	
		Primary	Secondary	Primary	Secondary
Al ₂ O ₃	Hexagonal	{0001}<11 $\bar{2}$ 0>	Several	1200	
BeO	Hexagonal	{0001}<11 $\bar{2}$ 0>	Several	1000	
MgO	Cubic (NaCl)	{110}<1 $\bar{1}$ 0>	{001}<110>	0	1700
MgO·Al ₂ O ₃	Cubic (spinel)	{111}<1 $\bar{1}$ 0>	{110}<1 $\bar{1}$ 0>	1650	
β -SiC	Cubic (ZnS)	{111}<1 $\bar{1}$ 0>		>2000	
β -Si ₃ N ₄	Hexagonal	{10 $\bar{1}$ 0}<0001>		>1800	
TiC, (ZrC, HfC, etc.)	Cubic (NaCl)	{111}<1 $\bar{1}$ 0>	{110}<1 $\bar{1}$ 0>	900	
UO ₂ , (ThO ₂)	Cubic (CaF ₂)	{001}<110>	{110}<1 $\bar{1}$ 0>	700	1200
ZrB ₂ (TiB ₂)	Hexagonal	{0001}<11 $\bar{2}$ 0>		2100	
C (diamond)	Cubic	{111}<1 $\bar{1}$ 0>			
C (graphite)	Hexagonal	{0001}<11 $\bar{2}$ 0>			
β -SiO ₂	Hexagonal	{0001}<11 $\bar{2}$ 0>			
CaF ₂ (BaF ₂ , etc.)	Cubic	{001}<110>			
CsBr	Cubic (CsCl)	{110}<001>			
TiO ₂	Tetragonal	{110}<1 $\bar{1}$ 0>	{110}<001>		
WC	Hexagonal	{10 $\bar{1}$ 0}<0001>	{10 $\bar{1}$ 0}<11 $\bar{2}$ 0>		

17.3 SLIP IN ALUMINA

The slip system for α -alumina (corundum) is given in Table 17.1. The primary slip plane is the basal plane, (0001); the slip direction is <11 $\bar{2}$ 0>. The arrangement of atoms on the slip plane was shown in Figure 12.12. For

the oxygen ions the close-packed direction is actually <1 $\bar{1}$ 00>; this is not the slip direction because we need to consider what happens to the aluminum ions, which occupy only two-thirds of the octahedral interstices. Slip along <11 $\bar{2}$ 0> preserves the stacking sequence of the aluminum ions. Temperatures around 1300°C are needed before significant plastic deformation is observed in single-crystal alumina. At even higher temperatures other slip systems become activated as summarized in Table 17.3.

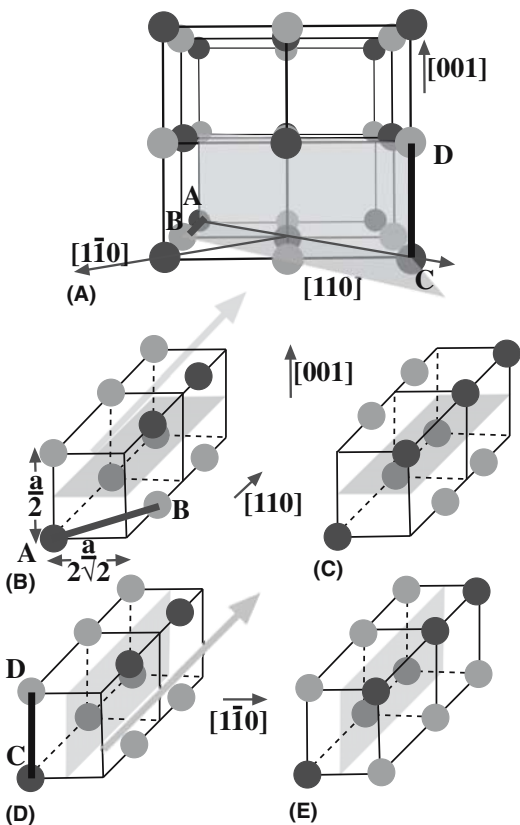


FIGURE 17.5 (a–e) Schematic comparing slip in the rocksalt structure on {100} and {110} planes.

TABLE 17.2 Comparison of Primary Glide Planes in Crystals Having a Rocksalt Structure

Crystal	Primary glide plane	Polarizability (10 ⁻³⁰ /m ³)			Lattice constant (nm)
		Anion	Cation	Total	
LiF	{110}	0.03	1.0	1.03	0.401
MgO	{110}	0.09	3.1	3.19	0.420
NaCl	{110}	0.18	3.7	3.88	0.563
PbS	{100}	3.1	10.2	13.3	0.597
PbTe	{100}	3.1	14.0	17.1	0.634

TABLE 17.3 Slip Systems in α -Alumina (Corundum)

System name	Slip system	Remarks
Basal	(0001)1/3<2 $\bar{1}$ 10>	Dominant system under shear superimposed on 1-atm pressure
Prismatic	{1 $\bar{2}$ 10}<10 $\bar{1}$ 0> {1 $\bar{2}$ 10}<10 $\bar{1}$ 1>	Occurs above 1600°C under shear superimposed on 1-atm pressure
Pyramidal	{1 $\bar{1}$ 02}<01 $\bar{1}$ 1> {10 $\bar{1}$ 1}<01 $\bar{1}$ 1>	Occurs above 1600°C under shear superimposed on 1-atm pressure

Because of the large Burgers vector involved the combined motion of partial dislocations may lead to slip. The background to this argument was presented in Chapter 12. Graphite is another hexagonal ceramic in which slip has been found to occur by the motion of partial dislocations.

17.4 PLASTIC DEFORMATION IN SINGLE CRYSTALS

There are many mechanisms that can lead to plastic deformation in single crystals, but the most important is slip. The two things that we need to consider are the inherent resistance to the movement of dislocations provided by the periodicity of the lattice and the orientation of the crystal with respect to the applied stress.

Lattice Resistance

The stress, τ_f , needed to move a dislocation along the slip plane is known as the Peirels–Nabarro (or frictional) stress and is given by

$$\tau_f = \mu \exp\left(-\frac{2\pi w}{b}\right) \quad (17.1)$$

The stress, which is clearly a function of the crystal structure and bonding, depends on b and w . You will recall from Chapter 12 that dislocation widths in covalent solids are quite narrow ($w \sim b$) compared with those in face-centered cubic (fcc) metals ($w \sim 10b$).

- For metals $\tau_f \sim 10 \text{ MPa} \sim 10^{-4} \mu$, these stresses are fairly small and dislocations can move freely. The yield stress is determined primarily by interactions between dislocations and other defects such as impurities.
- For simple ionic ceramics (e.g., NaCl and CaF₂) $\tau_f \sim 10\text{--}100 \text{ MPa} \sim 10^{-4} \mu\text{--}10^{-3} \mu$.
- For complex ionic (e.g., Al₂O₃) and covalent ceramics (e.g., SiC) $\tau_f \sim 1000 \text{ MPa} \sim 10^{-2} \mu$. Dislocations have low mobility and lattice resistance is the main obstacle.

Orientation

Plastic deformation depends not only on how easy it is for the dislocations to glide on their slip plane but also the orientation of the slip plane and the slip direction with the applied stress. If we consider a single crystal subject to uniaxial tension as illustrated in Figure 17.6 the shear stress, τ_r , acting on the slip plane in the slip direction is

$$\tau_r = \sigma \cos \phi \cos \psi \quad (17.2)$$

For some structures it is possible to orient the crystal so that τ_r on all operative slip systems is zero. If this is the

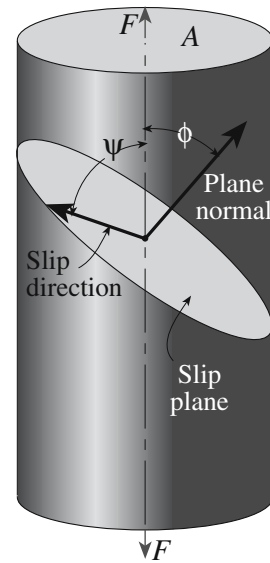


FIGURE 17.6 Geometry used to determine the critical resolved shear stress.

case, dislocation motion does not occur and the crystal will not plastically deform at stresses below the theoretical lattice strength. For example, in MgO τ_r is zero when σ is applied along $\langle 111 \rangle$. Under these loading conditions at elevated temperatures ($>300^\circ\text{C}$) slip may occur on the secondary slip system: $\{001\}\langle 110 \rangle$.

The critical resolved shear stress, τ_{crss} , is the minimum shear stress required to initiate slip for a particular slip system defined when $\sigma = \sigma_y$:

$$\tau_{\text{crss}} = \sigma_y (\cos \phi \cos \psi) \quad (17.3)$$

Figure 17.7a shows the stress–strain behavior for a single crystal that is favorably oriented for plastic flow. This type of behavior is seen in MgO and other ceramics with a rocksalt structure. There are three distinct stages:

- Stage I: Easy glide of dislocations with the possibility of large strains ($\sim 20\%$)
- Stage II: Interaction of dislocations on intersecting slip planes resulting in work hardening
- Stage III: Cross-slip

The value of τ_{crss} depends on test conditions such as temperature and strain rate as shown schematically in Figure 17.7b. We can again identify three distinct behaviors:

- Region I: τ_{crss} decreases with increasing temperature and decreasing strain rate. Thermal fluctuations enhance dislocation motion.

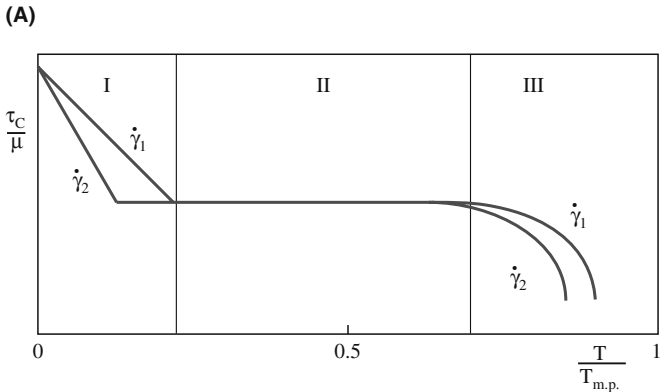
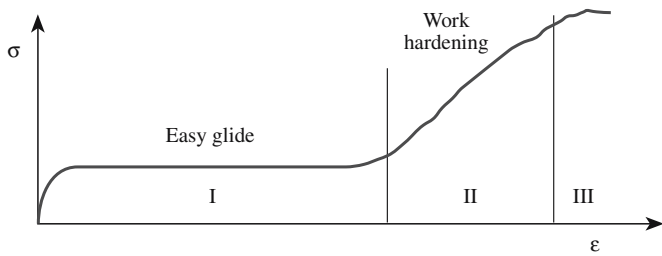


FIGURE 17.7 (a) Stress–strain curve for a crystal suitably oriented for plastic flow. (b) Temperature dependence of the normalized critical resolved shear stress for two strain rates, where $\dot{\gamma}_1 > \dot{\gamma}_2$.

- Region II: τ_{crss} is independent of temperature and strain rate. There is interaction between dislocations and between dislocations and other defects.
- Region III: τ_{crss} again decreases with increasing temperature and decreasing strain rate. At high temperatures diffusion processes can become important.

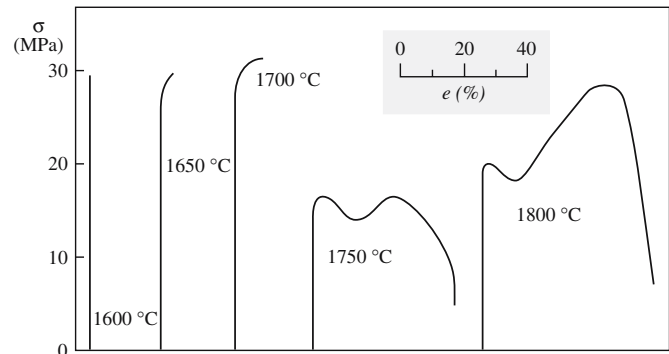


FIGURE 17.8 Stress–strain curves for polycrystalline MgO as a function of temperature.

17.5 PLASTIC DEFORMATION IN POLYCRYSTALS

Plastic deformation is more difficult in polycrystals than in single crystals because now we have to consider what happens at the grain boundaries. Grain boundaries act as barriers to dislocation motion and if adjacent grains are not favorably oriented for slip to continue, dislocations will pile up at the boundary.

A polycrystal needs five independent slip systems before it can undergo an arbitrary strain. This requirement is known as the von Mises criterion. A slip system is independent if the same strain cannot be produced from a combination of slip on other systems. From Table 17.4 you can see why MgO might be ductile when stressed as a single crystal but in polycrystalline form it is brittle except at high temperature where secondary slip systems operate. For polycrystalline MgO the brittle-to-ductile transition occurs at $\sim 1700^\circ\text{C}$ as shown in Figure 17.8.

TABLE 17.4 Independent Slip Systems for Some Ceramics

Lattice type	Crystal	Slip system	Number of independent systems
Rocksalt	MgO, NaCl, LiF, NaF	{110}<1 $\bar{1}$ 0>	2
Rocksalt	MgO, NaCl, LiF, NaF	{110}<1 $\bar{1}$ 0> {001}<1 $\bar{1}$ 0> {111}<1 $\bar{1}$ 0>	5 at high temperature
Fluorite	UO ₂ and CaF ₂	{001}<1 $\bar{1}$ 0>	3
	TiC and UC	{111}<1 $\bar{1}$ 0>	5
Spinel	MgAl ₂ O ₄	{111}<1 $\bar{1}$ 0>	5
Fluorite	UO ₂ and CaF ₂	{110}<1 $\bar{1}$ 0> {001}<1 $\bar{1}$ 0> {110}<1 $\bar{1}$ 0> {111}<1 $\bar{1}$ 0>	5 at high temperatures
Hexagonal	Al ₂ O ₃ , C (graphite), BeO	{0001}<11 $\bar{2}$ 0>	2
Hexagonal	Al ₂ O ₃ , C (graphite), BeO	{0001}<11 $\bar{2}$ 0> {1 $\bar{2}$ 10}<10 $\bar{1}$ 0> {1 $\bar{2}$ 10}<10 $\bar{1}$ 1> {1 $\bar{1}$ 02}<01 $\bar{1}$ 1> {10 $\bar{1}$ 1}<01 $\bar{1}$ 1>	5 at high temperatures
Sphalerite	ZnS, β -SiC	(111)<1 $\bar{1}$ 0>	5

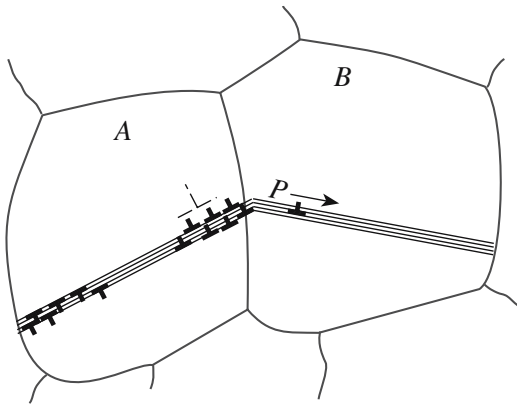


FIGURE 17.9 Illustration of slip propagation from grain A to grain B.

Some cubic materials, e.g., TiC and $MgAl_2O_4$, do have enough independent slip systems, but the Peierls–Nabarro stress is high making dislocations immobile except at high temperature.

The Hall–Petch relation (Eq. 14.8) indicates the effect of grain size, d , on the stress required to make the dislocation move in a polycrystalline sample. The origin of the relation is that the stress to operate a Frank–Read source increases as the size of the source decreases. If the grain size decreases, then the maximum size of the Frank–Read source also decreases. The result is the famous $d^{1/2}$ relationship.

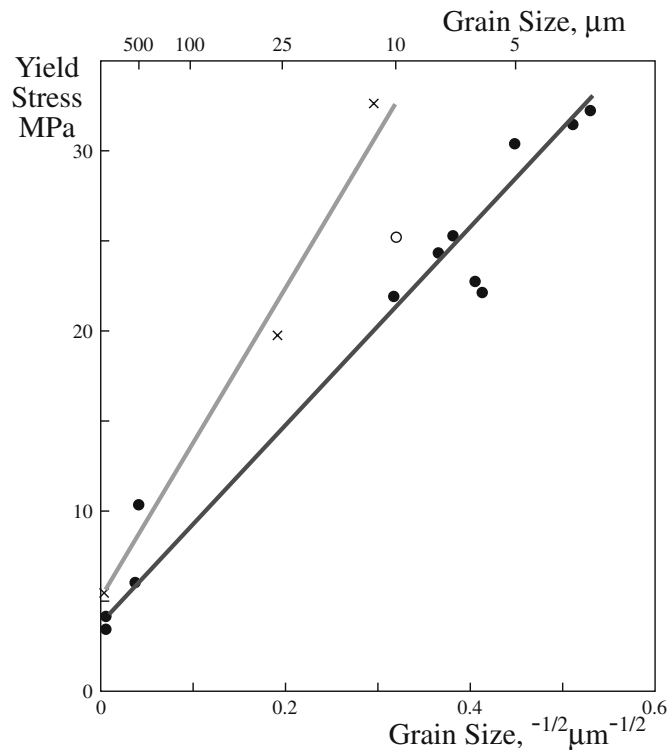


FIGURE 17.10 Grain size dependence of yield strength for KCl. The solid circles are for pure material with a $\langle 100 \rangle$ texture; the open circles are for pure material with a $\langle 111 \rangle$ texture. The crosses are for Sr-doped KCl.

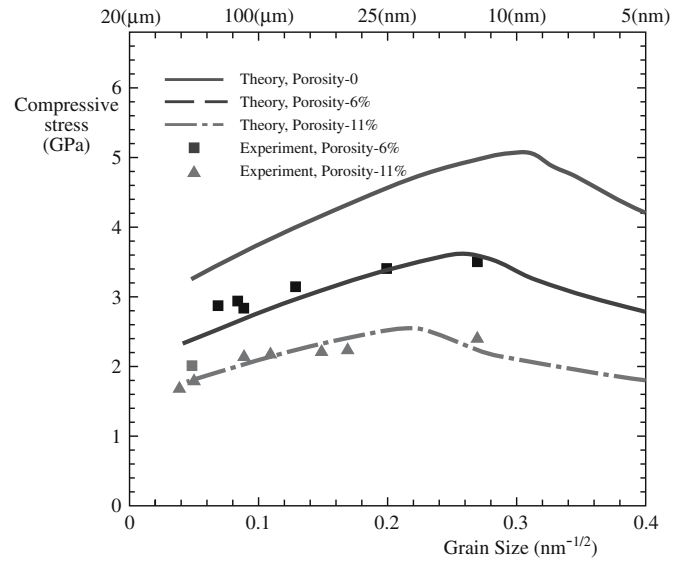


FIGURE 17.11 Compressive yield stress as a function of grain size for nanocrystalline TiO_2 at three levels of porosity.

So the grain size of a polycrystalline ceramic is important in determining the yield strength and the fracture strength of ceramics. Figure 17.9 illustrates the background to Eq. 14.8. Slip starts in the most favorably oriented grains. If the material is to plastically deform then slip must propagate from one grain to the next. Stress concentrations are built up at the grain boundary at P and these are greater when the length of the slip band, or the grain size, is large. For deformation to continue the stress must be sufficient to start dislocation motion in an adjacent grain, which will be easier for large grained samples. The increase in strength of polycrystalline KCl as the grain size decreases (an illustration of the Hall–Petch phenomenon) is shown in Figure 17.10.

In some cases the Hall–Petch equation appears to hold when the grain size is on the order of several nanometers. In these cases deformation cannot be due to dislocation glide and perhaps Eq. 14.8 is best thought of as a scaling law. Figure 17.11 shows a Hall–Petch plot for TiO_2 over a wide range of grain sizes. At the very smallest grain sizes studied the behavior is inverse or negative Hall–Petch. The reasons for this transition are not well understood and the transition does not appear to occur for all nanomaterials.

17.6 DISLOCATION VELOCITY AND PINNING

Figure 17.12 shows the stress dependence of dislocation velocity for CaF_2 . At low stresses the relationship has the form

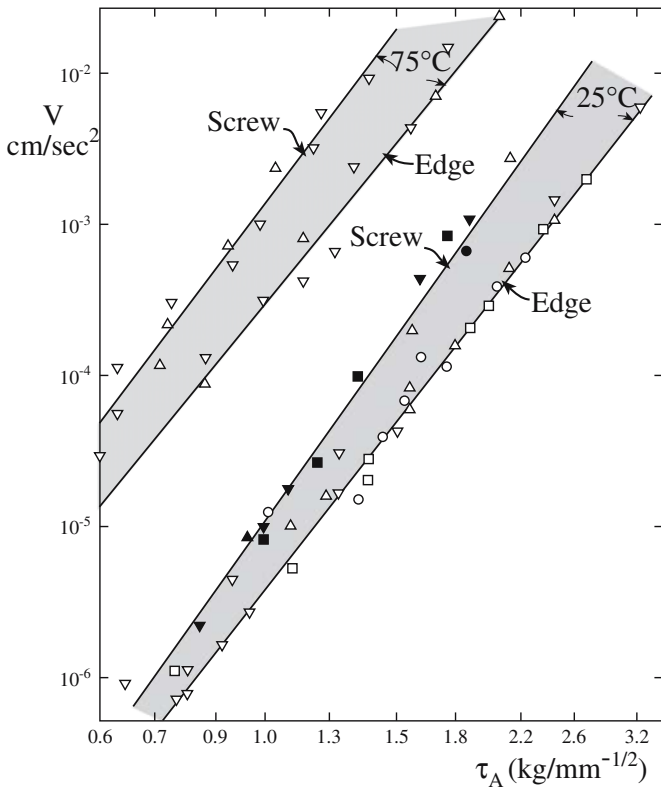


FIGURE 17.12 The stress dependence of dislocation velocity.

$$v = \left(\frac{\tau}{\tau_0} \right)^p \quad (17.4)$$

Both τ_0 and p are material constants: τ_0 is the shear stress for unit dislocation velocity and p is the velocity stress exponent that describes the stress dependence of the dislocation velocity. Values are given for some materials in Table 17.5. At very high stresses Eq. 17.4 does not hold, as the maximum dislocation velocity in a crystal equals the velocity of sound. Determination of dislocation velo-

TABLE 17.5 Values of the Constants in Eq. 17.4 for Some Materials (RT Except for Ge)		
Material	τ_0 (MPa)	p
Zn	0.03	1
Cu	0.03	1
Mo	64.8	7
Nb	48.3	16
Fe+3%Si	193.1	30
NaCl	1.45	8
LiF	11.7	25
Ge (440°C)	965 GPa	1

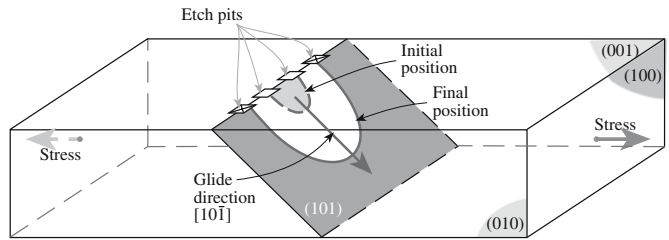
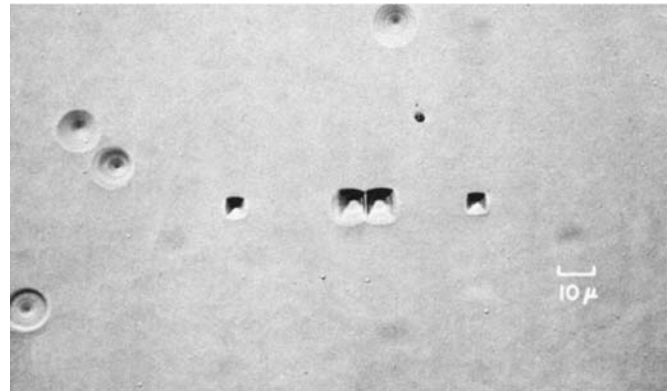


FIGURE 17.13 Etch pits showing the motion of a dislocation loop in single-crystal LiF.

city has been done using the etch-pit technique as illustrated in Figure 17.13 for LiF.

Dislocations in ceramics can be pinned by solute atoms just as they can in metals as shown in Figure 17.14. The dislocations are impeded because of their interaction with the stress field around the impurity. This effect has long been used to strengthen metals.

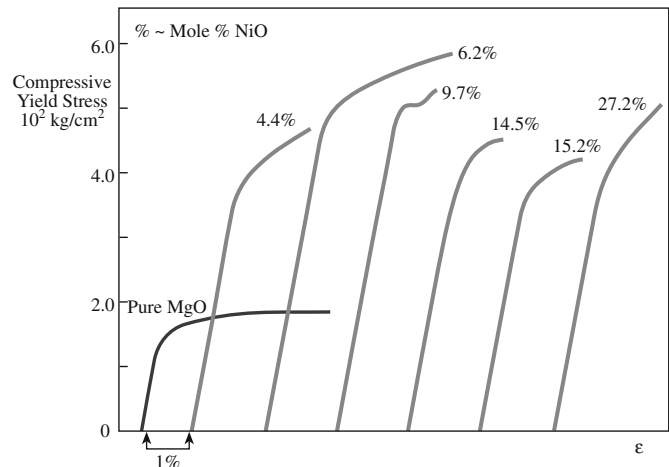


FIGURE 17.14 Illustration of solute hardening in MgO.

17.7 CREEP

Creep is time-dependent permanent deformation that is often due to diffusion processes rather than dislocation motion. Engineers need to consider creep in cases in which ceramic components will be used in load-bearing applications at high temperature. It is necessary to specify a particular maximum strain that is acceptable during the anticipated lifetime of the component.

In general, creep behavior of ceramics is similar to that of metals. However, in ceramics it usually occurs at higher temperatures, typically $>0.5 T_m$. In comparison, creep is a consideration in aluminum alloys at 100°C and in polymers at room temperature. Creep is particularly important in ice, which creeps extensively at low temperatures. The creep of ice is responsible for the movement of glaciers and the spreading of the Antarctic ice cap.

Figure 17.15 shows a general creep curve. There are three regimes:

- Transient or primary creep: Following a spontaneous elastic strain the creep rate (also referred to as the creep strain rate) decreases with time from an initially high value. This stage of creep is often represented by an equation of the form

$$\epsilon = \beta T^m \quad (17.5)$$

β is a constant and m varies from 0.03 to 1.0 depending on the material, stress, and temperature. In some ceramics (e.g., SiC fibers) this may be the only stage shown.

- Steady-state or secondary creep: Strain increases linearly with time, the creep rate is constant, and deformation may continue for a long time. This is the most important regime. The equation for secondary creep is

$$\epsilon = Kt \quad (17.6)$$

K is a constant that depends on stress and temperature. The mechanisms for this stage are discussed in the next sections.

- Tertiary creep: a rapid increase in creep rate just before failure. This stage is often missing for ceramics.

The creep behavior of a ceramic is determined by measuring the strain rate as a function of load. In the

STRAIN AND CREEP
Elastic strain: $\epsilon_0 = \sigma/E$ Creep rate: $\dot{\epsilon}_c = d\epsilon_c/dt$ ϵ_c is the creep strain.

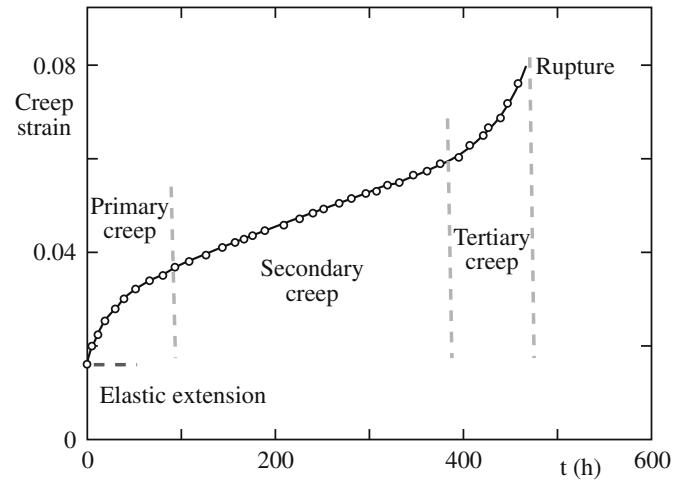


FIGURE 17.15 Creep curve illustrating three distinct regimes.

simplest approach a load is attached to the sample, which is heated, and the deformation is measured as a function of time. Because of the problems we mentioned earlier in performing tensile tests on ceramics the load is usually applied by bending. The disadvantage of bending tests is the inhomogeneous stress state that changes during creep deformation. The creep behavior of ceramics is different if the load is applied in tension or compression and compressive creep tests may, although rarely, be performed.

There are three mechanisms for creep and we will describe each of these in the following sections.

17.8 DISLOCATION CREEP

In this mechanism creep occurs by dislocation motion, i.e., glide and climb. For the climb-controlled process the creep rate can be expressed as

$$\dot{\epsilon} = \frac{\alpha D_L \mu b}{kT} \left(\frac{\sigma}{\mu} \right)^n \quad (17.7)$$

which we can simplify by taking all of the “constants” into a temperature-dependant constant Γ :

$$\dot{\epsilon} = \Gamma \sigma^n \quad (17.8)$$

This is a simple power law equation and when $n > 1$ we refer to it as power law creep. For climb n is in the range 4–5; for a glide-controlled process $n = 3$.

17.9 DIFFUSION-CONTROLLED CREEP

In this mechanism creep is due to atomic diffusion. There is no dislocation motion. If we consider the single crystal shown in Figure 17.16 Nabarro (1948) showed that vacancies would move from the faces under tension to those under compression. There will be a counter-flow of atoms and we obtain a permanent shape change as a result.

For Nabarro–Herring creep the creep rate is given by

$$\dot{\epsilon} = \frac{\alpha D_L \sigma \Omega}{d^2 kT} \quad (17.9)$$

In this case the constant, α , depends on the extent of grain-boundary sliding as determined by Herring (1950). For simple tension test measurements under steady-state conditions $\alpha = 13.3$.

We assume the following:

- The main source and sink for vacancies are grain boundaries.
- We are in equilibrium.
- There is no cavitation.

The following important points apply to Nabarro–Herring creep:

- The temperature has to be high enough to allow significant vacancy diffusion.
- Diffusion is considered to occur through the bulk of the material.

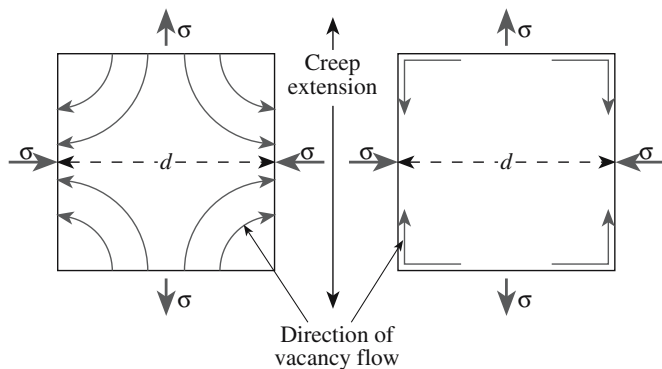


FIGURE 17.16 Illustration of Nabarro–Herring creep.

TERMS IN CREEP EQUATIONS

α	a constant
D_L	lattice diffusivity
k	Boltzmann's constant
b	Burgers vector
T	absolute temperature
σ	applied stress
μ	shear modulus
m	grain size exponent
n	stress exponent
ϕ	atomic volume
d	grain size
D_{gb}	grain boundary diffusivity
δ	grain boundary width
A	dimensionless constant
D	diffusion coefficient

- Because of the d^{-2} dependence the creep rate will increase with decreasing grain size (shorter diffusion distance).
- The creep rate is proportional to the applied stress (at least for lower stresses).
- There is a linear dependence between strain rate and stress.

At lower temperatures and for fine-grained ceramics grain boundary diffusion may be the dominant path. In these situations

the process is termed Coble creep (Coble, 1963) and the creep rate is

$$\dot{\epsilon} = \frac{150\Omega\delta D_{gb}\sigma}{\pi d^3 kT} \quad (17.10)$$

The important points to note from Eq. 17.10 are that

- Creep rate varies as d^{-3} ; hence it is important for very fine-grained ceramics.
- $D_{gb} > D_L$, so Coble creep is favored at lower temperatures.

Nabarro–Herring and Coble creep can take place in parallel so that actual creep rates will involve both components and both diffusion coefficients. In ceramics we also have a situation in which both anions and cations are diffusing adding further complications to the creep rate equations. If there is a large difference in the diffusion rates then the creep rate is controlled by the slower diffusing species along the faster diffusing path.

17.10 GRAIN-BOUNDARY SLIDING

Some ceramics have an intergranular film (IGF) formed during fabrication, often due to the addition of a sintering aid. If this phase softens at high temperature then we get creep by grain-boundary sliding. The glass viscosity, η , which is a function of temperature, controls the creep rate. As the temperature increases the viscosity decreases, and this is usually represented by an empirical relation known as the Vogel–Fulcher–Tammann (VFT) equation or sometimes simply the Fulcher equation:

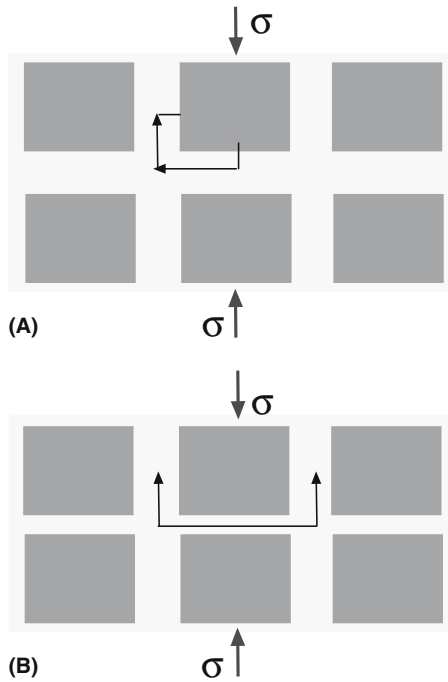


FIGURE 17.17 Illustration of the dissolution–precipitation mechanism that could be operative in ceramics containing a glassy phase at the GB.

$$\ln \eta = A + \frac{B}{T - T_0} \quad (17.11)$$

A , B , and T_0 are constants for a particular glass. The VFT equation works very well except at temperatures close to the glass transition temperature, T_g .

There are several mechanisms that can result in a permanent change in shape. In one mechanism the glass is squeezed out of the boundaries during compression flowing to those under tension. Proof of this mechanism comes from high-resolution TEM, which can be used to directly measure the thickness, w , of the IGF. In these cases

$$\dot{\epsilon} = \frac{\alpha \omega^3 \sigma}{\eta_0 d^3} \quad (17.12)$$

Another proposed mechanism is that of dissolution and reprecipitation, which is illustrated in Figure 17.17. Here grains dissolve in the liquid at points of high stress, and this solute then diffuses through the liquid and precipitates at regions of low stress. In this case the creep rate is

$$\dot{\epsilon} = \frac{\alpha \omega \sigma \Omega^{\frac{2}{3}}}{\eta_0 d^3} \quad (17.13)$$

This latter mechanism is similar to what happens during liquid-phase sintering (see Chapter 24). The requirements include the following:

- The solid must have a certain amount of solubility in the liquid.
- The liquid must wet the solid.

The composition of the IGF is important in determining overall creep behavior. For example, using Y_2O_3 as a sintering aid for silicon nitride ceramics has been found to be superior to using MgO . Other important aspects of the microstructure are the grain size and the volume fraction of liquid present.

17.11 TERTIARY CREEP AND CAVITATION

Tertiary creep represents the final stage of creep deformation and involves an acceleration of the creep rate followed by failure of the component. This stage does not occur in all ceramics, and as previously noted certain ceramics exhibit only primary creep. Tertiary creep involves the formation of cavities that lead to crack formation, often along grain boundaries. The cracks can propagate rapidly, particularly under tensile loading.

Although the nucleation of cavities does not seem to be well understood at present it is clear that cavitation depends on microstructure. Porosity and second-phase particles, which are sources of stress concentration (see Chapter 18), can act as nucleation sites for cavitation and subsequent crack growth. Remember pores can be found in most ceramics; even “pore-free” materials such as hot-pressed alumina may contain small pores. Cavitation also occurs in ceramics with IGFs. Nucleation of the cavities will usually occur at regions where the IGF is not homogeneous, e.g., nonwetted regions, gas bubbles, and impurity particles.

Figure 17.18 shows cavity size distribution data for two polycrystalline aluminas. One is Lucalox (there is no glassy phase) and the other is 99% pure alumina with a

glassy phase. The data were obtained using small-angle neutron scattering. For Lucalox the number of pores increases with increasing creep strain but their size does not increase—nucleation is the dominant process. For the alumina with a glassy phase both the number and size of the pores increase with creep strain—we are getting both nucleation and growth.

VISCOUS FLOW

Newton's law:

$$\tau = \eta d\gamma/dt$$

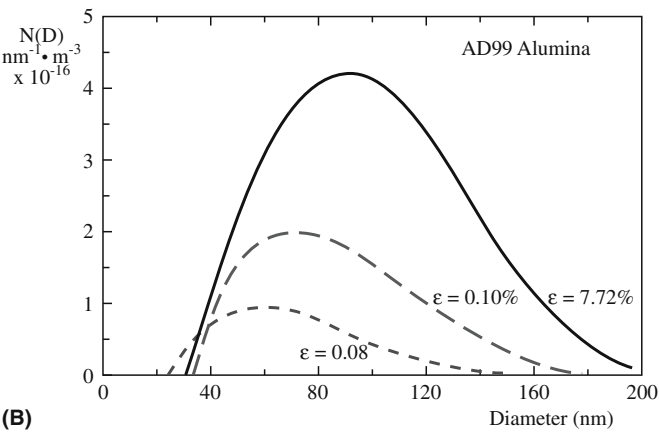
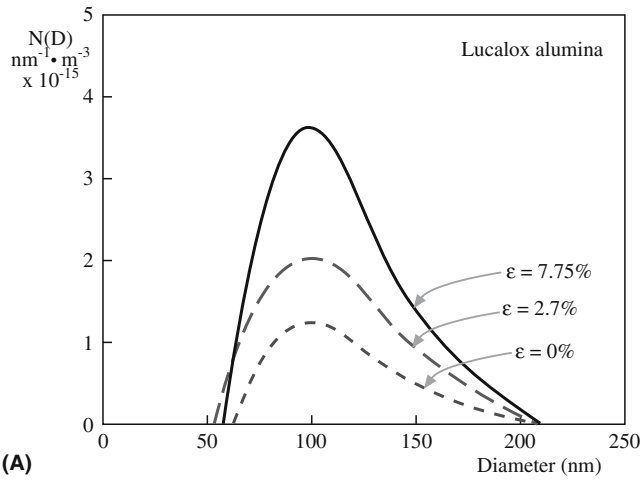
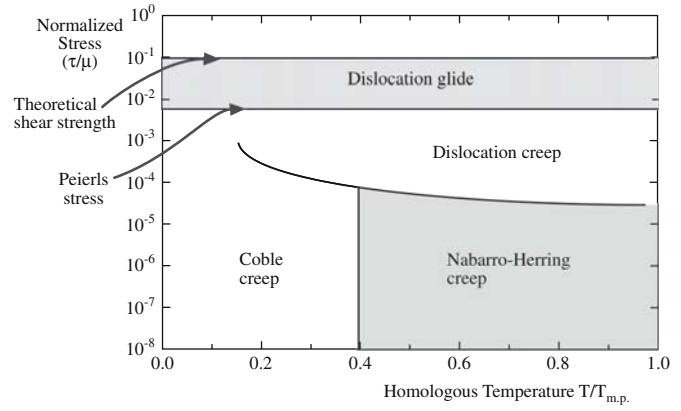
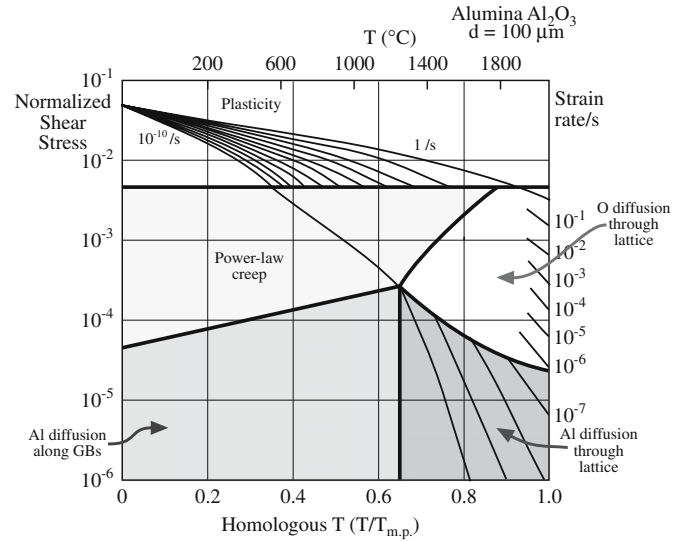


FIGURE 17.18 (a) Cavity-size distribution as a function of creep strain in alumina without a glassy phase (Lucalox). (b) Cavity-size distribution as a function of creep strain in alumina with a glassy phase (AD99).



(A)



(B)

FIGURE 17.19 (a) Schematic of creep deformation map for a polycrystalline ceramic. (b) Creep deformation map for Al_2O_3 .

TABLE 17.6 Creep Equation Exponents and Diffusion Paths for Various Creep Mechanisms

Creep mechanism	m	n	Diffusion path
<i>Dislocation creep mechanism</i>			
Dislocation glide climb, climb controlled	0	4–5	Lattice
Dislocation glide climb, glide controlled	0	3	Lattice
Dissolution of dislocation loops	0	4	Lattice
Dislocation climb without glide	0	3	Lattice
Dislocation climb by pipe diffusion	0	5	Dislocation core
<i>Diffusional creep mechanisms</i>			
Vacancy flow through grains	2	1	Lattice
Vacancy flow along grain boundaries	3	1	Grain boundary
Interface reaction control	1	2	Lattice/grain boundary
<i>Grain boundary sliding mechanisms</i>			
Sliding with liquid	3	1	Liquid
Sliding without liquid (diffusion control)	2–3	1	Lattice/grain boundary



FIGURE 17.20 Detail from a glass sculpture by Dale Chihuly.

17.12 CREEP DEFORMATION MAPS

From the previous sections you can see that there are a large number of creep mechanisms. These can be expressed by one general equation:

$$\dot{\epsilon} = \frac{AD\mu b}{kT} \left(\frac{b}{d}\right)^m \left(\frac{\sigma}{\mu}\right)^n \quad (17.14)$$

The various creep mechanisms give rise to different values of the exponents, m and n , as shown in Table 17.6. For a given ceramic a specific creep mechanism may dominate at certain temperatures and stresses. This can be represented on a creep deformation map as illustrated in Figure 17.19a for a general case and in Figure 17.19b for the specific case of Al_2O_3 . These maps are based on a large amount of experimental data.

17.13 VISCOUS FLOW

Viscous flow is an important mechanism for permanent deformation in glasses. It allows us to form complex shapes such as shown in Figure 17.20. Viscous flow is also a mechanism by which ceramics containing IGFs undergo creep. So it is a

characteristic that is both beneficial and deleterious, but unavoidable at high temperature.

Under most conditions oxide glasses behave as Newtonian fluids, i.e., the strain rate, $d\gamma/dt$, is a linear function of the applied shear stress, τ . An important consequence of this behavior is that when we draw glasses, such as during the formation of optical fibers, the cross section reduces at a constant rate. In other words, we do not get necking of narrow sections of the fiber. At high stress levels non-Newtonian behavior, which is common in polymers, may be observed in oxide glasses.

Models of viscous flow include the following:

Absolute-rate theory: Viscous flow is a thermally activated process involving a high-energy activated state. Viscosity follows an Arrhenius expression with activation energy for viscous flow, E_v . The preexponential term has a weaker dependence on temperature than the exponential term. This theory is applicable only over a narrow range of temperatures.

Free-volume theory: Molecular motion involves the availability of vacancies. The vacancy volume is the free volume, V_F , of the liquid, approximately the difference in volume of the liquid, V_L , and crystalline, V_C , forms. V_F is a function of temperature. D is a constant close to unity. The Williams–Landel–Ferry (WLF) equation uses a similar approach in which f_g is the fraction of free volume at T_g , about 0.025, and β_L and β_C are the volumetric thermal expansion coefficients of the liquid and solid, respectively.

Excess-entropy theory: There is a decrease in the configurational entropy, S_c , of a liquid when it is cooled down—fewer molecular arrangements are possible.

This makes deformation more difficult. E_s is proportional to the potential energy barrier for molecular rearrangement.

The Vogel–Fulcher–Tammann (VFT) equation is an empirical expression relating η to T and can be interpreted in terms of the different models. The VLT expression is accurate over a wide range of temperatures and is widely used in many practical applications.

The viscosity of a specific glass depends on temperature as shown in Figure 17.21. Glass blowing is often performed at viscosities of ~ 10 MPa·s. This is at the top end of the

EQUATIONS FOR VISCOUS FLOW

Arrhenius:

$$\eta = \eta_0 \exp\left(\frac{E_v}{RT}\right)$$

Turnbull and Cohen:

$$\eta = \eta_0 \exp\left(\frac{DV_c}{V_F}\right)$$

Williams–Landel–Ferry (WLF):

$$\eta = \eta_0 \exp\left[\frac{D}{f_g + (\beta_L - \beta_C)(T - T_g)}\right]$$

Adams–Gibbs:

$$\eta = \eta_0 \exp\left[\frac{E_s}{TS}\right]$$

Vogel–Fulcher–Tammann (VFT):

$$\eta = \eta_0 \exp\left[\frac{C}{T - T_0}\right]$$

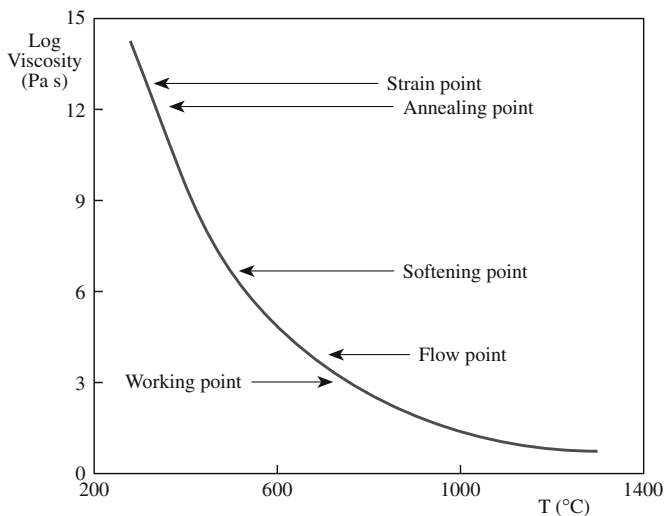


FIGURE 17.21 Temperature dependence of viscosity for a soda-lime-silica glass.

working range, which extends from 1 kPa·s to 10 MPa·s. Figure 17.22 shows a microblown feature formed in a silica scale on oxidized SiC at 1800°C, which for pure silica corresponds to the softening point. If the viscosity was at the fining temperature (~5 Pa·s) the gas would have been able to escape easily. If the viscosity were too high the glass would not have been able to deform in this way.

There is also time dependence to the viscosity, particularly near T_g and above. At these temperatures structural relaxation occurs.

17.14 SUPERPLASTICITY

Superplasticity is the ability of a material to sustain very large strains. From our discussions so far on the mechanical properties of ceramics you may think it unlikely that any ceramic would exhibit superplasticity. But superplasticity has been observed in, for example, tetragonal ZrO_2 stabilized with Y_2O_3 . Elongations of 800% were observed for ceramics stabilized with 3 mol% Y_2O_3 and 1038% for tetragonal zirconia stabilized with 2.5 mol% Y_2O_3 containing 5 wt% SiO_2 . The general requirements are that the grains should be

- Small (typically < 1 μm)
- Equiaxed

The mechanism for superplasticity in ceramics must clearly be different from that in metal alloys because there



FIGURE 17.22 Microblown silica shape formed on oxidized SiC.

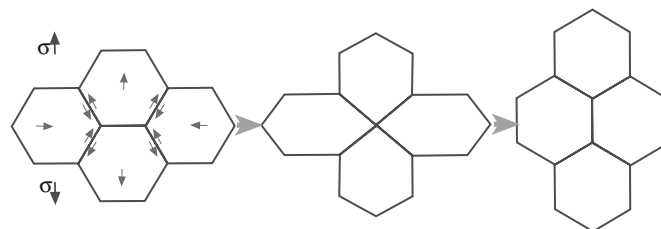


FIGURE 17.23 Model showing how grain switching can produce a shape change.

is no appreciable change in grain shape. Several models have been proposed. The one illustrated in Figure 17.23 involves grain switching and accounts for the constancy of grain shape during deformation, but cannot account for the increase in surface area resulting from plastic deformation. Other models involve grain boundary sliding, but again do not appear to fully account for the process.

Although superplasticity is a useful forming process for metals it tends not to work for ceramics because of the problem of cavitation and the requirement of high temperatures.

CHAPTER SUMMARY

Although we often think of the mechanical properties of ceramics entirely in terms of their brittleness, in this chapter we showed that plastic deformation is also important. The main difference between plasticity in ceramics and in metals is that for ceramics the primary mechanism

of plastic deformation may not be the motion of dislocations. If dislocations are involved then we are invariably at high temperatures. Plastic deformation is a key engineering design consideration in the use of ceramics in structural applications. Consequently, understanding creep behavior is essential, which means we have to understand point defects (Chapter 11) and in many cases the role of IGFs (Chapter 15). As an illustration of why we devoted an entire chapter to this topic remember the example from the final section; elongations in excess of 1000% have been observed in some ceramics. This is clearly not the conventional wisdom when it comes to ceramics and probably something that you would not have expected prior to reading this chapter. Unfortunately, we have not been able to come up with a clear explanation for this property.

PEOPLE IN HISTORY

Herring, W. Conyers, an exception to our rule, is Emeritus Professor of Applied Physics at Stanford University.

He has won many major awards and was elected to the National Academy of Sciences in 1968.

Nabarro, Frank Reginald Nunes (1916–2006) is another exception to our rule. He studied at Oxford and Bristol University. During World War II he worked on the explosive effect of shells and was made a member of the Order of the British Empire (OBE). In 1953 he became head of the physics department at the University of the Witwatersrand in South Africa. He is perhaps best known for Nabarro–Herring creep and the Peierls–Nabarro force.

von Mises, Richard (1883–1953) was born in Lemberg, Austria-Hungary, which is now Lviv, Ukraine. A mathematician and engineer he worked in a number of areas including statistics, probability theory, and mechanics. He died in Boston.

GENERAL REFERENCES

Cannon, W.R. and Langdon, T.G. (1983) “Creep of ceramics: Part 1,” *J. Mater. Sci.* **18**, 1–80; (1988) “Creep of ceramics: Part 2,” *J. Mater. Sci.* **23**, 1.

Chan, K.S. and Page, R.A. (1993) “Creep damage development in structural ceramics,” *J. Am. Ceram. Soc.* **76**, 803. A review of creep behavior.

Cook, R.F. and Pharr, G.M. (1994) “Mechanical properties of ceramics,” in *Materials Science and Technology*, Vol. 11, edited by M. Swain, VCH Publishers, Weinheim, p. 339.

Davidge, R.W. (1979) *Mechanical Behaviour of Ceramics*, Cambridge, University Press, New York.

Green, D.J. (1998) *An Introduction to the Mechanical Properties of Ceramics*, Cambridge University Press, Cambridge UK.

Nieh, T.G. and Wadsworth, J. (1990) “Superplastic ceramics,” *Annu. Rev. Mater. Sci.* **20**, 117.

Poirier, J.-P. (1985) “Creep of crystals: High-temperature deformation processes,” in *Metals, Ceramics and Minerals*, Cambridge University Press, Cambridge, UK.

Sprackling, M.T. (1976) *The Plastic Deformation of Simple Ionic Crystals*, Academic Press, London, UK.

Wachtman, J.B. (1996) *Mechanical Properties of Ceramics*, Wiley-Interscience, New York.

SPECIFIC REFERENCES

Buerger, M.J. (1930) “Translation-gliding in crystals of the NaCl structural type,” *Am. Mineral.* **15**, 174 and 226.

Coble, R.L. (1963) “A model for boundary diffusion controlled creep in polycrystalline materials,” *J. Appl. Phys.* **34**, 1679.

Gilman, J.J. (1959) “Plastic anisotropy of LiF and other rocksalt-type crystals,” *Acta Metall.* **7**, 608.

Hall, E.O. (1951) “The deformation and aging of mild steel: III. discussion of results,” *Proc. Phys. Soc.* **B64**, 747.

Herring, C. (1950) “Diffusional viscosity of a polycrystalline solid,” *J. Appl. Phys.* **21**, 437.

Nabarro, F.R.N. (1948) in *Report of a Conference on Strength of Solids*, The Physical Society, London, 75. The conference was held at Bristol University in the UK in 1947.

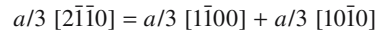
Petch, N.J. (1953) “The cleavage strength of polycrystals,” *J. Iron Steel Inst. (London)* **173**, 25.

Reusch, E. (1867) “Ueber eine besondere Gattung von Durchgängen im Steinsalz und Kalkspath,” *Ann. Phys. Chem.* **132**, 443 and 449.

EXERCISES

- 17.1 An MgO single crystal is loaded in uniaxial compression with the [001] direction parallel to the compression axis. Assuming that dislocation motion occurs on the primary slip system when the applied stress is 30 MPa, what is the inherent lattice resistance to dislocation motion?
- 17.2 The lattice parameter of MgO is $a = 0.4211$ nm. Calculate the distance between Mg^{2+} and O^{2-} ions prior to slip (Figure 17.5a and c) and at the midpoint position (Figure 17.5b and d) during slip on {100} and {110} planes.

- 17.3 Figure 17.14 shows the hardening effect of NiO additions to MgO. Based on what you know about these two ceramics would you expect the NiO/MgO system to show a complete range of solid solubility? You must justify how you arrived at your answer.
- 17.4 Figure 17.22 shows a microblown silica shape formed on SiC. What gas do you think would be formed at the SiO₂/SiC interface and lead to the shape shown? Would the gas be different at different temperatures?
- 17.5 For each of the ceramics listed in Table 17.1 will a tensile stress applied parallel to the *c* axis give a nonzero resolved shear stress?
- 17.6 The following dislocation reaction has been proposed for dislocation motion in graphite:



Is the reaction favorable as written? Justify your answer and state any assumptions that you make.

- 17.7 The addition of impurity atoms can pin dislocations in single crystals. The addition of small amounts (0.002%) of NdF₃ to CaF₂ can be very effective at increasing the yield stress because of the formation of point defect complexes. Using Kröger–Vink notation show that adding NdF₃ to CaF₂ can result in the formation of a defect complex.
- 17.8 Creep is a concern for structural ceramics at high temperatures. Discuss possible creep mechanisms for SiC and Si₃N₄.
- 17.9 A major multinational company hires you as a consultant because of your knowledge of ceramics. You are asked to recommend a ceramic that will have the maximum possible creep resistance at an operating temperature of 1200°C. What material would you select and why? Also consider how you would process it.
- 17.10 Using the data in Figure 17.21 determine the activation energy for viscous flow in the soda-lime-silica glass. Based on your knowledge of glass structures would you expect the activation energy to be higher or lower for a pure silica glass? Briefly justify your answer.

Fracturing: Brittleness

CHAPTER PREVIEW

The previous two chapters on mechanical properties described how we test ceramics, their elastic response, and how under certain conditions they can permanently deform. In this chapter we describe why and how ceramics break. The main topics are

- Fracture
- Toughening
- Fatigue

Some of these topics may already be familiar from classes on metals. The exception is probably toughening. Ceramics are not tough. Toughening makes the material absorb energy during fracture by mechanisms such as local phase transformations, plastic deformation near the crack tip, or crack bridging behind the crack tip. Fracture requires cracks. In fatigue crack growth occurs as a result of cyclic loading—even at small loads.

We begin this chapter by showing some of the key equations. The most important work is that of A.A. Griffith, the “Father of Fracture Mechanics.” Griffith showed the importance of flaws, which act as stress concentrators. Because it is almost impossible to make ceramics without flaws they often are the dominant cause of failure. So there is a link between this chapter and Chapter 16.

18.1 THE IMPORTANCE OF BRITTLENESS

Most ceramics are brittle at room temperature. That is they fracture with very little plastic deformation. Many archeologists believe that our very existence depended on the brittleness of ceramics, particularly flint. The fracture of flint, like cubic zirconia, diamond, and glass, is termed conchoidal, producing shell-like fracture surfaces. These surfaces are very sharp and were utilized in early stone tools to cut and shape wood and to butcher animals required for food. The hides were used for clothing and were attached to wooden frames to make shelters. Stone tools were necessary to cut vegetation and cultivate plants, allowing a change from a food-gathering economy to one of food production, which happened around the eighth millennium BCE in southwestern Asia. This revolutionary change from hunting to farming laid the foundation for civilization.

Bulletproof glass, which is a laminate of glass and polycarbonate, is a dramatic illustration of the utilization of brittle fracture. The glass absorbs the energy of the projectile either in elastic changes or ultimately in the creation of new surfaces when it fractures. The polymer

provides an additional mechanism for absorption of energy before the projectile exits the final layer. Table 18.1 gives the kinetic energy of several different types of handgun bullets.

The brittle behavior of ceramics is critical to the successful operation of ceramic armor. In addition to brittleness the basic requirements are that it be

- Hard
- Lightweight

The first ceramic used in this application was alumina backed with a laminate of fiberglass and polyester resin called “Doron.” Boron carbide (B_4C) ceramic armor was developed during the Vietnam War and used in the mid-1960s for both helicopter and infantry armor. It provides the same protection as alumina, but with a 20% savings in weight. A quarter-inch (0.64-cm) plate of B_4C can stop a 30-caliber armor-piercing projectile (one containing a tungsten carbide core). Boron carbide is being used during the current conflict in Iraq. Small arms protective inserts are made of boron carbide. They will stop up to a 7.62-mm round with a muzzle velocity of ~850 m/s.

TABLE 18.1 Kinetic Energy of Handgun Projectiles

Hand gun size	Missile size (g)	Missile velocity (m/s)	Energy (J)
0.38	10	243	295
0.22	2.6	305	133
0.45	15	259	503
0.357	10	381	725
9mm	8	332	440

Brittle fracture is used for shaping and machining ceramics after they have been fired. Ceramics can be modified to make them machinable: this is controlled fracture and is the approach we adopt with machinable glass-ceramics such as Macor (Chapter 26). Of course, many ceramics already are machinable and can be shaped into intricate and beautiful forms as illustrated in the carved marble sculpture shown in Figure 18.1.

In many of the applications in which we use or would like to use ceramics their brittleness can be a serious limitation:

- Space shuttle tiles are made of silica glass. We need to be concerned about the impact of space debris.
- Radomes are made of fused silica and silicon nitride. They have to be transparent to infrared (IR) and radio waves and resist the impact of atmospheric particles.
- Ceramic bearings are used in low-load applications (watch bearings of ruby or sapphire “jewels”), but for high-load and high-speed use metals are often preferred because ceramics have low fracture toughness.



FIGURE 18.1 Marble sculpture in a fountain outside the Pantheon in Rome.

It is important to remember that metals and polymers can also fracture in a brittle manner. But brittle fracture often occurs only at temperatures below room temperature.

18.2 THEORETICAL STRENGTH: THE OROWAN EQUATION

We will consider brittle fracture at the atomic level where we are separating two planes of atoms as shown in Figure 18.2a. In many crystalline materials fracture occurs along crystallographic planes that are relatively densely packed. These planes are known as cleavage planes. In MgO {100} is the cleavage plane. (It is interesting that {111} is the growth plane for MgO and that fluorite is exactly the opposite!) In glasses and in some crystals (diamond and cubic zirconia, for example) fracture is noncrystallographic.

Figure 18.2b shows a plot of stress versus distance. Note we are using X for distance (rather than r as we did in Chapter 3) because we are now thinking about planes of atoms rather than individual atoms. The curve is the

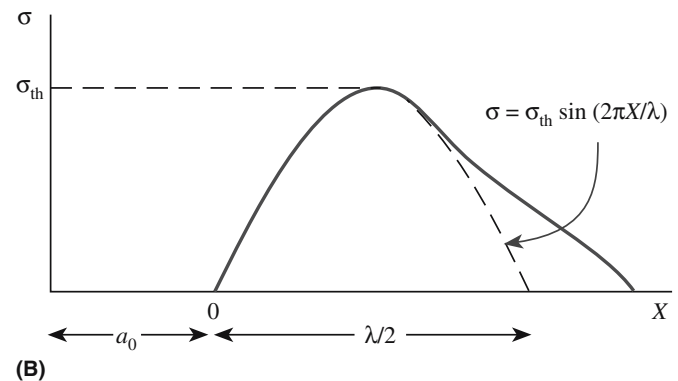
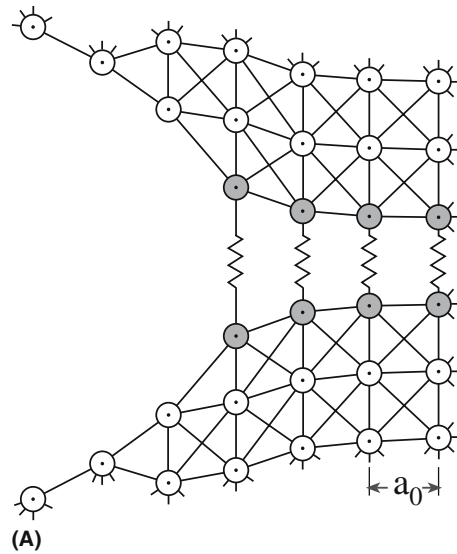


FIGURE 18.2 (a) Model of a crack tip. The interplanar spacing is a_0 . (b) Stress versus distance plot.

same; it is only the notation that changes. If a stress is applied that exceeds the theoretical strength, σ_{th} , then the ceramic will fracture. This is the strength of the ceramic if there is no plastic deformation and there are no defects. It is “theoretical” because we can rarely, if ever, achieve it. We would like to be able to obtain an expression for σ_{th} and there are several different approaches we can use. The one we have selected is simple, works well, and gives values similar to those obtained by more complex methods.

The part of the σ - X curve near to the equilibrium interplanar spacing, a_0 , can be approximated as being sinusoidal and we can write

$$\sigma = \sigma_{th} \sin(2\pi x/\lambda) \quad (18.1)$$

where x is the displacement of the planes beyond their equilibrium value and λ is the wavelength of the sine wave.

The two new surfaces created during fracture—the fracture surfaces—have a total energy 2γ , which must be equal to the work required to separate the two planes of atoms (i.e., it is the area under the curve or the integral of Eq. 18.1 between 0 and $\lambda/2$):

$$2\gamma = \int_0^{\lambda/2} \sigma_{th} \sin(2\pi x/\lambda) dx = \lambda \sigma_{th} / \pi \quad (18.2)$$

Rearranging Eq. 18.2 gives

$$\sigma_{th} = 2\pi\gamma/\lambda \quad (18.3)$$

For low stresses the material will be elastic, Hooke’s law will be obeyed, and we can write the Young’s modulus as

$$E = \sigma a_0/x \quad (18.4)$$

and

$$d\sigma/dx = E/a_0 \quad (18.5)$$

For small displacements we can make the approximation $\sin x \sim x$ and from Eq. 18.1 write

$$d\sigma/dx = 2\pi\sigma_{th}/\lambda \quad (18.6)$$

TABLE 18.2 Values of Theoretical Strength

Material	Direction	E (GPa)	γ (J/m ²)	σ_{th} (GPa)
α -Fe	<111>	132	2	30
Si	<111>	188	1.2	32
NaCl	<100>	44	0.25	6.3
MgO	<100>	245	1.2	37
Al ₂ O ₃	<0001>	460	1	46

TABLE 18.3 Comparison of Theoretical Strength and Actual Strength

Material	E (GPa)	Estimated theoretical strength (GPa)	Measured strength of fibers (GPa)	Measured strength of polycrystalline specimen (GPa)
Al ₂ O ₃	380	38	16	0.4
SiC	440	44	21	0.7

Combining Eqs. 18.5 and 18.6 gives

$$2\pi\sigma_{th}/\lambda = E/a_0 \quad (18.7)$$

By substitution of Eq. 18.3 we get the Orowan equation

$$\sigma_{th} = (E\gamma/a_0)^{1/2} \quad (18.8)$$

Theoretical strength thus depends on

- Surface energy
- Young’s modulus
- Lattice spacing

Putting in reasonable values for γ (see Chapter 13) and a_0 , we find that $\sigma_{th} \approx E/5$ to $E/10$. This is a useful relationship to remember. Values of σ_{th} for some materials calculated using the Orowan equation are given in Table 18.2. These values are possible only in very special forms such as silica fibers with pristine surfaces. Whiskers and fibers of sapphire and silicon carbide have been made with measured strengths of about $\sigma_{th}/2$ (Table 18.3).

For most polycrystalline ceramics, measured strengths are in the range of $E/100$ to $E/1000$ or even less. Why is there such a large discrepancy between theoretical and measured strengths? The reason is the presence of pre-existing cracks on the surface or inside the ceramic and sharp corners that may be introduced during processing. The presence of cracks does not mean that samples will fracture spontaneously; our teeth are full of cracks.

18.3 THE EFFECT OF FLAWS: THE GRIFFITH EQUATION

To explain the discrepancy between theoretical strength predicted by Eq. 18.8 and experimental data A.A. Griffith (1920) suggested that preexisting flaws in the materials act to concentrate stress. Figure 18.3 shows data obtained by Griffith for the tensile strength of glass fibers as a function of their diameter. As the fibers get smaller the probability of having a crack decreases and the size of the largest crack also decreases. Consequently, they get stronger. This is the basis of the “weak link” approach adopted in Weibull statistics that we described in Chapter 16. So there is a direct relationship between flaws and probability of failure.

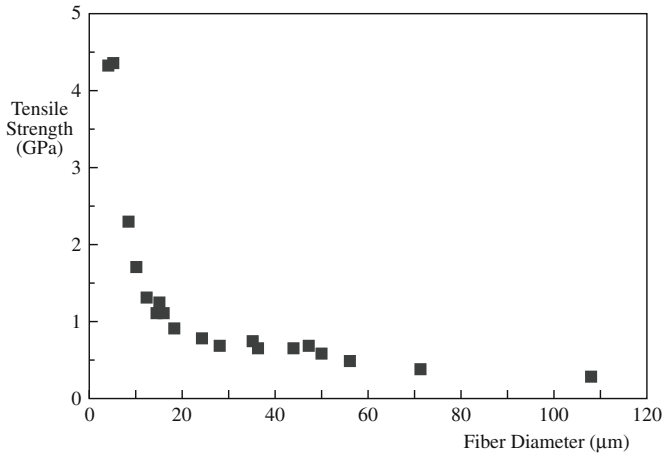


FIGURE 18.3 Tensile strength of a glass fiber as a function of fiber diameter.

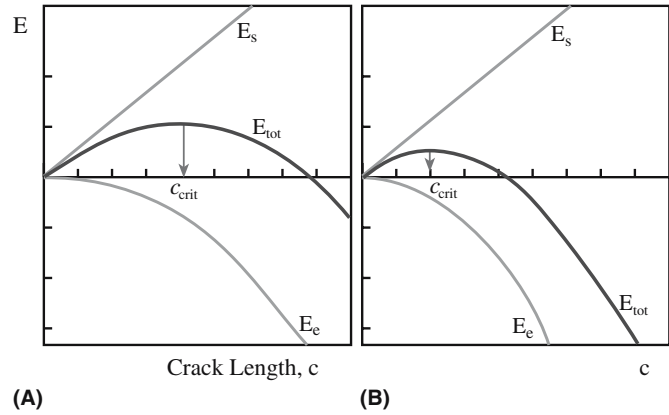


FIGURE 18.4 Plots of energy versus crack length. E_{tot} is the sum of E_s and E_e . The right plot corresponds to a greater applied stress (on this scale the stress is greater by $\sqrt{2}$ and c_{crit} is correspondingly reduced by a factor of 2).

Griffith’s approach is an energy balance: A crack will propagate when the additional energy created by the formation of the fracture surfaces, E_s , is offset by a decrease in the stored elastic energy, E_e , in the stretched bonds (this is the area under the stress–strain curve). The Griffith energy balance condition can be expressed as

$$\frac{dE_e}{dc} = \frac{dE_s}{dc} \quad (18.9)$$

Note that we are using E for energy to avoid any confusion with Young’s modulus (\mathcal{E}). The elastic energy term is

$$E_e = \pi\sigma^2 c^2 / \mathcal{E} \quad (18.10)$$

The surface energy term is

$$E_s = 4c\gamma \quad (18.11)$$

Because E_s scales linearly with c and E_e scales quadratically with c there is a maximum in the total energy E_{tot} of the system, which corresponds to the critical crack size, c_{crit} . This balance can be represented graphically as shown in Figure 18.4.

- A crack smaller than c_{crit} is stable, therefore the surface energy dominates.
- A crack larger than c_{crit} is unstable, therefore the released strain energy dominates.

SCRIBING

A simple illustration of the effect of surface flaws is the ease with which a sheet of glass can be “cut” after light scribing using a diamond tip.

For an atomically sharp crack of length $2c$, as illustrated in Figure 18.5, the energy balance approach shows that

$$\sigma_f = (2\mathcal{E}\gamma/\pi c)^{1/2} \quad (18.12)$$

Equation 18.12 is often called the Griffith equation and shows that fracture stress depends on the following:

- Young’s modulus (a property of the material)
- Surface energy (a property of the material)
- Crack length

Griffith confirmed this equation using experimental data on glass as shown in Figure 18.6. Although the energy balance approach works well, kinetic effects may also be present during fracture as demonstrated for the fracture of mica flake.

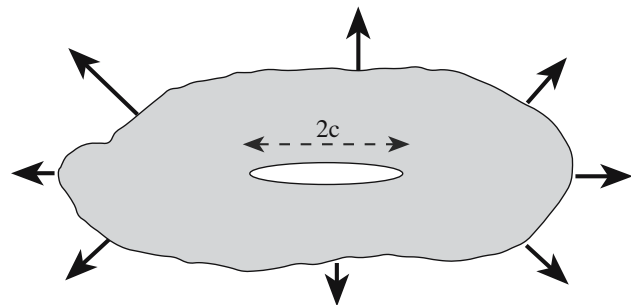


FIGURE 18.5 The “Griffith” crack of length $2c$.

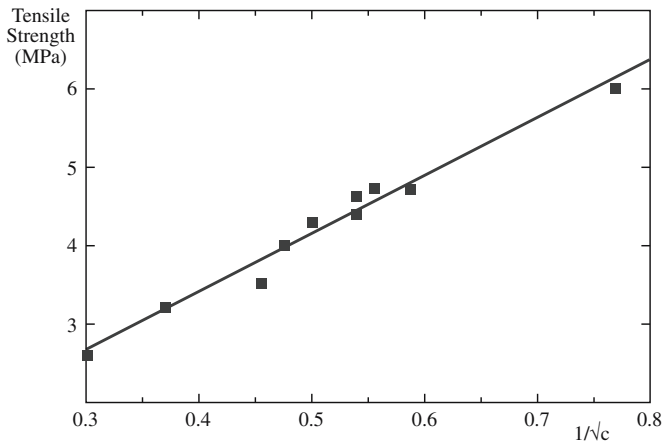


FIGURE 18.6 Verification of Eq. 18.12. The tensile strength of glass as a function of crack length.

18.4 THE CRACK TIP: THE INGLIS EQUATION

In our discussions of fracture so far we have assumed that the crack looks much like that shown in Figure 18.2a. The crack separates planes of atoms, is atomically sharp, and the only deformation is elastic ahead of the crack tip. This is the situation encountered in many ceramics at room temperature.

The maximum tensile stress at the crack tip, for the geometry in Figure 18.5, is

$$\sigma_m = 2\sigma(c/\rho)^{1/2} \quad (18.13)$$

where ρ is the crack tip radius. The ratio σ_m/σ is called the stress concentration factor. As an illustration of how large the stress concentration factor can be we will consider an example of a ceramic with a flaw size c of 50 μm . The stress concentration at the crack tip is about 1200.

For fracture to occur in an ideal brittle material, the maximum stress must reach the theoretical strength of the material to provide a mechanism for fracture, i.e., $\sigma_m = \sigma_{th}$. If we set the applied stress (σ) equal to the fracture stress (σ_f) then we obtain

$$\sigma_f = \left(\frac{E\gamma}{4c} \frac{\rho}{\alpha_0} \right)^{1/2} \quad (18.14)$$

From Eq. 18.14 you can see why sharp cracks are so deleterious to the strength of ceramics. For metals there is often a plastic zone ahead of the crack tip, which is due to dislocation motion. This leads to blunting of the crack tip and a corresponding decrease in stress concentration.

A crack in a brittle material passes between adjacent planes of atoms and a reasonable estimate for the tip radius is half the atomic spacing, therefore we can simplify Eq. 18.14:

$$\sigma_f = (E\gamma/8c)^{1/2} \quad (18.15)$$

The fracture process, although not far from ideal in ceramics, can be quite complex. Real cracks differ from those assumed in the model in that there is often no distinct crack edge. There will be attractive interactions between atoms on opposite sides of the crack when the spacing is quite small.

18.5 STRESS INTENSITY FACTOR

We introduced the stress intensity factors in Chapter 16. These are a combination of c and σ for different loading geometries with respect to crack position.

The most important geometry for ceramics is mode I, the opening mode. The mode I stress intensity factor is

$$K_I = \sigma Y \sqrt{c} \quad (18.16)$$

Y is a dimensionless term that depends on crack configuration and loading geometry. For a simple interior crack of length $2c$ and tensile loading $Y = \sqrt{\pi}$ (this is the original geometry considered by Griffith); for a surface crack under similar loading $Y = \sqrt{(\pi/2)}$.

The critical stress intensity factor for mode I loading, K_{Ic} , at which the crack will propagate and lead to fracture is known as the fracture toughness (sometimes denoted as T). Table 18.4 lists some values for

AI ALLOYS
Fracture toughness is $\sim 40 \text{ MPa}\cdot\text{m}^{1/2}$.

TABLE 18.4 Fracture Toughness for Several Ceramics

Ceramic	K_{Ic} (MPa·m ^{1/2})
Al ₂ O ₃	2.0–6.0
Al ₂ O ₃ (single crystal, 10 $\bar{1}$ 2)	2.2
Al ₂ O ₃ (single crystal, 0001)	>6.0
MgO	2.5
MgAl ₂ O ₄	1.9–2.4
Mullite (fully dense)	2.0–4.0
ThO ₂	1.6
Y ₂ O ₃	1.5
ZrO ₂ (cubic)	3.0–3.6
ZrO ₂ (partially stabilized)	3.0–15.0
SiC (hot pressed)	3.0–6.0
SiC (single crystal)	3.7
Si ₃ N ₄ (hot pressed)	3.0–10.0
TiC	3.0–5.0
WC	6.0–20.0
CaF ₂	0.80
KCl (single crystal)	~0.35
MgF ₂	1.00
SrF ₂	1.00
Aluminosilicate glass (Corning 1720)	0.96
Borosilicate glass (Corning 7740)	0.75
LAS (glass-ceramic)	2.00
Silica (fused)	0.80
Silica (96%)	0.70
Soda-lime silica glass	0.82

TABLE 18.5 Theoretical and Measured Values of G_c for Some Materials

Material	Theoretical $G_c = 2\gamma$ (N/m)	Measured G_c (N/m)
Glass	3.5	14
Plexiglass	11.4	480
MgO	14.9	17.5
High-strength steel	22.8	53,000
High-strength aluminum	7.0	17,000
High-strength titanium	10.5	105,000

ceramics. You can see that the values are generally low and a significant amount of research has been undertaken over the past 40 years or so to increase K_{Ic} . We will look at some of the approaches that have been used a little later in this chapter.

If the material is not perfectly brittle, i.e., there are energy dissipating mechanisms in addition to the creation of new surfaces, then we introduce a term G_c , which is an energy (its units are J/m^2) representing crack extension by all the available processes. You will find G_c referred to as total work of fracture, crack extension force, and strain energy release rate.

For plane stress (the sample is a thin plate)

$$K_{Ic} = \sqrt{\mathcal{E}G_c} \quad (18.17)$$

For plane strain (the sample is a thick block)

$$K_{Ic} = \sqrt{\frac{\mathcal{E}G_c}{1-\nu^2}} \quad (18.18)$$

When fracture occurs we can write

$$G_c = dE_s/dc = R \quad (18.19)$$

R is the crack resistance of the material and is called the crack resistance “force.” The material will fracture when $G_c = R$, i.e., the crack extension force is equal to the crack resistance force. If the fracture is entirely brittle, the energy is only required to create new surfaces, then $R = 2\gamma$. (Note: The surface energy term used here differs from that in Eq. 18.11 by a factor of two because G_c is associated with a single crack tip.)

Table 18.5 compares some measured values of G_c to some theoretical values based on surface energies. You can see that for MgO the two values are in good agreement. This is not the case for the metal alloys.

18.6 R CURVES

The crack resistance R is related to fracture toughness as we just described. It was assumed that R and T are independent of crack length. But this is not necessarily so.

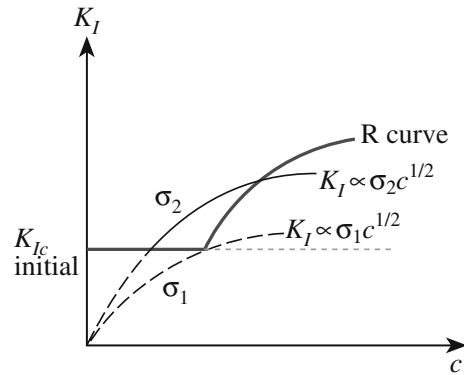


FIGURE 18.7 A material showing R curve behavior (bold curve) exhibits a region of stable crack growth and flaw tolerant behavior. The lighter curves σ_1 and σ_2 represent typical Griffith behavior.

The R curve, which is a plot of fracture toughness versus crack length, relates the crack resistance to crack length as shown in Figure 18.7. The fracture toughness increases as the crack grows. We can explain the shape of these curves by considering what happens in the wake of the crack. If there is a mechanism that bridges the crack then the energy required for crack propagation will increase. There are several mechanisms that can be envisaged, for example, a phase transformation associated with crack propagation, or ligaments that bridge the crack after the crack tip has passed. Both these mechanisms will be described when we discuss how we actually try to toughen ceramics.

Eventually a plateau is reached beyond which fracture toughness will not increase. This is the steady-state condition. The following implications apply to ceramics that show R curve behavior:

- Strength degradation is less dependent on flaw size (illustrated in Figure 18.8).
- Reliability is increased. There is a region where the strength is insensitive to crack size.
- Fatigue resistance is decreased.
- There is better thermal shock resistance.

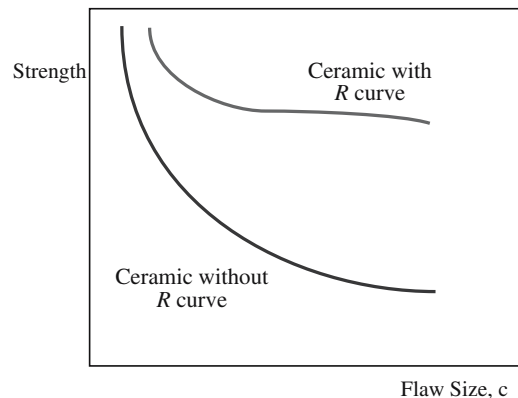


FIGURE 18.8 Effect of R curve behavior on strength. There is a region in which the strength is insensitive to flaw size.

18.7 FATIGUE AND STRESS CORROSION CRACKING

The cracks that we have been describing so far lead to rapid fracture. We call these “critical cracks.” Ceramics may contain many other cracks, called “subcritical cracks,” that can lead to time-dependent fracture. Static fatigue, also known as stress rupture, is where subcritical cracks grow under an applied load. Failure occurs gradually, is often unexpected, and may occur after a component has been in service for many years.

The slow growth of cracks is often the result of a combination of stress and corrosion. This is the field of stress corrosion cracking (SCC), which is important in metals such as gold jewelry alloys and many ceramics. Figure 18.9 shows experimentally measured crack velocities in soda-lime glass tested in nitrogen of

CORROSION AND FAILURE

The corrosion rate of silica glass in water is 10^{-17} m/s.
The rate of stress corrosion cracking (SCC) is 10^{-3} m/s.

varying relative humidity. We can identify three distinct regions:

Region I: Crack growth is sensitive to K_I and follows a relationship of the form

$$v = A^* \exp \alpha K_I \quad (18.20)$$

A^* and α are fitting parameters. From an engineering point of view this is the most important region.

Region II: Crack growth is independent of K_I .

Region III: Very rapid crack growth leads to fracture.

For many materials there exists a threshold value of K_I below which the crack will not grow. This value is not seen in Figure 18.9 because of the experimental difficulties in measuring very small values of crack velocity.

Figure 18.10 illustrates the process that is happening at the crack tip. The corresponding reaction, which involves breaking of Si–O bonds, is shown below:

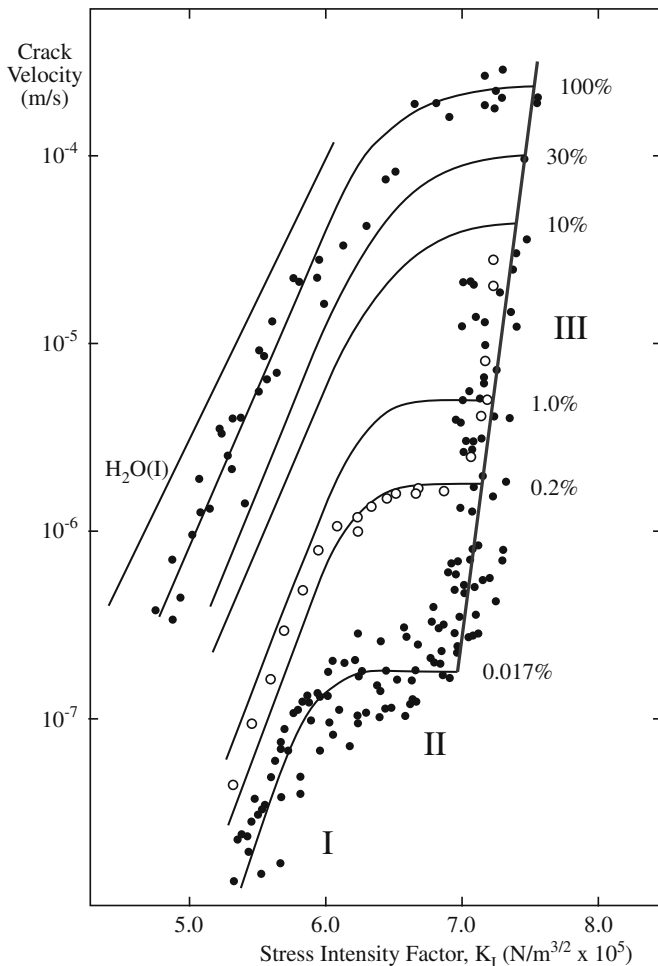


FIGURE 18.9 Crack velocity in soda-lime glass as a function of K_I , the stress intensity factor. The percentages indicate the relative humidity and the Roman numerals indicate the three regions of crack propagation.

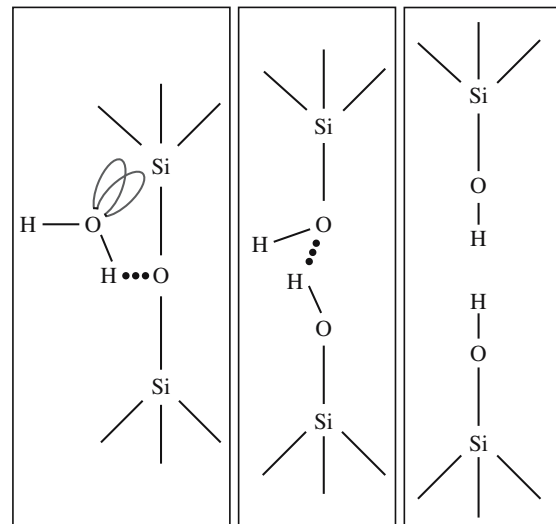
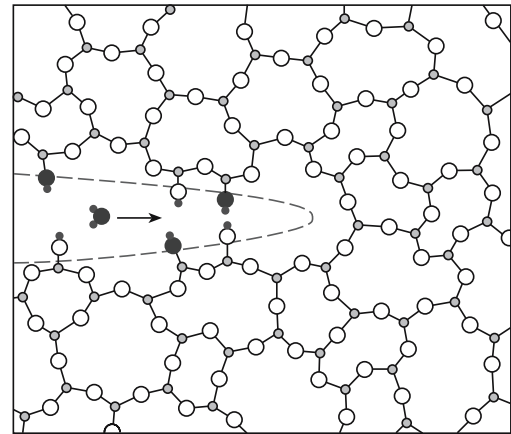
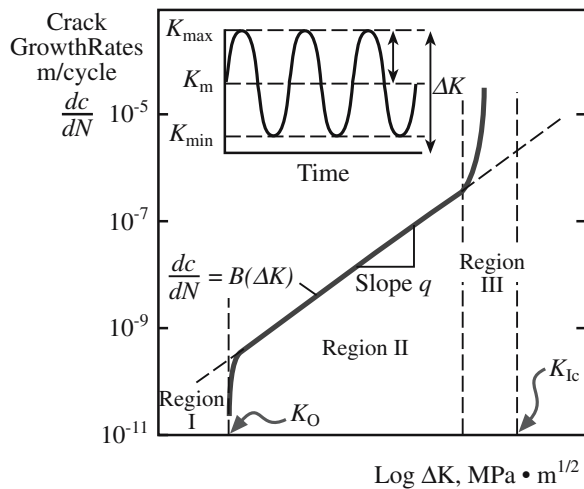
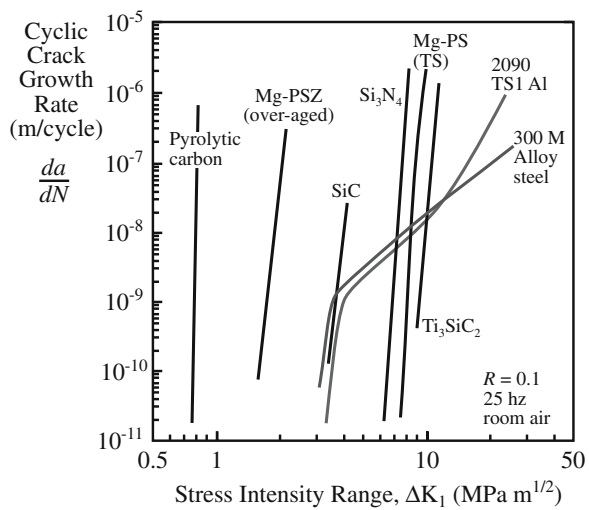


FIGURE 18.10 Environmental effects at the crack tip. A water molecule diffuses to the crack tip, chemisorbs, and rotates such that the lone pairs on the oxygen are aligned with the unoccupied electron orbitals of the Si atom.



(A)



(B)

FIGURE 18.11 (a) Log–log plot of crack growth rate versus K , which is defined in the inset. (b) Cyclic-fatigue crack growth rates for several ceramics and metal alloys as a function of applied stress intensity range, ΔK .



Other small polar molecules such as methanol (CH_3OH) and ammonia (NH_3) can promote SCC in glass. The main requirement is that they are small enough to fit into the crack, <0.3 nm.

Ceramics can also fail by cyclic fatigue. The mechanisms are complicated and not well understood. Fatigue failure in metals is pervasive and due to dislocation motion.

Because fatigue is due to propagation of cracks it will be related to K . During a fatigue cycle K will vary, so what we are actually interested in is ΔK , the difference between K at the maximum load (K_{max}) and K at the minimum load (K_{min}).

$$\Delta K = K_{\text{max}} - K_{\text{min}} \quad (18.21)$$

Figure 18.11a shows a schematic log–log plot of the crack growth rate (dc/dN), N is the number of cycles, against ΔK . We can identify three distinct regions:

Region I: The lower limit to the curve ΔK_T is the threshold stress intensity factor range for crack growth. In this range crack growth with cyclic loading is negligible, if indeed it occurs at all.

Region II: The plot is linear and the crack growth rate can be described by the following equation (sometimes called the Paris–Erdogan equation):

$$dc/dN = B(\Delta K)^q \quad (18.22)$$

B and q are materials constants, which are determined empirically.

Region III: At high ΔK values crack growth is very rapid and fracture would be characteristic of normal static failure.

Figure 18.11b shows examples of cyclic fatigue plots for several ceramics. The curves are linear and very steep implying a high value of q in Eq. 18.22 and that fracture is rapid. The fatigue fracture we see in metals is rare in ceramics.

18.8 FAILURE AND FRACTOGRAPHY

Here we discuss the appearance of different surfaces formed when a ceramic fractures; this is the topic of fractography and is always a postmortem analysis. Fractography is used not only to determine the failure mechanism but also the origin of fracture. Examples of where fractography is used include

- Dentistry, e.g., examination of teeth to improve survivability
- Liability cases, e.g., hip implants to determine who is to blame
- Disasters, e.g., space shuttle tiles to make sure problems do not reoccur

Figure 18.12 illustrates two different crack paths through a material. In Figure 18.12a the crack passes between grains and the fracture is termed intergranular. Intergranular fracture is most likely when the grain boundaries are weak. A striking example of intergranular fracture is shown in Figure 18.13a. The ceramic is AlN , which was prepared by sintering with Y_2O_3 added as a

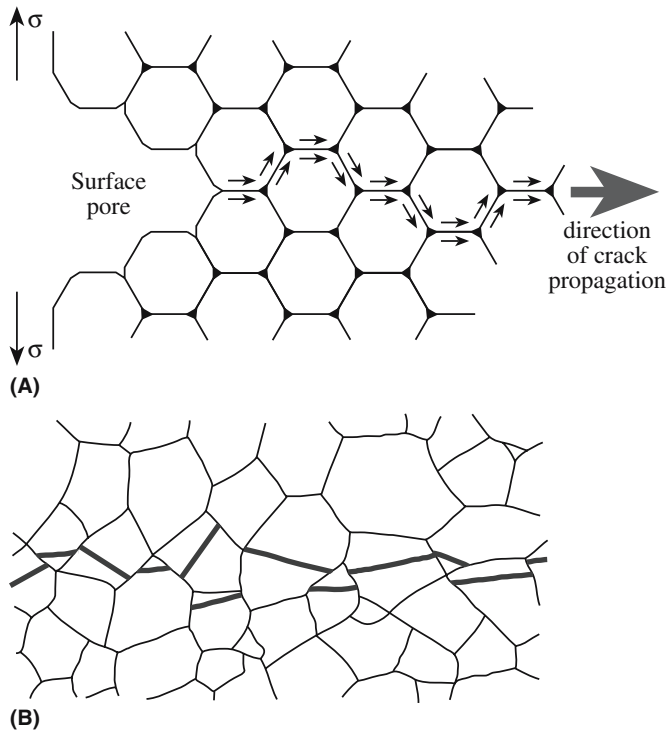


FIGURE 18.12 (a) Illustration of intergranular cracking. (b) Illustration of transgranular cracking.

sintering aid. The individual grains, which are faceted, can be clearly seen in the scanning electron microscopy (SEM) image.

In transgranular (or cleavage) fracture the crack passes through the grains as illustrated in Figure 18.12b. The fracture surface may be smooth or show steps, which form as the crack front moves for one plane to another. Figure 18.13b shows transgranular fracture in polycrystalline SiC. In conchoidal fracture there are no distinct cleavage planes. As mentioned earlier, conchoidal fracture occurs in flint, cubic zirconia, diamond, and glass.

When fracture surfaces are examined, in addition to determining the failure mechanism we also are often interested in the origin of fracture, which in turn might help identify the cause. By reassembling the pieces and looking for where cracks come together as illustrated in Figure 18.14 it is possible to determine crack initiation sites. These may be associated with flaws (e.g., pores or inclusions) introduced during processing.

The extent of crack branching provides information about the amount of energy associated with crack propagation. There will be more branching if the applied stresses are large or if there are large residual stresses that are released as the crack advances. The latter principle is utilized in tempered glass. Extensive crack branching occurs causing the glass to eventually break into many small pieces.

In glasses it is often quite easy to determine the origin of fracture as shown in Figure 18.15. We can identify three distinct regions on the fracture surface:

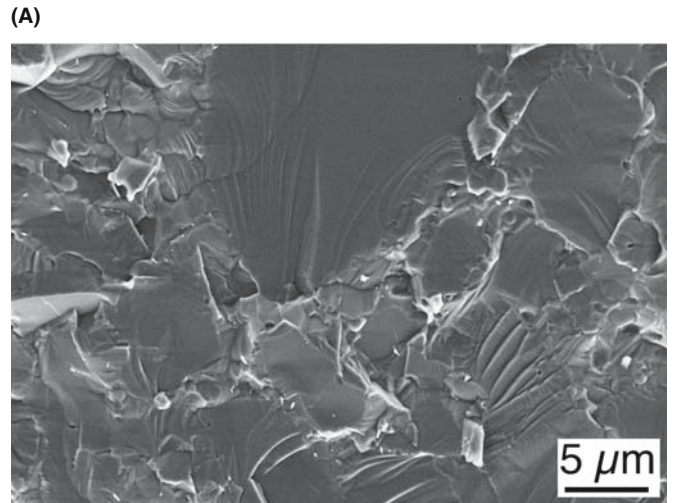
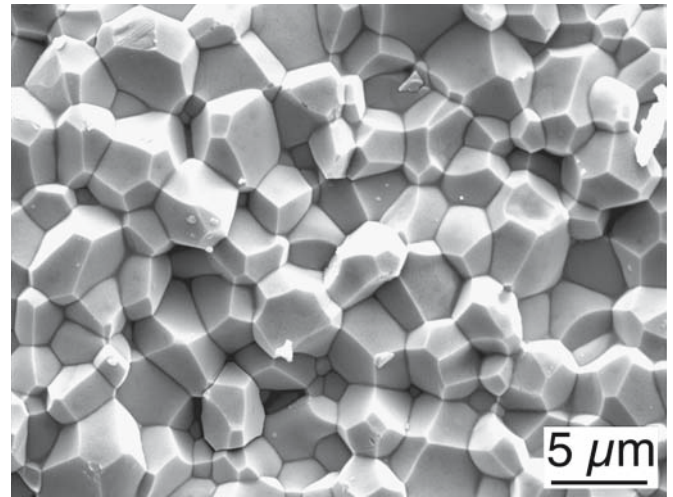


FIGURE 18.13 (a) The fracture surface of polycrystalline AlN. (b) The fracture surface of polycrystalline SiC.

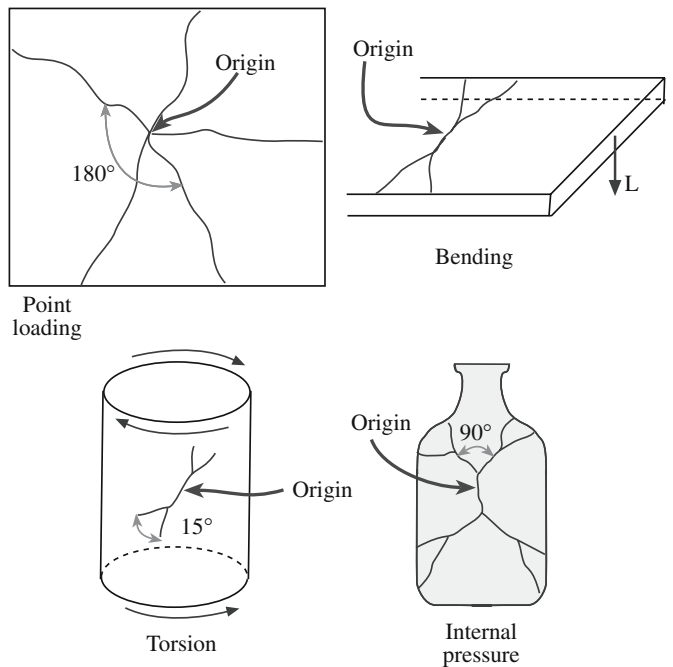


FIGURE 18.14 Determination of crack origin and failure mechanism by postmortem examination of glass fragments.

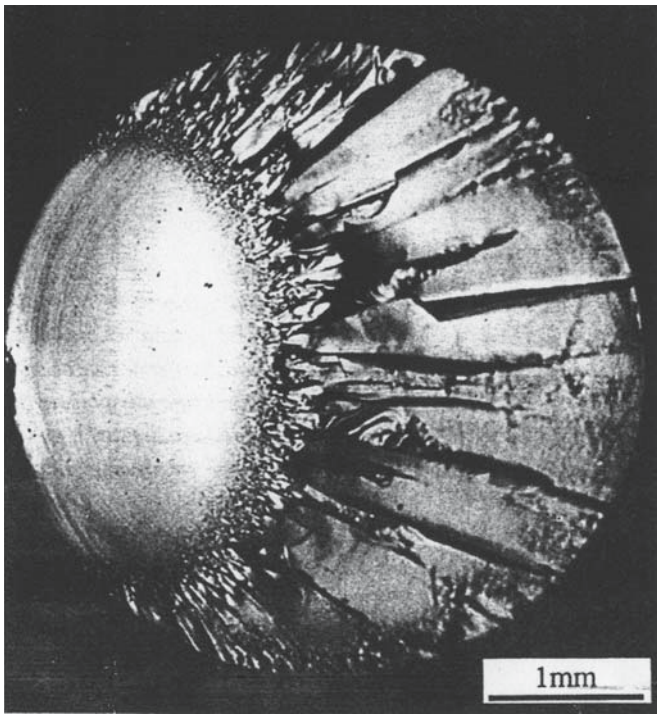
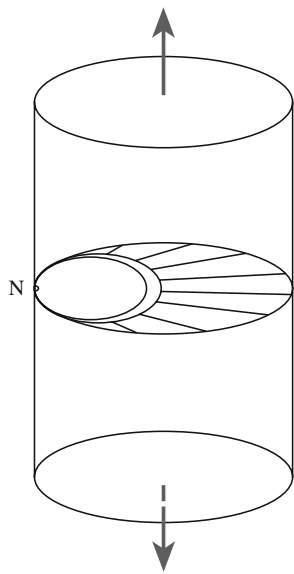
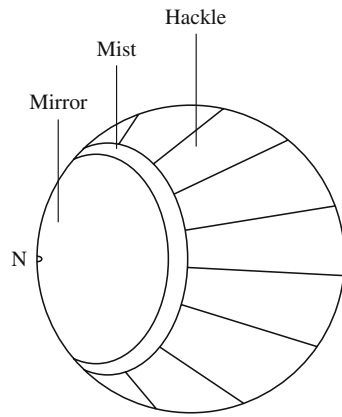


FIGURE 18.15 Fracture surface of a glass rod and corresponding schematics illustrating the distinct regions of the surface.

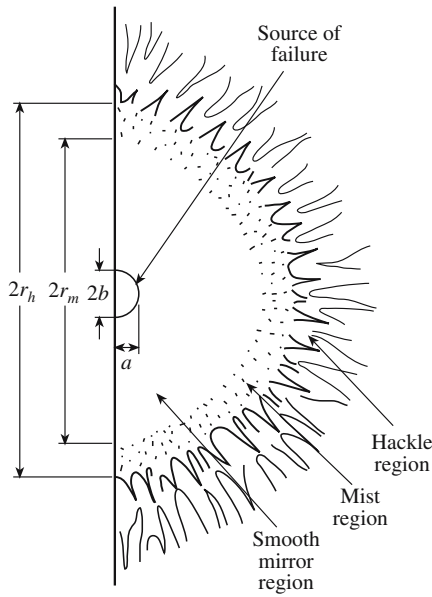
(A)



(B)



(C)



(D)

Mirror: The region around the crack origin. The crack travels in a single plane accelerating as it goes. The fracture surface is smooth and highly reflective. This can be seen in polycrystalline ceramics, but reflectivity is lower.

Mist: The crack deviates either because it reaches a critical velocity, intersects an inclusion, or there is a change in the internal stresses in the glass. The fracture surface is rougher and less reflective. This region is often difficult to see in polycrystalline ceramics.

Hackle: Crack branches forming larger ridges, further increasing the roughness of the fracture surface. By tracing the hackle lines backward we can usually determine the origin of fracture.

Hackle is also referred to as river patterns because the appearance is similar to a river branching into tributaries. Figure 18.16 illustrates river patterns on the fracture surface of an Nd-doped YAG single crystal that fractured during growth. The irregular shaped voids seen in the image are where failure originated.

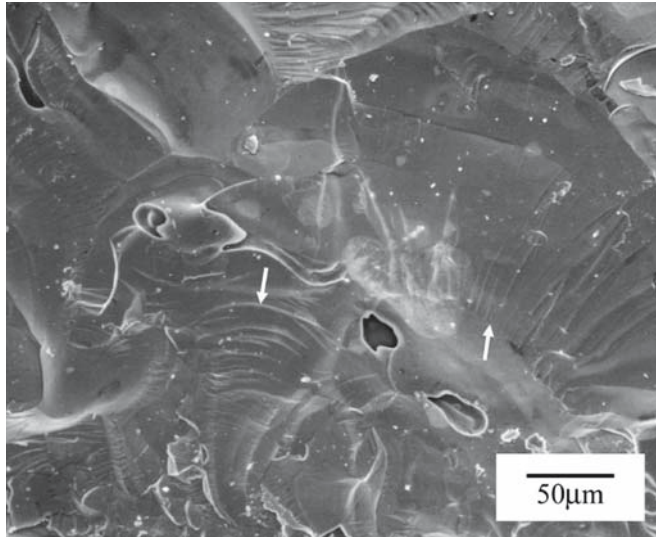


FIGURE 18.16 SEM image of the fracture surface of Nd-doped YAG. River marks are indicated by arrows.

18.9 TOUGHENING AND CERAMIC MATRIX COMPOSITES

Ceramics usually have low fracture toughness. For many engineering applications we must increase the toughness. The desire to toughen ceramics is not new. Toughening of brick using straw was known in 9000 BCE. The basic idea is how to stop crack movement thereby increasing the amount of energy required for crack propagation.

The toughening mechanisms for ceramics are summarized in Table 18.6. A stress–strain curve for a toughened ceramic is shown in Figure 18.17. In this particular case,

TOUGHENING

We want to increase G_c to toughen the ceramic.

TABLE 18.6 Classification of Toughening Mechanisms in Ceramics

General mechanism	Detailed mechanisms
Crack deflection	Tilt and twist out of the crack plane around grains and second-phase additions
Crack bowing	Bowing in the crack plane between second-phase crack-pinning points
Crack branching	Crack may subdivide into two or more roughly parallel cracks
Crack tip shielding by process zone activity	Microcracking Transformation toughening Ductile yielding in process zone
Crack tip shielding by crack bridging	Second-phase brittle fibers with partial debonding Frictional and ligamentary grain bridges Second-phase ductile ligament bridging

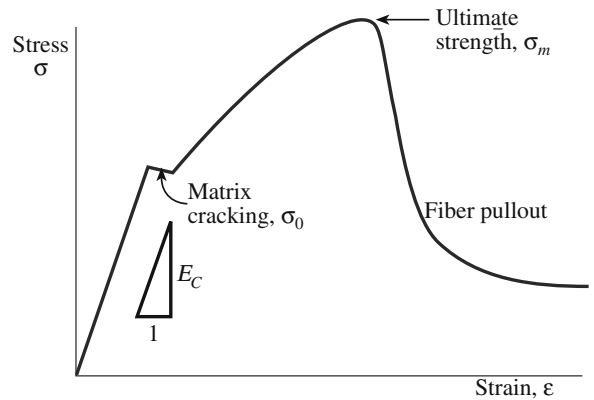


FIGURE 18.17 Schematic stress–strain curve for a tough fiber-reinforced ceramic matrix composite.

reinforcing the ceramic matrix [e.g., a lithium aluminosilicate (LAS) glass ceramic] with fibers (e.g., SiC) produced the desired toughening. The resulting fracture surface would look like that shown in Figure 18.18. Toughening is achieved by bridging of the crack surfaces behind the crack tip by the strong reinforcing phase. The stress intensity at the crack tip is reduced, which slows crack propagation. The fibers absorb energy as the crack front advances. An

additional energy-absorbing process that often accompanies crack bridging is fiber pullout away from the crack plane as

illustrated in Figure 18.19.

The following factors contribute to the fracture toughness of a composite:

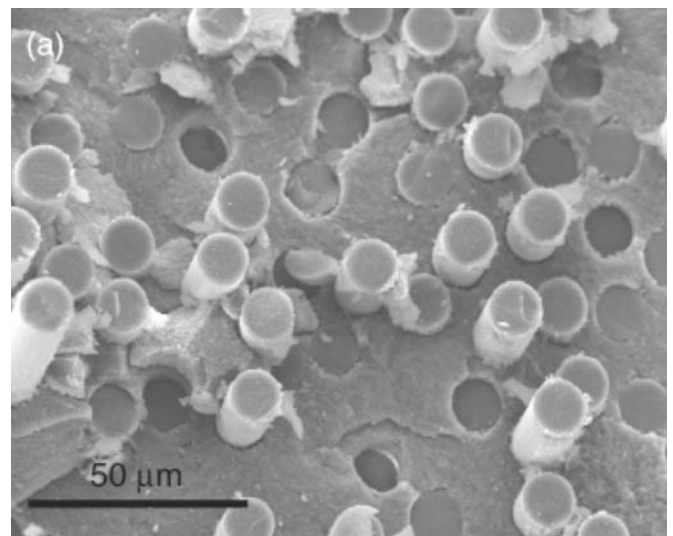


FIGURE 18.18 SEM image showing fiber pullout on the fracture surface of AlPO_4 -coated alumina/mullite fiber/ Al_2O_3 CMC, hot pressed at 1250°C for 1 h.

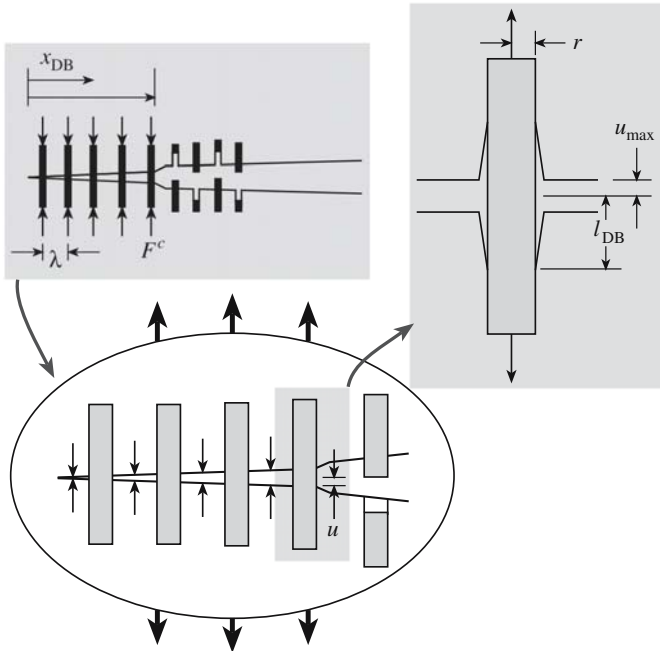


FIGURE 18.19 Illustration of a crack bridging mechanism with debonding and fiber pullout.

- Volume fraction of reinforcement. Figure 18.20 shows how fracture toughness increases for SiC whisker-reinforced ceramics as a function of increasing whisker content.
- Young's modulus of matrix and reinforcement. If a matrix is reinforced with high modulus, high strength fibers then more of the stress can be carried by the fibers.
- Strength of the matrix/reinforcement interface. In fiber-reinforced composites a strong interface can lead to transfer of the stress from the matrix to the fibers; a weak interface can lead to debonding and crack deflection.

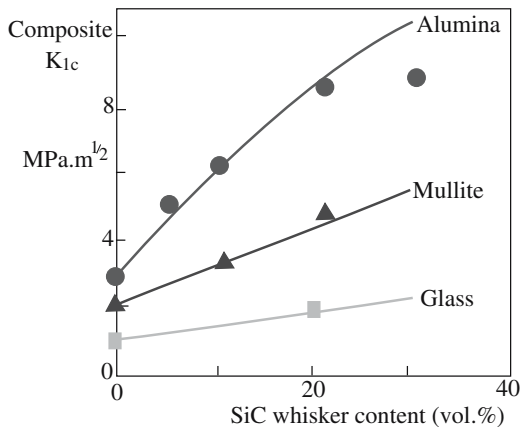


FIGURE 18.20 The effect of SiC whisker content on toughness enhancement in different matrices.

For the specific case in which toughening is due to elastic deformation of a partially debonded reinforcement with no interfacial friction, K_{Ic} has been determined to be

$$K_{Ic} = \sqrt{\{E_c G_m + \sigma_f^2 [(rV_f E_c \gamma_f)/(12E_f \gamma_i)]\}} \quad (18.23)$$

The subscripts c, m, and f refer to the composite, matrix, and reinforcement, respectively. Increases in fracture toughness are predicted by

- Increasing V_f
- Increasing E_c/E_f
- Increasing γ_f/γ_i

The last bullet implies that toughness is enhanced when the interface between the fiber and the matrix is weak. The crack will then pass around the fiber as shown in Figure 18.21.

An important toughening mechanism involves a phase transformation in zirconia (ZrO_2). The best-known example is zirconia-toughened alumina (ZTA), which contains 10–20 vol% of fine ZrO_2 particles. At elevated temperatures the equilibrium structure of ZrO_2 is tetragonal (t) and at low temperatures it is monoclinic (m). On cooling ZTA from the high temperatures required for fabrication the $t \rightarrow m$ transformation may occur in the zirconia particles. This transformation is accompanied by an increase in volume of about 3%.

The transformation is athermal, i.e., it is not time dependent and proceeds very rapidly. If the transformation takes place in the ZrO_2 particles during fabrication of ZTA ceramics, then the 3% volume change produces stresses in the alumina matrix around the transformed particle leading to microcracking. These microcracks increase the toughness of the ceramic by their ability to deflect and

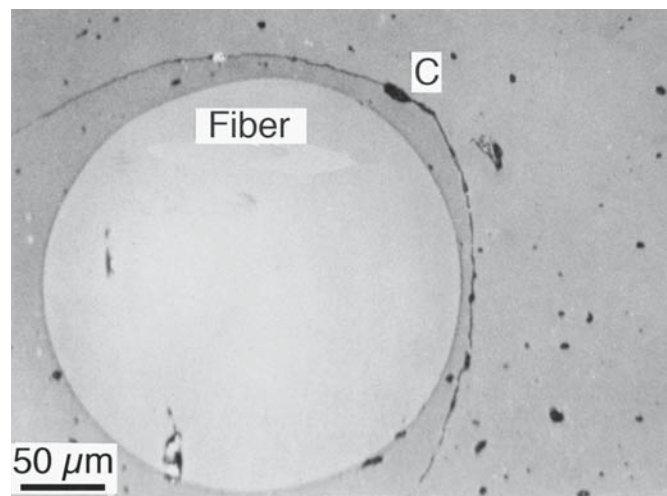


FIGURE 18.21 SEM image showing crack propagation around a saphikon (Al_2O_3) fiber in a calcium aluminosilicate (CAS) glass-ceramic.

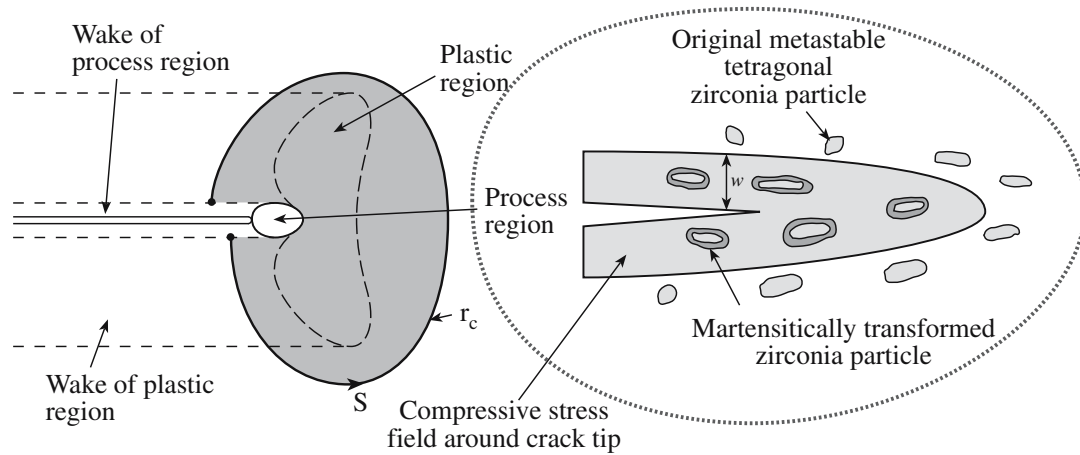


FIGURE 18.22 Illustration of transformation toughening in a ceramic matrix containing ZrO_2 particles.

bifurcate a propagating crack. Control of the extent of the microcracking determines the increase in toughness. The optimum conditions are when the particles are large enough to transform but only small enough to cause limited microcrack development. If microcracking becomes extensive then the cracks can interact resulting in a decrease in strength. Zirconia particle size is controlled by

- Milling prior to sintering
- Aging after sintering

If a stabilizing oxide, say 3 mol% Y_2O_3 , is added to the zirconia then it is possible to suppress the $t \rightarrow m$ transformation on cooling from the fabrication temperature. The ZrO_2 particles can be retained in the metastable tetragonal form at room temperature. Whether the transformation takes place depends on the amount of stabilizing oxide and the particle size. The presence of the alumina matrix makes it difficult for the volume expansion associated with the transformation to be accommodated. The constraint is such that small particles are less likely to transform than large particles. With a suitable combination of amount of stabilizing oxide and particle size it is possible to obtain a dispersion of metastable tetragonal particles.

Under the influence of the stress field at a cracktip these particles will transform athermally to the monoclinic state. This leads to transformation toughening and the toughening increment ΔK_T that can be achieved by this mechanism is

$$\Delta K_T = AV_{ZrO_2} \epsilon_T E_m w^{1/2} \quad (18.24)$$

A is a constant with a value close to unity, V_{zirc} is the volume fraction of the metastable particles, ϵ_T is the volume strain accompanying the transformation, E_m is Young's modulus of the matrix (often alumina), and w is the width of the process zone around a crack containing transformed particles (shown in Figure 18.22).

It is important to note that in contrast to ZTA toughened by microcracking, transformation toughening can lead to an improvement in both toughness and strength and, consequently, is the preferred toughening mechanism.

The effectiveness of the different toughening mechanisms for structural ceramics appears to decrease in the following order:

- Continuous fiber reinforcement—most effective
- Metal dispersed particles
- Transformation toughening
- Whiskers/platelet/particle reinforcement
- Microcracking—least effective

Some examples and associated toughness values are given in Table 18.7. It is worth remembering that although the values are higher, in some cases by an order of magnitude, than for single-phase polycrystalline ceramics, they are still much lower than most engineering metal alloys.

TABLE 18.7 The Effect of Different Toughening Mechanisms

Mechanism	Highest value achieved ($MPa \cdot m^{1/2}$)	Exemplary systems
Continuous fiber reinforced	>30	SiC–SiC; glass–SiC
	>25	Glass-ceramics–SiC
	~16	Si_3N_4 –SiC
Metal dispersed Transformation	~25	Al_2O_3 –Al; Al_2O_3 –Ni
	~20	ZrO_2 (MgO)
Platelet	~14	Si_3N_4 –SiC
Whisker	~11	Si_3N_4 –SiC
	~8.5	Al_2O_3 –SiC
Particle	~8	Si_3N_4 –SiC
	~10	Al_2O_3 – ZrO_2
Microcracking	~10	Al_2O_3 – ZrO_2

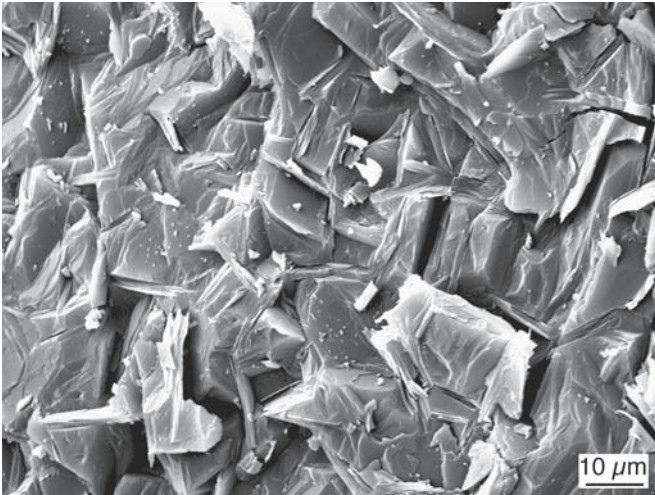


FIGURE 18.23 The fracture surface of Macor®.

18.10 MACHINABLE GLASS-CERAMICS

Machinable glass-ceramics (MGCs) rely on controlled fracture. In Macor®, a commercial MGC made by Corning, the crystalline phase is fluorophlogopite mica. The mica forms as randomly oriented grains in a borosilicate glass matrix. During machining cracks propagate along the glass–mica interface (intergranular) and material is removed. Figure 18.23 shows the fracture surface of Macor® where the mica crystals, which look like packs of cards, can be clearly seen. MGCs can be machined using either high-speed steel or tungsten carbide cutting tools. They can be used at high temperatures (up to 1000°C) and because of their high chemical resistance they are used for precision valves and nozzles in the chemical industry. Table 18.8 lists the composition of Macor® and some of its properties.

TABLE 18.8 Composition (wt%) and Properties of Macor® MGC

SiO_2	Al_2O_3	B_2O_3	K_2O	MgO	F
46	16	7	10	17	4
Property					Value
Coefficient of thermal expansion (ppm/°C)					7.4–12.6
Thermal conductivity ($Wm^{-1}°C^{-1}$)					1.46
Continuous operating temperature (°C)					800
Maximum no-load temperature (°C)					1000
Density (g/cm^3)					2.52
Young's modulus at 25°C (GPa)					66.9
Poisson's ratio					0.29
Shear modulus at 25°C (GPa)					25.5
Knoop hardness, 100g load					250
Modulus of rupture at 25°C (MPa)					94
Compressive strength (MPa)					345
Fracture toughness ($MPa \cdot m^{1/2}$)					1.53

18.11 WEAR

Wear resistance is the ability of a material to resist mechanical (or chemical-mechanical) abrasion. There are two main mechanisms that lead to removal of material from the surface of a ceramic:

- Grain pullout: In polycrystalline ceramics with weak grain boundaries
- Cracking: Fracture due to abrasion, gouging, or erosion

Wear resistance is usually closely associated with hardness and corrosion resistance. For example, Table 18.9 shows how erosion resistance correlates very directly with hardness. Erosion usually specifies wear of a material by an abrasive in a fluid, the type of situation encountered when ceramics are polished.

Although ceramics are generally characterized as being wear resistant their commercial use as wear parts is less than 10% of the overall market.

Alumina is the most commonly used wear-resistant ceramic. One of the early applications was in seal faces for rotary water pumps for automobiles. Alumina is particularly suitable because it is resistant to engine cooling fluids. Another application for alumina, which we mentioned in Chapter 16, is in total hip prosthesis. In terms of wear rates at the contact surfaces between the ball and socket, alumina is far superior to alternative metal and polymer systems.

Alumina and toughened zirconia ceramics are used in the wire drawing industry as capstans, pulleys, and guides. Improved product quality, longer component service life, and lower manufacturing costs have been attributed to the use of ceramics. For example, ceramic capstans last up to 10 times longer than carbide-coated capstans.

As with other mechanical properties there are standard tests to measure wear resistance. The main method is described in ASTM G99, which uses a pin-on-disk apparatus. This test is used to measure sliding wear of ceramics and ceramic coatings.

TABLE 18.9 Erosion Resistance versus Hardness for Several Ceramics

Material (in order of increasing erosion resistance)	Knoop hardness (kg/mm^2)
MgO	370
SiO_2	820
ZrO_2	1160
Al_2O_3	2000
Si_3N_4	2200
SiC	2700
B_4C	3500
Diamond	7000–8000

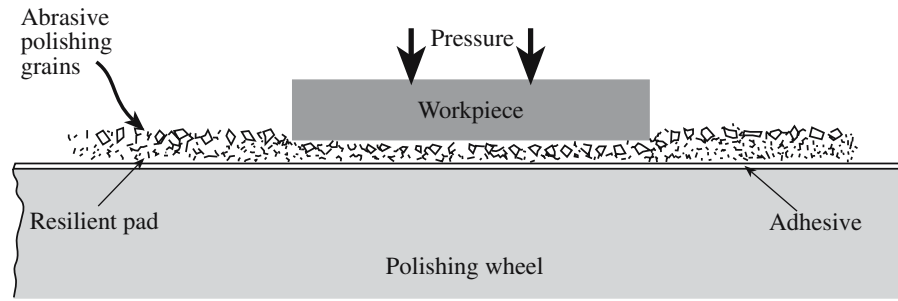


FIGURE 18.24 Illustration of the polishing process using abrasive grains held in a soft pad. This method is the one most often used in university metallography laboratories.

TABLE 18.10 Hardness of Selected Abrasives Used in the Polishing of Ceramics

Abrasive	Mohs hardness	Knoop hardness
Zirconia	8	1160
Garnet	8	1360
Calcined alumina	9	2100
Silicon carbide	9–10	2480
Boron carbide	9–10	2750
Cubic boron nitride	10	4500
Diamond	10	7000

18.12 GRINDING AND POLISHING

Grinding and polishing both use controlled fracture. Abrasives are the basis of an important ceramic industry. For example, the abrasive used in Emory paper is SiC; sand paper uses SiO₂. The historically important abrasive was jeweler's rouge (hematite). Now ceria (CeO₂) is often preferred for glass and ceramics and colloidal silica (e.g., Syton™) is used for Si. Abrasive particles are almost always ceramics (usually oxides, carbides, or diamond). The polishing action actually involves an interaction between two surfaces with the second surface being the abrasive particle. Figure 18.24 illustrates mechanical polishing using abrasive grains held in a soft pad. Table 18.10 lists some of the common abrasives used for polishing ceramics together with their hardness.

The abrasive is often applied as a slurry onto a soft pad. A series of polishing steps are used, with abrasives with decreasing particle size (eventually down to as low as 4 nm). The final step produces a smooth specular surface, which is good enough for film deposition.

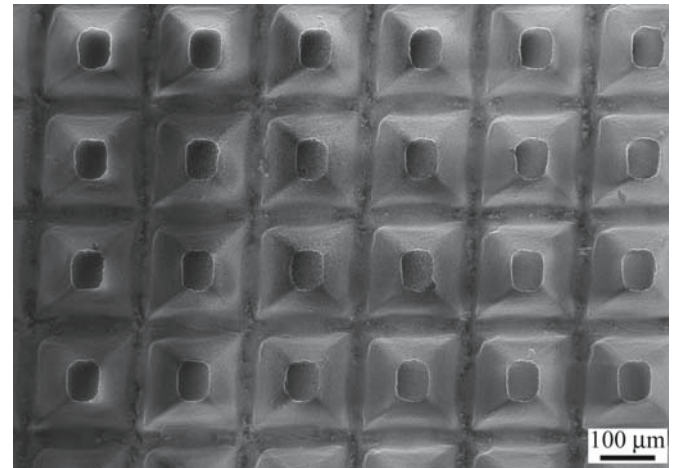


FIGURE 18.25 SEM image of ceria particles in a modern polishing cloth.

Chemical/mechanical polishing (CMP) may also be used. In this case an abrasive is used together with a chemical (usually either an acid or a caustic solution) that will produce an etching action. CMP is actually very complex and still not fully understood. Final CMP may involve an abrasive that is softer than the materials being polished.

An example of a modern commercial polishing cloth is shown in Figure 18.25. The pyramids are particles of ceria bound in a polymer on a flexible cloth. This type of fixed abrasive has an advantage over a slurry in that the abrasive is well controlled and can be easily changed/renewed and there is always a clear channel for the electrolyte to reach the polishing site.

CHAPTER SUMMARY

Although we often think of the brittleness of ceramics as a distinct disadvantage, the very existence of our civilization depended on this property. We make use of brittleness in many applications, such as sculpture and in polishing, but for reliable structural uses we often need better fracture toughness. One way to achieve this is to form a composite by adding some fibers to a ceramic matrix. The fibers provide additional mechanisms for energy absorption during fracture. The key work in understanding brittle fracture goes back to that of Griffith. He showed

that flaws act as stress concentrators, which lead to measured strengths significantly lower than those predicted by theory. The work of Griffith is the link to the Weibull statistics described in Chapter 16. By examining fracture surfaces, a process called “fractography,” we can often determine how and why a brittle material failed. This information can be useful in guiding processing methods to avoid stress concentrators such as porosity and inclusions.

PEOPLE IN HISTORY

Griffith, Alan Arnold (1893–1963), was known as “The Father of Fracture Mechanics” and “Bubble Griffith,” the first for his classic work in fracture mechanics and the role of flaws and the second for his work on soap films. He was a British aeronautical engineer who worked at Rolls-Royce from 1939 to 1960 designing turbojet engines.

Inglis, Sir Charles Edward (1875–1952), professor of Engineering at Cambridge University, was best known for his work on stress in metal plates when cracks are present.

Orowan, Egon (1901–1989) was born in Budapest, Hungary and died in Cambridge, Massachusetts. In addition to his work on fracture, he showed the importance of dislocation in plastic deformation. He joined MIT as a professor in 1950.

GENERAL REFERENCES

Davidge, R.W. (1979) *Mechanical Behaviour of Ceramics*, Cambridge University Press, Cambridge, UK.

Green, D.J. (1998) *An Introduction to the Mechanical Properties of Ceramics*, Cambridge University Press, Cambridge, UK.

Hull, D. (1999) *Fractography*, Cambridge University Press, Cambridge, UK.

Lawn, B. (1993) *Fracture of Brittle Solids*, 2nd edition, Cambridge University Press, Cambridge, UK.

Tabor, D. (2000) *The Hardness of Metals*, Oxford University Press, Oxford, UK. Reprint of the 1959 classic. Very readable.

Wachtman, J.B. (1996) *Mechanical Properties of Ceramics*, Wiley-Interscience, New York.

SPECIFIC REFERENCES

Garvie, R., Hannick, R.H.J., and Pascoe, R. (1975) “Ceramic steel?” *Nature* **258**, 703. First description of transformation toughening.

Griffith, A.A. (1920) “The phenomenon of rupture and flow in solids,” *Phil. Trans. R. Soc. Lond.* **A221**, 163. (1924) “The theory of rupture,” *Proc. 1st Int. Cong. Appl. Mech.* p. 55.

Inglis, C.E. (1913) “Stresses in a plate due to the presence of cracks and sharp corners,” *Trans. Inst. Naval Archit.* **A127**, 219. The Inglis equation (Eq. 18.13).

Johnson, J.W. and Holloway, D.G. (1966) “On the shape and size of the fracture zones on glass fracture surfaces,” *Phil. Mag.* **14**, 731. Also “Microstructure of the mist zone on glass fracture surfaces,” *Phil. Mag.* **17**, 899.

Obreimoff, J.W. (1930) “The splitting strength of mica,” *Proc. R. Soc. Lond.* **A127**, 290. Early study of the fracture of mica (Section 18.3).

Orowan, E. (1949) “Fracture and strength of solids,” *Rep. Prog. Phys.* **12**, 185.

EXERCISES

- 18.1 Carbon nanotubes have been proposed as a material for the next generation of ceramic armor. (a) What are the properties of carbon nanotubes that make them of interest for this application? (b) Are there practical limitations that are currently preventing their widespread use?
- 18.2 Calculate the theoretical strength of MgO. Are there any conditions under which this value would be attainable?
- 18.3 A sharp notch 0.1 mm long is introduced into the surface of a fused silica plate. The plate is then loaded to 100 MPa in tension normal to the notch. (a) Will the plate fracture? (b) If not, what is the applied stress that would lead to fracture? (c) If the plate was made of an LAS glass-ceramic what applied stress would lead to fracture?
- 18.4 A soda-lime silica plate failed at 100 MPa. (a) Estimate the flaw size and state any assumptions you make. (b) If the plate were made of fused silica and contained the same flaw size what is the maximum applied stress it could withstand without breaking? Assume the glass has $\mathcal{E} = 70$ GPa.
- 18.5 A manufacturer of silicon nitride jet engine parts found that a recent batch of samples became damaged during processing and had surface flaws about 50 μm deep. The normal average flaw size in these parts is about 10 μm . (a) Estimate the tensile strength of these samples. (b) Estimate the compressive strength of these samples.

- 18.6 You have been hired as a consultant and asked to choose the best ceramic for a load-bearing application. A vendor has offered you the following options; which one would you take and why? Are there any other factors that you need to consider before you make your final recommendation?

<i>Ceramic</i>	<i>Maximum flaw size (μm)</i>	<i>Average flaw size (μm)</i>
Si_3N_4	20	15
SiC	30	18
MgO	10	7
Al_2O_3	5	3

- 18.7 In Table 18.6 we list different toughening mechanisms for ceramic–matrix composites (CMCs). Illustrate each mechanism using a sketch and, where appropriate, indicate the differences between using particles, platelets, and fibers as the reinforcement.
- 18.8 Explain how the addition of zirconia particles can lead to toughening of a ceramic. Suggest other additions that might produce similar toughening effects.
- 18.9 Draw sketches similar to Figure 18.10 to indicate how (a) ammonia and (b) methanol might lead to stress corrosion cracking in glass.
- 18.10 Figure 18.13a shows the fracture surface of polycrystalline AlN. Can you see any evidence of transgranular failure?

Part VI

Processing

Raw Materials

CHAPTER PREVIEW

In this chapter we look at several important raw materials used in the ceramics industry. Obtaining the necessary raw materials is the first step in the fabrication of ceramic components. This topic used to be addressed by many Departments of Mining and Mineral Engineering. It is no less important today, but few such departments still exist. There are two basic sources for these raw materials:

- Naturally occurring minerals
- Synthetic minerals

For naturally occurring minerals we will describe, in general terms, their origin, the locations in which they can be found, and their relative abundance. Naturally occurring minerals require extraction, which is often a regional industry located close to abundant quantities of the natural deposit. Most minerals need to go through some form of physical or chemical processing before use. The collective term for these processes is *beneficiation*. When you understand how oxides are manufactured, it will be clear why they are often impure and why Si, Na, Ca are the major impurities.

Materials that do not occur in nature or are rare must be synthesized (so calling them minerals is a misnomer) and we describe the processes used for their synthesis. Carbides, nitrides, and borides are becoming more common, but are generally expensive and require special processing environments. For many nonoxides the main impurities are often components of the starting material that have not reacted, e.g., Al in AlN or Si in Si₃N₄.

There are many other raw materials that play important roles in specific ceramics, but rather than providing a comprehensive discussion about every raw material, we focus on representative examples of naturally occurring minerals and synthetic ones. There are two ways of looking at this topic: the mineral we start from and the material we want to form. Here, we mix the two approaches.

19.1 GEOLOGY, MINERALS, AND ORES

Figure 19.1 shows a schematic cross section of the earth. The earth has a mean radius of about 6370 km and consists of three distinct concentric layers. The outermost layer is known as the crust and is relatively thin. The continental crust ranges in thickness from about 20 to 60 km, averaging approximately 30 km. It is the minerals that occur here that are important to us as raw materials for ceramics.

The continental crust is composed primarily of the silicates of Mg, Fe, Al, and Ca, and the alkali metals plus Al and free SiO₂. Table 19.1 lists the abundance of the major elements in the continental crust. From this you can see that O, Si, and Al together account for almost 90 wt% of the elements in the crust.

Beneath the earth's crust is the mantle. This thick layer is thought to be composed of Mg silicates

and Fe silicates, free Fe, and minor Fe sulfides. Minerals in the mantle (and the core) are presently not accessible; for this reason we will not discuss them further. However, geologists can identify rocks that have moved from the mantle to the crust by natural processes. An ore is defined as a mineral from which a constituent can be profitably mined or extracted. Examples include hematite (Fe₂O₃), which is the major ore of Fe, and ilmenite (FeTiO₃), which is the major ore of Ti, but is also an Fe-containing mineral. Pyrophanite (MnTiO₃) is neither a Ti nor Mn ore, but is actually a rare mineral.

19.2 MINERAL FORMATION

Minerals are the constituents of rocks, which make up the entire inorganic,

MINES
The deepest mine is ~5 km deep.

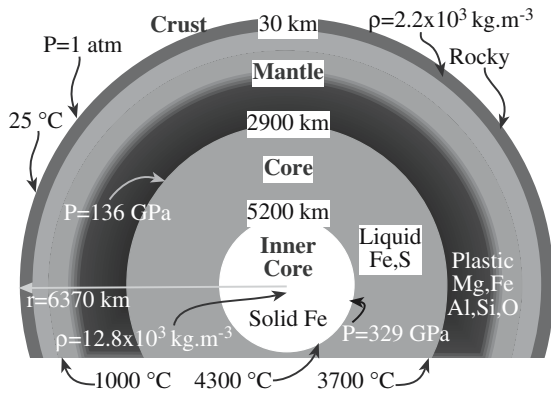


FIGURE 19.1 Schematic cross section of the earth.

TABLE 19.2 Major Oxides in Igneous Rocks and Their Ranges of Composition

Constituent (oxide)	Concentration (wt%)
SiO ₂	30–78
Al ₂ O ₃	3–34
Fe ₂ O ₃	0–5
FeO	0–15
MgO	0–40
CaO	0–20
Na ₂ O	0–10
K ₂ O	0–15

solid portion of the earth. Rocks are usually not composed of a single mineral; rather they are an aggregate of two or more minerals. Broadly speaking, geologists divide rocks into three types: igneous, metamorphic, and sedimentary.

Igneous rocks form when magma cools and solidifies. Magma is a complex molten material that originates deep within the earth. The word igneous comes from the Latin word *ignis*, which means “fire”; igneous rocks then are “formed from fire.” Magma is rich in the elements Si, O, Al, Na, K, Ca, Fe, and Mg. Table 19.2 shows the composition ranges for the major elements (expressed as oxides) in igneous rocks. These are the elements that when combined with SiO₂ form the silicate minerals. A limited number of silicate minerals accounts for over 90% of all igneous rocks.

All silicate minerals contain tetrahedral silicate [SiO₄] groups. Classification of the silicate minerals is based upon the way in which these groups combine, as described in Chapter 7.

The specific mineral crystallizing from magma depends both on the composition and temperature of the magma. The order of crystallization of the main silicate minerals is given by Bowen’s reaction series, which is shown in

TABLE 19.1 Abundances of the Major Elements in the Continental Crust

Element	wt%	at%	vol% of ion
Oxygen	47.2	61.7	93.8
Silicon	28.2	21.0	0.9
Aluminum	8.2	6.4	0.5
Total Iron	5.1	1.9	0.4
Calcium	3.7	1.9	1.0
Sodium	2.9	2.6	1.3
Potassium	2.6	1.4	1.8
Magnesium	2.1	1.8	0.3
Hydrogen	trace	1.3	0.0

IGNEOUS ROCK

- Granite*: magma cooled near the earth’s surface
- Rhyolite*: fine grain granite
- Obsidian*, pumice and scoria: volcanic origin
- Basalt*: very small grains of usually rapidly cooled lava
- Gabbro*: like basalt, but has larger grains
- Mafic*: dark igneous (e.g., basalt)
- Intermediate*: e.g., diorite; Mg and Fe rich
- Felsic*: light igneous (e.g., granite); quartz rich

Figure 19.2. Olivine and Ca feldspar form at high temperatures and may separate early from the melt. Other minerals solidify as the temperature falls. The last minerals to crystallize are K feldspar, muscovite mica, and quartz, the major constituents of granite. Finally, water in the magma

carries metals and S in solution through cracks in the surrounding rock and deposits them as sulfides in veins.

Metamorphic rocks have undergone structural and/or chemical transitions (metamorphism or metamorphosis)

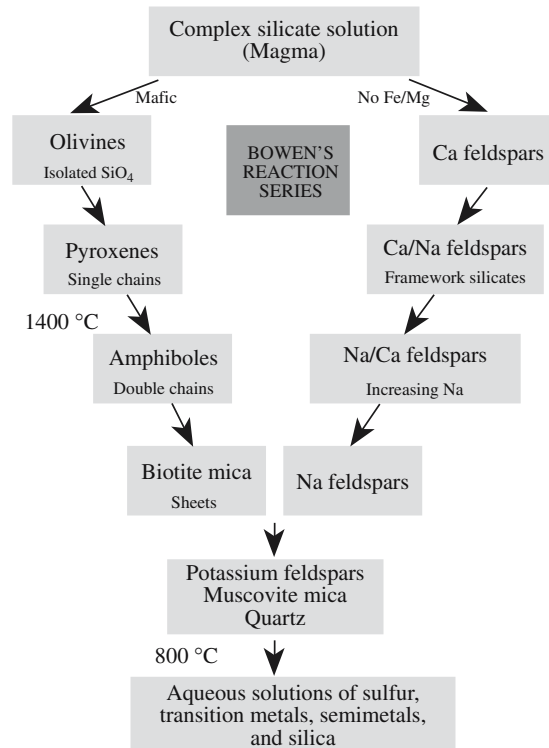


FIGURE 19.2 Bowen’s reaction series.

from their original form as a result of high temperatures and pressures deep beneath the earth's surface. These transitions occur in the solid state without melting and result in the formation of new minerals, such as kyanite, staurolite, sillimanite, andalusite, and some garnets. Other minerals, such as some of the igneous minerals, may be present in metamorphic rocks, although they are not necessarily the result of metamorphism.

The word "metamorphic" has a Greek origin coming from *meta* meaning "change" and *morphe* meaning "shape."

Sedimentary rocks are formed when small particles or precipitated crystals become cemented together. Sedimentary rocks are classified as either clastic or chemical.

Clastic sedimentary rocks form when rock particles produced by mechanical and chemical weathering are transported by water, ice, and wind to new locations where they become cemented together.

Chemical sedimentary rocks form when highly soluble ions, such as Na^+ , K^+ , Ca^{2+} , Mg^{2+} , Cl^- , F^- , $(\text{SO}_4)^{2-}$, $(\text{CO}_3)^{2-}$, and $(\text{PO}_4)^{3-}$, from existing rocks are dissolved in water and subsequently precipitate forming layers in oceans and lakes where they become cemented together. The composition of sedimentary rocks depends on the

- Composition of the original source rocks
- Chemical and mechanical resistance of each mineral component
- Distance traveled

Resistant minerals such as quartz are common constituents of sedimentary rocks, and some more rare minerals (e.g., garnet, rutile, and zircon) have similar properties. Feldspar is less resistant, but is so common that it is a major constituent of many sedimentary rocks. Precipitated minerals include the carbonates (e.g., calcite and dolomite), sulfates (e.g., gypsum and anhydrite), chlorides, and chalcedonic silica (e.g., chert and flint).

The three rock types are compared below; Figure 19.3 shows what is called the rock cycle.

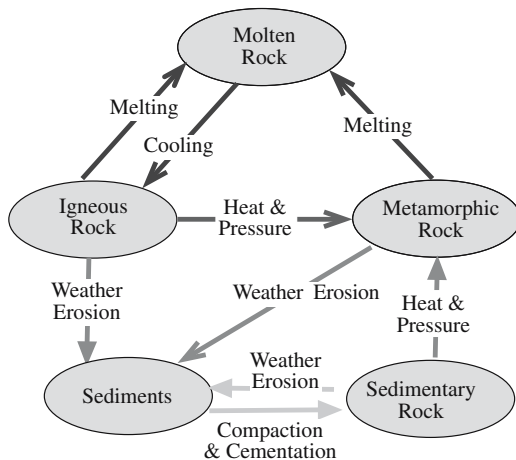


FIGURE 19.3 Simplified diagram of the rock cycle.

Igneous	Rocks are formed by cooling and solidification of magma.
Metamorphic	Rocks have undergone structural and/or chemical transitions.
Sedimentary	Rocks are formed when smaller particles become cemented.

19.3 BENEFICIATION

Beneficiation is the process through which most minerals need to go before they can be used to produce ceramics. Physical beneficiation includes crushing and grinding of coarse rocks. The particle size of the raw material may affect subsequent steps in the production process. An example that we use is producing alumina from bauxite, a process that involves a chemical reaction.

Chemical beneficiation includes processes of separating the desired mineral from unwanted waste products, for example, by dissolution in a suitable solvent followed by filtration. The Bayer process for producing alumina is also a good example of chemical beneficiation. Bauxite contains many impurities.

The purity of the raw materials will be reflected in the composition of the final product. For many ceramics careful control over purity is required. For these applications the raw materials are synthesized. Furthermore, several important ceramics do not occur naturally in mineral form and must be fabricated chemically. Synthesis of ceramic powders can have advantages not only in purity but also in allowing the generation of fine particle-sized powders having a well-defined morphology. We will show in Chapter 24 the importance of particle, size on the densification of a ceramic component by sintering.

19.4 WEIGHTS AND MEASURES

The SI unit of mass is the kilogram (kg), which is interesting for a few reasons. It is the only basic SI unit defined with a prefix (*kilo*) already in place, and it is the only one defined by reference to a physical object—a mass of platinum-iridium held at Sevres in France. To express the large quantities of material that we encounter in the extraction and processing of ores it is usual to use the metric ton (sometimes written tonne: symbol t):

$$1 \text{ t} = 1 \text{ Mg} = 10^3 \text{ kg}$$

Possible confusion exists because of special British and U.S. units that are still in use in these countries.

$$1 \text{ t} = 0.984 \text{ UK (long) ton}$$

$$1 \text{ t} = 1.103 \text{ US (short) ton}$$

The situation is even more complicated in the UK where the short ton is often used in mining

metal-containing ores, but the long ton is used in coal mining. We will use the metric ton (written simply as ton) unless specifically stated otherwise. You can see that for “ballpark” estimates of mass it really does not make much difference. When we discuss single crystals in Chapter 29 we will introduce units of mass that are used to describe very small quantities of a material.

Determining the quantity of all commercial minerals produced is straightforward. The United States Geological Survey maintains updated information on their website in the form of Mineral Commodity Summaries and the Minerals Yearbook. These sources provided most of the numbers given in this chapter. Obviously, like all commodities, the production of minerals may vary from year to year based on many different factors such as supply, demand, and reserves. The problems at the end of this chapter will help you think about some of those factors for specific minerals.

19.5 SILICA

Silica (SiO_2) is an important raw material for ceramics. The major use (accounting for about 38% of U.S. production) is in glass manufacture. For example, incandescent lamp bulbs are made of a soda-lime silicate glass containing about 70 wt% SiO_2 . The SiO_2 content of high-quality optical glasses can be as high as 99.8 wt%.

A major source of silica is sand. Industrial sand and silica sand are two terms used by the ceramics industry for sands that have a high percentage of SiO_2 . In some of the high-quality silica sand sources mentioned below the SiO_2 content is >99.5%.

Sand is defined by the American Society for Testing and Materials (ASTM) as granular rock particles that pass through a No. 4-mesh (4.75-mm aperture) U.S. standard sieve, are retained on a No. 200-mesh (75- μm aperture) sieve, and result from the natural disintegration or comminution of rock. Sands are also produced by physical beneficiation of rocks by crushing. These sands have various chemical compositions, determined by the type of rock being mined.

The United States is the largest producer of industrial sand in the world. The states of West Virginia, California, Illinois, Pennsylvania, Ohio, and New Jersey supply about 80% of all the high-quality silica sand used domestically. In Illinois and Missouri, practically all the glass-grade silica is derived from the St. Peter sandstone formation. Other quality deposits are the Oriskany sandstone deposits in West Virginia and Pennsylvania. Deposits are usually found in dune forms or in deposits lying 20–30 m under layers of silts, clays, and shales.

The mining of industrial silica is, in general, a regional market. Unless the material possesses unique characteristics,

TABLE 19.3 Abundance of Minerals in the Earth's Crust

Mineral groups	vol%
Feldspars	58
Pyroxenes, amphiboles	13
Quartz	11
Micas, chlorites, clay minerals	10
Carbonates, oxides, sulfides, halides	3
Olivines	3
Epidotes, aluminosilicates, garnets, zeolites	2

such as a certain grain size or shape, the geographic market of a plant rarely extends beyond 200 miles. This is because of the high transportation cost relative to the price of the materials and the extensive location of mines.

In recent years, environmental regulations have been placed on the mining of silica sand due to health risks associated with this product.

Quartz, the principal silica mineral, is a constituent of igneous rocks such as granite. It is also found in most metamorphic rocks, comprising a major portion of the sandstones, as well as in the pure form in veins running through other rocks. Optical quality quartz crystals are quite rare, but there are economically viable methods to produce quartz crystals as we will see in Section 29.11.

19.6 SILICATES

We discussed the silicates in Chapter 7. Here we discuss the use of these materials to form commercial ceramics.

Feldspar	70% is used for glass.
Kaolin	It is used in fine china, paper, and rubber.
Mica	Over 200,000t of low-quality mica is used each year.
Mullite	600,000t is used each year for refractory furnace blocks.

Feldspar

Feldspars constitute an abundant mineral group and make up an estimated 60% of the earth's crust, as shown in Table 19.3. They are present in many sedimentary deposits and are found in almost all igneous and metamorphic rocks.

The glass industry uses most of the feldspar produced. Feldspar is a source of Al_2O_3 , which improves the mechanical properties of glass such as its scratch resistance and its ability to withstand thermal shock. It is also used in whiteware bodies as a flux, which produces a glassy phase during firing increasing the strength and translucency of the body.

The Republic of Korea is the largest producer of feldspar in the world. Annual feldspar produc-

SILICA PRODUCTION

Annual production of silica in the United States is approximately 30 Mt, valued at around \$700 million.

tion in the United States is about 800,000t with a value of about \$45 million. The largest producing states are North Carolina, Connecticut, and California. The typical procedure for processing feldspar deposits is

- Drilling and blasting at the quarry
- Transporting to a mill for crushing and grinding (physical beneficiation)
- Froth flotation separating the minerals according to their relative wettability in aqueous solution (chemical beneficiation)
- Drying
- Grinding to a No. 20 mesh (841 μm aperture size) for glassmaking and below a No. 200 mesh (aperture size 74 μm) for most other ceramic applications

In the froth flotation process, air is bubbled through a water suspension containing the crushed minerals to form a foam or froth. The wetted particles (those that are hydrophilic) remain in the water suspension, whereas hydrophobic particles collect at the air bubble/water interface and can be removed from the liquid. Various agents, such as amino acids (having a high molecular weight), can be used to enhance the relative wettability of the solids in a mixture; these agents are adsorbed selectively on the surface of certain species in the mixture. The process is carried out in stages:

1. Remove mica
2. Remove iron-bearing minerals, especially garnet
3. Separate feldspar from a residue consisting mainly of quartz

Clays and Kaolin

Clay is the primary ingredient in traditional ceramics and is the general name given to the layer silicates with a grain size < 2 μm. Any of the layer silicates could qualify as a clay mineral. There are six types of commercial clays and these are listed in Table 19.4. They

are distinguished by their composition, plasticity, color, and firing characteristics.

Mechanical and chemical weathering of feldspars in igneous and metamorphic rocks forms kaolin, a key ingredient in China clay. It may be disintegrated *in situ* or transported by water or wind and redeposited elsewhere. Primary kaolin deposits are located at the site of the original rock. These typically contain large amounts of quartz and mica, which also formed during weathering. Large, primary kaolin deposits are found in southwest England, the Ukraine, and China.

Secondary kaolins were washed from the original weathering site, naturally beneficiated, and redeposited in large areas of pure kaolin. The major commercial deposits of secondary kaolin in the United States were formed 50 million years ago and occur as a continuous belt stretching along the ancient coastline from Alabama northeast to North Carolina.

Mica

The mica group consists of 37 minerals, known as phyllosilicates, which have a layered or platy texture. The Greek word “phylon” means leaf. Some of the mica minerals are listed in Table 19.5 together with the location of their principal sources. The micas are

classified as either true or brittle.

True micas contain univalent cations (e.g., Na⁺ or K⁺) between each set of layers and show perfect basal cleavage, allowing the crystals to be split into thin sheets. The cleavage flakes are flexible and elastic.

In brittle micas, the interlayer cations are divalent (e.g., Ca²⁺). The bond is stronger and although the layered structure still imparts basal cleavage they are more brittle. Brittle micas are uncommon minerals and not of any real interest.

Muscovite is the principal mica used because of its abundance and superior electrical properties. Phlogopite

MICA

The commercially important mica minerals are muscovite and phlogopite.

TABLE 19.4 Commercial Clays, Their Main Uses, and Annual U.S. Production

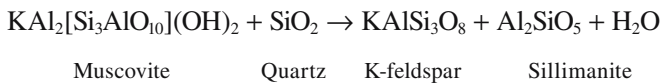
Type	Main uses	Annual U.S. Production (Mt)	Comments
Ball clay	Floor and wall tiles	1.3	Also called “plastic clay” because it improves workability
Bentonite	Sanitary ware	4.4	The United States imports bentonite from Canada
	Foundry sand bond		
Common clay	Absorbents	26	Also called “brick clay” Red color comes from iron
	Bricks		
Fire clay	Cement	0.3	Fireclay refractories contain 25–45% alumina
Fuller’s earth	Refractories	3.2	Textile workers (or “fullers”) cleaned raw wool by kneading it in a mixture of water and fine earth, which adsorbed oil, dirt, and other contaminants
Kaolin	Absorbents	7.2	Kaolinite is a hydrous aluminum silicate; kaolin is a white firing clay, primarily composed of kaolinite
	Paper		

TABLE 19.5 Principal Sources and Occurrence of Mica Minerals

Mineral	Chemical formula	M, H, or O	Type	Source
Muscovite	$KAl_2(Si_3Al)O_{10}(OH)_2$	M	True	United States, India, Brazil, Russia
Phlogopite	$KMg_3(AlSi_3O_{10})(OH,F)_2$	M,H	True	Madagascar, Canada, Mexico, Sri Lanka
Paragonite	$NaAl_2(Si_3Al)O_{10}(OH)_2$	M	True	United States, Switzerland, Italy
Biotite	$K(Mg,Fe)_3(Al,Fe)Si_3O_{10}(OH,F)_2$	M,H	True	United States, Canada, Ireland, Scotland
Lepidolite	$K(Li,Al)_3(Al,Si)_4O_{10}(F,OH)_2$	M,H,O	True	United States, Canada, Brazil, Sweden
Zinnwaldite	$KLiFeAl(AlSi_3O_{10})(F,OH)_2$	M	True	United States, Brazil, Scotland, Germany
Margarite	$CaAl_2(Al_2Si_2O_{10})(OH)_2$	M	Brittle	United States, Scotland, Italy, Austria
Clintonite	$Ca(Mg,Al)_3(Al_3Si)O_{10}(OH)_2$	M	Brittle	United States, Italy, Finland, Russia

is stable at higher temperatures and is used in applications in which a combination of high heat stability and electrical properties is required. Both are used in sheet and ground forms.

Micas occur in igneous, sedimentary, and metamorphic rocks in a great many contrasting geological environments. The reason for this range of occurrence is their wide thermal stabilities. Figure 19.4 shows a pressure–temperature diagram for muscovite mica. At very high temperatures (>600°C) it becomes unstable, breaking down in the presence of quartz to give potassium feldspar and sillimanite.



Muscovite occurs in low-grade metamorphic rocks where it forms from pyrophyllite ($Al_4[Si_8O_{20}](OH)_4$) and illite ($K_{1-1.5}Al_4[Si_{7-6.5}Al_{1-1.5}O_{20}](OH)_4$). It also occurs as a primary crystallizing mineral in igneous rocks, such as granites and pegmatites, and is a common constituent of sedimentary rocks, especially the arenites. Muscovite mica is locally common in many parts of the United States.

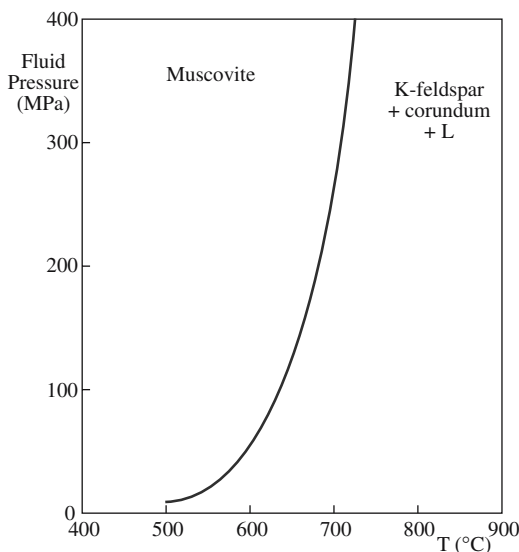


FIGURE 19.4 Pressure–temperature phase relations for the bulk composition $K_2O \cdot 3Al_2O_3 \cdot 6SiO_2 - 2H_2O$.

The largest producer of mica is Russia, which produces about one-third of the world’s annual supply of 300,000t. The United States produces about 75,000t of scrap and flake mica each year. Although historically the United States was a producer of sheet mica, domestic reserves have declined to zero and commercial production is all scrap and flake.

The principal use for ground mica is as a filler and extender in gypsum wallboard joint compounds where it produces a smooth consistency, improves workability, and prevents cracking. It is also found in paints, molded rubber products including tires, and toothpaste. Mica flakes are being used as a replacement for asbestos in brake linings and clutch facings.

India is the largest producer of muscovite sheet mica. Madagascar is the principal supplier of phlogopite sheet mica. The prices for sheet mica range from less than \$1/kg for low-quality material to more than \$2,000/kg for the highest quality. High-quality muscovite mica is used as a dielectric in capacitors.

Mullite

Mullite ($3Al_2O_3 \cdot 2SiO_2$) does not exist in nature in large quantities and must be produced synthetically. It has many properties that make it suitable for high-temperature applications. Mullite has a very small coefficient of thermal expansion (giving it good thermal shock resistance) and is creep resistant at high temperature. Most importantly, it does not react readily with molten glass or with molten metal slags and is stable in the corrosive furnace atmosphere. Hence it is used as a furnace lining and other refractory applications in the iron, steel making, and glass industries.

There are two commercial approaches to producing mullite:

- Sintering
- Fusing

Sintered mullite may be obtained from a mixture of kyanite (Al_2OSiO_4), a naturally occurring mineral found in metamorphic rocks, bauxite, and kaolin. This mixture (in the correct ratio) is sintered at temperatures up to about 1600°C. The sintered quality contains 85–90% mullite

with the balance being mainly glass and cristobalite (a crystalline polymorph of SiO₂). South Africa is the major producer of kyanite, about 165,000t/year. The United States has the largest resource of kyanite and these are located mainly in the Appalachian Mountains region and in Idaho. Andalusite and sillimanite are other aluminosilicate minerals, similar to kyanite, that can be used as a raw material for mullite.

By fusing the appropriate amounts of alumina and kaolin together in an electric-arc furnace at about 1750°C a higher purity mullite can be made. The fused product contains >95% mullite, the rest being a mixture of alumina and glass.

19.7 OXIDES

The raw materials used for oxide ceramics are almost entirely produced by chemical processes to achieve a high chemical purity and to obtain the most suitable powders for component fabrication. The important oxides are summarized in Table 19.6 and are discussed individually.

Alumina

Aluminum oxide (Al₂O₃, alumina, corundum) is the most widely used inorganic chemical for ceramics and is produced from the mineral bauxite using the Bayer process. Bauxite is a mixture of hydrated aluminum oxide with iron oxide (Fe₂O₃), silica (SiO₂), and titania (TiO₂) impurities. It results from the decay and weathering of aluminous rocks, often igneous, under tropical conditions. Like kaolin, bauxite occurs as both primary deposits and secondary deposits.

The Bayer process produces a nominal 99.5% Al₂O₃ product. The alumina can be prepared in a range of grades to suit specific applications. The grades differ by the size and shape of the crystals and the impurity content. The dominant impurity, accounting for up to 0.5%, is Na₂O. The crystal size can be adjusted to measure between 0.1 and 25 μm. Figure 19.5 shows a refinery that produces alumina from bauxite using the Bayer process.

The steps in the Bayer process are as follows:

Physical beneficiation: The bauxite from the mine is first ground, fairly coarsely, to a particle size of <1 mm. Grinding increases the total surface area of the particles, leading to a reduction in the processing time for the chemical reaction in the following step.

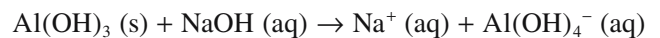
TABLE 19.6 Oxide Raw Materials

Alumina	Refractories, abrasives, substrates
Ceria	Catalysts, fuel cells, polishing (CMP)
Ferrites	Magnets
Magnesia	Refractories
Rutile and anatase	Paints
Zincite	Rubber, adhesives, varistors
Zirconia	Additives, furnace components



FIGURE 19.5 Alcoa refinery in Wagerup, Western Australia that supplies 15% of the world's alumina.

Digestion: The coarsely ground bauxite is treated with a sodium hydroxide (NaOH) solution at 150–160°C and 0.5 MPa total pressure. Most of the hydrated alumina goes into solution as sodium aluminate:



Filtration: The solid impurities, mainly SiO₂, TiO₂, and Fe₂O₃, remain undissolved and are separated by filtration.

Precipitation: After cooling, the filtered sodium aluminate solution is seeded with very fine gibbsite [a naturally occurring hydrated alumina, α-Al(OH)₃] and at the lower temperature the aluminum hydroxide reforms as the stable phase. Reducing the pH by bubbling CO₂ through the solution encourages precipitation.

Washing: The precipitate is filtered and washed to reduce the sodium content.

Calcination: The powder is calcined at temperatures in the range 1100–1200°C to convert the hydroxide to the oxide:



At this stage the alumina is in the form of agglomerates of small grains about 5–10 μm in diameter.

Milling: The powder is then milled to give the desired particle size and particle size distribution. The alumina produced in this way contains ≥99.5% Al₂O₃ and, as mentioned earlier, the major impurity is Na₂O. The powder may also contain small amounts, on the order of 0.001%, SiO₂. This level of purity is sufficient for many

TABLE 19.7 Composition of Calcined Aluminas

	Normal Na ₂ O (wt%)	Low Na ₂ O (wt%)	Reactive (wt%)
Al ₂ O ₃	98.9–99.7	99.5–99.8	>99.5
SiO ₂	0.02–0.05	0.07–0.12	0.04–0.08
Fe ₂ O ₃	0.04–0.05	0.04–0.06	0.01–0.02
Na ₂ O	0.3–0.6	<0.13	0.08

applications. Careful control of the precipitation conditions, thorough washing of the precipitate, and control of the calcination/milling conditions can give aluminas of up to 99.99% purity. The cost of normal calcined alumina is about \$0.60/kg and can go up to over \$2.00/kg for higher purity calcined aluminas. The price for metallurgical-grade (suitable for conversion into Al) alumina is around \$150/t.

Table 19.7 gives typical compositions of the main forms of calcined aluminas. The presence of Na₂O can be unacceptable. For example, the Na⁺ ion is mobile in an electric field and causes degradation of electrical insulation. Also during high-temperature processing a sodium β-alumina (Na₂O · 11Al₂O₃) phase can form that leads to a reduction in density, strength, thermal shock resistance, and corrosion resistance of the final product. Table 19.8 shows the Na₂O content required for various applications of calcined alumina prepared by the Bayer process.

Australia is the world's largest producer of bauxite, producing almost 60 Mt per year. The major regional producer of bauxite in the United States is Arkansas, with smaller deposits in Georgia, Alabama, and Mississippi. Domestic mines supply less than 1% of the U.S. bauxite requirement and hence the United States is a major importer of bauxite, importing over 10 Mt/year.

Of all the bauxite mined about 95% is converted to alumina. World production of alumina is about 50 Mt/year. The majority (about 90%) of the alumina is used for the production of aluminum; most of the rest goes into nonmetal uses such as specialty aluminas. It is this latter quantity that is of interest to us in ceramics. The primary suppliers of specialty aluminas in the United States are Alcoa, Alcan, Aluchem, LaRoche, and Reynolds.

TABLE 19.8 Soda Contents Required of Calcined Aluminas in Commercial Applications

Application	Median crystal size (μm)	Na ₂ O content range (%)
Electronic ceramics	<0.5–5	<0.02–0.1
Sodium vapor lamps	<0.5	<0.02–0.1
Structural ceramics	<0.5–5	0.02–>0.4
Fused abrasives	<0.5–1	0.2–>0.4
Ceramic fibers	<0.5–1	0.2–>0.4
High-technology refractories	0.5–3	<0.1–0.25
Spark plugs	2.5–>5	0.02–0.2

High-purity aluminas can also be prepared directly from aluminum metal, of which there are several routes as shown in Figure 19.6.

Magnesia

Magnesium oxide (MgO, magnesia) occurs naturally as the mineral periclase, a metamorphic mineral formed by the breakdown of dolomite, CaMg(CO₃)₂, and other magnesium minerals. Occurrences of periclase are rare and are of no commercial importance. The principal commercial sources of MgO are magnesite (MgCO₃) and magnesium hydroxide [Mg(OH)₂].

Major deposits of magnesite occur in many countries including China, Turkey, and Russia. The magnesite contains varying amounts of impurities including silica, iron, aluminum, manganese, and calcium, usually present in the form of various minerals, for example, quartz, talc, mica, and magnetite. After mining the ores must be beneficiated. The methods for beneficiation vary, for example, crushing, screening, washing, magnetic separation, and froth floatation.

After the impurities have been separated the magnesium carbonate is calcined. Calcining at temperatures between 800 and 900°C produces a very reactive fine-grained MgO called caustic magnesia. Sintered, or dead burned, magnesia is obtained by calcining the magnesium carbonate at temperatures above 1700°C. During this process the reactive crystals grow and lose their activated state.

Magnesia can be produced from seawater and magnesium-rich brines. About 60% of the U.S. production

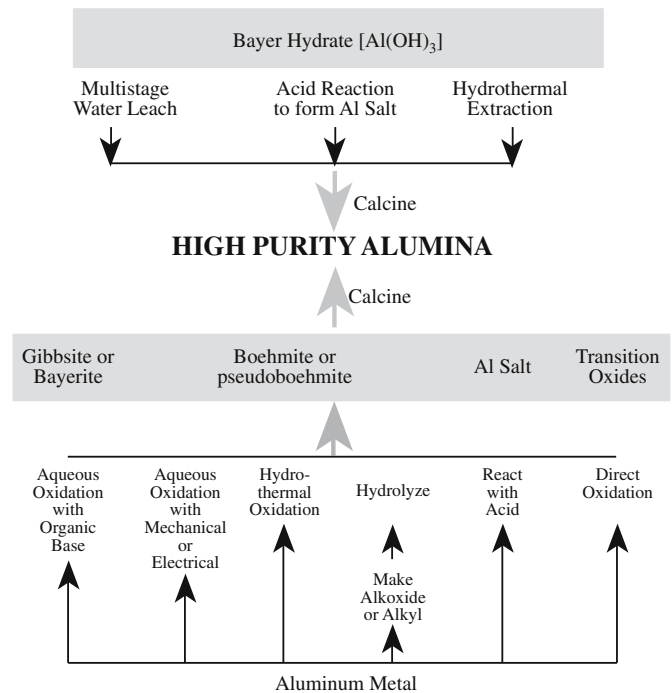
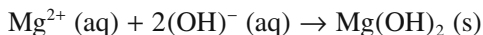


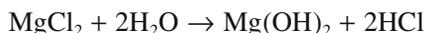
FIGURE 19.6 High-purity alumina production routes.

of magnesium compounds is from these sources. Seawater contains about 1.28 g Mg²⁺/kg. The most important process for the production of MgO from seawater is precipitation of magnesium hydroxide [Mg(OH)₂] from solutions of magnesium salts by a strong base:



The Mg(OH)₂ precipitate is washed, filtered, and calcined to produce MgO.

Another means of obtaining magnesia is from brines. This process is based on the decomposition of MgCl₂ at 600–800°C:



World magnesia production capacity is about 10 Mt/year: ~9.0 Mt from natural magnesite and ~1.5 Mt from seawater and brines. Prices for magnesia range from \$150/t to more than \$1200/t depending on purity.

The major application for magnesia is as a refractory lining in furnaces. In lesser quantities, it is made into a well-known milky solution and ingested. It is also used to manufacture other ceramics such as chrome-free spinels. Nonchrome spinel is not available in nature on an industrial scale. At Asahi Glass, spinel is produced by electrofusing magnesia with alumina.

Zirconia

Zirconium dioxide (ZrO₂, zirconia) is principally derived from zircon, ZrSiO₄, which occurs in igneous rocks such as granites and pegmatites. Decomposed pegmatites have been worked for zircon in Madagascar and Brazil. Zircon is also a constituent of some metamorphic rocks and also occurs as secondary deposits in beach sands in Australia, Brazil, India, and Florida. In these secondary deposits, which have been worked commercially, the zircon occurs together with other minerals such as ilmenite, rutile, and monazite.

There are a number of commercial approaches to producing pure zirconia from zircon. Zircon dissociates above 1750°C into ZrO₂ and SiO₂. Injection of zircon sand into a plasma (at temperatures >6000°C) results in dissociation and melting. The zirconia solidifies first, in the form of dendrites, and the silica solidifies as a glassy coating on the zirconia. The silica may be removed by leaching in boiling sodium hydroxide solution. The residue is washed and the zirconia is removed by centrifuging.

The main production method for zirconium oxide is electric arc melting of zircon between 2100 and 2300°C. Dissociation still occurs at these lower temperatures, but solid zirconia is produced along with liquid silica. The purity of the ZrO₂ produced is about 99%.

Another, although commercially less significant, source of zirconia is baddeleyite (impure monoclinic ZrO₂). Baddeleyite is found in small deposits and usually contains contaminants such as silica, iron oxide, and

titanium. Baddeleyite deposits are mined commercially in Brazil and South Africa.

Zirconium ores all contain varying amounts of hafnium, typically 1.5–3 wt% of the Zr content. As a result of the chemical similarity of Hf to Zr, separation techniques are expensive. Unless specifically required separation is not performed and technical grade zirconia is sold containing up to 3 wt% Hf.

Zincite

Zinc oxide (ZnO) occurs naturally as the mineral zincite. Chemically pure ZnO is white. Zincite is red because it contains up to 10% Mn; traces of FeO are usually also present. Naturally occurring sources of zincite are not commercially important. There are two production methods for forming zinc oxide:

- Oxidation of vaporized zinc metal in air
- Reduction of sphalerite (ZnS) with carbon and CO

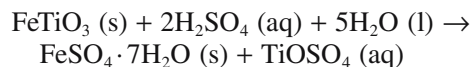
Sphalerite is a naturally occurring mineral and the most important ore of zinc. Large deposits are found in limestone of the Mississippi Valley, around Joplin, MO and Galena, IL. Significant deposits are also found in France, Mexico, Spain, Sweden, and the UK.

The largest consumers of ZnO are the rubber and adhesives industries. Zinc oxide is also found in some latex paints, tiles, glazes, and porcelain enamels, and is the most widely used material in the manufacture of varistors.

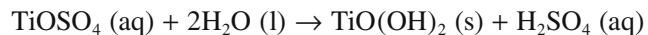
Rutile and Anatase

Rutile (TiO₂, titania) occurs as a constituent of igneous rocks such as granites and also in metamorphic derivatives such as gneiss. It also occurs as fine needles in slates, biotite mica, quartz, and feldspar. Economically the most important deposits are segregations in igneous rocks as found in Virginia, Canada, and Norway. Rutile is also an important constituent of beach sands resulting from denudation of rutile-bearing rocks, as in Australia, Florida, and India.

Titania is also produced by reacting ilmenite FeTiO₃ with sulfuric acid at 150–180°C to form titanyl sulfate, TiOSO₄:



Titanyl sulfate is soluble in water and can be separated from undissolved impurities and the precipitated iron sulfate by filtration. Hydrolyzing at 90°C causes the hydroxide TiO(OH)₂ to precipitate:



The titanyl hydroxide is calcined at about 1000°C to produce titania TiO₂.

19.8 NONOXIDES

Most of the important nonoxide ceramics do not occur naturally and therefore must be synthesized. The synthesis route is usually one of the following:

- Combine the metal directly with the nonmetal at high temperatures.
- Reduce the oxide with carbon at high temperature (carbothermal reduction) and subsequently react it with the nonmetal.

In this section we look at several important nonoxide ceramics. To show the variety of nonoxide ceramics we have taken examples of carbides, nitrides, and borides. There are of course many other nonoxide ceramics that are of interest.

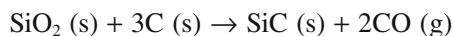
SiC	Abrasives, harsh-environment electronic packaging
TiC	Bearings, cutting tools
AlN	Electronic packaging, crucibles
Si ₃ N ₄	Future gas-turbine and diesel engine components
ZrB ₂	Crucibles and thermowell tubes (steel)
WC	Abrasives, cutting tools
C	Graphite: solid lubricant; diamond: abrasive

Silicon Carbide

Silicon carbide (SiC) is the most widely used nonoxide ceramic. Its major application is in abrasives because of its hardness (surpassed only by diamond, cubic boron nitride, and boron carbide). Silicon carbide does not occur in nature and therefore must be synthesized. It occurs in two crystalline forms: the cubic β phase, which is formed in the range 1400–1800°C, and the hexagonal α phase, formed at >2000°C.

Silicon carbide is synthesized commercially by the Acheson process, which involves mixing high-quality silica sand (99.5% SiO₂) with coke (carbon) in a large elongated mound and placing carbon electrodes in opposite ends. Each mound, or furnace, consists of about 3000 t of material. An electric current is passed between the electrodes resistively heating the coke in the mound to about 2200°C. The total electrical energy consumed during a standard furnace run is about 2 million kWh (about 7 TJ). The average power input during the furnace run is 9000–10,000 kW.

At the high temperatures the coke reacts with the SiO₂ to produce SiC plus CO:



Heating is continued (2–20 days depending on the size of the transformer and the furnace) until the reaction is completed on the inside of the mound. After cooling, the mound is broken up and sorted. The core contains high-



FIGURE 19.7 SiC produced by the Acheson process.

purity green hexagonal SiC crystals suitable for electronic applications. The purity of the SiC can be determined based on the color of the crystals.

- Light green 99.8% pure
- Dark green 99% pure
- Black 98.5%

Around the core is a zone of lower purity ($\geq 97.5\%$), which is suitable for abrasives. The outer layer consists of a mixture of SiC, unreacted SiO₂, and C that is reused in the next batch. Figure 19.7 shows examples of SiC crystals produced by the Acheson process.

The world's largest producer of SiC is China, which produces about 450,000 t/year. The largest U.S.-based manufacturer for SiC is Exolon in Hennepin, IL, which produces about 40,000 t of SiC annually. Figure 19.8 shows several of the furnaces at the Hennepin plant in various stages of production. The cost for SiC powders produced by the Acheson process is in the range \$10–\$40/kg.

Titanium Carbide

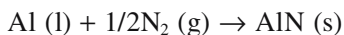
Titanium carbide (TiC) is another nonoxide ceramic that is not available in nature. It is prepared either by the carbothermal reduction of TiO₂ or by direct reaction between the elements titanium and carbon. As in many of these reactions high temperatures are required. The carburization temperature is between 2100 and 2300°C.

Aluminum Nitride

There are several large-scale methods for producing AlN, two of which are currently used in industry. One method is direct nitridation of aluminum:



FIGURE 19.8 The Exolon plant in Hennepin, IL. This plant is one of the newest SiC facilities in the world, producing both high-quality metallurgical and crystalline SiC annually. It is North America's only manufacturer of SiC. The plant features 16 furnaces operating off of four transformers.



Al powders are converted directly to the nitride at temperatures above the melting point of the metal. Careful process control is necessary to avoid coalescence of the metal prior to nitridation.

Reducing alumina using nitrogen or ammonia in the presence of carbon is another method to produce AlN:



The mixture of alumina and carbon is reacted with a nitrogen-containing atmosphere above 1400°C. Fine powders and extremely good control of mixing are required to result in complete conversion to AlN.

In both processes the major impurities are O (~1.0 wt%) and C (<0.07 wt%). Other impurities are silicon, iron, and calcium, which typically occur at levels <50 ppm each.

The main vendors for AlN powders are Advanced Refractory Technologies (in the United States); H.C. Starck and Elf Atochem (Europe); and Toyo Aluminum and Tokuyama Soda (Japan). The world market for AlN powder is about 200 t/year. Prices range from \$20/kg to \$180/kg depending on supplier, powder characteristics, and quantity.

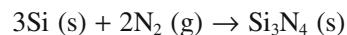
Many of the applications of AlN require it to be in consolidated in the form of substrates or crucibles. It is an electrical insulator and has a high thermal conductivity (better than Fe), which makes it attractive for use in electronic packaging. Aluminum nitride crucibles are used to contain metal melts and molten salts.

Silicon Nitride

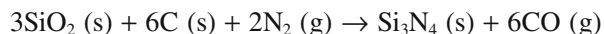
Silicon nitride (Si₃N₄) is another synthetic mineral. It occurs in two crystalline forms. The lower temperature α form is usually preferred as a raw material because the transformation to the β form during sintering favors the development of an elongated crystal structure. Several routes are available for the synthesis of Si₃N₄ powder, similar to those used to form AlN:

- Nitridation of Si powder
- Carbothermal reduction of silica in N₂
- Vapor phase reaction of SiCl₄ or silane (SiH₄) with ammonia

Most commercially available powder is made by reacting silicon powder with nitrogen at temperatures from 1250 to 1400°C according to the reaction

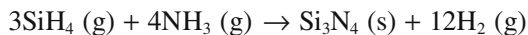


The powder generally consists of a 90:10 mixture of α-Si₃N₄ and β-Si₃N₄ polymorphs. Seeds of Si₃N₄ powder are often mixed with the silicon to hasten the reaction and to help prevent the formation of the undesired β phase. Nitrided powder contains impurities such as Fe, Ca, and Al originally present in the Si or picked up during subsequent milling. Higher purity Si₃N₄ powder can be made by carbothermal reduction in the range 1200–1550°C:



Although this process leads to powders with residual carbon and oxygen it produces high surface area powder with a high α content. Si₃N₄ seeds may again be used to speed up the reaction.

High-purity powders are also made via vapor phase reactions such as



Powder from these reactions is amorphous, but the product on heating to 1400°C is mostly α-Si₃N₄.

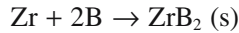
Worldwide production of Si₃N₄ is about 500t/year; Japan is the primary market. The cost for this powder is between \$30/kg and \$150/kg depending on the particle size and the quantity ordered.

Silicon nitride exhibits high strength at elevated temperatures and excellent thermal shock, creep, and oxidation resistance in hostile environments, which makes it ideal for gas turbine and diesel engine applications. The SiAlONs are variations on this theme. For example, SiAlON is being combined with boron nitride (BN) to produce a composite material that is reported to have incomparable thermal shock resistance.

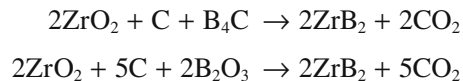
Zirconium Diboride

ZrB₂ is useful as a crucible material for metal melts because of its excellent corrosion resistance. It is also used in Hall–Heroult cells (for Al production) as a cathode and in steel refining where it is used as thermowell tubes.

Several different processes can be used to produce ZrB₂; these are similar to those used to form carbides and nitrides. Commercially, either a direct reaction between zirconium and boron



or carbothermal reduction of zirconia is used:



All these reactions must be carried out at high temperature in an inert atmosphere or in vacuum. The typical price of ZrB₂ powder is \$60–\$100/kg.

Tungsten Carbide

Tungsten carbide is a wear-resistant material used in the metalworking, mining, and construction industries for machine parts and dies that are subject to severe service conditions. It is produced by carburization of tungsten powder. The United States uses about 5500 t of WC each year.

Carbon

Graphite is one of three crystalline forms of carbon, the others being diamond and fullerenes. Graphite is unlike most of the nonoxide ceramics in that it occurs naturally in metamorphic rocks such as marble.

The graphite used in industry comes both from natural sources where it is mined in open pit and underground operations. The largest producers of natural graphite are China and India and total world production is around 1 Mt/year. Graphite is not currently mined in the United States, although the United States does produce about 300,000 t of synthetic graphite annually with a value of almost \$1 billion.

There are several methods used to produce synthetic graphite. Many of these involve heating nongraphitic carbons above 2500°C. For example, a high-purity form is produced by heating a calcined mix of petroleum coke and coal tar pitch to 3000°C. The high temperature allows the carbon atoms to order into the graphite structure. Synthetic graphite can also be obtained by chemical vapor deposition from hydrocarbons at lower temperatures (~1800°C).

Most of the synthetic graphite produced in the United States (>60%) is used in the massive electrodes in carbon-arc furnaces to melt steel and in much smaller battery electrodes. Other major applications include lubricants and carbon raisers in steelmaking. Synthetic graphite is used in replacement heart valves, an application we describe in Chapter 35.

The largest uses for natural graphite are in refractories (45%) and brake linings (20%). Natural graphite costs around \$500/t, whereas synthetic graphite costs over \$2000/t.

The quantity of industrial diamonds produced in the United States is much smaller than the amount of synthetic graphite. About 300 million carats or 60 t are produced each year with major applications in stone cutting and highway/building repair.

The fullerenes were discovered in 1985 and the related carbon nanotubes in 1991. Both are now available in commercial quantities, but at present they are very expensive and the applications are limited to specialty products such as Nanodesu bowling balls, which use fullerenes as an additive in a polymer coating.

CHAPTER SUMMARY

This chapter described the processes used to obtain the raw materials necessary to make ceramics. The significant points to remember from this chapter as you continue your study of ceramics are as follows:

- Where and how we get the raw materials will determine impurity concentrations in the final powder (e.g., Na is the major impurity in Bayer alumina).
- The abundance of a mineral may affect the cost of the final ceramic component (e.g., SiO₂ comes from sand; it is abundant and inexpensive. Glass bottles are cheap; the cost of an Si wafer is not related to the cost of sand).
- If the raw materials are not oxides then they have almost certainly been synthesized [e.g., we use 0.5 Mt of SiC (mostly for abrasives), which must be synthesized. The cost of the powder depends on how pure it is].
- Gemstones are found during mining, but are not abundant (e.g., about 200 mg of diamonds will come from 1 ton of ore; the market price of diamonds can justify this dilution).

PEOPLE & HISTORY

Acheson, Edward Goodrich (1856–1931), was an American chemist who worked with Thomas Edison before establishing his own laboratory. He developed a process for producing silicon carbide while trying to make synthetic diamonds. In 1891 he founded The Carborundum Co. to produce SiC for abrasives and was granted a patent in 1893 for SiC. In 1926, the U.S. Patent Office named his patent for SiC one of the 22 patents most responsible for the industrial age.

Bauxite is named after the small French town of Les Baux de Provence, which is near Arles.

Bayer, Karl Joseph (1847–1904) was an Austrian chemist (born in (Bielitz) who described the Bayer process in 1888.

Dana, James Dwight (1813–1895) was educated at Yale University and made contributions to the fields of geology, mineralogy, and zoology. He developed classification systems that are still in use in these fields today.

Graphite. The word is derived from the Greek word *graphein*, to write. Graphite is used as the “lead” in pencils among many other applications.

Kaolin refers to an area of Jiangxi province, which is why it is also called China clay.

Moissan, Ferdinand Frédéric-Henri (1852–1907) is known in the field of ceramics for his unsuccessful attempts at diamond synthesis (he actually produced SiC). Moissan was awarded the 1906 Nobel Prize in Chemistry for isolating fluorine on June 26, 1886. It was in Moissan’s laboratory at the University of Paris in France that tungsten carbide was first made.

Mullite is named after the Isle of Mull off the west coast of Scotland where the rare mineral is found.

Muscovite mica was first used in 1850 by James Dwight Dana and is derived from the term “Muscovy glass,” by which it was previously known because of its widespread use as a window-glass substitute in the old Russian state of Muscovy.

Phlogopite mica comes from the Greek word *phlogopos* meaning *fiery* in reference to the reddish color seen on some specimens of this mica.

GENERAL REFERENCES

Annual Minerals Review published in the *Bulletin of the American Ceramic Society* gives an annual update on the production status of a wide range of ceramic raw materials.

Evans, J.W. and DeJonghe, L.C. (1991) *The Production of Inorganic Materials*, Macmillan, New York. A readable description of how many metals and ceramics are produced.

Gribble, C.D. (1988) *Rutley’s Elements of Mineralogy*, 27th edition, Unwin Hyman, London. Classic resource on mineralogy including detailed descriptions of properties and occurrences of a wide range of minerals.

Mineral Commodity Summaries, published by the U.S. Department of the Interior, U.S. Geological Survey, provide extensive data on mineral production in the United States and the rest of the world.

Reed, J.S. (1995) *Introduction to the Principles of Ceramic Processing*, 2nd edition, Wiley, New York. Chapters 3 and 4 describe the extraction and synthesis of various ceramic raw materials.

SPECIFIC REFERENCES

Bowen, N.L. (1922), “The reaction principle in petrogenesis,” *J. Geol.* **30**, 177. Describes the eponymous reaction series.

Martin, E.S. and Weaver, M.L. (1993) “Synthesis and properties of high-purity alumina,” *Am. Ceram. Soc. Bull.* **72**, 71. Discussion of the pros and cons of different processes to produce alumina.

WWW

www.usgs.gov

U.S. Geological Survey. The Mineral Commodity Summaries and the Minerals Yearbook are here, and so much more.

EXERCISES

- 19.1 How many pounds of mullite are there in 1 ton of the material? How many kilograms?
- 19.2 What are the major impurities you would expect to find in high-quality deposits of silica sand?
- 19.3 Why do you think rock quartz is not used widely as a source of silica?
- 19.4 In the brief description of Edward Acheson we noted that the U.S. Patent Office named silicon carbide as one of the 22 patents most responsible for the industrial age. Why do you think this was such an important material?
- 19.5 What factors do you think contribute most to feldspar sales in the United States?

- 19.6 Why are magnesia sales related to steel production?
- 19.7 What is the difference between zircon and zirconia? Which of these, in single crystal form, is the diamond simulant?
- 19.8 A commercial supplier of ceramic powders sells 1 g of HfO_2 (purity 99%) for about \$2, but charges only 15 cents for the same amount of ZrO_2 (purity 99%). Both powders come from the ore zircon. Explain the differences in the price.
- 19.9 Quartz, basalt, and obsidian are all formed when magma cools (they are all igneous). Relate the microstructure of each of these materials to the expected relative rate of cooling of the magma. (We described obsidian in Chapter 2, you may need to look in a geology book for the microstructure of basalt.)
- 19.10 Synthetic graphite is used primarily for electrodes and as a carbon raiser in steel production, whereas the major applications of natural graphite are refractories and brake linings. Why does the source of graphite matter and what are some of the considerations end users might make in deciding where to buy their graphite?

Powders, Fibers, Platelets, and Composites

CHAPTER PREVIEW

The topic of this chapter is how to produce particles of a particular shape, chemistry, and size and then how to characterize them. We are going to describe the methods used to produce ceramic powders, from the traditional ball-milling technique to more recent vapor-phase approaches that can produce nanometer-sized particles. It is worth remembering that powder processing is used to produce some special metals (e.g., tungsten filaments for incandescent lamps), it is used in the pharmaceutical industry, for making catalysts, and it is used to prepare many food ingredients.

Producing powders of a consistent quality and composition is an important industry. In the United States the total market for powders of advanced ceramics (e.g., electronic and structural ceramics) alone is around \$1 billion per year.

To specify powders for particular applications and products we need to be able to determine their physical and chemical characteristics, often with a high degree of accuracy and with statistical significance. In this chapter we will describe the different analytical techniques used for particle characterization and also indicate which technique works best. In addition to powders there are other important dimensionally constrained forms of ceramics. Whiskers and fibers are long in one dimension but restricted in the other two. Ceramics in these forms are important reinforcement phases in composites, such as

- C fibers in polymer–matrix composites (PMCs)
- Al_2O_3 fibers in metal–matrix composites (MMCs)
- SiC whiskers in ceramic–matrix composites (CMCs)

If the particles are constrained in only one dimension, we have platelets. The amount of space we devote to platelets does not correlate with their commercial importance: remember that clay particles are platelets. The excuse is that most platelet particles are produced in nature while we are concentrating on particles we “design.”

If we limit the size in two or three dimensions to less than 100 nm, we have nanomaterials.

20.1 MAKING POWDERS

Many methods are available for the preparation of ceramic powders. These can be divided into just three basic types:

- Mechanical
- Chemical
- Vapor phase

Mechanical methods use coarse-grained materials that have generally been derived from naturally occurring minerals. They are subjected to a series of processes, collectively referred to as comminution, in which the particle

size is gradually reduced. The final step is known as milling, which produces particles of the desired size. Mechanical methods of powder production are used widely in the production of traditional ceramic products where high purity powders are not required and cost is one of the most important requirements.

Chemical methods, such as sol-gel processing, offer several advantages over mechanical methods because they allow exceptional control over particle morphology and purity. Chemical processes are used widely in the production of advanced ceramic materials.

Vapor-phase processes can be used to produce ceramic powders. They tend to be expensive, but offer many advantages, such as the ability to produce particles of nonoxides.

TABLE 20.1 Desirable Powder Characteristics for Advanced Ceramics

Powder characteristic	Desired property
Particle size	Fine ($<1\ \mu\text{m}$)
Particle size distribution	Narrow
Particle shape	Spherical or equiaxed
State of agglomeration	No agglomeration or soft agglomerates
Chemical composition	High purity
Phase composition	Single phase

Vapor phase techniques are also used to produce nanoparticles (particles with diameters of a few to 10s of nanometers).

Table 20.1 lists the desirable powder characteristics for advanced ceramics. For most processing methods we want a small particle size. The small size helps shape the product and during densification (sintering) at high temperature, allows higher density bodies at lower firing temperatures.

20.2 TYPES OF POWDERS

Powders can have a complex structure; to describe this structure it is necessary to follow a consistent terminology. The terminology we use follows that used in the ceramic processing industry.

- *Primary particles* are the smallest clearly identifiable unit in the powder. Primary particles may be crystalline or amorphous and cannot easily be broken down into smaller units.
- *Agglomerates* are clusters of bonded primary particles. Soft agglomerates are easily broken up; hard agglomerates, because of the stronger interparticle bonds, are more difficult to break up. Hard agglomerates should be avoided in ceramic powder processing as much as possible.
- *Particles* is a general term applied to both primary particles and agglomerates. Some of the techniques that we refer to in the next section measure particle size often with no distinction between agglomerates and primary particles.
- *Granules* are large agglomerates, usually 0.1–1 mm in diameter, that are formed by the addition of a granulating agent (e.g., a polymer binder). The mixture is tumbled, producing large, nearly spherical granules that flow freely and can be used to fill complex molds and in automated processes.
- *Flocs* are clusters of particles in a liquid suspension held together electrostatically.
- *Colloids* are very fine particles (they can be as small as 1 nm in diameter) held in fluid suspension by

POPULAR MILLING MEDIA

Porcelain ($\rho = 2.3\ \text{Mg/m}^3$)
 Alumina ($\rho = 3.6\ \text{Mg/m}^3$)
 Zirconia ($\rho = 5.5\ \text{Mg/m}^3$)
 Steel ($\rho = 7.8\ \text{Mg/m}^3$)
 Tungsten carbide ($\rho = 15.6\ \text{Mg/m}^3$)

Brownian motion. Consequently, colloidal particles will settle very slowly.

- *Aggregates* are coarse constituents, $>1\ \text{mm}$, in a mixture. The important example is the addition of gravel to cement to make concrete. In early concrete structures such as the Pantheon in Rome, pumice was used as aggregate.

20.3 MECHANICAL MILLING

For traditional raw materials like clay and the oxides produced from ores, it is often necessary to eliminate aggregates and to reduce the particle size. Compound formation during firing and densification during sintering require diffusion between neighboring particles. Diffusional processes are proportional to the square of the particle size.

The most common method for reducing particle size is ball milling. A ball mill is a barrel (usually made of a ceramic, although for small-scale milling in the laboratory a small plastic bottle works well) that rotates on its

axis and is partially filled with a grinding medium (called media) in the form of spheres, cylinders, or rods. Figure 20.1 shows a cross section of a ball mill. The quantity of the media is such that the rotation of the mill causes it to cascade, creating both shearing and crushing actions on the powder.

The media should have a high density (ρ) as this provides for the most effective collisions. The choice of media is also based on cost, wear resistance, and the possibility of introducing contamination into the powder.

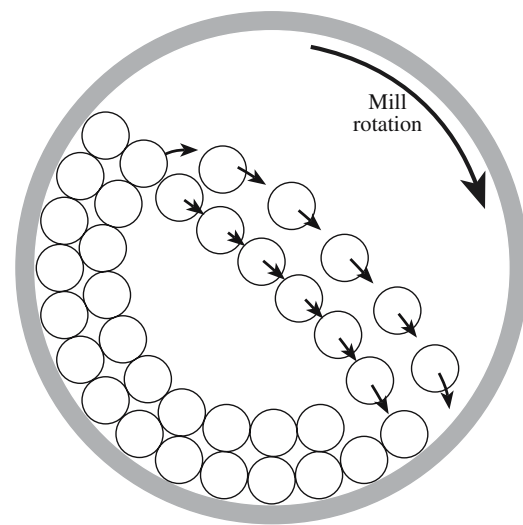


FIGURE 20.1 Cross section of a ball mill showing the movement of the media as the mill rotates about its axis.

TABLE 20.2 Possible Particles Sizes for Different Milling Techniques

Jaw crushers	to 5 mm
Cone crushers	to 5 mm
Crushing rolls	to ~1 mm
Hammer mill	to ~0.1 mm
Jet mill	1 to ~50 μm
Vibratory mill	1 to ~50 μm
Ball mill	0.5–10 μm
Attrition mill	0.1–5 μm
Roller mill	0.1–5 μm

Depending on the amount of powder to be milled, the size of the mill, and the final particle size required, the media could range from more than 8 cm in diameter to 0.6 cm, which is used for fine grinding. The powder is often milled in a liquid with a surface-active agent added. Ball milling eliminates aggregates and can typically reduce the particle size down to 1 μm.

The advantages of ball milling are that the equipment is

- Simple (although experimentally straightforward, there are many theoretical aspects that are quite complex)
- Inexpensive (at least for small batch sizes)

The disadvantages of ball milling are that it

- Cannot produce ultrafine particles
- Can add impurities to the powder from the media and the inside of the mill
- Is inefficient, less than 2% of the energy input goes into creating new surfaces

You have seen polished stones of hematite, quartz, etc. These are obtained by tumbling in the same type of mill—the “particle” size is just bigger. The biggest “ball” mill is the seashore, where pebbles are eventually changed into sand.

MILLING

The minimum particle size possible by ball milling is ~0.1 μm.

Vibratory milling is 10× faster than ball milling.

There are many other mechanical methods that can be used to achieve comminution. The possible particle size range for each is compared in Table 20.2; we describe three of the methods in more detail below.

Fluid-energy milling, also called *jet milling*, achieves particle size reduction by particle–particle impact in a high-velocity fluid, usually either compressed air or superheated steam. The powder is added to the fluid and injected into the grinding chamber at sonic or near-sonic velocity. The design of the chamber maximizes particle–particle impact while minimizing particle–wall impact. Coating of the walls of the chamber, e.g., with a polymer, can further reduce contamination. Fluid-energy milling can achieve controlled particle size (down to about 1 μm) with a narrow size

distribution. Table 20.3 shows examples of ceramic powders formed by fluid-energy milling. The main drawback with this method is collecting the fine powder that is mixed into the gas stream.

In *vibratory milling* the drum containing the media and powder is vigorously shaken. The collisions between the media are much more violent than they are in ball milling and this can shorten milling times. Polymer balls can be used as media and this means any contamination can be burned off during subsequent firing.

Attrition milling, or *agitated ball milling*, differs from conventional ball milling in that the milling chamber does not rotate. Instead, a slurry containing the particles and media is stirred continuously at frequencies of 1–10 Hz. The grinding chamber is aligned either vertically, as shown in Figure 20.2, or horizontally, with the stirrer located in the center of the chamber. The media consists of small spheres (0.2–5 mm) that make up between 60 and 90% of the available mill volume. Most attrition mills work on a continuous basis with the powder to be milled fed in at one end and the milled product collected at the other. Attrition mills are more energy efficient than the other methods we have described and can also handle higher solid contents in the slurry. The rapid milling time, because of the use of small media, helps reduce contamination.

TABLE 20.3 Examples of Ceramic Powders Produced by Fluid-Energy Milling

Material	Mill diameter		Grinding medium	Material feed rate		Average particle size obtained	
	cm	in.		kg/h	lb/h	μm	in.
Al ₂ O ₃	20.3	8	Air	6.8	15	3	0.00012
TiO ₂	76.2	30	Steam	1020	2250	<1	<0.00004
TiO ₂	106.7	42	Steam	1820	4000	<1	<0.00004
MgO	20.3	8	Air	6.8	15	5	0.0002
Dolomite	91.4	36	Steam	1090	2400	<44	<0.0018
Fe ₂ O ₃	76.2	30	Steam	450	1000	2–3	~0.0001

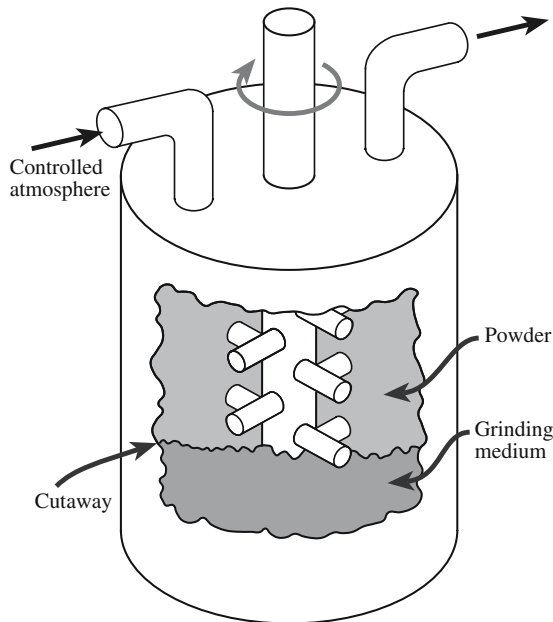


FIGURE 20.2 An attrition mill.

Lining the chamber with a polymer or a ceramic and using ceramic stirrers and media can further reduce contamination.

20.4 SPRAY DRYING

Spray drying is an example of powder production from solution. It is used widely for preparing ferrites, titanates, and other electrical ceramics. Fine droplets produced by an atomizer are sprayed into a drying chamber and the powder is collected (Figure 20.3). There are different types of atomizers. One uses ultrasonic atomization in which the solution is passed over a rapidly vibrating piezoelectric membrane. Droplet sizes in the range of $10\ \mu\text{m}$ to over $100\ \mu\text{m}$ can be produced.

In the drying chamber, the flow pattern of the hot air determines the completeness of moisture removal and the maximum temperature that the particles experience. Finally the particles are carried out of the chamber in the air stream and captured in a bag or another form of collector. The particles produced by spray drying are often agglomerated with a primary particle size less than $0.1\ \mu\text{m}$.

The variables in spray drying are

- Droplet size
- Solution concentration and composition
- Temperature and flow pattern of the air in the drying chamber
- Chamber design

For small-scale laboratory experiments nitrates and acetates are often used because of their relatively low

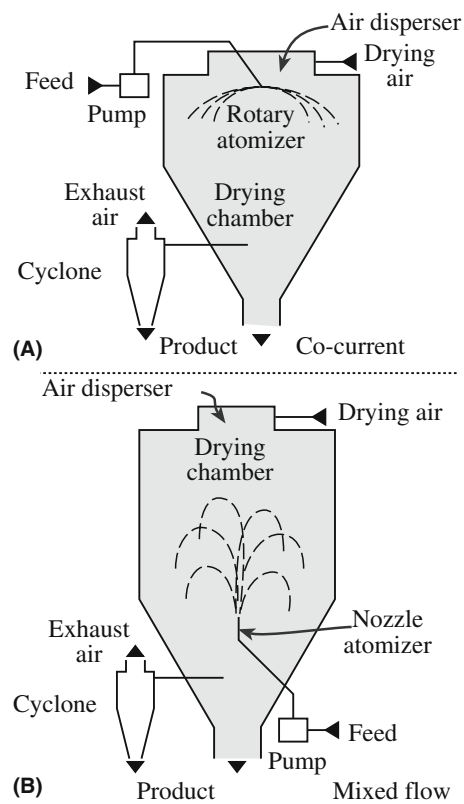


FIGURE 20.3 Spray dryers: (a) Centrifugal atomizer with cocurrent air flow. (b) Nozzle atomizer using mixed-flow conditions.

decomposition temperature. Chlorides and oxychlorides are frequently used in industrial spray-drying operations because of their high solubility in aqueous solutions. The capacities of industrial spray dryers are up to several hundred kilograms per hour. The spray drying process is not limited to aqueous solutions; for example, alcohol solutions of alkoxides can be used.

Table 20.4 lists examples of salt precursors and their decomposition temperatures. The decomposition of salts to oxides is an example of a solid-state reaction. These reactions are often referred to as calcination and are frequently governed by kinetics rather than thermodynamics. As a consequence, they may be carried out at temperatures much greater than those necessary based on thermodynamic calculations. A feature of the decomposition reactions is that they often result in the production of extremely fine particles.

TABLE 20.4 Salt Precursors and Their Decomposition Temperatures in Air

Precursor	T ($^{\circ}\text{C}$)
$\text{Zn}(\text{NO}_3)_2 \cdot 6\text{H}_2\text{O}$	360
$\text{Ni}(\text{NO}_3)_2 \cdot 6\text{H}_2\text{O}$	400
$\text{Ni}(\text{CH}_3\text{COO})_2 \cdot 4\text{H}_2\text{O}$	350
$\text{Fe}(\text{NO}_3)_3 \cdot 9\text{H}_2\text{O}$	200
MgSO_4	1000
$\text{Y}_2(\text{C}_2\text{O}_4)_3 \cdot 5\text{H}_2\text{O}$	500

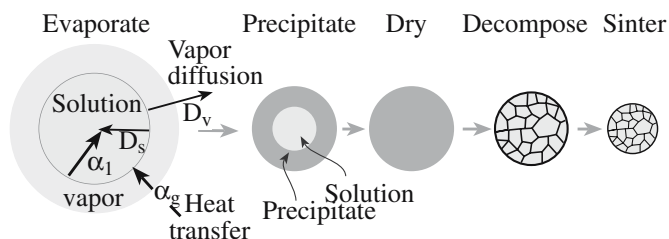


FIGURE 20.4 Stages in the spray pyrolysis process.

A variation of the spray drying process, known as spray pyrolysis, uses a higher temperature and a reactive (often an oxidizing) environment in the chamber. This allows the salts to be dried and decomposed directly. Figure 20.4 shows the stages in the spray pyrolysis process. In addition to producing powders this technique has been used to produce thin films and fibers.

20.5 POWDERS BY SOL-GEL PROCESSING

Sol-gel processing is one of the topics we describe in Chapter 22. It is best applied to the formation of films and fibers. We discuss the technique here because, although expensive, it can produce powders with a high surface area, which allows sintering to nearly full density at much lower temperatures than are normally required when the particles have been made by other techniques.

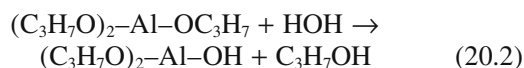
In most sol-gel processes the reactants are solutions of metal alkoxy compounds. Alkoxides result from the reaction of metals (Me) with alcohols. The general reaction is



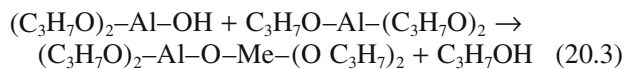
where R is an organic group. For ethanol, R is the ethoxy group C_2H_5 . Catalysts are often necessary to increase reaction rates. For example, aluminum will react with isopropanol at 80°C in the presence of a small amount of HgCl_2 . In this case the catalyst breaks down the protective oxide layer that forms on the aluminum.

A number of metal alkoxides are commercially available in high purity form. To make metal oxide powders from these organometallic precursors we start with a solution (a “sol”) of the metal alkoxide in alcohol. (The alcohol is usually the same one that was used for alkoxide formation.) Water is added to the alcohol solution. Two reactions then occur, which, using aluminum isopropoxide as an example, may be written as follows:

Reaction 1: Hydrolysis



Reaction 2: Condensation



The remaining alkoxy groups ($-\text{OR}$) of the condensation product can be hydrolyzed further to form a cross-linked, three-dimensional network of metal–oxygen bonds. The actual reactions that occur appear to be significantly more complex than those represented by Eqs. 20.2 and 20.3.

There are several variables in the sol-gel process:

- Rates of hydrolysis and condensation (relative differences in the rates can be used to modify the microstructure of the powder)
- Type of alkoxy (mixing of the alkoxides in the solution is achieved at a molecular level giving the powders a high degree of chemical homogeneity)
- Reaction temperature (affects the degree of polymerization of the gel)
- Amount of water added (affects the degree of polymerization of the gel)
- Solution pH (rates of hydrolysis and condensation can be increased by the addition of acids or bases, respectively)

Gelation times vary from seconds to several days. When the gel forms it may contain only about 5 vol% of the oxide. The dried gel is calcined to completely convert it to oxide. Powders produced by the sol-gel method are amorphous. A crystallization step is required to produce crystalline bodies, which is often performed after sintering.

20.6 POWDERS BY PRECIPITATION

To cause precipitation it is necessary to produce a supersaturated solution. This can be achieved, for example, by changing the pH or the temperature. A larger quantity of a soluble component (for example, a metal salt) can be dissolved in a solution at high temperature than at a lower temperature. For example, not only does sugar dissolve more quickly in hot tea than in iced tea, but more sugar dissolves. The relation between solubility and temperature for several ionic compounds is shown in Figure 20.5. There are some exceptions to prove the rule: cerium sulfate is less soluble at higher temperatures because its heat of solution is negative ($\Delta H_{\text{sol}} < 0$).

At a supersaturation that exceeds the concentration threshold for homogeneous nucleation, a large number of nuclei form suddenly. Their formation lowers the solution concentration below the concentration at which nucleation occurs, but enough excess solute remains for the existing nuclei to grow. If the solution is kept uniform, growth of all the particles proceeds at the same rate, producing

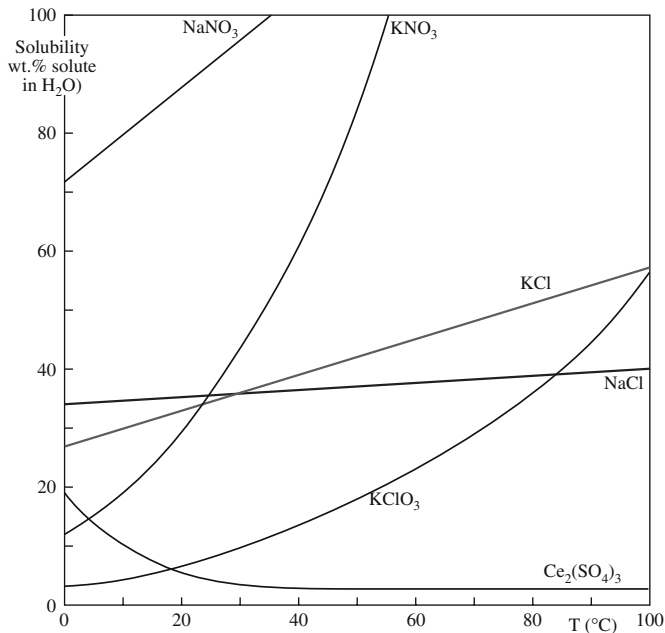


FIGURE 20.5 Solubility (grams of solute in 100g H₂O) versus temperature for several ionic compounds.

powders with extremely uniform size distribution. The variation of solute concentration with time during the nucleation and growth of particles from solution is shown in Figure 20.6.

PRECIPITATION

It is important to make sure that nucleation occurs homogeneously. Good housekeeping is essential as specks of dirt can act as nucleation sites causing heterogeneous nucleation.

This diagram is often referred to as a LaMer diagram after the work of LaMer and Dinegar.

Precipitation of mixed oxides is possible. For example, in the fabrication of nickel ferrite (a magnetic ceramic used for memories) a mixed aqueous solution of iron and nickel sulfates is used. The solution is kept at about

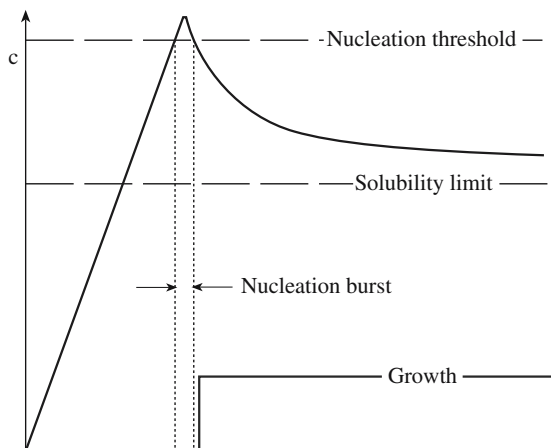


FIGURE 20.6 Concentration versus time for a solution in which the concentration is first increased to the point of nucleation (e.g., by evaporation) and then declines as a precipitate grows.

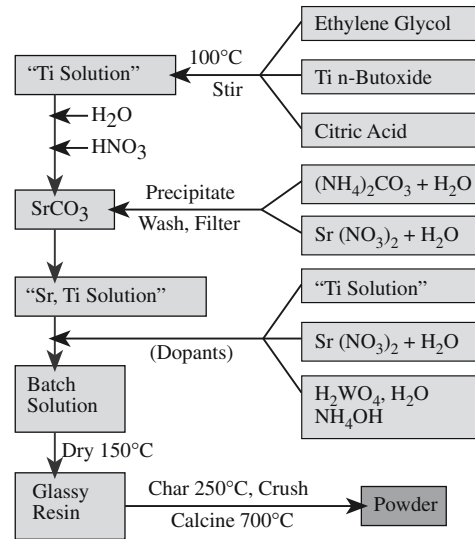


FIGURE 20.7 Flow chart for preparing SrTiO₃ powders by the Pechini method.

80°C and precipitation occurs when the pH is increased to around 11 with ammonium hydroxide. A mixed hydroxide precipitates, which is washed to remove the residual sulfate and dried to a powder with a particle size between 50 nm and 1 μm.

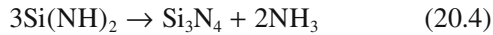
The Pechini method is a commercial process for the preparation of titanates and niobates for the capacitor industry. With slight modifications, it is also referred to as the “citrate gel” process or the “amorphous citrate” process. Figure 20.7 shows a flow chart for the preparation of strontium titanate powder. Metal ions from starting materials such as carbonates, nitrates, and alkoxides are complexed in aqueous solution with α-carboxylic acids such as citric acid. When heated with a polyhydroxyl alcohol, such as ethylene glycol, polyesterification occurs. On removal of the excess liquid a transparent resin is formed. The resin is heated to decompose the organic constituents, ground to break up large agglomerates, and finally calcined. The powders produced are not as uniform as those from the sol-gel process: they often contain hard agglomerates.

20.7 CHEMICAL ROUTES TO NONOXIDE POWDERS

Many important engineering ceramics are nonoxides, e.g., Si₃N₄ and SiC. These often do not exist in nature or are rare and so must be produced synthetically. In Chapter 19 we described how nonoxide powders are obtained by solid-state reactions, such as between SiO₂ and C to

produce SiC. We also described direct nitridation processes, such as the reaction between Al and N₂ to produce AlN. Now we are concerned with liquid-phase reactions that lead to the formation of nonoxides.

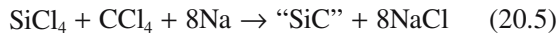
It is possible to produce submicron particles of α-Si₃N₄ by reacting silicon tetrachloride, a liquid at room temperature, and ammonia. The reaction involves the formation of silicon diimide [Si(NH)₂] as an intermediate phase.



This process is used commercially by Ube Industries in Japan to produce Si₃N₄. The particle morphology is controlled by the calcination time and temperature:

- Fine-grained equiaxed powders form at low temperatures
- Needle-like and coarse-grained hexagonal particles form at temperatures >1500°C.

Another example of a liquid-phase reaction used to produce precursors for nonoxide powders involves reductive dechlorination of halide solutions. An example is the reaction between silicon tetrachloride, carbon tetrachloride, and sodium in heptane at ~300°C:



The amorphous precursor can be crystallized by heating between 1400 and 1800°C in 5% H₂/Ar. This process has also been used to produce powders of TiB₂ and B₄C.

20.8 PLATELETS

Platelets are particles that are constrained in one dimension. They are commercially important because this is the shape of clay particles and mica. Another example of platelets previously encountered is SiC, which forms as flat hexagonal crystals by the Acheson process. An *in situ* process has been developed to produce platelet-reinforced-intermetallic composites. The reaction is



The SiC is in the form of platelets in an MoSi₂ matrix.

20.9 NANOPOWDERS BY VAPOR-PHASE REACTIONS

Vapor phase processes are relatively expensive, but there are several good reasons for using them to prepare powders, particularly when we want

- High purity
- Discrete and nonaggregated particles
- Nanoparticles with narrow size distributions

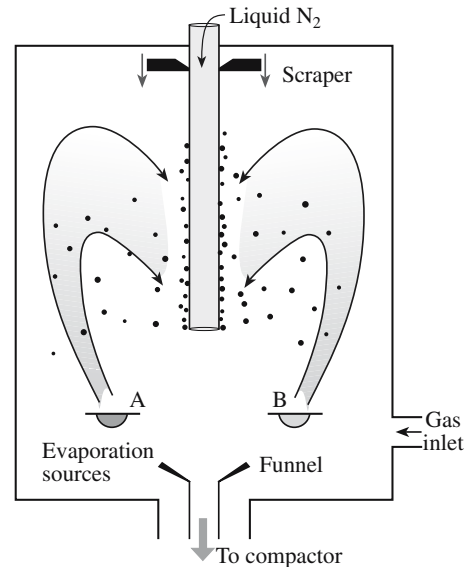


FIGURE 20.8 Schematic of a gas-condensation chamber for nanoparticle synthesis.

- Versatility in producing powders of oxides and nonoxides

Figure 20.8 illustrates a gas-condensation chamber developed specifically for this purpose. Material is evaporated from the two sources and condenses in the gas phase. The condensate is transported by convection to the liquid nitrogen cold finger. The clusters are scraped from the cold finger and collected via a funnel. It is possible to have the particles transferred directly into a cold press where they can be compacted. With this technique ceramic powders with very small particle size have been produced, e.g., TiO₂ powders with an average particle size of 10–15 nm.

Figure 20.9 shows a typical plasma reactor that can also be used to produce ceramic nanoparticles. The

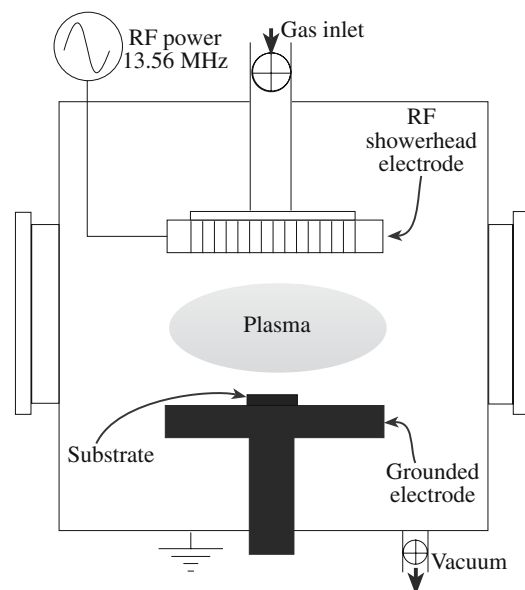


FIGURE 20.9 Schematic of a plasma reactor.

TABLE 20.5 Summary of Particle Size Analysis Techniques

<i>Method</i>	<i>Medium</i>	<i>Size (μm)</i>	<i>wt (g)</i>	<i>t</i>
Light microscopy	Liquid/gas	400–0.2	<1	S-L
Electron microscopy	Vacuum	20–0.002	<1	S-L
Sieving	Air	8000–37	50	M
	Air	5000–37	5–20	M
	Liquid	5000–5	5	L
	Inert gas	5000–20	5	M
Gravity sedimentation	Liquid	100–0.2	<5	M-L
Centrifuge sedimentation	Liquid	100–0.02	<1	M
Electrical sensing zone (Coulter counter)	Liquid	400–0.3	<1	S-M
Fraunhofer scattering	Liquid/gas	1800–1	<5	S
Mie scattering	Liquid	1–0.1	<5	S
Intensity fluctuation	Liquid	5–0.005	<1	S
X-ray line broadening	Air	<0.1	<1	S-M

gaseous reactants are introduced into an argon plasma where they are decomposed into free atoms, ions, and electrons. Quenching of these highly excited species results in the formation of ultrafine powders with sizes typically less than 20 nm.

20.10 CHARACTERIZING POWDERS

There are several techniques that can be used to obtain particle size and particle size distribution and these are compared in Table 20.5. The choice of technique depends on several factors, such as applicable particle size range, sample size required, and the analysis time. In addition, we often have to consider instrument cost, availability, ease of operation, and maintenance.

Obtaining accurate and representative measurements of particle size is not trivial. Beyond selecting the right experimental method to use, you may have to perform a statistical analysis of the data to obtain meaningful results.

20.11 CHARACTERIZING POWDERS BY MICROSCOPY

The most direct way to determine the size of a particle is to look at it. We described the various microscopy techniques in some detail in Chapter 10. If the size of the particle is >1 μm, then visible light microscopy (VLM) is fine. Particle size measurements are made either directly at the microscope or from micrographs (photographs taken using the microscope). The main challenge is in determining the size of three-dimensional grains on the basis of planar images. Several procedures have been employed for making these measurements. The Heyn intercept method is one of the most useful approaches, and is ideally suited for nonequiaxed grains. The number of grain or grain boundary intersections of a straight or

curved line is measured and from this information the grain size is determined. It is possible to make these measurements by hand using a ruler, but it would take a long time to obtain a statistically relevant sample. Using image-analysis methods on a computer a large number of particles can be measured quickly. The data are often then plotted as a histogram of frequency of occurrence versus particle size.

For submicron particles it is necessary to use an electron microscope. For scanning electron microscopy (SEM), and in particular transmission electron microscopy (TEM), the total amount of material that can be examined is quite small, and so it is essential to make sure that the sample examined is representative of the entire powder batch.

The digital readout on a TEM is not more than ±10% accurate. To obtain more accurate measurements you must first calibrate the magnification of the instrument.

20.12 SIEVING

Sieving is the oldest method to determine particle size distribution. Actually, sieving is used for sorting particles according to size rather than measuring their size. Typically, sieves with decreasing mesh size are stacked with the largest mesh at the top. The term “mesh size” denotes the number of openings per linear inch in the sieve screen. NBS (now NIST) developed the sieve numbering system based on the “fourth root of two” ratio; this series is known as the ASTM E-11 standard. This ratio (= 1.189) means that the sieve openings are an exact geometric series.

Table 20.6 lists the aperture (hole) size of standard sieves; this size corresponds closely to the ISO standard. As you can see sieving is not applicable to the smallest particle sizes (<5 μm), which are often used in the fabrication of components from advanced ceramics. But sieving is used in the traditional ceramics industry for size determination of raw materials. It is particularly suited for

TABLE 20.6 Aperture Size of U.S. Standard Sieves

Sieve number	Aperture (μm)	Sieve number	Aperture (μm)
3.5	5,660	60	250
4	4,760	70	210
5	4,000	80	177
6	3,360	100	149
7	2,830	120	125
8	2,380	140	105
10	2,000	170	88
12	1,680	200	74
14	1,410	230	63
16	1,190	270	53
18	1,000	325	44
20	841	400	37
25	707	600	30
30	595	1,200	15
35	500	1,800	9
40	420	3,000	6
45	354	8,000	3
50	297	14,000	1

powders with particle size $>56\mu\text{m}$. The particle size distribution obtained by sieving is normally only approximate because it is often too time consuming to sieve for long enough periods to achieve the final distribution of particles in the various sieves.

20.13 SEDIMENTATION

A spherical particle of diameter, d , falling through a viscous liquid, soon reaches a constant velocity, v , where its weight is balanced by a frictional force, F , exerted by the liquid as shown in Figure 20.10. Stokes' law gives the important relationship between F and v :

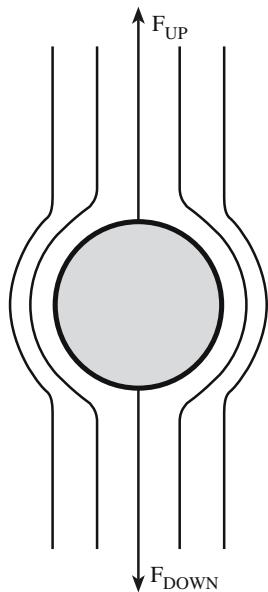


FIGURE 20.10 Illustration of the force balance during settling of a particle in a Newtonian fluid with laminar flow.

$$F = 3\pi\eta dv \tag{20.7}$$

where η is the viscosity of the liquid. Equating F to the effective weight of the particle (i.e., the downward force) gives

$$v = d(\rho_s - \rho_l)g/18\eta \tag{20.8}$$

where g is the gravitational constant and ρ_s and ρ_l are the densities of the particle and the liquid, respectively. Equation 20.8 is Stokes' equation from which we can determine d by measuring the sedimentation rate.

The sedimentation technique is reliable for particle size determination when d is in a size range of $2\text{--}50\mu\text{m}$. The falling rate of smaller particles is affected by Brownian motion resulting from collisions with the molecules of the liquid and other interactions between particles. Stokes' law is valid only for laminar or streamline flow (i.e., when there is no turbulence). The Reynolds number (Re) is a measure of when the process transitions from turbulent to laminar flow:

$$Re = v\rho_l d/\eta \tag{20.9}$$

Laminar flow is restricted to Reynolds numbers of less than 0.2.

If there is a narrow distribution of particle sizes then sedimentation is experimentally very simple. A dilute suspension of the particles is shaken in a tall graduated cylinder. After a few seconds the suspension becomes stagnant and the particles start to settle at a constant (terminal) velocity. A clear layer of liquid forms at the top of the cylinder and grows as the particles continue to settle. The velocity of the downward movement of the interface between the clear liquid and suspension is v , which can readily be obtained using a stopwatch and the cylinder graduations.

The technique becomes more complicated if there is a distribution of particle sizes. In these cases it is more usual to measure the particle concentration at some point in the fluid. One way of doing this is by determining the turbidity of the fluid (i.e., its clarity). We use either light or X-rays and measure the intensity of the transmitted beam as the powder settles. The ratio of the intensity of the transmitted beam, I , to that of the incident beam, I_0 , is given by the Beer-Lambert law:

$$I/I_0 = \exp(-KAcx) \tag{20.10}$$

where K is the extinction coefficient, A is the projected area per unit mass of particles, c is the concentration by mass of the particles, and x is the path length of the light through the suspension.

For a dilute suspension containing roughly equal amounts of two particle sizes, Figure 20.11 shows the way turbidity changes with time at a distance, L , below the top of the liquid. Turbidity is usually expressed in terms of nephelometric turbidity units (NTu). This is in reference to a specific type of measurement technique. A nephelometer specifically measures the light reflected into the detector by the particles.

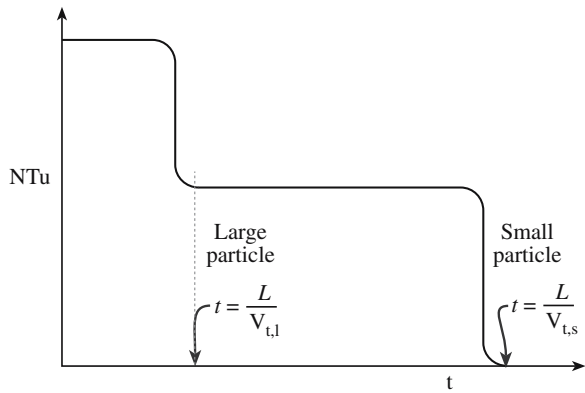


FIGURE 20.11 Result of sedimentation measurements using turbidity for two particle sizes in a solution; V_t is the terminal velocity.

The particle size can be determined from Stokes' equation. Clearly, if the particle size distribution is broad, the interpretation of turbidity measurements is not simple! Turbidity measurements are widely used to assess water quality. In the United States the allowable turbidity in drinking water is 1 NTu. Many drinking water utilities try to achieve levels as low as 0.1 NTu.

20.14 THE COULTER COUNTER

The Coulter counter, shown in Figure 20.12a, measures the number and size of particles suspended in an electrolyte by causing them to flow through a narrow orifice on

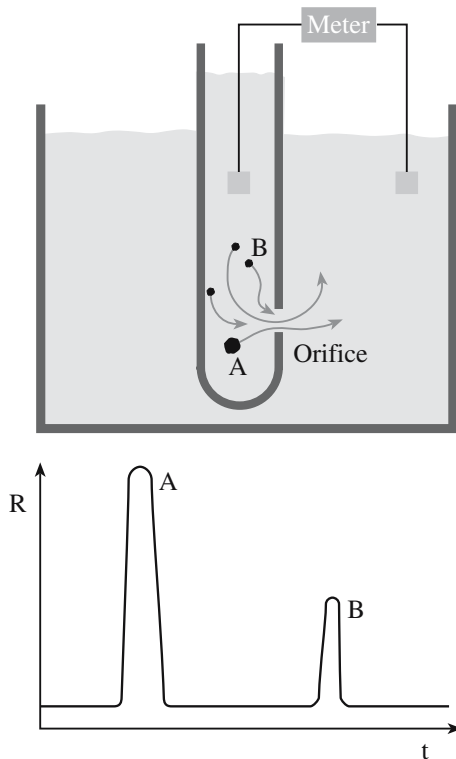


FIGURE 20.12 Results of Coulter counter measurements for two particle sizes A and B. R is the resistance between the electrodes, shown as shaded squares.

either side of which an electrode is immersed. As a particle passes through the orifice, it displaces an equivalent volume of electrolyte and causes a change in resistance, R . The magnitude of this change is proportional to the particle size.

The changes in R are converted to voltage pulses that are amplified, sized, and counted to produce data for the size distribution of the suspended particles. The peak height depends on the particle size as illustrated in Figure 20.12b. For peak A a larger particle passes through the orifice than for peak B. The peak width is a measure of how long it takes the particle to move through the orifice. The Coulter counter can measure particles in a size range 0.5–100 μm .

20.15 CHARACTERIZING POWDERS BY LIGHT SCATTERING

When a beam of light strikes a particle, some of it is transmitted, some is absorbed, and some is scattered. When the particles are larger than the wavelength of the incident light they cause Fraunhofer diffraction. The intensity of the forward-scattered light (i.e., light traveling in roughly the same direction as the incident light) is proportional to d^2 . Figure 20.13 shows examples of the light scattered from two particles of different sizes.

- Smaller particles scatter a small amount of light through a large angle.
- Large particles scatter a greater amount of light but through a smaller angle.

The relationship between scattering angle (θ) and d is

$$\sin \theta = 1.22\lambda/d \quad (20.11)$$

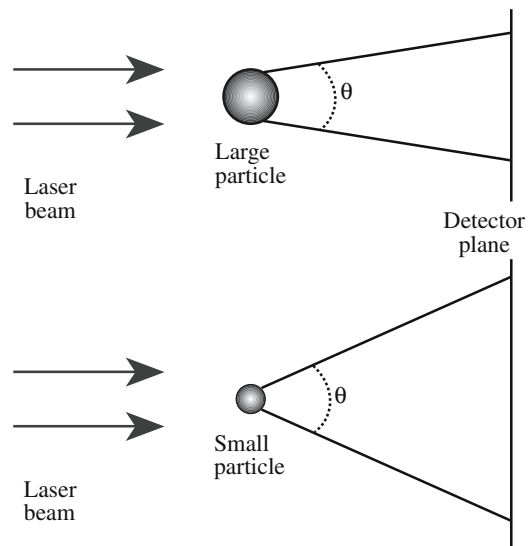


FIGURE 20.13 Scattering of light by large and small particles.

The light source is usually an He–Ne laser with $\lambda = 0.63\ \mu\text{m}$. For this wavelength the reliable particle size range is 2–100 μm . Light-scattering methods have the following advantages:

- Accuracy
- Speed
- Small sample size
- Can be automated

20.16 CHARACTERIZING POWDERS BY X-RAY DIFFRACTION

In Chapter 10 we discussed X-ray diffraction (XRD) and how it can be used to obtain crystallite size. Because of the widespread use of this technique and its applicability to very small particles we will reiterate some of the key points as they apply to characterizing powders. The width of the diffraction peaks, β , is related to d by the Scherrer equation:

$$d = 0.9\lambda/(\beta \cos \theta) \quad (20.12)$$

where λ is the X-ray wavelength and θ is the Bragg angle. From Eq. 20.12 you can see that as d increases, β decreases. When d is greater than about 0.1 μm the peaks are so narrow that their width cannot be distinguished from instrumental broadening. Consequently, XRD is most applicable to fairly small particle sizes. Figure 20.14 shows a

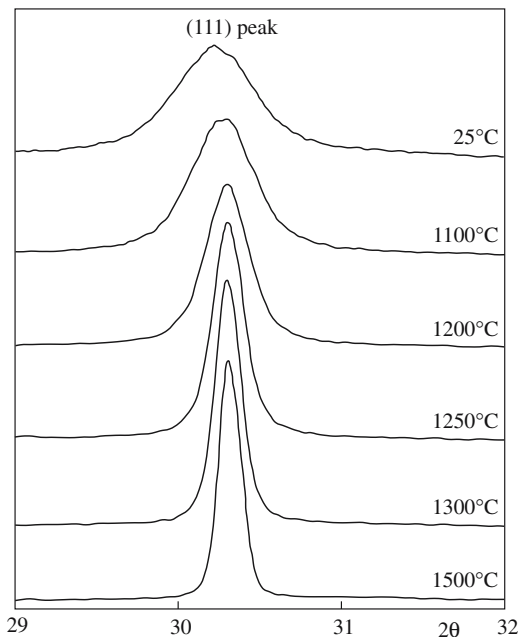


FIGURE 20.14 Illustration of X-ray line broadening for a $\text{ZrO}_2/3\ \text{mol}\% \text{Y}_2\text{O}_3$ powder prepared by hydrothermal synthesis.

series of XRD profiles for the 111 peak (arising from diffraction of the X-rays by the {111} planes) of a ZrO_2 powder doped with 3 mol% Y_2O_3 . Higher calcination temperatures lead to particle coarsening and a corresponding decrease in β .

It is important to remember that when determining particle size in a powder by measuring the width of X-ray peaks it is actually the size of the individual crystals that are being measured. As a consequence, if the particles are agglomerated XRD will give the size of the primary particles and *not* the agglomerate size.

Similarly, the reflections (spots) in an electron diffraction pattern will be broadened if the sample is composed of small crystals. Therefore diffraction in the TEM is not normally used to determine particle size because the number of particles that can be examined is fairly small and because it is better to just look at the image and make the measurements directly.

20.17 MEASURING SURFACE AREA (THE BET METHOD)

Surface-area methods rely on the adsorption of gases onto a particle surface at low temperature. The mass of gas adsorbed is measured as a function of gas pressure at a fixed temperature (typically liquid nitrogen).

The method developed by Brunauer, Emmett, and Teller (BET) to estimate the particle size relies on determining the surface area of the powder, which is calculated from the N_2 -isotherm observed at the boiling point of N_2 .

The BET equation is

$$P/[V_a(P_0 - P)] = (V_m C)^{-1} + (C - 1)P/[P_0 V_m C] \quad (20.13)$$

P is the gas pressure

P_0 is the saturation vapor pressure for the adsorbate at the adsorption temperature

V_a is the adsorbate volume at relative pressure P/P_0

V_m is the adsorbate volume per unit mass of solid for monolayer coverage

C is the BET constant

V_m is determined in the relative pressure ranges $P/P_0 \sim 0.05$ and $P/P_0 \sim 0.2$; according to BET theory this is the amount of nitrogen necessary to form a monomolecular layer on the particle. Since one nitrogen molecule requires a surface area of $0.162\ \text{nm}^2$, the surface area of the particle can be easily estimated in m^2/g .

A plot of $P/[V_a(P_0 - P)]$ versus P/P_0 gives a straight line from which V_m and C can be determined. The specific surface area, S , of the powder can then be calculated using

$$S = N_A \sigma V_m / V' \quad (20.14)$$

where N_A is Avogadro's number, V' is the molar volume = 22,410 cm³/mol, and σ is the cross-sectional area of the adsorbate molecule (0.162 nm² for N₂).

For spherical particles the particle radius, a , can be obtained from

$$a = 3/\rho S \quad (20.15)$$

where ρ is the density.

20.18 DETERMINING PARTICLE COMPOSITION AND PURITY

In addition to knowing particle size and particle size distribution of our powder we often need to know its composition and purity. Table 20.7 lists the composition of a typical high-purity alumina powder. Industrial ceramic powders can contain over 30 detectable elements, but in most cases less than 10 are present at levels greater than 0.01–0.05%. Many industries use wet chemical techniques such as precipitation and titration for such analysis. These techniques are used because they are often simple to perform and give a quick result. For example, in the industrial production of red lead (Pb₃O₄) it is necessary to determine the amount of free Pb and litharge (PbO). This analysis is typically done hourly and the results are used to modify the furnace temperature or throughput.

In addition to using wet chemistry there are numerous analytical methods that can give us chemical composition and impurity levels and these are summarized in Table 20.8.

The choice of technique depends on several factors:

- Type of material (is it readily soluble in common solvents, is the powder agglomerated)
- Amount of material (do we have milligrams or kilograms)
- Possible impurities (alkali metals, H, rare earths)
- Amount of impurities (ppm or percent)
- Availability and cost of instrument (do we need to use a national facility)

TABLE 20.7 Composition of a High-Purity Alumina Powder (wt%)

Oxide	%
Al ₂ O ₃	99.8
Na ₂ O	0.06
MgO	0.05
SiO ₂	0.03
Fe ₂ O ₃	0.03
U oxide	≤0.0005

TABLE 20.8 Chemical Analysis of Powders

Bulk techniques	Comments
Emission spectroscopy (ES)	Elemental analysis to the ppm level, frequently used for qualitative survey analyses, 5 mg powder sample
Flame emission spectroscopy (FES)	Quantitative analysis of alkali and Ba to the ppm level, ppb detectability for some elements, solution sample
Atomic absorption spectroscopy (AAS)	Industry standard for quantitative elemental impurity analyses; detectability to ppm level, solution sample
X-ray fluorescence (XRF)	Elemental analyses, detectability to 10 ppm, Z > 11, solid/liquid samples
Gas chromatography/mass spectrometry (GC/MS)	Identification of compounds and analysis of vapors and gases
Infrared (IR) spectroscopy	Identification and structure of organic and inorganic compounds, mg dispersed powder in transparent liquid or solid or thin-film sample
X-ray diffraction (XRD)	Identification and structure of crystalline phases, quantitative analysis to 1%, mg powder sample
Nuclear magnetic resonance (NMR)	Identification and structure of organic and inorganic compounds, sample to 5 mg for H and 50 mg for C

Of these factors, cost is often the most important. There are numerous choices:

- X-ray fluorescence (XRF) would not be a good choice to determine the amount of low-Z elements present.
- Flame emission spectroscopy (FES) is a good choice if we have very small amounts of the alkali metals.
- Nuclear magnetic resonance (NMR) can be used to determine H concentrations, but it is often expensive to use and not as widespread as atomic absorption spectroscopy (AAS).
- For phase determination and phase proportions in a powder mixture XRD is useful, allowing quantitative phase analysis down to ~1% in a powder sample.
- With a field-emission source in TEM, chemical analysis with atomic resolution is possible; the interaction volume can be as small as ~10⁻⁸ mm³.

20.19 MAKING FIBERS AND WHISKERS

Ceramic fibers and whiskers are used in the fabrication of composites where they are dispersed within a matrix, which may be a ceramic, a polymer, or a metal. The choice of matrix depends on the proposed applications for the composite. A primary consideration is the desired operating

temperature. Polymers are stable up to a maximum temperature of about 300°C, metals up to about 900°C, and ceramics are usable at temperatures >1800°C. Ceramics can be used as the reinforcement phase in all types of matrix. The major requirements are that they are strong and stiff.

Whiskers are small single crystals a few tens of micrometers in length with a diameter typically <1 μm. Whiskers have extremely high strengths, approaching the theoretical strength, because of the absence of crystalline imperfections such as dislocations.

20.20 OXIDE FIBERS

Oxide fibers have been commercially available since the 1970s. Control of the microstructure through careful processing is essential to obtain the desired properties, which for ceramic fibers for structural applications are

- Low porosity
- Small grain size (for low-temperature applications)
- Large grain size (for high-temperature applications where creep is a concern)
- High purity

Ceramic fibers cannot usually be produced by the techniques used to produce glass fibers because of the very high melting temperatures (often >2000°C) and the low viscosities when molten. There are four general methods to produce ceramic fibers:

- From slurry
- By sol-gel processing
- By chemical vapor deposition
- From polymer precursors

As you can see chemistry plays an important role and consequently there is overlap with Chapter 22. In this section we give one typical example of each of the methods, but bear in mind that it is possible to produce fibers of many other ceramics by similar routes.

Alumina Fibers from Slurry

A fiber developed in 1974 by DuPont and known as ‘Fiber FP’ was the first commercially produced alumina fiber. It has now been discontinued, but the process is a good illustration of the use of a slurry.

Step 1. Slurry formation. The slurry is an aqueous solution containing aluminum oxychloride [Al₂(OH)₅Cl] together with additions to stabilize the suspension (defloculents) and polymers to modify the viscosity. The viscosity must be adjusted such that the slurry is spinnable.

ALKYL CHAINS

Straight chains are always designated as normal, and the word is usually abbreviated to *n*-. So in *n*-butoxide the alkyl chain is CH₃CH₂CH₂CH₂-].

Step 2. Spinning. The slurry is extruded through a spinnerette into “green” fibers and dried. A similar process produces polymer fibers, such as nylon.

Step 3. Firing. The “green” fibers are fired initially at low temperatures to drive off the organic additives and convert the aluminum oxychloride to the oxide. It is during this

stage that shrinkage of the fiber is controlled. Firing at higher temperature causes sintering that results in solid fibers with a controlled amount of porosity and grain size. The resulting fiber is 99% α-Al₂O₃, 98% theoretical density, with a diameter of 10–20 μm and a grain size of ~0.5 μm. The mechanical properties of these fibers at room temperature are good, but the fibers are susceptible to grain growth at temperatures >1000°C, which leads to a considerable fall in strength.

Zirconia Fibers by Sol-Gel Processing

Step 1. Sol formation. Zirconium *n*-butoxide [Zr(*n*-OBu)₄] is mixed with hydrogen peroxide (H₂O₂), nitric acid (HNO₃), and a solution of yttrium nitrate [Y(NO₃)₃ · *n*H₂O]. The zirconium *n*-butoxide undergoes hydrolysis producing zirconium hydroxide and a molecule of alcohol.



Step 2. Gelation. After mixing the solution is heated to 60°C; at this temperature the alcohol evaporates. The viscous solution is passed through a spinnerette to produce gel fibers.

Step 3. Firing. The gel fibers are fired to produce a ceramic. The zirconia is stabilized in a cubic fluorite structure by the presence of yttrium in the structure. The polycrystalline fibers are typically 5–10 μm in diameter. The grain size depends on the sintering temperature. At temperatures ≤1000°C the grain size is <0.1 μm. If the sintering temperature is 1500°C the grains are ~1 μm in diameter.

Silicon Carbide Fibers by Chemical Vapor Deposition

Chemical vapor deposition often involves decomposition of a volatile gas to produce a nonvolatile solid. The reaction usually proceeds at high temperature and the solid is deposited onto some form of substrate. In the case of fiber formation the substrate is a wire. SiC can be formed by decomposing methyltrichlorosilane, CH₃SiCl₃:



The substrate or core in this case is a 10-μm-diameter tungsten wire. The deposit consists of fine crystals of

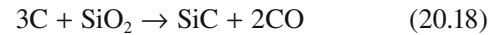
β -SiC oriented preferentially with the {111} planes parallel to the fiber axis. These fibers, which are sometimes called monofilaments, have diameters in the range of 100–150 μm . It takes about 20 seconds in the reactor to obtain a monofilament of 100 μm . Because of their large diameter and high Young's modulus, monofilaments are not flexible and, as a consequence, cannot be easily woven. The properties of the fiber are degraded above about 1000°C because of the formation of W_2C and W_5Si_3 .

POLYCRYSTALLINE Si

This is used by industry to manufacture Si boules. It is prepared by decomposing silanes onto high-purity Si cores.

In the mid-1970s, a process for obtaining SiC whiskers by pyrolyzing rice hulls was developed. Rice hulls are a waste byproduct of rice milling. For each

100 kg of rice milled, about 20 kg of rice hull is produced. The rice hulls contain silica, which comes from the soil and is closely mixed into the cellulose structure of the rice hull in fortuitously near ideal amounts for producing SiC. The rice hulls are heated (called “coking”) in an oxygen-free atmosphere at 700°C and the volatile constituents are driven off. The coked rice hulls, containing about equal amounts of SiO_2 and free carbon, are further heated in an inert or reducing atmosphere (flowing N_2 or NH_3 gas) between 1500 and 1600°C for about 1 hour to form SiC:



About 10% of the product is in the form of whiskers and the remaining product is in the form of particles, generally platelets. The whiskers may be separated out to give a 90–95% “pure” product.

SiC whiskers are used commercially in a number of different applications. Alumina reinforced with 25–30 wt% SiC whiskers is the material of choice for inserts used in high-speed cutting of nickel-based superalloys (for aerospace applications). However, whiskers do have a number of disadvantages over particles. It is difficult to produce homogeneous dispersions as the whiskers tend to form entangled agglomerates and, even if well dispersed, some orientation of the whiskers occurs leading to anisotropic properties.

Silicon Carbide Fibers from Organic Precursors

These processes allow the production of fibers (10–20 μm in diameter) thinner than those produced by chemical vapor deposition (CVD).

Step 1. Precursor synthesis. For SiC fibers the precursor is polycarbosilane, a high-molecular-weight polymer containing both Si and C. Polycarbosilane is synthesized by dechlorination of dimethylchlorosilane (a commercially available organic compound) by reacting it with sodium to produce polydimethylsilane. Thermal decomposition and polymerization of polydimethylsilane lead to polycarbosilane. The average molecular weight of the resulting polymer is about 1500.

Step 2. Melt spinning. The polymer is melt spun from a 500-hole nozzle at about 350°C under N_2 to obtain the so-called “preceramic continuous precursor fiber.”

Step 3. Firing. The precursor fiber is quite weak and must be converted to a strong SiC fiber by firing. The heat treatment involves several stages. Initially the precursor fiber is oxidized in air at 200°C to induce cross-linking of the polymer chains. Heating is continued slowly in N_2 . Above 200°C, the side chains containing hydrogen and methyl groups decompose. The conversion to SiC is complete above about 850°C.

The SiC is in the form of small (~2 nm) crystals of β -SiC. The fiber is not pure SiC as some oxygen remains from the low temperature heat treatment and also excess silicon and carbon are present. A typical composition is 59% Si–31% C–10% O.

20.22 GLASS FIBERS

“Glass fiber” is a generic term like “carbon fiber” or “steel.” There are many types of glasses, but from the point of view of composite technology only silica glasses are currently important. However, even within this group of glasses the composition, and hence properties, vary considerably. The composition of three glasses commonly used in fibers is given in Table 20.9.

The “E” in E glass is an abbreviation for electrical. E glass is a good electrical insulator and it has good strength

20.21 WHISKERS

SiC whiskers are the strongest materials known that are produced in commercial volumes. There are two methods that are used:

- Vapor–liquid–solid (VLS) process (this is described in Chapter 29)
- From rice hulls (described below)

TABLE 20.9 Approximate Chemical Compositions of Some Glasses Used in Fibers (wt%)

	<i>E glass</i>	<i>C glass</i>	<i>S glass</i>
SiO_2	55.2	65.0	65.0
Al_2O_3	8.0	4.0	25.0
CaO	18.7	14.0	—
MgO	4.6	3.0	10.0
Na_2O	0.3	8.5	0.3
K_2O	0.2	—	—
B_2O_3	7.3	5.0	—

and a reasonably high Young's modulus. This glass is based on the eutectic in the ternary $\text{CaO}-\text{Al}_2\text{O}_3-\text{SiO}_2$ with some substitution of B_2O_3 for SiO_2 and MgO for CaO . The B_2O_3 substantially lowers the liquidus temperature giving a longer working range and consequently makes fiber drawing easier. More than 90% of all continuous glass fiber produced is of the E glass type and is used mainly as a reinforcement in PMCs.

S glass is based on the $\text{SiO}_2-\text{Al}_2\text{O}_3-\text{MgO}$ system; this fiber has higher stiffness and strength (hence the designation "S") than E glass. It also retains its mechanical properties to higher temperatures. However, S glass is more difficult to draw into fibers due to its limited working range and is therefore expensive.

C glass has a high CaO content and this results in a glass with a high corrosion resistance in acid and alkaline environments.

Producing glass fibers is a well-established technology. Figure 20.15 shows a schematic of the conventional procedure for forming glass fibers. The raw materials are melted in a hopper and the molten glass is fed into electrically heated platinum-rhodium bushings; each bushing contains 200 holes at its base. The bushing diameter is 1–2 mm. A constant head of molten glass is maintained

E GLASS: E IS FOR ELECTRICAL
Most applications of E glass do not utilize its electrical properties.

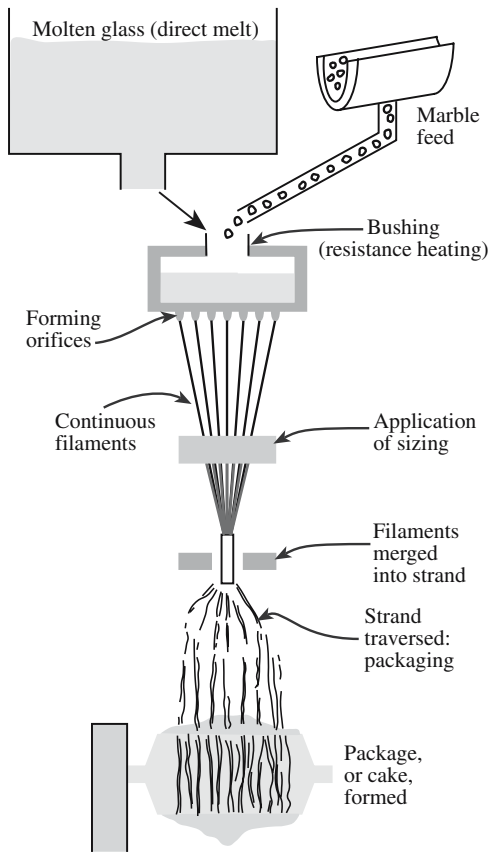


FIGURE 20.15 Fiber-forming process using either a glass melt or marble feed.

in the tank. The glass flows by gravity through the holes, forming fine continuous filaments that are gathered together and passed around a fast rotating collet, followed by drawing rapidly at a speed of 1–2 km/min. The diameter of the glass fibers depends on the diameter of the bushing orifice, the viscosity of the melt, which is a function of temperature and composition, and the head of glass in the hopper. Typically fibers produced in this way have a diameter on the order of 10 μm . A "size" consisting of an aqueous polymer emulsion is applied before the fibers are wound onto a drum. Sizing protects the

surface of the fibers from damage and also helps in handling the fibers by binding them into a strand.

Because optical fibers require much more precise control over composition and impurities than glass fibers for composites they are prepared by very different means; we describe the methods for preparing optical fibers in Chapter 32.

20.23 COATING FIBERS

The interface between fiber (or whisker) and matrix is the key to the overall mechanical properties of a composite. A weak interface allows a propagating crack to be deflected, which increases the toughness of the composite. A strong interface allows transfer of the load from the matrix to the fiber and produces an increase in modulus and stiffness of the composite. In CMCs we are usually more interested in producing a weak interface so that debonding occurs, which often leads to fiber pull-out by frictional sliding and substantial absorption of energy.

Figure 20.16 shows the effect of carbon coatings of increasing thickness (D_c) deposited on Nicalon™ (a

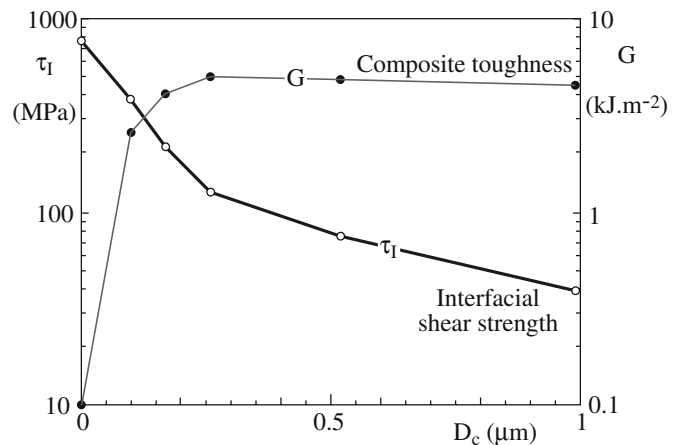


FIGURE 20.16 Effect of carbon coating thickness (D_c) on the mechanical properties of Nicalon™ fibers in a SiC matrix. Interfacial shear strength was measured by push-down testing and toughness from the area under the stress–strain curve during loading along the fiber axis.

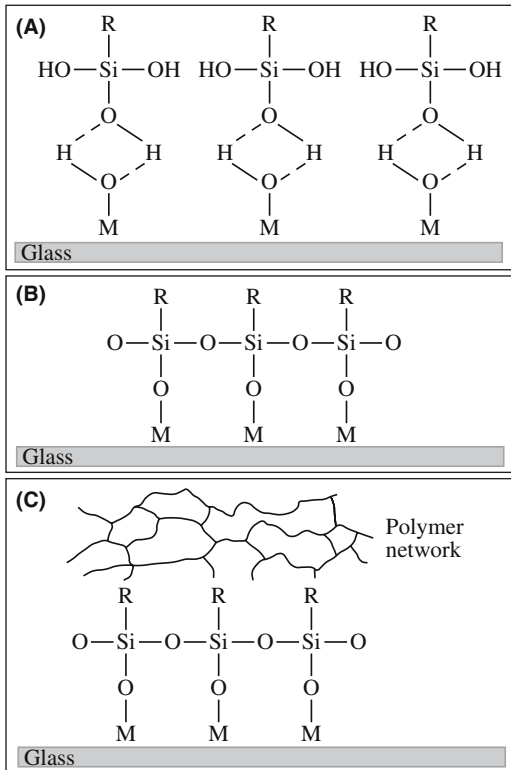


FIGURE 20.17 Illustration of the processes involved in joining a polymer and glass using silane coupling agents. (a) Hydrolysis of the silane to the corresponding silanol; (b) hydrogen bonding between hydroxyls on the silanol and those attached to the glass; (c) polysiloxane bonded to the glass following condensation during drying; and (d) bonding between the functional group R and the polymer.

commercial SiC fiber produced from polymer precursors) fibers prior to composite formation. The interfacial shear strength decreases with increasing coating thickness, but the macroscopic toughness increases.

When ceramic fibers are in contact with metals at elevated temperatures (e.g., during fabrication of MMCs) an extensive reaction can occur that leads to interfacial cracking and degradation in the properties of the composite. These reactions are particularly severe for titanium matrices, which are of interest for high-temperature applications. Applying a protective coating (called a diffusion barrier) can reduce the extent of the reaction. These coatings must be

- Thermodynamically stable
- Nonpermeable to migrating reactants
- Robust

Although it is difficult to meet all these requirements, particularly the first one, coatings that provide protection to ceramic fibers in titanium MMCs have been developed; examples include carbon and duplex C/TiB₂.

Glass fibers, widely used as reinforcements in PMCs, are often coated to improve their durability in aqueous

environments. Reaction with water can result in the formation of a weak porous surface on the fiber and to weak bonding between fiber and matrix. Coating a glass fiber with a coupling agent can lead to strong interfacial bonding. There are many types of coupling agents, and the principles of how they work can be illustrated with silane coupling agents. These have the general formula R-Si-X₃, where X represents hydrolyzable groups such as ethoxy (-OC₂H₅). The R group is chosen based on the type of polymer used for the matrix. The processes leading to bond formation between a glass fiber and a polymer matrix via the use of a silane coupling agent are illustrated in Figure 20.17.

20.24 MAKING CERAMIC-MATRIX COMPOSITES

Monolithic ceramics generally have reasonably high strength and stiffness but are brittle with low toughness. One of the main reasons for forming CMCs is to increase toughness. Naturally it is also hoped, and often found, that there is a concomitant improvement in strength and stiffness.

The development of CMCs has lagged behind MMCs and PMCs for two primary reasons:

- Most of the processing routes for CMCs involve high temperatures and can be employed only with high temperature reinforcements. It was not until fibers and whiskers of ceramics such as silicon carbide were readily available that there was much interest in CMCs.
- Differences in coefficients of thermal expansion, α , between the matrix and the reinforcement lead to thermal stresses on cooling from the processing temperature. These stresses can lead to cracking of the matrix.

The number of feasible methods for producing CMCs is limited and very few of these are commercially viable at the present time.

20.25 CERAMIC-MATRIX COMPOSITES FROM POWDERS AND SLURRIES

This is simply an extension of the powder route for producing monolithic ceramics. A powder of the matrix constituent is mixed with the toughening constituent, which is in particulate or whisker form, together with a binder. The mixture is then pressed and fired or hot pressed.

Difficulty can be experienced in obtaining a homogeneous mixture of the two constituents and high proportions of the toughening phase cannot be easily achieved. Additional problems may arise with whiskers. Whiskers tend to aggregate causing a significant reduction in the

packing efficiency. Also damage to the whiskers can occur during mixing and pressing, particularly when cold pressing.

Because of the difficulties encountered in obtaining homogeneous mixtures by conventional powder processing, wet processing is sometimes favored. It is essential that the constituents remain deflocculated, i.e., well dispersed, in the slurry. Deflocculation is achieved by control of the pH of aqueous solutions and by ultrasonic agitation of the slurry.

The slurry process can also be used to produce composites by tape casting. An example is the fabrication of laminated SiC whisker-reinforced mullite composites.

1. Mullite is mixed with an organic binder in a ball mill for 24 h. SiC whiskers, between 10 and 50 vol%, are added and mixed for a further 24 h.
2. The mix is tape cast to produce sheets having a thickness of 50–200 μm . The whiskers are all oriented with their long axes parallel and aligned to the edges of the tape.
3. Several sheets (40–80) are laminated together at 80°C and 35 MPa for 10 min.
4. The binder is burned out by heating the laminate to 600°C at a rate of 2°C/min. The hold time at this temperature is 2 hours.
5. The laminate is hot pressed at 1550–1850°C for 30–70 minutes at a pressure of 35 MPa. An oriented SiC whisker composite is produced.

Another slurry-based process to form CMCs involves passing the fibers (e.g., SiC) through a slurry of glass powder, water, and a binder. The bundles of fibers (called tows) impregnated with the slurry are wound on a mandrel to form a monolayer tape. The tape is cut into plies that are stacked into the required stacking sequence, e.g., unidirectional or cross-ply, prior to burnout of the binder. Hot pressing is used to consolidate the matrix. In glass-ceramic composite production some crystallization occurs during hot pressing, but an additional heat treatment may be required to complete devitrification.

20.26 CERAMIC–MATRIX COMPOSITES BY INFILTRATION

Melt infiltration techniques, although well established for MMCs, have met with only limited success for CMCs. The main problems are

- Reactions with the reinforcement due to the high melting temperatures of refractory ceramics and the reactivity of molten glasses
- Low rates of infiltration resulting from the high viscosities

The most successful of the melt techniques is matrix transfer molding, which was originally developed for glass

matrix composites but can also be used for glass-ceramic matrix composites. The advantage of matrix transfer molding is that it permits fabrication of components such as tubes, which are difficult to produce by other methods. In tube production, a preform and a glass slug are inserted into a cylindrical mold. Application of heat and pressure forces the fluid glass into the pores in the preform and, after cooling, the composite tube is ejected from the mold.

If a sol is poured over a preform it will infiltrate it because of its fluidity. The sol is then dried in a subsequent heat treatment. The processing temperature is normally low, thus reducing the risk of damage to the preform, and complex shapes can be produced. However, there are disadvantages of high shrinkage and low yield and consequently repeated infiltrations are necessary to increase the density of the matrix. Furthermore, for some materials temperatures higher than those needed just for drying are required to produce the desired ceramic, e.g., $\text{Zr}(\text{OH})_4$ needs to be calcined at about 550°C to give ZrO_2 .

Infiltration can be done in the vapor phase using a CVD process. In composite technology CVD is used, as we have already seen, to produce fibers. It is also used to coat fibers and to infiltrate porous preforms to form the matrix. In the latter case the process is called chemical vapor infiltration (CVI).

CVI is very similar to the CVD processes we have already described. The gaseous reactants infiltrate the heated substrate positioned in the reactor. A chemical reaction occurs in the gaseous state and deposition of the matrix takes place. The maximum deposition rate is about 2500 $\mu\text{m}/\text{h}$.

The best-established CVI process is for the production of carbon–carbon composites. It has also been employed for the production of a wide range of ceramic matrices including carbides (e.g., B_4C , SiC, TaC, and TiC), nitrides (e.g., BN and Si_3N_4), TiB_2 , and Al_2O_3 .

The advantages of CVI are

- Complex shaped preforms can be coated.
- Relatively low temperatures (800–1000°C) can be used.
- *In situ* fiber surface treatments can be made prior to densification.

The main disadvantages are that the process is time consuming and expensive.

20.27 IN SITU PROCESSES

The Lanxide process, developed by the Lanxide Corporation, involves the formation of a ceramic matrix by the reaction between a molten metal and a gas, e.g., molten aluminum reacting with oxygen to form alumina. Growth

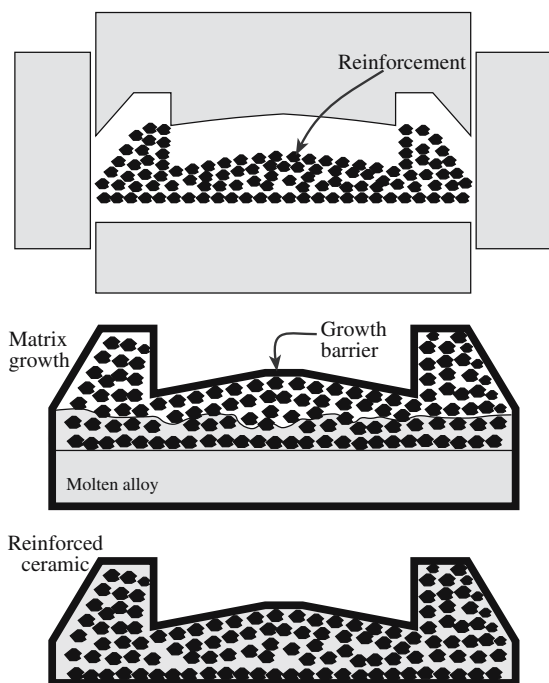


FIGURE 20.18 Illustration of the Lanxide process for making a shaped CMC.

of the ceramic occurs outward from the original metal surface and through a preform as illustrated in Figure 20.18. A preform is not a prerequisite. By simply placing powder particles above a liquid metal particulate reinforced composites may be produced. In both cases the only requirements are that the fibers/particles do not react with the gas and are wetted by the ceramic. One of the big advantages of this type of process is that near-net-shape forming is possible.

A number of novel techniques are being studied whereby the composite is formed *in situ* via a chemical reaction. One possible reaction is



Such reactions have the potential to give good homogeneous distributions of the toughening phase, and the raw materials may be less costly than the products, e.g., BN is expensive.

CHAPTER SUMMARY

In this chapter we described ceramic particles and their use in making composite materials. We paid particular attention to how ceramic powders are produced. The important characteristics of ceramics powders are size and size distribution, shape, and chemical composition

As is often the case, this is a big subject. For many traditional ceramic products cost is one of the overriding concerns; therefore the most inexpensive method of producing powders is often selected. For advanced ceramics products such as those used in the electronics industry, obtaining fine-grained uniform particles of high purity is often the dominant issue. For these applications chemical routes such as sol-gel are used for powder production. For nonoxide ceramics, such as Si_3N_4 , vapor-phase routes are used to produce powders. A major advantage of vapor-phase routes is that we can produce nanoparticles with narrow size distributions.

We also described the different analytical techniques used to characterize powders both in terms of their size and composition. To determine particle size it is necessary to choose a method that has sufficient sensitivity. Sieving is a low-cost method and is reliable when the particle size is greater than about $60\mu\text{m}$. But if the particles are smaller than this, as is often the case, then the use of light scattering or X-ray diffraction should be considered. In determining both particle size and chemical composition it is essential that the specimen we choose for analysis is representative of the entire powder sample.

Ceramics in the form of fibers and whiskers are often used as reinforcing phases in composites. We described the different methods used to produce whiskers and fibers and how they are incorporated into PMCs, MMCs, and, particularly for our interest, CMCs. One of the current directions in the production of CMCs is to produce the matrix and fiber *in situ*.

PEOPLE IN HISTORY

BET: Stephen Brunauer (1903–1986) was born in Budapest. Paul Emmett (1900–1985) was born in Portland, Oregon and was in the same Ph.D. class as Linus Pauling. Edward Teller, also born in Hungary (1908–2003), is also known for his work in physics.

Coulter, Wallace H. (1913–1998) was born in Little Rock, Arkansas. He patented the Coulter principle in 1953 and began production of the Coulter counter with his brother Joseph. The instrument was originally used to count blood cells. He established the Coulter Corporation in Miami Florida in 1961.

Reynolds, Osborne (1842–1912) published his famous paper that described the Reynolds number in 1883. The paper, “An experimental investigation of the circumstances which determine whether motion of water shall be direct or sinuous and of the law of resistance in parallel channels,” was published in the *Philosophical Transactions of the Royal Society*.

Stokes, Sir George Gabriel (1819–1903) was Master of Pembroke College, Cambridge, Lucasian Professor of Mathematics (a position once held by Sir Isaac Newton and now held by Stephen Hawking), and a former President of the Royal Society. Stokes was one of the foremost mathematicians of his time and established the field of hydrodynamics.

GENERAL REFERENCES

Allen, T. (1997) *Particle Size Measurements. Volume 1: Powder Sampling and Particle Size Measurements. Volume 2: Surface Area and Pore Size Determination*, 5th. edition, Chapman & Hall, London. Comprehensive guides to particle size, surface area, and pore size measurements covering experimental methods and data analysis.

Chawla, K.K. (1993) *Ceramic Matrix Composites*, Chapman & Hall, London. A detailed description of CMCs.

Evans, J.W. and DeJonghe, L.C. (1991) *The Production of Inorganic Materials*, Macmillan Publishing Company, New York. Standard description of powder processing. Covers more than ceramics.

Matthews, F.L. and Rawlings, R.D. (1994) *Composite Materials: Engineering and Science*, Chapman & Hall, London. A standard composite textbook. At a similar level to this text.

Rahaman, M.N. (1995) *Ceramic Processing and Sintering*, Marcel Dekker, Inc., New York. A detailed description of ceramic powder processing.

Reed, J.S. (1988) *Introduction to the Principles of Ceramic Processing*, John Wiley & Sons, New York. A detailed description of powder processing.

Ring, T.A. (1996) *Fundamentals of Ceramic Powder Processing and Synthesis*, Academic Press, San Diego. Again with more detail on milling.

Segal, D. (1989) *Chemical Synthesis of Advanced Ceramic Materials*, Cambridge University Press, Cambridge.

SPECIFIC REFERENCES

Brunauer, S., Emmett, P.H., and Teller, E. (1938) “Adsorption of gases in multimolecular layers,” *J. Am. Chem. Soc.* **60**, 309. The original BET paper; cited almost 7000 times.

LaMer, V.K. and Dinegar, R.H. (1950) “Theory, production and mechanism of formation of monodispersed hydrosols,” *J. Am. Chem. Soc.* **72**, 4847.

Messing, G.L., Zhang, S-C., and Jayanthi, G.V. (1993) “Ceramic powder synthesis by spray-pyrolysis,” *J. Am. Ceram. Soc.* **76**, 2707. A comprehensive review of spray pyrolysis.

Pechini, M.P. (1967) “Method of preparing lead and alkaline earth titanates and niobates and coating method using the same to form a capacitor,” U.S. Patent 3,330,697.

Suryanarayana, C. and Norton, M.G. (1998) *X-Ray Diffraction: A Practical Approach*, Plenum, New York. In particular, experimental module 6 shows how to determine particle size and experimental module 7 shows the method used to determine phase proportions in a powder mixture using XRD.

Vander Voort, G.F. (1984) *Metallography: Principles and Practice*, McGraw-Hill, New York, p. 435. Currently out of print. Although its title says it is for the metallurgist, it contains a detailed discussion of grain size determination that can be applied equally well to nonmetals. It gives a detailed description of the various methods and their pros and cons.

WWW

www.ube.com

Ube Industries in Japan, a commercial manufacturer of Si_3N_4 . There are currently no U.S. suppliers of Si_3N_4 powder.

EXERCISES

- 20.1 (a) Explain briefly the differences between jet milling, vibratory milling, and agitated ball milling. (b) Which technique would you use if you wanted to obtain a particle size of $<1\ \mu\text{m}$. (c) Which technique would you use if maintaining the purity of your powder was your primary concern.
- 20.2 Why does the sol-gel process allow outstanding control of purity and chemical homogeneity of ceramic powders?
- 20.3 In Section 20.6 we described the Pechini method for producing SrTiO_3 powders. Other multicomponent oxide powders such as $\text{YBa}_2\text{Cu}_3\text{O}_7$ (YBCO) have been made by a similar process. Identify suitable reactants to make YBCO powders by the Pechini method.

- 20.4 You have been employed as a consultant by a company making ceramic powders. Your first assignment is to recommend a technique for measuring particle sizes. An external analysis company has found that the powders typically have a size in the range of 5–30 μm . The powders are also sensitive to moisture. What technique(s) would you recommend and why?
- 20.5 You are given a sample of a whisker reinforced CMC. How would you go about determining the relative amount of whiskers in the composite and also the composition of the whiskers and matrix phases?
- 20.6 Compare the material costs involved in making a BN-reinforced Al_2O_3 CMC composite by (a) combining the individual constituents, and (b) using an *in situ* reaction involving AlN and B_2O_3 . Would you expect the two composites to have similar microstructures?
- 20.7 What are the different forms of commercially available fiber that contain mainly alumina and silica?
- 20.8 Assuming that Figure 20.14 was recorded using $\text{Cu-K}\alpha$ radiation, plot the change in particle size as a function of annealing temperature.
- 20.9 Are there any commercially available ceramic nanopowders? If so, what compositions are available and how much do they cost compared to a “conventional” powder of the same material?
- 20.10 Compare the use of scattering of visible light and that of X-rays to determine particle size distributions.

Glass and Glass-Ceramics

CHAPTER PREVIEW

The structure of glass, particularly silica glass, was introduced at the end of Chapter 7. In this chapter we discuss the different types of glass and some of their various applications. Then, in Chapter 26, we will concentrate on processing glass and the wide variations in compositions. Only two chapters have been devoted to glass due to space limitations; do not take this as a reflection on its importance. Glass is arguably our most important material. It is used for windows, containers, lenses, optical fibers, insulators, glazing and enameling, surgical knives, spectacular art, and road signs! Glass is usually recyclable and environmentally friendly. The Egyptians were great glassworkers, but they were not the first. Glass was actually used much earlier and obsidian, a natural black volcanic glass, was important during Paleolithic times. We can say that glass has played a major role in shaping our civilization.

However, there is some difficulty in defining a glass. We will discuss why the words glassy, vitreous, and amorphous are all used to describe glass and try to answer the question “what is glass”? Two thoughts should be kept in mind while studying this chapter:

- The assertion by Sturkey: “glass at high temperatures is a chemical solution.”
- If glass is a supercooled liquid, it is not a solid so it is not a ceramic (but it is).

The mechanical, optical, and electrical properties of glasses are discussed in detail, along with other ceramics, in those topical chapters.

21.1 DEFINITIONS

The classic definition of glass is based on the historical method of formation: this is a very unusual way of defining any material. The result is that glass is now defined in several different ways.

The classic definition: *Glass is a supercooled liquid.*

The problem with this definition is that in some cases a particular glass can be prepared that never has been in the liquid state.

The American Society for Testing and Materials (ASTM) definition: *An inorganic product of fusion that has cooled to a rigid condition without crystallizing.*

This essentially says the same thing as the classic definition but excludes polymer glass. It is clearly not ideal to rely on the method of production to define a class of materials. We would not consider doing this for crystalline materials.

Alternative definition 1: *Glass is a solid material that does not show long-range order.*

“No long-range order” means not longer than, say, one or two or three times the basic building block of the glass. This definition is consistent with experimental observations [X-ray diffraction (XRD), transmission electron microscopy (TEM), etc.] but it is clearly a little arbitrary since it depends on the size of the building block.

Alternative definition 2: *Glass is a liquid that has lost its ability to flow.*

This definition is consistent, but broader, than the one given by ASTM and uses a mechanical property to describe glass. It is actually close to the more modern physicist’s view of glass.

The main glasses we will discuss are the network oxide glasses, specifically the silicates. Then our definition of such a glass is

Alternative definition 3: *A solid assembly of vertex-sharing tetrahedra lacking long-range order.*

We are concerned only with ceramic glass, but you should know that there are metallic glasses and polymer glasses. How metallic glasses are formed provides a clue to why they exist: they have complicated compositions to “frustrate” crystallization when they are quenched quickly from the melt (a process known as splat quenching). For the same reason, glycerin can be a glass below -90°C . With this *understanding* in mind, we can discuss the basic features of glasses.

Structure

Glasses are essentially noncrystalline (or amorphous) solids often obtained by freezing supercooled liquids. Long-range order (LRO) in the atomic arrangement does not exist over distances greater than, say, 1 nm. The regular arrangement resulting from the distribution over long distances of a repeating atomic arrangement (unit cell), which is characteristic of a crystal, is missing. There is often evidence of a short-range order (SRO) in glasses, which corresponds to the atomic arrangement in the immediate vicinity of any selected atom. Numerous attempts have been made to explain the formation or the nonformation of glasses. We have two basic approaches:

- Consider the structure
- Consider the kinetics of crystallization

In the first case, we examine the geometry of the constituent entities that make up the glass, the nature of the interatomic bonds, or the strength of the bonds. In the second, we consider how the liquid transitions to a solid as the temperature drops below the melting point.

Glass Transition Temperature

We consider a plot of specific volume as a function of temperature as shown in Figure 21.1. This is a form of a time–temperature–transformation (TTT) diagram for a glass. On cooling the liquid from a high temperature, two phenomena may occur at the point of solidification, T_m .

- If the liquid crystallizes there is a discontinuous change in V and a discontinuity in the rate of cooling (associated with the heat of crystallization).
- If no crystallization occurs the liquid passes into a supercooled state and V decreases at about the same rate as above T_m .

At the glass transition temperature, T_g , the slope of the curve decreases to become close to that of the crystalline solid. This break in the cooling curve marks the passage

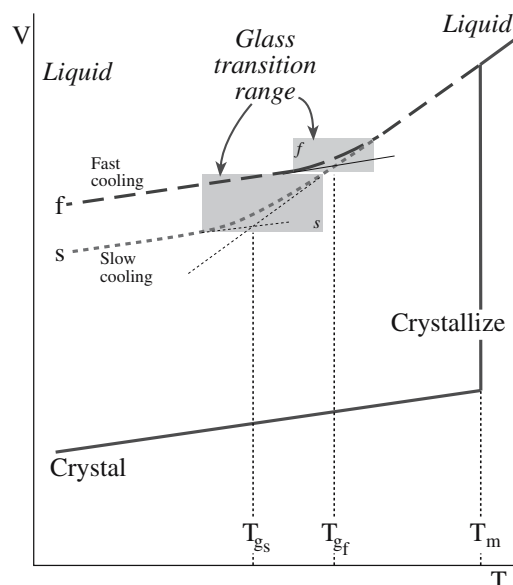


FIGURE 21.1 Plot of volume versus temperature for a liquid that forms a glass on cooling and one that forms a crystalline solid. The glass transition temperature, T_g , depends on the cooling rate and is not fixed like T_m .

TERMINOLOGY

The words “vitreous,” “amorphous” and “glassy” are not actually synonymous although they tend to be used interchangeably anyway.

Vitreous: from the Latin word for glass (*vitrum*)
Amorphous: means having no definite form (strictly speaking, shapeless from the Greek *amorphos*). Now the lack of ‘form’ implies ‘not crystalline.’ Liquids are generally without form, so a ‘solid liquid’ is amorphous.

from a supercooled liquid to a glass. Below T_g the glass structure does not relax very fast because it is now a solid. In the region of T_g the viscosity is about 10^{13} dPa·s. The expansion coefficient for the glassy state is usually about the same as that for the crystalline solid. If slower cooling rates are used so

that the time for the structure to relax is increased, the supercooled liquid persists to a lower temperature, and the resulting glass may have a higher density as shown graphically in Figure 21.1.

The physics of glass examines the concept of fragility; this is actually a property of glass-forming liquids above T_g and is a measure of the strength of the interatomic bonding. We will talk about water dissolving glass or glass containers for water; what is less well known is that you can freeze water into a glassy state by quenching it into liquid ethane. It is a fragile glass, but it is thought that most of the water in the universe exists in this state!

21.2 HISTORY

In Chapter 2 we gave a brief history of glass. We will expand on that discussion here. Glass, like flint, is intimately connected with human history because of the use of obsidian, which is a natural glass. Nobody knows for sure when the first glass objects were made. The oldest

finds date back to ~7000 BCE, or possibly even earlier. Methods of manufacturing glass for its own sake, and not just as a glaze for pots, had already been discovered in Mesopotamia by approximately 4500 BCE. The use of glass as the glaze in pottery dates back even earlier.

Around 3000 BCE Egyptian glassmakers systematically began making pieces of jewelry and small vessels from glass. Glass had both a functional and a decorative role. Pieces of glass jewelry have been found on excavated Egyptian mummies; an example is the turquoise blue glass figure shown in Figure 21.2. By about 1500 BCE Egyptian glassmakers during the reign of Touthmosis III had developed a technique to make usable hollowware. A most striking example is the core-formed bottle in the shape of a *bulti*-fish shown in Figure 21.3. This vessel was made between 1352 and 1336 BCE and was believed to be used to hold scented oil (based on the narrowness of the neck). The wave pattern is very typical of core-formed objects and was made by drawing a sharp object along the softened glass.

The Roman author Pliny the Elder (23–79 CE) explains the invention of glass in his encyclopedia *Naturalis Historia*:

There is a story that once a ship belonging to some traders in nitrum put in here [the coast of modern Lebanon] and that they scattered along the shore to prepare a meal. Since, however, no stones for supporting their cauldrons were forthcoming, they

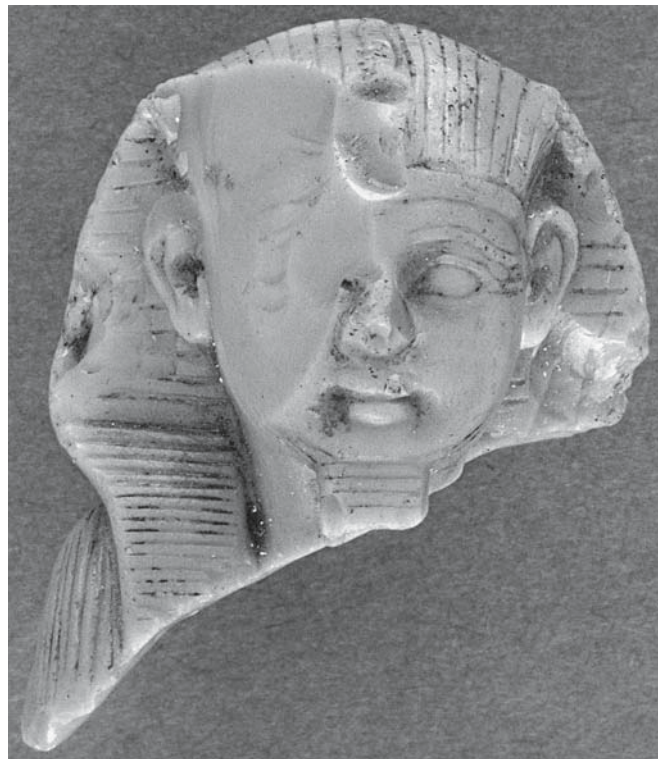


FIGURE 21.2 Glass head of a pharaoh (believed to be Amenophis II) as sphinx, 1400–1390 BCE. It was made by lost-wax casting and is ~3.2cm high.

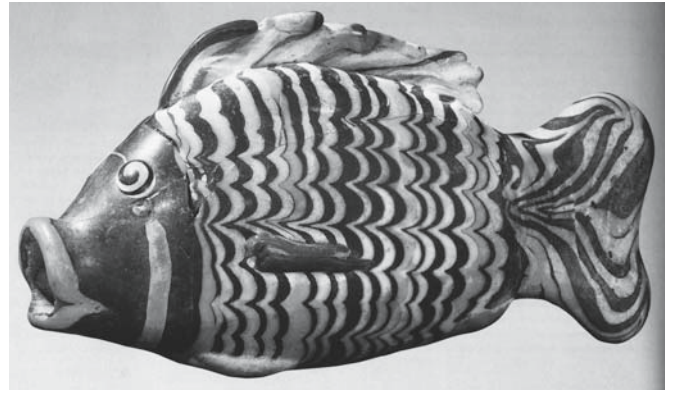


FIGURE 21.3 Core-formed bottle shaped like a *bulti*-fish, 1390–1336 BCE. This example is unusual because it is in polychrome glass. The length is ~14.5cm.

rested them on lumps of nitrum from their cargo. When these became heated and were completely mingled with the sand on the beach a strange liquid flowed in streams; and this, it is said, was the origin of glass.

Nitrum is a naturally occurring soda, an important ingredient in both ancient and modern glasses. The ashes of plants also provided the glassmaker with a rich source of sodium. The plants saltwort and glasswort (known as halophytes) were both used to supply sodium.

Aside: Gerard's Herbal (1633) says that 'saltwort was called Kali by the Arabians': hence the word *alkali* and the ashes are called *soda*.

One of the most common methods used to form glass is glassblowing. Although this technique was developed over two thousand years ago, the glassblowing pipe has not changed much over time. The main development that has been made in glassblowing is the automated blowing processes that are used to produce glass containers and light bulbs and the technique of blowing the glass inside a mold. Most of the important milestones in the history of glass, particularly in the twentieth century, are associated with developments in manufacturing technology. These developments have led to the low-cost production of commercial glasses, for example, window glass, and the use of glass in new applications, such as optical fibers.

Many of the topics summarized here have been rediscovered many times. Now that we have the tools, we can see that nature often preempted humans.

Ancient History

50,000 BCE to 1000 BCE. Glass is used in potter's colored glazes.

7000 BCE to 1500 BCE. Ancient glass artifacts (possibly as early as 10,000 BCE).

2600 BCE. Earliest actual dated glass.

1500 BCE. Egyptians are manufacturing glass articles.

- 1200 BCE. Earliest glass molding.
 100 BCE. Blown glass is invented with the glassblowing pipe (Romans in Syria).
 c100 BCE. In Alexandria the introduction of manganese oxide into the glass composition together with improvements in glass-melting furnaces resulted in the first successful production of colorless glass.
 450 CE. Stained glass was used.

Beginning to Engineer Glass

- 1200s. In Germany a new process was developed to make mirrors. The back of a piece of flat glass was coated with a lead-antimony layer to produce quality (“silvered”) mirrors. The mirror format remains essentially unchanged today.
 1268. Eye glasses described by Bacon. These had convex lenses for the correction of near sightedness.
 1291. Murano, a small island near Venice, became a glass center. Glass workers on Murano were generally not allowed to leave the island.
 c1590. The first telescope lenses were made in Italy and later, in 1604, in the Netherlands.
 1609. Glass was made in Jamestown, Virginia.
 1612. Publication of the textbook *L'Arte Vetraria* by Antonio Neri in Pisa. This was the first systematic account of the preparation of the raw materials for glassmaking.
 1676. George Ravenscroft, an English glassmaker, developed lead-crystal glass (also known as flint glass). The addition of lead oxide to the glass formula yielded a glass of high brilliance and a pure ring. It is not crystal, but it does contain a lot of lead and it is heavy.
 1688. Bernard Perrot, a glassmaker in France under Louis XIV, invented the plate-pouring process. This process allowed mirrors with a large surface area to be produced. Examples are the magnificent wall of mirrors in the Galerie des Glaces at Versailles.
 Late 1700s. Joseph von Fraunhofer (1787–1826), a German mirror maker and student of glassmaking technology, produced optical quality glasses for telescopes and microscopes. (Fraunhofer diffraction and the Fraunhofer Institutes are named in his honor.)

Modern Times

1857. William Clark of Pittsburgh patented a sheet-drawing process: a plate glass.
 1861. A British patent was granted to C.W. Siemens and F. Siemens. Their patent included a discussion of the application of the principle of regeneration to glass melting. Regenerative heating is still used in glass melting furnaces today.
 1865. A U.S. patent was issued for a press-and-blow process.
 1875. Corning Glass Works was incorporated. The company was founded by Amory Houghton Sr. (1812–

1882) and named after the town in upstate New York where it is still located. Houghton already owned the Brooklyn Flint Glass Works, but moved to Corning because real estate was cheaper there.

1881. Thomas Edison brought out his first incandescent electric lamps using glass bulbs made by the Corning Glass Works.
 1884. Otto Schott (1851–1935), Ernst Abbe (1840–1905), Carl Zeiss, and Roderick Zeiss established the Glastechnisches Laboratorium Schott und Genossen, which later became the Jenaer Glaswerk Schott und Gen and in 1952 the Schott Glaswerke. This company is now the leading European glass company.
 1893. The Enterprise Glass Company in the United States developed a press-and-blow mold that led to the widespread production of wide-mouth containers.
 1903. The automatic bottle-blowing machine invented by the American Michael Owens (1859–1923) began production. A machine for drawing large cylinders of glass that were then flattened into window glass was developed by another American, John Lubbers.
 1913. Emile Fourcault, a Belgian, developed a flat-glass machine for commercial operation.
 1917. Edward Danner at the Libbey Glass Company introduced an automatic method for tube making. The company remains in operation today and is the largest manufacturer of glass dinnerware in the United States.
 1926. The Corning ribbon machine for high-speed automatic production of glass light bulbs was developed.

Present Technology

1957. Corning introduced the Pyroceram[®] brand of glass-ceramics.
 1959. Sir Alastair Pilkington's float process for producing flat glass worked.
 1960. Glass-ceramics were patented by S. Donald Stookey of Corning Glass Works.
 1966. Optical fibers were developed.
 1975. Glass recycling became accepted/required.
 1980. An acid-leaching process was introduced for producing 99.6–99.9% silica fibers that resist devitrification up to 1370°C. These fibers were used as insulation for the space shuttle.
 1991. Schott produced an 8.2-m-diameter telescope blank from a glass-ceramic ZERODUR[®], which had been introduced in 1968.
 1997. Corning produces glass for the Subaru Telescope mirror. Weighing 27 t and more than 26 feet across it is one of the largest pieces of glass ever made.

New and improved methods for processing glass are being developed. One of the main thrust areas for these activities is our concern for the environment. Reducing energy costs and reducing polluting emissions are important in the modern glass industry.

21.3 VISCOSITY, η

Viscosity is a key property of glass. We need to know the viscosity of glass at different temperatures so that it can be formed, shaped, and annealed. The concept of viscous flow was described (and illustrated) in Chapter 17 because this is the process by which permanent deformation occurs in glasses. Viscosity is a mechanical property. Consider the tangential force, F , required to slide two parallel plates a distance d apart past one another when they are separated by a layer of viscosity, η :

$$\eta = (Fd)/(Av) \quad (21.1)$$

The common area is A and the velocity of the planes relative to one another is v . Essentially, then, viscosity is a measure of the liquid's response to a shearing. Liquids have viscosities measured in centipoises

(cP) and gases have viscosities measured in micropoises (μP). In the SI system we would say that liquids have viscosities in millipascal-seconds (mPa·s) while gas viscosities are tenths of micropascal-seconds ($\mu\text{Pa}\cdot\text{s}$) (so we stick with the poise).

Table 21.1 lists some of the viscosity values that are important for glass processing. The values given in Table 21.2 are used to define certain characteristics of a glass (again with an emphasis on processing). Many of the values listed in this table of viscosities are "standards." For example, ASTM C338-93(2003) is the "Standard Test Method" for determining the softening point of glass.

Determine the softening point of a glass by determining the temperature at which a round fiber of the glass, nominally 0.65 mm in diameter and 235 mm long with specified tolerances, elongates under its own weight at a rate of 1 mm/min when the upper 100 mm of its length is heated in a specified furnace at the rate of 5°C/min.

The viscosities of some common liquids are given in Table 21.2 for comparison. Notice that at the working point

TABLE 21.1 Viscosity Values for Glass Processing

Viscosity	Example
$10^{1.5}$ – $10^{-2.5}$ dPa·s	ASTM melting
$10^{3.7}$ – $10^{3.8}$ dPa·s	Casting plate glass
$10^{3.8}$ dPa·s	Seal glass to metal
$10^{5.3}$ dPa·s	Begin updrawing or downdrawing
10^6 dPa·s	Sinter glass powder to produce a porous body
10^8 dPa·s	Sinter glass powder to produce a solid body
$10^{11.3}$ – $10^{11.7}$ dPa·s	Glass deforms under gravity
$10^{12.7}$ – $10^{12.8}$ dPa·s	Practical annealing range (stress relief in seconds)

VISCOSITY AND POISE

If a force of 1 dyn is required to move an area of 1 cm² of liquid or gas relative to a second layer 1 cm away at a speed of 1 cm s⁻¹, then the viscosity is one P (poise).

$$1 \text{ P} = 1 \text{ dPa}\cdot\text{s}$$

the glass has a viscosity similar to that of honey at room temperature. For a typical soda-lime-silicate flat-glass composition this viscosity is achieved in the temperature range 1015–1045°C. The other key reference value to remember is that a solid has a viscosity of $>10^{15}$ dPa·s.

The viscosity of glass varies dramatically with temperature as shown in Figure 21.4a for various silicates. The fictive temperature, T_f , is the temperature at which the liquid structure is frozen into the glassy state and is defined by the crossing of the extrapolated curves from high and low temperatures on the η against T plot. The fictive temperature like T_g is related to structural transformations in glass; T_g is slightly lower.

Figure 21.4b shows the temperature dependence of viscosity for the main glass-forming oxides as a function of temperature. You will notice that from the slope of these lines we can obtain the activation energy for viscous flow, E_v

(see Section 17.13). Table 21.3 gives some values for η and some measured crystallization velocities, v . The latter term refers to the rate of movement of the solid/liquid interface. The very low v for SiO₂ is indicative of its excellent glass-forming ability: it is very difficult to crystallize a solidifying melt of SiO₂.

There are several methods for measuring viscosity; which is used depends on the expected value of the viscosity.

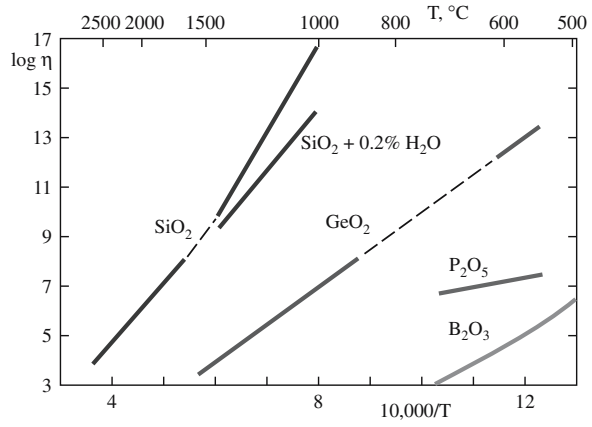
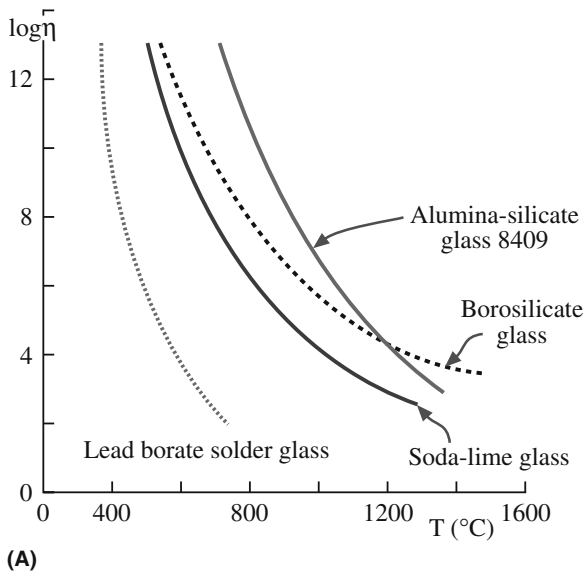
Mergules viscometer	$\leq 10^7$ dPa·s
Fiber elongation	$\leq 10^7$ to 10^9 dPa·s
Beam bending	$\leq 10^9$ to 10^{14} dPa·s

The schematics in Figure 21.5 illustrate the first two approaches to measuring η . The viscometer is used for

TABLE 21.2 Viscosity "Milestones"

Viscosity	Example
10^{-2} dPa·s	Water at 20°C
10^0 dPa·s	Light machine oil
10^1 dPa·s	Heavy machine oil
10^2 dPa·s	Olive oil at 20°C
10^4 dPa·s	Runny honey at 20°C; some measure it to be 10^2 dP·s
10^4 dPa·s	Glass at its working point; begin working at 10^3
$10^{7.6}$ dPa·s	Shortening point (deforms under its own weight; softening at $10^{7.7}$) ^a
10^8 dPa·s	Upper limit for low viscosity
10^{13} dPa·s	Annealing point (ASTM)
$10^{13.4}$ dPa·s	Glass at T_g
$10^{14.6}$ dPa·s	The strain point of glass (ASTM)
$>10^{15}$ dPa·s	Solid
10^{16} dPa·s	Upper limit for measuring viscosity

^aThe shortening point is also called the softening point.



(B) **FIGURE 21.4** (a) Viscosity as a function of temperature (T) for several silicate glasses: units of η are $\text{dPa}\cdot\text{s}$. (b) Viscosity as a function of temperature ($1/T$) for the main glass-forming oxides. Notice the effect that a small amount of water has on the viscosity of silica glass.

TABLE 21.3 Crystallization Velocities and Viscosities of Glass-Forming Liquids

Glass	T_m ($^{\circ}\text{C}$)	v_{max} (cm/s)	Temperature for v_{max} ($^{\circ}\text{C}$)	$\text{Log } \eta$ at T_m ($\text{dPa}\cdot\text{s}$)
Vitreous SiO_2	1734	2.2×10^{-7}	1674	7.36
Vitreous GeO_2	1116	4.2×10^{-6}	1020	5.5
P_2O_5	580	1.5×10^{-7}	561	6.7
$\text{Na}_2\text{O}\cdot 2\text{SiO}_2$	878	1.5×10^{-4}	762	3.8
$\text{K}_2\text{O}\cdot 2\text{SiO}_2$	1040	3.6×10^{-4}	930	
$\text{BaO}\cdot 2\text{B}_2\text{O}_3$	910	4.3×10^{-3}	849	1.7
$\text{PbO}\cdot 2\text{B}_2\text{O}_5$	774	1.9×10^{-4}	705	1.0

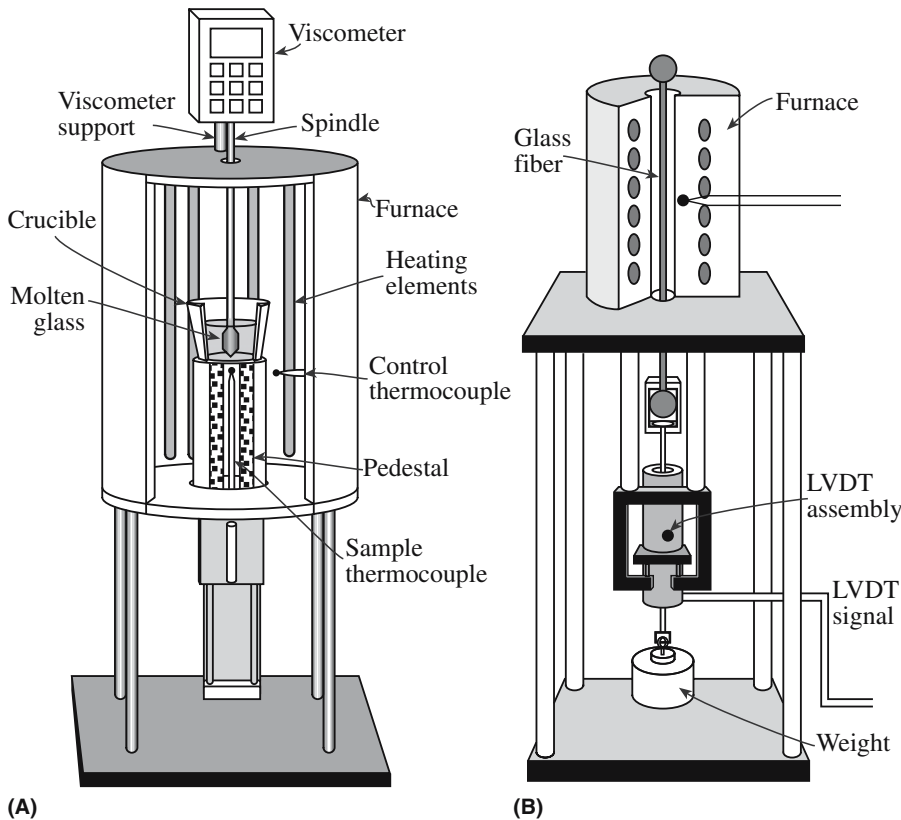


FIGURE 21.5 Schematic illustration of instruments used to measure viscosity: (a) a viscometer; (b) the fiber elongation method.

low viscosities and the method is similar to the concentric cylinder viscometer used to determine the sol-gel transition that we describe in Chapter 22. The spindle is rotated at an angular velocity, ω , and the resistance to its motion is measured.

For higher viscosities the fiber elongation method is used. A load is attached to a glass fiber, which can be heated to a range of temperatures. The strain rate of the fiber as it elongates is then measured.

21.4 GLASS: A SUMMARY OF ITS PROPERTIES, OR NOT

We can summarize what we *know* about glass—and probably be wrong.

Glass is inert. This depends on the environment. It is nearly true if the glass is a silicate and essential if it is going to contain radioactive waste, but not all glasses are inert. Bioglass[®] is designed not to be inert.

Glass is homogeneous. This depends on how the glass was formed and its composition. We can process glass to make it inhomogeneous.

Glass can be reshaped. This is generally true and is the reason why glass is so recyclable. Some glasses are designed so that they can be modified by light, by diffusion, by irradiation, etc.

Glass has a small expansion coefficient. This is usually true, but not all glass is Pyrex[™].

Glass is transparent. This is essential for optical fibers, but we can make it translucent or opaque (see Figure 21.2). Most early glasses were not very transparent because they contained impurities and inclusions.

Glass is cheap. This is true for window glass since the invention of the float-glass process. Thin films may be expensive. Some glass is colored red by doping it with Au. Some vases can cost >\$50k.

Glass is a bulk material. This is true unless we grow it as a thin film or it is present as an intergranular film (IGF) or pocket in, or on, a crystalline ceramic.

So the lesson is to beware of your preconceived ideas when thinking about glass.

The mechanical, optical, thermal, and electrical properties of glasses are discussed in detail, along with other ceramics, in those topical chapters. Here we just give some things to think about in relation to glass.

Some Mechanical Properties of Glass

The theoretical strength of silicate glass is around 10 GPa (using the criterion given in Section 18.2), but this is usually much reduced by the presence of surface flaws (cracks and seeds). Glasses are elastic but break in tension. They can be strengthened by creating a compressive surface layer (by ion exchange or tempering) or by

removing the surface flaws (acid polishing or applying a protective coating). Prince Rupert's drops are an interesting and entertaining illustration of the effect of residual stress on the mechanical properties of glass. Small gobs of molten glass are dropped into cold water to form tadpole-shaped drops. The surface cools much more rapidly than the center creating internal residual stresses and a very high surface tension. The solidified drops can be hit with a hammer without breaking. But if the tail is broken off the entire drop shatters into powder.

Some Electrical Properties of Glass

Glass usually has a high electrical resistivity because of the large band gap energy (see Chapter 30). In cases in which they are conductive the charge is carried by ions, with alkali ions (e.g., Na⁺) being the fastest. Thus conductivity increases significantly as T is increased and it is different for silicate glasses, borate glasses, and phosphate glasses because the glass network is different. The mixed alkali effect is an interesting phenomenon that occurs in glasses that contain more than one different alkali ion. The resulting conductivity has been found experimentally to be significantly lower than would be expected from simply adding their individual conductivities. This has applications in, e.g., high-wattage lamps.

The dielectric constant of glass is quite high but not high enough for some advanced memory applications such as dynamic random access memory DRAMS (see Chapter 31). The capacitance is a measure of the amount of charge stored and is related to the thickness of the dielectric. As the layer gets thinner the capacitance increases, but electrical breakdown can occur. SiO₂ glass has a high dielectric strength but not as high as some polymer dielectrics such as phenolic resin.

Some Optical Properties of Glass

Transmission in the ultraviolet (UV), visible, and infrared (IR) depends on several factors including Rayleigh scattering, which is determined by impurities. The IR edge and the UV edge are the values where transmission of these frequencies cut off. A UV edge blocker removes the UV while a UV edge transmitter allows it through.

Refraction depends on the refractive index and on dispersion. Reflection, which occurs at the surface, can be internal. Because the optical properties of glass are so important much of Chapter 32 is devoted to this topic.

Some Thermal Properties of Glass

Expansion coefficients of glass are generally smaller than for metals. But often we want to make the following connections to metals:

Glass-to-metal seals: an obvious important technological process

SiO₂: metal/insulator junctions for the electronics industry

Graded seals: for example, a graded seal structure can be constructed by joining a series of glass pieces, each of which has a slightly higher thermal coefficient of expansion (α)

Thermal conductivity is ~1% of that of a metal. The implications and applications of this fact are obvious.

21.5 DEFECTS IN GLASS

The idea is that although glass does not have a crystalline matrix, it can still contain point defects, precipitates, undergo segregation, and contain internal interfaces. Glass can be used to trap radioactive elements as point defects or as a “second phase.” The future value of this capability depends in part on how fast components can diffuse through glass. This applies to whether the radioactive material is diffusing out or other components are diffusing in (perhaps to leach out the trapped material).

21.6 HETEROGENEOUS GLASS

Just because glass is a “supercooled” liquid does not mean it must be homogeneous. Certain glasses can separate into two phases, which need not be a crystallization process. When these two phases are both glassy, there may either be no barrier to the separation (a spinodal decomposition) or, as in the case of liquid/liquid phase separation, there may be a nucleation step. In either case, diffusion is important.

The principle of immiscibility in glass is very important to today’s technology. For example, immiscibility plays a role in forming glass-ceramics, making Vycor® and opal glass, and in the precipitation in glass. Many of the binary and ternary oxides with silica as a component show miscibility gaps. A miscibility gap is a region in the phase diagram in which a liquid separates into two liquids of different composition (see Section 8.11). The following are examples of systems exhibiting this effect:

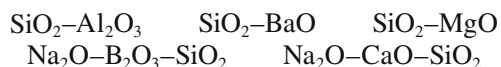


Figure 21.6 shows the SiO₂-Li₂O phase diagram. In the low-temperature silica-rich corner of the diagram one liquid phase separates into two chemically distinct, different liquid phases below the immiscibility dome. The dashed line represents the estimated region of immiscibility. The difficulty in making these measurements is that phase separation occurs at a lower temperature where the kinetics are slower. There is an interesting comparison with crystallization. Phase

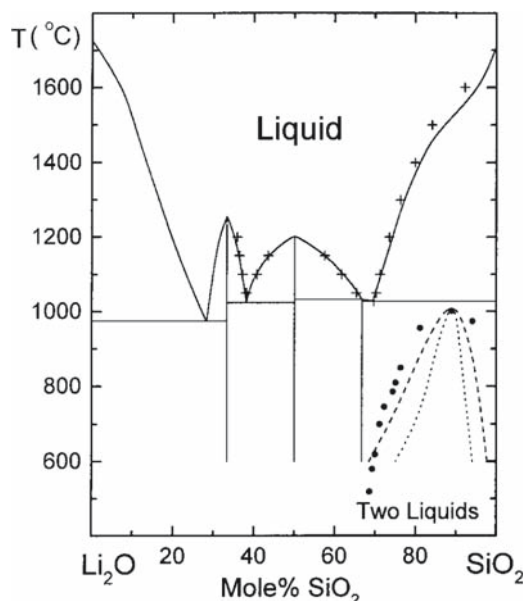


FIGURE 21.6 Region of liquid–liquid immiscibility for SiO₂-Li₂O. Notice that these occur only in the silica-rich end of the phase diagram.

segregation may be energetically less favorable than crystallization, but it is easier to accomplish because it requires only the segregation, not the correct rearrangement of the atoms. As a general rule for silica, immiscibility is increased by the addition of TiO₂, but decreased by the addition of Al₂O₃.

The Vycor process described in Chapter 8 uses the principle of phase separation. The resulting glass is 96% SiO₂ and 4% pores and is used as a filter and a bioceramic where porosity is important. It can be densified (after shaping) to allow processing of a pure SiO₂ shape at a lower temperature than for pure quartz glass.

21.7 YTTRIUM-ALUMINUM GLASS

Yttrium–aluminum (YA) glasses can be formed in the composition range ~59.8–75.6 mol% Al₂O₃. With 59.8–69.0 mol% Al₂O₃, a two-phase glass forms with droplets of one phase in the other. The glass can spontaneously crystallize to form YAG or a mixture of Al₂O₃ and YAlO₃ (YAP; P = perovskite). These YA glasses show a phenomenon known as polyamorphism, meaning that they exist with different amorphous structures.

21.8 COLORING GLASS

Although many applications for glass require a colorless product, for other applications colored glass is needed. Windows in a church do not look as impressive when all

the glass is colorless. Glass is often colored by adding transition-metal oxides or oxides of the rare-earth elements to the glass batch. Table 21.4 lists the colors produced by some of the common glass colorants. We will look at how these additives actually result in the formation of color in Chapter 32, but at this stage you should already know why glass bottles are often green. Bright yellow, orange, and red colors are produced by the precipitation of colloids of the precious metals. Au produces a ruby red coloration, but it is not cheap. CdS produces a yellow coloration, but when it is used in conjunction with Se it produces an intense ruby red color.

The questions are

- How does coloring “work”?
- What causes the colors?
- Is it the same as for crystals?

Glass is intentionally colored by adding dopants (we are creating point defects in the glass). The color of the glass depends on the dopant and its state of oxidation. The explanation is the same as for coloring crystals, but because the glass structure does not have LRO the absorption spectra can be broader.

Combinations of dopants can decolorize, mask, or modify the effect. For example, we can compensate for the coloring effect of Fe by adding Cr; if too much Cr³⁺ is added, Cr₂O₃ can precipitate out. When the glass is blown, these platelets of Cr₂O₃ can align to give “chromium aventurine.” Cu was used to produce Egyptian Blue glass. Co is present in some twelfth-century stained glass and, of course, was used in the glazes on Chinese porcelains in the Tang and Ming dynasties; the color it produces is known as cobalt blue.

In a CdS-doped glass, adding more Se can result in “Selenium Ruby.” The details of all these colorings will depend on just what glass batch is used and the firing conditions.

Corning makes microbarcodes (i.e., very small barcodes) by doping glass with rare earths (REs); the REs have particularly narrow emission bands. Of 13 RE ions tested, four (Dy, Tm, Ce, and Tb) can be excited with UV radiation used in fluorescence microscopy but do not interfere with other fluorescent labels. These microbarcodes can be used for biological applications since they are not toxic; tags using quantum dots may be less benign. These bar codes can even label genes. The REs can be used together to give more color combinations.

Special colored glasses include the following:

Ruby and cranberry glass. Ruby glass is produced by adding Au to a lead glass with Sn present. Cranberry glass, first reported in 1685, is paler (usually a delicate pink) because it contains less gold. The secret of making red glass was lost for many centuries and rediscovered during the seventeenth century.

Vaseline glass or uranium glass. Uranium produces a deep red when used in high-Pb glass. There are other uranium-containing glasses: the so-called “uranium depression-ware” glass (also called Vaseline glass), which has a green color. True “depression ware” is actually greener than Vaseline glass because it contains both iron and uranium oxides. What is special is that the glass actually fluoresces when illuminated with UV radiation (Vaseline ware more strongly because of the higher concentration of uranium). Since 1940 or so, only depleted uranium has been used as a dopant and that is quite plentiful, but for the previous 100 years, natural uranium was used. Figure 21.7 shows an example of Vaseline ware.

TABLE 21.4 Colors Produced by the Inclusion of Different Ions in a Glass

Copper	Cu ²⁺	Light blue (red ruby glass for Cu nanoparticles)
	Cu ⁺	Green and blue (includes turquoise blue)
Chromium	Cr ³⁺	Green
	Cr ⁶⁺	Yellow
	Cr ³⁺ + Sn ⁴⁺	Emerald green
Manganese	Mn ³⁺	Violet (present in some Egyptian glasses)
	Mn ²⁺	Weak yellow/brown (orange/green fluorescence)
Iron	Fe ³⁺	Yellowish-brown or yellow-green
	Fe ²⁺	Bluish-green
	FeS	Dark amber
Cobalt	Co ²⁺	Intense blue (especially if K ⁺ is present); in borates and borosilicates, pink
	Co ³⁺	Green
Nickel	Ni ²⁺	Grayish-brown, yellow, green, blue to violet, depending on glass
Vanadium	V ³⁺	Green in silicates; brown in borates
Titanium	Ti ³⁺	Violet (melting under reducing conditions)
Neodymium	Nd ³⁺	Reddish-violet
Praseodymium	Pr ³⁺	Light green
Cerium	Ce ³⁺	Green
	Ce ⁴⁺	Yellow
Uranium	U	Yellow (known as “Vaseline glass”)
Gold	Au	Ruby (ruby gold, Au nanoparticles)



FIGURE 21.7 Example of Vaseline ware produced by coloring with uranium.

21.9 GLASS LASER

Rare-earth elements (e.g., Nd) are used to dope glass to create lasers and other optical devices (Figure 21.8). The Nd-doped glass laser works like the ruby laser, although there are some differences that relate to the glass. The laser rod is about $\frac{1}{4}$ to $\frac{1}{2}$ inch diameter and is usually pumped by a helical lamp to give a discharge length longer than from a linear lamp. The energy is stored in a capacitor (e.g., 500 mF) with a charge voltage of ~ 4 kV giving a pulse duration of ~ 0.8 ms. The Nd:glass laser gives efficiencies up to 2%, which is four times that of the ruby laser, and the Nd:glass rod can be made even larger. Because the thermal conductivity of the glass is lower it requires more time to cool between firings.

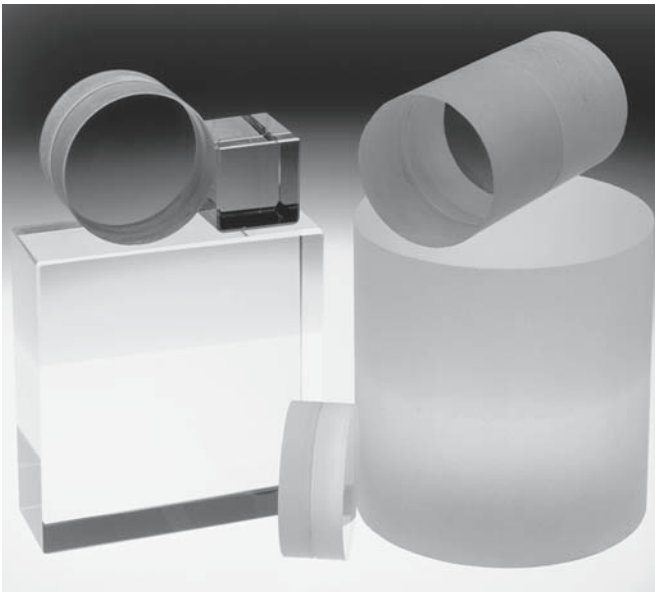


FIGURE 21.8 Examples of phosphate laser glass. Individual laser rods vary from 0.6 to 1.2 mm in diameter.

21.10 PRECIPITATES IN GLASS

Precipitation in glass is generally inevitable given time. The question is only how long it will take to occur, especially if nucleation is homogeneous (i.e., no seeds are present). We may introduce seeds to produce particular effects. Nucleation of crystals in glass follows the classic theory. We will examine the topic more in Chapter 26 and see there that precipitates can also cause the coloring of glass.

21.11 CRYSTALLIZING GLASS

We will address processing these materials in Chapter 26. Here we will explain what a glass-ceramic is and relate it to other two-phase ceramics. We can crystallize a droplet of glass, as shown in Figure 21.9, or a complete film, as shown in Figure 21.10. We can also crystallize a bulk object almost completely to produce a glass-ceramic. The basic idea is that there is sometimes a great advantage in processing a ceramic as a glass but producing the finished object as a polycrystalline body.

Opal glass has a milky (opalescent) appearance caused by the formation of small crystallites. Even window glass crystallizes; given time it devitrifies to form devitrite.

The visible light microscopy (VLM) image shown in Figure 21.11 illustrates the growth of perfectly symmetric individual crystals inside a glass matrix. The crystals and the matrix are all transparent, so the full shape shown here schematically can be appreciated. The SEM images in Figures 21.12 and 21.13 show that the glass and crystal

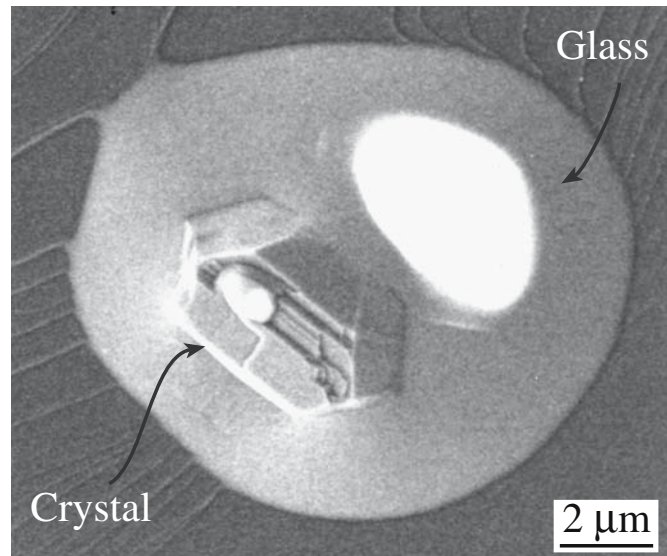


FIGURE 21.9 An example of crystallization in a glass droplet.

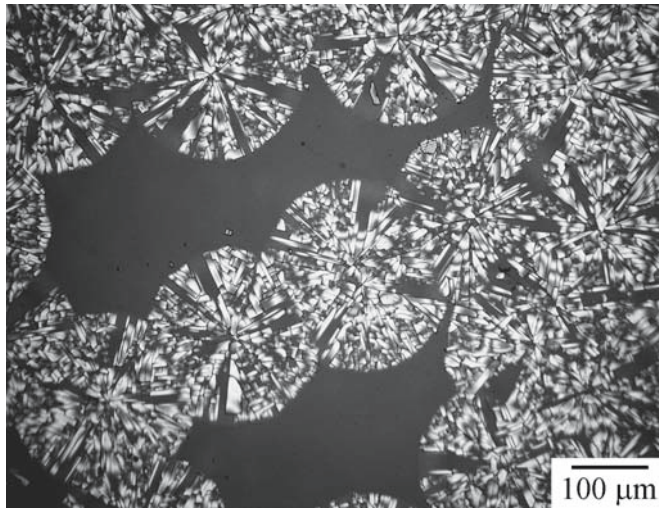


FIGURE 21.10 Spherulitic crystallization of an amorphous SiO_2 film on SiC. The spherulites are cristobalite.

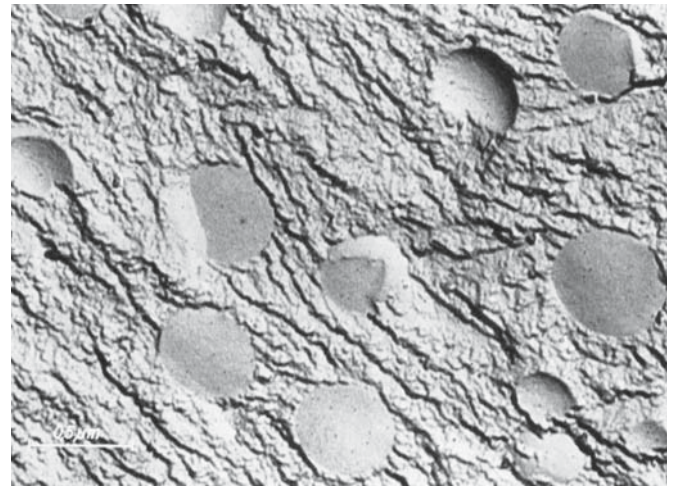
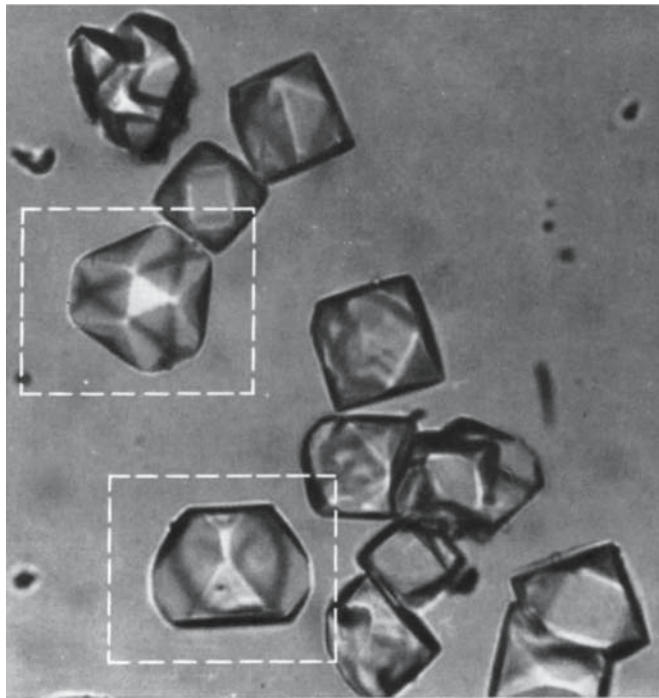
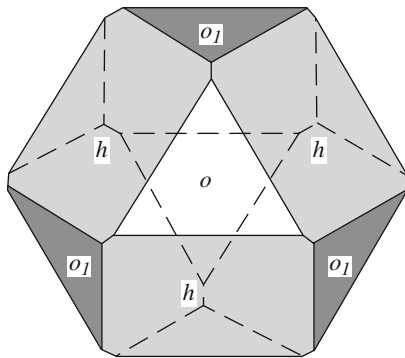


FIGURE 21.12 SEM image of crystallized glass. The glass is a binary Li–Be fluoride opal glass 40 mol% LiF, 60 mol% BeF_2 containing small amounts of Ag and Ce (0.001 and 0.01 mol%, respectively). The glassy droplets (BeF_2 rich) are surrounded by a crystallized matrix.

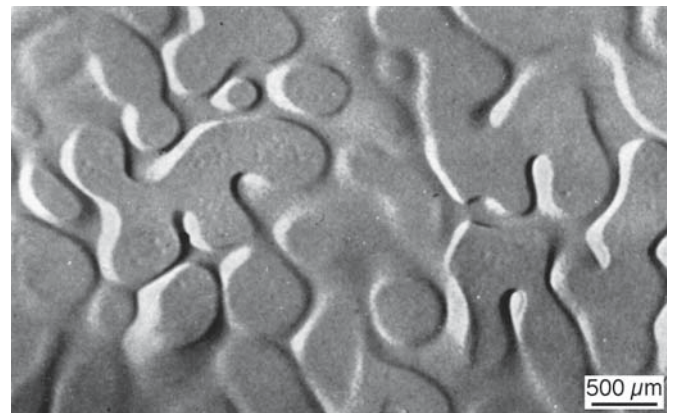


(A)

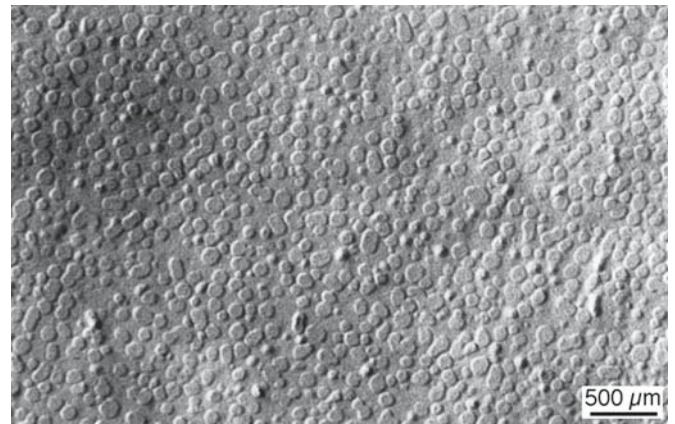


(B)

FIGURE 21.11 VLM image showing crystallization in a glass.



(A)



(B)

FIGURE 21.13 SEM images of (a) Na–Be and (b) K–Be fluoride glass 15 mol% KF (or NaF), 85 mol% BeF_2 . This glass is cloudy: if the droplets were smaller the glass would be clear. Replacing K by Rb actually reduced the droplet size to 10–20nm.

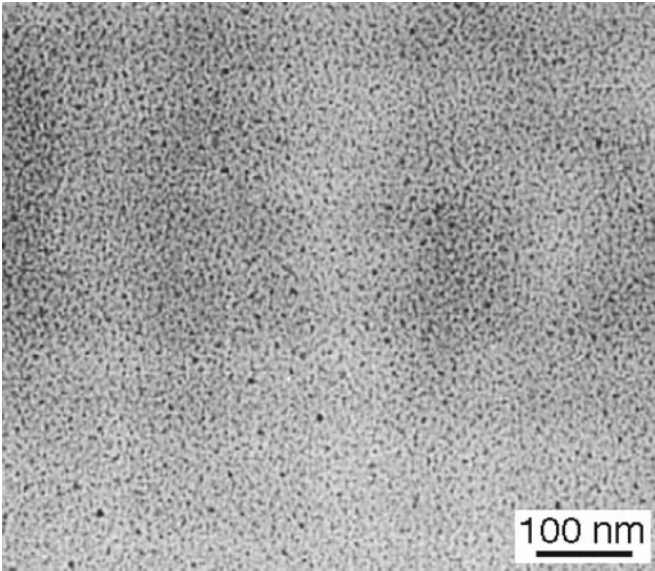


FIGURE 21.14 TEM image showing crystallization on a nanometer scale in an LAS glass-ceramic.

appear very different even on a fractured surface. Breaking a sample can quickly reveal a “grain” size down to $\sim 0.1 \mu\text{m}$. To probe the structure on a near-atomic level with high spatial resolution, TEM can be used as shown in Figure 21.14, but its use has been limited, in part because of the difficulties of preparing the TEM sample: the thickness of the sample tends to be greater than the dimensions of the crystalline phase.

FLUX AND MODIFIERS

The flux in a glaze is a modifier in glass. The clear glaze is glass: i.e., silica and alumina with added modifiers. The clear glaze may contain lead but Pb should not be used for modern food containers. Strong colored glazes also often contain heavy metals.

21.12 GLASS AS GLAZE AND ENAMEL

Glazes are everywhere, just as glass is. In this section we summarize the topic of complete books, namely the glazes on pottery and enamels. Glazing uses the viscous properties of glass to form a (usually) smooth continuous layer on a ceramic substrate (a pot); enameling does the same thing for a metal substrate. One thing that you will notice is that in general when it comes to ceramics, potters did it first. The science of ceramics is often still unraveling just what they did. (In materials science, ceramists usually did it first.)

First we summarize some terms in pottery. (The processing of pottery was summarized in Chapter 2.)

Underglaze. When a pot [white bisqueware (also called biscuit) is ideal] is decorated the first coating is the underglaze. This is essentially a paint layer made by mixing oxide, carbonate, sulfate, etc., an opacifying agent to make it opaque, and a flux to make it adhere better to the pot. The mixture is calcined, ground, and then usually com-

bined with a liquid to allow smooth application. The decorated pot is then typically coated with a clear glaze before it is fired. In the majolica technique, the pot is coated with an opaque white glaze first, then decorated, and then fired so that the colors bond to the white coating forming an in-glaze (rather than under) decoration.

Glaze crawling. The glaze separates from the underlying pot—it dewets the pot surfaces during firing.

Crackle glazes. If the coefficient of thermal expansion, α , of the glaze is greater than that of the underlying ceramic, the glaze may fracture as it cools; this crackling can easily be achieved using higher concentrations of Na or K in the glaze. In most technological applications this is not desirable. Some glazes, however, are designed to have a pattern of hair-like cracks for an artistic effect; these are then known as crackle glazes. Fast cooling produces a finer pattern of crazes.

Celadon, tenmoku, raku, and copper glazes are particular glazes found in the ceramics art world.

Celadon glazes (first produced 3500 years ago) vary from light blue to yellow green and can be quite dark. The color is produced by iron (between 0.5 and 3.0 wt% Fe_2O_3 added to the glaze). The glazed pot is then fired a second time at about 1300°C . An example of Korean celadon pottery is the small water container, 23 cm tall, given to former U.S. President Harry Truman in 1946 by the government of Korea. It is now valued at \$3 million.

Tenmoku glaze (from the Sung Dynasty) is dark brown or even black; 5–8 wt% Fe_2O_3 is included in the glaze to produce the effect. An interesting variation of the tenmoku glaze is the oil-spot tenmoku where bubbles begin to form in the glaze as it starts to melt; if the potter catches them just in time, they leave spots all over the surface. If a tenmoku glaze is fired in reducing conditions, the Fe_2O_3 is partially reduced to FeO , which acts as a modifier instead of an intermediate in glass terms. Hence this glaze behaves differently under oxidizing and reducing conditions, and the color will change. Copper glazes may use 0.5 wt% CuCO_3 as the Cu source, but it breaks down to give CuO during firing, and this reacts with CO in the furnace to give particles of Cu in the glaze. These particles of Cu provide the red color.

Raku glazes often appear metallic as if produced by coating with a Ti metal. One modern method of raku glazing involves firing the pots in the usual way, plunging them into a reducing environment (like sawdust), and then quenching them before they can oxidize. These glazes are often the exception to the rule in that they can change with time. This is simply because they oxidize when treated as other pots. The glaze is thus not as inert as others and is used only for decoration. (However, see the historical note on Chojiro Rakuyaki.)

Crystalline glazes. These are decorative glazes but are directly related to the formation of technologically important glass-ceramics. The crystals form by slowly cooling the glaze to allow a few large crystals to grow. The growth is interesting since the glaze is typically only ~0.5 mm thick and the crystals must therefore form as platelets. A seed of TiO_2 is usually used to nucleate the crystal in a low-viscosity glaze giving what is termed “rutile break-up,” which is actually the formation of PbTiO_3 . The chemistry of the glaze is thus important, with SiO_2 and Al_2O_3 being low and PbO between 8 and 10 wt%. The growing crystal tends to incorporate Fe from the glaze, but can also preferentially exclude other dopants.

Modern potters tend to use Zn as the modifier and produce willemite crystals. [Willemite is a somewhat rare zinc mineral (except as kidney stones), but is abundant at Franklin, NJ.] The technique is tricky because the addition of large amounts of Zn (a network modifier) to the glaze causes its viscosity to remain low even at low temperatures, so that it tends to run off the pot! The crystals appear to grow out from a seed as in the spherulitic growth seen by VLM in Figure 21.15. Each spherulite is actually a mass of radiating crystals that is similarly aligned with respect to the center of the spherulite.

Opaque glazes. If crystals are added to the molten glaze it can be made opaque. SnO_2 was for long the standard, but zircon is much cheaper; ZnO_2 is used to make zircon glazes white. TiO_2 is used less because larger rutile crystals are a golden color and thus make the glaze yellow. We can also make the glaze opaque by forming crystals (e.g., wollastonite; CaSiO_3) using a suitable thermal treatment, or by trapping gas (F_2 or air), or by causing a liquid/liquid phase separation. Matt glazes



FIGURE 21.15 Illustration of spherulitic crystallization in a glass.

SPHERULITES

Dana described spherulites in obsidian in 1863; these are the snowflakes in snowflake obsidian. In 1879 Rutley noted that artificial glass may develop a spherulitic structure.

are produced by forming very small crystals (e.g., wollastonite for a “lime matt” and willemite, Zn_2SiO_4 , for a “zinc matt”) across the surface of the glaze. The wollastonite



FIGURE 21.16 Example of glaze color produced by nanoparticles.

can be formed by adding calcite (also known as whiting) to an SiO_2 -based glaze. An alternative is to add so much crystalline material to the glaze that it remains unchanged by the firing. A satin or vellum glaze, with smaller crystal sizes, might contain 18% SnO_2 or ZnO and 4% TiO_2 in a high-lead glaze fired at 1000°C .

Color in glass and glaze is the subject of much active research, with the realization that some colors are produced by nanoparticles in the glass/glaze as for the luster-glazed plate in Figure 21.16. In general Ag and Au nanoparticles produce the gold color and Cu nanoparticles produce the red color; in the case of Cu especially, the ions may be reduced to the metal during processing. Explanations for the color of glazes are actually more complicated than for glass because the glaze is supported by a substrate and does not have to be transparent, so it can be a thin film or a multilayer and fired in a reducing or oxidizing environment. So this is a very large topic condensed into a paragraph! Cipriano Piccolpasso described luster preparation in 1557. Who says the use of nanomaterials is new!

Colored glazes must use stable ceramic pigments if the color is to be consistent over repeated batches (e.g., for industrial production of sanitaryware, tiles, etc.). Cheaper metal oxide colorants can be used when

variability is acceptable or desirable as in the pottery crafts. Of course, many glaze colorants are the same as we use for coloring glass (see Table 21.4). Co_3O_4 is a black powder but <1% gives a glaze a deep blue color, although it is usually added as the carbonate. Since Co^{2+} is present when it dissolves, it changes the viscosity of the glaze. Cr_2O_3 (2–3% can be added, but only 1.5% will dissolve in the glaze) is intriguing because you expect green but can produce red, yellow, pink, or brown. The red can occur if Pb is present in the original glaze; if Zn is present, the glaze becomes brown unless Pb is also present when the glaze becomes yellow. MnO_2 (added as the carbonate) gives a brown glaze but can produce red, purple, or even black; the color depends in part on how much Na is present in the initial glaze. CuO is equally interesting: 1–2% added to an Na-rich glaze gives turquoise whereas up to a 3% addition produces a clear green/blue. If even more CuO is added the glaze can have a metallic appearance like pewter. If the glaze (0.3–2% CuO) is fired in a reducing atmosphere, the classic copper red is formed. This color is caused by the presence of colloidal Cu. If you see the bright yellow glaze, this might be the CdS/CdSe yellow (also produces orange and red) glaze. If Pb is present, then PbS can form, which makes the glaze black. Zircon is used in industry to help stabilize these Cd-based colors. In fact, $(\text{V,Zr})\text{SiO}_4$ (vanadium zircon blue) and $(\text{Pr,Zr})\text{SiO}_4$ (praseodymium zircon yellow) are most important in the whitewares industry. Uranium is added to glazes but tends to produce a dark brown rather than the pale yellow found in Vaseline glass; it can be yellow or bright red/orange, but this depends on the glaze composition.

Salt glaze. The pot is reacted with salt in the furnace while at temperature. In practice, the potter actually throws salt over the pot when it is in the kiln. The technique was used by early potters in Iran and by the English in the 1700s. You will see many examples in Germany where a blue coloring is often produced using metal oxides. The salt reacts with the clay forming a glass layer on the surface; essentially the process is high-temperature soda corrosion of the fired clay.

The term enamel usually implies a glaze applied to a metal, but it can be a glaze applied on top of a glaze. The market for enamel is large varying from toilet fixtures (whitewares) to jewelry. Enamel is the ever-lasting paint with the organic component replaced by glass.

21.13 CORROSION OF GLASS AND GLAZE

We think of glass as being inert. Citric acid and acetic acid (present in lemon and vinegar, respectively) can chelate with metal ions present in a glass and form water-soluble complexes. (A chelate is a complex compound with a central metal atom attached to a large molecule, a ligand, in a ring or cyclic structure like the claw of a crab.) The

effect can actually be greater than for what we think of as stronger acids (sulfuric, nitric, and hydrochloric acids readily attack metals and skin). The Ca, Mg, and Al ions usually increase the chemical durability of a glass, but they will react with these “food” acids. The tannic acid present in red wine and tea can have a similar effect. Thus Pb can be released from glass when the glass is in contact with acid (even fruit juice). This means that we should not use Pb in glazes either; however, this has often been done because such glazes can be so brightly colored.

Silicate glass is strongly corroded by HF. The process of “frosting” glass light bulbs was carried out for many years by blowing HF vapor into the glass envelope and then evacuating it after a short period.

Glass dissolves in water, particularly at elevated temperature and pressure: we use this fact to grow all the quartz crystals used by industry. Dishwashers make glass dull. Roman glass (Figure 21.17) is iridescent because the glass has reacted with acid in the soil. (The iridescence was not present in Roman times.) The corrosion products form several distinct layers and, hence, generate the interference known as iridescence. It can easily be duplicated as shown by Tiffany and others.

Not all glass is attacked as readily. As described in Chapter 8, we leach one component of a phase-separated glass during the preparation of Vycor but leave the other intact.

It is possible to minimize these reactions to some extent by adding inhibitors, such as Zr or Be, to the glass. This question of reactivity is closely related to the phenomenon of ion exchange.



FIGURE 21.17 Example of iridescence in Roman glassware.

H⁺ can replace alkali ions when glass is weathered.
 K⁺ can replace Na⁺ and Na⁺ can replace Li⁺ when we want to strengthen the surface of glass.
 Ag⁺ and Cu⁺ can replace Na⁺ to “stain” glass.

A special feature here is that we have point defects (and large defects) in glass just as we do in crystals. Our challenge is to understand what determines the properties (e.g., diffusion) of such defects when we do not have a reference lattice.

21.14 TYPES OF CERAMIC GLASSES

Not all glass is based on the silica tetrahedron. The structural units are summarized in Table 21.5 and some representation glass compositions are given in Table 21.6.

Silicate Glass (Soda-Lime Glass)

This is based on SiO₂–Na₂O–CaO (usually containing MgO and Al₂O₃). It is relatively inexpensive and durable and is widely used in the building and packaging industries. Its α is not negligible and it is not a good insulator. The main uses are in sheet glass, bottles, tableware, and in the light industry for envelopes (bulbs). The alkaline aluminosilicate glasses (SiO₂–Al₂O₃–RO, where R is the alkali) have low αs, are durable, and are better electrical insulators. They also have a high strain point. Uses include combustion tubing, envelopes for halogen lamps, and substrates in the electronics industry.

Silicates	SiO ₄
Borates	BO ₃
Phosphates	PO ₄
Fluorides	F
Chalogenides	S

Lead Glass

Generally the composition will be a lead-alkali silicate glass SiO₂–PbO–R₂O, so the PbO replaces the CaO in soda-lime glass. These glasses have a high resistivity, a large α, a low softening temperature, and a long working range. The reason that Pb glass has been used to make so-called lead crystal glass is that it has a high refractive index. Besides being used in art objects, it is used for lamp tubing, TVs (the “bulbs”), and thermometer tubing. In a traditional English lead crystal the concentration of PbO will be at least 30%: an EU directive required that glass must contain ≥24% to be considered lead crystal. Then the EU had to exempt crystal glass from recycling laws! Lead glass used for radiation shielding may contain as much as 65% PbO. Applications include TV tubes, although Ba glass may be used in the face or panel of the TV. (The electrons hitting the TV screen can create X-rays that the glass must then absorb.) Lead-borate glasses can be used as glass solder—they contain little SiO₂ or Al₂O₃ and are quite inert.

Flint glass is a high-dispersion, lead-alkali silicate glass originally made by melting flint rock, which is a

TABLE 21.6 Approximate Composition (wt%) of Some Commercial Glasses

Glass	SiO ₂	Al ₂ O ₃	Fe ₂ O ₃	CaO	MgO	BaO	Na ₂ O	K ₂ O	SO ₃	F ₂	ZnO	PbO	B ₂ O ₃	Se	CdO	CuO
Container flint	72.7	2.0	0.06	10.4		0.5	13.6	0.4	0.3	0.2						
Container amber	72.5	2.0	0.1	10.2		0.6	14.4	0.2	S-0.02	0.2						
Container flint	71.2	2.1	0.05	6.3	3.9	0.5	15.1	0.4	0.3	0.1						
Container flint	70.4	1.4	0.06	10.8	2.7	0.7	13.1	0.6	0.2	0.1						
Window green	71.7	0.2	0.1	9.6	4.4		13.1		0.4							
Window	72.0	1.3		8.2	3.5		14.3	0.3	0.3							
Plate	71.6	1.0		9.8	4.3		13.3		0.2							
Opal jar	71.2	7.3		4.8			12.2	2.0		4.2						
Opal illumination	59.0	8.9		4.6	2.0		7.5			5.0	12.0	3.0				
Ruby selenium	67.2	1.8	0.03	1.9	0.4		14.6	1.2	S-0.1	0.4	11.2		0.7	0.3	0.4	
Ruby	72.0	2.0	0.04	9.0			16.6	0.2		Trace						0.05
Borosilicate	76.2	3.7		0.8			5.4	0.4					13.5			
Borosilicate	74.3	5.6		0.9		2.2	6.6	0.4					10.0			
Borosilicate	81.0	2.5					4.5						12.0			
Fiber glass	54.5	14.5	0.4	15.9	4.4		0.5			0.3			10.0			
Lead tableware	66.0	0.9		0.7		0.5	6.0	9.5				15.5	0.6			
Lead technical	56.3	1.3					4.7	7.2				29.5	0.6			
Lamp bulb	72.9	2.2		4.7	3.6		16.3	0.2	0.2				0.2			
Heat absorbing	70.7	4.3	0.8	9.4	3.7	0.9	9.8	0.7		Trace			0.5			

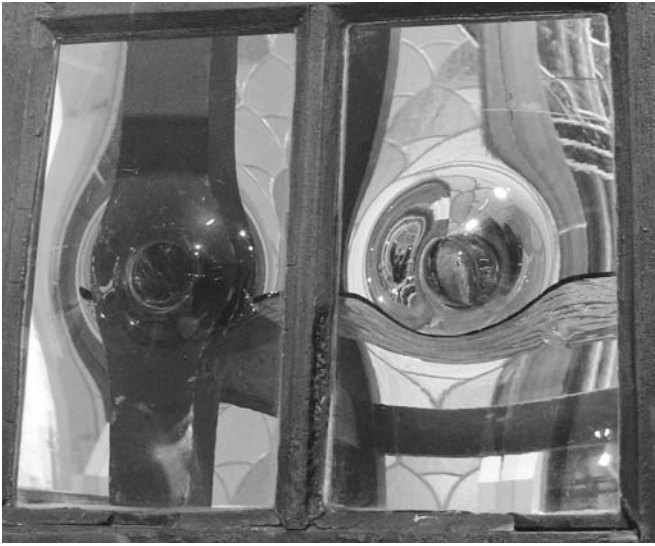


FIGURE 21.18 Crown glass with bull's eye.

particularly pure form of silica. Note that this rock is now calcined and is still used extensively in the pottery industry.

Crown glass based on soda-lime glass, has quite a low dispersion. It is still made by initially blowing the glass, flattening it, and transferring it to the pontil (a solid iron rod rather than the blow pipe) where it is spun until it is in the form of a disc that could be 1.5 m in diameter (Figure 21.18). The disk shows concentric ripples from the spinning and has a bull's eye at the center of the crown. The disk can be very smooth having been flame annealed without mechanical polishing. Historically, windowpanes could be cut around the bull's eye or could contain it.

Borate Glass (Borosilicate Glass)

The alkali borosilicates, $\text{SiO}_2\text{-B}_2\text{O}_3\text{-R}_2\text{O}$ (R is the alkali), are special for their low α . They are durable and have useful electrical properties. The cookware material Pyrex™ is a borosilicate. Borosilicate glass is widely used in the chemical processing industry. Some borate glasses melt at very low temperatures ($\sim 500 \pm 50^\circ\text{C}$), so they can be used to join together other glasses. Zinc-borosilicate glass, known as passivation glass, contains no alkalis, so it can be used for Si electronics components.

Fused Silica

Being essentially pure SiO_2 , this is the silicate glass for high-temperature applications. It has a near zero α [known as ultralow expansion (ULE) silica]. This is used for telescope mirrors and substrates. ULE® glass containing 7% TiO_2 is being used for photolithography masks [for extreme ultraviolet lithography (EUVL) at a wavelength of 13.4 nm, extreme UV]. Another silica glass that can be used for 157-nm lithography was made by removing the water and

adding fluorine ions to change the composition of the silica; this process allows transmission of wavelengths down to 157 nm. We have already discussed Vycor, which can be pure (porous) silica after we remove the second phase.

Phosphate Glass

Phosphate glasses are important because they are semi-conducting; one application is in the manufacture of electron multipliers (hence amplifiers) using Er doping (with Er_2O_3). The cations here are usually V and P, but Oak Ridge National Laboratory (ORNL) developed a lead indium phosphate glass that has a high index of refraction, a low melting temperature, and is transparent over a wide range of wavelengths. Since it can also dissolve significant concentrations of rare-earth elements (it was designed to be a container for radioactive waste), it is being explored for new optically active devices (e.g., fiberoptic amplifiers and lasers). Nd-doped (using Nd_2O_3) phosphate glasses are being used in solid-state lasers (1.054 μm wavelength). The typical composition is $60\text{P}_2\text{O}_5\text{-}10\text{Al}_2\text{O}_3\text{-}30\text{M}_2\text{O}$ (or MO); the Nd concentrations is $\sim 0.2\text{-}2.0$ mol%. Calcium phosphate glass will be discussed more extensively in Chapter 35.

Chalcogenide Glass

Based on As, Se, and Te, these glasses are IR transparent. They are nonoxide semiconductors and are used in special electronic devices and lenses. The devices use the abrupt change in electrical conductivity that occurs when a critical voltage is exceeded. The applications have to be special because these glasses are not durable and have low softening temperatures.

Fluoride Glass

In general, halide glasses are based on BeF_2 and ZnCl_2 and are used in optical waveguides (OWG) where the cost can be justified.

21.15 NATURAL GLASS

It surprises some people that not only does glass occur in nature, but it is relatively common. Tektites are formed within the impact craters of meteors. Moldavite is a green glass from Moldavia in the Czech Republic; Libyan Desert Glass formed the same way but is yellow. Fulgarites are fragile tubes of glass that can be formed when lightning strikes a sandy soil. Obsidian is the glass formed in volcano flows. The usual black color is due to impurities; green and red obsidian also occur. Obsidian was used to make tools during the Paleolithic period. The advantages of using glass for scalpels have only recently been rediscovered: the cut made by a glass knife is particularly even

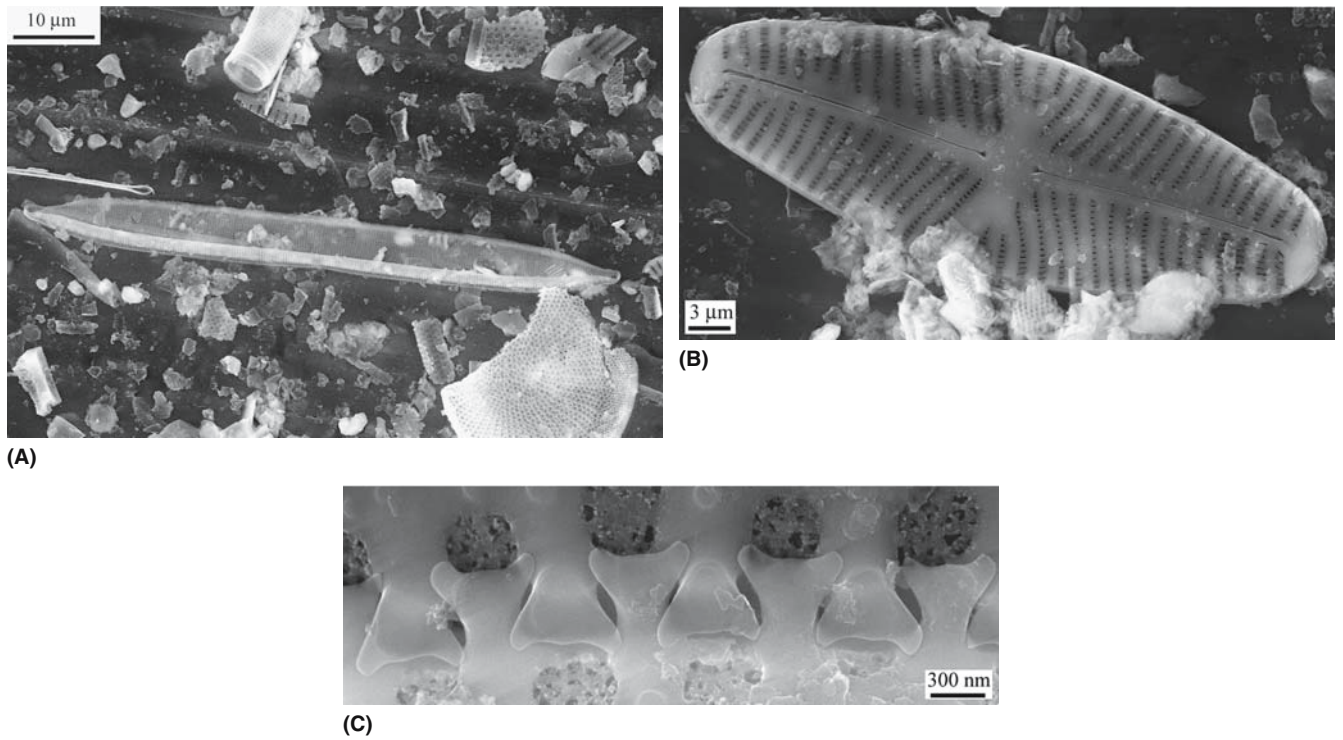


FIGURE 21.19 SEM images of diatoms.

so it heals fast. It has been proposed that the Aztec civilization may not have developed metallurgy because it was so adept at using obsidian and there are many sources of obsidian in the volcanic mountain ranges of Peru and Ecuador in particular.

Pumice is another glass formed in volcanic eruptions. It can be very porous if it contains a high concentration of gas. Pumice is thus the porous form of obsidian.

Trinitite is not really a natural glass but one that we might say forms unintentionally. This glass has been found at the Trinity site where the nuclear bomb was exploded in New Mexico.

Diatoms are included in this topic because they are both interesting and surprising. Not all living things on earth are based on carbon. Diatoms are small aquatic microorganisms, or one-celled plants, that live by ingesting silica that is dissolved in water; we usually think of seawater, but it can be a freshwater lake. The diatoms then use the silica to form and grow a pair of shells as illustrated in Figure 21.19. The two shells resemble a pillbox. The shells come in many varieties—there are thousands of species of diatoms. When the microorganisms die, their siliceous skeletons have formed layers up to 3000 feet thick: they are not rare! The result is that there are regions in which deposits of silica have built up to form what is known as diatomite or diatomaceous earth. The comparable process for carbon-based creatures would be the formation of limestone and chalk. Diatoms do contain chlorophyll, so they are plant colored while alive.

The Venus Flower Basket (*Euplectella*) is a sponge that lives in the deepest parts of the oceans in the tropics. It

has a skeleton that looks like a mesh of glassy silica fibers (Figure 21.20). Each fiber actually consists of coaxial cylindrical layers with different optical properties. It is reminiscent of the cladding used today on commercial optical fibers, but nature did it eons earlier. The optical properties of the natural fibers are not as good as those of human-made fibers but they are more resistant to breaking. Note that these layers are deposited at ambient water temperatures!

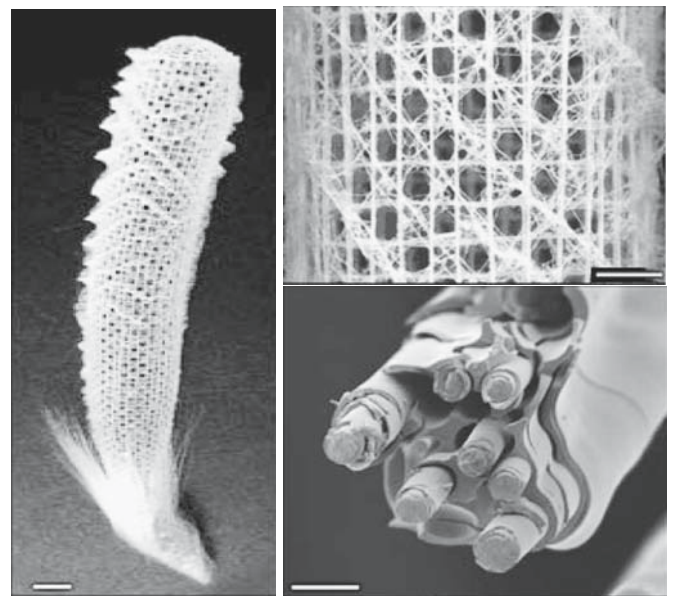


FIGURE 21.20 Sea sponge.

21.16 THE PHYSICS OF GLASS

We will now discuss glass from the physicist's point of view. We have left this topic for last so as either to confirm your excitement or not completely put you off the subject.

The idea is that glass is a condensed phase just as liquids and crystals are. The atomic interactions can be described by a potential energy function, ϕ .

If we describe the energy of a glass plotted against the coordinates of the glass, we would find a multidimensional energy hypersurface, which is multiply dented with structured valleys. The glass structure corresponds to one of those valleys, but there may be another valley or a minimum not far away on the surface. Then we have the concept of polymorphism, in which the glass can have several distinct amorphous structures. (The comparison to crystalline materials is instructive!)

The experimental observation is that the viscosity of some glasses decreases suddenly above T_g in a non-Arrhenius way. It is as if the structure of the glass collapsed because it was fragile (the term fragile refers only to the liquid, not the glass). Hence fragility is a property of some glass-forming liquids above T_g although we talk about fragile and strong glasses. If we plot $\log \eta$ versus T_g/T (the reduced T_g as shown in Figure 21.21), then the curve would be straight if it was for Arrhenius-like behavior. For SiO_2 and other highly polymerized network glasses (strong glass formers), it is nearly straight. If the bonds are not directional, the plot deviates significantly from Arrhenius behavior; this is a fragile glass former. Two approaches have been used to explain this behavior:

- Free volume
- Configurational entropy

Each connects η to the macroscopic quantities of either volume or entropy. A newer approach considers factors affecting the kinetics of the transformation. There are

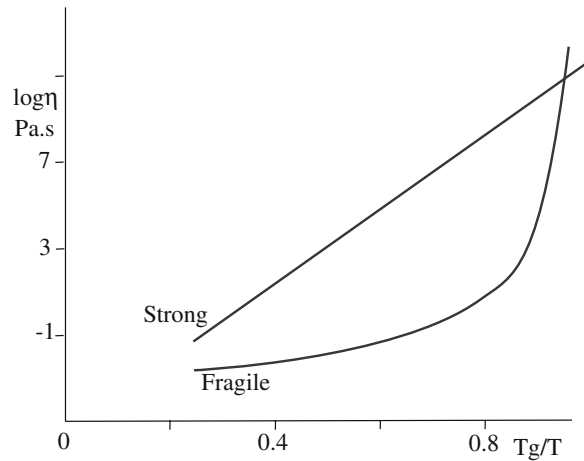


FIGURE 21.21 Viscosity versus temperature for strong and fragile liquids.

fast relaxation processes (known as β processes) and low-frequency processes, which contribute to the dynamic structure factor. In the glass's vibrational spectra detected by Raman or neutrons, these features are known as the boson peak. The boson peak is large for strong glass formers; low-frequency excitations in a glass suggest intermediate-range order: so more order indicates a stronger glass.

The molar heat capacity, c_p , is a well-defined quantity. At very low temperatures ($T < 1$ K: a temperature familiar to physicists but less so to ceramists), glasses show a linear term in c_p due to an anharmonic contribution. At $T \sim 5\text{--}10$ K, an excess vibrational (harmonic) contribution causes a bump in c_p . The excess vibrational contribution to c_p at this bump (call it $c_p - c_D$) can be plotted against the fragility of the glass. The resulting correlation suggests that the excess vibration and the fragility have a related origin. So SiO_2 , a particularly strong glass, has a large c_p/c_D , whereas a fragile glass like CKN [$\text{Ca}_{0.4}\text{K}_{0.6}(\text{NO}_3)_{1.4}$] has a small c_p/c_D .

CHAPTER SUMMARY

This chapter has been placed after powders but before processing because we are still emphasizing the material. Because glass is an extremely important material the history of this topic is particularly rich. Remember that glazes on pots and enamels on metals are essentially two variations on a single theme—protecting other materials by coating them with glass. The variety of glasses is large and we have touched on only a small range here. Remember that historically, silica-based glass was for a long time synonymous with the word glass. So, it has dominated our thinking about glass. New glasses are being developed that may contain no Si and the properties may be very different; there is not just one material called glass any more than there is one material called crystal. Glass will crystallize given time; although glass-ceramics were the new materials of the 1960s, they were already old friends to the potter. The basic science of glass is more difficult than for crystals because we have no “frame of reference.” However, there are point defects in glass (remember the origins of color). Glass has both internal and external interfaces and does have special structural features. Of its many important properties, transparency and viscosity must be the most important, although for many applications the small, or controllable, expansion coefficient is the key to the value of glass.

As we explained from the beginning, glass appears throughout our discussion of ceramics. The processing of glass is treated in Chapter 26, mechanical properties are discussed in Chapter 18, and Bioglass is discussed in Chapter 35. The reason we treat glass separately is partly historical and partly because its behavior is often so different from crystalline ceramics, which emphasizes the point we made in Chapters 5 through 7, bonding and structure determine the properties and thus the applications.

PEOPLE IN HISTORY

- Bacon, Roger, a Franciscan Friar, described reading glasses made using two lenses in 1268. Salvino D'Armato of Pisa is sometimes credited with the invention in 1284.
- Cassius, Andreas (1685) in the book "*De Auro*" describes how to produce this ruby red color, which thus became known as "Purple of Cassius."
- La Farge, John (patent No. 224,831; February 24, 1880); a "Colored-Glass Window," the original patent on opal glass, was followed shortly by Louis Comfort Tiffany's patent (No. 237,417; February 8, 1881) with the same title, "Colored-Glass Window."
- Lipperhey, Hans was a lens grinder in the Netherlands; he applied for a patent for the telescope in 1608.
- Pascal, Blaise (1623–1662) was born in Clermont-Ferrand, France and died in Paris. The SI unit of pressure (stress) is named after him. He argued against Descartes in favor of the existence of vacuum.
- Perrot, Bernard (1619–1709) was a well-known early French glassmaker.
- Poiseuille, Jean Louis Marie (1799–1869) was the French physician after whom we name the Poise.
- Prince Rupert of Bavaria (1619–1682) was the grandson of James I of England and nephew of Charles II. He introduced his drops to England in the 1640s, where they became party pieces in the court of Charles II. The famous diarist Samuel Pepys wrote about them in his diary on January 13, 1662.
- Rakuyaki, Chojiro (died 1859) was the first member of the family to begin the tradition of raku. Their home is now an exquisite museum illustrating tea bowls made by 15 generations.
- van Leeuwenhoek, Anton (1632–1723) was born in Delft, Holland and worked as a cloth merchant; he devised a simple microscope that succeeded so well because he was a skilled lens grinder. The microscope itself was invented in the 1500s and was used by Robert Hooke.
- Warren, Bertram Eugene (1902–1991; at M.I.T. 1930–1976) is known for his textbook on X-ray diffraction and his studies of the structure of glass and carbon black. These began small-angle scattering research into nonperiodic and nearly periodic structures.

THE HISTORY OF GLASS

- Allen, D.(1998) *Roman Glass in Britain*, Shire Pub. Ltd., Bucks, UK.
- Boyd, D.C. and Thompson, D.A.(1980) *Glass*, 3rd edition (Kirk-Othmer: *Encyclopedia of Chemical Technology*, Vol. 11, p. 807).
- Bray, C.(2001) *Dictionary of Glass Materials and Techniques*, University of Pennsylvania Press, Philadelphia, PA.
- Douglas, R.W. and Frank, S.(1972) *A History of Glass Making*, Foulis & Co, London, UK. A very readable history of glassmaking with some super illustrations and photographs.
- Newby, M.S.(2000) *Glass of Four Millennia*, Ashmoleum Museum, Oxford, UK.
- Stern, E.M.(2001) *Roman, Byzantine and Early Medieval Glass 10 BCE–700 CE*, H. Cantz Publishers, Ostfildern-Ruit, Germany.
- Stookey, S. Donald (2000) *Explorations in Glass*, American Ceramic Society, Westerville, OH. About 70 pages of essential reading.
- Zerwick, C.(1990) *A Short History of Glass*, H.N. Abrams Inc., New York.

JOURNALS

J. Non-Cryst. Solids; J. Chem. Phys.; J. Appl. Phys.; J. Mater. Sci.

GENERAL REFERENCES

- Bach, H. and others (1998–) *The Schott Series on Glass and Glass Ceramics*, Springer, Berlin. Superb series from specialists at one of the leading glass companies.
- Bailey, M. (2004) *Oriental Glazes*, A & C Black, London. One of the Ceramic Handbooks series of texts aimed at the practicing potter.
- Brow, R.K. (2000) "Review: The structure of simple phosphate glasses," *J. Non-Cryst. Solids* **263 and 264**, 1.
- Creber, D. (2005) *Crystalline Glazes*, A&C Black, London. One of the Ceramic Handbooks series.
- Davies, J. (1972) *A Glaze of Color*, Watson-Guptill Pubs, New York. Very practical insights for the potter.

- Doremus, R.H. (1994) *Glass Science*, 2nd edition, John Wiley & Sons Inc., New York. An essential text if you study glass. The discussion of definitions is very clear.
- Höland, W. and Beall, G. (2002) *Glass-Ceramic Technology*, American Ceramic Society, Westerville OH. The book on glass-ceramics. Dr. George Beall has the greatest number of patents (100 in 2004) granted to a single individual in Corning's history.
- Ilsley, P. (1999) *Macro-Crystalline Glazes: The Challenge of Crystals*, The Crowood Press, Ramsbury, Wilts, UK. Beautiful illustrations from an experimentalist.
- Morey, G.W. (1954) *The Properties of Glass*, 2nd edition, Reinhold Publishing Co., New York. Includes a useful discussion of viscosity.
- Paul, A. (1982) *Chemistry of Glasses*, Chapman & Hall, London, UK.
- Pfaender, H.G. (1982) *The Schott Guide to Glass*, Chapman & Hall, London, UK. A small, enjoyable text with color illustrations.
- Rawson, H. (1967) *Inorganic Glass-Forming Systems*, Academic Press, New York. Another of the standards on glass.
- Shimbo, F. (2003) *Crystal Glazes*, 2nd edition, Digital Fire Co., Medicine Hat, Alberta, Canada.
- Stoemer, E.F. and Smol. J.P. (1999) *The Diatoms*, Cambridge University Press, Cambridge, UK. Concerned primarily with applications of these diatomaceous materials. Very comprehensive.
- Sturkey, S.D. (2000) *Explorations in Glass*, American Ceramics Society, Westerville, OH. A "must-read" for anyone interested in glass. Particularly nice discussion on opal glass.
- Taylor, J.R. and Bull, A.C. (1986) *Ceramic Glaze Technology*, Pergamon Press, New York. An excellent resource on glazes.
- Wiggington, M. (1996) *Glass in Architecture*, Phaidon Press, London.
- Zarzycki, J. (1991) *Glasses and the Vitreous State*, Cambridge University Press, Cambridge, UK.

SPECIFIC REFERENCES

- Aizenberg, J., Weaver, J.C., Thanawala, M.S., Sundar, V.C., Morse, D.E., and Fratzl, P. (2005) "Skeleton of *Euplectella* sp.: Structural hierarchy from the nanoscale to the macroscale," *Science* **309**, 275.
- Angell, C.A. (1985) in *Strong and Fragile Glass Formers in Relaxation in Complex Systems*, edited by K.I. Ngai and G.B. Wright, National Technical Information Service, U.S. Department of Commerce, Springfield, VA, 3.
- Angell, C.A. (1995) "Formation of glasses from liquids and biopolymers," *Science* **267**, 1924. A particularly important review.
- Angell, C.A. (2002) "Liquid fragility and the glass transition in water and aqueous solutions," *Chem. Rev.* **102**, 2627. Much more relevant than it might appear.
- Bondioli, F., Manfredini, T., Siligardi, C., and Ferrari, A.M. (2004) "A new glass-ceramic pigment," *J. Eur. Ceram. Soc.* **24**, 3593.
- Kim, S.S. and Sanders, T.H., Jr. (2000) "Calculation of subliquidus miscibility gaps in the $\text{Li}_2\text{O-B}_2\text{O}_3\text{-SiO}_2$ system," *Ceram. Int.* **26**, 769.
- Knowles, K.M. and Freeman, F.S.H.B. (2004) "Microscopy and microanalysis of crystalline Glazes," *J. Microsc.* **215**, 257.
- Pye, L.D., Montenero, A., and Joseph, I. (2005) *Properties of Glass-Forming Melts*, CRC Press, Boca Raton, FL. A collection of chapters on current aspects of molten glass.
- Rössler, E. and Sokolov, A.P. (1996) "The dynamics of strong and fragile glass formers," *Chem. Geol.* **128**, 143.
- Strahan, D. (2001) "Uranium in glass, glazes and enamels: History, identification and handling," *Studies Conservation* **46**, 181.
- Tangeman, J.A., Phillips, B.L., Nordine, P.C., and Weber, J.K.R. (2004) "Thermodynamics and structure of single- and two-phase yttria-alumina glasses," *J. Phys. Chem. B* **108**, 10663.
- Vogel, W. (1971) *Structure and Crystallization of Glasses*, The Leipzig Ed., Pergamon Press, Oxford, UK.
- Zhu, D., Ray, C.S., Zhou, W., and Day, D.E. (2003) "Glass transition and fragility of $\text{Na}_2\text{O-TeO}_2$ glasses," *J. Non-Cryst. Sol.* **319**, 247.

WWW

- www.bell-labs.com
Bell Labs
- www.corning.com
The site for the Corning Glass Company
- www.cmog.org
The Corning Museum of Glass
- www.glass.org
The site for the NGA (National Glass Association)

www.pilkington.com

The site for Pilkington Glass, a key developer of glass based in the UK

www.schottglass.com

The site for Schott Glass with descriptions of new glass developments

www.focusmm.com/pasabahce/co_hi.htm

Describes the history of the wonderful Pasabahce glass of Turkey

www.doge.it/murano/muranoi.htm

The history of Murano glass

www.ortonceramic.com

A source for testing equipment

www.britglass.org.uk

The site for the British Glass Manufacturers' Confederation

www.jlsloan.com/lct1.htm

Julie L. Sloan's site describing the rivalry between La Farge and Tiffany in developing opal glass

EXERCISES

- 21.1 What causes refraction in glass?
- 21.2 Why is smoky quartz smoky?
- 21.3 If you increase the wavelength, how does the refractive index change?
- 21.4 What is dispersion and why does glass cause it?
- 21.5 If Pb were added to a typical lead crystal glass, what weight percent would be added? What atomic percent of Pb would the glass then contain? What is actually added in industrial practice and will this practice continue in the future?
- 21.6 If you are given crystalline SiO_2 , quartz glass, silica gel, and a sample of liquid SiO_2 , how would you analyze the bonding of the Si in each case? Would you detect a difference?
- 21.7 How would you expect the properties of GeO_2 glass to differ from those of SiO_2 glass? Be as quantitative as possible.
- 21.8 We can make glass based on B and on P. What will the bonding characteristics of these two glasses be? Suggest three modifiers for each glass. Compare the densities you expect for these glasses.
- 21.9 Libyan Desert glass was produced naturally. Is pressure or temperature the more important factor? Explain your reasoning as quantitatively as possible.
- 21.10 Na is a network modifier for SiO_2 glass. How would Li and K compare to Na in this role? Similarly Ca is present in soda-lime glass; if the Ca were replaced by an equal atomic percent of Mg or Ba, how would the properties of the glass change?

Sols, Gels, and Organic Chemistry

CHAPTER PREVIEW

Extensive research and development in the past decade have resulted in increasing awareness of the importance of chemical synthesis, particularly using organic precursors, in the processing and fabrication of ceramics. The sol-gel process is one method that is used commercially in many applications, such as forming coatings on window glass. It is also used, as we have previously described, for forming powders and fibers. The process gives us excellent control of product purity and composition for the simple reason that we start with pure materials. It allows us to deposit films and coatings on a range of different surfaces, enabling a flexibility that is not present in many vapor-phase methods.

We can summarize the key advantages offered by the sol-gel process.

- It uses relatively low temperatures.
- It can create very fine powders.
- It produces compositions not possible by solid-state fusion.

There are some disadvantages of the sol-gel process.

- The cost of the raw materials (the chemicals) may be high. As an example, MgO powder with a purity of 98% is available in small quantities for \$30/kg. Magnesium ethoxide, a chemical source for making MgO, costs about \$200/kg.
- There is often a large volume shrinkage and cracking during drying (we have to remove the “organics”).
- Organic chemistry often uses confusing terminology and is avoided by ceramists whenever possible.

In Chapter 20 we described how sol-gel processing (and other chemical methods) is used to make ceramic powders and fibers. So, why do we need another chapter on this topic? There are two main reasons. First, to use sol-gel processing scientifically you must understand the chemistry (the terminology and the reactions). Second, chemical methods for making powders are going to be even more important in the future because they can be used to make nanoparticles and even to coat them.

22.1 SOL-GEL PROCESSING

The sol-gel process consists of two steps. First we form a *sol*. Then we transform this into a *gel*. In ceramic synthesis, two different sol-gel routes have been identified and depend on the gel structure.

- Particulate gel—using a network of colloidal particles
- Polymeric gel—using an array of polymeric chains

THE TERM SOL-GEL

It is convention to use the term “sol-gel” rather than “sol/gel,” although the latter might be more correct; “sol” and “gel” are two independent concepts.

DEFINITION OF SOL AND GEL

Colloidal particles or molecules are suspended in a liquid or solution, a “*sol*.” The sol is mixed with another liquid, which causes formation of a continuous three-dimensional network, a “*gel*.”

The process that occurs depends on the form of the sol, i.e., whether it is a solution or a suspension of fine particles. A flow diagram indicating each of

the processes is shown in Figure 22.1.

In this chapter we are concerned only with the polymeric gel route because this is the approach that is most useful to ceramists. This method has been successful in preparing a range of advanced ceramics such as lead zirconate titanate (PZT) and the high- T_c oxide superconductors.

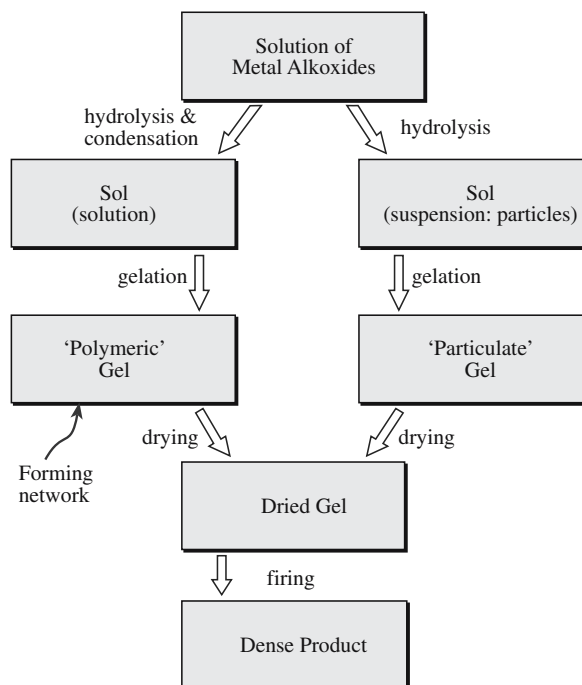


FIGURE 22.1 Flow chart comparing sol-gel processing using a solution and a suspension of fine particles.

The significant advantage of sol-gel processing of ceramic powders is that homogeneous compositions can be prepared at temperatures lower than required for conventional powder processes. Furthermore, the reactants used in sol-gel processing are available in very high purities, which allows the formation of high-purity powders of crystalline ceramics and glasses.

A commonly studied approach for synthesizing oxides has been to hydrolyze the appropriate metal alkoxides. There are several advantages to using metal alkoxides as precursors for ceramic powders. Most of the alkoxides of interest can be easily prepared or are commercially available and can be readily purified prior to use. Interaction of alkoxides with water yields precipitates of hydroxides, hydrates, and oxides. The precipitate particles usually range in size from 0.01 to 1 μm , depending on the hydrolysis conditions. So we can easily produce nanoparticles.

22.2 STRUCTURE AND SYNTHESIS OF ALKOXIDES

Alkoxides have the general formula $\text{M}(\text{OR})_z$, where M is usually a metal, but can also be a nonmetal such as Si, and R is an alkyl chain. Table 22.1 lists some common alkoxides used in the preparation of ceramics.

The nomenclature adopted for the simple alkoxides follows the basic rules of organic chemistry:

METAL ALKOXIDE $\text{M}(\text{OR})_z$

For convenience we will say “metal alkoxide” even when referring to alkoxides of nonmetals such as silicon and boron.

TABLE 22.1 Examples of Metal Alkoxides

Name	Chemical formula	Physical state
Aluminum <i>S</i> -butoxide	$\text{Al}(\text{O}^i\text{C}_4\text{H}_9)_3$	Colorless liquid, $T_B \sim 203^\circ\text{C}$
Aluminum ethoxide	$\text{Al}(\text{OC}_2\text{H}_5)_3$	White powder, $T_M 130^\circ\text{C}$
Aluminum isopropoxide	$\text{Al}(\text{O}^i\text{C}_3\text{H}_7)_3$	White powder, $T_M 118.5^\circ\text{C}$
Antimony ethoxide	$\text{Sb}(\text{OC}_2\text{H}_5)_3$	Colorless liquid, $T_B 95^\circ\text{C}$
Barium isopropoxide	$\text{Ba}(\text{O}^i\text{C}_3\text{H}_7)_2$	Off-white powder
Boron ethoxide	$\text{B}(\text{OC}_2\text{H}_5)_3$	Colorless liquid, $T_B 117.4^\circ\text{C}$
Calcium methoxide	$\text{Ca}(\text{OCH}_3)_2$	Off-white powder
Iron ethoxide	$\text{Fe}(\text{OC}_2\text{H}_5)_3$	$T_M 120^\circ\text{C}$
Iron isopropoxide	$\text{Fe}(\text{O}^i\text{C}_3\text{H}_7)_3$	Brown powder
Silicon tetraethoxide	$\text{Si}(\text{OC}_2\text{H}_5)_4$	Colorless liquid, $T_B 165.8^\circ\text{C}$
Silicon tetraheptoxide	$\text{Si}(\text{OC}_7\text{H}_{15})_4$	Yellow liquid
Silicon tetrahexoxide	$\text{Si}(\text{OC}_6\text{H}_{13})_4$	Colorless liquid
Silicon tetramethoxide	$\text{Si}(\text{OCH}_3)_4$	Colorless liquid, $T_B 121\text{--}122^\circ\text{C}$
Titanium ethoxide	$\text{Ti}(\text{OC}_2\text{H}_5)_4$	Colorless liquid, $T_B 122^\circ\text{C}$
Titanium isopropoxide	$\text{Ti}(\text{O}^i\text{C}_3\text{H}_7)_4$	Colorless liquid, $T_B 58^\circ\text{C}$
Yttrium isopropoxide	$\text{Y}(\text{O}^i\text{C}_3\text{H}_7)_3$	Yellowish-brown liquid

Methoxide	$\text{R} = \text{CH}_3$	Example is $\text{B}(\text{OCH}_3)_3$
Ethoxide	$\text{R} = \text{C}_2\text{H}_5$	Example is $\text{Si}(\text{OC}_2\text{H}_5)_4$
Propoxide	$\text{R} = \text{C}_3\text{H}_7$	Example is $\text{Ti}(\text{O}^i\text{C}_3\text{H}_7)_4$ (<i>n</i> - and <i>iso</i> -)
Butoxide	$\text{R} = \text{C}_4\text{H}_9$	Example is $\text{Al}(\text{O}^i\text{C}_4\text{H}_9)_3$ (<i>n</i> -, <i>iso</i> -, <i>sec</i> -, and <i>tert</i> -)

In these molecular formulas, the superscripts *n*, *t*, *s*, and *i* refer to normal, tertiary, and secondary or isoalkyl chains, each of which is illustrated for the butoxide group in Figure 22.2. These are common names and do not follow the Commission on the Nomenclature of Organic Chemistry of the International Union of Pure and Applied Chemistry (IUPAC). In the case of higher alkoxides, i.e., those with five or more C atoms, the nomenclature is derived strictly from IUPAC conventions. For example, the alkoxide group $(\text{CH}_3)_3\text{CCH}_2\text{CH}_2\text{O}^-$ would be referred to as 2,2-dimethylbutoxide. The old name is neohexoxide.

Most metal alkoxides contain lower aliphatic alkyl groups and are coordinated complexes and not single molecules. Figure 22.3 shows an example of a coordination complex of aluminum isopropoxide consisting of three molecules.

Even when using the IUPAC convention there is still the distinct possibility of encountering confusion when reading the literature. For example, silicon tetraethoxide

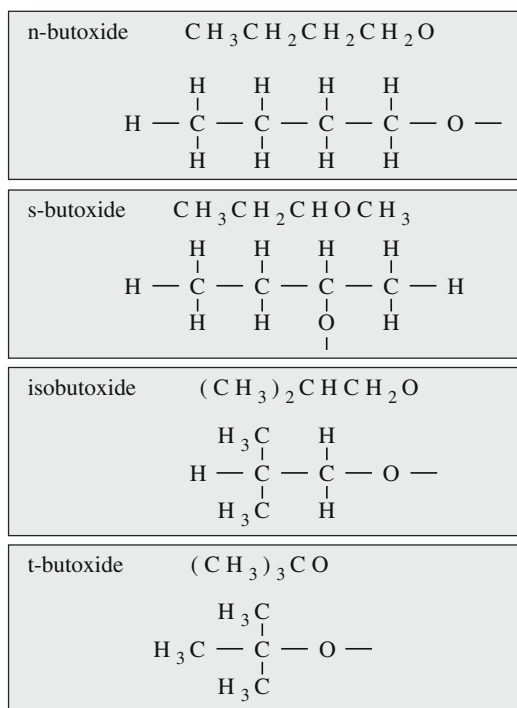


FIGURE 22.2 Illustration of nomenclature for metal alkoxides.

may be referred to as tetraethylsilicate, tetraethylorthosilicate (TEOS), and tetraethoxysilane!

The first alkoxide to be synthesized was silicon tetraisopentoxide (formerly called silicon tetraisooamyloxide), made by a reaction between silicon tetrachloride and isopentanol (formerly isoamyl alcohol):



Many alkoxides are available commercially, particularly those of Si, Al, Ti, B, and Zr. These are not generally

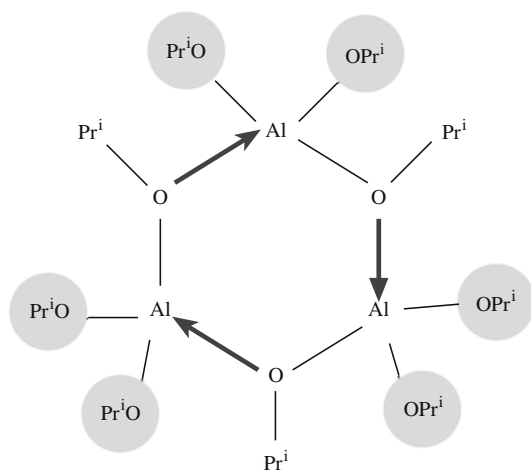


FIGURE 22.3 Three-molecule coordination complex of aluminum isopropoxide.

TABLE 22.2 Alkoxides of Metals with Different Electronegativities

Alkoxide	Electronegativity of metal	State
$\text{Na}(\text{OC}_2\text{H}_5)$	0.9	Solid (decomposes above ~530 K)
$\text{Ba}(\text{O}^i\text{C}_3\text{H}_7)_2$	0.9	Solid (decomposes above ~400 K)
$\text{Y}(\text{O}^i\text{C}_3\text{H}_7)_3$	1.2	Solid (sublimes at ~475 K)
$\text{Zr}(\text{O}^i\text{C}_3\text{H}_7)_4$	1.4	Liquid (boiling point 476 K at 0.65 kPa)
$\text{Al}(\text{O}^i\text{C}_3\text{H}_7)_3$	1.5	Liquid (boiling point 408 K at 1.3 kPa)
$\text{Ti}(\text{O}^i\text{C}_3\text{H}_7)_4$	1.5	Liquid (boiling point 364.3 K at 0.65 kPa)
$\text{Si}(\text{OC}_2\text{H}_5)_4$	1.8	Liquid (boiling point 442 K at atmospheric pressure)
$\text{Fe}(\text{OC}_2\text{H}_5)_3$	1.8	Liquid (boiling point 428 K at 13 Pa)
$\text{Sb}(\text{OC}_2\text{H}_5)_3$	1.9	Liquid (boiling point 367 K at 1.3 kPa)
$\text{B}(\text{O}^i\text{C}_4\text{H}_9)_3$	2.0	Liquid (boiling point 401 K at atmospheric pressure)
$\text{Te}(\text{OC}_2\text{H}_5)_4$	2.1	Liquid (boiling point 363 K at 0.26 kPa)

expensive materials, for example, TEOS, a colorless liquid, costs about \$40/kg. However, nonstandard alkoxides, for example, $\text{Ba}(\text{OC}_2\text{H}_5)_2$, are more expensive. Barium isopropoxide is an off-white powder and costs about 250 times as much as TEOS (\$10/g). A 10% w/v solution of $\text{Ba}(\text{OC}_2\text{H}_5)_2$ in ethanol will cost about \$2/ml.

22.3 PROPERTIES OF ALKOXIDES

The properties of metal alkoxides depend on the electronegativity of the metal. Pauling's electronegativity scale was given in Chapter 3.

Alkoxides of alkali metals, e.g., sodium alkoxides, and alkaline earth metals are ionic solids. Alkoxides of Ge, Al, Si, Ti, and Zr are often covalent liquids. Since most alkoxides are either liquids or volatile solids (examples are given in Table 22.2), they can be purified by distillation to form exceptionally pure oxide sources as shown in Table 22.3.

TABLE 22.3 Effect of Distillation on the Purity of Silicon Tetraethoxide

Form/impurity	Mn	Cr	Fe	Co	Ni	Cu
As supplied (ppb)	10	15	86	0.7	<200	<200
Once distilled (ppb)	0.8	2	31	0.3	11	<20

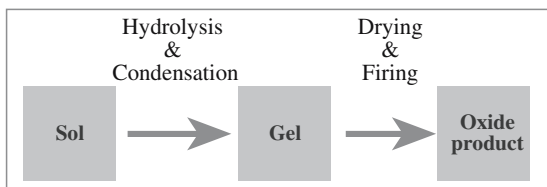


FIGURE 22.4 The basic steps in the sol-gel process using metal alkoxides.

22.4 THE SOL-GEL PROCESS USING METAL ALKOXIDES

The three basic steps in the sol-gel process are summarized in Figure 22.4. The conversion of the sol to a gel occurs by hydrolysis and condensation reactions. The gel is converted into the oxide by drying and firing. We will now look at each of these steps in a little more detail.

Preparing the Sol

The sol-gel process can be used to make single or multi-component oxides. First we will consider the case of a one-component system—silica. Of the many available silicon alkoxides, TEOS is commonly used. It is insoluble in water, but water is necessary for the hydrolysis reaction; hence we need to select a solvent for both the alkoxide and water. Ethanol is a suitable solvent, and a typical formulation contains three main components: 43 vol% $\text{Si}(\text{OC}_2\text{H}_5)_4$, 43 vol% $\text{C}_2\text{H}_5\text{OH}$, and 14 vol% H_2O .

For small-scale sol-gel processing in the laboratory the equipment is relatively simple and inexpensive:

- Three-necked flask (contains the mixed solutions)
- Mechanical stirrer (the mixture is stirred constantly)
- Reflux condenser (needed to prevent the solution from evaporating)
- Constant temperature bath (the rate of hydrolysis depends on temperature)

Multicomponent sols can be prepared by mixing different precursors, which are selected to give eventually an oxide of the desired composition. Table 22.4 gives examples of typical formulations for both single-component and multicomponent alkoxide solutions. There may be problems if the hydrolysis rates of the precursors are different, and this can create inhomogeneities in the subsequent gel. We can allow for this possibility by partially hydrolyzing the less reactive component [e.g., $\text{Si}(\text{OC}_2\text{H}_5)_4$] before adding the more reactive one [e.g., $\text{Ti}(\text{O}^i\text{C}_3\text{H}_7)_4$].

For some metals, such as the alkali metals and alkaline earth metals, it is not possible or it is inconvenient to use alkoxides because they are either unavailable or difficult to prepare. You can see from Table 22.2 that alkoxides of these metals are solids

SAMPLE RECIPE

PZT thin films can be prepared using a solution of zirconium butoxide [$\text{Zr}(\text{O}^n\text{C}_4\text{H}_9)_4$] and titanium propoxide [$\text{Ti}(\text{O}^n\text{C}_3\text{H}_7)_4$] in 2-methoxyethanol ($\text{CH}_3\text{OCH}_2\text{CH}_2\text{OH}$) mixed with lead acetate trihydrate [$(\text{CH}_3\text{CO}_2)_2\text{Pb} \cdot 3\text{H}_2\text{O}$] that is also dissolved in 2-methoxyethanol.

with low volatility. In many cases they also have low solubility. In these situations alternative reactants must be found. Metal salts such as acetates and citrates, which are soluble in organic solvents, are a viable alternative. Many of these can be obtained in a high-purity analytical grade. In cases in which we use both alkoxides and metal salts it is usual to first form a solution of all the components that are to be added as alkoxides. Then add the salts as solutions in alcohol or, if this is not possible, in the water that is to be used for the hydrolysis reaction. The final solution is homogenized by stirring.

TABLE 22.4 Formulations for Single-Component and Multicomponent Alkoxide Solutions

Precursor	One component: 100 mol% SiO_2				Two components: 94 mol% SiO_2 + 6 mol% TiO_2				Three components: 15 mol% Li_2O + 3 mol% Al_2O_3 + 82 mol% SiO_2			
	Solution concentration (wt%/100 g)	Oxide content (vol%/100 ml)	mol	g/mol	Solution concentration (wt%/100 g)	Oxide content (vol%/100 ml)	mol	g/mol	Solution concentration (wt%/100 g)	Oxide content (vol%/100 ml)	mol	g/mol
$\text{Si}(\text{OC}_2\text{H}_5)_4$	45	43			11	11			35	34		
$\text{Ti}(\text{OC}_3\text{H}_7)_4$					1	1						
$\text{Al}(\text{OC}_4\text{H}_9)_3$									1	1		
LiNO_3									3	1		
$\text{C}_2\text{H}_5\text{OH}$	40	43	4		36	41	14		29	34	4	
H_2O	16	14	4		52	47	50		33	30	8	
Oxide (Si + Ti + Al + Li)			1	11.3			1	3.15			1	10.6

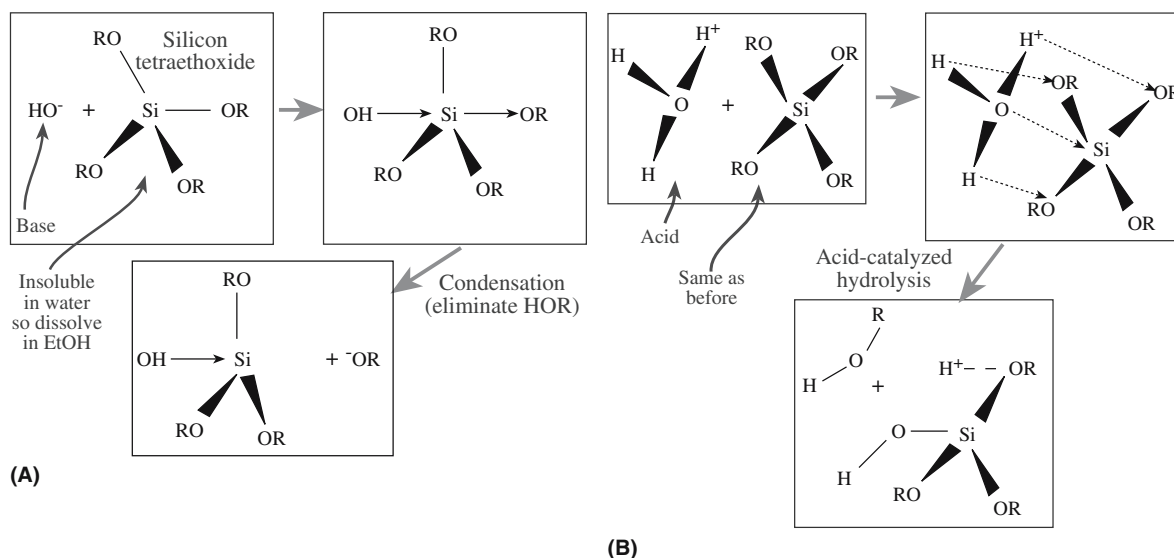


FIGURE 22.5 Schematic showing reaction mechanisms for (a) acid- and (b) base-catalyzed hydrolysis of silicon alkoxides.

Hydrolysis and Condensation

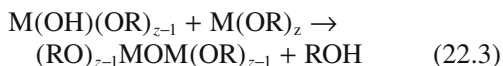
Metal alkoxides undergo hydrolysis very easily (meaning they react with water). In many cases they are so sensitive to moisture that special precautions must be taken in handling and storage (e.g., the use of an N_2 glove box and dehydrated solvents). The product vendor will provide information on the sensitivity of the compound.

During the initial stage of hydrolysis an alcohol molecule, ROH, is expelled.



This is an example of a condensation reaction involving the elimination of an alcohol (e.g., ethanol).

The hydroxy metal alkoxide product can react by a further condensation reaction to form polymerizable species.



Hydrolysis can be carried out either under basic or acidic conditions as shown in Figures 22.5 for TEOS. In the context of sol-gel processing, acid-catalyzed conditions are defined as $pH < 2.5$; base-catalyzed conditions are defined as $pH > 2.5$. Of course, this is not our usual definition of acid and base, where a neutral pH is 7, but corresponds to the point of zero charge (PZC) at which the surface is electrically neutral.

Hydrolysis may go to completion leading to the formation of the silicic acid monomer. But this generally does not occur except at low pH and high water concentrations.

CONDENSATION REACTIONS

The class of organic reactions in which two molecules combine eliminating water or another simple molecule. This produces thermosetting polymers and phenolformaldehyde, nylon, and polycarbonates.

The silicic acid monomer is not stable and condensation of silanol groups (Si–OH) leads to polymer formation before silanol groups substitute for all the alkoxy groups. This

process is illustrated for a general case in Figure 22.6a.

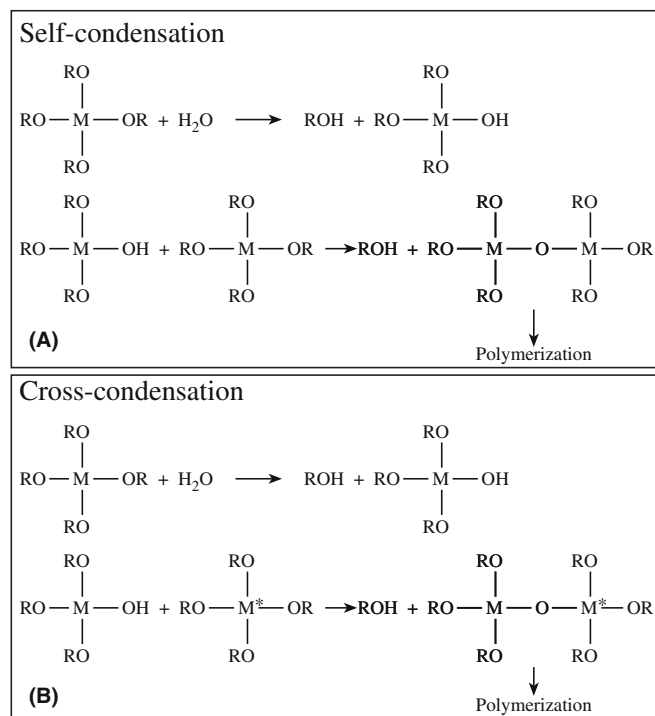


FIGURE 22.6 Schematic showing condensation reactions in (a) single metal alkoxide solutions and (b) mixed metal alkoxide solutions.

For different metal alkoxides the situation is shown in Figure 22.6b.

The experimental variables used in the first stage of the sol-gel process determine the kinetics of the hydrolysis of the sol to form a gel and have a major influence on gel structure. The relevant variables are

- Alkoxide concentration
- Reaction medium
- Concentration of catalyst [The rates of hydrolysis and condensation can be affected by the addition of small amounts of acid (e.g., HCl) or base (e.g., NH₄OH), respectively.]
- Temperature

The Sol-Gel Transition

Viscosity is a key parameter that is used to determine when the sol-gel transition occurs. At the transition there is an abrupt increase in viscosity. The structural changes that occur during gelation for acid-catalyzed and base-catalyzed reactions are illustrated in Figure 22.7.

Viscosity can be measured by two simple methods:

- Capillary flow—most common
- Rotation—using “Couette flow”

The Ostwald viscometer, illustrated in Figure 22.8, is an example of a capillary method used to study the sol-gel

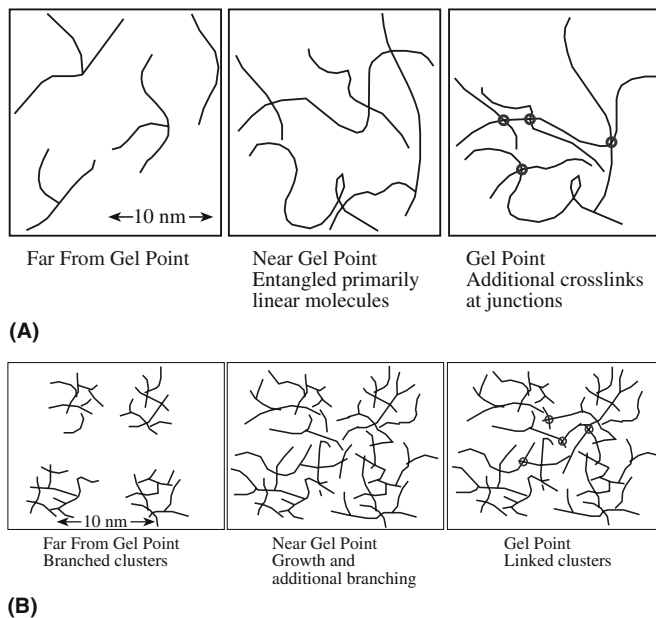


FIGURE 22.7 Illustration of (a) acid- and (b) base-catalyzed polymerization and gelation.

transition. The solution is introduced into the viscometer such that it reaches levels B and C. Liquid is then drawn up into the left-hand limb until the liquid levels are above A and at the bottom of the right-hand bulb. When the liquid is released the time for the left-hand meniscus to pass between marks A and B is measured. Since the pressure at any instant driving the liquid through the capillary is proportional to its density we write

$$\eta = k\rho t \quad (22.5)$$

where k is a constant known as the viscometer coefficient, ρ is the density of the liquid, and t is the flow time. The capillary measurement is simple to operate and quite precise (0.01–0.1%).

Rotational methods are particularly suitable for studying the flow of non-Newtonian liquids. An

example is the concentric cylinder (or Couette) viscometer. The liquid is sheared between concentric cylinders, which are moving relative to one another. The outer cylinder can be rotated (or oscillated) at a constant rate and the shear measured in terms of the deflection of the inner cylinder, which is suspended by a torsion wire. Alterna-

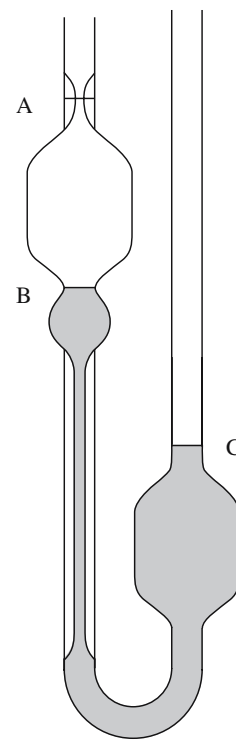


FIGURE 22.8 An Ostwald viscometer. The liquid is initially at B and C, then is drawn up to A.

tively, the inner cylinder can be rotated with the outer cylinder stationary and the resistance offered by the motor measured. The coefficient of viscosity is given by

$$\eta = K\theta/\omega h \quad (22.6)$$

where K is an instrument constant (usually obtained by calibration with a liquid of known η), ω is the angular velocity of the rotating cylinder, and h is the effective height of the liquid in contact with the cylinders. This method is essentially the same as the Mergules viscometer (Section 21.3) that is used to measure the viscosity of glass melts; the temperature is very different.

Drying and Firing

After gelation, the gel usually consists of a weak skeleton of amorphous material containing an interconnected network of small liquid-filled pores. The liquid is usually a mixture of alcohol and water, which must be removed. Shrinkage during this step is usually large.

There are several different methods used to dry gels. Each method produces a dried gel with a specific microstructure. In most cases we obtain either an aerogel or a xerogel, but other microstructures are possible as shown in Table 22.5.

The drying process is complicated, particularly when we want to form monolithic ceramics. One problem is cracking, which is more likely with high drying rates and thick (>1 cm) gels. A number of procedures have been developed to increase drying rates while avoiding cracking:

- Increase the pore size of the gel.
- Decrease the liquid/vapor interfacial energy; e.g., use a solvent with a low γ_{lv} .
- Strengthen the gel.
- Use supercritical (hypercritical) drying: the liquid is removed above its critical temperature, T_c , and critical pressure, p_c . The values of T_c and p_c for the commonly

used sol-gel liquids are water: 647 K and 22 MPa, and ethanol: 516 K and 6.4 MPa.

During firing, further changes occur as the gel densifies. The driving forces for these changes are as follows:

- The large surface area of the dried gel. A xerogel has a solid/vapor interfacial area of 100–1000 m²/g. Reduction of the surface area provides a driving force for densification.
- The low cross-linked density of the dried gel. The free energy, ΔG_f (298 K), of the polymerization reaction (Eq. 22.7) is -14.9 kJ/mol, and this acts as a driving force for increasing the amount of cross-linking.



- Structural relaxation of the solid skeletal phase of the gel as the structure approaches that of a supercooled liquid (if the gel forms a glass) or a crystal line solid (if the gel forms a crystalline ceramic).

SHRINKAGE

During drying: Linear shrinkage 50%, volume shrinkage 90%

During firing: Linear shrinkage 20%, volume shrinkage 50%

22.5 CHARACTERIZATION OF THE SOL-GEL PROCESS

Many techniques, in addition to measuring viscosity changes, have been used to follow the transitions that occur during sol-gel processing. There are the two parts of the process in which we are interested:

1. The transition from sol to gel
2. The transition from gel to oxide

Examples of techniques used to characterize sol-gel processes and the type of information they can provide are listed in Table 22.6. We described most of these techniques in Chapter 10.

TABLE 22.5 The Various Types of Dried Gels

Type	Drying conditions	Microstructure
Aerogels	In an autoclave, the fluid is removed by hypercritical evacuation	A network consisting of ~95% porosity
Xerogels	Natural evaporation	Dried gel has about 40–60% of the fired density and contains small pores (as small as 2 nm)
Sonogels	Gel exposed to ultrasound in the 20-kHz range prior to autoclave treatment	Assists in the formation of multicomponent gels
Cryogels	Freeze dried	Finely divided powder, not suitable for producing monolithic ceramics
Vapogels	A fluid stream of SiCl ₄ is injected into acidified water; this allows rapid gel formation; the gel is then dried to a xerogel	Allows incorporation of additives into the gel, e.g., GeO ₂ if the fluid stream also contains GeCl ₄

TABLE 22.6 Methods Used to Characterize Sol-Gel Processes

<i>Technique</i>	<i>What is measured</i>	<i>How it is used</i>
Ellipsometry	Thickness, optical constants of films	To measure film thickness changes, for example, during drying
Fourier transform IR spectroscopy	Vibrational frequencies of chemical bonds, qualitative and quantitative identification of functional groups	Chemical changes during gelation, drying, and firing
Raman spectroscopy	Vibrational frequencies of chemical bonds, compound identification, structural order and phase transitions	Chemical and structural changes during gelation, drying, and firing
Solid-state nuclear magnetic resonance (NMR) spectroscopy	Interaction between nuclear magnetic moments in atoms in the sample with rf electromagnetic waves, sensitive indicator of structural and chemical bonding properties; phase identification and characterization of local bonding environment	Polymerization kinetics, time evolution of condensed species The chemical shifts in ²⁹ Si NMR are functions of the state of silicon polymerization
Transmission electron microscopy	Crystallinity and phase identification by diffraction, microstructure at high spatial resolution	Transformation from amorphous to crystalline during firing; experiments can be performed <i>in situ</i>
X-ray diffraction	Crystallinity and phase identification, averaged microstructural information	Transformation from amorphous to crystalline during firing; experiments can be performed <i>in situ</i>

22.6 POWDERS, COATINGS, FIBERS, CRYSTALLINE, OR GLASS?

Sol-gel processing is versatile because it can be used to produce ceramics in a number of different forms:

Powders—because we can make very small particles and control the composition

Example application: bioactive glass powders, with a composition of SiO₂–CaO–P₂O₅

Coatings—because the sol is a viscous liquid and can be applied to a substrate by spinning

Example application: TiO₂-based antiglare coatings on glass

Example application: coat steel with alumina to improve wear resistance

Fibers—because we can pull a thread out that is liquid and dry it, coat it, etc.

Example application: SiO₂ fibers used for space shuttle tiles

Crystalline or Glass? We have the choice.

Example application: high-purity porous silica glass for filtration

Powders

Powders can be obtained via a sol-gel process using metal alkoxides or a combination of metal alkoxides and metal salts. Because the mixing of the constituents is achieved at a molecular level, the powders are chemically homogeneous. Powders produced by the sol-gel method are usually amorphous. This characteristic, together with their high surface area, allows them to be sintered to nearly full

density at temperatures lower than are normally required when the particles have been made by other techniques. For example, gel-derived mullite powders can be sintered to full density at <1300°C, whereas the sintering temperature is ~1600°C for crystalline mullite powders. However, the cost of the raw materials limits the use of the sol-gel method in producing many ceramic powders except for those used for specialty applications.

Coatings and Films

Ceramic coatings can be prepared using a sol-gel process involving metal alkoxides. The coatings may be formed by

- Dipping
- Spinning
- Spraying
- Lowering (similar to dipping except the substrate remains stationary and the liquid is lowered)

Spinning is widely used for applying sol-gel coatings, and one particular application is to produce thin coatings of PZT for microelectromechanical systems (MEMS). Alkoxide-derived coatings are used for both antireflective layers on glass substrates and solar reflecting coatings on flat glass. Table 22.7 lists a number of applications for sol-gel films and coatings.

The advantages of forming coatings via sol-gel reactions are

- Large areas
- Uniform composition

TABLE 22.7 Applications of Sol-Gel Films and Coatings

Field	Property	Examples
Electronic	Ferroelectric	BaTiO ₃ , PZT
	Piezoelectric	PZT
	High-Tc superconductor	YBa ₂ Cu ₃ O ₇
	Ferrimagnetic	Doped Fe ₂ O ₃
	Transparent conductors	Indium tin oxide
Optical	Antireflective	TiO ₂ /SiO ₂
	Solar reflecting	TiO ₂ /Pd
	Electrooptic	PLZT
Protective	Corrosion resistant	SiO ₂
	Abrasion resistant	Organic modified silicates
Biomaterials	Barrier films	YSZ
	Bone cell regeneration	Calcium apatites

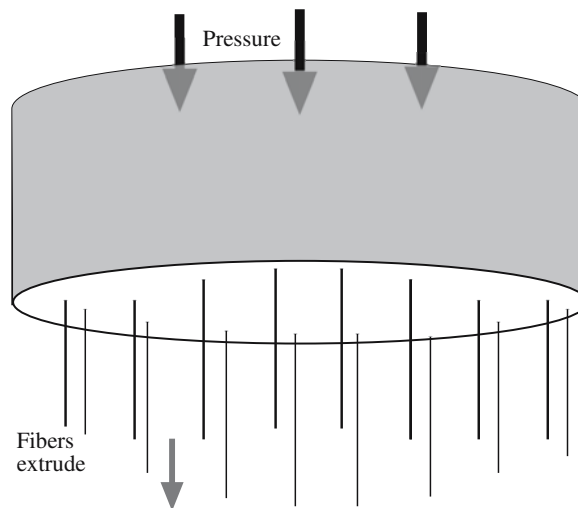
- Conformal coating of irregularly shaped substrates, e.g., fibers
- High purity
- Microstructural control, i.e., pore volume (0–65%), pore size (<0.4 nm to >5.0 nm), and surface area (<1–250 m²/g)
- Less expensive than vapor-phase processes such as chemical vapor deposition (CVD) and sputtering
- Fibers

In Chapter 20 we described various methods of making ceramic fibers including the sol-gel process. Fibers can be drawn directly from viscous sols, which are usually made by acid-catalyzed hydrolysis using low H₂O:M ratios. At viscosities greater than about 1 Pa·s (glycerine has a viscosity of ~1 Pa·s at room temperature) the sol is sticky and we can produce fibers by forcing the sol through a spinnerette, illustrated in Figure 22.9. The spinnerette can be rotated to produce a yarn. This process is used commercially to produce polymer fibers.

Applications for sol-gel-derived fibers include

- Reinforcement in composites
- Refractory textiles
- High-temperature superconductors

Examples of fibers produced by sol-gel are

**FIGURE 22.9** Illustration of a spinnerette used to produce fibers and yarn.

- SiO₂
- SiO₂–TiO₂ (10–50 mol% TiO₂)
- SiO₂–Al₂O₃ (10–30 mol% Al₂O₃)
- SiO₂–ZrO₂ (10–33 mol% ZrO₂)
- SiO₂–Na₂O–ZrO₂ (25 mol% ZrO₂)

The properties of some commercial sol-gel fibers are given in Table 22.8.

Glasses

Glasses can be synthesized using the sol-gel process. This process makes it possible to form a disordered glass network, not directly at high temperatures from the melt, but at low temperatures by chemical polymerization in a liquid.

The Owens-Illinois Company started an investigation of bulk glass systems formed by the sol-gel process in 1967. The dried gels were melted and fabricated by conventional techniques. They found the following advantages:

- Lower melting temperatures could be used (the gel is already amorphous).

TABLE 22.8 Properties of Commercial Gel-Derived Ceramic Fibers

Producer	Name	Composition	Tensile strength (MPa)	Tensile modulus (GPa)	Density (g/cm ³)
3M	Nextel 312	Al ₂ O ₃ , SiO ₂ , B ₂ O ₃	1750	154	2.70
3M	Nextel 440	Al ₂ O ₃ , SiO ₂ , B ₂ O ₃	2100	189	3.05
3M	Nextel 480	Al ₂ O ₃ , SiO ₂ , B ₂ O ₃	2275	224	3.05
Du Pont	PRD-166	Al ₂ O ₃ , ZrO ₂	2100	385	4.20
Du Pont	FP	α-Al ₂ O ₃	1400	3853	3.90
Sumitomo		Al ₂ O ₃ , SiO ₂	Average 2200	Average 230	3.20

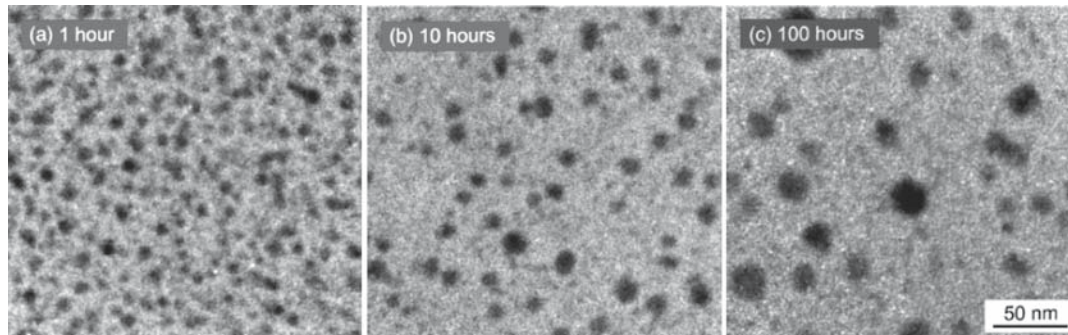


FIGURE 22.10 Use of sol-gel processing to produce Si nanoparticles in a glass matrix. (a–c) The time indicates the length of the heat treatment.

- It was not necessary to stir the melt (the gel is homogeneous).

It was also found that glasses fabricated from gels and those of the same composition made from oxide powders had essentially the same physical properties. But the work was discontinued because of the high cost of the gels compared to the cost of the traditional powders. And, in terms of processing considerations, the gel must be heated very slowly to the melting temperature to ensure that any residual organics and water are removed, otherwise a very seedy and foamy melt can be obtained.

Sol-gel processing can really be justified only for glasses of certain compositions such as those with high melting temperatures and high viscosity glasses that are difficult to melt conventionally. But glass coatings made by the sol-gel process are still important commercially.

Monolithic Ceramics

There are basically two routes that can be used to produce monolithic ceramics via a sol-gel process:

- Firing: use xerogels or aerogels
- Compaction and firing: use gel-derived powders

Making monolithic ceramics directly by a sol-gel process is still a challenge. The main issue is how the gel can be dried without introducing cracks in the dried body. The advantages of using a sol-gel route compared

to conventional ceramic methods is that we are working in uncontaminated conditions and using lower temperatures.

The compaction-and-firing process is similar to traditional methods for producing ceramics from powders except that the powders are derived from the sol-gel process. The pros and cons are the same as those mentioned in forming powders using this method.

Particles in Sol-Gel Films

Since the sol-gel films are essentially amorphous in their as-prepared state, we can heat treat them to grow nanoparticles that are then embedded inside an amorphous matrix. The amorphous SiO(C) film in Figure 22.10 was produced by pyrolysis of a sol-gel precursor. The cohydrolysis of triethoxysilane and methyl-diethoxysilane (in a molar ratio of 9:1) used addition of acidic water (pH 2.25)

to produce the xerogel. The xerogel was pyrolyzed at 1000°C for 1 hour to produce an Si-rich glass. The films were heated for a further 10 hours and then 100 hours to produce the images shown here.

The dark regions in the images are O depleted and Si rich. High-resolution transmission electron microscopy (HRTEM) showed that these were crystalline Si nanoparticles (which have potentially interesting luminescent properties). So not only does this type of study produce an interesting material, but it also sheds light on Ostwald ripening and devitrification of a glass.

MONOLITHIC CERAMICS

The instruction to build a wall in “monolithic” concrete indicates that it should be a wall of concrete built in place and then hardened into a solid unbroken mass. Hence a monolithic ceramic is “built” *in situ*.

CHAPTER SUMMARY

You should know that sols and gels are different concepts and that sol-gel uses both. You cannot avoid learning the basic organic chemistry: it is messy and has confusing terminology but is amazingly versatile and can produce nanomaterials routinely. Sol-gel processing is a method that can be used to form ceramic powders, thin films and coatings, fibers, and monolithic ceramics. The advantages of sol-gel processing are that we have excellent control of the

composition, purity, and homogeneity of our product; how much control depends on the purity of the chemicals with which we start. It also allows us to process materials at lower temperatures than any other method because we have small reactive particles. The disadvantages are that the reactants are often expensive and there are problems in producing bulk ceramic components because of shrinkage. Sol-gel processes are used commercially to produce fibers, coatings, and coated fibers, particularly of ceramics with a high SiO₂ content (because processing temperatures are much lower). It is also particularly suited to producing thin films of multicomponent oxides such as PZT, which have application in MEMS; and how can you put a more uniform coating on a nanoparticle?

PEOPLE IN HISTORY

- Couette, Maurice Frédéric Alfred (1858–1943) was professor of physics at the University of Angers in France. During his lifetime he published only seven papers. The idea for a viscometer based on shearing a liquid between two surfaces came from his Ph.D. thesis.
- Ostwald, Wilhelm (1853–1932) won the Nobel Prize in Chemistry in 1909. He held academic positions at several institutions and from 1887 until his retirement in 1906 was Professor of Physical Chemistry at Leipzig University. His famous students included Arrhenius (Nobel Prize 1903), Van't Hoff (Nobel Prize 1901), and Nernst (Nobel Prize 1920).

GENERAL REFERENCES

- Bradley, D.C., Mehrotra, R.C., and Gaur, D.P. (1978) *Metal Alkoxides*, Academic Press, London. This is essential reading if you want to find out more. It gives a detailed account of the history and synthesis of metal alkoxides, together with a full list of references.
- Brinker, C.J. and Scherer, G.W. (1990) *Sol-Gel Science: The Physics and Chemistry of Sol-Gel Processing*, Academic Press, Boston. This is the comprehensive treatment of sol-gel processing. It is the essential resource for those working (or planning to work) in this field. Brinker and Scherer and their co-workers have done extensive work on the densification of gels that form glasses. For more information and specifics on this topic, find these papers in your library: Brinker, C.J., Roth, E.P., Scherer, G.W., and Tallant, D.R. (1985) "Structural evolution during the gel to glass conversion," *J. Non-Cryst. Sol.* **71**, 171; Brinker, C.J., Scherer, G.W., and Roth, E.P. (1985) "Sol → gel → glass: II. Physical and structural evolution during constant heating rate experiments," *J. Non-Cryst. Solids* **72**, 345; Scherer, G.W., Brinker, C.J., and Roth, E.P. (1985) "Sol → gel → glass: III. Viscous sintering," *J. Non-Cryst. Solids* **72**, 369.
- Hübert, T., Schwarz, J., and Oertel, B. (2006) "Sol-gel alumina coatings on stainless steel for wear protection," *J. Sol-Gel Sci. Techn.* **38**, 179.
- Iler, R.K. (1979) *The Chemistry of Silica*, Wiley, New York. Every aspect of the chemistry of silica in aqueous systems, including polymerization, gelation, gel structure, and applications, is discussed in this classic text.
- Johnson, J.F., Martin, J.R., and Porter, R.S. (1977) "Determination of viscosity," in *Physical Methods of Chemistry*, edited by A. Weissberger and B.W. Rossiter, Vol. 1 Part 6 of *Techniques of Chemistry*, Wiley, New York, p. 63. Detailed descriptions of measuring viscosity.
- Rahaman, M.N. (1995) *Ceramic Processing and Sintering*, Marcel Dekker, New York. Chapter 5 covers sol-gel processing, especially for drying procedures.
- Segal, D. (1989) *Chemical Synthesis of Advanced Ceramic Materials*, Cambridge University Press, Cambridge. Concise description of the various chemical routes to fabricate ceramics. Contains a large number of references.

JOURNALS AND CONFERENCES

- For coverage of current sol-gel research, the most widely used journals are *J. Non-Cryst. Solids*, *J. Mater. Res.*, *J. Am. Ceram. Soc.*, *J. Sol-Gel Sci. Techn.*, and *J. Mater. Sci.*
- The Materials Research Society has sponsored meetings since 1984 under the title *Better Ceramics Through Chemistry* and has published proceedings.

SPECIFIC REFERENCES

- Ebelman, J.J. and Bouquet, M. (1846) *Ann. Chem. Phys.* **17**, 54. Ebelman was the first person to describe alkoxide synthesis. This paper reported the synthesis of boron methoxide, ethoxide, and pentoxide by the reaction of boron trichloride with the appropriate alcohol. These alkoxides can be used in the synthesis of borosilicate glasses.
- Piau, J.M., Bremond, M., Couette, J.M., and Piau, M. (1994) "Maurice Couette, one of the founders of rheology," *Rheol. Acta* **33**(5), 357.

- Roy, D.M. and Roy, R. (1955) "Synthesis and stability of minerals in the system $\text{MgO-Al}_2\text{O}_3\text{-SiO}_2\text{-H}_2\text{O}$," *Am. Min.* **40**, 147. For studying phase equilibria in minerals homogeneous samples are essential. Hydrolysis of alkoxides was used to synthesize the powders. Rustum Roy of Pennsylvania State University was one of the pioneers in using sol-gel techniques for preparing ceramics.
- Scherer, G.W. (1990) "Stress and fracture during drying of gels," *J. Non-Cryst. Solids* **121**, 104. Model for drying gels.

EXERCISES

- 22.1 Sol-gel coatings are usually prepared using either dipping or spinning. What are the advantages and disadvantages of the two methods?
- 22.2 Why would spinning rather than dipping be used to produce PZT films for applications such as MEMS?
- 22.3 The ceramic fibers listed in Table 22.8 are made by sol-gel processing. (a) Why do you think this processing method was chosen? (b) What starting chemicals would be suitable for making these fibers? (c) Are there any alternative approaches that could be used to produce these ceramic fibers? If so, what are they and how do they compare to sol-gel?
- 22.4 Discuss the economic issues involved in using the sol-gel process to form ceramic powders.
- 22.5 Explain why ^{29}Si NMR can be used to study the amorphous-to-crystalline transition in a silica gel. [Note: You may find the following references of use: Brown, I.D. and Shannon, R.D. (1973) "Empirical bond-strength bond-length curves for oxides," *Acta Crystallogr. A* **29**, 266; Smith, K.A., Kirkpatrick, R.J., Oldfield, E., and Henderson, D.M. (1983) "High-resolution ^{29}Si nuclear magnetic-resonance spectroscopic study of rock-forming silicates," *Am. Mineral.* **68**, 1206.]
- 22.6 What is the difference between a particulate gel and a polymeric gel?
- 22.7 What would be appropriate starting chemicals for producing $\text{YBa}_2\text{Cu}_3\text{O}_7$ films by sol-gel?
- 22.8 Explain briefly the problems with shrinkage as they apply to sol-gel processing.
- 22.9 Compare the raw materials costs of preparing PZT powders by conventional solid-state reactions and sol-gel processing. What are the pros and cons of each approach?
- 22.10 Nylon is prepared by a condensation reaction. Compare this process to that occurring during sol-gel processing of ceramics using metal alkoxides.

Shaping and Forming

CHAPTER PREVIEW

This is the pottery chapter! Many of the techniques that are now being used to shape high-tech ceramics have been used by potters for millennia, but have been refined for today's high-tech applications and for new ceramic materials. We will try to relate shaping to the potter's craft throughout the chapter.

We can just process dry powder and sinter it, but it is much more common to add some amount of liquid, just as the potter adds water to clay; we then shape the object and fire it. Shaping transforms an unconsolidated powder mixture into a coherent, consolidated body having a chosen geometry. The selection of a shaping operation for a particular product is very dependent on the size and dimensional tolerances of the product, the requisite microstructural characteristics, the levels of reproducibility required, economic considerations, and of course the required shape. We cover shaping of glass in Chapters 21 and 26 so here we will consider the similarities in processing glass and crystalline ceramics. Similarly, we discuss thick films in Chapter 27; here we concentrate on three-dimensional (3D) objects varying from fish-hooks to turbine blades. However, we will cover slip casting, which we used only in a limited way for thin films.

23.1 THE WORDS

There is a special vocabulary for shaping ceramics because it is an ancient art. Once the constituent powders have been prepared in the desired purity and particle size most ceramic products must be fabricated into useful shapes. Many shaping methods are used for ceramic products and these can be grouped into three basic categories, which are not necessarily independent.

1. Powder compaction: dry pressing, hot pressing, cold isostatic pressing, etc.
2. Casting: using a mold with the ceramic as, or containing, a liquid or slurry
3. Plastic forming: extrusion, injection molding, etc.—using pressure to shape the green ceramic

Powder compaction is simply the pressing of a free-flowing powder. The powder may be dry pressed (i.e., without the addition of a binder) or pressed with the addition of a small amount of a suitable binder. The pressure is applied either uniaxially or isostatically. The choice of pressing method depends on the shape of the final product. We make simple shapes by applying the pressure uniaxially; more complex shapes require isostatic pressing.

Casting ceramics is carried out at room temperature and generally requires the ceramic powder particles to be suspended in a liquid to form a slurry; note this process

is quite unlike the casting of metals. The slurry is then poured into a porous mold that removes the liquid (it diffuses out through the mold) and leaves a particulate compact in the mold. This process is known as slip casting. The process has been used to form many traditional ceramic products (e.g., sanitary ware) and more recently has been used in forming advanced ceramic products (e.g., rotor blades for gas turbines). The other main casting process for ceramics is tape casting, which, as you would guess, is used to make thick films or sheets and is described in Chapter 27.

Plastic forming consists of mixing the ceramic powder with a large volume fraction of a liquid to produce a mass that is deformable (plastic) under pressure. Such processes were developed and used originally for clay and have since been adapted to polymeric materials. For traditional clay-based ceramics the liquid is mainly water. For ceramic systems that are not based on clay, an organic may be used in place of, or in addition to, water. The binders are often complex and contain multiple components to achieve the required viscosity and burn-out characteristics.

Table 23.1 lists the major methods that are included in each of the above categories and the types of shape that can be produced. First some of the words:

Binder is a component that is added to hold the powder together while we shape the body.

Slurry is a suspension of ceramic particles in a liquid.

TABLE 23.1 Various Shaping Methods for Ceramic Components

Shaping method	Type of feed material	Type of shape
Dry pressing	Free-flowing granules	Small and simple
Isostatic pressing	Fragile granules	Larger and more intricate
Extrusion	Plastic mass using a viscous polymer solution	Elongated with constant cross section
Injection molding	Organic binder giving fluidity when hot	Complex
Slip casting	Free-flowing cream	Mainly hollow

Plasticizer is the component of a binder that keeps it soft or pliable; it improves the rheological properties. *Green* is a ceramic before it is fired. Brown, white, or gray potter's clays are well known green ceramics. *Slip* is the liquid-like coating used to form the glaze when fired.

Some of the shaping methods we will describe in this chapter produce a ceramic compact that is strong enough to be handled and machined; however, it is not fully dense and the bonds between the grains are not strong. This is called the "green" state and represents a transition state between the loose powder and the high-density sintered product. Other shaping methods, those that involve the use of high temperatures and pressures, can directly produce a very dense sintered product. Much of what we talk about here has a parallel in the field of powder metallurgy; the theme is often *processing powders*, which are not necessarily ceramic powders (e.g., they could be pharmaceuticals).

23.2 BINDERS AND PLASTICIZERS

It is often necessary to add a binder to the ceramic powder. The binder has two functions. In some shaping methods, such as extrusion, the binder provides the plasticity necessary for forming. The binder also provides the dry (green) shape with strength sufficient to survive the handling process between shaping and sintering. One of the most important requirements for the binder is that we must be able to eliminate it from the compact during the firing process without any disruptive effect: polymers are thus often ideal binders.

In pottery, the binder is often water that is present in sufficient quantity to make the clay easily shaped with the shape being retained during firing. The idea is that we then add a plasticizer to optimize the rheology of the material. Note that these processes are not exclusive to ceramics but are general to powder processing. The distinction between binder and plasticizer is sometimes not too clear.

BINDERS

Poly (vinyl alcohol) (PVA) and poly (ethylene glycol) (PEG) are the two of the most popular binders for dry-pressing ceramics:

PVA provides a high green strength.
PEG provide a high green density.

Binders can also be used when metal powders are processed; PMC is *precious-metal clay*.

23.3 SLIP AND SLURRY

The word slip appears to come (according to Webster's) from the Old English words meaning cream: the suspension of curds in the liquid when making cheese; the cheese was actually sieved through a "slippe clothe."

In general, slip consists of fine (<10µm) ceramic-powder particles that are suspended in a fluid. In the pottery industry, the liquid is usually water. The suspension can have a solid content up to ~60 vol%. Deflocculents are added to the slip to modify the electrical environment of each particle so that the particles repel each other.

Deflocculants: Since deflocculation is defined as the process by which flocules present in a liquid break up into fine particles producing a dispersion, a deflocculant is an additive that causes this process. In other words, deflocculation is the opposite of coagulation. (A flocule is a small piece of matter or a flock.)

Colloids: Colloids are defined very generally as any substance that consists of particles substantially larger than ordinary molecules but much too small to be visible without optical magnification (~1 nm to 10µm). They can be linked or bonded together in various ways. Colloidal systems can take several forms; the one relevant to us is the dispersion of one substance in another. Brownian motion has interested scientists for generations. Slip is a colloid. We can change the properties of the slip by adding flocculants or deflocculants.

Slurry: Clay particles are suspended in a liquid (water in the case of pottery). As the amount of water is decreased it becomes more solid. Glazes used in pottery have the same base as the clay but with more water content. Potter's clay is made by first producing a slip from naturally occur-

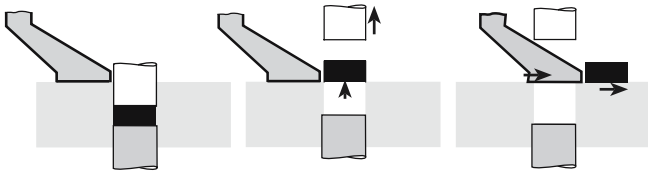


FIGURE 23.1 The stages in dry pressing.

ring clays. The slip is repeatedly filtered to produce a consistency that is constant over long periods of manufacture. Slabs of clay are then formed from this colloid by allowing most of the water to evaporate. The final product may be shaped by extrusion and packaged to prevent further loss of water.

23.4 DRY PRESSING

Dry pressing is ideally suited to the formation of simple solid shapes and consists of three basic steps: filling the die, compacting the contents, and ejecting the pressed solid.

Figure 23.1 shows a schematic diagram of the double-action dry-pressing process. In a double-action press both the top and bottom punches are movable. When the bottom punch is in the low position a cavity is formed in the die and this cavity is filled with free flowing powder. In dry pressing the powder mixture will contain between 0 and 5 wt% of a binder. (So, dry does not imply that there is no binder.) Once the cavity has been filled, the powder is struck off level with the top of the die. The top punch descends and compresses the powder either to a predetermined volume or to a set pressure. During pressing the powder particles must flow between the closing punches so that the space between them is uniformly filled. A particle size distribution of between 20 and 200 μm is often preferred for dry pressing: a high volume fraction of small particles causes problems with particle flow and also results in sticking of the punches. The pressures used in dry pressing may be as high as 300 MPa, depending upon material and press type, to maximize the density of the compact. After pressing, both punches move upward until the bottom punch is level with the top of the die and the top punch is clear of the powder-feeding mechanism. The compact is then ejected, the bottom punch is lowered, and the cycle is repeated.

Because the dry-pressing process is so simple and involves low capital equipment costs it is the most widely used high-volume forming process for ceramics. Production rates depend on the size and shape of the part and on the type of press used. For large components such as refractories or complex parts such as grinding wheels the production rates are 1–15 parts per minute. During a tour of the Wedgwood factory, you will see dinner plates being dry pressed in a continuous process. Simpler or smaller

shapes such as seal rings and nozzles can be produced at rates up to several hundred per minute. Small flat parts such as insulators, chip carriers, or cutting tools can be produced at rates up to several thousand per minute.

23.5 HOT PRESSING

Pressing can also be performed at high temperatures; this process is known as hot pressing. The die assembly used for hot pressing is very similar to that described in Section 23.4 for dry pressing. The main difference is that in hot pressing the die assembly is contained within a high-temperature furnace as shown in Figure 23.2. During hot pressing the ceramic powders may sinter together to form a high-density component.

We can summarize the advantages of this process.

- The powder does not have to be of the highest quality.
- Large pores that are caused by nonuniform mixing are easily removed.
- We can densify at temperatures lower (typically half the melting temperature of the material) than those needed for conventional pressureless sintering.
- Extensive grain growth or secondary recrystallization does not occur when we keep the temperature low during densification.
- We can densify covalently bonded materials such as B₄C, SiC, and Si₃N₄ without additives.

The principal disadvantage is also important.

- Dies for use at high temperatures are expensive and do not generally last long.

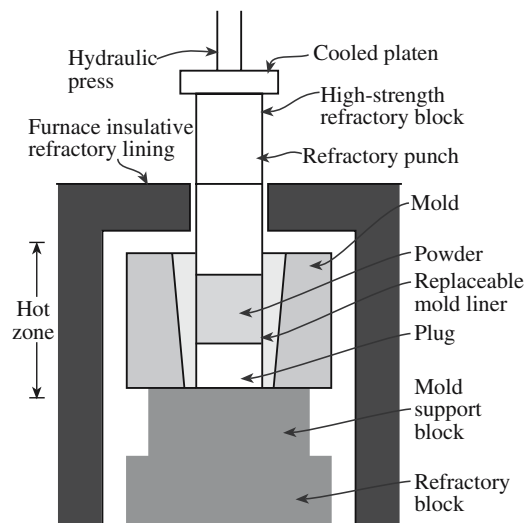


FIGURE 23.2 Schematic showing the essential elements of a hot press.

TABLE 23.2 Hot Pressed Products

Product	Types of material
Optical windows	IR: MgF ₂ , ZnS, ZnSe; visible: Y ₂ O ₃ , MgAl ₂ O ₄
Ceramic armor	B ₄ C, TiB ₂ , SiC, Al ₂ O ₃
Cutting tools	Al ₂ O ₃ particle-reinforced TiC, Si ₃ N ₄ , Si ₃ N ₄ -AlN-Al ₂ O ₃
Tooling (molds and dies)	Al ₂ O ₃ -SiC _w composites, SiC, Al ₂ O ₃
Sputtering targets	Cr-SiO, TiN, Si ₃ N ₄ , B ₄ C, Al ₂ O ₃
Heat engine components	Si ₃ N ₄ , SiC
Ceramic bearings	Si ₃ N ₄
Microwave absorbers	MgO-SiC particulate composites, BeO-SiC, Al ₂ O ₃ -SiC
Varistors	ZnO
Electrooptic materials	PLZT
Titanates	BaTiO ₃ , CaTiO ₃
Microelectronic packages	Cofired W-metallized AlN
Resistors	Si ₃ N ₄ matrix with particulates of TiB ₂ , TiC, TiN, or SiC as the dispersed conducting phase

Most metals are of little use as die materials above 1000°C because they become ductile, and the die bulges. Special alloys, mostly based on Mo, can be used up to 1000°C at pressures of about 80 MPa. Ceramics such as Al₂O₃, SiC, and Si₃N₄ can be used up to about 1400°C at similar pressures. Graphite is the most widely used die material and can be used at temperatures up to 2200°C and pressures between 10 and 30 MPa. The difficulty is that a graphite die will tend to produce a very reducing environment. (You can make an Al₂O₃ sample vanish using a graphite die!)

However, graphite does have many properties that make it suitable for a die.

- It is easy to machine (but the dust is toxic if inhaled—like coal dust).
- It is inexpensive.
- Its strength increases with increasing temperature.
- It has good creep resistance.
- It has excellent thermal conductivity.
- It has a relatively low coefficient of thermal expansion.

Hot pressing, like dry pressing, is limited to simple solid shapes, such as flat plates, blocks, and cylinders. More complex or large shapes are difficult and often impossible to produce by hot pressing. Hot pressing is widely used in the research laboratory for processing very dense, high-purity ceramic components. Although it is extensively used in university and government laboratories, the technique is limited as a production tool because of its high cost and low productivity. For any mass-produced ceramic product there would be considerable commercial pressure for a company to find a less expensive alternative. However, some commercial hot-pressed ceramic products are available. These products require a

small grain size, a high density (low porosity), or low impurity levels. Examples of such products are given in Table 23.2.

Isostatic pressing involves the application of hydrostatic pressure to a powder in a flexible container. The advantage of applying pressure in all directions is that there is more uniform compaction of the powder and more complex shapes can be produced than with uniaxial pressing. Isostatic pressing can be performed either with or without applied heat.

23.6 COLD ISOSTATIC PRESSING

There are many variations on using the cold isostatic press (CIP); here we just emphasize some basic themes. Figure 23.3 illustrates the so-called wet-bag CIP process. Powder is weighed into a rubber bag and a metal mandrel is inserted that makes a seal with the mouth of the rubber bag. The sealed bag is placed inside a high-pressure chamber that is filled with a fluid (normally a soluble oil/water mixture) and is hydrostatically pressed. The pressures used can vary from about 20 MPa up to 1 GPa depending upon the press and the application. For production units the pressure is usually ≤400 MPa. Once pressing is complete, the pressure is released slowly, the mold is removed from the pressure chamber, and the pressed component is removed from the mold.

The advantages of the wet-bag process are

- Wide range of shapes and sizes can be produced
- Uniform density of the pressed product
- Low tooling costs

The disadvantages are

- Poor shape and dimensional control (particularly for complex shapes)

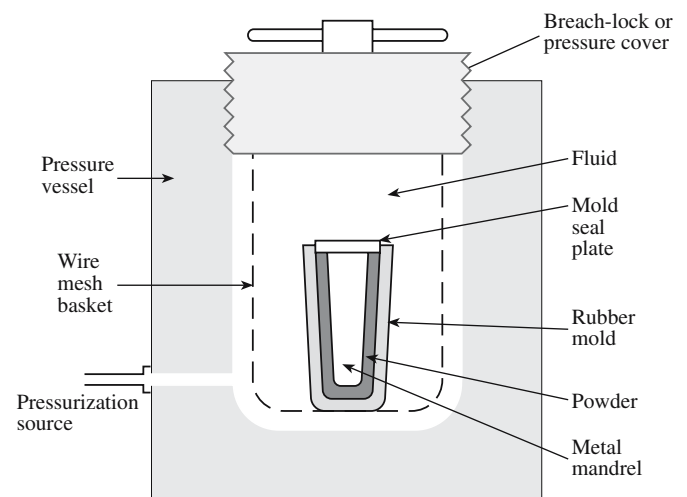


FIGURE 23.3 Schematic of a wet-bag isostatic pressing system.

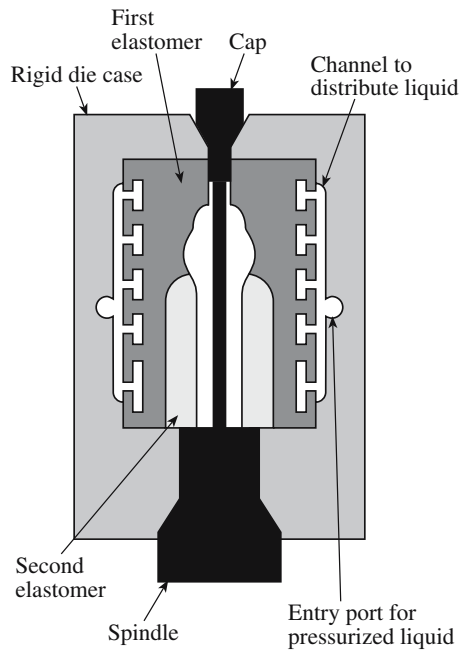


FIGURE 23.4 Schematic of a die for dry-bag isostatic pressing of a spark plug insulator.

- Products often require green machining (described in Section 23.14) after pressing
- Long cycle times (typically between 5 and 60 minutes) give low production rates

A small wet-bag isostatic press, used to produce laboratory samples and low-volume production parts, might have an internal diameter of 150 mm and a depth of 460 mm. Large wet-bag presses may have cavity diameters >1.8 m and lengths up to 3.7 m. The wet-bag CIP process can be automated.

A schematic diagram of a mold for the dry-bag CIP is shown in Figure 23.4. The main distinction of the dry-bag process is that the rubber mold is now an integral part of the press. The high-pressure fluid is applied through channels in the mold. After pressing, the pressed part is removed without disturbing the mold. Hence, the dry-bag press can be readily automated. Fully automated units are widely available and have been operating in the high-volume production of ceramic parts for over 20 years.

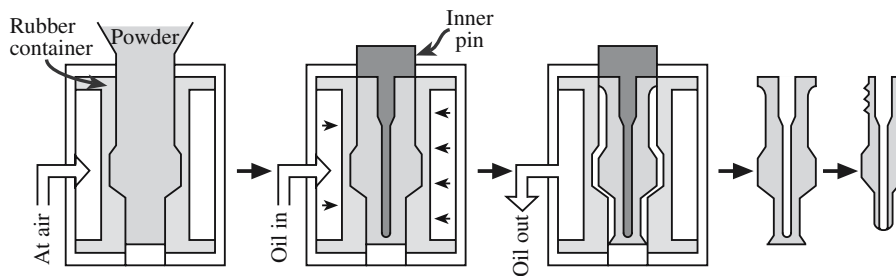


FIGURE 23.5 Making spark plugs. Hydrostatic pressure is applied by pumping oil around the rubber container, which is part of the press and thus easily removed.

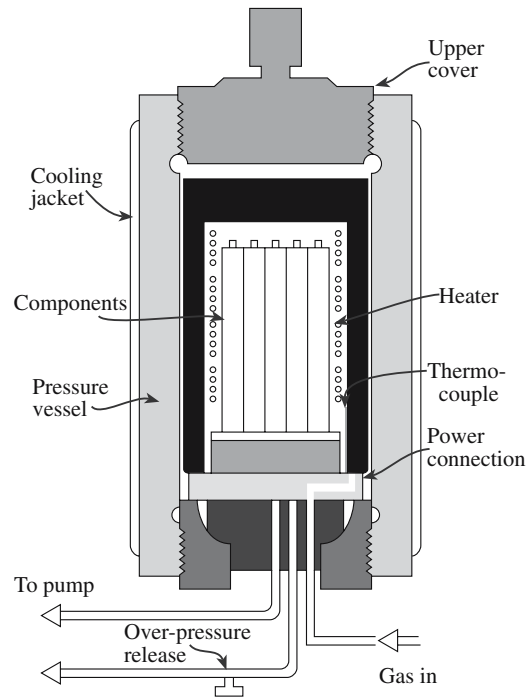


FIGURE 23.6 Schematic of a hot isostatic pressing apparatus.

Production rates of up to 1 part per second are being achieved industrially.

The dry-bag CIP has been used for many years to press spark plug insulators. The steps in this process are shown in Figure 23.5. Notice the insertion of the inner pin in the mold. The world's largest producers of spark plugs produced by this method are Champion and AC Spark Plug.

23.7 HOT ISOSTATIC PRESSING

The hot isostatic press (HIP) uses the simultaneous application of heat and pressure. We refer to this process as HIPing and the product as being HIPed (but you will see variations on these abbreviations). A furnace is constructed within a high-pressure vessel and the objects to be pressed are placed inside. Figure 23.6 shows a typical HIP arrangement. Temperatures can be up to 2000°C and pressures are typically in the range of 30–100 MPa. A gas

is used as the pressure medium, unlike the CIP in which a liquid is often used. Argon is the most common gas that is used for HIPing, but oxidizing and reactive gases can also be used. Note that the high-pressure vessel is not inside the furnace.

There are two variants of HIPing:

- Encapsulated: using a deformable container
- Not encapsulated: it is shaped and sintered first, then HIPed

In the original HIPing method the ceramic powder was filled into a deformable metal can and then subjected to heat and pressure. This method was subsequently modified for small particle sized powders. The powder compact was preformed to the desired shape by a process such as dry pressing or injection molding. The green compact was then encapsulated in a glass envelope that could be removed from the product after HIPing as shown in Figure 23.7.

The second variant does not involve encapsulation. The ceramic powder is first compacted using another shaping method such as dry pressing or injection molding. It is then sintered at relatively high temperatures in a furnace to close all the surface pores, which prevents the entry of the gas during subsequent HIPing. The steps in this process, which is sometimes referred to as sinter-plus-HIP, are shown in Figure 23.8.

Now HIPing is used for a wide variety of ceramic (and metallic) components, such as alumina-based tool bits and the silicon nitride nozzles used in flue-gas desulfurization plants by the utility industry. The advantages of the HIPing process are becoming more important as interest in structural ceramics such as Si_3N_4 grows.

Nonoxide ceramics can be HIPed to full density while keeping the grain size small and not using additives. Very high densities combined with small grain sizes (because of the relatively low temperatures) lead to products with

HIP AND HIPING

Used initially for fabricating the cladding for nuclear fuel elements. It was called “gas-pressure bonding.”

We use the acronym HIP to identify the press and HIPing to identify the action. You will also see HIP used to mean HIPing and you will see HIPing spelled HIPping! We then say a sample has been HIPed rather than HIPped. Only nano is HYPed.

special mechanical properties. HIPing has also been applied to the formation of piezoelectric ceramics such as BaTiO_3 , SrTiO_3 , and lead zirconate titanate (PZT) for use in acoustic wave filters and oscillators.

Uses: produces dense materials without growing the grains

Disadvantage: cost

23.8 SLIP CASTING

The slip is poured into a mold (usually plaster of Paris: $2\text{CaSO}_4 \cdot \text{H}_2\text{O}$) that has been made by casting round a model of the required shape, which was itself suitably enlarged to allow for the shrinkage of the cast ceramic on drying and sintering. The fineness of the powder (in the slip) and the consequent high surface area ensure that electrostatic forces dominate gravity so that settling does not occur. The electrochemistry of the slip is quite complex: Na silicate (or soda ash) is added to the slip to deflocculate the particles. The water passes, via capillary action, into the porous plaster leaving a layer of the solid on the wall of the mold. (We consider this model in Section 25.7.) Once a sufficient thickness has been cast, the surplus slip is poured out and the mold and cast are allowed to dry. These steps are shown in Figure 23.9. This variant of slip casting, which is the most widely used, is also called drain casting. A very effective technique used by some potters is to produce a multilayer slip, parts of which are removed before firing.

Slip casting is a low cost way to produce complex shapes and in the traditional pottery industry it is the accepted method for the production of teapots, jugs, and figurines, although handmade items will likely be hand-thrown. Large articles, such as wash-hand basins and other whitewares, are also mass produced by slip casting. (Whitewares are not necessarily white.) One of the telltale

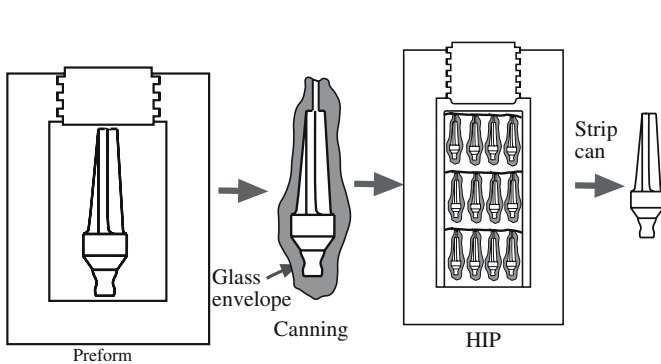


FIGURE 23.7 Individual steps of cold preforming, canning, HIPing, and stripping in the standard HIPing process.

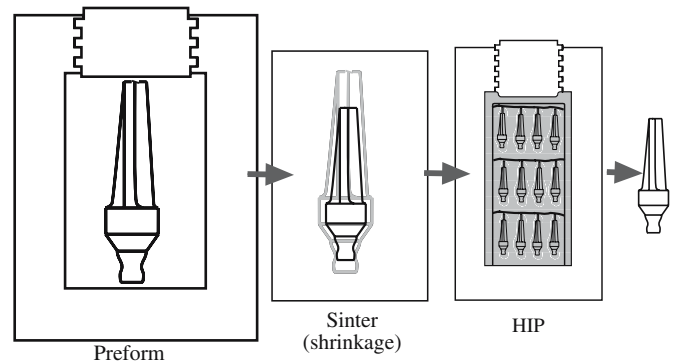


FIGURE 23.8 Individual steps of cold forming, sintering, and HIPing in the sinter plus HIPing process.

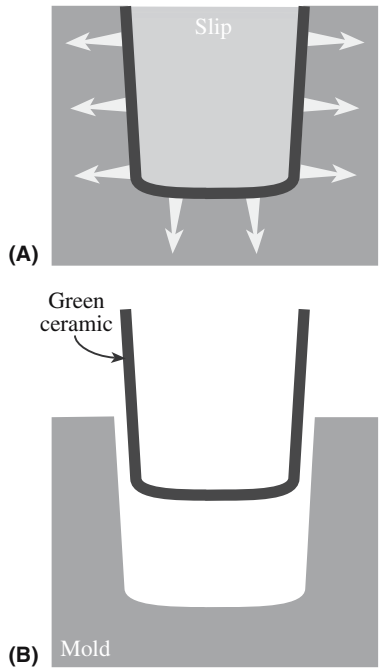


FIGURE 23.9 Schematic illustrating the drain-casting process. (a) Fill the mold with slip; the mold extracts liquid, forming a compact along the mold walls; (b) after excess slip is drained and after partially dried, green ceramic is removed.

signs of a ceramic product made by slip casting is that it is hollow. Another variant of the slip casting process is solid casting. In solid casting, slip is continually added until a solid cast is made. These items will not be hollow—relatively, they will be heavier.

Slip casting is also used in the fabrication of some technical and structural ceramics. It is the standard method used to make alumina crucibles and has been successfully used to make complex structural ceramic components such as gas-turbine rotors. The technique of doctor-blading, which we discuss in Chapter 27, is just another method of shaping the slip—ensuring that the slip is spread as a uniform layer.

23.9 EXTRUSION

Extrusion involves forcing a deformable mass through a die orifice (like toothpaste from a tube). The process is widely used to produce ceramic components having a

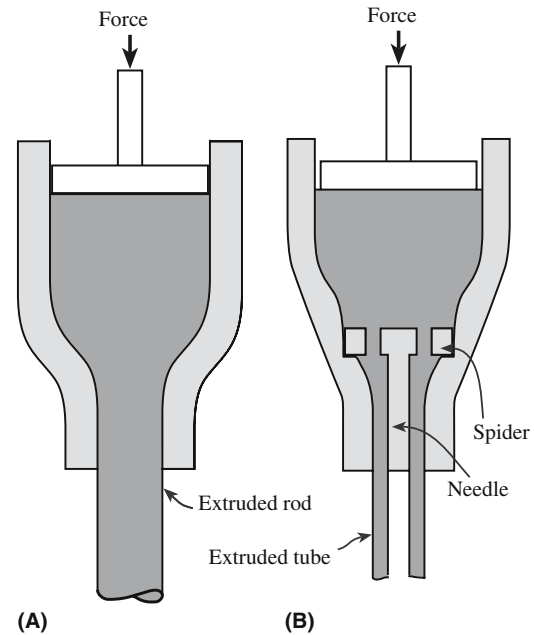


FIGURE 23.10 Extrusion of (a) a rod and (b) a tube.

uniform cross section and a large length-to-diameter ratio such as ceramic tubes and rods as illustrated in Figure 23.10. Clay with a suitable rheology for the extrusion process (essentially a paste) can be made by controlling the amount of water. Clay-free starting materials, such as Al_2O_3 , are mixed with a viscous liquid such as polyvinyl alcohol or methylcellulose and water to produce a plastically deformable mass. Table 23.3 lists the compositions of some extrusion bodies. Extrusion of polymers has been used since the 1860s; it was originally used to process natural rubber. An extrusion press like those shown in Figure 23.11 is standard equipment in the potter's barn.

Extrusion is also used to produce the alumina shells for sodium vapor lamps and the honeycomb-shaped catalyst supports for automotive emission-control devices (see Chapter 37). The catalyst supports are designed to give a high surface area and can consist of hundreds of open cells per square centimeter with wall thicknesses $<100\mu\text{m}$. To produce these shapes, cordierite ceramic powder is mixed with a hydraulic-setting polyurethane resin. The mix is extruded into a water bath at a rate that matches the rate of cure of the polyurethane (about 2 mm/s). It is then fired to produce the final ceramic.

TABLE 23.3 Examples of Compositions of Extruded Bodies (Composition in vol%)

Refractory alumina		High alumina		Electrical porcelain	
Alumina ($<20\mu\text{m}$)	50	Alumina ($<20\mu\text{m}$)	46	Quartz ($<44\mu\text{m}$)	16
Hydroxyethyl cellulose	6	Ball clay	4	Feldspar ($<44\mu\text{m}$)	16
Water	44	Methylcellulose	2	Kaolin	16
AlCl_3 (pH > 8.5)	<1	Water	48	Ball clay	16
		MgCl_2	<1	Water	36
				CaCl_2	<1



(A)



(B)

FIGURE 23.11 Extruding clay. Manual and electric extruders.

23.10 INJECTION MOLDING

Injection molding is another technique that is widely used in shaping thermoplastic polymers. A thermoplastic polymer is one that softens when heated and hardens when cooled. Such processes are totally reversible and may be

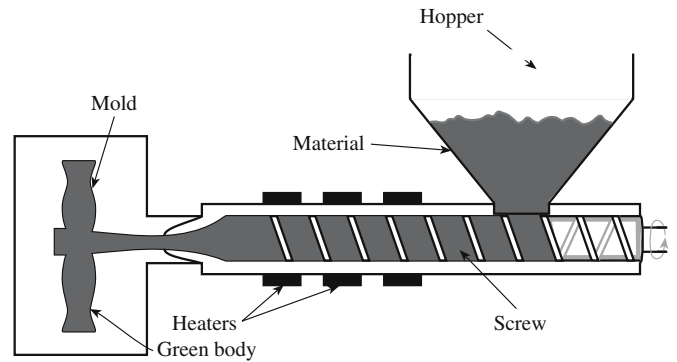


FIGURE 23.12 Cross-sectional side view of a screw-type machine.

repeated. Injection molding can be applied to shaping and forming ceramic components if the ceramic powder is added to a thermoplastic polymer. When forming ceramics by injection molding, the polymer is usually referred to as the binder (but we could instead have called the material a ceramic-loaded polymer). The ceramic powder is added to the binder and is usually mixed with several other organic materials to provide a mass that has the desired rheological properties. Table 23.4 shows the additives that have been used to form SiC shapes by injection molding. The organic part of the mix accounts for about 40 vol%.

The plastic mass is first heated, at which point the thermoplastic polymer becomes soft and is then forced into a mold cavity as shown in Figure 23.12. The heated mixture is very fluid and is not self-supporting (this is different from the situation encountered in extrusion). The mixture is allowed to cool in the mold during which time the thermoplastic polymer hardens. Because of the large volume fraction of organic material used in the mixture, there is a high degree of shrinkage of injection-molded components during sintering. Shrinkage of 15–20% is typical, so precise control of component dimensions is difficult. However, complex shapes are retained with very little distortion during sintering since the densities, although low, are uniform.

TABLE 23.4 Additives for Injection Molding of SiC

Function	Example	Quantity (wt%)	Volatilization temperature
Thermoplastic resin	Ethyl cellulose	9–17	200–400°C
	Polyethylene		
	Polyethylene glycol		
Wax or high-temperature volatilizing oil	Paraffin	2–3.5	150–190°C
	Mineral oils		
	Vegetable oils		
Low-temperature volatilizing hydrocarbon or oil	Animal oils	4.5–8.5	50–150°C
	Vegetable oils		
	Mineral oils		
Lubricant or mold release	Fatty acids	1–3	
	Fatty alcohols		
	Fatty esters		
Thermosetting resin	Epoxy		Gives carbon 450–1000°C
	Polyphenylene		
	Phenol formaldehyde		

Injection molding is used to fabricate ceramic components with complex shapes; because cycle times can be rapid, injection molding can be a high-volume process. The major limitation is that the initial tooling costs of the mold can be quite high. The mold to fabricate an individual turbine blade can be >\$10,000 and a mold for a turbine rotor may be >\$100,000, but such molds are reusable since they are never subjected to high temperatures.

23.11 RAPID PROTOTYPING

Rapid prototyping (RP) or solid freeform fabrication (SFF) is a relatively recent approach to forming ceramic components. There are various forms of RP techniques, but they are based on a common principle: a computer directly controls the shaping process by accessing computer-aided design (CAD) files. We can thus use RP to form a 3D component without the use of a die or a mold. RP techniques are used commercially for fabrication of parts from polymers for design verification and form-and-fit applications; these techniques have more recently been applied to forming parts out of ceramics.

In this section we will look at just two of the several RP methods

Stereolithography (SLA)

Fused deposition modeling (FDM)

Both these methods have been successfully used to form ceramic components. The SLA process is illustrated in Figure 23.13. In SLA the component is formed from an epoxy resin. As the z-stage elevator is lowered, an ultraviolet (UV) laser beam whose position is controlled by a computer cures successive layers of the uncured resin. In this way a 3D component is made one layer at a time. It can take many hours to build a large complex object. But this is still rapid compared to the time taken to form a component by, e.g., injection molding, where fabrication of the tools can take a considerable amount of time. To form ceramic components by SLA the polymer must be

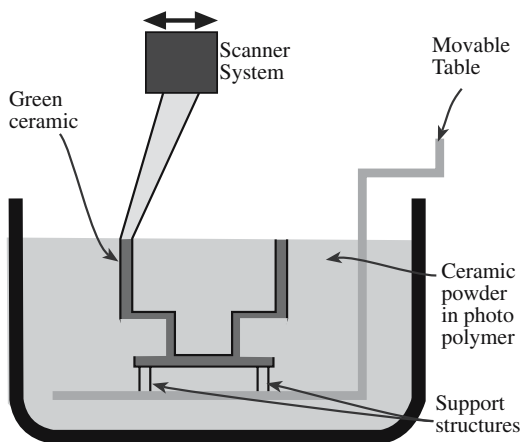


FIGURE 23.13 Schematic representation of the SLA SFF process.

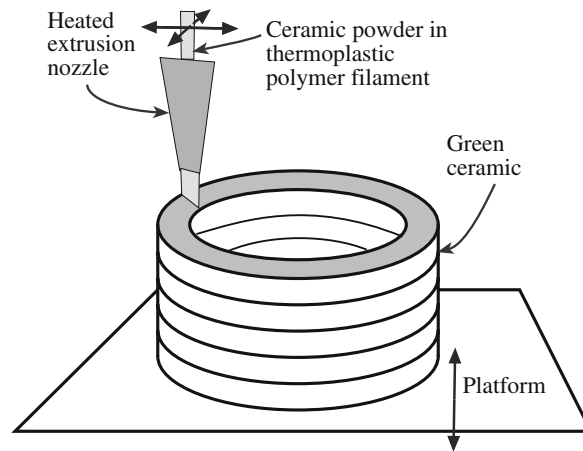


FIGURE 23.14 Schematic representation of the fused deposition (FD) SFF process.

loaded with ceramic powders. Si_3N_4 , SiO_2 , and Al_2O_3 powders have all been used for SLA.

In FDM the source material is a thermoplastic polymer filament that is heated and extruded to form the product as shown in Figure 23.14. The product is formed in a layer-by-layer manner similar to building up layers of icing on a cake. The computer controls the x - y position of the filament and the deposition rate. The filament can be loaded with up to 60 vol% ceramic powders; once the part is completed the binder is removed and the part is sintered. Most of the work in the RP of ceramic parts by FDM has involved Si_3N_4 . The feasibility of making components out of Al_2O_3 , SiO_2 , and PZT has also been demonstrated. The abbreviation FDC (fused deposition of ceramics) is used to identify this special application of FDM.

23.12 GREEN MACHINING

To obtain the desired shape of a ceramic product it is often necessary to machine it. Machining can be performed either before or after the product has been sintered. If the machining is done before sintering, while the component is still in the green state, the process is called green machining. The advantages of green machining compared to machining the sintered product are that there is a considerable reduction (10 \times) in machining time and a 20 \times reduction in cost because of less tool wear and the possibility of using cheaper tools. Table 23.5 compares the use

TABLE 23.5 Comparison of Cutting Speed versus Tool Life

Tool material	Cutting speed (m/min)	Work-piece material removed (cm^3)	Relative cost factor
Cubic BN	30	8.2	\times
Ti-coated carbide	30	13.1	\times
Co-coated WC	30	19.7	\times
Diamond	90	8500	10 \times

of different tool materials in the green machining of an Si compact before nitriding it to form Si_3N_4 .

In the processing of spark plug insulators the final processing step prior to firing involves green machining as shown earlier in Figure 23.5.

23.13 BINDER BURNOUT

In pottery, the binder burnout is the removal of water from the shaped clay. The rest of the firing process causes structure changes and transformations in the silicate itself. Forming methods for engineering ceramics, like injection molding, produce green bodies that can contain 30–50 vol% of organic binder. We generally want to remove this binder without cracking or distorting the ceramic compact. Binder burnout is one of the most likely stages to form defects in the processing of a ceramic: macroscopic defects, such as cracks and blisters, can be introduced at this stage, and these will affect the mechanical strength and other properties. An additional complication is that the binder system used in fabricating many commercial ceramic parts often consists of several components. These components have different boiling points and decomposition temperatures.

The components with low boiling points (e.g., waxes) may be removed by evaporation at fairly low temperatures.

Oxidation or decomposition at higher temperatures removes high-molecular-weight components.

For oxide ceramics, the binder can be oxidized to form H_2O , CO , and CO_2 when the green compact is heated in air. Binder burnout in air generally presents no problem. However, there are some situations in which binder burnout in air can be a problem. An example is the use of poly(vinyl butyral) with Al_2O_3 where carbon residues can be as high as thousands of parts per minute even after burnout in air at 700°C for 24 hours. Nonoxide ceramics generally cannot be heated in oxidizing environments and binder burnout in inert or reducing atmospheres is more difficult. Pyrolysis of many binders in these environments is not well understood and most binders leave some carbonaceous residue that could be detrimental to the subsequent sintering stage.

The process of binder removal is kept slow to reduce the possibility of macrodefects being produced. Figure 23.15 shows a plot of a binder removal cycle. In this plot a pressurized gas, called a *sweep gas*, has been passed over the part to help sweep away the vapor. The cycle time also depends on the size of the part. Thin sections take much shorter times than thick sections. The *debinding* time is proportional to the square of the section thickness of the compact—the familiar parabolic kinetics seen in our discussion of reactions in Chapter 25.

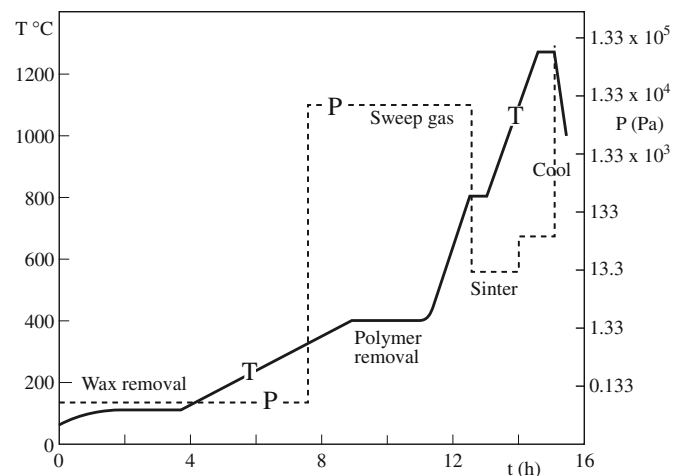


FIGURE 23.15 Pressure-induced binder removal cycle.

Binder burnout continues to be an active area of ceramics research with one of the main thrusts being in developing models of binder decomposition and diffusion.

23.14 FINAL MACHINING

Ideally the shaping and forming processes that are employed would produce the ceramic component in the desired shape with the specified dimensional tolerances and with an acceptable surface finish. However, in many cases this is not the situation and some final machining (after firing/sintering) of the ceramic is necessary. Generally final machining is required to

- Meet dimensional tolerances
- Improve the surface finish
- Remove surface flaws

Machining fired ceramics can be expensive and can represent a significant fraction of the total fabrication costs. Ceramic materials are difficult to machine because they are hard and brittle. The tooling costs are high because diamond tools are likely to be required or if conventional tools are used the tool life is very short. Also the time required to machine ceramics is long because if high tensile loads are applied to the ceramic part it might fracture.

Mechanical approaches to machining ceramics include the following:

- *Grinding* uses tools in which abrasive particles are embedded in a softer matrix such as glass, rubber, or polymer resin, or even a metal (as for WC in Co).
- *Lapping* uses loose abrasive particles placed on a soft cloth.
- *Sandblasting* uses abrasive particles accelerated by compressed air and directed through a nozzle at high velocity.

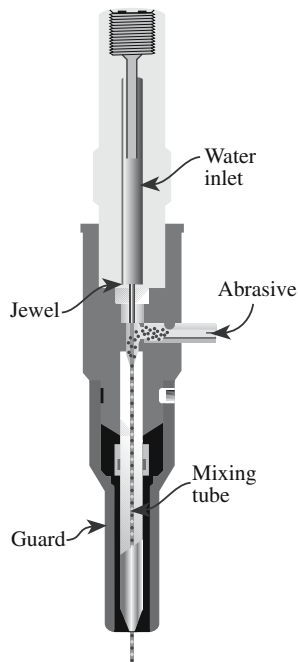


FIGURE 23.16 Schematic of the abrasive waterjet cutting process.

- *Water-jet machining* uses a high-pressure (~400 MPa pumping pressure) water jet to transport the abrasive particles to the ceramic surface.

The water-jet method is gaining popularity as a high-speed method for machining hard ceramics. Figure 23.16 shows the basic components of an abrasive water-jet cutter. Cutting rates depend on the material being cut and can vary from 130 mm/min for glass to 5 mm/min for a dense hard ceramic such as TiB₂. In a water-jet, the water is pressurized to ~380 MPa and is forced through a sapphire orifice at a velocity of up to about 750 m/s; in the abrasive jet, the speeds may be a little lower, but garnet powder is pulled into the water stream and acts as the abrasive to cut through, e.g., 25 mm of Ti or steel. It can also cut through ceramics and glass. Of course, dentists use the same technique when working on our teeth. The Grand Canyon was formed on a larger scale by essentially the same process. Masons use sandblasting to clean the surfaces of old stone buildings.

23.15 MAKING POROUS CERAMICS

In many traditional applications for ceramics, particularly in structural and electrical applications, the sintered ceramic component is required to have minimum porosity. However, in a growing number of applications, for example, in ceramic humidity and gas sensors, porosity is not just desirable, it is required. Several different methods can be used to produce porous structures.

- Use large particles with a very small size distribution to avoid dense packing.
- Underfire a green compact to leave a large amount of fine pores.
- Add organic particles (diameter >20 μm) to the powder mixture; when these burn out they will leave behind porosity. We use a controlled version of this technique elsewhere to produce mesoporous photonic materials.
- Use a binder system that contains a foaming agent and produces a large amount of gas bubbles in the mixture.
- Impregnate a foam that has a continuous porosity and then burn it out.
- Use a glass composition that phase separates and then leaches out (e.g., using an acid) one of the phases to produce porous glasses.

Mesoporous materials, which have quite a uniform distribution and a very high density of pores, were discussed in Chapter 15.

23.16 SHAPING POTTERY

We stated at the beginning that this chapter is the pottery chapter. We will now summarize areas in which many of the techniques described above have been used, in some cases for millennia, in pottery; then we can do the same for glass. Classical porcelain can be as thin as a sheet of paper (<0.2 mm). Bone china, so called because even today it is made by adding ~50% bone ash to a conventional hard-porcelain clay mixture, can be so thin that it is translucent. This ingredient is so critical that the UK imports bone ash from Argentina.

Paper clay is a relatively new material for the potter being a mixture of clay and paper in approximately equal amounts by volume. The paper (cellulose fiber) gives added strength to the green body so it can even be made into a sheet that can then be cut and shaped before firing. The firing burns out the organics and leaves a ceramic body that is lighter than usual. Figure 23.17 shows a sheet of paper clay being lifted off the plaster “substrate” (see also Section 25.7). As you might guess, there are many variations on this process, which of course are related to the ancient use of straw in making house bricks.

Throwing a pot, as shown in Figure 23.18, is the process of producing hollow clay objects on a revolving pottery wheel. Potters may use their hands as shown here, or other tools—the step to industry is then a small one.

Coiling, pinching, and slabbing are used to form large pottery objects. Their common feature is that the total thickness of the ceramic piece is kept constant so that the drying and firing process will be even. Wedging is not a shaping process, although the end result is a slab of clay. Rather, it is the process used to remove porosity from clay before it is used to make a pot. This is now carried out mechanically in a pug mill. If you pinch the clay or carve



FIGURE 23.17 Removing paper clay from the substrate.



FIGURE 23.18 Throwing a pot.

it, you can combine different colored clays and shape and fire them to produce the neriage (marbled) style of the potters version of millefiore.

23.17 SHAPING GLASS

Glass can be shaped by many different processes.

Casting or molding has produced, for example, the 20-inch-thick Palomar telescope mirror and the submilli-

meter-thick molded-glass aspheric lenses that are used in everything from laser printers to optical disc storage devices and optical communications systems.

Pressing needs a mold that will be gray cast iron (to 1000°C), stainless steel (can be used for borosilicates at 1185°C and glass ceramics at 1480°C), or even bronze. Usually, though, the mold is cooled. The process uses a viscosity of ~4 kP and has been applied to objects weighing from 5 g to 15 kg. The finished object can be fire-polished. This process, shown in Figure 23.19, is quite

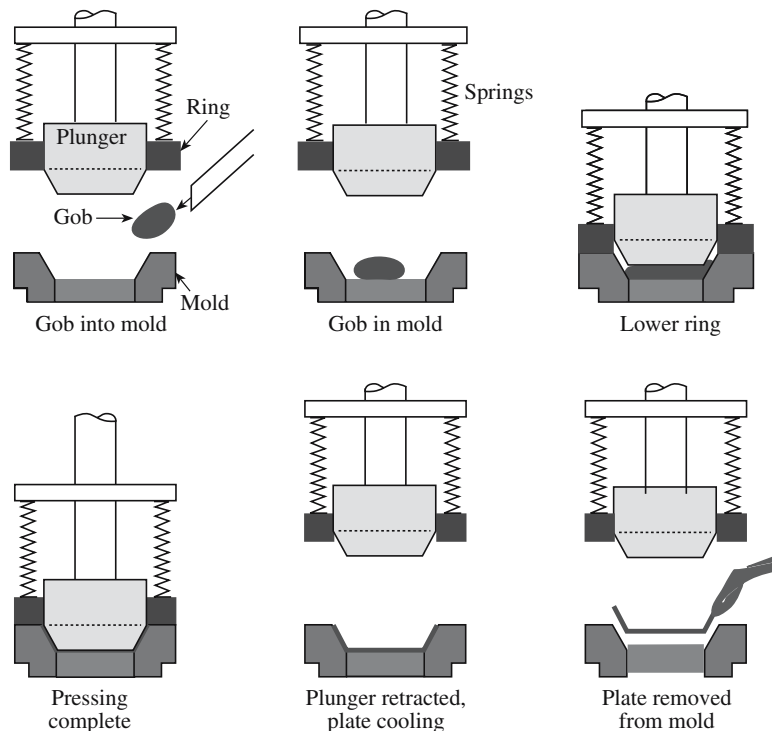


FIGURE 23.19 Automated pressing glass.

similar to the HIPing technique shown in Figure 23.2 and predates it, of course.

Sagging or slumping is a simple method whereby the glass is heated so that it “slumps” into the mold. The technique can also be used for clay; effectively it is pressing, with gravity providing half the press.

Glass blowing was clearly in use in the first century BCE. The temperature is critical since it determines the working range. There will be other factors such as the air pressure, the role of gravity, and the centrifugal force produced by the blower. The craftsman will produce free-blown objects or can blow the glass inside a mold. When a ribbon or hub machine is used, the glass is invariably blown into a mold.

Drawing is used for glass tubes and sheets. For tubes the variations include Danner (e.g., tubes for fluorescent lights), Vello (large diameter tubes), downdrawn tubes (used for vacuum tubes or uses a vacuum), and updrawn tubes (for glass thermometers). Sheets are drawn in the same way: using a slot orifice, with an overflow pipe, using updraw or floating.

Spinning is used for fibers and is very reminiscent of the beginnings of industry (the spinning jenny).

Rolling is an old technique that is still in use. It is similar to slabbing in pottery.

The lost wax process of forming glass shapes has been used since the fifth century CE. Originally, the molten glass was poured into an outer mold made of beeswax, which could easily be removed.

Inlays in glass, such as sandwiched-gold glass, was made perhaps as early as ~250 BCE. Gold leaf is pressed between two layers of glass.

Final machining using Vycor (the “cor” is from Corning), Macor, or similar specially treated glasses. (Vycor contains “built-in” pores; Macor contains small grains of mica.)

Core forming was one of the earliest methods used to shape glass (see Figure 21.3). A shape was fashioned in clay and the glass was then trailed around the core until it completely covered it. It could be heated further so that the coils fused together. When cool, the clay core would be removed leaving a stand-alone glass vessel.

CHAPTER SUMMARY

In this chapter we described the methods used to shape and form ceramic components. There are a number of possible choices and the best one depends on the types of shapes being produced, the cost of the component, and the number of units being made. For predominantly covalently bonded ceramics it is necessary to use shaping techniques that involve the application of pressure and heat if the objective is to obtain a high-purity material. Because ceramics cannot be softened in the same way as polymers and metals it is often necessary to form a plastic mixture of the ceramic prior to shaping. These methods may leave a large amount of organic residue that must be removed during sintering. Binder removal is tricky because it can lead to the formation of voids and cracks in the ceramic component. Machining of ceramics is often performed when they are in the green state—before sintering. This is because the presintered component is much softer and tooling costs are significantly reduced. A relatively recent approach to forming ceramic components is rapid prototyping. The advantage of this technique is that 3D parts can be made without using a die or a mold. The technique has been well established for producing parts made of polymeric materials and is now being extensively investigated for forming ceramic components.

PEOPLE IN HISOTRY

Brown, Robert, the Scottish botanist (1773–1858), among other activities studied the movement of particles (pollen and inorganic) in water and thus recognized Brownian motion.

Champion, Albert founded two companies—Champion and AC Spark Plug. In the 1990s, between them they produced over one-half of the world’s spark plugs. McDougal (1949) gives a review of these two companies.

Hamada, Shoji (1892–1978) was born in Tokyo. His home and his pottery are in Mashiko, which is a ceramics town just a short drive north of Tsukuba.

Kawai, Kanjiro (1890–1966) lived in Kyoto in a house that is now another wonderful museum.

Leach, Bernard Howell (1887–1979) is probably the best-known British potter. He was born in Hong Kong and worked in Japan (with Shoji Hamada) and at St. Ives in England.

Spode, Josiah (1733–1797) founded his pottery in 1770 at Stoke. He developed the formula for bone china that is still used.

Tomimoto, Kenkichi (1795–1835) was born and raised in Japan and helped make style part of everyday Japanese pottery.

Wedgwood, Josiah (1730–1792) was born in Burslem, Staffordshire. He joined the firm of Thomas Wheildon at Fenton, who gave him the freedom to experiment, and founded a factory in Etruria with his business

partner Thomas Bentley. He was elected a Fellow of the Royal Society for inventing the pyrometer: he used the fact that porcelain shrinks in the furnace to measure the temperature of the furnace. His daughter, Susannah, had a son, Charles Darwin.

Yanagi, Soetsu (1889–1961) created the mingei (folk art) movement in Japan in the 1920s; this movement has influenced much of Japan's stunning pottery.

GENERAL REFERENCES

For information on modeling binder removal see the papers by Barone and Ulicny (1990), Stangle and Aksay (1990), Evans *et al.* (1991), and Matar *et al.* (1993).

Birks, T. (1998), *The Complete Potter's Companion*, Bulfinch Press, Boston. Photos of techniques are especially clear and instructive.

Engineered Materials Handbook, Volume 4, *Ceramics and Glasses*, ASM International. Section 3 covers, in considerable detail, many aspects of shaping and forming as practiced in industry.

Leach, B. (1944) *A Potter's Book*, Faber & Faber Ltd., London.

Onoda, G.Y. and Hench, L.L. (1978) *Ceramic Processing Before Firing*, Wiley-Interscience, New York.

Peterson, S. (2003) *The Craft and Art of Clay*, 4th edition, The Overlook Press, Woodstock, NY. Much more than shaping; glazes, kilns, design, history.

Rahaman, M.N. (1995) *Ceramic Processing and Sintering*, Marcel Dekker, New York. Less well known than Reed but very useful.

Reed, J.S. (1988) *Introduction to the Principles of Ceramic Processing*, John Wiley, New York. A classic text on processing.

Richerson, D.W. (2006) *Modern Ceramic Engineering*, 3rd. edition, CRC Press, Boca Raton, FL. Chapter 13 describes the important shape-forming processes.

Solid Freeform Fabrication Symposium Proceedings (held annually, University of Texas, Austin). The formation of ceramic components by RP or SFF is a developing field. These proceedings give current information.

SPECIFIC REFERENCES

Barone, M.R. and Ulicny, J.C. (1990) "Liquid-phase transport during removal of organic vehicle in injection moulded ceramics," *J. Am. Ceram. Soc.* **73**, 3323.

Evans, J.R.G., Edirisinghe, M.J., Wright, J.K., and Crank, J. (1991) "On the removal of organic vehicle from moulded ceramic bodies," *Proc. R. Soc. (London)* **A432**, 321.

German, R.M. (1987) "Theory of thermal debinding," *Int. J. Powder Met.* **23**, 237. Classic article on this topic.

Gault, R. (2005) *Paper Clay (Ceramics Handbook)*, 2nd edition, A&C Black, London.

Mater, S.A., Edirisinghe, M.J., Evans, J.R.G., and Twizell, E.H. (1993) "The effect of porosity development on the removal of organic vehicle from ceramic or metal mouldings," *J. Mater. Res.* **8**, 617.

McDougal, T.G. (1949) "History of AC spark plug division, General Motors Corporation," *Am. Ceram. Soc. Bull.* **28**, 445.

Stangle, G.C. and Aksay, I.A. (1990) "Simultaneous momentum, heat and mass transfer with chemical reaction in a disordered porous medium: Application to binder removal from a ceramic green body," *Chem. Eng. Sci.* **45**, 1719.

WWW

www.stratasys.com/NA/index.html
A commercial supplier of FDM equipment and software.

www.optima-prec.com
For molded glass lenses

www.raku-yaki.or.jp
The Raku Museum

www.ceramicsmuseum.alfred.edu
The site for Alfred's museum.

www.omax.com
For information on abrasive waterjets.

www.pottery-making.org
Pottery Making Illustrated.

EXERCISES

- 23.1 Explain briefly why melting and solidification can be used for shaping glasses (as well as many metals and polymers) but in general not for forming crystalline ceramics.
- 23.2 Briefly describe the differences between hot pressing and cold pressing.

- 23.3 Explain why hot pressing is often used when ceramics with a small grain size are required. For what applications must grain growth be minimized?
- 23.4 Why are graphite dies widely used for hot pressing? Under what conditions would the use of graphite not be appropriate?
- 23.5 Which method would you choose to form each of the following shapes; briefly justify your choice. (a) A cylinder; (b) a tube; (c) a cube; (d) a teapot; (e) a rotor blade; (f) a spark plug insulator; (g) an insulator for a power cable.
- 23.6 Why is it necessary to use an organic binder when forming a ceramic component by extrusion? What are the main requirements for the binder?
- 23.7 Why is it difficult to use injection molding for near net shape manufacturing?
- 23.8 Briefly explain why it is better to machine in a ceramic component when it is in its green state rather than when it has been fired.
- 23.9 Keramica is a new company that wants to manufacture alumina furnace tubes and they hire you as a consultant. You are asked to propose a process for the fabrication of such tubes. Give a general description of the process you would propose. Explain the roles of the different steps involved.
- 23.10 Porcelain figurines are manufactured worldwide in large quantities. In most cases, many figures are made with an identical shape. As you know, such figures are often hollow. Explain the process used to form such figures economically.

Sintering and Grain Growth

CHAPTER PREVIEW

Sintering is the process of transforming a powder into a solid body using heat. Why is there a whole chapter on sintering? Partly for historical reasons—it has traditionally been the principal method of processing ceramic bodies. Sintering is still the most important process in making bulk ceramics, but the process is not unique to ceramics. There is a large field known as “powder metallurgy” that considers many of the concepts and problems that we address for ceramics. One of the reasons for processing metals by sintering is to control the grain size, which is precisely what we usually need to do in ceramics.

We can discuss the topic at different levels of complexity. The phenomenon is quite straightforward and involves deciding how best to pack particles (that are usually modeled as spheres), understanding the movement of grain boundaries (GBs), and knowing how the packing geometry and GB migration is affected by the need to balance surface tensions (interface energies). The quantitative analysis of the process is much more difficult since it involves transport of several different species with different chemical driving forces. In multiphase systems, quantitative analysis is not yet possible.

The other point to emphasize is that for many years the aim of sintering has been to make dense ceramics. The terms sintering and densification were almost used interchangeably. Today, there are many uses for porous ceramics and these materials must also be sintered. The aim is then different and the process must change accordingly. Most of the time we assume that the material we are sintering is single phase, so we make some assumptions that will not necessarily be valid for multiphase materials that also need to be sintered.

24.1 THE SINTERING PROCESS

The idea of sintering is to join particles together without melting them. We may, however, use an additive that does melt. The particles can be crystalline or amorphous—we can sinter glass marbles as long as we do not melt them: of course, the particles need not be spheres. At too high a temperature, the marbles also deform.

The problems involved in sintering can be appreciated by examining Figure 24.1. We often model sintering by packing spheres of various sizes together. If we use spheres of only one radius, then the maximum initial density would be 74%. Note, that the schematic in Figure 24.1 is only an idealized two-dimensional picture of the packing of circles! Figure 24.1b shows a disordered structure of the same size “spheres” so there is even more open space. If we fill this space with smaller spheres we can achieve a much higher “density,” as you see in the adjacent region. Also keep in mind that the object is to produce a product like that shown in Figure 24.2, which is a sintered SiC radiant-heat U tube. The actual structure of the sintered body will look something like that shown in Figure 24.3. The SiC particles involved in forming the tube in Figure

24.2 will tend to be strongly faceted parallel to the close-packed planes, {111} if cubic or (0001) if hexagonal.

Consider the logic of the sintering process:

- When crystalline powder particles join together, the junction is a GB.
- It is likely that the solid body thus formed will not be 100% dense, so it will contain pores.
- Pores are a structural component of the solid body (see Chapter 15). They often behave like grains of a different material.
- Although sintering explicitly involves solid powder grains, a liquid may form if a component that has a low melting temperature is present. This is then known as liquid-phase sintering (LPS) (Section 24.7). We must thus consider films, tubes, and droplets (or particles) of noncrystalline material. There may be no trace of the liquid when the sample is examined at room temperature after sintering; such a liquid is referred to as a transient phase.
- After and during sintering, some grains will grow, consuming others. This process is known as grain growth and is essentially an Ostwald ripening process.

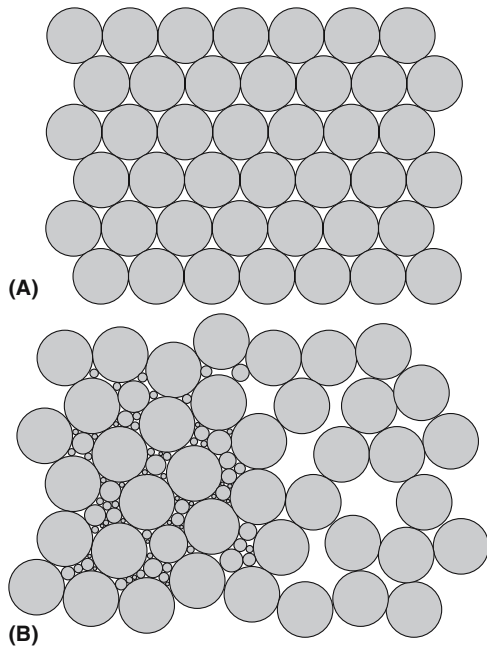


FIGURE 24.1 Model grain/shape distributions in 2D; packing identical spheres can never achieve less than 26% porosity: (a) ideal planar packing, (b) less-dense packing of larger spheres, part with inserted smaller spheres giving a higher local density.

Note: this topic is often referred to as solid-state sintering. We have to be careful about making assumptions. It is often implicitly assumed in our analysis that all grains have the same composition. This chapter will include a real example of the packing of spheres, namely the formation of opal. (We also include the inverse opal.)

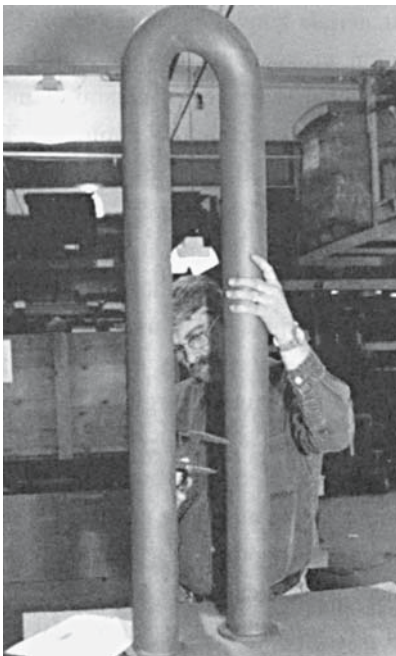


FIGURE 24.2 A radiant U tube produced by sintering SiC.

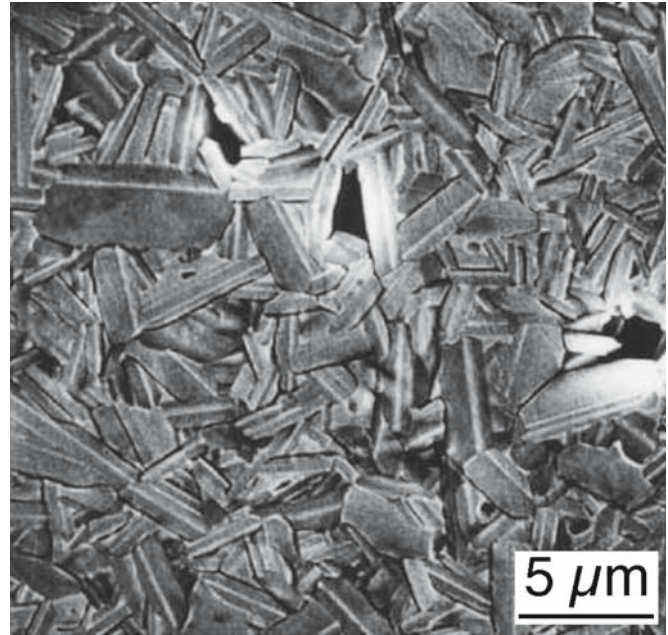


FIGURE 24.3 SiC processed with addition of Al_2O_3 at 2050°C ; etched polished surface.

- How do we maintain a porous structure? (Why do we want some materials to be porous?)
- How do we achieve full density?
- How do we maintain the shape of the green body?
- What changes in the analysis/process if the grains do not all have the same composition?

We are often preoccupied with grain boundaries, but triple junctions may be even more important in the sintering process since these may be open pipes for transporting material. Part of the reason for this bias is that triple junctions are very difficult to study and to model (see Section 14.9).

The topic of capillary forces was introduced in Section 13.6. This topic is extremely important in sintering when there is a liquid phase present. The overall “plan” of our discussion is shown in Figure 24.4.

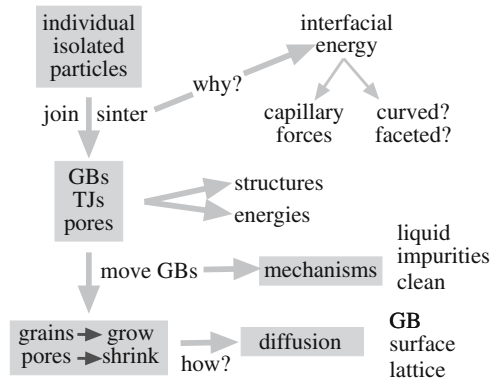


FIGURE 24.4 Thinking about sintering: some of the concepts and processes.

24.2 THE TERMINOLOGY OF SINTERING

Since sintering is an ancient process, it has its own language, much of which preceded the scientific analysis.

Green bodies. All types of unfired ceramic are included. Volatiles. During processing we may remove volatile materials; even though we think of sintering as a solid-state phenomenon, the gas phase is important. The gaseous component may form as water or other solvents are removed or as organics undergo burnout.

Hot pressing is the addition of pressure (uniaxial or hydrostatic) while sintering. This is a large topic, so we address it again in a separate section.

Desintering is the reverse of sintering and may be associated with the reverse of densification.

A monolithic ceramic is a uniform ceramic piece.

The importance of the shape of the particles before and during sintering is an extra complication. Corners and sharp junctions are difficult to treat in any continuum model of sintering.

24.3 CAPILLARY FORCES AND SURFACE FORCES

A curved surface will always want to become flat as we discussed in Chapter 13. The result is that there is a pressure difference, ΔP , between the inside and the outside of a curved surface.

$$\Delta P = 2\gamma/r \quad (24.1)$$

Here γ is the surface free energy and r is the radius of the sphere. The radius of curvature r is positive or negative depending on whether the center of radius is inside or outside the material, respectively. Consequently, negative pressure is exerted on the concave surface.

We should remember that the principle that leads to Eq. 24.1 assumes that there is only one value of the surface energy; the surface energy is assumed to be isotropic. When the particle size of the powder is small, the powder has a large surface area in comparison with a similar volume of bulk solid. We can say that a small particle, which is assumed to be a sphere, has surface properties that are different from those of a bulk solid because it has a large surface-to-volume ratio and because its surface has a small radius of curvature.

In sintering, we see the effect of this curvature first when grains (viewed as spheres) join together. This is the curvature of the initial particle surfaces. Then the GBs will move: this is the same effect but for internal surfaces and leads to grain growth during sintering.

24.4 SINTERING SPHERES AND WIRES

Models in Sintering

We first summarize the steps that must occur during sintering and then consider simplified models that allow us to examine aspects of these different processes. We need to examine the following processes:

- How do two grains join together?
- How do we remove pores once they are formed? This is the essential step in densification.
- Why do we want to densify the material?
- Why do some grains absorb others and how does this occur?

After the ceramic has been shaped as a green body, it must be fired, often at very high temperatures, to develop useful properties. The sintering process has several distinct stages.

- We consolidate the product during firing.
- We remove the pores between the starting particles.
- The components shrink.
- Some grains grow while others shrink.

The simplest model is that of two spheres in two dimensions shown in Figure 24.5. Notice that the two

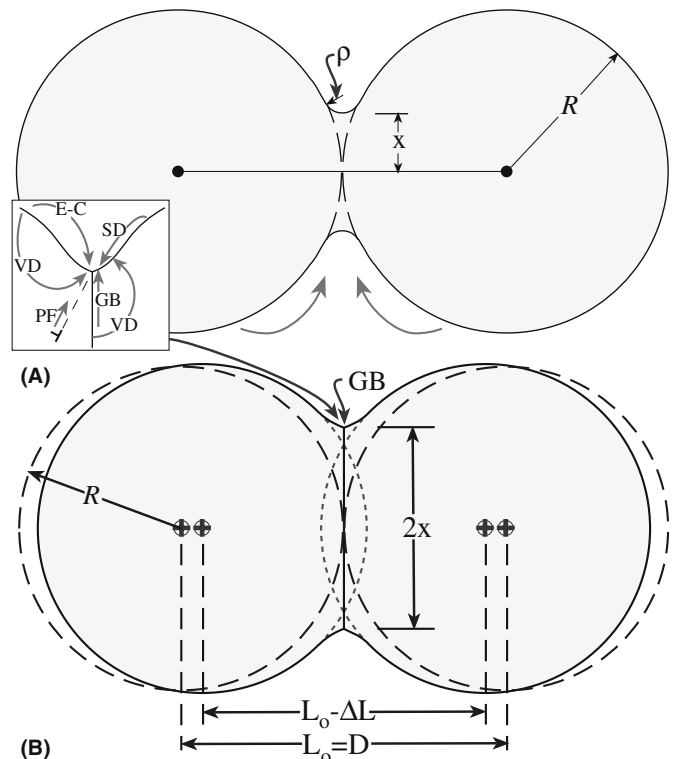


FIGURE 24.5 (a, b) Sintering and curvature. The two-sphere model showing the transport paths, the two curvatures (ρ and x), and the process leading to densification.

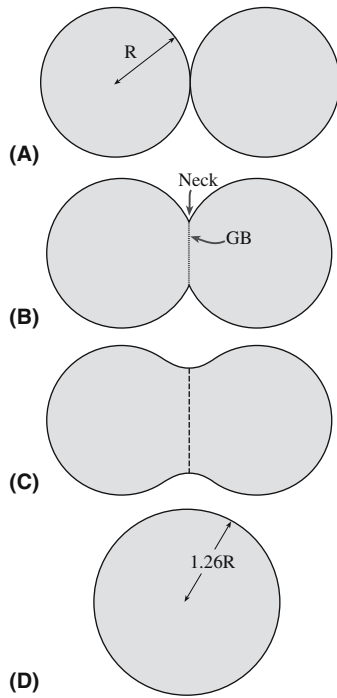


FIGURE 24.6 Coalescence of two spheres (a–d).

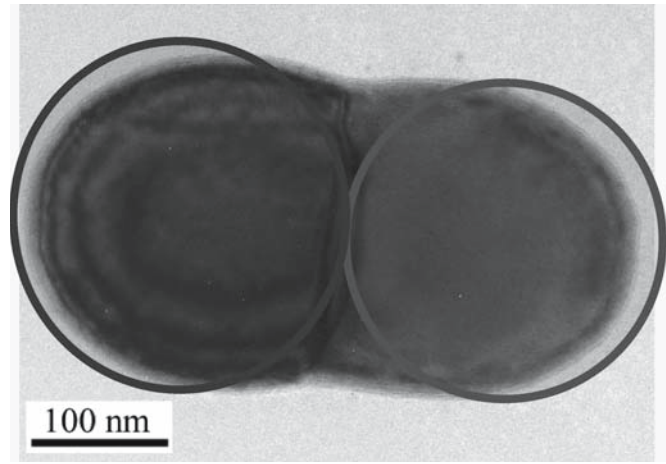


FIGURE 24.7 Two Si spheres partly sintered (TEM image).

spheres can no longer be spherical if we have started to form the neck as shown in Figure 24.5a. Notice also that in Figure 24.5b the centers of the two spheres must have moved toward one another. We know the situation at the start and at the end; the question is, what happens in the middle? We can even do the experiment of joining two such spheres as shown schemetically in Figure 24.6. Figure 24.7 shows experimental results for the nearly nanoscale case. This schematic of the two spheres emphasizes some important points and omits others.

- There are two radii to consider (x and ρ).
- There will be a GB between the two spheres if they are single crystals; if they are glass spheres, then there is no GB; if the spheres are polycrystalline there will be many GBs.
- There is always a GB groove where the GB meets a free surface.

Changes that occur during the firing process are related to (1) changes in grain size and shape and (2) changes in pore size and shape. Before firing, a powder compact is composed of individual grains and may contain as much as 60 vol% porosity. The amount of porosity will depend on the size and size distribution of the powder particles and the shaping method (see Chapter 23). To maximize properties such as compressive strength, translucency, and thermal conductivity, we want to eliminate as much of this porosity as possible (i.e., we want a dense ceramic). This objective can be achieved during firing by the transfer of material from one part of the structure to another. There are several mechanisms for material transfer and some of the processes are listed in Table 24.1. Note that sink and source refer to matter, not defects.

As sintering progresses, the two spheres move together. This movement is the essential step in densification.

We can extend this analysis to three or more spheres as shown in Figure 24.8 and then to three dimensions. With three spheres we introduce another degree of freedom: the outer spheres can also move together until they form a pore. A model experiment that avoids this movement uses a wire that is wound on a reel and sintered; the experiment can, in principle, be adapted for ceramics, but it may be using straight fibers.

TABLE 24.1 Mechanisms and Transport in Sintering (Diffusion to the Neck)

Mechanism	Transport path	Source
SD	Surface diffusion	Surface
VD	Volume diffusion	Surface
E-C	Evaporation–condensation	Surface
GB	GB diffusion	GB
VD	Volume diffusion	GB
PF	Plastic flow	Dislocations

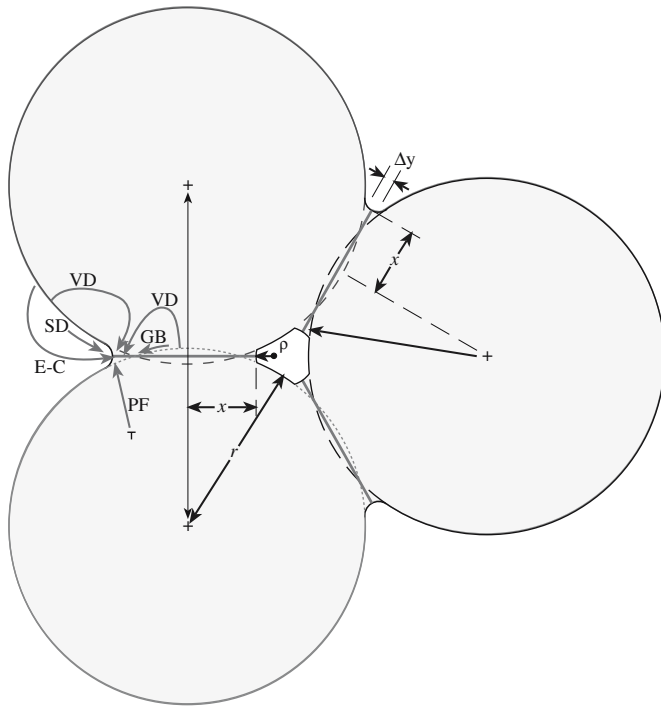


FIGURE 24.8 Sintering three spheres; showing the diffusion paths from the GB to the neck surface and the development of a pore (2D projection).

24.5 GRAIN GROWTH

For a grain structure to be in metastable equilibrium the surface tensions must balance at every junction between the GBs. It is theoretically possible to construct a three-dimensional polycrystal in which the boundary tension forces balance at all faces and junctions, but in a real random polycrystalline aggregate there are always going to be boundaries with a net curvature in one direction and thus curved triple junctions. Consequently, a random grain structure is inherently unstable and, on heating at high temperatures, the unbalanced forces will cause the boundaries to migrate toward their center of curvature.

The effect of grain-boundary curvatures in **two dimensions** is shown in Figure 24.9. It has been assumed that equilibrium at each two-dimensional (2D) GB junction results in angles of 120° . Therefore, if a grain has six boundaries they can be planar (i.e., flat) and the structure metastable. However, if the total number of boundaries around a grain is less than six, each boundary must concave inward. These grains will therefore shrink and eventually disappear during sintering. Large grains, on the other hand, will have more than six boundaries and will grow. The free-energy change that gives rise to grain growth is the decrease in the surface area between the fine-grained material and the larger-grain-sized product and the corresponding lowering of the grain-boundary energy.

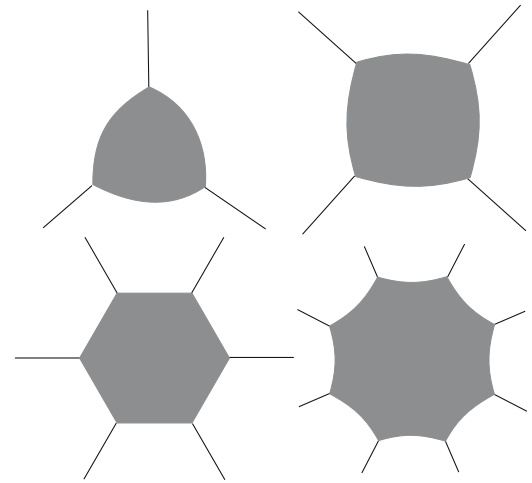


FIGURE 24.9 Angles and grains. In 2D the grains shrink if there are fewer than six sides and expand if there are more than six sides.

The effect of the pressure difference caused by a curved GB is to create a difference in free energy (ΔG) on two sides of the boundary; this is the driving force that makes the boundary move toward its center of curvature.

$$\Delta G = 2\gamma V/r \quad (24.2)$$

where V is the molar volume. We might expect that the rate at which the boundary moves is proportional to its curvature and to the rate at which the atoms can jump across the boundary.

24.6 SINTERING AND DIFFUSION

There is a significant difference between the paths for matter transport shown in Figure 24.8. Transfer of material into the “pore” must occur if the porosity of the compact is to shrink. You can imagine that in three dimensions (3D), this requires that matter transfer from the bulk of the grain, from the GB between particles, or from the outer surface by diffusion through the grain or through the GB. (Alternatively, you can think of vacancies moving out from the pores.)

For the case of matter transport from the grain boundary to the neck by lattice diffusion, we can derive an equation for the rate of growth of the neck area between particles.

$$\frac{x}{r} = \left(\frac{40\gamma a^3 D^*}{kT} \right)^{1/5} r^{-3/5} t^{1/5} \quad (24.3)$$

Here, the volume of the diffusing vacancy is a^3 and D^* is the self-diffusion coefficient. In view of the approximations in the model, it is not worth learning this equation, but notice the terms involved.

With diffusion, in addition to the increase in contact area between particles, particle centers move toward one another. We can derive an equation for the rate of this approach.

$$\frac{\Delta V}{V_0} = \frac{3\Delta L}{L_0} = 3 \left(\frac{20\gamma a^3 D^*}{\sqrt{2}kT} \right)^{2/5} r^{-6/5} t^{2/5} \quad (24.4)$$

The decrease in densification rate gives rise to an apparent end-point density if experiments are carried out for similar time periods as shown in Figure 24.10. The same comments hold for the details (beware) and the suggested trends (good). It is seen that the sintering rate steadily decreases with time, so that merely sintering for longer periods of time to obtain improved properties is impractical. Once again, control of particle size is very important.

Consider how the curved GB in Figure 24.11 moves; the classical picture for the change in energy as an atom changes its position is shown in Figure 24.12, but reality is clearly much more complex. This diagram is drawn to show the (100) surface of MgO. If the curved interface is actually normal to the plane of the figure, the GB is pure tilt in character. It is clear from Figure 24.12 that not all the ions move in the same direction. If you select different ions in Figure 24.11 you can appreciate that some move

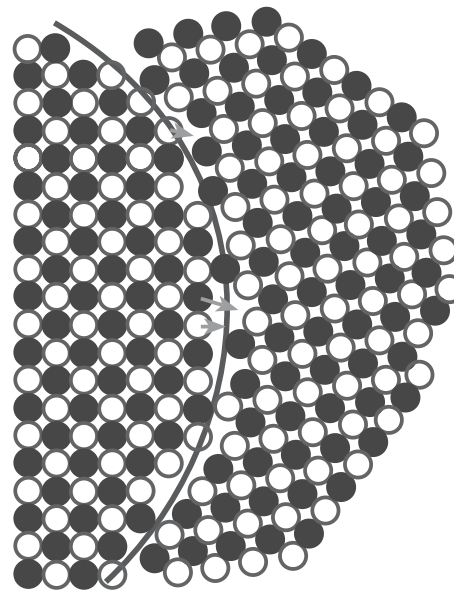


FIGURE 24.11 Atomistic model for GB migration.

to the right while others may move at 90° to this direction. (This should remind you of atom motion during the glide of dislocations.) Some ions cannot move until others have moved, as a result of Coulomb interactions. The frequency of atomic jumps in the forward direction is given by

$$f_{AB} = v \exp(-\Delta G^*/RT) \quad (24.5)$$

The frequency of reverse jumps is given by

$$f_{BA} = v \exp(-\Delta G^* + \Delta G/RT) \quad (24.6)$$

The frequency factor, v , has, for solids, a value of about 10^{13} Hz.

For the net growth process

$$U = \lambda(f_{BA} - f_{AB}) \quad (24.7)$$

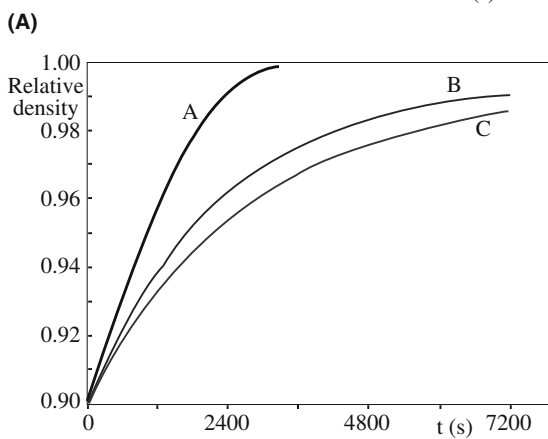
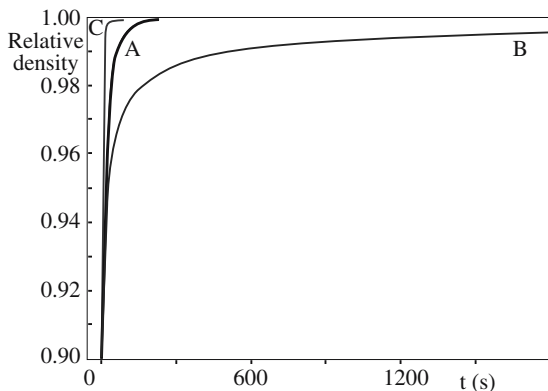


FIGURE 24.10 Calculated densification curves at final stage of sintering at 1727°C for alumina powder compacts for grain size of (a) 0.8 μm and (b) 4.0 μm at 90% density. The curves are calculated using different equations but show the same trends.

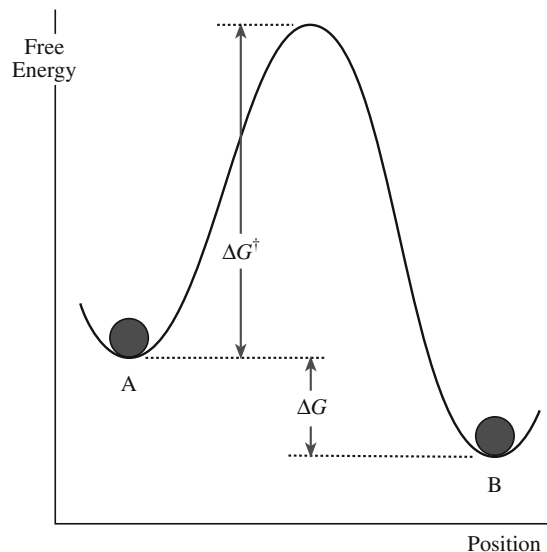


FIGURE 24.12 Activation barrier model for GB migration.

Here λ is the distance of each jump, and U is given by

$$U = v\lambda \left[\frac{\gamma V}{RT} \left(\frac{1}{r_1} + \frac{1}{r_2} \right) \right] \exp \frac{\Delta S^*}{R} \exp \left(-\frac{\Delta H^*}{RT} \right) \quad (24.8)$$

The important result is that the rate of growth increases exponentially with temperature.

When considering ceramic sintering processes, you should always remember that the oxidation state of the cations may vary depending on the environment. For example, when CeO_2 is sintered at high temperatures the Ce^{4+} may be partially reduced to Ce^{3+} , which can cause cracking in the compact. Such cracking will, of course, change the available diffusion paths.

24.7 LIQUID-PHASE SINTERING

Liquid-phase sintering is the sintering of a powder in the presence of a liquid; the liquid generally solidifies below the sintering temperature. The details depend on the interfacial energies: is the liquid wetting or not? Either way liquid may be present in triple junctions (TJs), quadruple junctions (QJs), and GBs because it simply cannot get to the external surface. If it can reach the outer surface then we have another capillary geometry as shown in Figure 24.13. As the sample cools after processing, the still-molten liquid can be drawn back into the grains because of differences in the thermal expansion coefficients. We then see liquid at the GBs in the image. We may also precipitate out crystalline material as the glass cools.

The densification of LPS materials takes place in three stages:

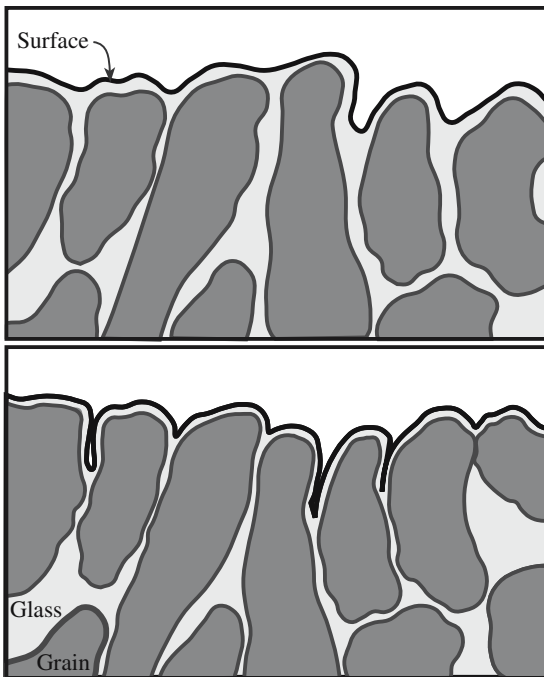


FIGURE 24.13 Liquid at surfaces.

TABLE 24.2 Applications of LPS

Material	Application
BaTiO ₃ /LiF/MgO	Capacitors
BaTiO ₃ /SiO ₂	Capacitors
Co/WC; TiC/Mo/Ni	Cutting tools
Fe/Al ₂ O ₃ /C	Friction materials
Al ₂ O ₃ /glass	Grinding materials
Si ₃ N ₄ /Y ₂ O ₃	Metal-working tools
Clay/feldspar/flint	Porcelain
Si ₃ N ₄ /MgO; SiC/B	Refractories
Al ₂ O ₃ /MgO/SiO ₂	Refractories
AlN/Y ₂ O ₃	Substrate
ZnO/Bi ₂ O ₃	Varistor

- The solid particles quickly rearrange when the liquid forms.
- Solute reprecipitation takes place if this is thermodynamically possible (if some solid can dissolve in the liquid).
- Microstructural coarsening occurs with slow solid-state sintering of the solid.

In the first stage, capillary forces play a major role as voids are removed from the body.

There are several points we should keep in mind.

- Glass may dissolve the matrix, which may reprecipitate elsewhere on the grains.
- Diffusion through the glass is almost always faster than through a structured GB.
- Crystal/glass interface energies *do* depend on the orientation of the interface.

Some of the difficulties include the following:

- The composition of the glass may not be uniform.
- When the layer is thin it may be more appropriate to call it an absorption layer.
- The viscosity of glass changes with T .
- The composition of the glass in equilibrium with crystal changes with T .
- The viscosity of glass changes with changes in composition.
- The expansion coefficient of glass will generally not be the same as the crystal grains.

Examples of processing using LPS are given in Table 24.2; it is a useful exercise to identify the liquid in each case.

24.8 HOT PRESSING

We noted in Section 24.1 that we are able to sinter glass spheres as long as we do not melt them. This process is a special sintering situation because we do not form GBs.

You can imagine that if we heat the spheres to a temperature below T_g we can decrease the viscosity significantly and then apply a pressure so that the spheres will plastically deform (change shape) so as to fill the empty space, especially if we did this in a vacuum. The deformation of the glass spheres occurs by viscous flow. (We will see this again when discussing paté de verre in Section 26.14.) Exactly the same process happens if the particles are crystalline, except that the deformation of the particles occurs by other mechanisms (movement of crystal-lattice defects); the precise deformation mechanism will depend on the temperature of the treatment and the applied pressure. In this case GBs are formed. Hot pressing allows us to produce material with very little porosity; since the temperature is not taken too high, grain growth is minimized.

Hot forging is the application of a uniaxial stress while the samples are held at temperature. Discontinuous hot forging has been used to extract the temperature dependence of the so-called constitutive sintering parameters for alumina. This analysis showed for alumina that creep and densification during sintering are kinetic processes that are both controlled by GB diffusion. Such studies of sintering are aimed at producing a set of constitutive para-

eters that will allow the sintering behavior of materials to be predicted even if the shape of the body is complex or if materials are being cosintered. These parameters include viscosity, a viscous Poisson's ratio, and the sintering stress. This stress is the driving force for sintering and results from the interfacial energies associated with pores and GBs. In this situation, the concept of viscosity is not taken to imply that the material is liquid, but rather that the strain rate is linearly related to the strain rate of the free sample and, through a uniaxial viscosity, E_p , to the stresses in the material.

24.9 PINNING GRAIN BOUNDARIES

When grains grow to be so large that they are nearly the same size as the specimen in one or more dimensions, grain growth stops or becomes very slow. Similarly, inclusions increase the energy necessary for the movement of a grain boundary and inhibit grain growth. If we consider a moving GB, the total interface energy is decreased when it reaches an inclusion as shown in Figure 24.14a–d: the energy decrease is proportional to the cross-sectional

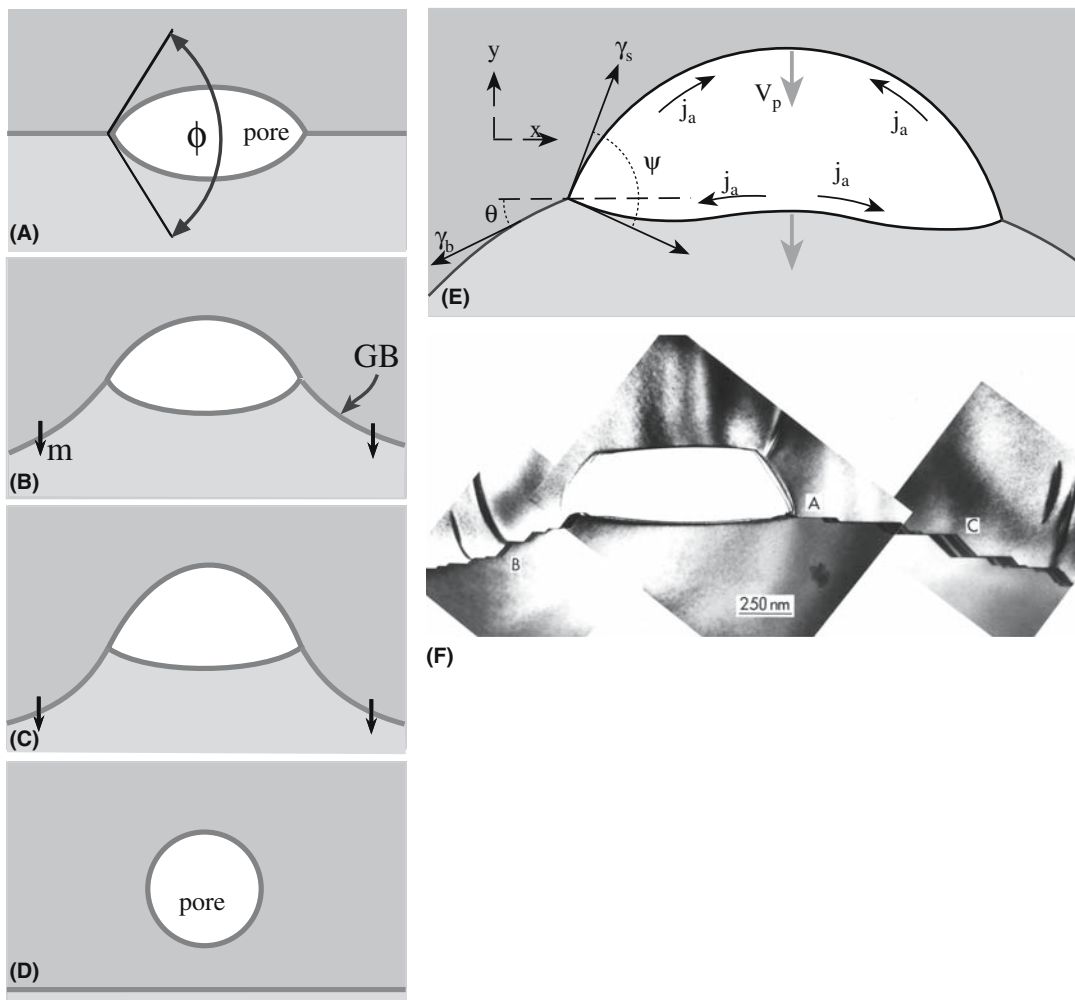


FIGURE 24.14 (a–e) GB/pore interaction: the break-away process.

area of the inclusion because we remove that much GB. (This assumes that the surface energies are the same, which you know is not necessarily true.) The total energy must be increased again to pull the GB away from the inclusion.

Consequently, when a number of inclusions are present on a grain boundary, its normal curvature becomes insufficient for continued growth after some limiting size is reached. We can estimate this limiting grain size using a simple equation.

$$d_l \approx d_i / f_{di} \quad (24.9)$$

Here d_i is the particle size of the inclusion and f_{di} is the volume fraction of inclusions.

For the process shown in Figure 24.14a–d, the boundary approaches, becomes attached to, and subsequently breaks away from a pore; the diagrams have been drawn so as to encourage you to think about how the shape of the pore will change. Actually, the process is similar whether the obstacle is a pore or a particle; just the details of the interface differ. The image in Figure 24.14F reminds us that the pore will probably be faceted in a material like alumina, although the details of the faceting may vary with temperature. Another possibility is that the grain boundary drags the obstacle, which remains attached to the boundary as it moves. If the obstacle is a particle, the second phase gradually becomes concentrated at boundary intersections and agglomerates into larger particles as grain growth proceeds.

Now if we take TJs into account the picture becomes more complicated as shown in Figure 24.15: the TJ becomes the pinning defect.

In the next section, we consider what is really happening at the atomistic scale, namely dissolution and precipitation. Inhibition of grain growth by solid-phase inclusions has been observed for MgO additions to Al_2O_3 and for CaO additions to ThO_2 .

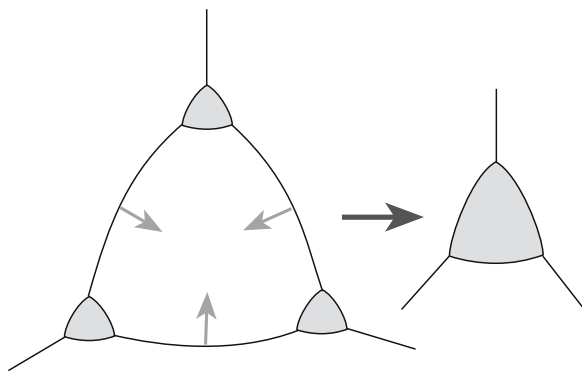


FIGURE 24.15 Coalescence of three TJs due to grain shrinkage and associated increase of material in the pocket.

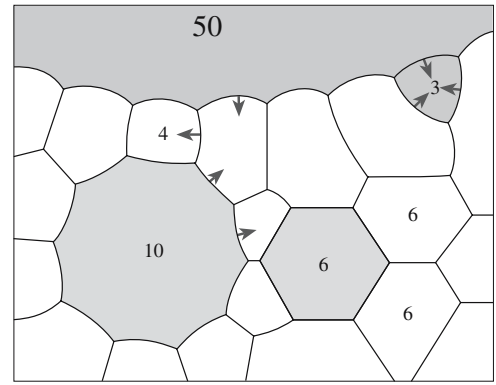


FIGURE 24.16 Growth of the largest grain.

24.10 MORE GRAIN GROWTH

The classic idea is suggested in Figure 24.16: large grains grow while small grains shrink. The direction of GB movement is always toward the center of curvature (which reduces the area of the interface). The idea behind this schematic is to apply the principle of balancing interfacial tensions, which we illustrated in Figure 24.9, to a polycrystal. The problem is that the diagram is 2D so it can be misleading. Figure 24.17 makes the problem clear. The same area is shown before and after annealing; the dashed lines in Figure 24.17b show the original position of the GBs (from Figure 24.17a). The grain that is smallest in the

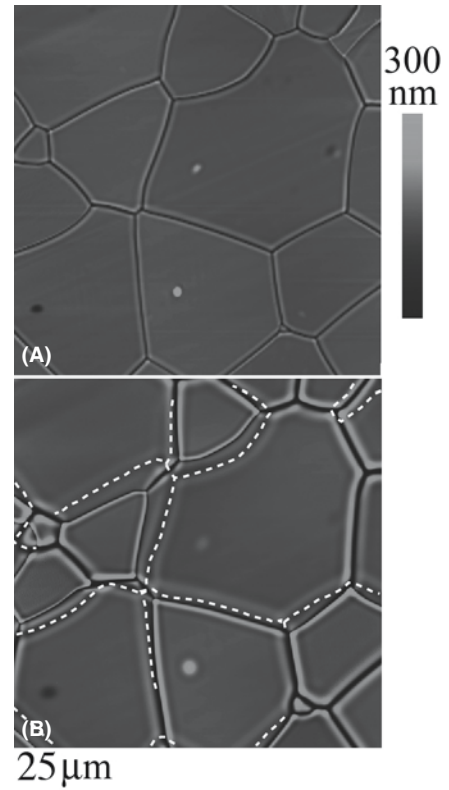


FIGURE 24.17 (a, b) AFM of grooves at migrating GBs.

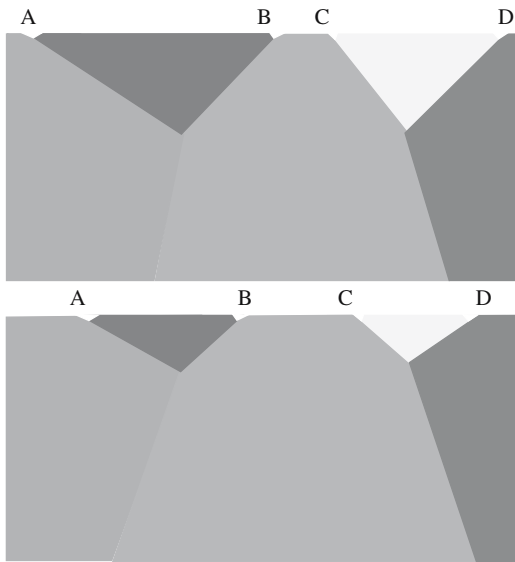


FIGURE 24.18 Side view schematic of “small grain” growing.

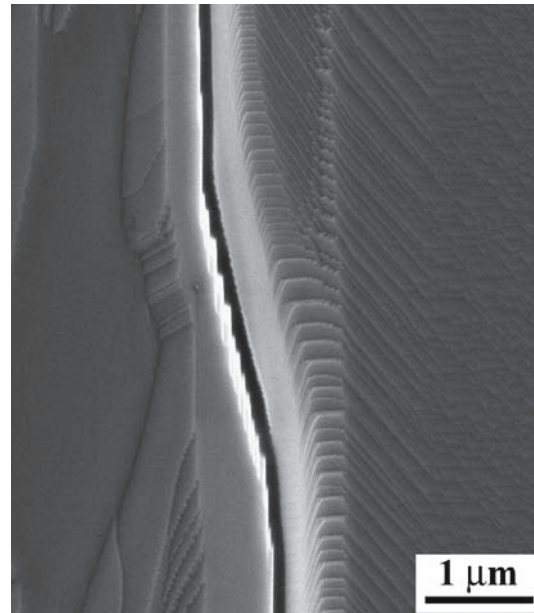


FIGURE 24.19 GB movement in bicrystals showing the large- and small-scale faceting.

original atomic force microscopy (AFM) image has grown. (Aside: look back at Figure 14.34 and then look again at the upper part of these two figures.) The schematic in Figure 24.18 provides the explanation for the growth of the smallest grain. This *small* grain is actually a *large* grain but only part of it is seen at the polished surface. Thus grains that appear to be large and many sided can shrink while others that appear to be small and have fewer than six sides can grow.

You can appreciate how GBs move from Figure 24.11. Matter is transported across the grain boundary from one grain to the other. The example shown here is a curved $\langle 100 \rangle$ tilt boundary in MgO. On the atomic scale, the motion takes place by ions moving from one facet to the other as would occur for the GB shown in Figure 24.19. We know the direction of migration in this case because it is a bicrystal and we can see the remnant groove. In Figure 24.11, these facets are only atomic in size, but are clearly recognizable.

Some final points: moving MgO GBs have been observed in real time using a transmission electron micrograph (TEM) with a heating holder going to $\sim 2000^\circ\text{C}$. Diffusion-induced GB migration (DIGM) has been reported in ceramics. The difficulty is that all observations are made after cooling the specimen to room temperature. Diffusion along GBs (as opposed to across them) is an important process in sintering.

An image and two EBSD patterns from Al_2O_3

are shown in Figure 24.20. One DP is from the large grain on the right and the other is from the point marked X. You can see that the two DPs are related by a mirror running down the middle of the page so that grain X and the large grain are basal-twin related. EBSD is able to determine the orientations of very large numbers of grains and thus to produce an orientation map. The value in grain growth studies is clear from Figure 24.20. The basal-twin boundary has not moved. Even more importantly, most of the GB above it has not moved, although one facet has started to move and this will eventually move the whole GB: the mobility of the GB depends on its orientation.

24.11 GRAIN BOUNDARIES, SURFACES, AND SINTERING

Crystallography is important in determining the geometry of surfaces, glass/crystal interfaces, and grain boundaries. For example, at temperatures at least as high as 1450°C , Al_2O_3 shows a strong tendency to facet parallel to the basal plane when heated in air, although the $\{11\bar{2}0\}$ and $\{10\bar{1}2\}$ planes are also favored. The presence of glass enhances this faceting, since it increases the kinetics of the process. The crystallography of surfaces during sintering is clearly important in understanding the behavior of pores during this process.

ELECTRON BACKSCATTERED DIFFRACTION (EBSD)

Although we have always known that diffraction occurs in scanning electron microscopy (SEM), EBSD is a relatively new technique, partly because of the experimental challenge of recording electron diffraction patterns that are noisy; however, image processing solves this problem. The power of the technique is that you can collect X-ray energy-dispersive spectrometry (XEDS) data at the same time, so you have an image, the chemistry, and the crystallography from the same area.

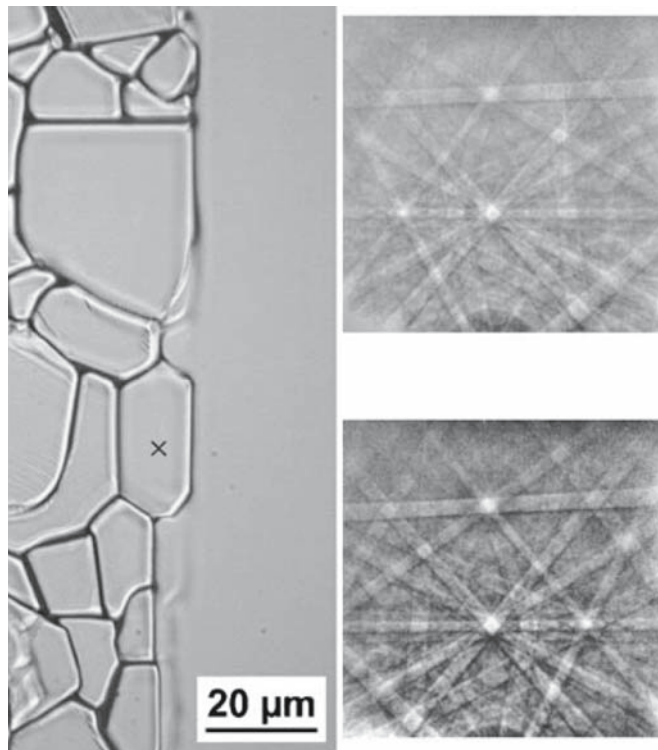


FIGURE 24.20 SEM image and two EBSD patterns from a series of engineered GBs in Al_2O_3 . The upper DP is from point X and the lower is from the large grain on the left showing the basal-twin relationship.

Particles that are initially spherical will facet when a powder is heated to the sintering temperature. Thus, again using alumina as the example, particles may join with their basal facets parallel to one another so that either a single crystal or a twinned bicrystal may form ($\Sigma = 7, 13, 21,$ and 39 may also be favored). The twin interface is a low-energy grain boundary, and the bicrystal “grain” will effectively have twice the volume of the initial particles; if the grains are slightly rotated away from the exact twin misorientation, secondary dislocations will form in the resulting interface. Such an unusually large particle may initiate exaggerated grain growth. Twin boundaries are found in many large grains in sintered materials. This process can occur even for a high-angle grain boundary such as the $\Sigma = 13$ boundary (rotate nearly 30° about the $[0001]$ axis); a high-resolution image of a $\Sigma = 13$ boundary, which was formed by hot-pressing together two crystals of Al_2O_3 , showed that the interface appears to very abrupt.

Several parameters are involved in determining whether special GBs will form during sintering.

- The kinetics of faceting
- The crystallography and size of the surface steps
- The crystallography of the facet planes

Since sintering of Al_2O_3 usually takes place at temperatures in excess of 1600°C , such faceting will almost cer-

tainly occur both before and during sintering. At higher temperatures, roughening transitions may become important, but we have no observations on this process for ceramics.

24.12 EXAGGERATED GRAIN GROWTH

A primary requirement in many sintering processes is the need to control the grain size. In ceramics, we usually refer to secondary recrystallization as discontinuous or exaggerated grain growth. The process occurs when some small fraction of the grains grows to a large size, consuming the surrounding smaller grains. Once a grain grows in size to a point at which it has many more sides than the neighboring grains, the curvature of each side increases, and it grows more rapidly than the smaller grains with fewer sides. An example of exaggerated grain growth is shown in Figure 24.21.

Aside: Classical primary recrystallization is the nucleation and growth of new strain-free grains in a matrix of heavily deformed material. The driving force arises from the decrease in strain energy. There is an induction period as the system forms stable nuclei.

Secondary recrystallization is particularly likely to occur when continuous grain growth is inhibited by the presence of impurities or pores. Under these conditions the only boundaries able to move are those with a curvature much larger than the average. Secondary recrystallization is common for titanate and ferrite ceramics in which grain growth is frequently inhibited by minor amounts of second phases or by porosity during the sintering process. The result is that both the sintering of the ceramic and the resultant properties change. Excessive grain growth is frequently detrimental to mechanical properties.

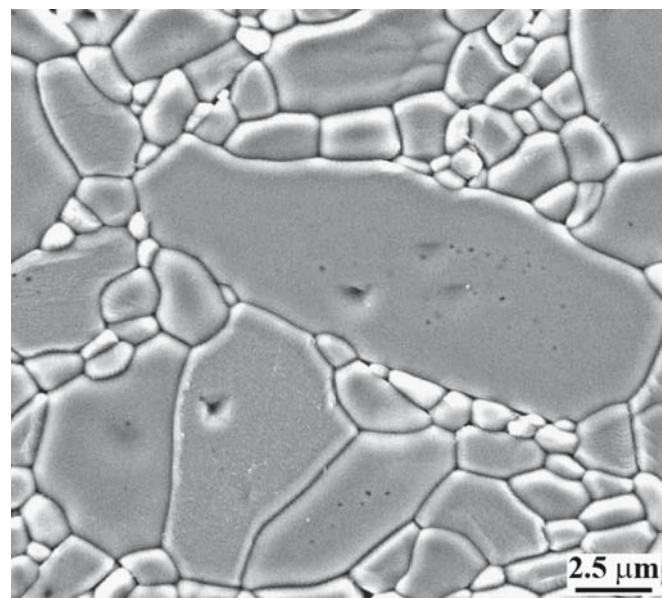


FIGURE 24.21 Elongated exaggerated grain in Al_2O_3 .

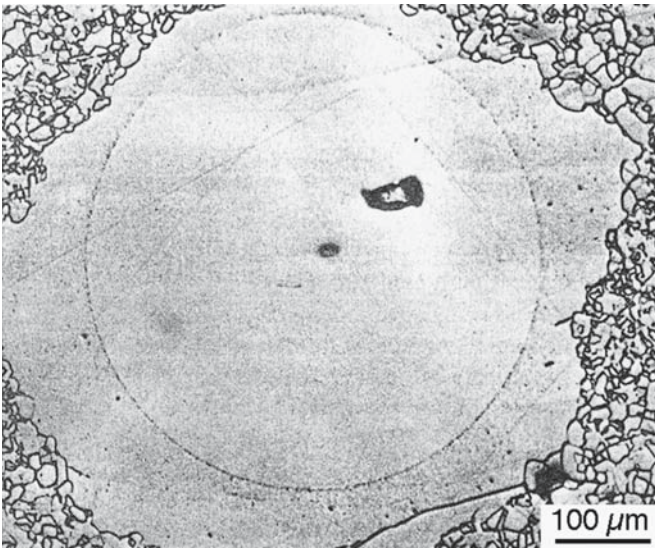


FIGURE 24.22 Using a single-crystal sphere to model exaggerated grain growth in Al_2O_3 doped with 1 wt% MgO ; at 1800°C for 60 minutes.

Modeling grain growth experimentally is illustrated in Figure 24.22. Such studies are an extension of the measurement of GB migration.

In Ostwald ripening the driving force is the reduction of total energy. The mechanism may require diffusion of one component through the other, as shown in Figure 24.23, which thus imposes an activation barrier.

An application in which secondary recrystallization has been useful is in the development of textured ceramics in which the preferred orientation is produced by seeding. (More about this is given later.) The magnetically hard ferrite, $\text{BaFe}_{12}\text{O}_{19}$, may thus be produced with large grain sizes. For this ferrimagnet it is desirable to obtain a high density as well as a high degree of preferred orientation in the sintered product. Particles of the powdered material can be oriented to a considerable extent by subjecting them to a high magnetic field while forming. On sintering there was a 57% alignment after heating to 1250°C . On further heating at 1340°C the preferred orientation

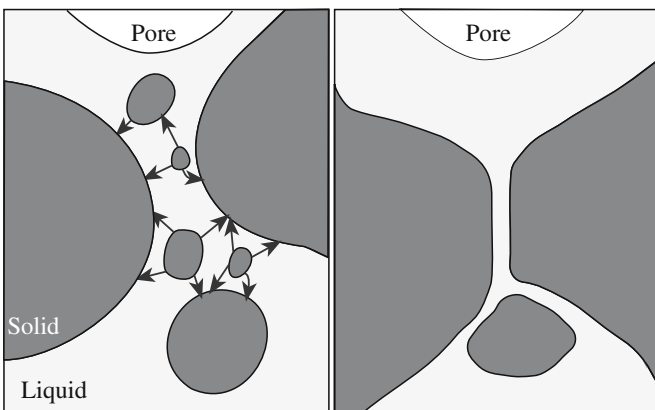


FIGURE 24.23 Schematic of Ostwald ripening.

increased to 93% alignment, corresponding to the structural change brought about by secondary recrystallization. It seems apparent that the few large grains in the starting material are more uniformly aligned than the fine surrounding material. These grains serve as nuclei for the secondary recrystallization process and give rise to a highly oriented final product.

24.13 FABRICATING COMPLEX SHAPES

We consider shaping in Chapter 23, but mention some additional features here. The method used depends on the material. Either brute force or a plasticizer should be used. The classic example is pottery—we mold the clay. Then we have the alumina thermal conduction module (TCM), cordierite honeycombs, Si_3N_4 fishhooks, and carbide blades for kitchen knives.

The TCM process involves sintering as many as 40 layers of ceramic. Vias are drilled through the layers before firing (which is much easier and cheaper to do than after firing) but must still line up after sintering when each layer will have shrunk considerably.

The mechanism can be changed with liquids. A significant proportion of ceramic products used in low-temperature applications are predominantly crystalline materials containing a minor amount of a glass phase (as noted in Section 24.7), for example, alumina substrates used in the electronic packaging industry usually contain 96% Al_2O_3 and 4% of a silicate glass. The liquid phase may be a glass added to the crystalline ceramic compact or a mixture of oxides that becomes liquid at the sintering temperature.

Liquid-phase sintering occurs most readily when the liquid completely wets the surfaces of the solid particles at the sintering temperature. The liquid in the narrow channels results in the development of a substantial capillary pressure, as illustrated in Figure 24.13. For submicrometer sizes, capillaries with diameters in the range of $0.1\text{--}1\ \mu\text{m}$ develop pressures on the order of 7 MPa for silicate liquids.

The capillary pressure developed between the particles results in dissolution of material into the liquid and its subsequent precipitation elsewhere.

The degree of wetting depends on the relationship between the interfacial and grain-boundary energies according to the relationship

$$\cos \phi/2 = (1/2)(\gamma_{ss}/\gamma_{sl}) \quad (24.10)$$

Here γ_{ss} is the grain-boundary energy, γ_{sl} is the interfacial energy, and ϕ is the dihedral angle, as illustrated earlier.

- When $\phi > 120^\circ$ the second phase forms as isolated pockets at the GBs.
- When ϕ is $60^\circ\text{--}120^\circ$ the second phase partially penetrates along the GBs.

- When $\phi < 60^\circ$ the second phase is stable along the entire GB length forming triangular prisms at the TJs.
- When $\phi = 0$ the grains are completely separated by the second phase.

The resulting microstructure for each of these cases is shown in Figure 14.33. The process of LPS is also important in forming dense powder compacts of nonoxide ceramics such as the nitrides. In these ceramics, where the bonding is predominantly covalent, atomic mobility is limited and sintering to high density is difficult in the absence of a liquid phase or without the application of high pressure.

An example of such a system is AlN, which is important as a substrate material for electronic packaging applications because of its high thermal conductivity. Its ability to remove heat from a mounted device is decreased if oxide is present in the GBs. It is made commercially by sintering AlN powder and Y_2O_3 at temperatures above $1800^\circ C$. The Y_2O_3 reacts at high temperature with the oxide coating on the AlN grains to form a liquid phase. On cooling, the liquid phase crystallizes to form Y–Al oxides (particularly YAG). These phases are located mainly at triple points.

24.14 POTTERY

Since ceramic studies began with pottery, we should consider how sintering relates to pottery. In pottery, the green body is the clay pot before it is fired; in this state it can easily be shaped. The binder is generally water. A slurry or slip is prepared by adding just enough water to the clay to ensure that the viscosity of the green body is low. Some pots are given a low temperature (biscuit or bisque) firing to remove the water and binder and to give the pot some mechanical strength so that it can then be glazed and fired to a higher temperature to give the final ceramic body. The processes occurring during the firing of a pot are much more complex than sintering alumina, for example, because phase transformations occur simultaneously with the sintering. One important process that occurs is the formation of glass in the silicate body, which allows sufficient mobility for the surface tension to consolidate the article and thus reduce porosity. Shrinkage at this stage can be 40%. The same liquid-forming process occurs externally in the formation of salt glazes as we saw elsewhere; in this case, the NaCl reacts with the silicate to produce a low-viscosity glass—the glaze.

24.15 PORES AND POROUS CERAMICS

The challenge in sintering porous ceramics is the need to avoid rather than attain densification. Figure 24.24 shows a rather uniform distribution of pores in a sintered body.

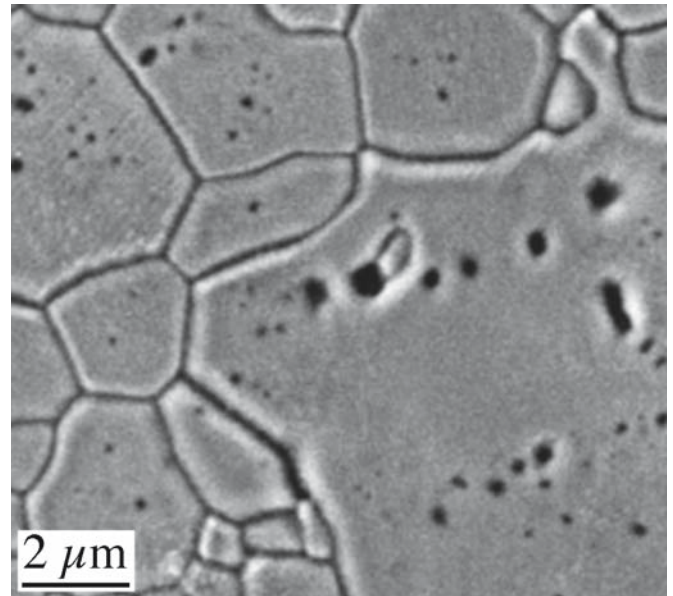


FIGURE 24.24 Pores trapped in grains.

Many of these pores have become isolated within the grains so that further reduction in their size will require lattice diffusion unless another GB migrates and intersects them during further processing.

Pillared interlayered clays (PILCs) are a special group of porous ceramics. We saw in Chapter 7 that clays are layered materials. The idea behind PILCs is to intercalate a large polyoxocation between the silicate sheets, forcing the sheets to separate, and then to convert these large particles into large metal-oxide clusters by heating to cause dehydration and dehydroxylation. Although some processes involve heating to only $400^\circ C$ —not too high, some of the PILCs are stable to above $700^\circ C$. The metal-oxide clusters are then called pillars and permanently hold the clay layers apart. The interlayer spacing is still small, the size of the molecules, and the new material has a microporous structure. The intercalation process is also known as a cation-exchange reaction, but we do not need to exchange anything; we can intercalate Na between the layers of graphite or $MoSi_2$, for example. The process studied most uses montmorillonite, but mica, vermiculite, and other layered materials have also been examined. The polycation $Al_{13}O_4(OH)_{24}(H_2O)_{12}$ (known as Al_{13}) is widely used, and the resulting materials are then referred to as Al-pillared clays. Today, a wide range of cations can be incorporated into the pillars. These PILCs are used as catalyst supports; the active metal is intercalated between the widely spaced sheets giving an extremely high surface area. By changing the active cation, many different reactions involving organic-compound conversion can be catalyzed. The idea of pillaring has been extended to layered titanates, for example; in principle, any layered material can be used. While these materials are primarily used in catalysis at present, they are also potential hosts for storing waste materials.

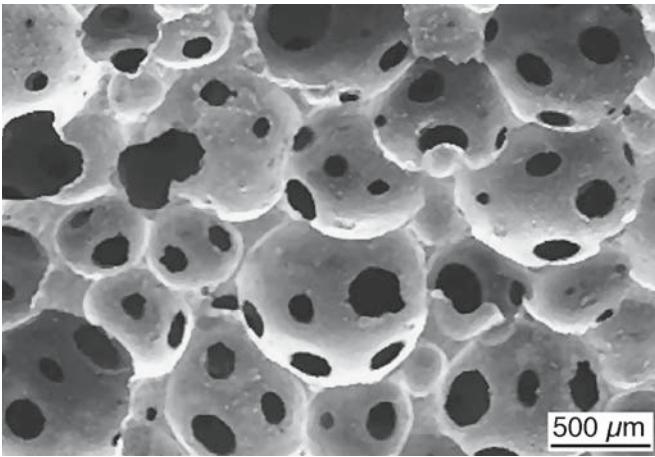


FIGURE 24.25 Porous ceramic.

The IUPAC definition of porous describes three ranges of pore sizes: microporous (<2nm), mesoporous (2–50 nm), and macroporous (>50 nm). In 1992 a new porous material similar in many ways to the natural zeolites and known as MCM-41 was patented; the name stands for Mobil Composition of Matter No. 41. Actually this is just one of a family of mesoporous molecular sieves known as M41S. It has a hexagonal array of mesopores giving channels 1.5–10 nm in diameter and a surface area of up to 700 m²/g. The mechanism proposed for their formation is referred to as liquid-crystal templating (LCT), which is similar to one model proposed for the formation of natural zeolites. The idea is that we start with two phases and burn out one leaving a porous medium. MCM-41 is essentially a honeycomb structure (it has hexagonal symmetry), but it could have been an ordered foam. Honeycombs and foams are two forms of cellular ceramics.

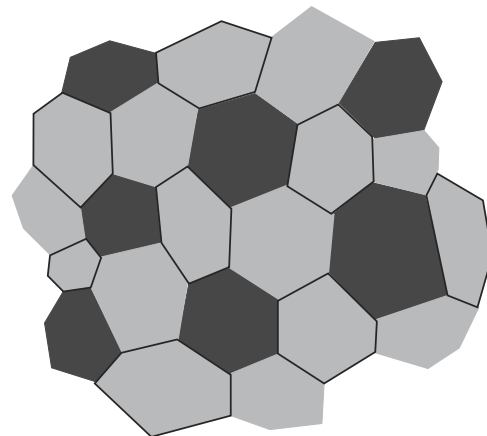
We can also make porous (cellular) ceramics by simply adding air to the green body before firing; this is exactly how nature produces pumice of course, except the green body is molten glass. By analogy with pumice, a simple route is to add pores to a slurry. This is essentially the route taken to make MCM-41; such materials may be referred to as reticulated ceramics—the result of a replication process. A completely different approach is to foam a liquid that contains the ceramic precursor (the approach used by nature to form pumice). We can use mechanical agitation, bubbling gas through the liquid, or generating the gas in the liquid. An example of a structure produced by this method is shown in Figure 24.25. (Compare this to the pores in Chapter 15.)

24.16 SINTERING WITH TWO AND THREE PHASES

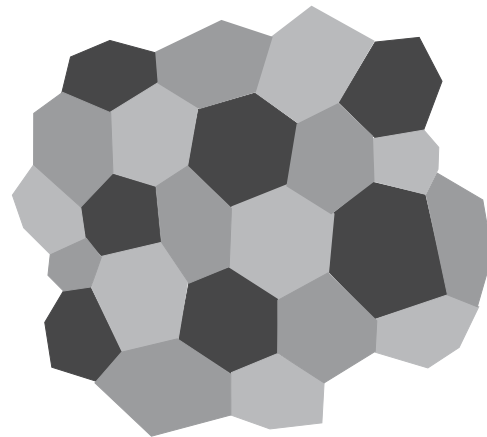
What is new? There are two situations: (1) reactions occur between the components and (2) no reaction occurs. You can see from the schematic in Figure 24.26 that this is related to the tiling problem. In a 2D cross-sectional view

of a two-phase structure, you must see both GBs and phase boundaries (PBs). In Figure 24.26a we have two phases. If the GBs in phase B move, we can generate a microstructure of isolation grains of phase A inside a single-crystal matrix of phase B. (Phase A could, for example, be porosity.) A three-phase system could, in principle, contain only PBs with no GBs (or the GBs could disappear by “local” grain growth inside that particular phase). The grains of the three phases shown here cannot grow unless we have diffusion of material A along the interface between phases B and C, for example. As was the case for Figure 24.16, the situation in 3D will be more complex with more connections and the likelihood of percolation phenomena.

Two images of a two-phase material are shown in Figure 24.27: the material is ZTA 30% (zirconia-toughened alumina with 30 vol% YSZ, which itself contains 10 molar% yttria). The smaller grains are in the as-sintered material; the larger grains are after heat treating at 1600°C for 30 hours. In both cases, the microstructure closely resembles Figure 24.26a, showing that the phases remain dispersed after a long anneal. You can imagine the three-phase situation if we add a nonreaction metal (e.g., Nb) to the two oxide phases. The result would be a cermet (ceramic/metal composite), a type of composite material



(A)



(B)

FIGURE 24.26 Schematics of multiphase ceramics; (a) two phases and (b) three phases.

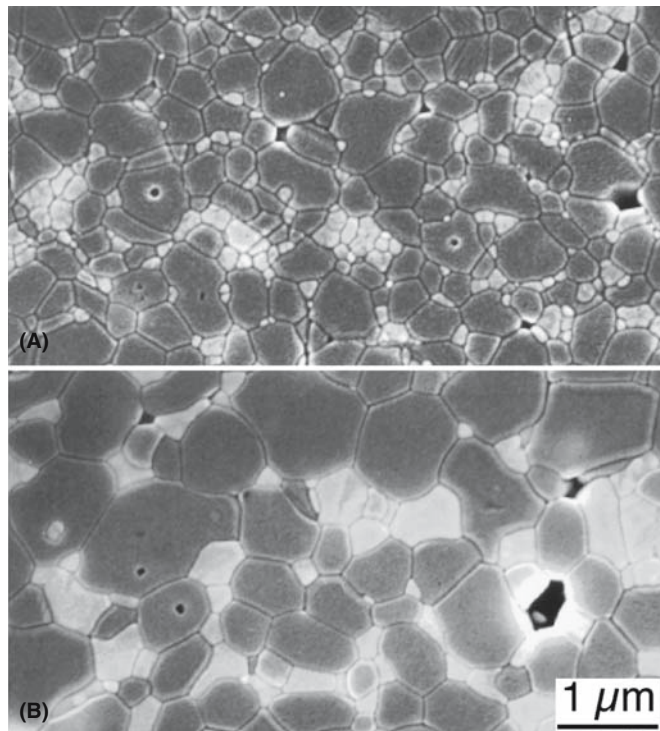


FIGURE 24.27 Two-phase ceramics. (a) As sintered and (b) heat treated at 1600°C for 30 hours. ZTA 30% (zirconia-toughened alumina with 30 vol% YSZ containing 10 molar% yttria).

widely used in different compositions. You can see how the materials can quickly become complicated. The only requirement is that the different phases are not reacting. One phase could be a glass (or even a polymer), in which case we need not worry about GBs in that phase.

24.17 EXAMPLES OF SINTERING IN ACTION

Some of these examples are discussed in detail elsewhere in the text. Here we are concerned with why the sintering process is used.

Why do we use translucent polycrystalline alumina rather than single-crystal alumina, which is transparent, in alumina lamp envelopes? Why use alumina and not yttria for this application: the yttria would allow the lamp to operate at higher temperatures producing a whiter light? The answer in both cases is the cost; both would be technologically possible. The alumina envelope is particularly interesting because of the use of MgO to limit grain growth.

Templated growth of materials like BaTiO₃ presents an attractive route to producing a textured ceramic. Templated grain growth of alumina was discussed above. The principle involved here is the use of a seed to initiate exaggerated grain growth.

Nanomaterials are very reactive, which means that we can usually sinter nanoparticles at temperatures that are

much lower than for conventional powders. However, they are also reactive even when you do not want them to be. In this case we can coat the nanoparticles to induce a repulsion or simply to physically prevent them from joining.

Materials are bonded together during packaging in IC fabrication using several different technologies, such as anodic bonding, Si-fusion bonding, surface-activated bonding, and intermediate thin-film bonding. In each scheme, heat is applied to sinter two surfaces together. Diffusion bonding of Si wafers may require very little diffusion if the wafers are nearly atomically flat. We can improve the bonding by applying a voltage; this is the anodic bonding process and is used to join Si to SiO₂.

Millefiore paperweights are essentially formed using sintering. The individual canes of glass are bonded together in a glass matrix: the essential point is that the canes do not melt.

24.18 COMPUTER MODELING

Sintering can be modeled in many different ways. One particularly interesting approach is to use Surface Evolver to model how the shape of spheres will change when they are placed in contact. In the calculation, which can in principle be extended to many more contacting spheres, the surface is allowed to move with a velocity that depends on the local curvature of the surface. At this time, the model assumes isotropic surface energies and sintering occurs by an evaporation/condensation mechanism. The approach is illustrated in Figure 24.28a, which shows two spheres that have started to sinter together. The surface of the sphere on the right is represented as a triangular mesh; the triangles are essentially small facets of a particular surface orientation. The total surface area determines the surface energy, since it is isotropic. Surface Evolver lets the surface change toward a minimum value under some constrained conditions and a grain boundary, with energy proportional to its area, is included in the calculation. The gradient of the energy is a force that is then converted to give the velocity of the interface. The motion of the surface is some multiple of the velocity; this scale factor can then be regarded as the time step, which is used in determining the dynamics of motion. The GB energy and the surface energy are related in the usual way through Young's equation so that the calculation can be run for different GB-to-surface energy ratios, which influences the development of the neck geometry as shown in Figure 24.28b.

Many other aspects of sintering are now becoming amenable to computer modeling and a new understanding of the relative importance of the different stages of sintering and the different diffusion parameters will become more widely available in the near future. Indeed, most sintering models come from what has been termed the pre- "computer-simulation age." New models are already relating these different processes at the different stages.

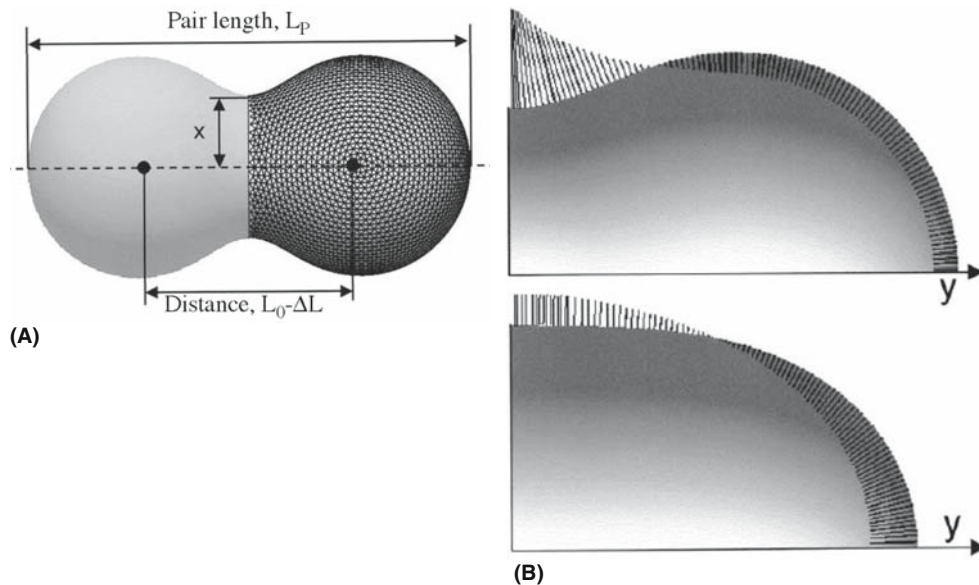


FIGURE 24.28 (a, b) Modeling sintering using Surface Evolver.

CHAPTER SUMMARY

The fundamental feature of the sintering process is the joining together of two particles without either of them melting. This process can take place fully in the solid state, although there may be a liquid involved as in the case of LPS. In fact, liquids in the form of a binder are common in commercial processes. In practice, the process may be even more complex because phase transformations may occur at the same time as sintering, and there may be more than one phase present. A full understanding of sintering makes use of everything we learned about GBs, grain growth, diffusion, and second phases in the form of pores. Computer modeling is beginning to be applied to sintering and should become more commonplace in the future.

PEOPLE IN HISTORY

Coble, Robert (Bob) L. (1928–1992) was best known for showing that small additions of MgO made it possible to form polycrystalline translucent alumina (Lucalox). This occurred while he was at the General Electric Research Laboratory in Schenectady, New York. He joined MIT in 1960. [More about this appears in the special alumina issue of *J. Am. Ceram. Soc.* **77**(2), 1994.] He is also known for Coble creep.

Kingery, W. David (1926–2000) was awarded the Kyoto Prize in 1999. David Kingery put the *science* into *ceramic science* for two generations of ceramicists. His books, including those exploring the link between the (really) old ceramics and the new, are always worth studying.

GENERAL READING

Exner, H.E. (1979) *Principles of Single-Phase Sintering*, in *Reviews on Powder Metallurgy and Physical Ceramics* **1**, 1–251. Freund Pub. House, Tel-Aviv, Israel. Not just ceramics; a very useful review.

German, R.M. (1996) *Sintering Theory and Practice*, Wiley, New York. The standard reference. Not only concerned with ceramics.

Kang, S.-L.L. (2005) *Sintering: Densification, Grain Growth and Microstructure*, Elsevier, Oxford. Very readable.

Kuczynski, G.C. *et al.* (Eds.) *Sintering Processes*, Materials Science Research; Plenum Press (now Springer), New York. Another series of Proceedings from the 1960s and 1970s. More classic discussions.

Microporous and Mesoporous Materials. This journal is a source for current research. *Sintering and Related Phenomena*. Proceedings from the 1960s and 1970s. Many classic discussions.

SPECIFIC REFERENCES

Ashby, M.F. (1974) "A first report on sintering diagrams," *Acta Met.* **22**, 275.

Casellas, D., Nagl, M.M., Llanes, L., and Anglada, M. (2005) "Microstructural coarsening of zirconia-toughened alumina composites," *J. Am. Ceram. Soc.* **88**(7), 1958.

Clay and Clay Minerals. The journal of The Clay Minerals Society.

- Gil, A., Gandía, L., and Vicente, M. (2000) "Recent advances in the synthesis and catalytic applications of pillared clays," *Catal. Rev.-Sci. Eng.* **42**(1&2), 145. A comprehensive review.
- Green, D.J. and Colombo, P. (2003) "Cellular ceramics: intriguing structures, novel properties, and innovative applications," *MRS Bull.* (April), 296.
- Kingery, W.D. (1959). "Densification during sintering in the presence of a liquid phase 1. theory," *J. Appl. Phys.* **30**, 301. The LPS paper.
- Maximemko, A.L. and Olevsky, E.A. (2004) "Effective diffusion coefficients in solid-state sintering," *Acta Mater.* **52**, 2953. An example of the use of computer modeling to analyze the role of different diffusion processes in the various stages of sintering.
- Mortensen, A., (1997) "Kinetics of densification by solution-precipitation," *Acta Mater.* **45**, 749. Quite recent update to the classic studies of LPS by Kingery.
- Swinkels, F.B. and Ashby, M.F. (1981) "A second report on sintering diagrams," *Acta Met.* **29**, 259.
- Tikare, V. and Cawley, J.D. (1998) "Numerical simulation of grain growth in liquid phase sintered materials-I. model," *Acta Mater.* **46**, 1333.
- Wakai, F. and Aldinger, F. (2003) "Sintering through surface motion by the difference in mean curvature," *Acta Mater.* **51**, 4013. Uses Surface Evolver to examine sintering.
- Zhou, Y. and Rahaman, M.N. (1997) "Effect of redox reaction on the sintering behavior of cerium oxide," *Acta Mater.* **45**, 3635. Sintering CeO_2 as Ce^{4+} is reduced to Ce^{3+} .
- Zuo, R. and Rödel, J. (2004) "Temperature dependence of constitutive behavior for solid-state sintering of alumina," *Acta Mater.* **52**, 3059. Includes a discussion of hot-forging of alumina.

EXERCISES

- 24.1 You have sintered your ceramic at 1800°C for 12 hours and attained 95% theoretical density. You then continue to heat treat it for another 12 hours at the same temperature but detect no change in density. Could the grain size of the material have changed?
- 24.2 You have two 1 μm -diameter spheres of amorphous Si and two similar spheres of crystalline Si. You bring the two pairs of spheres into contact without any applied pressure and heat for 1 hour at 1000°C. Discuss all the differences you will find when comparing the two pairs of dumbbells.
- 24.3 You place two spheres of crystalline MgO in contact without applying pressure. You find that each sphere experiences a stress due to contact with the other. Why is this so?
- 24.4 A sample consists of two slabs of TiO_2 separated by a 100 nm film of silica. The sample is heated to 1500°C. What do you expect to occur? How would you make use of information on the Hamaker constant in discussing this material?
- 24.5 A translucent alumina is prepared commercially by adding up to 200 ppm of MgO before sintering at 1800°C. This addition allows the alumina to be sintered to full density. Summarize the possible reasons for this effect and suggest an alternative additive.
- 24.6 What would be the advantages and disadvantages of making Na-vapor lamp envelopes using yttria instead of alumina?
- 24.7 You are given batches of powder of LiF, NaCl, and KCl; each has a grain size (grain diameter) of 100 nm. You cold isostatic press (CIP) each sample to 95% density and then sinter each at 1100°C. After 5 hours you remeasure the percent density. What results do you expect to see?
- 24.8 A glass contains pores that are 1 μm in diameter and are filled with N_2 at 0.8 atm pressure. If the surface tension of the glass is 28 Pa and the relative density is 0.85, what will the pore size be when the gas pressure just balances the pressure due to the surface tension? Repeat this calculation for pores that are 0.1 μm and 10 μm in diameter and discuss the changes.
- 24.9 In a sample of MgO held at 1500°C grains of MgO grew from 1 μm diameter to 10 μm diameter in 1 hour. If the grain boundary diffusion energy is 250 kJ/mol, what will the grain size be after 2 hours and 4 hours? If the experiment were repeated at 1600°C, how would these results change?
- 24.10 Imagine making a close-packed material by filling a container with 20- μm -diameter glass spheres. You then heat this "material" for 12×10^3 seconds at 650°C and the "material" shrinks by 5 vol%. You take an identical sample and find that the same shrinkage is achieved in 360 seconds at 700°C. Assuming that the surface energy of the glass is 0.3 J/m², calculate the viscosity of the glass at each temperature and deduce an activation energy.

Solid-State Phase Transformations and Reactions

CHAPTER PREVIEW

A phase transformation occurs when one material changes its composition or structure. The transformation can be caused by a change in temperature so that no other material is involved or it may involve the reaction with another material, which may or may not be a ceramic, and may be in the liquid or gaseous phase. In this chapter, we will restrict the discussion to phase transformations in which the ceramic is in the solid state. Whenever a phase transformation occurs, a phase boundary must move.

Phase transformations occur at interfaces and require the interface to move. A solid-state phase transformation occurs when the interface between two grains that are chemically or structurally different moves. If the grains are chemically the same but have different structures, the process is referred to as a (structural) phase transformation and local atomic movements can induce the change; if the grains have a different chemistry, then long-range diffusion must occur and the process is most likely part of a solid-state reaction. Clearly there are many features in common with grain growth where the grains are chemically and structurally the same. In particular, the ideas of curvature and capillarity carry over. This chapter thus builds on our discussion of all types of interfaces.

25.1 TRANSFORMATIONS AND REACTIONS: THE LINK

In Chapters 14 and 15 we discussed grain boundaries (GBs) and phase boundaries (PBs), respectively. These two chapters described the interfaces and crystal defects. In Chapter 24 we examined how the movement of GBs can lead to sintering, grain growth, and densification. In this chapter we examine how the movement of PBs leads to transformations and reactions. Some examples of reactions involving the movement of a PB are given in Table 25.1: not all of these are solid-state reactions.

How special is this topic for ceramics? These processes do occur in metal/semiconductor systems. In ceramics, solid-state reactions usually involve the movement of two species because the species are likely to be charged and we must maintain electrical neutrality. The special feature in ceramics is therefore the movement of charge and the requirement for overall electrical neutrality. We can thus apply a voltage to the system and cause an electric or ionic current to flow. As in other systems, the slower moving species will control the rate of the reaction.

The reason phase transformations are so important for ceramics is that ceramics are usually processed in the solid state. A major difficulty in studying these processes is that they usually occur at high temperatures.

We will consider three types of phase transformation: (1) crystal \rightarrow crystal, (2) glass \rightarrow crystal, and (3) crystal \rightarrow amorphous. Transformations (1) and (2) are closely related to solidification from the melt and dissolution into a liquid. Solidification is a major theme in Chapter 29. There are two topics to address:

Do atoms move further than atomic distances?
Is charge transferred during the process?

We can put these questions another way: is the driving force due to a gradient in the chemical potential or in the electrochemical potential? It is important to remember that phase diagrams describe the equilibrium state. Phase transformations occur because the system is not in its equilibrium state. We can change P , T , or c and then examine how long it takes to reach equilibrium and how we can get there. Our main tool will be our understanding of point defect mobility and diffusion. In general, we will

TABLE 25.1 Reactions by PB Movement

System	<i>Examples of special features and challenges</i>
Calcination	Removing CO ₂ and other gases during firing
Dehydration	Removing water before and during firing
Gas/solid reactions	Vapor phase at high <i>T</i> : oxidation or corrosion
Hydration reactions	Cement; changes over long time periods
NiO/Al ₂ O ₃	Large structure change at one interface, less at the other
NiO/CoO	Need diffusion data; Darken equation required
Precipitation	With control: glass-ceramics Lacking control: devitrification of glass
Transport through a fluid	Important for glass crystallization; e.g., after nucleation
Vitrification	Phase separation in glass Pottery; salt glazes

consider model systems, but even then, the data available are often not very good.

25.2 THE TERMINOLOGY

As described in Chapter 5 the polymorphic form of a material that has the lowest free energy is the most stable. The free energy, *G*, of each phase is given by the usual relation $G = E - TS$. At absolute zero, the entropy term (*TS*) is zero and the phase with the lowest internal energy will be most stable. However, at higher temperatures other polymorphic forms can exist despite their higher internal energy because of the dominance of *TS* (see Figure 5.10).

- Polymorphic transformation: The chemistry is unchanged.

Polymorphic transformations can be classified into two general types, depending on the kind of changes occurring in the crystal. Displacive transformations, as the name suggests, involve displacements of the atoms only; there is no structural rearrangement. The displacive transformation that has been extensively studied in metals is the martensite transformation. Martensitic transformations are actually quite common in ceramics, but they are generally not as rapid as in metals even though they are transformations.

Reconstructive phase transformations are associated with high activation energies. The structural change involves breaking of bonds. The energy required is at least partly recovered when the new structure is formed. Reconstructive transformations are frequently sluggish and, consequently, the high-temperature forms can often be cooled to room temperature without reverting to the thermodynamic stable form.

- Displacive transformations: atoms remain attached to the same neighbors.
- Reconstruction transformations: bonds are broken and atoms are rearranged.

The driving force for reactions is either a chemical potential or an electrochemical potential. The electrochemical potential takes account of the fact that in ceramics we have charged defects and these charged defects may move at different rates.

25.3 TECHNOLOGY

From a general technological viewpoint, not only are polycrystalline ceramics almost always very impure by metallurgical standards (3N, i.e., 99.9%, being typical high purity), but also it is common practice to add other oxides to enhance densification during processing. If the concentration of the additives exceeds the solubility, a second phase may form. Remembering our discussion in Section 24.1, imagine sintering blue and yellow colored marbles. If the temperature stays low, the marbles remain distinct but deform and rearrange to form a dense material. If the temperature increases the glasses may mix to give a uniform green glass, which in our analogy is the reacted material. Whether a reaction takes place therefore depends on factors such as the temperature; changes in the morphology of reactants can be affected by other considerations.

New Materials

Solid-state reactions are also used to produce new materials. For example, although equimolar Mg–Al spinel (i.e., MgAl₂O₄ or MgO·Al₂O₃) powder is available commercially, nonequimolar Mg–Al spinel powders may be less easy to obtain. (A similar processing method is used to produce many of the spinel-structured ferrites.) These spinel powders may have useful properties since they can be used to produce polycrystalline compacts that deform more readily than the equimolar material. Such materials can be prepared by firing an intimate mixture of the equimolar spinel with high-purity alumina powder. A closely related process (structurally the opposite) occurs when γ -alumina is transformed to α -alumina, for example, when alumina is prepared from boehmite.

YBCO, (Sr,Ba)TiO₃, BSSCO, and PZT are all essentially prepared by combining oxides or their precursors.

Multiphase Materials

There is a growing interest in the development of multiphase ceramics. Both the processing and the use of each of the materials described above may involve a solid-state reaction and the movement of a phase boundary. There are, of course, many other situations in which solid-state

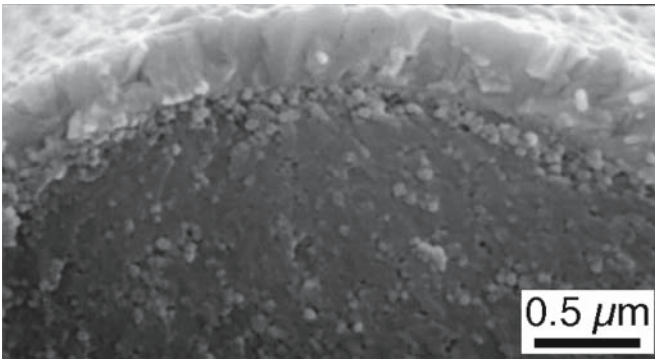


FIGURE 25.1 Technical application 1. Monazite on alumina fibers as a barrier layer in a ceramic-matrix composite.

reactions are important. In electronic packaging, chromium is first bonded to alumina and the copper conduction lines are then, in turn, bonded to the chromium. It is likely that thin spinel layers are formed in the process. Ore reduction is another important example, as illustrated by the reduction of hematite to Fe via magnetite and wüstite. A special case is the reaction that can take place when fibers are encapsulated in a matrix to enhance mechanical properties of the matrix as illustrated in Figure 25.1. If the fiber reacts with the matrix, the two are no longer able to deform independently and the mechanical properties of the composite are degraded. For this reason barrier layers may be used to coat the fibers before enclosing them in the matrix.

Growth of Thin Films

The first example shown in Figure 25.2 occurred when YBCO was grown on a substrate of ZrO_2 . The intermediate layer grew by a solid-state reaction during the deposition. This can be a problem since complicated multilayer devices are needed for many new applications. The use of

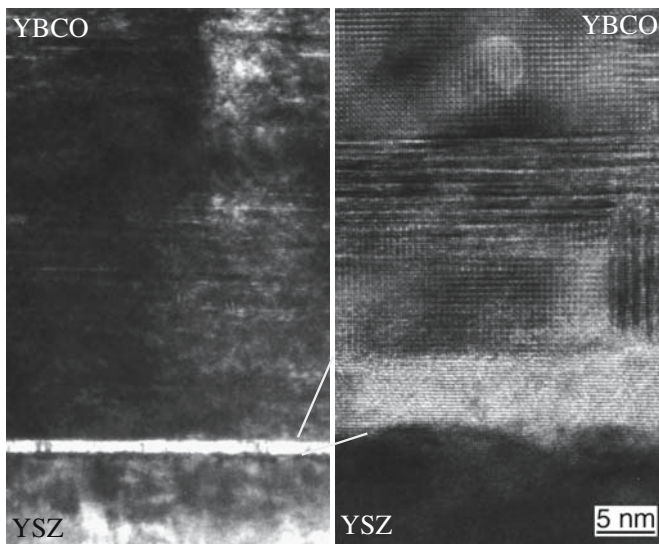


FIGURE 25.2 Technical application 2. YBCO on YSZ.

ferroelectric materials almost always involves manufacturing multilayers. It is essential that the layers should not react with one another.

Changing Properties

We can add a second phase to modify the mechanical properties of a ceramic. An example we discussed in Chapter 18 is the toughening of alumina using zirconia. In this application again, the materials should not react (which is why zirconia is used).

Degrading Thermal Barrier Coatings

A model thermal barrier coating (TBC) is shown in Figure 25.3. The white band separates the Al-rich bond coat from the underlying Ni-rich superalloy. Capping the structure is the columnar YSZ TBC. The role of the bond coat, as its name implies, is to ensure that the coating continues to adhere to the metal during oxidation. Between the bond coat and the YSZ is an oxide layer that forms during oxidation (the overlayer or thermally grown oxide—TGO). Between the bond coat and the superalloy is a thin reaction layer.

Impurity Phases

A well-known example of this process is the addition of MgO to alumina to permit sintering to theoretical density as required for the production of translucent alumina tubing (see Section 24.17). If, in this example, MgO is added in excess of the solubility limit (~210 ppm is used; the actual solubility varies with temperature), then spinel is formed, which may in turn react with Na during use to produce a precipitate of β''' -alumina. This reaction can cause the failure of sodium-vapor lamps. Since oxides are frequently processed at high temperatures, it is also likely that the vapor pressure can become appreciable for certain additive oxides.

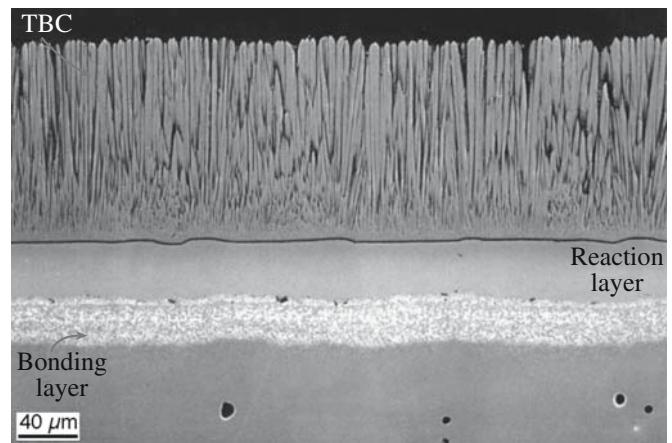


FIGURE 25.3 Technical application 3. TBC on a metal with a reaction layer and a bonding layer.

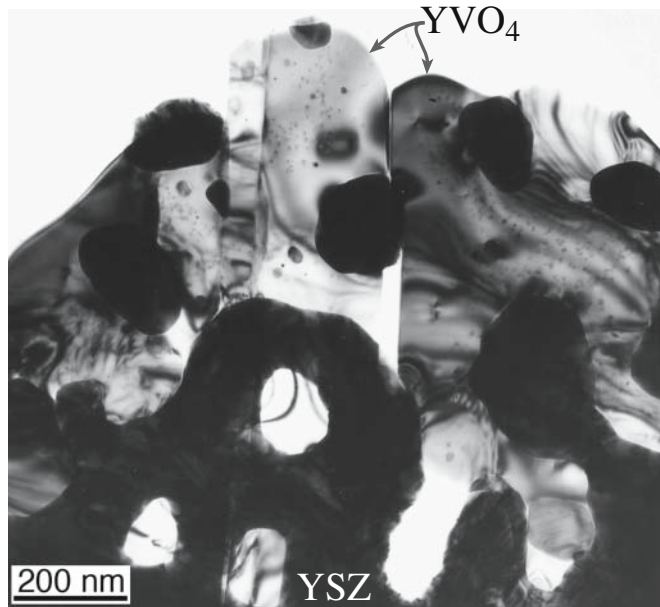


FIGURE 25.4 Corrosion of YSZ by V_2O_5 vapor.

Corrosion of Oxides

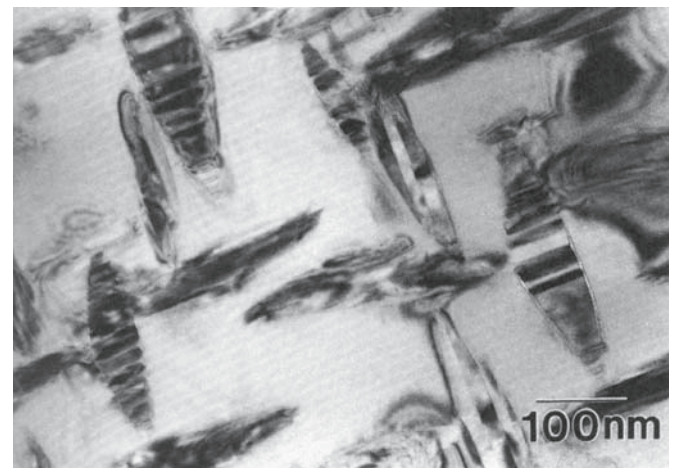
Even sapphire and YSZ can be corroded at relatively low temperatures. Figure 25.4 shows polycrystalline YSZ being corroded by V_2O_5 vapor to form a reaction layer of YVO_4 . This process may actually be important when a burning fuel contains V and the TBC contains YSZ. The Y that is stabilizing the YSZ diffuses out to react with the V_2O_5 to form YVO_4 . The result is that the Y is no longer available to stabilize the ZrO_2 , which therefore undergoes a phase change and can fracture.

25.4 PHASE TRANSFORMATIONS WITHOUT CHANGING CHEMISTRY

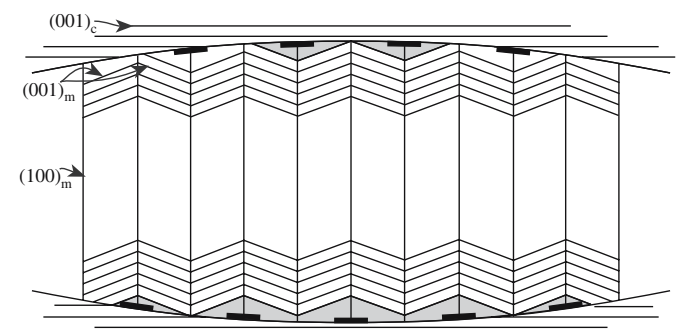
Phase transformations are, of course, closely linked to phase diagrams, but remember that if a phase transformation is occurring, then the system is not in equilibrium and the equilibrium phase diagram can be used only as a guide. Metastable phases may form during a reaction. The stability of a phase is determined by the relative value of G . Although the chemistry does not change, the redistribution of charge can be very significant, leading, for example, to the piezoelectric effect. Polymorphic transformations do not change the chemistry of the material. Since displacive transformations do not require a change in the first coordination of the atoms, there is no bond breaking, only bond bending. The distorted form is a derivative structure of the starting material usually losing one or more symmetry elements. Displacive transformations to lower temperature forms commonly result in twins. As we saw in Chapter 14, a crystal is twinned when one portion of the lattice is a mirror image of the neighboring portion, the mirror being the twinning plane. This can lead to the for-

mation of twinned “particles” as shown in Figure 25.5a. An idea of how this might occur can be obtained by considering Figure 25.5b. The particle effectively contracts along its length by the $(001)_c$ planes rotating to the $(001)_m$ planes of twin-variant 1 and back to the $(001)_m$ planes of twin-variant 2 so there is no long-range shear. Where $(001)_{m1}$ planes change to $(001)_{m2}$ planes we form a twin boundary. Depending on the details of the crystallography (which planes match best), the twin boundaries may lie along the short (as here) or long axis.

A displacive transformation is diffusionless and requires only a shear of the parent structure to produce the new phase; consequently the rate of transformation at any temperature occurs nearly instantly. An important example of the displacive transformation is the change from tetragonal to monoclinic ZrO_2 . In this example there is a 5 vol% increase during cooling, which can result in internal stresses in the ceramic and lead to weakening or even fracture. However, the controlled transformation of ZrO_2 particles in a ceramic matrix (e.g., Al_2O_3) can be used to strengthen the matrix. (We discussed fracture of ceramic materials in Chapter 18.) The addition of MgO , CaO , or Y_2O_3 , to ZrO_2 can stabilize the cubic (fluorite) structure. When ZrO_2 transforms from the cubic to the



(A)



(B)

FIGURE 25.5 Twins in transformed particles: (a) experimental observation and (b) a possible mechanism.

tetragonal phase or from the tetragonal to the monoclinic phase the volume changes. This volume change is the key to using such mechanisms in toughening ceramics since it relaxes local stresses at a crack tip.

Barium titanate is cubic with a perovskite structure. However, at room temperature (actually below the Curie temperature of 120°C) it is tetragonal with a spontaneous electric polarization in the direction of the *c*-axis (only the higher temperatures form is shown in Figure 7.2). In this ferroelectric condition a crystal of BaTiO₃ has a domain structure.

The classic example of a reconstructive phase transformation in ceramics is the transformation between the low and high forms of SiO₂: the distorted form of quartz structure is stable at the lower temperature. Twins are again often formed during reconstructive phase transformations when these lead to a decrease in symmetry since the change can often occur in symmetry-related ways; the twins are then related by the “lost” symmetry element.

25.5 PHASE TRANSFORMATIONS CHANGING CHEMISTRY

For short-range or long-range chemistry changes it is necessary for ions to move. Atoms diffuse and charge is transferred. If charge is moved an electric field may develop in the material or we can influence the transformation by applying an electric field. The structure may also change, so the beginning of the process (the nucleation stage) may be controlled by the difficulty in changing the structure. At a later stage diffusion almost invariably controls such reactions.

The reaction can be considered as involving three steps.

1. Transport to the interface
2. Reaction at the interface
3. Transport away from interface of the product and heat

As usual, the slowest step controls the rate. The rate of such reactions is controlled by gradients in the chemical potential or, if there is a local variation in charge, by the electrochemical potential.

This concept is very important because the chemical potential and the electrical potential can act in opposite directions. There are many model and technological applications of this concept.

Silver sulfides provide a model system for studying this effect partly because the processes occur at relatively low temperatures.

In oxides such as ZrO₂, flow of oxygen ions can be measured and related to the difference in oxygen partial pressure across the ZrO₂ layer since an electrochemical potential is generated.

In the formation of NiAl₂O₄ by solid-state reaction, we have diffusion of Al³⁺ ions and Ni²⁺ ions. If the Al³⁺ ion moves faster than the Ni²⁺ ion, then we would build up charge; this would create an electric field that would then act to reverse the flow of ions rather than allow a build-up of charge. (More details are provided in Section 25.9.)

Precipitation

Precipitation usually involves a change in local chemistry. Since we are creating a new particle, we form a new PB (see Chapter 15). As the particle grows, this PB moves. The balance between kinetics (of interface motion and diffusion) and energy (of the new bulk and the new PB) may determine the shape of the particle during growth. Three factors in particular must be considered.

1. Number of particles per unit volume
2. Shape of the particles
3. Size of the particles (and hence volume fraction of the precipitate)

As for metals, we can change *T* or the chemical potential. Particles in ceramics have not been as widely used as in metals because we do not need to pin dislocations. However, particles can still inhibit GB motion, act as sinks for impurities, or modify mechanical properties. The widespread occurrence and usefulness of precipitation in ceramics are becoming more fully recognized. Things happen slowly in ceramics. If there is a good alignment between the matrix and the precipitate, the transformation can occur by the movement of dislocations as in Figure 25.6, which shows a plate of hematite growing in an Ni–Fe spinel matrix. Notice that the interfacial dislocations bow out in the direction of movement and that the plate thickens as they move.

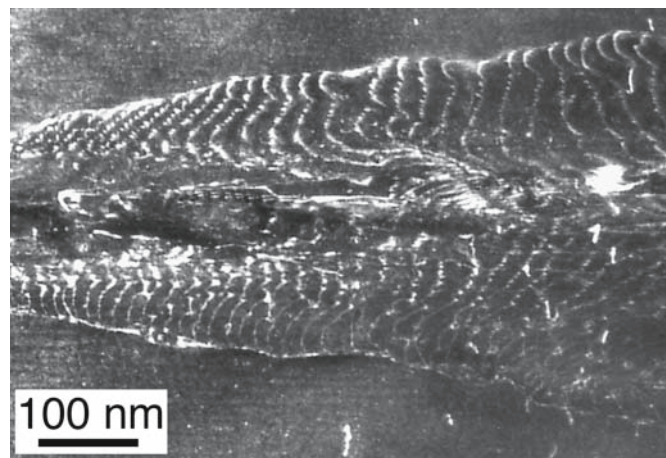


FIGURE 25.6 Movement of interfacial dislocations between hematite and NiFe₂O₄ spinel during oxidation leading to thickening of the precipitate.

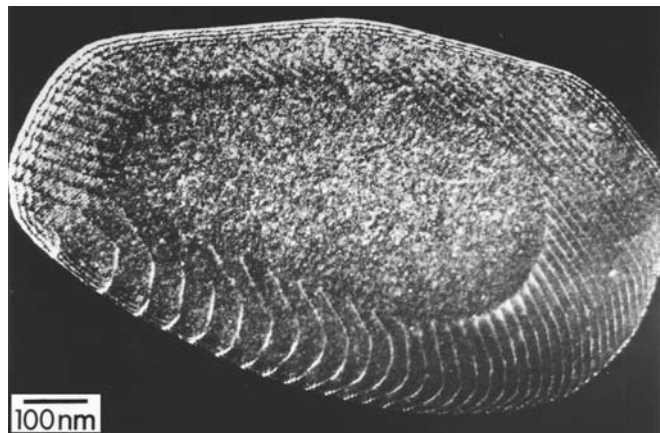


FIGURE 25.7 Growing particle of spinel in a matrix of Fe-doped Al_2O_3 during internal reduction.

Internal Oxidation and Reduction

The thought experiment: imagine a 1-mm cube of Fe-doped Al_2O_3 in which all the Fe is in the 3+ state. Now heat the cube in a reducing atmosphere at $\sim 1500^\circ\text{C}$. The matrix is unchanged (it is Al_2O_3), but the Fe^{3+} is reduced to Fe^{2+} . Initially, this phase change can happen only at the surface where the oxygen activity has been lowered, but then the “reduction” front moves into the cube like a PB (but there is no change in phase). The Fe^{2+} is no longer soluble in the matrix and precipitates out as FeAl_2O_4 spinel. The result is that we can see where the front has passed through by where the precipitates, such as that in Figure 25.7, have formed. (Notice the curvature of the dislocations implying their direction of movement.) The converse process, namely internal oxidation, can be demonstrated using a similar cube of Fe(II)-doped NiO.

25.6 METHODS FOR STUDYING KINETICS

We need to understand what controls the rate of a phase transformation. We can monitor both chemical and structural changes to address the sometimes subtle question—which change (chemistry or structure) occurs first? The answer depends on why the phase change itself occurs. The experimental techniques we use are those given in Chapter 10, so we just give some specific illustrations here. The classical approach used to study the kinetics of solid-state reactions between two ceramic oxides is to react a bulk diffusion couple in much the same way as, for example, when studying the Kirkendall effect in metals.

Using Weight Change

We can weigh the sample and plot the fraction that has reacted as a function of time as illustrated in Figure 25.8. Microbalances now allow us to make this technique very

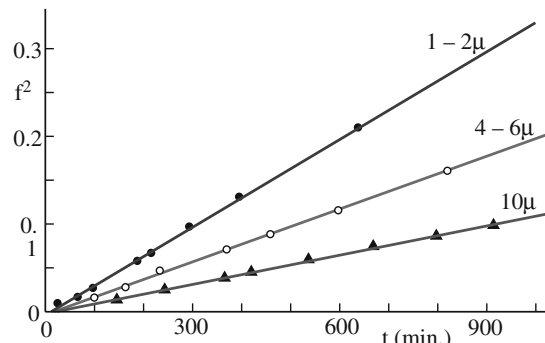


FIGURE 25.8 Reaction by weight. f^2 is the square of fraction reacted.

sensitive. A modern microbalance can weigh samples up to 3.5 g with an accuracy of 0.1 μg . A quartz-crystal microbalance (QCM) can actually measure mass changes in the nanogram range. So we use a piezoelectric ceramic, a thin plate of quartz, to make the device, which then allows us to study reactions in ceramics (and other materials).

Using Visible Light Microscopy, the Microprobe, and Scanning Electron Microscopy

The reacted microstructure is often best analyzed using low-voltage scanning electron microscopy (LVSEM) in the backscattered-electron (BSE) imaging mode. The low voltage means that we need only a thin conductive coating (if any) to prevent an insulator from charging. The BSE mode allows the phases present to be readily recognized because the backscatter coefficients are likely to be different for the reactants and the reaction product.

Using Transmission Electron Microscopy

The movement of a particular PB is illustrated in Figure 25.9. A spinel particle has been grown on the edge of a

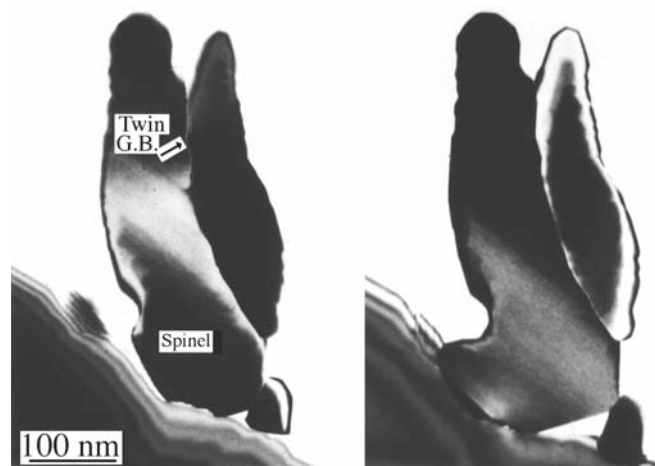


FIGURE 25.9 Particle of Ni–Al spinel growing on an Al_2O_3 thin film.

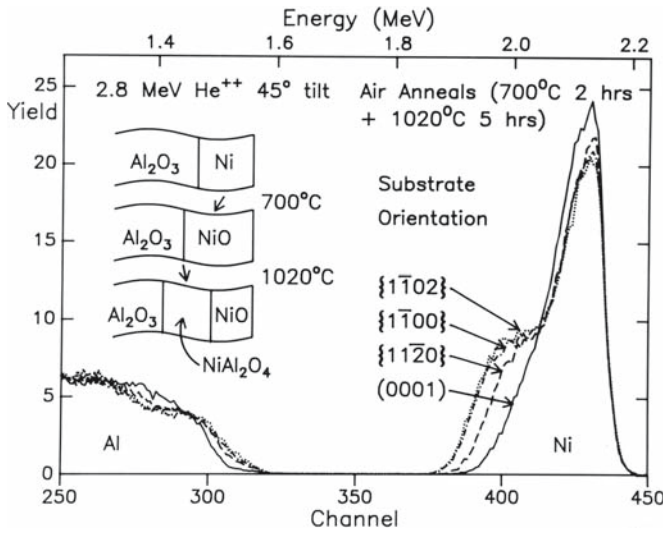


FIGURE 25.10 Rutherford backscattering spectrometry (RBS) of a reaction between NiO and Al₂O₃ substrates for different surface orientations.

thin film of Al₂O₃ by reacting the film with NiO vapor, looked at in the transmission electron micrograph (TEM), replaced in the reaction chamber, and looked at again. You can see that the spinel has grown into the Al₂O₃. In this case, the PB moves in the solid state, but the NiO is provided from the vapor phase. The spinel particle changes only where it grows into the sapphire.

Using Rutherford Backscattering Spectrometry

This technique is very direct and measures the thickness of a reaction layer. The lateral resolution is the width of the ion beam (~0.1 μm). An example from a thin layer of NiO reacting with differently oriented surfaces of Al₂O₃ is illustrated in Figure 25.10. The thickness of the spinel is obtained by fitting the data to a simulated profile (using RUMP) and shows in this example that the rate of growth of the spinel layer does indeed depend on the orientation of the surface.

25.7 DIFFUSION THROUGH A LAYER: SLIP CASTING

We consider the kinetics of slip coating or slip casting for two reasons: (1) as a model for the transport of a reactant through a planar boundary layer, and (2) because it is a very important aspect of ceramic processing. The model actually applies to reduction, oxi-

HOW THIS PARABOLIC RELATIONSHIP ARISES

- *J* is proportional to *dx/dt*: *J* depends on velocity.
- *J* is also proportional to 1/*x*: Δ*P* is the driving force.

So, *dx/dt* is proportional to 1/*x*: hence it is parabolic.
 When *x* is very small, *dx/dt* is very large.
 When *x* is very large *dx/dt* is very small.

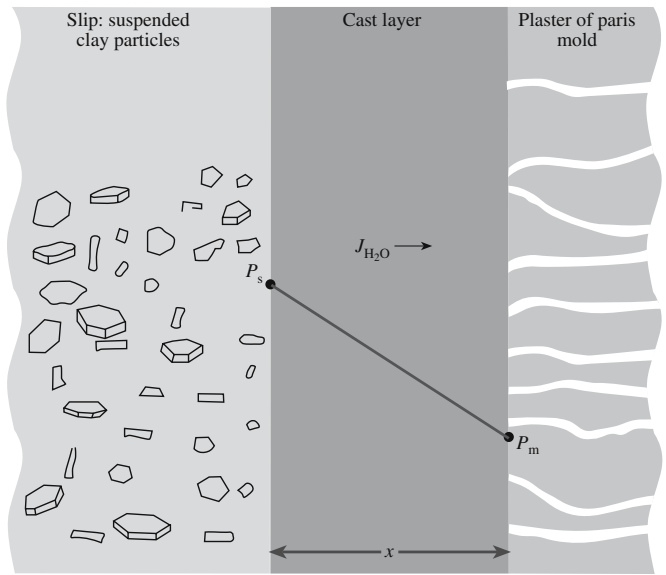


FIGURE 25.11 Schematic of slip drying to form a slip-cast layer.

duction, and MgO/Al₂O₃ reactions. In slip casting, a mold is made from gypsum (Plaster of Paris: CaSO₄·2H₂O). Gypsum contains fine capillaries that remove water from a slip at a predictable rate. The clay particles in the slip are platelets as shown in Figure 25.11, so a more compact layer forms as the water is removed. In the compacted cast layer there are fewer capillaries, so it becomes more difficult to remove more water. Hence as the thickness increases, the rate of material transported decreases.

We can write an expression for the flow (current) of atoms (the transport equation) as

$$J = \frac{KdP}{dx} \quad (25.1)$$

The water pressure gradient is *dP/dx*; *K*, the permutation coefficient, depends on the particle size, the viscosity, and *T*. The pressure at the surface of the slip, *P_s* is 1 atm. The pressure at the slip/mold interface, *P_m* is determined by the surface tension in the capillaries (which are assumed to have a fixed radius *r_c*).

$$\Delta P = P_s - P_m = \frac{2\gamma}{r_c} \quad (25.2)$$

The flux can also be expressed as a volume (proportional to ρ⁻¹) multiplied by the velocity of the slip/layer interface

$$J = \frac{1}{(\kappa\rho)} \frac{dx}{dt} \quad (25.3)$$

Combining Eqs. 25.1 through 25.3 gives

$$J = 1/(\kappa\rho) \frac{dx}{dt} = K \frac{dp}{dx} = -K \frac{\Delta p}{x} = -K \frac{2\gamma}{r_c x} \quad (25.4)$$

Then by rearranging we get an expression for the interface velocity

$$\frac{dx}{dt} = -K\kappa\rho \frac{2\gamma}{r_c x} \quad (25.5)$$

If we integrate, we find that x^2 is proportional to t , so the kinetics are parabolic. κ is a volume factor relating to the difference between water and the clay particles.

A pot can be slip cast to a thickness of several millimeters in a few hours. The potter would then pour off the remaining slip, let the pot dry and shrink, and remove it from the mold, which can then be reused.

25.8 DIFFUSION THROUGH A LAYER: SOLID-STATE REACTIONS

In solid-state reactions, the reactants are initially in contact and combine chemically to form the reaction product. The kinetics of the initial stage of such a reaction depend on the parameters of the interface (the crystallography of the contacting surfaces, etc.). The fundamental point is that we start with one interface and immediately create two new interfaces. We will consider the example of NiO/Al₂O₃. Similar systems include MgO/Al₂O₃ and FeO/Fe₂O₃.

The mechanism for such reactions, as proposed by Wagner, is the counterdiffusion of cations. It has been found that this mechanism does occur for purely ionic materials. Counterdiffusion of cations in ionic systems is dictated by charge-balance considerations rather than cation mobilities. Thus significant deviations from the predicted balance may occur when electronic carriers (i.e., electrons and holes) are present.

The initial position of the interface between the reactant oxides can be labeled by “inert” Pt markers or recognized by the presence of voids. Some early measurements were not in agreement with this model but may have suffered from the fact that inert markers can move even though they remain inert.

25.9 THE SPINEL-FORMING REACTION

The phase transformation at the Al₂O₃/spinel phase boundary involves both a change in the distribution of cations and a change in the structure of the oxygen sublattice. At the spinel/NiO interface the oxygen sublattice remains cubic, although misfit dislocations may be introduced. It is not possible to observe directly the movement of particular interfaces using bulk samples. Techniques can be

used that allow the actual movement of individual interfaces to be studied and the kinetics of the earliest stages of the reactions to be determined.

When alumina and NiO react to form a layer, the equation is



There are many possible reaction paths. The chosen path may depend on whether the reaction occurs in air. In all three cases, electrical neutrality is maintained.

There are three main possibilities:

1. 2B³⁺ ions move in one direction; electrons or O²⁻ ions move in the opposite direction.
2. 3A²⁺ ions move in one direction; electrons or O²⁻ ions move in the opposite direction.
3. 2B³⁺ move in one direction and 3A²⁺ move in the opposite direction.

These processes are summarized in Figure 25.12. Mechanisms 1 and 2 require that O²⁻ diffuse, which may not be likely, or that electrons can move, which may be the case in semiconducting oxides unless it is prevented. The third mechanism is the counterdiffusion of cations,

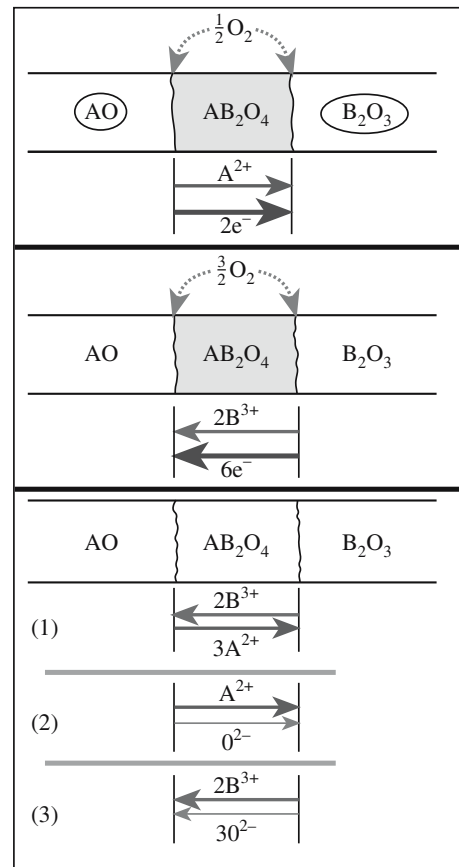


FIGURE 25.12 Mechanisms for the reaction between AO and B₂O₃.

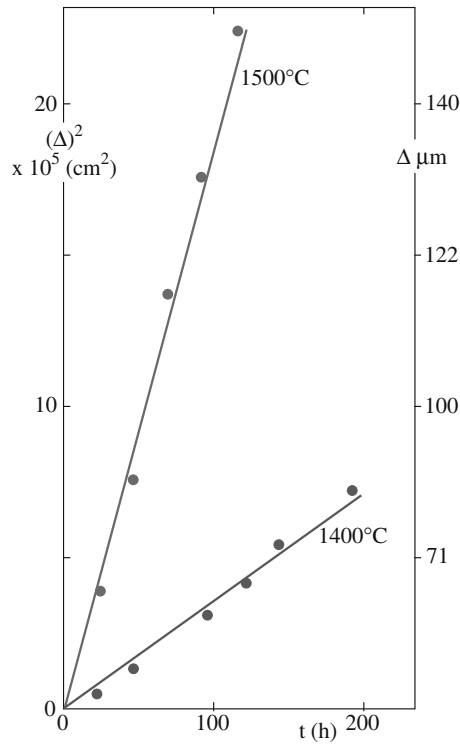


FIGURE 25.13 Kinetics of the reaction between bulk NiO and bulk Al₂O₃ to form spinel.

which avoids the build-up of electric charge but does not require O²⁻ ions or electrons to move: it is a purely ionic process. When thickness is plotted against time for the bulk reaction (Figure 25.13), the gradient of the straight line depends on *T* and we can directly determine a value for the diffusion coefficients.

We know that if there is a charge build-up then we will have an electrochemical potential, η_i , rather than the simple chemical potential, μ_i . These two potentials are related by taking account of ϕ , the electrical potential acting on this charge.

$$\eta_i = \mu_i + Z_i F \phi \quad (25.7)$$

The subscript *i* refers to the *i*th species, which has an effective charge of Z_i , and *F* is the Faraday constant. The current is the product of charge and velocity.

$$j_i = c_i v_i \quad (25.8)$$

Remember that velocity is mobility times force.

$$v_i = -B_i \cdot \text{Force} = -B_i \frac{1}{N} \frac{d\eta_i}{dx} \quad (25.9)$$

and

$$j_i = \frac{c_i B_i}{N} \frac{\partial \eta_i}{\partial x} \quad (25.8)$$

We can then define a diffusion coefficient, D_i .

$$D_i = -\frac{RTB_i}{N} \quad (25.10)$$

The parabolic rate law holds when the reaction layer is thick. When trying to be quantitative, there is the obvious question how to “mark” the location of the original interface. An additional complication arises if AO and AB₂O₄ are both cubic but not lattice matched; then misfit dislocations must be present at the interface and these can move only if point defects on the O sublattice move.

25.10 INERT MARKERS AND REACTION BARRIERS

We saw examples of structures in which reactions would destroy the device in Section 25.1—this is where we need barriers. When we study the kinetics of reactions we would like to mark the initial location of the interface(s)—this is where we need markers. In both cases, the barrier/marker must be inert; it should not participate in any reaction. This topic can be illustrated by two examples:

- Behavior of rows of Pt particles forming a marker layer
- Failure of a coating on a fiber during formation of a fiber-reinforced composite

We will consider the example of diffusion couples prepared by depositing an In₂O₃ thin film on a cleaved bulk single-crystal substrate of MgO and identify the location of the initial interface by an array of Pt particles as illustrated in Figure 25.14. The Pt particles are prepared

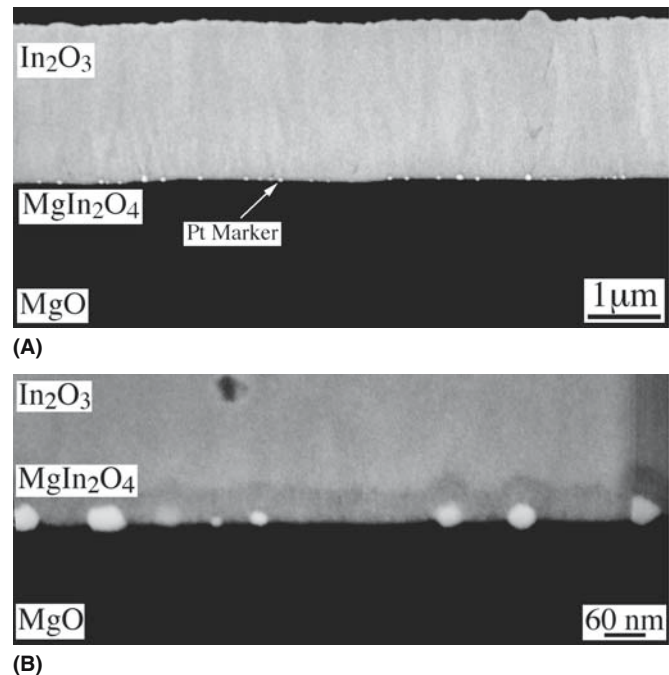


FIGURE 25.14 SEM backscattered electron images of an as-deposited In₂O₃ film on MgO with Pt markers.

by first sputter coating the MgO substrate with a 2-nm-thick continuous film of Pt. The Pt-film/MgO-substrate couple is then heated to 1175°C for 5 minutes. This heat treatment causes the Pt film to dewet the MgO surface and thus form small islands. This array of small Pt particles then serves as the marker layer. After dewetting, thin films of MgIn₂O₄ and In₂O₃ can be deposited onto the decorated substrate using pulsed-laser deposition (PLD). This intermediate MgIn₂O₄ layer acts as the nucleation layer for the reaction product so that the markers do not affect the initial nucleation of the spinel. (It can also be grown on the MgO before depositing the Pt.)

Markers of various compositions and sizes have been used in numerous studies to track the movement of interfaces in a wide variety of material systems. In many of these studies, the markers were intended to serve as a fixed reference point and typically are used to aid in determining which species were diffusing during a reaction process. When a material is used as a marker it is usually assumed to be inert, i.e., the marker should neither affect nor be affected by the reaction process. Direct analysis of these thin-film diffusion couples can show directly whether the markers are inert and how they behave during such reactions. The markers may affect the reaction process or the reaction process may cause the markers to move. The interface between the marker and the surrounding matrix plays a critical role in determining the inertness of the marker. This is especially significant when diffusion couples are reacted in an applied electric field.

The idea of a barrier layer is to prevent two materials coming into contact that would react. Applications include protecting reinforcing fibers and separating layers in multilayer thin films. Such barrier layers could also be used to exclude water from hydrophobic layers.

25.11 SIMPLIFIED DARKEN EQUATION

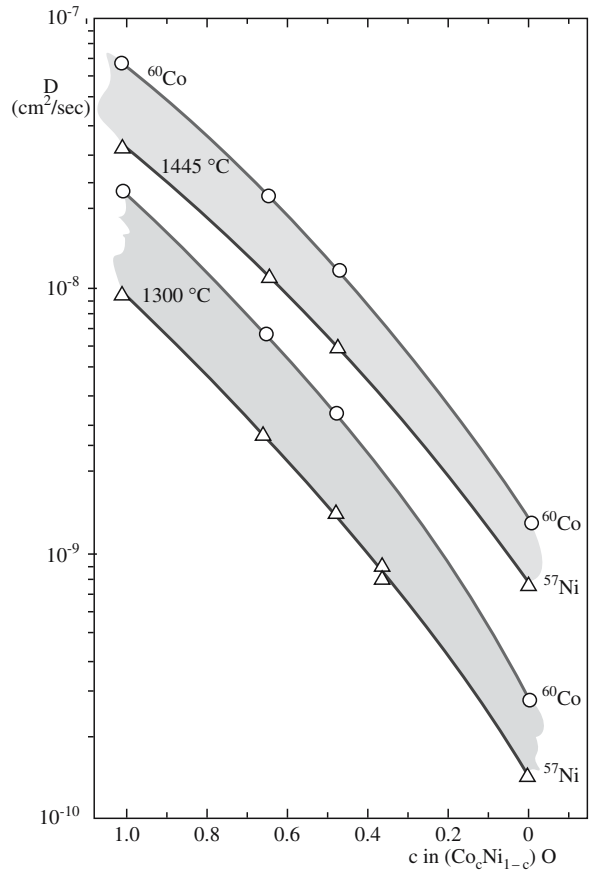
The diffusion coefficient actually will depend on the composition. Consider NiO/CoO, which is a nearly ideal solid solution. The activity coefficient is ~1.

$$\mu_i = \mu_i^0 + RT \ln c \quad (25.11)$$

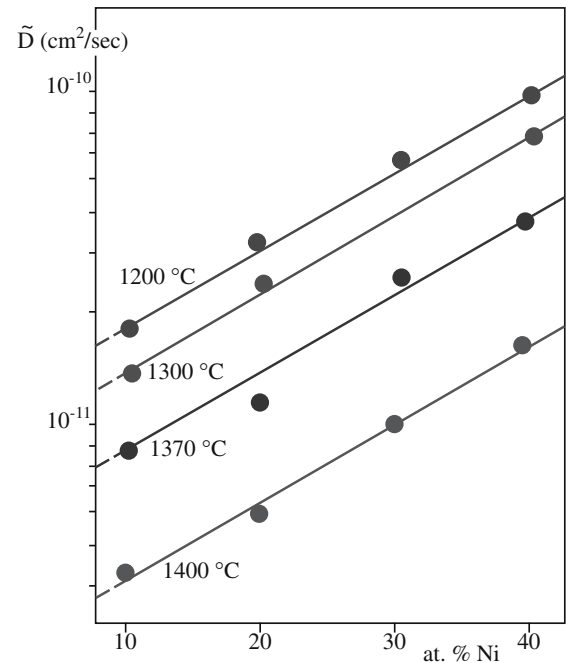
We can write an “average” diffusion coefficient as

$$\tilde{D} = D \frac{T}{Co} x_{Co} + D \frac{T}{Ni} (1 - x_{Co}) \quad (25.12)$$

In this equation, which is known as the Darken equation, x indicates the mole fraction of Co or of Ni. The equation assumes local equilibrium everywhere and that \tilde{D} is a chemical or interdiffusion coefficient in a chemical potential gradient. The matrix is Co_{*x*}Ni_{*1-x*}O. D is plotted as a function of concentration for both Ni and Co diffusing in the mixed oxide at 1300°C and 1445°C in Figure 25.15a.



(A)



(B)

FIGURE 25.15 D as composition varies: (a) using tracer diffusion at two values of T in CoO–NiO mixed oxide and (b) diffusivities for MgO–NiO mixed oxides.

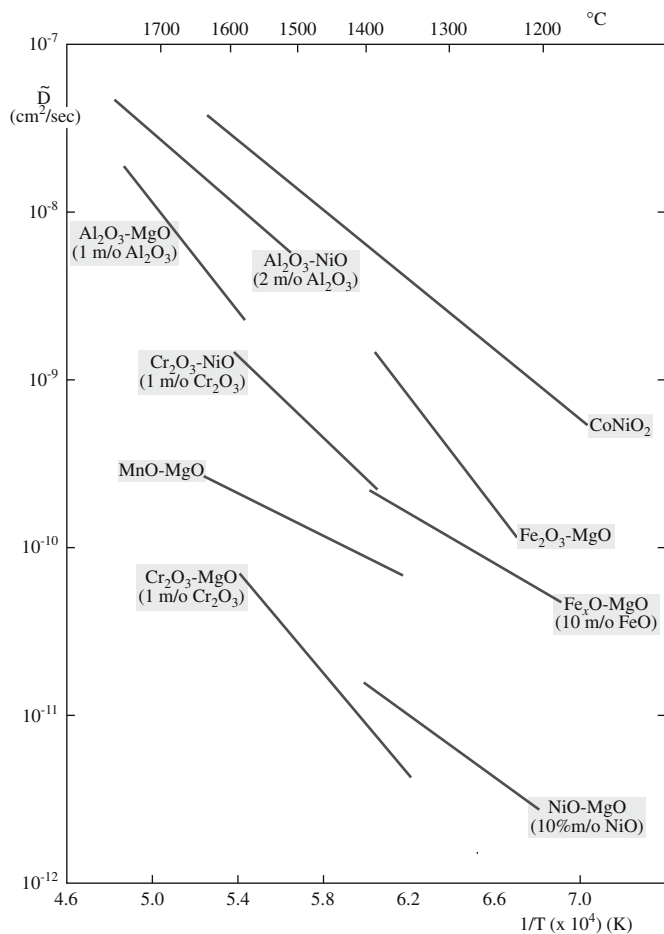


FIGURE 25.16 Dependence of diffusion coefficients on T for different oxides.

The mean value from Eq. 25.12 is plotted in Figure 25.15b. \bar{D} can also be plotted as a function of temperature as shown for many more oxide systems in Figure 25.16.

This analysis is useful but be cautious. The oppositely charged point defects Ni^{3+} and $\text{V}^{\prime\prime}$ form an associated defect, which diffuses at a different rate. You can measure D but modeling \bar{D} is difficult; essentially predictions are tricky.

25.12 THE INCUBATION PERIOD

The initial stage of a solid-state reaction was historically referred to as the “incubation period.” Early studies of such reactions in oxides lacked the required spatial resolution so that measurements were not made until the reaction layer was $\sim 1 \mu\text{m}$ thick (the resolution limit for chemical analysis in a microprobe operating at $\sim 30 \text{ kV}$). Often, the reactants were not initially in ideal contact. The nucleation of spinel or other reaction products can now be detected at a very early stage using TEM. The kinetics of such early stages of reactions are often controlled by the difficulty of nucleating the reaction product, which may indicate a crystallographic factor. Thus, for example, the basal plane in Al_2O_3 tends to dissolve less readily than, say, a pris-

matic plane so reactions at basal planes tend to nucleate more slowly than on prismatic planes. (More is given in Section 25.14.)

25.13 PARTICLE GROWTH AND THE EFFECT OF MISFIT

The lattice misfit at moving phase boundaries is accommodated by misfit dislocations, lattice rotations, etc. An important consideration will be the role of size in determining these effects; neither misfit dislocations nor lattice rotations may be necessary when the new phase is very small. The chemical abruptness of the interface is particularly interesting when the oxygen sublattice is almost common to the two materials as we saw in Section 15.6 for the $\text{NiO}/\text{NiFe}_2\text{O}_4$ interface. This interface can then move by only the cations moving. However, if misfit dislocations are present, as in Figure 15.3, then the anions must also move.

The growth of β -alumina into spinel shown in Figure 25.17a is an example of a special situation in which the misfit between the precipitates and the matrix is very

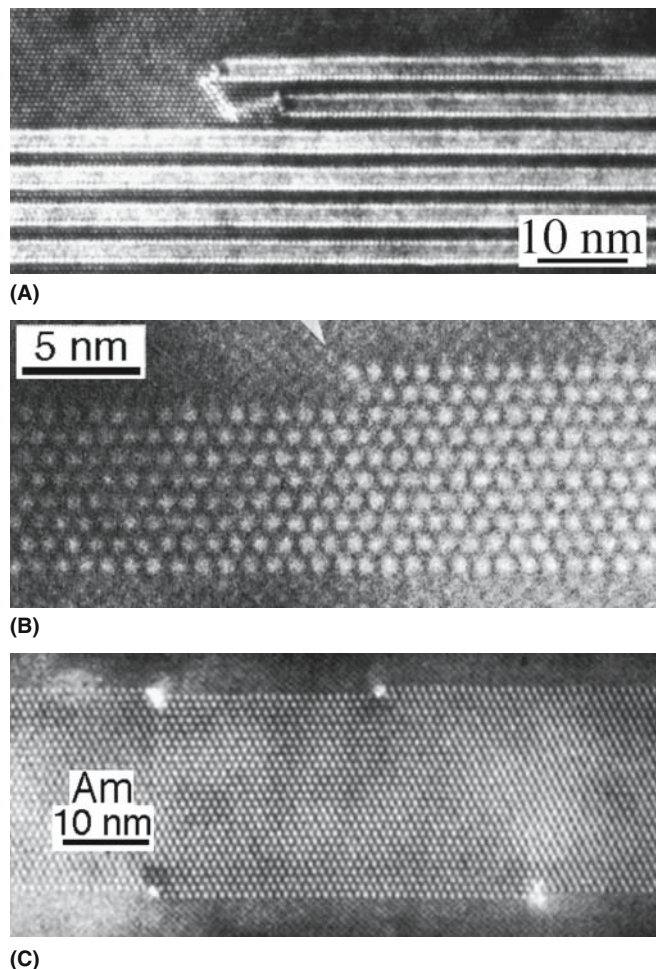


FIGURE 25.17 Chemical reactions by movement of steps on in interface. a) $\beta\text{-Al}_2\text{O}_3$ growing in spinel; (b,c) amphibole growing in orthopyroxene.

small along one plane, thus creating a low-energy interface. This situation is not unique as shown in Figure 25.17b. The result of such a reaction is the formation of particles that appear to be very large in one direction: the particle may be large in two directions—hence a platelet. Isolated steps move across the larger surface. Incidentally, always remember that most observations of such phenomena are made at room temperature.

25.14 THIN-FILM REACTIONS

Understanding how phase boundaries in oxides move is essential for a comprehensive understanding of solid-state reactions between ceramic oxides. The factors that determine the mobility of a phase boundary may involve the usual aspects of structure, bonding, and chemistry. Because thin-film reactions can be carried out at low temperatures, the morphology of the interface can easily be “frozen in.” Grain boundaries and other defects can affect the rate of a reaction in several ways. They can act as short-circuit paths to allow more rapid diffusion of reactants, or simply act as nucleation sites for the growth of a new structure. Evidence for both of these mechanisms was found in the study of the reduction of Fe-doped Al_2O_3 . It has also been shown that grain boundaries are a necessary product of the growth of spinel into alumina.

By combining TEM and field emission gun (FEG)-SEM we find that the formation of spinel occurs more quickly along GBs in thin-film reaction couples as illustrated in Figure 25.18. At the earliest stages of these reactions, the kinetics are controlled by the interface mobility rather than by diffusion through the reactant.

Thin-film reaction couples can be prepared by growing thin films on a specially prepared substrate; PLD works well for the deposition but molecular beam epitaxy (MBE) and chemical vapor deposition (CVD) could be used equally well.

This geometry offers many advantages over bulk samples.

- The reaction temperatures can be much lower than with bulk reaction couples.
- The cooling rate can be very rapid.
- We control the microstructure, crystallography, and morphology of the substrate.
- We can study the same interface before and after the reaction.
- We can thus directly study the role played by steps on the surface of the substrates and grain boundaries in the thin films.
- We can use a combination of materials or a graded reactant.

MISFIT AND SPINEL FORMATION

When NiO and Al_2O_3 react, the lattice misfit at the initial NiO/ Al_2O_3 interface (when perfectly aligned) is shared almost equally between the NiO/ NiAl_2O_4 and the NiAl_2O_4 / Al_2O_3 interfaces. However, when NiO and Fe_2O_3 react, the misfit at the NiO/ NiFe_2O_4 interface is close to zero so that nearly all the misfit is accommodated at the NiFe_2O_4 / Fe_2O_3 interface.

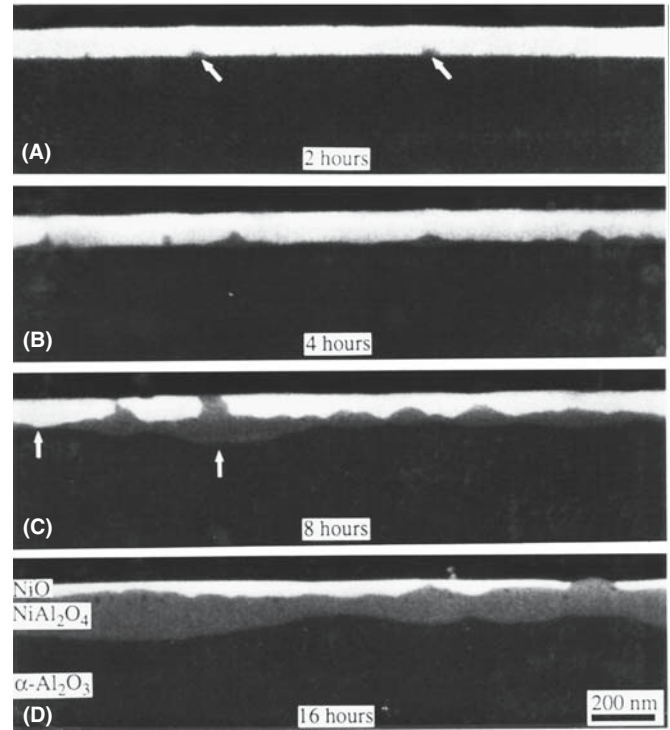


FIGURE 25.18 SEM images of reactions at GBs in thin films of NiO deposited on (0001) Al_2O_3 .

- We can grow material M_1 on a single crystal of material M_2 , or vice versa, and thus predetermine the location of grain boundaries.
- We can control the oxidation state of the reactants.

This approach overcomes the difficulty encountered using classical bulk diffusion: we know that there is intimate contact between the substrate and the thin film. If the materials are not in direct contact, the earliest stages of the reaction will likely involve a vapor-phase component.

The key feature is always that phase boundaries move during solid-state reactions. Defects and grain boundaries influence both the mechanisms and the rates of solid-state reactions, but with bulk reactants you do not know where to start. The volume probably changes during

the reaction.

When the epilayer contains grain boundaries, the thin-film approach allows us to examine how the nucleation rate depends on the type of grain boundary (misorientation, grain-boundary plane, etc.) intersecting the phase boundary. The growth of the product will depend on the nucleation site.

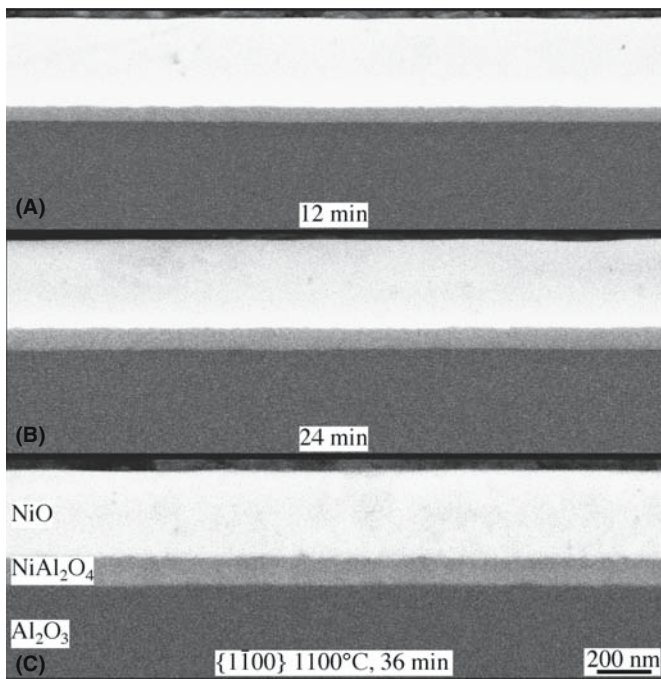


FIGURE 25.19 SEM images of growth of spinel between thin films of NiO and (0001) Al₂O₃ when an initial buffer layer of spinel is present.

If, as is often drawn schematically, a continuous reaction layer forms, then the volume change may be accommodated by an expansion normal to this layer (analogous to the tetragonal distortion in semiconductor multilayers). If the reaction occurs initially along the triple junction where a grain boundary meets the substrate, the constraints are very different. The thin film can become extensively deformed in accommodating this volume change. There is, for example, an ~7% volume expansion when NiO reacts with Al₂O₃ to form the spinel.

Two types of reaction sample are illustrated in Figures 25.18 and 25.19. In the first, the reactant material is grown directly on the substrate so as to examine the *nucleation* of the reaction product and to quantify the role of grain boundaries in the polycrystalline material. We can easily reverse the layer/

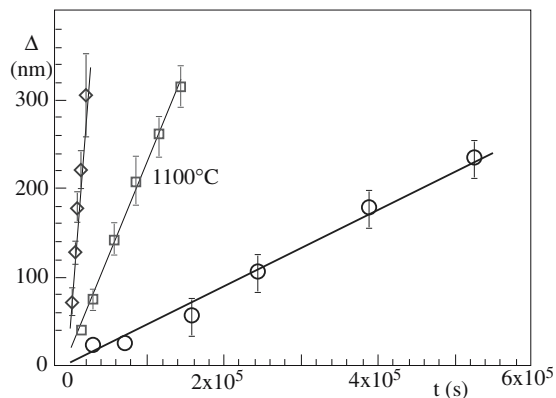


FIGURE 25.20 Kinetics of reactions between thin films of NiO deposited on (0001) Al₂O₃ when an initial buffer layer of spinel is present.

substrate geometry to examine the role of grain boundaries in the two materials separately.

In the second type of sample a **buffer layer** of the reaction product or a **reaction-barrier layer** is grown before growing the reactant layer. This geometry allows us to quantify the *kinetics of the reaction* separately from the nucleation. We can then examine the morphological development of the two moving interfaces and the effect of lattice misfit on this morphology. The expansion that occurs when the spinel forms can be readily accommodated if a buffer layer is present forming a uniform layer

as you can see in Figure 25.19. In this case, the kinetics can be deduced directly as shown in Figure 25.20. Notice that t and Δ are much smaller than in Figure 25.13 and that the kinetics are linear. At the early stages of the reaction, the rate is determined by the interface.

This reaction geometry can be extended to a situation in which there are several reaction products as illustrated for the Al₂O₃/Y₂O₃ system in Figure 25.21. Finally we should note that reactions often take place more easily at surfaces since there is no volume constraint.

A special thin-film reaction (though it becomes more general as it proceeds) is the corrosion of a ceramic by a metal or another ceramic. Phase

DIFFUSION COUPLES

The diffusion couple (approximately 1 mm thick) is placed between two Pt electrodes with the thin film in contact with the cathode and the bulk MgO substrate in contact with the anode as illustrated in Figure 25.23a. The reaction takes place in air with a voltage of -10 V applied across the sample. T depends on the material, ~1350°C for In₂O₃/MgO but as low as 700°C for Fe₂O₃/MgO. A second diffusion couple, without the applied field, is placed with the thin film down on a piece of Pt foil to ensure similar reaction conditions. The two samples are kept close together to ensure they are reacted at the same temperature.

GROWING AIN IN AN ELECTRIC FIELD

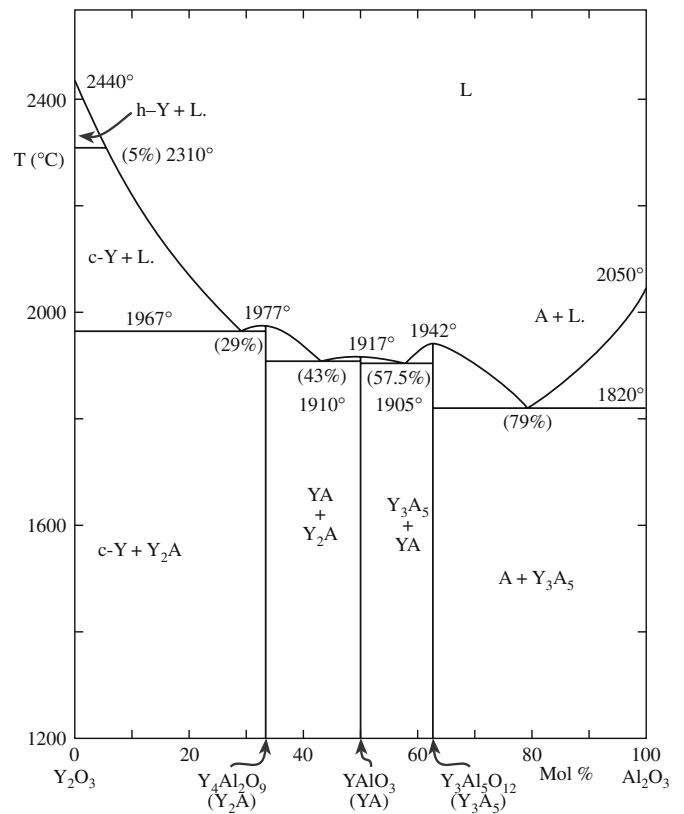
Place a single-crystal of α -Al₂O₃ between two Pt electrodes in an N₂-rich environment. The Pt electrodes act as chemically inert conductors with a high melting temperature. We have to scratch the Pt electrodes with an abrasive to roughen the surface and thus allow the nitrogen to reach the entire surface of the Al₂O₃. If N₂ transport across the surface is inadequate, the Al³⁺ cations arriving at this surface would either evaporate or form an alloy with the Pt electrodes. After the furnace is evacuated to 10⁻⁶ torr and heated to remove excess water, backfill with a 5% H₂/95% N₂ gas mixture and react.



(A)



(B)



(C)

FIGURE 25.21 Forming YAG by a thin-film reaction: (a) intermediate state; (b) final state for the same film; (c) the equilibrium phase diagram.

boundaries form during the corrosion process just as they do when a metal oxidizes or when an oxide is reduced; the only special feature is that the action takes place close to the surface, so there are fewer constraints. Figure 25.22 illustrates the PB formed when K_2O vapor corrodes (reacts with) alumina. The DP shows that the two phases are topotactically aligned.

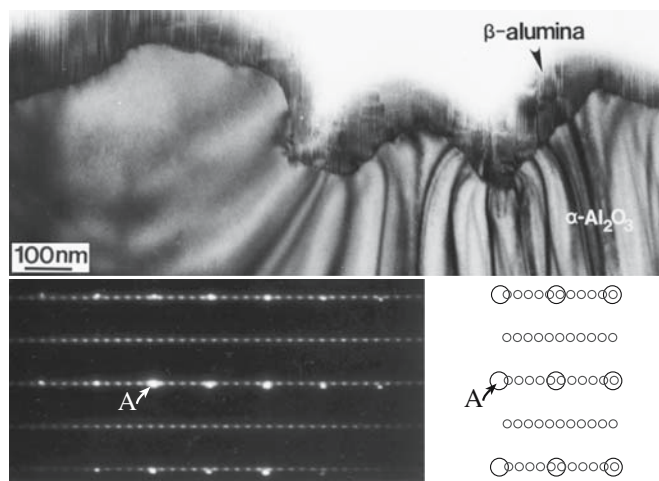


FIGURE 25.22 Corrosion of Al_2O_3 by reaction with K_2O vapor showing a TEM image, the DP, and a schematic of the DP.

25.15 REACTIONS IN AN ELECTRIC FIELD

Diffusion in ionic materials occurs primarily by the movement of charged species. Therefore, the application of an electric field can provide a very powerful driving force for mass transport. There have been numerous studies on the effects of electric fields on transport phenomena. Several studies have been performed on the evaporation of alkali halides in the presence of an external field. These investigations showed that the application of an electric field enhanced the evaporation of the crystal species. Similar studies have been performed on oxide ionic conductors, including ZrO_2 and β -aluminas. However, only a few experiments have been performed on classical insulating oxides such as α - Al_2O_3 and MgO (perhaps because they are insulators).

Polycrystalline diffusion couples can be studied in a similar way. Results show an increased transport and consequently an increase in the growth of the reaction product. However, the polycrystalline nature of the compacts makes it difficult to separate the influence of grain boundary diffusion and bulk diffusion.

This thin-film geometry can also help us understand how an electric field affects heterogeneous solid-state reactions and transport phenomena. The spinel-forming

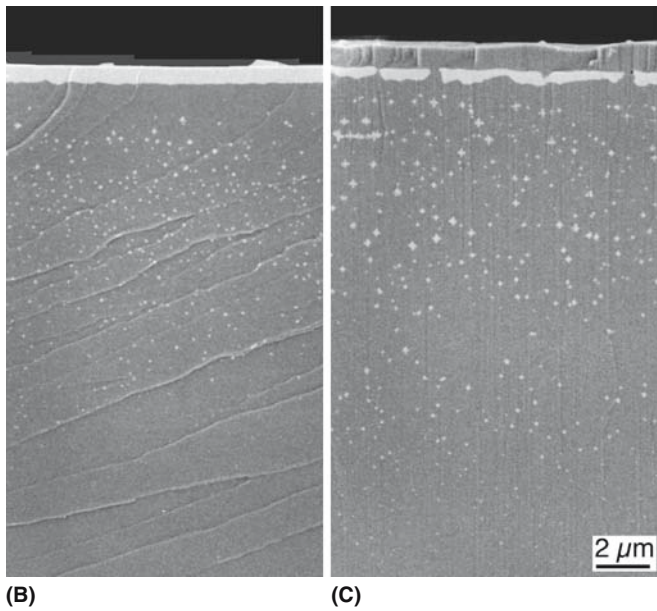
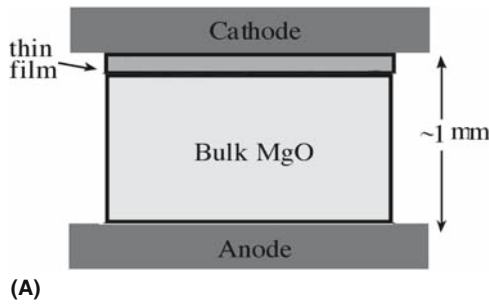


FIGURE 25.23 Reaction between a thin film of Fe_2O_3 and a layer of MgO in an electric field at 1150°C for 2 hours: (a) schematic of the set up; (b) no applied field; (c) 2 kV/cm applied field. The MgO has grown on top of the spinel. The reaction is fastest at GBs in the thin film.

reaction between MgO and Fe_2O_3 deposited on thin single-crystal films of iron oxide on $\{001\}$ MgO using PLD is shown in Figure 25.23a. The diffusion couples are then reacted at elevated temperatures under an applied electric field. The electric field can increase mass transport in the bulk and can change the resulting microstructure and the interface topology as shown in Figure 25.23b and c. The controlled nature of the experiment and the simple reaction geometry allow the transport phenomena and reactions to be examined directly. We can study the reaction with NiO instead of MgO with the electronic contribution to the process removed by including layers of ZrO_2 next to the Pt electrode.

We can grow thin films of AlN on sapphire by applying an electric field to a sample heated in a nitrogen-rich atmosphere with an extremely low oxygen partial pres-

sure. By applying an electric field with an appropriate electrode material, at elevated temperatures, across Al_2O_3 , a flux of Al^{3+} cations toward the cathode is induced. The cations arriving at the surface of the Al_2O_3 then react with a nitrogen gas atmosphere to form a thin epitaxial film of AlN on the Al_2O_3 . The hydrogen portion of the mixture serves to help reduce the oxygen activity in the gas atmosphere so that Al_2O_3 does not reform. Under the reaction conditions used for the formation of these films, it is estimated that the partial pressure of oxygen in the chamber is between 10^{-21} and 10^{-26} ! For a more accurate determination, we would need to know the amount of water vapor in the chamber. The gas mixture used for this study is critical: e.g., using 99.999% N_2 gas results in the formation of only Al_2O_3 (the oxygen activity is too high). The Al_2O_3 is reacted at, e.g., 1250°C for 2 hours. The properties of AlN make it an interesting material for applications in the microelectronics industry: it has a large bandgap, good thermal conductivity, high-temperature stability, and chemical inertness. Thin AlN films on basal Al_2O_3 substrates are used as buffer layers for the growth of GaN on alumina.

25.16 PHASE TRANSFORMATIONS INVOLVING GLASS

The crystallization of glass is so well established that it is responsible for the development of a whole class of materials known as glass-ceramics. There is therefore a large body of literature on this subject. When glass is present in a GB, there is an additional constraint on the crystallization since a second “nucleating” interface is present. For example, it is possible that a glass that will crystallize on

a free surface may not do so in a GB due to the competition between the two “seed” grains. There is a growing number of studies of the crystallization of glass in different systems, but few relationships between the new crystals and the crystalline grains have been reported. Much

of the work on this topic has been carried out on commercially available material where other elements may be present in the glass.

Glass can dissolve crystal. The kinetics of dissolving crystalline sapphire in a $\text{CaO-Al}_2\text{O}_3\text{-SiO}_2$ melt are shown in Figure 25.24. We see parabolic kinetics—it is a diffusion-controlled reaction. Glass can penetrate polycrystalline compacts and dissolve or redistribute the crystalline phase. In the case of polycrystalline MgO , further heat treatment caused the glass to crystallize as monticellite. A particularly interesting observation in this study was that the impurities, which were present in the sintered

NUCLEATING AGENTS

Different types are used to promote the process of crystallization.

The Pt group and noble metals: concentration $\sim 0.05\%$

Fluorides (e.g., Na_2AlF_6 or Na_2SiF_6): concentration 2–4%

TiO_2 : concentration 2–21 wt%

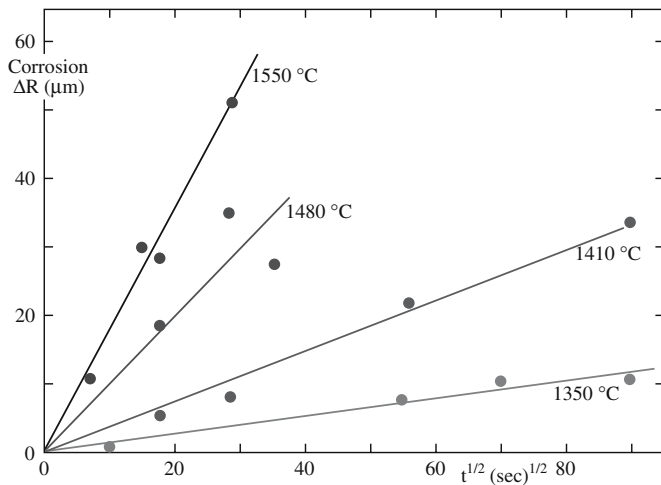


FIGURE 25.24 Dissolution of sapphire in a CaO–Al₂O₃–SiO₂ silicate melt.

MgO (primarily ZrO₂: a grain-growth inhibitor), were swept into the residual glass regions between the crystalline monticellite grains (known as the snow-ploughing process).

Glass can crystallize. Glass-ceramic materials are produced by the controlled crystallization of appropriate glasses. The glass-ceramic typically consists of 95–98 vol% of very small crystals, generally <1 μm in size, with the residual glass phase making up the rest of the pore-free material. When these materials are fabricated, the required shape is produced using conventional glass-forming techniques. To obtain small crystals of uniform size in the glassy matrix, a uniform density of nuclei of the order of 10¹²–10¹⁵ cm⁻³ is required. Selected nucleating agents are added to the batch during the melting operation and a controlled heat treatment is performed.

The role of the different nucleating agents and the mechanism that leads to a subsequent volume crystallization are not yet entirely clear. For the metals, the solubility decreases as *T* in the glass melt decreases and small metallic particles precipitate out. In the case of oxide nucleating agents, the crystallization process appears to take place by an induced phase separation (demixing) followed by crystallization. (We considered phase separation of glasses in Section 21.11). For a TiO₂-nucleated Li₂O–Al₂O₃–SiO₂ glass-ceramic, the nucleation involves a phase separation on a scale of ~5 nm followed by the formation of a crystalline TiO₂-rich nucleating phase.

As a result of carefully controlled thermal treatment, the initial glass is converted into a polycrystalline material in which the final properties depend on the nature of the precipitated phases, the final degree of crystallinity, the size of the crystallites, etc. The material is generally opaque, although translucent and even transparent glass-ceramics have been produced. The small size of the grains and the absence of porosity are characteristics of glass-ceramics. These result in excellent mechanical properties. This is explained in part by the action of the microcrystal-

lites, which limit the propagation of flaws. (See also the discussion in Section 21.11, including the mention of devitrite.)

25.17 POTTERY

The phase transformations that take place in pottery and glazes on pottery have not been studied as extensively as the model NiO/Al₂O₃ reaction in part because the processes are complex and perhaps because they are not the basis of high-tech applications. The glazes are usually silica based with high concentrations of dopants to lower *T_g* or produce other special properties. The best example of a phase transformation in a glaze is the crystallization glaze discussed in Section 21.12. What happens when we heat clay therefore depends on the clay, which depends on where you are since most clay firing is local. The topic is enormous and varied. When we glaze the pot, the formation and behavior of the different glazes depend not only on the composition of the glaze but also on the firing temperature and environment.

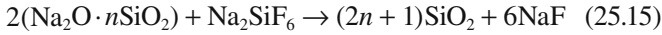
25.18 CEMENT

Cement is not only an extremely important ceramic but is also a very complex one. One factor in this complexity results from the importance of hydration reactions. Cements are, by definition, powder ceramics that react with a liquid (usually, though not necessarily, water) to undergo a chemical reaction to form a solid structure. A cement paste is the suspension of this powder in a liquid phase. Some cement pastes require the presence of air or CO₂ to harden, while others can harden under water. Pozzolanic cements are Si- or Al-based powders that can react with water providing Ca(OH)₂ is also present. The situation can be further confused by the presence of non-reactive constituents that are added to change the rheology of the mixture. The rheological properties change as the fresh cement hardens. This setting process is thus quite like the solidification of glass, but it takes place at ambient temperature and involves a change in structure. (So, it is completely different.) The two fundamental (do not say basic, since the basicity of CaO is an important factor here) reactions with CO₂ and H₂O are illustrated by these simple equations.



The water content can vary producing different hydrate phases. If sulfur is present (in gypsum) the reaction becomes more complex and leads to the formation of the mineral ettringite, Ca₆Al₂(SO₄)₃(OH)₁₂·26H₂O, during the hydration of Portland cement.

In an alkali silica cement, we see a new setting/hardening reaction with quartz becoming a factor.



We have mentioned cement terminology in Chapter 2: C is CaO, S is SiO₂, and A is Al₂O₃. CA is the main constituent in calcium aluminate cement (referred to as CAC). In high-alumina cement (HAC), the Al₂O₃ content ranges from 40% to 80%; it contains some C₂S but no C₃S. Its value is that it sets much more quickly than Portland cement.

For reasons that are obvious, pores are an important component in concrete and are the main flaw in the material. This is unfortunate in a material primarily needed for its strength.

Not all cement is based on CS_x or CA_x. A group of cements known as glass ionomer cements (GICs) is used as cements in dentistry. The reaction involves an ion-leachable alumina-silicate glass and an aqueous solution of polyalkenoic acid. The resulting cement consists of glass particles in a polysalt matrix. This is a specialty topic with far-reaching applications.

25.19 REACTIONS INVOLVING A GAS PHASE

The gas phase becomes important when a vapor is either intentionally used in a reaction or is created during a reaction, as is the case in the decomposition of a product. The problem is illustrated by the carbonate reaction shown in Figure 25.25; many ceramics are processed from their

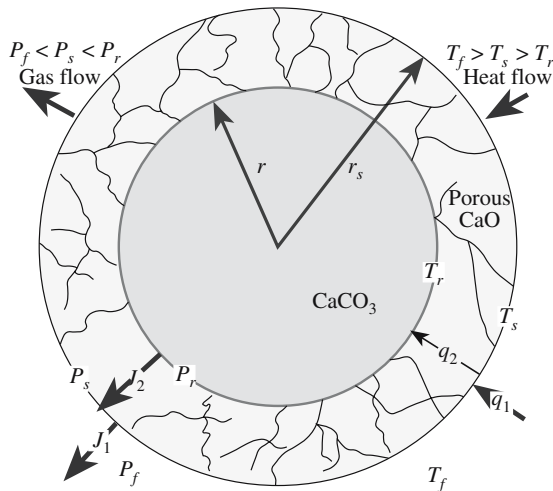
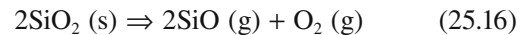


FIGURE 25.25 Schematic of the processes involved in decomposing a carbonate.

salts rather than from the oxides themselves. As the CaCO₃ decomposes to form the oxide, emitting CO₂, heat moves into the core of the particle and CO₂ move outward. The result is the formation of another reaction layer, which further slows down decomposition. Of course, in this case we can expect the CaO to be porous so that the CO₂ can evolve quite easily.

When SiO₂ dissociates, the situation is not so simple. This reaction is important not just because

SiO₂ itself is important, but also because SiO₂ is present in glass, furnace bricks, and alumina furnace tubes.



At 1320°C we can write the reaction coefficient in terms of the partial pressures.

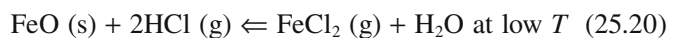
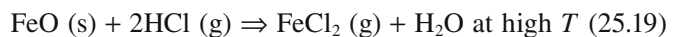
$$K_{\text{eq}} = \frac{(P_{\text{SiO}})^2 p_{\text{O}_2}}{(a_{\text{SiO}_2})^2} = 10^{-25} \quad (25.17)$$

Assuming the concentration of SiO₂ is unity (it is the principal component), we can express P_{SiO} in terms of the oxygen partial pressure. [We are using pO₂ (as is conventional) to represent the partial pressure of O₂ but P_x to represent the partial pressure of X—to keep the notation clear!]

$$P_{\text{SiO}} = \frac{K_{\text{eq}}^{1/2}}{p_{\text{O}_2}^{1/2}} \quad (25.18)$$

This equation indicates that the oxygen partial pressure controls the vaporization of the silica. For example, if the pO₂ is 10⁻¹⁸ atm (a reasonable value in a reducing atmosphere of H₂ or CO), then the P_{SiO} will be ~3 × 10⁻⁴, which is quite high, so the SiO₂ evaporates. Hence SiO₂ would not be a good refractory in a dry reducing atmosphere. The effect can be minimized by adding a small amount of H₂O if H₂ is present.

A similar situation arises when an oxide is reacted in a chloride gas. This reaction is actually used in growth of thin films by vapor transport.



The reaction of the active gas with the ceramic increases the vapor transport. What we are actually doing is controlling the chemical potential (concentration) of the reaction

gases and hence controlling the rate of deposition. We can apply Fick's law:

$$\frac{dn}{dt} = -AD \frac{\partial c}{\partial x} = -AD \frac{\Delta c}{L} = -AD \frac{c_h - c_c}{L} \quad (25.21)$$

With some manipulation we can express the concentration difference as a pressure difference and see that the diffusion from hot (h) to cold (c) is driven by the concentration gradient and the direction of the reaction is just due to the enthalpy of the reaction. At equilibrium we can write an expression for ΔG .

$$\Delta G_h = -RT \ln \left(\frac{P_{\text{FeCl}_2} P_{\text{H}_2\text{O}}}{P_{\text{HCl}}} \right) \quad (25.22)$$

In a closed system, the initial amount of HCl is B atm. Then two molecules of HCl gives one molecule of FeCl_2 and one molecule of H_2O .

$$P_{\text{HCl}} = B - 2P_{\text{FeCl}_2} + P_{\text{H}_2\text{O}} = P_{\text{FeCl}_2} \quad (25.23)$$

and

$$\Delta G_{h,c}^0 = -RT \ln \left[\frac{P_{\text{FeCl}_2}^2}{(B - 2P_{\text{FeCl}_2})^2} \right] \quad (25.24)$$

25.20 CURVED INTERFACES

The equation given by Thompson and Freundlich (the Thompson–Freundlich equation) relates the concentration in equilibrium with a curved surface to that in equilibrium with an infinite flat surface.

$$RF \ln \left(\frac{c_a}{c_{pi}} \right) = \frac{2E}{a} \frac{M}{\rho} \quad (25.25)$$

Here c_a is the concentration at the curved interface, c_{pi} is the concentration at the planar interface, M is the molecular weight, E is the interfacial energy, and ρ is the density. Thus the concentration in equilibrium for a curved surface differs from that for a flat surface. This result is not due just to the reduction of surface area. This phenomenon is known as the Gibbs–Thompson effect.

CHAPTER SUMMARY

The key idea for solid-state reactions and phase transformations is that they occur by the movement of interfaces no matter what phase is involved. A phase transformation can occur by one interface moving, but even if a reaction starts at one interface, we will have two interfaces as soon as a reaction product forms. When either a solid-state reaction or a phase transformation occurs, the system is not in equilibrium and the equilibrium phase diagrams can serve only as a guide to what the final product will be. Diffusion of point defects is an essential feature in solid-state reactions, but understanding the kinetics of these processes is not necessarily straightforward because the diffusion coefficients change as the composition of the phase changes (the Darken equation). The situation can be even more complex if the structure of the reaction product is also new and if misfit dislocations form at the phase boundary. The use of slip casting to explain the physical basis of parabolic reaction kinetics is extremely instructive and builds on a real ceramic process. Like slip casting; many phase transformations in ceramics involve the transfer of water or a gas phase; the setting of cement and the corrosion of TBCs are two such examples.

PEOPLE IN HISTORY

Schmalzried, Hermann (1932–) is an exception to the rule. Formerly a postdoc with Carl Wagner, Hermann has been a mentor and inspiration to many of the current generation of researchers in the field of solid-state reactions in ceramic systems and is profusely thanked by the authors.

Wagner, Carl was born May 25, 1901 in Leipzig and died December 10, 1977 in Göttingen. He wrote the seminal text with Schottky and laid the foundations for understanding corrosion and reactions between oxides.

GENERAL REFERENCES

Christian, J.W. (2002) *The Theory of Transformations in Metals and Alloys* (Part I + II), 3rd edition (Hardcover), Elsevier, UK. 1216 pages written by the expert: not easy reading.

Porter, D.A. and Easterling, K.E. (1992) *Phase Transformations in Metals and Alloys*, 2nd edition, CRC Press, New York. Although written for metallic systems, this text is at just the right level and is still the standard.

Schmalzried, H. (1981) *Solid State Reactions*, 2nd edition, Verlag Chemie, Weinheim, Germany and (1995) *Kinetics of Reactions*, VCH (now Wiley-VCH), Weinheim, Germany. Two texts by the master. Very condensed!

SPECIFIC REFERENCES

- Butman, M.F., Smirnov, A.A., Kudin, L.S., and Munir, Z.A. (2000) "Determination of the sign of the intrinsic surface charge in alkali halides from ionic sublimation measurements," *Surf. Sci.* **458**, 106. Using an electric field to study ion vaporization.
- Clarke, D.R. and Levi, C.G. (2003) "Materials design for the next generation of thermal barrier coatings," *Annu. Rev. Mater. Res.* **33**, 383. Discusses the background to Figure 25.3.
- He, T. and Becker, K.D. (1997) "Optical in-situ study of a reacting spinel crystal," *Solid State Ionics* **101–103**, 337. Studying solid-state reactions by weighing the products.
- Johnson, M.T., Schmalzried, H., and Carter, C.B. (1997) "The effect of an applied electric field on a heterogeneous solid-state reaction," *Solid State Ionics* **101–103**, 1327.
- Odler, I. (2000) *Special Inorganic Cements*, E&FN Spon, London. A very helpful resource.
- Smith, D.C. (1998) "Development of glass-ionomer cement systems." *Biomaterials* **19**, 467.

EXERCISES

- 25.1 Two cubes (400 μm long on each side) of NiO and Al_2O_3 are reacted at 1600°C. Assuming that the reaction takes place without significant movement of electrons or oxygen and that a reaction layer is produced that is 100 μm thick, what are the respective thicknesses of the remaining NiO and Al_2O_3 ?
- 25.2 Given the densities of some of the polymorphs of SiO_2 , should it be possible to convert β -cristobalite to some of the other forms by applying pressure? Briefly explain the reasoning behind your answer and indicate to which of the four forms, if any, the transformation might occur.
- 25.3 Calcium carbonate (CaCO_3) exists in two polymorphic forms, calcite and aragonite. The standard state enthalpy of calcite is -1207.37 kJ/mol , while that of aragonite is -1207.74 kJ/mol . The entropies of aragonite and calcite under the same conditions are $88 \text{ J mol}^{-1} \text{ K}^{-1}$ and $91.7 \text{ J mol}^{-1} \text{ K}^{-1}$, respectively. What is the stable polymorph at 25°C and 1 atm? Is there a temperature above which the other polymorph would be the equilibrium phase? If so, what is that T ? If not, why not?
- 25.4 You want to prepare a sample of mullite by reacting alumina and silica powders. If the activation energy is 210 kJ/mol and the reaction is 10% complete at 1400°C, how long will it take to convert 50% to mullite at 1400°C and at 1500°C? How will you determine that 50% has indeed been converted?
- 25.5 You place two perfect crystals of alumina and magnesia in contact with flat (0001) and (111) surfaces in contact. What orientation will you choose to produce the fast reaction when you heat these to 1400°C for 1 hour? You make the assumption that oxygen does not move during this heat treatment, but this cannot be strictly true. Explain.
- 25.6 You react two samples of alumina and magnesia at 1400°C for 1 hour. This time the MgO is a perfect single crystal but the alumina is 100-nm grain size polycrystalline material. Will the reaction proceed more quickly or more slowly on average?
- 25.7 Explain the geometry of the precipitates in Figure 25.5 and the defects they contain.
- 25.8 Consider Figure 25.13. What can you determine about the activation energies involved and the diffusion processes.
- 25.9 Consider Figure 25.21. How do you explain the experimental observations in the images in view of the phase diagram and other factors you know about these materials?
- 25.10 Consider Figure 25.24. What can you determine about the energies involved in this reaction?

Processing Glass and Glass-Ceramics

CHAPTER PREVIEW

Glass has changed the world more than any other material. In Chapter 21 we described some of the different types of glass and their properties. In this chapter we will look at the main methods used to fabricate glass products. In terms of the volume of glass that is produced each year, glass processing could be said to be the most important processing method for ceramics. The largest segments of the market are

- Flat glass for windows
- Containers (including bottles, jars, and tableware)

These products are formed using essentially two methods [one is recent (in glass terms) the other has its roots in antiquity]:

- The float glass process
- Blowing

We will also look at some processes that are used to modify glass for specific uses such as the application of thin-film coatings for solar radiation control and tempering and laminating for safety glass. In the last section of this chapter we will examine how glass-ceramics are produced.

This chapter does not cover the processing of some special glass products. For example, the processing of optical fibers is described in Chapter 32, but we introduce the important ideas here. Optical fibers must meet stringent quality requirements. We must understand these requirements to understand why the elaborate processing methods are necessary.

This chapter covers three closely related topics:

- Processing as dictated by applications
- Shaping
- Treating

26.1 THE MARKET FOR GLASS AND GLASS PRODUCTS

More than half of the total worldwide ceramics market is glass products, accounting for over \$50 billion/year. Figure 26.1 shows the distribution of glass sales. The market for manufactured glass products emphasizes three main types of glass:

- Hollow glass (bottles, drinking glasses, lamp bulbs, glass containers) 35%
- Flat glass (mirrors, windows) 30%
- Fiberglass (includes glass fiber) 17%

Hollow glass includes most of the container glass and tableware we use (i.e., consumer glassware). Table 26.1 lists examples of the applications for these product categories.

26.2 PROCESSING BULK GLASSES

Glass production starts with a mixture of raw materials, which for glass manufacture often contain a high proportion of naturally occurring minerals (for example, sand and limestone). However, some industrial chemicals such as sodium carbonate (Na_2CO_3) and alumina (Al_2O_3) are also used. The mixture containing the raw materials in the

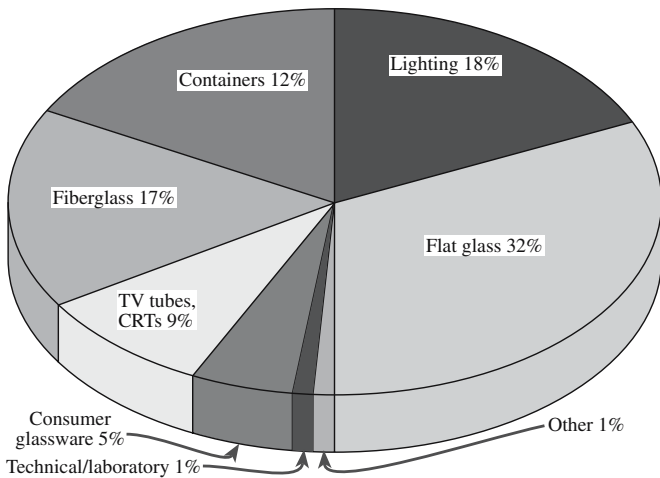


FIGURE 26.1 Percent distribution of glass sales; total: \$48,260 million.

TABLE 26.1 Glass Product Types and Applications

Glass product type	Applications
Flat glass	Automotive: cars and trucks Architectural: commercial buildings, storefronts Residential: windows, doors, sunrooms, skylights Patterned glass: shower doors, privacy glass Blanks for microscopes and telescopes
Containers/tableware	Beverage Liquor, beer, wine Food Pharmaceutical, drugs Glasses, plates, cups, bowls, serving dishes
Fiberglass and glass fiber	Wool: insulation, filters Textile: plastic or rubber tire reinforcements, fabrics, roof shingle and roll goods reinforcement
Specialty glass	Optical communications Artware, stained glass, lead and lead crystal, lighting TV picture tubes and flat-panel displays, ovenware and stovetop Ophthalmics, aviation, tubing, foamed glass, marbles

appropriate amounts is known as the *batch*. The batch contains a mixture of glass formers, modifiers, and intermediates; the amount of each component depends on the application of the final glass product. In Table 26.2 we link the different ways of giving a batch composition and the sources of some of the raw materials.

FLAT GLASS RAW MATERIALS

- Limestone, CaCO_3
- Silica sand, SiO_2
- Soda ash, Na_2CO_3
- Alumina hydrate, $\text{Al}_2\text{O}_3 \cdot 3\text{H}_2\text{O}$
- Burnt dolomite, $\text{CaO} \cdot \text{MgO}$

Batch melting depends on the source of energy, the refractory used to contain the glass, details of the batch,

processes occurring during melting, and fining (see Section 26.3).

We must also consider the possibility of oxidation and/or reduction of the glass, homogenization processes, and defect in the glass.

By far the greatest amount of flat glass is soda-lime silicate glass. You must be familiar with the terminology used in the glassmaking industry: soda is sodium oxide (Na_2O) and lime is calcium oxide (CaO), so soda-lime silicate glass consists mainly of Na_2O , CaO , and SiO_2 . Glass manufacturers often use the common names for these oxides, which are not always the generally recognized scientific name. If you are unsure of the composition of a particular mineral then you need to look at its formula.

All manufacturers of flat glass use basically the same formula, but they never actually use the compounds Na_2O or CaO . Values of the components are usually given in weight percent (wt%). Typical values are 72 wt% SiO_2 , 14 wt% Na_2O , wt% CaO , 4 wt% MgO , and 1 wt% Al_2O_3 . The molecular formula for a glass of this composition can be calculated as follows.

Step 1: Divide the wt% of each component in the batch by its molecular weight.

Oxide	wt (g)	Molecular weight (g/mol)	wt%/molecular weight (mol)	Ratio
SiO_2	72	60.1	1.20	120
Na_2O	14	62.0	0.23	23
CaO	9	56.1	0.16	16
MgO	4	40.3	0.10	10
Al_2O_3	1	102.1	0.01	1

Step 2: Divide each ratio by the smallest ratio in column 4. This gives the number in column 5.

Step 3: Write out the molecular formula for the glass. The molecular formula of our flat glass is then $\text{Al}_2\text{O}_3 \cdot 10\text{MgO} \cdot 16\text{CaO} \cdot 23\text{Na}_2\text{O} \cdot 120\text{SiO}_2$.

To make the batch it would not be economical to use only synthesized or pure ingredients. For most glasses a large proportion of the batch is made up of naturally occurring minerals that have been through a beneficiation process. Table 26.3 (top) shows the typical batch constituents used to make the $\text{Al}_2\text{O}_3 \cdot 10\text{MgO} \cdot 16\text{CaO} \cdot 23\text{Na}_2\text{O} \cdot 120\text{SiO}_2$ glass. To determine how much of the raw material

we need to add to the batch to obtain the desired amount of oxide in the final glass, we need to know the fraction of that oxide in the raw material. For the principal raw materials used in glass making this fraction is given in column 5 in Table 26.2. For example, during melting limestone will decompose as follows:

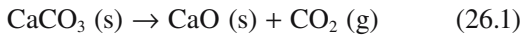
TABLE 26.2 Principal Raw Materials Used in Glassmaking

<i>Material</i>	<i>Alternative name</i>	<i>Theoretical formula</i>	<i>Oxides</i>	<i>Fraction</i>	<i>Batch</i>	<i>Purpose</i>
Alumina	Calcined alumina	Al ₂ O ₃	Al ₂ O ₃	1.000	1.000	
Aluminum hyd.	Hydrated alumina	Al ₂ O ₃ · 3H ₂ O	Al ₂ O ₃	0.654	1.531	
Aplite (typical composition)	—	—	Al ₂ O ₃	0.240	4.167	Source of Al ₂ O ₃
	—	—	Na ₂ (K ₂)O	0.100	—	
	—	—	SiO ₂	0.600	—	
	—	—	CaO	0.060	—	
Feldspar	Microcline (composition of commercial spar)	K ₂ O · Al ₂ O ₃ · 6SiO ₂	Al ₂ O ₃	0.180	5.556	Source of Al ₂ O ₃
			K ₂ (Na ₂)O	0.130	—	
			SiO ₂	0.680	—	
Nepheline syenite (typical composition)	—	—	Al ₂ O ₃	0.250	4.000	Source of Al ₂ O ₃
	—	—	Na ₂ (K ₂)O	0.150	—	
	—	—	SiO ₂	0.600	—	
Calumite	Calcium-aluminum silicate	2CaO · MgO · 2SiO ₂ 2CaO · Al ₂ O ₃ · SiO ₂ 2(CaO · SiO ₂)	SiO ₂	0.380		
			Al ₂ O ₃	0.117		
			CaO	0.400		
			MgO	0.080		
Kyanite (90% concentrate)	—	Al ₂ O ₃ · SiO ₂	Al ₂ O ₃	0.567	1.763	
	—	—	SiO ₂	0.433	—	
Kaolin	China clay	Al ₂ O ₃ · 2SiO ₂ · 2H ₂ O	Al ₂ O ₃	0.395	2.57	
			SiO ₂	0.465	—	
Cryolite	Kryolith	Na ₃ AlF ₆	—	—	—	Flux and opacifier in opal glasses
Antimony oxide	—	Sb ₂ O ₃	Sb ₂ O ₃	1.000	1.000	
Arsenious oxide	White arsenic	As ₂ O ₅	As ₂ O ₅	1.160	0.860	Fining and decolorizing
Barium carbonate	—	BaCO ₃	BaO	0.777	1.288	Source of BaO
Barium oxide	Baryta	BaO	BaO	1.000	1.000	
Barium sulfate	Barytes	BaSO ₄	BaO	0.657	1.523	Flux and fining
Boric acid	Boracic acid	B ₂ O ₃ · 3H ₂ O	B ₂ O ₃	0.563	1.776	Source of B ₂ O ₃
Borax	—	Na ₂ O · 2B ₂ O ₃ · 10H ₂ O	B ₂ O ₃	0.365	2.738	Source of B ₂ O ₃
	—		Na ₂ O	0.163	6.135	
	Anhydrous borax (“Pyrobor”)		Na ₂ O · 2B ₂ O ₃	B ₂ O ₃	0.692	
	—	—	Na ₂ O	0.308	3.245	
Lime, burnt	Quick lime	CaO	CaO	1.000	1.000	
Lime, hydrated	Calcium hydrate	CaO · H ₂ O	CaO	0.757	1.322	
Limestone	Calcium carbonate	CaCO ₃	CaO	0.560	1.786	Source of CaO
Calcium carbonate	Whiting	CaCO ₃	CaO	0.560	1.786	Source of CaO
Lime, dolomitic	Burnt dolomite	CaO · MgO	CaO	0.582	1.720	Source of CaO and MgO
			MgO	0.418	2.390	
Dolomite	Raw limestone (dolomitic)	CaO · MgO · 2CO ₂	CaO	0.304	3.290	Source of CaO and MgO
			MgO	0.218	4.580	
Lime, hydrated, dolomitic	Finishing lime	CaO · MgO · 2H ₂ O	CaO	0.423	2.363	Source of CaO and MgO
			MgO	0.304	3.290	
Litharge	Lead oxide, yellow	PbO	PbO	1.000	1.000	
Red lead	Minium	Pb ₃ O ₄	PbO	0.977	1.024	Source of PbO
Bone ash	Calcium phosphate	3CaO · 2P ₂ O ₅ + xCaCO ₂	CaO	0.372	2.700	
			P ₂ O ₅	0.628	1.592	
Iron oxide, red	Rouge	Fe ₂ O ₃	Fe ₂ O ₃	1.000	1.000	Color
Potassium hydroxide	Caustic potash	KOH	K ₂ O	0.838	1.194	Source of K ₂ O
Potassium nitrate	Saltpeter	KNO ₃	K ₂ O	0.465	2.151	Source of K ₂ O
Potassium carbonate.	Calcined potash	K ₂ CO ₃	K ₂ O	0.681	1.469	Source of K ₂ O
Glassmaker’s potash	Potassium carbonate, hydrated	K ₂ CO ₃ · $\frac{3}{2}$ H ₂ O	K ₂ O	0.570	1.754	Source of K ₂ O
Sand	Glass sand, quartz	SiO ₂	SiO ₂	1.000	1.000	
Soda ash	Sodium carbonate compl.	Na ₂ CO ₃	Na ₂ O	0.585	1.709	Source of Na ₂ O
Sodium nitrate	Saltpeter chili	NaNO ₂	Na ₂ O	0.365	2.741	Oxidizing and fining
Salt cake	Sodium sulfate	Na ₂ SO ₄	Na ₂ O	0.437	2.290	Oxidizing and fining
Zinc oxide	—	ZnO	ZnO	1.000	1.000	

TABLE 26.3 Batch Composition and Sources in the United States

<i>Raw material</i>	<i>Oxides supplied</i>	<i>Fraction of oxide</i>	<i>Weight of oxide required (g)</i>	<i>Weight of raw material in batch (g)</i>
Limestone	CaO	0.560	90	61
Silica sand	SiO ₂	1.000	720	720
Soda ash	Na ₂ O	0.585	140	239
Alumina hydrate	Al ₂ O ₃	0.654	10	15
Burnt dolomite	CaO	0.582	90	96
	MgO	0.418	40	

<i>Source</i>	<i>U.S.A. location</i>
Silica sand	Bank sand Sandstone Jersey shore
Soda ash	Trona deposits Allegheny mountains Wyoming
Limestone	Dolomite All over, e.g., Alabama
Feldspars	In pegmatites North Carolina
B ₂ O ₃	Borax California



The fraction of CaO (molecular weight: 56.1 g/mol) in CaCO₃ (molecular weight: 100.1 g/mol) is 0.560, or 56%. Hence, for each kilogram of limestone added to the batch the melt will contain only 0.56 kg of CaO. So using the raw materials listed above, and by bearing in mind the fraction of each oxide provided by each mineral, we can determine the batch composition for a 1 kg melt of flat glass. These are the numbers given in Table 26.3 (top). Note that the lime comes from both burnt dolomite and limestone. A batch weighing 2t can be measured to an accuracy of 0.1%.

Table 26.3 (bottom) shows where we might actually have to go to obtain these raw materials. [If we are making bottles and jars the batch will likely contain cullet, recycled glass; see Section 37.7.]

After the batch has been thoroughly mixed, it is melted at high temperature to form a homogeneous liquid melt. For small-scale melting of glass the batch will be placed in a crucible. For glass-melting experiments in the laboratory it is common to use Pt, or a Pt alloy such as Pt-5% Au or Pt-20% Rh crucibles.

These crucibles are very expensive, but they can withstand high temperatures, they do not contaminate the glass melt, and they can be easily cleaned and reused. Other crucible materials, usually used for larger batch sizes, include silica, alumina, and mullite.

Large-scale industrial production of glass is carried out in continuous furnaces called tanks. Glass-melting tanks are the second largest industrial furnaces, the largest being the blast furnaces used in making iron and steel. Figure 26.2 shows the inside of a glass-melting tank and Figure 26.3 shows a schematic of a glass-melting tank for producing glass containers. The tanks are typically 10–40m long, 3–6 m wide, and 1–1.5 m deep and contain over 2kt of molten glass. (The largest glass-melting furnaces

are 100 m long and 13 m wide.) The furnace is constructed of alumina/zirconia refractories that can withstand the high temperature and corrosive environment of the melt (see Chapter 9). The life of a tank furnace is about 8 years.

With reference to Figure 26.3: The batch is loaded into the hopper (1). In industry, the batch-loading compartment is referred to as the “doghouse.” In region (3) the batch begins to melt. The surface temperature of the melt peaks in region (4). During the melting process it is important to control the homogeneity of the mixture and the oxidation state of the components. Region (5), the throat, divides the furnace into two parts—the melting end and the conditioning, or working, region to the right. In the working region the melt is cooled down to about 1300°C and the glass viscosity increases. The glass travels through narrow tunnels called the forehearth (7), where the temperature is further lowered to 1000–1100°C, and on to the forming

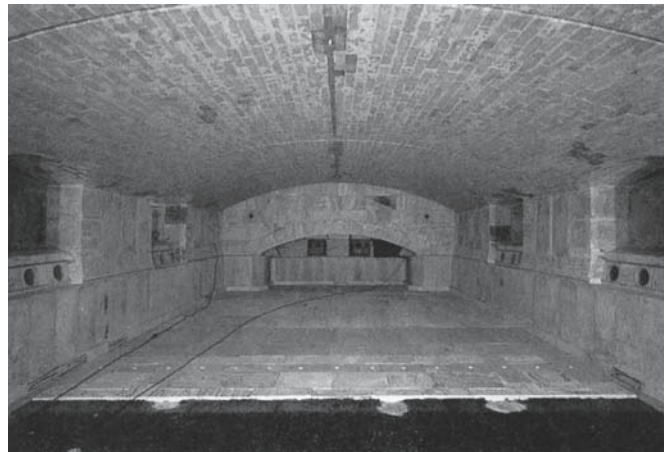


FIGURE 26.2 Inside a typical glass melting tank.

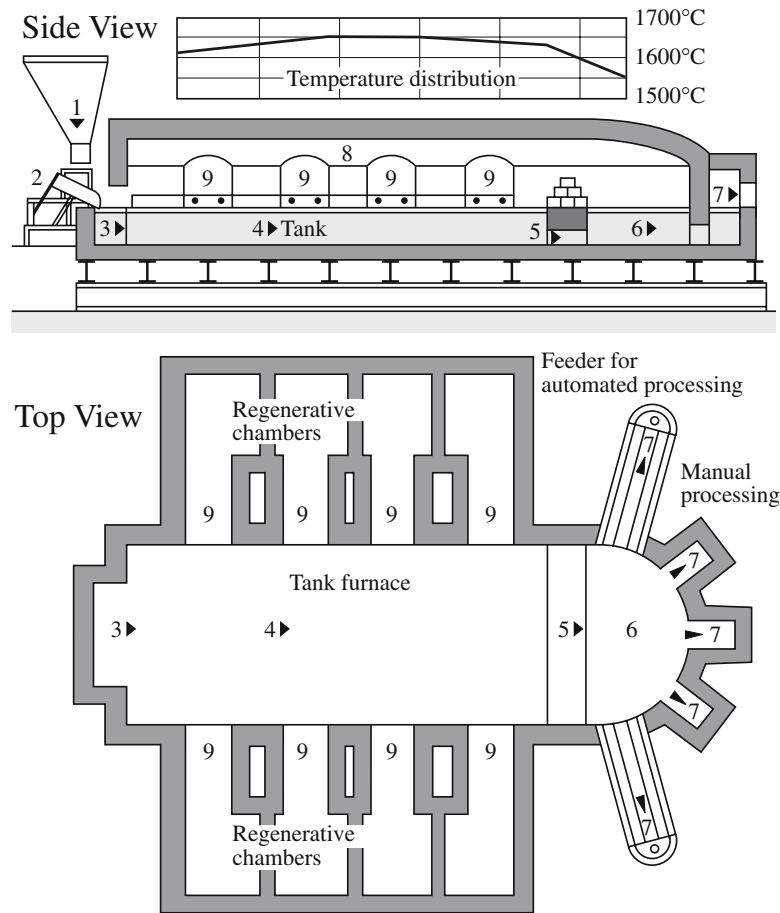


FIGURE 26.3 Schematics of a glass melting tank for producing containers.

machines. Depending upon the requirements of the forming machines, the glass may be delivered in the form of a continuous stream (as shown in Figure 26.4) or in discrete amounts, called gobs. The viscosity of glass at the

working point is 10^4 dPa-s (see Chapter 21). The regenerative chambers, region (9), are used to preheat the fuel gases and air to increase the combustion efficiency of the furnace.

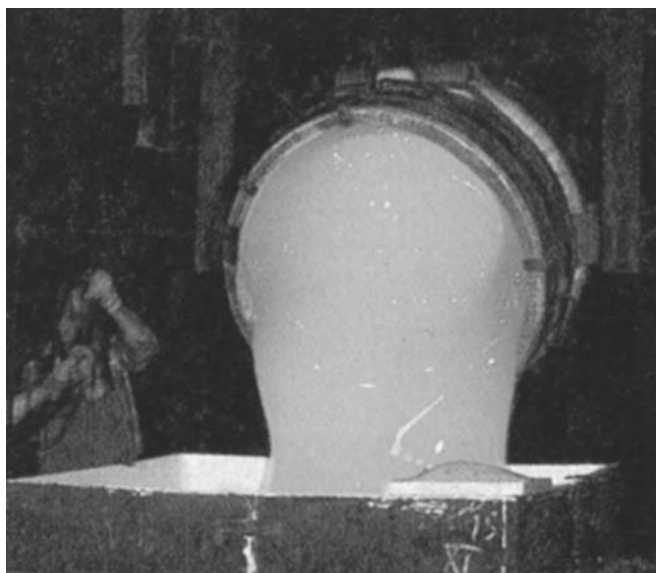


FIGURE 26.4 Pouring molten glass into a mold.

26.3 BUBBLES

The temperature required to form a glass melt varies with the composition of the batch. Typically melting temperatures are in the range 1300–1600°C. At this stage of the process the melt may contain many gas bubbles, mainly CO₂ and SO₂, from the dissociation of carbonates and sulfates. Bubbles also come from reactions between the glass melt and the refractories. Gas bubbles (which are known as seeds or blisters if the size is >0.5 mm) are usually undesirable in the final product because they affect its appearance. Bubbles are eliminated during melting by a process known as fining.

Fining can be achieved by increasing the temperature of the molten glass by about 150°C to reduce its viscosity. From Stokes' law (or by comparing the rise of bubbles in Cola versus liquid soap) we know that the drift velocity

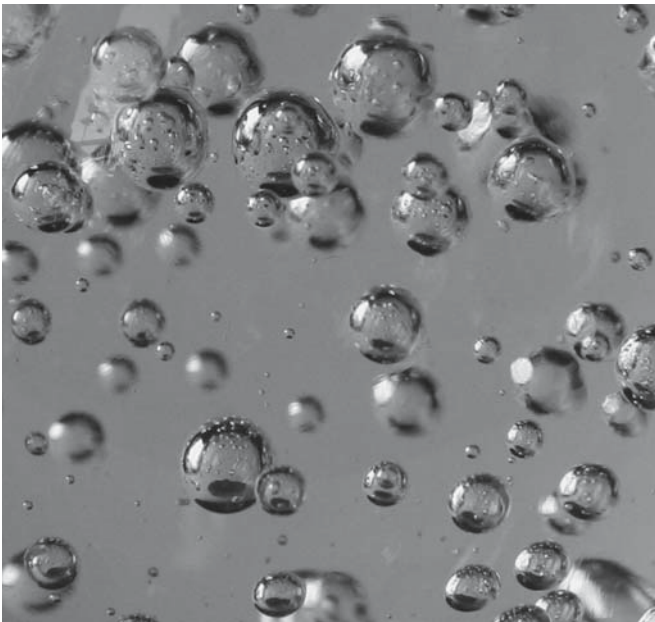


FIGURE 26.5 Example of a bubble deliberately blown in glass.

- Rolling
- Drawing
- The float process

The float process is so important to the glass industry that we will discuss it separately in the next section. In this section we will discuss the formation of flat glass by rolling and drawing. Figure 26.6 shows an example of a method for producing flat glass by rolling. The molten glass flows from the tank furnace over a refractory lip and between a set of water-cooled rollers where it solidifies into a continuous ribbon. The glass ribbon is transported over rollers into a tunnel-like annealing furnace (called a lehr in the glassmaking industry). Inside the lehr, the glass is first reheated to between 600 and 800°C. On the way through the lehr the temperature decreases slowly in a carefully controlled manner to minimize the development of internal stresses within the glass.

The glass thickness is controlled by a combination of factors:

- The rotational speed of the rollers
- Their spacing
- The glass pull rate

of the bubbles toward the surface of the melt is increased as the viscosity of the melt is decreased.

Fining is also traditionally achieved by adding fining agents, such as Na_2SO_4 or NaCl , to the melt at the end of the melting process. The fining agent decomposes as shown in Eq. 26.2 to produce a large quantity of gas bubbles, which coalesce with existing bubbles, increasing their volume and hence taking them to the surface faster.



Arsenic oxide, As_2O_3 , is another fining agent (giving a mixed-valence effect), but it is not so widely used today because it is toxic. The reaction involving arsenic oxide is a little more complicated than that shown for Na_2SO_4 , but the effect is the same. Fining will occur toward the end of region (4) in Figure 26.3. Modern systems will also use mechanical bubblers.

In some studio glass and tableware, bubbles are introduced intentionally as illustrated in Figure 26.5.

26.4 FLAT GLASS

Flat glass is not necessarily flat but is generally flatish! Historically, glass windows were not made in the way they are now. There are three basic methods for producing flat glass:

DEFECTS IN GLASS MELTS

Stones: opaque particles of rock or batch material embedded in the glass

Cords: thin string of inhomogeneity

Seed or blister: elongated bubble (~0.5 mm)

Typical pull rates are 0.5–5 m/min producing sheets 3–15 mm thick and up to 3.6 m wide.

A drawing process can also be used to produce flat glass. A solid metal plate is dipped into a bath of molten glass and then slowly withdrawn from the melt. This process would present no problems if we were interested in producing a glass rod (Figure 26.7). Producing a planar sheet is problematic because the sheet would neck down to a narrow ribbon. This difficulty is overcome by cooling the sheet as it is drawn; it is passed between two coolers as shown in Figure

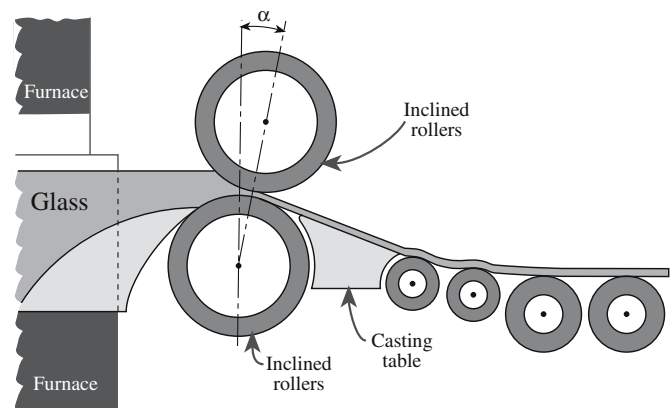


FIGURE 26.6 Continuous casting of flat glass.

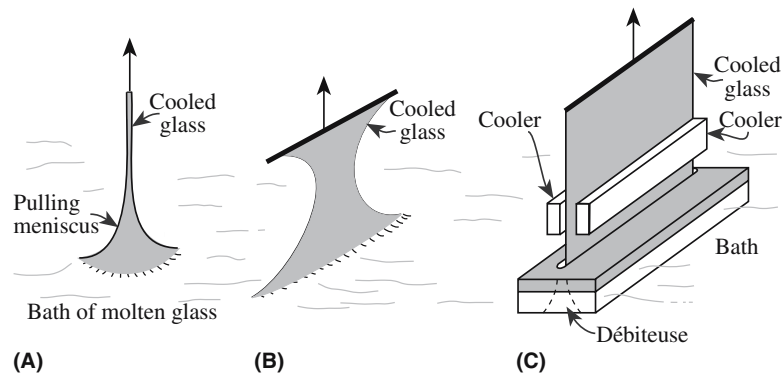


FIGURE 26.7 Principle of drawing from molten glass: (a) a circular rod; (b) problem of pulling a planar sheet; (c) use of a débiteuse and cooling to allow the formation of a sheet of constant width.

26.7c. These coolers solidify the glass and produce a sheet of fixed width. (We will see a similar process used in crystal growth in Section 29.6.)

There are several variations on the drawing process and these are illustrated schematically in Figure 26.8, which gives a different view of Figure 26.7.

In the Fourcault process the glass is drawn through a slot in a clay block (called the débiteuse or draw bar). The glass sheet is pulled upward through a system of steel rollers about 7 m high. The sheet at the mouth of the débiteuse is cooled at its edges in order to retain the width. As the glass travels upward it is annealed in a vertical lehr. After annealing and cooling the glass can then be cut into sections.

In the Pittsburgh process, the draw bar is completely submerged where it lowers the temperature of the glass below the meniscus. This modification allows increased drawing rates.

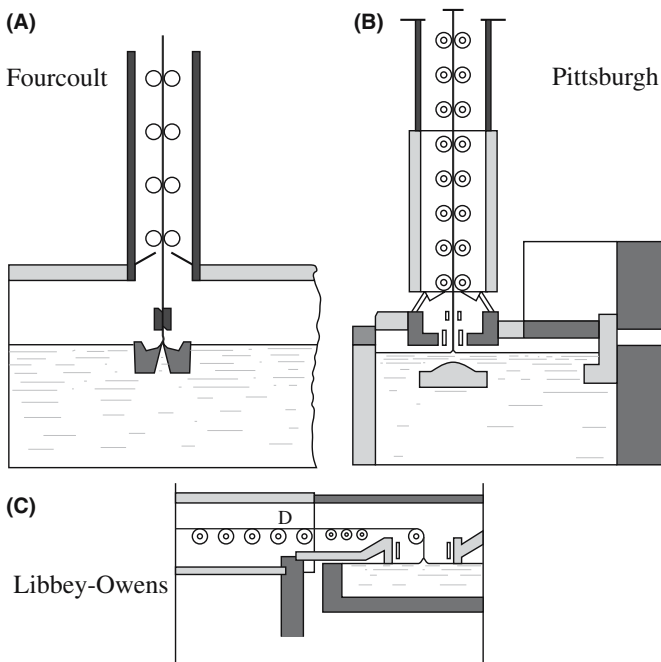


FIGURE 26.8 Drawing processes for window glass. (a) Fourcault, (b) Pittsburgh, and (c) Libbey-Owens.

In the Libbey–Owens or Colburn–Libbey–Owens process the drawn glass sheet is bent through 90°, ~1 m above the surface of the bath, on a polished chrome-nickel alloy roll; there is no débiteuse. The glass then travels into a horizontal lehr for annealing.

By the mid 1900s these three processes were responsible for the world’s entire production of flat glass, with 72% being made by the Fourcault process, 20% by the Colburn–Libbey–Owens process, and 8% by the Pittsburgh process. These processes have now been replaced almost entirely by the float process.

Plate glass is flat glass that has been ground and polished to produce two perfectly plane and parallel faces with a high quality optical finish. The surface of a flat glass sheet is flattened by grinding it between two cast-iron wheels with sand abrasive and water lubricant. As the grinding progresses, the particle size of the abrasive is decreased producing a very fine satin surface. The operation is completed by polishing the sheet with a suspension of iron oxide on felt pads; this abrasive is known as rouge because of its color (see Chapter 36). The processing of plate glass can be entirely mechanized with continuous simultaneous grinding and polishing on both faces. However, the float-glass process has almost entirely ended this older method of manufacturing plate glass. The quality of float-glass may not be quite as high as that of plate glass, but the cost is considerably lower because of the elimination of the mechanical grinding and polishing operations.

26.5 FLOAT-GLASS

The float process was developed in 1959 by Pilkington in the UK and revolutionized the flat-glass industry. It has been hailed as one of the major inventions on the twentieth century. Worldwide, there are only ~170 float-glass plants, but these have a combined output of 3000 miles of flat glass, 4–8 feet wide, each day. Annually these plants produce the equivalent of a ribbon of glass over one million miles long. Over 90% of the world’s window glass is produced using the float process.

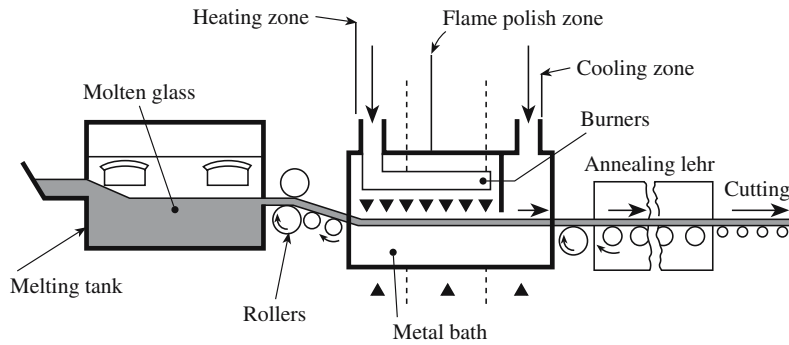


FIGURE 26.9 Schematic diagram of the float glass process.

A schematic of the float process is shown in Figure 26.9. Molten glass is fed from the furnace between two rollers onto a bath containing molten tin at about 1000°C (the melting temperature of tin is 232°C). The tin bath is 4–8 m wide and up to 60 m long. Equilibrium between gravitational forces and surface tension produces a sheet of uniform thickness. The equilibrium thickness, h_e , can be calculated using an equation derived by Langmuir:

$$h_e = \left\{ \frac{(\gamma_{Gv} + \gamma_{Gt} + \gamma_{tv})2\rho_t}{g\rho_G(\rho_t - \rho_G)} \right\}^{1/2} \quad (26.3)$$

There are three interfacial energy (γ) terms between the different phases glass (G), air (v), and tin (t); g is the acceleration due to gravity, which has a value of 9.806 m/s², ρ_G and ρ_t are the density of the glass and tin, respectively.

In practice, it is possible to produce glass thicknesses between about 2 mm and 20 mm using the float process, depending upon the glass viscosity and the drawing speed. At the exit, the temperature of the glass is decreased to ~600°C, at which point the tin is still fluid, but the glass can be removed in a “rigid” condition. The glass ribbon leaves the bath and enters the lehr for annealing. The glass leaves the lehr at ~200°C, is cooled to room temperature, and is cut to size. The main advantage of the float process is the production of planar glass sheets with a high optical quality—the planarity approaches that of plate glass without the need for polishing. Moreover, the output rate is 5–10 times higher than the drawing rate for window glass. About 25 t of finished glass can be produced per hour by the float process.

On the negative side, the equipment requires careful control of the atmosphere above the bath, which must be neutral or slightly reducing to avoid oxidation of the bath

and the maintenance of constant surface tension, which controls the thickness of the sheet. The atmosphere is approximately 90% N and 10% H. The hydrogen ensures that there is an oxygen-free environment: molten tin is easily oxidized. The glass can, itself, be affected adversely by the presence of oxygen, which can make the surface appear hazy. Purity and reliability are therefore critical factors in float-glass manufacture. Approximately 5 m³ of hydrogen is required for each ton of glass produced.

26.6 GLASSBLOWING

The classic glassblowing pipes are made from iron tubes about 100–150 cm in length with an opening about 1 cm in diameter. At one end the tube had a mouthpiece and at the

other end it has a button-like extension. The glassmaker gathers a gob of molten glass on one end then blows through the mouthpiece to form a hollow shape as demonstrated in Figure 26.10. This process was important historically because by blowing glass with a pipe it was possible not only to produce simple round shapes but also other thin-

walled objects. By blowing the glass into a wooden mold it became possible to produce items with a standard reproducible shape. The glassblowing pipe was also the first step in making flat glass. The glass was blown into a large cylindrical body, cut along its length, and “ironed” flat while it was still hot and soft. This is known as muffle glass and is still used today to make traditional stained glass.

Today the glassworker’s blowpipe is very similar to the original design and works in the same way. The original blowing technique is used now mainly for specialty glass applications such as glass ornaments and studio-art glass.

GLASS THICKNESS

It is instructive to estimate the value of h_e . A reasonable value for the glass/Sn interfacial energy is ~1 J/m², the surface free energy of molten tin is 0.68 J/m², the density of Sn is 7.5 g/cm³, the surface free energy of a molten soda-lime-silicate glass is 0.35 J/m², and the density for a silicate glass is 2.5 g/cm³, hence h_e is ~9 mm. This calculated value is actually slightly higher than the actual equilibrium thickness, ~7 mm. Remember that we are using only an estimate for the energy of the glass/Sn interface.



FIGURE 26.10 Demonstration of blowing glass into a mold. Note the worker's bench, the annealing burners, and the box of frit.

To produce hollow glassware for bottles and jars the original blowing technique has been mechanized. The process starts by forming a blank or preform (called a parison) by blowing into or pressing a gob of glass as illustrated in Figure 26.11. (The hole into the furnace is called the parison hole; traditionally, the glassblower would gather a glob, or gob, of glass on the blowpipe and roll it to make the parison.) After the initial shaping process, the parison is blown by compressed air to the final shape. With today's automated techniques, from parison to final product can take less than 10 seconds.

- The blow-and-blow process is used to make narrow-neck containers (Figure 26.11a).
- The press-and-blow process is used to make wide-mouth jars (Figure 26.11b).

Figure 26.12 shows the ribbon machine developed in 1926 by Corning for high-speed production of light bulbs. In this process a stream of molten glass is made into a ribbon by passing it through a pair of rollers. The ribbon

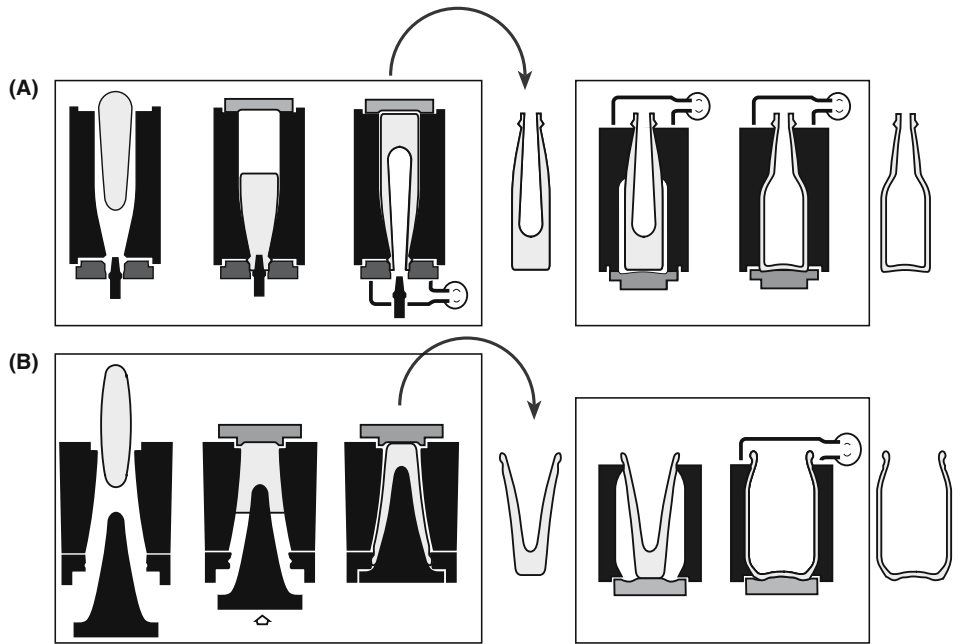


FIGURE 26.11 Automatic fabrication of hollow ware: (a) formation of the blank by blowing followed by blowing in a mold (blow and blow); (b) formation of the blank by pressing followed by blowing (press and blow).

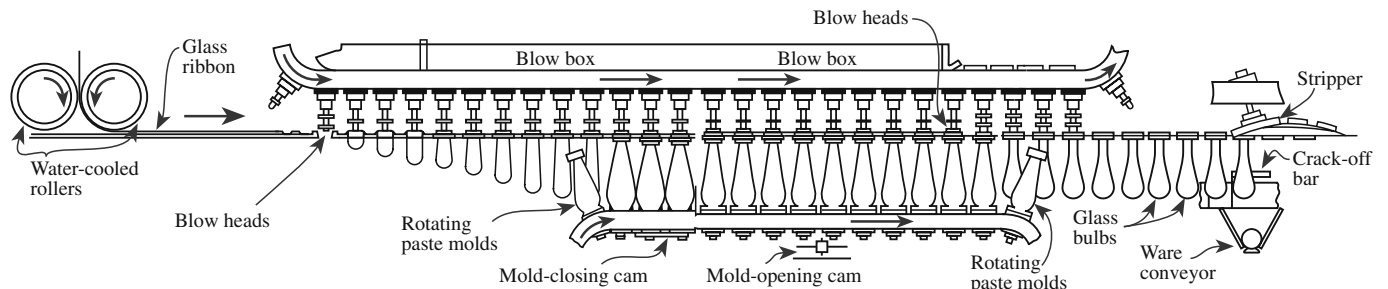


FIGURE 26.12 The Corning ribbon machine for glass lamp bulbs.

passes under a series of blowheads that are attached to a rotating turret (the blowhead turret). Air is puffed into the glass and the glass begins to take the form of a blown shell. The glass shell is then enveloped by a mold mounted on a rotating turret below the blowhead turret. The shells are blown to their final form while in the mold. The finished shells are cracked away from the ribbon, collected, and carried through the annealer. More than 50 light bulb shells (in single molds) can be made per second in one machine!

26.7 COATING GLASS

Coated glass also has a long history. Stained glass used in church windows has long used flashed glass, which is clear glass with a coating of a colored glass. Today we use many other types of coatings, but flashed glass is still used in the glass studio (see Section 26.14).

Normal window glass transmits between 75% and 90% of the incident radiation. We can apply thin coatings to the surface to alter the radiation and heat-transmission characteristics. In architectural applications, coatings on glass are used to reduce the amount of energy needed to heat buildings in the winter and cool them in the summer. One way to do this is by allowing the transmission of visible light while reducing the transmission of infrared (IR) radiation (heat). Such glass would reduce the amount of energy required to air condition a room in the summer.

One conventional way to reduce the transmission of heat is to add a component to the glass batch that strongly absorbs radiation in the IR region. When FeO is added to the glass formulation, the product strongly absorbs radiation in the 0.7–2.5 μm range. Since the absorption sharply increases above 0.6 μm , the transmitted visible light does have a noticeably green tint. But this can be corrected to a certain extent by adding other components (commonly Se and Co). A 6-mm-thick glass window that contains FeO may absorb ~50% of the total incident radiation but only ~25% of the radiation in the visible part of the electromagnetic spectrum.

Thin films are also used to control the light-transmission characteristics of window glass by reflecting a large amount of IR radiation.

Such films allow a higher retention of heat in a room during the winter, thus reducing the energy costs associated with heating. Normal flat glass can be coated with metallic or nonmetallic layers to maintain a high degree of visible light transmission combined with a considerable amount of heat reflection (40–60%). Thin (10–20 nm) metal films of Cu, Ag, and Au are all used commercially; each gives a very high reflec-

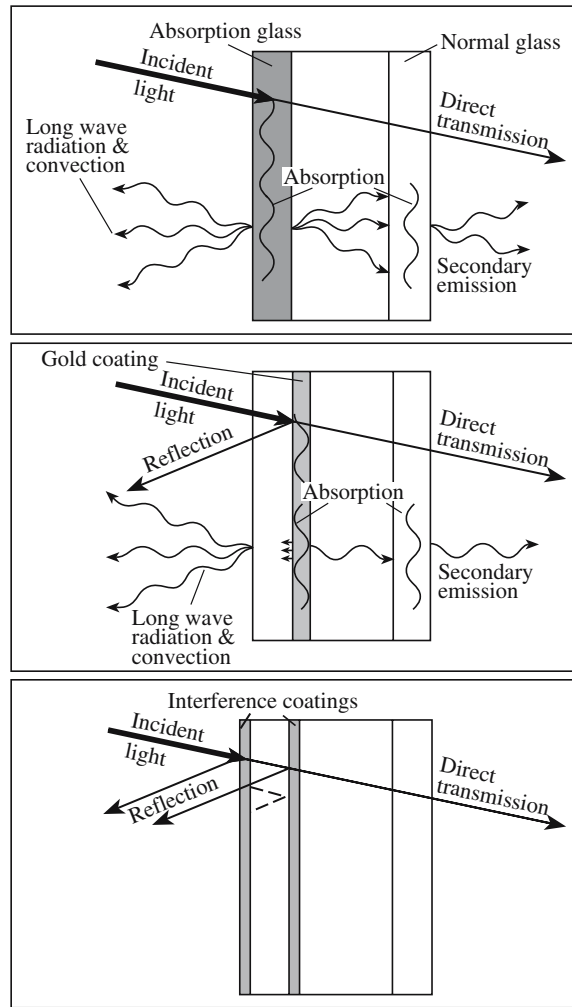


FIGURE 26.13 Illustration of approaches for solar protective double glazing with absorbing and reflecting panes.

tivity. The metal layer is deposited using physical vapor deposition (PVD) techniques such as evaporation and sputtering (see Chapter 28). Metal coatings can also be applied using dipping and spraying techniques, followed by firing to densify the coating (see Chapter 27).

Single-layer and multilayer coatings of oxides are also used to enhance reflectivity in the near IR. These coatings work because of optical interference effects and usually have a thickness about one-quarter of the wavelength of the radiation such that the primary wave reflected off the first interface is 180° out of phase with the secondary wave reflected from the second interface. The result is destructive interference of the two waves. Thin films of TiO_2 , Ti_3N_4 , CrN_x , and Zn_2SnO_4 are all used commercially for this application.

Figure 26.13 shows a schematic diagram summarizing the principles behind solar radiation control panels. For solar-

MULTILAYER COATING

An example of the effectiveness of a multilayer coating, which works on the interference principle, is the $\text{Sb}_2\text{S}_3/\text{CaF}_2$ superlattice. For 11 alternating layers of Sb_2S_3 ($n = 2.70$) and CaF_2 ($n = 1.28$), the reflectance is 0.9999 at $\lambda = 1 \mu\text{m}$.

protective double glazing, a coated glass pane is combined with an uncoated pane.

Radiation can also be modified using electrochromism. Electrochromism is the production of color by applying an electrical field. Electrochromic compounds such as WO_3 are coated on the glass using a variety of thin film techniques. The point defect reaction is reversible.



When a direct current (dc) voltage is applied, the optical absorption characteristics of the compound change. The gain/loss of color occurs by the inclusion/elimination of the M^+ ion. In this case, the M^+ ion can be H^+ , Li^+ , Na^+ , or Ag^+ . The absorption characteristics of electrochromic materials can thus be tailored for specific applications simply by adjusting the applied voltage.

26.8 SAFETY GLASS

Flat glass often breaks due to impact or to the application of a relatively low applied pressure. At most temperatures, the failure occurs in a brittle manner and results in the production of a number of sharp fragments, which, of course, can cause serious injury. Special treatment of the glass can make it less susceptible to breaking and can thus reduce the chance of injury. Hence the United States and many other countries require the use of safety glass in buildings and vehicles. There are two forms of safety glass:

- Tempered
- Laminated

Tempered glass (or toughened glass as it is also often called) is made by quickly heating flat glass to about 150°C above T_g . (Remember: the viscosity at the T_g is $\sim 10^{13}$ dPa·s.) For a soda-lime silicate glass $150 + T_g$ is $525\text{--}545^\circ\text{C}$. The glass is then blasted with cold air. The outside of the glass cools much more quickly than the inside. Hence the inside is still contracting after the surface has already solidified. The result is that the outer surface layer is subject to compression and the inside layer is subject to tension. This tempering process changes the behavior of the glass when it breaks. For example, when a sheet of tempered glass breaks, the fragments are small and almost regularly shaped with no sharp edges. The principle used in the tempering process is the same as

CRACKLE GLASS

Crackle glass has been produced for its artistic appearance for over 150 years (perhaps since the sixteenth century in Venice). The glass is heated to $\sim 1000^\circ\text{C}$ and then plunged into water causing cracks to form across the surface; if reheated and blown further the cracks heal on the interior; a similar effect is produced in glazes.

that used to make crackle glass: the internal stress at the surface is different from that in the bulk.

The other form of safety glass is laminated glass, which consists of two or more glass sheets (usually float glass) joined with a layer of an elastomeric polymer such as poly (vinyl butyral) (PVB). The glass layers are bonded to the polymer by a combination of pressure and heating. When laminated glass is broken, the broken pieces of glass are stuck to the polymer and the broken sheet remains transparent. Car windshields are laminated glass in which the two bonded sheets are both tempered glass. If a stone breaks the windshield when the car is moving, the polymer sheet holds the fragments of glass together so that they do not cause injury to the occupants of the car. The side and rear windows of an automobile are routinely made from tempered glass.

The front and rear windows of an automobile are often curved. The flat glass is shaped before the tempering process because the tempered condition would disappear at the bending temperature. One of the advantages of laminated glass over tempered glass is that laminated glass can be processed further; for example, it can be cut and drilled. Bulletproof glass is thick laminated glass (25–60 mm thick) consisting of at least four layers of glass laminated with an elastomeric polymer.

26.9 FOAM GLASS

Because we do not usually want glass to contain large numbers of bubbles, we reduce the number of bubbles in the glass melt using the fining process. The opposite approach is used to make foam glass: additional gases or gas-bearing materials are added to the melt producing a large quantity of bubbles.

One of the major applications of foam glass is in the manufacture of insulating panels for buildings. Insulating panels made from foam glass can be light, rigid, and good thermal insulators. As usual for porous materials, the thermal property is due to the low heat conductivity of the bubbles (i.e., pores).

- Foam glass is the porous ceramic of the glass world.
- Bubbles may be intentionally included in art glass.

26.10 SEALING GLASS

Special glasses have been developed that are used as the “glue” usually between another glass and a metal. The main challenge is engineering α while controlling

the chemistry and keeping the sealing temperature reasonable.

Borosilicate (alkaline earth/alumina) glass is used to seal glass to W (lighting applications).

Borosilicate (Na) glass is used to seal glass to Mo.

Borosilicate (K) glass, with a high concentration of B (20% B₂O₃), is used to bond to Kovar (Westinghouse's trade name for the Fe–Ni–Co magnetic alloy that has α close to that of the glass).

Pb glass is used if electrical insulation of a joint is critical.

26.11 ENAMEL

Ceramic enamel compositions are used for a wide variety of applications, including decorative coatings for glassware and china. In industry they are used in coating baths, stovetops, etc. They are used whenever a metal requires a coating that is more durable than paint. It is also used to form colored borders around glass sheets used as automotive windshields. The reason for the colored borders is to enhance the appearance and to decrease the degradation of the underlying adhesives by ultraviolet (UV) radiation. The enamel compositions consist of a glass frit (a powdered glass), a colorant, and an organic vehicle. The mixture is applied to the required part and then fired to burn off the organic vehicle and to fuse the enamel to the surface of the substrate.

In the art world, enameling is carried out using small furnaces and grams of powdered glass; in industry, square meters of surface can be enameled uniformly. The principle is the same, only the scale differs. A large piece like a cast-iron bath would be shot-blasted to clean it, coated with a ground coat that will bond to the Fe, dried, and heated to nearly 1000°C. It is then sprinkled with dry enamel frit while still hot and brought back to temperature. Five such coatings of enamel would be routine. The composition of the enamel must be chosen so that it is in compression after cooling. The composition would be modified on curved regions to maintain this compression.

Color is produced in ways similar to other glass. (We discussed color in glass in Section 21.8.) As recently as 1999, the French Consumer Safety Committee considered the safety of the use of UO₂ dye to make enamels for the preparation of jewelry and enameled tiles. Old yellow enamels contained up to 9% UO₂ and frits using nondepleted U are certainly more “radioactive” than those of today. The committee noted that having 50% Pb in the frit might help absorb the radiation, but this increased the toxicity of the frit powder! Safety in enameling is therefore always a concern because the technique uses powders.

26.12 PHOTOCROMIC GLASS

PHOTOSENSITIVE AND PHOTOCROMIC

Photosensitive: the glass is sensitive to light.

Photochromic: the color is changed by exposure to light.

Photosensitive glass is the glass analog of photographic film where Au or Ag atoms (as halide particles) are affected by the action of light. Such glass

is used in printing and image reproduction. Heat treating after exposure to light can cause a permanent change in the glass. Photochromic glass (discovered at Corning in the 1960s), darkens when exposed to light but then returns to its original clear state when the light is removed; hence it is used in sunglasses or other ophthalmic lenses. The light affects small (~5 nm or a little larger) AgCl_xBr_{1-x} crystals in the glass. To manufacture photochromic glass the glass must be heated to over 1400°C, shaped, and then annealed again at 550–700°C to allow the small halide crystals to form in the initially homogeneous glass. Large flat glasses are not generally affordable, but the new approach is to use sol-gel processing (Chapter 22) to form a photochromic layer on conventional preformed glass sheets.

The principle is that the near-UV radiation generates electron-hole pairs in the halide particles. The electrons are trapped by the interstitial Ag ions producing Ag colloids on the surface of the halide particle. The activation energy for this process is only 0.06 eV so the Ag ion moves easily in the halide; in addition, a small amount of Cu increases the effect by at least an order of magnitude. This is the same process used in photography and is explained by the same Gurney–Mott theory. The metal particles formed in the process are 1–5 nm in size, but because the halide must be >5 nm to show the effect the second annealing T is critical.

26.13 CERAMMING: CHANGING GLASS TO GLASS-CERAMICS

Worldwide sales of glass-ceramic products exceed \$500 million a year. The highest volume is in cookware and tableware consumer items (such as plates and bowls) and domestic ovens (stovetops and stove windows). In this section we will look at how these commercially important ceramics are processed.

Glass-ceramics are formed by controlled crystallization of a glass. They consist of a high density (maybe >95 vol%) of small crystals in a glass matrix. The important feature of the processing of glass-ceramics is that the crystallization must be controlled. As usual, crystallization occurs in two stages:

- First the crystals are nucleated.
- Then the crystals grow.

The rate at which these two processes occur is a function of temperature. We can control the nucleation process by

adding a nucleating agent (typically either TiO₂ or ZrO₂) to the glass batch.

Initially the glass batch is heated to form a homogeneous melt. The shape of the desired object is formed from the glass at the working point by the usual processes such as pressing, blowing, rolling, or casting. Remember, the viscosity of the glass is ~10⁴ dPa·s at the working point (like honey). After annealing to eliminate internal stresses, the glass object then undergoes a thermal treatment that converts it into a glass-ceramic. The first part of the heat treatment is nucleation. The optimum nucleation temperature generally corresponds to a glass viscosity of 10¹¹–10¹² dPa·s. During this step, which may last for several hours, an extremely high density (10¹²–10¹⁵/cm³) of nuclei forms. Following nucleation, *T* is increased to allow growth to occur. The crystal-growth step, like nucleation, may take several hours. The optimum temperature for crystal growth is selected to allow for the maximum development of the crystalline phase without viscous deformation of the object. Figure 26.14 shows the complete processing cycle for a glass-ceramic.

The glass-ceramic process uses the same rapid forming techniques employed in glassworking, permitting the economical production of objects with complex shapes or thin walls that are difficult or impossible to produce with other, more traditional, ceramic-forming techniques.

The most important and useful glass-ceramic system is the Li₂O–Al₂O₃–SiO₂ (LAS) family that was first developed at the Corning Company by Stookey. One commercial LAS glass-ceramic is Pyroceram®, which has β-spodumene (LiAl[Si₂O₆]; α = ~10⁻⁶/°C) as the major crystalline phase. The low α, together with excellent high temperature stability and insensitivity to thermal shock, means that these materials find applications as cookware, benchtops, hot-plate tops, ball bearings, and matrices for fiber-reinforced composites.

If the crystallization temperature is kept ≤900°C the crystalline phase that is formed in LAS glass-ceramics is

ION EXCHANGE

Glass can be strengthened by ion exchange in which small ions in the surface layer are replaced by larger ions, which put the surface into compression.

Step 1: Rapid exchange of Na⁺ or K⁺ with H⁺ or H₃O⁺ from solution:



This step is usually controlled by diffusion and exhibits *t*^{-1/2} dependence.

Step 2: Loss of soluble silica in the form of Si(OH)₄, resulting from breaking of Si–O–Si bonds and the formation of Si–OH (silanols) at the glass solution interface:



This stage is usually reaction controlled and exhibits *t*^{1.0} dependence.

Step 3: Condensation and repolymerization of an SiO₂-rich layer on the surface depleted of alkalis and alkaline-earth cations.

Step 4: Migration of Ca²⁺ and PO₄³⁻ groups to the surface through the SiO₂-rich layer forming a CaO–P₂O₅-rich film on top of the SiO₂-rich layer, followed by growth of the amorphous CaO–P₂O₅-rich film by incorporation of soluble calcium and phosphates from solution.

Step 5: Crystallization of the amorphous CaO–P₂O₅ film by incorporation of OH⁻, CO₃²⁻, or F⁻ anions from solution to form a mixed hydroxyl, carbonate, fluorapatite layer.

β-quartz. The β-quartz crystals are <0.1 μm in diameter. Crystal sizes below the wavelength of visible light (λ = 0.7–0.4 μm), a good match in refractive index between the glass and the crystal phase, coupled with a low birefringence result in high transparency. Table 26.4 lists the compositions and applications of some commercial transparent LAS glass-ceramics based on β-quartz.

Application 1: Machinable glass-ceramics are derived from the K₂O–MgO–Al₂O₃–SiO₂ system containing some fluorine. In Macor® the crystalline phase is potassium fluorophlogopite [KMg₃(AlSi₃O₁₀F₂)]. Phlogopite is a mica mineral and the plate-like mica crystals are randomly oriented in the glass phase as shown in Figure 18.23. Macor® can be machined to precise tolerances

(±0.01 mm) and into intricate shapes using conventional steel tools: they can be drilled, cut, or turned on a lathe.

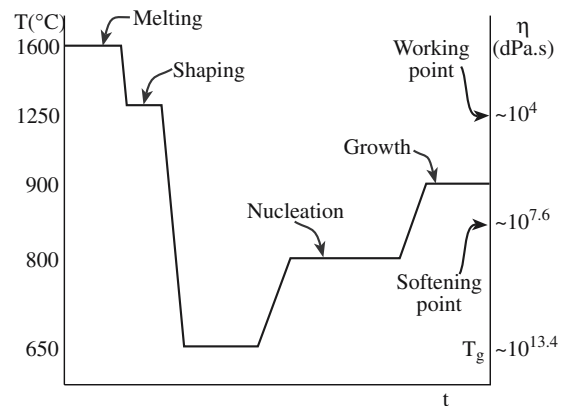


FIGURE 26.14 Processing cycle for a glass-ceramic.

TABLE 26.4 Base Compositions and Applications of Transparent Glass-Ceramics Based on Quartz Solid Solutions

Material	Composition, wt%														Commercial application
	SiO ₂	Al ₂ O ₃	MgO	Na ₂ O	K ₂ O	ZnO	Fe ₂ O ₃	Li ₂ O	BaO	P ₂ O ₅	F	TiO ₂	ZrO ₂	As ₂ O ₃	
Vision	68.8	19.2	1.8	0.2	0.1	1.0	0.1	2.7	0.8	—	—	2.7	1.8	0.8	Transparent cookware
Zerodur	55.5	25.3	1.0	0.5	—	1.4	0.03	3.7	—	7.9	—	2.3	1.9	0.5	Telescope mirrors
Ceran	63.4	22.7	u	0.7	u	1.3	u	3.3	2.2	u	u	2.7	1.5	u	Black infrared transmission cooktop
Narumi	65.1	22.6	0.5	0.6	0.3	—	0.03	4.2	—	1.2	0.1	2.0	2.3	1.1	Rangetops; stove windows

u = unknown

Application 2: Another commercial fluoromica glass-ceramic called Dicor[®] has been developed for dental restorations. Dicor has better chemical durability and translucency than Macor. It is based on the tetrasilic mica, $KMg_{2.5}Si_4O_{10}F_2$, which forms fine-grained (~1 μm) anisotropic flakes. Dicor dental restorations are very similar to natural teeth both in hardness and appearance. They are easy to cast using conventional dental laboratory methods and offer significant advantages over traditional metal–ceramic systems.

Application 3: Calcium phosphate, $Ca_3(PO_4)_2$, glasses can be made into glass-ceramics to form a material resembling the mineral part of bone. Since bone is porous, the first step is to produce a foam glass. This is achieved by decomposing carbonate in the glass melt. The foam glass simultaneously undergoes a controlled crystallization, transforming it into a porous glass-ceramic. The dimensions of the interconnections between the pores must be sufficient to allow the ingrowth of living bone tissue, which ensures a permanent joint with the surface of the prosthesis.

In principle, any glass can be converted to a glass-ceramic by finding a suitable nucleation agent and the appropriate heat treatment. In practice, a number of technical factors (among which is the production of the base glass) limit the choice.

We can use the phenomenon of photosensitivity to make a machinable glass! For example, we could use CorningWare ($Li_2O \cdot Al_2O_3 \cdot SiO_2$) as the starting material and then add <1 wt% Cu, Ag, or Au. The idea behind the technique is similar to the photochromic glass, but we then leach out the Li_2SiO_3 crystals to leave a high density of small voids in the glass.

1. Irradiate the glass with UV (Figure 26.15).
2. Anneal Au^0 agglomerates (small particles); nuclei for crystalline ceramic Li_2SiO_3 ($2SiO_2 \cdot Li_2O$).
3. Place the glass in dilute HF to dissolve the Li_2SiO_3 (dissolution is 10× faster than for the glass). This method can produce densities of 3.6×10^4 holes/square inch.

4. Reexpose the glass to UV (no mask) and anneal; all is then polycrystalline, e.g., with 0.001% Au, 0.001–0.03% AgCl, or 0.001–1.00% Cu_2O .

Before leaving the topic we should mention that this is not the only way to prepare glass-ceramics. Another group of these materials used for dentistry go by the label In-Ceram[®]. The material is prepared as a porous crystalline ceramic (alumina, spinel, and zirconia have all been used) and then infiltrated with an La-rich glass. The resulting glass-infiltrated ceramic can be quite translucent, can be colored to match other teeth, and is mechanically tough (for a ceramic). It can be coated with porcelains for improved appearance.

26.14 GLASS FOR ART AND SCULPTURE

Today, the glass art world is very active with more abstract pieces by Chihuly and others being hung in many public buildings (e.g., the Victoria and Albert Museum in London; Figure 26.16). Exhibitions travel round the United States and the world. The field is actually much wider than you might imagine.

The glass harp produces the “sound of the universe” according to Goethe. The musician Gluck gave an entire concert using the glass harp in London in 1746. Sound is

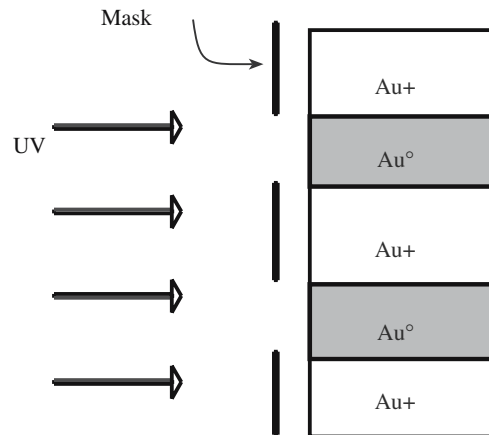


FIGURE 26.15 Process for making porous glass.

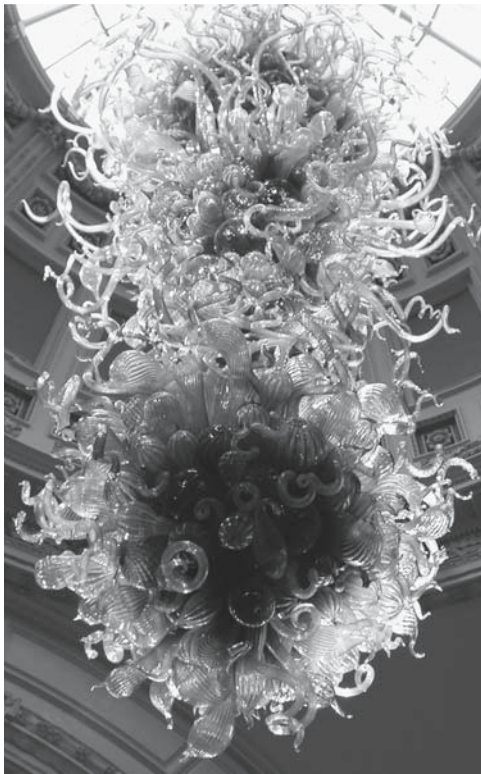


FIGURE 26.16 Chihuly installation at the Victoria and Albert Museum in London.

made when a wine glass “sings”: run your finger around the rim. The sound is thus produced by making the glass vibrate rather than by making the air in the container vibrate (like blowing over a bottle). Benjamin Franklin made a glass armonica (Mozart wrote music for the armonica): he placed glasses inside one another (not touching) and rotated them on a spindle to make playing easy! Galileo actually explained the resonance phenomenon in 1638. The tone will depend on the mechanical (elastic) properties of the glass.

Murano, a small island near the city of Venice, was the center of glass making for many years. The location was chosen to stop glassworkers from moving away from the vicinity of Venice. It is still famous for its art glass and the glass companies provide free boat taxis from the mainland to encourage customers. The millefiore insets seen in paperweights and glass sculptures, and illustrated in Figure 26.17, are usually associated with Murano. Actually, the technique had already been used in the first century CE.

Paté de verre is an art glass made by sintering pieces of glass, including powder, to make objects with distributions of color that would not be possible if the glass were melted. Essentially, the millefiore glass of Murano is made by this technique but now with larger “particles.” It is now being used by industry for the same purpose. The classical sintering technique for processing ceramic powders is thus being used to produce unique glass objects.

MARBLES

Marble King in Virginia makes 10⁶ marbles every day.

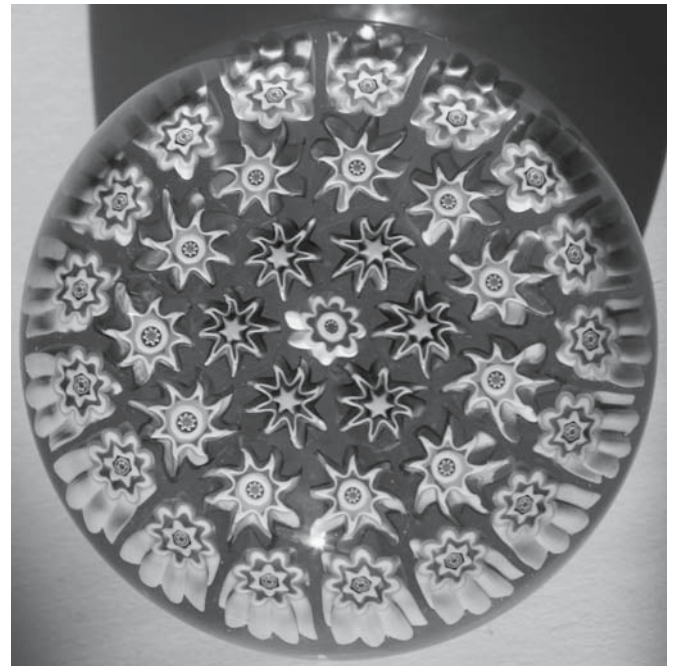


FIGURE 26.17 Millefiore paperweight showing the different glass canes used.

Art glass, usually in the form of figures and vases, became popular in the 1800s with Lalique, Gallé, Daum Frères, Tiffany, and others as illustrated in Figure 26.18.

Between 1886 and 1936, the father and son team of Leopold and Rudolph Blaschka produced the Harvard glass flowers (shown in Figure 26.19) for use in teaching botany (there are other collections, but this is the best known). Tiffany produced similar specimens for the



FIGURE 26.18 Small vase by Daum Frères.



FIGURE 26.19 Example of a Harvard flower.

art market. The idea is that the color of glass does not change with time and the flowers are three-dimensional. Actually, the Blaschkas used wire, paint (especially in the early years), varnish, and glue to enhance the models at the time. Thus they will not be quite as inert to the atmosphere as hoped, but they are superb examples of lampworking (heating a soda-rich glass and shaping it by pulling and pinching with various tools including tweezers).

In some countries, the best-known form of art glass is the stained-glass window (Figure 26.20). Since it was first



FIGURE 26.20 Example of drawing in stained glass.

developed in the early twelfth century stained glass has been made using several different techniques.

Pot-metal glass is bulk glass that has been colored by adding metal oxides in the usual way (Cu for red, Fe for green, Co for blue, etc.). Since the glass must be thick enough for the window, light transmission was often reduced (making the church dark).

Flash glass is produced by dipping a gob of clear glass into a pot of colored glass. When the glass is then blown, the two layers are thin. The colored layer remains only a fraction of the total thickness. If the glass were uniformly colored but not flashed, it would transmit too little light (old church windows make for dark interiors); if the glass were uniformly colored but thin so as not to decrease the light it would have insufficient mechanical strength. The layer can be abraded to produce variations in color on the one piece of glass. Details in the window images can be drawn on the glass using an iron oxide pigment. The drawing is then fired to incorporate it into the glass.

26.15 GLASS FOR SCIENCE AND ENGINEERING

Lenses have been made using glass since microscopes and telescopes were first invented. When visible light is used, this is still generally the case. For transmitted light, the challenge is usually to minimize absorption; some telescopes, such as that on Mount Palomar, use a very wide coated glass reflector. The critical factor is now not transmission but thermal expansion.

Stepper lenses are used in producing very large-scale integration (VLSI) chips using photolithography. The stepper lens is the opposite of an enlarging lens—it shrinks the circuit pattern and prints it onto the semiconductor surface. (The term stepper is used to denote the step-and-repeat exposure system.) In 1997 the line width was $0.25\ \mu\text{m}$; it is now around $60\ \text{nm}$. The challenge then is to focus light, which has a wavelength much larger than the required resolution.

The Hale Telescope is a 200-inch telescope that was built in ~1949 using a Pyrex blank manufactured by Corning Glass works. Schott Glass has since produced a telescope with a dish that is 8.2m wide; it is made from Zerodur®, Schott's glass ceramic, using a centrifugal casting process. An interesting link between art and science is the proposal by David Hockney that some of the masters used mirrors and lenses to help compose their paintings. Glass lenses range in size from the end of a fiber used in near-field scanning optical microscopy (NSOM) (see Chapter 10) to the Fresnel plate that was used in lighthouses.

Glass is one of our most important building materials. In 1851, the windows in the Crystal Palace used 300,000 panes, which accounted for 33% of England's annual production of glass. Biosphere 2 (built in the late 1980s) relies entirely on glass to separate the interior from Biosphere 1.

Glass fibers are used in textiles for clothing. The spacesuits used on the Apollo lunar missions were made from glass fiber industrial fabrics.

Glass microspheres are used, for example, in traffic signs and drug delivery. We will describe radiotherapy glasses used in the treatment of unoperable cancers in more detail in Chapter 35. The key process is forming uniform glass spheres. We will also discuss Bioglass in Chapter 35 but not ceramic cremation tiles for after-life applications.

FORMING MICROSPHERES

1. Glass melting
 - a. Select chemically pure raw materials (oxides) that do not contain any impurities that would form undesirable radioisotopes during neutron irradiation.
 - b. Mix the raw materials.
 - c. Melt the raw materials to form homogeneous glass.
2. Spheroidization (microsphere formation):
 - a. Crush the glass to particles of the desired size.
 - b. Inject particles into a gas-oxygen flame to melt each particle and form a solid glass sphere (flame spray powder).
 - c. Collect microspheres in a suitable container.
3. Sizing: screen or separate microspheres into desired size range.

Traffic signs and road marking tape contain spheres that are $\sim 200\mu\text{m}$ in diameter and act as microlenses.

In the Ballotini flame drawing process, glass powder is injected into a flame that draws it up a tower until it melts and forms spheres ($1\text{--}60\mu\text{m}$ diameter) dropping outside the flame and cooling under gravity. Filaments used to make the biprism for electron holography are made in the laboratory

using a variation on the same principle.

CHAPTER SUMMARY

The production of glass is a multibillion dollar industry. The widespread use of glass products has gone hand-in-hand with developments in glass processing. Arguably the most significant recent development was the float glass process, which allowed high-volume production of very high-quality glass sheets for architectural and transportation applications. Our city skylines certainly are influenced by the use of glass. More recent developments have led to improvements in the energy efficiency of buildings by controlling the transmission and absorption properties of glass. This is part of the “green” revolution in architecture.

Glass processing, which is an industry and art, has its own language. It is necessary to learn that language: in particular, frit, cullet, lehr, fining, gob, and ribbon. The processing terms are from engineering: floating, rolling, drawing, tempering, laminating, and ceramming.

PEOPLE IN HISTORY

Abbe, Ernst (1840–1905) was a professor of optics who worked with Schott, the glassmaker, and Zeiss, the lensmaker, in Jena.

Burne-Jones, Sir Edward Coley (1833–1898) designed stained glass working with William Morris.

Gallé, Émile (1846–1904) was a pioneer in the Art Nouveau movement; he used wheel cutting, acid etching, casing (i.e., layers of various glass), including metallic foils and air bubbles. He called his experiments “marquetry of glass.” When you see heavy pieces of deeply colored, nearly opaque glasses, which use several layers of glass and are then carved or etched to form plant motifs, you think of Gallé.

Lalique, René (1860–1945) was one of the creators of Art Nouveau glass. Etched clear glass is a particular trademark.

Littleton, Harvey K. (born 1922 in Corning, New York) was the University of Wisconsin professor who introduced Chihuly, Lipofsky, and others to glass and began the American Glass Movement.

Owens, Michael (1859–1923) invented the automatic bottling machine.

Schott, Otto (1851–1935) see Abbe.

Stookey, S. Donald (another exception to the rule) is one of the greatest scientific creators from Corning Glass.

Trancrede de Dolomieu, Guy S. (1750–1801) was a French professor of mineralogy. The mineral dolomite is named after him.

Zeiss, Carl Friedrich (1816–1888) gave his name to the optics company that was, for many years, based in Jena.

GENERAL REFERENCES

Bach, H. and Krause, D. (Eds.) (1999) *Analysis of the Composition and Structure of Glass and Glass Ceramics*, Schott Series on Glass and Glass Ceramics, Springer, Berlin.

Bach, H. and Krause, D. (Eds.) (1997) *Thin Films on Glass*, Schott Series on Glass and Glass Ceramics, Springer, Berlin.

- Bach, H. and Neuroth, N. (1995) *The Properties of Optical Glass*, Schott Series on Glass and Glass Ceramics, Springer, Berlin.
- Bach, H., Baudke, F.G.K., and Krause, D. (2000) *Electrochemistry of Glass and Glass Melts*, Schott Series on Glass and Glass Ceramics, Springer, Berlin.
- Beall, G.H. (1992) "Design and properties of glass-ceramics," *Annu. Rev. Mater. Sci.* **22**, 91. For more information about the different types of glass-ceramic written by the expert.
- Ellis, W.S. (1998). "The story of the substance that changed the world," *Glass*. Avon, New York. Includes more on the glass harp and marbles.
- McMillan, P.W. (1979) *Glass-Ceramics*, 2nd edition, Academic Press, London. The standard glass-ceramics text.
- Pfaender, H.G. (1983) *Schott Guide to Glass*, Van Nostrand Reinhold, New York. A concise overview of glass-forming processes.
- Schultes, E.S. and Davis, W.A. (1982) *The Glass Flowers at Harvard*, Botanical Museum of Harvard University, Cambridge, MA.
- Tooley, F.V. (1983) *The Handbook of Glass Manufacture*, 3rd edition, Volumes I and II, Ashlee Publishing Co., New York. A comprehensive manual for industrial glass formation. Designed primarily for the person in industry.
- Waseda, Y. and Toguri, J.M. (1998) *The Structure and Properties of Oxide Melts*, World Scientific Pub. Co., Singapore. A compact book concerned primarily with silicate melts.
- Varshneya, A.K. (1994) *Fundamentals of Inorganic Glasses*, Academic Press, Boston. One of the most comprehensive books on glasses. Chapter 20 is on the fundamental aspects of glassmaking.
- Zarzycki, J. (1991) *Glasses and the Vitreous State*, Cambridge University Press, Cambridge. This book was originally published in French as *Les Verres et l'Etat Vitreux* in 1982. The English edition does include an updated bibliography and some additional information not in the original version.

SPECIFIC REFERENCES

- Langmuir, I. (1933) "Oil lenses on water and the nature of monomolecular expanded films," *J. Chem. Phys.* **1**, 756.
- McNally, R.S. and Buschini, N. (1993) "The Harvard glass flowers: Materials and techniques," *JAIC* **32**, 231.
- Miller, J. (2004) *20th-Century Glass*, Dorling Kindersley Ltd, London. Among the best.

EXERCISES

- 26.1 Describe how cords and stones could be removed.
- 26.2 How much glass in your area is recycled as cullet?
- 26.3 Why did ancient glass batches contain so much alkali content?
- 26.4 Why is tin used in the float glass process?
- 26.5 We process the glass to remove bubbles and thus avoid stresses in the glass. Is this statement true or false? Explain your answer.
- 26.6 On ceramming a glass, we produce a density of $10^{15}/\text{cm}^3$ nuclei. How far apart are the nuclei and how does this affect the resulting grain size?
- 26.7 Why has the art of glass produced so much new interest? Is it new? Discuss.
- 26.8 Figure 26.1 shows the distribution of glass sales. Using the internet or otherwise, compare these with the figures for Al, steel, and Cu. Discuss your results.
- 26.9 Estimate the cost of an automobile's windows assuming they are made from tempered glass.
- 26.10 What are the compositions of some of the common sealing glasses?

Coatings and Thick Films

CHAPTER PREVIEW

The term “thick film” does not just refer to film thickness but rather to layers or a coating made by certain processing techniques. Most of the methods that we describe in this chapter involve suspending ceramic particles either in a solution or in a mixture of organic solvents (known as the *vehicle*). It will be necessary to remove all the volatile material from the coating to produce a dense adherent ceramic layer. Many of the processes described in this chapter are relatively inexpensive (at least compared to those used to produce thin films that we describe in Chapter 28) and simple.

Tape casting is used to produce flat sheets of many different ceramics for applications as substrates, capacitor dielectrics, and fuel cell electrolytes. Some of the techniques described in this chapter, for example, spin coating, are useful only for producing films on flat substrates. However, dip coating and electrophoretic deposition can be used to coat complex shapes. We finish by describing how thick-film circuits are made. In this application the ceramic is used as the substrate onto which the films are deposited and as important ingredients of the pastes that are used to form the circuits. The principle of the technology is not difficult, but controlling the processes may be.

All of these techniques are important in industry and you should know the *language* of thick films, e.g., slurry, slip, and paste.

27.1 DEFINING THICK FILM

A thick film will typically have a thickness in the range 10–25 μm ; thin films are usually $<500\text{ nm}$. However, what really distinguishes thick films and thin films, more than just their relative thickness, is the way in which they are produced. Thin films are often deposited using vacuum techniques such as sputtering and molecular beam epitaxy (MBE). We describe these techniques and consider acronyms and hyphens in Chapter 28. Thick films are deposited from a solution or paste, which must be dried and then often sintered to produce the final coating.

There are several advantages of thick-film processing:

- Simple
- Easy to automate
- Rapid
- Inexpensive
- Versatile
- Coating of complex substrates

In addition to describing some of the methods used to apply thick ceramic films to a substrate, we also describe the tape casting process. Films produced by tape casting are not used as coatings but as self-supporting ceramic sheets (down to 25 μm thick) that are widely used in the production of thick-film circuits.

27.2 TAPE CASTING

Tape casting is used to make flat ceramic sheets having a thickness up to about 1 mm. The process was developed during the

1940s for capacitor dielectrics. The production of ceramic capacitors is still one of the most important applications of tape casting.

In tape casting, a slurry (also called a slip) containing a powdered ceramic together with a complex mixture of solvents and binders is spread onto a moving polymer (such as MylarTM) sheet as shown in Figure 27.1. In the early form of tape casting the slurry was actually spread onto moving plaster-of-Paris plates. The use of a polymer sheet was patented in 1961 and since then the process has

TAPE CASTING

Band casting and the doctor-blade process are other names.

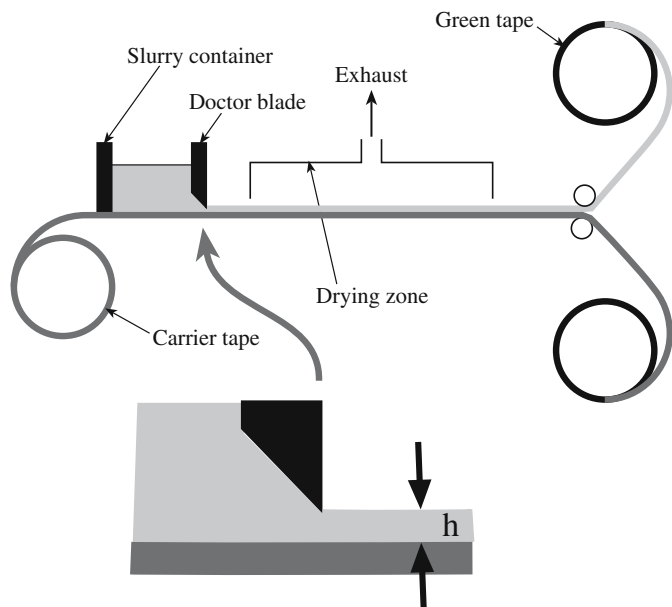


FIGURE 27.1 Schematic diagram of the tape casting process.

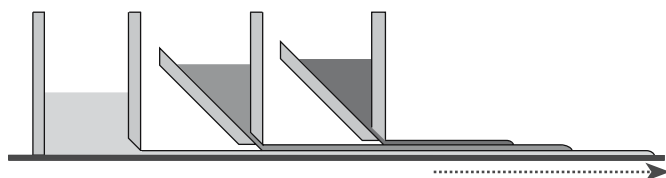


FIGURE 27.2 Illustration of a triple doctor blade for producing multilayer tapes.

not significantly changed. The principle of the process is essentially identical to spreading plaster on a wall, icing on a cake, or painting.

The thickness of the deposited layer is determined by the height of the doctor blade above the polymer sheet. Multilayer films are possible using the approach illustrated in Figure 27.2. The special feature of the doctor blade is that it produces a very uniform thickness. A typical doctor blade assembly is shown in Figure 27.3. The cast tape is dried, peeled from the polymer sheet, and reeled up to wait for further processing. At this stage of the process the tape is flexible because it still contains a

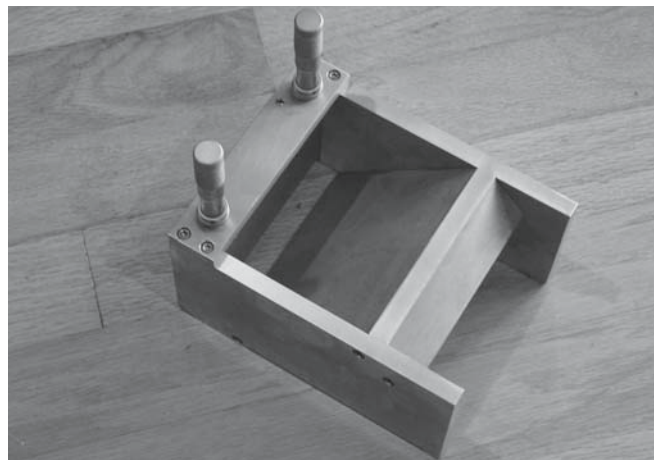


FIGURE 27.3 Typical doctor blade assembly.

high percentage of organics in the form of the polymer binder and is referred to as being “green.” This term is used to describe any unfired but shaped ceramic.

The preparation of the slurry is very important. A slurry formulation used in processing alumina sheets for use as substrates for electronic devices is shown in Table 27.1.

- The solvent controls the viscosity of the slurry allowing it to be spread on the polymer sheet.
- The binder holds the ceramic particles together until the tape is sintered and must be removed during the sintering process.
- Plasticizers increase the flexibility of the green tape.
- Dispersants (deflocculants) avoid settling of the powder particles.

Dispersants work by a process known as steric hindrance. The long-chain organic molecules such as those in Menhaden fish oil (a long-chain fatty acid) attach themselves to the ceramic particles with their long molecular tails pointing outward. This orientation prevents the particles from getting too close together and hence reduces the extent of agglomeration or settling. Menhaden fish oil is a natural product and is widely used in the ceramics industry because it is cheap.

TABLE 27.1 Materials for the Preparation of Alumina Slurries for Tape Casting

Milling step	Material	Function	wt%
Stage 1: Mill for 24 hours	Alumina powder	Substrate material	59.6
	Magnesium oxide	Grain growth inhibitor	0.15
	Menhaden fish oil	Dispersant	1.0
	Trichloroethylene	Solvent	23.2
	Ethyl alcohol	Solvent	8.9
Stage 2: Add to above and mill for 24 hours	Poly(vinyl butyral)	Binder	2.4
	Poly(ethylene glycol)	Plasticizer	2.6
	Octyl phthalate	Plasticizer	2.1

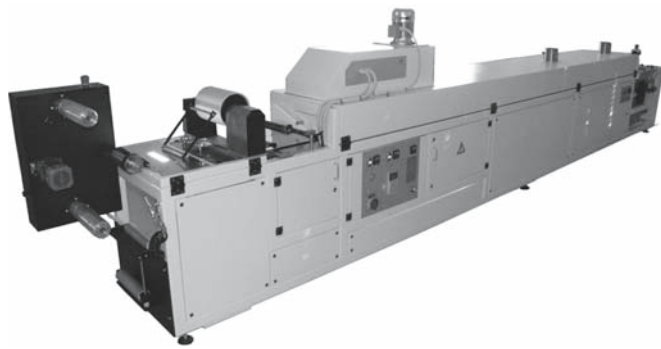


FIGURE 27.4 Example of an industrial tape casting machine.

Extensive shrinkage occurs during drying and firing of the tape because of the large volume fraction of organics in the slurry. For example, when the alumina slurry shown in Table 27.1 is cast to a thickness of 1.50 mm it will dry to produce a 0.75-mm green tape (about a 50% reduction). When sintered, the tape will shrink further to a final thickness of about 0.60 mm.

Figure 27.4 shows a commercial tape-casting machine for the continuous production of ceramic tape. These machines range in size from 2 m to more than 35 m in length and from about 100 mm to more than 1.25 m in width. The size determines the rate at which tapes can be produced. Typical casting speeds are on the order of 0.15 m/min. For quick drying compositions the casting speed can be as high as 2 m/min. In industrial production it is often important to have continuous measurement of the tape thickness. These measurements can be made through a hole in the support plate downstream of the doctor blade. Several different approaches are used commercially: (1) X-ray backscattering from below, (2) X-ray transmission involving instrument heads below and above (a technique commonly used in the aluminum industry to measure the thickness of Al plates), or (3) reflecting visible light at an angle from the top surface of the cast tape. The X-ray transmission method is generally preferred because of its greater accuracy.

Figure 27.5 illustrates the production of an integrated circuit (IC) package that uses tape cast alumina sheets.

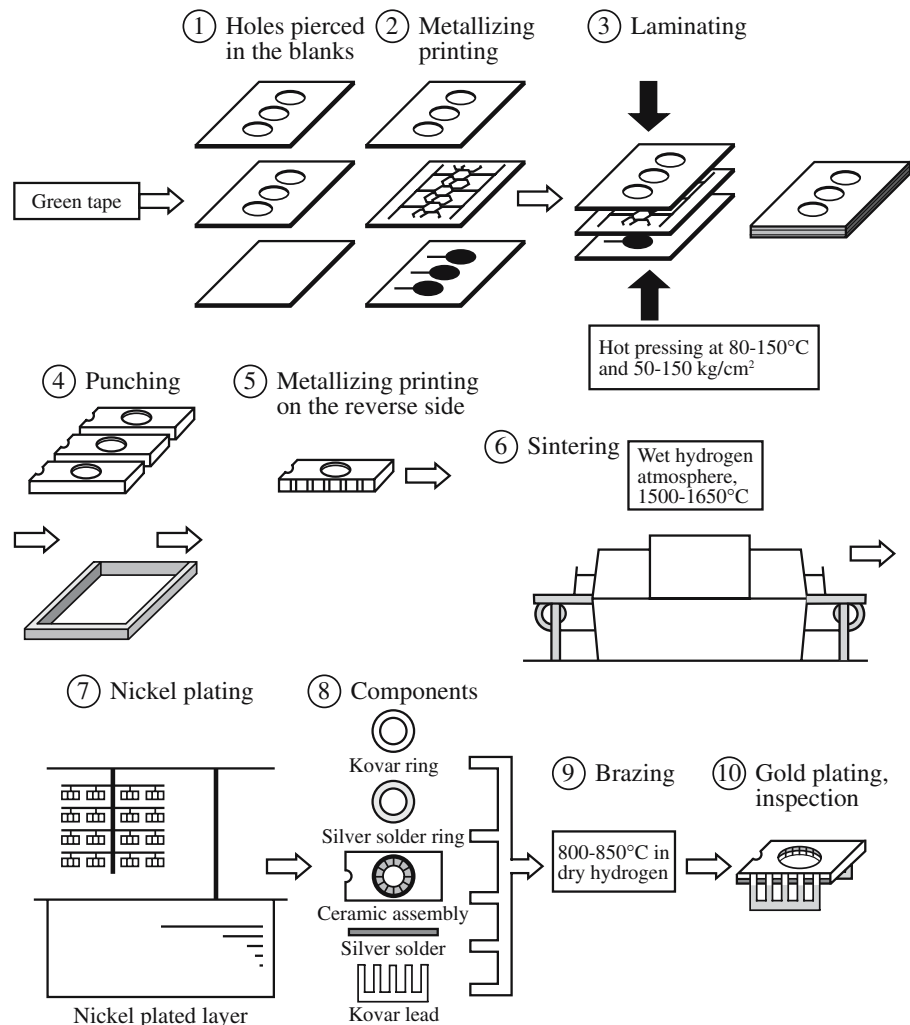


FIGURE 27.5 The steps in the production of an integrated-circuit package.

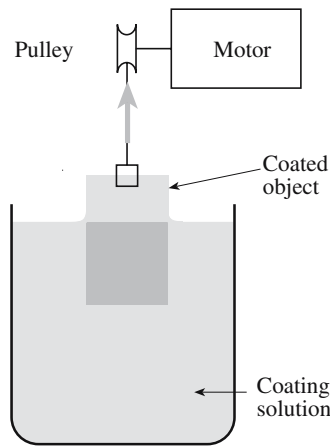


FIGURE 27.6 Schematic of a simple dip coating process.

The green tape can easily be punched to produce holes or vias, which are an important part of the processing of IC packages. In addition an ink or paste made of a mixture of metallic powder (tungsten or molybdenum), organic binders, and solvents is screen printed onto the green tape. The tape is then fired in a wet hydrogen atmosphere to produce a strongly adherent metal layer on the sintered alumina. We describe the screen printing process in more detail in Section 27.7.

DIP COATING
The high-tech version of the dipping process used to glaze pottery.

27.3 DIP COATING

A ceramic film can be formed very easily on a substrate by dip coating as illustrated in Figure 27.6. The starting material usually consists of metal alkoxides, but solutions of metal salts, such as nitrates, may be used instead. The substrate, or object to be coated, is lowered into the solution and withdrawn at rates between 10 and 30 cm/min. It is necessary that the solution wets and spreads over the surface of the substrate and so the contact angle must be

low. The final film is obtained after firing the coated object. Dip coating has the following advantages:

- It is simple.
- It is inexpensive.
- Complex shapes can be coated.
- Planar substrates can be coated on both sides at once.

The thickness, t , of the liquid film depends on the viscosity, η , of the solution and the speed, v , with which the object is withdrawn from the solution and is given by

$$t = 0.944 \left(\frac{\eta V}{\gamma_{lv}} \right)^{1/6} \left(\frac{\eta V}{\rho g} \right)^{1/2} \quad (27.1)$$

where γ_{lv} is the liquid-vapor interfacial energy, ρ is the density of the solution, and g is the acceleration due to gravity. The

thickness will, of course, be less in the final fired film due to shrinkage. There are several applications for dip-coated ceramic films as shown in Table 27.2.

27.4 SPIN COATING

Spin coating, like dip coating, starts with a solution that is often a mixture of metal alkoxides. The basic idea is illustrated in Figure 27.7 and there are two variants:

- Static
- Dynamic

In the static spin process, a few volumes of solution is dropped onto the substrate and allowed to spread until it covers most of the surface. Once the liquid has reached a specified diameter the chuck is accelerated to a predetermined speed, on the order of 20,000 rpm.

TABLE 27.2 Applications of Dip Coated Sol-Gel Preparations

Film use	Composition	Conditions
Mechanical protection	SiO ₂	Multistep process; alternating dips and firings at >400°C; increase thickness by 100 nm each cycle
Chemical protection	SiO ₂	Great care in drying; minimize cracking and crazing
Transparent electrode	In ₂ O ₃ -SnO ₂	Single dip process
Antireflecting	Na ₂ O-B ₂ O ₃ -SiO ₂	
Specific absorption	TiO ₂ -SiO ₂ Cr ₂ O ₃ -SiO ₂ Fe ₂ O ₃ -SiO ₂	
Catalytic		Low temperature gelling below 400°C ensures a porous film that has a high surface area
Photo mode	TiO ₂	
Ionic mode	β-Al ₂ O ₃ Ta ₂ O ₅	

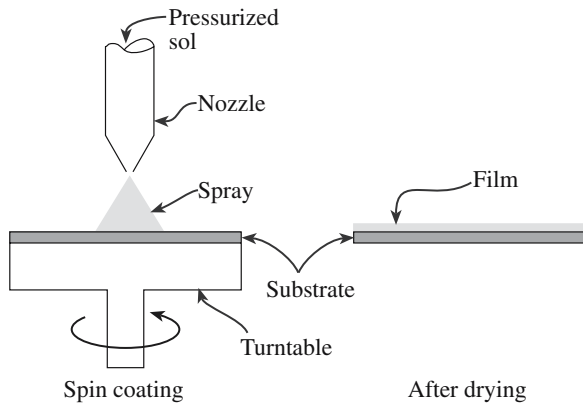


FIGURE 27.7 Schematic of the spin coating process.

In the dynamic spin process the solution is dispensed onto the substrate surface, which is spinning at a low speed of about 500rpm. After the liquid has spread the rotation speed is increased to produce the final film. The dynamic spin process is better for producing uniform coatings on larger diameter substrates.

Spin coating can be used only for single-side coatings and generally is applicable only to fairly simple planar shapes. Also spinning of very large objects is impractical. The thickness of the coating varies inversely with the angular velocity ($\omega^{-2/3}$) of the spin coater and is proportional to the viscosity of the solution ($\eta^{1/3}$). Spin coating is used widely in industry for forming polymer coatings, in particular for the deposition of photoresist layers prior to the patterning of semiconductor devices. Although not widely used for producing ceramic films, spin coating has

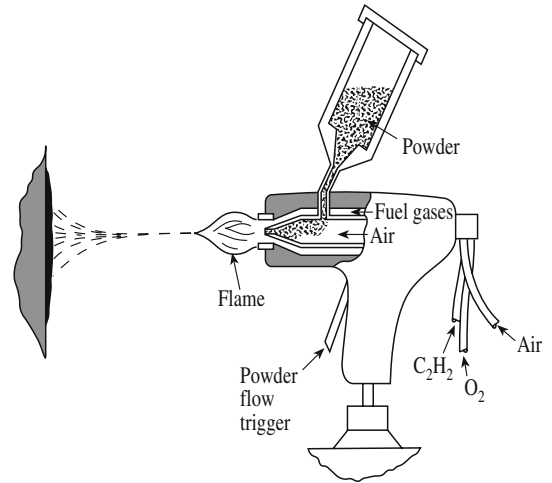


FIGURE 27.8 Thermal spraying with a gas combustion/powder gun.

found some application in forming films of piezoelectric materials for microelectromechanical systems (MEMS).

27.5 SPRAYING

Forming ceramic coatings by spraying is an important industrial process, in particular for applying wear-resistant and thermal-barrier coatings. There are several different types of the spraying process. In thermal spraying, illustrated in Figure 27.8, the powder is melted or softened by passing it through an oxyacetylene flame. A variant of the basic thermal spray process called plasma spraying, which utilizes a plasma heat source, is illustrated in Figure 27.9. The plasma temperature is typically $>28,000^{\circ}\text{C}$, well

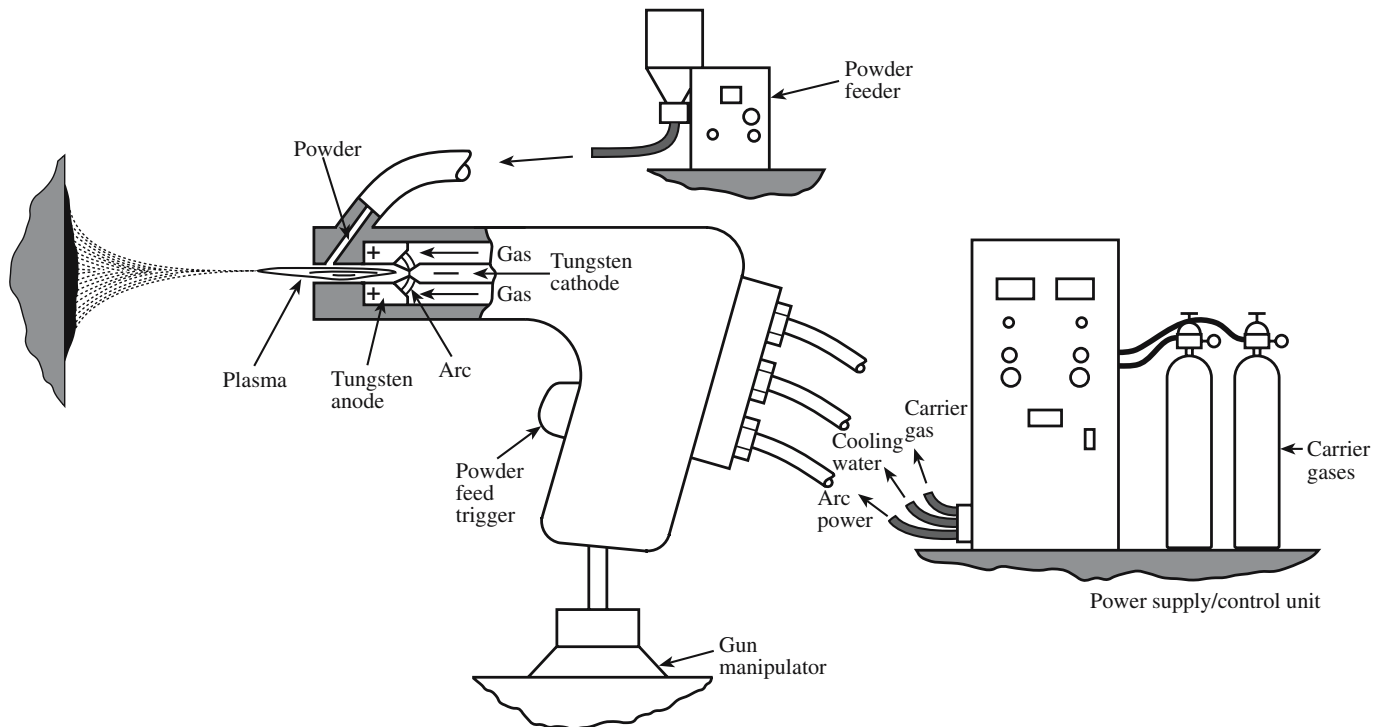


FIGURE 27.9 Thermal spraying using a plasma arc.

above that attained in gas combustion processes. The velocity of the plasma/droplet stream that exits the

nozzle is usually subsonic, although high-velocity plasma torches with constricted nozzle designs are available. Thermal spray processes are generally suitable for applying any material that melts or becomes plastic in the heating cycle and does not degrade at high temperature.

Plasma spraying is widely used in forming wear-resistant coatings on diesel engine components and for producing thermal barrier coatings on metals for gas turbine engines. The efficiency of gas turbine engines depends on the maximum temperature that can be sustained by the rotor blades during continuous operation. Applying a ceramic coating (called a thermal barrier coating) to the metal can allow the engine temperature to be increased by between 50 and 200°C without the temperature of the metal increasing significantly. There is a corresponding improvement (up to about 12%) in engine efficiency with considerable financial savings. Thermal barrier coatings must have the following properties:

- High coefficient of thermal expansion
- Low thermal conductivity
- Chemically stable in the gas turbine environment
- Thermal shock resistant

SPRAY PAINTING CARS
The paint contains TiO₂ powder.

for thermal barrier coatings. Figure 27.10 shows a schematic representation of the cross section of such a coating. An Ni–Cr–Al–Y alloy (called the bond coat in Figure 27.10) provides an adherent interlayer between the metal component and the ceramic coating. Joining metals and ceramics is not a trivial issue and the approach mentioned here is just one of the methods that we mention in this book.

The source material for spraying can be a solution that is forced through a spray gun onto a heated substrate. In this case the spraying is not “thermal” and is more akin to paint spraying. The glass industry uses this approach for depositing conductive layers of SnO₂ on glass.

27.6 ELECTROPHORETIC DEPOSITION

Electrophoresis is the movement of charged particles through a liquid under the influence of an external electric field. Electrophoretic deposition, which is very similar

to the electrodeposition process used to form metal coatings, can be used to form a ceramic coating up to 0.6 mm thick on a metallic substrate. The substrate forms one of the electrodes in an electrochemical cell as illustrated in Figure 27.11. The main advantage

EXAMPLE OF ELECTROPHORETIC DEPOSITION
For β-Al₂O₃ coatings the ceramic powder is suspended in an organic liquid mixture composed of nitromethane (CH₃NO₂) and benzoic acid (C₆H₅CO₂H). The benzoic acid produces a positive charge on the surface of the β-Al₂O₃ particles by adsorption of protons. The particles can be used to coat a negatively charged electrode.

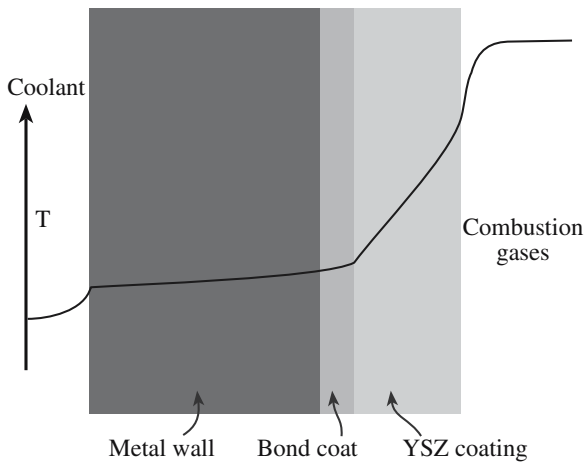


FIGURE 27.10 Schematic representation of a thermal barrier coating. The relative temperatures in the different parts of the coating are indicated.

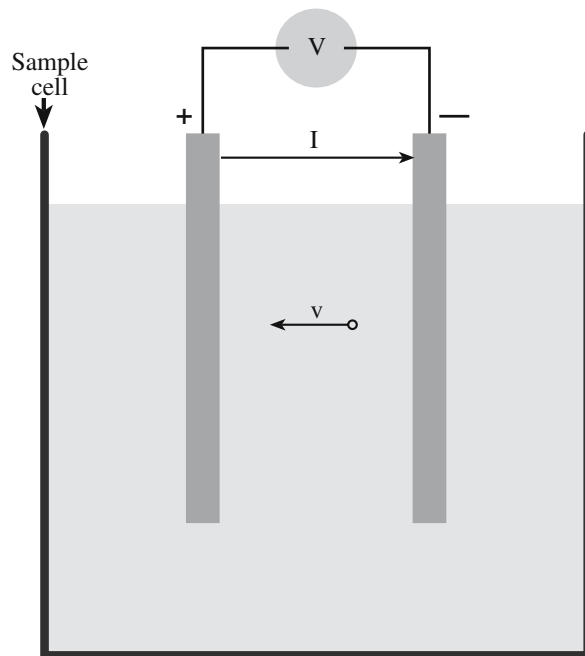


FIGURE 27.11 Schematic diagram of a particle electrophoresis cell.

of electrophoretic deposition is that coatings can be formed on nonplanar objects.

The particles that will form the coating are suspended in a liquid, which produces a surface charge on the particles, for example, by the adsorption of protons. When a particle with charge q is placed in an electric field, E , it experiences a force, F

$$F = qE \quad (27.2)$$

This force accelerates the particle toward the oppositely charged electrode. The particle also experiences a retarding force due to friction as it moves through the fluid. You will recall from Chapter 20 that Stokes' law gives the retarding force due to viscous flow:

$$F = 3\pi\eta d v \quad (27.3)$$

where v is the terminal velocity. We can write this as

$$v = \frac{qE}{3\pi\eta d} \quad (27.4)$$

In terms of mobility, μ

$$\mu = \frac{v}{E} = \frac{q}{3\pi\eta d} \quad (27.5)$$

From Eq. 27.5 we would expect that particle mobility would be increased for small particles in a solution of a low viscosity. This assumption is not entirely true. For example, the mobility of Li^+ ions in aqueous solution is lower than that of K^+ ions even though $r_{\text{K}^+} = 133 \text{ pm}$ compared to $r_{\text{Li}^+} = 60 \text{ pm}$. The discrepancy can be accounted for by considering solvation effects. Solvent molecules can cluster around an ion increasing its effective size. Small ions are the source of stronger electric fields than large ions, hence solvation is more extensive in the case of small ions giving them a larger effective size and lower drift velocities. A similar effect can occur for charged ceramic particles moving through a liquid during electrophoretic deposition.

The zeta potential, ζ , which is illustrated in Figure 27.12, is the potential on the surface of the charged particle moving through the liquid.

For a particle in a dilute electrolyte solution ζ is given by

$$\zeta = \frac{q}{2\pi\kappa\epsilon_0 d} \quad (27.6)$$

where κ is the dielectric constant of the liquid and ϵ_0 is the permittivity of a vacuum (a universal constant = $8.85 \times 10^{-12} \text{ F/m}$).

We can now obtain an expression for μ in terms of ζ :

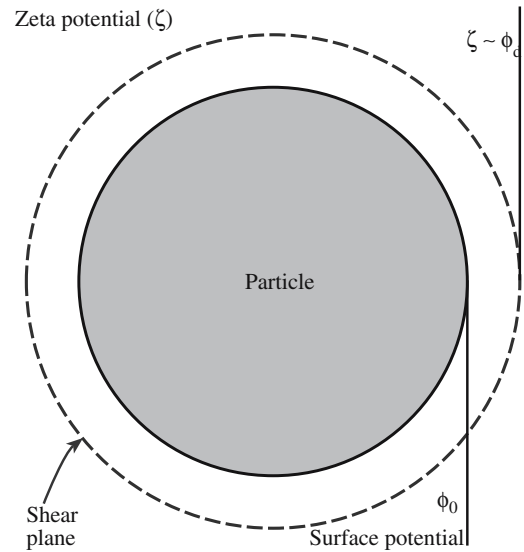


FIGURE 27.12 Illustration of the ζ potential and the effective size of a charged particle.

$$\mu = \frac{2\kappa\epsilon_0\zeta}{3\eta} \quad (27.7)$$

For concentrated electrolytes we use the Helmholtz–Smuluchowski equation to give us the mobility:

$$\mu = \frac{\kappa\epsilon_0\zeta}{\eta} \quad (27.8)$$

The important point from both Eqs. 27.7 and 27.8 is that mobility is proportional to κ . For rapid coating we want to use a liquid with a high dielectric constant. The advantage of using aqueous solutions is clear—water has a high dielectric constant. Dielectric constants of some other liquids are given in Table 27.3.

Figure 27.13 shows the electrophoretic mobility of TiO_2 particles in aqueous solutions of potassium nitrate (KNO_3); in this plot, σ_0 is the surface charge density,

TABLE 27.3 Dielectric Constants of Certain Liquids at 25°C and Zero Frequency

Nonpolar molecules		Polar molecules	
Methane	1.70 (at 173°C)	Water	78.54 80.37 (20°C)
Carbon tetrachloride	2.274	Ammonia	16.9 22.4 (–33°C)
Cyclohexane	2.105	Hydrogen sulfide	9.26 (–85°C)
Benzene	2.274	Methanol	32.63
		Ethanol	24.30
		Nitrobenzene	34.82

27.7 THICK-FILM CIRCUITS

Thick-film circuits are single or multilayer structures produced by depositing a layer, or layers, of a specially formulated paste or ink onto a suitable substrate. Thick-film technology began in the early 1960s when DuPont introduced a thick-film resistor system for application in miniaturized circuits. IBM used thick-film materials in their family of IBM/360 computers. Currently the worldwide market for thick-film circuits and devices is around \$14 billion. Most thick-film circuits are still used in electronic applications such as in computers (Figure 27.14).

There are three basic classes of thick-film material (conductors, resistors, and dielectrics) and all have at least one component that is a ceramic. They are supplied in the form of a paste or ink, which contains the following:

- The functional inorganic component or components; this is in the form of a fine powder.
- An organic binder; this is used to provide the green strength.
- A low boiling point organic solvent; this provides the required viscosity to allow the paste to be deposited onto the substrate.

Screen Printing and Processing

Thick-film materials are deposited onto flat substrates by screen printing. The origins of screen printing date back more than 3000 years when the Chinese used “silk screen” printing to deposit multilayered colored patterns onto fabrics. A similar process is still used today to print designs and logos onto T-shirts.

Figure 27.15 shows a schematic diagram of the screen-printing process. The paste is forced through holes in a screen using a rubber squeegee. The viscosity of the ink is determined by the type and amount of organic solvent added to the formulation. Common solvents include pine oil, terpeneol, and butyl carbitol acetate. The ideal thick-

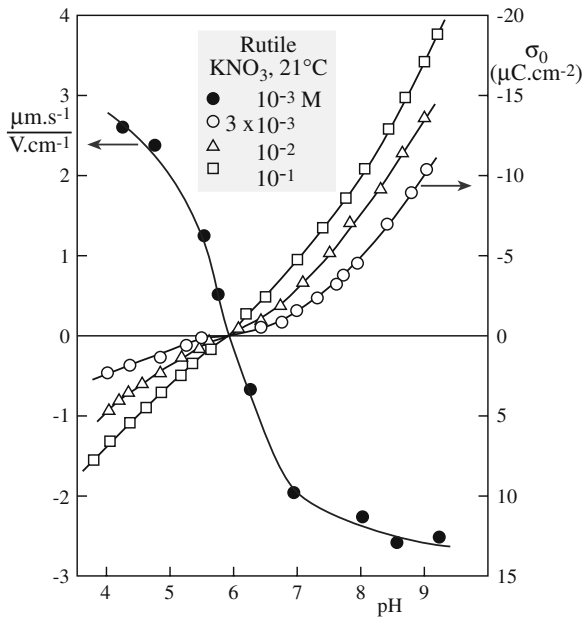


FIGURE 27.13 The surface charge density and electrophoretic mobility as functions of pH for rutile in aqueous solutions of potassium nitrate.

which was measured using the Brunauer, Emmett, and Teller (BET) method. The mobility is a function of the solution pH.

- In acidic solutions the surface of the TiO_2 particles has a positive charge due to cation adsorption.
- In basic solutions the powder particles have a negative charge due to the adsorption of anions.

At a pH of 5.9 the mobility is zero: this point is referred to as the isoelectric point (IEP). At the IEP the ζ potential is zero. Table 27.4 shows IEPs for several different oxides. Acidic oxides such as SiO_2 have low IEPs and basic oxides such as MgO have high IEPs.

TABLE 27.4 Isoelectric Points of Some Oxides

Material	Nominal composition	IEP
Quartz	SiO_2	2
Soda-lime silica glass	$\text{Na}_2\text{O}-0.58 \text{CaO} \cdot 3.70 \text{SiO}_2$	2-3
Potassium feldspar	$\text{K}_2\text{O} \cdot \text{Al}_2\text{O}_3 \cdot 6\text{SiO}_2$	3-5
Zirconia	ZrO_2	4-6
Apatite	$10\text{CaO} \cdot 6\text{PO}_2 \cdot 2\text{H}_2\text{O}$	4-6
Tin oxide	SnO_2	4-5
Titania	TiO_2	4-6
Kaolin (edges)	$\text{Al}_2\text{O}_3 \cdot \text{SiO}_2 \cdot 2\text{H}_2\text{O}$	5-7
Mullite	$3\text{Al}_2\text{O}_3 \cdot 2\text{SiO}_2$	6-8
Chromium oxide	Cr_2O_3	6-7
Hematite	Fe_2O_3	8-9
Zinc oxide	ZnO	9
Alumina (Bayer process)	Al_2O_3	8-9
Calcium carbonate	CaCO_2	9-10
Magnesia	MgO	12

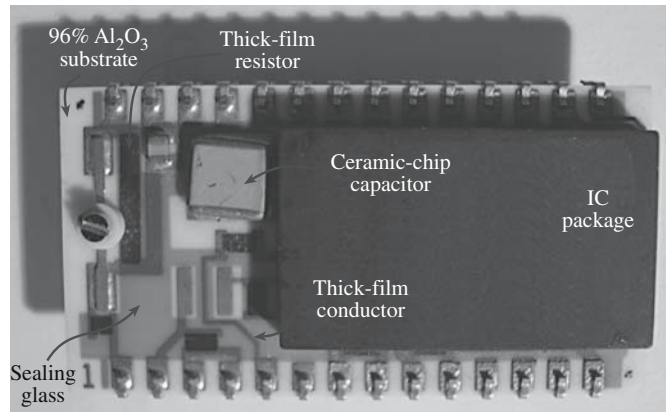


FIGURE 27.14 A typical thick film circuit used in a personal computer showing the different components.

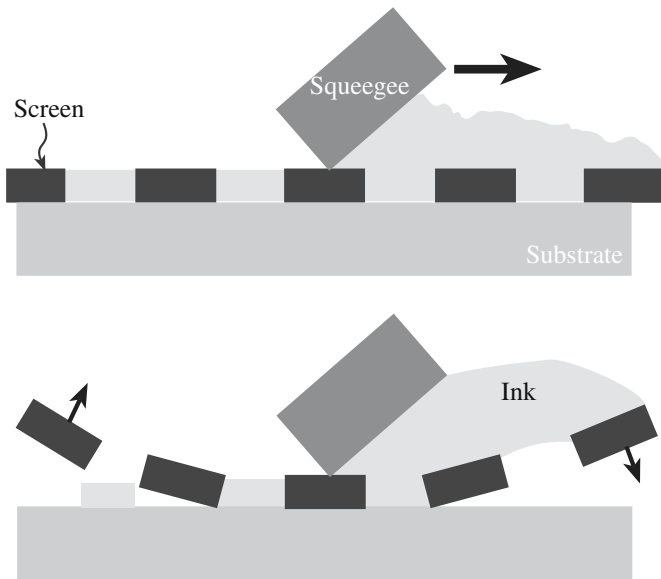


FIGURE 27.15 The screen printing process for depositing thick film circuits. The ink is forced through the screen, which then snaps away leaving a film on the substrate.

film paste should have a low viscosity at a high shear rate produced when the squeegee traverses the screen so that material transfer onto the substrate occurs. The viscosity should remain low for a short time after the squeegee passes and the screen snaps off of the substrate so that the printed film can level to fill in the unevenness from the screen wires. The viscosity should then increase rapidly to a very high value to prevent spreading of the deposited film.

The equipment used to deposit thick-film pastes is similar to that used in printing T-shirts, but for electronic applications much higher precision in the placement of material and thickness control is required. It is possible to produce circuit lines having a width of $5\ \mu\text{m}$ and a thickness of $5\ \mu\text{m}$. After printing, the substrates (coated with the wet paste) are moved to a drying oven where the low boiling organic solvents are removed. The circuit lines still contain the organic binder, which gives the green strength to the deposited film.

The choice of binder is as important as the choice of solvent. The binder contributes to the overall rheological properties of the paste, but it must be removed completely during firing. Ethyl cellulose is a common binder for air-fired materials. Binders for firing in inert or reducing atmospheres must be chosen carefully to avoid leaving a carbon residue in the fired film; suitable choices include nitrocellulose and copolymers of ethylene and vinyl acetate.

The furnace is a belt furnace with a well defined temperature profile as shown in Figure 27.16. The time at peak temperature is between 6 and 10 minutes during which time the inorganic components sinter together and bond to the substrate.

Substrates for Thick-Film Circuits

Substrates for thick-film circuits generally have to satisfy the following requirements:

- A uniform surface (surface roughness between 20 and $40\ \mu\text{m}$ is typical)
- Minimum distortion or bowing ($0.010\text{--}0.22\ \text{cm/cm}$)
- The ability to withstand processing temperatures of up to 1000°C
- Tight dimensional tolerances ($\pm 0.07\text{--}0.10\ \text{mm}$ size; $\pm 0.02\text{--}0.10\ \text{mm}$ thickness)
- Strength
- High thermal conductivity
- High electrical resistivity
- Chemically compatible with paste constituents
- Low dielectric constant
- Inexpensive

Alumina ($96\% \text{Al}_2\text{O}_3$ with 4% of a glass containing MgO , CaO , and SiO_2) is the most common substrate material because it meets all of the above requirements to an acceptable degree. The substrates themselves are frequently made by tape casting, which we described in Section 27.2.

When a circuit will be used in conditions in which a significant amount of heat will be transferred through the substrate but the thermal conductivity of alumina is not high enough, then alternative materials may be used. For many years the only alternative to Al_2O_3 was beryllia (BeO). The disadvantages of BeO are its cost and high toxicity in both vapor and powder form as encountered in processing. Aluminum nitride (AlN) is another option; it not only has a high thermal conductivity but is closely matched in coefficient of thermal expansion to silicon in the temperature range $25\text{--}400^\circ\text{C}$ ($\alpha_{\text{Si}} = 4.0\ \text{ppm}/^\circ\text{C}$; $\alpha_{\text{AlN}} = 4.3\ \text{ppm}/^\circ\text{C}$). The three substrates are compared in Table 27.5.

Although the properties of AlN make it very well suited for electronic packaging, there have been several problems in commercializing:

- Most commercial AlN substrates have thermal conductivities $\sim 170\ \text{W m}^{-1}\ \text{K}^{-1}$, which is considerably lower than the theoretical thermal conductivity of $320\ \text{W m}^{-1}\ \text{K}^{-1}$.

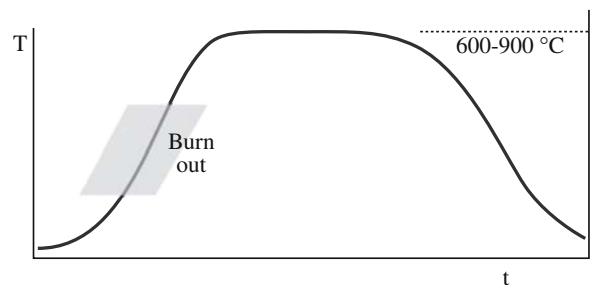


FIGURE 27.16 Typical thick film circuit firing profile.

TABLE 27.5 Properties of Different Substrate Materials (AlN sublimes)

Property	Units	96% Al ₂ O ₃	BeO	AlN
Thermal conductivity	W m ⁻¹ K ⁻¹	15–20	230–260	120–210
Coefficient of thermal expansion (RT –400°C)	10 ⁻⁶ °C ⁻¹	7.2	8.3	4.3
Electrical resistivity	Ω · cm	>10 ¹⁴	>10 ¹⁴	>10 ¹⁴
Dielectric constant (RT at 1 MHz)	Unitless	9.4	6.7	8.6
Dielectric loss (RT at 1 MHz)	Unitless	0.0001	0.0003	0.0002
Dielectric strength	kV/mm	15	10	15
Density	g/cm ³	3.75	2.85	3.3
Melting temperature	°C	2030	2530	2300
Modulus of rupture	MPa	358	280	280–350
Knoop hardness	GPa	19.6	9.8	11.8
Modulus of elasticity	GPa	303	345	331

- AlN powder costs more than four times that of alumina powder.
- The adhesion of pastes designed for alumina is low on AlN unless the surface is preoxidized prior to deposition.

Thick-Film Conductors

The general requirements for thick-film conductors are

- Low electrical resistivity
- Good adhesion to the substrate
- Good line definition

In addition there may be the following considerations:

- Ability to be wire bonded or soldered for external connections
- Resistant to electromigration
- Compatible with other thick film components such as resistors and dielectrics
- Acceptable cost

The functional material in a thick-film conductor is a metal. The important metals and alloys used in thick-film conductors, together with some of their characteristics, are listed in Table 27.6. There are two mechanisms for achieving adhesion of the metal film to the substrate:

- Frit bonding. A small amount (2–10%) of glass powder is added to the paste formulation. During firing the glass softens, wets the substrate, and penetrates into the metal network to develop an interlocking structure. The most common glasses used in frit-bonded conductors are lead borosilicates, e.g., 63 wt% PbO–25 wt% B₂O₃–12 wt% SiO₂.
- Reactive bonding. A small amount (0.1–1%) of CuO or CdO is added to the paste formulation. During firing the oxides react with the alumina substrate to form a copper or cadmium spinel, CuAl₂O₄ or CdAl₂O₄, respectively.

Frit bonding is the most common method, but there are several advantages to reactive bonding. First, very small amounts of additive are needed, which means that the electrical resistivity of the conductor is kept as low as possible. Second, the surface of the conductor is nearly pure metal, which enhances the attachment of thin Au or Al wires during wire bonding. Some thick-film conductor compositions are termed “mixed bonded” and these contain a glass frit together with a mixture of oxides.

Thick-Film Resistors

The functional phase in thick-film resistors is a mixture of electrically conducting (or semiconducting) ceramic powders such as ruthenium dioxide (RuO₂), bismuth ruthenate (Bi₂Ru₂O₇), lead ruthenate (Pb₂Ru₂O₆), and Ag–Pd–PdO mixtures for use in air-fired pastes and tantalum nitride (TaN) for nitrogen-fired pastes. The resistance of thick-film resistors is specified in terms of sheet resistance, which has units of ohms/square (Ω/□).

TABLE 27.6 Metals and Alloys Used in Thick Film Conductors

Metal or alloy	Principal features
Ag	\$ Highest conductivity; Ag ion migrates; tarnishes; seldom in microcircuits; migrates through glass and between conductors
Pd–Ag Pt–Ag	\$\$ Pd inhibits migration but lowers conductivity \$\$ Smaller quantity of Pt replaces palladium in the binary alloy
Au	\$\$\$\$ Highly conductive and chemically inert; reliable bonds to Au wire; high solubility in common solders makes soldering difficult
Pd–Au	\$\$\$\$ Compared with Au the solubility in solder is reduced but conductivity is impaired
Pt–Au	\$\$\$\$ Reliable solderable alternative to Au; not so conductive
Cu	\$ High conductivity; fire in reducing atmospheres to achieve excellent solderability
Ni	\$ Can fire in air but not solderable from the furnace

\$ lowest cost; \$\$\$\$ highest cost.

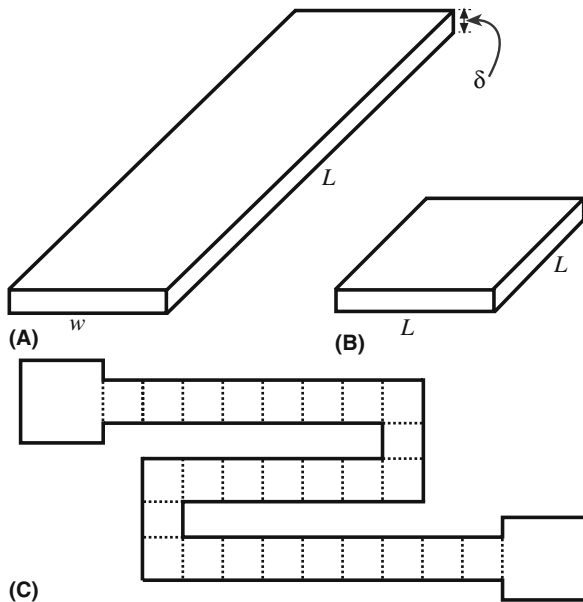


FIGURE 27.17 (a–c) Illustration of sheet resistance.

The concept of sheet resistance is illustrated in Figure 27.17a, which shows a sheet resistor of length l , width w , and thickness d , having a resistance, R given by

$$R = \frac{\rho l}{dw} \quad (27.9)$$

where ρ is the resistivity. If the resistor is square in shape, as in Figure 27.17b, then $l = w$ and Eq. 27.9 becomes

$$R = \frac{\rho}{d} \quad (27.10)$$

For a given material and thickness, all square sheets have the same resistance independent of the size of the square. The resistance of such squares is known as the sheet resistance. Figure 27.17c shows a complex thick-film resistor configuration, but the resistance can easily be determined by dividing it into squares, counting the number of squares per strip, and multiplying by the sheet resistance.

Thick-film resistors are available with sheet resistance values in the range from 0.1 to 10M Ω/\square . By blending different quantities of conductive material and an electrically insulating glass the resistivity is controlled. For a high sheet resistance formulation the ratio of conductor to glass would be about 70/30.

An important parameter for thick-film resistors is their temperature coefficient of resistivity (TCR), which is a measure of how much the resistance changes with temperature. It is defined as the slope of the change in resis-

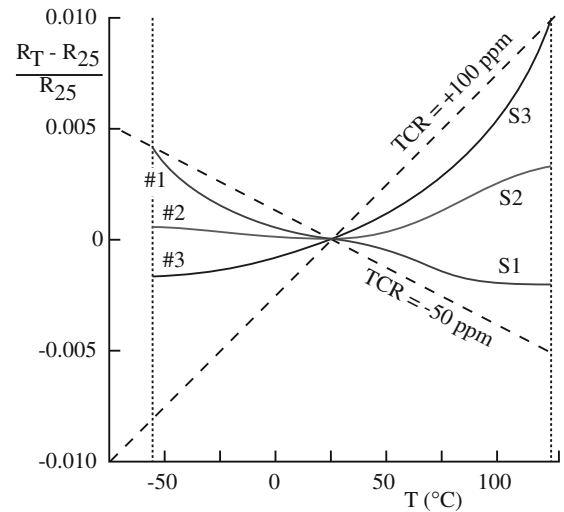


FIGURE 27.18 Typical resistance versus temperature profiles for thick-film resistors.

tance ($\Delta R/R$) versus temperature as illustrated in Figure 27.18. The TCR limits specified for a particular formulation are the slopes of the two lines passing through the reference points on the curve that bound the resistance deviation. Typically the reference temperature is 25°C and the temperature range is -55°C to $+125^\circ\text{C}$. TCR values for thick-film resistors are typically less than ± 100 ppm/°C.

Resistor patterns are designed so that the average value of the fired resistor is lower than the required value. The final resistor is then trimmed using a laser, or an abrasive jet, to remove material and increase the resistance to within $\pm 1\%$ of the desired value.

SHEET RESISTANCE

It depends only on the thickness of the resistor and its resistivity.

Thick-Film Dielectrics

Dielectrics are used in several difficult applica-

tions in thick-film circuits:

- To isolate circuit lines in multilayer structures
- As a dielectric layer in thick-film capacitors
- To encapsulate circuit components

For multilayer applications the functional material is commonly a glass or a glass-ceramic. It must have a low dielectric constant and be thermal expansion matched to the substrate to prevent stresses that can cause the substrate to bow. The film must also be stable as it may be subjected to many firing cycles in the fabrication of a multilayer structure.

For thick-film capacitor applications the dielectric composition will contain a material with a high dielectric

constant such as barium titanate. Encapsulants are used to protect resistors from harmful environmental conditions such as high humidity and reactive organic solvents, and to protect silver-containing conductors from silver migration. The glass is chosen so that it can be fired at low temperatures to avoid significant refiring of the thick-film

resistors (which would change their resistance values). Typical firing temperatures for encapsulant glasses are $\sim 500^{\circ}\text{C}$. Most glass formulations used in the thick-film industry are proprietary. But to achieve low softening temperatures the glass used for encapsulation will probably contain a significant amount of either PbO or B_2O_3 .

CHAPTER SUMMARY

The term thick-film refers to layers and coatings made by certain types of processing techniques. Such films are usually not prepared using vacuum conditions. In this chapter we described most of the techniques that are used to produce thick ceramic films. Some of these processes are extremely simple and inexpensive such as dip coating, which can be accomplished, at a minimum, with simply a beaker and a pair of tweezers. However, processes such as thermal spraying require specialized equipment.

In this chapter we described tape casting. This process is used to make flat sheets. Although this is a means of shaping and could have been described in the “shaping” chapter we described it here because it shares a common feature with the other thick film coating methods: it uses a slurry. It also is the process most often used to make ceramic substrates for thick-film circuits. Ceramics are a major component of thick-film circuits. Even in thick-film conductors, ceramics are important in ensuring adhesion between the metal layer and the substrate (which is invariably also a ceramic).

GENERAL REFERENCES

- Budinski, K.G. (1988) *Surface Engineering for Wear Resistance*, Prentice Hall, Englewood Cliffs, NJ. Describes various thermal spray techniques.
- Kuo, C.C.Y. (1991) in *Engineered Materials Handbook Volume 4: Ceramics and Glasses*, ASM International, pp. 1140–1144. A brief review of thick film circuits.
- Mistler, R.E. (1995) in *Ceramic Processing*, edited by R.A. Terpstra, P.P.A.C. Pex, and A.H. De Vries, Chapman & Hall, London. A detailed discussion of tape casting.
- Rahaman, M.N. (1995) *Ceramic Processing and Sintering*, Marcel Dekker, New York. Covers many of the processing techniques for ceramic films and coatings at a level similar to this book.

SPECIFIC REFERENCES

- Howatt, G.N., Breckenridge, R.G., and Brownlow, J.M. (1947) “Fabrication of thin ceramic sheets for capacitors,” *J. Am. Ceram. Soc.* **30**, 237. The original description of tape casting. Howatt obtained a U.S. patent (2,582,993) for the process in 1952.
- Parks, J.L., Jr. (1961) *Manufacture of Ceramics*, U.S. Patent 2,966,719. Patent for the use of polymer film in tape casting process.

EXERCISES

- 27.1 The slurry formulation for tape casting barium titanate sheets consists of the following ingredients: barium titanate powder, phosphate ester, methyl ethyl ketone, ethanol, acrylic resin, benzyl butyl phthalate, and poly(ethylene glycol). (a) Explain the function that each of the ingredients has in the formulation. (b) What would be the usual amounts (in wt%) of each of the ingredients in a typical tape cast formulation?
- 27.2 Explain why shrinkage of a cast tape occurs during drying and firing. Which of the ingredients in the above formulation would you expect to be lost at each stage of the process? Justify your answer.
- 27.3 Of the methods described in this chapter which one would you choose to produce a uniform $10\ \mu\text{m}$ coating of BaTiO_3 on a 5-cm-diameter silicon wafer? Justify your choice.
- 27.4 Of the methods described in this chapter which one would you choose to produce a uniform $100\ \mu\text{m}$ coating of Al_2O_3 on a 5-mm-diameter steel rod? Justify your choice.
- 27.5 Would thermal spraying be a suitable technique for forming thick films of aluminum nitride (AlN)? Explain the reasoning for your answer.
- 27.6 Alumina substrates for electronic packaging usually contain 96% Al_2O_3 and the remaining 4% is a mixture of CaO – MgO – SiO_2 . Why do you think these constituents are added to the alumina and what effect, if any, do you think they will have on the properties of a 96% alumina substrate compared to a 99.5% alumina substrate?

- 27.7 In glass formulations used in thick-film inks alkali metal constituents are avoided. Why?
- 27.8 Who are the major vendors for thick-film materials?
- 27.9 Rank the thick-film conductors in Table 27.6 in terms of electrical conductivity starting with the most conductive. Is the trend consistent with their cost?
- 27.10 Figure 27.14 shows a thick-film circuit. (a) What is the role of the sealing glass? (b) Why is it green? (c) What properties are important for the sealing glass?

Thin Films and Vapor Deposition

CHAPTER SUMMARY

Thin films are often deposited relatively slowly so that the growth can be strongly influenced by the substrate, which plays a key role in determining film microstructure and properties. The substrate is much more important in growing thin films than it is for thick films and is a crucial factor if we want to grow oriented (epitactic) films. At the end of this chapter we describe some of the requirements for the substrate. The growth techniques described in this chapter involve vacuum chambers and are generally expensive so that thick films are grown by other methods, particularly when epitaxy is not required. Much of this topic is carried over from the semiconductor industry and is often not thought of as ceramic processing. However, without thin films of Si oxide and Si nitride, “Silicon Valley” might still be green fields.

28.1 THE DIFFERENCE BETWEEN THIN FILMS AND THICK FILMS

In Chapter 27 we described how thick films of ceramics are produced. The difference between thick films and thin films is not really the thickness of the layer; it is how the layer is formed. In general, thin films are ≤ 500 nm in thickness whereas thick films may be several tens of micrometers in thickness or even thicker depending upon the particular application. Thin films are generally prepared from the vapor phase whereas for thick films we use a solution or slurry. Furthermore, thin films are often crystallographically oriented in a particular way with respect to the underlying substrate. This orientation relationship, known as epitaxy, is determined by the crystal structures and lattice parameters of the film and the substrate. In general, thick films and coatings have no specific orientation and contain a large number of randomly oriented crystalline grains.

28.2 ACRONYMS, ADJECTIVES, AND HYPHENS

The thinnest thin films are almost exclusively formed from the vapor or gaseous phase and although there are many different deposition techniques they can be divided into two basic classes:

- Physical vapor deposition (PVD)
- Chemical vapor deposition (CVD)

Chemical vapor deposition techniques use either gas phase reactions or gaseous decomposition as the source of material. Physical vapor deposition techniques rely on excitation of a source (sometimes called the target) that is usually solid to produce the necessary material for film formation. In addition to the basic difference in the way that material transfer from the vapor phase to the solid phase is accomplished, there are other differences between CVD and PVD. For example, CVD is often used to produce thicker films (i.e., films >1 μm in thickness). The reason is that the growth rate by CVD is on the order of micrometers per minute (e.g., 2 $\mu\text{m}/\text{min}$), whereas for PVD techniques the growth rate is often orders of magnitude lower (e.g., growth rates in the range 0.01 – 0.03 $\mu\text{m}/\text{min}$ are typical). There are other differences that will become evident as we describe the different techniques in the following sections.

Thin-film technology is replete with acronyms and several of the main ones you will encounter are listed in Table 28.1. Molecular beam epitaxy (MBE) is the only acronym that assumes a crystalline structure and alignment of the thin film. Molecular-beam evaporation would be much better, especially when used to grow amorphous films!

We defined epitaxy in Chapter 15. Incidentally, the grammatically correct adjective from epitaxy is epitactic or better still epitaxial, but epitaxial has come to be accepted even by the *Oxford English Dictionary* because it is now so widely used. In many of the deposition techniques, it is not clear where the hyphen(s) should be (if there should be one) but thin-film growth is always the way to grow thin films and adverbs are never hyphenated to parts of verbs.

TABLE 28.1 Some Common Acronyms in Thin-Film Technology

<i>CVD technique</i>	<i>Chemical vapor deposition</i>	<i>PVD technique</i>	<i>Physical vapor deposition</i>
APCVD	Atmospheric-pressure CVD	MBE	Molecular-beam epitaxy
LECVD	Laser-enhanced CVD	PLD	Pulsed-laser deposition
LPCVD	Low-pressure CVD	IBAD	Ion-beam-assisted deposition
MOCVD	Metal-organic CVD	RE	Reactive evaporation
PECVD	Plasma-enhanced CVD		

28.3 REQUIREMENTS FOR THIN CERAMIC FILMS

There are four general characteristics that we usually want to control when growing ceramic thin films:

- Crystal structure
- Stoichiometry
- Phase
- Surface morphology/topography

We will now look at each of these characteristics and explain the rationale behind why they are important. The thin film may be crystalline, often epitaxial, or sometimes polycrystalline or amorphous. The reason for requiring crystallinity is that for thin films we are often making use of a particular electronic, optical, or magnetic property of the material. These properties are frequently anisotropic. Hence we want to ensure that the film is crystalline and oriented in the correct way to optimize the desired property. This alignment is best achieved by judicious choice of substrate and, therefore, we make use of epitaxy. Many properties of ceramic thin films are affected by the presence of grain boundaries. In epitaxial films it is often possible to control the types of grain boundary that are produced. Generally these boundaries are low-angle grain boundaries, but they can be high-angle grain boundaries that may be associated with large distortions.

The correct stoichiometry, or composition, is necessary because for some materials they exhibit the required property only within a certain composition range. An example is the high-temperature superconductors whose structures we described in Chapter 7. For $\text{YBa}_2\text{Cu}_3\text{O}_{6+x}$ (YBCO), the value of the superconducting transition temperature depends on the value of x . When x is close to one the transition temperature is ~ 90 K. When $x = 0.3$ the transition temperature is reduced to 30 K. The change in oxygen stoichiometry is associated with a change in the structure of the material. Many technologically important ceramics exist in different crystalline forms. Another

example is BaTiO_3 . The ferroelectric form of BaTiO_3 is tetragonal.

The final characteristic is the film surface. In general we want to have smooth films, but this requirement is not universal and is really based on what we want to do with the film. If the film is part of a multilayer structure, i.e., there are going to be other layers deposited on top, then it is clearly important for the underlying surface to be smooth. If the film is to be patterned using photolithographic techniques (the same techniques used to pattern semiconductor devices) then smooth surfaces are essential. Some properties are dependent upon surface roughness. For example, rough surfaces can contribute strongly to propagation losses in films used for guiding microwave radiation.

From the above discussion you can see that there are several stringent requirements for ceramic thin films. For this reason, there are numerous techniques that have been used to form such films. Some techniques work better for some materials whereas other techniques work better for other materials. We describe some of the techniques used to form ceramic thin films in the following sections, but this is not a comprehensive list.

28.4 CHEMICAL VAPOR DEPOSITION

Chemical vapor deposition involves either

- Chemically reacting a volatile compound of a material to be deposited, with other gases, to produce a non-volatile solid or
- Pyrolysis (decomposition) of a compound at high temperature to produce a solid.

In either case the solid forms as a film on a suitably placed substrate. It is important that the reaction takes place only on the substrate surface. If the reaction takes place in the gas stream above the substrate then particulates will form. Under these conditions the film will have a low density and a large number of voids. There are several different geometries for a CVD reactor and some of these are illustrated in Figure 28.1. The substrates are usually placed on a graphite slab, which acts as a susceptor for radiofrequency induction heating. The gases are introduced into the reactor chamber, sometimes in the presence of an inert carrier gas such as argon. As an example of a CVD reaction consider the formation of SiC from silicon tetrachloride (SiCl_4) and methane (CH_4):



Silicon tetrachloride is a liquid at room temperature and can easily be vaporized (it boils at 57.6°C) and transported to the reactor chamber. Methane can be supplied as a high-purity gas directly from a bottle. The reaction between SiCl_4 and CH_4 to produce SiC films occurs at 1400°C . Two aspects of the temperature are important:

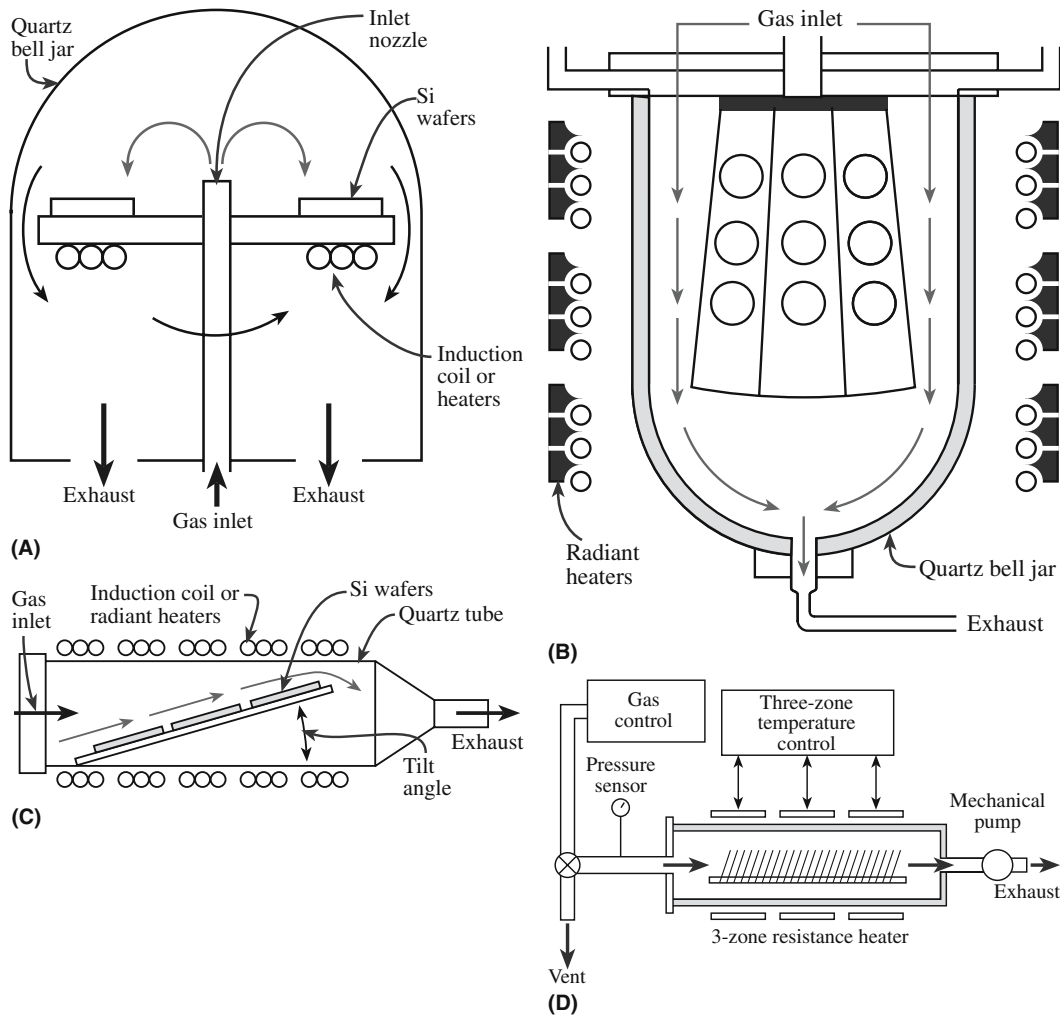
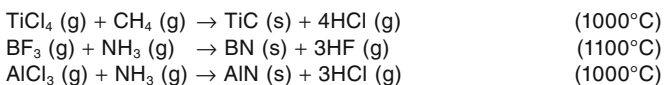


FIGURE 28.1 Examples of CVD reactor configurations: (a) pancake, (b) barrel, (c) horizontal, (d) LPCVD.

- It must be sufficiently high so that the reaction occurs.
- If an epitactic deposit is required, it must be high enough to allow the condensing species to diffuse across the crystal surface to find their required lattice crystal positions.

A variety of oxide, carbide, nitride, and boride films and coatings can be readily prepared by CVD techniques as shown in Table 28.2. The reacting compounds must exist in a volatile form and must be sufficiently reactive in the gas phase. Examples of other reactions that can be used to produce ceramic films by CVD are given below:



ELECTRONIC GRADE SILICON (EGS)

The annual worldwide production capacity is $>10^7$ kg. It is all made by CVD.

Chemical vapor deposition is one of the most important deposition techniques for forming ceramic films and coatings. We described two examples in Chapter 20 in which CVD is used in composites. It is used to form SiC fibers by the reaction between CH_3SiCl_3 and H_2 on a tungsten wire. It is also used to form the matrix phase in a ceramic matrix composite (CMC) by a process known as chemical-vapor infiltration. In later chapters we describe the CVD technique again, e.g., it is used in the formation of optical fibers.

Before we leave this section there is one additional example of the importance of CVD. All of the electronic grade silicon (EGS) used in the fabrication of silicon wafers is made by CVD. The highest purity EGS is made by decomposition of silane (SiH_4), which itself can be prepared in extremely high purity. The substrate is an electrically heated U-shaped rod made of single crystal silicon. The silane decomposes to form silicon, which deposits on the U-shaped rod in the form of

TABLE 28.2 Examples of Ceramic Films and Coatings Produced by CVD				
Film	Substrate	Reactants	Deposition T (°C)	Crystallinity ^a
Si	Si	Either SiCl ₂ H ₂ , SiCl ₃ H, or SiCl ₄ + H ₂ SiH ₄ + H ₂	1050–1200 600–700	E P
Ge	Ge	GeCl ₄ or GeH ₄ + H ₂	600–900	E
SiC	Si	SiCl ₄ , toluene, H ₂	1100	P
AlN	Sapphire	AlCl ₃ , NH ₃ , H ₂	1000	E
In ₂ O ₃ :Sn	Glass	In-chelate, (C ₄ H ₉) ₂ Sn(OOCH ₃) ₂ , H ₂ O	500	A
ZnS	GaAs, GaP	Zn, H ₂ S, H ₂	825	E
CdS	GaAs, sapphire	Cd, H ₂ S, H ₂	690	A
Al ₂ O ₃	Si	Al(CH ₃) ₃ + O ₂	275–475	A
	Cemented carbide	AlCl ₃ , CO ₂ , H ₂	850–1100	A
SiO ₂	Si	SiH ₄ + O ₂	450	A
		SiCl ₂ H ₂ + 2N ₂ O	900	
Si ₃ N ₄	SiO ₂	SiCl ₂ H ₂ + NH ₃	~750	A
SiNH	SiO ₂	SiH ₄ + NH ₃ (plasma)	300	A
TiO ₂	Quartz	Ti(OC ₂ H ₅) ₄ + O ₂	450	A
TiC	Steel	TiCl ₄ , CH ₄ , H ₂	1000	P
TiN	Steel	TiCl ₄ , N ₂ , H ₂	1000	P
BN	Steel	BCl ₃ , NH ₃ , H ₂	1000	P
TiB ₂	Steel	TiCl ₄ , BCl ₃ , H ₂	>800	P

^aE, epitaxial; P, polycrystalline; A, amorphous.

a columnar “feather-like” polycrystalline layer as shown in Figure 28.2. The overall thickness of this layer can exceed 5 cm, so CVD can be used to produce very “thick” films!

28.5 THERMODYNAMICS OF CHEMICAL VAPOR DEPOSITION

Thermodynamics indicates whether a particular chemical reaction is feasible. However, it will not provide any information about the speed of the reaction and film growth rates. Even if a reaction is thermodynamically possible, if

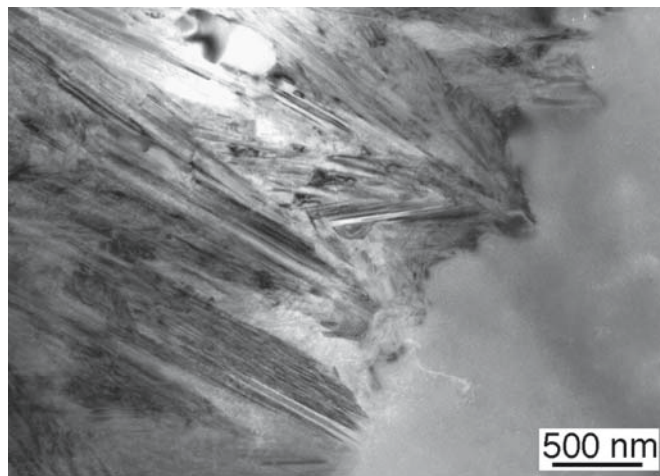


FIGURE 28.2 TEM image showing a polysilicon layer grown on a single crystal Si rod by CVD.

it proceeds at very low rates then it will not be commercially useful.

We can calculate the standard free energy, ΔG^0 , of many reactions using tabulations of thermodynamic data. Consider the reaction between TiCl₄ and CH₄:



To find the standard free energy, ΔG_r^0 , for this reaction we need to consider the standard free energies for forming the reactants and the products from their elements in the standard state at the temperature of interest. If we assume a reaction temperature of 1200 K we can look up ΔG^0 for the individual reactions below:

Ti + 2Cl ₂	→ TiCl ₄	$\Delta G_1^0 = -610 \text{ kJ}$
C + 2H ₂	→ CH ₄	$\Delta G_2^0 = 42 \text{ kJ}$
1/2H ₂ + 1/2Cl ₂	→ HCl	$\Delta G_3^0 = -102 \text{ kJ}$
Ti + C	→ TiC	$\Delta G_4^0 = -171 \text{ kJ}$

From basic thermodynamics we know

$$\Delta G_r^0 = \sum \Delta G^0 \text{ products} - \sum \Delta G^0 \text{ reactants} \quad (28.3)$$

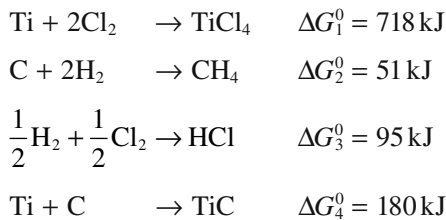
Hence, for the reaction in Eq. 28.2

$$\Delta G_r^0 = (\Delta G_4^0 + \Delta G_3^0) - (\Delta G_2^0 + \Delta G_1^0) \quad (28.4)$$

The numbers are

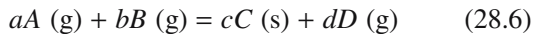
$$\Delta G_r^0 = [-171 + 4(-102)] - (42 - 610) = -11 \text{ kJ} \quad (28.5)$$

The negative value of ΔG_r^0 indicates that the reaction will proceed spontaneously at 1200 K to produce TiC. Consider a similar calculation at 298 K instead of 1200 K. The calculated values for ΔG^0 are now



Therefore, at a temperature of 298 K the value of ΔG_r^0 is +109 kJ. The positive value of ΔG_r^0 indicates that the reaction between TiCl_4 and CH_4 to form TiC will not proceed spontaneously at room temperature.

We now consider a generalized chemical reaction between two gases *A* and *B* to produce a solid *C* and another gas *D*.



The equilibrium constant for this reaction is

$$K = [C]^c [D]^d / [A]^a [B]^b \quad (28.7)$$

where [] indicates the equilibrium activity of each component of the reaction. As usual, we can take the activity of a pure stable component as unity. Pressures may be used to approximate the activities of the gaseous species, hence

$$K \approx (pD)^d / (pA)^a (pB)^b \quad (28.8)$$

where (*p*) are the equilibrium pressures of the reactants and products. The driving force for growth may be expressed as

$$\Delta G_r^0 = -RT \ln K \quad (28.9)$$

R, the gas constant, is $8.314 \text{ J K}^{-1} \text{ mol}^{-1}$.

It is usually desired that the concentration of the volatile reactant species be fairly high so that the transport of reactants to the substrate is very rapid. If the concentration of reactants is too low, it will be difficult to produce a reasonable flow of material to the substrate surface. Thus, we want the value of *K* to be small. Assuming that the reaction to produce TiC was carried out in a closed system (so that the HCl was not being removed), the value of $\ln K$ would be 1.1. [Sometimes the equilibrium constant term is expressed as a logarithm in base 10 (log) rather than as a natural logarithm, ln; the desired value would then be $\log K = 0.5$.] When $\ln K$ is very large, the driving force is very large, which tends to produce a polycrystalline film rather than

CVD

This is an empirical method of film growth guided by thermodynamics.

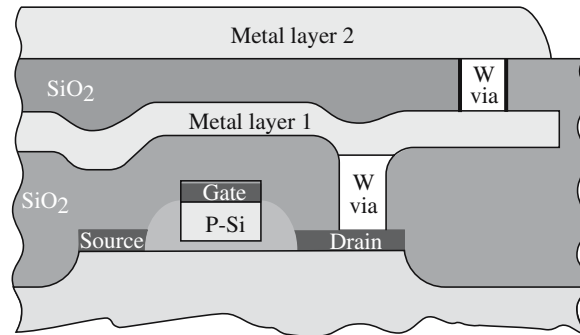


FIGURE 28.3 Schematic cross section of a multilayer metallization to a polysilicon gate field effect transistor. The contacts to the source and drain are silicides. Tungsten is used to provide vertical interconnects through vias in the oxide layer.

single-crystal epitaxial films. The use of thermodynamics implies that chemical equilibrium has been attained. Although this may occur in a closed system, it is generally not the case in an open system such as a flow reactor, where gaseous reactants and products are continuously introduced and removed.

28.6 CHEMICAL VAPOR DEPOSITION OF CERAMIC FILMS FOR SEMICONDUCTOR DEVICES

Ceramic films are widely used in the fabrication of semiconductor devices. The two materials that are presently of major interest are silicon dioxide (SiO_2) and silicon nitride (Si_3N_4). These are deposited as thin films using CVD.

SiO_2 films can be deposited with, or without, dopants. Undoped it has multiple uses:

- Insulating layer between multilevel metallizations (Figure 28.3)
- Implantation or diffusion mask
- Capping layer over doped regions to prevent outdiffusion during thermal cycling

A suitable reaction to produce SiO_2 is the oxidation of silane (SiH_4) at 450°C :



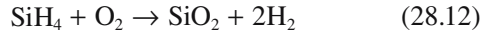
Above 600°C water vapor is produced:



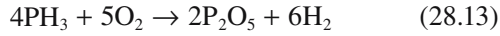
The SiO_2 film produced by either of the above two reactions is amorphous.

For some applications we need doped SiO_2 films. Dopant species include boron and phosphorus. Doped oxide films are made by introducing dopant compounds such as phosphine (PH_3)

or diborane (B₂H₆) into the gas stream along with SiH₄ and an oxygen source. The chemical reactions for phosphorus-doped oxides are



and



Phosphorus-doped silica films are used as

- Insulators between metal layers
- Device passivation
- Diffusion sources

One application that we will describe in a little more detail is the use of phosphorus-doped glass (called P-glass in the semiconductor industry) as an insulator between polysilicon gates and the top metallization in a metal oxide semiconductor field effect transistor (MOSFET). The P-glass is used because steps formed by the polysilicon gate make uniform deposition of the metal film impossible. The P-glass layer is deposited by CVD and then heated until it softens and flows: this process is called reflow. The reflow characteristics depend on the concentration of P in the glass, which is typically between 6 and 8 wt%. Silica doped with both P and B is also used for the reflow process. Typical concentrations are 1–4 wt% B and 4–6 wt% P. The borophosphosilicate glass (BPSG) has the advantage of lower flow temperatures; however, care must be taken to carefully control the dopant concentrations, otherwise separation of a B-rich phase can occur.

Si₃N₄ layers deposited by CVD are important in the fabrication of certain semiconductor devices. One area is in the so-called LOCOS (local oxidation of silicon) process. This method is used in both bipolar and metal oxide semiconductor (MOS) devices to isolate active device regions. The process works as follows: A layer of Si₃N₄ is deposited on the silicon wafer by CVD either by reacting silane and ammonia at temperatures between 700 and 900°C



or by reacting dichlorosilane and ammonia between 700 and 800°C



Like the SiO₂ films described earlier the Si₃N₄ is amorphous. The exposed regions of the silicon wafer are then oxidized whereas the areas covered by Si₃N₄ are protected. The oxidizing agent cannot diffuse through the Si₃N₄ layer to reach the silicon surface. However, oxidation does occur a small distance below the edges of the silicon nitride layer. If the oxide layer is sufficiently thick, the edges of

the nitride film are pushed up and away from the silicon surface. After oxidation the Si₃N₄ layer is removed.

Si₃N₄ layers are also used for passivating Si devices because they act as an extremely good barrier to the diffusion of water and Na. These impurities can cause device metallization to corrode or devices to become unstable.

28.7 TYPES OF CHEMICAL VAPOR DEPOSITION

There are several forms of CVD and each form has its own acronym. If the process takes place at atmospheric pressure (AP) it is referred to simply as CVD or APCVD. In APCVD systems the gas flow is almost exclusively parallel to the surface. The reactor configurations shown in Figure 28.1 are all examples of configurations used for APCVD.

When lower pressures are used the operation is low-pressure CVD (LPCVD). The gas pressure is usually in the range 0.5–1 torr for LPCVD reactors, distinguishing it from APCVD systems operating at 760 torr. In LPCVD reactors the substrates are mounted vertically.

If a plasma is used to generate ions or radicals that recombine to give the desired film, the process is plasma-enhanced CVD (PECVD). In PECVD it is possible to use much lower substrate temperatures because the plasma provides energy for the reaction to proceed. A major commercial application of PECVD is the formation of silicon nitride films for passivation and encapsulation of semiconductor devices. At this stage of the fabrication process the device cannot tolerate temperatures much above 300°C. High temperatures would still be required if crystalline or epitaxial films were required. Many nitrides have been prepared in thin-film form by PECVD, including AlN, GaN, TiN, and BN. A more complete list of films deposited by PECVD is given in Table 28.3.

PECVD has also been used to fabricate carbon nanotubes and other one-dimensional nanostructures such as boron carbide nanowires and nanosprings. A convenient precursor for boron carbide nanowires is orthocarborane (C₂B₁₀H₁₂).

MOCVD is distinguished from other forms of CVD in that the precursors are metalorganic compounds. MOCVD is widely used in the semiconductor industry but not so widely used in forming ceramic films. One example of a ceramic film formed by MOCVD is AlN, where the precursors are trimethyl aluminum [TMAI = Al(CH₃)₃] and ammonia (NH₃)



LECVD (laser-enhanced CVD) uses a laser beam to enhance reactions at the substrate surface. One feature of this technique is that it is possible to “write” materials on the substrate: the deposit is formed only where the scanned light beam hits the substrate.

TABLE 28.3 PECVD Reactants, Deposition Temperatures, and Growth Rates

<i>Film</i>	<i>T (K)</i>	<i>Rate (cm/s)</i>	<i>Reactants</i>
a-Si	573	10 ⁻⁸ -10 ⁻⁷	SiH ₄ ; SiF ₄ -H ₂ ; Si-H ₂
c-Si	673	10 ⁻⁸ -10 ⁻⁷	SiH ₄ -H ₂ ; SiF ₄ -H ₂ ; Si-H ₂
C (graphite)	1073-1273	10 ⁻⁵	C-H ₂ ; C-N ₂
CdS	373-573	10 ⁻⁶	Cd-H ₂ S
SiO ₂	523	10 ⁻⁸ -10 ⁻⁶	Si(OC ₂ H ₅) ₄ ; SiH ₄ -O ₂ , N ₂ O
GeO ₂	523	10 ⁻⁸ -10 ⁻⁶	Ge(OC ₂ H ₅) ₄ ; GeH ₄ -O ₂ , N ₂ O
SiO ₂ /GeO ₂	1273	3 × 10 ⁻⁴	SiCl ₄ -GeCl ₄ + O ₂
Al ₂ O ₃	523-773	10 ⁻⁸ -10 ⁻⁷	AlCl ₃ -O ₂
TiO ₂	473-673	10 ⁻⁸	TiCl ₄ -O ₂
B ₂ O ₃			B(OC ₂ H ₅) ₃ -O ₂
Si ₃ N ₄ (H)	573-773	10 ⁻⁸ -10 ⁻⁷	SiH ₄ -N ₂ , NH ₃
AlN	1273	10 ⁻⁶	SiCl ₄ -N ₂
GaN	873	10 ⁻⁸ -10 ⁻⁷	GaCl ₃ -N ₂
TiN	523-1273	10 ⁻⁸ -5 × 10 ⁻⁶	TiCl ₄ -H ₂ + N ₂
BN	673-973		B ₂ H ₆ -NH ₃
SiC	473-773	10 ⁻⁸	SiH ₄ -C _n H _m
TiC	673-873	5 × 10 ⁻⁸ -10 ⁻⁶	TiCl ₄ -CH ₄ + H ₂
B _x C	673	10 ⁻⁸ -10 ⁻⁷	B ₂ H ₆ -CH ₄

28.8 CHEMICAL VAPOR DEPOSITION SAFETY

Safety issues are particularly important for CVD since many of the source compounds are toxic and disposal of waste products, e.g., HCl, is often problematic. Additional problems can occur if the reactants are pyrophoric (ignite in contact with air). Table 28.4 lists some of the source gases used in CVD and their potential hazards. Silane is widely used in the semiconductor industry and was the cause of a major explosion and fire at a manufacturing plant in Moses Lake, WA. The incident caused a number

of critical injuries and resulted in the plant being closed for several months.

28.9 EVAPORATION

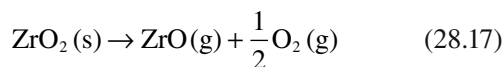
Experimentally, evaporation is a very simple method for forming thin films. The source is either a liquid or a solid that is heated to produce a flux of atoms or molecules. In general, it will be necessary to melt the material if the vapor pressure is <10⁻³ torr at its melting temperature. Most metals fall into this category and so liquid sources

TABLE 28.4 Hazardous Gases Used in CVD

<i>Gas</i>	<i>Corrosive</i>	<i>Flammable</i>	<i>Pyrophoric</i>	<i>Toxic</i>	<i>Bodily hazard</i>
Ammonia (NH ₃)	X			X	Eye and respiratory irritation
Arsine (AsH ₃)		X		X	Anemia, kidney damage, death
Boron trichloride (BCl ₃)	X				
Boron trifluoride (BF ₃)	X				
Chlorine (Cl ₂)	X			X	Eye and respiratory irritation
Diborane (B ₂ H ₆)		X	X	X	Respiratory irritation
Dichlorosilane (SiH ₂ Cl ₂)	X	X			
Germane (GeH ₄)		X		X	
Hydrogen chloride (HCl)	X				
Hydrogen fluoride (HF)	X				Severe burns
Hydrogen (H ₂)		X			
Phosphine (PH ₃)		X	X	X	Respiratory irritation, death
Phosphorus pentachloride (PCl ₅)	X				
Silane (SiH ₄)		X	X	X	
Silicon tetrachloride (SiCl ₄)	X				

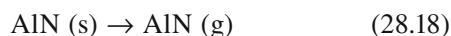
are used. Some metals reach sufficiently high vapor pressures below their melting temperature (e.g., Cr) and can be used as solids.

Evaporation of metals is generally straightforward because they evaporate either as atoms or as clusters of atoms. However, most compounds dissociate when heated and therefore the vapor composition will be different from that of the source. Consequently, the stoichiometry of the deposited film will also be different from that of the source. An example of an oxide that dissociates on heating is ZrO_2



Films formed directly from evaporation of ZrO_2 tend to be metal rich. To maintain the desired stoichiometry it is necessary to perform the evaporation in an oxygen-rich environment. This is called reactive evaporation (RE). A similar approach needs to be used with SiO_2 , GeO_2 , TiO_2 , and SnO_2 .

Some ceramics sublime, i.e., they go from a solid to a vapor without dissociation, for example



Thus film stoichiometry would be maintained in the deposit. Several oxides also behave in this way, for example, B_2O_3 , GeO , and SnO .

For some ceramics the high sublimation temperatures require special heating sources for evaporation. One such source is a focused electron beam. The process is then called electron beam (or simply e-beam) evaporation.

28.10 SPUTTERING

An example of a simple sputtering system is shown in Figure 28.4. Atoms are dislodged from a solid target through the impact of energetic gaseous ions. The usual sputtering gas is argon, which is ionized forming a plasma. An argon plasma has a characteristic purple color, which you see during sputter coating of samples for scanning electron microscopy (SEM) and transmission electron microscopy (TEM) analysis. The plasma forms as a result of collisions between energetic electrons in the gas and the argon atoms. The positive Ar^+ ions in the plasma are attracted toward the cathode (the *target*) and the electrons toward the anode (the *substrate*). The energy of the Ar^+ depends on the value of the applied electric field, but is sufficient to cause atoms to be ejected from the target surface. When an ion reaches the target it collects an electron, supplied via the external circuit from the anode, and become a neutral atom that returns to the gas to be reionized. A

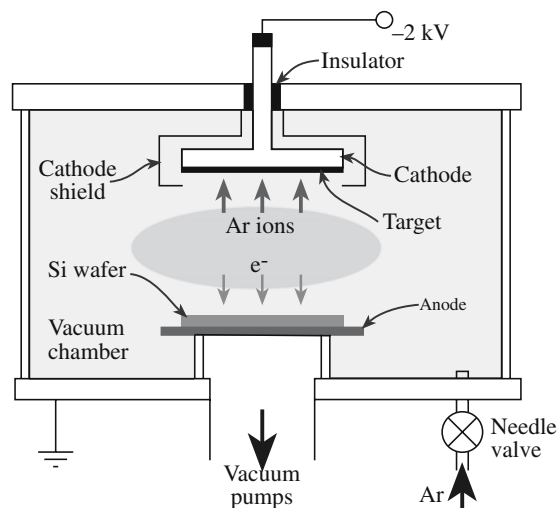


FIGURE 28.4 Schematic of a sputtering system.

substrate placed facing the cathode will be coated with a film of the material sputtered off the target surface. [If you have any experience with sputter coating samples for electron microscopy you will realize that the inside walls of the vacuum chamber also become coated.] A wide range of ceramics can be deposited by sputtering; some examples are given in Table 28.5.

There are several characteristics of the sputtering process that need to be considered before using this technique for film growth:

- It does not involve melting and therefore materials with high melting points can be deposited.
- It is a relatively slow process.
- It may be difficult to maintain stoichiometry of a multicomponent target due to the different sputtering rates of the constituents.
- When the substrate and target are facing each other (on-axis configuration) the growing film may be damaged by bombardment by energetic species from the plasma.

As with CVD and evaporation, there are various types of sputtering. The process we have described so far is DC sputtering, also called diode or cathodic sputtering. It is the easiest process to visualize, but cannot be used for insulating targets. There are two approaches for ceramics:

- Reactive sputtering uses DC sputtering of a metal target in a reactive gas environment. For example, we can make AlN films by sputtering an Al target in either nitrogen or ammonia (mixed in with the working gas, Ar).
- RF sputtering uses an alternating RF signal between the electrodes. Typical frequencies are between 5 and 30 MHz.

Ar IN PLASMA FORMATION

It is used because of its high mass, which creates a high momentum and more ejected particles from the target.

TABLE 28.5 Ceramic Sputtering Targets

<i>Material</i>	<i>Applications</i>
<i>Oxides</i>	
Al ₂ O ₃	Insulation, protective films for mirrors
BaTiO ₃ , PbTiO ₃	Thin-film capacitors
CeO ₂	Antireflection coatings
In ₂ O ₃ -SnO ₂	Transparent conductors
LiNbO ₃	Piezoelectric films
SiO ₂	Insulation
SiO	Protective films for mirrors, infrared filters
Ta ₂ O ₅ , TiO ₂ , ZrO ₂ , HfO ₂ , MgO	Dielectric films for multilayer optical coatings
Yttrium aluminum garnet (YAG), yttrium iron garnet (YIG), gadolinium gallium garnet (GGG, Gd ₃ Ga ₅ O ₁₂)	Magnetic bubble memory devices
YVO ₃ -Eu ₂ O ₃	Phosphorescent coating on special currency papers
YBa ₂ Cu ₃ O ₇	High-temperature superconductors
<i>Fluorides</i>	
CaF ₂ , CeF ₃ , MgF ₂ , ThF ₄ , Na ₃ AlF ₆ (cryolite)	Dielectric films for multilayer optical coatings (antireflection coatings, filters, etc.)
<i>Borides</i>	
TiB ₂ , ZrB ₂	Hard, wear-resistant coatings
LaB ₆	Thermionic emitters
<i>Carbides</i>	
SiC	High-temperature semiconduction
TiC, TaC, WC	Hard, wear-resistant coatings
<i>Nitrides</i>	
Si ₃ N ₄	Insulation, diffusion barriers
TaN	Thin-film resistors
TiN	Hard coatings
<i>Silicides</i>	
MoSi ₂ , TaSi ₂ , TiSi ₂ , WSi ₂	Contacts, diffusion barriers in integrated circuits
<i>Sulfides</i>	
CdS	Photoconductive films
MoS ₂ , TaS ₂	Lubricant films for bearings and moving parts
ZnS	Multilayer optical coatings
<i>Selenides, tellurides</i>	
CdSe, PbSe, CdTe	Photoconductive films
ZnSe, PbTe	Optical coatings
MoTe, MoSe	Lubricants

28.11 MOLECULAR-BEAM EPITAXY

Molecular-beam epitaxy is a technique that has mainly been used by the semiconductor industry for producing thin films of compound semiconductors (e.g., GaAs and InP) used in the fabrication of LEDs, laser diodes, etc. Because these inorganic semiconductors are ceramics it should not be surprising that the technique can also be used to grow other ceramic thin films, such as the high-temperature superconductor YBa₂Cu₃O₇. In fact, MBE is ideal for ceramics that have layered structures because it allows precise sequential deposition of single monolayers.

A diagram of an MBE system is shown in Figure 28.5. The materials to be deposited are usually evaporated from

separate furnaces called Knudsen effusion cells, which are bottle-shaped crucibles with a narrow neck. A resistance heater wound around the cell provides the heat necessary to evaporate the material. As in the case of conventional evaporation the source may be solid or liquid depending upon its vapor pressure. The rate of deposition of each species is determined by the vapor pressure above the source, which is a strong function of temperature. The temperature of each of the Knudsen effusion cells therefore controls the flux of atoms reaching the substrate.

Molecular-beam epitaxy of semiconductors requires the use of an ultrahigh vacuum (UHV) chamber (background pressure 10⁻⁸–10⁻¹⁰ torr). For oxide ceramics background pressures of ≤10⁻⁴ torr are more common. The high vacuum requirement of MBE presents a problem for the growth of

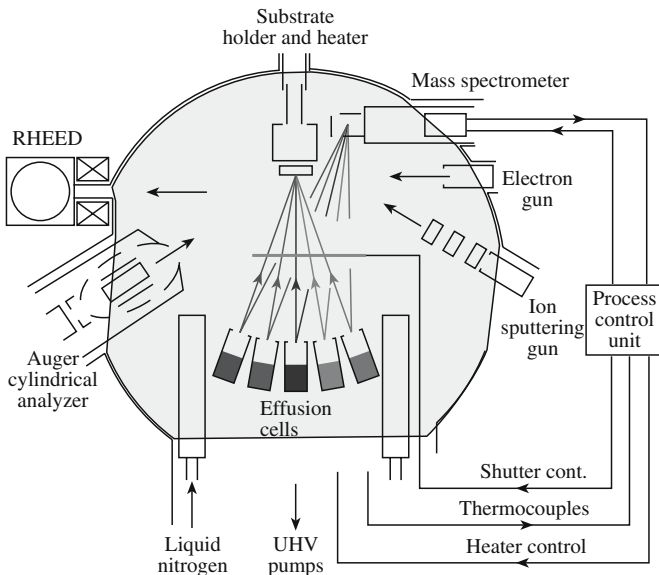


FIGURE 28.5 Schematic of an MBE system.

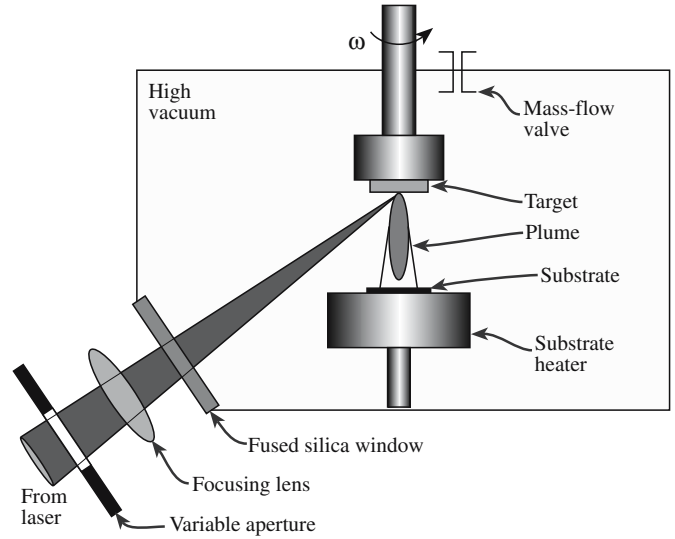


FIGURE 28.6 Schematic of a PLD system.

many multicomponent oxides such as the high-temperature superconductors because most of these compounds require oxygen pressures much higher than this to form. This limitation has been overcome by the use of highly oxidizing gases, such as NO_2 , atomic O, or O_3 , near the surface of the growing film, while the background pressure is maintained as low as possible.

In addition to the requirement of high vacuum or UHV environments, other features of MBE limit its use:

- The equipment is expensive (>\$1 million) so the value added must be high.
- Deposition rates are low: $\leq 1 \mu\text{m/h}$ is typical.

28.12 PULSED-LASER DEPOSITION

In pulsed-laser deposition (PLD) a laser beam is used to ablate material from a solid target. The experimental arrangement, which is very simple, is shown in Figure 28.6. However, the laser–target interactions are very complex and result in the formation of a plume of material (often visible and brightly colored) that contains all the necessary components (often in the correct proportions) for film growth.

PRESSURE

Pressure is often quoted in the non-SI units of torr, 1 torr being equivalent to 1 mmHg. The SI unit for pressure is the pascal, Pa. One Pa is equal to one newton per square meter (N/m^2). To convert between torr and Pa, simply multiply the pressure in torr by 133.3 to obtain the pressure in Pa ($750 \text{ torr} = 10^5 \text{ Pa}$).

PLD GROWTH OF BaTiO_3 THIN FILMS CONDITIONS

Chamber evacuated to $<5 \mu\text{torr}$
 Pressure during deposition 400 mtorr of O_2
 KrF excimer laser $\lambda = 248 \text{ nm}$
 Pulse repetition rate 50 Hz
 Pulse energy 85 mJ
 Target to substrate distance 4 cm
 Substrate temperature 750°C

Excimer lasers operating in the UV are the laser of choice for most PLD systems. The operating wavelengths used in commercial systems are shown in Table 28.6. Pulse energies up to 500 mJ are used with repetition rates up to several hundred hertz.

Pulsed-laser deposition offers several advantages over other PVD methods:

- The interaction of the laser beam and the target produces a plasma consisting of species having high kinetic energy, which enables epitaxial film growth at low substrate temperatures.
- Growth of films having complex stoichiometry can be achieved.
- The irradiation source is outside the deposition chamber allowing flexibility. Multiple chambers can

TABLE 28.6 Excimer Laser Wavelengths

Excimer molecule	Wavelength (nm)
F_2	157
ArF	193
KrCl	222
KrF	248
XeCl	308
XeF	351

use a single laser and the irradiation source can be easily changed.

- Relatively high deposition rates ($>10\text{nm/s}$) can be achieved.
- It is fairly inexpensive.

But it also has several drawbacks:

- It is difficult, at present, to cover large substrates uniformly since the plume peaks in the forward direction.
- The technique is line of sight.
- It is difficult to coat a large number of substrates at once.
- Laser–target interactions can result in the deposition of large (micrometer-sized) particles on the surface of the film. This presents problems if we want to produce multilayer structures.

28.13 ION-BEAM-ASSISTED DEPOSITION

There are two forms of ion-beam-assisted deposition (IBAD). The first is a dual-ion-beam system in which one source is used to sputter a target to provide a source of atoms for deposition (the same process we described in Section 28.10). Simultaneously a second ion beam is aimed at the substrate and bombards the depositing film. In the second configuration, shown in Figure 28.7, an ion source is combined with an evaporation source.

The use of ion bombardment during film growth can modify film properties. For example, IBAD of SiO_2 with 300eV O_2^+ ions during growth can change the refractive index. It is also possible to

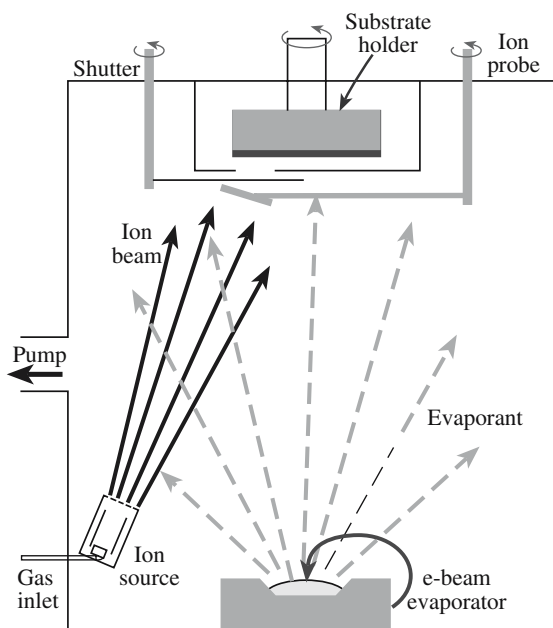


FIGURE 28.7 Ion-beam-assisted deposition system.

- Increase film adhesion
- Modify grain shape
- Induce crystallization

These changes are possible because the incident ion beam may

- Alter surface chemistry
- Create extra nucleation sites
- Increase the surface mobility of the adsorbed atoms
- Raise film temperature leading to higher reaction and diffusion rates

28.14 SUBSTRATES

There are many considerations when choosing a substrate for thin-film growth:

- *Chemical compatibility.* There should be no deleterious reactions between the film and the substrate. For the high temperatures ($\geq 700^\circ\text{C}$) used during the growth of many ceramic thin films this requirement may be quite restrictive.
- *Matched coefficient of thermal expansion (α).* In cases in which the film and substrate are different it will be almost impossible to achieve an exact match in α . A significant difference in α should be avoided because it can cause poor adhesion and cracking of the film. The latter problem is particularly relevant to ceramics, which are often brittle. Brittle materials are particularly weak in tension and therefore it is better if $\alpha_{\text{film}} < \alpha_{\text{substrate}}$; this will put the film in compression.
- *Surface quality.* The surface of the substrate is important because it is here that film nucleation and growth occur. The surface of a single-crystal substrate can contain a variety of defects of different sizes, from emergent dislocations, to surface steps, to scratches due to polishing. The defects are important because they can act as preferential sites for nucleation. Figure 28.8 shows the nucleation of islands of Fe_2O_3 at step edges formed in a Al_2O_3 substrate by high-temperature annealing. This type of orientation mechanism is known as graphoepitaxy, in which the topography of the substrate surface controls the microstructure of the film.
- *Cleanliness.* It is important to ensure that each substrate is cleaned before film deposition. For example, single-crystal MgO substrates are often packaged in mineral oil prior to shipping to avoid the reaction between the MgO and water vapor that results in the formation of $\text{Mg}(\text{OH})_2$. The oil can be removed by soaking in acetone. Many laboratories develop their own in-house cleaning procedures. The main steps involve degreasing in organic solvents, possibly followed by a high-temperature anneal.

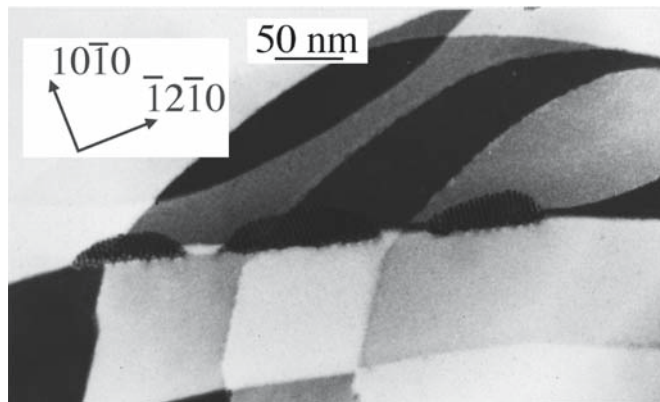


FIGURE 28.8 Growth at surface steps.

- *Substrate homogeneity.* In many single-crystal substrates this is not a problem. But in materials that are heavily twinned, such as LaAlO_3 and LaGaO_3 , twin boundaries that propagate through the substrate can act as nucleation sites. In bicrystal and polycrystal substrates the presence and orientation of the grain boundaries affect film microstructure and properties.

- *Thermal stability.* Phase transformations occurring during heating and cooling can result in the generation of stresses within the film. Perovskite substrates undergo phase transformation.

If we want to form epitaxial films, then we also need to consider the following:

- *Lattice mismatch.* In semiconductor systems lattice mismatches of only a few percent, or less, are desired to reduce the number of dislocations in the film. In ceramic thin films larger mismatches (generally $<15\%$) are tolerated because higher defect densities in the film are acceptable. In some situations a certain number of defects are actually beneficial to film properties (they can provide pinning sites in high-temperature superconductors that can trap magnetic flux lines).
- *Crystal structure.* A close match in the lattice parameters of the film and substrate is one important requirement for epitaxial growth. There must also be a reasonable number of coincident lattice sites on either side of the interface. Frequently, although not always, this means that the film and substrate should have similar crystal structures. The higher the number of coincident sites, the better the chance of good epitaxy.

CHAPTER SUMMARY

Thin films of ceramic materials are important both scientifically and commercially. For example, the operation of semiconductor devices relies on thin dielectric layers. In this chapter we described some of the main techniques used to produce such films. The common feature of all techniques for growing thin films is that we require a vacuum chamber. Deposition may occur at atmospheric pressure (e.g., some versions of CVD), but prior to deposition the chamber was evacuated. The choice of technique is based on several factors, including the type of material being deposited, whether we need an epitaxial layer, and often the cost. The substrate plays an important role in the growth of thin films and thus we need to know the properties of the substrate and how to prepare it. Some of the techniques we described, such as PECVD, are important not only for growing thin films but also for producing nanostructures such as nanowires and nanosprings.

PEOPLE IN HISTORY

Pascal, Blaise (1623–1662) was a French mathematician and philosopher who invented the first digital calculator to help his father, a tax collector. Among his other notable contributions to mathematics and science was laying the foundation for the theory of probability. The SI unit of pressure, the pascal, Pa, is named after him.

Torricelli, Evangelista (1608–1647) was born in Faenza (the home of faience pottery). He invented the barometer and worked in geometry. He died in Florence and the unit of pressure, torr, is named after him.

GENERAL REFERENCES

Chrisey, D.B. and Hubler, G.K. (1994) *Pulsed Laser Deposition of Thin Films*, Wiley, New York. A comprehensive survey of PLD and an excellent resource for information about materials grown by this technique.

Ohring, M. (1992) *The Materials Science of Thin Films*, Academic Press, Boston. Covers many aspects of thin-film deposition of all types of material. A very useful resource.

Pierson, H.O. (1992) *Handbook of Chemical Vapor Deposition (CVD): Principles, Technology, and Applications*, Noyes Publications, Park Ridge, NJ. Everything you want to know about CVD. Chapter 7 covers CVD of ceramics.

Smith, D.L. (1995) *Thin-Film Deposition: Principles and Practice*, McGraw-Hill, New York. A comprehensive handbook on thin-film growth.
Thin Solid Films. An international journal devoted to thin films.

SPECIFIC REFERENCES

- Adams, A.C. (1988) "Dielectric and polysilicon film deposition," Chapter 6 in *VLSI Technology* 2nd edition, edited by S.M. Sze, McGraw-Hill, New York. Gives an overview of the use of ceramic insulating layers in semiconductor device fabrication.
- Kubaschewski, O., Evans, E.L., and Alcock, C.B. (1967) *Metallurgical Thermochemistry*, 4th. edition, Pergamon Press, Oxford. A good standard thermodynamics text with lots of useful data collected in appendices.
- Phillips, J.M. (1996) "Substrate selection for high-temperature superconducting thin films," *J. Appl. Phys.* **79**, 1829.

EXERCISES

- 28.1 What reactive gases would be suitable for forming the following ceramic thin films by reactive sputtering?: (a) Al₂O₃, (b) TaN, (c) TiC, (d) CdS.
- 28.2 Name two of the ways that you might use to make sputtering targets.
- 28.3 Thin films can grow by three distinct mechanisms. Name the three mechanisms and explain how they differ.
- 28.4 Why is it often desirable to form thin films at the lowest possible substrate temperature?
- 28.5 What advantages are there, if any, of working at high substrate temperature?
- 28.6 What reactant gases might you use for making the following films by CVD?: (a) ZrC, (b) TaN, (c) TiB₂.
- 28.7 Consider the data given below:

Reaction	A	B	C
TiCl ₄ = Ti + 2Cl ₂	180,700	1.8	-34.65
2TiN = 2Ti + N ₂	161,700	—	-45.54
SiCl ₄ = Si + 2Cl ₂	155,600	3.64	-43.90
SiC = Si + C	14,000	1.3	-5.68
C + 2H ₂ = CH ₄	-16,500	12.25	-15.62
$\frac{1}{2}$ H ₂ + $\frac{1}{2}$ Cl ₂ = HCl	-21,770	0.99	-5.22
SiO ₂ = Si + O ₂	215,600	—	-41.50

The values of A, B, and C are given for $\Delta G^0 = A + BT \log T + CT$ (ΔG^0 in cal.). From these data determine whether it would be thermodynamically feasible to form the following ceramic films by CVD at a temperature of 850°C. (a) TiN from the nitridation of TiCl₄, (b) SiC from the reaction between SiCl₄ and methane, and (c) SiO₂ from the oxidation of SiCl₄.

- 28.8 What technique would you use to produce a 100-nm thin film of AlN on silicon? Explain why you chose your technique and its pros and cons.
- 28.9 What technique would you use to produce a 5-nm thin film of BaBiO₃ on MgO? Explain why you chose your technique and its pros and cons.
- 28.10 Which of the techniques described in this chapter is most suitable for producing thin films on large substrates? What is the largest substrate that can be coated?

Growing Single Crystals

CHAPTER PREVIEW

We will now describe the important methods used to produce single crystals of ceramic materials. Single crystals are important in many applications ranging from synthetic gemstones for jewelry to hosts for solid-state lasers. The method that is selected to grow a particular type of crystal depends on several factors. The selection criteria are determined by the properties of the material—whether a suitable solvent can be found, if the solid melts congruently or incongruently, or if it sublimates, and the economic factors—the volume of material to be produced and the capital equipment costs. Remember that without the growth of ceramic single crystals, the Si Age would never have happened.

29.1 WHY SINGLE CRYSTALS?

For some applications, ceramic materials must be prepared as single crystals. When used as substrates for thin-film growth [e.g., silicon-on-sapphire (SOS) technology or the growth of superconductor thin films] it is the crystalline perfection of a single crystal that is important. In optical applications, e.g., the use of ruby and yttrium–aluminum–garnet (YAG) for laser hosts and quartz and sapphire for optical windows, single crystals are used to minimize scattering or absorption of energy. In piezoelectric materials, e.g., quartz, the optimum properties are obtained in single-domain single crystals. Table 29.1 lists some of the applications that utilize the desirable optical, electrical, magnetic, or mechanical properties of ceramic single crystals.

Because preparing single crystals is in most cases a more difficult and expensive process than preparing the same compositions in polycrystalline form they are often much more expensive than their polycrystalline counterparts. For example, you can buy 99.9% pure MgO powder in small quantities for about \$2/gram. Single crystal slices of MgO of the same purity cost about \$300/gram! The increased cost of the single crystal not only involves the extra processing costs but may also include costs associated with orienting, cutting, and polishing.

When used for jewelry, synthetic single crystals can be more costly than naturally occurring ones. For example, the cost of a gem-grade faceted synthetic diamond may be 10 times that of an equivalent natural diamond. However, flux-grown emeralds and rubies are about one-tenth the cost of natural stones of comparable quality. (The synthetic stones are often much more perfect than the natural ones.) Large single crystals of cubic ZrO₂, which are used

as diamond simulants, are available only as synthetics. In its pure form the cubic polymorph of zirconia is not stable at room temperature and must be stabilized by the addition of CaO, MgO, or Y₂O₃. The cubic form of ZrO₂ does exist in nature; it was discovered in 1937 as tiny crystals in an amorphized piece of zircon (ZrSiO₄), but it is not abundant.

29.2 A BRIEF HISTORY OF GROWING CERAMIC SINGLE CRYSTALS

Although crystal growth is a relatively new industry, we can trace its origin back to 2500 BCE when salt was purified by crystallization. Systematic work in crystal growth started in c. 1600 CE with the growth of crystals from aqueous solution and in c. 1850 from the melt and the vapor.

Hydrothermal growth. Growth of large single crystals of a ceramic material using the hydrothermal growth method was first demonstrated for α -quartz. This method uses an aqueous solution that is usually heated and pressurized. The growth process closely reproduces the growth of amethyst in nature. The principle is essentially the same as used for growing salt or copper sulfate crystals in high school. Silica is soluble in water, which is where diatoms find their silica. The special feature of the hydrothermal growth of quartz is the use of pressure to increase the solubility of SiO₂ in H₂O.

Flux growth. First practiced by French and German chemists and mineralogists in the late 1800s, this technique is also known as molten-salt growth. Flux growth did not become an important method for forming single crystals until the 1950s. A particularly significant

TABLE 29.1 The Uses of Single Crystals

Semiconductor devices	
1. Diodes	Si, Ge
2. Photodiodes	Si, GaAs, Cd _x Hg _{1-x} Te
3. Transistors	Si, GaAs, SiC
4. Thyristors	Si
5. Photoconductive devices	Si, Cd _x Hg _{1-x} Te
6. Integrated circuits	Si, GaAs
7. Light-emitting diodes	GaAs, GaN, SiC
8. Radiation detectors	Si, Ge, CdTe, YAG
9. Strain gauges	Si
10. Hall effect magnetometers	InSb
Mechanical components	
1. Abrasives and cutting tools	SiC, Al ₂ O ₃
2. Substrates	Diamond, Al ₂ O ₃
Magnetic devices	
1. Transformer cores	Ferrites
2. Electric motors	Ferrites
3. Tape heads	Ferrites
4. Microwave circulators	Garnets
Piezoelectric devices	
1. Resonant bulk wave devices	SiO ₂ , LiTaO ₃
2. Surface wave devices	SiO ₂ , LiNbO ₃ , AlN
Optical devices	
1. Windows	Al ₂ O ₃
2. Lenses	CaF ₂
3. Polarizers	CaCO ₃
4. Laser hosts	YAG, Al ₂ O ₃ , alexandrite
5. Magneto-optical devices	YIG
6. Electro-optic devices	LiNbO ₃ , ADP, KDP
7. Nonlinear devices	ADP, KDP, LiNbO ₃
Jewelry	
Pyroelectric devices	
X-ray and particle optical devices	
1. Collimators and focusing elements	SiO ₂

contribution during this time was the growth of BaTiO₃ single crystals using a KF flux at Bell Telephone Laboratories in New Jersey. These crystals were of interest to Bell Labs for ferroelectric storage elements for digital computers and telephone switching systems. Single crystals were preferred over polycrystalline sintered BaTiO₃ ceramics because the single crystals had a more rectangular hysteresis loop and lower coercive fields. (See Chapter 31 for more on ferroelectric ceramics.)

Verneuil, Czochralski, and Bridgman. The Verneuil process, also known as the flame-fusion method, was first described in 1902 by Auguste Verneuil. His original apparatus has been preserved and is in the Museum of Arts and Sciences (Musée des Arts et Métiers) in Paris. This process was used in the early 1900s to make synthetic rubies. Although the initial application for these crystals was in jewelry, their hardness made them suitable for bearings in clocks and watches, which eventually has become their main use. Other methods for growing crystals from the melt followed. Pulling the crystal from the melt was first practiced by Czochralski (Cz) in 1917. He grew crystals of low-melting temperature metals including Sn, Pb, and Zn. Single crystals of Ge and Si were first

produced by the Cz method in 1950. This process is now used in the semiconductor industry for preparing very large single crystals of Si and, with some slight modifications, it can be used to produce single crystals of compound semiconductors (e.g., GaAs). The first oxide crystals to be grown extensively by the Cz process were calcium tungstate (CaWO₄), a laser host. Melt growth of single crystals in crucibles was first used by Bridgman and the method was significantly improved by Stockbarger and became known as the Bridgman–Stockbarger method.

Two melt-growth techniques that have emerged since 1950 are zone refining and the floating-zone (FZ) method; some of the thin-film methods discussed in Chapter 28 can also be thought of as melt techniques. Zone refining is used to purify single crystals (also for polycrystals). Although zone refining is applicable to all types of single crystal, its use is widespread only in the semiconductor industry where crystal purity is of great concern. The FZ method was first applied to the growth of Si crystals. It has since been used to form single crystals of other ceramics but is mainly limited to high-purity Si.

Although vapor-phase techniques are widely used to make thin films they are not used extensively in the growth of large single crystals. One of the most interesting vapor-phase methods is the vapor–liquid–solid (VLS) mechanism first identified by Wagner and Ellis. This mechanism allows the growth of thin single-crystal whiskers that can be used as reinforcements in ceramic-matrix composites (see Chapter 20). It is also widely discussed regarding the growth of nanotubes, nanowires, and nanosprings.

29.3 METHODS FOR GROWING SINGLE CRYSTALS OF CERAMICS

The growth of single crystals involves one of the following changes of state:

- Liquid (pure or solution) → solid
- Gas → solid

The atomic or molecular species in a fluid are, on average, arranged randomly. During crystal growth they must move to the correct sites in the ordered structure of the crystalline phase. If crystal growth is too rapid, disordered regions (crystal lattice defects such as dislocations) are trapped in the crystal or many smaller crystals with varying orientations are nucleated thereby destroying the desired single-crystal perfection. The growth process involved in producing a single crystal must therefore be slow and so it requires precise control over the growth conditions (e.g., temperature) for prolonged periods.

Several different methods are used commercially to grow single crystals. These methods, which can be divided into melt, solution, and vapor-phase techniques, are summarized in Table 29.2. Here, the operating cost does not include the cost of labor, the skill refers only to the diffi-

TABLE 29.2 Factors Relevant to the Choice of a Growth Technique for Crystal Production

	<i>Equipment investment</i>	<i>Operating costs</i>	<i>Skill needed</i>	<i>Development needed</i>	<i>Range of materials</i>	<i>Growth rate</i>	<i>Crystal perfection</i>
Cz	High	Medium	Medium	Medium	Many	Rapid	High
Bridgman	Low	Medium	Low	Little	Many	Medium	Medium
Verneuil	Medium	Low	High	Little	Some	Rapid	Low
Skull melting	High	Medium	Medium	Medium	Some	Rapid	Medium
Flux	Medium	Medium	Low	Much	Few	Slow	Variable
Hydrothermal	Very high	High	Medium	Much	Few	Slow	Variable
UHP	Very high	High	High	Much	Few	Slow	Variable
Gas phase	Low	Low	Low	Varies	Few	Very slow	Variable

culty in using the equipment, not in developing the process, the crystal perfection assumes the optimum conditions, not the fastest, and the rate of flux growth depends on the complexity of the reaction—as is the case with growth of emerald.

The method chosen depends on the type of crystal, the application for that crystal, and the required size. The most widely used growth technique is the Cz process because it can produce very large dislocation-free crystals of silicon. It is also used to form single crystals of many oxides. For oxides containing more than one cation the general requirement for forming a crystal by the Cz process is that the material melts congruently. In such cases crystal growth of compounds by pulling is similar to growing elemental crystals. If the compound melts incongruently the Cz method can still be used, if special precautions are taken, or an alternative method, e.g., growth from solution or from a flux, may have to be used.

Most methods of single-crystal growth seek to control the nucleation of the crystalline phase. This is achieved by arranging for the crystal to grow on a “seed” (which is the nucleus). The seed crystal is usually a single crystal of the same composition as the crystal to be grown. It is often oriented in such a way as to facilitate growth of one specific crystalline orientation. In the Bridgman–Stockbarger method a seed crystal is not used. In this method advantage is taken of the tendency for crystals to grow more rapidly in one crystallographic direction than in another.

Vapor-phase techniques are not as widely used as growth from the melt or solution because the growth rate is generally slow or only small crystals can be grown. However, two vapor-phase techniques have commercial application: the growth of whiskers or small islands (e.g., SiC and GaN) by the VLS process and the growth of SiC and nanotubes by sublimation processes.

Many other techniques can be used to produce single crystals; solid–solid phase transformations or growth from gels are modern examples. Although such methods may be useful in the laboratory for producing small single crystals of ceramics they are not currently of commercial importance.

29.4 MELT TECHNIQUE: VERNEUIL (FLAME-FUSION)

The Verneuil, or flame-fusion, method is illustrated in Figure 29.1. It is a well-established technique for growing single crystals of oxides that have high melting temperatures. The largest application of the Verneuil method is for the growth of sapphire and ruby.

For growing sapphire crystals, high-purity aluminum oxide powder of a uniform particle size is fed at a controlled rate down a tube at the end of which the particles are melted by an oxyhydrogen flame. The molten particle then falls into a shallow (~20- μm -deep) pool of liquid on top of a seed crystal. The pool of liquid is held on the seed crystal by surface tension. The seed is lowered into the annealing zone of the furnace at the

same rate as the new material arrives, thus growing the crystal. The growing crystal cools slowly helping to reduce strains and minimizing the chance of forming lattice defects. It is always preferable to anneal the crystal from the growing temperature without first cooling to room temperature. If the crystal is first cooled to room temperature and then annealed it is much more difficult to remove any defects that have formed. Remember that the crystal will still contain point defects as these are equilibrium defects at high T and so cannot easily be annealed out. Since a gas flame and powder are used in the process, trapped pores are common defects.

SINGLE-CRYSTAL TERMINOLOGY

A large single crystal in the as-grown form is often referred to as a *boule*, from the French word for ball, or as an *ingot* (which may also be used to describe a polycrystal).

When a boule is cut into flat sections, the single-crystal slices are typically referred to as *wafers*.

When the wafers are cut into small units (usually either square, rectangular, or circular) they are referred to as *substrates* or *windows*.

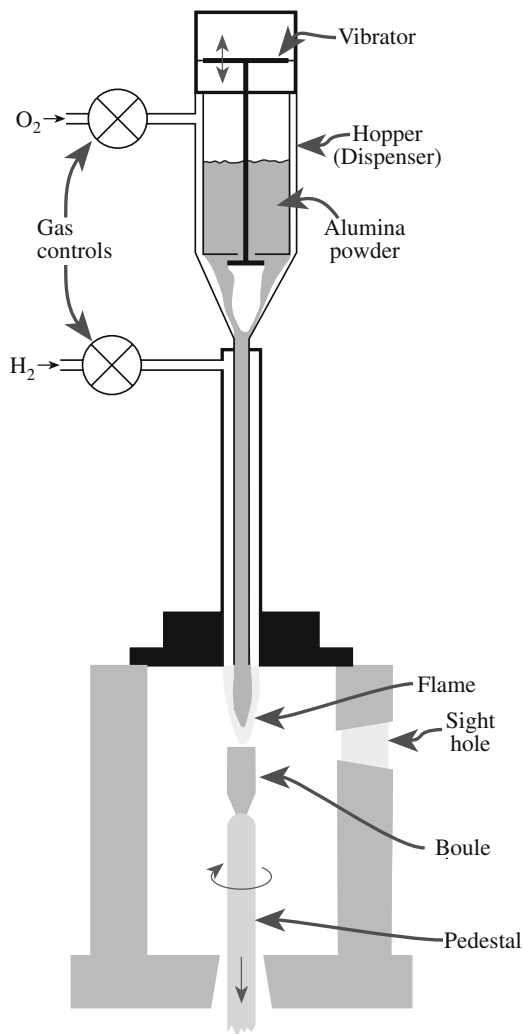


FIGURE 29.1 The Verneuil technique.

To produce artificial rubies and sapphires various transition metal oxides are added to the alumina feed powder. For rubies, between 1 and 3 at% Cr₂O₃ gives the char-

STALAGMITES

The Verneuil technique is related to the growth of stalagmites in nature. Liquid drips (from the stalactite) onto the stalagmite, but instead of settling there and freezing (like a stalagmite icicle would) some of the mineral content is deposited as the water evaporates.

acteristic deep red color. Artificial blue sapphires are obtained when a mixture of 1 at% TiO₂ and 2 at% FeO is added to the feed powder.

One advantage of the Verneuil method is that it does not use a crucible to contain the melt—only a shallow pool of liquid is present throughout the growth process. An important constraint of liquid-to-solid transitions for crystal growth is the reaction of the melt with the container. For crystals with a high melting temperature (the situation we often encounter in ceramics) this constraint becomes especially severe. Even if reactivity is not a problem it is still difficult to find suitable containers that can withstand very high temperatures without melting or degrading. The other advantages of the Verneuil method are that it is relatively inexpensive and quick. Crystals can easily be obtained in a matter of hours (typical growth rates are 10⁻² m/h) compared with the months needed for some solution techniques.

The main disadvantage of the Verneuil process is that there is relatively poor control over the growth parameters, particularly the temperature, because of the very small melt volume. As a consequence the quality of the crystal is often inferior to that obtained by, for example, the Cz method. Typically, Verneuil-grown crystals have high dislocation densities, which makes them most suitable for applications in which such imperfections are not so important (e.g., jewelry or jewel bearings). Very large single crystals cannot be produced by the Verneuil method. Verneuil-grown boules may be up to 9 cm in diameter. Table 29.3 lists some of the ceramic crystals that have been grown by the Verneuil method. Verneuil sapphire is used as the starting material (crackle) for Cz sapphire.

The FZ method shares many similarities with the Verneuil method. The main difference is that the source is a dense polycrystalline rod of the same composition as the desired single crystal, rather than the free-flowing powder used in the Verneuil method, but it still uses a constrained volume of liquid. The advantage of

TABLE 29.3 Crystals Grown by Verneuil and Arc-Image Techniques

Material		Comments	T _M (°C)
Al ₂ O ₃	Corundum, sapphire	Growth in a variety of directions; best growth in a cone of directions 60° from c	2040
Al ₂ O ₃ : Cr	Ruby	Verneuil	
MgAl ₂ O ₄	Magnesium-aluminum spinel	Verneuil	2130
3Al ₂ O ₃ ·2SiO ₂	Mullite	Verneuil	1810
CaWO ₄	Scheelite	Verneuil	1530
TiO ₂	Rutile	Verneuil	1830
ZrO ₂	Zirconia	Verneuil	2700
Y ₂ O ₃	Yttria	Verneuil	2400
MgFe ₂ O ₄	Magnesium (nonstoichiometric) spinel	Arc-image	>1200
NiFe ₂ O ₄	Nickel ferrite	Arc-image	>1200

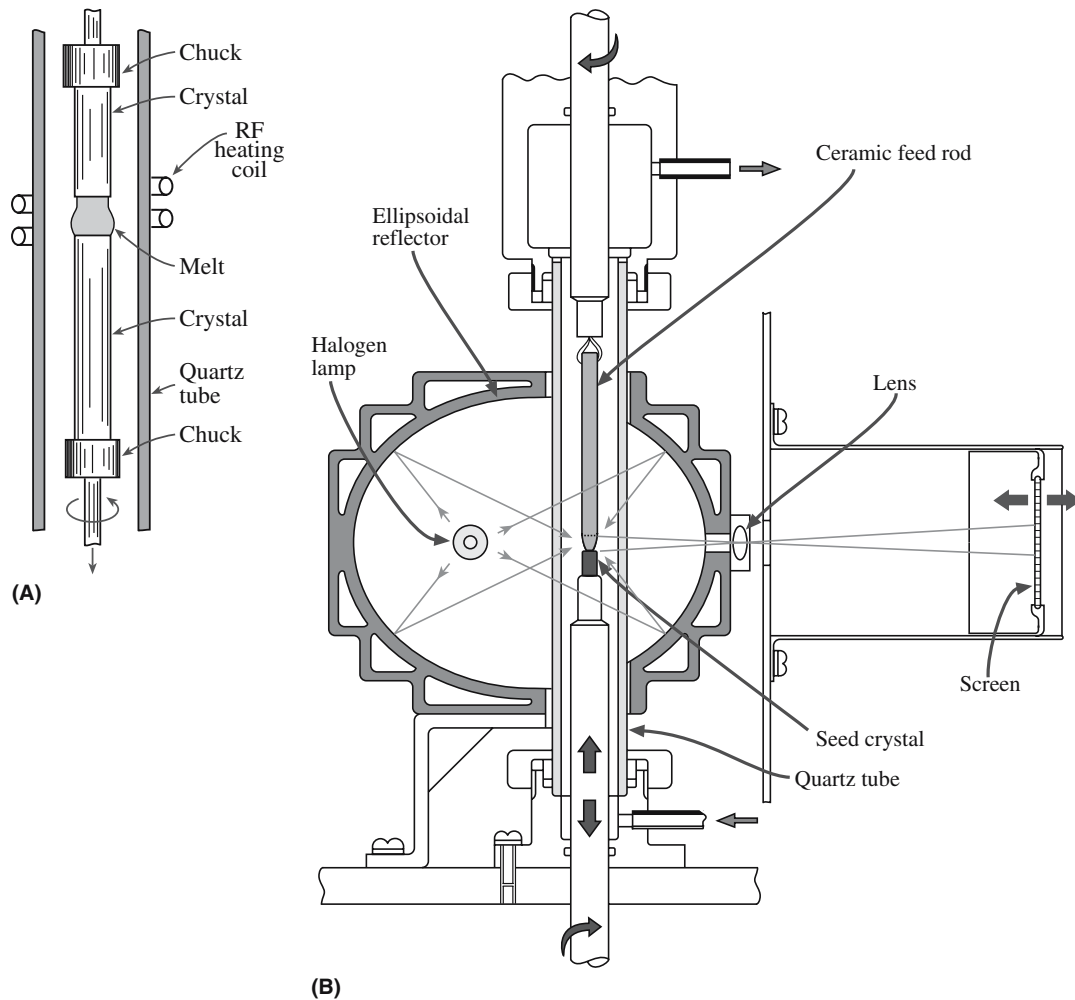


FIGURE 29.2 (a) Vertical float zone. (b) Arc image furnace.

the FZ method is that like the Verneuil method, no crucible is used: the material is its own crucible as shown in Figure 29.2a. A thin region of melt is again held in place by surface tension, this time between two parts of the feed rod. Not having a container removes one possible source of contamination; this is why the FZ method is used to produce high-resistivity silicon. The disadvantages of the FZ method are that it is not as amenable as the Cz method for producing very large high-quality single crystals. For ceramics the FZ method may use the arc-image heating method to attain the necessary high temperatures.

29.5 MELT TECHNIQUE: ARC-IMAGE GROWTH

Several techniques for growing single crystals combine aspects of the FZ method and the Verneuil flame fusion method, but the heat source is not a flame. One such “modified” FZ growth technique is called arc-image growth. Heat is supplied using a focused light source. Figure 29.2b shows a schematic arrangement of the

arc-image growth process. The radiation from the light source is focused by parabolic reflectors and allows sample temperatures $>2500^{\circ}\text{C}$ to be attained. If a controlled or inert atmosphere is needed around the sample then it can be enclosed in a suitable transparent tube (envelope). MgFe_2O_4 , and NiFe_2O_4 , have both been grown by this technique. The main advantage of using arc-image heating is that it is easy to provide a clean high-temperature environment with a controllable atmosphere (which is particularly important when Fe cations are involved).

29.6 MELT TECHNIQUE: CZOCHRALSKI

A schematic diagram of the Cz technique is given in Figure 29.3a. The melt is kept at a temperature just above its freezing point and a seed crystal, rigidly fixed to a rotating tube, is lowered into the surface of the melt. The temperature of the melt is reduced until the molten material begins to freeze onto the seed. Pulling is then started and more material solidifies onto the crystal as it is withdrawn. The shape of the meniscus is determined by the

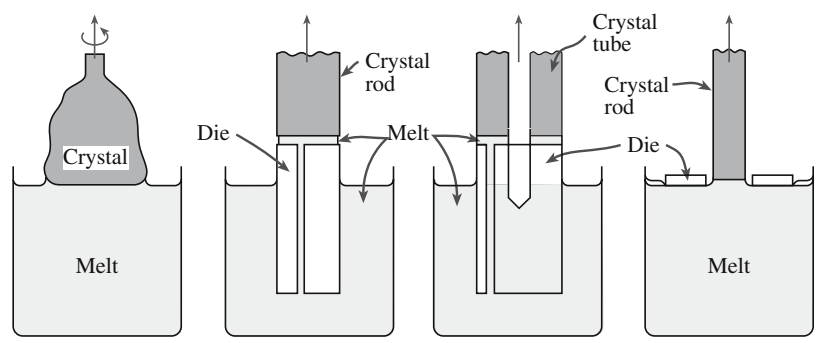
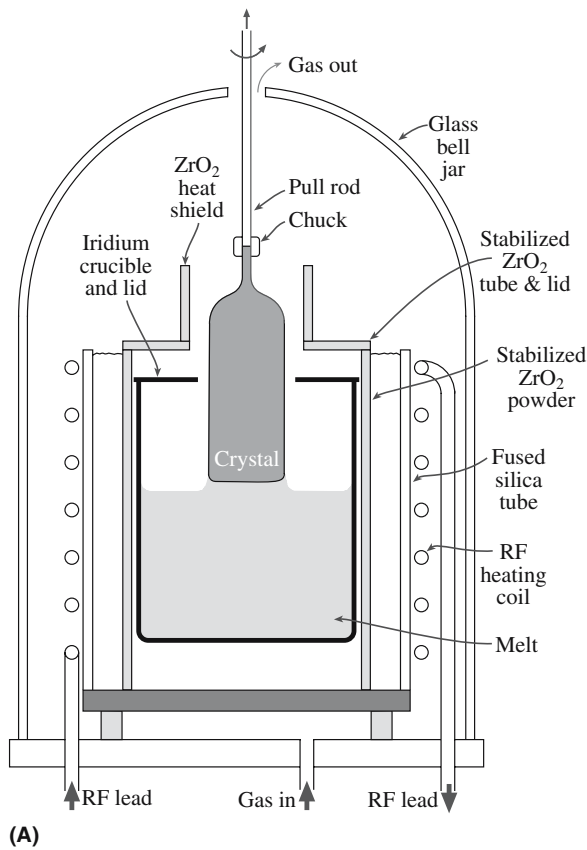


FIGURE 29.3 (a) The Czochralski technique for pulling crystals. (b) Modifications to Czochralski. Compared with the conventional geometry (left).

surface tension of the liquid. The seed crystal is normally rotated as it is withdrawn to average out any thermal asymmetries in the heating elements. This rotation also produces a stirring action, which can help homogenize the melt. At the same time, it accelerates crucible erosion and hence can introduce additional impurities into the melt. In cases in which the impurity concentration must be kept to a minimum the crucible containing the melt and the crystal

can be rotated at the same rate and in the same direction! For nonoxide crystals the whole apparatus is maintained in an inert environment (e.g., Ar). Table 29.4 summarizes the relevant growth conditions that have been used to produce different crystals. A variation is to use a die to produce tubes, fibers, or sheets of sapphire or garnet as illustrated in Figure 29.3b. Actually single-crystal tubes can be produced inside single-crystal tubes.

TABLE 29.4 Materials Grown by the Cz Technique (for Crystals ~2cm in Diameter)

Material	T_M (°C)	Crucible	Atmosphere	Pulling rate (mm/h)	Rotation rate (rpm)
Zn	419	Pyrex	Vacuum	400–800	10–30
GaSb	712	Graphite	Hydrogen	50–100	10–30
FeGe ₂	866	Alumina	Vacuum	5–20	20–50
Bi ₁₁ GeO ₂₀	930	Platinum	Oxygen	5–15	10–50
Ge	937	Graphite	H ₂ /N ₂	60–120	20–50
ZnWO ₄	1200	Platinum	Air	8–16	50–100
GaAs	1237	Silica	Arsenic	20–30	10–30
LiNbO ₃	1250	Platinum	Oxygen	3–8	20–30
Sr _x Ba _{1-x} Nb ₂ O ₆	1400	Platinum	Oxygen	3–6	10–20
Si	1420	Silica	Argon	100–200	10–20
MnFe ₂ O ₄	1500	Iridium		3–6	10–20
CaWO ₄	1650	Rhodium	Air	8–16	50–100
LiTaO ₃	1650	Iridium	Nitrogen	8–15	20–40
Y ₃ Al ₅ O ₁₂	1950	Iridium	Nitrogen	1–3	40–60
Al ₂ O ₃	2037	Iridium	Argon	1–3	30–50
MgAl ₂ O ₄	2100	Iridium	Argon	4–8	20–40



FIGURE 29.4 Lower part of sapphire boule grown by the Cz technique, the boule was 100–150mm diameter; 300mm long.

Figure 29.4 shows part of a sapphire boule produced by the Cz process. Sapphire boules can be up to 150mm in diameter and 600 mm in length and weigh >40 kg. Most sapphire is grown in the *r*-plane orientation (the growth axis is normal to the *r* plane). If an Si crystal is grown with a 300 mm (12 inches) diameter to a length of 0.5 m, the crystal weighs ~82 kg.

To determine the factors that affect the growth rate of the crystal we need to consider the heat flow in the system. The heat input, q_{in} , to the crystal across the crystal/melt interface is given by the sum of the heat associated with crystallization, q_L , and the heat flow from the melt, q_M :

$$q_{in} = q_L + q_M \quad (29.1)$$

q_L is given by

$$q_L = A\rho_s\Delta H_{fus} \frac{dx}{dt} \quad (29.2)$$

where A can be considered to be the area of the crystal at the liquid–solid interface. Actually, A is the area of the isotherm that goes through a point in the liquid close to the interface; however, very close to the interface this area is approximately the liquid–solid interfacial area. The density of the solid is ρ_s , ΔH_{fus} is the heat of crystallization (fusion), and dx/dt is the rate of growth. To a good approximation the growth rate can be considered equal to the pulling rate, which from Eq. 29.2 we can see is inversely proportional to A . Therefore the faster the crystal grows, the smaller its diameter.

The heat flow from the melt, q_M , is given by

$$q_M = Ak_L \frac{dT}{dx_L} \quad (29.3)$$

where k_L is the thermal conductivity of the liquid and dT/dx_L is the thermal gradient in the liquid. q_{in} is also the heat flow down the crystal, which is given by

$$q_{in} = Ak_s \frac{dT}{dx_s} \quad (29.4)$$

where k_s is the thermal conductivity of the crystal and dT/dx_s is the thermal gradient in the crystal. By substituting Eqs. 29.2, 29.3, and 29.4 into Eq. 29.1 we find

$$Ak_s \frac{dT}{dx_s} = A\rho_s\Delta H_{fus} \frac{dx}{dt} + Ak_L \frac{dT}{dx_L} \quad (29.5)$$

Upon rearranging

$$\frac{dx}{dt} = \frac{1}{\rho_s\Delta H_{fus}} \left(k_s \frac{dT}{dx_s} - k_L \frac{dT}{dx_L} \right) \quad (29.6)$$

If the pulling rate exceeds the value of dx/dt given by Eq. 29.6 the crystal separates from the melt; if it less than that given by Eq. 29.6, then A will increase. Figure 29.5 shows the rings that develop around a single crystal as it grows with dx/dt constantly changing to keep A constant.

According to Eq. 29.6 the maximum growth rate possible occurs when dT/dx_L approaches 0 (if dT/dx_L becomes negative the liquid would be supercooled and the interface would advance rapidly and dendritic growth would occur). The maximum growth rate, $(dx/dt)_{max}$, is then given by

$$\left(\frac{dx}{dt} \right)_{max} = \frac{1}{\rho_s\Delta H_{fus}} \left(k_s \frac{dT}{dx_s} \right) \quad (29.7)$$

We can see from Eq. 29.7 that the value of $(dx/dt)_{max}$ depends on the temperature gradient in the solid. The largest gradients in the solid may be obtained by deliberately introducing large heat leaks from the growing crystal; one method is to water-cool the seed holder. However, the high rates obtained under such conditions are generally not



FIGURE 29.5 Growth rings on crystal surface: top section of Si crystal after removing seed.

useful because the crystal perfection under such growth conditions is usually not very high. Typically, growth rates for good crystal quality are 10^{-4} – 10^{-2} mm/s, 30–50% slower than the maximum values given by Eq. 29.7.

The Cz process has the following principal advantages:

- Excellent control over the growth conditions produces very high quality crystals.
- It is relatively fast.
- Very large crystals can be produced.

A particular feature of the Cz process is that it is possible to produce dislocation-free single crystals. As discussed in Chapter 12, dislocations are not equilibrium defects. Therefore it is, in principle, possible to produce crystals that are free of dislocations. Although a small number of dislocations in a single crystal of most ceramics does not normally present any problems, this must be avoided if we are using the ceramic for its electrical/semi-conducting properties. Dislocation-free crystals can be achieved once growth has started on the seed if the diameter of the crystal is slowly reduced to a minimum size. The minimum size is the size that can still support the weight of the crystal to be grown (without deforming plastically and multiplying the number of dislocations). Typically the minimum size is ~3 mm in diameter and 30 mm long; a 3-mm-diameter sapphire rod will support ~200 kg. During this period, the crystal-melt surface becomes strongly concave as illustrated in Figure 29.6 so that dislocations present in the initial seed can glide to the sidewalls of the crystal. Dislocation glide is facilitated if the glide plane makes a large angle to the growth axis. For crystals with a diamond-cubic structure the glide plane is {111}; for crystals with a rocksalt (NaCl) structure the glide plane is {110} (unless it is not—see Section 17.2). Subsequent growth is slowly modified to give the desired crystal diameter and a dislocation-free crystal is then pulled. The dislocation density in Cz sapphire boules is typically in the range of 10^3 – 10^4 cm⁻².

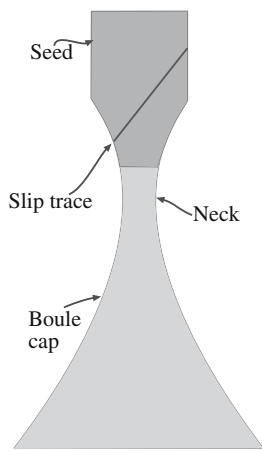


FIGURE 29.6 Schematic illustration of neck-down and flare-out geometries for growing dislocation-free crystals.

There are several disadvantages to the Cz process.

- It is applicable only to materials that melt congruently or nearly congruently (see Sections 8.10 and 29.10).
- The melt must be contained in a crucible; this is a problem for reactive high-temperature melts.
- The capital cost is high. A Cz furnace used to produce 8-inch-diameter sapphire boules costs \$400,000. For larger boules the furnace can cost \$1 million.

Despite these disadvantages the Cz technique is the most important crystal-growth technique for producing large high-quality single crystals.

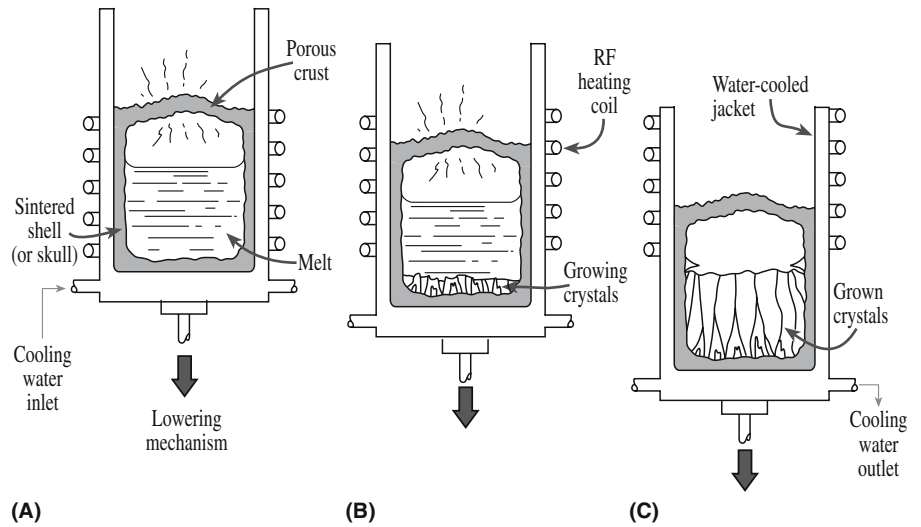
29.7 MELT TECHNIQUE: SKULL MELTING

One of the problems with growing single crystals of ceramic materials is that they often have very high melting temperatures. When molten, the liquid can be extremely corrosive to any crucible. In skull melting the melt is contained within a frozen shell of the material itself—the material acts as its own crucible. In perhaps the first application of the skull melting process the technique was combined with crystal pulling to produce single crystals of manganese ferrite. Later (1961) the same method was successfully applied to the growth of single crystals of sapphire and YAG. [The technique is also known as induction skull melting (ISM) and is used for casting Ti and Ti alloys—for the same reason.]

The most important economic application of the skull melting technique for ceramics has been the production of cubic zirconia ($T_M = 2700^\circ\text{C}$), which is manufactured at rates in excess of 300 tonnes (1.5 billion carats) per year. Cubic zirconia is the best of the diamond simulants and the growth of large (centimeter-sized) crystals became feasible only with the use of the skull melting technique (Figure 29.7). The zirconia powder containing some small pieces of Zr metal is contained in a water-cooled assembly and heated by means of high-frequency induction heating (see Section 9.6). The Zr metal is used to couple with the high-frequency radiation. Once the temperature has reached 1100°C the zirconia becomes electrically conducting and itself acts as a susceptor. The material close to the water-cooled walls remains solid, thus forming a dense sintered shell or “skull.” The rest of the zirconia liquefies. To induce crystallization, the melt is lowered slowly (~1 cm/h) from the heating coil, as shown in Figure 29.7b. Crystal growth begins at the base of the melt and large columnar crystals (to ~7 cm long) can be produced.

The cost of cubic ZrO_2 crystals varies depending on supply and demand. The selling price for single crystals is only ~\$0.80 g⁻¹. This makes them a low-cost commodity material for the gem trade and necessitates large-scale production to make the process economically feasible. However, once the crystals have been oriented, cut, and polished for use as substrates for thin-film growth (e.g., the high-temperature superconductors) the equivalent cost

FIGURE 29.7 (a–c) The skull melting process.



is $\sim \$150 \text{ g}^{-1}$ [$\sim \$50$ for a single $1 \times 1 \times 0.05\text{-cm}$ -thick (100) oriented substrate].

29.8 MELT TECHNIQUE: BRIDGMAN–STOCKBARGER

The Bridgman–Stockbarger technique is illustrated in Figure 29.8. The powdered charge is melted in a crucible, which is often a refractory metal Pt, Ir, or Mo. This technique necessitates that the melt does not significantly react with the crucible. The furnace is designed such that there is a sharp drop in temperature just below the bottom tip of the crucible in its initial position.

The crucible is lowered (typically at a rate of 1 to 30 mm/h) so that the tip enters the colder zone causing the nucleation of crystals. The crystals grow fastest in particular crystallographic directions and crystals growing at angles greater than half the cone angle terminate at the

walls of the cone; only those crystals oriented so that the growth is favored in the axial direction persist into the bulk of the charge as the crucible is lowered into the cooler zone. As a result the upper part of the crucible finally contains either a single crystal or a few large crystals. One of the problems associated with the Bridgman–Stockbarger method occurs if the crystal expands on freezing (this happens in covalently bonded crystals Si and Ge—as it does with ice). The crucible acts as a constraint on the growing crystal and the expansion usually leads to large stresses, which can result in the introduction of dislocations and low-angle grain boundaries (GBs) and even cause the crucible to burst. It is difficult to produce single crystals with dislocation densities less than 10^4 cm^{-2} by this technique. There are other geometries for the Bridgman–Stockbarger technique. One configuration is the horizontal configuration in which the crystal is grown horizontally in a boat.

The Bridgman–Stockbarger method has been used primarily in the growth of alkali halides and alkaline-earth halides (e.g., LiF and CaF_2). Table 29.5 summarizes some

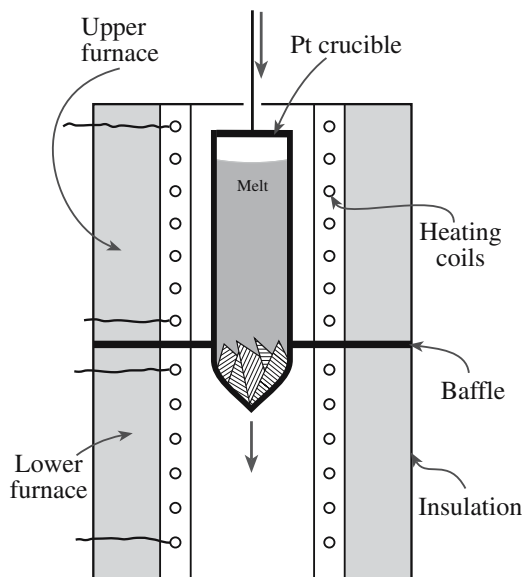


FIGURE 29.8 The Bridgman–Stockbarger technique.

TABLE 29.5 Typical Conditions for Bridgman–Stockbarger Growth

Crystal	T_M ($^{\circ}\text{C}$)	Growth rate (mm/h)	Crucible
Al_2O_3	2037	2–8	Molybdenum
ZnS	1850	0.5–2	Silica supported by graphite
FeAl_2O_3	1790	5–10	Iridium
GaAs	1238	2–6	Sand-blasted silica
Cu	1083	6–60	Graphite powder
Ge	937	50–150	Graphite- or carbon-coated silica
As	814	5–12	Thick-walled silica
AgBr	434	1–5	Pyrex
NaNO_2	271	3–6	PTFE ^a
K	63.7	1–4	Stainless steel coated with paraffin
Ar	–189.2	0.7–1.5	Mylar

^aPTFE, polytetrafluoroethylene.

of the other crystals that have been grown by this method. This table is by no means complete; indeed, several thousand different crystals have been reported. In many cases the furnace tube is filled with an inert gas to protect the charge and crucible. If the crystal is volatile, and the crucible is silica or pyrex, the crucible may also be sealed.

29.9 MELT TECHNIQUE: HEAT-EXCHANGE METHOD

The heat-exchange method (HEM) (also known as the Schmid–Viechnicki method) is best known for its use in growing large crystals of sapphire. Sapphire crystals of 34 cm diameter and 65 kg in weight are grown in a production facility, up from the initial 20 cm diameter, 20 kg weight. (These values should be compared to a maximum diameter of 15 cm for Cz growth.) Sapphire is particularly challenging since it is essential to use low thermal gradients during growth and cool down to prevent cracking of the boule. The furnace is shown schematically in Figure 29.9. The furnace has several special features:

- Heat extraction and input can be controlled independently.

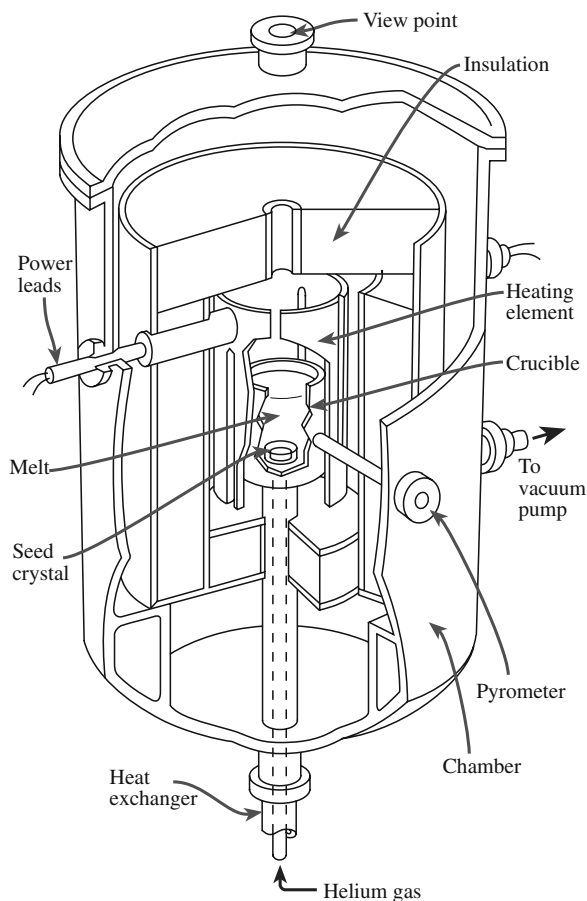


FIGURE 29.9 Illustration of the heat-exchange (Schmid–Viechnicki) method.

- The boule can be annealed *in situ* after growth.
- Nothing moves mechanically.

In the HEM technique, the Mo crucible, the seed, the melt, and the growing crystal are all located in the heat zone. Heat is removed using a W He-gas heat exchanger and is thus a temperature gradient technique (TGT). The technique uses directional solidification of the melt from a seed that is in contact with the heat exchanger placed at the base of the crucible. The furnace elements melt the sapphire crackle and control the temperature of the liquid. The temperature of the seed is allowed to increase to melt back its surface and then growth begins by lowering the temperature of the seed and the melt. Crystallization is a three-dimensional process. The whole process takes about 72 hours and is followed by a similar annealing period. Growth of (0001) boules is most difficult because the solid/liquid interface is convex toward the liquid in the HEM process, which increases solidification stresses. The situation can be remedied by carefully controlling the temperature gradients. The resultant boule has a flat top surface making a large fraction suitable for preparing windows, etc.

Fluorite crystals for use in ultraviolet (UV) ($\lambda = 193$ nm) and vacuum ultraviolet (VUV) (vacuum UV; $\lambda = 157$ nm) lithography up to 20 cm diameter have been grown using a modified TGT, which is another variation on the directional solidification approach to crystal growth. The inner diameter of the high-purity graphite crucible used is 300 mm. An interesting feature of this method is the use of 2 wt% PbF_2 to scavenge oxygen impurities. Blocks of the $\text{CaF}_2/\text{PbS}_2$ mixture are pressed into the crucible with a (111) seed at the bottom. The vacuum is kept at $\sim 10^{-3}$ Pa with a graphite lid on the crucible to minimize vaporization and the thermal gradient can be controlled by changing the position of the crucible in the furnace or adjusting the flow of cooling water to the bottom of the crucible support. Crystals of CaF_2 up to 250 mm diameter can also be grown by the Bridgman method. In either case, a temperature of $\sim 1500^\circ\text{C}$ is used for the growth.

29.10 APPLYING PHASE DIAGRAMS TO SINGLE-CRYSTAL GROWTH

An important consideration in the crystal growth of oxides containing several cations is whether the melting is congruent or incongruent. The discussion in this section builds on that in Section 8.10. If the compound melts congruently then crystal growth will proceed easily. For example, the crystal could be grown by the Cz method in a way similar to growth of an elemental crystal.

Crystals of lithium niobate, LiNbO_3 , can be readily grown using the Cz process. Its large nonlinear optical coefficients have led to an intense interest in this material. Figure 29.10 shows part of the $\text{Li}_2\text{O}-\text{Nb}_2\text{O}_5$ phase diagram. The congruent melting temperature is not exactly at the

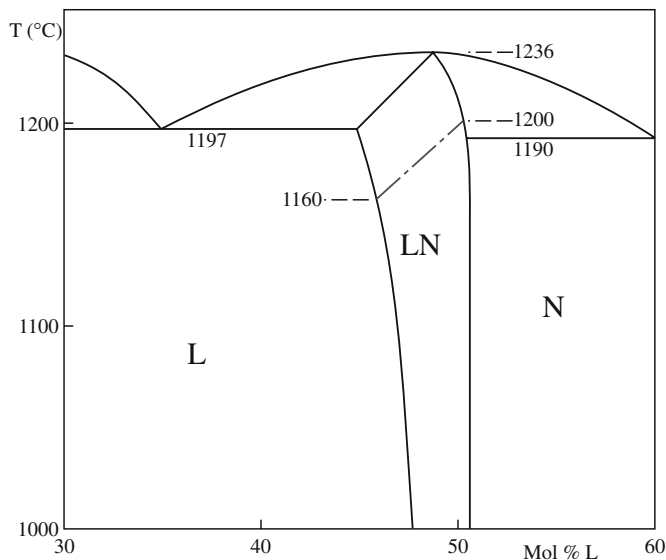


FIGURE 29.10 Part of the $\text{Nb}_2\text{O}_5\text{-Li}_2\text{O}$ phase diagram.

stoichiometric composition but at 51.4 mol% Nb_2O_5 . Solidifying a melt of the composition 48.6% Li_2O and 51.4 mol% Nb_2O_5 can produce a high-quality single crystal, but the cation stoichiometry will not be 1 : 1. To obtain stoichiometric $\text{Li}_{1.00}\text{Nb}_{1.00}\text{O}_3$ it is necessary to cool a melt containing excess Li_2O . For example, referring back to Figure 29.10, a melt of composition 55 mol% Li_2O and 45 mol% Nb_2O_5 will solidify below $\sim 1200^\circ\text{C}$ producing a stoichiometric solid. During growth of the crystal the melt will become depleted in Nb. To counteract this loss it is necessary to ensure the melt is homogenized by stirring; if a large melt volume is used, and a moderately sized crystal is grown, the composition change will be small.

As noted in Section 8.10, pure cubic BaTiO_3 cannot be grown from a melt of that composition because, as shown in Figure 8.23, the hexagonal phase is in equilibrium with the liquid at the solidification temperature (1618°C). The hexagonal phase transforms to the cubic phase at 1460°C , but the phase change is very slow and thus the hexagonal phase can persist at room temperature. The hexagonal form of BaTiO_3 is not ferroelectric. Its structure contains the required TiO_6 octahedra, but the linking of the octahedra is different from that found in cubic BaTiO_3 . In cubic BaTiO_3 the octahedra share corners; in hexagonal BaTiO_3 some of the octahedra share faces.

Cubic BaTiO_3 can, however, be grown from a melt composition containing 35 mol% BaO and 65 mol% TiO_2 , which solidifies below 1460°C , the temperature below which the cubic form is stable. The melt is held just above its solidification temperature, a seed crystal is dipped into its surface, and the crystal is pulled from the melt at a rate of 0.5–1.0 mm/h. The seed crystal is rotated during growth

so that the liquid near the crystal does not become depleted in Ba. Only a fraction of the melt can be obtained as single-crystal BaTiO_3 since the whole of it solidifies, forming a mixture of cubic BaTiO_3 and $\text{Ba}_6\text{Ti}_{17}\text{O}_{40}$, when the BaO content falls to about 32 mol%.

If the desired compound melts incongruently it is often easier just to use a technique like flux growth to obtain single crystals.

29.11 SOLUTION TECHNIQUE: HYDROTHERMAL

In the hydrothermal method single crystals are grown from an aqueous (hydro) solution. Although many crystals have been grown hydrothermally, α -quartz crystals are the only ones that are produced on a large scale. For this reason we will describe the method used for growing large α -quartz crystals, although the system used for other materials (including emerald and ruby) is very similar. An important feature is that the low-symmetry form of quartz is produced directly since T is low.

Pure finely divided particles of mineral quartz are placed at the bottom of a tall cylindrical autoclave that is 80% filled with a basic solution, for example, 0.5 M NaOH. Suitably oriented seed crystals of α -quartz are held in wire frames near the top of the autoclave.

AUTOCLAVE

An autoclave is a thick-walled vessel, usually made of steel, which allows us to carry out reactions under pressure and at high temperatures. (The original definition implied a self-closing vessel with internal pressure sealing its joints; the closure is now made externally.)

Thermometers allow temperature control within the chamber. The seed crystals are usually naturally occurring quartz, since this usually has a very low dislocation density. The base of the autoclave is kept at 400°C ; in this section the quartz fragments dissolve so it is called the *dissolving* section. The top of the autoclave, which is called the *growth* section, is maintained at a temperature some 40°C cooler than the dissolving section. The α - β transition in quartz occurs at 573°C . For highly perfect single crystals, growth should be carried out below the transition temperature. The solution at the bottom of the autoclave will saturate and move by convection to the growth zone where the seed crystals are located. In the growth zone the solubility is lower, the solution becomes supersaturated, and material is deposited onto the seed crystals. Figure 29.11 shows a schematic of an autoclave used for hydrothermal growth. The baffle shown in the lower half of the autoclave is a perforated metal disk separating the dissolving and growth sections and helping to localize the temperature differential. For piezoelectric applications, the principal faces of the seed crystals are $\{0001\}$ and the crystals grow at ~ 1 mm/day in both $\langle 0001 \rangle$ directions producing crystals weighing over a kilogram in a few weeks. Figure 29.12 shows a hydrothermally grown α -quartz crystal. Table 29.6 lists other ceramic

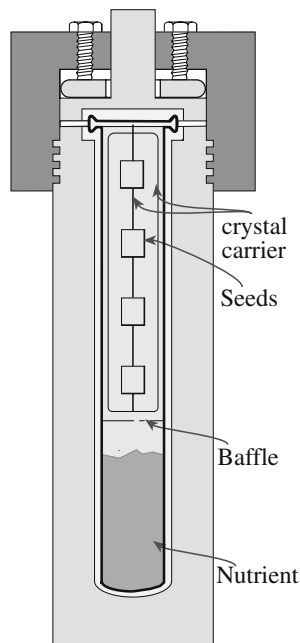


FIGURE 29.11 A silver-lined laboratory hydrothermal autoclave, about 35cm long. It can be much longer.

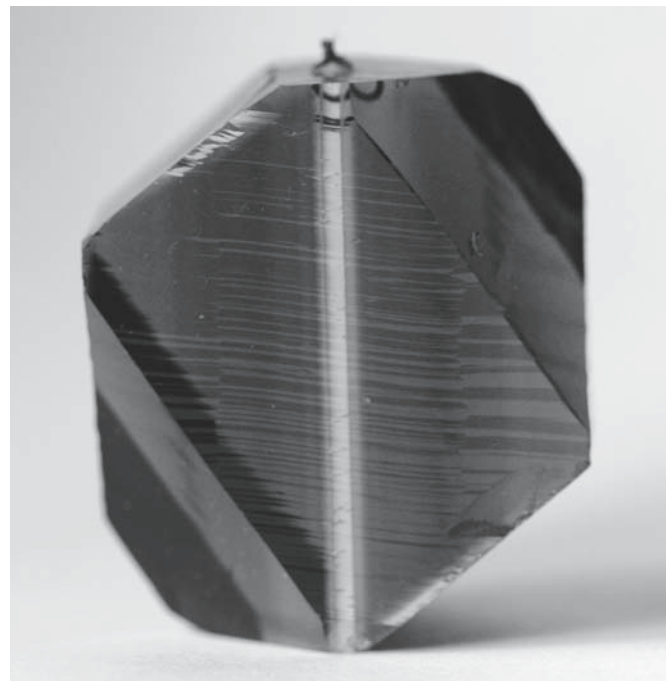


FIGURE 29.12 Hydrothermally grown quartz crystal; note the colorless seed and the Pt support wire at the top.

TABLE 29.6 Examples of Hydrothermally Grown Crystals

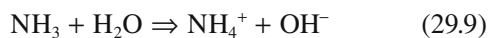
Crystal	Solvent	Growth zone temperature (°C)	Dissolution zone temperature (°C)	Pressure or degree of fill
α -SiO ₂	1 N Na ₂ CO ₃	360	400	80%
	1.0M NaOH + 0.025 M Li ₂ CO ₃ + 0.1 M Na ₂ CO ₃	374	397	88%
LiGaO ₂	3.5 M NaOH	385	420	70%
BiTi ₂ O ₁₂ , Bi ₁₂ TiO ₂₀	KF	550~600	—	>70~80%
K(Ta,Nb)O ₂	15 M KOH	650	690	1000 atm
KNbO ₃ , KTaO ₃	KOH	400~600	450~680	70~80%
PbTiO ₃ , PbZrO ₃	KF	570	585~590	50~55%
Pb(Ti _x Zr _{1-x})O ₃	>10wt% KF	580	~618	83%
R ₃ Al ₃ (BOH) ₂ Si ₄ O ₁₉	H ₃ BO ₃ + NaCl or NaF	400~700	—	1000~3000 atm
AlPO ₄ , GaPO ₄	6.1 M H ₃ PO ₄ , 3.8 M ADP	150	300	80%
(Mn,Fe,Zn) ₈ [Be ₆ Si ₆ O ₂₄]S ₂	1% NaOH or 8% NH ₄ Cl	450	480~500	1500~2000 atm
Na ₂ ZnGeO ₄	30wt% NaOH	250~300	253~310	50~90%
NiFe ₂ O ₄	0.5 N NH ₄ Cl	470~480	—	70~75% (1100~1300 atm)
Fe ₃ O ₄	10 M NaOH	500	550	1000 atm
ZnFe ₂ O ₄	NaOH	400	—	—
Y ₃ Fe ₅ O ₁₂	1~3 M Na ₂ CO ₃ or 1~3 M NaOH	400~750	—	200~1350 atm
	20 M KOH	350	360	88%
Y ₃ Ga ₅ O ₁₂	1~3 M Na ₂ CO ₃ or 1~3 M NaOH	400~500	—	1000~3000 atm
	K ₂ CO ₃	500	550	~1000 atm
α -Al ₂ O ₃	2~3 M Na ₂ CO ₃ or 1 M K ₂ CO ₃	390~490	500~540	75~82% (1100~1600 atm)
	10% K ₂ CO ₃ or 10% KHCO ₃	530~600	540~640	50~70%
	4 M K ₂ CO ₃	370	390	85%
Y ₃ Al ₅ O ₁₂	HCl	—	—	—
CaWO ₄	2 M K ₂ CO ₃	550	600	1000 atm
SrWO ₄ , BaWO ₄	4wt% NaOH	380	430	60~70%
	7~10wt% NaOH	410~485	450~500	70%
CdWO ₄	5~7 wt% NH ₄ Cl or 15~20 wt% LiCl or 30~40wt% NaCl	430~485	450~500	65~70%
	7wt% NH ₄ Cl or 16~25wt% LiCl	430~455	450~470	75%
SrMoO ₄ , BaMoO ₄	5~7 wt% NH ₄ Cl or 15~20 wt% LiCl or 30~40wt% NaCl	430~485	450~500	65~70%
	5.45 M KOH + 0.7 M LiOH	353	467	83%
PbO	1 N LiOH	430	450	60%
ZnS	2~5 M NaOH	350~380	410~560	50~80%

single crystals grown by the hydrothermal method and the experimental conditions used.

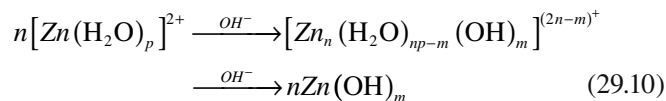
29.12 SOLUTION TECHNIQUE: HYDROTHERMAL GROWTH AT LOW TEMPERATURE

Low temperatures are suitable for nanowires etc. because they do not have to grow very large! An example is the growth of ZnO nanorods. The early stage of growth on a sapphire substrate is shown in Figure 29.13. The principle of the synthesis is the hydroxylation of Zn^{2+} ions in an aqueous solution in the presence of hexamethylenetetramine [HMTA: $(CH_2)_6N_4$].

The hydrolysis reactions are



This promotes the hydroxylation of Zn^{2+} ions in solution to form dissolved complexes, which are precursors to nucleation of the ZnO precipitate phase.



Though this route has been used for the synthesis of ZnO nanorods in solution, crystal growth can occur on substrates when they are exposed to the vapor phase above a

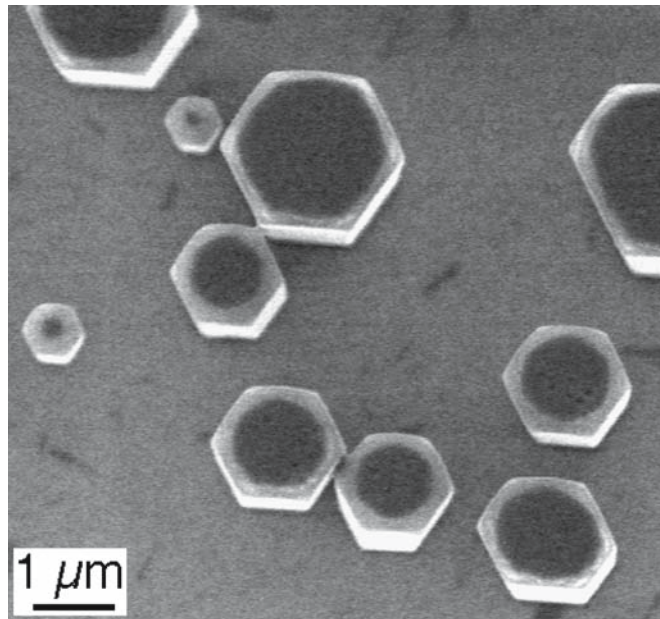


FIGURE 29.13 Hydrothermal ZnO nanorods seen nearly end on.

dilute aqueous solution containing 0.025 M $Zn(NO_3)_2$ and 0.025 M HMTA maintained in the range 70–90°C for 1–3 hours.

29.13 SOLUTION TECHNIQUE: FLUX GROWTH

Crystals of many ceramics can be obtained by cooling a solution of the required compound in a suitable flux or solvent (serving the role of water in Section 29.11). The common fluxes include KF, PbO, and PbF_2 . The flux is selected to give minimum contamination:

- PbO and Bi_2O_3 are good fluxes for the growth of oxides because Pb and Bi atoms are so large that they do not fit into many lattices.
- Alkali metal ions do not fit well into many lattices either because the sizes or the charges are wrong.

To illustrate the flux-growth process for growing single crystals we will look at three examples.

Yttrium iron garnet ($Y_3Fe_5O_{12}$ or YIG) is ferromagnetic. Approximately 52.5 mol% PbO, 44 mol% Fe_2O_3 , and 3.5 mol% Y_2O_3 are mixed together in a Pt

crucible and heated to 1250–1350°C. After the melt has homogenized it is cooled at a rate of 0.5°C/h. The solidified melt contains crystals of Fe_2O_3 , $PbFe_{12}O_{19}$, and the required $Y_3Fe_5O_{12}$. The mixture is crushed and digested in nitric acid to free the crystals from the flux. In any flux-growth process it is important to have a solvent that dissolves the flux but does not affect the desired crystals. The crystals are separated magnetically at temperatures above and below the appropriate Curie temperatures. The garnet crystals are equiaxed and can also be picked out of the crushed mixture visually.

$BaTiO_3$ crystals have been prepared using a KF flux containing 30% $BaTiO_3$. The mixture is homogenized at 1150–1200°C for about 8 hours. The temperature is then lowered to 900°C and the flux is poured off. The $BaTiO_3$ crystals are allowed to cool in the furnace to room temperature. A characteristic feature of flux-grown $BaTiO_3$ crystals is that they form pairs of triangular plates (“butterfly twins”) as shown schematically in Figure 29.14. The cooling rate determines the plate thickness making it possible to form thin sheets directly, without them having to be cut from larger single crystals. In some cases a small amount of iron, about 0.2 wt% Fe_2O_3 , is added to the starting mix. Iron assists in the formation of large area plates. However, a small amount of Fe^{3+} is then incorporated in the $BaTiO_3$ lattice on Ti^{4+} sites. The charge difference is compensated for by the replacement of an equivalent number of O^{2-} ions by F^- ions.

Although many details of the process used are kept secret, emeralds [$Be_3Al_2(SiO_3)_6$] can be produced by dissolving BeO, Al_2O_3 , and SiO_2 in an Li_2O – MoO_3 flux using

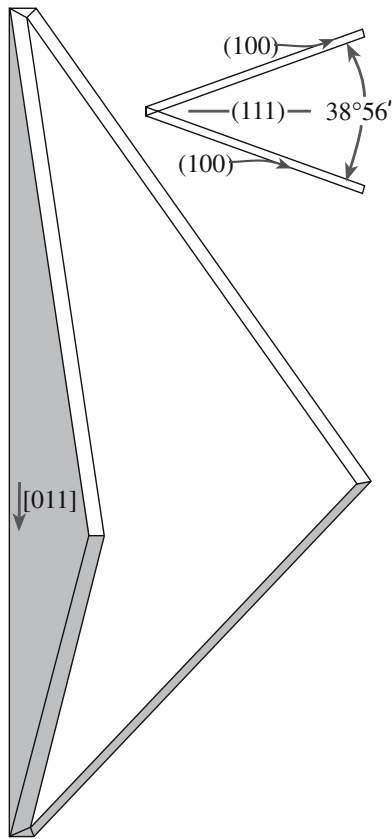


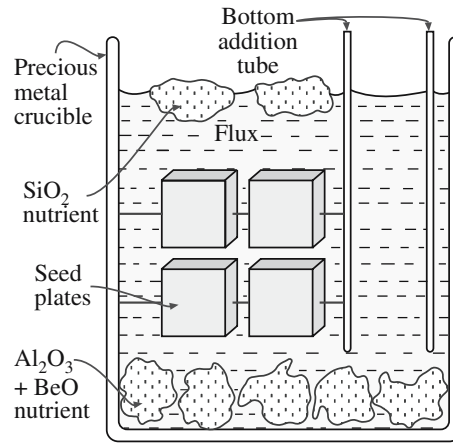
FIGURE 29.14 Butterfly twins in BaTiO₃.

an arrangement shown in Figure 29.15; emeralds can grow to ~60 g in 10–12 months. Synthetic rubies can be produced using a PbF₂ flux; rubies can grow to 600 g in 8 months. The synthetic crystals are ~10% of the price of natural ones. The primary commercial manufacturer of emerald and ruby in the United States is Chatham in San Francisco, which produces 20% (1 t/year) of the worldwide production of synthetic emeralds and about 70% (700 kg/year) of the worldwide production of flux-grown rubies.

The main advantage of the flux-growth method is that it can be used for a wide variety of materials. Single crystals of materials that undergo phase transitions, melt incongruently, or have a high vapor pressure at their melting temperature can all be grown using flux growth. The major disadvantages are as follows:

- Impurities may be trapped in the crystal.
- Growth is slow compared to melt-growth methods.
- Growth of very large crystals is not possible.

For these reasons flux growth is a useful research tool for growing small crystals (typical crucible volumes between 50 and a few hundred cubic centimeters), but it is not used widely for the production of industrial single crystals apart from gemstones. Many ceramics have been produced as single crystals by the flux-growth process. The literature contains a large amount of information about suitable fluxes for several thousand materials. Table 29.7 gives a few examples.



(A)



(B)

FIGURE 29.15 Flux growth of emerald: (a) schematic; (b) emeralds.

TABLE 29.7 Fluxes Used for the Growth of Ceramics

Material	Flux
Al ₂ O ₃	PbF ₂ + B ₂ O ₃
B	Pt
BaFe ₂ O ₄	Na ₂ CO ₃
BaTiO ₃	Bi ₂ O ₃
BeAl ₂ O ₄	PbO, Li ₂ MoO ₃ , PbMoO ₄
CeO ₂	NaF + B ₂ O ₃
Fe ₂ O ₃	Na ₂ B ₄ O ₇
GaAs	Ga, Sn
GaFeO ₃	Bi ₂ O ₃ + B ₂ O ₃
GaP	Ga
Ge	In, Sn + Pb
GeO ₂	Li ₂ Mo ₂ O ₇ , Li ₂ W ₂ O ₇
KNbO ₃	KF, KCl
KTa _x Nb _{1-x} O ₃	K ₂ CO ₃
MgFe ₂ O ₄	Bi ₂ O ₃ + B ₂ O ₃
NiFe ₂ O ₄	Na ₂ B ₄ O ₇
PbZrO ₃	PbF ₂
SiC	Si
TiO ₂	Na ₂ B ₄ O ₇ + B ₂ O ₃
Y ₃ Al ₅ O ₁₂	PbO + B ₂ O ₃ , PbO + PbF ₂
Y ₃ Fe ₅ O ₁₂	PbO, PbO + PbF ₂ , BaO + B ₂ O ₃
ZnO	PbF ₂
ZnS	ZnF ₂
ZnTe	In, Ga, Sn, Bi, Pb

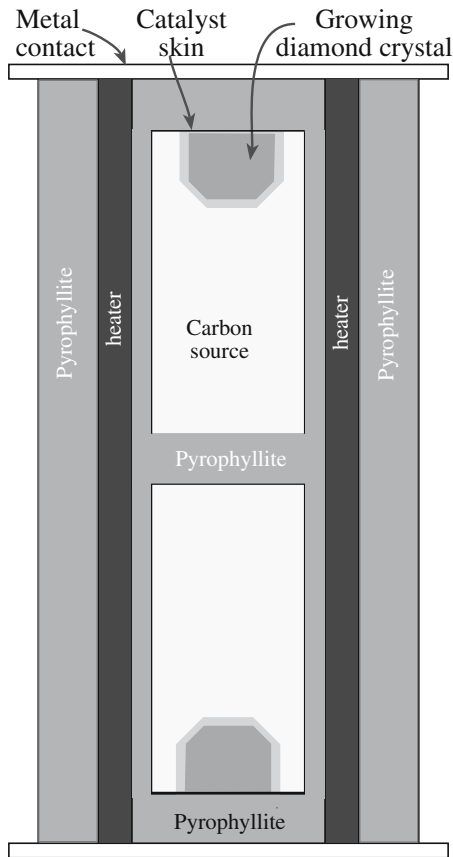


FIGURE 29.16 Chamber for diamond growth.

29.14 SOLUTION TECHNIQUE: GROWING DIAMONDS

In addition to their importance in jewelry, diamonds also have important industrial applications such as in diamond-impregnated cutting tools and as abrasives. The world use of diamonds is about 26t (26Mg) per year, of which about 16t is synthetic. The synthetic diamond industry is a \$1 billion/year business.

The carbon phase diagram was shown in Figure 8.7. From this diagram you can see that diamond is in fact the metastable form of C under ambient conditions, with graphite being the stable form. Diamond is stable at pressures as low as 1 GPa if T is $\sim 25^\circ\text{C}$, although the rate of the transformation is extremely slow if the pressure is lower. However, diamonds can be synthesized from graphite at very high temperature ($\sim 3300\text{ K}$) and very high pressure ($\sim 13\text{ GPa}$). A more practical method involves the use of a solution (the flux again) and shares similarities with the other solution methods described above.

The credit for the first synthesis of diamonds goes to Bundy *et al.* of the General Electric Company, although the Swedish company ASEA may have synthesized diamonds in 1953. In each case, the product was diamond grit suitable for grinding and polishing uses. In 1970 researchers at GE succeeded in synthesizing large (up to about 1 ct in weight) single-crystal diamonds. The arrangement for

growing large diamonds is shown in the schematic diagram in Figure 29.16. The pyrophyllite (a hydrous aluminum silicate) tube is inserted into a ring of tungsten carbide through which the hydraulic pressure is applied. Pyrophyllite is used because at high temperature and under high pressure it extrudes to form a gasket that bonds well to the tungsten carbide pistons and seals the tube to maintain the applied pressure. Heating is achieved by passing an electric current through the tube. The temperature gradient within the tube is such that the center is between 10 and 30°C hotter than the ends. The carbon source (any carbon-containing compound may be used, even peanuts) is dissolved in the solvent, often Ni, Fe, or an Ni-Fe alloy. The solvent forms a thin film on the surface of the seed and transport of carbon from the source to the crystal takes place by temperature-difference solution growth (similar to what happens in the hydrothermal process). The diamond seed crystals favor the formation of diamond instead of graphite. Growth rates depend on the solvent and the orientation of the seed crystal, but are 3 to 5 mm/day.

29.15 VAPOR TECHNIQUE: VAPOR-LIQUID-SOLID

The VLS mechanism was first used to grow Si whiskers. (Other whiskers were identified some years earlier.) The catalyst-mediated whisker-growth process is illustrated in Figure 29.17 for the growth of SiC whiskers. The process begins with melting a solid catalyst particle (e.g., steel), so that it forms a liquid ball on a suitable surface (in this case, a graphite slab). The ball forms a liquid interface between the growing SiC whiskers and the vapor phase. Carbon (in the form of methane CH_4) and silicon (in the form of SiO) in the vapor feed are extracted by the liquid catalyst, which in turn becomes supersaturated. Crystal growth occurs by precipitation from the supersaturated liquid at the solid-liquid interface. Whiskers produced by the VLS process characteristically have a spherical cap.

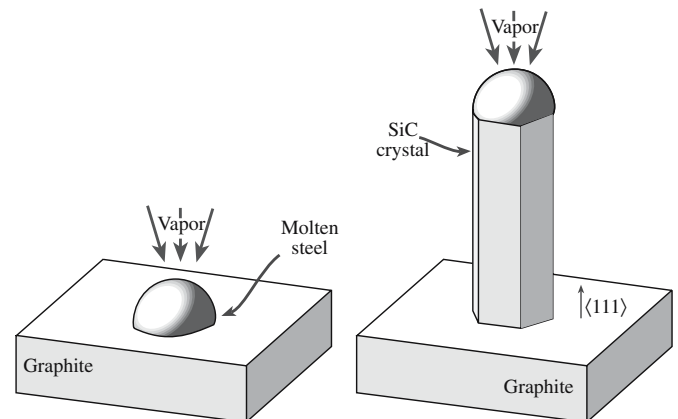


FIGURE 29.17 VLS process for growing SiC whiskers.

One of the drawbacks of the VLS process is that it is extremely slow. This leads to high production costs and limited availability, which together combine to make the whiskers extremely expensive (\$800/kg in 1994). Also although SiC has been classified as a nonhazardous material, there are health concerns associated with very small whiskers. This problem may be even more important with the increasing production of the smaller whiskers known as nanowires and nanotubes.

The VLS mechanism has been identified in the growth of other ceramic whiskers including Al_2O_3 , BeO , and B_4C . It has been proposed as a method for producing nanotubes, and is often assumed to be the principal feature of such growth processes.

29.16 VAPOR TECHNIQUE: SUBLIMATION

Single crystal SiC is of interest for a number of applications including high-temperature electronic devices and blue-light-emitting diodes. For these applications the preparation of large high-quality boules is necessary from which individual wafers can be sliced. At atmospheric pressure SiC sublimates, so single crystals cannot be produced by melt growth techniques such as the Cz process. However, a sublimation technique has been developed that can produce boules up to 30 mm in diameter. The cross section of a reaction chamber is shown schematically in Figure 29.18. A seed crystal and a polycrystalline source material are placed at opposite ends of a cylindrical container, along which a temperature gradient of 10–20°C/cm is established (2300–2500°C at the source and 2100–2200°C at the seed). SiC sublimates from the source

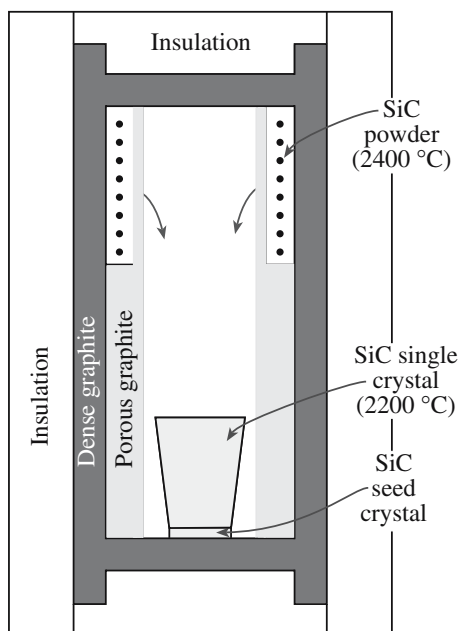


FIGURE 29.18 Modified sublimation process for SiC single crystals.

and the products condense onto the cooler seed. The process is carried out at a low argon pressure (200 Pa), allowing boules of 20 mm in length and up to 30 mm in diameter to be produced at a rate of about 4 mm/h.

SiC wafers produced from the boules are very expensive. A single SiC wafer 30 mm in diameter and 0.3 mm thick can cost upward of \$3000. By comparison, an Si wafer of this size costs less than \$20.

29.17 PREPARING SUBSTRATES FOR THIN-FILM APPLICATIONS

Conversion of the boule into polished substrates requires several operations. The exact number and type of steps involved in this process depend on the material involved and the application for the substrates. The following sequence would be typical for the preparation of single-crystal substrates of ceramics.

- The top and bottom (sometimes called the *seed* and *tang* ends, respectively) of the boule are removed using a diamond-tipped saw.
- The surface orientation of the boule is determined by an X-ray method (typically Laue back-reflection). The boule is mounted in such a way that when it is cut the slices have the desired surface orientation.
- Wafers are sliced from the boule using a diamond-tipped saw or a set of diamond-coated wires. When the wire saw is used many slices can be cut in one run (like slicing a hard-boiled egg). The substrate thickness essentially depends on the slicing operation, although the final value depends on subsequent polishing operations.
- The wafers are polished (see Section 18.12).
- The wafers are diced up to produce individual substrates of the desired size. In some cases the substrates are cut so that the edge is aligned along a particular crystallographic orientation. This orientation is also set by X-ray methods.

29.18 GROWING NANOWIRES AND NANOTUBES BY VAPOR-LIQUID-SOLID AND NOT

There is great interest in growing single crystals that are smaller than 100 nm in one, two, or three dimensions. The techniques being used are variations on those listed above but deserve separate mention because of the special features involved. The detailed mechanisms involved in the growth are not fully understood. The essential feature is that the “substrate” is small.

The VLS technique has probably attracted most attention. Essentially this is an extension of that used by Wagner and Ellis to grow the original Si whiskers, which were themselves nanowires. Vapor-liquid-solid growth of

Si required a catalyst particle, but not all wire growth requires a heterogeneous catalyst. We can grow arrays of ZnO wires by depositing islands of catalyst on a substrate and providing a vapor so that the wires will grow only where the catalyst particle is. In some cases, it appears that the catalyst may be solid throughout the process. In other similar processes there is no catalyst. Nature grows rutile and asbestos fibers using crystal anisotropy.

Carbon nanotubes started the excitement in nanotechnology, although the Nobel Prize was awarded for the buckyball (Chapter 7). We can construct these nanotubes by rolling the sheet of graphite shown in Figure 29.19a (known as a graphene sheet) and joining the sides. Now we can join the sheets so that A meets B, or C meets D, but we can also make A meet E. You will realize that this corresponds to the formation of a screw dislocation that runs along the tube and really does have a hollow core! Then we could wrap other sheets around the first (not necessarily of the identical construction). The tubes can

be grown by several methods include arc-discharge and pulsed-laser deposition; both methods can produce quite large quantities; it has been claimed that tons of high-quality nanotubes will be produced (which will be needed for the space elevator). For technological applications we might prefer to grow arrays of aligned tubes. We can do this using Fe-oxide particles as the catalyst and 9% acetylene in N_2 as the feedstock; the growth temperature need only be $\sim 600^\circ C$. Such aligned structures can already be grown from the pores of mesoporous SiO_2 , on glass substrates, porous Si, porous alumina, etc. Ni catalysts have been used with plasma-assisted CVD at $660^\circ C$. We can use the C nanotubes themselves as templates (or substrates) to grow tubes (or wires) of other materials.

We can now grow tubes of many ceramics. The array of TiO_2 nanotubes shown in Figure 29.19b was grown from a Ti foil placed in an electrolyte of 0.5% HF in water using a Pt cathode. The anodization voltage was kept at

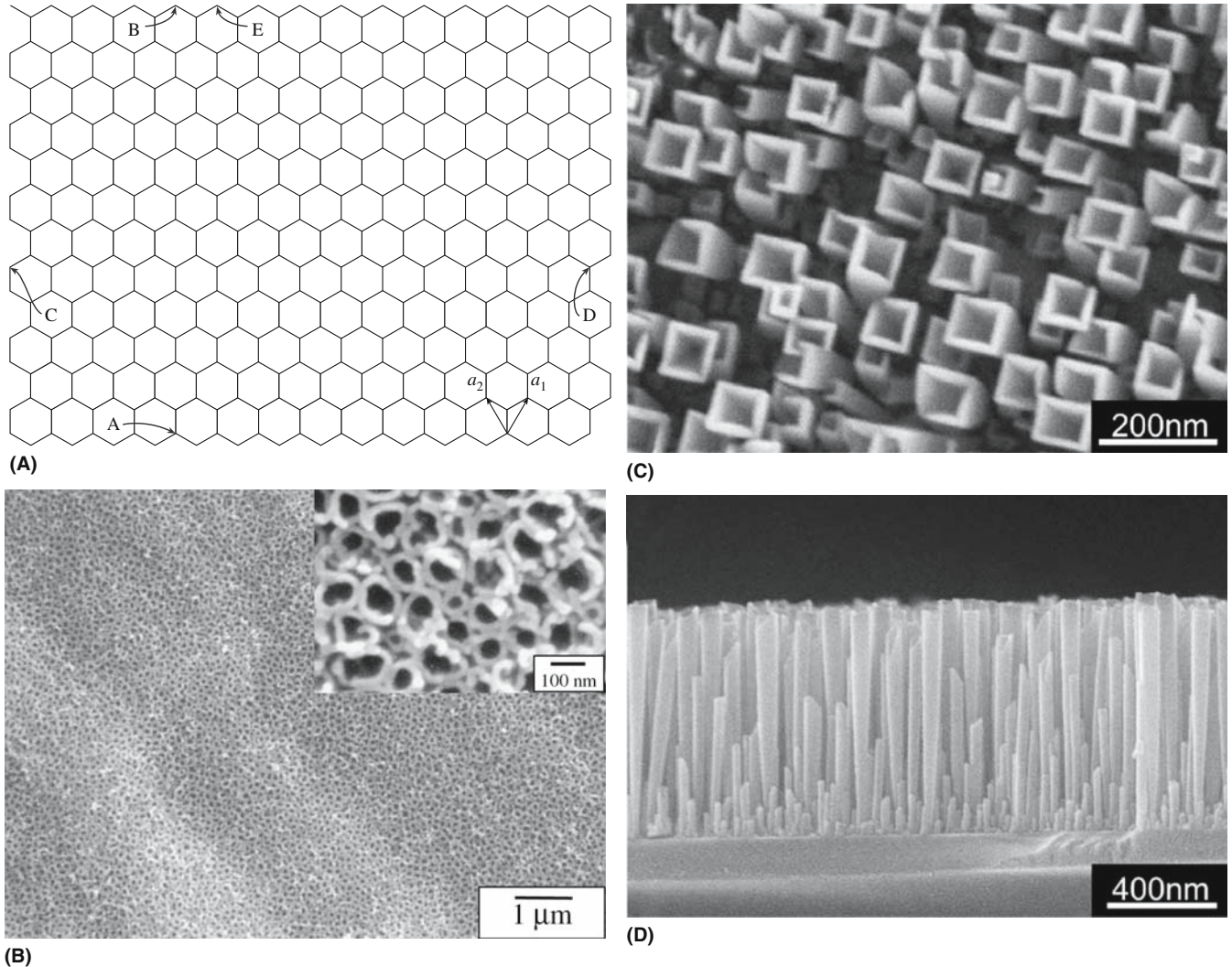


FIGURE 29.19 (a) Graphene sheet illustrating how carbon nanotubes are formed. (b) TiO_2 nanotubes. (c) and (d) IrO_2 nanotubes.

~20 V and this structure was produced in ~45 minutes. The sample was cleaned in pure water and sintered at up to 880°C transforming the as-grown anatase to rutile. The resulting material has many possible applications (it resembles MCM-41 structurally) since it has all the

chemical properties of rutile. The nanotubes of IrO₂ in Figure 29.29c and d have a square cross section because they are single crystal with sides parallel to {001} planes. We can grow nanotubes of other oxides such as MgO and NiO, and nanotubes of nonoxides such as BN.

CHAPTER SUMMARY

Many methods can be used to grow single crystals of ceramic materials. To produce large crystals the methods can be classified as melt growth, solution growth, or vapor growth. For solution growth a suitable solvent must be found for the material. Because it is possible to find a solvent for most materials (the literature contains solvents for several thousand materials), solution-growth techniques are applicable to a very wide range of ceramics. Melt-growth techniques generally require that the material melts congruently or nearly congruently—so knowledge of the phase diagram for the material is important—and this fact alone eliminates many materials from consideration. The significant advantage of melt-growth techniques is that, particularly in the case of the Cz method, very high quality crystals can be produced. Vapor growth of bulk material is generally used only to produce single crystals of ceramics like SiC that cannot be made by either melt or solution techniques, or for growing nanocrystals.

Many of the methods used for thin-film growth produce single crystals—the emphasis in this chapter is that the crystals “stand alone.”

PEOPLE IN HISTORY

Bridgman, Percy Williams was born in Cambridge, Massachusetts in 1882 and joined the faculty of Harvard University in 1908. He is best known for his research on the effects of high pressure on materials and was awarded the Nobel Prize in Physics in 1946 “for the invention of an apparatus to produce extremely high pressures, and for the discoveries he made therewith in the field of high pressure physics.” Bridgman made contributions to many fields including crystallography and devised a method for growing single crystals, which bears his name. He died in 1961.

Czochralski, Jan was born on October 23, 1885 in Kcynia, which is now in Poland. He was the eighth child of a carpenter (died 1953). He went to Berlin to study chemistry in 1904 and by 1910 was working on the processing of Cu. The story is that in 1913 he was writing up his notes on a study of crystallizing metals while sitting next to a crucible with molten Sn. Absentmindedly, instead of dipping his pen in the inkpot, he dipped it in the crucible and withdrew it quickly. He observed a thin thread of solidified metal hanging at the tip of the nib. His observation led to a new crystal growth technique, which he published in 1917.

Verneuil, August Victor Louis (1856–1913) was a French chemist who reported his method for growing ruby in 1902.

GENERAL REFERENCES

Brice, J.C. (1986) *Crystal Growth Processes*, Blackie, Glasgow. A clear description of all the major (and most of the minor) techniques used to produce single crystals and a useful discussion on method selection.

Elwell, D. and Scheel, H.J. (1975) *Crystal Growth from High Temperature Solutions*, Academic Press, New York. An excellent place to look for fluxes for crystal growth.

Hazen, R.M. (1999) *The Diamond Makers*, Cambridge University Press, Cambridge. Fascinating; it reads like a novel.

Hurle, D.T.J., Ed. (1994) *Handbook of Crystal Growth*, Vol. 2, *Bulk Crystal Growth*, North-Holland, Amsterdam.

Journal of Crystal Growth. An international journal that publishes articles that deal with all aspects of crystal growth, from nucleation and growth theories to apparatus and instrumentation.

Laudise, R.A. (1970) *The Growth of Single Crystals*, Prentice-Hall, Inc, Englewood Cliffs, NJ. The standard reference for crystal growth; summarizes materials grown by different methods.

Nassau, K. (1980) *Gems Made by Man*, Chilton Book Company, Radnor, PA. An excellent and highly readable account of the techniques used to produce artificial gemstones. Contains lots of history and background information on the processes and their inventors.

Nassau, K. and Nassau, J. (1980) in *Crystals: Growth, Properties, and Applications*, edited by H.C. Freyhardt, Springer-Verlag, New York.

O'Donoghue, M. (1988) *Gemstones*, Chapman & Hall, London. The processing and properties of gemstones. Chapter 10 discusses synthetic and imitation stones.

Scheel, H.J. and Fukuda, T. (2004) *Crystal Growth Technology*, Wiley, Chichester. In Chapter One, this text points out that Czochralski used the Bridgman technique in his laboratory and that the Cz technique should have been called the Teal–Little–Dash technique after the group who first produced large (nearly) dislocation-free crystals of Ge.

SPECIFIC REFERENCES

- Aleksandrov, V.I., Osiko, V.V., Prokhorov, A.M., and Tatarintsev, V.M. (1978) in *Current Topics in Materials Science*, Vol. 1, edited by E. Kaldis, North Holland Publishers, Amsterdam, p. 421. Discussion of skull melting.
- Bundy, F.P., Hall, H.T., Strong, H.M., and Wentorf, R.H. (1955) “Man-made diamonds,” *Nature* **176**, 51. First description of diamond synthesis. Hazen (1999) indicates that synthetic diamonds may have been made prior to this publication from GE.
- Ivanov, P.A. and Chelnokov, V.E. (1992) “Recent developments in SiC single-crystal electronics,” *Semicond. Sci. Technol.* **7**, 863. On using SiC for blue LEDs.
- Keck, P.H. and Golay, M.J.E. (1953) “Crystallization of silicon from a floating liquid zone,” *Phys. Rev.* **89**, 1297. First description of the FZ method.
- Khattak, C.P. and Schmid, F. (2001) “Growth of the world’s largest sapphire crystals,” *J. Cryst. Growth* **225**, 572.
- Montforte, F.R., Swanekamp, F.W., and Van Uitert, L.G. (1961) “Radio-frequency technique for pulling oxide crystals without employing a crucible susceptor,” *J. Appl. Phys.* **32**, 959. First application of the skull melting process combined with crystal pulling to produce single crystals.
- Nassau, K. and Van Uitert, L.G. (1960) “Preparation of large calcium-tungstate crystals containing paramagnetic ions for maser applications,” *J. Appl. Phys.* **31**, 1508. Describes the first use of the Cz process to grow ceramic crystals (CaWO₄).
- Pfann, W.G. (1952) “Principles of zone melting,” *Trans AIME* **194**, 747. The zone refining process.
- Remeika, J.P. (1954) “A method for growing barium titanate single crystals,” *J. Am. Chem. Soc.* **76**, 940. Growth of BaTiO₃ by flux growth at Bell Labs.
- Schmid, F. and Viechnicki, D. (1970) “Growth of sapphire disks from melt by a gradient furnace technique,” *J. Am. Ceram. Soc.* **53**, 528.
- Stockbarger, D.C. (1936) “The production of large single crystals of lithium fluoride,” *Rev. Sci. Instr.* **7**, 133. Described improvements to the Bridgman process.
- Tairov, Yu.M. and Tsvetkov, V.F. (1978) “Investigation of growth processes of ingots of silicon carbide single crystals,” *J. Cryst. Growth* **43**, 209; (1981) “General principles of growing large size single crystals of various silicon carbide polytypes,” *J. Cryst. Growth* **52**, 146. Describing the sublimation technique for growing large boules.
- Teal, G.K. and Little, J.B. (1950) “Growth of germanium single crystals,” *Phys. Rev.* **78**, 647. Teal and Little of Bell Telephone Laboratories were the first to produce single crystals of Ge and Si by the Cz method.
- Tomaszewski, P.E. *Professor Jan Czochralski (1885–1953)*. <http://www.ptwk.org.pl/art2.htm>.
- Vergés, M.A., Mifsud, A., and Serna, C.J. (1990) “Formation of rod-like zinc oxide microcrystals in homogeneous solutions,” *J. Chem. Soc. Faraday Trans.* **86**, 959. Low-T growth of ZnO.
- Wagner, R.S. and Ellis, W.C. (1964) “Vapor-liquid-solid mechanism of single crystal growth,” *Appl. Phys. Lett.* **4**, 89; (1965) “Vapor-liquid-solid mechanism of crystal growth and its application to silicon,” *Trans. Met. Soc. AIME* **233**, 1053. The description of the VLS mechanism. Now used for more than Si.
- Ziegler, G., Lanig, P., Theis, D., and Weyrich, C. (1983) “Single-crystal growth of SiC substrate material for blue-light emitting diodes,” *IEEE Transact. Electr. Dev.* **ED-30**, 227. (See Tairov *et al.*, 1978.)

EXERCISES

- 29.1 Describe the Verneuil method for producing ruby. What are the advantages and disadvantages of this process?
- 29.2 Briefly describe how ruby could be produced by the Czochralski (Cz) process. Under what situations, if any, would it be preferable to use the Cz process rather than the Verneuil process for ruby growth?
- 29.3 Why are crystals of cubic zirconia grown by the skull melting technique?
- 29.4 There are several different geometries for the Bridgman–Stockbarger method. Comparing the vertical and horizontal geometries, what are the advantages and disadvantages of each?
- 29.5 Knowledge of phase diagrams is very important for understanding the growth of single crystals from the melt. Using the case of BaTiO₃ explain the considerations involved when producing single crystals of incongruently melting solids using melt growth techniques such as the Cz method.
- 29.6 Why are flux growth methods widely used in the production of synthetic gems? Are there are disadvantages that you can think of in using these methods for this particular application?

- 29.7 A company wishing to start producing single crystals of AlN has called you in as a consultant. What advice would you give them concerning the type of methods that would be suitable?
- 29.8 Draw up a list of as many different substrate materials as you can that have been used in the growth of thin films of the high-temperature superconductors. In your list make note of the surface orientation (if it is given) and the surface condition (was it polished, cleaned, annealed, etc.) of the substrate.
- 29.9 Using the information you gathered for question 29.8 add to your list one method that could be used to produce each type of single crystal from which the substrates were obtained.
- 29.10 By carefully reviewing the literature, present a detailed discussion of the method of growing diamond using the “flux” method. You should give quantities, diagrams, and references.

Part VII

Properties and Applications

Conducting Charge or Not

CHAPTER PREVIEW

Ceramics show the widest range of electrical properties of any class of material. At one extreme we have high-temperature superconductors, which have no resistance to an electrical current. At the other extreme we have electrical insulators. Ceramic superconductors have not yet fulfilled many of the expectations and predications for useful applications, whereas insulating ceramics are used for a number of critical applications such as packages for integrated circuits. Without the use of insulating ceramics the development of powerful personal computers would not have been so rapid. Between the two extremes are ceramics that behave very much like metals, and there are the semiconductors, which are all ceramics. Ceramics with metal-like conductivity are used as electrodes and in thick-film resistors. Semiconductors such as SiC are important for high-temperature electronics. In this chapter we will explain why ceramics show such a diverse range of electrical properties. The important concepts are related to our earlier discussion of bonding and energy bands.

In some ceramics the only species that can move in an applied electric field are the ions in the structure. Generally, the movement of ions is slow, but in a class of ceramics called fast ion conductors, they can move very rapidly. In cubic zirconia the diffusion of oxygen ions at high temperature is particularly fast, and this ceramic is used as the electrolyte in solid oxide fuel cells. Fuel cells are becoming a key part of a diverse energy plan for the twenty-first century.

We will begin by describing the conduction mechanisms in ceramics and looking at some specific applications. We will finish by describing one of the most fascinating developments in ceramics—high-temperature superconductors.

30.1 CERAMICS AS ELECTRICAL CONDUCTORS

Ceramics are usually thought of as electrical insulators and indeed a great many of them are. Since the first uses of electricity it has been necessary to have good electrical insulators to isolate current-carrying wires. The expansion of the electrical industry and, in particular, the use of the electric telegraph required enormous numbers of porcelain insulators for telegraph poles. From 1888 ceramics based on steatite began to be used for the same purpose. Today ceramics are still used to provide insulating supports in the power lines that criss-cross the country.

The distinction between materials as electrical conductors and materials as insulators was made in the eighteenth century. Although historically the insulating properties of ceramics have often been one of their most

important properties, many ceramics are actually very good electrical conductors and some are even superconductors. Ceramics show the broadest range of electrical properties of any of the classes of material. The values of electrical conductivity for ceramics vary over an enormous range—over 24 orders of magnitude!—as shown in Figure 30.1.

Table 30.1 lists the important parameters that are used in discussions of electrical conductivity. As we have done elsewhere in this book we will use SI units (unless there is a good reason for not doing so, such as the use of electron volts for band gap energies). If another system is widely used the appropriate conversion factor is given. Electrical conductivity is in general a tensor of the second rank. Fortunately, the electrical properties of materials can largely be understood by assuming that they are isotropic and σ is simply a scalar.

The conduction mechanisms in ceramics can be quite complex and may involve the movement of electrons,

ELECTRIC TOWN

In 1881 Godalming became the first town in the world to have a public electricity supply.

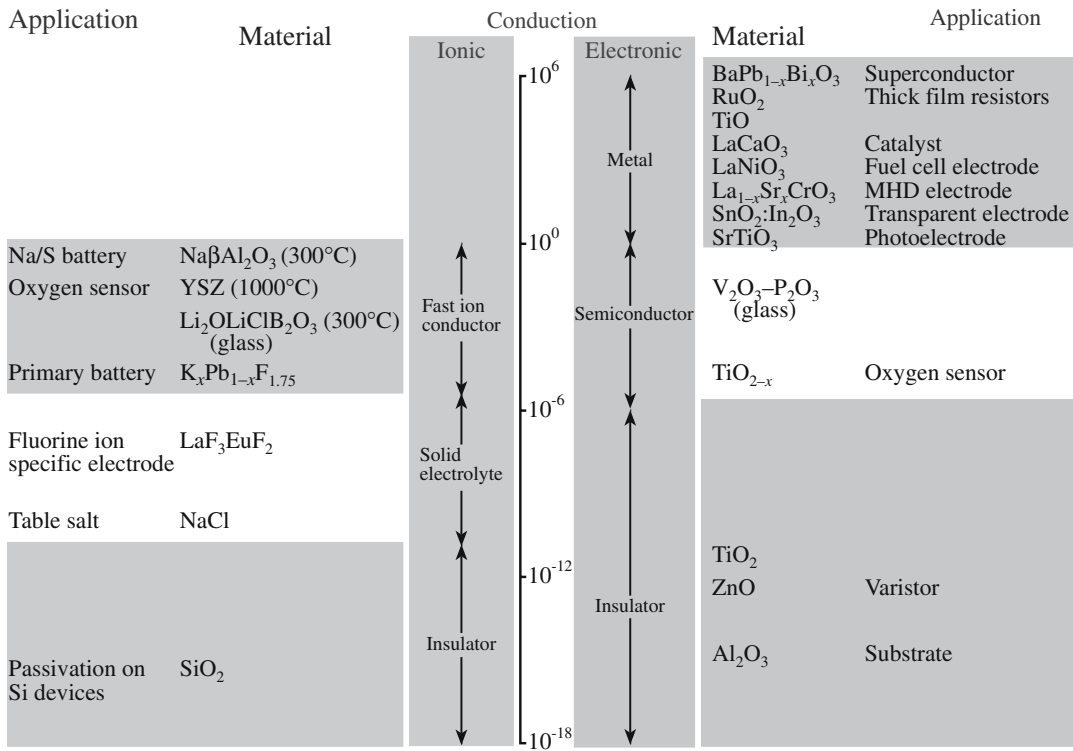


FIGURE 30.1 Range of conductivities of ceramics.

holes, and ions; in some cases they may be “mixed,” with more than one type of charge carrier responsible for current flow. In the case of ceramic superconductors the current is carried by electron pairs (Cooper pairs). So this is really very different and is discussed separately.

In comparing values of σ and ρ it is useful to remember the simple relationship between them:

$$\sigma = \frac{1}{\rho} \quad (30.1)$$

TABLE 30.1 Terms and Units Used

Parameter	Definition	Units/value	Conversion factor
E_g	Band gap energy	eV	1 eV = 1.602×10^{-19} J (eV is a much more convenient unit for E_g)
E_f	Fermi energy		
σ	Conductivity	S/m	1 S = $1 \Omega^{-1}$
I	Current	A	
J	Current density	$C m^{-2} s^{-1}$	
v	Drift velocity	m/s	
ξ	Electric field strength	V/m	
μ	Mobility	$m^2 V^{-1} s^{-1}$	Subscripts e and h will be used to represent electron and hole mobility, respectively; the units are the same in both cases
R	Resistance	Ω	
ρ	Resistivity	$\Omega \cdot m$	
V	Voltage	V	
q	Electron charge	1.602×10^{-19} C	Sometimes e
t	Transference number	Dimensionless	
K	Boltzmann constant	1.381×10^{-23} J/K	
T	Temperature	K or °C	
T_c	Critical temperature for superconductivity	K	0 K = -273°C

30.2 CONDUCTION MECHANISMS IN CERAMICS

Electrical conductivity is given by

$$\sigma = nq\mu \quad (30.2)$$

The importance of Eq. 30.2 is that it applies to all materials and it shows that the two factors affecting σ are

- Number of charge carriers, n
- Their mobility, μ

When we consider the effect of variables such as composition, structure, and temperature on σ we are concerned with their effect on n and μ .

If more than one type of charge carrier is contributing to σ then we can define a partial conductivity for each. For example, if σ were due to the movement of electrons and cations with a charge Z , then for electrons

$$\sigma_e = \mu_e (n_e q) \quad (30.3)$$

and for cations

$$\sigma_+ = \mu_+ (n_+ Zq) \quad (30.4)$$

The total is

$$\sigma_{\text{tot}} = \sigma_e + \sigma_+ \quad (30.5)$$

If a ceramic is an electron conductor, i.e., $t_e = 1$, then to determine n we need to know E_g . We usually consider the three situations shown in Figure 30.2, where the band gap is either zero, narrow, or wide.

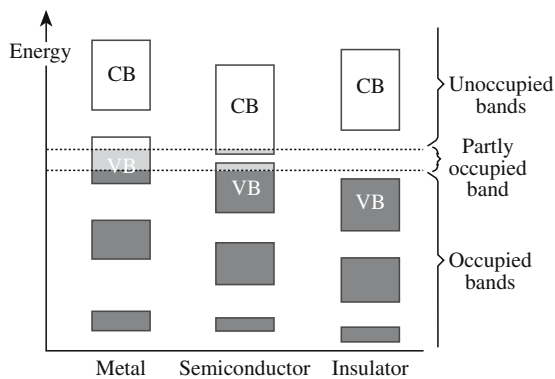


FIGURE 30.2 Schematic of electron energy bands in solids. The valence band (VB) and conduction band (CB) are indicated.

TABLE 30.2 Transference Numbers of Cations, t_+ , Anions, t_- , and Electrons or Holes, $t_{e,h}$ in Several Materials

Ceramic	T ($^{\circ}\text{C}$)	t_+	t_-	$t_{e,h}$
NaCl	400	1.00	0.00	
	600	0.95	0.05	
KCl	435	0.96	0.04	
	600	0.88	0.12	
KCl + 0.02% CaCl ₂	430	0.99	0.01	
	600	0.99	0.01	
AgCl	20–350	1.00		
AgBr	20–300	1.00		
BaF ₂	500		1.00	
PbF ₂	200		1.00	
CuCl	20			1.00
	366	1.00		
ZrO ₂ + 7% CaO	>700		1.00	<10 ⁻⁴
Na ₂ O·11Al ₂ O ₃	<800	1.00 (Na ⁺)		<10 ⁻⁶
FeO	800	10 ⁻⁴		1.00
ZrO ₂ + 18% CeO ₂	1500		0.52	0.48
ZrO ₂ + 50% CeO ₂	1500		0.15	0.85
Na ₂ O·CaO·SiO ₂ glass		1.00 (Na ⁺)		
15% (FeO·Fe ₂ O ₃)·CaO·SiO ₂ ·Al ₂ O ₃ glass	1500	0.1 (Ca ²⁺)		0.9

The real band structure of a material is actually a complex three-dimensional shape. Even so these simple representations can be used to illustrate many of the important electronic properties of materials. When E_g is zero, as in the case of most metals, there are free electrons present at any temperature above 0 K. The total number of free electrons is equal to the number of valence electrons per atom multiplied by the number of atoms in the metal. E_g in a metal is not zero, but it is very small. For example, if we have a metal crystal consisting of

10^{23} atoms and the width of the energy band is 1 eV then the separation between the energy levels would be only 10^{-23} eV (1.6×10^{-42} J). This would be the minimum amount of energy required to excite an electron into a vacant level.

A narrow band gap is usually defined as being in the range of 0.02 to about 2.5 eV. When E_g is toward the lowest end of this range there is a significant fraction of electrons in the conduction band. Materials with a narrow band gap are usually referred to as semiconductors.

- Silicon: $E_g = 1.12$ eV
- Gallium arsenide: $E_g = 1.42$ eV

Both Si and GaAs are ceramics.

TABLE 30.3 Band Gap Energies for Various Ceramics

Material	E_g (eV)	Material	E_g (eV)	Material	E_g (eV)
Halides					
AgBr	2.80	BaF ₂	8.85	CaF ₂	12.00
KBr	0.18	KCl	7.00	LiF	12.00
MgF ₂	11.00	MnF ₂	15.50	NaCl	7.30
NaF	6.70	SrF ₂	9.50	TlBr	2.50
Oxides					
Al ₂ O ₃ (sapphire)	8.80	CdO	2.10	Ga ₂ O ₃	4.60
MgO (periclase)	7.7	SiO ₂ (fused silica)	8.30	UO ₂	5.20
CoO	4.0	CrO ₃	2.0	Cr ₂ O ₃	3.3
CuO	1.4	Cu ₂ O	2.1	FeO	2.4
Fe ₂ O ₃	3.1	MnO	3.6	MoO ₃	3.0
Nb ₂ O ₅	3.9	NiO	4.2	Ta ₂ O ₅	4.2
TiO ₂ (rutile)	3.0–3.4	V ₂ O ₅	2.2	WO ₃	2.6
Y ₂ O ₃	5.5	ZnO	3.2	BaTiO ₃	2.8–3.2
KNbO ₃	3.3	LiNbO ₃	3.8	LiTaO ₃	3.8
MgTiO ₃	3.7	NaTaO ₃	3.8	SrTiO ₃	3.4
SrZrO ₃	5.4	Y ₃ Fe ₅ O ₁₂	3.0		
Carbides and Nitrides					
AlN	6.2	BN	4.8	C (diamond)	5.33
SiC (α)	2.60–3.20a				
Chalcogenides					
PbTe	0.275	PbS (galena)	0.350	PbSe	0.400
CdTe	1.450	CdSe	1.850	CdS	2.420
ZnSe	2.600	ZnS	3.600		

Materials with a wide band gap (>2.5 eV) are considered to be electrical insulators because the probability of an electron being in the conduction band at room temperature is extremely small. However, the probability is not zero and so we should think of these materials as wide-band-gap semiconductors. SiC ($E_g = 2.6\text{--}3.0$) is an example of a wide-band-gap semiconductor and is used in sensors in aircraft and fuel cells that can operate in hostile environments at temperatures up to 600°C where conventional silicon-based electronics cannot function.

Band gap energies for a number of ceramics are listed in Table 30.3.

30.3 NUMBER OF CONDUCTION ELECTRONS

This section follows directly from Section 4.8. The number of electrons in the conduction band, n_i , is

$$n_i = \int_{E_c}^{E_{top}} N_c(E) f(E) dE \quad (30.6)$$

- $N_c(E) dE$ is the density of states in the conduction band and represents the number of energy levels over which

the electrons can be distributed (i.e., the number of allowed energy states).

- $P(E)$ is the Fermi–Dirac function giving the probability of an electron being in the conduction band.

$$f(E) = \left\{ \frac{1}{1 + \exp\left(\frac{E - E_f}{kT}\right)} \right\} \quad (30.7)$$

The evaluation of n_i is quite straightforward if we make the following assumptions:

1. $E - E_f \gg kT$. This is often the case since at room temperature $kT \sim 0.025$ eV and $E - E_f$ is usually >5 eV. We can now omit the +1 in Eq. 30.7. [We are in effect replacing Fermi–Dirac statistics by Boltzmann statistics.]

2. The excited electrons occupy states near the bottom of the conduction band. Under these conditions they behave as free particles for which the state distribution function is known.

3. The upper limit of the integration in Eq. 30.6 is taken as ∞ since the probability of occupancy of a state by an electron rapidly approaches zero as the energy increases through the band.

Under these assumptions we can write

$$n_i = N_c \exp\left(-\frac{E_c - E_F}{kT}\right) \quad (30.8)$$

E_F lies midway between E_C and E_V in an intrinsic material (i.e., one that has few impurities) and since $N_C \sim 10^{25} \text{ m}^{-3}$ we can simplify Eq. 30.8 as

$$n_i = N_c \exp\left(-\frac{E_g}{2kT}\right) \sim 10^{25} \exp\left(-\frac{E_g}{2kT}\right) \quad (30.9)$$

The important things to remember from this series of equations are that

- n depends on E_g and T .
- As we increase T we increase n .

30.4 ELECTRON MOBILITY

As electrons move through a solid under the influence of ξ they experience a number of collisions (in a process called scattering) that decreases μ . There are three scattering mechanisms:

- *Phonon*. This is the major factor affecting μ (of both electrons and holes). A phonon is the quantum unit of lattice vibrational energy as described later in Chapter 34. The higher the temperature the greater the vibrational amplitude of the atoms in the lattice and the greater the number of phonons. As a result, scattering increases and μ decreases with increasing temperature.

$$\mu \propto T^{-m} \quad (30.10)$$

- *Electron–electron*. At room temperature the mean distance between electron–electron collisions is about 10 times that of electron–phonon collisions so electron–phonon scattering is dominant.
- *Polaron*. This mechanism occurs only in ionic crystals and involves the interaction between the electron and the ions in the crystal. The electron can cause local distortion of the lattice known as a polaron as illustrated in Figure 30.3. When the interaction is sufficiently strong (small polaron) the electron may be trapped at a particular lattice site, reducing μ and decreasing σ .

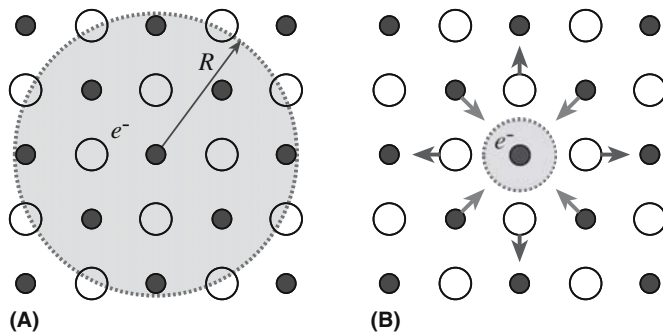


FIGURE 30.3 Illustration of (a) a large polaron of radius R , formed in a metal oxide MO and (b) a small polaron, showing the distortion of the lattice around an electron trapped at a metal.

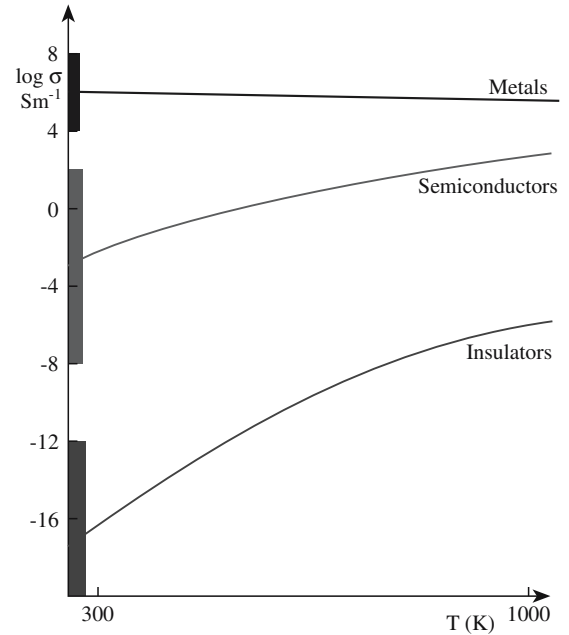


FIGURE 30.4 Conductivity variations with temperature for the different classes of electrical conductor. The shading indicates the range of values at room temperature.

30.5 EFFECT OF TEMPERATURE

For a material where $E_g = 0$, i.e., one in which n does not vary significantly with T , σ decreases with increasing temperature because of the decrease in μ :

$$\sigma \propto \frac{n}{T^m} \quad (30.11)$$

For materials where $E_g > 0$ (i.e., materials that we would classify as semiconductors or insulators), σ rises with T because of the temperature dependence of n as shown by Eq. 30.9:

$$\sigma \propto \exp\left(-\frac{E}{2kT}\right) \quad (30.12)$$

Figure 30.4 shows the typical T dependence of σ for the three broad classes of electrical behavior.

Because it is possible to make practical use of the variation in σ or ρ with T it is often beneficial to classify materials based on this variation. (From a practical point of view we usually consider changes in ρ rather than changes in σ .) The temperature dependence of resistivity may be expressed by an empirical equation

$$\rho_2 = \rho_1 [1 + \alpha_R (T_2 - T_1)] \quad (30.13)$$

where ρ_1 is the resistivity at T_1 and ρ_2 is the resistivity at T_2 . The parameter α_R is known as the temperature coefficient of resistivity or TCR. For materials where $E_g = 0$ the TCR is typically positive. These materials are called positive temperature coefficient (PTC) materials. Most materials that show semiconducting or insulating properties are negative temperature coefficient (NTC) materials. Some ceramics, for example BaTiO_3 , that do have energy band gaps are actually PTC materials. This type of behavior has nothing to do with conduction across the band gap but is actually a grain boundary (GB) effect.

30.6 CERAMICS WITH METAL-LIKE CONDUCTIVITY

The general electrical characteristics of metals are

- $\sigma \geq 10^4 \text{ S/m}$
- $t_e = 1$
- $n = 10^{22} - 10^{23} \text{ cm}^{-3}$
- $d\sigma/dT$ is small and negative.

Remember that Ω^{-1} (ohm^{-1}) is S (siemens). Some ceramics, for example TiO and VO, show metallic-like electronic conductivity where the conduction is due to the movement of free electrons. To explain this behavior we will consider the example of TiO.

TiO has a structure based on rocksalt with vacancies in both the metal and oxygen sublattices. One-sixth of the titaniums and one-sixth of the oxygens are missing as illustrated in Figure 30.5. The 2p orbitals from the oxygen atoms form a filled valence band. The bands formed by the 4s and 4p orbitals on the Ti are at a

TRANSITION METALS
Transition metals have partially filled d orbitals.

ELECTRON CONFIGURATIONS

Ti	$1s^2 2s^2 2p^6 3s^2 3p^6 3d^2 4s^2$
Ti ²⁺	$1s^2 2s^2 2p^6 3s^2 3p^6 3d^2$
Ti ⁴⁺	$1s^2 2s^2 2p^6 3s^2 3p^6$

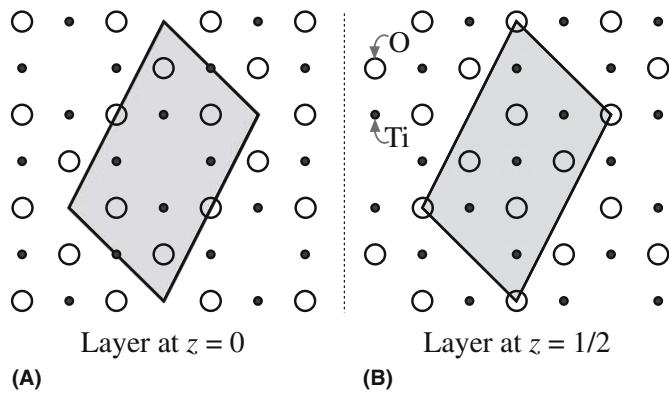


FIGURE 30.5 The structure of TiO. (a) The (100) plane. (b) The (200) plane. Both show the absence of alternate ions along $\langle 110 \rangle$ directions. The resultant superlattice has a monoclinic unit cell as indicated by the shaded region.

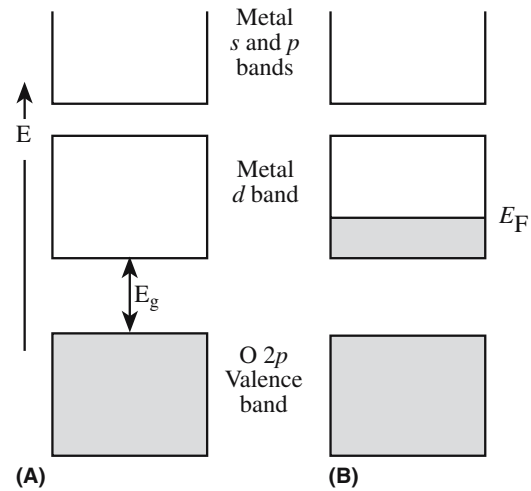


FIGURE 30.6 Energy bands of a transition metal oxide: (a) d band empty; (b) metallic oxide with d band partially filled.

much higher energy. The metal d orbitals form a band below that of the metal s and p orbitals as illustrated in Figure 30.6.

The divalent titanium ion, Ti^{2+} , in TiO has two 3d electrons and so the metal d band shown in Figure 30.6 is partially filled. It is this partially filled band, which you will notice resembles the energy level diagram for a metal shown in Figure 30.2, that leads to metallic conductivity in TiO. Looking at Figure 30.6 it is easy to see why titanium dioxide, TiO_2 , is an insulator. In the formation of the Ti^{4+} ion, both the two 4s electrons and the two 3d electrons are given up to form oxygen ions. So the 3d band (the conduction band in the solid) is empty at $T = 0 \text{ K}$. The band gap, E_g , in TiO_2 is 3 eV. This is a relatively small E_g for an insulator and indicates some covalent character in the Ti–O bond.

So why aren't MnO, CoO, and NiO, which are also monoxides of the first row transition metals and have the rocksalt structure, metallic-like conductors?

To answer this question we need to consider the interaction between the d orbitals and the formation of the d band in metal oxides. In the rocksalt structure the d_{xy} , d_{yz} , and d_{xz} orbitals (collectively known as the t_{2g} orbitals) on adjacent metal atoms overlap. The extent of the overlap is less than it would be in the pure metal because in the oxides the metal atoms are not nearest neighbors. Consequently the d bands are narrower than they would be for the metal. (We are referring to the widths of the bands themselves and not the size of the band gap.) As we go across the first row transition elements (from Ti to Ni) there is an increase in nuclear charge and a corresponding

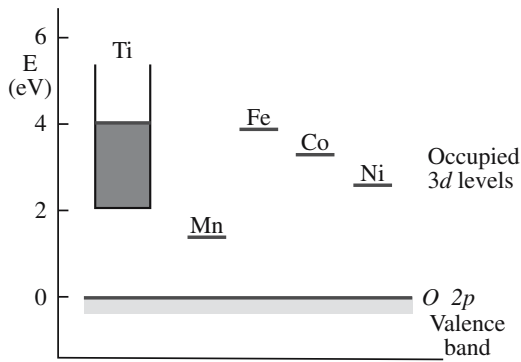


FIGURE 30.7 Electronic energy levels of some 3d monoxides, deduced from spectroscopic measurements. The energy zero has been taken as the top of the oxygen 2p valence band.

contraction in the size of the d orbitals. As the d orbitals become smaller the extent of overlap decreases and the 3d band becomes narrower, eventually forming a localized state as illustrated in Figure 30.7.

Some oxides of the second and third row transition elements also exhibit metallic-like properties, for example, ReO_2 and ReO_3 . In these compounds the metal electron energy levels of interest are the 5d, rather than the 3d as in the case of the first row transition metals.

Figure 30.8 shows the σ versus temperature behavior for several oxides. For some of the oxides we have already

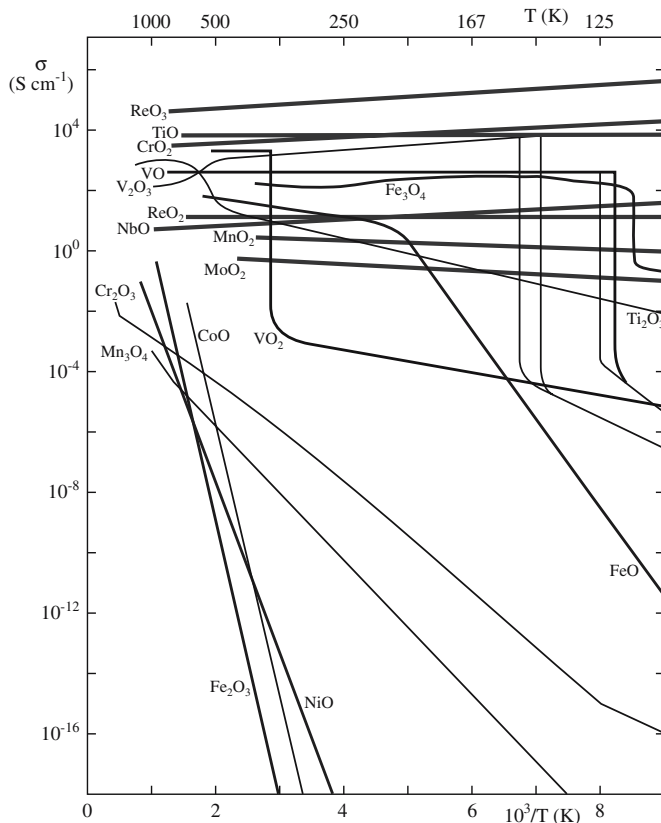


FIGURE 30.8 Temperature dependence of the electrical conductivity of several electronically conducting oxides.

mentioned, e.g., ReO_3 , TiO , CrO_2 , and ReO_2 , $d\sigma/dT$ is small and negative, just like it is for most metals.

30.7 APPLICATIONS FOR HIGH- σ CERAMICS

There are many applications for ceramics that have metal-like conductivity. We will look at two examples:

- Resistors
- Electrodes

Resistors

The requirements for most resistors are that they are

- Ohmic
- Small TCR

Components with R in the range 10^3 – $10^8 \Omega$ are the major requirements of the electronic industry. These are fabricated from electronically conducting ceramics with σ in the range 10^5 – 10^6 S/m . Resistance is not an intrinsic property of a material. It is influenced by the specimen configuration, i.e., its thickness and length. The relationship between R and σ is

$$R = \frac{l}{\sigma A} \quad (30.14)$$

where A is the cross-sectional area of the specimen perpendicular to the direction of the current flow and l is the distance between the two points at which the voltage is measured. To make a 10^5 - Ω resistor of length 10 cm from a material with $\sigma = 10^6 \text{ S/m}$ would require a cross-sectional area of 10^{-12} m^2 . Using a strip with a $1 \mu\text{m}^2$ cross section would be possible, but it is not usually economically feasible. There are two methods that are used to make high-resistance components using high- σ ceramics:

1. Increase the aspect ratio (length to width) of the conductive layer by patterning
2. Mix the conductive phase with a highly resistive one

Thin-film resistors usually make use of the first approach. For example, thin films ($\sim 10 \text{ nm}$ thick) of indium tin oxide (ITO) are deposited onto glass, or sometimes sapphire, substrates by sputtering or chemical vapor deposition (CVD). After deposition the films are patterned to achieve a large aspect ratio. If the substrate is in the form of a rod a spiral groove is cut into the film.

Thick-film resistors are made by diluting a conductive oxide with an electrical insulator such as glass. (The practical aspects of thick-film processing were described in

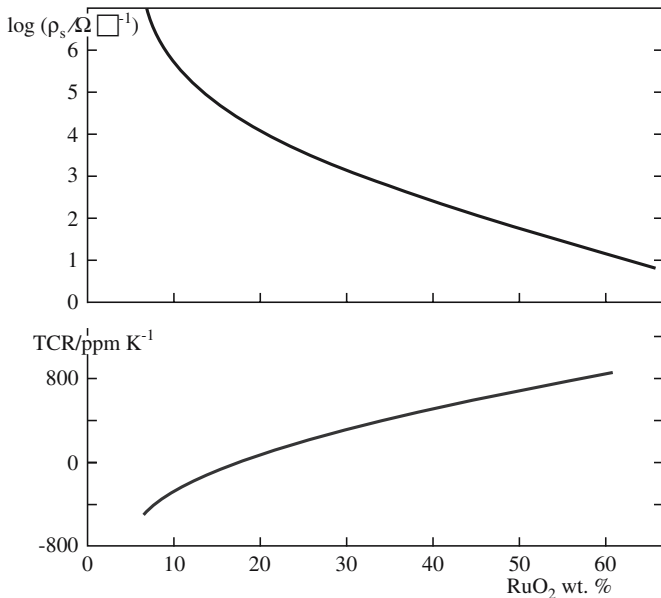


FIGURE 30.9 Electrical characteristics of RuO₂ thick-film resistors.

Chapter 27.) Ruthenium dioxide (RuO₂) and mixed metal oxides containing ruthenium, such as Bi₂Ru₂O₇, are widely used as the conducting component. These oxides have σ in the range of 10⁵–10⁶ S/m. The glass is usually a lead borosilicate of composition typically (in wt%) 52PbO–35SiO₂–10B₂O₃–3Al₂O₃. The final thickness of the resistor after processing is in the range of 10–15 μ m. The resistors normally have high resistivities and negative TCRs for low concentrations of the conductive component and low resistivities and positive TCRs for high concentrations as shown in Figure 30.9. This behavior is the result of a combination of the positive TCR of the conductive particles and the negative TCR of the regions between them.

The distribution of the conductive particles and the contact between them also determines the resistance of the deposited film. Final resistance values are obtained either by sand blasting, where the thickness of the film is reduced, or by laser trimming, to increase the effective length of the resistor. These procedures would be performed after the resistor has been fired, but before the application of the protective glaze coating.

Electrodes

High- σ ceramics are used as electrodes in a number of applications:

- Fuel cells
- Humidity sensors
- Displays

The question we need to ask ourselves again is: What is special about ceramics?

Temperature Stability. LaCrO₃ was developed in the 1960s for electrodes in magnetohydrodynamic (MHD)

generators where the electrode had to withstand temperatures up to 2000°C and the corrosive potassium atmosphere in the generator. LaCrO₃ has a melting temperature of 2500°C and $\sigma = 100$ S/m at 1400°C. MHD generators are now of little interest, but LaCrO₃ has been used as an electrode in solid oxide fuel cells. LaCrO₃ has the perovskite structure that we described in Chapter 7.

Porous. In humidity and gas sensors the electrode must be electrically conductive, produce a porous coating (to allow the vapors to reach the sensor), and be stable in the sensing environment. RuO₂ is used as an electrode in humidity sensors. One example of the sensing element is a solid solution of TiO₂ in MgCr₂O₄. This type of sensor is used in microwave ovens where it detects the rapid rise in humidity corresponding to the onset of cooking. There is a fall in ρ when the ceramic is exposed to humid atmospheres, the result of dissociation of water molecules:



Several other materials have been developed for humidity sensors and the electrical responses of three different ones are shown in Figure 30.10.

Transparent. For applications in which a transparent electrode is required metals are completely unsuitable. Metals, because of their very small E_g , can absorb all wavelengths of visible light and are, as a result, opaque in the visible part of the electromagnetic spectrum. Only metal layers <1 μ m will be transparent. A ceramic used as a transparent electrode is indium tin oxide (ITO). A typical electrode composition is 90In₂O₃–10SnO₂. Transparent electrodes are important for many electrooptic devices,

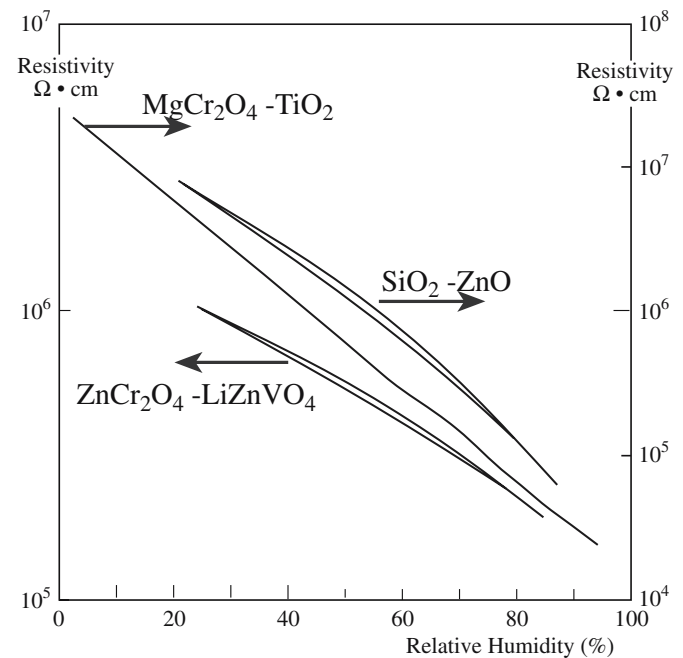


FIGURE 30.10 Electrical response of three ceramic humidity sensors at room temperature and 1 kHz.

liquid crystal displays (LCDs), light-emitting diodes (LEDs), and solar cells.

30.8 SEMICONDUCTING CERAMICS

Semiconductors have a small E_g as shown in Figure 30.2. In semiconductors σ is proportional to n and μ (for both electrons and holes). In general, there are three ways free electrons and holes may be generated in ceramics:

- Excitation across the band gap (*intrinsic* semiconductors)
- Introduction of impurities/dopants (*extrinsic* semiconductors)
- Departures from stoichiometry (*nonstoichiometric* semiconductors)

Most oxide semiconductors are either doped to create extrinsic defects or are annealed under conditions in which they become nonstoichiometric.

Intrinsic Semiconductors

For every electron that is excited into the conduction band, a hole is produced in the valence band.

The number of electrons in the conduction band is

$$n = N_c \exp\left(-\frac{E_g}{2kT}\right) \quad (30.16)$$

Similarly, the number of holes in the valence band is

$$p = N_v \exp\left(-\frac{E_g}{2kT}\right) \quad (30.17)$$

The densities of states are given by

$$N_c = 2\left(\frac{2\pi m_e^* kT}{h^2}\right)^{3/2} \quad (30.18)$$

and

$$N_v = 2\left(\frac{2\pi m_h^* kT}{h^2}\right)^{3/2} \quad (30.19)$$

where m_e^* and m_h^* are the effective masses of the electrons and holes, respectively. For many ceramics m_e^* and m_h^* are

not known and we make the (often incorrect) assumption that $m_e = m_e^* = m_h^*$, where m_e is the rest mass of the electron.

If we use the subscript i to denote intrinsic carrier concentrations, we can write

$$n_i = p_i \quad (30.20)$$

and

$$np = n_i p_i = n_i^2 \quad (30.21)$$

Therefore

$$n_i = (N_c N_v)^{1/2} \exp\left(-\frac{E_g}{2kT}\right) \quad (30.22)$$

If $N_c = N_v$ then

$$n_i = N_c \exp\left(-\frac{E_g}{2kT}\right) \quad (30.23)$$

The intrinsic conductivity is given by

$$\sigma_i = qn_i(\mu_e + \mu_h) \quad (30.24)$$

MOBILITIES OF ELECTRONS AND HOLES

In ceramics these depend upon their interaction with the lattice. Typical values are very small ($\leq 0.1 \text{ cm}^2 \text{ V}^{-1} \text{ s}^{-1}$): orders of magnitude lower than in Si and GaAs.

Equation 30.24 is similar to Eq. 30.2, but we are now considering μ_e and μ_h .

The intrinsic conductivity of many pure oxide semiconductors is generally very low because of their large E_g compared to Si and GaAs. To illustrate this point we will compare the room temperature conductivities of Cu_2O , a semiconducting oxide $E_g = 2.1 \text{ eV}$, and GaAs, a III-V semiconductor $E_g = 1.4 \text{ eV}$.

The largest applications for semiconductors use extrinsic material. The entire electronic materials industry is built around doped silicon. However, there are applications that require intrinsic semiconductors. One such application is X-ray detectors used on transmission electron microscopes (TEMs) and scanning electron microscopes (SEMs) for chemical analysis. Unfortunately it is essentially impossible to produce pure silicon. Even electronic grade silicon contains small amounts of boron (a p-type dopant). To create "intrinsic" material a dopant is added that produces an excess of electrons that combine with the holes formed by the residual boron. The process involves diffusing lithium atoms into the semiconductor. Ionization of the lithium produces electrons that recombine with the holes. It is possible to produce germanium crystals with much higher purity, and intrinsic Ge detectors are used on some TEMs.

Extrinsic and Nonstoichiometric Semiconductors

An extrinsic semiconductor contains impurities that are present either accidentally or, as is most often the case, that have been intentionally added. The effect of these impurities on the energy band diagram is that they introduce additional energy levels into the band gap as illustrated in Figure 30.11. These new energy levels are often close to the band edges.

If the impurity level is just above the valence band the impurity is an “acceptor” because it can accept electrons leaving holes in the valence band. If the impurity can supply electrons into the conduction band it is a “donor” and the level is located just below the bottom of the conduction band. If the impurity acts as an electron donor the semiconductor is known as an n-type semiconductor because the electrons (or negatively charged species) are the majority charge carriers. If the impurity acts as an electron acceptor then the semi-

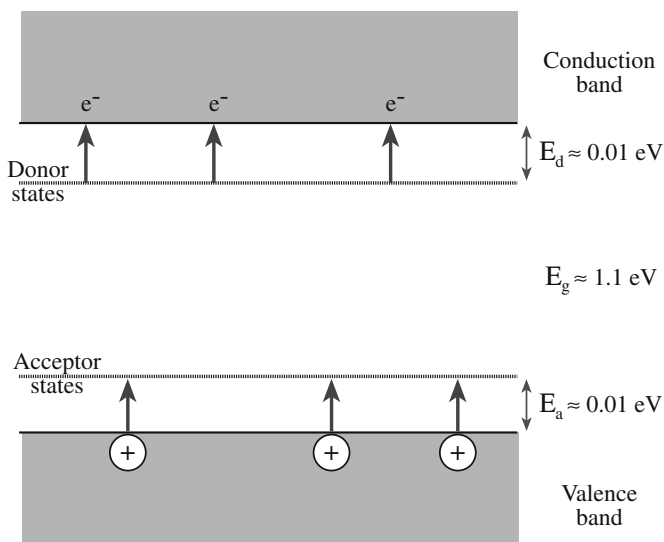


FIGURE 30.11 Effect of doping on band structure.

WORKED EXAMPLE

1. Calculate N_c and N_v (Eqs. 30.18 and 30.19) (density of states):

$$\text{Cu}_2\text{O: we will assume } m_c^* = m_h^* = 9.11 \times 10^{-32} \text{ kg} \\ \Rightarrow N_c = N_v = 2.49 \times 10^{19} \text{ cm}^{-3}$$

$$\text{GaAs: } m_c^* = 0.067m_e = 6.10 \times 10^{-32} \text{ kg,} \\ m_h^* = 0.48m_e = 4.37 \times 10^{-31} \text{ kg} \Rightarrow \\ N_c = 4.31 \times 10^{17} \text{ cm}^{-3} \text{ and} \\ N_v = 8.26 \times 10^{18} \text{ cm}^{-3}$$

2. Calculate n_i (Eq. 30.23):

$$\text{Cu}_2\text{O: } n_i = 45.11 \text{ cm}^{-3}; \text{ GaAs: } n_i = 2.85 \times 10^6 \text{ cm}^{-3}$$

3. Calculate σ (Eq. 30.24):

The last parameters we need before we can calculate n_i are μ_e and μ_h . In ionic solids these values are often not well known, but are several orders of magnitude lower than for the covalent semiconductors.

$$\text{Cu}_2\text{O: } \mu_e = 0.2 \text{ cm}^2 \text{ V}^{-1} \text{ s}^{-1} \text{ and } \mu_h = 0.1 \text{ cm}^2 \text{ V}^{-1} \text{ s}^{-1}.$$

(Reasonable estimates.) For GaAs see Table 30.4.

$$\text{Cu}_2\text{O: } \sigma = 2.17 \times 10^{-18} \text{ S/cm;} \\ \text{GaAs } \sigma = 5 \times 10^{-9} \text{ S/cm}$$

These are room temperature values for “pure” materials.

conductor is known as a p-type semiconductor because holes (or positively charged species) act as the majority charge carriers.

At low temperatures the number of charge carriers is determined by the donor and acceptor ionization energies. At sufficiently high temperatures full ionization of the impurities is achieved and the carrier densities become independent of temperature. This region is called the “exhaustion” or “saturation” region. At even higher temperatures the thermal energy is enough to excite electrons across the energy band gap and the material behaves like an intrinsic semiconductor. These three regions are shown in Figure 30.12.

Nonstoichiometric semiconductors are very similar to extrinsic semiconductors, and can really be con-

TABLE 30.4 Mobilities of Various Semiconductors

Semiconductor	Electron mobility ($\text{m}^2 \text{ V}^{-1} \text{ s}^{-1}$)	Hole mobility ($\text{m}^2 \text{ V}^{-1} \text{ s}^{-1}$)
α -SiC	0.04	~0.02
Si	0.15	0.049
Ge	0.39	0.18
GaAs	0.85	0.30
InAs	3.30	0.02
InSb	8.00	0.17
Diamond	0.18	0.12
PbS	0.06	0.02
GaSb	0.30	0.065
CdS	0.04	—
CdSe	0.065	—
CdTe	0.12	0.005
GaP	0.015	0.012
AlN	—	0.001
PbSe	0.09	0.07
PbTe	0.17	0.093
AgCl	0.005	—
SnO ₂	0.016	—
SrTiO ₃	0.0006	—
Fe ₂ O ₃	10 ⁻⁵	—
TiO ₂	2 × 10 ⁻⁵	—
Fe ₃ O ₄	—	10 ⁻⁵
CoFe ₂ O ₄	10 ⁻⁸	10 ⁻¹²
FeO, MnO, CoO, NiO	—	~10 ⁻⁵

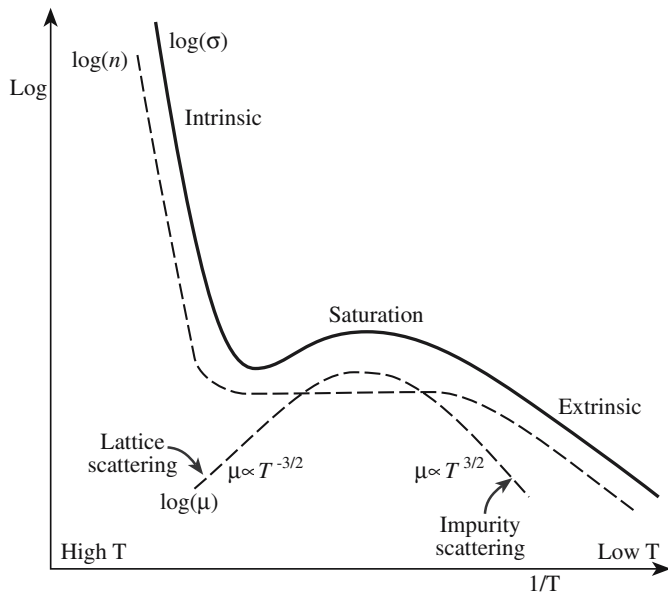


FIGURE 30.12 Temperature dependence of σ for an extrinsic semiconductor. The dashed lines show the individual contributions of n and μ to σ .

sidered together. The main difference is that the electronic defects rather than being due to impurity atoms are the result of changes in the stoichiometry of the crystal. We still use the designations n- and p-type to describe the majority charge carrier and the defect adds levels into the band gap that lead to increased levels of conductivity, particularly at room temperature and below.

30.9 EXAMPLES OF EXTRINSIC SEMICONDUCTORS

Zinc Oxide: An n-Type Semiconductor

In Section 11.7 we described the result of heating ZnO in Zn vapor. The excess Zn atoms occupy interstitial sites. One electron is produced for every Zn interstitial as shown using Kröger-Vink notation:



The requirement of electroneutrality means that the concentration of interstitials is equal to the concentration of electrons:

$$[\text{Zn}_i] = [e'] = Kp_{\text{Zn}}^{1/2} \quad (11.14)$$

Because σ depends on the number of charge carriers it will be proportional to the zinc vapor pressure:

$$\sigma \propto p_{\text{Zn}}^{1/2} \quad (30.25)$$

The oxygen dependence can be considered in a similar way and gives

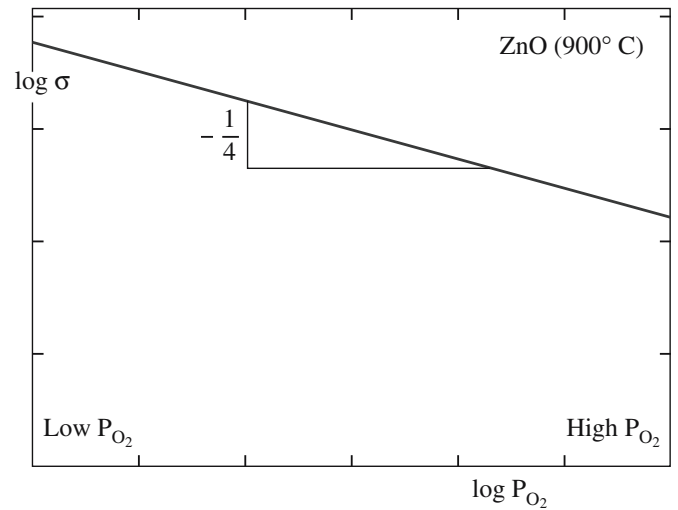


FIGURE 30.13 Effect of oxygen pressure on the electrical conductivity of ZnO.

$$[\text{Zn}_i] = [e'] = Kp_{\text{O}_2}^{-1/4} \quad (30.26)$$

Now σ will vary with the oxygen partial pressure as shown in the log-log plot in Figure 30.13:

$$\sigma \propto p_{\text{O}_2}^{-1/4} \quad (30.27)$$

Figure 30.14 shows the energy band diagram for Zn_{1+x}O illustrating the positions of the donor levels. E_1 and E_2 are

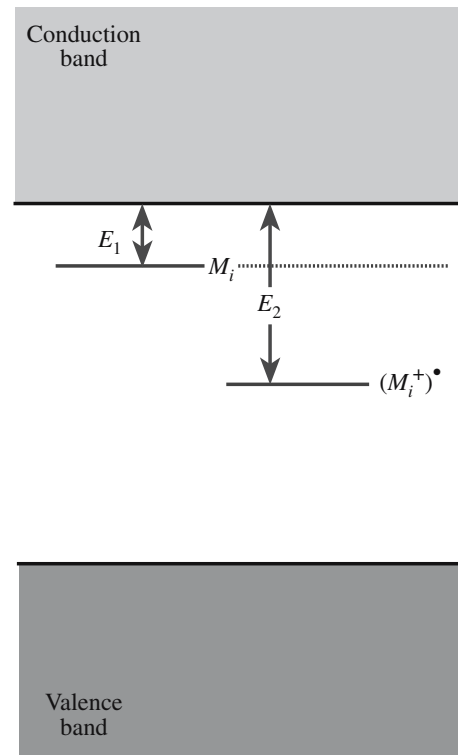
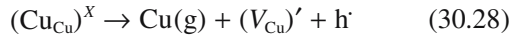


FIGURE 30.14 Schematic representation of the energy levels in Zn_{1+x}O .

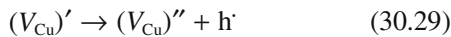
the first and second ionization energies for Zn. At low temperatures the electrons would not be excited into the conduction band and would be localized at the donor level. As the temperature rises, the fraction of electrons in the conduction band increases. At a sufficiently high temperature all the impurity atoms will be ionized.

Copper Oxide: A p-Type Semiconductor

If we start with stoichiometric Cu₂O and remove a copper atom to form a copper vacancy, the charge balance requires formation of a hole as shown using Kröger–Vink notation:



For a possible second ionization state



The above processes are shown on an energy band diagram in Figure 30.15.

We can also consider that a hole forms by the production of vacancies on the cation sublattice when $p\text{O}_2$ is increased. The overall reaction can be represented as

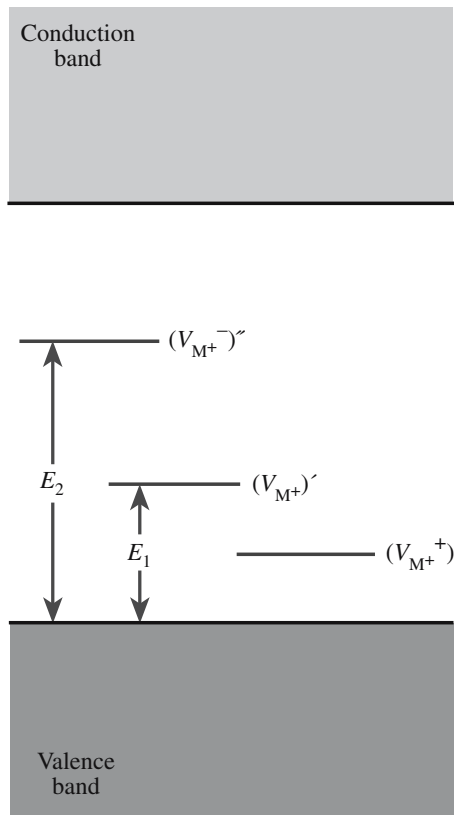
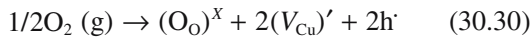


FIGURE 30.15 Schematic representation of energy levels in a deficit semiconductor such as Cu_{2-x}O.

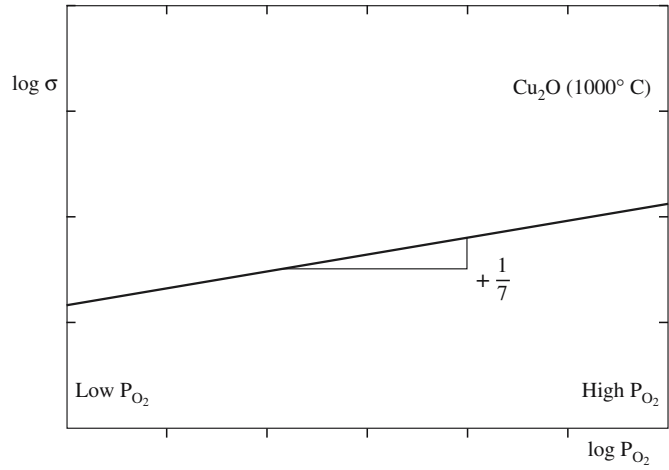


FIGURE 30.16 Conductivity of Cu₂O as a function of $p\text{O}_2$.

(You will recognize Eq. 30.30 as being similar to Eq. 11.8.)

Using the same approach that we used for ZnO we can obtain a relationship between $p\text{O}_2$ and σ :

$$\sigma \propto [\text{h}^{\cdot}] = K(T)^{1/4} p\text{O}_2^{1/8} \quad (30.31)$$

Experimentally, as illustrated in Figure 30.16, σ is found to be proportional to $p\text{O}_2^{1/7}$, which is in reasonable agreement with Eq. 30.31.

There are many examples of impurity semiconductors and a partial list is given in Table 30.5.

30.10 VARISTORS

A varistor is used in an electric circuit as protection against large voltage pulses, i.e., a surge protector. Such devices are particularly important in protecting micro-electronic devices. ZnO is the most widely used and important material for varistors.

Under normal operating conditions a small current will flow through the varistor. If the voltage rises above some threshold value (for example, the result of a voltage

TABLE 30.5 Partial List of Impurity Semiconductors

<i>n-Type</i>					
TiO ₂	Nb ₂ O ₅	CdS	Cs ₂ Se	BaTiO ₃	Hg ₂ S
V ₂ O ₅	MoO ₂	CdSe	BaO	PbCrO ₄	ZnF ₂
U ₃ O ₈	CdO	SnO ₂	Ta ₂ O ₅	Fe ₃ O ₄	
ZnO	Ag ₂ S	Cs ₂ S	WO ₃		
<i>p-Type</i>					
Ag ₂ O	CoO	Cu ₂ O	SnS	Bi ₂ Te ₃	MoO ₂
Cr ₂ O ₃	SnO	Cu ₂ S	Sb ₂ S ₃	Hg ₂ O	MnO
NiO	Pr ₂ O ₃	CuI			

spike in the power supply) a large current will flow through the varistor to ground before it can damage the circuit. To operate in this way a varistor must have a highly nonlinear I - V relationship, as shown in Figure 30.17.

- At low applied voltages the varistor behaves in an ohmic manner, i.e., there is a linear I - V relationship.
- When the applied voltage reaches a threshold value known as the breakdown voltage a large current flows, following a power law:

$$I \propto V^\alpha \quad (30.32)$$

The exponent α is used as a figure of merit for the varistor and can be as high as 70 for ZnO, although values in the range 25–45 are more typical. For SiC $\alpha \sim 5$.

A significant difference between a varistor and a diode is that varistors can be used in both ac and dc circuits. Compare the plot shown in Figure 30.17 with what would be seen for a Zener diode.

The microstructure of a ZnO varistor is the key to its operation. Grains of about 15–20 μm in diameter are separated by a Bi-rich intergranular film (IGF) that varies in thickness from 1 nm to 1 μm , as illustrated in Figure 14.38. Varistor action is a result of a depletion region formed on either side of the IGF. To explain varistor behavior we use an approach very similar to that used to describe Schottky barriers in metal–semiconductor junctions.

Figure 30.18a shows an energy level diagram for two ZnO grains separated by an IGF. The bismuth that segregates to the GB results in the formation of acceptor levels. The way that the bismuth dopants produce these sites is not well understood, but possibly they stabilize acceptor defects such as Zn vacancies at the GB. At equilibrium the Fermi levels on each side of the boundary must line up, as shown in Figure 30.18b. This requirement is necessary because at equilibrium the probability of occupation of any quantum level must be independent of position. When this occurs, the conduction and valence bands bend, resulting in an energy barrier (height $e\phi$) at the GB. Con-

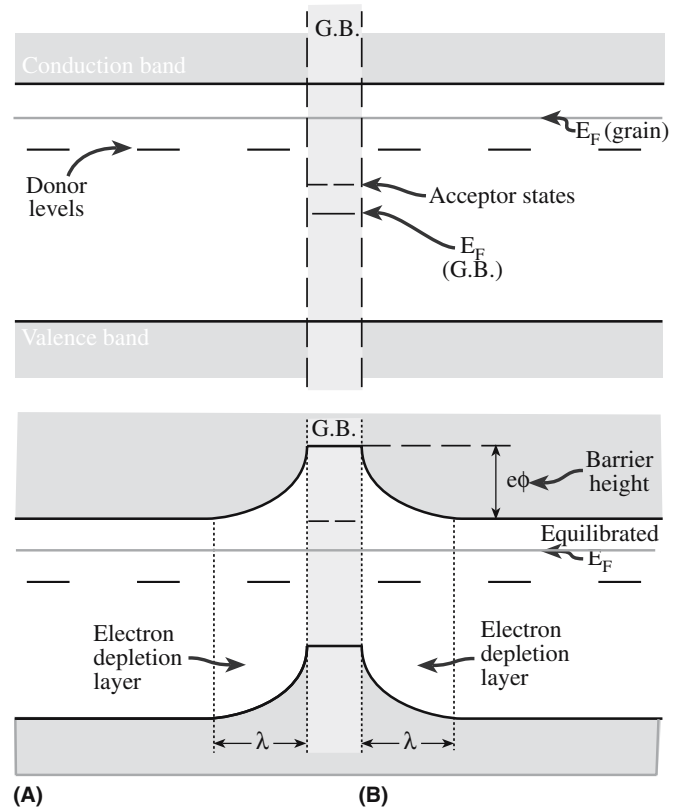


FIGURE 30.18 Proposed band diagram for two semiconducting ZnO grains separated by an IGF: (a) showing the location of acceptor sites in the IGF; (b) at equilibrium. Application of a potential decreases the barrier height.

duction band electrons must surmount this energy barrier for conduction to occur. When a potential is applied across the varistor the size of the energy barrier is reduced. Conduction is provided by thermal activation of electrons across the barrier (at low fields) or tunneling (high fields). At the breakdown voltage the energy barrier is zero and a massive increase in electrical conduction occurs.

Varistor breakdown is reversible and if the applied voltage is decreased below the breakdown value the varistor will return to ohmic behavior. The breakdown voltage is typically in the range of tens to hundreds of volts.

- Single-crystal silicon diodes (avalanche or Zener) are used only for low-voltage applications.
- ZnO varistors are used for both low- and high-voltage applications.

30.11 THERMISTORS

Thermally sensitive resistors (thermistors) have high TCRs produced by one of the following mechanisms:

1. Excitation across the band gap—intrinsic semiconductor behavior resulting in an exponential decrease in ρ over a wide temperature range (NTC).

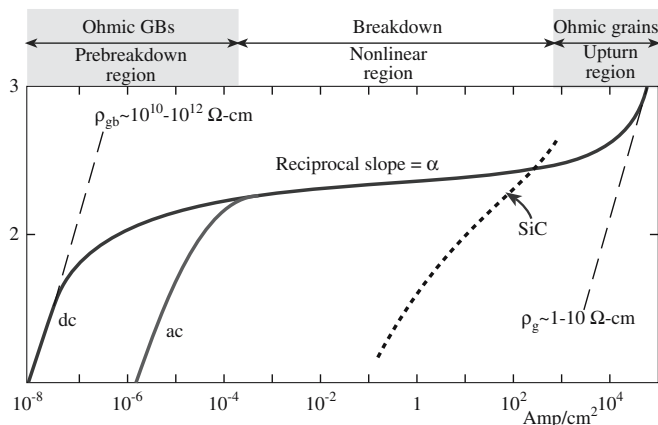


FIGURE 30.17 Typical I - V characteristic for a ZnO varistor.

2. A structural phase transformation causing a change from semiconducting behavior to metallic conduction, which causes a large decrease in ρ over a small temperature range (NTC).

3. A change in the conductivity of the GB, which produces a large increase in ρ over a small temperature range (PTC).

In semiconductors such as SiC where NTC behavior is expected ρ varies with T according to

$$\rho(T) = \rho_{\infty} \exp(B/T) \quad (30.33)$$

ρ_{∞} is approximately independent of temperature and B is a constant related to the energy required to excite the electrons into the conduction band. By differentiation we can obtain an expression for α :

$$\alpha_R = d\rho/\rho dT = -B/T^2 \quad (30.34)$$

α_R is usually expressed either as a percentage change in resistivity, e.g., $-3\% \text{ K}^{-1}$, or in terms of ppm changes per degree change in temperature, e.g., ppm/ $^{\circ}\text{C}$. Table 30.6 shows the properties of thermistors based on Mn_3O_4 with partial replacement of the Mn by Ni, Co, and Cu.

NTC materials are used in many applications to either sense temperature or to respond to changes in temperature. One application is temperature sensors to measure the temperature of the cooling water in an automobile engine.

The behavior of PTC materials is very different from NTC materials. Commercial PTC devices rely on the changes associated with the ferroelectric Curie temperature (θ_c). Typical PTC behavior is shown in Figure 30.19. In regions AB and CD the material is showing NTC behavior. But at the Curie temperature (θ_c) there is a large positive change in ρ .

Polycrystalline lanthanum-doped BaTiO_3 (BLT) is one example of a PTC material. The effect is associated with GBs and is not observed in single crystals. At the GB there is a potential barrier (ϕ) preventing electron movement from one grain to an adjacent one (very similar to that caused by the IGF in ZnO). The GB resistance, R_{gb} is

$$R_{gb} \propto \exp(\phi/kT) \quad (30.35)$$

TABLE 30.6 Properties of Thermistor Compositions Based on Mn_3O_4 at 25°C

Composition (cat.%)						
Mn	Co	Ni	Cu	$\rho_{25}/\Omega \cdot m$	B/K	$\alpha_R/\%K^{-1}$
56	8	16	20	10^{-1}	2580	-2.9
65	9	19	7	1	2000	-2.2
70	10	20		10	3600	-4.0
85		15		10^2	4250	-4.7
94		6		10^3	4600	-5.1

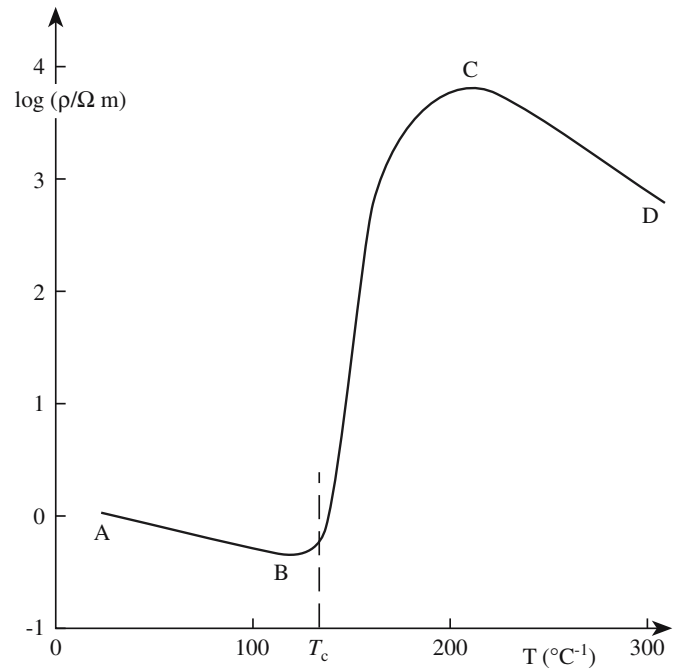


FIGURE 30.19 Typical characteristics of a PTC thermistor material.

Above θ_c

$$R_{gb} \propto \exp\left[N\left(1 - \frac{T_{cw}}{T}\right)\right] \quad (30.36)$$

where N is a temperature-independent constant for the particular material and includes specific details about the electronic structure of the grain boundary and T_{cw} is the Curie-Weiss temperature ($\sim\theta_c$).

30.12 WIDE-BAND-GAP SEMICONDUCTORS

Wide-band-gap semiconductors refer to materials that have a band gap between about 2 and 5 eV. At present one of the most interesting wide-band-gap semiconductors is SiC, which has an E_g from 2.4 to 5.1 eV. These materials are important because they can be used at much higher temperatures than Si or GaAs because the thermal generation of electron-hole pairs is much lower. SiC exists in a number of different polytypes each having different properties as shown in Tables 30.7 and 30.8.

TABLE 30.7 Summary of Band Structures for SiC Polytypes

	3C	6H	4H	2H
Direct band gap (eV)	5.14	4.4	4.6	4.46
Indirect band gap (eV)				
Experimental	2.39	3.0	3.26	3.35
Theory	2.4	2.4	2.8	3.35

TABLE 30.8 Summary of Properties for n-Type SiC ($N_D = 6 \times 10^{16} \text{ cm}^{-3}$) at Room Temperature

Polytype	Electron mobility ($\text{cm}^2 \text{ V}^{-1} \text{ s}^{-1}$)	E_D (meV)	m_{ii}^*/m_e	m_{e}^*/m_e
4H	700	33	0.19	0.21
15R	500	47	0.27	0.25
6H	330	95	1.39	0.35

30.13 ION CONDUCTION

Ion movement can make a major contribution to σ , particularly if the material has a large E_g . Conductivity resulting from ion migration is important in several ceramics. It is also the major conduction mechanism in ionic salts such as the halides.

When we describe the mobility of ions we often use the absolute mobility, B :

$$B = \frac{v}{F} = \frac{v}{zeE} \quad (30.37)$$

where v is the drift velocity and F is the applied force (which in this case is the electrical potential, i.e., $F = Zq\xi$, where Z is the charge on the ion.)

B is related to μ :

$$\mu = ZqB \quad (30.38)$$

Substituting Eq. 30.38 into Eq. 30.2 gives

$$\sigma = nZq^2B \quad (30.39)$$

The absolute mobility, and hence σ , is directly related to the diffusion coefficient, D , through the Nernst–Einstein equation:

$$D = kTB \quad (30.40)$$

The diffusion coefficient is given by an Arrhenius equation, which means that there is an activation energy that must be overcome for the ions to move through the material as illustrated in Figure 30.20. We can

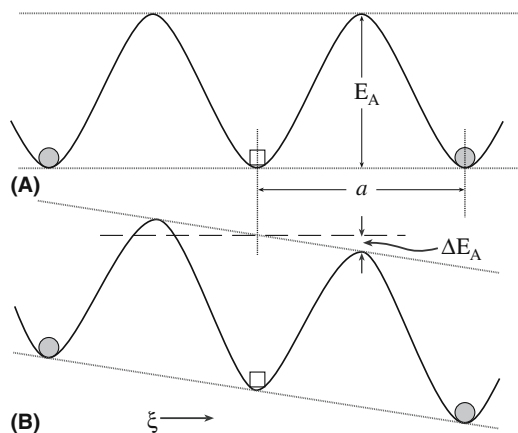


FIGURE 30.20 Potential energy barrier to ion movement. (a) In the absence of an applied field and (b) with an applied field. E_A is the activation energy and a the jump distance between ion sites.

then give σ in terms of D , which is what we did in Section 11.15:

$$\sigma = \frac{ne^2D}{kT} \quad (11.53)$$

The following factors contribute to ionic mobility:

- *Size.* It is easier to move a small ion than a large one.
- *Charge.* A highly charged ion will polarize, and be polarized by ions of opposite charge as it moves past them. This will increase E_A .
- *Lattice geometry.* Some structures contain channels that facilitate the ion movement. A large number of vacant sites can help.

30.14 FAST ION CONDUCTORS

Materials that show exceptionally high ionic conductivity are referred to as “fast ion” conductors or “superionic” conductors. The conductivities are comparable to those of electrolyte solutions, but are still low compared with metal-like electron conductivity. There are two important types of fast ion conductor:

1. The β -aluminas: nonstoichiometric aluminates, for example
 - $\text{Na}_2\text{O} \cdot 11\text{Al}_2\text{O}_3$ (β -alumina)
 - $\text{Na}_2\text{O} \cdot 8\text{Al}_2\text{O}_3$ (β' -alumina)
 - $\text{Na}_2\text{O} \cdot 5\text{Al}_2\text{O}_3$ (β'' -alumina)

They all have a layer structure, as illustrated earlier in Figure 7.12, that is composed of spinel blocks of close-packed O^{2-} ions with Al^{3+} in tetrahedral and octahedral interstices. Planes containing Na^+ and O^{2-} ions separate the spinel blocks. It is within these planes that the mobility of the Na^+ ions is high. The conductivity is highly anisotropic; it is high within the Na^+ -containing planes and negligible in the perpendicular direction.

2. Cubic stabilized zirconia stabilized usually with either CaO or Y_2O_3 .

These materials have oxygen ion transport numbers very close to 1.0. To understand how they are able to conduct large oxygen ions it is necessary to consider their defect structure. The correct composition of an oxide with the fluorite structure oxide would be MO_2 . The addition of CaO to ZrO_2 , for example, drops the metal-to-oxygen ratio below 2.0, and the formula of the oxide becomes $\text{Ca}_x\text{Zr}_{1-x}\text{O}_{2-x}$. As we showed in Section 11.7, the Ca^{2+} ions substitute for Zr^{4+} ions and we have compensating oxygen vacancies. For each substitutional Ca^{2+} , we must create one anion vacancy. The result of this enormous defect population is to greatly increase the diffusion coefficient for oxygen to the extent that this material becomes a very fast oxygen-ion conductor.

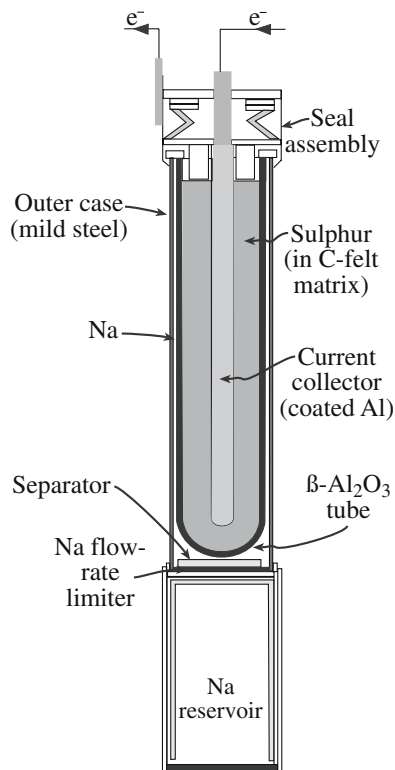


FIGURE 30.21 Schematic of a “central sulfur” cell. Typically, the electrolyte tube is some 300 mm long and 30 mm in diameter.

Stable ceramics that have completely ionic conductivity can be used as solid-state electrolytes. Two examples are the Na–S battery and the solid oxide fuel cell.

OTHER USES OF CERAMICS IN BATTERIES

- Hg battery—HgO is the cathode.
- Ni–Cd battery—hydrated NiO (NiOOH·H₂O) is the cathode.
- Li battery—MnO₂ is the cathode.

TABLE 30.9 Efficiency of Various Batteries

Type	Efficiency (Wh/kg)
Nickel–cadmium (Ni–Cd)	7–50
Nickel–metal hydride (Ni–H)	20–100
Sodium–sulfur	75–200

Figure 30.21. It is often convenient to place the S inside the β -alumina tube since the ceramic has far superior corrosion resistance to that of the mild steel outer casing. On connection to the external circuit the Na gives up electrons forming Na⁺ ions. These diffuse through the β -alumina to react with the S to produce the sulfide according to the reaction



The reverse reaction occurs on recharging. The cell runs at about 300°C with both Na and S in the liquid state. The cell reaction is extremely energetic, and the heat required to maintain the cell at its operating temperature is readily supplied by the cell reaction itself.

Despite being used by the Ford Motor Company in a series of test vehicles the disadvantages of the Na–S battery, not least of all its cost (~\$50,000 each), have limited its adoption for electric vehicle applications.

A different application proposed for Na–S batteries is for spacecraft. Since electrical power systems make up a major part of a spacecraft’s weight and batteries are typically the largest component of the power system, it is critical to improve the efficiency of spacecraft batteries.

Battery efficiency is measured in terms of specific energy, or watt-hours of energy output per kilogram of battery weight (Wh/kg), and values for several batteries are given in Table 30.9. In 1996 an Na–S battery was flight tested during a space shuttle mission. Although cost is not as much of an issue with spacecraft as it is with automobiles, there are still technological challenges in using Na–S batteries. One of these challenges is producing a suitable casing. Steel containers, even with protective coatings, can easily be dented or scratched, leading to corrosion and rapid failure.

30.15 BATTERIES

A battery operates on the principle of a Galvanic cell; a chemical reaction is used to produce electricity. The materials that are involved in the reaction form the electrodes and the reaction takes place by the passage of ions through an electrolyte. The formation of ions during the chemical reaction involves the transfer of electrons to or from the electrodes. In a galvanic cell these are not allowed to pass through the electrolyte but must travel around an external circuit, driven by a potential difference created between the electrodes. It is the electron movement through the external circuit that can be used to do work.

β -Alumina is used as an electrolyte in high-energy-density Na–S batteries. The concept of a battery based on the reaction of Na and S was first proposed in 1967 as an alternative to the conventional lead-acid battery. The Na and S are separated by a membrane of β -alumina, usually in the form of a closed-end thin-walled tube as shown in

30.16 FUEL CELLS

A fuel cell is another example of a galvanic cell and supplies electrical energy in the same way as a battery. The essential difference between the two types of cell is that the electrodes of a fuel cell do not deteriorate chemically. Therefore, if a fuel cell is fed a constant supply of fuel it

TABLE 30.10 Fuel Cells and Their Applications

Fuel cell	Electrolyte	Anode fuel	Cathode gas	Operating T(°C)	Applications
Alkaline fuel cell (AFC)	KOH solution	H ₂	O ₂	60–90	Spacecraft, submarines
Proton exchange membrane fuel cell (PEMFC)	Proton conductive polymer membrane	H ₂	O ₂ (in air)	60–90	Transportation vehicles, stationary power plants, cogeneration plants, portable power supplies
Direct methanol fuel cell (DMFC)	Proton conductive polymer membrane	Methanol	O ₂ (in air)	90–120	Transportation vehicles, stationary power plants, cogeneration plants, portable power supplies
Phosphoric acid fuel cell (PAFC)	Phosphoric acid	H ₂	O ₂ (in air)	200	Stationary power plants, cogeneration plants
Molten carbonate fuel cell (MCFC)	Molten alkaline carbonate	H ₂ , CH ₄ , or coal gas	O ₂ (in air)	650	Stationary power plants, cogeneration plants
Solid oxide fuel cell (SOFC)	Ceramic solid electrolyte	H ₂ , natural gas, coal gas	O ₂ (in air)	800–1000	Stationary power plants, cogeneration plants

will supply continuous electrical energy. The fuel is hydrogen or a hydrogen-rich source (e.g., methanol or formic acid).

The first practical fuel cell was developed in the 1950s at Cambridge University in the UK. The cell used Ni electrodes and an alkaline electrolyte. Pratt and Whitney further modified the alkaline fuel cell as it was called in the 1960s for NASA’s Apollo program. The cells were used to provide on board electrical power and drinking water for the astronauts. The alkaline fuel cell proved successful, but it was an order of magnitude too expensive for terrestrial applications and demanded pure hydrogen and oxygen to operate.

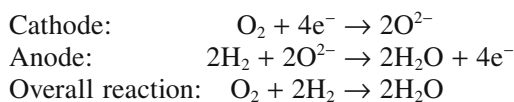
Table 30.10 lists the different types of fuel cell that are being investigated together with some of their potential applications. Fuel cells are one of the leading research topics at the present time with the goal of reducing the dependence on fossil fuels and associated problems of global warming.

There are two types of fuel cell that use ceramics:

- Molten carbonate fuel cell (MCFC)
- Solid-oxide fuel cell (SOFC)

The main difference between the two types is in the electrolyte. The MCFC uses a molten carbonate immobilized in a porous LiAlO₂ matrix. The SOFC uses a ceramic membrane of cubic stabilized zirconia. An illustration of the operation of a SOFC is shown in Figure 30.22.

The cell reactions are



A single fuel cell supplies a dc voltage of <1 V. If larger voltages are required the cells must be stacked

together in series. Commercially voltages up to ~200 V can be attained. The current produced is proportional to the area over which the reaction occurs. The best fuel cells at present provide a maximum current density of 0.5–2 A/cm².

MCFCs and SOFCs can be made by assembling individual plate cells into stacks, just like the design of the original voltaic pile. For SOFCs producing 5–200 kW ceramic plates from 150 mm to 300 mm square are required. This requirement presents a problem because it is difficult to produce large thin flat dense plates of ceramics. Siemens-Westinghouse developed an alternative tubular design; it is straightforward to extrude long tubes (see Section 23.9). The disadvantage of the tube design

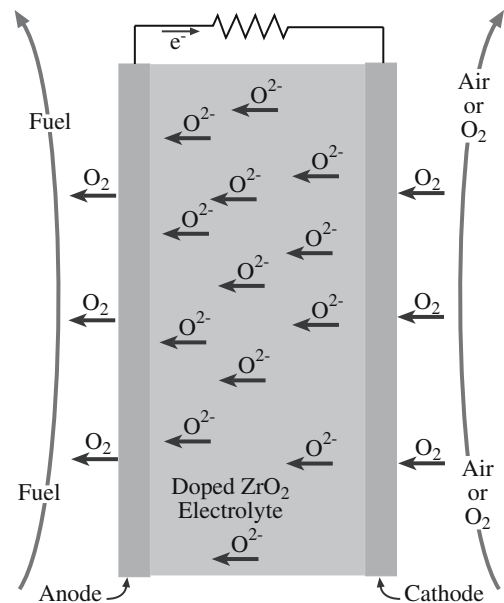


FIGURE 30.22 Simple representation of an SOFC using cubic zirconia.

is that it has high thermal inertia and a long warming time.

Fuel cells offer significant advantages over many other power sources. They are

- Silent
- Low maintenance
- Efficient (they are not limited to the Carnot efficiency—i.e., the maximum theoretical efficiency that can be obtained from an engine employing combustion)
- Nonpolluting (the product is distilled water)

These advantages are the reasons for the continued research efforts. However, we still do not know whether fuel cell technology can be made commercially viable (at the present time it is not).

A principle similar to that used in the SOFC can be applied to oxygen sensors for applications including monitoring of automobile exhaust emissions to increase engine efficiency and reduce emissions. Figure 11.17 can be compared to Figure 30.22 to see the similarities. Oxygen control is also important in several metallurgical processes such as gas carburizing and the bright annealing of stainless steel.

30.17 CERAMIC INSULATORS

More typically we think of ceramics as being good electrical insulators and there are many ceramics that have $\rho > 10^{14} \Omega \cdot \text{cm}$. Examples of common ceramic insulators include

- Aluminum oxide (Al_2O_3)
- Mullite ($3\text{Al}_2\text{O}_3 \cdot 2\text{SiO}_2$)
- Forsterite ($2\text{MgO} \cdot \text{SiO}_2$)
- Beryllium oxide (BeO)
- Aluminum nitride (AlN)

In an electrical insulator there is a wide energy gap between the bottom of the conduction band and the top of the valence band. Figure 30.23 shows the energy band diagram for MgO. The valence band is formed by the 2p energy levels of oxygen (O^{2-} ions) and the conduction band is formed from the empty 3s orbitals of the Mg^{2+} ions. The energy band gap is $\sim 8\text{eV}$ and the concentration of thermally excited electrons in the conduction band of MgO is low right up to its melting point, 2800°C . MgO is therefore an excellent high temperature insulator.

Very wide energy band gaps ($>6\text{eV}$) are associated with compounds that have high fractions of ionic character in their bonding. Ions have a stable noble gas electron configuration. To excite an electron from the valence band to the conduction band involves making the electron configuration of the ions different from those of the noble gases. This process is energetically unfavorable.

In general, compounds with wide band gaps have

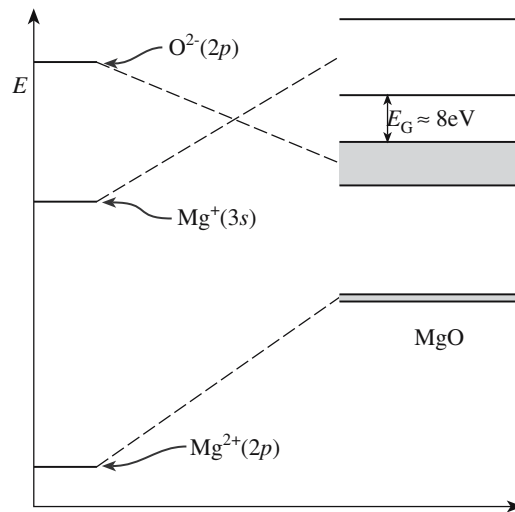


FIGURE 30.23 Energy band diagram for MgO.

- Predominantly ionic bonding
- Consist of atoms (ions) of low Z

Some ceramics having large values of E_g are listed in Table 30.3. No entirely satisfactory relationship has been established between the ionic character of the bond and the atom size on E_g . In a homologous series of oxides, such as the oxides of the alkaline-earth metals, E_g increases with increasing ionic potential, ϕ , of the cation as shown in Figure 30.24.

In a series of isoelectronic compounds (i.e., compounds with an identical total number of electrons) E_g increases

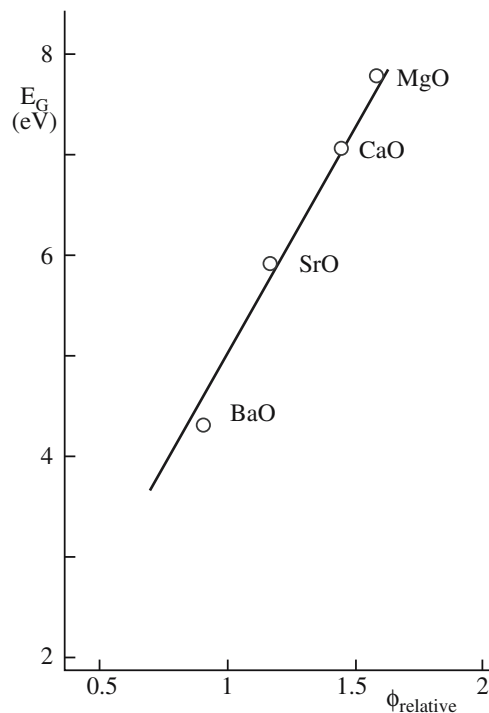


FIGURE 30.24 Effect of bond ionicity on E_g for metal oxides MO ($\phi = Z/r$).

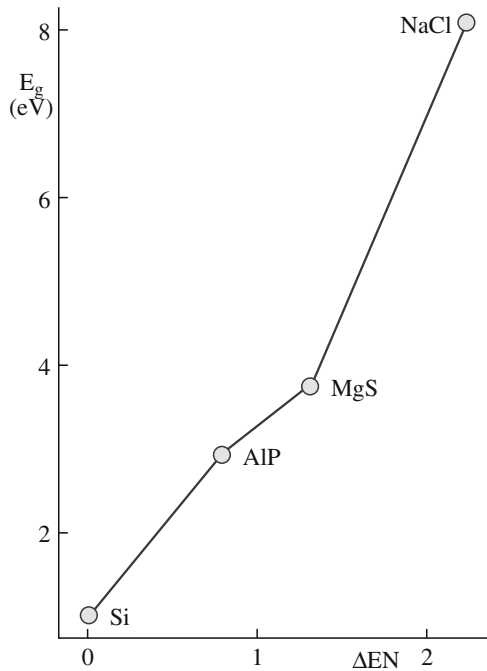


FIGURE 30.25 Correlation of E_g and electronegativity difference (ΔEN).

with the increasing ionic character of the interatomic bond as shown in Figure 30.25. Understanding this relationship is quite straightforward. As the fraction of covalent character in a bond increases the electrons in that bond are more equally shared and hence electron transfer becomes easier.

The presence of point defects in the lattice can be viewed as being donor or acceptor species in the same way that we considered defects in semiconductor crystals. Figure 30.26 shows another version of an energy band

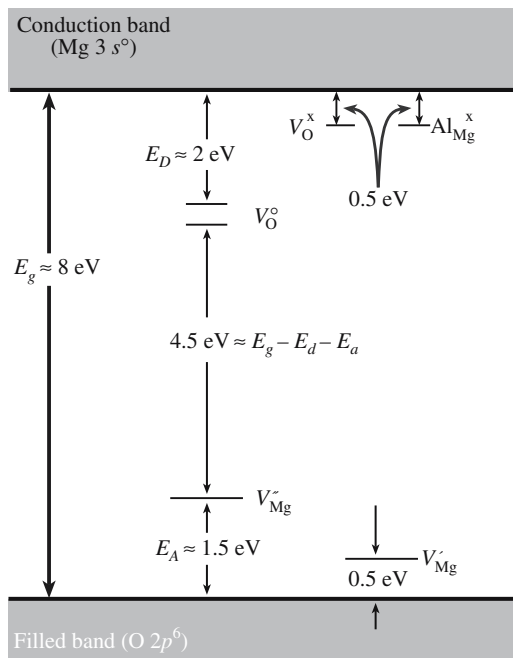


FIGURE 30.26 Defect levels in MgO.

diagram for MgO, this time with the estimated defect energy levels included. If the crystal contains oxygen vacancies (i.e., it has been reduced) these can become ionized:



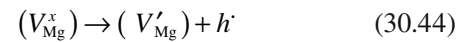
You will notice that Kröger–Vink notation is useful for describing this process. The energy for ionization is 0.5 eV and can be represented as a level just below the bottom of the conduction band—the oxygen vacancy is behaving as a donor.

The oxygen vacancy can become doubly ionized:

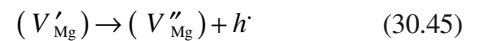


The energy for this second ionization process is ~2 eV and can be represented as another donor level.

In a similar way we can represent acceptor sites within the band diagram for MgO as being due to the oxidation of MgO, i.e., the introduction of magnesium vacancies and corresponding holes. The following reactions show the origin of the acceptor levels:

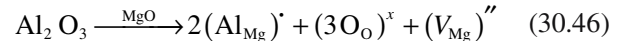


and

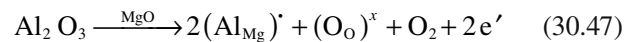


The energies for these two processes are 0.5 eV and ~1.5 eV, respectively. Even though these ionization energies are relatively small compared to the band gap, the concentration of these defects is extremely low. Even at temperatures >2000°C the number of cation and anion vacancies in MgO is only about one per billion lattice sites.

The addition of substitutional and interstitial point defects can also introduce additional energy levels. Using MgO as our example let us consider the incorporation of Al_2O_3 . There are two defect reactions we can envision:



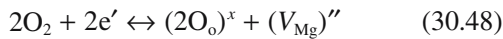
and



In Eq. 30.46 the incorporation of Al into Mg sites is compensated for by the formation of a magnesium vacancy. This type of incorporation is termed ionically compensated because an ionic defect has compensated for the charge difference. The second reaction, given by Eq. 30.47, is electronically compensated because electrons (or in some cases holes) are compensating for the charge difference resulting from the substitution of a divalent cation

for a trivalent one. Acceptor levels are introduced by ionic compensation, and electronic compensation corresponds to the introduction of donor levels in the energy gap.

Combining Eqs. 30.46 and 30.47 we can write



Stoichiometric oxides such as MgO are very difficult to reduce and hence the reaction represented by Eq. 30.48 is strongly to the right throughout all accessible ranges of temperature and oxygen activity. Even highly doped compositions are not electrically conductive at room temperature. The defects with a positive effective charge are donors; these have given up an electron to become ionized positively relative to the perfect lattice. Correspondingly, defects with a negative effective charge are acceptors, having accepted electrons relative to the perfect lattice.

Dislocations are defects that also create additional energy levels within the band gap. They act as acceptors as shown in Figure 30.27. Note that the dislocation-acceptor levels are usually in the upper half of the band gap. Dislocations are particularly deleterious to the behavior of semiconductors. One of the main factors that limited the increase in the size of silicon wafers has been the need to grow dislocation-free single crystals. At the beginning of the semiconductor industry in the 1960s wafer sizes were limited to 2-inch-diameter wafers; now 18-inch-diameter wafers are possible because of better control of the growth parameters.

To understand why dislocations act as acceptors consider the illustration of a dislocation in silicon shown in Figure 12.11. The dislocation creates dangling bonds, which act as electron traps to satisfy the requirement of each silicon atom to achieve a noble gas electron configuration.

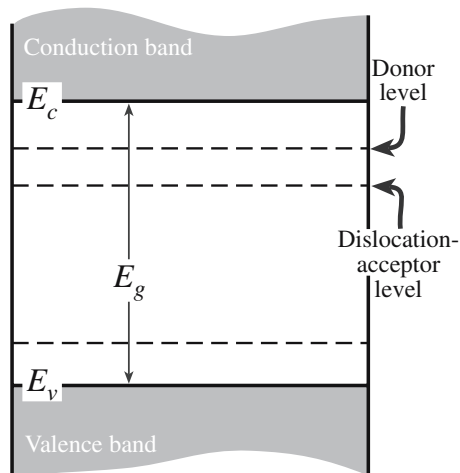


FIGURE 30.27 Effect of dislocations on the energy band diagram of a semiconductor.

CHARGE BALANCE

Reminder: Reactions expressed using Kröger–Vink notation must be charged balanced, just like regular chemical reaction equations.

Ceramics with high ρ are important for a number of applications, many of which utilize more than just the high ρ . Other properties such as high strength, stability at elevated temperature, high thermal conductivity, and hermeticity (impervious to the environment) are also important.

One application that you may be familiar with is the use of alumina ceramics as the insulator in spark plugs. The insulator must be able to withstand a peak voltage of about 10kV at each spark discharge, a pressure pulse of about 10MPa, and the thermal radiation from the combustion temperature that is typically 2000°C. This combination of requirements can be met only by a ceramic.

A very visible application of ceramic insulators is as power line insulators. For this application the strength of the ceramic is very important because the insulator supports a considerable weight. The insulator must also be resistant to weather damage and to absorption of water, which can lead to arcing. One ceramic used for this application is porcelain. A typical porcelain composition would lie in the following ranges: clays [e.g., kaolinite $Al_2(Si_2O_5)(OH)_4$], 40–60 wt%, flux [e.g., orthoclase $(KAlSi_3O_8)$], 15–25 wt%, and quartz or bauxite filler, 30–40 wt%. The porcelain is known as a “silicious porcelain” if quartz is used as the filler and an “aluminous porcelain” if bauxite is used.

The above applications are visible uses for ceramic insulators. The two applications that we are going to emphasize next may not be ones that immediately come to mind when you think of ceramic insulators, but they are extremely important and, in fact, the development of personal computers and other electronic devices owes much to the use of insulating ceramics.

30.18 SUBSTRATES AND PACKAGES FOR INTEGRATED CIRCUITS

Substrates and packages for integrated circuits (ICs) constitute the largest application for ceramic insulators. The following properties are required:

- High ρ
- High thermal conduction
- Low dielectric constant
- Hermetic

Three ceramics are usually used for this application:

- Al_2O_3
- BeO
- AlN

Alumina ceramics dominate, but there are important reasons why BeO and AlN are used in certain applications. Table 30.11 compares the properties of these three

TABLE 30.11 Physical Properties of Substrate Materials

Property	96%Al ₂ O ₃	99.5% Al ₂ O ₃	BeO	AlN	Mullite	Glass-ceramics
Density (g/cm ³)	3.75	3.90	2.85	3.25	2.82	2.5–2.8
Flexural strength (MPa)	400	552	207	345	186	138
Thermal expansion from 25 to 500°C (ppm/°C)	7.4	7.5	7.5	4.4	3.7	3.0–4.5
Thermal conductivity at 20°C (W m ⁻¹ K ⁻¹)	26	35	260	140–220	4	4–5
Dielectric constant at 1 MHz	9.5	9.9	6.7	8.8	5.4	4–8
Dielectric loss at 1 MHz (tan δ)	0.0004	0.0002	0.0003	0.001–0.0002	0.003	>0.002

ceramics and some others that have also been used as substrates and packages. BeO and AlN are used in situations in which high thermal conductivity is needed. Heat removal from power electronics and from integrated circuits is determined mainly through the substrate; one factor that influences the heat transfer rate is the thermal conductivity of the substrate material. Effective thermal management is important in improving the reliability of electronic devices.

AlN has a theoretical thermal conductivity of 320 W m⁻¹ K⁻¹ and values as high as 285 W m⁻¹ K⁻¹ have been experimentally measured for single crystals. Commercial AlN substrates are available with a thermal conductivity up to about 200 W m⁻¹ K⁻¹ at room temperature. The thermal expansion of AlN (3.9 × 10⁻⁶ K⁻¹) from room temperature to 500K is very similar to that of silicon (3 × 10⁻⁶ K⁻¹) over the same temperature interval, which helps to avoid cracking due to thermal misfit stresses between substrate and device. This consideration is particularly important for large silicon chips. AlN also does not have the inherent toxicity problems associated with BeO.

30.19 INSULATING LAYERS IN INTEGRATED CIRCUITS

Layers of SiO₂ have several uses in the production of silicon ICs:

- Device isolation
- Isolation of multilevel metallization
- Surface passivation
- The gate oxide in metal–oxide–semiconductor (MOS) structures
- Barrier layer during dopant incorporation.

SiO₂ layers can be obtained by direct oxidation by one of the following reactions:

Dry oxidation:



Wet oxidation:



Dry oxidation is slow, but produces a uniform relatively defect-free layer that is electrically very reliable. Wet oxidation is more frequently used for masking operations because the growth rate is faster, however, the layers are not as uniform as those produced by dry oxidation.

The oxide layer formed on the silicon surface is what is known as a protective oxide. The growth rate initially follows a linear rate law, i.e., the oxide thickness, *x*, increases linearly with time, *t*

$$x \propto t \quad (30.51)$$

For the two processes the activation energies are

$$E_A = 1.96 \text{ eV for wet oxidation}$$

$$E_A = 2.0 \text{ eV for dry oxidation}$$

These values are close to the energy required to break the Si–Si bond, 1.83 eV.

After a layer of approximately 100 nm has formed the growth kinetics follow a parabolic rate law, i.e., the oxide thickness increases with the square root of time:

$$x \propto \sqrt{t} \quad (30.52)$$

Diffusion through the oxide layer follows an Arrhenius law (Eq. 3.13):

$$E_A = 1.24 \text{ eV for dry oxidation}$$

$$E_A = 0.71 \text{ eV for wet oxidation}$$

These activation energies are close to those for the diffusivity of oxygen and water vapor through fused silica, respectively. Fused silica has a structure very similar to that of thermal SiO₂.

When very thin SiO₂ layers are required such as a gate oxide in an MOS-field effect transistor (MOSFET) or when an SiO₂ layer is required as an insulating layer between layers in a multilevel device the CVD process is used. The dielectric is an active component of the storage capacitor in dynamic RAMs, and its thickness determines the amount of charge that can be stored (see Chapter 31).

In a complementary metal-oxide semiconductor (CMOS) device oxidation of polysilicon is necessary for electrical isolation. A thermal oxide can be produced on polysilicon in a manner similar to that produced on single crystal silicon.

30.20 SUPERCONDUCTIVITY

There are two properties that a material must possess to be considered a superconductor:

1. $\rho = 0$
2. $B = 0$ (described in Chapter 33)

Zero resistivity is observed in a superconductor at all temperatures below a critical temperature, T_c , as illustrated in Figure 30.28. At T_c the material changes from a state of normal conduction to the superconducting state. In the superconducting state an induced current will flow indefinitely: without loss. This behavior has been demonstrated experimentally when a current has been run through a closed ring of a superconducting metal for over two and a half years without any measurable decay.

Superconductivity has been observed in *all* the classes of materials: metals, ceramics, and polymers. Of all the elements in the periodic table only 27 are known to become superconducting under ordinary pressure. Niobium is the element with the highest T_c , 9.2 K, whereas for tungsten T_c is only 0.0154 K. An interesting fact is that metals having the highest σ , e.g., Cu, Ag, and Au, are not superconducting even at extremely low temperatures, if at all. It is the metals that are the poorer electrical conductors that make

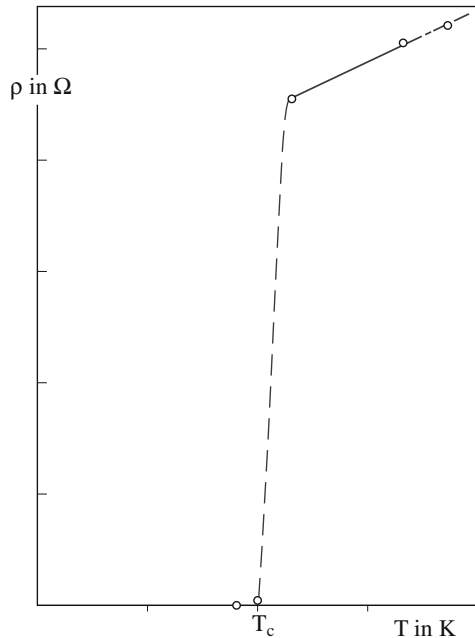


FIGURE 30.28 Plot of ρ versus T for a superconductor.

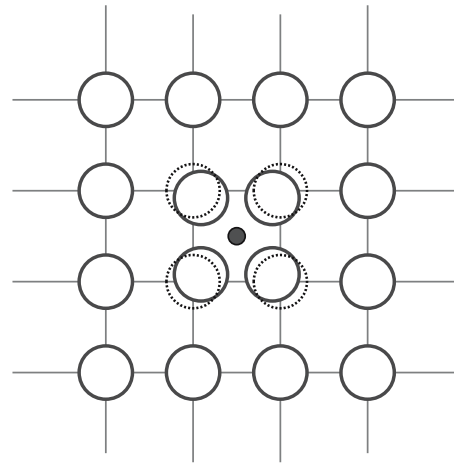


FIGURE 30.29 Illustration of lattice distortion around a free electron, which leads to the formation of Cooper pairs.

the better superconductors, albeit still at very low temperatures. Low-temperature superconductors (LTSC) have a T_c up to about 20 K. High-temperature superconductors (HTSC) are usually defined as having a T_c above the boiling temperature of liquid nitrogen.

The BCS theory (after Bardeen, Cooper, and Schrieffer) provides an explanation for superconductivity at low temperatures. The theory is complicated, but the basis is that there exists an attractive force between electrons that have about the same energy. This force causes them, under the right circumstances, to move in pairs. These are the so-called Cooper pairs. The criterion for superconductivity is that this attraction should be greater than the natural repulsion between like charges. T_c corresponds to the binding energy needed to hold the Cooper pairs together in a superconducting state.

The origin of the attractive force is that in a lattice of positive ions, an electron will attract the positive ions toward itself. In this region the lattice will be slightly denser as shown in Figure 30.29. To a passing electron the local lattice distortion will appear as an increase in positive charge density and it will be attracted toward it. The two electrons pair up in this way through their interaction with the lattice.

If the lattice is vibrating through thermal effects pairing will not be possible, but at very low temperatures where the vibration amplitude is small, the attractive force can be dominant. The electrons are held together by a binding energy of only about 10^{-4} eV. The separation of the electrons in the pair (called the coherence length) for most LTSC is 100 nm. Interatomic spacings are on the order of 0.3 nm, so two bound electrons can be as far apart as 300 lattice spaces. The large coherence length means that defects such as dislocations, GBs, and impurities are too small to have much effect on superconducting behavior.

The existence of these bound electron pairs alters the energy band diagram for a superconductor by introducing

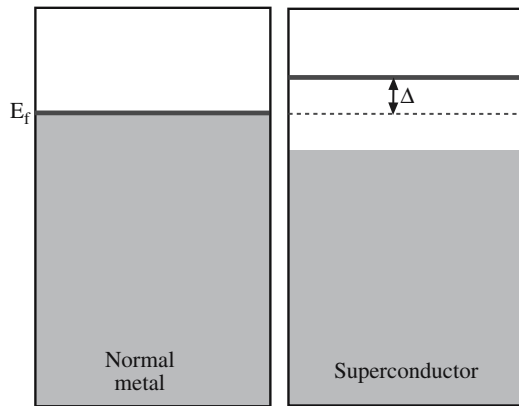


FIGURE 30.30 Band diagram for a superconductor.

a small gap at E_F , known as the superconducting gap, Δ . The difference in the band structure of a material in the superconducting state and in the nonsuperconducting state is illustrated in Figure 30.30. The energy of this gap corresponds to the binding energy of the electron pairs. An energy 2Δ is needed to break a Cooper pair. The relationship between Δ and T_c is given by the BCS theory:

$$2\Delta = 3.5kT_c \quad (30.53)$$

- For LTSC $\Delta \sim 1$ meV
- For HTSC $\Delta \sim 1$ –10 meV

The BCS theory predicts an ultimate limiting value of T_c of 30 K for electron pairing via lattice vibrations (phonons). This limit was enough to stop many researchers from pursuing careers in superconductivity. But clearly the BCS theory, in its entirety, cannot be applicable to HTSC where $T_c \gg 30$ K. In these materials pairing of the electrons still occurs, but the mechanism that allows this pairing needs to be determined.

30.21 CERAMIC SUPERCONDUCTORS

The earliest nonmetallic superconductors were NbO and NbN. Both materials have a rocksalt crystal structure. What was significant about the discovery of superconductivity in these materials (they are of no practical use) is that they linked the phenomenon to ceramics and cubic crystal structures.

Superconductivity in a multicomponent oxide was first observed in SrTiO₃. Although T_c was determined to be only 0.3 K, SrTiO₃ has the very important perovskite struc-

TABLE 30.12 Critical Temperatures of Some Ceramic Superconductors

Compound	T_c (K)
$\text{La}_{2-x}\text{M}_x\text{CuO}_{4-y}$ M = Ba, Sr, Ca $x \sim 0.15$, y small	38
$\text{Nd}_{2-x}\text{Ce}_x\text{CuO}_{4-y}$ (electron doped)	30
$\text{Ba}_{1-x}\text{K}_x\text{BiO}_3$ (isotropic, cubic)	30
$\text{Pb}_2\text{Sr}_2\text{Y}_{1-x}\text{Ca}_x\text{Cu}_3\text{O}_8$	70
$\text{R}_1\text{Ba}_2\text{Cu}_{2+m}\text{O}_{6+m}$ R: Y, La, Nd, Sm, Eu, Ho, Er, Tm, Lu	
$m = 1$ (123)	92
$m = 1.5$ (247)	95
$m = 2$ (124)	82
$\text{Bi}_2\text{Sr}_2\text{Ca}_{n-1}\text{Cu}_n\text{O}_{2n+4}$	
$n = 1$ (2201)	~10
$n = 2$ (2212)	85
$n = 3$ (2223)	110
$\text{Tl}_2\text{Ba}_2\text{Ca}_{n-1}\text{Cu}_n\text{O}_{2n+4}$	
$n = 1$ (2201)	85
$n = 2$ (2212)	105
$n = 3$ (2223)	125

ture, which, as shown in Chapter 7, is the structural building block of all presently known HTSC.

The beginning of HTSC started in 1986 with the discovery of superconductivity in the compound $\text{La}_2\text{BaCuO}_4$, which has $T_c \sim 38$ K. This discovery was of monumental importance because the classic BCS theory for superconductivity predicted a maximum value of T_c of only 30 K!

Many more HTSC were simply obtained by systematic substitution of elements into the basic perovskite unit. Certainly in the early days many scientists said that research in HTSC was more akin to cooking than any area of science!

The elements yttrium and lanthanum are interchangeable in terms of chemical properties (they are in the same group in the periodic table) although they differ in size. The same is true of strontium and barium in Group II of the periodic table. The idea behind the substitution of the large element for a smaller element was based on observations that T_c could be raised under an applied pressure. Substitution of a larger element for a smaller one was thought to produce an internalized pressure effect. Table 30.12 lists some of these compounds and their T_c .

Tables 30.13 compares properties of HTSC and LTSC; v_F is the velocity of propagation of conduction electrons through crystal.

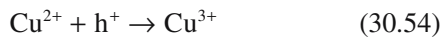
TABLE 30.13 Comparison of Superconductors in the Normal State

Material	Number of conduction electrons (n) (electrons/cm ³)	Fermi velocity (v _F) (m/s)	Mean free path (λ _e) (nm)	ρ (@ 100K) (μΩ·cm)	χ (nm)
Al	180 × 10 ²¹	2.0 × 10 ⁶	130	0.3	1600
Nb	56 × 10 ²¹	1.4 × 10 ⁶	29	3	38
LSCO	5 × 10 ²¹	0.1 × 10 ⁶	~5	~100	~1.5
YBCO	7 × 10 ²¹	0.1 × 10 ⁶	~10	~60	~1.0

- The obvious difference is T_c . The fact that $T_c \sim 10^2$ K means that the binding energy is ~ 10 meV, as compared to < 1 meV in LTSC.
- The ceramics have higher ρ than the metals at 100 K. But ρ is comparable to some of the best ceramic electrical conductors, such as CrO₂ and TiO.
- For HTSC χ is only ~ 1.0 nm, which means that the pairing behavior is almost on an atomic scale and the superconducting properties will be dependent on atomic scale defects. (Compare χ with the width of a dislocation or GB.) Such defects therefore scatter the electron pairs and reduce the critical current density. For metals χ is large, e.g., $\chi = 1.6 \mu\text{m}$ in pure Al, $\chi = 38$ nm in pure Nb.
- χ is anisotropic. For YBCO $\chi_{ab} \sim 1.5$ nm and $\chi_c \sim 0.4$ nm. A major problem in HTSC is to find a crystal defect that pins the flux vortices, but does not disrupt current flow.

We showed the structures of HTSC in Chapter 7. Superconductivity essentially takes place within the CuO₂ planes. The Cu–O chains can be considered as a “charge-reservoir” that is needed to transfer charge into the CuO₂ planes. Charge carriers are added by doping: adding oxygen to YBa₂Cu₃O₆, which enters the compound as O²⁻ and forms Cu–O chains. To maintain charge balance, electrons are removed from the Cu–O planes and the remaining holes are mobile (hence conduction) and form Cooper pairs below T_c .

In LTSC Cooper pairs, with a charge of $-2e$, are responsible for current flow. In most of the HTSC the Cooper pairs have a positive charge, $+2e$. In other words they are positive holes and the charge transfer process can be written as



One of the consequences of a hole-hopping process involving a two-dimensional array of copper ions is that the superconducting current is very anisotropic. Hopping tends to occur between copper ions that have the smallest separation from each other, namely those in the plane. The distance between copper ions on adjacent planes is much

larger than within the planes; hence charge hopping between planes is much less efficient.

There are many potential applications for HTSC, but the actual realization of these has in many cases not occurred. The major problem is being able to fabricate the ceramics into useful and usable shapes. Ceramics are inherently brittle and this alone makes the fabrication of long wires and tapes extremely difficult. These would be essential for domestic and industrial power transmission (some limited progress has been made in this area as we describe in Chapter 37). The low χ also makes practical applications more difficult to achieve because we have to be concerned about defects.

The most likely route to widespread practical application is to use the HTSC in the form of a thin film and utilize the Josephson effect. The original observation of this effect was made using a junction consisting of two superconductors separated by a very thin insulating layer (~ 1 nm). In thin films the “insulating” region can be orientation changes across a GB as shown in Figure 14.37.

The I – V characteristics of a Josephson junction are very nonlinear as shown in Figure 30.31. The key features are as follows:

- When $V = 0$, a direct current flows.
- When a small voltage is applied $I = 0$.
- At V_c the electrons are no longer paired and normal electron tunneling occurs with associated resistive losses.

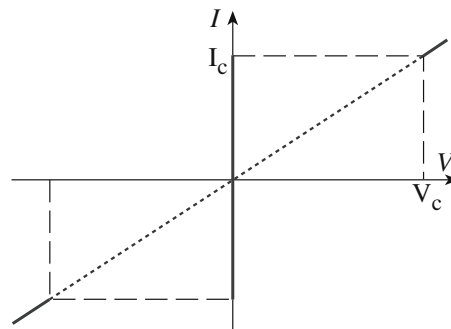


FIGURE 30.31 I – V characteristics of a Josephson junction.

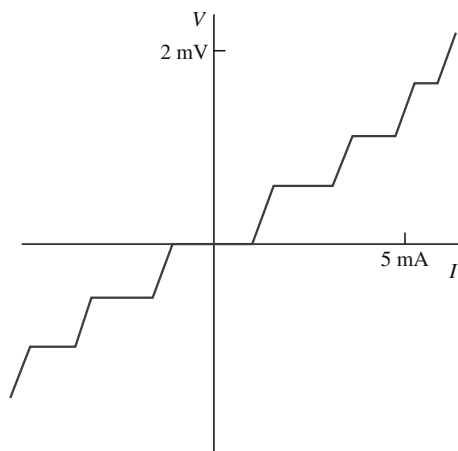


FIGURE 30.32 Effect of incident microwave radiation on the I – V characteristics of a Josephson junction.

If a Josephson junction is irradiated with microwaves of frequency f , the I – V behavior shows a series of steps, called Shapiro steps, as shown in Figure 30.32. These steps correspond to supercurrents across the junction when the condition for the absorption of microwave photons is satisfied (this is called the ac Josephson effect). Similar behavior is seen when we expose the junction to a magnetic field. How Josephson junctions can be used to detect very small magnetic fields is described in Chapter 33.

CHAPTER SUMMARY

We can explain the wide range of electrical properties shown by ceramics by considering their electron band structure. Some oxides show metallic-like levels of conductivity consistent with either a partially filled valence band or a small E_g . These materials are used as electrodes and conductors. Most ceramics fall into the category of having a medium to wide E_g . Semiconducting ceramics are used in a variety of sensors. The most important application is to “sense” anomalous voltages. As with the more familiar Si and GaAs, which are also ceramics, the conductivity of all semiconductors can be changed by doping. Unlike Si and GaAs we can use stoichiometry changes to modify σ . Ceramics having the largest E_g usually show a significant degree of ionic bonding and any conductivity is mainly associated with ion transport. The important technological example is cubic ZrO_2 , which is the electrolyte in solid oxide fuel cells. Fuel cells are one of the key components of a “hydrogen economy.” We finished this chapter with superconductors. The structure of these materials is already familiar from Chapter 7 and the importance of GBs as weak links from Chapter 14.

PEOPLE IN HISTORY

Bardeen, John (1908–1991) received the 1972 Nobel Prize in physics with Cooper and Schrieffer for the BCS theory. It was his second Nobel Prize! He won his first in 1956 for his role in the invention of the transistor.

Cooper, Leon Neil (1930–) received the Nobel Prize in physics with Bardeen and Schrieffer for the BCS theory. Cooper pairs are named after him.

Drude, Paul Karl Ludwig (1863–1906) was a German physicist who developed a theory for electron conduction. Drude’s theory provided an atomistic basis for understanding electron motion in metals and ceramics. In its original version it contained several inaccuracies, which were corrected by the application of quantum mechanics.

Grove, Sir William Robert (1811–1896) was a British scientist who in 1839 discovered the principle on which fuel cells are based. His cell, which was composed of two Pt electrodes both half immersed in dilute H_2SO_4 , one electrode fed with O_2 and the other with H_2 , was not a practical method for energy production.

Onnes, Heike Kamerlingh (1853–1926) was a Dutch physicist who succeeded in liquefying helium in 1908 and discovered superconductivity in mercury in 1911. He wrote at the time: *Mercury has passed into a new state, which on account of its extraordinary electrical properties may be called the superconducting state.* He received the Nobel Prize in physics in 1913.

Schrieffer, John Robert (1931–) received the Nobel Prize in physics with Bardeen and Cooper for the BCS theory.

GENERAL REFERENCES

Cox, P.A. (1987) *The Electronic Structure and Chemistry of Solids*, Oxford University Press, Oxford. A very good description of electronic properties.

- Cyrot, M. and Pavuna, D. (1992) *Introduction to Superconductivity and High-Tc Materials*, World Scientific, Singapore. A clear introduction to the field. Treats the theoretical models at a level above that used here but within the range of most upper division MSE undergraduates and graduate students.
- Duffy, J.A. (1990) *Bonding, Energy Levels and Bands in Inorganic Solids*, Longman Scientific and Technical, Harlow, Essex, UK. Straightforward description of energy bands in solids.
- Hench, L.L. and West, J.K. (1990) *Principles of Electronic Ceramics*, Wiley, New York. Comprehensive background to electronic ceramics.
- Moulson, A.J. and Herbert, J.M. (1992) *Electroceramics*, Chapman & Hall, London. An excellent account of the properties and applications of electroceramics.
- Owens, F.J. and Poole, C.P. Jr. (1996) *The New Superconductors*, Plenum Press, New York.

SPECIFIC REFERENCES

- Bardeen, J., Cooper, L.N., and Schrieffer, J.R. (1957) "Theory of superconductivity," *Phys. Rev.* **108**, 1175. The BCS theory in all its technical detail.
- Josephson, B.D. (1962) "Possible new effects in superconductive tunneling," *Phys. Lett.* **1**, 251. The eponymous junction.
- Nye, J.F. (1985) *Physical Properties of Crystals*, Clarendon Press, Oxford. This is the standard reference for tensor representation. Chapter XI covers transport properties including electrical conductivity. The representation of σ by tensors is not necessary to understand the electrical behavior of materials. Its significance becomes clear when we want to specify certain properties of anisotropic single crystals.

JOURNALS

- Solid State Ionics*. An international journal published by Elsevier.
- Journal of Electronic Materials*. Published by ASM.
- Journal of Materials Science: Materials in Electronics*. Published by Springer.

JOURNALS DEVOTED TO SUPERCONDUCTIVITY AND ITS APPLICATIONS

- The field of high-temperature superconductivity experienced unprecedented growth during the late 1970s and 1980s. The important aspects of much of that research have been compiled in several books. Even so the field is still producing new developments, although of a much more incremental nature, and journals are the best place to find out what is happening. The following journals deal exclusively with superconductivity.
- Physica C*. Published by Elsevier.
- Journal of Superconductivity* since January 2006 renamed the *Journal of Superconductivity and Novel Magnetism*. Published by Springer.
- Superconductor Science and Technology*. Published by the Institute of Physics (IOP).

OTHER JOURNALS REPORTING DEVELOPMENTS IN HTSC

- Many other journals have regular contributions in the area of HTSC. The major resources are listed below.
- Journal of Applied Physics*. Published by the American Institute of Physics (AIP).
- Applied Physics Letters*. Also published by AIP. Consists of three page papers covering important developments in applied physics. A repository for many of the early papers covering processing of HTSC films.
- Physical Review B*, *Physical Review Letters*, *Japanese Journal of Applied Physics*, *Journal of Materials Science: Materials in Electronics*.

EXERCISES

- 30.1 Using Table 30.2 explain the following: (a) Why do t_+ and t_- change for NaCl as the temperature is increased from 400 to 600°C. (b) How would you expect these numbers to change if the temperature was increased further to 700°C? (c) Why is t_c zero?
- 30.2 At what temperature would the probability of finding an electron in the conduction band of diamond be the same as the probability of finding an electron in the conduction band of silicon at 25°C?
- 30.3 Using appropriate sketches compare the ion arrangements in the electrical conductor TiO shown in Figure 30.5 to those in the electrical insulator MgO.
- 30.4 In glasses containing alkali metal oxides such as Na₂O, the current is carried almost entirely by the alkali metal ion. (a). What is the transference number for alkali metal ions in this case? (b) Sketch the potential energy barrier for ion transport (i.e., redraw Figure 30.20 for a glass). (c) Why does your figure look different from Figure 30.20?
- 30.5 Calculate the probability of an electron being in the conduction band of MgO at a temperature of 2000°C.

- 30.6 The Hope diamond exhibited at the Smithsonian Institution in Washington, D.C. is a striking blue. Would you expect this stone to be electrically conducting? Explain how you arrived at your answer. Make sure to mention any assumptions you make.
- 30.7 What is the HTSC that currently has the highest T_c ? Are there any practical problems related to the use of this material?
- 30.8 In ZrO_2 (fluorite structure) ion conduction is the result of anion motion. In Li_2O (antifluorite structure) would you consider the anions or cations to be more mobile? (b). How might you increase ion conductivity in Li_2O ? In both cases explain how you arrived at your answer. (c) Now repeat (a) and (b) for MgO .
- 30.9 GaN is a wide-band-gap semiconductor. (a) What is E_g for GaN? (b) Describe some possible applications for GaN.
- 30.10 Dislocations have been shown to decrease the mobility of electrons in a semiconductor. Using the illustration of a dislocation in Figure 12.11 explain why you think they have a detrimental effect on μ .

Locally Redistributing Charge

CHAPTER PREVIEW

In this chapter we describe ceramic dielectrics. A dielectric is by definition an electrical insulator (ρ is high and E_g is large). That means that dielectric behavior is a property associated with certain ceramics and polymers but not a property associated with metals. We begin with a background section. Some of this material may have been covered before but perhaps not specifically in terms of ceramics.

Dielectrics in the context of this chapter are more than just passive insulators. For example, in BaTiO_3 and related perovskites structural changes create permanent electric dipoles that cause the material to become polarized. Among other things, polarization allows the material to store large amounts of charge: this is a prerequisite for a capacitor. Without dielectrics, computers cannot function; some of today's greatest challenges for the electronics industry concern dielectrics more than semiconductors.

The following key topics are discussed in this chapter:

- Dielectrics are polarizable: the separated charges cause an electric field that we characterize by the dielectric constant.
- Dielectrics can be self-polarizing: this is the ferroelectric effect. These ceramics are used in capacitors because of their high dielectric constant.
- The dimensions of a dielectric may change when it is polarized: this is the piezoelectric effect and is used in microelectromechanical systems (MEMS), sonar, and medical ultrasound imaging.
- The spontaneous polarization of a dielectric depends strongly on T ; this is the pyroelectric effect that we use for infrared (IR) detection (e.g., intruder alarms and thermal imaging).

31.1 BACKGROUND ON DIELECTRICS

All materials contain electrically charged particles. At a minimum these are the electrons and protons that are part of the constituent atoms. Many ceramics also contain ions, which are charged. In a dielectric, charges have a limited mobility and they will move only when they have enough energy to overcome their inertia. When an insulator receives a charge, it retains that charge, confining it within the localized region in which it was introduced. However, a conductor allows charge to flow freely and redistribute itself within the material. The distinction between conductors and nonconductors (and it is not always a clear one) arises from the relative mobility of charge within the material.

The terms “dielectric,” “nonconductor,” and “insulator” are often used interchangeably. However, we often specify dielectrics as materials that are not only electrically insulating but also have a high dielectric constant, κ .

Table 31.1 lists the important parameters discussed in this chapter and their units.

Polarization Mechanisms

Even though no charge is transferred when a dielectric is placed in an electric field there is a redistribution of charge, which occurs by the formation and movement of electric dipoles. There is an associated dipole moment, μ , having both magnitude and direction

$$\mu = qd \quad (31.1)$$

where d is the separation of the positive and negative ends of the dipole. The dipole direction is, by convention, taken to point from the negative end to the positive end.

When a dielectric material is placed in an electric field the induced dipoles, and any permanent dipoles, become aligned. The material is now polarized and

TABLE 31.1 Terms and Units Used to Describe Dielectric Behavior

Parameter	Definition	Units/value	Conversion factor
C	Capacitance	F, farads	$1\text{ F} = 1\text{ C/V} = 1\text{ A}^2\text{ s}^4\text{ kg}^{-1}\text{ m}^{-2}$
ϵ_0	Permittivity of a vacuum	$8.85 \times 10^{-12}\text{ F/m}$	
ϵ	Permittivity	F/m	
ϵ_r	Relative permittivity (ϵ/ϵ_0)	Dimensionless	
κ (same as ϵ_r)	Dielectric constant	Dimensionless	
P	Polarization	C/m^2	
Q	Charge	C, coulombs	$1\text{ C} = 1\text{ A s}$
μ	Dipole moment	$\text{C}\cdot\text{m}$	
V	Voltage	V	
q or e	Electron charge	0.16 aC	
D	Dielectric displacement	C/m^2	$D = Q/A$
θ_c	Curie temperature	K	$0\text{ K} = -273^\circ\text{C}$
T_{ow}	Curie-Weiss temperature	K	
E_c	Coercive field	V/m	
χ	Dielectric susceptibility	Dimensionless	
ξ	Electric field strength	V/m	
C	Curie constant	K	

the polarization (or dipole moment per unit volume) is given by

$$P = Nqd \quad (31.2)$$

where N is the number of dipoles.

There are four possible polarization mechanisms in a dielectric:

- Electronic
- Ionic
- Dipolar (also called molecular or orientation)
- Interfacial (also called space charge)

These mechanisms are each illustrated in Figure 31.1.

Electronic When an electric field is applied to an atom, there is a displacement of the electrons relative to the nucleus. The electrons will concentrate on the side of the nucleus near the positive end of the field. The atom acts as a temporarily induced dipole. This effect occurs in all materials (because all materials contain atoms), but the magnitude is small because d is very small. Typical displacements are $\sim 1\text{ \AA}$ giving $\mu \sim 1.6 \times 10^{-37}\text{ C}\cdot\text{m}$. Electronic polarization is the only possible mechanism in pure materials that are covalently bonded and does not contain permanent dipoles (e.g., diamond and silicon).

Ionic This occurs when an ionically bonded material is placed in an electric field; it is common in many ceramics (e.g., MgO , Al_2O_3 , NaCl). The bonds between the ions are elastically deformed. Consequently the charge is minutely redistributed. Depending on the direction of the field, the cations and anions move either closer together or further apart. These temporarily induced dipoles cause polarization

POLARIZATION MECHANISMS

A note: In some texts you will find that the polarization mechanism occurring in BaTiO_3 is described as dipolar and in others as ionic. We prefer the former because BaTiO_3 contains permanent dipoles (a condition of dipolar polarization) that are being oriented in an electric field. Although the permanent dipoles in BaTiO_3 are the result of ion displacements, the term ionic polarization refers to the movement of any ions in an electric field (whether the material has a permanent dipole or not).

and may also change the overall dimensions of the material. The dipole moment is usually small because, once again, the displacements involved are very small. Typically the ion displacements are only 10–100 \AA .

Dipolar This mechanism is generally uncommon in ceramics because

most of the permanent dipoles cannot be reoriented without

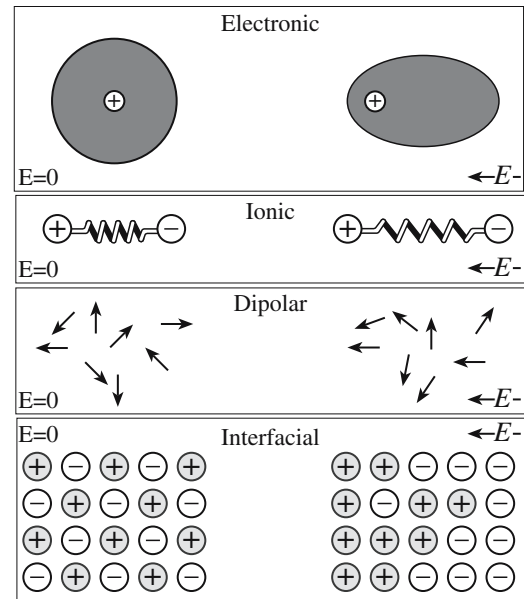


FIGURE 31.1 Illustration of the different polarization mechanisms in a solid.

destroying their crystal structure. But there are some very important exceptions and it is these materials that will form a large part of this chapter. The prototypical example is barium titanate. The structure is shown in Figure 7.2. At room temperature the octahedrally coordinated Ti^{4+} ion is displaced slightly from its ideal symmetric position causing the crystal structure to become tetragonal and permanently polarized. When an alternating electric field is applied to a crystal of barium titanate, the Ti^{4+} ion moves back and forth between its two allowable positions to ensure that the polarization is aligned with the field.

Interfacial A charge may develop at interfaces (such as grain or phase boundaries and free surfaces) normally as a result of the presence of impurities. The charge moves on the surface when the material is placed in an electric field. This type of polarization is not well understood, although it has considerable practical interest because most real materials and, in particular, many ceramics, are not pure.

The total P for the material is then the sum of all the individual contributions:

$$P = P_{\text{electronic}} + P_{\text{ionic}} + P_{\text{dipolar}} + P_{\text{interfacial}} \quad (31.3)$$

Relating P and κ

The dielectric constant is an important materials property and is a measure of the ability of an insulating material to store charge when subjected to an electric field; as you might expect, it is directly related to P .

We can develop an equation relating P and κ by beginning with a simple parallel plate capacitor. From electromagnetic theory we know that the total charge per unit area of a capacitor plate, D_0 , is proportional to the applied electric field ξ . The constant of proportionality is ϵ_0 :

$$D_0 = Q/A = \epsilon_0 \xi \quad (31.4)$$

If we now place a dielectric between the parallel plates we write

$$D = \epsilon \xi \quad (31.5)$$

D is also known as the dielectric displacement and represents the extra charge that can be stored because of the presence of the dielectric. So we can rewrite Eq. 31.5 as

$$D = \epsilon_0 \xi + P \quad (31.6)$$

By substituting Eq. 31.5 into Eq. 31.6 we obtain

$$\epsilon \xi = \epsilon_0 \xi + P \quad (31.7)$$

By simple rearrangement we can write

TABLE 31.2 Dielectric Constants of Various Ceramics

Material	κ at 1 MHz	Material	κ at 1 MHz
Diamond	5.5–6.6	Al_2O_3	8.8
SiO_2	3.7–3.8	MgO	9.6
NaCl	5.9	BaTiO_3	3000
Mica	5.4–8.7	Pyrex glass	4.0–6.0
Soda-lime glass	7.0–7.6	TiO_2	14–110
Steatite ($\text{SiO}_2 + \text{MgO} + \text{Al}_2\text{O}_3$)	5.5–7.5	Forsterite ($2\text{MgO} \cdot \text{SiO}_2$)	6.2
Cordierite ($\text{SiO}_2 + \text{MgO} + \text{Al}_2\text{O}_3$)	4.5–5.4	Mullite	6.6
High-lead glass	19	Vycor glass	3.9

$$P = (\kappa - 1)\epsilon_0 \xi = \chi \epsilon_0 \xi \quad (31.8)$$

where χ is a measure of the ratio of the bound charge/free charge (i.e., P/Q). For dielectrics that polarize easily κ will be large and, in turn, a large quantity of charge can be stored.

Table 31.2 lists κ for a range of materials. Many ceramics and glasses have κ in the range of 4–10. Polarization is electronic only in covalent ceramics such as diamond and is a combination of electronic and ionic in materials such as MgO. Some ceramics, in particular BaTiO_3 and other titanates and zirconates, have very large κ due to their permanent dipole moments.

Frequency Dependence of Polarization

When a dielectric is placed in an alternating electric field the dipoles attempt to maintain alignment with the field. This process requires a finite time that is different for each polarization mechanism. At the relaxation frequency the dipoles will only just be able to reorient themselves in time with the applied field. At this frequency the dielectric is “lossy” and energy is lost in the form of heat. The dielectric loss is at a maximum when the frequency of the external field coincides with the relaxation frequency of a given polarization mechanism. This is the principle behind the microwave oven. It operates at the relaxation frequency of water molecules and the heat generated warms the food.

At frequencies above the relaxation frequency the dipoles will no longer be able to keep up with changes in the applied field and the contributing polarization mechanism becomes effectively “frozen” and no longer contributes. Figure 31.2 shows the variation of polarization with frequency for a hypothetical material that exhibits all four of the polarization mechanisms.

- At optical frequencies only electronic polarization is operative.
- Dipolar and ionic contributions are small at high frequencies because of the inertia of the molecules and

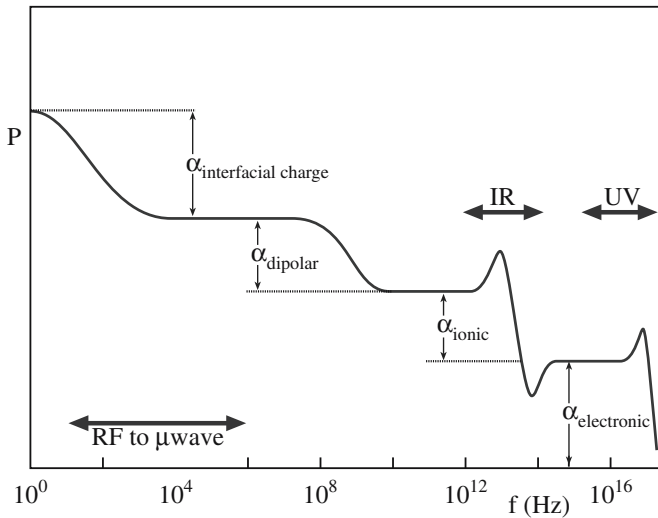


FIGURE 31.2 Frequency dependence of polarization.

ions. The peaks occurring at $\sim 10^{13}$ and $\sim 10^{15}$ Hz are due to resonance effects where the external field is alternating at the natural vibrational frequency of the bound ions or electrons, respectively.

Dielectric Strength

A dielectric will be able to withstand a certain applied electric field strength before it breaks down and current flows. High dielec-

REAL AND IMAGINARY COMPONENTS OF ϵ

The permittivity under an alternating field can be represented mathematically as the sum of real (ϵ') and imaginary (ϵ'') parts:

$$\epsilon = \epsilon' - j\epsilon'' \quad (\text{Box 31.1})$$

In an alternating electric field the phase angle of the electric flux density lags behind that of the electric field due to the finite speed of polarization. The delay angle δ is

$$\tan \delta = \epsilon''/\epsilon' \quad (\text{Box 31.2})$$

The electric power loss per unit time (also called the dielectric loss) is proportional to $\tan \delta$. Typical values are given in Table 31.3.

TABLE 31.3 Dielectric Loss for Some Ceramics and Glasses at 25°C and 1 MHz

Material	Tan δ
LiF	0.0002
MgO	0.0003
KBr	0.0002
NaCl	0.0002
TiO ₂ (\parallel c)	0.0016
TiO ₂ (\parallel a,b)	0.0002
Al ₂ O ₃ (\parallel c)	0.0010
Al ₂ O ₃ (\parallel a,b)	0.0010
BaO	0.0010
KCl	0.0001
Diamond	0.0002
Mg ₂ SiO ₄ (forsterite)	0.0003
Fused silica glass	0.0001
Vycor (96 SiO ₂ -4B ₂ O ₃) glass	0.0008
Soda-lime silica glass	0.0100
High-lead silica glass	0.0057

TABLE 31.4 Dielectric Strengths for Various Ceramics

Material	Dielectric strength (MV/cm at 25°C)
Al ₂ O ₃ (99.5%)	0.18
Al ₂ O ₃ (94.0%)	0.26
High-voltage porcelain	0.15
Steatite porcelain	0.10
Lead glass	0.25
Lime glass	2.5
Borosilicate glass	5.8
Fused quartz	6.6
Quartz crystal	6.0
NaCl [100], [111], [110]	2.5, 2.2, 2.0
Muscovite mica	10.1

tric strengths are important in applications in which the thickness of the material is going to be small, e.g., in capacitors. Values of dielectric strength for several ceramics are given in Table 31.4. Note the very high value of mica, which is one of the reasons it was used in early ceramic disk capacitors.

Nonlinear Dielectrics

Nonlinear dielectrics have permanent dipoles that interact to give a polarization in the absence of an applied electric field. These materials are the ferroelectrics. The topic shares many similarities with ferromagnetism described in Chapter 33. For example, above a critical temperature, the Curie temperature θ_c , the spontaneous polarization is destroyed by thermal disorder. A plot of P versus ξ is shown in Figure 31.3 and demonstrates hysteresis. This behavior is similar to that produced by a ferromagnet when it is cycled through an alternating magnetic field. The description is based on the domain structure of ferroelectrics.

When the dipoles in a crystal are randomly oriented there is no net P . When a field is applied, the dipoles begin to line up with the electric field. The total dipole moment changes either by the movement of the walls between domains or by the nucleation of new domains. Eventually the field aligns all of the dipoles and P_s is obtained. When all the dipoles are aligned in the same direction the material is "poled."

When the field is subsequently removed a remnant polarization P_r exists due to the coupling between adjacent dipoles. The material is permanently polarized in the

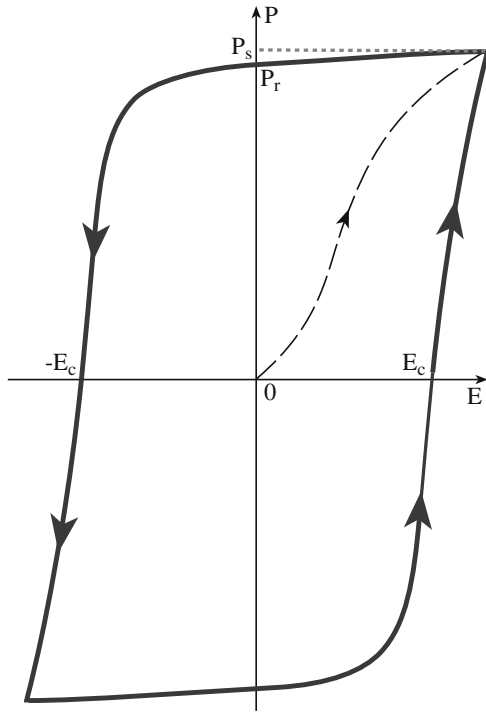


FIGURE 31.3 Hysteresis curve for a typical ferroelectric.

TABLE 31.5 Noncentrosymmetric Crystals

Crystal system	Noncentrosymmetric		
	point groups	Piezoelectric	Pyroelectric
Triclinic	1	Yes	Yes
Monoclinic	2	Yes	Yes
	m	Yes	Yes
Orthorhombic	mm2	Yes	Yes
	222	Yes	No
Tetragonal	4	Yes	Yes
	$\bar{4}$	Yes	No
	422	Yes	No
	4mm	Yes	Yes
	$\bar{4}2m$	Yes	No
Trigonal	3	Yes	Yes
	32	Yes	No
	3m	Yes	Yes
Hexagonal	6	Yes	Yes
	$\bar{6}$	Yes	No
	622	Yes	No
	6mm	Yes	Yes
	$\bar{6}m2$	Yes	No
Cubic	23	Yes	No
	432	No	No
	$\bar{4}3m$	Yes	No

absence of an electric field. This property is the key to ferroelectricity.

When the direction of ξ is reversed the dipole orientation switches to become aligned with the new field direction. As the strength of the reverse field is increased, P_s will eventually occur with the opposite polarization. As the field alternates a hysteresis loop is produced. The area contained within the loop is related to the energy required to cause the polarization to switch directions. Linear dielectrics (which is most of them) do not show significant hysteresis in an alternating electric field.

There is a structural requirement for ferroelectricity. There are a total of 32 different symmetry point groups, 21 of which do not possess a center of symmetry. Ferroelectrics are part of a small subgroup of noncentrosymmetric crystals. Related properties are piezoelectricity and pyroelectricity. Dielectrics belonging to all but one of the groups of noncentrosymmetric crystals are piezoelectric. Pyroelectric crystals form a further subgroup of 10 types of crystal having especially low symmetry as shown in Table 31.5.

- All ferroelectrics are pyroelectric and piezoelectric.
- All pyroelectrics are piezoelectric.
- All piezoelectrics are not pyroelectric.
- All pyroelectrics are not ferroelectrics.

31.2 FERROELECTRICITY

FERROELECTRICS

Ferroelectrics do not contain iron. The term comes from the analogy with ferromagnetism, which also does not require iron.

Ferroelectrics exhibit an electric dipole moment in the absence of an external electric field. The direction of the dipole moment may be switched by the application of an alternating field. This property of polarization reversal and remanence cannot be predicted by looking only at the structure of a material; it must be determined experimentally.

Ferroelectricity is a property that is associated not only with ceramics. Certain polymers such as polyvinylidene fluoride (PVDF) and copolymers between PVDF and trifluoroethylene are ferroelectric. PVDF is a semicrystalline polymer. The crystalline conformation has an orthorhombic unit cell (mm2).

A ferroelectric crystal consists of regions called domains. Within each domain the polarization is in a common direction, but in adjacent domains the polarization is in a different direction as illustrated in Figure 31.4. The net polarization then depends on the difference in volumes of the two domain orientations. If the volumes are equal the material will not exhibit a net polarization. By etching in a suitable chemical we can see the domain structure. This is analogous to the process we described in Section 12.3 to reveal dislocations.

Domain walls separate adjacent domains and are transition regions in which the direction of polarization

Domain walls separate adjacent domains and are transition regions in which the direction of polarization

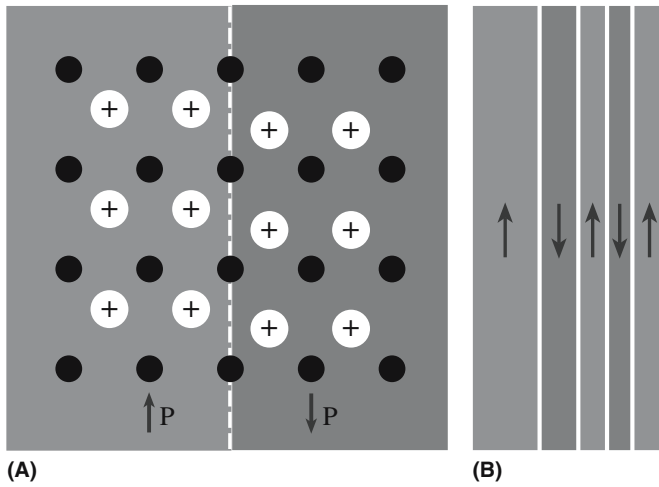


FIGURE 31.4 (a) Schematic showing ionic displacements in two 180° ferroelectric domains. (b) Domain structure showing several 180° domains of different sizes.

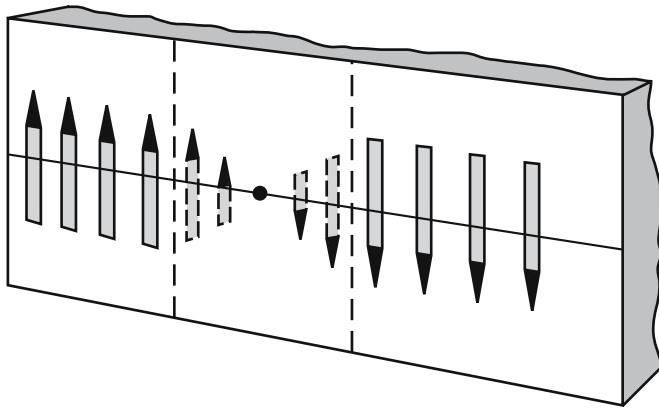


FIGURE 31.5 Illustration of a 180° domain wall. The width is ~0.2–0.3 nm.

changes. They have a width on the order of one lattice parameter (~0.2–0.3 nm), but this varies with temperature and crystal purity. This is less than one hundredth as thick as the Bloch walls between magnetic domains in ferromagnets (see Chapter 33). Figure 31.5 illustrates a domain wall in a ferroelectric. There are actually two types:

- 90° wall—polarization vectors are in adjacent domains at right angles.

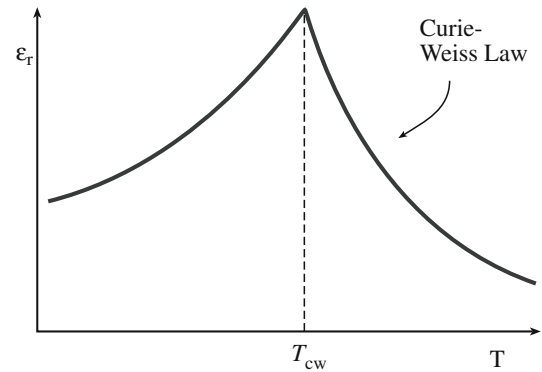


FIGURE 31.6 Relative permittivity of a ferroelectric as a function of T .

- 180° wall—polarization vectors in adjacent domains are antiparallel.

The wall energy is of the order of 10 mJ/m². This value can be compared to typical grain-boundary (GB) energies that range from 0.1 to 0.3 J/m² for low-angle boundaries, 0.5–0.6 J/m² for high-angle tilt boundaries, and 0.8–0.9 J/m² for high-angle twist boundaries. As a consequence, it is, in general, easier to move domain boundaries than it is to move GBs.

Ferroelectricity depends on temperature. Above θ_c ferroelectric behavior is lost and the material becomes paraelectric. The change from the ferroelectric to the non-ferroelectric state is accompanied either by a change in crystal symmetry (e.g., as in BaTiO₃) or by an order–disorder transition such as in the organic ferroelectric compound triglycine sulfate (TGS).

The relative permittivity shows a characteristic peak at T_{cw} as shown in Figure 31.6 and falls off at higher temperatures following the Curie–Weiss law:

$$\epsilon_r - 1 = \chi = C/(T - T_{cw}) \quad (31.9)$$

Curie constants and Curie temperatures for several ferroelectric ceramics are given in Table 31.6.

- For ferroelectrics that undergo a first-order transition [e.g., BaTiO₃, (Ba, Sr)TiO₃, PbTiO₃, and KNbO₃] $T_{cw} < \theta_c$. For example, experimental measurements on polycrystalline BaTiO₃ have shown that T_{cw} can be more than 10°C less than θ_c . A first-order transition involves a discontinuous change in P with T .

TABLE 31.6 Curie Temperatures and Curie Constants for Several Ferroelectric Ceramics							
Ceramic	Structure	θ_c (K)	C (K)	Oxide	Structure	θ_c (K)	C (K)
SrTiO ₃	Perovskite	~0	7.0×10^4	LiNbO ₃	Ilmenite	1470	
BaTiO ₃	Perovskite	393	12.0×10^4	LiTaO ₃	Ilmenite	890	
PbTiO ₃	Perovskite	763	15.4×10^4	Cd ₂ Nb ₂ O ₇	Pyrochlore	185	7.0×10^4
CdTiO ₃	Perovskite	1223	4.5×10^4	PbNb ₂ O ₆	Tungsten bronze	843	30.0×10^4
KNbO ₃	Perovskite	712	27.0×10^4				

- For ferroelectrics that undergo a second-order transition (e.g., triglycine sulfate, Rochelle salt, and dihydrogen phosphate) $T_{cw} \sim \theta_c$. The change in P is continuous for a second-order transition.

31.3 BaTiO₃: THE PROTOTYPICAL FERROELECTRIC

Barium titanate (BaTiO₃) was the first ceramic in which ferroelectric behavior was observed and is probably the most extensively investigated of all ferroelectrics. Its discovery made available ks up to two orders of magnitude greater than had been known before. This property was very soon utilized in capacitors and BaTiO₃ remains the basic capacitor dielectric in use today (although not in its pure form). There are several reasons why BaTiO₃ has been so widely studied:

- Relatively simple crystal structure
- Durable
- Ferroelectric at room temperature ($\theta_c = 120^\circ\text{C}$)
- Easily prepared as a polycrystalline ceramic, single crystal, or thin film

Structure and Structural Transformations

Above θ_c the unit cell of BaTiO₃ is cubic (point group m3m) with the ions arranged as shown in Figure 7.2.

Recap: Each Ba²⁺ is surrounded by 12 nearest-neighbor oxygen ions; each Ti⁴⁺ has six oxygen-ion neighbors. Together the Ba²⁺ and O²⁻ ions form a face-centered cubic (fcc) arrangement with Ti⁴⁺ fitting into the octahedral interstices. The octahedral site is actually expanded because of the large Ba²⁺ ions ($r_{\text{Ba}^{2+}} = 0.136 \text{ nm}$). The Ti⁴⁺ ion is quite small ($r_{\text{Ti}^{4+}} = 0.064 \text{ nm}$) giving a radius ratio with oxygen of $r_{\text{Ti}^{4+}}/r_{\text{O}^{2-}} = 0.44$. This value is close to the limiting value (≥ 0.414) for a coordination number of 6. The result is that the Ti⁴⁺ often finds itself off-centered within its coordination octahedron. This is why it is sometimes referred to as the “rattling” titanium ion (think back to Pauling’s rules). The direction of off-centering may be along one of the 6 $\langle 001 \rangle$ directions, one of the 8 $\langle 111 \rangle$ directions, or one of the 12 $\langle 110 \rangle$ directions.

At temperatures greater than θ_c the Ti⁴⁺ has no fixed nonsymmetrical position and hence there is no permanent dipole moment. The crystal is paraelectric; it can be polarized only while it is in an applied electric field.

On cooling BaTiO₃ below θ_c the structure spontaneously changes to the tetragonal form (point group 4mm) with a dipole moment along the c axis. The magnitude and direction of the ion displacements accompanying this transformation are given in Figure 31.7.

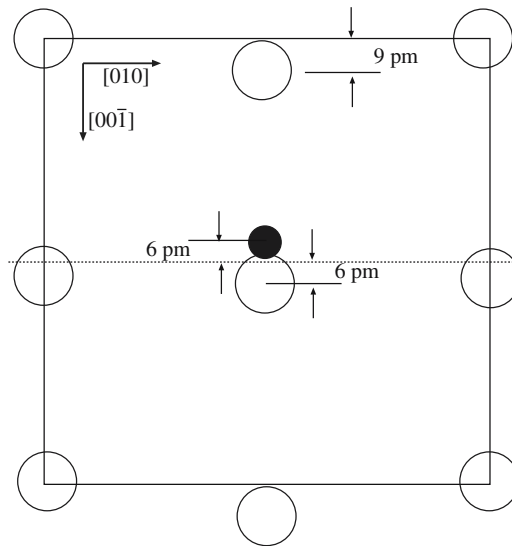


FIGURE 31.7 [100] projection of BaTiO₃ showing ion displacements below θ_c (not to scale).

There are other structural transformations that occur in BaTiO₃, these are shown in Figure 31.8.

- Below 0°C the unit cell is orthorhombic with the polar axis parallel to a face diagonal. Application of an electric field along $[011]$ causes the domains to adopt this direction of Ti⁴⁺ off-centering.
- Below -90°C the structure is rhombohedral with the polar axis along a body diagonal. The Ti⁴⁺ is off-centered along $[111]$.

Because these transformations both occur below room temperature they are not commercially important.

The phase changes that occur in BaTiO₃ are characterized by an expansion of the original cubic lattice in the direction of the spontaneous polarization and a contraction in the perpendicular direction. The temperature dependence of the lattice parameters of BaTiO₃ in the four phases is shown in Figure 31.9.

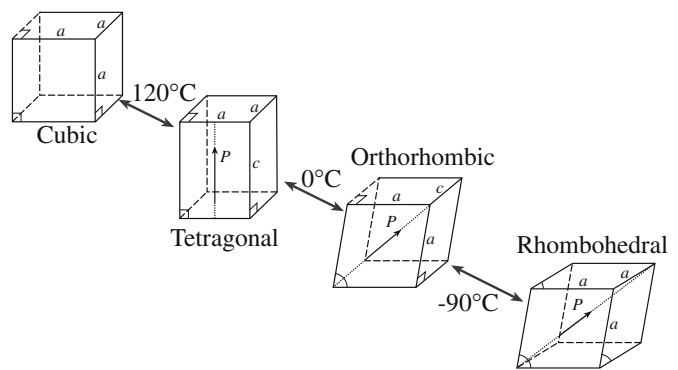


FIGURE 31.8 BaTiO₃ polymorphs showing direction of polarization.

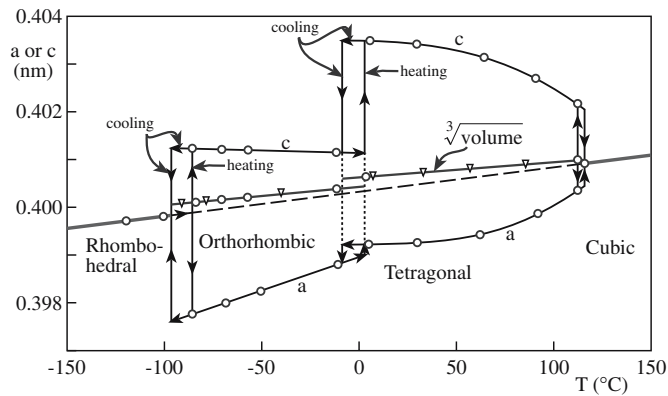


FIGURE 31.9 Experimental measurements of lattice parameters of BaTiO₃ as a function of T . Note the change in volume at each transition and the hysteresis in the lattice parameters.

Properties of BaTiO₃

Barium titanate is ferroelectric and, by implication, also pyroelectric and piezoelectric. The characteristic of a ferroelectric is that it is polarized in the absence of an applied electric field and the direction of polarization can be reversed. Figure 31.10 shows a rectangular hysteresis loop for a single-domain single crystal of BaTiO₃. This loop was obtained at room temperature using a 50 Hz supply. E_c is 0.1 MV/m and P_s is 0.27 C/m².

In tracing out the hysteresis loop both 180° and 90° changes in domain orientation take place. The almost vertical portions of the loop are due to the reversal of spontaneous polarization as antiparallel 180° domains nucleate and grow as illustrated in Figure 31.11. This process corresponds to the Ti⁴⁺ moving from one of its off-center sites along the c axis to the other site. There is a potential barrier to this movement as indicated by Figure 31.12.

The motion of domain walls in ferroelectrics is not simple. In an electric field a 180° wall in BaTiO₃ appears to move by the repeated nucleation of steps by thermal fluctuations along the parent wall. Domains misoriented by 180° tend to switch more easily than 90° domain walls since no net physical deformation is required; domains misoriented by 90° are inhibited from changing orienta-

tion by the strain that accommodates switching of c and a axes.

The almost horizontal portions of the hysteresis loop represent saturated states in which the crystal is a single domain during a cycle. Defects and internal strains within the crystallites impede the movement of domain walls. Domain wall mobility has been found to decrease with time (even without an applied mechanical or electrical stress or thermal changes). This is due to internal fields associated with charged defects, redistribution of lattice strains, and accumulation of defects at domain walls.

The hysteresis loop of a polycrystalline BaTiO₃ ceramic has a higher E_c and lower P_r than the single crystal.

The size of the hysteresis loop also depends on temperature as shown in Figure 31.13. At low temperatures the loops are fatter and E_c is greater, corresponding to

the larger energy required for domain reorientation. At higher temperatures E_c decreases until at θ_c no hysteresis remains and the material becomes paraelectric.

Figure 31.14 shows the temperature dependence of the dielectric constant of single-crystal BaTiO₃. The high value of κ appears over a very short temperature range, close to θ_c and far from room temperature. For this reason pure BaTiO₃ is not particularly useful as a dielectric. Ideally κ must be

- High at room temperature
- Stable over as wide a T range as possible

There are several approaches that can be used to lower θ_c and increase κ at room temperature:

- A solid solution can be formed with an isostructural compound (see Section 31.4).
- The grain size can be reduced as shown in Figure 31.15.
- Mechanical stresses (compressive or tensile) in thin films can be induced because of differences in the lattice parameter between the film and the substrate, e.g., values of θ_c for BaTiO₃ thin films on MgO and on Pt are lower than for bulk material.

CALCULATION OF THE DIPOLE MOMENT FOR BaTiO₃

Using Eq. 33.1 we need to consider the distances that the Ti⁴⁺ and O²⁻ ions are displaced from their regular (cubic) lattice positions (assuming the position of the Ba²⁺ ions is fixed). The charge is the product of q and the ion charge. The dipole moments are then

$$\mu(\text{Ti}^{4+}): \quad (1.602 \times 10^{-19} \text{ C}) (4) (0.06 \times 10^{-8} \text{ cm}) \\ = 3.84 \times 10^{-28} \text{ C}\cdot\text{cm}$$

$$\mu(\text{O}^{2-} \text{ top}): \quad (1.602 \times 10^{-19} \text{ C}) (2) (0.09 \times 10^{-8} \text{ cm}) \\ = 2.88 \times 10^{-28} \text{ C}\cdot\text{cm}$$

$$\mu(\text{O}^{2-} \text{ side}): \quad (1.602 \times 10^{-19} \text{ C}) (2) (0.06 \times 10^{-8} \text{ cm}) \\ = 1.92 \times 10^{-28} \text{ C}\cdot\text{cm}$$

Now we need to include the number of each of the types of ions per cell. There is a single Ti⁴⁺/cell, there is a top-face O²⁻/cell, and there are two side-face O²⁻/cell.

The total dipole moment per unit cell is

$$\mu = \mu(\text{Ti}^{4+}) + \mu(\text{O}^{2-} \text{ top}) + 2\mu(\text{O}^{2-} \text{ side}) \\ = 1.056 \times 10^{-27} \text{ C}\cdot\text{cm}$$

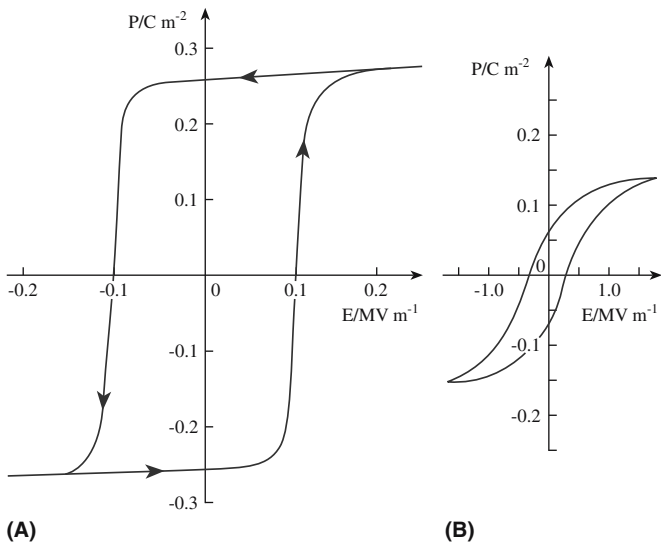


FIGURE 31.10 Hysteresis loops for BaTiO₃. (a) Single-domain single crystal. (b) Polycrystalline ceramic.

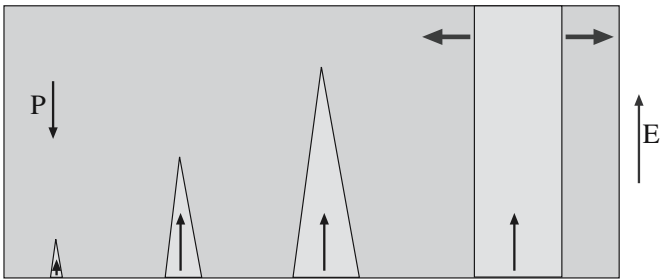


FIGURE 31.11 Illustration of the growth of a ferroelectric domain in a field ξ .

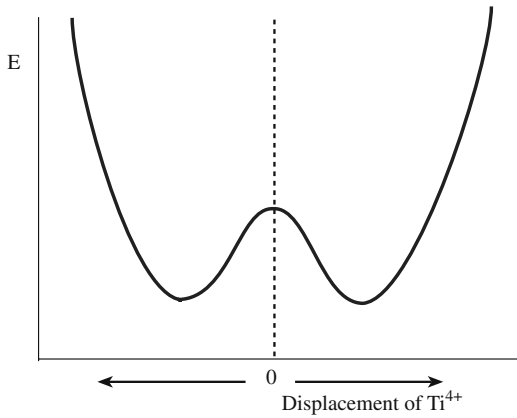


FIGURE 31.12 Potential energy wells for Ti⁴⁺ as a function of displacement within the octahedral site.

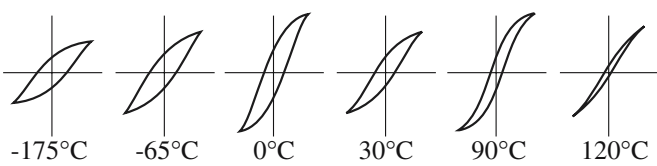
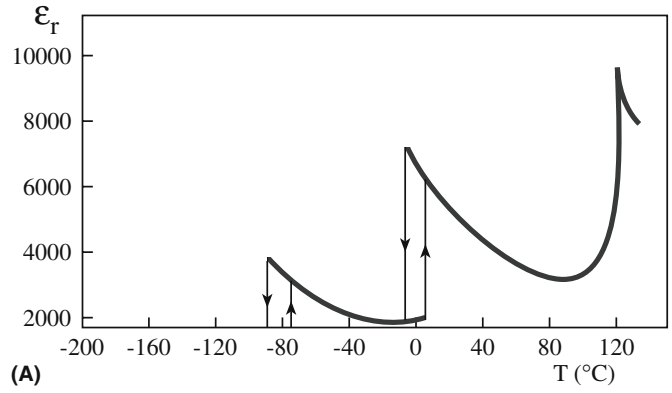
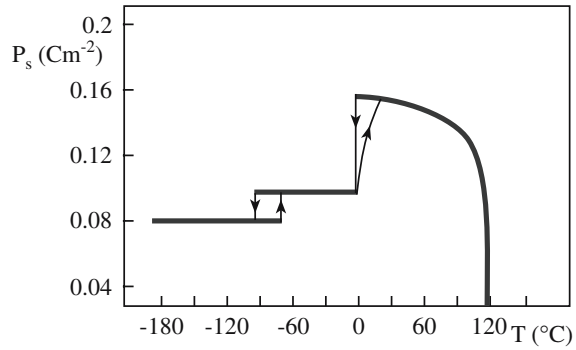


FIGURE 31.13 Hysteresis loops for BaTiO₃ as a function of T .



(A)



(B)

FIGURE 31.14 (a) Dielectric constant and (b) spontaneous polarization of single-crystal BaTiO₃ as a function of T . (Compare to Figure 31.9.)

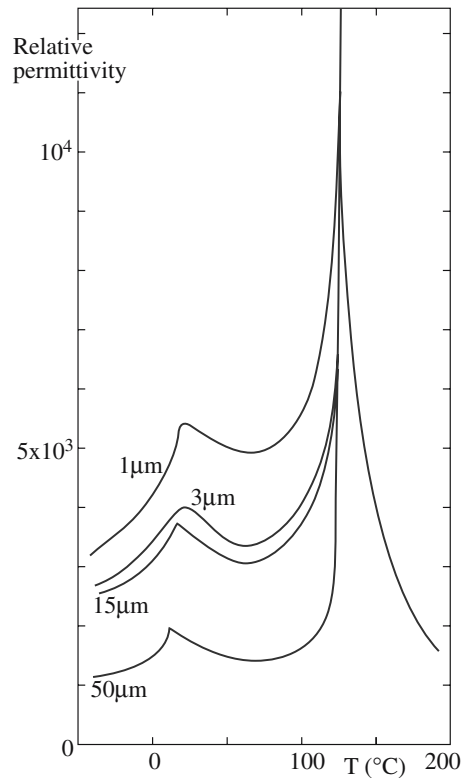


FIGURE 31.15 Effect of grain size on the dielectric constant of BaTiO₃.

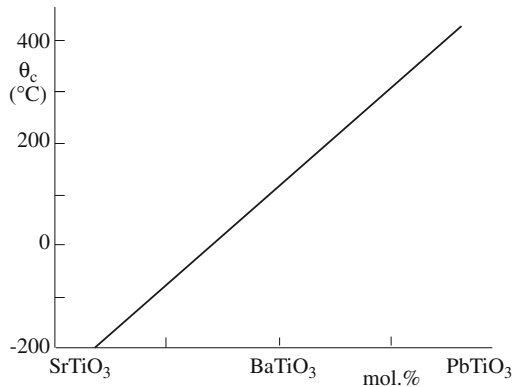


FIGURE 31.16 Effect of substitution on θ_c for BaTiO₃ solid solutions with SrTiO₃ and PbTiO₃.

31.4 SOLID SOLUTIONS WITH BaTiO₃

BaTiO₃ is rarely used in its pure form because, as mentioned in the previous section, high κ occurs only over a very short temperature range that is far from room temperature. Solid solutions with an isostructural compound can broaden θ_c as well as shifting it to lower temperatures. One important solid-solution phase is that formed between BaTiO₃ and SrTiO₃. These solid solutions are often referred to as BST. Solid solutions of BaTiO₃ and PbTiO₃ lead to an increase in θ_c over that of pure BaTiO₃. The effect on the substitution of either Sr²⁺ or Pb²⁺ for Ba²⁺ in BaTiO₃ is shown in Figure 31.16.

31.5 OTHER FERROELECTRIC CERAMICS

Table 31.7 lists some other ferroelectric ceramics, although it does not include the large number of solid-solution phases that are ferroelectric. Many ferroelectric ceramics have a perovskite structure above θ_c , but this is not a prerequisite. For example, LiNbO₃ has an ilmenite (FeTiO₃) structure and Cd₂Nb₂O₇ has a pyrochlore structure (the mineral pyrochlore is CaNaNb₂O₆F).

TABLE 31.7 Some Other Ferroelectric Ceramics	
Compound	θ_c (°C)
SrTiO ₃	-245
PbTiO ₃	490
KNbO ₃	435
KTaO ₃	-260
Cd ₂ Nb ₂ O ₇	-85
PbNb ₂ O ₆	570
LiNbO ₃	1200

31.6 RELAXOR DIELECTRICS

BaTiO₃ and most related compositions show little change in dielectric properties with frequency until the gigahertz range is reached. Relaxor dielectrics are a class of perovskite ferroelectrics that shows significant changes in κ and $\tan \delta$ with frequency. The classic high- κ relaxor is lead magnesium niobate (PbMg_{1/3}Nb_{2/3}O₃ or PMN), which was first synthesized in the late 1950s.

In addition to the high κ of many relaxor compositions they also have a broad peak in the permittivity versus temperature range, even in the absence of additives and even in the form of single crystals. This behavior is attributed to nanoscale (~10 nm)-ordered regions, which are too small to yield the sharp phase transition of normal ferroelectrics. As a result, spontaneous polarization and associated ferroelectric properties are retained over a very broad temperature range. Another attractive feature of relaxors is that dense polycrystalline ceramics are achievable at relatively low sintering temperatures ($\leq 900^\circ\text{C}$), which allows a significant reduction in the amount of Pd used in Ag-Pd metallizations for electrodes in multilayer capacitors (see Section 31.7).

One of the difficulties with most relaxor compositions containing Pb and Nb is that they have a tendency to form the lower κ pyrochlore-type rather than perovskite structures. The pyrochlore-type phase found in PMN has the composition Pb_{1.83}Nb_{1.71}Mg_{0.29}O_{6.39}. It has a room temperature κ of 130 and is paraelectric.

There are a whole range of lead-containing relaxors based on lead zinc niobate (PZN), lead iron niobate (PFN), lead iron tungstate (PFW), and solid solutions with each other and with BaTiO₃ (BT), PbTiO₃ (PT), and SrTiO₃ (ST). Some of the solid-solution phases are PMN-PT, PMN-PT-PZN, PMN-PZN, PFN-PFW, PFN-PMN, and PFW-PT.

31.7 CERAMIC CAPACITORS

Capacitance is defined as the total charge stored by the capacitor divided by the applied potential:

$$C = Q/V \quad (31.10)$$

This depends on the

- Dielectric between the conductors
- Area of each conductor, A
- Separation between them, d

For a parallel plate capacitor in a vacuum

$$C = \epsilon_0 A/d \quad (31.11)$$

When a dielectric is present polarization occurs and permits additional charge to be stored. The ability of the

dipoles in the dielectric to polarize and store charge is reflected by ϵ :

$$C = \epsilon A/d \quad (31.12)$$

Or in terms of κ

$$C = \kappa \epsilon_0 A/d \quad (31.13)$$

There are three main types of capacitors:

- Ceramic
- Paper or polymer film
- Electrolytic (aluminum or tantalum)

Frequency ranges in which these capacitor types are usable and the capacitance values of each type are shown in Table 31.8. Ceramic capacitors occupy about 30% of the total capacitor market with sales of over 80 billion discrete units per year.

We can distinguish three basic types of ceramic capacitors:

- Film capacitors used in memory devices
- Single-layer discrete capacitors, usually disc capacitors
- Multilayer chip capacitors (MLCCs)

Each of these types will be described separately. Film capacitors that are used in memory devices are integrated with the other circuit components. However, disc capacitors and MLCCs are discrete components.

Categories of Ceramic Capacitor Dielectric

Ceramic capacitors are generally classified into three types (1, 2, 3 or I, II, III) based on their properties.

Class 1 or *NPO* capacitors have $\kappa < 15$ and are mainly used for electrical insulation such as substrates, power line insulators, and spark plug insulators. Medium κ class 1 capacitors are used in the following:

- High-power transmitter capacitors in the frequency range 0.5–50 MHz because of their low $\tan \delta$

TABLE 31.8 Frequency and Capacitance Ranges for Capacitor Types

Capacitor	Maximum usable frequency (Hz)	Range of capacitance values (μF)
Mica	10 G	0.1– 10^{-6}
Paper/polymer	10 G	100– 10^{-6}
Ceramic	10 G	10^3 – 10^{-6}
Al electrolytic	10 k	10^6 –0.1
Ta electrolytic	10 k	10^3 –0.1

NOTATION FOR C

We use C for capacitance and C for the Curie constant. There is really no way around this potential confusion; fortunately both terms rarely occur in the same equation.

- Stable capacitors for general electronic use in the frequency range 1 kHz–100 MHz because of the stability of capacitance with temperature
- Microwave resonant cavities operating between 0.5 and 50 GHz because of their stability and low $\tan \delta$

Class 2 capacitors consist of high dielectric constant ceramics based on BaTiO_3 . The two main subclasses are Z5U and X7R after the scheme shown in Table 31.9 that was devised by the Electronics Industries Association (EIA) in the United States for specifying the variability of capacitance with temperature in the range of practical interest. For maximum capacitance θ_c is shifted close to room temperature and broadened. Shifters form solid solution phases with BaTiO_3 . Depressor additives result in broadening of the peak and concentrate at the GBs. The compositions and properties of some Z5U and X7R dielectrics are shown in Tables 31.10 and 31.11, respectively.

Class 3 capacitors are based on either BaTiO_3 or SrTiO_3 (usually X7R type) and have very high “apparent” dielectric constants ($\kappa = 50,000$ – $100,000$), which are achieved by producing either a surface layer on the grains or at the GBs that is electrically insulating while the grains themselves are conducting or semiconducting. This can be achieved in two ways:

- The ceramic is first heated to a high temperature (900–1000°C) under reducing conditions (usually a H_2/N_2 mixture) that makes it semiconducting and then the surface layer is reoxidized by heating in oxygen at a lower temperature.
- The GBs can be made insulating by diffusing a low melting point mixture of metal oxides such as CuO , MnO , and Bi_2O_3 . The very thin (10 μm) insulating layers and the high GB area produce very high capacitances.

The properties of these dielectrics are similar to those in class 2, but their working voltages are between 2 and

TABLE 31.9 EIA Coding of Class 2 Capacitors

Code	Temperature range ($^{\circ}\text{C}$)	Code	Capacitance change (%)
X7	–55 to +125	D	± 3.3
X5	–55 to +85	E	± 4.7
Y5	–30 to +85	F	± 7.5
Z5	+10 to +85	P	± 10
		R	± 15
		S	± 22
		T	+22 to –33
		U	+22 to –56
		V	+22 to –82

TABLE 31.10 Composition and Properties of Z5U Dielectrics

Component	Composition (wt%)			Role
	1	2	3	
BaTiO ₃	84–90	65–80	72–76	Base material
CaZrO ₃	8–13	—	—	Shifter
MgZrO ₃	0–3	—	—	Depressor
SrTiO ₃	—	7–11	5–8	Shifter
CaTiO ₃	—	7–11	4–6	Depressor
BaZrO ₃	—	7–11	7–10	Shifter
CaSnO ₃	—	—	2–4	Shifter
Other oxides (e.g., Nb ₂ O ₅)	1–3	8–13	0–3	Acceptors
κ (25°C, 1 kHz)	5700–7000	5500–6500	11,500–13,000	
Tan δ	≤0.03	≤0.03	≤0.03	

25 V. The big advantage is that simple disc capacitors can be produced with large capacitances >1 μF.

Disk Capacitors

Figure 31.17 shows an example of a ceramic disk capacitor. Disc diameters range from 2 to 30 mm and dielectric thicknesses range from 50 μm to 2 mm.

These capacitors are common, but from a practical standpoint can store only a limited amount of charge. To increase the storage capacity it would be necessary to increase the overall size or decrease the distance between the plates. The first option would make the component too bulky. The second option would increase the possibility of dielectric breakdown.

The first disc capacitors used mica sheets. Mica has a very high dielectric strength (see Table 31.4) and can readily be cleaved into thin sheets. Disk capacitors are now made from BaTiO₃-based compositions using traditional ceramic processing

methods. The powder is mixed with between 5 and 10 vol% of an organic binder and pressed into a disk. Alternatively they can be punched from extruded ribbon or tape. The green ceramic is then sintered at between 900 and 1300°C in air to produce a dense material. After sintering Ag paint is applied to the major surfaces and the discs are briefly refired at 600–800°C. Tinned copper wires are soldered to the metallized ceramic disc before the whole assembly is immersed in a polymer (usually an epoxy resin).

Disc capacitors are made using all classes of capacitor dielectric allowing a wide range of capacitances:

- 0.1–1000 pF using class 1 dielectrics
- 1000–100 000 pF using class 2 dielectrics
- 0.1–2 μF using class 3 dielectrics

MLCC ADVANTAGES

- Small
- Inexpensive
- Good frequency response
- Can be surface mounted
- High capacitance
- Easy to make

Multilayer Chip Capacitors (MLCCs)

The largest class of ceramic capacitors produced, in numbers and in value, is

TABLE 31.11 Composition and Properties of X7R Dielectrics

Component	Composition (wt%)			Role
	1	2	3	
BaTiO ₃	90–97	85–92	86–94	Base material
CaZrO ₃	2–5	4–8	—	Shifter
BaCO ₃	0–5	—	—	Stoichiometry adjuster
SrTiO ₃	—	3–6	—	Shifter
Bi ₂ O ₃	—	—	5–10	Depressor, flux
Other	2–5	1–4	2–6	
κ (25°C, 1 kHz)	1600–2000	1800	1400–1500	
Tan δ	<0.025	<0.025	<0.015	



FIGURE 31.17 Ceramic disc capacitor.

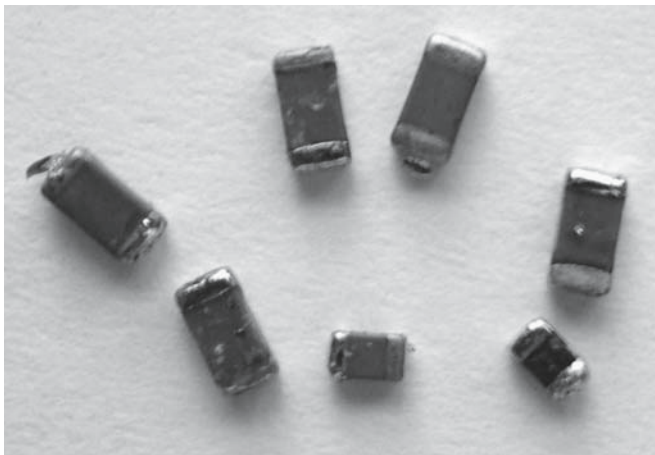
the MLCC. More than 80 billion “chips” are manufactured worldwide each year.

Figure 31.18 shows several MLCCs and a schematic of their structure. The external dimensions range from 1.25 mm × 1 mm × 1 mm thick up to 6 mm × 6 mm × 2.25 mm thick. The interelectrode spacing is typically about 20 μm. Capacitance values have been produced from 1 pF up to 300 μF. Class 1 and class 2 dielectrics are mainly used for MLCCs. Increased performance has been obtained using relaxor dielectrics, such as PFN and PMN.

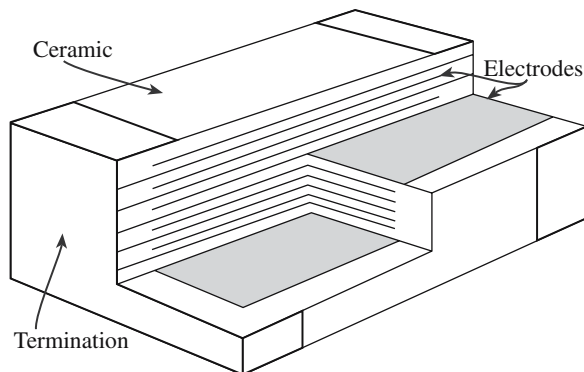
Fabricating MLCCs

There are several different ways to make MLCCs. The basic steps include the following:

- Preparing the slurry. The slurry may contain up to 35 vol% of liquid. Water-based slurries containing a latex binder are often used, although for some powder formulations an organic based slurry is required.
- Tape casting
- Drying
- Cutting dried sheets typically into 15-cm squares



(A)



(B)

FIGURE 31.18 (a) Ceramic MLCC. (b) Schematic showing electrode structure.

- Screen printing Ag–Pd electrodes. The cost of the electrode materials is a big concern. In fact, the noble metals account for more than half the cost price of MLCCs. Alternative nonprecious metals such as copper and nickel have been used. A different approach to reducing the cost of metallization is the “fugitive” electrode process. The electrodes are made of carbon, which is removed during sintering in air. The remaining cavities are then pressure infiltrated with either molten lead or a tin–lead alloy to produce the electrodes.
- Stacking the electroded sheets
- Laminating
- Dicing
- Burning out the binder. This step of the process must be very carefully controlled. There is a lot of binder to be removed and if burnout is too rapid the sheets may delaminate.
- Sintering. Typical sintering temperatures are 1200–1400°C in air. If nonprecious metals are used the furnace atmosphere must be very carefully controlled to avoid oxidation. Atmospheres of N₂ and H₂ + N₂ have been used.
- Application of external electrodes. The ends of the chips can be dipped into an Ag–Pd ink. Pure Ag can be used (which is cheaper), but it must be coated with Ni to increase solder leach resistance and then by Sn to maintain solderability.

31.8 CERAMIC FERROELECTRICS FOR MEMORY APPLICATIONS

An important potential application for ferroelectrics is their incorporation as thin films into dynamic random access memories (DRAMs). The majority of the memory in a computer is DRAM. Information is stored in millions of tiny capacitors, each representing a single bit. The capacitors used in DRAM chips are fabricated directly onto the silicon substrate.

The dielectrics currently used in DRAMs are

- SiO₂, which can be produced by thermal oxidation of Si
- A combination of SiO₂ and Si₃N₄ (which is often referred to as “ONO” because the dielectric consists of alternating layers of SiO₂ and Si₃N₄)

The bottom electrode is the doped (often n-type) silicon substrate; the top electrode is either polysilicon or aluminum. The limitation of both SiO₂ and Si₃N₄ is that they have low κ .

The dielectric constant of SiO₂ is 3.9. A 100-nm-thick SiO₂ film will yield a capacitance of $3.4 \times 10^{-16} \text{ F}/\mu\text{m}^2$ (31 fF/μm²).

The dielectric constant of Si₃N₄ is 6. A 100-nm Si₃N₄ film will yield a capacitance of 53 fF/μm².

To push memory densities beyond 64 Mbits using SiO₂ or ONO dielectrics it has been necessary to develop very complicated three-dimensional structures such as trench capacitors.

Being able to use a dielectric with a large κ would allow a decrease in the required surface area, would avoid stacking and trenching, and would allow planar configurations. Such configurations are easier and cheaper to fabricate and provide high production yields.

Thin films of BST have been the most widely studied dielectric for ferroelectric DRAMs (FRAMs or FeRAMs). The highest capacitance reported for a BST dielectric is 145 fF/ μm^2 , which was achieved with a 20 nm film of a material having $\kappa = 325$. Prototype BST capacitor DRAMs were first reported in 1995, but have not been widely used commercially because of the advances in other storage technologies.

31.9 PIEZOELECTRICITY

Piezoelectricity is a reversible property possessed by a select group of materials that does not have a center of symmetry. When a dimensional change is imposed on the dielectric, polarization occurs and a voltage or field is created. This is the direct effect. When an electric field is applied to a dielectric, polarization may change its dimensions. This is the inverse effect, also called electrostriction. Dielectric materials that display this reversible behavior are piezoelectric.

The ξ produced by the stress T is

$$\xi = gT \quad (31.14)$$

The strain, S , produced by ξ is

$$S = d\xi \quad (31.15)$$

The piezoelectric coefficients d and g are related by Young's modulus, \mathcal{E} :

$$\mathcal{E} = 1/gd \quad (31.16)$$

- High- d coefficients are desirable for dielectrics that are utilized in motional or vibrational devices such as sonar and transducers in ultrasonic cleaners.
- High- g coefficients are desirable for dielectrics used to produce voltages in response to mechanical stress, such as in gas igniters.

The equations of state that describe a piezoelectric crystal in regard to its electric and elastic properties are, in their general form:

$$\text{Direct effect} \quad D = dT + \epsilon^T \xi \quad (31.17)$$

$$\text{Inverse effect} \quad S = s^E T + d\xi \quad (31.18)$$

STRESS AND STRAIN

We use S for the strain and T for the stress (not ϵ and σ , which are more typical) to avoid possible confusion with permittivity, which is almost always represented by ϵ .

The only new variable here is s , the material compliance (inverse of stiffness). The superscripts in Eqs. 31.17 and 31.18 denote the parameters that are held constant. For example,

s^E is the compliance at constant ξ .

When written in matrix form these equations relate the properties to the crystallographic directions. For ceramics and other crystals the piezoelectric constants are anisotropic. For this reason, they are expressed in tensor form. The directional properties are defined by the use of subscripts. For example, d_{31} is the piezoelectric strain coefficient where the stress or strain direction is along the 1 axis and the dielectric displacement or electric field direction is along the 3 axis (i.e., the electrodes are perpendicular to the 3 axis). The notation can be understood by looking at Figure 31.19.

Another important parameter of a piezoelectric is the electromechanical coupling coefficient, k , which is a measure of the ability of the material to convert electrical energy to mechanical energy or vice versa.

For the direct effect

$$k^2 = \frac{\text{mechanical energy converted to electrical energy}}{\text{input mechanical energy}} \quad (31.19)$$

For the indirect effect

$$k^2 = \frac{\text{electrical energy converted to mechanical energy}}{\text{input electrical energy}} \quad (31.20)$$

Since the conversion of electrical energy to mechanical energy (or vice versa) is always incomplete, k^2 is always

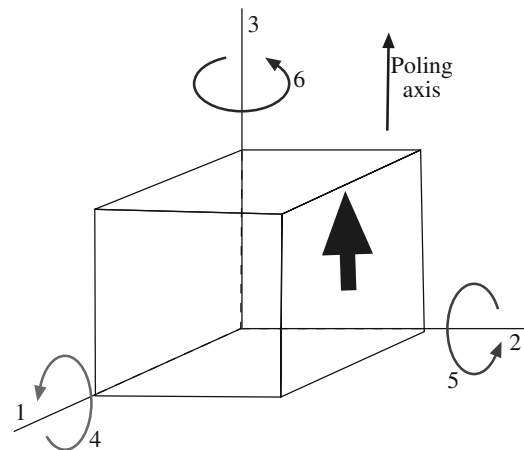


FIGURE 31.19 Notation of axes for a piezoelectric ceramic.

TABLE 31.12 Properties of Some Piezoelectric Ceramics

Material	Piezoelectric constant C/N	Electromechanical coupling factor (<i>k</i>)
Quartz (× cut)	$d_{21} = 2.25 \times 10^{-12}$ $d_{33} = 2.3 \times 10^{-12}$	0.1
BaTiO ₃	$d_{31} = -75 \times 10^{-12}$	0.48
PZT	$d_{33} = 374 \times 10^{-12}$	0.67
Lead metaniobate	$d_{33} = 85 \times 10^{-12}$	0.42
Lithium niobate	$d_{33} = -1 \times 10^{-12}$ $d_{15} = 68 \times 10^{-12}$	0.4
Rochelle salt (45° × cut)	$d_{14} = 870 \times 10^{-12}$	0.78

<1, and so *k* is also <1. Values of *k* in piezoelectric ceramics range from 0.1 to 0.9 as shown in Table 31.12. Rochelle salt is the classic example of a piezoelectric because *k* is so large.

31.10 LEAD ZIRCONATE–LEAD TITANATE (PZT) SOLID SOLUTIONS

Solid solutions between lead zirconate (PbZrO₃) and lead titanate (PbTiO₃) are known by the acronym PZT and are the most widely used of all piezoelectric ceramics.

Lead zirconate is orthorhombic at room temperature: *a* = 0.588 nm, *b* = 1.176 nm, and *c* = 0.820 nm. It is antiferroelectric with $\theta_c = 231^\circ\text{C}$. The dipoles due to the displacement of the Zr⁴⁺ ion from the center of the octahedral site are in opposite directions in adjacent unit cells so that the net *P* is zero.

Lead titanate is isomorphous with BaTiO₃ with *a* = 0.390 nm and *c* = 0.415 nm. It is ferroelectric at room temperature with a $\theta_c = 495^\circ\text{C}$ (the highest known value among perovskite ferroelectrics).

The PZT phase diagram is shown in Figure 31.20. The significant feature of this phase diagram is the morphotropic phase boundary (MPB) at a composition where the

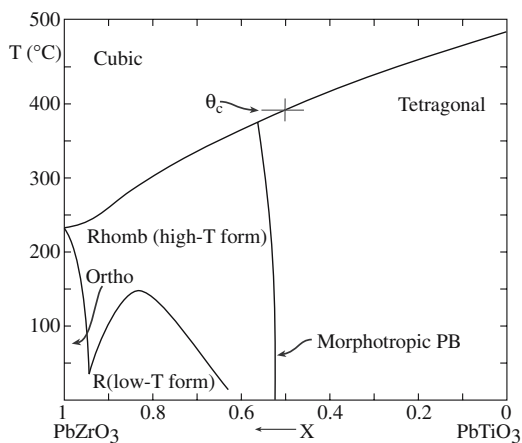


FIGURE 31.20 The PZT phase diagram.

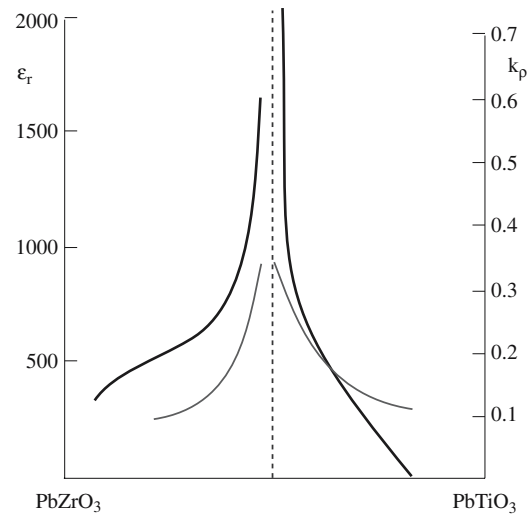


FIGURE 31.21 Dielectric constants and coupling coefficients for PZT compositions near the MPB.

PZ:PT ratio is almost 1 : 1. At an MPB there is an abrupt change in the structure with composition at a constant temperature. PZT compositions near the MPB have both high *k* and high κ as shown in Figure 31.21. This is where commercial PZT compositions are chosen.

PZT ceramics often contain dopants (in the range 0.05 to 5 at%) to modify the properties of the material for specific applications.

Examples:

1. Donors, e.g., replacing Zr⁴⁺ with Nb⁵⁺ or replacing Pb²⁺ with La³⁺. To maintain electroneutrality the addition of these dopants is usually compensated for by the formation of Pb²⁺ vacancies. Donors enhance domain reorientation, and materials produced with these additives are characterized by rectangular hysteresis loops, low *E_c*, high *P_r*, high κ , maximum *k*, high tan δ , high elastic compliance, and reduced aging. Typical applications are in areas in which high sensitivity is required, such as hydrophones, sounders, and loudspeakers.

2. Acceptors, e.g., replacing Zr⁴⁺ with Fe³⁺ with the concomitant formation of oxygen vacancies. Domain reorientation is limited, and hence acceptor additives lead to poorly developed hysteresis loops, lower κ , low tan δ , low compliance, and high aging rates. Typical applications are in high-power devices such as sonar and ultrasonic transducers.

3. Isovalent, e.g., replacing Pb²⁺ with Ba²⁺ or Sr²⁺ or replacing Zr⁴⁺ with Sn⁴⁺. The substituting ion is of the same valence and approximately the same size as the replaced ion. Solid-solution ranges with these additives are usually quite high and may result in lower θ_c . Hysteresis loops may be poorly developed without additional additives. Other properties include lower tan δ , low compliance, and higher aging rates. These ceramics are used in high-drive applications such as torpedo guidance.

PZT ceramics can be made by normal powder processing methods. The main difficulty is the high volatility of PbO. To retain as much PbO as possible sintering may be performed with the component surrounded by a lead-rich powder such as PZ and enclosed in a lidded crucible. Even with these precautions there is usually some (typically 2–3%) loss of PbO, which is compensated for by adding additional PbO to the starting batch. A note about safety: lead is toxic and exposure to lead compounds has a cumulative effect. It is therefore necessary that evaporation is controlled.

**MEDICAL ULTRASOUND IMAGING
FREQUENCY RANGES**

Abdominal, obstetrical, and cardiological applications:
2–5 MHz
Pediatric and peripheral vascular applications:
5–7.5 MHz
Small objects (e.g., the eye) and intracardiac and intravascular applications: 10–30 MHz
As in other forms of microscopy, a higher frequency (lower λ) gives better resolution: $\sim 50\mu\text{m}$ at 30 MHz

**31.11 APPLICATIONS FOR
PIEZOELECTRIC CERAMICS**

Applications for piezoelectric ceramics utilize one of the two piezoelectric effects:

Direct effect—a voltage is produced by means of a compressive stress.

Inverse effect—an applied ξ produces small movements. In an alternating field the piezoelectric will vibrate.

Direct Effect

The first commercial piezoelectric BaTiO₃ devices were phonograph pickups marketed by Sonotome Corporation in the mid-1940s. These used a so-called bimorph design in which an electrode layer separated two strips of the piezoelectric material. Bimorphs are no longer used for this application because they do not produce a high enough quality sound reproduction and most people use CDs now.

The direct effect is used in high-voltage spark generation for some gasoline engine ignition systems and manually operated gas lighters. In the latter example, widely used to ignite natural gas water heaters and other gas-fired domestic appliances, lever-amplified hand pressure generates the voltage. Two electroded piezoelectric cylinders are placed back to back and a force applied to the cylinders generates a spark across the electrodes. If this force is not applied quickly the voltage generated will disappear as the charge leaks away. Typical spark energies are $\sim 3\text{mJ}$.

Indirect Effect

Actuators are an important and growing market for piezoelectric ceramics. In applications requiring precise

mechanical control there is a need for a variety of types of actuators. Examples include the positioning of circuit components during the fabrication of integrated and positioning of lenses and mirrors in precise optical equipment. They are also used as positioners for atomic force microscopy (AFM) and scanning tunneling microscopy (STM).

The natural resonance frequency of a piezoelectric crystal may be used as a frequency standard. Quartz is the material of choice. Quartz crystal resonators provide highly stable crystal-controlled clocks and watches (constant to 1 part in 10⁹) and control fixed frequencies in communications equipment.

Other resonant uses include selective wave filters and transducers for sound generation as in sonar. PZT ceramics also dominate the market for resonators for ultrasonic cleaners and drilling devices.

Piezoelectric transducers are key components in medical ultrasound imaging and are used both as the acoustic source and the detector (pulse-echo technique). The uses for ultrasound are numerous and include examination of the fetus in the mother’s womb as shown in Figure 31.22 and high-resolution imaging of intravascular structures. PZT is the ceramic of choice for this application mainly because it has a high κ and is inexpensive compared to some of the other options such as polymer piezoelectrics.



FIGURE 31.22 Medical ultrasound image using ceramic piezoelectric transducers. (Scale is in centimeters.)

31.12 PIEZOELECTRIC MATERIALS FOR MICROELECTROMECHANICAL SYSTEMS

Microelectromechanical systems (MEMS) are devices capable of sensing and responding to a mechanical or an electrical stimulus. One common MEMS device that is in commercial production is the miniature accelerometer (a device used to measure acceleration) used

to control the deployment of an automobile airbag. Ferroelectric and piezoelectric ceramics are materials that fit well into the field of MEMS because of their combined and related electrical/mechanical properties. The ceramic need not be both ferroelectric and piezoelectric. But if it is ferroelectric then polycrystalline material can be used because it can be poled before use. In nonferroelectric piezoelectric materials such as ZnO it is necessary to use single crystals with a single domain orientation.

The most widely studied ceramics for MEMS applications are the PZTs because of their high κ and high k . Thin films of PZT have been used in the fabrication of a range of different MEMS and can be integrated with silicon IC processing methods. Figure 31.23 illustrates some of the process steps used to fabricate a cantilever beam microsensor such as an accelerometer. The actual processing sequence requires over 50 individual steps.

MEMS APPLICATIONS USING PIEZOELECTRIC THIN FILMS

- Accelerometers
- Acoustic sensors
- Infrared detectors
- Hot-wire anemometers
- Microvalves
- Micropumps
- Stepper motors

PZT films can be prepared using physical vapor deposition (PVD) methods such as sputtering, chemical vapor deposition (CVD), and solution processing. Vapor deposition provides uniform films with good step coverage and uses methods that are standard in microfabrication facilities. However, there is often a problem with obtaining films of the correct stoichiometry because of the high vapor pressure of PbO. Solution techniques such as sol-gel processing are simple and inexpensive and give good stoichiometry control but result in poor step coverage.

31.13 PYROELECTRICITY

Pyroelectric materials exhibit a spontaneous polarization that is a strong function of temperature because the dipole moments vary as the crystal expands or contracts. This was observed in the mineral tourmaline in the seventeenth century. Pyroelectricity occurs in organic crystals such as triglycine sulfate (TGS), ceramics such as LiTaO₃, and polymers such as PVDF.

The electric field developed across a pyroelectric crystal can be extremely large when it is subjected

PYROELECTRICS

LiTaO ₃ (single crystal):	$p = 230 \mu\text{C m}^{-2} \text{K}^{-1}$
(Sr,Ba)Nb ₂ O ₆ (single crystal):	$p = 550 \mu\text{C m}^{-2} \text{K}^{-1}$
PZT (polycrystalline):	$p = 380 \mu\text{C m}^{-2} \text{K}^{-1}$

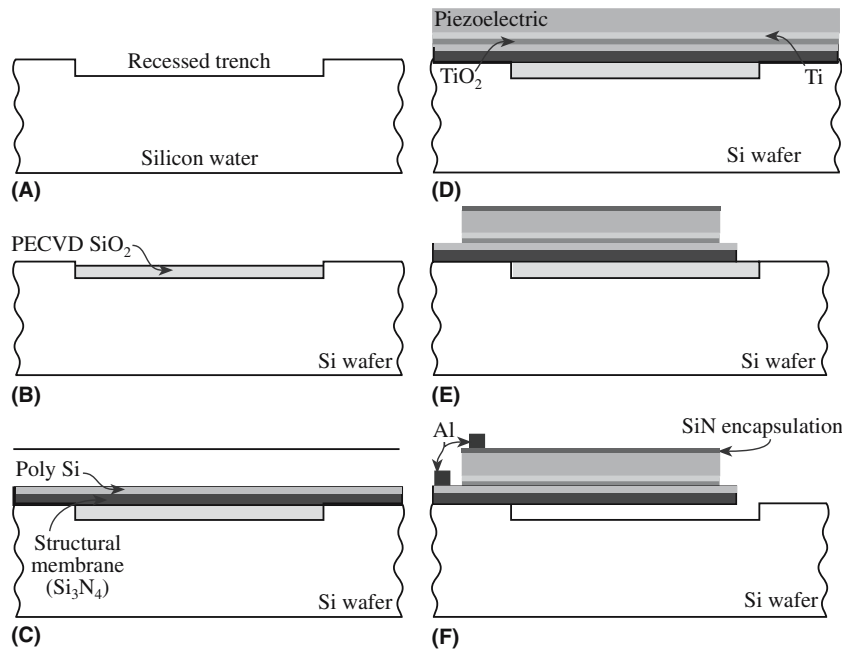


FIGURE 31.23 Steps in the production of a MEMS cantilever. (a) Create trench by etching; (b) deposit SiO₂ layer by pressure-enhanced chemical vapor deposition (PECVD); (c) deposit Si₃N₄ followed by polysilicon; (d) deposit the piezoelectric film on an electrode/diffusion barrier system; (e) pattern and etch; (f) apply metal contacts and sacrificial etch.

to a small change in temperature. A pyroelectric coefficient, p , can be defined as the change in D due to a change in T :

$$p = \frac{\partial D}{\partial T} \quad (31.21)$$

For example, a crystal with a typical pyroelectric coefficient of $10^{-4} \text{C m}^{-2} \text{K}^{-1}$ and $\kappa = 50$ develops a field of 2000V/cm for a 1K temperature change.

31.14 APPLICATIONS FOR PYROELECTRIC CERAMICS

Pyroelectric ceramics can be used to detect any radiation that produces a change in the temperature of the crystal, but are generally used for IR detection. Because of their extreme sensitivity a rise in temperature of less than one-thousandth of a degree can be detected. This property finds application in devices such as intruder alarms, thermal imaging, and geographic mapping.

CHAPTER SUMMARY

The uses of dielectrics range from capacitors for storing charge to ultrasound imaging for medical applications. We separate “dielectrics” from “insulators,” which we described in Chapter 30, because dielectrics have permanent electric dipoles. If the resultant polarization is spontaneous we have ferroelectrics. This topic is essentially exclusive ceramic materials. Although some polymers are ferroelectric they do not find as wide use as ceramics. And metals cannot be ferroelectric because the charge is not localized.

The requirement of a permanent dipole moment limits useful dielectrics to a select few crystal structures. So the topic of crystallography is once again important, but we cannot predict ferroelectricity by considering only crystal structure. The most important of the ferroelectric crystals are perovskites. By now you should be gaining an appreciation of the significance of this crystal structure and we still have some important magnetic perovskites to describe in Chapter 33.

PEOPLE IN HISTORY

- Hankel, Wilhelm Gottlieb (1814–1899) (father of Herman Hankel) proposed the word piezoelectricity in 1881. He taught for 10 years in Halle and then moved to Leipzig in 1849 where he was Professor for 40 years. His thesis was titled “De thermoelectricitate crystallorum”. Pierre and Jacques Curie had discovered piezoelectricity in 1880.
- Seignette, Pierre (1660–1719) was a French pharmacist who first prepared Rochelle salt in c. 1675. In the early literature the phenomenon of ferroelectricity was more often referred to as “Seignette-electricity” or “Rochelle-electricity.”
- Valasek, Joseph (1897–1993) discovered ferroelectricity in the 1920s during an investigation of the anomalous dielectric properties of Rochelle salt, $\text{NaKC}_4\text{H}_4\text{O}_6 \cdot 4\text{H}_2\text{O}$. Rochelle salt is named after the town of La Rochelle (France) where it was first prepared. Valasek was on the faculty at the University of Minnesota from 1919 until he retired in 1965.
- Von Hippel, Arthur Robert (1898–2003) reported the ferroelectric properties of BaTiO_3 in 1946. Since then over a hundred pure materials and many more mixed crystal systems that are ferroelectric have been found. He was on the faculty of MIT from 1936 until he retired in 1964. His starting salary was only \$3,500 per year and he is reported to have sold textbooks to pay for medical bills for his children. The Materials Research Society has named one of its major awards in recognition of von Hippel’s contribution to “dielectrics, semiconductors, ferromagnetics, and ferroelectrics.”

GENERAL REFERENCES

- Jaffe, B., Cook, W.R., Jr., and Jaffe, H. (1971) *Piezoelectric Ceramics*, Academic Press, London. Now a little dated in view of more recent developments in the field. But the basic science remains the same.
- Jona, F. and Shirane, G. (1993) *Ferroelectric Crystals*, Dover, New York. First published by Pergamon Press, Oxford, England and The Macmillan Company, New York in 1962 as Volume I in the International Series of Monographs on Solid State Physics. A comprehensive description of many types of ferroelectric crystal. Somewhat dated: the Dover edition was not updated from the 1962 Pergamon edition.
- Lines, M.E. and Glass, A.M. (1977) *Principles and Applications of Ferroelectric and Related Materials*, Clarendon Press, Oxford.
- Moulson, A.J. and Herbert, J.M. (1990) *Electroceramics*, Chapman & Hall, London. An outstanding and very readable coverage of the entire field of electronic ceramics including applications for capacitors. Highly recommended.

SPECIFIC REFERENCES

Smolenskii, G.A. and Agranovskaya, A.I. (1958) "Dielectric polarization and losses of some complex compounds," *Sov. Phys. Tech. Phys.* **3**, 1380. The first synthesis of PMN relaxors.

JOURNALS AND CONFERENCES DEVOTED TO FERROELECTRIC MATERIALS

The Materials Research Society (MRS) has offered a number of symposia under the title *Ferroelectric Thin Films*.

Integrated Ferroelectrics. An international journal published by Gordon and Breach since 1992 devoted to research, design, development, manufacturing, and utilization of integrated ferroelectrics. These are devices that combine ferroelectric films and semiconductor IC chips.

Journal of Materials Science: Materials in Electronics.

WWW

www.uoguelph.ca/~antoon/gadgets/caps/caps.html

A general site on capacitors: explains that NPO is "negative-positive-zero", and emphasizes that all capacitors are polarized.

EXERCISES

- 31.1 What technique would you use to obtain the data shown in Figure 31.9?
- 31.2 Explain why the hysteresis loops of single crystal and polycrystalline BaTiO₃ shown in Figure 31.10 have different E_c and P_s . Would you expect this behavior?
- 31.3 What would be the appropriate EIA code for a capacitor that is required to have a capacitance at room temperature that changes by no more than $\pm 4.7\%$ in the temperature range -55 to $+125^\circ\text{C}$?
- 31.4 (a) The dielectric strength of lead glass has been measured at two temperatures, 25°C and 200°C . The values obtained are 0.25 MV/cm and 0.05 MV/cm . Explain why these values are different. (b) A similar study was performed using a 100-nm -thick Al₂O₃ film that had been obtained by anodizing Al. The dielectric breakdown was measured to be 16 MV/cm . Why is this value so much higher than that for the polycrystalline Al₂O₃ ceramics listed in Table 31.4?
- 31.5 Describe how you would expect the polarization of the following ceramics to vary as a function of frequency. Start at 1 MHz and go up to visible light frequencies: (a) diamond, (b) Al₂O₃, (c) BaTiO₃, (d) MgO, (e) AlN.
- 31.6 Explain the trend in the hysteresis loops shown in Figure 31.13. Sketch the situation at 150°C .
- 31.7 A parallel plate capacitor is required to store a charge of $50\text{ }\mu\text{C}$ at a potential of 5 kV . The separation between the electrodes is $500\text{ }\mu\text{m}$. Determine the plate area if the following dielectrics are used: (a) mica, (b) MgO, (c) BaTiO₃, (d) Al₂O₃. In each case would the dielectric be able to withstand the applied field?
- 31.8 Estimate the polarization of diamond. Diamond has a diamond-cubic structure with $a = 0.357\text{ nm}$.
- 31.9 Estimate the polarization of MgO. MgO has a rocksalt structure with $a = 0.421\text{ nm}$.
- 31.10 Write out using Kröger–Vink notation the effect of the donor and acceptor additions described in Section 31.10.

Interacting with and Generating Light

CHAPTER PREVIEW

In this chapter we examine four key properties of ceramic materials all of which we can classify as *optical*. (1) Ceramics can be transparent, translucent, or opaque for one particular composition. (2) The color of many ceramics can be changed by small additions: additives, dopants, or point defects. (3) Ceramics can emit light in response to an electric field or illumination by light of another wavelength. (4) Ceramics can reflect and/or refract light. We will discuss why these effects are special for ceramics and how we make use of them.

The optical properties of ceramics result in some of their most important applications. In their pure form, most dielectric single crystals and glasses are transparent to visible light. This behavior is very different from that of metals and semiconductors, which, unless they are very thin ($<1\ \mu\text{m}$), are opaque. Many ceramics and glasses also show good transparency to infrared (IR) radiation. This property has led to the use of glasses for optical fibers for high-speed communications.

We can produce polycrystalline ceramics that are highly transparent. The ability to make translucent and transparent polycrystalline ceramics was developed in the 1960s when it was discovered that small additions of MgO to Al_2O_3 powder could produce a fully dense ceramic by sintering. This product is widely used in streetlights (the golden glow).

If a transparent ceramic or glass is doped, for example, by the addition of transition metal ions, the material becomes colored. We will discuss the different types of colors that can be produced in ceramics. The doping of Al_2O_3 with Cr^{3+} produces ruby, which is used as an optical cavity in a solid-state laser. The ruby laser was the first solid-state laser. There are now many more examples of solid-state lasers using colored ceramics and glasses as the optical cavity. We will describe how solid-state lasers work and the different wavelengths of radiation that can be produced. Phosphors produce light as a result of excitation by, e.g., electron irradiation. Again, we are using doped ceramics for this application because, as we will see, doping changes the electronic band structure of the ceramic.

32.1 SOME BACKGROUND FOR OPTICAL CERAMICS

Electromagnetic Spectrum, the Terminology and Units

Table 32.1 lists some of the major terms, and their units, that we will encounter in this chapter. It also lists the important physical constants that are needed to describe the optical properties of materials. The electromagnetic spectrum embraces a wide range of wavelengths, from the very short γ rays to the long radio waves.

The portion of the spectrum that the human eye can detect is quite small. To put this in context, the full electromagnetic spectrum is

shown in Figure 32.1. Radiation with a single wavelength is referred to as monochromatic; λ and f are related through c :

$$f = \frac{c}{\lambda} \quad (32.1)$$

The frequency never changes regardless of the density of the medium through which the monochromatic light passes; however, the velocity of propagation and λ do change. For a high-density medium, such as glass, the velocity is lower than it would be in a vacuum and, consequently, λ is proportionally smaller. (A dense medium has a lower c .) The light waves are retarded because of the interaction of the electro-

λ AND COLOR

Ultraviolet (UV) is short λ
 Blue is 390 nm
 Green is 550 nm
 Red is 770 nm
 IR is long λ

TABLE 32.1 Terms and Units Used in Optics

Parameter	Definition	Units/value	Conversion factor
λ	Wavelength	m	$1 \text{ \AA} = 10^{-10} \text{ m}$
f	Frequency	Hz	
v	Velocity	m/s	
n	Refractive index	Dimensionless	
Δn	Birefringence	Dimensionless	
c	Speed of light	$2.998 \times 10^8 \text{ m/s}$	
R	Reflected light	Dimensionless	Ratio given by Eq. 32.6
T	Transmitted light	Dimensionless	Ratio given by Eq. 32.2
E_g	Band gap energy	eV	$1 \text{ eV} = 0.1602 \text{ aJ}$
I	Intensity	cd	
ϵ_0	Permittivity of a vacuum	$8.85 \times 10^{-12} \text{ F/m}$	See also Section 31.1
R_∞	Molar refractivity		Directly proportional to electronic polarizability (see Section 31.1)
N_0	Avogadro's number	$6.022 \times 10^{23} \text{ mol}^{-1}$	
r_c	Linear electrooptic coefficient	m/V	
R	Quadratic electrooptic coefficient	m^2/V^2	
P	Polarization	C/m ²	See also Section 31.1
E_c	Coercive field	V/m	

magnetic radiation and the electrons of the atoms that make up the material.

The Nature of Light

Maxwell's equations describe how an electromagnetic wave originates from an accelerating charge and propagates in free space with a speed of $2.998 \times 10^8 \text{ m/s}$. An electromagnetic wave in the visible part of the spectrum may be emitted when an electron changes its position relative to the rest of an atom, involving a change in dipole moment. Light can also be emitted from a single charge moving at high speed under the influence of a magnetic field: because the charge follows a curved trajectory it is accelerating and, as a consequence, radiating. (The same principle is used to produce high-energy X-rays at a synchrotron.)

An electromagnetic wave in free space comprises an electric field **E** and a magnetic induction field **B** that lie in mutually perpendicular directions in a plane normal to

the wave propagation direction as shown in Figure 32.2. Remember that a dielectric material reacts to electromagnetic radiation because the opposite electrical charges are displaced in opposite directions; this dielectric property is the underlying reason for refraction and absorption in glass.

Absorption and Transmission

The classical description of the absorption of electromagnetic radiation by materials indicates that it occurs by two basic mechanisms:

- *Electronic transitions*: electrons are excited from the valence band into unfilled energy states in the conduction band.
- *Absorption*: the light excites vibrational and rotational vibrating modes in the dielectric material since it is associated with an oscillating electric field.

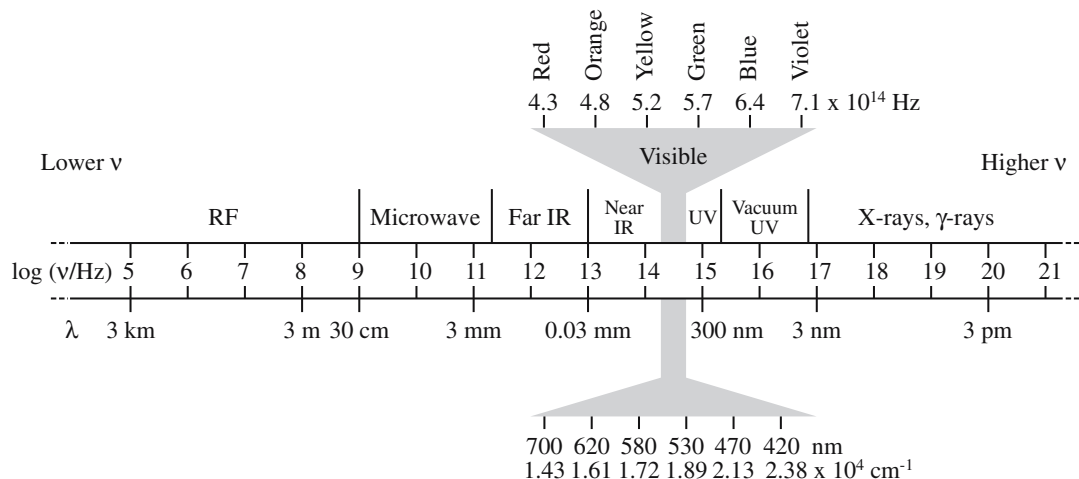


FIGURE 32.1 The electromagnetic spectrum. The visible region has been expanded for clarity. It is actually a very small part of the spectrum.

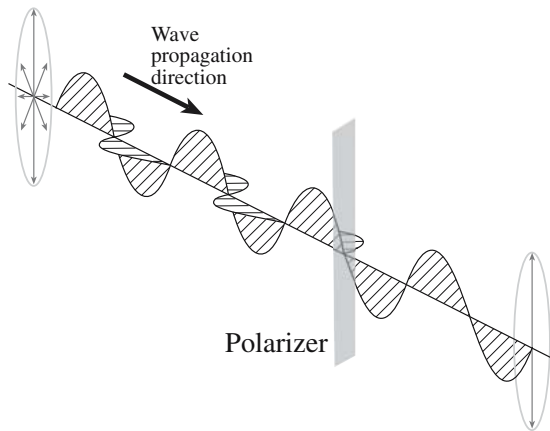


FIGURE 32.2 Polarization of light.

For a single-phase material we can express the fraction of light transmitted, T , as

$$T = I/I_0 = \exp(-\beta x) \quad (32.2)$$

where I is the transmitted intensity, I_0 is the intensity of the incident light, x is the optical path length (the thickness as seen by the light beam), and β is the absorption coefficient. Equation 32.2 is a mathematical representation of Lambert's law, which simply states that the fraction of light that is transmitted by a material does not depend on the intensity of the incident light. The parameter β varies with λ ; this variation is important because it causes color when light is transmitted. If the absorption is due to a particular dopant ion then Eq. 32.2 is modified by setting β equal to ϵC ; C is the concentration of the absorbing ion and ϵ is the absorption per unit concentration. This is the Beer-Lambert law. In real life, we also have scattering by defects in the bulk or at the surface.

Ultraviolet absorption corresponds to electronic transitions from the filled valence band to the unfilled conduction band: the larger E_g is, the greater the range of transparency in the UV. Infrared absorption occurs by elastic vibrations.

Refraction

Refraction is the phenomenon that is responsible for making lenses work. The ratio of the velocity of light in a vacuum to that in any other medium is known as the refractive index, n . Expressed mathematically, n is given by the simple equation

$$n = \frac{c}{c_m} \quad (32.3)$$

where c_m is the velocity of light in the material (the medium). Since c_m is always less than c , values of n are always greater than unity and range from 1.0003 (air) to approximately 3.0 for very dense solids. Clearly n is not a constant for any ceramic, since it depends on c_m ; n is a

function of λ . The variation of n with λ produces a dispersion of the light:

$$\text{Dispersion} = dn/d\lambda \quad (32.4)$$

The ability of a substance to refract or "bend" light waves is sometimes described as refringence. Crystals having one unique axis (optic axis) along which the index of refraction is different from the index along the other orthogonal axes are known as uniaxial birefringent crystals. The magnitude of the difference between the two indices of refraction is referred to as the birefringence, or simply, Δn . It is defined as

$$\Delta n = n_e - n_o \quad (32.5)$$

where n_e is the index of refraction of a light wave vibrating in a plane parallel to the optic axis but traveling in a direction perpendicular to the optic axis, n_o is the index of refraction of a wave vibrating parallel to either of the other axes and traveling in the direction of the optic axis, o is the ordinary ray, and e is the extraordinary ray. The value of the birefringence may be positive or negative. Glass cannot be birefringent because it is isotropic. Ceramics from all noncubic crystal systems do show birefringence.

Ceramic applications of refraction are numerous: from the glass spheres used in road signs to the sparkle in diamonds. The trilobite eye made use of refraction in calcite (Section 32.16).

Reflection

The amount of light reflected from a surface of a material in air is determined by the refractive index of the reflecting medium. At normal incidence, the fraction, R , of light reflected (in medium 1) from the interface between two dielectric materials (1 and 2) is given by Fresnel's equation:

$$R = (n_2 - n_1)^2 / (n_2 + n_1)^2 \quad (32.6)$$

For air ($n_1 \sim 1$) and "optical" glass ($n_2 \sim 1.5$) R is $\sim 4\%$, whereas lead-crystal glass ($n_2 \sim 2.1$) gives an R of $\sim 13\%$. Equation 32.6 will be very important when we use dielectrics as antireflection coatings (ARCs); we then have to consider two interfaces. The thickness of the films and the nature of the reflecting surface will also be important. Ceramic applications of reflection are numerous but are often linked to refraction.

32.2 TRANSPARENCY

Dielectrics generally show good transmission in the visible part of the electromagnetic spectrum as shown in Figure 32.3. In the UV, absorption corresponds to electronic transitions from the filled valence band to the unfilled

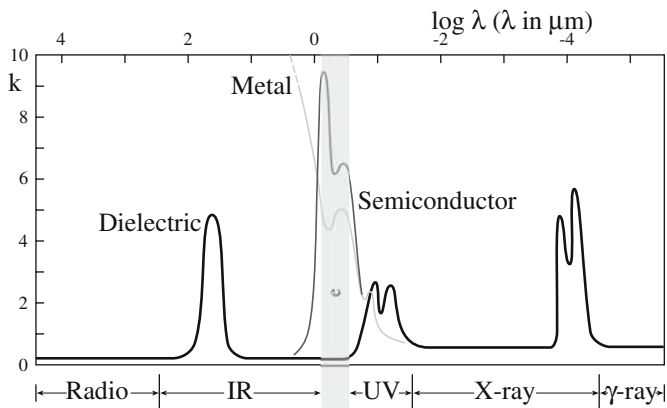


FIGURE 32.3 Comparison of the frequency variation of absorption for metals, semiconductors, and dielectrics. The visible region of the spectrum is shaded.

conduction band. Ceramics with large values of E_g are transparent to shorter UV wavelengths. In the IR, absorption by elastic vibrations is the result of loss of transparency. This absorption occurs at longer wavelengths for materials that contain large ions held together by weak interatomic forces: large ions and weak bonds lead to low frequencies, i.e., small f , which implies large λ , i.e., long wavelength. Transparency in the microwave and radio frequency (RF) region is critical for radomes that house the guidance system on missiles. Ceramics are the only materials that are suitable for this application.

32.3 REFRACTIVE INDEX

Refraction is the bending of a beam of light when it enters a dielectric. The physical reason for this is that the velocity of light is different inside the dielectric. We are used to this happening in water or glass but in crystals the situation can be more complex when crystals are anisotropic. The classic example is calcite, which is illustrated in Figure 32.4.

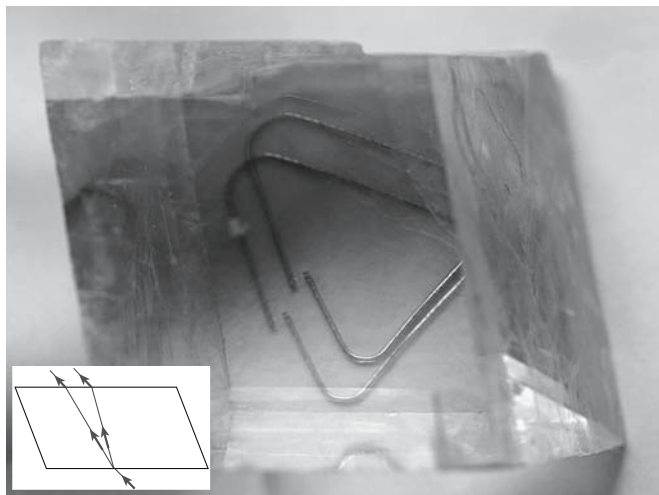


FIGURE 32.4 Birefringence in calcite: two images of one paperclip.

The refractive index of several ceramic materials is given in Table 32.2. We have seen that the value of n is a function of λ . It normally decreases as λ increases and this trend is illustrated for a range of ceramics in Figure 32.5. The reason for this behavior is that colorless solids and glasses have characteristic frequencies in the UV where they become opaque. For example, the important characteristic frequencies for glasses occur at $\lambda \approx 100$ nm. The dispersion as a function of λ for several ceramics is shown in Figure 32.6. Dispersion is important in creating “fire” in gemstones (see Chapter 36). Several factors influence n .

- *Ion size.* Materials containing large ions have large values of n because large ions are more easily polarized than small ions. The Lorentz–Lorentz equation quantifies the relationship between polarizability, α , and n .

TABLE 32.2 Refractive Indices of Some Glasses and Crystals

	Average refractive index	Birefringence
Glass composition		
From orthoclase (KAlSi_3O_8)	1.51	
From albite ($\text{NaAlSi}_3\text{O}_8$)	1.49	
From nepheline syenite	1.50	
Silica glass, SiO_2	1.458	
Vycor glass (96% SiO_2)	1.458	
Soda-lime–silica glass	1.51–1.52	
Borosilicate (Pyrex) glass	1.47	
Dense flint optical glasses	1.6–1.7	
Arsenic trisulfide glass, As_2S_3	2.66	
Crystals		
Silicon chloride, SiCl_4	1.412	
Lithium fluoride, LiF	1.392	
Sodium fluoride, NaF	1.326	
Calcium fluoride, CaF_2	1.434	
Corundum, Al_2O_3	1.76	0.008
Periclase, MgO	1.74	
Quartz, SiO_2	1.55	0.009
Spinel, MgAl_2O_4	1.72	
Zircon, ZrSiO_4	1.95	0.055
Orthoclase, KAlSi_3O_8	1.525	0.007
Albite, $\text{NaAlSi}_3\text{O}_8$	1.529	0.008
Anorthite, $\text{CaAl}_2\text{Si}_2\text{O}_8$	1.585	0.008
Sillimanite, $\text{Al}_2\text{O}_3 \cdot \text{SiO}_2$	1.65	0.021
Mullite, $3\text{Al}_2\text{O}_3 \cdot 2\text{SiO}_2$	1.64	0.010
Rutile, TiO_2	2.71	0.287
Silicon carbide, SiC	2.68	0.043
Litharge, PbO	2.61	
Galena, PbS	3.912	
Calcite, CaCO_3	1.65	0.17
Silicon, Si	3.49	
Cadmium telluride, CdTe	2.74	
Cadmium sulfide, CdS	2.50	
Strontium titanate, SrTiO_3	2.49	
Lithium niobate, LiNbO_3	2.31	
Yttrium oxide, Y_2O_3	1.92	
Zinc selenide, ZnSe	2.62	
Barium titanate, BaTiO_3	2.40	

$$\alpha = \frac{3\epsilon_0 n^2 - 1}{N_0} \frac{M}{n^2 + 2\rho} = \frac{3\epsilon_0}{N_0} R_\infty \quad (32.7)$$

where M is molar weight and ρ is density.

The refractive index of SiO_2 glass can be raised by adding GeO_2 . This has important implications in the fabrication of optical fibers (Section 32.11).

- **Structure.** Less dense polymorphs of a particular material will have a more open structure and thus a lower n than their denser counterparts. We can illustrate this with the case of SiO_2 , which can exist as a glass or in several crystallographic forms: $n_{\text{glass}} = 1.46$, $n_{\text{tridymite}} = 1.47$, $n_{\text{cristobalite}} = 1.49$, and $n_{\text{quartz}} = 1.55$.

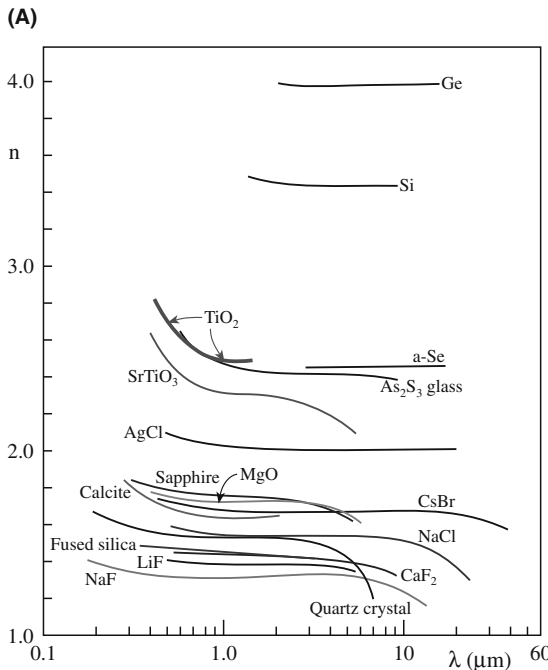
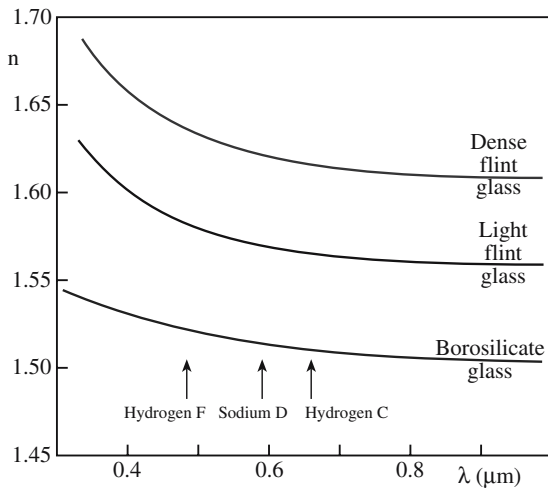


FIGURE 32.5 (a) Change in n with λ for several commercial glasses. (Hydrogen F, Sodium D, and Hydrogen C refer to specific light sources that have $\lambda = 589$, 486 , and 656 nm, respectively.) (b) Change in n with λ for several ceramics and glasses.

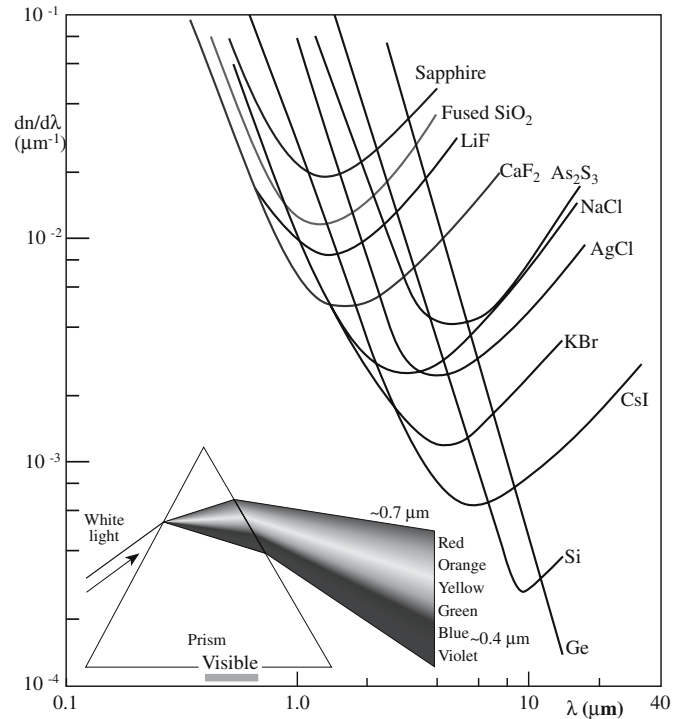


FIGURE 32.6 Dispersion as a function of wavelength for a number of ceramics. The inset is the classic illustration of dispersion, a prism separating white light into its spectral components.

- **Crystallographic direction.** Glasses and crystals with a cubic structure are optically isotropic. In all other crystal systems n is higher along close packed directions.
- **Stress.** The application of tensile stress to an isotropic material causes an increase in n normal to the direction of the applied stress and decreases n along the stressed direction. The situation is the exact opposite if a compressive stress is applied. The change of n with applied stress is known as stress birefringence.

32.4 REFLECTION FROM CERAMIC SURFACES

Using Eq. 32.6 we can determine the reflectivity from the surface of various ceramics and glasses. The reflectivity is about 4% from a surface with $n = 1.5$ and about 10% for a surface with $n = 1.9$. A high reflectivity is often important for aesthetic reasons. The high reflectivity, $R = 13\%$, of lead “crystal” glass, glass that contains a high amount of PbO , is due to its high refractive index, $n = 2.1$. The reflectivity is more than twice that of normal silicate glasses. High reflectivity is important for gemstones, where it affects the brightness and sparkle of the stone. This is partly the result of the cutting skills of the jeweler and the fact that gemstones have high values of n . The refractive index of diamond is 2.4.

High reflectivity for glazes and enamels is also important, and can be achieved by using glass formulations with

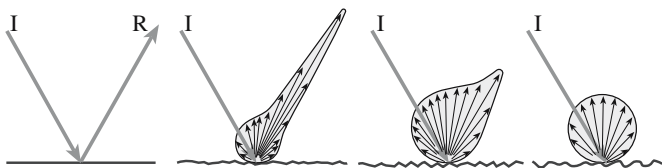


FIGURE 32.7 Effect of surface roughness on reflectivity. I, incident; R, reflected.

a high PbO content. However, it is important to test the formulation carefully to make sure that high concentrations of Pb do not leach out into food and beverage items. (Hence there is a protocol for the leach-testing of glazes; see Section 2.5).

The reflectivity of a glaze or enamel is reduced if the surface is rough. Roughness causes considerable diffuse reflection from the surface as illustrated in Figure 32.7.

- Specular reflection is light reflected at a single angle (conventional reflection).
- Diffuse reflection occurs when light is reflected through a range of different angles.

In some situations we do not want a high reflectivity. In fact, we want to minimize the reflectivity as far as possible. One very

effective way of reducing the reflectivity of a glass surface is to coat it with an antireflection (AR) coating (giving an ARC). A good ARC can cut the percentage of light reflected from $>5\%$ to $<0.2\%$. One example is the purple colored ARC on binocular and camera lens. Catalogs for optical equipment will often indicate whether the lens has an ARC applied. The principle behind how an ARCs works is illustrated in Figure 32.8. The coating is applied onto the glass

A LIGAND
A ligand is any molecule or ion that is bonded to a metal ion.

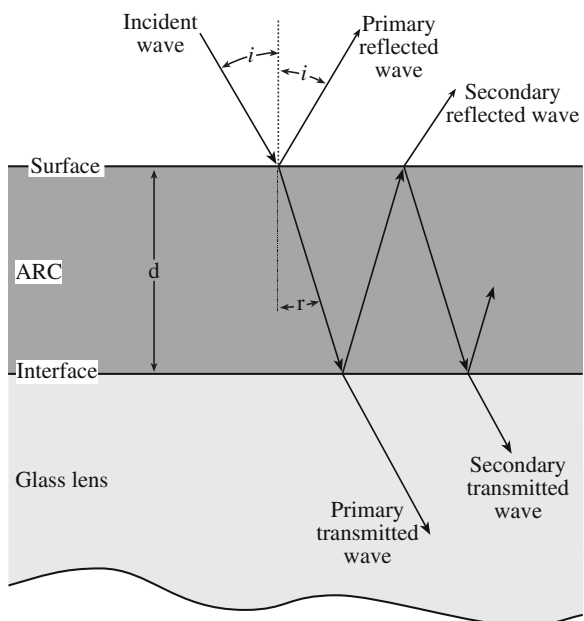


FIGURE 32.8 Illustration of how an ARC works.

surface so that its thickness is one-quarter of the wavelength of the incident light. For an ARC optimized for green light ($\lambda = 530 \text{ nm}$), which is in the center of the electromagnetic spectrum (and where the eye is most sensitive), the thickness of the ARC should be about 130 nm ($0.13 \mu\text{m}$). Light reflected from the top surface of the coating is exactly out of phase with light reflected from the glass surface, and so there is destructive interference and no net reflected beam. Magnesium fluoride (MgF_2) is a widely used ARC material and is usually applied onto the glass surface by a physical vapor deposition (PVD) process such as evaporation. A single layer of MgF_2 ($d = \lambda/4$) will reduce the reflectance of glass from about 4% to a little more than 1% over the visible spectrum. Antireflective coatings are also applied to glass for architectural applications to help with radiation control (see Section 26.7).

32.5 COLOR IN CERAMICS

We discussed colorants in history throughout Chapter 2,

F centers in crystals in Section 11.9, and the origins of color in glass in Section 21.8; we will discuss color more in Chapter 36.

Most dielectric ceramics and glasses are colorless because of their large E_g . They become colored when energy states are added within the band gap. These new levels allow electron transitions to occur within the visible part of the electromagnetic spectrum.

The most common way to color a ceramic is by adding transition metals (TM), particularly Ti, V, Cr, Mn, Fe, Co, and Ni, where the 3d is partly filled.

To explain how the addition of a TM to a colorless ceramic makes it colored we use the ligand field theory. In ceramics the most common ligand is oxygen, the O^{2-} ion. To understand the behavior of a transition metal once it is placed in a ligand field we need to consider the shapes of the d orbitals (see Figure 3.2). There are five of them and they are designated d_{xy} , d_{xz} , d_{yz} , $d_{x^2-y^2}$, and d_{z^2} . In a free ion, all the d orbitals are degenerate (i.e., they have the same energy). However, when the ion is put into a crystal the energy of the d orbitals is affected by the ligands.

Consider the case of the Ti^{3+} ion, which contains only a single 3d electron. If the Ti^{3+} ion is in an octahedral site (i.e., it is surrounded by six anions arranged at the corners of an octahedron) the energy of the $d_{x^2-y^2}$ and d_{z^2} orbitals is raised relative to the free Ti^{3+} ion because of repulsion from the surrounding anions. The energy of the other three orbitals is lowered, as illustrated in Figure 32.9a. If the Ti^{3+} ion were placed in a tetrahedral site (i.e., it is surrounded by four anions arranged at the corners of a tetrahedron), the energy of the $d_{x^2-y^2}$ and d_{z^2} orbitals is lowered with respect to the d_{xy} , d_{xz} , and d_{yz} orbitals. The total splitting for d orbitals is in the range of 1–2 eV, being lower

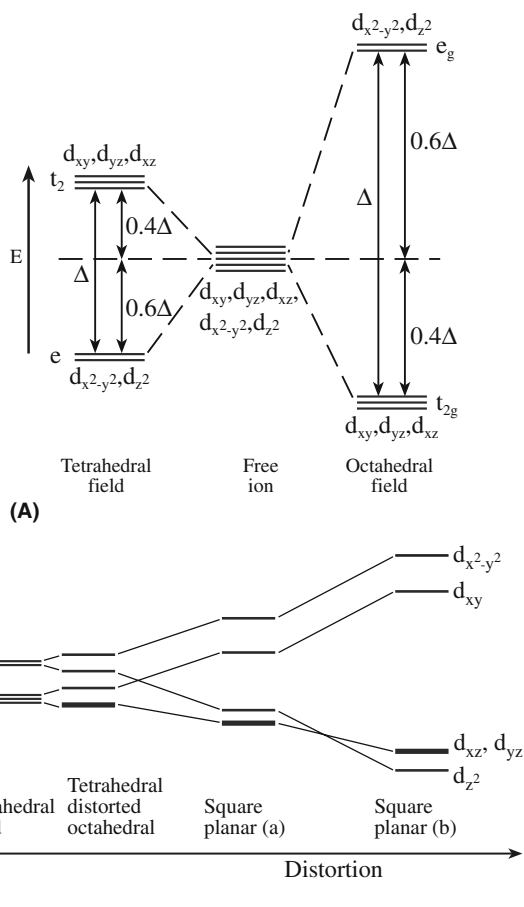


FIGURE 32.9 (a) Splitting of the d orbitals in a ligand field. (b) Splitting of d orbitals in a distorted octahedral ligand field in corundum.

for a tetrahedral ligand field than for an octahedral field. Hence absorption of light, associated with electronic transitions between the lower and upper d levels, generally occurs in the visible or near IR regions of the spectrum.

The situation is actually a little more complicated if we consider corundum, because the octahedral sites are slightly distorted. This distortion produces further splitting of the energy levels as illustrated in Figure 32.9b.

We can use a similar argument to show how the addition of rare earth (RE) elements, with incomplete f shells, also causes color. Table 32.3 shows the colors produced

TABLE 32.3 Optical Absorption of Rare Earth Ions in Oxide Glasses

Ion	Number of f electrons	Color
Ce ³⁺	1	Green
Pr ³⁺	2	Green
Nd ³⁺	4	Violet
Sm ²⁺	6	Green
Eu ²⁺	7	Brown
Dy ²⁺	10	Brown
Ho ³⁺	10	Yellow
Er ³⁺	11	Pink

by the addition of RE ions to oxide glasses. Rare earth ions tend to color glass less strongly than do transition metal ions and the spectra usually consist of a large number of weak bands.

Other sources of color in ceramics include the following:

- F centers in alkali halides, which result from heating in alkali vapor. An F center in metal halides consists of a halide ion vacancy that has trapped an electron. This process creates additional energy levels between the valence band and the conduction band. A similar situation is found in MgO heated in Mg vapor: the F center consists of two electrons trapped at an oxygen vacancy. F centers are one example of so-called color centers in ionic materials involving electrons and holes. (See Section 11.9; F is Farben.)
- Defects produced by X-ray or neutron bombardment. Irradiation of colorless quartz crystals with X-rays will result in the formation of a dark brownish gray to black color of “smoky quartz.” Coloration is due to the formation of a color center, a hole color center this time. If the smoky quartz is heated to several hundred °C it will become clear again.
- Defect states produced as a result of nonstoichiometry. This occurs in, e.g., TiO₂ and ZrO₂.

32.6 COLORING GLASS AND GLAZES

To color glass, TM oxides or RE oxides are added to the glass batch. Color is produced through selective light absorption by the TM or RE ion, which is incorporated into the glass structure. The mechanism essentially uses a solution approach to coloring. The color results when the absorbing ion removes light of certain wavelengths, so we see the complementary color in transmission.

Uses for colored glass include not only the obvious stained glass windows and Tiffany lampshades but also the glazes used to seal and decorate cups and pots. Adding Pb to make X-ray-absorbing glass is essentially the same process/motivation: the intent is to absorb the X-rays.

32.7 CERAMIC PIGMENTS AND STAINS

We color ceramics using inorganic pigments and stains that are relatively insoluble in the ceramic they are coloring; they should also be unaffected chemically and physically. This is not the same approach used for glass.

Table 32.4 shows the types of environment and temperatures that ceramic pigments must withstand. The colorant may be mixed directly with the ceramic body (this is called a body stain). An example is the coloring of

TABLE 32.4 Ceramic Environments for Colors

T (°C)	Environment	Colorant type	Use
700–900	Molten leaded/unleaded borosilicate glass	Enamel or overglaze colors	Tableware, tile decoration
900–1000	Molten lead/unleaded borosilicate or alkali borosilicate glasses	Low-temperature glaze stains, underglaze colors, colored pellets and granules	Tableware, wall and floor tiles
950–1200	Siliceous bodies	Body stains, brick surface colorants, colored pellets and granules	Tableware, floor tiles, fancies, bricks
1100–1350	Molten alkali/lime glasses	Glaze stains	Tableware, tiles, sanitary ware

house bricks—not all house bricks are the same color. If the stain is used to produce a glaze then actually we are coloring a glassy phase and coating the ceramic. An example of this approach is the glazing of sanitary ware and tiles (coloring whitewares). There are several classification systems for ceramic pigments. One of the most widely used is that drawn up by the Color Pigments Manufacturers Association (CPMA), formerly the Dry Color Manufacturers Association (DCMA), in the United States. This system provides a structural classification of pigments as summarized in Table 32.5. Fourteen classes of pigment and over 50 broad pigment subcategories cover all the principal mixed-metal oxide pigments manufactured today. However, it does not cover the full range of possible pigments. For example, nonoxide compounds, such as the Cd-based pigments, are not included.

In the CPMA classification, one commercially important class of pigments is the zircon pigments. Zircon is

PIGMENTS

Much of the information is covered in the patent literature. Zircon–vanadium blue was one of the most significant innovations in color technology for several decades. Seabright was also responsible for the praseodymium yellow and the zircon–iron coral pink.

zirconium silicate, and the first patent for a zircon-based pigment was issued in the 1930s. Zircon pigments fall into two categories.

- Lattice type. The dopant ion replaces a Zr^{4+} ion in the zircon lattice, e.g., vanadium blue (V^{4+} replaces Zr^{4+}) and praseodymium yellow (Pr^{4+} replaces Zr^{4+}).
- Encapsulated type. Discrete particles of the colorant are trapped inside zircon crystals, e.g., the iron coral pink where very fine particles of red Fe_2O_3 are incorporated in zircon crystals.

A different important class of pigments is the family of cadmium pigments. These are substitutional solid solutions between CdS and CdSe (both end members have the same crystal structure). Cadmium sulfide has a band gap $E_g = 2.6\text{ eV}$. This provides absorption of violet and some blue but none of the other colors, leading to a yellow color. CdSe has $E_g = 1.6\text{ eV}$ and is black. When CdSe is added to CdS the band gap of the material decreases and the color changes. This process is analogous to what we do in doping the III–Vs used to make light-emitting diodes (LEDs) in Section 32.12.

The achievable colors range from the yellow of CdS, through orange, to bright red and maroon as the percentage of CdSe is increased (Table 32.6). (The red is known

TABLE 32.5 CPMA Classification of Mixed-Metal Oxide Inorganic Pigments

Pigment system, CPMA number	Main components	Color
I. Baddeleyite 1-01-4	Zr–V	Yellow
II. Borate 2-02-1	Co–Mg	Red-blue
III. Corundum-hematite 3-03-5	Cr–Al	Pink
IV. Garnet 4-07-3	Ca–Cr–Si	Green
V. Olivine 5-08-2	Co–Si	Blue
VI. Periclase 6-09-8	Co–Ni	Gray
VII. Phenacite 7-10-2	Co–Zn–Si	Blue
VIII. Phosphate 8-11-1	Co–Ni	Gray
IX. Priderite 9-13-4	Ni–Ba–Ti	Primrose
X. Pyrochlore 10-14-4	Pb–Sb	Yellow
XI. Rutile-cassiterite 11-15-4	Ni–Sb–Ti	Yellow
XII. Sphene 12-25-5	Cr–Sn–Si	Pink
XIII. Spinel 13-26-2	Co–Al	Blue
XIV. Zircon 14-42-2	Zr–Si–V	Blue

TABLE 32.6 Colors in the CdSe–CdS System

CdSe (mol%)	CdS (mol%)	Color
12.6	87.4	Orange
20.0	80.0	Orange-red
36.0	64.0	Light red
43.0	57.0	Dark red
49.0	51.0	Brown
54.5	45.5	Dark brown

as selenium ruby.) The red color is particularly significant because, for now, the only other additive that can produce the red color in glass is the metal Au. The stability of the selenide pigment is somewhat limited; it will oxidize at 650°C with a resultant loss of color. But if the pigment is encapsulated in a zircon matrix then it has the properties of zircon and is stable to at least 1300°C and is relatively inert in many environments.

A problem, of course, with Cd-containing pigments (like Pb in glass) is the toxicity of Cd. In some countries, e.g., Sweden, home of Orrefors and Kosta Boda, the use of Cd is prohibited. There is increasing pressure worldwide to reduce the use of potentially harmful or toxic species, such as Cd and Pb; there is therefore a growing need for developing suitable alternatives. Even if these additives can be managed during processing, it is difficult to control them during recycling; legislation can be aimed at the initial use (to protect the worker) or at recycling (e.g., so that heavy metals no longer enter the water supply).

32.8 TRANSLUCENT CERAMICS

Polycrystalline ceramics are often opaque, even though the single crystal may be transparent and E_g is large. We can also make glass that is not clear or is even opaque. The loss of transparency is due to scattering of the incident light, which can have several possible causes as illustrated in Figure 32.10.

- *Porosity.* The transmission decreases markedly with small increases in porosity as shown in Figure 32.11.

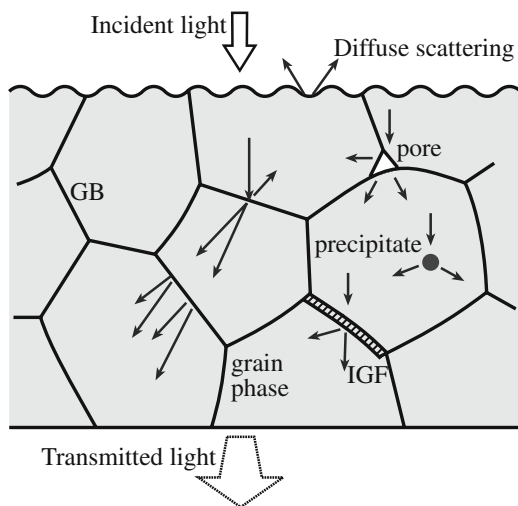


FIGURE 32.10 Mechanisms for loss of transparency due to scattering. GB, grain boundary; IGF, intergranular film. Details of the individual defects are described in Chapters 12–15.

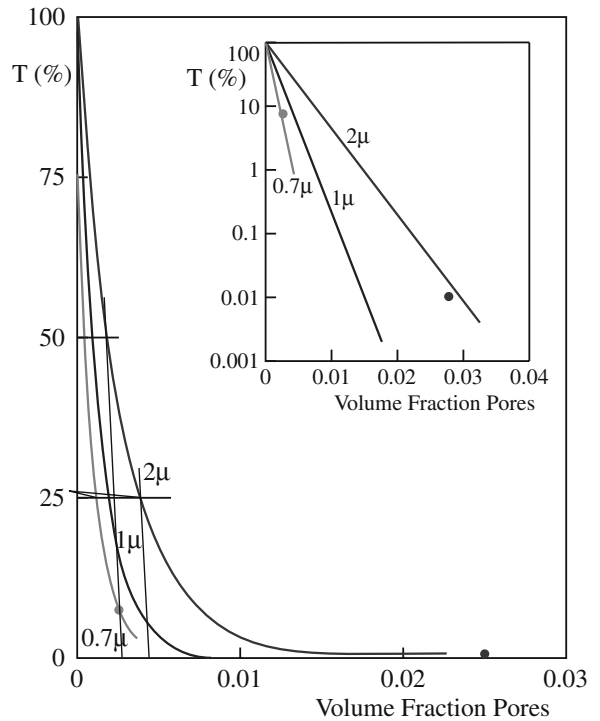


FIGURE 32.11 Effect of porosity on the transparency of polycrystalline alumina.

When the pore size is close to the λ of visible light then the scattering is maximized. This scattering can be engineered by controlling the sintering conditions or by hot pressing. Table 32.7 shows examples of processing conditions that have been shown to produce translucent ceramics.

- *Differences in n .* In general, light scattering can occur at grain boundaries (GBs) where refractive indices are discontinuous; this is especially easy for noncubic (i.e., anisotropic) structures. A similar situation can occur in multiphase materials, such as ceramics densified by liquid-phase sintering, where there may be an intergranular film (IGF). Matching refractive indices between different phases can reduce scattering losses. This approach is used in making high-quality bone china.
- *Grain size, r .* The effect of grain size on scattering is shown in Figure 32.12. Scattering is at a maximum when r is close to λ of visible light. For grain sizes smaller than the wavelength of the incident radiation, the scattering increases with r and is proportional to λ^{-4} . Scattering decreases rapidly as r increases and for large r it reaches a constant value.

The oldest glass objects in museums are opaque. Frosted glass appears to be opaque because light is scattered at the surface.

TABLE 32.7 Sintering Additives and Conditions of Various Translucent Ceramics

Ceramic	Sintering additive (wt%)	Transmissivity (%)	λ (μm) and specimen thickness (mm)	Sintering conditions
Al_2O_3	MgO (0.25)	40–60	0.3 ~ 2 (1)	$T = 1850\text{--}1900^\circ\text{C}$ $t = 16$ hours Atmosphere: H_2
	Y_2O_3 (0.1), MgO (0.05)	70	0.3 ~ 1.1 (0.5)	$T = 1700^\circ\text{C}$ $t = 5$ hours Atmosphere: H_2
	MgO (0.05)	40	~0.9	$T = 1700^\circ\text{C}$ $P = 0.06$ Pa
	Y_2O_3 , La_2O_3 , ZrO_2 (0.1–0.5), MgO (0.55–1.0), MgO (0.05)	80	Visible light (~1)	$T = 1700^\circ\text{C}$ Atmosphere: H_2
CaO	CaF ₂ (0.2–0.6)	40–70	0.4–8 (1.25)	$T = 1725\text{--}1800^\circ\text{C}$ $t = 17\text{--}30$ hours Atmosphere: H_2
				$T = 1200\text{--}1400^\circ\text{C}$ $t = 0.5\text{--}2$ hours $P = 0.5\text{--}0.8$ GPa
MgO	LiF, NaF (1)	80–85	1–7 (5)	$T = 1000^\circ\text{C}$ $t = 15$ minutes $P = 10$ MPa <i>in vacuo</i>
	NaF (0.25)	Clear	Visible light	$T = 1600^\circ\text{C}$ $t = 111$ hours Atmosphere: O_2

32.9 LAMP ENVELOPES

An important application of transparent ceramics is found in the familiar high-intensity yellow streetlights that are common along major highways. These lamps are known as sodium-vapor lamps because during operation they contain sodium vapor that is being heated to a high temperature. Figure 32.13 shows the construction of a typical sodium-vapor lamp. The plasma temperature inside the lamp is 3700°C and the lamp envelope reaches a peak temperature of 1200°C ; the Na vapor pressure is ~ 100 torr.

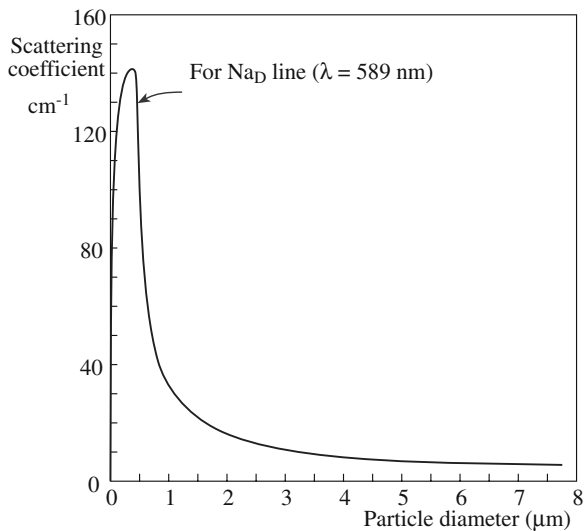


FIGURE 32.12 Effect of particle size on the scattering of light.

The requirements for the envelope material are therefore very stringent: it has to be transparent to visible light, stable at high temperature, and must contain the corrosive Na plasma. It needs to be inexpensive because about 16 million units are made each year. The sodium-vapor lamp was made possible by the development of very dense

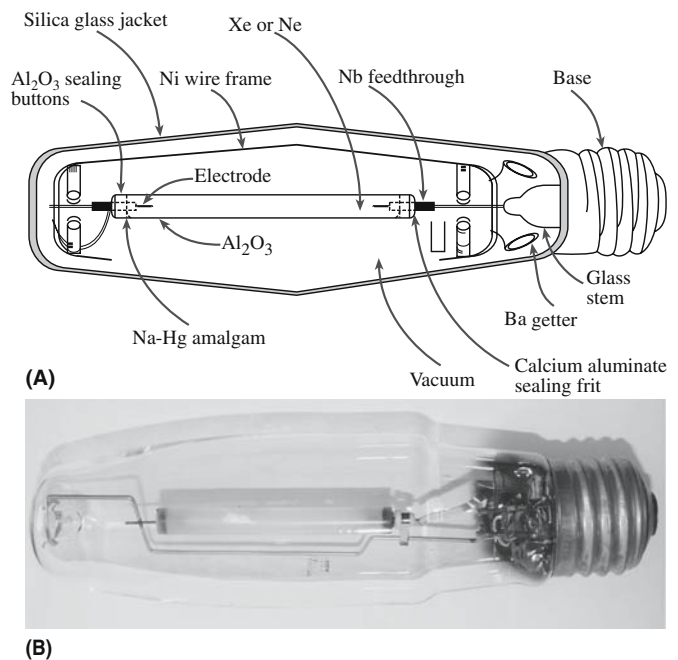


FIGURE 32.13 (a) Construction of an Na-vapor lamp. (b) An actual lamp.

TABLE 32.8 Fundamental Properties of Candidate Lamp-Envelope Materials

Property	Al_2O_3	Y_2O_3	MgO	$3Al_2O_3 \cdot 2SiO_2$	$MgAl_2O_4$	$Y_3Al_5O_{12}$
E_G (eV)	7.4	5.6	>5	≥ 5	>5	>5
σ (S/m)	$<2 \times 10^{-12}$	Low	Low	$<10^{-7}$	Low	Low
α ($10^{-6} K^{-1}$; 300–1300 K)	8.2	7.9	13.5	5.3	9.0	8.6
Strength (MPa)	310	150	206	270	184	410
\mathcal{E} (GPa)	405	164	307	220	277	290
k at 300 K ($W m^{-1} K^{-1}$)	29	13	25	6	15	13
R_{TS}	2707	1508	1242	1389	1077	2137
T_M (K)	2323	2737	3073	2101	2408	2243
Vapor pressure (Pa at 1500 K)	3×10^{-9}	1×10^{-10}	2×10^{-5}	2×10^{-5}	2×10^{-6}	—
Relative emissivity ($-\lambda_{0.75}$) (μm)	5.56	7.9	8.2	4	5.7	5.8

ceramic envelopes that did not contain any light-scattering porosity. The addition of small amounts of magnesia (MgO) allows us to sinter a compact of fine Al_2O_3 powder to theoretical density—free of porosity.

Table 32.8 compares the properties of Al_2O_3 to some of the other materials evaluated as candidate lamp-envelope materials. In addition to satisfying the materials selection criteria given above, Al_2O_3 also has a significant advantage over the other materials listed in Table 32.8 because it has superior thermal shock resistance.

32.10 FLUORESCENCE

Fluorescence occurs when light that is incident on a specimen causes the emission of light of another color; the effect is shown in Figure 32.14. This is most dramatic when the incident light is UV (and the observer is in a darkened room), but it also occurs with other wavelengths. Short wavelength UV is 254 nm; long wavelength UV is 300–388 nm (IR would be >780 nm). The wavelength of the emitted radiation is longer than that of the illuminating light; this is known as Stokes' law of fluorescence. The energy of the emitted light is therefore lower, with the

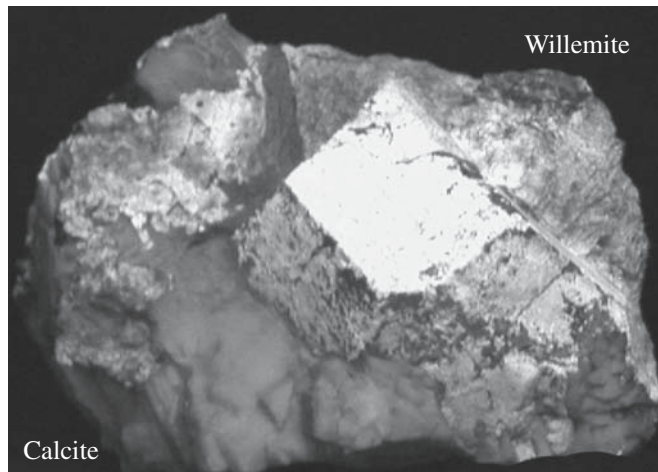


FIGURE 32.14 Fluorescent minerals.

difference in energy causing heating in the sample. Many naturally occurring minerals show fluorescence, but only some are spectacular.

Calcite, halite (with Mn)	red
Fluorite, opal	green
Adamite	yellow/green
Willhemite	green
Scheelite	blue
Scapolite	yellow

Scapolite has a complicated crystal structure and is formed by the alteration of plagioclase feldspars. Incidentally, diamond, sapphire, and ruby all fluoresce, but as with the materials above, the color depends on the UV wavelength used. A given specimen can also show different colors depending on the distribution of impurities. Trace elements can be included in synthetic gemstones to make them fluoresce and thus be easily identifiable.

Phosphorescence. UV radiation excites electrons to a higher energy state. When the UV is removed, the decay to the ground state usually takes seconds but can take years. A material that phosphoresces for 12 hours would have many uses (see Section 32.12).

Flash is the initial color produced when a UV lamp is first directed at certain fluorescent samples. The emitted wavelength then changes as exposure continues.

Thermoluminescence. This is essential fluorescence caused by heating a mineral to allow electrons that are trapped in high-energy states to drop back to the ground state. Heating chlorophane, a variety of fluorite, can produce a green light but only once.

Triboluminescence. Light can be produced by rubbing or striking a ceramic. Fracturing mica or rubbing a sphenite crystal causes light emission.

Cathodoluminescence. Instead of UV radiation, this luminescence is produced by irradiating the sample with electrons (and therefore it usually occurs in a vacuum). This is the phenomenon used in cathode ray tubes (CRTs) (including old TV screens) that were coated on the inside with a ceramic phosphor.

32.11 THE BASICS OF OPTICAL FIBERS

Light is transmitted from one end of an optical fiber to the other by total internal reflection (TIR) as illustrated in Figure 32.15. Modern optical fibers use a composite construction with a core of refractive index n_1 and a cladding with a lower refractive index, n_2 , such that $(n_1 - n_2)$ is typically in the range of 0.005–0.05. Light will remain in the fiber when the critical angle of incidence, i_c , is met or exceeded. To determine i_c we make use of Snell's law (which can be derived from Maxwell's equations):

$$n_2/n_1 = \sin i/\sin r \quad (32.8)$$

At i_c the angle of refraction, r , must be 90° and so we can write

$$n_2/n_1 = \sin i_c/\sin 90^\circ = \sin i_c/1 \quad (32.9)$$

The requirement for TIR sets a limit on the angle of the light incident on the fiber that will be trapped in the core of the fiber. This condition is expressed in terms of the numerical aperture (NA) of the fiber, defined as the sine of the acceptance angle for incident radiation.

$$\sin i_c = (n_2^2 - n_1^2)^{1/2} \quad (32.10)$$

Although light can be transmitted along a glass fiber in air, there are large losses due to scattering arising from surface defects on the fiber. The most important optical fibers consist of a high-purity glass core encased in an equally high-purity cladding. In most cases the cladding is glass, but polymer claddings are also used when a suitable glass cladding is not available or when it is important to reduce costs.

Kao and Hockham suggested the concept of sending optical signals along glass fibers in 1966. Initiated at the Standard Telecommunications Laboratory (STL) in the UK, optical fibers were crossing the Atlantic Ocean by

1988 and the Pacific Ocean by 1996 (but STL had disappeared). The first low-loss fibers were made at the Corning Glass Works. The fibers were made by a CVD process known as outside vapor-phase oxidation (OVPO) and produced an early fiber with a loss of 20 dB/km (which means that 1% of the light remains after traveling 1 km).

Materials

- Processing: how to make the fibers
- Applications: how they work and what goes wrong
- Materials: which glasses to choose

There are four classes of glass optical fiber.

1. Pure fused silica and doped silica glasses are used for telecommunications because of the requirement of very low transmission loss over long distances. These now form the backbone for trunk transmission in most developed countries, and in undersea intercontinental routes, and many millions of kilometers have been installed throughout the world. For applications in laser surgery pure silica-based glass fibers are used as they have a low transmission loss at $1.06\ \mu\text{m}$ and have high strength and durability.

2. Multicomponent oxide glasses such as $\text{Na}_2\text{O}-\text{CaO}-\text{SiO}_2$ (NCS) and $\text{Na}_2\text{O}-\text{B}_2\text{O}_3-\text{SiO}_2$ (NBS) are used for applications requiring light transmission over short distances such as in image bundles, in optical faceplates on CRTs, and in IR imaging devices. The glass is of lower optical quality than silica glass, but can be processed in bulk by conventional melting techniques and is relatively cheap.

3. Fluoride glasses based on $\text{ZrF}_4-\text{BaF}_2-\text{LaF}_3-\text{AlF}_3-\text{NaF}$ (ZBLAN) have been widely investigated because they have potentially very low losses. The ultimate attenuation has been calculated to be $\sim 10^{-2}\ \text{dB/km}$ at $2.5\ \mu\text{m}$. Heavy-metal fluoride glasses are made by melting together high-purity fluoride powders at $\sim 800^\circ\text{C}$ and casting preforms. The impurity levels ($\sim 10-1000\ \text{ppb}$) have meant that the very low losses have not yet been achieved.

4. Chalcogenide glasses based on AsGeS have been investigated. The raw materials used to make these glasses are volatile and so the glasses are usually made in sealed silica ampoules in a rocking furnace. The resulting glass is reasonably stable and can be machined into preforms or drawn in a fiber from the melt.

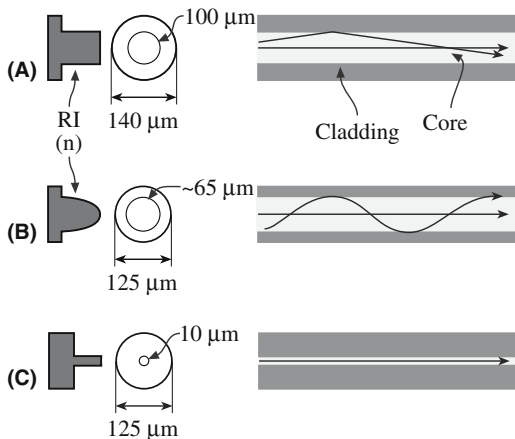


FIGURE 32.15 Total internal reflection (TIR) along an optical fiber. (a) Step index fiber; (b) graded index fiber; (c) single mode fiber. The plot on the left is a variation of RI ($= n$).

Fabrication

Three methods are used to make glass optical fibers:

- Double crucible method
- Rod-in-tube method followed by drawing
- Chemical vapor deposition (CVD) techniques to make preforms followed by drawing

The double crucible method and the rod-in-tube method are used primarily for higher-loss fibers made

from multicomponent glasses, such as those used in imaging bundles. Pure fused silica and doped silica fibers are drawn from a preform that has been made using a CVD process.

The *double-crucible method*: The glasses for the core and cladding are made by melting together the constituent oxides (or fluorides) and then pulling the fiber. This technique is suitable for glasses that have low working temperatures (<1200°C) such as NBS and NCS glasses.

The *rod-in-tube method*: A preform consisting of a rod of the core glass is formed inside a tube of the cladding glass. The preform can be made either by drawing a rod of core glass and a tube of cladding glass from the melt, or by machining a rod and tube from bulk glass. The preform is then drawn into a fiber by elongation in a furnace. Glass is drawn into a fiber when the viscosity is in the range of $10^3 - 10^5$ dPas. The drawing process, which is normally performed vertically downward, is a balance between the downward viscous forces and the surface tension of the molten region.

Several variations of the CVD process are used to make preforms:

- MCVD—modified chemical-vapor deposition
- OVD—outside vapor deposition
- VAD—axial vapor deposition

The MCVD process was developed by Bell Laboratories in the United States and became the standard method. The other processes are very similar except for the details of the geometry. The MCVD process is illustrated in Figure 32.16. The cladding is a tube of pure silica that is

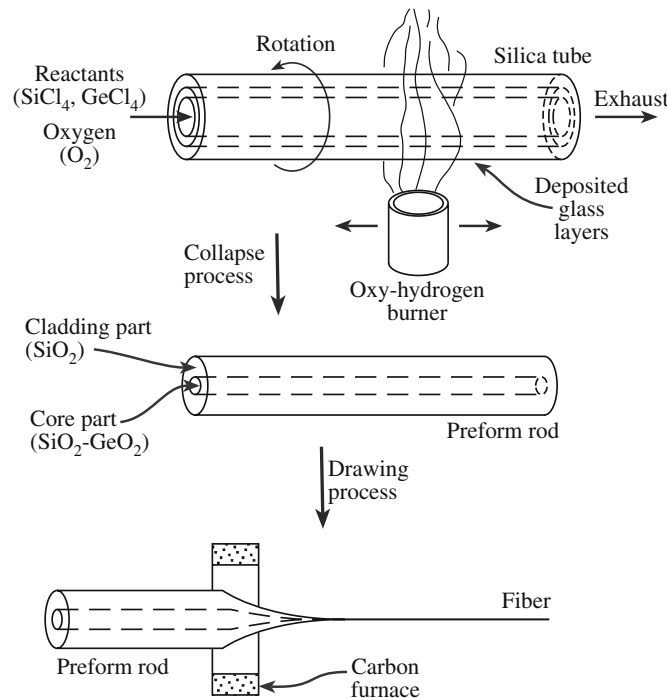
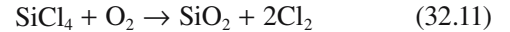
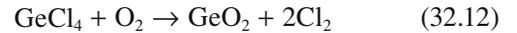


FIGURE 32.16 Steps in the metalorganic chemical vapor deposition (MOCVD) process for forming optical fiber preforms.

mounted in a special lathe. The core, which must have a higher n than the cladding, is formed inside the tube by the following reactions:



and



The burners that traverse the tube heat the vapors and oxidize the halides. Glass particles are deposited on the wall of the tube and are remelted to give clear glassy layers. The deposition rate is typically 1 g/min. When sufficient deposit has been achieved the tube is collapsed to give a preform. The GeO_2 has the effect of lowering n . Adding 10 mol% GeO_2 to pure SiO_2 raises n by 0.012. By varying the ratio of GeCl_4 to SiCl_4 in the gas stream with time it is therefore possible to produce graded-index fibers.

Drawing the Preform

The preform is drawn in a carbon-resistance furnace or zirconia induction furnace; these furnaces can provide the required temperature (>2000°C) while still having a reasonable operating life. The temperature required for drawing optical fibers is much greater than for conventional glass fibers because of their higher purity (the cladding is pure SiO_2). The furnace is mounted in a tall tower with a preform feed-screw mounted above. Drawing is achieved using a capstan, with the fiber being wound onto a drum that can hold several kilometers of fiber. A coating applicator is mounted above the capstan and fibers are coated on-line with a polymer to give mechanical protection. Drawing speeds of >10 m/s are possible in production; the drawing speed is mainly limited by the stability of the polymer coating process. A single preform can yield up to 100 km of fiber. A schematic of a typical fiber drawing apparatus is shown in Figure 32.17.

Silica fibers may be joined in an electric arc. The two ends are aligned and the arc is struck. The fibers are fed toward each other at a controlled rate so they are fused with minimal distortion of the core; joint losses can be very low (<0.1 dB). We then have to polish the ends of the fiber.

Operation

An important characteristic for optical fibers is loss or attenuation. Attenuation in fibers is normally measured in decibels per kilometer (dB/km). The optical loss, in dB, measured over 1 km is written as $10 \log I_{\text{in}}/I_{\text{out}}$ where I_{in} and I_{out} are the input and output optical power.

The optical signal can be attenuated primarily by two factors.

1. *Absorption.* Photons interact with electronic and vibrational transitions in the glass in the UV and IR regions, respectively. In the UV, absorption is due to electronic transitions across the band gap. Absorption occurs at shorter wavelengths for a larger band gap. In the IR, absorption is due to a coupling of the electromagnetic field to lattice vibrations.

2. *Scattering.* Fluctuations in composition and density of the glass occur as it cools down below T_g ; the resulting scattering is a form of Rayleigh scattering. We can describe the intrinsic loss, L , mathematically by

$$L = A \exp(e/\lambda) + B \exp(-g/\lambda) + C\lambda^{-4} \quad (32.13)$$

where A , B , C , e , and g are constants characteristic of the glass. These loss mechanisms combine to give a loss spectrum as shown in Figure 32.18. For silica the minimum loss of 0.15 dB/km occurs at a wavelength of 1.55 μm . ZBLAN is a fluoride glass with even lower loss, 0.02 dB/km at 2.55 μm . These losses are theoretical minima and difficult to achieve in practical situations.

There are many extrinsic sources of loss:

- Absorption caused by transition metal impurities (e.g., Fe, and Cu)

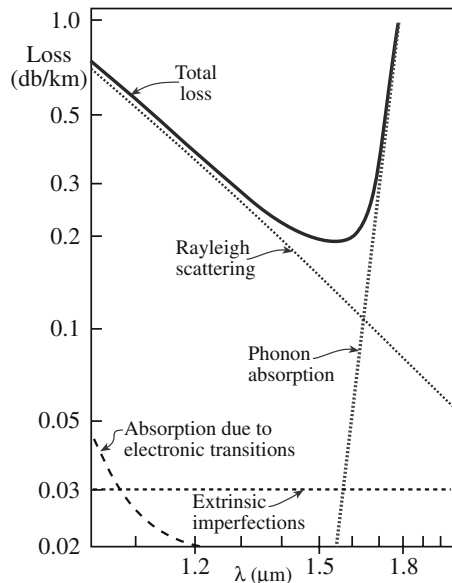


FIGURE 32.18 Loss spectrum for fibers.

- Absorption caused by the OH group
- Scattering caused by defects in the glass such as particulate contamination and bubbles
- Scattering caused by manufacturing defects such as changes in the fiber diameter along its length and frozen-in stresses

The minimum loss in commercial silica fibers used for optical communications is typically 0.2 dB/km at 1.55 μm . In fluoride fibers the lowest reported loss is 0.4 dB/km at 2.35 μm .

32.12 PHOSPHORS AND EMITTERS

When a material is placed in an electric field or irradiated with light, it may itself radiate light: either electric or optical energy is absorbed and optical energy is then radiated. A material that exhibits this phenomenon is called a phosphor and the light radiated is called luminescence (see Section 32.10). Luminescence can be fluorescence or phosphorescence. The difference is the time for which emission occurs.

- Fluorescence occurs very quickly: $<10^{-8}$ s.
- Phosphorescence is slow emission over ~ 1 s or even longer.

Table 32.9 lists the applications of various phosphors.

Light-emitting diodes and III–V lasers are devices that use a direct-band-gap semiconductor to convert electrical energy into visible light. They have long been used for materials with $E_g \sim 1$ eV (the familiar red), but now GaN (with a wider band gap, large v , and smaller λ) gives us a blue emitter.

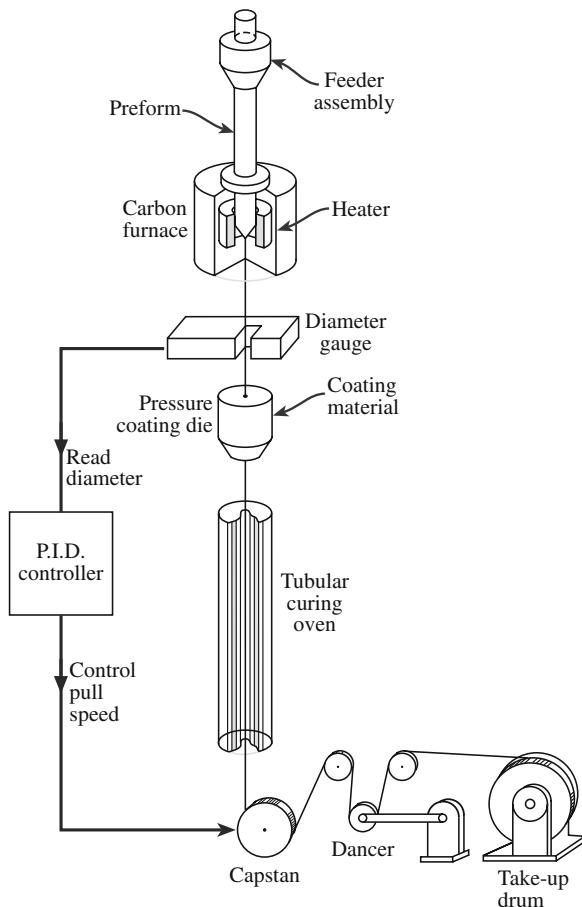


FIGURE 32.17 The fiber drawing tower.

TABLE 32.9 Applications of Various Phosphors

Applications	Excitation methods	Phosphors	Color
Color TV	18–27 kV e-beam	ZnS: Ag, Cl ZnS: Cu, Au, Al Y ₂ O ₂ S: Eu	Blue Green Red
Cathode ray tube	1.5–10 kV e-beam	Zn ₂ SiO ₄ : Mn	Green
Electron microscope	50–3000 kV e-beam	(Zn,Cd)S: Cu, Al	Green
Numerical display	~20 kV e-beam	ZnO	Green
Fluorescent lamps	254 nm UV	Ca ₁₀ (PO ₄) ₆ (F,Cl) ₂ : Sb, Mn	White
Fluorescent Hg lamps	365 nm UV	Y(V,P)O ₄ : Eu	Red
Copying lamps	254 nm UV	Zn ₂ SiO ₄ : Mn	Green
X-ray multipliers	X-ray	CaWO ₄ Gd ₂ O ₂ S: Tb	Blue/white Yellow/green
Scintillators	Radiation	NaI: Tl	Blue
Electroluminescence	10–5 × 10 ac/dc	ZnS: Cu, Mn, Cl	Green
Solid-state lasers	Visible light (near UV – near IR)	Y ₃ Al ₅ O ₁₂ : Nd (YAG)	IR

32.13 SOLID-STATE LASERS

The word “laser” was originally an acronym for “light amplification by the stimulated emission of radiation”; now it is just a word—so there is no capitalization. A laser produces coherent (in phase) monochromatic (single λ) radiation. It consists of the active medium, called the optical cavity, which in the case of a solid-state laser is an insulating crystal or glass containing a specific dopant. The optical cavity is typically 10 cm long and 1 cm in diameter. One end is coated to form a partially transparent mirror while the other end is fully reflecting. The operation of the laser is based on electronic excitation of the active medium using a pump source, which is usually a flash lamp or flash tube, as shown in Figure 32.19, or another laser. The excited electrons relax back to the ground state by emitting light. As light is reflected to and fro between the mirrors it is amplified.

The two most important solid-state lasers are:

1. The ruby laser uses a single crystal of Al₂O₃ containing about 1.6×10^{19} Cr³⁺/cm³. The active electronic states are d levels of the Cr³⁺.

NOTATION

$^4I_{11/2}$ is an example of a term symbol having the form $^{2S+1}L_J$, which is used to describe arrangements of electrons in orbitals. The superscript is $2S + 1$ where S is the overall spin $S = \sum m_s$. The symbol is the overall $L = \sum m_l$. The subscript is a quantum number, J , that considers spin-orbit coupling; J has values from $L + S$, $L + S - 1$, to $|L - S|$.

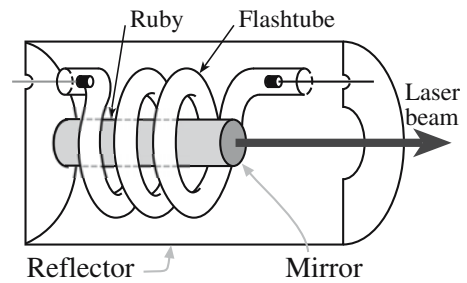


FIGURE 32.19 Schematic of the components of a ruby laser.

2. The Nd–YAG laser uses a single crystal of Y₃Al₅O₁₂ containing 1.4×10^{20} Nd³⁺/cm³. The active electronic states are the f levels of Nd³⁺.

The properties of the ruby and Nd–YAG laser are summarized in Table 32.10. The Cr³⁺ transition is a three-level system: the laser transition returns the electrons to the ground state. The emission occurs in the red part of the visible spectrum ($\lambda = 694$ nm). The Nd³⁺ transition is a four-level system: emission occurs near 1.06 μ m and the terminating state lies above the

TABLE 32.10 Characteristics of Typical Solid-State Laser Crystals

Crystal	Active center	Concentration of active centers (cm ⁻³)	Spontaneous fluorescence lifetime	Wavelength
Ruby	Cr ³⁺	1.6×10^{19}	3 ms	694.3 nm
YAG: Nd	Nd ³⁺	1.4×10^{20}	230 μ s	1.061 μ m, 1.064 μ m, 1.839 μ m (77 K), 0946 μ m (77 K), 1.318 μ m
NaF–(F ₂ ⁻)	(F ₂ ⁻) color center	2×10^{17}	40 ns	Tunable, 0.99–1.22 μ m
Nd _{0.5} La _{0.5} P ₅ O ₄	Nd ³⁺	2×10^{21}	150 μ s	1.05 μ m

ground state. The four-level system is shown schematically in Figure 32.20.

Doped oxide glasses are also used as the optical cavities in solid-state lasers. A wide range of dopants and glasses can be used as indicated in Table 32.11. The advantages of using glass as a laser medium is that glass is optically isotropic and producible in a variety of sizes and shapes of high optical quality. In addition, its chemical composition can be varied to tailor laser parameters for specific applications. However, because the thermal conductivity of glass is usually poor compared to its crystalline counterparts, glass lasers are limited to pulsed and low average-power operation. Crystalline lasers are more appropriate for continuous and high-average-power operation.

POLING
 Poling is the process of polarizing a ferroelectric material by applying a high electric field for a short time.

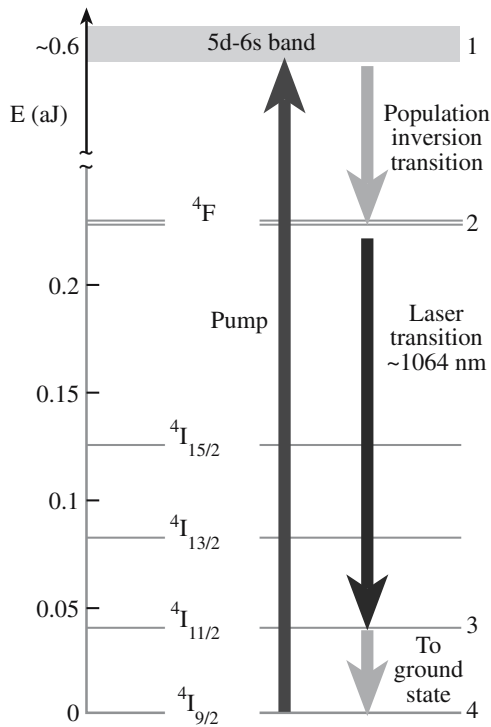


FIGURE 32.20 The four-level system for lasers.

32.14 ELECTROOPTIC CERAMICS FOR OPTICAL DEVICES

Electrooptic Effect

By applying an E field the optical properties, especially n , of electrooptic (EO) materials can be changed. Many transparent solids and liquids show EO effects, but only a few of these are useful for practical applications.

If an electrooptic ceramic is noncentrosymmetric then δn is proportional to E . Examples of such materials include piezoelectric crystals and some poled ferroelectric ceramics; this is known as the linear or Pockels effect. If the material is initially centrosymmetric, then δn is proportional to E^2 ; this is known as the quadratic or Kerr effect.

Such materials include isotropic crystals, unpoled ferroelectric ceramics, and all liquids.

We saw in Section 32.1 that EO materials are birefringent: i.e., they have two orthogonal optic axes that are characterized by different indices of refraction; Δn is referred to as the birefringence in Eq. 32.5. The value of Δn may be positive or negative. If an E field is applied parallel to one optic axis, then one refractive index is changed with respect to the other. As a result Δn is changed and the state of polarization of light propagating through the material is altered. Quadratic EO materials are not generally birefringent unless they are subjected to a properly aligned E field.

The general relationship between Δn and E is

$$\Delta n = n^3(r_c E + R E^2) \quad (32.14)$$

Table 32.12 lists the values of r and R for several EO ceramics. The higher the EO coefficient, the lower the applied voltage necessary to perform a particular function.

TABLE 32.11 Glass Laser Ions and Hosts

Ion	Transition	Wavelength (μm)	Sensitizer	Host glasses
Nd ³⁺	⁴ F _{3/2} → ⁴ I _{9/2}	0.92		Borate, silicate (77 K)
	⁴ F _{3/2} → ⁴ I _{11/2}	1.05–1.08	Mn ²⁺ , UO ₂ ²⁺	Borate, silicate, phosphate, fluorophosphates, germanate, tellurite, fluoroberyllate
	⁴ F _{3/2} → ⁴ I _{13/2}	1.32–1.37		Borate, silicate, phosphate
Tb ³⁺	⁵ D ₄ → ⁷ F ₄	0.54		Borate
Ho ³⁺	⁵ I ₇ → ⁵ I ₈	2.06–2.08	Yb ³⁺ , Er ³⁺	Silicate
Er ³⁺	⁴ I _{13/2} → ⁴ I _{15/2}	1.54–1.55	Yb ³⁺	Silicate, phosphate, fluorophosphate
Tm ³⁺	³ H ₄ → ³ H ₆	1.85–2.02	Yb ³⁺ , Er ³⁺	Silicate
Yb ³⁺	² F _{5/2} → ² F _{7/2}	1.01–1.06	Nd ³⁺	Borate, silicate

TABLE 32.12 Electrooptical Properties of Several Ceramics

Material	κ	n at 633nm	r_e m/V	R m^2/V^2
Ceramic				
PLZT 8.5/65/35	5000	2.50	—	38.6×10^{-16}
PLZT 9/65/35	5700	2.50	—	3.8×10^{-16}
PLZT 9.5/65/35	5500	2.50	—	1.5×10^{-16}
PLZT 8/70/30	5400	2.48	—	11.7×10^{-16}
PLZT 8/40/60	980	2.57	1.02×10^{-10}	—
PLZT 12/40/60	1300	2.57	1.20×10^{-10}	—
PLZT 14/30/70	1025	2.59	1.12×10^{-10}	—
Single crystal				
LiNbO ₃ (r_{33})	37	2.20	0.32×10^{-10}	—
LiNbO ₃ (r_{13})	37	2.29	0.10×10^{-10}	—
BaTiO ₃ (r_{33})	373	2.36	0.28×10^{-10}	—
BaTiO ₃ (r_{51})	372	2.38	8.20×10^{-10}	—
KNbO ₃ (r_{33})	30	2.17	0.64×10^{-10}	—
KNbO ₃ (r_{42})	137	2.25	3.80×10^{-10}	—
Strontium barium niobate ($T = 560$ K)	119	2.22	0.56×10^{-10}	—
Strontium barium niobate ($T = 300$ K)	3400	2.30	13.40×10^{-10}	—
Ba ₂ NaNb ₅ O ₁₅	86	2.22	0.56×10^{-10}	—

Solid Solutions in the PLZT System

The most important EO ceramics are solid-solution phases in the PbZrO₃-PbTiO₃-La₂O₃ system known collectively as PLZT materials.

- The general chemical formula is $Pb_{1-x}La_x(Zr_zTi_{1-z})_{1-x/4}O_3$.
- The structure of PLZT is based on the perovskite, ABO₃ (see Section 7.3).

The linked network of oxygen octahedra has B ions (Ti⁴⁺, Zr⁴⁺) occupying the sites within the oxygen octahedra (B sites) and A ions (Pb²⁺, La³⁺) situated in the interstices (A sites) created by the linked octahedra. When off-valent ionic substitutions are made into this structure (e.g., La³⁺ for Pb²⁺) electrical neutrality is automatically maintained by the creation of A-site or B-site vacancies.

The PLZT phase diagram at room temperature is shown in Figure 32.21. The compositions are specified by three successive numbers, e.g., 8.5/65/35, which represent, from left to right, the La, Zr, and Ti atomic concentrations.

Ferroelectric PLZT ceramics possess crystalline phases that belong principally to the tetragonal and rhombohedral crystal systems. These materials are classified as uniaxial, because they have two or more crystallographically equivalent directions lying in a plane that is perpendicular to the 4-fold (tetragonal case) or 6-fold (rhombohedral case) axis. They are also optically negative (i.e., $n_e - n_o < 0$), with Δn values typically ranging from about -0.018 to near zero. These

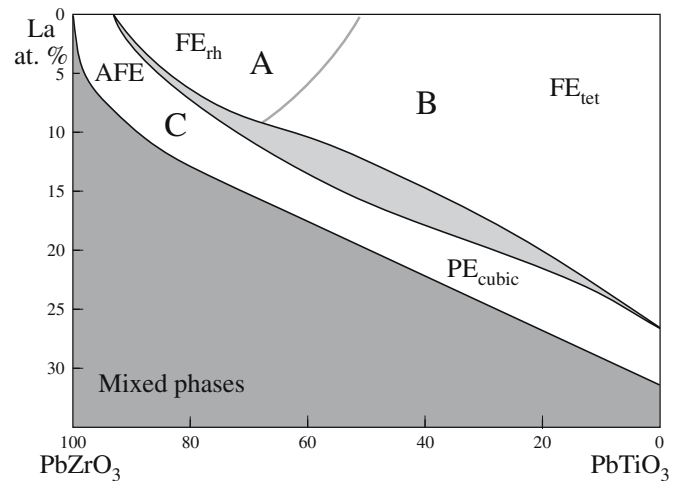


FIGURE 32.21 The PLZT phase diagram. A, memory; B, linear; C, quadratic.

PLZT COMPOSITION

When expressed as 8.5/65/35, the PLZT contains 8.5 at% La and the Zr/Ti ratio is 65/35.

values are low because of the low distortion of the unit cell. In their ferroelectric (FE) state the polar *c* axis is typically only about 1% longer than the *a*

axis, which is why domain reorientation is easy in these materials. Domain reorientation produces a change in the optical properties. The magnitude of the observed EO effect is dependent on both the strength and direction of the *E* field.

PLZT ceramics display optically uniaxial properties on both a microscopic and a macroscopic scale once polarized. The optic axis coincides with the polarization.

TABLE 32.13 Transparent Electrooptical Ceramics

Composition	Notation	Composition	Notation
(Pb,La)(Zr,Ti)O ₃	PLZT	(Pb,La)(Hf,Ti)O ₃	PLHT
(Pb,Ba,Sr)(Zr,Ti)O ₃	PBSZT	(Pb,Sn)(In,Zr,Ti)O ₃	PSIZT
(Pb,Ba,La)Nb ₂ O ₆	PBLN	(Pb,La)(Zn,Nb,Zr,Ti)O ₃	PBLNZT
K(Ta,Nb)O ₃	KTN	Pb(Sc,Nb)O ₃	PSN
(Pb,La)(Mg,Nb,Zr,Ti)O ₃	PLMNZT	(Ba,La)(Ti,Nb)O ₃	BLTN
(Pb,La,Li)(Zr,Ti)O ₃	PLLZT	(Sr,Ba)Nb ₂ O ₆	SBN

The macroscopic or effective birefringence is designated by $\overline{\Delta n}$. On a macroscopic scale, $\overline{\Delta n}$ is equal to zero before electrical poling and has some finite value after poling, depending on the composition and the degree of polarization. The $\overline{\Delta n}$ value is an important quantity because it is related to the optical phase retardation, Γ , of the material.

The phenomenon of optical phase retardation in an EO poled ceramic occurs when entering linearly polarized monochromatic light is resolved into two perpendicular components c_1 and c_2 . Because of the different refractive indices, n_e and n_o , the propagation velocity of the two components will be different and will result in a phase shift or “retardation.” Γ is a function of both $\overline{\Delta n}$ and the path length t :

$$\Gamma = \overline{\Delta n}t \tag{32.15}$$

Although at present PLZT is the most important EO ceramic, there are other transparent ceramics that exhibit EO characteristics; some of these are listed in Table 32.13. Many of these ceramics are based on solid solutions in the lead zirconate–lead titanate (PZT) system and are structurally related to PLZT. Notable exceptions are the niobates, such as KTN (potassium tantalum niobate or $\text{KTa}_{1-x}\text{Nb}_x\text{O}_3$ with $x \sim 0.35$), which are also based on the perovskite structure. NTT has shown n for KTN changing by a factor of 20× the change produced in LiNbO_3 using an applied field of 60 V/mm² (achieved by applying 1.2 V across a 20- μm sample), but the limiting factor is the growth of high-quality crystals.

Electrooptic Characteristics of PLZT Ceramics

Depending on composition PLZT ceramics display one of the three major types of EO characteristics shown in Figure 32.22.

1. *Memory.* The P versus E hysteresis loop is narrow, indicating low E_c . This characteristic occurs for the rhombohedral FE phase; a typical composition is 8/65/35. The EO memory effect depends on the fact that $\overline{\Delta n}$ can be set to different values by applying (and removing) an E field. Once set, $\overline{\Delta n}$ remains constant as long as $E = 0$. The vari-

ation of $\overline{\Delta n}$ is usually plotted in terms of the normalized remnant polarization P_r/P_R because P_r is an easily measured parameter that depends on domain switching. Intermediate remnant states can be achieved by removing the applied E field prior to reaching E_c .

2. *Linear* (Pockels effect). This effect is characterized by a square hysteresis loop having a large E_c . It occurs for tetragonal type compositions at the PbTiO_3 -rich end of the solid-solution range such as 8/36/60. $\overline{\Delta n}$ is linear with respect to E ; from a practical point of view, grain size has a very significant effect on the linearity.

3. *Quadratic* (Kerr effect). A slim hysteresis loop with zero, or very low P_r , is obtained between the FE and paraelectric (PE) compositions; a typical composition is 9.5/65/35. At room temperature they are essentially cubic, but the application of E enforces a transition to the rhombohedral or tetragonal FE phase, and the optical anisotropy increases with E^2 .

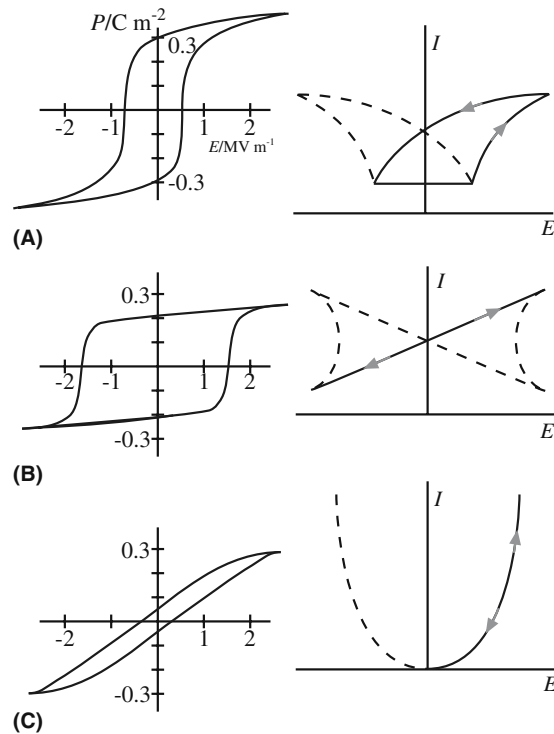


FIGURE 32.22 Electrooptic characteristics of PLZT: (a) memory, (b) linear, (c) quadratic. I is the light output versus applied field E (see A, B, and C in Figure 32.21).

Making Transparent PLZT Ceramics

For a ceramic to be useful as an EO material it must be transparent. In single-crystal form ferroelectric materials possess high optical transparency and useful EO properties. In the form of polycrystalline ceramics they can also possess such properties if special precautions are taken during processing. To create a transparent ceramic it is necessary to limit the amount of sources that can lead to light scattering (the main culprits were discussed in Section 32.8). Hot pressing can produce a high-density product with low porosity. If the pore size is reduced to a value less than the wavelength of light ($\lambda_{\text{yellow}} \sim 0.5 \mu\text{m}$) then the pores will have only a minor scattering effect. The presence of impurities can be reduced by using high purity starting materials or by preparing the powders by a sol-gel process using metal alkoxides (see Chapter 22). The use of liquid or solution techniques also helps to ensure good intermixing between the various components. As noted above, for noncubic materials light scattering can occur at GBs, where refractive indices are discontinuous. In PLZT the optical anisotropy is reduced by doping with La, which brings the ratio between c and a lattice parameters close to unity.

Applications Using PLZT Electrooptic Ceramics

There are several applications for EO ceramics and two basic modes of operation for EO devices.

- Transverse—the E field is applied in a direction normal to the light propagation direction.
- Longitudinal—the E field is applied along the light propagation direction.

Linear materials are used primarily for high-speed modulation of the intensity, amplitude, phase, frequency, or direction of a light beam. Quadratic materials are used principally for light valves and shutters.

Here we will briefly describe four applications for PLZT ceramics.

1. Flash goggles are used by military pilots to prevent them from being blinded by a very bright flash! The arrangement consists of three components as illustrated in Figure 32.23. Under normal illumination the PLZT plate allows the plane of polarization to be turned by 90° when a voltage of $\sim 800 \text{ V}$ is applied to the interdigitated gold electrodes. The light passes through the analyzer and into the pilot's eyes. An intense flash of light is detected by a photodiode that forms part of the circuit connected to the PLZT plate, and removes the voltage applied to the electrodes. The plane of polarization of the incident light is not rotated and the analyzer blocks most of the light. The switching times are $\sim 100 \mu\text{s}$ and transmission ratios are 1000:1. For this application the PLZT is a slim-loop

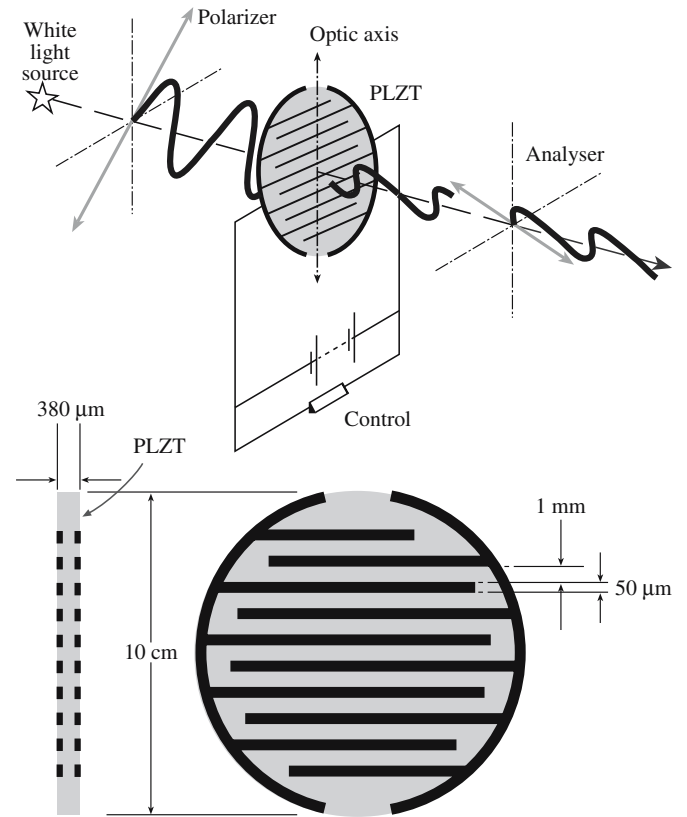


FIGURE 32.23 Illustration of the operation of flash goggles and the interdigitated electrode arrangement.

quadratic material of typical composition 9.2/65/35, with almost zero birefringence when $E = 0$.

This application uses an arrangement similar to that used for a voltage-controlled color filter. Now a variable voltage is used that determines what part of the visible spectrum is blocked. When the applied voltage is zero no light is transmitted. At the voltage at which the green light is retarded by $\lambda/2$ “white” light is transmitted (i.e., green plus part of everything else). Further increases in the voltage produce conditions at which the blue is extinguished resulting in the transmission of yellow light (i.e., red and green are transmitted). In a similar way voltage conditions can be reached at which either the red or the green is excluded and the resulting colors are transmitted. Again the PLZT is of the slim-loop quadratic variety.

2. PLZT elements can be used in reflective displays as shown in Figure 32.24. P_1 and P_2 are polarizers that are set up in the parallel position. When no voltage is applied to the indium tin oxide (ITO) electrodes, light passes through both polarizers and the PLZT plate and is reflected from the reflecting surface into the eye. If a voltage ($\sim 200 \text{ V}$) is applied to the PLZT the light experiences a retardation of $\lambda/2$ and is extinguished at P_2 . The activated segments appear dark against a light background. The PLZT is again of the 9.5/65/35 type, so it has a slim-loop quadratic. PLZT displays are much more expensive and

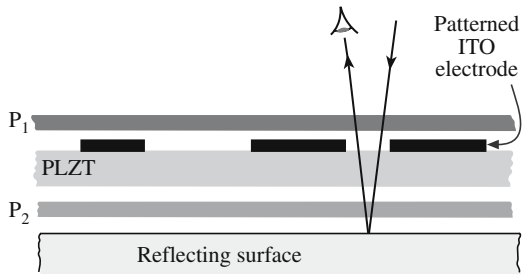


FIGURE 32.24 Basic layout of a PLZT reflective display.

require much higher operating voltages (>100 V) than the liquid crystal variety, but offer faster switching times. The main applications are in military and automotive markets.

3. Figure 32.25 shows an image storage device using PLZT that operates on the basis of light scattering by domain boundaries in the unpoled material. The PLZT is of the memory type with a composition 7/65/35 and a grain size of $\sim 4.5 \mu\text{m}$. To start, the device is uniformly irradiated and the PLZT is poled to P_r . The image to be stored is focused onto the photoconductive film (e.g., CdS or ZnS) while a voltage ($\sim 200 \text{ V}$ and opposite to that of the poling voltage) is applied across the transparent electrodes. This causes regions of the ferroelectric to become depoled. The image can then be read by passing light through the plate and focusing the unscattered light so that it passes through an aperture and onto a film. Regions that have become depoled scatter the light to a greater extent than the poled regions. Repoling the PLZT can erase the display.

4. Optical signals in telephone systems are routed by first converting them to their electronic equivalents, switching them electronically, and then reconverting them to the optical form. Thin-film optical switches allow the process of switching to be done optically, avoiding the need for electronic conversion. An example of a thin film optical switch using PLZT is shown in Figure 32.26. The PLZT layer can be deposited onto the sapphire substrate by a variety of methods including sputtering, CVD, and sol-gel. The lattice mismatch between the (0001) plane of sapphire and (111) plane of the PLZT is quite small ($\sim 2\%$), and this facilitates the formation of an epitaxial layer with the planar relationship $(0001)_s \parallel (111)_{\text{PLZT}}$.

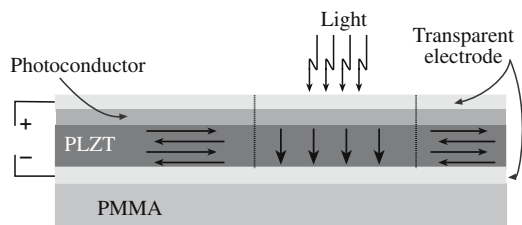


FIGURE 32.25 Schematic of an image storage device using a field-induced polarized PLZT film.

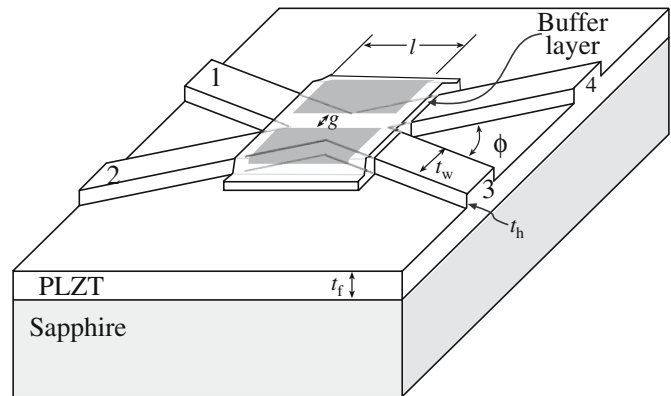


FIGURE 32.26 An example of a PLZT thin film optical switch on sapphire.

When there is no voltage applied to the metal electrodes light entering at 1 will exit at 3. If a large enough voltage V is applied, total internal reflection (TIR) of the light will occur between the electrodes causing the signal to now exit at 4. TIR occurs because the voltage reduces n .

The critical angle for TIR is

$$\theta_c = \sin^{-1}(1 - 0.5n^2RV^2) \quad (32.16)$$

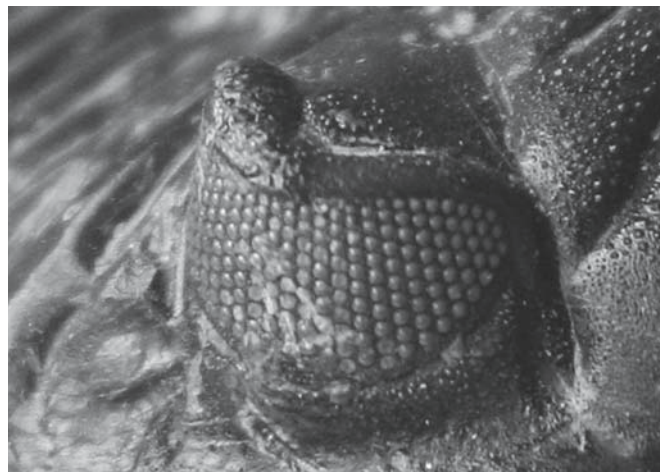
The change in n causing TIR is regarded as being due to the Kerr effect. If we use a 9/65/35 quadratic PLZT with $R = 380 \text{ nm}^2/\text{V}^2$, $n = 2.5$, and with a 2° angle between the guides (i.e., $\theta_c = 88^\circ$) then the switching voltage is 1.4 V.

32.15 REACTING TO OTHER PARTS OF THE SPECTRUM

So far we have concentrated on how ceramics interact with light in the UV, visible, and IR parts of the spectrum. This emphasis is because these interactions are often the most useful and the ones that we are likely to notice. The response of ceramics to γ -rays is becoming of increased interest because of their use for radiation detectors (primarily aimed at locating radioactive material that might be used for “dirty bombs”). Ceramics have long been used to detect high-energy radiation. One example is Tl-doped NaI used as a scintillation detector on early X-ray diffractometers. The thallium causes the crystal to fluoresce in the violet part of the spectrum ($\lambda = 420 \text{ nm}$). The goal is to make lower cost devices that can be portable, for example, incorporated into pagers and cell phones.

The basic requirements of a scintillator for γ -rays are as follows:

- High light yield (>20 k photons generated per incident γ -ray)
- A fast response time (<100 ns)
- High density and high Z
- Scintillation λ matches that of the light sensor (usually an Si diode or photomultiplier)



(A)

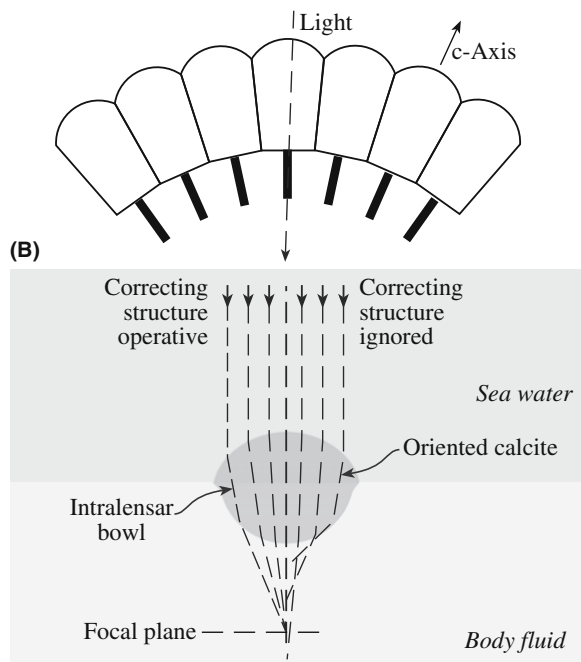


FIGURE 32.27 Trilobite eye.

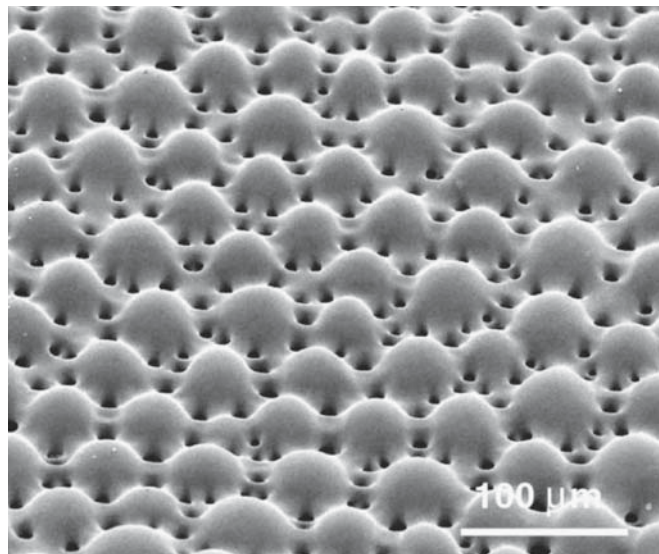
Ce-doped YAG (which is yellow) is one ceramic that meets these requirements and the estimated cost for single crystals is $< \$0.05 \text{ mm}^{-3}$.

32.16 OPTICAL CERAMICS IN NATURE

We will use many of the concepts introduced in this chapter when we discuss gemstones in Chapter 36. Nature does make use of these concepts in surprising ways. Figure 32.27 shows the eye of a trilobite. Trilobites existed for over 300 million years. The eye

ECHINODERMATA

This is a group of animals that includes sea urchins and sea stars, one of which is the brittlestar (*Ophiocoma wendtii*).



(A)

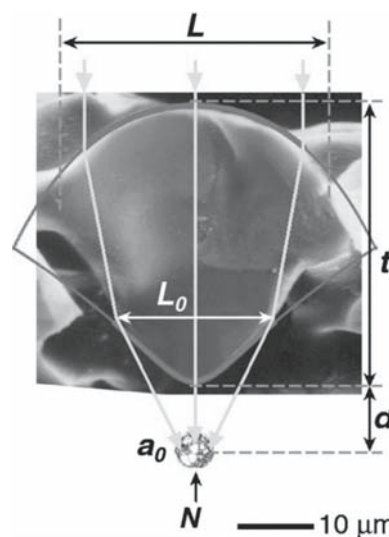


FIGURE 32.28 The brittlestar lens: (a) plan view of an array; (b) cross section.

shown here is an array of calcite crystals, which direct the light to a point. So at least some of the trilobites could see because their eyes were inorganic crystals. We may think of this as being an oddity because the trilobites are extinct (although they did survive for ~ 300 million years). However, it has now been shown that brittlestars use a similar structure to detect light. The scanning electron microscopy (SEM) image in Figure 32.28 shows an array of calcite lenses on the surface of the dorsal arm plate.

The cross section through one of these lenses demonstrates how the light is focused onto the nerve and even how the spherical aberration is corrected.

CHAPTER SUMMARY

At the simplest level the optical properties of ceramics are critical to society because glass is transparent, diamonds are not opaque, the development of television required phosphors, nearly all lighting depends on glass, the future of communications relies on glass fibers and periodic amplifiers, etc. Microscopy developed using glass lenses and led to our understanding of biology. We tend to use color when glazing (or there are no patterns). The general idea is that light affects and is affected by the electrons in the ceramic and this interaction is determined by the bonding in the ceramic. The interaction actually causes the speed of light to change inside a ceramic. The key properties of the material are then described by average quantities such as the dielectric constant and the refractive index. Crystallography comes in again because many ceramics are anisotropic; one particularly well-known case is calcite.

PEOPLE IN HISTORY

- Coble, R.L. (Bob) (1928–1992) developed Lucalox[®], a transparent polycrystalline alumina (Al₂O₃) ceramic, at the GE laboratory in Schenectady in 1961; GE is still a major supplier of lamp envelopes but Sylvania, Osram and others also manufacture the envelopes now.
- Maxwell, James Clerk (1831–1879) developed the electromagnetic wave theory of light.
- Seabright, Clarence A. (1914–2002) in the United States was one of the key contributors to the development of ceramic pigments: (1948) Ceramic Pigments, US Patent 2,441,367; (1961) Yellow Ceramic Pigments, US Patent 3,012,898; (1965) Iron Ceramic Pigment, US Patent 3,166,430.
- van Royen, Willebrod Snell (1581–1626), the Dutch scientist, first described Snell's law; the derivation is given in standard textbooks on electromagnetism (Panofsky and Philips, 1961) or optics (Born and Wolf, 1970).

GENERAL REFERENCES

- Aggarwal, I.D. and Lu, G. (Eds.) (1991) *Fluoride Glass Fiber Optics*, Academic Press, Boston. Contains a series of chapters written by leading experts in the field detailing the structure, processing, and properties of fluoride glasses and their application as optical fibers and use in other optical devices.
- Agulló-López, F., Cabrera, J.M., and Agulló-Rueda, F. (1994) *Electrooptics: Phenomena, Materials, and Applications*, Academic Press, London. Gives a very detailed description of all aspects of electrooptic materials. Two of the chapters cover applications. It also provides information about how electrooptic coefficients are determined experimentally.
- Born, M. and Wolf, E. (1970) *Principles of Optics*, 4th edition, p. 110, Pergamon, Oxford. Standard optics text.
- Haertling, G.H. (1991) "Electrooptic ceramics and devices", in *Engineered Materials Handbook Volume 4: Ceramics and Glasses*, ASM International, p. 1124. Haertling and Land (1971) developed the PLZT system of transparent ferroelectric ceramics.
- Kingery, W.D., Bowen, H.K., and Uhlmann, D.R. (1976) *Introduction to Ceramics*, 2nd edition, Wiley, New York. Chapter 13 covers the optical properties of ceramics and glasses.
- Moulson, A.J. and Herbert, J.M. (1990) *Electroceramics*, Chapman & Hall, London. Covers the entire field of electronic ceramics. Chapter 8 is devoted to electrooptic ceramics. Highly recommended.
- Robbins, M. (1994) *Fluorescence*, Geoscience Press Inc., Phoenix, AZ. Many examples including color illustrations and a comprehensive bibliography.
- Taylor J.R. and Bull, A. (1986) *Ceramics Glaze Technology*, Pergamon, Oxford. Great book for information on glazes with examples.
- Warren, T.S., Gleason, S., Bostwick, R.C., and Verbeek, E.R. (1999) *Ultraviolet Light and Fluorescent Minerals: Understanding, Collecting and Displaying Fluorescent Minerals (Rocks, Minerals and Gemstones)*, Gem Guides Book Co.

SPECIFIC REFERENCES

- Aizenberg, J. and Hendler, G. (2004) "Designing efficient microlens arrays: Lessons from nature," *J. Mater. Chem.* **14**, 2066. This and the earlier papers make fascinating reading.
- Burchfield, R.W. (1998) *The New Fowler's Modern English Usage*, revised 3rd edition, Clarendon Press, Oxford, p. 371. Explains why we prefer electrooptic.
- Coble, R.L. (1961) "Sintering crystalline solids: I. Intermediate and final stage models; II. Experimental test of diffusion models in powder compacts," *J. Appl. Phys.* **32**, 787.
- DCMA (1982) *Classification and Chemical Description of the Mixed Metal Oxide Inorganic Colored Pigments*, 2nd edition, Metal Oxides and Ceramic Colors Subcommittee, Dry Color Manufacturers Association, Arlington, VA. Now called the Color Pigments Manufacturers Association (CPMA).

- Haertling, G.H. and Land, C.E. (1971) "Hot-pressed (Pb,La)(Zr,Ti)O₃ ferroelectric ceramics for electrooptic applications," *J. Am. Ceram. Soc.* **54**, 1. This is the original citation for transparent PLZT ceramics.
- Kaiser, P. (1973) "Spectral losses of unclad fibers made from high-grade vitreous silica," *Appl. Phys. Lett.* **23**, 45. Developed the MCVD process.
- Kao, K.C. and Hockham, G.A. (1966) "Dielectric-fiber surface waveguides for optical frequencies," *Proc. IEE* **113**, 1151.
- Kapron, F.P., Keck, D.B., and Maurer, R.D. (1970) "Radiation losses in glass optical waveguides," *Appl. Phys. Lett.* **17**, 423. Report of the first low-loss optical fibers.
- Kerr, J. (1875) *Wied. Ann.* **18**, 213. The "Kerr" effect.
- Miyauchi, K. and Toda, G. (1975) "Effect of crystal-lattice distortion on optical transmittance of (Pb,La)(Zr,Ti)O₃ system," *J. Am. Ceram. Soc.* **58**, 361. Doping PLZT with La to reduce the optical anisotropy.
- Nassau, K. (1980) *Gems Made by Man*, Chilton Book Company, Radnor, PA.
- Nassau, K. (1983) *The Physics and Chemistry of Color: The Fifteen Causes of Color*, Wiley, New York. The classic book on the sources of color in ceramics.
- Panofsky, W.K.H. and Phillips, M. (1961) *Classical Electricity and Magnetism*, Addison-Wesley, Reading, MA.
- Pockels, F. (1884) *Abh. Gottinger Ges. d. Wiss.* **39**, 169. The "Pockels" effect.
- Tilley, R. (2000) *Colour and the Optical Properties of Materials*, Wiley, New York. Strongly recommended.

WWW

Saphikon (www.saphikon.com) gives current examples of using alumina fibers in medicine.

EXERCISES

- 32.1 Explain why BaTiO₃ is a linear electrooptic material below T_c but a quadratic electrooptic material above T_c .
- 32.2 PLZT ceramics belonging to either the tetragonal or rhombohedral crystal systems are classified as optically uniaxial. Which other crystal system or systems are also optically uniaxial?
- 32.3 Several methods have been used to produce PLZT thin films. Try to find as many methods as you can and discuss the pros and cons of each.
- 32.4 Prior to the development of transparent alumina ceramics the material of choice for the lamp-envelope market was silica-based glass. Explain why such materials are not suitable for use in the sodium vapor lamp but dominate the incandescent, fluorescent, and electric discharge lamp-envelope market.
- 32.5 With the increasing demand for optical fiber communication systems new glass and fiber processing methods are being investigated. One such example is the sol-gel route for silica fibers. What advantages do you think the sol-gel route would offer over the present CVD processes? Can you think of any disadvantages of the sol-gel route?
- 32.6 The single crystals required for solid-state lasers are often made by the Czochralski process. Describe the advantages and disadvantages of using this process for producing single crystals of ruby and YAG.
- 32.7 Explain briefly why the transparency range of single crystal NaCl is much greater than for single crystal MgO.
- 32.8 Why are house bricks different colors? (You can answer this in 2 minutes or 2 hours.)
- 32.9 How is the numerical aperture (NA) of a fiber linked to the NA of a camera lens?
- 32.10 What causes refraction in glass?

Using Magnetic Fields and Storing Data

CHAPTER PREVIEW

If you were asked to give an example of a magnetic material instinctively you would probably say iron. It is a good example, but in its pure form iron is not a very useful magnet. Ceramics can be magnetic too and they were the first magnets known to humans. About 600,000t of ceramic magnets are produced each year making them, in terms of volume, commercially more important than metallic magnets. The largest market segment is hard ferrites (permanent magnets) that are used in a range of applications including motors for electric toothbrushes and windshield wipers in automobiles, refrigerator door seals, speakers, and stripes on the back of the ubiquitous credit and ATM cards. Soft ferrites can be magnetized and demagnetized easily and are used in cell telephones, transformer cores, and, now to a somewhat lesser extent, magnetic recording.

Ferrite is a term used for ceramics that contain Fe_2O_3 as a principal component.

Magnetism has probably fascinated more people, including Socrates and Mozart (listen to *Così fan tutte*), over the years than any other materials property. For over four thousand years the strange power of magnets has captured our imagination. Yet it remains the least well understood of all properties. In this chapter we will start by describing some of the basic characteristics of magnetic materials, which often contain one of the first row transition metals, Fe, Co, or Ni. The electron arrangement in the 3d level of these atoms is the key. The manganates are a very interesting class of magnetic ceramic. Although they are not new, the recent discovery that they exhibit colossal magnetoresistance (just like the giant magnetoresistance observed in metal multilayers only *much* bigger) has renewed interest in these materials. Structurally the manganates are very similar to the high-temperature superconductors (HTSCs). The similarity may be more than coincidental.

33.1 A BRIEF HISTORY OF MAGNETIC CERAMICS

Applications of magnetism began with ceramics. The first magnetic material to be discovered was lodestone, which is better known now as magnetite (Fe_3O_4). In its naturally occurring state it is permanently magnetized and is the most magnetic mineral. The strange power of lodestone was well known in ancient times. In c. 400 BCE Socrates dangled iron rings beneath a piece of lodestone and found that the lodestone enabled the rings to attract other rings. They had become magnetized. Even earlier (~c. 2600 BCE) a Chinese legend tells of the Emperor Hwang-ti being guided into battle through a dense fog by means of a small pivoting figure with a piece of lodestone embedded in its outstretched arm. The figure always pointed south and was probably the first compass. The term lodestone was coined by the British from the old English word *lode*, which meant to *lead* or *guide*.

Figure 33.1 shows an ancient Chinese compass. The spoon or ladle was carved out of lodestone and rests on a

polished bronze plate. The rounded bottom of the spoon swivels on the plate until it points south. Although this compass has been found to work it was used apparently for quasimagical rather than navigational purposes.

Magnetite is found in many parts of the world and is an important iron ore used for steel making. The word *magnet* comes from the Greek word *magnes*, which itself may derive from the ancient colony of Magnesia (in Turkey). Magnetite was mined in Magnesia 2500 years ago. Today, large deposits of magnetite are found at Kiruna in Sweden and in the Adirondack region of New York.

Commercial interest in ceramic magnets really started in the early 1930s with the filing of a Japanese patent describing applications of copper and cobalt ferrites. In 1947 J.L. Snoeck of N.V. Philips Gloeilampenfabrieken performed a detailed study of ferrites, and the following year Louis Néel published his theory of ferrimagnetism. This latter study was particularly important because most of the ceramics that have useful magnetic properties are ferrimagnetic. The first commercial ceramic magnets were produced in 1952 by researchers at the Philips Company,

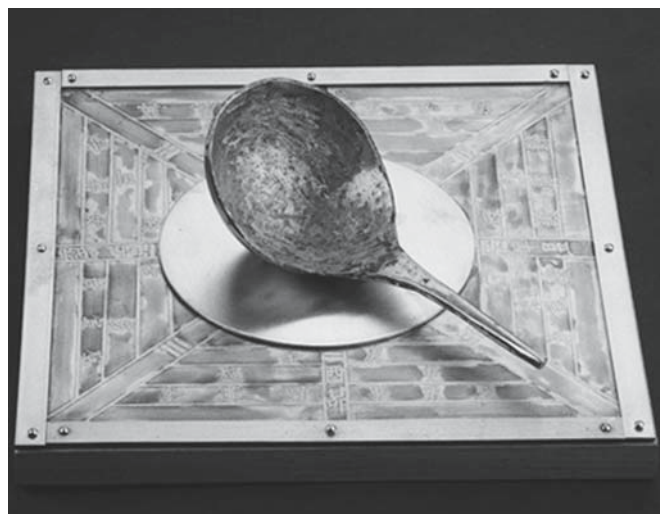


FIGURE 33.1 An ancient Chinese compass.

the same company that introduced the compact audiocassette in 1963.

33.2 MAGNETIC DIPOLES

The Danish physicist Hans Christian Oersted discovered that an electric current (i.e., moving electrons) gives rise to a magnetic force. In an atom, there are two possible sources of electron motion that can create a magnetic dipole and produce the resultant macroscopic magnetic properties of a material. Mag-

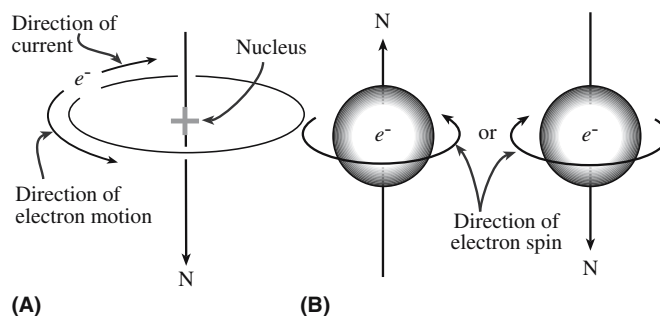


FIGURE 33.2 Generation of atomic magnetic moments by (a) electron orbital motion around the nucleus; (b) electron spin around its axis of rotation.

netic dipoles are small internal magnets with north and south poles.

MAGNETIC MOMENTS

The fundamental magnetic moment is the Bohr magneton, μ_B , which has a value of $9.27 \times 10^{-24} \text{ A}\cdot\text{m}^2$.

The orbital magnetic moment, μ_{orb} , of a single electron is

$$\mu_{\text{orb}} = \mu_B \sqrt{l(l+1)} \quad (\text{Box 33.1})$$

l is the orbital shape quantum number (see Chapter 3).

The spin magnetic moment of an electron is

$$\mu_s = 2\mu_B \sqrt{m_s(m_s+1)} \quad (\text{Box 33.2})$$

In ceramics where the magnetic behavior is due to the presence of transition metal ions with unpaired electron spins in the 3d orbital the magnetic moment of the ion due to electron spin, μ_{ion} , is

$$\mu_{\text{ion}} = 2\mu_B \sqrt{S(S+1)} \quad (\text{Box 33.3})$$

$$S = \sum m_s$$

- *Orbital motion.* Equivalent to a small current loop generating a very small magnetic field. The direction of the magnetic moment is along the orbit axis as illustrated in Figure 33.2a.
- *Spin.* Origin of the fourth quantum number, m_s , that we used in Chapter 3. The magnetic moment is along the spin axis as shown in Figure 33.2b and will be either up ($m_s = +1/2$) or in an antiparallel down direction ($m_s = -1/2$).

The magnetic moment due to electron spin is, when present, dominant

TABLE 33.1 Magnetic Moments of Isolated Transition Metal Cations

Cations	Electronic configuration	Calculated moments using Eq. B3	Measured moments (μ_B)
Sc ³⁺ , Ti ⁴⁺	3d ⁰	0.00	0.0
V ⁴⁺ , Ti ³⁺	3d ¹	1.73	1.8
V ³⁺	3d ²	2.83	2.8
V ²⁺ , Cr ³⁺	3d ³	3.87	3.8
Mn ³⁺ , Cr ²⁺	3d ⁴	4.90	4.9
Mn ²⁺ , Fe ³⁺	3d ⁵	5.92	5.9
Fe ²⁺	3d ⁶	4.90	5.4
Co ²⁺	3d ⁷	3.87	4.8
Ni ²⁺	3d ⁸	2.83	3.2
Cu ²⁺	3d ⁹	1.73	1.9
Cu ⁺ , Zn ²⁺	3d ¹⁰	0.00	0.0

TABLE 33.2 Terms and Units Used in Magnetism

Parameter	Definition	Units/value	Conversion factor
H	Magnetic field strength	A/m	$1 \text{ A/m} = 4\pi \times 10^{-3} \text{ oersted (Oe)}$
H_c	Coercive field	A/m	
H_{cr}	Critical field	A/m	
M	Magnetization	A/m	
B	Magnetic flux density Magnetic induction	T	$T = \text{Wb m}^{-2} = \text{kg A}^{-1} \text{ s}^2 = \text{V s m}^{-2}$ $= 10^4 \text{ gauss (G)}$
μ_0	Permeability of a vacuum	$4\pi \times 10^{-7} \text{ H/m}$	$1 \text{ H} = 1 \text{ J s}^2 \text{ C}^{-2}$
μ	Permeability	H/m	$1 \text{ H/m} = 1 \text{ Wb m}^{-1} \text{ A}^{-1}$
μ_r	Relative permeability	Dimensionless	
χ	Susceptibility	Dimensionless	
μ_{ion}	Net magnetic moment of an atom or ion	$\text{A} \cdot \text{m}^2$	
μ_s	Spin magnetic moment	$\text{A} \cdot \text{m}^2$	
μ_{orb}	Orbital magnetic moment	$\text{A} \cdot \text{m}^2$	
μ_B	Bohr magneton	$9.274 \times 10^{-24} \text{ A} \cdot \text{m}^2$	
θ_c	Curie temperature	K	$0 \text{ K} = -273^\circ \text{C}$
θ_N	Néel temperature	K	
T_c	Critical temperature for superconductivity	K	
C	Curie constant	K	

over that due to orbital motion. Table 33.1 lists values of μ_{ion} calculated for some first row transition metal ions using Eq. Box 33.3. You can see that, in general, the calculated values agree well with the experimental values. This agreement shows that we are justified in considering only the contribution of the spin magnetic moment to the overall magnetic moment.

When an electron orbital in an atom is filled, i.e., all the electrons are paired up, both the orbital magnetic moment and the spin magnetic moment are zero.

33.3 THE BASIC EQUATIONS, THE WORDS, AND THE UNITS

Table 33.2 lists the important parameters used in this chapter and their units. The situation regarding units is more complicated for magnetism than for almost any other property. The reason is that some of the older units, in particular the oersted (Oe) and the gauss (G), are still in widespread use despite being superseded, in the SI system, by A/m and T, respectively.

The properties of most interest to us in the description of magnetic behavior are

- μ
- χ

These terms are, of course, related to each other and by considering the role of H to macroscopic measures such as M and B .

The usual starting point to arrive at expressions for μ and χ is to consider a coil of wire in a vacuum as illustrated in Figure 33.3a. A current, I , passed through the wire generates a magnetic field H

$$H = IN \tag{33.1}$$

where N is the number of turns of wire per meter. The magnetic induction or magnetic flux density, B , is related to H by

$$B = \mu_0 H \tag{33.2}$$

μ_0 is a universal constant.

When a material is placed inside the coil, as shown in Figure 33.3b, it becomes “magnetized.” The magnetic

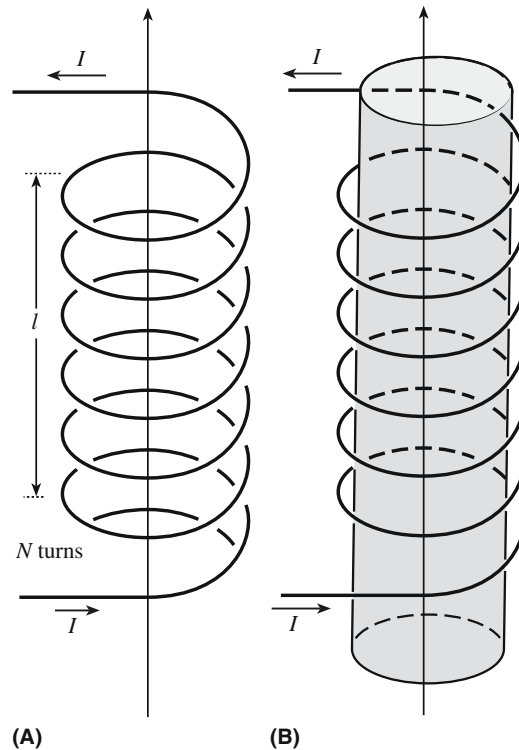


FIGURE 33.3 Generation of a magnetic field by current flowing in a coil of wire (a) in a vacuum; (b) with a material present.

moment produced in the material by the external field changes B :

$$B = \mu_0 H + \mu_0 M \quad (33.3)$$

M represents the response of the material to H , which is linear, and the ratio gives

$$\chi = M/H \quad (33.4)$$

By simple substitution we get

$$B = \mu_0(1 + \chi)H \quad (33.5)$$

B/H is then the permeability:

$$B/H = \mu_0(1 + \chi) = \mu \quad (33.6)$$

The ratio of the permeabilities gives us the relative permeability:

$$\frac{\mu}{\mu_0} = 1 + \chi = \mu_r \quad (33.7)$$

There are many qualitative similarities between magnetic parameters and those we used to describe dielectrics in Chapter 31. In the former case, the material is responding to an applied magnetic field, and in the latter case, it is responding to an applied electric field.

- H and the electric field strength ξ (V/m). Both are the external driving force, which causes the orientation of either magnetic or electric dipoles resulting in magnetization or polarization, respectively.
- B and the polarization P (C/m²). Both correspond to the total field after dipole orientation.
- χ and dielectric constant, κ . Both are dimensionless “constants” that describe the magnitude of a material’s response to the applied field. They are both properties of a material and depend on the types of atoms, the interatomic bonding, and, the crystal structure.
- μ_0 and the permittivity of a vacuum ϵ_0 are constants. They are reference values to establish the strength of a materials response to H or ξ , respectively.

The similarities described above are not surprising. In both cases, we are concerned with the relationship between an external field and the dipoles within a material. Despite these similarities the physical

nature of the dipoles and their origin is very different. In the case of a dielectric, the dipoles are electric; there is a separation of positive and negative charges. These dipoles can be permanent or induced. In a magnetic material, the dipoles are, of course, magnetic in origin and are due to electron motion.

A note on terminology: In most materials science textbooks, as we have done here, H is defined as the magnetic field or the applied magnetic field and B as the magnetic flux density. In many physics textbooks B is referred to as the magnetic field and H is often ignored. The physics convention is adopted for purely historical reasons, but it does have the advantage of reducing the number of terms we need to consider. Also H has nothing to do with a material whereas B is a measure of the response of a material to an applied magnetic field. Another point to note is that B and H are both vector quantities and because the magnetic properties of a material are anisotropic (different along different directions in the crystal) they should actually be represented by a second-rank tensor.

33.4 THE FIVE CLASSES OF MAGNETIC MATERIAL

There are five main types of magnetic behavior and these can be divided into two general categories:

- Induced
- Spontaneous

Table 33.3 summarizes the properties of the five classes. We can find examples of each in ceramics.

33.5 DIAMAGNETIC CERAMICS

Most ceramics are diamagnetic. The reason is that all the electrons are paired during bond formation and as a result the net magnetic moment due to electron spin is zero. Table 33.4 lists χ for several diamagnetic materials. Cu, Au, and Ag are diamagnetic even though their atoms have unpaired valence electrons. When the atoms combine to form the metal the valence electrons are shared by the crystal as a whole (to form the electron gas) and, on average, there will be as many electrons with $m_s = +1/2$ as with $m_s = -1/2$.

Most diamagnetic ceramics are of no commercial significance and of little scientific interest, at least not for their magnetic behavior. The one exception is the ceramic superconductors, which are perfect diamagnets below a critical magnetic field.

χ AND μ

Susceptibilities are generally used when the response to an applied magnetic field is weak (of interest only to physicists!). Permeabilities are used when the response is large—of great interest to engineers!

MAXWELL EQUATIONS

The magnetic, electric, and optical properties of a material are all related mathematically through the Maxwell equations.

TABLE 33.3 Magnetic Classification of Materials

Class	Critical temperature	χ	Temperature variation of χ	Spontaneous magnetization	Structure on atomic scale
Diamagnetic	None	-10^{-6} to -10^{-5}	Constant	None	Atoms have no permanent dipole moments
Paramagnetic	None	$+10^{-5}$ to $+10^{-3}$	$\chi = C/T$	None	Atoms have permanent dipole moments; neighboring moments do not interact
Ferromagnetic	θ_C	Large (below θ_C)	Above θ_C , $\chi = C/(T - \theta)$, with $\theta \approx \theta_C$	Below θ_C , $M_s(T)/M_s(0)$ against T/θ_C follows a universal curve; above θ_C , none	Atoms have permanent dipole moments; interaction produces parallel alignment
Antiferromagnetic	θ_N	As paramagnetic	Above θ_N , $\chi = C/(T \pm \theta)$, with $\theta \neq \theta_N$, below θ_N , χ decreases, anisotropic	None	Atoms have permanent dipole moments; interaction produces antiparallel alignment
Ferrimagnetic	θ_C	As ferromagnetic	Above θ_C , $\chi \approx C/(T \pm \theta)$, with $\theta \neq \theta_C$	Below θ_C , does not follow universal curve; above θ_C , none	Atoms have permanent dipole moments; interaction produces antiparallel alignment; moments are not equal

33.6 SUPERCONDUCTING MAGNETS

The net effect is that the whole of the magnetic flux appears to have been suddenly ejected from the material and it behaves as a perfect diamagnet. This phenomenon is known as the Meissner effect and is usually demonstrated by suspending a magnet above a cooled pellet of the superconductor.

When a superconductor in its normal (i.e., nonsuperconducting) state is placed in a magnetic field and then cooled below its critical temperature the induced magnetization, M , exactly opposes H and so from Eq. 33.3, we can write

$$B = 0 \quad (33.8)$$

LONDON PENETRATION DEPTH

Although there is no magnetic field in the bulk of a superconductor it does penetrate below the surface to a depth of between 0.2 and 0.8 μm .

CRITICAL MAGNETIC FIELDS FOR YBCO

H_{c1} (T) $\parallel c \sim 0.1$ $\parallel a,b \sim 0.01$
 H_{c2} (T) $\parallel c \sim 50$ $\parallel a,b \sim 200$
 $\parallel c$ field along the c axis of the unit cell
 $\parallel a,b$ field in the basal plane
 These H_{c2} values are enormous. The world's most powerful magnet is about 40 T.

There is an upper limit to the strength of the magnetic field that can be applied to a superconductor without changing its

TABLE 33.4 Magnetic Susceptibilities for Several Diamagnetic Materials

Material	χ (ppm)
Al ₂ O ₃	-37.0
Be	-9.0
BeO	-11.9
Bi	-280.1
B	-6.7
CaO	-15.0
CaF ₂	-28.0
C (diamond)	-5.9
C (graphite)	-6.0
Cu	-5.5
Ge	-76.8
Au	-28.0
Pb	-23.0
LiF	-10.1
MgO	-10.2
Si	-3.9
Ag	-19.5
NaCl	-30.3

diamagnetic behavior. At a critical field H_{cr} the magnetization goes toward zero and the material reverts to its normal state. For most elemental superconductors M rises in magnitude up to H_{cr} and then abruptly drops to zero; this is Type I behavior.

A few elemental and most compound superconductors, including all HTSCs, exhibit Type II behavior. Above a certain field, H_{c1} , magnetic flux can penetrate the material without destroying superconductivity. Then at a (usually much) higher field, H_{c2} , the material reverts to the normal state. These two behaviors are compared in Figure 33.4.

When a Type II superconductor is in the "mixed" state it consists of both normal and superconducting regions. The normal regions are called vortices, which are arranged parallel to the direction of the applied field. At low temperature the vortices are in a close-packed arrangement and vibrate about their equilibrium positions, in the same way that atoms in a solid vibrate. If the temperature is high enough the vortex motion becomes so pronounced that the

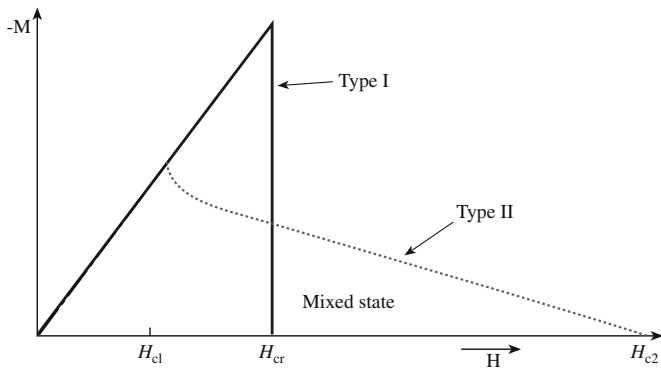


FIGURE 33.4 Magnetization behavior of Type I and Type II superconductors as a function of the applied field.

arrangement randomizes and the vortex lattice “melts.” Defects in the material can trap or pin vortices in place and higher temperatures are then needed to cause “melting.” Pinning is of considerable practical importance because it enables higher currents to flow through the material before superconductivity is lost.

One of the most exciting potential applications of the Meissner effect is magnetic levitation (maglev) for advanced high-speed transportation. Pilot maglev trains that can reach speeds of more than 550 km/h have already been developed in Japan, and other countries have plans to develop maglev train services. The first U.S. maglev train was scheduled for the campus of Old Dominion University in Virginia with plans to complete construction by 2003. But the project has suffered a continuation of major setbacks since then.

Although ceramic superconductors have not been used for the generation of large magnetic fields, because it is difficult to form them into long wires, they have been made into superconducting quantum interference devices (SQUIDs). The essential component of a SQUID is the Josephson junction, a thin (~1 nm) insulating layer between two superconductors through which weak supercurrents consisting of Cooper pairs can tunnel without an applied voltage. The insulating barrier can be a deposited thin film or, in the case of some of the ceramic superconductors, a high-angle grain boundary (GB), such as that shown in Figure 14.37, which works well.

A SQUID can be used to detect very small ($\sim 10^{-15}$ T) changes in B . When a Josephson junction is exposed to a magnetic field steps are produced in the I - V behavior. This is similar to what happens when the junction is irradiated with microwaves (as we showed in Chapter 30). Each step corresponds to a quantum change in B . Uses for SQUIDs include the following:

- They can detect small changes in magnetic field strength at the earth’s surface that can then be related

TABLE 33.5 Magnetic Susceptibilities for Several Paramagnetic Materials

Material	χ (ppm)
Al	+16.5
Ca	+40.0
Ce	+2450
CeO ₂	+26.0
Cr	+180
Cr ₂ O ₃	+1965
Li	+14.2
Mg	+13.1
Na	+16.0
Ti	+153.0
TiO ₂	+5.9

to the underlying geological structure (e.g., thickness of the crust, movement of magnetic poles over time, etc.).

- Magnetic imaging using scanning SQUID microscopy. This allows local magnetic fields to be measured at the surface of a sample.
- Searching for submarines. When a submarine moves through the water, the metal hull slightly disturbs the earth’s magnetic field and this small distortion can be measured.
- The human brain can be imaged by detecting small magnetic fields produced as a result of the currents due to neural activity. This area of research is called magnetoencephalography (MEG) and is being used to study epilepsy.

33.7 PARAMAGNETIC CERAMICS

The magnetic moment is due to unpaired electron spins. Magnetic susceptibilities are positive as shown in Table 33.5, because the magnetic moments line up with H and this leads to an increase in B . However, adjacent magnetic dipoles essentially behave independently; there is no interaction between them. It is this lack of an interaction that separates paramagnetic materials from ferromagnets.

Most first row transition metals, e.g., Ti and Cr, are paramagnetic because they have unpaired electrons in their 3d orbitals (see Table 33.1). The number of unpaired electrons per atom is determined using

Hund’s rule (Section 3.5).

Nontransition metals, e.g., Na, may be paramagnetic due to the alignment of the spin moment of some of the valence electrons with the applied field. This effect, known as Pauli paramagnetism, is much weaker than that due to unpaired 3d electrons and involves electrons moving into a higher energy level and changing their spin direction. This process can happen only if the gain in magnetic

REFERENCE POINTS

$B = 10^{-12}$ T at the Earth’s surface.

The human body produces a magnetic field of $\sim 10^{-10}$ T.

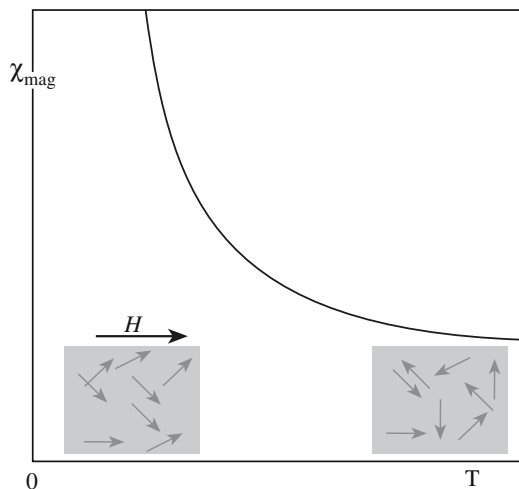


FIGURE 33.5 Schematic showing how χ varies with T for a paramagnetic solid. The insets indicate the direction of the magnetic dipoles in the solids.

energy is more than the energy needed for electron promotion. Some oxides containing transition metal or rare earth ions, such as CeO_2 and Cr_2O_3 , are also paramagnetic.

The temperature dependence of paramagnetic susceptibility is shown in Figure 33.5 and follows the Curie law:

$$\chi = \frac{C}{T} \quad (33.9)$$

There are currently no commercial applications for paramagnetism.

33.8 MEASURING χ

The most straightforward way to obtain χ is the classical Gouy method. The material, in the form of a rod, is attached to one arm of a sensitive balance. It is then placed between the poles of a magnet. If the sample is paramagnetic its energy is lower when it is inside the magnetic field, and so there is a force, F , drawing it into the field. If the sample is diamagnetic its energy is less if it is outside the field, and so F is in the opposite direction.

Qualitatively the sign of χ can be determined by whether the force on the sample (the apparent weight change measured by the balance) is positive or negative. We can quantify the value of χ using Eq. 33.10:

$$F = \frac{1}{2} A \chi H^2 \quad (33.10)$$

where A is the cross-sectional area of the sample.

Other methods can be used to determine magnetization and susceptibility, but all rely either on measuring the force exerted on

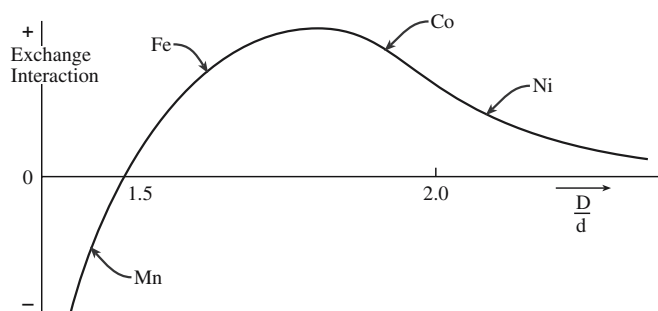


FIGURE 33.6 The Slater–Bethe curve showing the magnitude and sign of J as a function of D/d .

the sample by the magnetic field (as in the Gouy method) or on detecting currents induced in a circuit placed close to the magnetic material. The main disadvantage of the Gouy method is that it requires quite a large sample (~grams).

33.9 FERROMAGNETISM

The origin of ferromagnetism, like paramagnetism, is the presence of unpaired electron spins. However, in a ferromagnetic material there is an interaction between adjacent dipoles. Of the first row transition metals only Fe, Co, and Ni are ferromagnetic. So why is Cr paramagnetic not ferromagnetic? The reason is due to a quantum mechanical exchange interaction between the 3d orbitals on adjacent atoms, which is represented mathematically by the exchange integral, J . If $J > 0$ there is an interaction between adjacent magnetic dipoles causing them to line up and the material is ferromagnetic (below the Curie temperature, θ_c). If $J < 0$ adjacent dipoles are antiparallel and the material is antiferromagnetic (below the Néel temperature, θ_N).

The magnitude and the size of J depend on the interatomic separation, D , and the diameter, d , of the electron orbital under consideration as shown in Figure 33.6 (the Slater–Bethe curve) for the case of the 3d orbitals of Fe, Co, and Ni.

D can be determined simply by looking up the atomic radius of the element and doubling it, e.g., for Fe $r = 0.124 \text{ nm}$ and $D = 0.248 \text{ nm}$. The value of d can be estimated using Eq. Box 3.2 in Section 3.2. For the 3d orbitals of Fe $r = 0.159 \text{ nm}$. Hence D/d is 1.56, as shown in Figure 33.6. J is more difficult to determine. It is related to the overlap of the electron orbitals and involves integrating the products of the wavefunctions for the electron orbitals on adjacent atoms.

If there is significant overlap of the 3d orbitals then, by the requirements of the Pauli exclusion principle, the spins must be antiparallel ($J < 0$). If the separation is too large then

MEASURING χ

It is important to determine χ to know if a material is a superconductor. Having a very low electrical resistivity or an abrupt drop in resistivity is not a defining criterion. A strong magnet has a large value of χ .

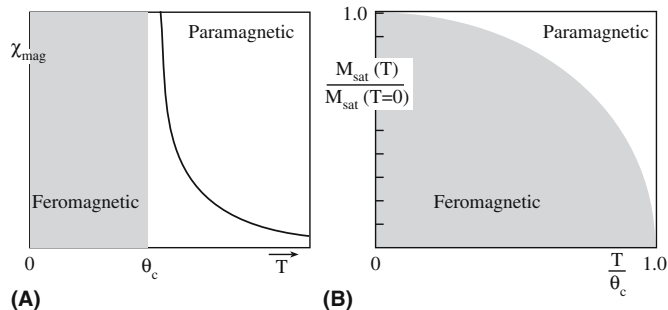


FIGURE 33.7 Schematic showing how (a) χ varies with T ; (b) M varies with T for a ferromagnet.

there is no appreciable interaction. However, in the case of iron, cobalt, and nickel the exchange interaction is large and positive and the electron spins are parallel.

The magnetic susceptibility of a ferromagnetic material varies with temperature (Figure 33.7a) according to the Curie–Weiss law:

$$\chi = C/(T - \theta_c) \quad (33.11)$$

You will recognize this type of variation as being very similar to an order–disorder transition. Above θ_c the material become paramagnetic because of randomization of the spin magnetic moments. M decreases from its maximum value at 0 K and vanishes at θ_c as shown in Figure 33.7(b).

Chromium dioxide (CrO_2) is at present the most important ferromagnetic ceramic. It is used as magnetic media in audio and video recording tapes. In this application, the CrO_2 is not in the pure form but is usually doped to improve its properties.

CrO_2 has the rutile (TiO_2) structure (Figure 6.11). The Cr^{4+} ions are located at the corners of the unit cell and there is a distorted CrO_6 octahedron in the center. The lattice parameters are $a = 0.437$ nm and $c = 0.291$ nm. CrO_2 does not occur in nature and is usually manufactured by thermal decomposition of CrO_3 at $\sim 500^\circ\text{C}$ under high pressure (>200 MPa) in the presence of water.

33.10 ANTIFERROMAGNETISM AND COLOSSAL MAGNETORESISTANCE

In an antiferromagnet there is exact cancellation of the magnetic moments. We can think of an antiferromagnetic material as consisting of two ferromagnetic lattices in which the spin magnetic moments are equal in magnitude but opposite in direction. Above θ_N the antiferromagnetic spin alignments are randomized and the material becomes paramagnetic. The temperature dependence of the magnetic susceptibility is shown in Figure 33.8.

The following oxides are antiferromagnetic:

MnO ($\theta_N = 122$ K)	NiO ($\theta_N = 523$ K)
CoO ($\theta_N = 293$ K)	FeO ($\theta_N = 198$ K)

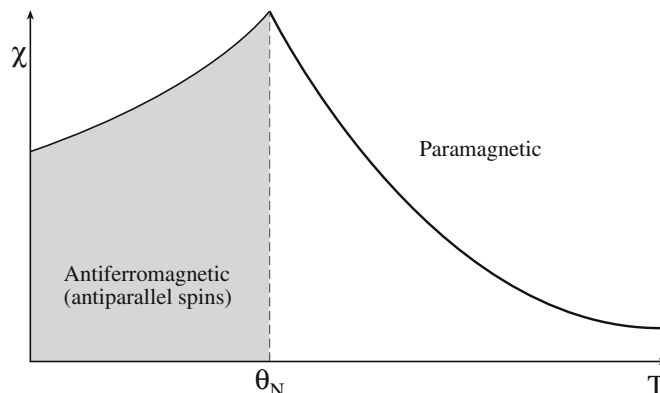
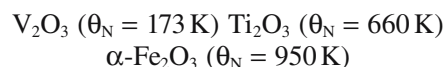


FIGURE 33.8 Schematic showing how χ varies with T for an antiferromagnetic material. At θ_N it becomes paramagnetic.

They all have the rocksalt (NaCl) structure and magnetic dipoles on adjacent $\{111\}$ planes are antiparallel. The magnetic interaction between the cations occurs indirectly through the oxygen ions and is known as a “superexchange” interaction. Along $\langle 100 \rangle$ there is overlap of the Ni d_{z^2} orbitals and the O p_z orbital as illustrated in Figure 33.9. The Pauli exclusion principle governs the spin direction in the overlapping orbitals and, as a result, the adjacent Ni ions have opposed spins.

We have direct evidence of the orientation of the spin magnetic moments in antiferromagnetic materials from neutron diffraction studies. Neutrons have a magnetic dipole moment. In neutron diffraction the neutron beam is responding not only to atom positions but also to their magnetic moments. (X-rays give us information on atom positions and electron distribution.) Above θ_N , the neutron diffraction pattern consists of reflections due to the periodic arrangement of the crystal structure. Below θ_N extra reflections appear in the pattern because the neutrons are “seeing” two sets of cations, with different magnetic moments. The magnetic unit cell is therefore twice the size of the crystallographic unit cell as shown in Figure 33.10.

Antiferromagnetism is not limited to oxides with a rocksalt structure. The following antiferromagnets have a corundum structure:



Although the ceramics we have mentioned so far in this section have no applications that use their magnetic

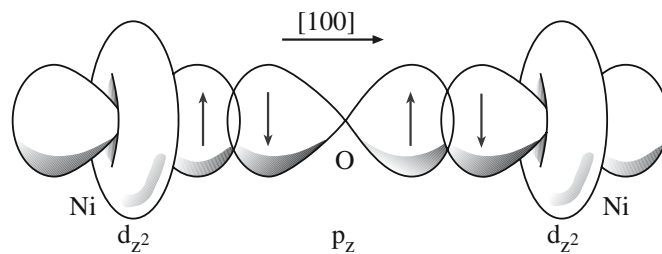


FIGURE 33.9 Overlap between Ni d_{z^2} orbitals and O p_z orbitals in Ni.

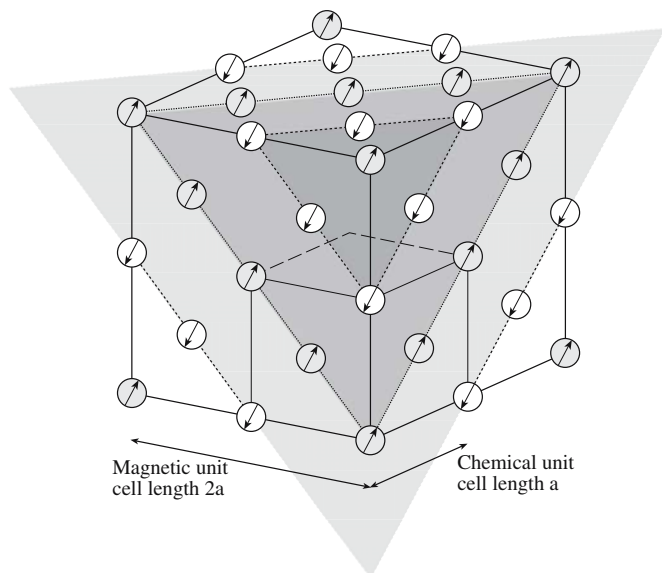


FIGURE 33.10 Comparison of structural and magnetic unit cells of NiO.

properties, there are manganate ceramics in the $\text{La}_{1-x}\text{A}_x\text{MnO}_3$ ($0 \leq x \leq 1$; A = Sr, Ca, Ba) system that are antiferromagnetic and exhibit colossal magnetoresistance (CMR). In CMR the resistance drops dramatically in an applied magnetic field. It is related to, but much greater than, giant magnetoresistance (GMR) found in multilayers of ferromagnetic and nonferromagnetic metals (e.g., 30 Co/Cu bilayers). In these structures there is an interaction between the ferromagnetic layers that can cause antiferromagnetic ordering of magnetic moments in adjacent layers.

So individually each Co layer is ferromagnetic, but the multilayer structure is actually antiferromagnetic. The extent of the interaction depends on the thickness of the nonferromagnetic layer and H . All current hard disk drives make use of this technology.

The manganates have the layered perovskite structure similar to that found in the YBCO superconductor (see Section 7.16). This similarity is particularly interesting and may lead to increased understanding of both types of material. The nature of the interactions in the manganites is complicated. They show a metal–insulator transition and a ferromagnetic–antiferromagnetic transition associated with CMR.

33.11 FERRIMAGNETISM

In a ferrimagnet the magnetic moments of one type of ion on one type of lattice site in the crystal are aligned antiparallel to those of ions on another lattice site. Because

ZnFe_2O_4

In ZnFe_2O_4 [$\text{Fe}^{\text{III}}(\text{Zn}^{\text{II}}\text{Fe}^{\text{III}})\text{O}_4$] all the magnetic Fe^{3+} are on octahedral sites and are separated by a plane of O^{2-} ions. The material is antiferromagnetic because the superexchange interaction involving the two Fe^{3+} ions resembles that shown in Figure 33.9.

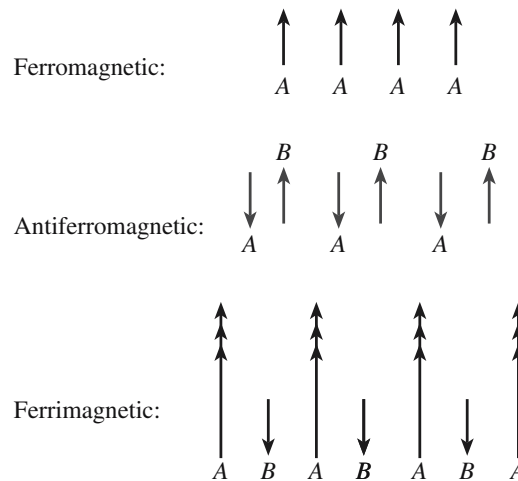


FIGURE 33.11 Schematic comparing dipole alignments in ferromagnetic, antiferromagnetic, and ferrimagnetic materials.

the magnetic moments are not of the same magnitude they only partially cancel each other and the material has a net M . Ferrimagnetism has several similarities to ferromagnetism in that the cooperative alignment between magnetic dipoles leads to a net magnetic moment even in the absence of an applied field. Ferrimagnetism is lost above θ_c . The difference between ferromagnetism, antiferromagnetism, and ferrimagnetism in terms of the spin alignments is illustrated in Figure 33.11.

The easiest way to consider what happens in a ferrimagnet is to look at the prototypical ferromagnetic material, magnetite. Magnetite has an inverse spinel structure (Section 7.2). The formula can be written as $\text{Fe}^{\text{III}}(\text{Fe}^{\text{II}}\text{Fe}^{\text{III}})\text{O}_4$,

i.e., in the classic spinel form AB_2O_4 . The Fe^{2+} ions and half of the Fe^{3+} ions are in octahedral sites and the other half of the Fe^{3+} cations are in tetrahedral sites. The spins of the Fe ions on the octahedral sites are parallel, but of a different magnitude. The spins of the Fe ions on the tetrahedral sites are antiparallel to those in the octahedral sites. The situation is illustrated in Figure 33.12, which shows one-eighth of the magnetite unit cell. The alignment of the spins is the result of an exchange interaction involving the O^{2-} ions. The antiparallel alignment of the Fe^{3+} ion in the octahedral site and the Fe^{3+} ion in the tetrahedral site is usually explained by a superexchange reaction similar to that used to explain antiferromagnetism.

A mechanism to account for the parallel spin alignment between the Fe^{3+} in the octahedral site and the octahedrally coordinated Fe^{2+} was proposed by Zener and is called the “double exchange” mechanism. The idea is that an electron from the Fe^{2+} ion ($3d^6$) is transferred to the oxygen in the face-centered position of the subcell shown in Figure 33.12. At the same time there is transfer of an

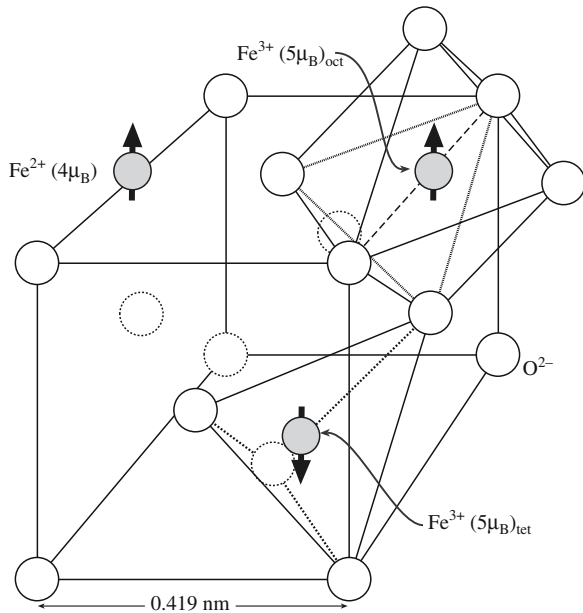


FIGURE 33.12 Subcell of magnetite showing the location of Fe ions and their spin moments.

electron with parallel spin to the Fe^{3+} ion. The process is illustrated in Figure 33.13 and shares similarities with the electron-hopping model of conduction in transition metal oxides. (Note: a requirement of Zener's model is that the cations have different charges.)

Ferrimagnetic ceramics have the spinel (almost exclusively inverse), the garnet, or the magnetoplumbite structure. Table 33.6 lists some examples of ferrimagnetic

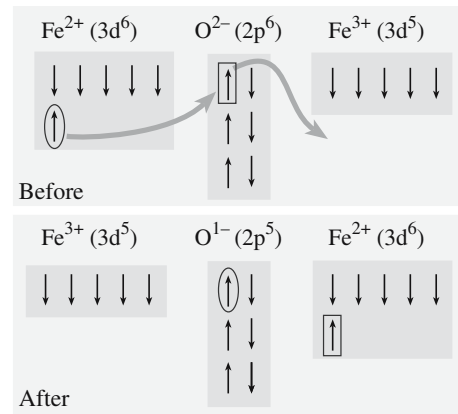


FIGURE 33.13 Illustration of the double exchange interaction in magnetite.

spinel and their properties. The magnetic moments in this table were calculated taking account of only the number of unpaired 3d electrons; the units are Bohr magnetons and the minus sign denotes an antiferromagnetic coupling.

The most important and widely studied magnetic garnet is yttrium–iron garnet (YIG), which has the formula $\text{Y}_3\text{Fe}_2(\text{FeO}_4)_3$ [remember garnet is $\text{Ca}_3\text{Al}_2(\text{SiO}_4)_3$]. We can write the formula of YIG as $\text{Y}_3^c\text{Fe}_2^d\text{Fe}_3^e\text{O}_{12}$ where the superscripts refer to the type of lattice site occupied by each cation. The cell shown in Figure 33.14 is actually one of the eight subcells that form the YIG unit cell, which contains 160 atoms. In the subcell the a ions are in a body-centered cubic (bcc) type arrangement with the

TABLE 33.6 Magnetic Properties of Several Ferrimagnetic Ceramics

Material	θ_c (K)	B_{sat} (T) at RT	Calculated moments			Experimental
			T site	O site	Net	
Spinel ferrites [AO · B₂O₃]						
$\text{Fe}^{3+}[\text{Cu}^{2+}\text{Fe}^{3+}]\text{O}_4$	728	0.20	–5	1.73 + 5	1	1.30
$\text{Fe}^{3+}[\text{Ni}^{2+}\text{Fe}^{3+}]\text{O}_4$	858	0.34	–5	2 + 5	2	2.40
$\text{Fe}^{3+}[\text{Co}^{2+}\text{Fe}^{3+}]\text{O}_4$	1020	0.50	–5	3 + 5	3	3.70–3.90
$\text{Fe}^{3+}[\text{Fe}^{2+}\text{Fe}^{3+}]\text{O}_4$	858	0.60	–5	4 + 5	4	4.10
$\text{Fe}^{3+}[\text{Mn}^{2+}\text{Fe}^{3+}]\text{O}_4$	573	0.51	–5	5 + 5	5	4.60–5.0
$\text{Fe}^{3+}[\text{Li}_{0.5}\text{Fe}_{1.5}]\text{O}_4$	943		–5	0 + 0.75		2.60
$\text{Mg}_{0.1}\text{Fe}_{0.9}[\text{Mg}_{0.9}\text{Fe}_{1.1}]\text{O}_4$	713	0.14	0–4.5	0 + 5.5	1	1.10
Hexagonal ferrites						
$\text{BaO} : 6\text{Fe}_2\text{O}_3$	723	0.48				1.10
$\text{SrO} : 6\text{Fe}_2\text{O}_3$	723	0.48				1.10
$\text{Y}_2\text{O}_3 : 5\text{Fe}_2\text{O}_3$	560	0.16				5.00
$\text{BaO} : 9\text{Fe}_2\text{O}_3$	718	0.65				
Garnets						
$\text{YIG}\{\text{Y}_3\}[\text{Fe}_2]\text{Fe}_3\text{O}_{12}$	560	0.16			5	4.96
$(\text{Gd}_3)[\text{Fe}_2]\text{Fe}_3\text{O}_{12}$	560				16	15.20
Binary oxides						
EuO	69					6.8
CrO_2	386	0.49				2.00

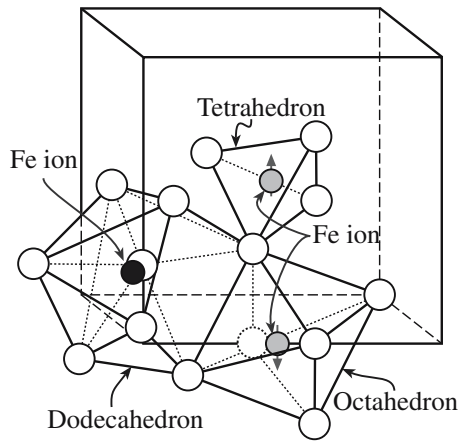


FIGURE 33.14 Structural units in a subcell of YIG. For clarity not all the atoms are shown and only one of each example of the polyhedra is shown.

c and *d* ions lying on the cube faces. Each *a* ion is in an octahedral site, each *c* ion is on a dodecahedral site, and each *d* ion is on a tetrahedral site as illustrated in Figure 33.14.

The net magnetic moment in YIG, as in other ferrimagnetic ceramics, arises from an uneven contribution from antiparallel spins; the magnetic moments of the *a* and *d* ions are aligned antiparallel as are those of the *c*

and *d* ions. For every two Fe^{3+} on a sites, there are three Fe^{3+} ions on *d* sites giving a measured magnetic moment of $\sim 5\mu_B$.

The mineral magnetoplumbite has the approximate composition $\text{PbFe}_{7.5}\text{Mn}_{3.5}\text{Al}_{0.5}\text{Ti}_{0.5}\text{O}_{19}$. The commercially important ferrimagnetic ceramic barium hexaferrite ($\text{BaO} \cdot 6\text{Fe}_2\text{O}_3$) is isostructural with magnetoplumbite. A schematic of the crystal structure of $\text{BaO} \cdot 6\text{Fe}_2\text{O}_3$ is shown in Figure 33.15. The hexagonal unit cell is very large and contains 64 atoms. Magnetization is easiest along the *c* axis. Also shown in Figure 33.15 is a simplified representation of the spin magnetic moments of the Fe^{3+} ions in $\text{BaO} \cdot 6\text{Fe}_2\text{O}_3$. The actual arrangements are more complicated.

There is a range of hexagonal ferrimagnetic ceramics containing BaO. These are usually classified based on their chemical formula:

- M-type compounds, $(\text{MO})(\text{Fe}_2\text{O}_3)_6$, e.g., $(\text{BaO})(\text{Fe}_2\text{O}_3)_6$
- W-type compounds, $(\text{BaO})(\text{MO})_2(\text{Fe}_2\text{O}_3)_8$ or M_2W , e.g., $(\text{BaO})(\text{CoO})_2(\text{Fe}_2\text{O}_3)_8$
- Y-type compounds, $(\text{BaO})_2(\text{MO})_2(\text{Fe}_2\text{O}_3)_6$ or M_2Y , e.g., $(\text{BaO})_2(\text{MnO})_2(\text{Fe}_2\text{O}_3)_6$
- Z-type compounds, $(\text{BaO})_3(\text{MO})_2(\text{Fe}_2\text{O}_3)_{12}$ or M_2Z , e.g., $(\text{BaO})_3(\text{MgO})_2(\text{Fe}_2\text{O}_3)_{12}$

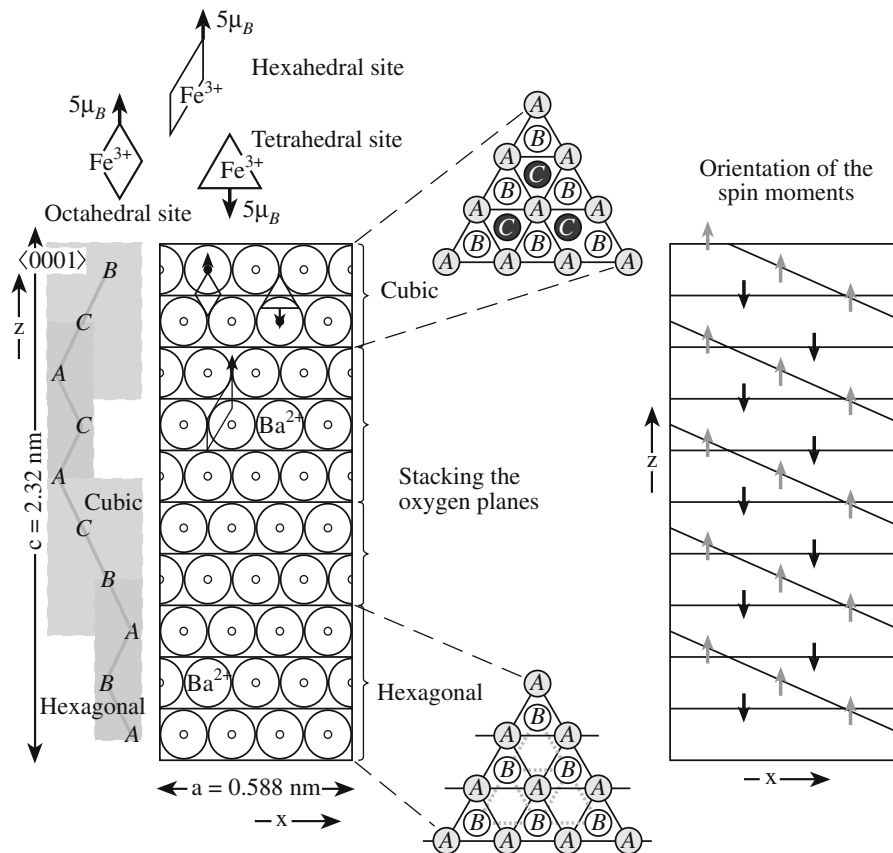


FIGURE 33.15 Schematic of the barium ferrite crystal structure showing the structural units and the magnetization directions.

TABLE 33.7 Magnetic Properties of Fe in Magnetic Ceramics

Ion	Number	Site	Spin direction	Ion moment (μ_B)	Total moment (μ_B)
Fe ²⁺	1	Octahedral	↑	4	4
Fe ³⁺	1	Octahedral	↑	5	5
Fe ³⁺	1	Tetrahedral	↓	5	-5

- X-type compounds, (BaO)₂(MO)₂(Fe₂O₃)₁₄ or M₂X, e.g., (BaO)₂(FeO)₂(Fe₂O₃)₁₄
- U-type compounds, (BaO)₄(MO)₂(Fe₂O₃)₁₈ or M₂U, e.g., (BaO)₄(ZnO)₂(Fe₂O₃)₁₈

33.12 ESTIMATING THE MAGNETIZATION OF FERRIMAGNETS

We can estimate saturation values of M and B by knowing the crystal structure and lattice parameter of the material and the orientation of the spin magnetic moments. We will illustrate this approach for magnetite. The magnetic moments of each type of ion are summarized in Table 33.7. The Fe³⁺ ions interact antiferromagnetically and the net magnetic moment is due only to the Fe²⁺ ions. Using Eq. Box 33.3 we can calculate the magnetic moment of an Fe²⁺ ion as $4.9\mu_B$. There are eight Fe²⁺ ions per unit cell so the total magnetic moment per cell is $8 \times 4.9 = 39.2\mu_B$.

M is therefore

$$39.2 [\mu_B] \times 9.27 \times 10^{-24} [A \cdot m^2 \mu_B^{-1}] / (0.837 \times 10^{-9} [m])^3 = 6.17 \times 10^5 A/m$$

which is in fairly good agreement with the measured value of $5.3 \times 10^5 A/m$.

B is

$$B_s = \mu_0 M_s = 4\pi \times 10^{-7} \times 6.17 \times 10^5 = 0.78 T$$

This value is close to the measured value of 0.6 T.

An interesting characteristic of both these values is that if the classical value of the spin magnetic moment is taken for Fe²⁺, i.e., $4\mu_B$, then both M and B are closer to the measured values, even though for isolated cations Eq. Box 33.3 provides much better agreement with the experimental data. The reason for this discrepancy is not obvious.

33.13 MAGNETIC DOMAINS AND BLOCH WALLS

A ferromagnetic or a ferrimagnetic material is divided into many small regions or domains. Pierre Weiss was the first to recognize the presence of magnetic domains and

therefore they are often named after him. Within each domain the direction of magnetization is the same. When the material is in its unmagnetized state the net magnetization is zero, i.e., there are as many domains magnetized in one direction as there are in the antiparallel direction. This situation is illustrated for several different domain structures in Figure 33.16. The energy of the material is lowered when the domains are smaller. For the configurations shown in Figure 33.16 the overall energy decreases from left to right. The triangular domains are called closure domains and complete the magnetic flux path with the solid; this also lowers the overall energy.

In the boundary region between the different domains there is a gradual change in magnetic dipole orientation as illustrated in Figure 33.17. The bound-

ary regions are known as domain walls or Bloch walls after the man who did much of the early work on this subject. The thickness of the domain wall is a tradeoff between the requirement for a small angle between adjacent spins, which would necessitate a thick wall, and the tendency for the magnetic dipoles to be aligned with a specific crystallographic orientation, requiring a thin wall.

There is also a domain structure in antiferromagnetic materials, with wall separating each domain:

- In S walls the magnetization direction is rotated across the wall.
- In T walls there is a change in orientation characteristic of twinning.

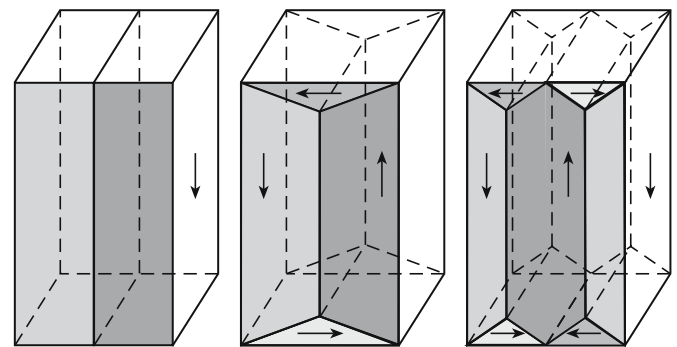


FIGURE 33.16 Examples of domain structures, each having zero net magnetization.

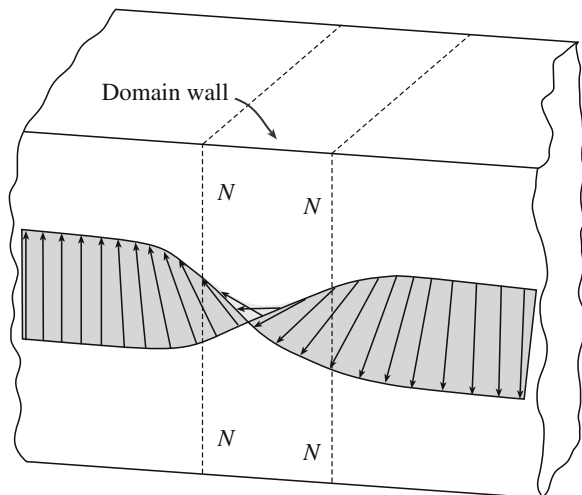


FIGURE 33.17 Change in magnetic dipole orientation through a domain wall. All moments lie in the plane of the wall.

33.14 IMAGING MAGNETIC DOMAINS

There are many different ways to image magnetic domain structures in a material. All the “microscopy” techniques we described in Chapter 10 can be used, although, in some cases, deviations from the usual operating procedure are necessary to obtain the desired images. It is also possible to use X-ray topography to study magnetic domains. In this section, we will briefly describe three techniques: the oldest, one of the newest, and the trickiest.

Visible Light Microscopy (VLM)

Examination of a magnetic material by simple VLM will not reveal any information about the domain structure because the direction of magnetization does not change the appearance of the surface in any way. Transmitted light requires that the specimens are transparent and so very thin ($<0.1\ \mu\text{m}$) samples must be used. The first approach, known as the Bitter technique, “decorates” the domain boundaries with magnetic particles suspended in a liquid. The particles are attracted to where the domain boundaries intersect the surface and this allows the domain pattern to be observed. The Bitter technique is applicable to all types of magnetic material, but specimen preparation is important to avoid introducing surface strains that can distort the domain structure. A Bitter pattern obtained in the hexagonal ferrite $\text{Co}_2\text{Ba}_2\text{Fe}_{28}\text{O}_{46}$ is shown in Figure 33.18.

An alternative means of observing magnetic domain structures in the VLM is to use polarized light. Domains magnetized in opposite directions will rotate the plane of polarization in opposite senses. Using an appropriate analyzer it is possible to vary the intensity of the light coming from each domain and produce corresponding intensity changes in the image. The effect of M on the transmitted light intensity is called the Faraday effect. The Faraday effect in a thin film of a substituted YIG, $(\text{BaTb})_3(\text{FeGa})_5\text{O}_{12}$, is shown in Figure 33.19.

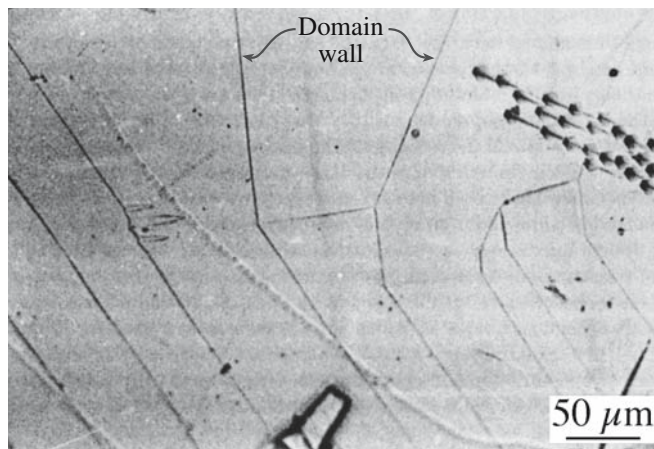


FIGURE 33.18 Magnetic domains on the basal surface of a hexagonal ferrite, $\text{Co}_2\text{Ba}_2\text{Fe}_{28}\text{O}_{46}$, revealed by the Bitter technique.

The effect of M on the reflected light intensity is known as the Kerr effect. The polar Kerr effect refers to a situation in which the sample has a component of M normal to the surface and normal incidence illumination is used. The longitudinal Kerr effect is used when M is parallel to the surface and the illumination is oblique.

Magnetic Force Microscopy (MFM)

Magnetic force microscopy is closely related to scanning tunneling microscopy (STM) and atomic force microscopy (AFM). In MFM the tip is coated with a ferromagnetic thin film that detects magnetic force variations on the sample surface. The tip is scanned over the surface of the sample (it does not actually touch) as in STM. Interactions between magnetic domains in the sample and the ferromagnetic coating result in a force on the tip, which



FIGURE 33.19 Domain pattern in a YIG thin film revealed by the Faraday effect. The stripes are $12\ \mu\text{m}$ wide.

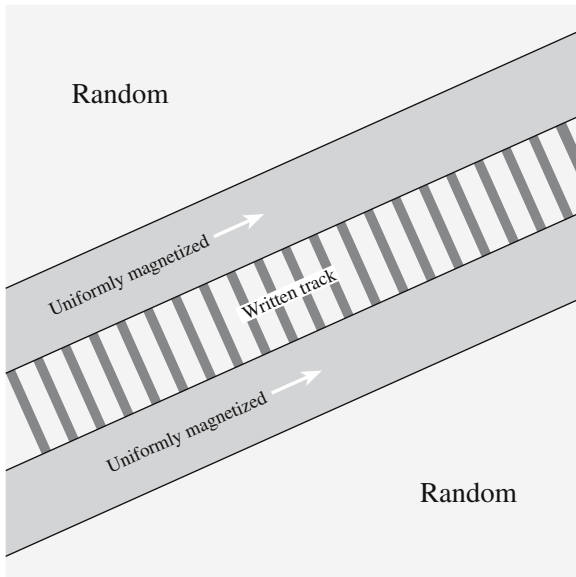


FIGURE 33.20 Schematic of MFM of a magnetized pattern on a hard drive.

depends upon the orientation of the domains. Different orientations produce a different force and this is how the different magnetized regions can be determined. Figure 33.20 illustrates how an MFM image of a magnetic tape would appear. The bright and dark stripes in the center of the image are regions where the direction of magnetization is different.

Transmission Electron Microscopy (TEM)

Because electrons are charged they experience a force—the Lorentz force—as they move through a magnetic field. This force causes them to be deflected by a small angle. The deflections are in different directions in different domains. The domain walls cannot be imaged under normal bright-field imaging conditions but they can be seen by either underfocusing or overfocusing the image (Fresnel images) or by displacing the objective aperture (Foucault images).

33.15 MOTION OF DOMAIN WALLS AND HYSTERESIS LOOPS

When an external magnetic field is applied to a ferromagnetic or ferrimagnetic material the domain boundaries begin to move. They move in such a way that domains in which the magnetization direction is aligned with H grow at the expense of the unaligned domains. The change in B with H is shown in Figure 33.21. Initially the movement of the domain walls is reversible and B increases only slightly with increasing H . As the field increases the favorably oriented domains grow more easily and μ increases. At very large H the unaligned domains will rotate and saturation will be reached in which all the domains are aligned in the same direction.

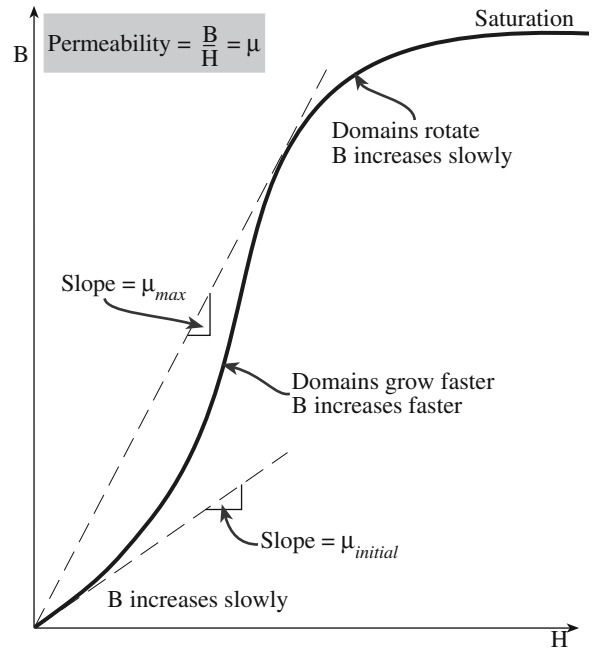


FIGURE 33.21 The effect of H on B . The ratio is μ .

When the field is removed, there is a resistance to domain wall motion preventing reorientation of the domains. As a result there is a residual magnetization, known as remanence (B_r), and the material acts as a permanent magnet.

If H is then applied in a direction opposite to what was originally used then domains grow with an alignment in the new direction. A certain field, called the coercive field, H_c , is needed to completely randomize the domains. Further increases in H eventually align the domains to saturation in the new direction. The behavior of a ferromagnetic or a ferrimagnetic material in an alternating magnetic field is shown in Figure 33.22. The size of the

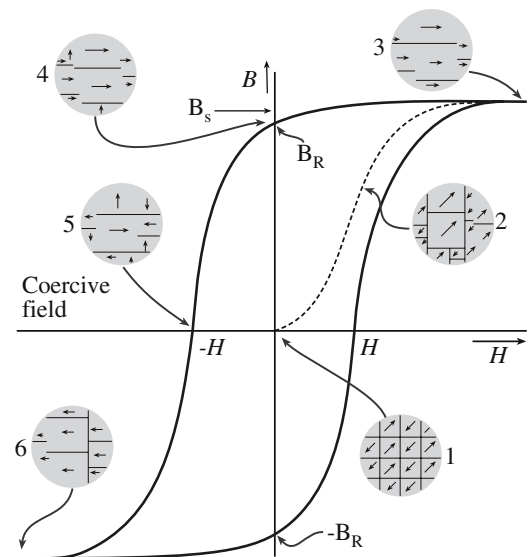


FIGURE 33.22 The variation of B as H alternates. The insets illustrate the domain structure at various points along the hysteresis curve.

TABLE 33.8 Classes of Magnetic Ceramic

Structure	Composition	Applications
Spinel (cubic ferrites)	1 MeO:1Fe ₂ O ₃ MeO = transition metal oxide, e.g., Ni,Co, Mn, Zn	Soft magnets
Garnet (rare earth ferrites)	3 Me ₂ O ₃ :5Fe ₂ O ₃ Me ₂ O ₃ = rare earth metal oxide, e.g., Y ₂ O ₃ , Gd ₂ O ₃	Microwave devices
Magnetoplumbite (hexagonal ferrites)	1 MeO:6Fe ₂ O ₃ MeO = divalent metal oxide from group IIA; e.g., BaO, CaO, SrO	Hard magnets

hysteresis loop, i.e., the values of B_r and H_c , vary from material to material.

- When H_c is small (typically $<10^3$ A/m) the material is a *soft* magnet.
- When H_c is large (typically $\gg 10^3$ A/m) the material is a *hard* magnet.

Hard and soft do not have any connection to the mechanical properties of the material. There are examples of metals and ceramics that exhibit hard and soft behavior.

33.16 HARD AND SOFT FERRITES

The important ferrimagnetic ceramics form three groups depending on their crystal structures as summarized in Table 33.8. When we are considering possible applications it is more useful, at least to the engineers who are designing and building magnetic components, to specify the materials as hard or soft. These designations, as mentioned in Section 33.15, are based on the size of the $B-H$ hysteresis loop, i.e., on the difficulty in reversing the direction of magnetization for the material. Hysteresis loops for hard and soft magnetic materials are compared schematically in Figure 33.23.

Convention: magnetic oxides that contain Fe^{3+} ions are called ferrites. This terminology does not distinguish between the crystal structures; do not confuse it with the chemical name. We often say that ferrites contain Fe_2O_3 as a principal component.

Hard Ferrites

Hard ferrites, which are used to fabricate permanent magnets, must have large

- H_c
- B_r

To satisfy these requirements, it is necessary to use materials with crystal structures that exhibit a large magnetic anisotropy and to prevent the growth and rotation of

magnetic domains (by, for example, controlling the grain size so that each grain becomes a single domain). Barium ferrite and oxides with a magnetoplumbite structure are the preferred choice.

Philips introduced ferrite magnets commercially in 1952 under the trade name “Ferroxdure.” About 550,000 t of hard ferrites are produced annually ($>95\%$ of the hard magnet market). This is more than metallic magnets. There are a number of reasons why ferrite magnets are commercially so important, not least of which is that the raw materials are relatively cheap and widely available and the manufacturing processes are simple.

Hard ferrite magnets are found in the following:

- Starter motors in automobiles
- Loudspeakers
- Rotors for cycle dynamos
- Windscreen wiper motors
- Mixed with a flexible polymer in door-catches and decorative magnets for refrigerators

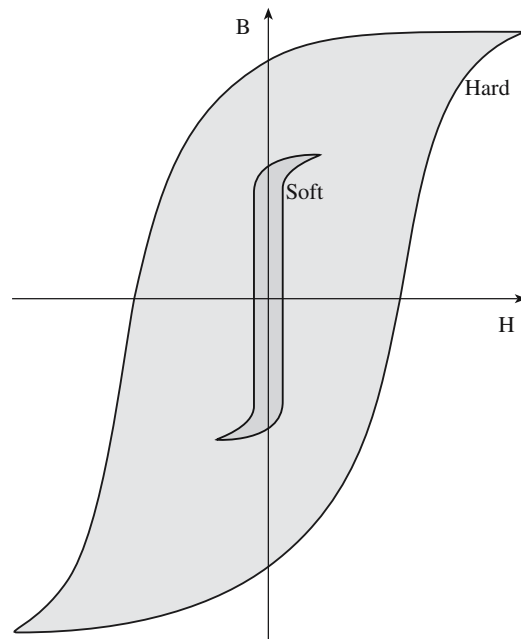


FIGURE 33.23 Comparison of the size and shape of hysteresis loops for hard and soft magnets.

TABLE 33.9 Properties of Several Hard Magnets

Material	Composition (wt%)	B_r (T)	H_c (A-turn m^{-1})	$(BH)_{max}$ (kJ/m ³)	θ_c (°C)	ρ ($\Omega \cdot m$)
Tungsten steel	92.8 Fe 6 W 0.5 Cr 0.7 C	0.95	5,900	2.6	760	3.0×10^{-7}
Cunife	20 Fe 20 Ni 60 Cu	0.54	44,000	12	410	1.8×10^{-7}
Sintered alnico	34 Fe 7 Al 15 Ni 35 Co 4 Cu 5 Ti	0.76	125,000	36	860	—
Sintered ferrite	BaO–6Fe ₂ O ₃	0.32	240,000	20	450	$\sim 10^4$
Cobalt rare earth	SmCo ₅	0.92	720,000	170	725	5.0×10^{-7}
Sintered neodymium–iron–boron	Nd ₂ Fe ₁₄ B	1.16	848,000	255	310	1.6×10^{-6}

- DC motors in fuel pumps
- Household appliances such as electric shavers, food mixers, and coffee grinders
- Magnetic strips on credit cards, ATM cards, etc.

Table 33.9 compares some of the important properties of hard ferrites with hard metal alloy magnets such as alnico and high-energy ($BH \geq 80 \text{ kJ/m}^3$) rare earth magnets such SmCo₅.

Soft Ferrites

The prime requirement for a soft ferrite is that a high M can be produced using a small H . This means that soft ferrites should have

- High μ
- Low H_c

Soft ferrites therefore have narrow hysteresis loops. During changes in field direction the domains are rapidly and easily realigned with the changing magnetic field. Consequently, domain wall motion and/or magnetization rotation must be easy. Domain wall motion is particularly sensitive to the microstructure of the material and characteristics such as grain size and grain-boundary structure,

the presence of inclusions or pores within the grains, impurity levels, and stresses all reduce domain wall motion. Porosity is particularly common in many sintered ceramics and ferrites are certainly no exception. As a result magnetization rotation plays an important role in reaching B_s . Soft ferrites should also have high electrical resistivities (not a problem for most ceramics!) because this limits eddy current losses.

Soft ferrites are generally used in applications in which the direction of H is frequently changing such as high-frequency inductors and transformers and magnetic elements in microwave components. There are plenty of household examples in which soft ferrites are used:

- Magnetic recording and data storage media
- Transformer cores in telephones
- Numerous applications in radios and televisions, such as line transformers, deflection coils, tuners, and rod antennas

Table 33.10 compares some of the relevant properties of metal and ceramic soft magnets. Spinel ferrites based upon the (Mn,Zn,Fe)O₄ system are examples of commercially important soft magnets. The market for soft ferrites is about 50,000t per year. These are usually marketed under the trade name *Ferroxcube*.

TABLE 33.10 Properties of Several Soft Magnets

Material	Composition (wt%)	μ_i	B_s (T)	Hysteresis loss/cycle (J/m ³)	ρ ($\Omega \cdot m$)
Iron	99.95 Fe	150	2.14	270	1.0×10^{-7}
Silicon-iron (oriented)	97 Fe, 3 Si	1,400	2.01	40	4.7×10^{-7}
45 Permalloy	55 Fe, 45 Ni	2,500	1.60	120	4.5×10^{-7}
Supermalloy	79 Ni, 15 Fe, 5 Mo, 0.5 Mn	75,000	0.80	—	6.0×10^{-7}
Ferroxcube A	48 MnFe ₂ O ₄ , 52 ZnFe ₂ O ₄	1,400	0.33	~ 40	2,000
Ferroxcube B	36 NiFe ₂ O ₄ , 64 ZnFe ₂ O ₄	650	0.36	~ 35	10^7

Garnets also tend to be soft magnets but are not as widely used as the cubic ferrites: they are more expensive. There was a great deal of interest in the late 1960s and 1970s in magnetic garnets for use in bubble memory. A magnetic bubble is a small (from about 0.05 μm up to 10 μm) cylindrical region, which has M in the opposite direction to H .

A bubble memory is nonvolatile, which means that once information is stored it remains even when the power is removed (just like current hard drives). Bubble memories used a thin layer (usually about 4 μm) of a magnetic garnet (a typical formulation being $\text{Y}_{2.6}\text{Sm}_{0.4}\text{Ga}_{1.2}\text{Fe}_{3.8}\text{O}_{12}$) deposited by liquid phase epitaxy onto a substrate of gadolinium gallium garnet (GGG). The strain induced by the lattice misfit and differences in the coefficient of thermal expansion between the two garnets resulted in an anisotropic axis normal to the film.

By the mid-1970s most of the large electronic companies were working on bubble memories and by the late 1970s there were several commercial products. By the 1980s the bubble memory market was dead. One of the reasons was the introduction of larger and faster hard drives.

33.17 MICROWAVE FERRITES

When a magnetic field is applied to a spinning electron it precesses around the field direction in much the same way that a spinning top precesses around the direction of a gravitational field. In ferromagnetic and ferrimagnetic materials the electron spins are coupled and the magnetization vector, M , will precess around the field direction as shown in Figure 33.24. The interaction between electromagnetic waves and the precessing spin magnetic moments in the ferrite has been used to make waveguides for microwaves. Microwaves are electromagnetic radiation with frequencies in the range of 1–300 GHz ($\lambda = 30\text{cm}$ to

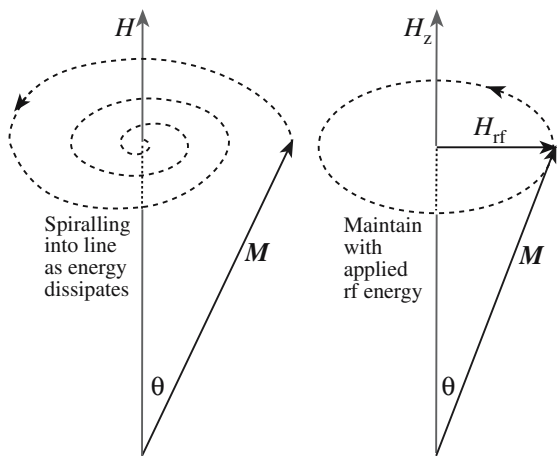


FIGURE 33.24 Illustration of the precessional motion of the magnetization vector.

3 mm). As they travel along the waveguide their behavior is modified.

An important example is known as Faraday rotation, which involves the rotation of the plane of polarization of a plane wave as it travels through the waveguide. A plane-polarized wave is equivalent to two circularly polarized waves, polarized in opposite senses (i.e., a right-polarized and a left-polarized component). Each component interacts very differently with the precessing spins and encounters different permeabilities, which affect the velocities of the two waves. The left component is retarded relative to the right, causing a clockwise rotation of the plane of polarization.

The most direct application of Faraday rotation is to use waveguides in the same way that polarizers and analyzers are used in light optics: to accept or reject plane polarized waves.

There are several different types of microwave devices. Isolators allow transmission of microwave radiation in one direction (they are used to prevent unwanted reflected signals). Gyrotors are used to rotate the plane of polarization. There are other, more complicated devices, such as phase shifters and circulators. Garnets are widely used in microwave engineering because their properties can be tailored for the specific application. A garnet that is currently used in radar phase shifters is $\text{Y}_{2.66}\text{Gd}_{0.34}\text{Fe}_{4.22}\text{Al}_{0.68}\text{Mn}_{0.09}\text{O}_{12}$.

Microwave ferrites are used in radar-absorbing paint, which is used to make planes such as the F-117 Nighthawk and the B-2 Spirit “stealthy.”

33.18 DATA STORAGE AND RECORDING

Magnetic recording is a major technology for electronic information mass storage. Its presence is ubiquitous in audio and video cassette tapes, floppy disks, computer hard disks, credit cards, etc. The magnetic audio recorder was invented in 1898. Video recorders were first introduced in 1955 primarily for use by broadcasters before they became widely available for commercial use. Now magnetic recording equipment has spread to almost every household with sales exceeding \$50 billion per year.

Magnetic recording materials such as magnetic tapes and floppy disks are collections of very fine magnetic particles supported on a flexible polymer such as polyethylene terephthalate (PET). The basic features of magnetic recording are illustrated in Figure 33.25. A minute part of the magnetic tape is magnetized by a signal from a magnetic head and data are stored in a form of the magnetization direction. The properties of the material used for this purpose are quite specific:

- H_c must be high enough to maintain magnetization but sufficiently low to allow stored data to be erased
- Chemically stable

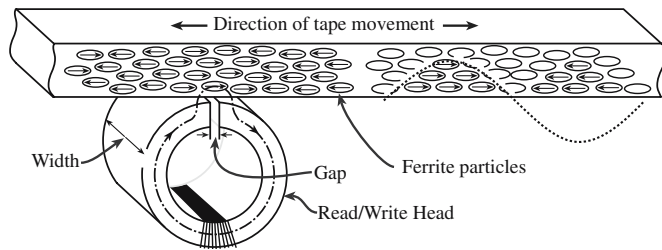


FIGURE 33.25 Illustration of the principal features of longitudinal recording.

- Small (<1 μm), uniformly distributed acicular particles
- Uniform distribution of particles
- Cheap

Three types of ceramic particles are currently used as magnetic media: $\gamma\text{-Fe}_2\text{O}_3$, $\text{Co-}\gamma\text{-Fe}_2\text{O}_3$, and CrO_2 . Their properties are given in Table 33.11. Iron oxide particles were first used in magnetic recording in the 1930s and now account for 90% of this market. The standard method for making $\gamma\text{-Fe}_2\text{O}_3$ involves dehydrating goethite ($\alpha\text{-FeOH}$) to hematite ($\alpha\text{-Fe}_2\text{O}_3$) followed by reducing the hematite to magnetite (Fe_3O_4) and finally oxidizing the magnetite to maghemite ($\gamma\text{-Fe}_2\text{O}_3$).

Various experimental modifications have been made to the process over the years to produce $\gamma\text{-Fe}_2\text{O}_3$ particles that have the required shape and uniformity for use as magnetic media. The $\gamma\text{-Fe}_2\text{O}_3$ particles typically have lengths in the range of 100–700 nm and aspect ratios up to 10. H_c of $\gamma\text{-Fe}_2\text{O}_3$ is at the low end of the useful range for magnetic recording. As a result it is more useful at recording signals in the low frequency range. Cobalt-modified $\gamma\text{-Fe}_2\text{O}_3$ particles were developed to increase H_c . These particles were widely used in audio-cassette tapes (before the advent of CDs and iPods) and also on some videocassette tapes. The reason for the higher H_c is not well understood.

The process for producing chromium dioxide (CrO_2) particles for magnetic media was developed by the DuPont Company in the 1960s. Because of the higher uniformity in size and shape of the particles CrO_2 tends to have a

much higher H_c than $\gamma\text{-Fe}_2\text{O}_3$. This makes CrO_2 more suitable for high-density recording. It also has a high M giving a large range of response and thus a high quality of reproduction. The small particle size and the very uniform particle size distribution mean that CrO_2 tapes have much lower noise (less background hiss on audio tapes; less “snow” on video pictures). Chromium dioxide is widely used in tapes for videocassettes and for professional audio-tapes. The drawbacks of CrO_2 are

- Low θ_c
- Toxicity
- It is abrasive to some types of recording head
- Magnetic properties degrade slowly with time

But the main drawback that prevented its more widespread use in audiotapes is that it is more expensive than $\gamma\text{-Fe}_2\text{O}_3$.

Ferrites can be used to store a considerable amount of information, but in many applications are being replaced by optical information storage such as CDs and DVDs.

Magnetic materials are used in the read and write heads of magnetic storage drives. The most significant change since the beginning of this technology and the use of conventional recording heads using magnetic induc-

tance was the introduction of magnetoresistive (MR) and then GMR recording heads. These allowed data to be stored more densely and read more quickly. GMR is now used in most modern hard drives.

Ceramic CMR materials may produce the next big change. In CMR resistance does not change by a few percent but by orders of magnitude. Applications for these materials are being developed.

The use of barium ferrite for high-density recording applications has been investigated because it is chemically stable and can have $H_c \sim 480 \text{ kA/m}$. The hexagonal particles can, in principle, be oriented with their c axis normal to the tape surface as shown in Figure 33.26. This is known as a perpendicular medium and can give very high recording densities. Hexagonal ferrites are used in the magnetic strips on credit cards and ATM cards. In these applications we want the data to be permanent.

MAGHEMITE

The name *maghemite* was first suggested in 1927. It is a combination of the first syllables of *magnetite*, which has the same structure, and *hematite*, which has the same composition.

TABLE 33.11 Physical and Magnetic Properties of Magnetic Particles

Magnetic particle	Particle length (μm)	Aspect ratio	Specific surface area (m ² /g)	H_c (kA/m)	B_s (T)	θ_c (°C)
$\gamma\text{-Fe}_2\text{O}_3$	0.3–0.6	10	20–30	20–32	0.5	675
$\text{Co-}\gamma\text{-Fe}_2\text{O}_3$	0.3–0.4	10	20–30	30–70	0.5	400
CrO_2	0.2–0.7	10–20	24–40	30–50	0.5	113
Fe (metal)	0.2–0.4	~6	40–50	75–130	2.0	770

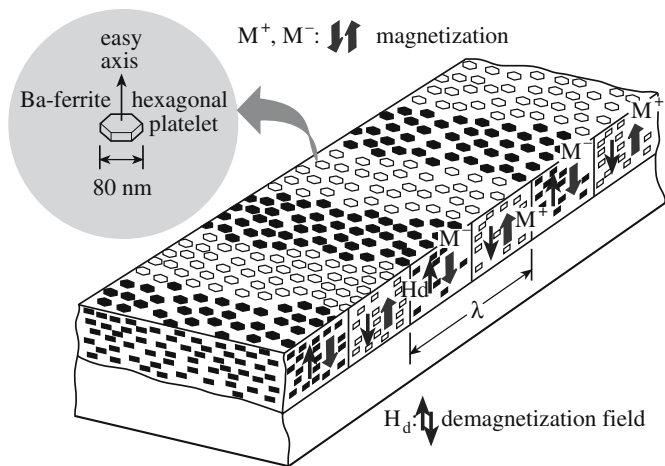


FIGURE 33.26 The principle of perpendicular recording.

33.19 MAGNETIC NANOPARTICLES

Magnetic ceramic nanoparticles are becoming of increasing interest in a number of areas. One of these areas is using them for the location and detection of viruses: a viral nanosensor. The approach is illustrated in Figure

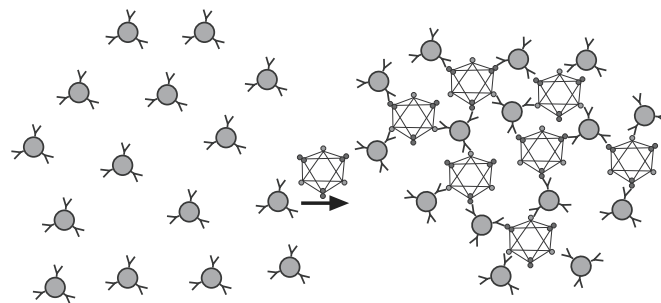


FIGURE 33.27 Diagram of a viral-induced nanoassembly of magnetic nanoparticles.

33.27. Iron oxide particles (~50 nm in diameter) with a dextran coating are covered with antibodies. The antibodies are chosen for a specific virus (e.g., herpes simplex virus or adenovirus). When these specially coated nanoparticles are then exposed to the virus they will form clusters that would be large enough to be visible on a nuclear magnetic resonance (NMR) or magnetic resonance imaging (MRI) scan. This approach has already been demonstrated in the laboratory using viral particles in solution. The idea is that it might eventually be used to detect viruses in human body fluid or tissue.

CHAPTER SUMMARY

In this chapter we described the different magnetic properties of ceramics. Most ceramics are diamagnetic, a very weak and commercially unimportant property. The most important magnetic properties of ceramics arise because of the presence of unpaired electron spins, primarily in the 3d orbitals of Fe. Ferrites, a class of magnetic ceramics containing Fe_2O_3 , are used in a wide variety of applications, and their production constitutes a multibillion dollar industry. Ferrites can be classified according to their structure, and there are three structural types: spinel or cubic ferrites, garnets, and hexagonal ferrites. The cubic ferrites, of which $\gamma\text{-Fe}_2\text{O}_3$ (maghemite) is the most ubiquitous example, are soft magnetic materials and hence the direction of magnetization can be relatively easily changed in an alternating magnetic field. Maghemite was used extensively in audiotapes and floppy disks (which have now largely been replaced by iPods and CDs). The magnetic garnets are used in microwave applications including ingredients on radar-absorbing paint for stealthy airplanes. The hexagonal ferrites, such as $\text{BaO} \cdot 6\text{Fe}_2\text{O}_3$, are hard or permanent magnetic materials. They are more difficult to demagnetize. Barium hexaferrite is used in many applications from small electric motors in automobiles, to the magnetic seal on a refrigerator, to the magnetic strip on credit cards. Manganates, which have the technologically important layered perovskite structure, exhibit a property called colossal magnetoresistance and offer potential in a number of technologies from read/write heads in magnetic recording, sensors, and spin-polarized electronics.

PEOPLE IN HISTORY

Bitter, Francis (1902–1967) was born in Weehawken, New Jersey. In 1931 he discovered a method for visualizing magnetic domains. In 1934 he joined the Department of Mining and Metallurgy at M.I.T. (where he spent most of his career) and helped establish a high field magnet laboratory. During WW II, he worked in England on methods to demagnetize German mines in the English Channel. His work after the war led to the establishment of the National Magnet Laboratory, which after his death was renamed the Francis Bitter National Magnet Laboratory.

Bloch, Felix (1905–1983) was born in Zurich, Switzerland. He received his Ph.D. in 1928 from the University of Leipzig where he worked with Heisenberg. Upon Hitler's rise to power Bloch left Europe and moved to the United States where he accepted a position at Stanford University. He was awarded the 1952 Nobel Prize in Physics for the development of the NMR technique.

Curie, Pierre (1859–1906) was born in Paris. In 1895 he obtained his Doctor of Science degree and was appointed Professor of Physics at the Sorbonne. In his early studies on crystallography, together with his brother Jacques, he discovered the piezoelectric effect. Later, he turned his attention to magnetism and showed that the magnetic properties of a given substance change at a certain temperature (the Curie temperature). He was awarded the Nobel Prize in physics in 1903 (together with his wife Marie) for their work in radioactivity. On April 19, 1906 he was killed in a street accident in Paris.

GMR was discovered in 1988; CMR was discovered in 1993.

Josephson, Brian David (1940–) was born in Cardiff, Wales and discovered the Josephson effect while a 22-year-old graduate student at the University of Cambridge. He won the Nobel Prize in physics in 1973 for his discovery.

Lenz (pronounced *lents*), Heinrich Friedrich Emil (1804–1865) was born in Dorpat, Russian Empire (now Tartu, Estonia) and formulated his eponymous law of electromagnetism in 1833. He participated in a round-the-world expedition in 1823–1826 and made extremely accurate measurements of the properties of seawater.

London, Fritz (1900–1954) was born in Breslau, Germany (now Wroclaw, Poland). He fled Nazi Germany in 1933 and came to the United States in 1939 where he became naturalized in 1945. Together with his younger brother Heinz he formulated the London equations of superconductivity.

Meissner, Walther (1882–1974) and his graduate student Robert Ochsenfeld (1901–1993), both Germans working in Berlin, discovered in 1933 that a superconducting material repels a magnetic field—behaving as a perfect diamagnet. The effect became known as the Meissner (or Meissner–Ochsenfeld) effect.

Oersted, Hans Christian (1777–1851) was a Danish physicist and philosopher. He demonstrated the fundamental relationship between electricity and magnetism on July 21, 1820 during a lecture on electricity at the University of Copenhagen. He showed that a compass needle is deflected when a wire carrying an electric current is placed near it. In addition to his work in electricity and magnetism, Oersted was the first to prepare pure metallic aluminum (1825).

Weiss, Pierre Ernest (1865–1940) was born in Mulhouse in the Alsace region of eastern France. He proposed the domain theory of ferromagnetism in 1907 while he was working at the Polytechnic Institute in Zurich.

GENERAL REFERENCES

Cullity, B.D. (1972) *Introduction to Magnetic Materials*, Addison-Wesley, Reading MA. A standard, but now dated, text on magnetism.

Jakubovics, J.P. (1994) *Magnetism and Magnetic Materials*, The Institute of Materials, London. A good overview (and brief), it includes more methods for measuring magnetic susceptibility.

Kittel, C. (1986) *Introduction to Solid State Physics*, 6th edition, Wiley, New York. Chapter 14 describes diamagnetism and paramagnetism and Chapter 15 describes ferromagnetism and antiferromagnetism. The approach is quite mathematical and goes deeper into the fundamentals than we do.

Moulson, A.J. and Herbert, J.M. (1990) *Electroceraamics*, Chapman & Hall, London. A very good text on this topic.

Owens, F.J. and Poole, C.P., Jr. (1996) *The New Superconductors*, Plenum Press, New York. A gentle introduction to ceramic superconductors includes a very readable account of the flux lattice.

Purcell, E.M. (1985) *Electricity and Magnetism*, 2nd edition, McGraw-Hill, New York. An E&M reference. Purcell shared the 1952 Nobel Prize in physics with Bloch.

Standley, K.J. (1972) *Oxide Magnetic Materials*, 2nd edition, Clarendon Press, Oxford. A very useful reference on this topic. Described the structure of manganates before their commercial importance was realized.

SPECIFIC REFERENCES

Kato, Y. and Takei, T. (1932) Japanese patent 98,844. The first commercial applications of ferrites.

Néel, L. (1948) “Proprietés magnetiques des ferrites—ferrimagnetisme et antiferromagnetisme,” *Ann. Phys.* **3**, 137. The original description of ferrimagnetism. Néel won the 1970 Nobel Prize in physics for his work on antiferromagnetism and ferrimagnetism.

Perez, J.M., Simeone, F.J., Saeki, Y., Josephson, L., and Weissleder, R. (2003) “Viral-induced self-assembly of magnetic nanoparticles allows the detection of viral particles in biological media,” *J. Am. Chem. Soc.* **125**, 10192. Description of a viral nanosensor using iron oxide nanoparticles. This group is at Harvard Medical School.

Roth, W.L. (1960) “Neutron and optical studies of domains in NiO,” *J. Appl. Phys.* **31**, 2000. The first description (and naming) of domain boundaries in antiferromagnets.

Shull, C.G. and Smart, J.S. (1949) “Detection of antiferromagnetism by neutron diffraction,” *Phys. Rev.* **76**, 1256. The original neutron diffraction studies on antiferromagnetic materials.

Smit, J. and Wijn, H.P.J. (1959) *Ferrites*, Wiley, New York. More detailed description of magnetoplumbite ferrites.

- Snoeck, J.L. (1947) *New Developments in Ferromagnetic Materials*, Elsevier, New York. The first major published study of ferrites.
- Weiss, P. (1906) "The variation of ferromagnetism with temperature," *Compt. Rend.* **143**, 1136. Weiss domains.
- Williams, D.B. and Carter, C.B. (1996) *Transmission Electron Microscopy: A Textbook for Materials Science*, Plenum, New York. The Lorentz technique is described on pp. 534–537.
- Zener, C (1951) "Interaction between the d-shells in the transition metals," *Phys. Rev.* **81**, 440 and "Interaction between the d-shells in the transition metals 2: Ferromagnetic compounds of manganese with perovskite structure," *Phys. Rev.* **82**, 403. These two papers have been cited collectively almost 4000 times and describe the double exchange mechanism. Clarence Zener spent a short time (1940–1942) as an instructor at Washington State University when it was still known as Washington State College.

EXERCISES

- 33.1 Diamagnetism is present in all materials. Why do we not usually need to consider its contribution when we determine χ for a paramagnetic material using a Gouy balance?
- 33.2 You are given a sample of a ceramic powder that you believe to be paramagnetic. You have access to a Gouy balance. Explain how you would determine χ for your powder and what possible sources of error there might be.
- 33.3 In Section 33.4 we said that there are two general categories of magnetic behavior. Assign each of the five main types of magnetic response, diamagnetism, paramagnetism, ferromagnetism, antiferromagnetism, and ferrimagnetism, into one of the two categories. Explain briefly how you arrived at your assignments.
- 33.4 Al_2O_3 , BeO, diamond, MgO, NaCl, and Si are all diamagnetic. Explain this observation.
- 33.5 You perform experiments using a Gouy balance using sintered rods of Al_2O_3 , BeO, CeO_2 , and TiO_2 . What sign would you expect to obtain for χ for each material? Would you get a different result if you replaced the oxide with its corresponding metal?
- 33.6 How would the magnetic properties of magnetite change if it were a normal spinel?
- 33.7 Sketch the position of the atoms in the perovskite unit cell that you would expect for the CMR compound $\text{La}_{0.5}\text{Ca}_{0.5}\text{MnO}_3$.
- 33.8 The compounds in the $\text{La}_{1-x}\text{A}_x\text{MnO}_3$ system contain both Mn^{3+} and Mn^{4+} ions and are collectively called "manganites." Is the use of this term correct scientific usage or not? Briefly explain your answer.
- 33.9 Liquid phase epitaxy (LPE) was used for forming thin garnet films for magnetic bubble memories. Describe the basic principles behind this technique. Would sputtering or evaporation be good alternative techniques for such films? Explain how you arrived at your answer.
- 33.10 Compare the energy and width of domain boundaries with values for grain boundaries. Based on the values you obtain discuss the relative ease of movement of the two types of boundary.

Responding to Temperature Changes

CHAPTER PREVIEW

Heat is essentially the vibration of atoms in a material. Consequently thermal properties reflect the type and strength of interatomic bonding and the crystal structure. The important thermal properties of any material are

- Heat capacity
- Coefficient of thermal expansion
- Thermal conductivity

Thermal properties of ceramics differ from those of metals whenever free (conduction) electrons are involved, such as in thermal conductivity. However, heat transfer by phonon (lattice vibration) transport can in some cases be more effective than through the movement of electrons. We describe melting and vaporization of ceramics as the temperatures for these transformations tend to be high, which can be critical in certain applications, such as the tiles on the space shuttle, but present problems during processing. It should also be obvious by now that heat affects many of the properties of ceramics such as Young’s modulus, electrical conductivity, magnetic behavior, and dielectric constant. There are major applications that utilize the varied thermal properties of ceramics, from high thermal conductivity substrates for electronic packaging to enormous mirror blanks for telescopes that have “zero” expansion.

34.1 SUMMARY OF TERMS AND UNITS

Table 34.1 lists the important parameters used in this chapter and their units. The SI unit of temperature is kelvin (K), but as you will have realized by now °C is often used in presenting data in materials science. As mentioned in Chapter 1, the numerical value of a temperature difference or temperature interval expressed in °C is equal to the numerical value of the same temperature difference or interval when expressed in K. This point is worth remembering when coefficients of thermal expansion or thermal conductivities are compared for different materials.

34.2 ABSORPTION AND HEAT CAPACITY

When a solid absorbs an amount of heat, dq , its internal energy, E , rises by an amount dE where

$$dE = dq \tag{34.1}$$

The increase in internal energy is largely due to the increased vibrational amplitude of the atoms about their

equilibrium positions. This vibrational motion represents the thermal energy of the solid. There are other mechanisms for heat absorption, but these are either negligible or absent entirely. However, we will list them here and very briefly describe them because they relate to some concepts that have been described in earlier chapters such as point defects.

- *Rotational*: Rotational absorption is important in liquids and gases where the molecules are free to rotate, but this contribution is negligible in solids.
- *Electronic*: Absorption by conduction electrons is very small, but it can be used to provide information about the electronic structure of a solid, so from that point of view it is useful.
- *Defect formation*: The formation of Frenkel and Schottky defects can contribute, although usually only at high temperatures.
- *Phase transformations*: These involve absorption by structural, magnetic, and ferroelectric transformations in certain materials.

Heat capacity is a measure of the amount of energy required to raise the temperature of a material. At room

TABLE 34.1 Summary of Terms Used to Describe the Thermal Properties of Materials

	Definition	Units/value
α	Linear coefficient of thermal expansion	$^{\circ}\text{C}^{-1}$ or K^{-1}
C_v	Heat capacity at constant volume	J/K
c_v	Molar heat capacity at constant volume	$\text{J mol}^{-1} \text{K}^{-1}$
C_p	Heat capacity at constant pressure	J/K
c_p	Molar heat capacity at constant pressure	$\text{J mol}^{-1} \text{K}^{-1}$
ΔS_f	Entropy of fusion	$\text{J mol}^{-1} \text{K}^{-1}$ or $\text{J g-atom}^{-1} \text{K}^{-1}$
ΔS_v	Entropy of vaporization	$\text{J mol}^{-1} \text{K}^{-1}$ or $\text{J g-atom}^{-1} \text{K}^{-1}$
k	Thermal conductivity	$\text{W m}^{-1} \text{K}^{-1}$
T_b	Boiling temperature	$^{\circ}\text{C}$ or K
T_m	Melting temperature	$^{\circ}\text{C}$ or K
R_{TS}	Thermal shock resistance	W/m
θ_D	Debye temperature	$^{\circ}\text{C}$ or K
R	Gas constant	$8.314 \text{ J mol}^{-1} \text{K}^{-1}$

temperature the specific heat capacity of many ceramics is between 0.75 and $1.0 \text{ J g}^{-1} \text{K}^{-1}$. For example, granite (an igneous silicate rock) has a specific heat capacity of $0.79 \text{ J g}^{-1} \text{K}^{-1}$ at 25°C , which means that it takes about 0.8 J of energy to raise the temperature of 1 g of granite by 1 K. Water has a specific heat capacity of $4.184 \text{ J g}^{-1} \text{K}^{-1}$ at 25°C ; this value is more than five times greater than that of granite. This difference is crucial in regulating the earth's temperature. It takes five times more energy to increase the temperature of water by 1 K than it does to increase the temperature of granite. If the earth's surface were composed entirely of rock (i.e., there were no oceans) then daytime temperatures would be extremely high. The oceans also help limit the temperature drop at night, because they have absorbed more energy during the day, which is released at night. If the earth had no oceans temperature swings between day and night would be very large.

When referring to heat capacity, and in particular when various other sources are consulted, it is necessary to be careful about terminology. Here are the definitions of all the terms you are likely to encounter:

- Heat capacity is the amount of heat required to change the temperature of an object by 1 K. The units of heat capacity are J/K.
- Specific heat capacity is the amount of heat required to change the temperature of 1 g of a substance by 1 K. The units of specific heat capacity are $\text{J g}^{-1} \text{K}^{-1}$.
- Molar heat capacity is the amount of heat required to change the temperature of 1 mol of a substance by 1 K. The units of molar heat capacity are $\text{J mol}^{-1} \text{K}^{-1}$.

In the literature you will find that “heat capacity” is often used to describe all these three terms. But it is usually obvious from the units given what term is actually the correct one to use. The next term is really the confusing one. Fortunately it is not used now, but it does occur from time to time in some of the older literature so beware:

- Specific heat is the ratio of the heat capacity of a substance to the heat capacity of water. This term is a unitless ratio and was used when the heat capacity of water was unity. In the SI system of units the heat capacity of water is not unity.

Heat capacities of solids are always functions of temperature, as illustrated for several ceramics in Figure 34.1. Note the units are $\text{J g-atom}^{-1} \text{K}^{-1}$. At absolute zero the internal energy of a solid is a minimum and the heat capacity is zero. As the temperature rises the heat capacity increases, which is indicative of the various mechanisms by which energy is absorbed. The heat capacity approaches a classical limit of $3R$ ($\sim 25 \text{ J mol}^{-1} \text{K}^{-1}$) at a sufficiently high temperature that differs from one solid to another. This statement is essentially the Dulong–

Petit law. The crystal structure and composition of a material do not appreciably affect heat capacity but n does: e.g., c_p is $3R$ for Cu but $6R$ for MgO.

The temperature at which the heat capacity becomes constant, or varies only slightly with temperature, is the Debye temperature, θ_D . Values of θ are typically in the range of $T_m/5$ to $T_m/2$ and depend on

- Bond strength
- E
- T_m

For example, in diamond, where the covalent bonds are very strong, θ_D is $\sim 2000 \text{ K}$. However, the value of θ_D for NaCl is 281 K .

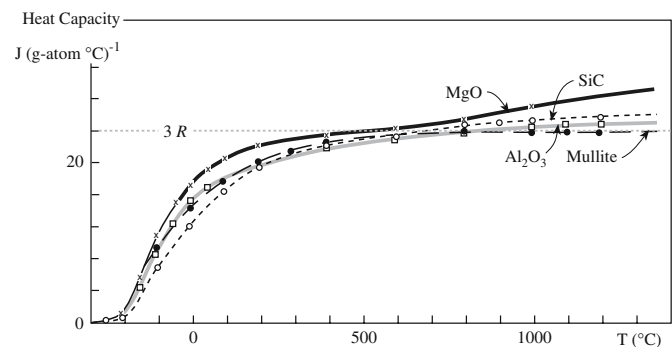


FIGURE 34.1 Heat capacity of some ceramics as a function of temperature.

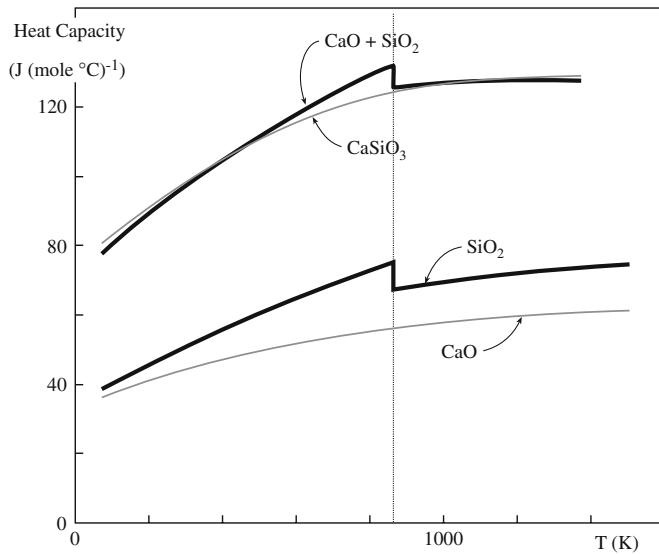


FIGURE 34.2 Heat capacity of SiO₂ as a function of temperature.

Abrupt changes in heat capacity are observed over a narrow temperature range when a material undergoes a structural transformation or some other change in order. The example shown in Figure 34.2 is for quartz (a polymorph of SiO₂), which undergoes a displacive α - β phase transformation at 573°C. Similar changes in heat capacity occur in glasses at the glass transition temperature, T_g , because of the increase in configurational entropy in the liquid. Anomalous heat capacities are also associated with the alignment of magnetic dipoles in ferromagnetic materials and the alignment of electric dipoles in ferroelectrics.

The heat capacity of a material can be calculated, depending on the temperature range of interest, using one of two equations. At very low (cryogenic) temperatures

$$c_p \cong c_v = K \left(\frac{T}{\theta_D} \right)^3 + \gamma T \quad (34.2)$$

where K is a constant equal to $1940 \text{ J mol}^{-1} \text{ K}^{-1}$ and γ is the electronic heat capacity coefficient. Values of θ_D and γ are tabulated in several lists of thermodynamic properties. These values are generally widely available for metals and somewhat more obscure for most ceramics. The overall contribution of Eq. 34.2 to the heat capacity of a material is small and is really of importance only if you wish to obtain a fundamental understanding of the nature of a material or if you are designing systems to operate at cryogenic temperatures.

At high temperature (usually above room temperature) heat capacities can be calculated using the empirical relation

$$c_p = a + bT + cT^{-2} \text{ J mol}^{-1} \text{ K}^{-1} \quad (34.3)$$

where a , b , and c are “constants,” which have been tabulated for a wide range of materials.

34.3 MELTING TEMPERATURES

One of the very useful properties of many ceramics is their high T_m as shown in Table 34.2. This property makes ceramics without equal for application at high temperature, such as refractories and thermal barrier coatings. There is a direct correlation between T_m and bond strengths. Also, ceramics with the highest values of T_m tend to have a significant fraction of covalent character to their bonding as shown in Table 34.3; this table is calculated using Eq. 4.24 and values of Pauling electronegativities given in Figure 3.4. However, T_m does not correlate directly with the fraction of covalent character of the bond or ionic potential (ϕ) of the cation as shown for the oxides of the alkaline earth elements in Table 34.4, which is calculated in the same manner. (The values of ionic radii are given in Table 4.6.)

Compounds with very high fractions of ionic character to their bonds such as the alkali halides NaCl and LiF tend to have lower values of T_m than their corresponding oxides. The reason is the greater ionic charges (e.g., O^{2-} rather than Cl^-) involved and hence the stronger electrostatic attraction. We can illustrate this point for the two compounds Li₂O and LiF. Bond energies for ionic compounds can be obtained using Eq. 34.4 (this is simply the Born-Landé equation given in Chapter 4 written for a single bond):

$$E_{\text{bond}} = \frac{Z_1 Z_2 e^2}{4\pi\epsilon_0 r_0} \left(1 - \frac{1}{n} \right) \quad (34.4)$$

For Li₂O we have $r_{\text{Li}^+} = 0.068 \text{ nm}$ and $r_{\text{O}^{2-}} = 0.140 \text{ nm}$, so $r_0 = 0.208 \text{ nm}$. Taking $n = 10$, and substituting into Eq. 34.4 we get a value of $E_{\text{bond}} = 1.997 \times 10^{-18} \text{ J}$.

For LiF we have $r_{\text{Li}^+} = 0.068 \text{ nm}$ and $r_{\text{F}^-} = 0.133 \text{ nm}$, so $r_0 = 0.201 \text{ nm}$. Taking $n = 10$ and substituting into Eq. 34.4 we get a value of $E_{\text{bond}} = 1.033 \times 10^{-18} \text{ J}$.

So we would expect Li₂O to have a higher T_m than LiF, and if you look at Table 34.2 you will see that for Li₂O $T_m = 1570^\circ\text{C}$ while for LiF $T_m = 848^\circ\text{C}$.

The entropy difference between the solid and the liquid at T_m is

$$\Delta S_f = \frac{\Delta H_f}{T_m} \quad (34.5)$$

RICHARD'S RULE

$$\Delta S_f = 8.4 \text{ J g-atom}^{-1} \text{ K}^{-1}$$

Values of ΔS_f are shown in Table 34.2. They are positive because the liquid is

always more disordered than the solid, but vary considerably from the empirical prediction known as Richard's

TABLE 34.2 T_m and ΔS_f for Selected Ceramics

Compound	T_m ($^{\circ}\text{C}$)	ΔS_f ($\text{J mol}^{-1} \text{ }^{\circ}\text{C}^{-1}$)	Compound	T_m ($^{\circ}\text{C}$)	ΔS_f ($\text{J mol}^{-1} \text{ }^{\circ}\text{C}^{-1}$)
Oxides					
Al ₂ O ₃	2054 ± 6	47.70	Mullite	1850	
BaO	2013	25.80	Na ₂ O (α)	1132	33.90
BeO	2780 ± 100	30.54	Nb ₂ O ₅	1512 ± 30	58.40
Bi ₂ O ₃	825		Sc ₂ O ₃	2375 ± 25	
CaO	2927 ± 50		SrO	2665 ± 20	25.60
Cr ₂ O ₃	2330 ± 15	49.80	Ta ₂ O ₅	1875 ± 25	
Eu ₂ O ₃	2175 ± 25		ThO ₂	3275 ± 25	
Fe ₂ O ₃	Decomposes at 1735K to Fe ₃ O ₄ and oxygen		TiO ₂ (rutile)	1857 ± 20	31.50
Fe ₃ O ₄	1597 ± 2	73.80	UO ₂	2825 ± 25	
Li ₂ O	1570	32.00	V ₂ O ₅	2067 ± 20	
Li ₂ ZrO ₃	1610		Y ₂ O ₃	2403	≈38.70
Ln ₂ O ₃	2325 ± 25		ZnO	1975 ± 25	
MgO	2852	25.80	ZrO ₂	2677	29.50
Halides					
AgBr	434		LiBr	550	
AgCl	455		LiCl	610	22.60
CaF ₂	1423		LiF	848	
CsCl	645	22.17	Lil	449	
KBr	730		NaCl	800	25.90
KCl	776	25.20	NaF	997	
KF	880		RbCl	722	23.85
Silicates and other glass-forming oxides					
B ₂ O ₃	450 ± 2	33.20	Na ₂ Si ₂ O ₅	874	31.00
CaSiO ₃	1544	31.00	Na ₂ SiO ₃	1088	38.50
GeO ₂	1116		P ₂ O ₅	569	
MgSiO ₃	1577	40.70	SiO ₂ (high quartz)	1423 ± 50	4.6
Mg ₂ SiO ₄	1898	32.76			
Carbides, nitrides, borides, and silicides					
B ₄ C	2470 ± 20	38.00	ThN	2820	
HfB ₂	2900		TiB ₂	2897	
HfC	3900		TiC	3070	
HfN	3390		TiN	2947	
HfSi	2100		TiSi ₂	1540	
MoSi ₂	2030		UC	2525	
NbC	3615		UN	2830	
NbN	2204		VB ₂	2450	
SiC	2837		VC	2650	
Si ₃ N ₄	At 2151 K partial pressure of N ₂ over Si ₃ N ₄ reaches 1 atm		VN	2177	
			WC	2775	
TaB ₂	3150		ZrB ₂	3038	
TaC	3985		ZrC	3420	
TaSi ₂	2400		ZrN	2980 ± 50	
ThC	2625		ZrSi ₂	1700	

TABLE 34.3 Predominantly Covalent Ceramics with Very High Melting Temperatures

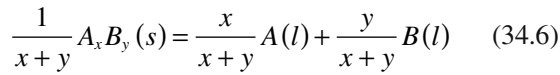
Ceramic	T_m ($^{\circ}\text{C}$)	Covalent character of bond (%)
HfC	3890	70
TiC	3100	78
WC	2775	85
B ₄ C	2425	94
SiC	2300	88
C (diamond)	3727	100

TABLE 34.4 Melting Temperatures of Alkaline Earth Metal Oxides

Oxide	T_m ($^{\circ}\text{C}$)	Covalent character (%)	ϕ (nm^{-1}) = Z/r
BeO	2780	37	57
MgO	2852	27	28
CaO	2927	21	20
SrO	2665	21	17
BaO	2017	18	15

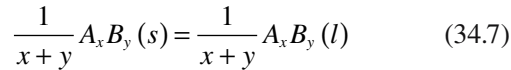
rule. Richard's rule holds fairly well for many elements (e.g., Au, Ti, Pb, Na, K, B) but not for compounds.

We can consolidate the values in Table 34.2 with Richard's rule by considering the processes involved when a compound, AB , melts. The overall melting reaction is

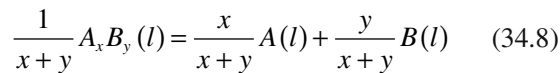


$$\Delta S_1 = \Delta S_f$$

This reaction can be broken down into two steps. First,



which gives ΔS_2 and corresponds to a hypothetical melting process in which the compound retains its ordered structure in the liquid phase. This step is followed by



which gives $\Delta S_3 = \Delta S_m$ and represents disordering of the compound in the liquid to form a random solution. For this latter step the entropy change is given by the "entropy of mixing," which is

$$\Delta S_m = -R[X_A \ln X_A + X_B \ln X_B] \quad (34.9)$$

where X_A and X_B are the atom fractions of A and B, respectively. For our particular example we can write the entropy of mixing as

$$\Delta S_3^0 = -R \left[\frac{x}{x+y} \ln \left(\frac{x}{x+y} \right) + \frac{y}{x+y} \ln \left(\frac{y}{x+y} \right) \right] \quad (34.10)$$

The entropies associated with each of the melting reactions given above are related as follows:

$$\Delta S_1 = \Delta S_2 + \Delta S_3 \quad (34.11)$$

We will now apply this approach to a real compound, MgO.

The entropy of fusion for MgO, given in Table 34.2, is $\Delta S_f = 12.9 \text{ J g-atom}^{-1} \text{ K}^{-1}$, i.e., $\Delta S_1 = 12.9 \text{ J g-atom}^{-1} \text{ K}^{-1}$. The entropy of mixing, ΔS_3 , can be calculated from Eq. 34.7 as

$$\begin{aligned} \Delta S_3^0 &= -8.314 \left[\frac{1}{2} \ln \left(\frac{1}{2} \right) + \frac{1}{2} \ln \left(\frac{1}{2} \right) \right] \\ &= -8.314 \ln \left(\frac{1}{2} \right) = 5.76 \text{ J g-atom}^{-1} \text{ K}^{-1} \quad (34.12) \end{aligned}$$

Using Eq. 34.11 this gives the entropy for the hypothetical melting reaction of $7.14 \text{ J g-atom}^{-1} \text{ K}^{-1}$. This value, which is closer to Richard's rule, does not consider a mixing contribution but only the vibrational change on melting such as occurs for an element. By assuming that we can apply Richard's rule as shown above then it is possible to determine ΔS_1 (ΔS_f), where such values are not available in the literature, and hence obtain ΔH_f .

34.4 VAPORIZATION

Most ceramics have very high T_b . Consequently their vapor pressures are negligible at room temperature and become appreciable only at high temperature. Also very few ceramics vaporize without a molecular change. The result is that the vapor composition is usually not the same as that of the original liquid or solid. A practical consequence is that when we try to grow ceramic thin films by evaporation as described in Chapter 28 the film may have a stoichiometry different from that of the source. Some of the phenomena that can occur when compounds evaporate are shown in Table 34.5.

TABLE 34.5 Possible Reactions during the Evaporation of Compounds

Reaction type	Chemical reaction ($M = \text{metal}$, $X = \text{nonmetal}$)	Examples	Comments
Evaporation without dissociation	$MX(s \text{ or } l) \rightarrow MX(g)$	SiO, B ₂ O ₃ , GeO, SnO, AlN, CaF ₂ , MgF ₂	Compound stoichiometry maintained in deposit
Decomposition	$MX(s) \rightarrow M(s) + (1/2)X_2(g)$ $MX(s) \rightarrow M(l) + (1/n)X_n(g)$	Ag ₂ S, Ag ₂ Se III-V semiconductors	Separate sources are required to deposit these compounds
Evaporation with dissociation Chalcogenides ($X = \text{S, Se, Te}$) Oxides	$MX(s) \rightarrow M(g) + (1/2)X_2(g)$ $MO_2(s) \rightarrow MO(g) + (1/2)O_2(g)$	CdS, CdSe, CdTe SiO ₂ , GeO ₂ , TiO ₂ , SnO ₂ , ZrO ₂	Deposits are metal-rich; separate sources are required to deposit these compounds Metal-rich discolored deposits; dioxides are best deposited in O ₂ partial pressure (reactive evaporation)

TABLE 34.6 Temperature at Which the Vapor Pressure Is 10^{-4} torr (1.3×10^{-2} Pa)

Oxide	T_m ($^{\circ}\text{C}$)	T (vapor pressure = 10^{-4} torr)
PbO	890	550 $^{\circ}\text{C}$
TiO ₂	1640	$\sim 1300^{\circ}\text{C}$
ZrO ₂	2700	$\sim 2200^{\circ}\text{C}$

In many multicomponent oxide ceramics the vapor pressure of each component may be different. This effect is particularly noticeable in lead-containing compounds such as lead zirconium titanate (PZT), an important piezoelectric ceramic. PZT contains PbO, ZrO₂, and TiO₂ in the form of a solid solution. PbO is significantly more volatile than the other two oxides (Table 34.6). As a result if PZT films are heated during processing then significant Pb loss can occur, leading to a change in film stoichiometry and dramatically different properties. If Pb loss is to be avoided then special precautions must be taken. For example, we can compensate for Pb loss by making our starting films Pb rich.

34.5 THERMAL CONDUCTIVITY

At all temperatures the atoms in a solid are vibrating about their equilibrium positions with a set of characteristic frequencies, ν , with values as high as 10^{12} Hz at room temperature. The energies of the lattice vibrations are quantized and given by

$$E = \left(n + \frac{1}{2} \right) h\nu \quad (34.13)$$

where n is an integer, which is zero at 0 K, and h is Planck's constant. At absolute zero the atoms have $E = h\nu/2$: the zero point energy. If the solid is heated E will increase in integer steps of $h\nu$ and similarly if the solid is cooled the vibrational energy will decrease in steps of $h\nu$. You can see immediately that there is a similarity between this process and the absorption or emission of light (*photons*). And so the name *phonon* is used as the quantum unit of lattice vibrational energy.

Wave-particle duality applies equally to phonons as it does to photons. Thus, phonons possess the characteristics of both waves and particles. In ceramics the conduction of heat is primarily due to the movement of phonons. When a ceramic is heated we can think in terms of an increase in the number of phonons. When there is a temperature dif-

ference phonons move from the high temperature end, where their concentration is high, to the lower temperature end, where their concentration is lower. The driving force is the concentration gradient, just as it is in the diffusion of matter. The rate of heat flow dq/dt is proportional to the temperature gradient dT/dx , where the constant of proportionality is the thermal conductivity, k :

$$\frac{dq}{dt} = -kA \frac{dT}{dx} \quad (34.14)$$

where A is the cross-sectional area normal to the direction of heat flow.

Thermal conductivity depends on three factors:

1. Heat capacity C
2. Average particle velocity, v
3. Mean free path of a particle between collisions, l

From the kinetic theory of gases the thermal conductivity of an ideal gas is

$$k = \frac{1}{3} Cvl \quad (34.15)$$

v AND l FOR ELECTRONS AND PHONONS

For electrons in a metal at room temperature, $v \sim 10^6$ m/s and $l \sim 10$ nm.

For phonons in a ceramic at room temperature, $v \sim 10^3$ m/s and $l \sim 1-4$ nm.

The phonon mean free path greatly increases with decreasing temperature; it is $\sim 10 \mu\text{m}$ at 20 K.

Debye (in 1914) applied Eq. 34.15 to phonon conduction to describe thermal conductivity in dielectric solids. Then C is the heat capacity of the phonons, v is the phonon velocity, and l is the phonon mean free path.

Phonon conduction in ceramics is very different from that found in metals where the free electrons are the source of the thermal conductivity. The mobility of phonons is usually significantly lower than that of electrons because they are scattered by lattice vibrations (i.e., other phonons). Consequently ceramics generally have low thermal conductivities. However, the phonon mechanism can be very effective and it is often a surprise to realize that the thermal conductivity of some ceramics is actually higher than that of metals! At temperatures above ~ 50 K, diamond has the highest thermal conductivity of any known material. The thermal conductivity of a gem quality diamond is in the range of $2000-2500 \text{ W m}^{-1} \text{ K}^{-1}$ at room temperature whereas that of copper is $400 \text{ W m}^{-1} \text{ K}^{-1}$. Values for the room temperature thermal conductivity of some selected ceramics are given in Table 34.7.

VIBRATIONAL AMPLITUDES

In a solid these may be as large as 0.02–0.03 nm.

Ceramics having high thermal conductivities generally share the following characteristics:

TABLE 34.7 The Thermal Conductivity of Some Ceramics

Material	k ($Wm^{-1}K^{-1}$)	Material	k ($Wm^{-1}K^{-1}$)
Al ₂ O ₃	30.0–35.0	Spinel (MgAl ₂ O ₄)	12.0
AlN	200.0–280.0	Soda–lime–silicate glass	1.7
BeO	63.0–216.0	TiB ₂	40.0
MgO	37.0	PSZ	2.0
SiC	84.0–93.0	SiAlON	21.0
SiO ₂	1.4	Si ₃ N ₄	25.0
Cordierite (Mg–aluminosilicate)	4.0	Forsterite	3.0

- Strong interatomic bonding
- Simple crystal structure
- Comprise light elements that are close together in the periodic table

From Table 34.7 you can see that BeO and AlN are examples of ceramics with high thermal conductivity and both these materials satisfy the conditions given above.

Figure 34.3 shows the thermal conductivity of single crystal alumina as a function of temperature. At very low temperatures the mean free path, l , of the phonons becomes comparable to the size of the specimen and k depends mainly on the heat capacity, which increases with T^3 . The thermal conductivity reaches a maximum at some low temperature (~ 40 K in this case). As the temperature increases k decreases because there are more phonons

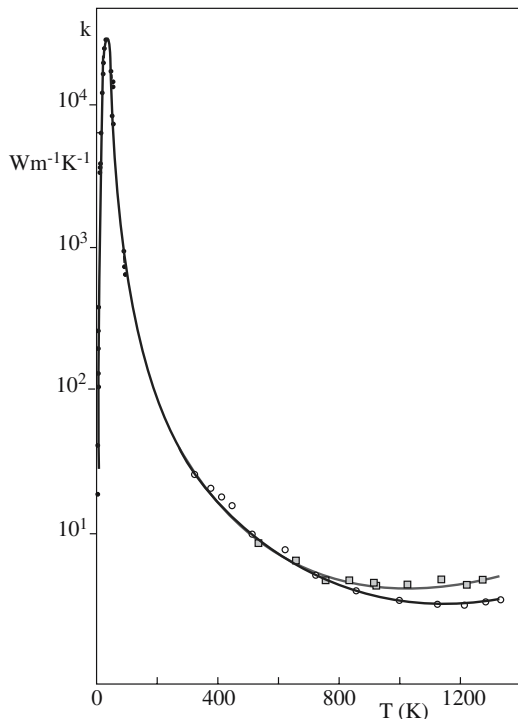


FIGURE 34.3 Thermal conductivity of single crystal aluminum oxide over a wide temperature range. The variation in the data above 800 K is due to the differences in the experimental method used.

around with which to collide and more chances of a scattering event taking place. The interactions between phonons was first described by Rudolf Peierls (1929) who identified two types of scattering processes:

- Umklapp (from the German *umklappen*, which means “flipping over”)
- Normal

The normal process has no effect on the thermal resistance. However, the umklapp process leads to an increase in thermal resistance with temperature given by

$$l \propto \frac{1}{T} \tag{34.16}$$

Eventually l decreases to a value close to the interplanar spacing and k due to phonon transport becomes temperature independent. The temperature variation of l for several ceramics is shown in Figure 34.4.

At high temperatures part of the thermal energy may also be transferred by radiation. The radiant energy conductivity, k_r , is given by

$$k_r = \frac{16}{3} \sigma n^2 T^3 l_r \tag{34.17}$$

where σ is the Stefan–Boltzmann constant, n is the refractive index, and l_r is the mean free path of the photons responsible for radiant heat transfer.

Some single crystals and glasses have good transparency in the visible and infrared (IR) parts of the electromagnetic spectrum and l_r can become large. In most polycrystalline ceramics, l_r is very short because of absorption and scattering, mainly due to the presence of pores. For opaque materials $l_r \sim 0$ and radiation transfer is negligible except at very high temperatures.

At the other extreme when l_r is very large there is no interaction with the material and radiation heat transfer

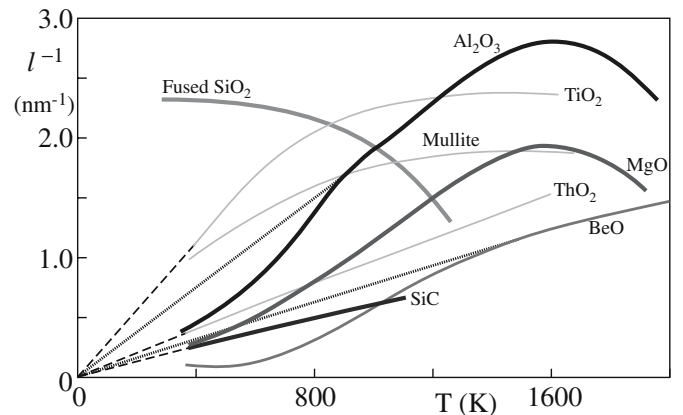


FIGURE 34.4 Inverse phonon mean free paths for several crystalline oxides and for vitreous silica.

becomes a surface effect. The contribution of k_r to the overall thermal conductivity becomes significant only when l_r is small compared with the sample size but large compared with atomic dimensions.

In ceramics with mobile electrons or holes there is a third mechanism that can contribute to thermal conductivity. The electronic thermal conductivity k_e is

$$k_e \propto \exp\left(-\frac{E_g}{kT}\right) \quad (34.18)$$

where E_g is the band gap energy and k is Boltzmann's constant.

In most ceramics the electronic contribution to the overall thermal conductivity is negligible. However, it can be significant in electrically conducting and semiconducting ceramics such as SiC, TiC, and graphite.

34.6 MEASURING THERMAL CONDUCTIVITY

There are several methods available to measure k , but no single one is appropriate for all ceramics because of their wide range of thermal conductivities. The laser flash method illustrated in Figure 34.5 is

one of the most popular. In this technique a laser pulse is used to rapidly heat one face of the ceramic, which is in the form of a thin plate. A typical laser would be an Nd:glass laser producing radiation with $\lambda \sim 1060\text{nm}$. The energy of each laser pulse is $\sim 15\text{J}$. An IR detector measures the temperature of the face remote from the laser. The time taken for the peak in the temperature profile to reach the remote face of the sample and the reduction in the peak temperature are measured. These measurements provide us with the thermal diffusivity, D_{th} , and the heat capacity, c_p . If the density, ρ , of the ceramic is known then k can be obtained using

MgO

$l \sim 3\text{ nm at } 200^\circ\text{C.}$
 $l \sim 0.6\text{ nm at } 1000^\circ\text{C.}$
 $a_{\text{MgO}} = 0.421\text{ nm.}$

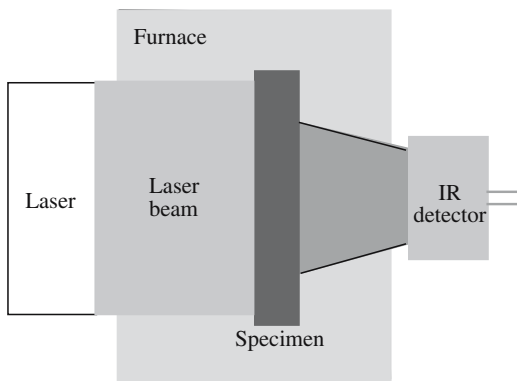


FIGURE 34.5 Schematic of the laser flash method used for measuring thermal conductivity of ceramics.

$$k = \rho c_p D_{th} \quad (34.19)$$

The measurements can be performed at room temperature or at a range of higher temperatures by enclosing the sample in a furnace.

34.7 MICROSTRUCTURE AND THERMAL CONDUCTIVITY

As mentioned in Chapter 1, thermal conductivity depends on microstructure. Anything that changes the local atomic arrangement or induces elastic strains in the lattice will decrease l .

- *Impurities.* The presence of impurities disrupts the normal lattice arrangement. As temperature increases the effect of the impurity becomes less because l approaches the dimensions of the unit cell. The effect on k is illustrated for solid solutions in the isomorphous system MgO–NiO in Figure 34.6.
- *Porosity.* The thermal conductivity of air is only $0.026\text{ W m}^{-1}\text{ K}^{-1}$, significantly less than most crystalline ceramics. Consequently ceramics containing a high volume fraction of porosity have

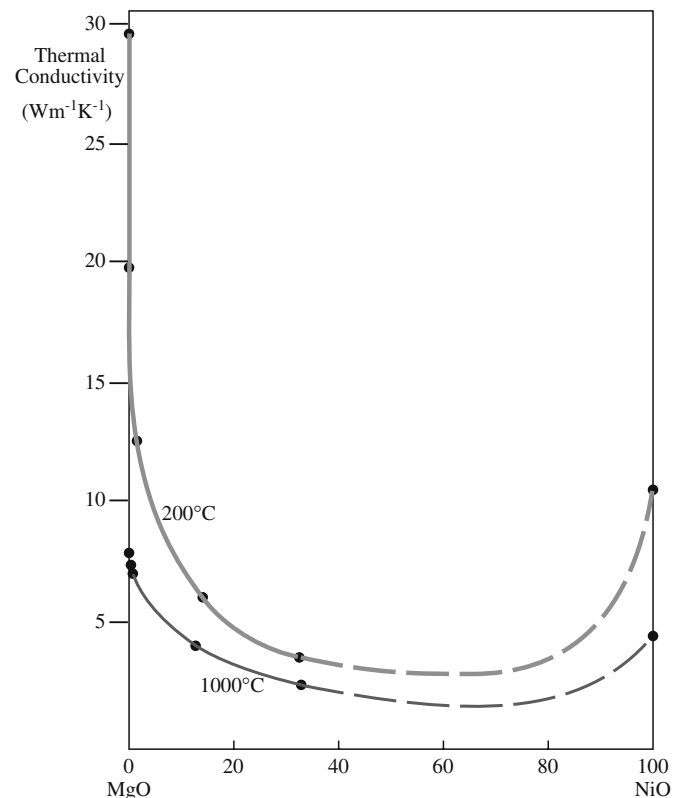


FIGURE 34.6 The thermal conductivities of solid solutions in the MgO–NiO system.

low values of k . This property is used to good effect in designing materials for thermal insulation such as the tiles used on the outside of the space shuttle to protect it during reentry into the earth's atmosphere. The tiles consist of a porous mat of SiO_2 fibers as showed earlier in Figure 15.19. The SiO_2 provides the high strength and high melting temperature requirements of the tile and the porous microstructure ensures a very low k .

- **Grain size.** The mean free path of phonons at room temperature is significantly smaller than typical grain sizes in ceramics. As a result phonon scattering at grain boundaries is not important in reducing k in most practical applications. Figure 34.7 shows the temperature dependence of k for CaF_2 , TiO_2 , and Al_2O_3 in single crystalline and polycrystalline form. The deviation in the relative thermal conductivities at higher temperatures is due to the contribution from photon conductivity.
- **Dislocations.** A dislocation consists of a core in which the structure and density of the material is altered. Around the core there is a long-range strain field. Both these regions can cause phonon scattering. The thermal resistance associated with dislocations is proportional to the dislocation density. There is no theory that so far accounts entirely satisfactorily for the magnitude of phonon scattering by dislocations. If you want to delve into some of the theories that have been proposed much of the original work has been discussed by Nabarro (1987).

Most practical ceramics are multiphase materials in which each constituent will, in general, have a different k . The value of k for the heterogeneous material is dependent upon the amount and distribution of the different phases.

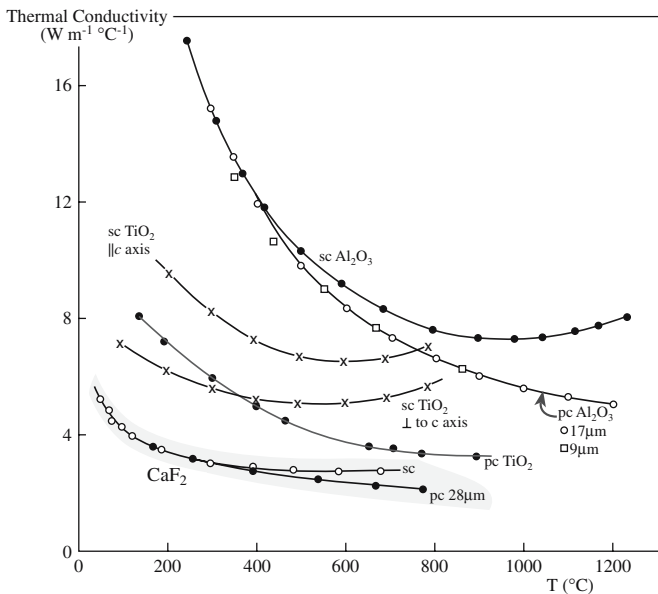


FIGURE 34.7 Comparison of the thermal conductivity of single crystal (sc) and polycrystalline (pc) ceramics.

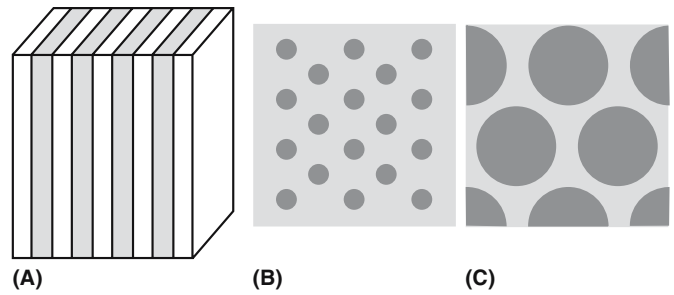


FIGURE 34.8 Three models for the distribution of two phases in a material. (a) Parallel slabs, (b) continuous matrix phase, discontinuous particulate dispersion, and (c) large isolated grains separated by a continuous minor phase.

There are three idealized kinds of phase distributions for which equations have been derived to estimate k of the bulk material and these are illustrated in Figure 34.8 with examples summarized in Table 34.8.

1. For parallel slabs with heat flow parallel to the phase boundary:

$$k_m = V_1 k_1 + V_2 k_2 \quad (34.20)$$

where V_1 and V_2 are the volume fractions of the two phases.

2. For parallel slabs with heat flow perpendicular to the phase boundary:

$$k_m = \frac{k_1 k_2}{V_1 k_2 + V_2 k_1} \quad (34.21)$$

3. For a continuous major phase:

$$k_m = k_c \left[\frac{1 + 2V_d \left(1 - \frac{k_c}{k_d}\right) / \left(\frac{2k_c}{k_d} + 1\right)}{1 - V_d \left(1 - \frac{k_c}{k_d}\right) / \left(\frac{k_c}{k_d} + 1\right)} \right] \quad (34.22)$$

where k_c is the thermal conductivity of the continuous phase, k_d is the thermal conductivity of the dispersed phase, and V_d is the volume fraction of the dispersed phase.

TABLE 34.8 Examples of Models for Phase Distribution^a

Parallel slabs	Continuous matrix	Continuous minor
Furnace linings	Dispersed impurities	Common microstructure
Thermal barrier coatings	Common two-phase microstructure	Grain-boundary phase
Cutting tool coatings	Dispersed-particle composites	Glass-bonded ceramic
Enamels	Immiscible phases	Cermet such as Co-bonded WC
Layered composites		Reaction-sintered SiC

^a See Figure 34.8.

34.8 USING HIGH THERMAL CONDUCTIVITY

One of the most important applications of high- k ceramics is as substrates and packages for electronic devices as shown in Figure 34.9. Due to the complexity and density of modern electronic devices, efficient thermal management is important. Removal of heat from the semiconductor is essential to prevent thermally induced damage.

Alumina (96 wt% Al_2O_3) is the most commonly used substrate material. It has a thermal conductivity in the range $15\text{--}20\text{ W m}^{-1}\text{ K}^{-1}$. The higher k alternatives are AlN, SiC, and BeO. Aluminum nitride is the most promising because it combines a high k and a high electrical resistivity (unlike SiC), it is nontoxic (unlike BeO), and it has a coefficient of thermal expansion closely matched to Si in the temperature range $25\text{--}400^\circ\text{C}$. Theoretically AlN has $k = 320\text{ W m}^{-1}\text{ K}^{-1}$. However, in polycrystalline AlN k is typically in the range $50\text{--}200\text{ W m}^{-1}\text{ K}^{-1}$. One of the reasons that commercially available materials show a wide range in k and values lower than predicted by theory is because of the presence of impurities, mainly oxygen. When oxygen replaces nitrogen, an aluminum vacancy is formed. We can represent this process using Kröger–Vink notation (we gave the details of this notation in Chapter 11):



The aluminum vacancy leads to phonon scattering because its scattering cross section, Γ , for phonons is large: Γ is proportional to the relative difference in mass between the original site occupant and the new site occupant.

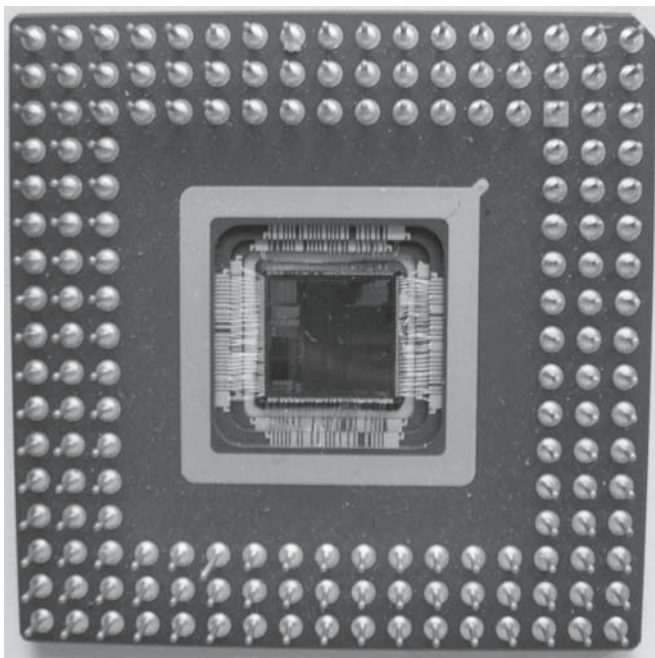


FIGURE 34.9 A ceramic pin-grid-array package (96% pure Al_2O_3) with multilayer Au metallization.

$$\Gamma \propto \frac{\Delta M}{M} \quad (34.24)$$

Aluminum has an atomic weight of 27 and the vacancy has zero weight. So for our example $\Delta M/M$ is 1. When an N atom is replaced by O on the anion sublattice $\Delta M/M = 0.1$. As a result the scattering cross section is smaller.

We can reduce the oxygen content in polycrystalline AlN by adding rare earth or alkaline metal oxides (such as Y_2O_3 and CaO) to the initial powder. During sintering the additive reacts with the oxide coating on the AlN grains forming a liquid. The liquid helps in densification (as described in Section 24.7) and also acts as an oxygen “getter,” removing Al_2O_3 from the bulk of the grains. During cooling the liquid concentrates mainly at triple points leaving mostly clean and sharp AlN–AlN grain boundaries as shown in Figure 1.4.

The record-high thermal conductivity of diamond makes it an obvious choice for consideration as a substrate for high power electronic devices. One method that has been successful in producing diamond films is chemical vapor deposition (CVD). The CVD diamond films are polycrystalline, but can still have $k > 2000\text{ W m}^{-1}\text{ K}^{-1}$. The high cost of diamond films still precludes their widespread use.

34.9 THERMAL EXPANSION

We know from our everyday experiences that when we heat most materials they expand and when we cool them they contract. The linear coefficient of thermal expansion, α , indicates how much the dimensions of a solid change with temperature:

$$\alpha = \frac{\Delta l}{\Delta T l_0} \quad (34.25)$$

where Δl is the change in length of the sample, l_0 is the original length, and ΔT is the temperature interval.

Figure 34.10 shows a typical bond–energy curve. At 0K the atoms are separated by the equilibrium spacing, r_0 , which corresponds to the minimum in the bond–energy curve. The atoms will be in their lowest vibrational energy state, corresponding to the zero point energy $h\nu/2$ and possess the minimum amplitude of vibration, x_0 . When the solid is heated its energy increases as shown by the horizontal lines in Figure 34.10. The width of the trough in the bond–energy curve represents the average vibrational amplitude of the atoms for a specific energy (or T). The average distance between the atoms is represented by the mean position along this line. A solid expands when heated because the bond–energy curve is asymmetric. If the curve was symmetric (the dashed curve in Figure 34.10) the average vibrational amplitude would increase with increasing temperature, but there would be no increase in the interatomic separation.

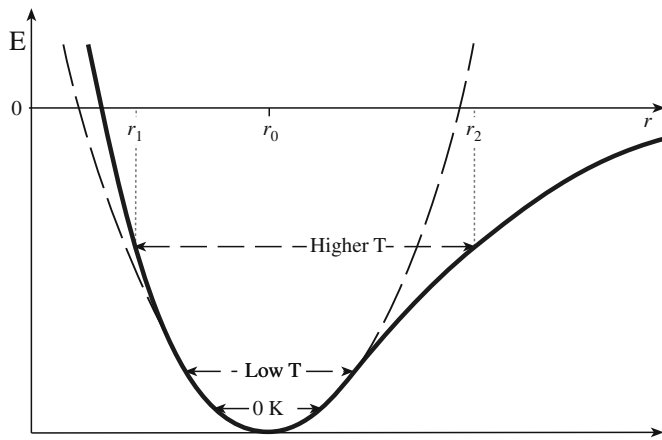


FIGURE 34.10 A typical bond-energy curve.

As described in Chapter 4 the shape of the bond-energy curve depends on the strength and type of the interatomic bonding:

- The greater the bond strength the deeper and narrower the trough in the bond-energy curve and the smaller the value of α .
- The more ionic the bonding the more asymmetric the curve. Ionically bonded materials will, in general, have higher values of α than covalently bonded ones.
- As melting temperature increases α decreases as shown in Figure 34.11.

AN EXAMPLE—MgO

$$\alpha = 13.5 \times 10^{-6} \text{ } ^\circ\text{C}^{-1} = 13.5 \text{ ppm}/^\circ\text{C}$$

$$\alpha(^\circ\text{C}^{-1}) \times 10^6 = 13.5; \alpha(10^6 \text{ } ^\circ\text{C}^{-1}) = 13.5$$

Heating MgO from 25°C to 50°C ($\Delta T = 25^\circ\text{C}$) increases a (0.421 nm at 25°C) by only 0.14 pm.

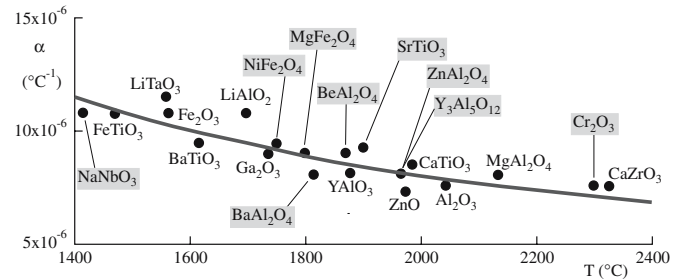


FIGURE 34.11 Plot of the average coefficient of thermal expansion versus melting temperature for many ceramics.

Values of α for various ceramics are given in Table 34.9. For most ceramics α lies between about 3×10^{-6} and $15 \times 10^{-6} \text{ } ^\circ\text{C}^{-1}$. Since α is a function of temperature, usually increasing with increasing temperature as shown in Figure 34.12, a mean value is often quoted for a particular material over a stated temperature range.

The values in Table 34.8 are mean values and the temperature range over which these values are applicable is given. Most values of α found in the literature are room temperature values and from a practical point of view it would be incorrect to use these values when considering an application over a different temperature range.

TABLE 34.9 Mean Thermal Expansion Coefficients of Various Ceramics

Ceramic	α (ppm/ $^\circ\text{C}$)	Ceramic	α (ppm/ $^\circ\text{C}$)
Binary oxides			
α - Al_2O_3	7.2–8.8	ThO_2	9.2
BaO	17.8	TiO_2	8.5
BeO	8.5–9.0 (25–1000)	UO_2	10.0
Bi_2O_3 (α)	14.0 (RT–730 $^\circ\text{C}$)	WO_2	9.3 (25–1000)
Bi_2O_3 (δ)	24.0 (650–825 $^\circ\text{C}$)	Y_2O_3	8.0 (<i>c</i> axis)
Dy_2O_3	8.5	ZnO	4.0 (<i>a</i> axis)
Gd_2O_3	10.5	ZrO_2 (monoclinic)	7.0
HfO_2	9.4–12.5	ZrO_2 (tetragonal)	12.0
MgO	13.5		
Mixed oxides			
$\text{Al}_2\text{O}_3 \cdot \text{TiO}_2$	9.7 (average)	Cordierite	2.1
$\text{Al}_2\text{O}_3 \cdot \text{MgO}$	7.6	$\text{MgO} \cdot \text{SiO}_2$	10.8 (25–1000)
$5\text{Al}_2\text{O}_3 \cdot 3\text{Y}_2\text{O}_3$	8.0 (25–1400)	$2\text{MgO} \cdot \text{SiO}_2$	11.0 (25–1000)
$\text{BaO} \cdot \text{ZrO}_2$	8.5 (25–1000)	$\text{MgO} \cdot \text{TiO}_2$	7.9 (25–1000)
$\text{BeO} \cdot \text{Al}_2\text{O}_3$	6.2–6.7	$\text{MgO} \cdot \text{ZrO}_2$	12.0 (25–1000)
$\text{CaO} \cdot \text{HfO}_2$	3.3 (25–1000)	$2\text{SiO}_2 \cdot 3\text{Al}_2\text{O}_3$ (mullite)	5.1 (25–1000)
$\text{CaO} \cdot \text{SiO}_2$ (β)	5.9 (25–700)	$\text{SiO}_2 \cdot \text{ZrO}_2$ (zircon)	4.5 (25–1000)
$\text{CaO} \cdot \text{SiO}_2$ (α)	11.2 (25–700)	$\text{SrO} \cdot \text{TiO}_2$	9.4 (25–1000)
$\text{CaO} \cdot \text{TiO}_2$	14.1	$\text{SrO} \cdot \text{ZrO}_2$	9.6
$\text{CaO} \cdot \text{ZrO}_2$	10.5	$\text{TiO}_2 \cdot \text{ZrO}_2$	7.9 (25–1000)
$2\text{CaO} \cdot \text{SiO}_2$ (β)	14.4 (25–1000)		

TABLE 34.9 *Continued*

<i>Ceramic</i>	α (ppm/°C)	<i>Ceramic</i>	α (ppm/°C)
Borides, nitrides, carbides, and silicides			
AlN	5.6 (25–1000)	SiC	4.3–4.8
B ₄ C	5.5	TaC	6.3
BN	4.4	TiB ₂	7.8
Cr ₃ C ₂	10.3	TiC	7.7–9.5
HfB ₂	5.0	TiN	9.4
HfC	6.6	TiSi ₂	10.5
MoSi ₂	8.5	ZrB ₂	5.7–7.0
β -Mo ₂ C	7.8	ZrC	6.9 (25–1000)
NbC	6.6	ZrSi ₂	7.6 (25–2700)
Si ₃ N ₄	3.1–3.7	ZrN	7.2
Halides			
CaF ₂	24.0	LiCl	12.2
LiF	9.2	Lil	16.7
LiBr	14.0	MgF ₂	16.0
		NaCl	11.0
Glasses			
Soda-lime glass	9.0	Fused silica	0.55
Pyrex	3.2		

34.10 EFFECT OF CRYSTAL STRUCTURE ON α

Cubic crystals like MgO are isotropic because they have uniform thermal expansion along the three crystallographic axes. Single crystals of noncubic structures are

anisotropic and have different values of α along different crystallographic directions. Some examples are given in Table 34.10. In a polycrystalline sample of an anisotropic material such as Al₂O₃, α would be intermediate between the single crystal values for each of the different orientations.

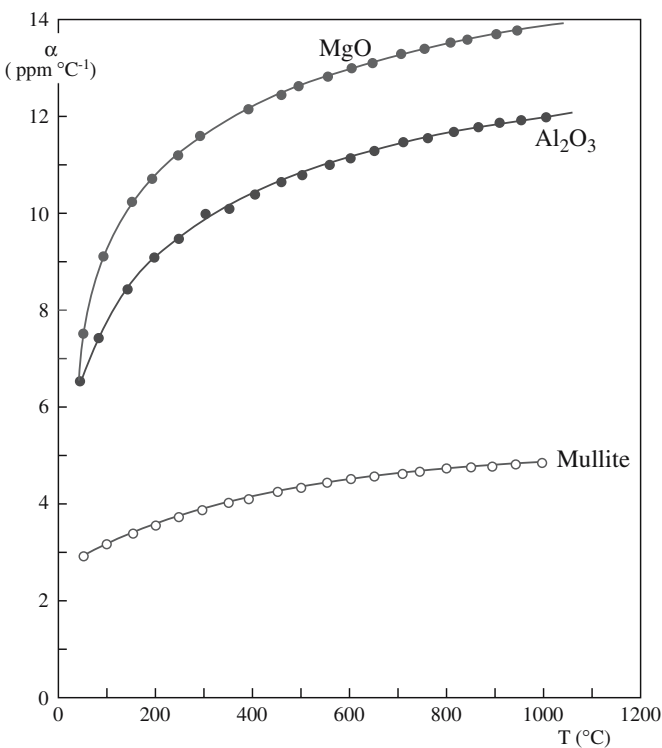


FIGURE 34.12 Thermal expansion coefficients versus temperature for some ceramic oxides.

Some silicate minerals such as quartz (SiO₂) and cordierite (Mg₂Al₄Si₅O₁₈) have very low coefficients of thermal expansion (for cordierite α is actually negative along the *c* axis!). This property is attributed to the very open three-dimensional structure of many silicates. Cordierite is a ring silicate made up of [SiO₄]⁴⁻ tetrahedral units as described in Chapter 7. During heating, thermal energy can be absorbed by rearrangement of these tetrahedral units by tilting or rotating.

Structural changes that occur in a ceramic during heating can also produce a change in α . An example is shown in Figure 34.13 for BaTiO₃. Similar changes are

TABLE 34.10 Thermal Expansion Coefficients for Some Anisotropic Crystals (ppm/°C)

<i>Crystal</i>	<i>Normal to c axis</i>	<i>Parallel to c axis</i>
Al ₂ O ₃	8.3	9.0
Al ₂ TiO ₅	-2.6	+11.5
3Al ₂ O ₃ · 2SiO ₂	4.5	5.7
TiO ₂	6.8	8.3
ZrSiO ₄	3.7	6.2
CaCO ₃	-6	25
SiO ₂ (quartz)	14	9
NaAlSi ₃ O ₈ (albite)	4	13
C (graphite)	1	27

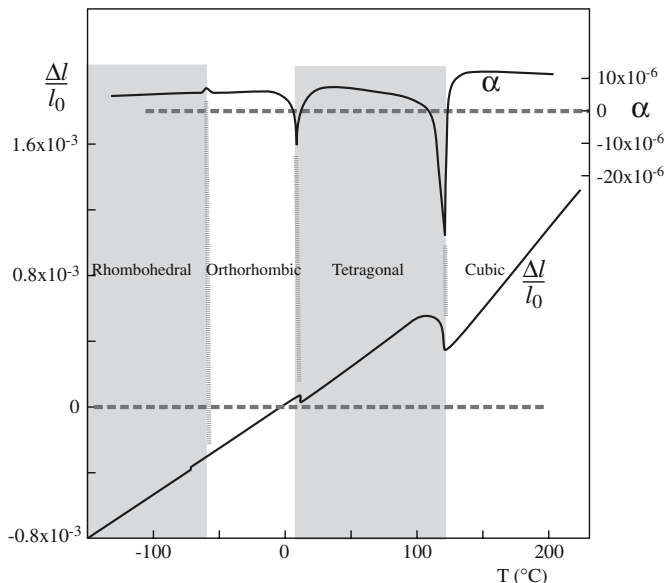


FIGURE 34.13 The coefficient of thermal expansion of BaTiO₃ as a function of temperature.

seen in the crystalline forms of SiO₂. Displacive phase transformations usually produce sudden changes in α . Reconstructive phase changes, which involve bond breaking, usually occur more slowly and are often characterized by hysteresis.

34.11 THERMAL EXPANSION MEASUREMENT

The usual method of measuring α is to record mechanically the change in length of a test piece as it is heated in an instrument called a push-rod dilatometer, which is illustrated in Figure 34.14. The data that are obtained are plotted as $\Delta l/l_0$ versus T as shown in Figure 34.15. The slope of a line at any temperature is α . Accuracies of commercial dilatometers can be as good as 0.5%.

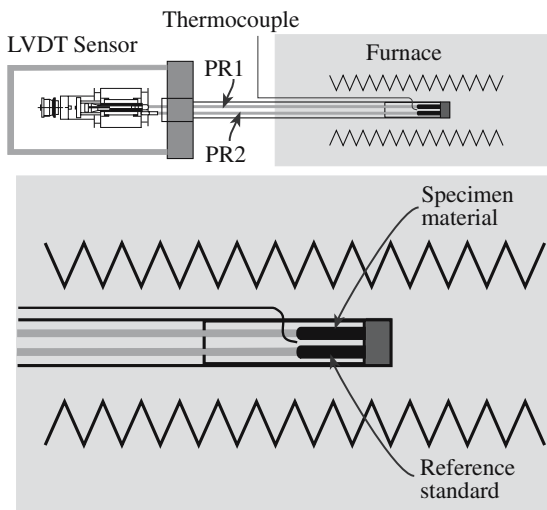


FIGURE 34.14 Schematic of a double pushrod differential dilatometer.

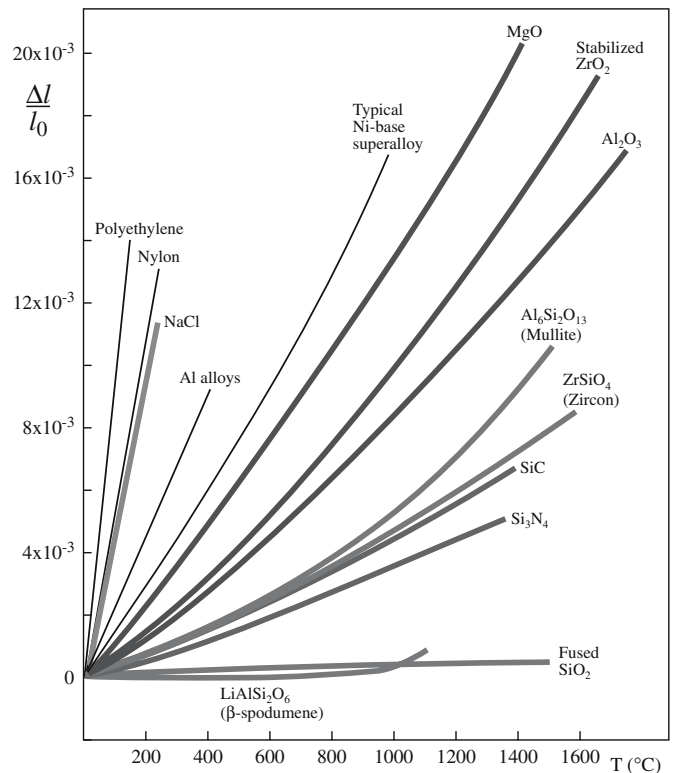


FIGURE 34.15 Thermal expansion characteristics of several polycrystalline ceramics.

A typical plot of $\Delta l/l_0$ versus T for a commercial silicate glass is shown in Figure 34.16. The sudden increase in α in the temperature range 500–600°C is associated with the change from the glassy state into the supercooled liquid (i.e., T_g). The temperature range over which this change occurs depends not only on the glass composition but also on the thermal history of the glass and the rate of heating (remember T_g is not an absolute value). The decrease in length at about 700°C corresponds to the dilatometric softening temperature (T_d), which is due to the viscous flow of the sample under the stresses imposed by

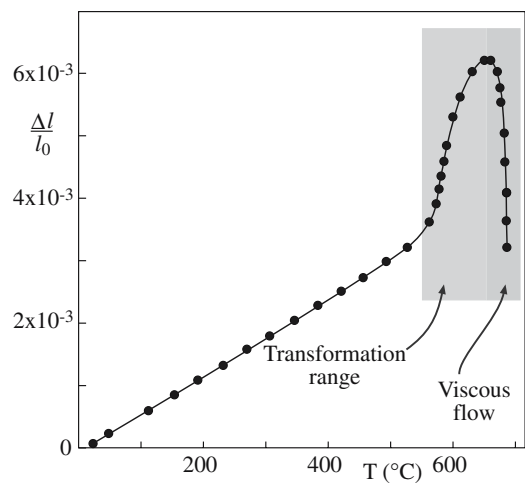
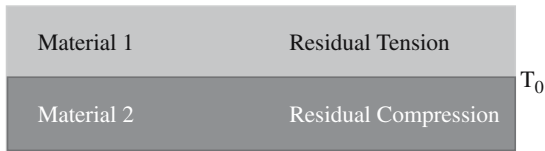


FIGURE 34.16 Typical data for thermal expansion of a commercial silicate glass.



$$\alpha_1 > \alpha_2$$

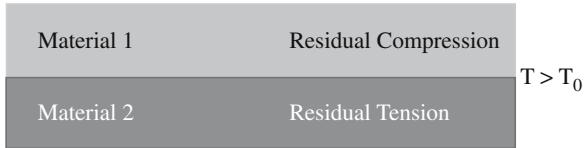


FIGURE 34.17 Stresses generated in a layered structure due to differences in α .

the dilatometer. Measurement of α for a glass should always be done on well-annealed samples.

34.12 IMPORTANCE OF MATCHING α s

Thermal expansion plays a key role when two or more materials are combined in situations in which they will be subjected to changes in temperature. Consider the situation illustrated in Figure 34.17. On heating, material 1 (with the higher α) will experience a compressive stress during heating while material 2 (with the lower α) will experience tensile stresses. On cooling back down, material 1 will be in tension while material 2 will be in compression. These stresses can lead to

- Bowing
- Delamination
- Cracking

Here are some important examples:

- *Glazes on ceramics.* Most types of pottery and white-ware are coated with a glaze for both aesthetic reasons and to make the body impermeable to liquids. The glaze (like most glasses) is strong in compression yet weak in tension. Typical compressive stresses in a glaze are on the order of 70 MPa. If tensile stresses are generated they can cause cracking of the glaze as illustrated in Figure 34.18.
- *Metal to ceramic bonding.* In the packaging of semiconductor devices it is often necessary to join a ceramic (the substrate on which the “chip” is mounted) to a metal (the lead frame that provides connections to and from the outside world). The most common substrate material is a 96% wt% Al_2O_3 ceramic ($\alpha = 7.2 \times 10^{-6} \text{ }^\circ\text{C}^{-1}$). The Kovar metal alloys (e.g., 29%

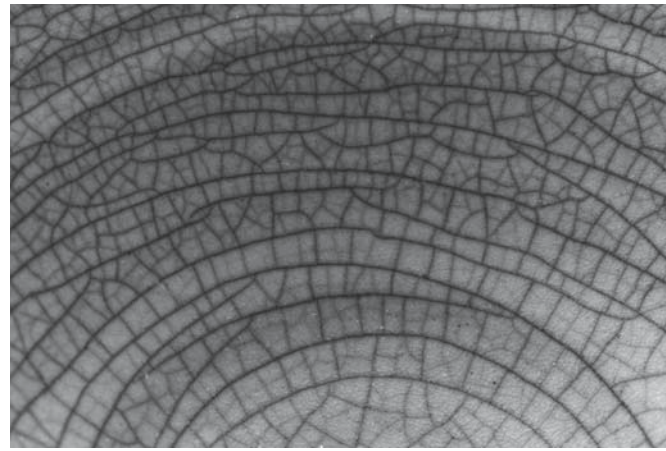


FIGURE 34.18 Artistic cracking in a glaze as a result of stresses generated due to differences in α .

Ni, 17% Co, 54% Fe; $\alpha = 5.1 \times 10^{-6} \text{ }^\circ\text{C}^{-1}$) were developed to have α s as close as possible to alumina.

- *Glass to metal seals.* In incandescent lamps the tungsten wire coil is fused to the glass lamp bulb to form a vacuum tight seal. The best seal is achieved when the glass and metal have similar values of α . Tungsten has $\alpha = 4.5 \times 10^{-6} \text{ }^\circ\text{C}^{-1}$. A typical glass composition for matching with tungsten is an alkali alumina borosilicate (72.9 SiO_2 , 4.5 Al_2O_3 , 14.5 B_2O_3 , 3.5 Na_2O , 2.4 K_2O , 1.2 BaO) which has $\alpha_{20-300^\circ\text{C}} = 4.5 \times 10^{-6} \text{ }^\circ\text{C}^{-1}$.
- *Porcelain enameled metals.* Porcelain enameling is an established technology for bonding a coating of glass on to ferrous metal objects (e.g., stoves). The coefficient of thermal expansion of the glass must be closely matched to that of steel ($\alpha_{1025 \text{ steel}} = 16 \times 10^{-6} \text{ }^\circ\text{C}^{-1}$).
- *Thin films.* Differences in α between a thin film and a substrate can lead to film stress. In a thin film (where the thickness of the film is considerably less than that of the substrate), the thermal stress, σ_f , in the thin film is

$$\sigma_f = \frac{(\alpha_s - \alpha_f) \Delta T \mathcal{E}_f}{(1 - \nu_f)} \quad (34.26)$$

where α_f and α_s are the coefficients of thermal expansion of the film and substrate, respectively, \mathcal{E}_f is the Young’s modulus of the film, and ν_f its Poisson ratio.

34.13 APPLICATIONS FOR LOW- α

Glass-ceramics, such as the lithium-aluminosilicates (LAS), can be designed to have very low, in fact near zero, α s over a wide temperature range making them particularly suitable as supports for telescope mirrors. Tele-

EXAMPLE OF THERMAL STRESS

Determine the thermal stress in a TiC coating deposited onto 1025 stainless steel by CVD at 1000°C:

$$\alpha_{1025 \text{ steel}} = 16 \times 10^{-6} \text{ }^\circ\text{C}^{-1} \quad \alpha_{\text{TiC}} = 8 \times 10^{-6} \text{ }^\circ\text{C}^{-1}$$

$$\mathcal{E}_{\text{TiC}} = 450 \text{ GPa} \quad \nu_{\text{TiC}} = 0.19$$

Substitution into Eq. 34.26 gives $\sigma_f = 1.67 \text{ GPa}$ at 0°C.

TABLE 34.11 Comparison of Thermal Shock Parameters for a Number of Ceramics^a

Material	MOR (MPa)	\mathcal{E} (GPa)	α (ppm/K)	k ($W\ m^{-1}\ K^{-1}$)	R_{TS} (W/m)
SiAlON	945	300	3.0	21	22,050
Hot-pressed Si ₃ N ₄	890	310	3.2	15–25	13,458
Reaction-bonded Si ₃ N ₄	240	220	3.2	8–12	2,727
SiC (sintered)	483	410	4.3	84	23,012
Hot-pressed Al ₂ O ₃	380	400	9.0	6–8	633
Hot-pressed BeO	200	400	8.5	63	3,706
PSZ	610	200	10.6	2	575

^aPoisson's ratio was taken to be 0.25 for all materials.

scopes are precise optical instruments and the resolution is very sensitive to the alignment of the mirrors and other optical components. Support materials with low α s minimize thermally induced strains. A commercial glass ceramic that is used for this application is known as Zerodur™. In addition to the very low α , Zerodur is stable up to 800°C and insensitive to thermal shock. The world's largest optical mirror is located at the Parnal Observatory in the Atacama Desert in Chile. The mirror, which is made of a polished Zerodur base coated with aluminum, is 8.2m in diameter with a surface area of more than 50 m².

34.14 THERMAL SHOCK

Thermal shock resistance is the ability of a material to withstand failure due to rapid changes in temperature. Ceramics and glasses are much more likely to develop thermal stress than metals because

- They generally have lower k
- They are brittle

Rapid cooling of a ceramic or a glass is more likely to inflict thermal shock than heating, since the induced surface stresses are tensile. And, as you know, crack formation and propagation from surface flaws are more probable when the imposed stress is tensile.

The thermal shock resistance (R_{TS}) of a material can be estimated using

$$R_{TS} = \sigma_f k / (\mathcal{E} \alpha) \tag{34.27}$$

where σ_f is the fracture stress (which for ceramics is often taken as the flexural strength or MOR) and \mathcal{E} is Young's

modulus. For high thermal shock resistance we want a ceramic with

- High σ_f
- High k
- Low \mathcal{E}
- Low α

Values to calculate R_{TS} for several ceramics are given in Table 34.11. As an example, the R_{TS} of SiC is 2.3×10^4 W/m, while that of Al₂O₃ is 740 W/m. Ceramics such as SiC and Si₃N₄, which also have a high R_{TS} , are the most useful for components that are loaded at high temperature.

Silica glass (SiO₂) has an R_{TS} of 5.27×10^3 W/m. Addition of other components to the glass lowers \mathcal{E} and increases α , hence decreasing R_{TS} . Soda-lime-silicate glasses such as those used for holding beverages are very susceptible to thermal shock as you have probably found out at one time or another because of their high $\alpha = 9.2 \times 10^{-6} \text{ }^\circ\text{C}^{-1}$. Modification of R_{TS} can most easily be accomplished by changing α . The other parameters in Eq. 34.23 do not vary significantly with glass composition. If the CaO and Na₂O contents are reduced and B₂O₃ is added then a borosilicate glass is formed. This is known as Pyrex™ glass ($\alpha = 3.3 \times 10^{-6} \text{ }^\circ\text{C}^{-1}$), which is much more resistant to thermal shock. Most cookware and the majority of laboratory glassware are Pyrex. From a practical point of view a soda-lime-silicate glass will fail if the temperature difference is $\geq 80^\circ\text{C}$ (so pouring boiling water into a glass beaker will certainly crack it). Pyrex glass can withstand temperature differences of 270°C before failure. Glass-ceramics with their extremely low α have very high thermal shock resistance and can withstand temperature changes of $>1000^\circ\text{C}$.

CHAPTER SUMMARY

The thermal properties of ceramics, like many of their other physical properties, vary over a very wide range. A good example is that of thermal conductivity. Diamond, a ceramic material, has the highest known thermal conductivity, whereas the thermal conductivity of a multiphase ceramic such as partially stabilized zirconia is three orders of magnitude lower. Thermal properties of ceramics are dominated primarily by the nature of the interatomic bonding (bond strength and ionicity). In practical ceramics we, of course, have to consider the presence of defects, impurities, and porosity as these all affect thermal properties.

PEOPLE IN HISTORY

Debye, Petrus (Peter) Josephus Wilhelmus (1884–1966) was born in the Netherlands and became a naturalized American citizen in 1946. In 1912 he proposed the idea of quantized elastic waves, called phonons. From 1940 to 1952 Debye was Professor of Chemistry at Cornell University. He won the Nobel Prize in Chemistry in 1936.

Thomson, William (Lord Kelvin) (1824–1907), Scottish mathematician and physicist, was born in Belfast, Ireland. He proposed his absolute scale of temperature in 1848. During his life he published more than 600 papers and was elected to the Royal Society in 1851. He is buried in Westminster Abbey next to Isaac Newton.

GENERAL REFERENCES

Berman, R. (1979) in *The Properties of Diamond*, edited by J.E. Field, Academic Press, London, p. 3. Discusses the thermal conductivity of diamond and the effect different impurities have on this property.

Kingery, W.D., Bowen, H.K., and Uhlmann, D.R. (1976) *Introduction to Ceramics*, 2nd edition, Wiley, New York, pp. 583–645. A very detailed chapter on thermal properties. The discussion of photon conductivity and the thermal properties of glasses are covered in more depth than we do.

Lynch, C.T. (1975) Ed., *CRC Handbook of Materials Science, Volume III: Nonmetallic Materials and Applications*, CRC Press, Cleveland. Relevant data for thin-film deposition are given on pp. 128–145. A useful resource for vapor pressures of various ceramics.

Rosenberg, H.M. (1988) *The Solid State*, 3rd. edition, Oxford University Press, Oxford, p. 96. Has a clear discussion of phonon scattering mechanisms.

SPECIFIC REFERENCES

Debye, P. (1912) “The theory of specific warmth,” *Ann. Phys.* **39**, 789. An English translation of this classic paper appears in *The Collected Papers of P.J.W. Debye* (1954), Interscience, New York, p. 650.

Debye, P. (1914) *Vorträge über die Kinetische Theorie*, B.G. Teubner, Leipzig. The original source. In German.

Hultgren, R., Orr, R.L., Anderson, P.D., and Kelley, K.K. (1963) *Selected Values of Thermodynamic Properties of Metals and Alloys*, Wiley, New York. Useful lists of thermodynamics properties.

Kubaschewski, O., and Alcock, C.B. (1979) *Metallurgical Thermochemistry*, 5th edition, Elsevier, Oxford. More thermodynamic properties.

Nabarro, F.R.N. (1987) *Theory of Crystal Dislocations*, Dover, New York, p. 746. The Dover edition is essentially a republication of the work first published by the Clarendon Press, Oxford in 1967.

Peierls, R. (1929) “The kinetic theory of thermal conduction in crystals,” *Ann. Phys.* **3**, 1055.

EXERCISES

- 34.1 Show that Eq. 34.4 gives energy in units of J.
- 34.2 The melting temperature of MgO is 3073 K while that of NaCl is 1074 K. Explain the reason for this difference.
- 34.3 Consider the structure of graphite. Would you expect the thermal conductivity to be the same parallel to the basal plane and perpendicular to the basal plane? If not, why not?
- 34.4 (a) Would you expect the thermal conductivity of crystalline quartz to be higher or lower than that of fused quartz? (b) Would you expect the differences in k to increase or decrease with increasing temperature? Explain the reasoning behind your answers.
- 34.5 Using the criteria given in Section 34.5 rank the following ceramics in order of increasing thermal conductivity: B_4C , UO_2 , TiO_2 , and Si_3N_4 . Explain the reasoning for your ranking.
- 34.6 Why is thermal transfer by radiation important only at high temperatures?
- 34.7 An AlN ceramic substrate contains 0.05 vol% porosity. Calculate the thermal conductivity of the ceramic at room temperature.
- 34.8 Which has the greater effect on the thermal conductivity of an AlN ceramic, 0.05 vol% porosity or 0.5 vol% of an $Y_3Al_5O_{12}$ second phase?
- 34.9 Would hot pressing or reaction bonding be the best method to produce Si_3N_4 components for applications in which sudden changes in temperature will occur? Explain how you arrived at your answer.
- 34.10 Would the alkali alumina borosilicate glass given in Section 34.12 be a good choice to glaze a mullite crucible? If not, would you be better off using a soda-lime–silicate glaze or a pure silica glaze?

Ceramics in Biology and Medicine

CHAPTER PREVIEW

Bioceramics are ceramics used for the repair and reconstruction of human body parts. There are many applications for bioceramics; currently the most important is in implants such as alumina hip prostheses. Alumina is classified as an inert bioceramic because it has very low reactivity in the body. However, bioactive materials have the ability to bond directly with bone. The advantages are

- Earlier stabilization of the implant
- Longer functional life

Bioactive ceramics are relatively weak compared with common implant metals and high strength ceramics such as alumina and zirconia. As a result they are often used as coatings, relying on the mechanical strength and toughness of the substrate. An important bioactive ceramic is hydroxyapatite (HA). Natural bone is a composite in which an assembly of HA particles is reinforced by organic collagen fibers. Hydroxyapatite-reinforced polyethylene composites have been developed in an attempt to replicate the mechanical behavior of bone.

A major problem with this topic stems from the realization that you cannot replace bone if you do not understand why bone has such incredible mechanical properties. So if you work in this field you must learn about biology.

35.1 WHAT ARE BIOCERAMICS?

A comprehensive definition of a biomaterial was provided at the National Institutes of Health (NIH) Consensus Development Conference on the Clinical Applications of Biomaterials in the United States:

A biomaterial is any substance, other than a drug, or combination of substances, synthetic or natural in origin, which can be used for any period of time, as a whole or as a part of a system which treats, augments, or replaces any tissue, organ, or function of the body.

This definition was significantly simplified in 1986 at the European Society for Biomaterials Consensus Conference:

Biomaterial—a non-viable material used in a medical device intended to interact with biological systems.

A bioceramic is defined as a ceramic used as a biomaterial (which is great if you know what a ceramic is). The

field of bioceramics is relatively new; it did not exist until the 1970s. However, many bioceramics are not new materials. One of the most important is Al_2O_3 , which we first encountered as a constituent of many traditional ceramic products. Bioceramics are typically classified into subgroups based upon their chemical reactivity in the body.

The subgroups are listed in Table 35.1 and their relative reactivities are compared in Figure 35.1.

If a nearly inert material is implanted into the body it initiates a protective response that leads to encapsulation by a nonadherent fibrous coating about $1\ \mu\text{m}$ thick. Over time this leads to complete isolation of the implant. A similar response occurs when metals and polymers are implanted. In the case of bioactive ceramics a bond forms across the implant–tissue interface that mimics the body's natural repair process. Bioactive ceramics such as HA can be used in bulk form or as part of a composite or as a coating. Resorbable bioceramics, such as tricalcium phosphate (TCP), actually dissolve in the body and are replaced by the surrounding tissue. It is an important requirement, of course, that the

PROSTHESIS

A prosthesis is an artificial replacement for a part of the body.

TABLE 35.1 Classification Scheme for Bioceramics

Nearly inert bioceramics
<i>Examples:</i> Al ₂ O ₃ , low-temperature isotropic (LTI) carbon; ultra LTI carbon; vitreous carbon; ZrO ₂
<i>Tissue attachment:</i> Mechanical
Bioactive ceramics
<i>Examples:</i> HA; bioactive glasses; bioactive glass-ceramics
<i>Tissue attachment:</i> Interfacial bonding
Resorbable bioceramics
<i>Examples:</i> Tricalcium phosphate (TCP); calcium sulfate; trisodium phosphate
<i>Tissue attachment:</i> Replacement
Composites
<i>Examples:</i> HA/autogenous bone; surface-active glass ceramics/poly(methyl methacrylate) (PMMA); surface-active glass/metal fibers; polylactic acid (PLA)/carbon fibers; PLA/HA; PLA/calcium/phosphorus-based glass fibers
<i>Tissue attachment:</i> Depends on materials

dissolution products are not toxic. As in the case of HA, TCP is often used as a coating rather than in bulk form. It is also used in powder form, e.g., for filling space in bone.

Figure 35.2 shows a number of clinical uses of bioceramics. The uses go from head to toe and include repairs to bones, joints, and teeth. These repairs become necessary when the existing part becomes diseased, damaged, or just simply wears out. There are many other applications of bioceramics including pyrolytic carbon coatings for heart valves and special radioactive glass formulations for the treatment of certain tumors. We will describe these latter two applications toward the end of this chapter. In the next section we will look at the advantages and disadvantages of ceramics as biomaterials as compared to the use of polymers and metals. We note that nanomaterials show interesting possibilities for such applications, but may pose as many health problems in other situations.

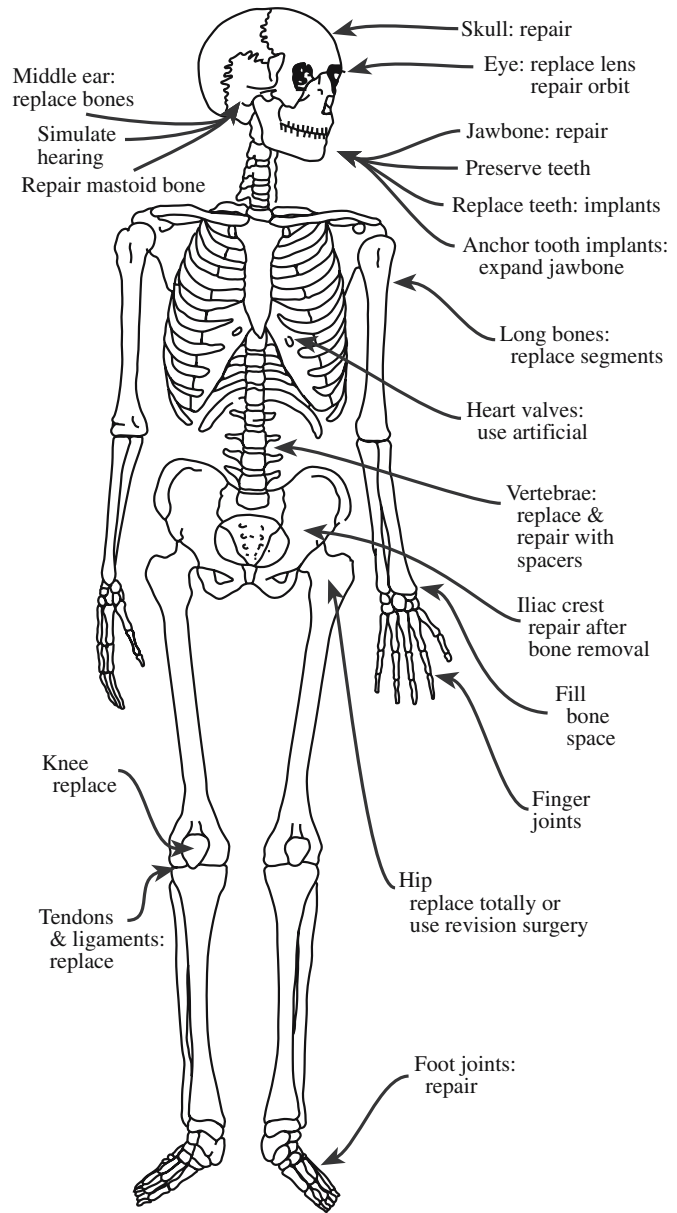


FIGURE 35.2 Illustration of the head-to-toe clinical uses for bioceramics.

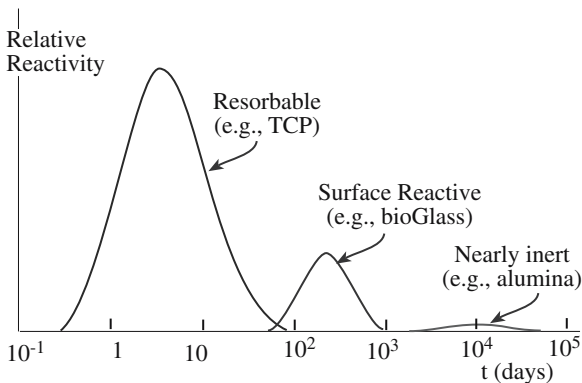


FIGURE 35.1 Relative reactivity of the different classes of bioceramic. TCP is tricalcium phosphate.

35.2 ADVANTAGES AND DISADVANTAGES OF CERAMICS

In the selection of a material for a particular application we always have a choice. Materials selection is a critical part of any component design process and is especially important for implants and other medical devices.

The three main classes of material from which we can select for a load-bearing application are metals, polymers, and ceramics. Table 35.2 is a comparative list of the significant physical properties of different biomaterials from each of the three classical material classes. Table 35.3 compares the behavior of these different classes relevant to their potential use as implants.

TABLE 35.2 Significant Physical Properties of Different Biomaterials

Material	Density ($g\text{cm}^{-3}$)	UTS (MPa)	Compressive strength (MPa)	E (GPa)	K_{Ic} ($\text{MPa m}^{1/2}$)	Hardness (Knoop)	α ($\text{ppm}/^\circ\text{C}$)	Fracture surface energy (J/m^2)	Poisson's ratio	k ($\text{Wm}^{-1}\text{K}^{-1}$)
HA	3.1	40–300	300–900	80–120	0.6–1.0	400–4,500	11	2.3–20	0.28	
TCP	3.14	40–120	450–650	90–120	1.20		14–15	6.3–8.1		
Bioglasses	1.8–2.9	20–350	800–1200	40–140	~2	4,000–5,000	0–14	14–50	0.21–0.24	1.5–3.6
A-W glass	3.07	215	1080	118	2					
ceramic										
SiO_2 glass	2.2	70–120		~70	0.7–0.8	7,000–7,500	0.6	3.5–4.6	0.17	1.5
Al_2O_3	3.85–3.99	270–500	3000–5000	380–410	3–6	15,000–20,000	6–9	7.6–30	0.27	30
PSZ	5.6–5.89	500–650	1850	195–210	5–8	~17,000	9.8	160–350	0.27	4.11
Si_3N_4	3.18	600–850	500–2500	300–320	3.5–8.0	~22,000	3.2	20–100	0.27	10–25
SiC	3.10–3.21	250–600	~650	350–450	3–6	~27,000	4.3–5.5	22–40	0.24	100–150
Graphite	1.5–2.25	5.6–25	35–80	3.5–12	1.9–3.5		1–3	~500	0.3	120–180
LTI-ULTI	1.5–2.2	200–700	330–360	25–40			1–10		0.3	2.5–420
Carbon fiber	1.5–1.8	400–5000	330–360	200–700						
Glassy carbon	1.4–1.6	150–250	~690	25–40		8,200	2.2–3.2	500–8,000	0.4	0.3–0.5
PE	0.9–1.0	0.5–65		0.1–1.0	0.4–4.0	170	11–22	300–400		0.20
PMMA	1.2	60–70	~80	3.5	1.5	160	5–8.1			
Ti	4.52	345	250–600	117	60	1,800–2,600	8.7–10.1	~15,000	0.31	
Ti/Al/V alloys	4.4	780–1050	450–1850	110	40–70	3,200–3,600	8.7–9.8	~10,000	0.34	
Ti/Al/Nb/Ta alloys	4.4–4.8	840–1010		105	50–80			~17,000	0.32	
Vitallium- stellite alloys	7.8–8.2	400–1030	480–600	230	120–160	3,000	15.6–17.0	~5,000	0.30	
(Co–Cr–Mn)										
Low C steel	7.8–8.2	540–4000	1000–4000	200	55–95	1,200–9,000	16.0–19.0	~50,000	0.20–0.33	46
Fe–Cr–Ni alloys										

TABLE 35.3 General Comparison of Materials for Implants

Material class	Advantages	Disadvantages
Polymers	Resiliant Tough Easy to fabricate Low density	Weak Low \mathcal{E} Not usually bioactive Not resorbable
Metals	Strong Wear resistant Tough Easy to fabricate	Can corrode in a physiological environment High \mathcal{E} High density Not usually bioactive Not resorbable
Ceramics	Biocompatible Wear resistant Certain compositions lightweight	Low tensile strength Difficult to fabricate Low toughness Not resilient

The main advantage of ceramics over other implant materials is their biocompatibility: some are inert in the physiological environment while others have a controlled reaction in the body. The main disadvantages of most bioceramics are

- Low toughness (which can affect reliability)
- High \mathcal{E} (which can lead to stress shielding, see Section 35.3)

One of the main ways of increasing the toughness of ceramics is to form a composite. The ceramic may be the reinforcement phase, the matrix, or both. An example of a polymer–matrix composite (PMC) reinforced with a bio-ceramic is polyethylene (PE) reinforced with HA particles. The toughness of the composite is greater than that of HA and, as we will see in Section 35.8, \mathcal{E} is more closely matched to that of bone. Bioceramics are also used as coatings on metal substrates. An example is a bioactive glass coating on stainless steel, which utilizes the strength and toughness of steel and the surface-active properties of the glass.

35.3 CERAMIC IMPLANTS AND THE STRUCTURE OF BONE

The requirements for a ceramic implant depend on what its role in the body will be. For example, the requirements for a total hip prosthesis (THP) will be different from those for a middle ear implant. However, there are two basic criteria:

1. The ceramic should be compatible with the physiological environment.
2. Its mechanical properties should match those of the tissue being replaced.

Most bioceramic implants are in contact with bone. Bone is a living material composed of cells and a blood supply encased in a strong composite structure. The composite consists of collagen, which is flexible and very tough, and crystals of an apatite of calcium and phosphate, resembling calcium hydroxyapatite; we will proceed as if it is HA. It is the HA component that gives bone its hardness. The acicular apatite crystals are 20–40 nm in length and 1.5–3 nm wide in the collagen fiber matrix. Two of the various types of bone that are of most concern in the use of bioceramics are

- Cancellous (spongy bone)
- Cortical (compact bone)

Cancellous bone is less dense than cortical bone. Every bone of the skeleton has a dense outer layer of compact bone covering the spongy bone, which is in the form of a honeycomb of small needle-like or flat pieces called trabeculae. Figure 35.3 is a schematic showing a longitudinal section of a long bone. The open spaces between the trabeculae are filled with red or yellow bone marrow in living bones. Because of its lower density, cancellous bone has a lower \mathcal{E} and higher strain-to-failure ratio than cortical bone, as shown in Table 35.4. Both types of bone have higher \mathcal{E} than soft connective tissues, such as tendons and ligaments. The difference in \mathcal{E} between the various types of connective tissues ensures a smooth gradient in mechanical stress across a bone, between bones, and between muscles and bones.

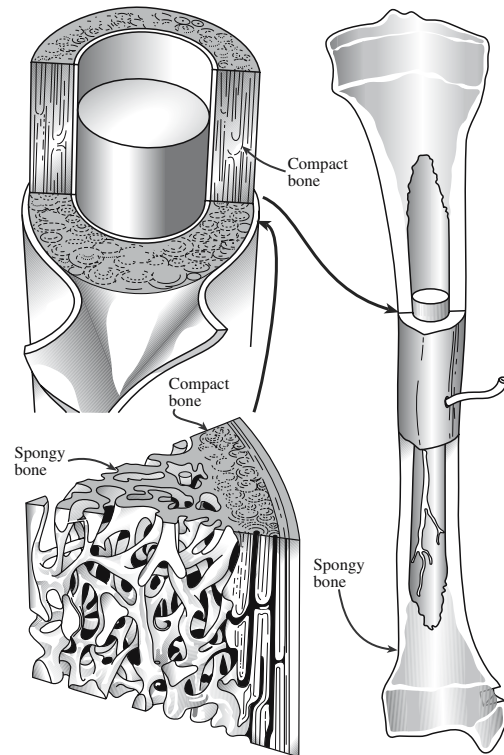


FIGURE 35.3 Longitudinal section showing the structure of long bone.

TABLE 35.4 Mechanical Properties of Skeletal Tissues

Property	Cortical bone	Cancellous bone	Articular cartilage	Tendon
Compressive strength (MPa)	100–230	2–12		
Flexural strength (MPa)	50–150	10–20	10–40	80–120
Strain to failure	1–3%	5–7%	15–50%	10%
E (GPa)	7–30	0.5–0.05	0.001–0.01	1
K_{Ic} (MPa m ^{1/2})	2–12			
Compressive stiffness (N/mm)			20–60	
Compressive creep modulus (MPa)			4–15	
Tensile stiffness (MPa)			50–225	

The mechanical properties of the implant are clearly very important. Figure 35.4 compares E of various implant materials to that of cortical and cancellous bone.

- E of cortical bone is 10–50 times less than that of Al_2O_3 .
- E of cancellous bone is several hundred times less than that of Al_2O_3 .

If the implant has a much higher E than the bone it is replacing then a problem called *stress shielding* can occur. Stress shielding weakens bone in the region at which the applied load is lowest or is in compression. (Bone must be loaded in tension to remain healthy.) Bone that is unloaded or is loaded in compression will undergo a biological change that leads to resorption. Eliminating stress shielding, by reducing E , is one of the primary motivations for the development of bioceramic composites.

STRESS SHIELDING

This occurs when a high- E implant material carries nearly all the applied load.

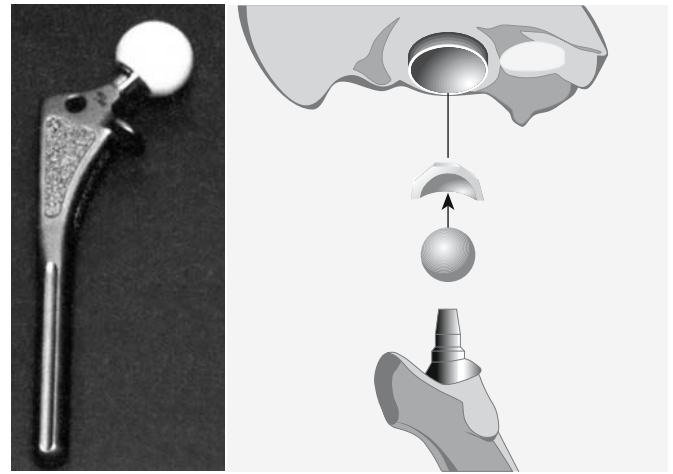


FIGURE 35.5 Medical grade alumina used as femoral balls in THP. The schematic shows how the femoral ball fits into the socket.

35.4 ALUMINA AND ZIRCONIA

Al_2O_3 and ZrO_2 are two nearly inert bioceramics. They undergo little or no chemical change during long-term exposure to body fluids. High-density, high-purity (>99.5%) alumina is used in a number of implants, particularly as load-bearing hip prostheses and dental implants. By 2006, >10⁶ hip prostheses used an alumina ball for the femoral-head component.

Figure 35.5 shows three femoral components of THP with alumina balls. The U.S. Food and Drug Administration (FDA) approved the use of alumina in this type of application in 1982.

Although some alumina dental implants are made from single crystals, most alumina implants are very fine-grained polycrystalline Al_2O_3 . These are usually made by pressing followed by sintering at temperatures in the range of 1600–1800°C. A small amount of MgO (<0.5%) is added, which acts as a grain growth inhibitor and allows a high-density product to be achieved by sintering without

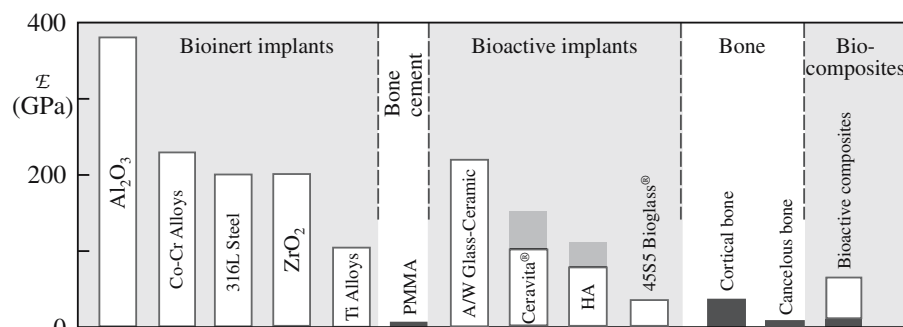


FIGURE 35.4 Young's modulus (E) for various implants compared with bone.

TABLE 35.5 Physical Characteristics of Al₂O₃ Bioceramics

Property	Commercially available high alumina ceramic implants	ISO Standard 6474
Alumina content (wt%)	>99.7	≥99.51
SiO ₂ + Na ₂ O (wt%)	<0.02	<0.01
Density (g/cm ³)	3.98	≥3.94
Average grain size (μm)	3.6	<4.5
Hardness (Vickers, HV)	2400	>2000
Bending strength (MPa, after testing in Ringer's solution)	595	>450

pressure. Table 35.5 lists the physical characteristics of Al₂O₃ bioceramics. The International Standards Organization (ISO) requirements are also given. The most current ISO standard relating to alumina for implants is ISO 6474: 1994, *Implants for Surgery—Ceramic Materials Based on High Purity Alumina*. The ISO is the international agency specializing in standards at the highest level. Individual countries also have their own standards organizations.

An important requirement for any implant material is that it should outlast the patient. Because of the probabilistic nature of failure in ceramics it is not possible to provide specific and definite lifetime predictions for each individual implant. This was the approach that we discussed in Section 16.14. [See the discussion of Figure 16.27, a diagram showing applied stress versus probability of time to failure (SPT) for medical-grade alumina.] It shows, as you might expect, that increased loads and longer times increase the probability of failure. Results from aging and fatigue studies show that it is essential that Al₂O₃ implants be produced with the highest possible standards of quality assurance, especially if they are to be used as orthopedic prostheses in younger patients.

Although alumina ceramics combine excellent biocompatibility and outstanding wear resistance they have only moderate flexural strength and low toughness. This limits the diameter of most alumina femoral head prostheses to 32 mm. Zirconia ceramics have higher fracture toughness, higher flexural strength, and lower \mathcal{E} than alumina ceramics as shown in Table 35.2. However, there are some concerns with ZrO₂:

There is a slight decrease in flexural strength and toughness of zirconia ceramics exposed to bodily fluids. The reason is associated with the martensitic transformation from the tetragonal to the monoclinic phase.

BLOMEDICAL APPLICATIONS OF Al₂O₃

There are many other applications of alumina as an implant material including knee prostheses, ankle joints, elbows, shoulders, wrists, and fingers.

A MOIETY

A moiety is a group of atoms that forms a distinct part of a large molecule.

A similar transformation has been observed to occur in aqueous environments.

The wear resistance of zirconia is inferior to that of alumina. In ceramic/ceramic combinations the wear rate of zirconia can be significantly higher than that of alumina. In combination with ultrahigh-molecular-weight polyethylene (UHMWPE) excessive wear of the polymer occurs.

Zirconia may contain low concentrations of long half-life radioactive elements such as Th and U, which are difficult and expensive to separate out. The main concern is that they emit α -particles (He nuclei) that can destroy both soft and hard tissue. Although the activity is small, there are questions concerning the long-term effect of α radiation emission from zirconia ceramics.

35.5 BIOACTIVE GLASSES

Bioactive materials form an interfacial bond with surrounding tissue. Hench and Andersson (1993) give the following definition:

A bioactive material is one that elicits a specific biological response at the interface of the material, which results in the formation of a bond between tissues and the material.

The first and most thoroughly studied bioactive glass is known as Bioglass[®] 45S5 and was developed at the University of Florida. Bioglass[®] 45S5 is a multicomponent oxide glass with the following composition (in wt%): 45% SiO₂, 24.5% Na₂O, 24.4% CaO, and 6% P₂O₅.

The majority of bioactive glasses are based on the same four components and all current bioactive glasses are silicates. However, the structure of Bioglass[®] 45S5 is different from that of the silicate glasses we described in Chapter 7. Bioactive glasses have a random, two-dimensional sheet-like structure with a low density. This is a result of the relatively low SiO₂ content. (You can compare the bioglass composition with that of other silicates given in Table 21.6.) Bioglass is mechanically weak and has low fracture toughness. Both these properties are related to the glass structure.

Bioactive glasses can readily be made using the processes developed for other silicate glasses. The constituent oxides, or compounds that can be decomposed to oxides, are mixed in the right proportions and melted at high temperatures to produce a homogeneous melt. On cooling a glass is produced. Because bioactive glasses are going to be used inside the body it is necessary to use high-purity starting

materials and often the melting is performed in Pt or Pt alloy crucibles to minimize contamination.

Bioactive glasses have certain properties that are relevant to their application in the body.

Advantages: There is a relatively rapid surface reaction that leads to fast tissue bonding. There are five reaction stages on the glass side of the interface. The reaction rates and mechanisms at each of the five stages have been determined by Fourier transform infrared (FTIR) spectroscopy. Bonding to tissue requires a further series of reactions that are at present not as well defined. But the bonding process starts when biological moieties are adsorbed onto the SiO_2 -hydroxycarboapatite layer. In addition, E is in the range 30–35 GPa, close to that of cortical bone (see Figure 35.4).

Disadvantages: They are mechanically weak. Tensile bending strengths are typically 40–60 MPa. In addition, the fracture toughness is low.

As a result of this combination of properties bioactive glasses are not found in load-bearing applications, rather they are used as coatings on metals, in low-loaded or compressively loaded devices, in the form of powders, and in composites. The first successful use of Bioglass[®] 45S5 was as a replacement for the ossicles (tiny bones) in the middle ear. The position of these bones (the malleus, incus and stapes) is illustrated in Figure 35.6.

Cone-shaped plugs of bioactive glasses have been used in oral surgery to fill the defect in the jaw created when a

tooth is removed. Bioactive glass implants have also been used to repair the bone that supports the eye (the orbital socket).

In powder form, bioactive glasses have been used in the treatment of periodontal disease and for the treatment of patients with paralysis of one of the vocal cords. When mixed with autologous bone they have been used in maxillofacial reconstruction (i.e., mixed with natural bone to rebuild a jaw).

35.6 BIOACTIVE GLASS-CERAMICS

We know that glass-ceramics are produced by ceramming a glass (see Chapter 26): converting it to a largely crystalline form by heat treatment. Several glass-ceramic compositions are bioactive. Their behavior in the body is very similar to that of the bioactive glasses, i.e., they form a strong interfacial bond with tissue.

- Cerabone[®] A-W is a glass-ceramic containing oxyfluoroapatite (A) and wollastonite (W).
- Ceravital[®] is primarily now used in middle ear operations.
- Bioverit I[®] is a class of bioactive machinable glass.

Cerabone[®] A-W glass-ceramic is produced by crystallization of a glass of the following composition (in wt%): 4.6 MgO, 44.7 CaO, 34.0 SiO_2 , 6.2 P_2O_5 , and 0.5 CaF_2 . The crystalline phases are oxyfluoroapatite

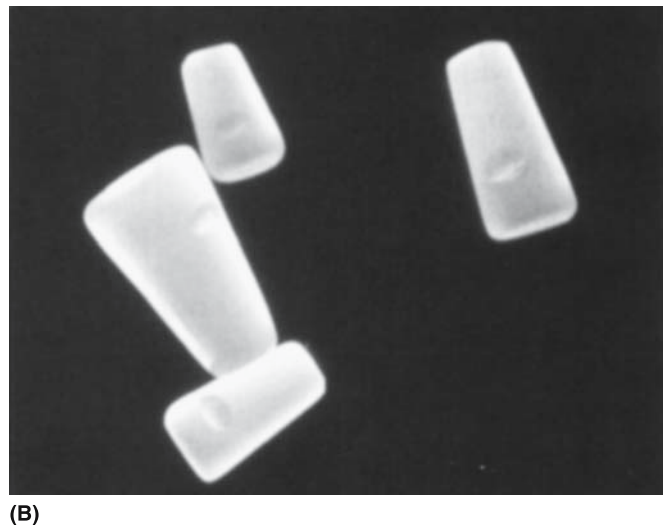
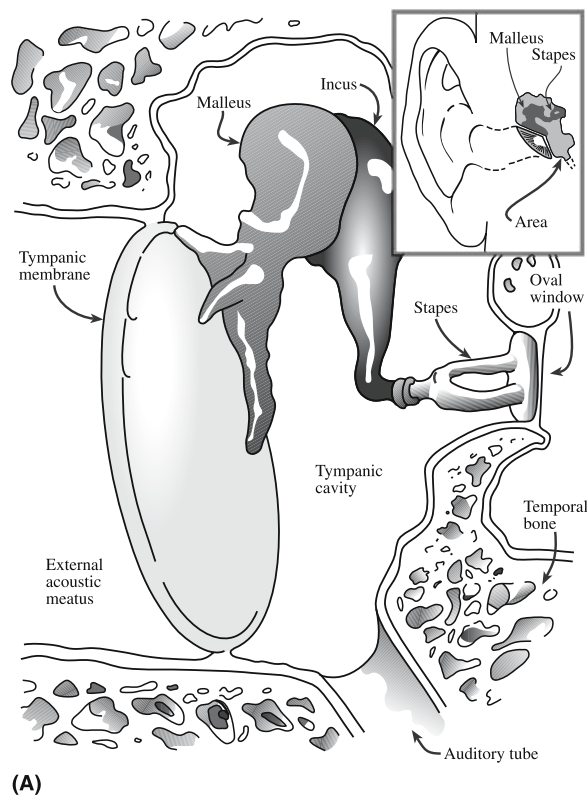


FIGURE 35.6 (a) The middle ear cavity and the auditory ossicles. (b) Ear implants.

TABLE 35.6 Composition Range in wt% of Bioverit® Glass Ceramics

Constituent	Composition range	Composition 1	Composition 2
SiO ₂	29.5–50	30.5	38.7
MgO	6–28	14.8	27.7
CaO	13–28	14.4	10.4
Na ₂ O/K ₂ O	5.5–9.5	2.3/5.8	0/6.8
Al ₂ O ₃	0–19.5	15.9	1.4
F	2.5–7	4.9	4.9
P ₂ O ₅	8–18	11.4	8.2
TiO ₂	Additions	—	1.9

[Ca₁₀(PO₄)₆(O,F)₂] as the A phase and β-wollastonite (CaO·SiO₂) as the W phase. These phases precipitate out at 870°C and 900°C, respectively. The composition of the residual glassy phase is (in wt%) 16.6 MgO, 24.2 CaO, and 59.2 SiO₂. The properties of A-W glass-ceramic are shown in Table 35.2. The applications include vertebral prostheses, vertebral spacers, and iliac crest prostheses.

Ceravital® refers to a number of different compositions of glasses and glass-ceramics that were developed in the 1970s in Germany for biomedical applications. The only field in which Ceravital® glass-ceramics are clinically used is in the replacement of the ossicular chain in the middle ear. In this application the mechanical properties of the material are sufficient to support the minimal applied loads.

Bioverit I® consists of two crystalline phases in a glass matrix. The key crystalline component that makes this glass-ceramic machinable is mica. We have already described the idea behind machinable glass-ceramics in Section 18.10. For bioactivity, the other crystalline phase is apatite. The type and amounts of each phase depend on the initial glass composition. Table 35.6 shows the typical composition range of Bioverit I® glass-ceramics. Composition 1 produces fluorophlogopite mica and apatite. Composition 2 produces tetrasilicic mica and apatite. There are several clinical applications of bioactive machinable glass-ceramics, such as spacers in orthopedic surgery and middle ear implants.

35.7 HYDROXYAPATITE

The apatite family of minerals has the general formula A₁₀(BO₄)₆X₂. In HA, or more specifically calcium hydroxyapatite, A = Ca, B = P, and X = OH. The mineral part of teeth and bones is made of an apatite of calcium and phosphorus similar to HA crystals. Natural bone is ~70% HA by weight and 50% HA by volume.

Hydroxyapatite is hexagonal (space group is *P6₃/m*) with *a* = 0.9432 nm and *c* = 0.6881 nm. The hydroxyl ions lie on the corners of the projected basal plane and occur at equidistant intervals [one-half of the cell (0.344 nm)] along columns perpendicular to the basal plane and paral-

lel to the *c* axis. Six of the 10 Ca²⁺ ions in the unit cell are associated with the hydroxyls in these particular columns. One group of three Ca²⁺ ions describing a triangle, surrounding the OH group, is located at *z* = 0.25 and the other set of three is located at *z* = 0.75. The six phosphate (PO₄)³⁻ tetrahedra are in a helical arrangement from levels *z* = 0.25 to *z* = 0.75. The network of (PO₄)³⁻ groups provides the skeletal framework that gives the apatite structure its stability. (It is complicated but certainly crystalline and very natural!)

Substitutions in the HA structure are possible. Substitutions for Ca, PO₄, and OH groups result in changes in the lattice parameter as well as changes in some of the properties of the crystal, such as solubility. If the OH groups in HA are replaced by F⁻ the anions are closer to the neighboring Ca²⁺ ions. This substitution helps to further stabilize the structure and is proposed as one of the reasons that fluoridation helps reduce tooth decay as shown by the study of the incorporation of F into HA and its effect on solubility. Biological apatites, which are the mineral phases of bone, enamel, and dentin, are usually referred to as HA. Actually, they differ from pure HA in stoichiometry, composition, and crystallinity, as well as in other physical and mechanical properties, as shown in Table 35.7. Biological apatites are usually Ca deficient and are always carbonate substituted: (CO₃)²⁻ for (PO₄)³⁻. For

TABLE 35.7 Comparative Composition and Crystallographic and Mechanical Properties of Human Enamel, Bone, and HA Ceramic

	Enamel	Cortical bone	HA
Constituents (wt%)			
Calcium, Ca ²⁺	36.0	24.5	39.6
Phosphorus, P	17.7	11.5	18.5
(Ca/P) molar	1.62	1.65	1.67
Sodium, Na ⁺	0.5	0.7	Trace
Potassium, K ⁺	0.08	0.03	Trace
Magnesium, Mg ²⁺	0.44	0.55	Trace
Carbonate, CO ₃ ²⁻	3.2	5.8	—
Fluoride, F ⁻	0.01	0.02	—
Chloride, Cl ⁻	0.30	0.10	—
Total inorganic	97.0	65.0	100
Total organic	1.0	25.0	—
Absorbed H ₂ O	1.5	9.7	—
Crystallographic properties			
Lattice parameters (±0.03 nm)			
<i>a</i>	0.9441	0.9419	0.422
<i>c</i>	0.6882	0.6880	0.6880
Crystallinity index	70–75	33–37	100
Crystallite size, nm	130 × 30	25 × 2.5–5.0	
Products after sintering >800°C			
	HA + TCP	HA + CaO	HA
Mechanical properties			
<i>E</i> (GPa)	14	20	10
Tensile strength (MPa)	70	150	100

this reason you will sometimes see biological apatites referred to as carbonate apatite and not as hydroxyapatite or HA.

For use in biomedical applications, HA is prepared in one of two forms: either dense or porous.

We will now discuss how these two forms are produced and some of the applications for each.

The methods used to produce **dense HA** are ones that we have already encountered in Chapter 23. The simplest is to dry press HA powder. Mold pressures are typically 60–80 MPa. The powder may also be mixed with a small amount of a binder. Suitable binders are 1 wt% cornstarch and water, steric acid in alcohol, or low-molecular-weight hydrocarbons. After pressing, the green ceramic is sintered in air. Sintering temperatures are up to 1300°C with dwell times at peak temperature of several hours.

By using hot isostatic pressing (HIP) techniques, we can achieve densification at much lower temperatures (900°C vs. 1300°C). The use of lower sintering temperatures not only saves on energy costs but prevents the formation of other calcium phosphate phases, such as TCP, which usually form when HA is sintered at $T > 900^\circ\text{C}$.

HIPing has also been used to form HA ceramics. HIPing results in products with more uniform densities than those obtained by uniaxial pressing and higher compressive strength.

The disadvantage of both hot pressing and HIPing is the equipment costs.

There are many applications for dense HA in both block form and as particles as listed in Table 35.8. One important application is replacements for tooth roots following extraction. The implants help minimize alveolar ridge resorption and maintain ridge shape following tooth loss, which affects millions of people.

The particular advantage of **porous HA** is that it permits ingrowth of tissue into the pores, providing biological fixation of the implant. The minimum pore size necessary is $\sim 100\mu\text{m}$. When used as a bone graft substitute, the porous HA should mimic the framework (or

stromal component) of the bone. The ideal microstructure for regeneration of cortical bone is an interconnected porosity of 65% with pore sizes ranging from 190 to 230 μm . The ideal graft substitute for cancellous bone would consist of a thin framework of large (500–600 μm) interconnected pores.

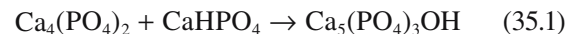
Several methods have been used to produce porous HA ceramics. Remember that historically much of ceramic processing was concerned with

trying to produce components that were fully dense. So to produce porous components, particularly where we need to control pore size, often requires ingenuity and a rethink. We discussed porous ceramics in Section 23.15, so will just point out special features for producing porous HA ceramics.

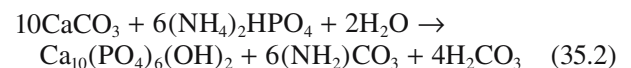
- Sintering HA powders
- Make a cement
- Use a natural template

Sintering HA powders, or a mixture of suitable reactant powders, uses naphthalene particles that volatilize during heating to create an interconnected porous network. Similar approaches have been used to produce foam glass (Section 26.9) and in the fugitive electrode method of producing multilayer chip capacitors (MLCCs) (Section 31.7).

By mixing water-setting HA cements with sucrose granules, porosity can be created when the sucrose is dissolved prior to the cement setting. One example of an HA cement is that obtained by the following reaction in an aqueous environment:



The natural-template method was developed in 1974. It can produce porous HA powders. A suitable template was found to be the calcium carbonate (CaCO_3) skeleton of reef-building corals, such as those found in the South Pacific. The reaction to produce HA involves a hydrothermal exchange reaction of carbonate groups with phosphate groups, which can occur via the following chemical reaction:



The HA structure produced by this exchange reaction replicates the porous marine skeleton, including its interconnected porosity. Hydroxyapatite grown on *Porites* and *Goniopora* coral skeleton templates can be used to mimic

DENSE HA

Porosity <5 vol%
Pore size <1 μm diameter
Grain size >0.2 μm

RESORPTION

Resorption is the process of reabsorbing biological material.

TABLE 35.8 Applications for Dense HA Ceramics

Application	Form
Augmentation of alveolar ridge for better denture fit	Blocks
Orthopedic surgery	Blocks
Target materials for ion-sputtered coatings	Blocks
Filler in bony defects in dental and orthopedic surgery	Particles
Plasma sprayed coatings on metal implants	Particles
Filler in composites and cements	Particles

the stroma of cortical bone and cancellous bone, respectively.

35.8 BIOCERAMICS IN COMPOSITES

The main reason for forming composites is to improve the mechanical properties, most often toughness, above that of the stand-alone ceramic. For bioceramic composites we often are trying to increase K_{IC} and decrease \mathcal{E} .

The first bioceramic composite was a stainless-steel fiber/bioactive glass composite made of Bioglass® 45S5 and AISI 316L stainless steel. The composite was made by first forming a preform of the discontinuous metal fibers, then impregnating it with molten glass, and finally heat treating the composite to develop the desired mechanical properties.

For effective stress transfer between the glass matrix and the reinforcing metal fibers when the composite is under load, there must be a strong glass-metal bond. This requires that the glass wet the metal surface during processing. Wetting is achieved by oxidizing the metal fibers before they are immersed in the glass. Chemical analysis across the glass-metal interface showed that there is Fe diffusion from the oxide into the glass and Si diffusion from the glass into the oxide. The composition gradient across the interface indicates chemical interaction between the two phases, which leads to improved adhesion.

Assuming that the fibers are aligned in the direction of the applied load, and that there is good adhesion with the matrix such that the elastic strains are equal in both components, we can write

$$\sigma_c = \sigma_f V_f + \sigma_m V_m \quad (35.3)$$

The subscripts c, f, and m refer to the composite, fiber, and matrix, respectively, and V is the volume fraction of each phase. If we assume 45 vol% of steel fibers and $\sigma_f = 530$ MPa and $\sigma_m = 42$ MPa, then $\sigma_c = 262$ MPa. This value, which is close to experimentally measured values, represents a significant strengthening above that of the glass alone.

One of the potential problems associated with forming composites is that of mismatch in α between the two components, which is significant for glass and steel. For reinforcing fibers for which the difference in α with the glass phase is even greater than that with steel, e.g., Ti, it is necessary to change the composition of the glass to lower its α .

AISI 316L
$\alpha = 20.0 \times 10^{-6} \text{ }^\circ\text{C}^{-1}$ (to 200°C)
$\alpha = 21.8 \times 10^{-6} \text{ }^\circ\text{C}^{-1}$ (to 400°C)
BIOGLASS® 45S5
$\alpha = 18.0 \times 10^{-6} \text{ }^\circ\text{C}^{-1}$ (to 450°C)

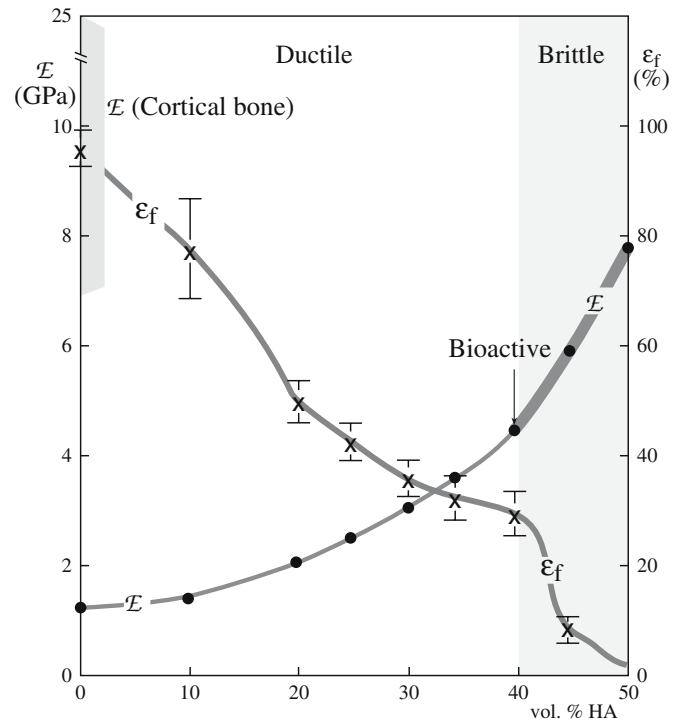


FIGURE 35.7 Effect of volume fraction of HA on \mathcal{E} and strain to failure of HA-reinforced PE composites, in comparison to cortical bone.

Other current bioceramic composites of interest are

- Ti-fiber-reinforced bioactive glass
- ZrO₂-reinforced A-W glass
- TCP-reinforced PE
- HA-reinforced PE

Hydroxyapatite-reinforced PE is a good illustration of a composite that can have properties that are not available in a single material. These composites were developed as a bone replacement that would have a matched modulus, be ductile, and bioactive. Figure 35.7 shows how increasing the volume fraction of HA to 0.5 in a composite can be achieved with \mathcal{E} in the range of that of cortical bone. When the volume fraction of HA in the composite is increased above about 0.45 the fracture mode changes from ductile to brittle. For clinical applications a volume fraction of 0.4 has been found to be optimum. The HA-reinforced PE composite is designated commercially as HAPEX™ and several thousand patients have received middle ear implants made from this material. The technology was granted regulatory approval by the FDA in the United States in 1995.

35.9 BIOCERAMIC COATINGS

Applying a glass or ceramic coating onto the surface of a substrate allows us to have the best of both worlds. We have the bulk properties of the substrate and the surface properties of the coating. There are three main reasons for applying a coating:

1. Protect the substrate against corrosion
2. Make the implant biocompatible
3. Turn a nonbioactive surface into a bioactive one

There are four substrate-coating combinations:

1. Polycrystalline ceramic on ceramic
2. Glass on ceramic
3. Polycrystalline ceramic on metal
4. Glass on metal

Bioceramic coatings are often used on metallic substrates in which the fracture toughness of the metal is combined with the ability of the coating to present a bioactive surface to the surrounding tissue. The use of a bioceramic coating on a metal implant can lead to earlier stabilization of the implant in the surrounding bone and extend the functional life of the prosthesis. Under the proper conditions a cementless prosthesis should remain functional longer than a cemented device in which stability is threatened by fracture of the bone cement.

The important ceramic coatings are HA and TCP. We described the structure and properties of HA, a bioactive ceramic, in some detail in Section 35.6. Tricalcium phosphate is a resorbable bioceramic. It occurs in two polymorphs, α -whitlockite and β -whitlockite. The β form is the more stable. When TCP is implanted into the body it will eventually dissolve and be replaced by tissue. The role of resorbable bioceramics is to serve as scaffolding, permitting tissue infiltration and eventual replacement. Essentially, this is the same function as bone grafts. Tricalcium phosphate has been clinically applied in many areas of dentistry and orthopedics. Bulk material, available in dense and porous forms, is used for alveolar ridge augmentation, immediate tooth root replacement, and maxillofacial reconstruction. However, because bulk TCP is mechanically weak, it cannot be used in load-bearing applications. Therefore, TCP is often used as a coating on metal substrates.

The most widely used method for applying coatings of HA and TCP is plasma spraying. We already described this technique in Section 27.5; it is one of the methods used to produce thermal barrier layers. Plasma spraying uses a plasma, an ionized gas, that partially melts the HA particles and carries them to the surface of the substrate. For HA coatings the starting material is pure 100% crystalline HA particles in the 20–40 μm range. One of the advantages of plasma spraying is that the substrate remains at a relatively low temperature (generally less than 300°C;

the plasma temperature may exceed 10,000°C!) so the mechanical properties of the metal are not compromised. The coating thickness typically averages 40–60 μm with a residual porosity <2%.

Hydroxyapatite coatings prepared by plasma spraying typically contain considerable amounts of amorphous calcium phosphate and small amounts of other crystalline phases. Heat treating the coating can increase crystallinity and also improve the adhesion to the substrate. However, this process is not usually done because of economic factors and concerns about the adverse effects it might have on the mechanical properties of the substrate.

In addition to plasma spraying other methods have been used to apply HA coatings:

- Electrophoretic deposition when line-of-sight deposition is not possible
- Sputtering when very thin coatings are needed
- HIPing when we need a very dense material

Electrophoretic deposition (see Section 27.6 for a description of the technique) can be used to coat porous surfaces that cannot be completely coated by line-of-sight techniques such as plasma spraying. But the adhesion of the HA particles to the substrate and each other is weak and high-temperature sintering after deposition is usually necessary.

Sputtering has been used to produce thin (1 μm) HA coatings. The deposited films are amorphous because the sputtered components do not possess enough kinetic energy to recombine in a crystalline form. Heat treatment at 500°C is enough to crystallize the amorphous film. Durability of thin sputtered films in the body has not yet been demonstrated.

HIPing is a technique we encountered earlier, but not in the context of forming films. If a metal implant is coated with HA particles then HIPing can be used to form a dense adherent coating. To achieve a uniform application of pressure on the HA particles an encapsulation material (e.g., a noble metal foil) is necessary. As mentioned earlier, HIPing allows the use of lower sintering temperatures than pressureless techniques; as a result there is less chance of altering the microstructure or mechanical properties of the metal substrate.

There are several requirements for HA coatings used for prosthetic devices:

- Correct crystalline phase
- Stable composition
- Dense
- Good adhesion to the substrate
- High purity
- No change to the substrate

Plasma sprayed coatings often contain a mixture of crystalline and amorphous phases, which may be undesirable. The adhesion of plasma-sprayed HA coatings to

metal substrates is principally mechanical, and so surface roughness of the substrate plays an important role.

Bioactive glass coatings are also important for implant devices. These are usually applied by one of the following techniques:

- Enameling
- Flame spraying
- Dip coating

Flame spraying is similar to plasma spraying except that the carrier gases are not ionized and the temperatures are considerably lower than in plasma spraying. In dip coating, the metal implant is preoxidized to provide a suitable surface for wetting of the molten glass. The heated metal is then dipped into the molten glass.

Enameling is a traditional method of applying glass coatings and uses a particulate form of the glass called a frit, which is formed when molten glass is quenched in water. The resulting coarse particles of the frit are ground to a fine powder that is applied to the metal substrate by painting, spraying, or dipping. The coated article is then heated to soften the glass and form a uniform coating. In traditional enameling the adhesion between the glass and metal is improved by using what enamellers call a “ground coat.” This is a mixture of metal oxides that reacts chemically with both the metal and the glass enabling the formation of a chemical bond. However, this approach has not proved to be successful with bioactive glasses and alternative approaches are being used.

35.10 RADIOTHERAPY GLASSES

Radioactive yttrium aluminosilicate (YAS) glasses have been used to provide *in situ* irradiation of malignant tumors in the liver. Although primary liver tumors are relatively rare in the United States (about 3000–4000 deaths per year in the United States, 1.2 million worldwide) they are almost always lethal. And most of these tumors are inoperable due to various medical complications. Irradiating the tumors inside the body allows the use of large (>10,000 rads) localized doses of radiation directly to the tumor while minimizing damage to surrounding healthy tissue. And this procedure represents an important tool in treating this disease.

YAS glasses are particularly suitable because they are

- Not toxic
- Easily made radioactive
- Chemically insoluble while the glass is radioactive

The sol-gel process has been used to produce high purity YAS glass spheres. The radioactive isotope produced when the YAS glass spheres are irradiated is ^{90}Y , a β emitter with a half-life of 64.1 hours. The average penetration of β -particles (electrons) in human tissue is 2.5 mm (maximum pen-

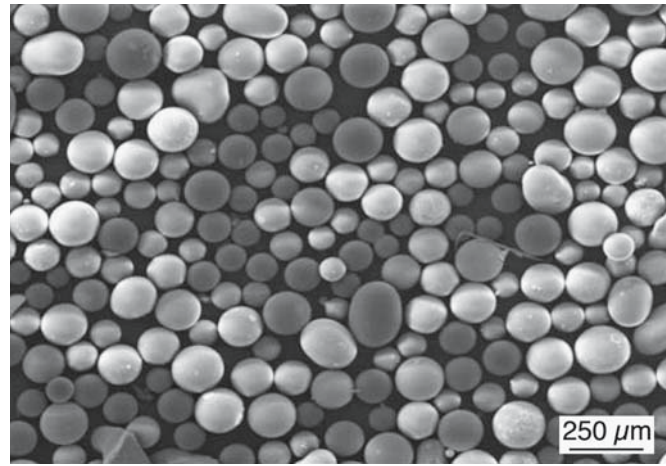


FIGURE 35.8 Lithium calcium borate glass microspheres produced by passing through a flame at 1400°C.

etration ~10 mm). For the radioactive material to reach the site of the tumors between 1 and 15 million microspheres are injected into the hepatic artery, which is the primary blood supply for the target tumors. Treatment time takes 2–4 hours. The size of the microspheres is 15–35 μm in diameter, which allows the blood to carry them into the liver, but they are too large to pass completely through the liver and enter the circulatory system. The microspheres concentrate in the tumor because it has a greater than normal blood supply. And there they irradiate it with β -particles. Since the half-life of ^{90}Y is 64.1 hours, the radioactivity decays to a negligible level in about 3 weeks.

Although the use of radiotherapy glass spheres in treating liver cancer is still at a relatively early stage the results appear promising. The commercially available product called TheraSphereTM made by MDS Nordion is approved in the United States and Canada for treating patients with inoperable liver cancer. Other medical applications for these glass spheres have been considered such as the treatment of cancers of the kidney and brain.

Figure 35.8 shows lithium calcium borate (LCB) glass microspheres that were spheroidized by passing them through a high-temperature flame. A similar process is used to make the smaller YAS microspheres. The LCB microspheres are subsequently converted into hollow hydroxyapatite microspheres that have potential application in drug delivery.

35.11 PYROLYTIC CARBON HEART VALVES

Carbon is an important bioceramic. It combines outstanding biocompatibility and chemical inertness. Carbon exists in many forms, some of which have been discussed in earlier chapters. The most important form of carbon for biomedical applications is a type of pyrolytic graphite known as the low-temperature isotropic form (LTI carbon).

LTI

Low T refers to the forming $T < 1500^\circ\text{C}$. For ceramics 1500°C is not a high T .

Low-temperature isotropic carbon is an example of what are referred to as turbostratic carbons. These have a disordered structure based on graphite (and thus are also called turbostratic graphite). In turbostratic carbon the ABABA stacking sequence is disrupted through random rotations or displacement of the layers relative to each other. The individual LTI carbon crystallites are only ~10nm in size and are arranged randomly in the bulk material. This microstructure leads to the material having isotropic mechanical and physical properties, unlike graphite in which the properties are highly anisotropic. The density and mechanical properties of LTI are influenced by the number of carbon vacancies in each of the layers and distortions within each plane. The densities range from 1400 kg/m³ up to a theoretical maximum of 2200 kg/m³.

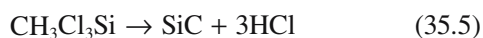
High-density LTI carbons are the strongest bulk form of turbostratic carbon; we can increase their strengths further by adding Si. The material then consists of discrete submicrometer β-SiC particles randomly dispersed in a matrix of roughly spherical micrometer-sized subgrains of pyrolytic carbon; the carbon itself has a “subcrystalline” turbostratic structure, with a crystallite size typically <10nm. This is analogous to the microstructure produced during precipitation hardening of metals.

A chemical vapor deposition (CVD) process (see Section 28.4) involving the codeposition of carbon and SiC is typically used to produce the LTI–Si alloys. Two possible reactions are

1. Decomposition of propane:



2. Decomposition of methyltrichlorosilane



The articles to be coated are suspended within a fluidized bed of granular particles, usually ZrO₂. The reactions take place in the range of 1000–1500°C and the products coat the components as well as the ZrO₂ particles.

One of the major applications for LTI carbon is in making prosthetic heart valves as shown in Figure 35.9. This is one of the most demanding applications for bio-



FIGURE 35.9 LTI pyrolytic carbon-coated heart valve.

materials. The first use of LTI carbon in humans for prosthetic heart valve was in 1969. The majority of artificial heart valves currently use Si-alloyed LTI pyrolytic carbon.

35.12 NANOBIOCERAMICS

By 2012, there will be books on the uses of nanoparticles and there are already hundreds of research papers. There may also be books discussing the toxicity of these materials. The asbestos fibers linked to respiratory illness have widths <250 nm; amphibole (red or blue asbestos) fibers are ~75–240 nm wide, therefore definitely counting as nanoparticles.

Examples of a microbarcode made by Corning are shown in Figure 35.10. The information is coded into the small glass bars so that they fluoresce. The pattern can then be read by illuminating the glass with UV; otherwise it is not only too small to see but the information could not be detected.

The magnetite nanocrystals we discussed in Chapter 33 are used by nature in ways we do not fully understand, but they appear to allow certain species to detect the earth’s magnetic field and use it to navigate.

TiO₂ nanoparticles are used in sunscreen to protect the skin from UV radiation. The particles used for this application are typically 10–100 nm in diameter and block both UVA (320–400 nm) and UVB (290–320 nm) irradiation.

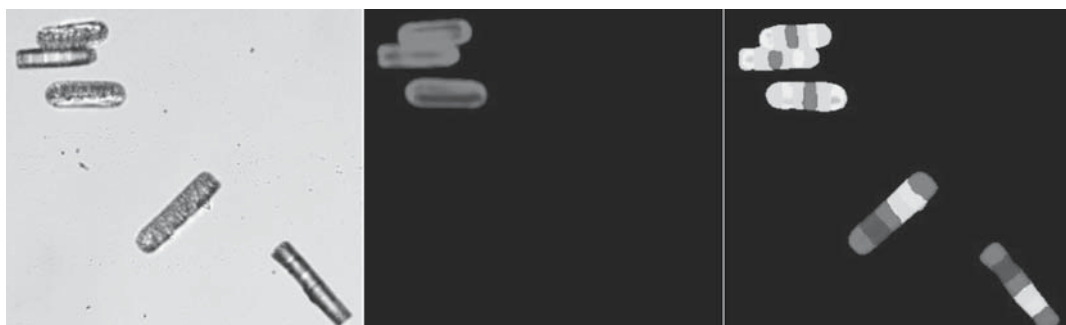


FIGURE 35.10 Microbar codes from Corning. The cylindrical bars are typically 100 μm long and 20 μm in diameter.

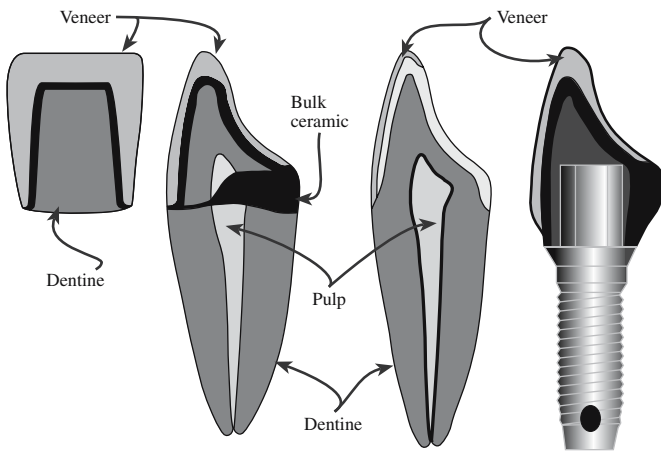


FIGURE 35.11 Tooth restoration.

There is some concern that these nanoparticles (and those of ZnO) are so active that they might catalyze the breakdown of DNA, but they do not appear to penetrate the outer layers of the skin. The positive aspect of this is the potential for using these same TiO₂ nanoparticles for photo-killing of malignant cells—known as photodynamic therapy. TiO₂ and ZnO particles are actually being coated with silica so that the particle surface is more inert. (A use for core-shell nanoparticles.)

35.13 DENTAL CERAMICS

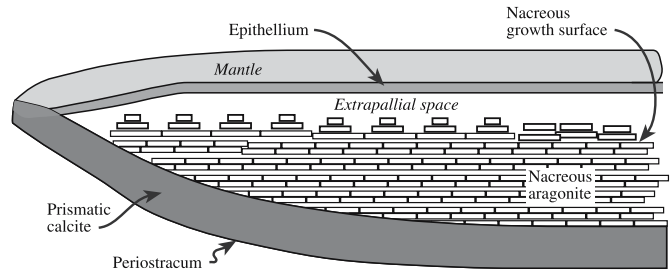
The felspathic porcelains (porcelain's based on feldspar) are used as the veneer to “cap” the front of a tooth for cosmetic reasons; these veneers are ~500 μm thick. Today, this material is mainly replaced by glass, although the name may not have changed. Leucite is added to modify the thermal expansion coefficient. Dicor is the glass-ceramic developed by Corning for construction of replacement teeth. The tooth is cast as a glass using a lost-wax mold and then cerammed. Alumina has also been used to form the tooth, although porosity causes failure during “use.” One way to improve this is to infiltrate the alumina with a lanthanum-containing glass (known commercially as In-Ceram). The different restorations are shown schematically in Figure 35.11.

DENTAL RESTORATIONS

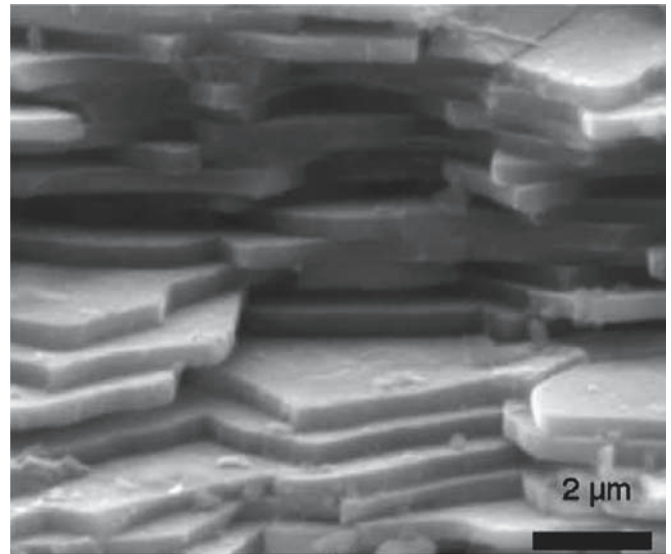
- Feldspathic veneers
- Porcelain jacket crowns (PJC's)
- Metal-ceramic crowns
- Inlays and onlays
- Implants

35.14 BIOMIMETICS

The topic of biomimetics was actually mentioned earlier but not using the new name. The principle underlying the development of biomimetics is “learning from nature.”



(A)



(B)

FIGURE 35.12 (a) Schematic of the abalone shell. (b) Abalone slabs.

Biomimetics can potentially lead to an enormous subset of ceramics. Not only are the materials important but their topology and microstructure are also special. The aim is to mimic natural materials

that have special behaviors, but to do it with “better” (i.e., ceramic) materials.

Shells (especially the abalone shell). Biological organisms can deposit inorganic layers. The abalone shell consists of layers of aragonite with ~5 wt% organic material (protein, etc.) between the layers to toughen it. A schematic cross section and a scanning electron microscopic (SEM) image of the aragonite layers are shown in Figure 35.12.

Coral. Coral is used “as harvested” or after processing in the manufacture of bone grafts. It is a natural porous ceramic and can be converted to porous HA (see Section 35.7). Surgeons in the United States perform ~500,000 bone grafts each year.

Petrified wood. A natural material is infiltrated by a ceramic.

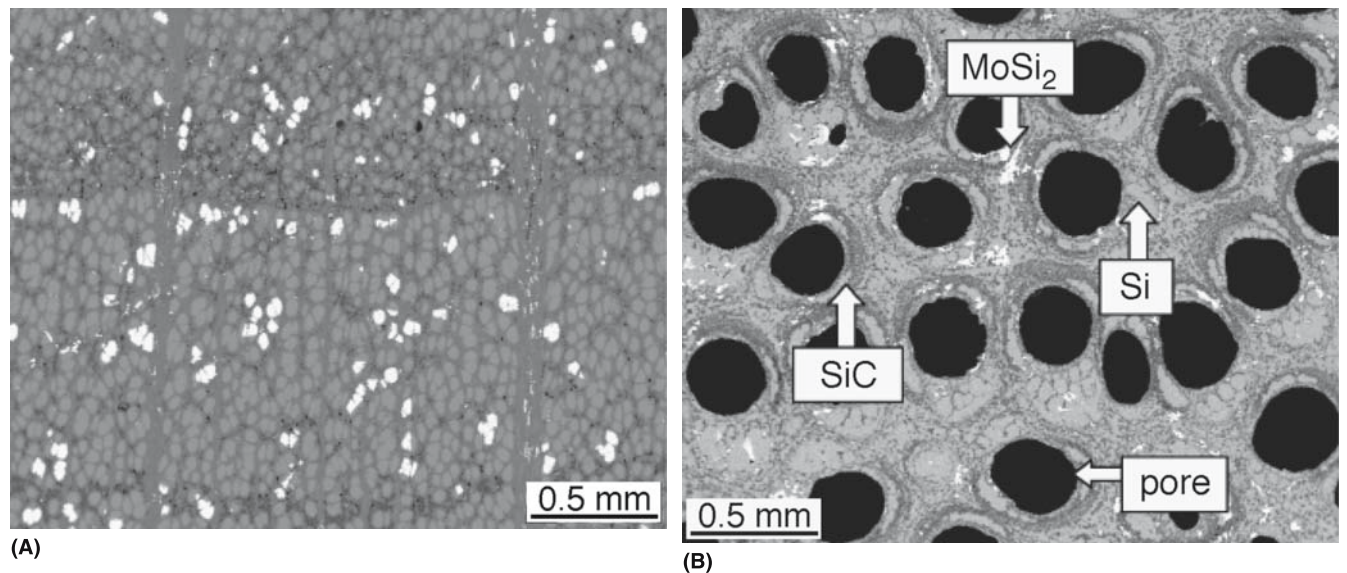


FIGURE 35.13 Wood converted into ceramics by a reactive melt-infiltration process.

Petrified wood provides a good illustration of the surprising potential of biomimetics in a way that is analogous to the conversion of coral. Wood can be intentionally converted into biomorphic, microcellular SiC-based ceramics using a reactive melt-infiltration process, or more specifically liquid-Si infiltration (LSI). The images shown in Figure 35.13 illustrate the possibility: the microstructure of the resulting composite depends on the nature of

the wood used. Beech, pine, and rattan produce very different microstructures which are of course different in cross section and longitudinally. In this example, the infiltrating liquid was a molten Si-M alloy (Mo, Ta, Ti, and Fe were explored as the metal, M). For Mo, this produces an MoSi₂/Si composite. The LSI technique has been used previously to produce SiC and Si₃N₄; the special feature here is the biomimetic structure produced by the wood.

CHAPTER SUMMARY

Bioceramics is a relatively new field and an increasingly important one. Bioceramics are implanted into the human body to replace existing parts that have become diseased, damaged, or worn out. More than 1 million hip prostheses using alumina components have been performed. Alumina is a very important bioceramic because it is biocompatible—it does not produce any adverse reactions in the body. One of the disadvantages of alumina is that it is also an example of what is termed a nearly inert bioceramic: it does not allow interfacial bonding with tissue. When bioactive ceramics and glasses are implanted into the body they undergo chemical reactions on their surface leading to strong bond formation. The most important bioactive ceramic is hydroxyapatite, which is very similar to the mineral part of teeth and bones. Hydroxyapatite is brittle and mechanically weak, but if it is combined with a polymer a composite can be produced that is ductile and has \mathcal{E} close to that of bone. Hydroxyapatite and other bioactive ceramics and glasses are often used as coatings on metal supports. This allows the excellent mechanical properties of the metal to be combined with the biocompatibility of ceramics. Another ceramic material that is used in the form of a coating is pyrolytic carbon. The application here is artificial heart valves, which is a very demanding materials application: reliability is critical. We concluded the chapter with a brief discussion of biomimetics (which is related to bionics, etc.) and emphasize that this will become a large field in itself but the materials must be understood to take full advantage of this potential.

GENERAL REFERENCES

Hench, L.L. and Wilson, J.K. (Eds.) (1993) *An Introduction to Bioceramics*, World Scientific, Singapore.
A collection of chapters on different aspects of bioceramics written by experts in the field. This is an excellent resource.

- LeGeros, R.Z. and LeGeros, J.P. (Eds.) (1998) *Bioceramics, Volume 11, Proceedings of the 11th International Symposium on Ceramics in Medicine*, World Scientific, Singapore. The most recently published proceedings in this annual conference series. Covers the latest developments in all aspects of the field of bioceramics.
- Marieb, E.N. (1998) *Human Anatomy and Physiology*, 4th edition, Benjamin Cummings, Menlo Park, CA. For a more detailed description of bone.
- Park, J.B. (1984) *Biomaterials Science and Engineering*, Plenum, New York. A textbook covering all aspects of biomaterials. The section covering ceramic implant materials is quite brief, but there is information about polymers and metals and a general background about the field.
- Ravaglioli, A. and Krajewski, A. (1992) *Bioceramics: Materials, Properties, and Application*, Chapman & Hall, London. Covers the history of bioceramics, scientific background to the field, and state of the art as of 1991.
- Shackelford, J.F. (Ed.) (1999) *Bioceramics: Applications of Ceramics and Glass Materials in Medicine Mater. Sci. Forum*, **293**. A recent monograph on bioceramics.
- Williams, D.F. (1999) *The Williams Dictionary of Biomaterials*, Liverpool University Press, Liverpool. The latest collection of definitions used in the field of biomaterials.
- Yamamuro, T., Hench, L.L., and Wilson, J. (Eds.) (1990) *Handbook of Bioactive Ceramics, Volume I: Bioactive Glasses and Glass Ceramics, Volume II: Calcium Phosphate and Hydroxylapatite Ceramics*, CRC Press, Boca Raton, FL. A collection of articles on bioactive and resorbable bioceramics.

JOURNALS AND CONFERENCE PROCEEDINGS

The following journals and conference proceedings contain reports of advances in bioceramics.

Bioceramics. This is the title of the Proceedings of the International Symposium on Ceramics in Medicine.

The symposium has been held annually since 1988.

Biomaterials. 1980–present (volume 27)

Biomedical Materials and Engineering. Covers all aspects of biomaterials and includes details of clinical studies. Usually found with medical journals rather than physical science or engineering publications.

Journal of Biomedical Materials Research. (Now volume 80; 4 volumes in both ‘A’ and ‘B’.)

Journal of Materials Science Materials in Medicine. Emphasising the materials science aspects.

Journal of the American Ceramic Society. Covers the entire ceramics field including bioceramics.

Nature. A journal with a wide readership. Publishes important news articles having a significant impact on the field.

SPECIFIC REFERENCES

Annual Book of ASTM Standards, 13.01, *Medical Implants*, ASTM, Philadelphia. The American Society for Testing and Materials (ASTM) has developed several standards related to bioceramics for surgical implants: the *Annual Book of ASTM Standards*.

Bokros, J.C., LaGrange, L.D., Fadali, A.M., Vos, K.D., and Ramos, M.D. (1969) *J. Biomed. Mater. Res.* **3**, 497. First use of carbon heart valves in humans.

Bonfield, W., Grynopas, M.D., Tully, A.E., Bowman, J., and Abram, J. (1981) “Hydroxyapatite reinforced polyethylene—a mechanically compatible implant,” *Biomaterials* **2**, 185.

Brömer, H., Pfeil, E., and Käs, H.H. (1973) German Patent 2,326,100. Patent for Ceravital.

Chakrabarti, O., Weisensel, L., and Sieber, H. (2005) “Reactive melt infiltration processing of biomorphic Si–Mo–C ceramics from wood,” *J. Am. Ceram. Soc.* **88**(7), 1792.

DiB: *Definitions in Biomaterials* (1987) D.F. Williams (Ed.), Elsevier, Amsterdam, 6. Includes a discussion of biocompatibility.

Ducheyne, P. and Hench, L.L. (1982) “The processing and static mechanical properties of metal fibre reinforced bioglass[®],” *J. Mater. Sci.* **17**, 595. Diffusion across a bioglass–metal interface.

Galletti, P.M. and Boretos, J.W. (1983) “Report on the Consensus Development Conference on Clinical Applications of Biomaterials” *J. Biomed. Mater. Res.* **17**, 539. Defined “biomaterial.”

Hench, L.L. (1991) “Bioceramics: From concept to clinic,” *J. Am. Ceram. Soc.* **74**, 1487. An excellent review on this topic.

Hench, L.L. and Andersson, O. (1993) “Bioactive glasses,” in *An Introduction to Bioceramics*, edited by L.L. Hench and J.K. Wilson, World Scientific, Singapore, 41.

Klawitter, J.J. and Hulbert, S.F. (1971) “Application of porous ceramics for the attachment of load bearing orthopedic applications,” *J. Biomed. Mater. Res.* **2**, 161. Determined that a minimum pore size of 100 μm is necessary for bone ingrowth.

Mehmel, M. (1930) *Z. Kristallogr.* **75**, 323. One of two original determinations of the structure of hydroxyapatite. The structure was originally taken to be the same as that of fluorapatite, Ca₁₀(PO₄)₆F₂, which had already been resolved.

- Merwin, G.E., Wilson, J., and Hench, L.L. (1984) in *Biomaterials in Otology*, edited by J.J. Grote, Nijhoff, The Hague, pp. 220–229. Description of bioglass.
- Náray-Szabó, S. (1930) *Z. Kristallogr.* **75**, 387. The other paper on the structure of hydroxyapatite.
- Posner, A.S., Perloff, A., and Diorio, A.F. (1958) “Refinement of the hydroxyapatite structure,” *Acta Cryst.* **11**, 308. Determined atom positions, bond lengths, and lattice parameters for the HA crystal structure.
- Roy, D.M. and Linnehan, S.K. (1974) “Hydroxyapatite formed from coral skeletal carbonate by hydrothermal exchange,” *Nature* **247**, 220. Developed the natural-template method for making porous HA.
- Sarakiya, M. (1994) “An introduction to biomimetics: A structural viewpoint,” *Microsc. Res. Techn.* **27**, 360. A very useful introduction.
- Sato, T. and Shimada, M. (1985) “Transformation of yttria-doped tetragonal ZrO₂ polycrystals by annealing in water,” *J. Am. Ceram. Soc.* **68**, 356. Described the martensitic transformation in ZrO₂ in aqueous environments.
- Wang, Q., Huang, W., Wang D., Darvell, B.W., Day, D.E., and Rahaman, M.N. (2006) “Preparation of hollow hydroxyapatite microspheres,” *J. Mater. Sci: Mater. Med.* **17**, 641.

WWW

www.mds.nordion.com/therasphere/
The TheraSphere® web site.

EXERCISES

- 35.1 Briefly compare and contrast the suitability of metals, ceramics, and polymers for use in biomedical applications. In your answer consider the following factors: biocompatibility, mechanical properties, and ease of processing.
- 35.2 Alumina (Al₂O₃) ceramic implants are required to have a small grain size (<4.5 μm). (a) Why do you think a small grain size is important? (b) How does the addition of MgO to the powder mixture help to keep the grain size small? (c) Are there any other ways that could be used to limit the extent of grain growth?
- 35.3 Explain why tetragonal zirconia polycrystal (TZP) and Mg-partially stabilized zirconia (PSZ) ceramics have higher toughness than alumina ceramics.
- 35.4 The Weibull modulus of an alumina bioceramic is given as 8.4. (a) What does a value of $m = 8.4$ imply? (b) For an implant made out of a metal the value of $m \sim 100$. What implications would this have for lifetime predictions for the metal component compared to the alumina component? (c) How does the value of m affect the design of a component for a load-bearing application?
- 35.5 The composition of Bioglass® 45S5 is 45% SiO₂, 24.5% Na₂O, 24.4% CaO, and 6% P₂O₅. (a) Classify each of the oxide constituents of 45S5 as either network formers, modifiers, or intermediates. (b) What would the composition of Bioglass® 45S5 be in mol%? (c) Explain briefly how the structure of 45S5 differs from the silicate glasses described in Chapter 7 and what implications this difference has on the properties of 45S5.
- 35.6 The substitution of ions in the HA structure can change the lattice parameters of the unit cell. Explain how you think the substitution of Ca²⁺ for the following ions would change both the a and c lattice parameters: Sr²⁺, Ba²⁺, Pb²⁺, Mg²⁺, Mn²⁺, and Cd²⁺.
- 35.7 According to ASTM Standards [American Society for Testing and Materials (1990) *Annual Book of ASTM Standards*, Section 13, F 1185–1188] the acceptable composition for commercial HA is a minimum of 95% HA, as established by X-ray diffraction (XRD) analysis. Describe how XRD can be used to determine phase proportions in a mixture.
- 35.8 We mentioned that in steel fibers/bioactive glass composites it was important that there was chemical interaction between the two components to ensure stress transfer during loading. We have just formed a bioceramics company and want to hire you as a consultant. We want you to determine whether such interactions have occurred in a composite we have just made. What analytical technique or techniques would you use for your evaluation? Explain the reasoning behind your answer and some of the pros and cons of the technique or techniques you chose.
- 35.9 One of the advantages of plasma spraying for producing HA coatings on metallic implants is that the substrate temperature can be kept relatively low. What possible mechanisms can lead to a loss in the mechanical strength of a metal if it is exposed to high temperatures? (You can limit your discussion to the cases of Ti alloys and stainless steel.)
- 35.10 Explain why the mechanical properties of turbostratic carbons such as LTI are different from those of graphite. Both are forms of carbon and are chemically identical.

Minerals and Gems

CHAPTER PREVIEW

We begin this chapter by explaining why we are including gems in a text on ceramics. Gems have been intimately linked with many developments in the use of ceramics or have been the motivation for what has become a leap forward in ceramic processing or application. We saw earlier how the efforts by August Verneuil in the early 1900s to produce synthetic ruby led to an industry that produces 2×10^5 kg of single-crystal Verneuil sapphire each year. Similarly, flux-growth techniques and hydrothermal quartz owe much to the desire to create gems. Gemstones use some special properties of ceramics: they can be transparent but with a range of colors, they scatter light (the sparkle), and the valuable ones are generally very stable (the less valuable ones have often been treated); actually most gemstones have been processed in some way. We will discuss the well-known gems and a few of the lesser known gems (for their special features). The most important gems are diamond, ruby, sapphire, and emerald. However, many other gems that are less well known may often be more valuable. Incidentally, the weight of a gemstone is usually given in carats (5 ct = 1 g). We will also use this chapter to summarize the links between some preceding topics, including history. If a friend hands you a blue (or red, yellow, green, or colorless) faceted sparkling stone and asks you to identify it (because you studied ceramics) what do you do or say? So when you read this chapter, keep asking yourself—what ceramic science is involved here.

36.1 MINERALS

Mining and mineral engineering are not always popular topics today. Many gemstones and mineral specimens are found during mining operations. Most minerals are then processed by physical or chemical means. Ceramists should have some knowledge of mineral processing because this can be the clue to understanding why certain impurities are present in powders used to produce high-tech ceramics (hence our discussion of raw materials in Chapter 19), but minerals and gemstones have many commercial in addition to decorative (ornamental) uses.

Grinding is a particularly simple example of physical processing. It has been used to make pigments, early cosmetics, and the ingredients for the potter's slip. It is a key step in modern ore processing (Chapter 19), but it has been used for centuries to make powders.

Grind hematite to produce the red pigment *ochre*

Grind cinnabar to produce the major component of *vermillion*

Crush lapis lazuli like the Persians did to make *ultramarine*

Grind azurite like the ancient Egyptians to produce the blue pigment *azure*

Grind tin oxide like the Romans to make a white cosmetic paste

Be cautious about using ground *talc* on your body

Of course, grinding is also the principle of the abrasives industry. Powders may be made by grinding or used for grinding/polishing as discussed in Section 18.12.

A crystal of galena was used in the cat's whisker radio (in the "point-contact" diode); Cu wire was slowly moved across the galena crystal to tune the device. Thin slices of tourmaline crystals were used in making the pressure gauges that measured the power dissipated by the first atom bomb explosions (tourmaline is piezoelectric).

Chalcedony is "non-crystalline" quartz. Examples of chalcedony are agate, jasper, and carnelian; they form by hydrothermal growth—hence the banding you see on

NATURAL GLASS THREAD

Pele's hair (the Hawaiian goddess of volcanoes, not the soccer player) consists of natural threads of basalt glass often containing crystals of olivine. Like obsidian and pumice it forms in volcanic eruptions.

stones in museum shops. The color depends on the impurities and not much impurity is needed (it can easily be changed/dyed). We will discuss flint and opal separately, although they are closely related. Flint tools, like obsidian tools, were used thousands of years ago. Flint consists of fine-grain silica (the black color is caused by trapped carbon) and fractures like obsidian, producing sharp edges that are ideal for cutting.

Alabaster, gypsum ($\text{CaSO}_4 \cdot 2\text{H}_2\text{O}$), and Plaster of Paris ($2\text{CaSO}_4 \cdot \text{H}_2\text{O}$) are all calcium sulfate (the last of these has been treated to produce the hemihydrate). Fine-grain gypsum is easily carved: fractures do not propagate far. Alabaster ornaments were made in Assyria (Iraq) before 2000 BCE and Plaster of Paris was used by the Egyptians in ~3000 BCE in making mortar.

36.2 WHAT IS A GEM?

Gems are often characterized as expensive sparkling stones. The value is not necessarily as obvious as we might hope. Even so, you will probably spend significant money on gems. A gem can be real (natural), synthetic (grown in the laboratory or factory), or a simulant (one material made to look like another).

Gems can provide a link between ceramics, geology, crystallography, mechanical testing, solid-state, physical, and inorganic chemistry, and electrical engineering. They provide the ceramist with many challenges, such as identify this ceramic (gem) without removing it from the gold band in which it is set. Table 36.1 lists some of the best-known gemstones with some of their special features.

One challenge is to identify a particular gemstone.

The scientist's way is to use X-ray diffraction (XRD), X-ray energy-dispersive spectrometry (XEDS), wavelength-dispersive spectroscopy (WDS), or comparable techniques for chemical analysis.

The gemologist's way is to use the refractive index or the thermal and/or electrical conductivity.

The difference, of course, is that the gemologist must often identify the gemstone in the field (in the home, in the mine, or really in the field) without taking the sample to the laboratory. With experience, you can, for example, "feel" if a stone is a good thermal conductor.

Some examples of questions you might be asked:

- Is this stone really diamond not cubic zirconia (CZ), white sapphire, or even moissanite?
- Why is the Black Prince's Ruby so dark? (It is in the English Crown Jewels and it is not a ruby.)
- Is this stone peridot or green glass? (If you cannot tell need you care?)
- Is this natural turquoise? (Probably, but the better question is: has it been treated?)

TABLE 36.1 Gemstones

Hard and resistant to chemicals	Chrysoberyl, BeAl_2O_4 Corundum, Al_2O_3 Quartz and chalcedony, SiO_2 Spinel, $\text{MgO} \cdot \text{Al}_2\text{O}_3$
Gem carbonates (not so hard)	Calcite, CaCO_3 Malachite, $\text{Cu}_2(\text{OH})_2\text{CO}_3$ Rhodochrosite, MnCO_3
Gem phosphates (not so hard)	Apatite, $\text{Ca}_5(\text{F}_2\text{Cl})(\text{PO}_4)_3$ Turquoise, a complex hydrated phosphate of copper and aluminum
Gem silicates (hard and durable)	Beryl, $\text{Be}_3\text{Al}_2(\text{SiO}_3)_6$ Feldspar group gems: aluminum silicates in combination with calcium, potassium, or sodium Garnet group gems: silicates of various combinations of magnesium, manganese, iron, calcium, aluminum, and chromium Jadeite, $\text{NaAl}(\text{SiO}_3)_2$ Nephrite, complex calcium, magnesium, or iron silicate Peridot, $(\text{Mg}, \text{Fe})_2\text{SiO}_4$ Rhodonsite, MnSiO_3 Topaz, $\text{Al}_2(\text{F}_2\text{OH})_2\text{SiO}_4$ Tourmaline, a complex borosilicate of aluminum and iron Zircon, ZrSiO_4

- Are there defects in my emerald? (Yes.)
- Is natural emerald better than synthetic emerald? (Synthetic emerald is usually more perfect.)
- Should I wash my opal with water or with alcohol? (No.)

The questions emphasize the need for techniques to aid the eye in examining these materials, or the need to understand the structure and chemistry of gemstones when handling them.

36.3 IN THE ROUGH

The traditional mining of gemstones is illustrated in Figure 36.1. Since many mines are in less developed countries and very small stones can be very valuable, the mining tends to rely on manual labor. Open mines like the one shown in Figure 36.1 are inexpensive to establish and in many cases have not changed in centuries. Miners then and now often have to endure brutal conditions. The following quotation, which is believed to be dated about 1830 BCE, describes the conditions suffered by Egyptian turquoise miners in the Sinai:

[The Pharaoh] dispatched the Seal-Bearer of the God, the Overseer of the Cabinet, and Director of *Lances*, Hor-ur-Re, to this mining area. This land was reached in the 3rd month of the second season [June, an almost unbearably hot season in Sinai],



(A)



(B)

FIGURE 36.1 Open cast mining in the Magok region of Myanmar (Burma).

although it was not at all the season for coming to the mining area. The Seal-Bearer of the God says to the officials who may come to this mining area at this season:

Let not your faces flag because of it. Behold ye, Hat-Hor [Egyptian goddess of the Sinai mines] turns it to good. I have seen (it so) with regard to myself. I came from Egypt with my face flagging. It was difficult, in my experience, to find the (proper) skin for it, when the land was burning hot, the highland was in summer, and the mountains branded an (already) blistered skin. When the day broke for my leading to the camp, I kept on addressing the craftsmen about it: "How fortunate is he who is in this mining area!" But they said: "Turquoise is always in the mountain, but it is the (proper) skin which has to be sought at this season. We used to hear the like, that ore is forthcoming at this season, but, really, it is the skin that is lacking for it in this difficult season of summer!"

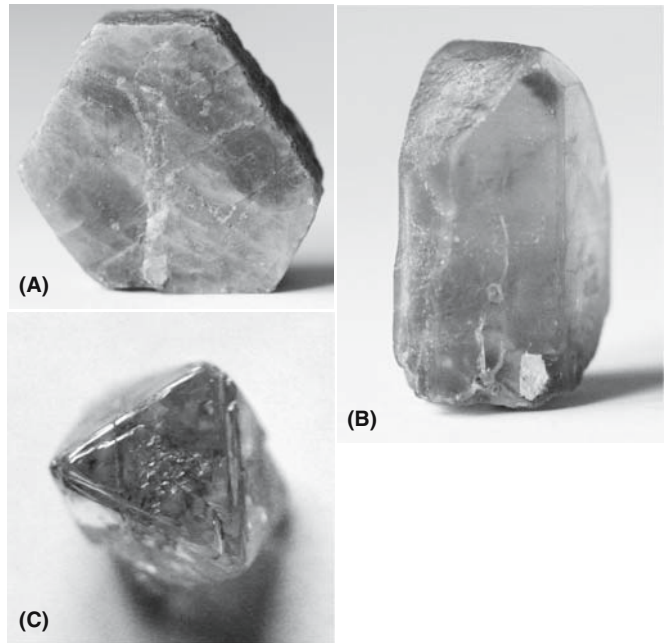


FIGURE 36.2 As-collected samples of rough (a) sapphire, (b) peridot, and (c) diamond.

Examples of gemstones *in the rough* are shown in Figure 36.2; many of these natural stones have shapes that are determined by their crystallography. Sources of sapphire, ruby, emerald, and diamond are given in Table 36.2. Sapphire tends to grow with a hexagonal shape as seen in these images; the best quality natural sapphire is shaped like a double hexagonal pyramid. Many of the harder gemstones (especially diamonds, sapphires, and garnets) are found in rivers where they have been deposited after removal from their native (natural) softer matrix.

Some specimens of natural gemstones are much larger than you might think. Just to remind you: amethyst *cathedrals* and *wheels* are the result of natural hydrothermal growth. The cathedrals can be >2m tall.

36.4 CUTTING AND POLISHING

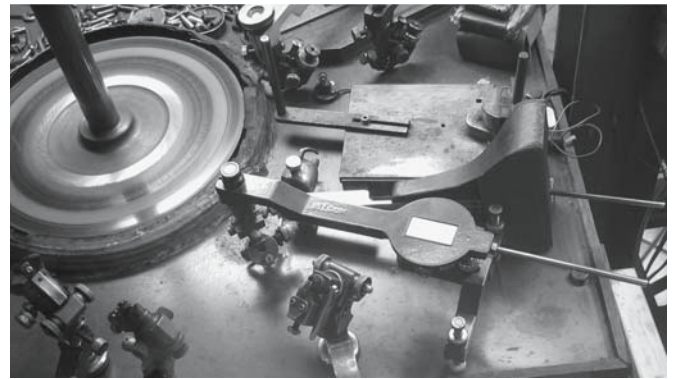
Agates started to be polished in Idar-Oberstein in the 1800s and the city is now a center for polishing gemstones. Antwerp and Amsterdam have been the centers for

TABLE 36.2 Gemstone Locations

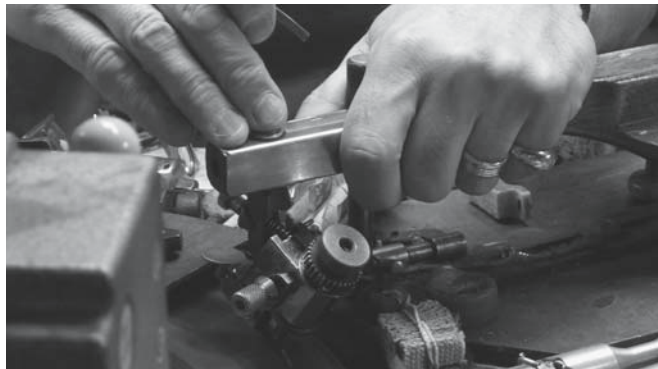
Ruby	Myanmar (formerly Burma)
Sapphire	India
Emerald	Colombia
	Madagascar
Diamonds	Russia
	South Africa (the Kimberley pipe)
Tanzanite	Tanzania
Amethyst	Brazil (Minas Gerais)



(A)



(C)



(B)



(D)

FIGURE 36.3 Equipment used for polishing gemstones.

diamond cutting for many years, although much of this trade is now carried out in Asia. The basic tools are the saw and the polishing wheel. The saw will be tipped with SiC, alumina, or diamond for precision work. Originally, the polishing pads used jeweler's rouge, but they now use various compounds including syton™, alumina, zirconia, and ceria. For most polishing, the process actually used has both a chemical and mechanical component and is thus known as chemical/mechanical polishing (CMP). The professional polisher uses a dop stick and wheel. In the diamond trade this has been partly automated using a tripod device [not unlike the tripod used for polishing transmission electron microscopy (TEM) samples] to replace, or to help steady the hand of the polisher; these are illustrated in Figure 36.3.

There are numerous books describing the shapes produced by polishers of gemstones. Figure 36.4 shows the main parts of a faceted stone to illustrate the terminology. For faceted stones the upper part is called the crown and consists of the table and the bezel. The girdle separates the crown from the pavilion, which is also called the base or the back. If a face is polished on the pavilion parallel to the table, it is called the culet. If you can see straight through the stone from the table through the culet, then the stone has a window. The shape of a brilliant-cut diamond is designed so that the light will all be reflected back to the source place directly in front of it—the

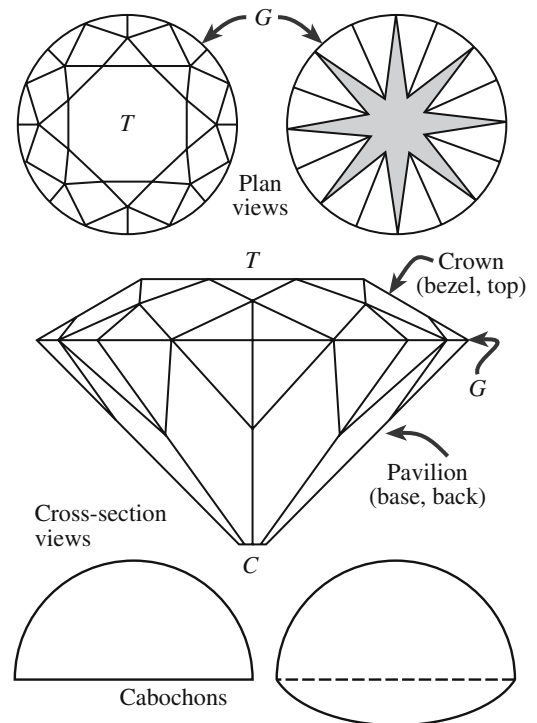


FIGURE 36.4 Different regions of polished (cut, faceted) stones and two cross sections of cabochons. T, table; C, culet; G, girdle.

pavilion facets act as mirrors. The term *en cabochon* refers to the shape (a cabochon—like a skull) shown in the lower part of Figure 36.4, which is essentially a non-faceted stone.

The {111} plane of diamond is the hardest plane to polish, which is why diamonds were initially left with {111} surfaces and just the tip polished off. Small naturally occurring octahedral crystals of diamond are quite common.

Carving minerals and gemstones is an old art. An example of a rock crystal bowl is shown in Figure 36.5. Old jade statues, fluorite bowls, and alabaster figures are museum pieces, but new ones are still being produced. The challenge in carving the harder minerals and gemstones is simply that they are hard and you reduce the weight of the stone as you carve it.



FIGURE 36.5 Examples of natural mineral specimens that have been shaped: (a) Buddha in garnet; 45 mm tall (b) rock-crystal bowl (~150 mm diameter).

36.5 LIGHT AND OPTICS IN GEMOLOGY

The gemologist judges diamonds by the four Cs: color, clarity, cut, and carat (weight). Here cut may actually mean cleave followed by polish. You would rather avoid cutting a stone since that wastes material. Remember, 1 carat is 0.2 g (about the weight of a carat—the small seed used in ancient Egypt as a unit of weight). Since diamonds can be expensive you may also encounter points (there are 100 points in 1 carat).

The following important optical properties contribute to the attractiveness associated with precious gems:

Color. Color is one of the main features we consider when choosing a gemstone. There are many different reasons for these colors: Cr makes emerald green and rubies red.

Refractive index. The higher the value of the refractive index (n or RI) of a properly cut gem, within limits, the more light will return to the eye of the viewer, resulting in brilliance, sometimes also termed life or liveliness. Diamond has a particularly high value of $n = 2.417$.

Dispersion. The dispersion is usually given as the difference in n for the b and g Fraunhofer solar spectrum lines. The Fraunhofer lines serve as reference markers across the spectrum. The b line is in the green part of the spectrum and the g line is in the violet part. The dispersion is 0.044 for diamond, one of the highest values for a natural gemstone. Dispersion causes rays of light to be split into their colored components that then emerge in slightly different directions to produce what the trade calls *fire*.

We discuss the causes of color in gemstones separately, but the point to remember here is that color is determined by the wavelength of the light, λ , and the n of a crystal depends on λ (dispersion). Table 36.3 gives examples of n of minerals and related materials, which are determined by measuring the critical angle on a hand-held refractometer (Figure 36.6) or a bench-top goniometer-style refractometer (Figure 36.7). Not all materials are transparent to visible light when they are too thick (i.e., we think of them as being opaque). Sphalerite, for example, is a gray crystal, but it is an orange gemstone with an n of 2.36.

Absorption. The other factor that is particular to different materials is the optical absorption. The absorption spectrum can easily distinguish different gems. Although laboratory instruments are best, gemologists can use a hand-held spectrometer. Hematite is gray unless the light passes through it, in which case it appears red (hence its name). A streak of hematite will appear red for the same reason; hematite with powder on the surface appears red. The reason for the red color is that hematite absorbs blue

TABLE 36.3 Refractive Index of Gemstones and Related Crystals

Al ₂ O ₃ , α-alumina	1.761, 1.769	KCl (sylvite)	1.49
AlSb	3.2, 3.2	MgAl ₂ O ₄	1.723
CaF ₂ (fluorite)	1.434	MgF ₂ (sellaite)	1.378, 1.39, 1.378
CaS (oldhamite)	2.137	MgO (periclase)	1.735
CdS, cubic	2.506, 2.529	Mn ₃ O ₄ (hausmannite)	2.15, 2.46
CdS, hexagonal (greenockide)	2.32	Mullite, 3Al ₂ O ₃ -2SiO ₂	1.64
CdTe, cubic	2.5	PbO (litharge)	2.535, 2.665
Cordierite	1.54	PbS (galena)	3.91
Diamond, natural	2.419	Sb ₂ O ₃ (senarmontite)	2.087
Fe ₂ O ₃ (hematite)	2.91, 3.19	Sb ₂ O ₃ (valentinite)	2.18, 2.35, 2.35
Fe ₂ O ₃ (maghemite)	2.63	SiC (moissanite)	2.648, 2.691
Fe ₃ O ₄ (magnetite)	2.42	SiC (wurtzite structure)	2.654
GaAs	3.309	Silica Aerogel 1	1.05
GaP	3.2	SiO ₂ (alpha quartz)	1.544, 1.553
GaSb	3.8	SiO ₂ (cristobalite)	1.484, 1.487
Ge mullite, 3Al ₂ O ₃ -2GeO ₂	1.664	SiO ₂ (tridymite)	1.475, 1.476, 1.479
Glass (fused quartz)	1.46	SnO ₂ (cassiterite)	2.006, 2.097
Glass 96% silica	1.458	ThO ₂ (thorianite)	2.2
Glass borosilicate	1.474	TiO ₂ (anatase)	2.488, 2.561
Glass Corning Pyrex® 7740	1.474	TiO ₂ (brookite)	2.583, 2.584, 2.7
Glass Corning Vycor® 7907	1.458	TiO ₂ (rutile)	2.9, 2.609
Glass GE 214 fused-quartz	1.4585	ZnO (zincite)	2.013, 2.029
HgO (montroydite)	2.37, 2.5, 2.65	ZnS (sphalerite)	2.356
Ice	1.31	ZnS (wurtzite)	2.356, 2.378
InAs	3.5	ZnSe	2.89
InP	3.1	ZnTe, cubic	3.56
InSb	3.96	ZrO ₂ (baddeleyite)	2.13, 2.19, 2.2

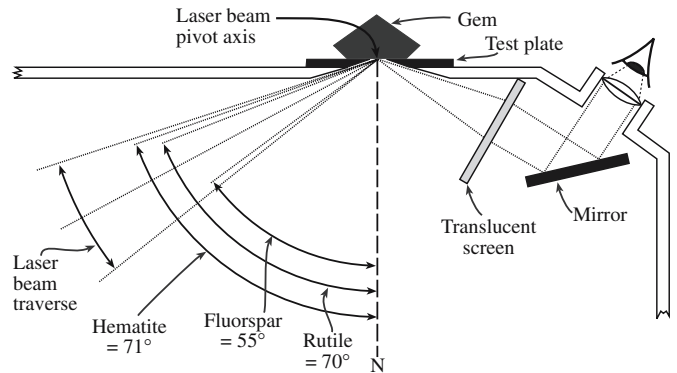
light. Two types of absorption spectrometer are used: one based on prisms and the other using a diffraction grating; both are shown in Figure 36.8. The wavelengths that are absorbed are well defined and are characteristic of both the doping (if it colors the stone) and the matrix itself as

illustrated in Figure 36.9, where you can clearly see stones with the same color clearly differentiated.

Facets. The faceted gemstone is ideally shaped to optimize its sparkle, which is simply saying we want to maximize the amount of light that is reflected back to the



(A)



(B)

FIGURE 36.6 (a) Portable jeweler's refractometer for measuring the critical angle; (b) the optics of determining the critical angle using the refractometer.



FIGURE 36.7 Goniometer-style refractometer.

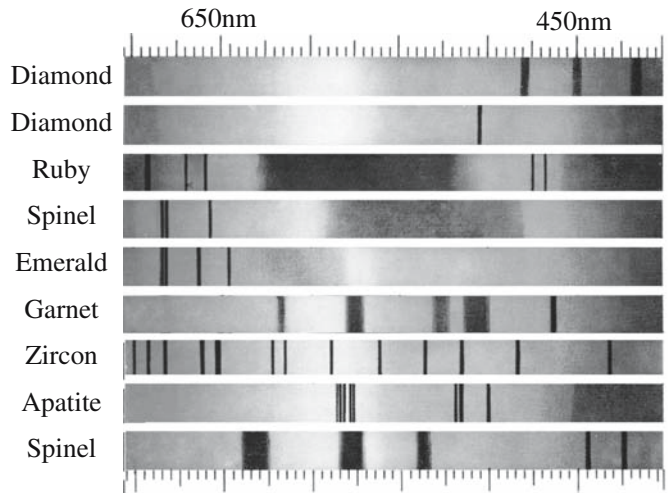
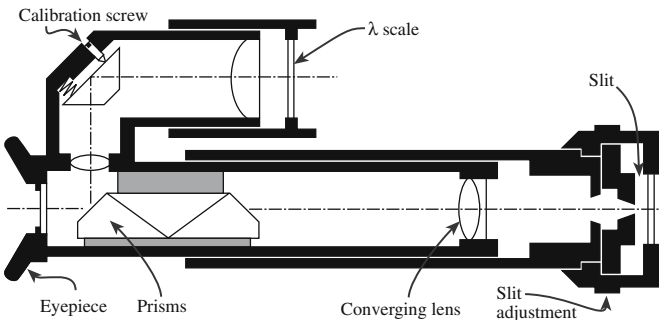


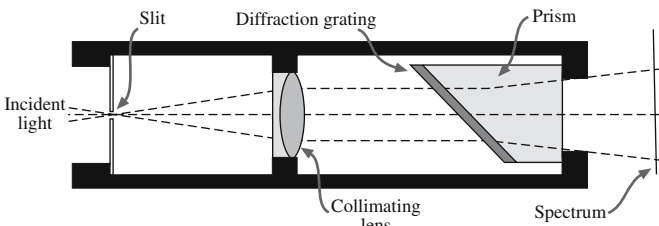
FIGURE 36.9 Spectra from different minerals.



(A)



(B)



(C)

FIGURE 36.8 (a) Photograph of a spectrometer. (b) The prism spectrometer and (c) the absorption spectrometer.

observer as shown schematically in Figure 36.10. The object of faceting then is to make the most of internal reflection. Note that the facets that you see on most gemstones are not crystallographic planes; the gemologist essentially never uses XRD to orient the sample!

Immersion. A simple method for estimating the refractive index is to use liquid immersion. The stone is immersed in a series of liquids of known refractive index (values of the n for different liquids are given in Table 36.4). The idea is that the gemstone will “disappear” when placed in a liquid that has the same n (Figure 36.11). The principle is that there is no longer a change in refractive index at the surface of the stone so that even if it is faceted, it will not reflect light internally. Of course, the technique is not good if the solvent can penetrate the stone or dissolve any filler.

Reflection. A more accurate method for determining the n of a gemstone is to measure the critical angle (the Brewster angle, θ_B) for reflection using a reflectometer. The principle is that the refractive index of a material is given by

$$n = (\sin \theta_I) / (\sin \theta_E) \quad (36.1)$$

Here the angle is defined as the angle to the normal ($\theta_I =$ incident angle; $\theta_E =$ exit angle). In the reflectometer, we place the gemstone in contact with the prism, the n of which is chosen to be large. We then adjust the incident angle until it is θ_B and deduce the n of the stone from Eq. 36.2:

$$n_{\text{gemstone}} = n_{\text{prism}} \times \sin \theta_B \quad (36.2)$$

Figure 36.6b illustrates the optics of the reflectometer.

Pleochroism. When n of a crystal varies with the direction in which light travels through it, the absorption can be different in different directions. The crystal then shows a different color when viewed in different direc-

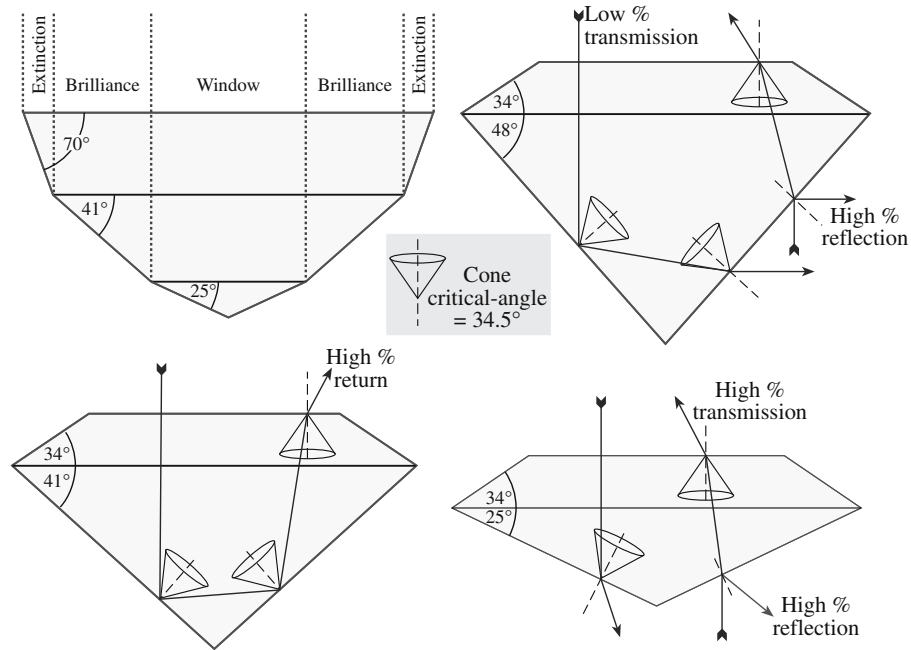
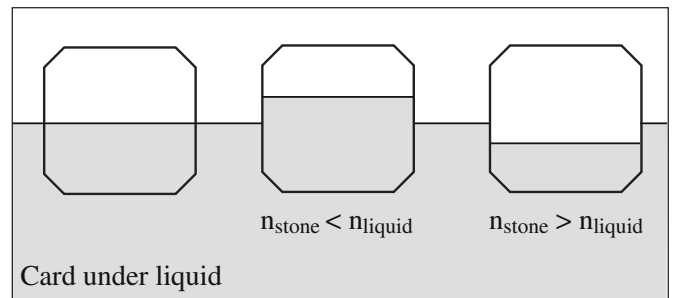
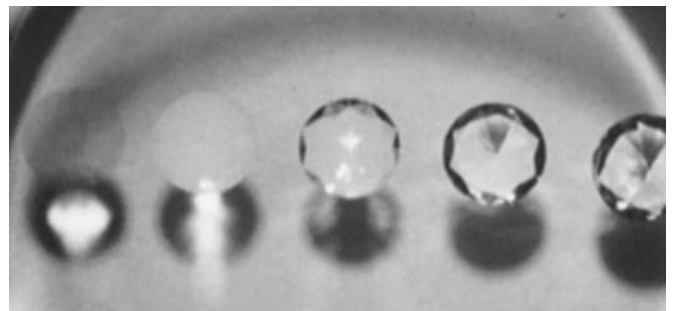


FIGURE 36.10 The origin of the sparkle in gemstones: total internal reflection (TIR).

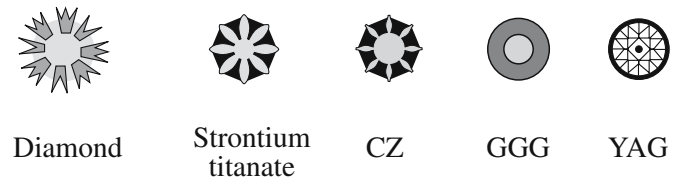
tions and this gives another method for identifying the crystal. If there are two distinct directions, the crystal is said to be dichroic (tetragonal, trigonal, and hexagonal crystals). Iolite (cordierite, $Mg_2Al_4Si_5O_{18}$) and tanzanite [the purple form of zoisite, $Ca_2Al_3(SiO_4)_3(OH)$] are two of the best-known examples. Crystals can show three colors: orthorhombic, monoclinic and triclinic crystals are trichroic. Pleochroic means either dichroic or trichroic. The dichroscope (Figure 36.12) is a simple hand-held device that is used to estimate the dichroism of a gemstone. It uses a crystal of calcite to separate the polarized rays and then compare them side by side to see how the color differs. Calcite has a strong double refraction. You have to rotate the stone since dichroism will not be present when viewing along the optic axis. In the laboratory you



(A)



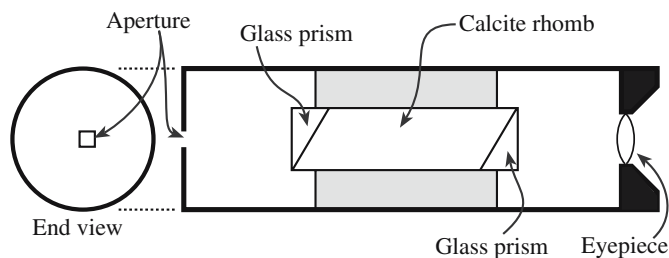
(B)



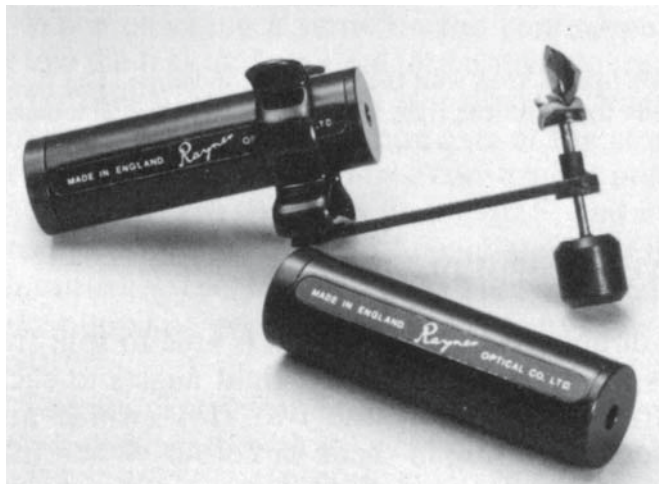
(C)

FIGURE 36.11 Determining the shadow patterns when stones are immersed in methyl iodide or liquid of other n . Different liquids are given in Table 36.4.

TABLE 36.4 Refractive Index of Liquids	
Liquid	n
Water	1.33
Ethyl alcohol	1.36
Acetone	1.36
Amyl alcohol	1.41
Glycerine	1.46
Olive oil	1.48
Toluene	1.49
Xylene	1.49
Benzol	1.50
Clove oil	1.53
Ethyl dibromide	1.54
Monobromobenzene	1.56
Bromoform	1.60
Monoiodobenzene	1.62
α -Monobromonaphthalene	1.66
Methylene iodide	1.74



(A)



(B)

FIGURE 36.12 A dichroscope for estimating the dichroism of a stone and the optics on which it is based.

might use the polarizing visible light microscope (VLM) instead of the hand-held device.

36.6 COLOR IN GEMS AND MINERALS

We will treat color separately for the different minerals and just add a few notes here; the importance of dopants is clear from Table 36.5. There are several different causes of color in gemstones. Most are associated with local trapped charges.

- Metal ions can give up an electron that may remain trapped locally; tsavorite is green because of the V^{3+} , but the same ion causes tanzanite to be purple.
- When we have two metal ions in different oxidation states, we can have intervalence charge transfer. The interplay between Fe^{2+} and Ti^{4+} causes the blue in blue sapphire and blue kyanite but also makes dravite brown; Mn^{2+} and Ti^{4+} combine to cause elbaite to be yellow.
- Instead of using a reactor or other source of radiation, natural ionizing radiation can excite electrons in the crystal. Fluorite can be red, green, or purple due to natural irradiation. The same irradiation can cause topaz to be brown (see below).

- The arrangement of defects (as in labradorite feldspar) or of grains (as in opal) can cause diffraction of the light.
- The mineral may be a semiconductor as in the case of sphalerite.

Blue. The common blue stones are sapphire, lapis, and irradiated topaz. Less common gemstones include blue diamond, although such stones could be common if irradiated more often.

Green. The green stones include emerald, malachite, and both uvarovite and tsavorite garnets.

Red. The red stones include ruby and both pyrope and almandite garnet (almandine).

Yellow. Yellow stones are less common but include citrine, yellow sapphire, and yellow diamond.

The color of ruby red and emerald green is the result of a transition metal in a ligand field (Section 32.5). In both cases the coloring ion is Cr^{3+} substituting for an Al^{3+} ion. Ruby is red corundum (Al_2O_3) containing about 1% Cr_2O_3 . The Cr^{3+} ion, which is only a little larger than Al^{3+} , is easily accommodated into the corundum structure. The five 3d orbitals in the Cr^{3+} ion split in the distorted octahedral ligand field. This is a slightly more complicated case than for the simple octahedral ligand field we described in Section 32.5 and involves further splitting of the 3d levels (see Figure 32.9). Nevertheless absorption of selected values of λ in the visible spectrum is due to electron transitions. Absorption is strongest in the green and violet and least in the red and blue regions; this gives ruby its red color with a slight purple overtone. In emerald

TABLE 36.5 Transition Element Dopants and Color

Titanium	Blue sapphire (with iron), blue zoisite (tanzanite)
Vanadium	Grossular garnet (tsavorite), green vanadium beryl, synthetic corundum (alexandrite simulant), some synthetic emeralds, blue/violet sapphire
Chromium	Ruby, emerald, ^a red spinel, pyrope garnet, chrome grossular garnet, demantoid garnet, uvarovite garnet, ^b chrome diopside, green jadeite, pink topaz, alexandrite, hiddenite
Manganese	Rhodochrosite, ^b rhodonite, ^b spessartite garnet, ^b rose quartz, morganite variety of beryl, andalusite
Iron	Sapphire, sinhalite, ^b peridot, ^b aquamarine, blue and green tourmaline, enstatite, amethyst, almandine garnet ^b
Cobalt	Synthetic blue and green spinel, synthetic blue quartz (except for a rare blue spinel, cobalt is not found in any natural transparent gemstone); cobalt glass
Nickel	Chrysoprase, synthetic green and yellow sapphires
Copper	Diopside, malachite, ^b turquoise, ^b synthetic green sapphire

^aIn UK and Europe only beryl colored by chromium may be described as emerald.

^bIdiochromatic gemstones.

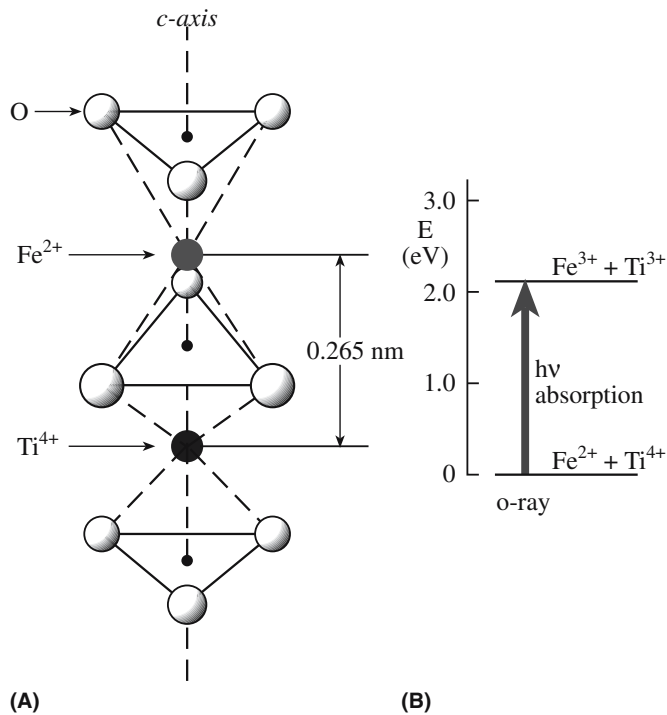
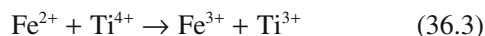


FIGURE 36.13 (a) Illustration of the combined effect of incorporation of Ti and Fe in sapphire. The distance between the dopant cations is 0.265 nm. (b) The corresponding energy band diagram for the excitation showing how a gemstone with blue coloration is obtained by absorption.

the color is again due to the Cr^{3+} ion replacing Al^{3+} in a distorted octahedral arrangement very similar to that in corundum. Emerald without the chromium impurity is beryl, which has the chemical formula $3\text{BeO} \cdot \text{Al}_2\text{O}_3 \cdot 6\text{SiO}_2$ or $\text{Be}_3\text{Al}_2\text{Si}_6\text{O}_{18}$. Because of the presence of the other constituents (it is a ring silicate) the overall bonding is a little weaker and the ligand field is less strong. As a result the splitting of the energy levels is different with strong absorption occurring in the yellow-red and violet and strong transmission in the blue-green regions.

For *sapphire blue*, the color results from a charge transfer mechanism. Sapphire shares the corundum structure with ruby, but the impurities are now small amounts of both iron and titanium oxides. Both Fe^{2+} and Ti^{4+} take the place of Al^{3+} in the corundum structure. If they are present on adjacent sites, as shown in Figure 36.13, then an interaction between them becomes possible. In this configuration there is enough overlap of the d_z^2 orbitals of the two ions that it is possible for an electron to transfer from the Fe^{2+} ion to the Ti^{4+} ion as follows:



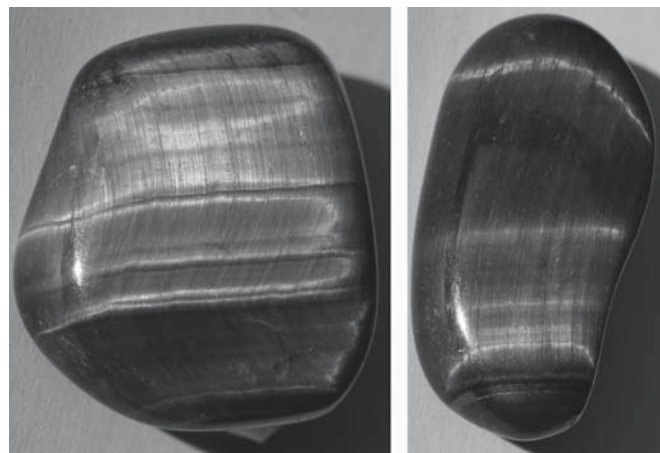
The energy of the combination on the right side of Eq. 36.3 is 2.11 eV higher than that on the left side, as shown in Figure 36.13. If light of this energy falls on blue sapphire, it is absorbed while producing the charge transfer

shown in Eq. 36.3. The blue color can be produced by doping with Ni or Co but the mechanism is different.

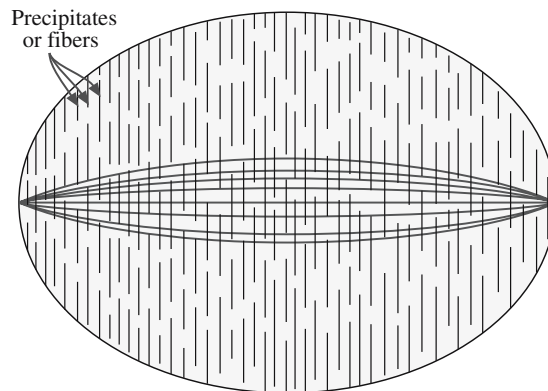
36.7 OPTICAL EFFECTS

Chatoyancy. The scattering of light by aligned fibers or channels within a matrix gives the optical effect seen in the minerals cat's eye and tiger-eye; the effect is termed chatoyancy. The crystals are cut *en cabochon* with the long axis parallel to the fibers, because you do not need the internal reflection from the surfaces. Tiger-eye (or tiger's eye) is quartz that contains oriented fibers of crocidolite; the mineral started as crocidolite (a form of asbestos) and was partly replaced by silica, which then becomes the matrix to the crocidolite fibers. This effect is shown together with others caused by interference in Figure 36.14.

Precious, or oriental, cat's eye is the rarest and most highly prized form of chrysoberyl; it is a green mineral called cymophane; the chatoyant effect is due to parallel arrays of pores.



(A)

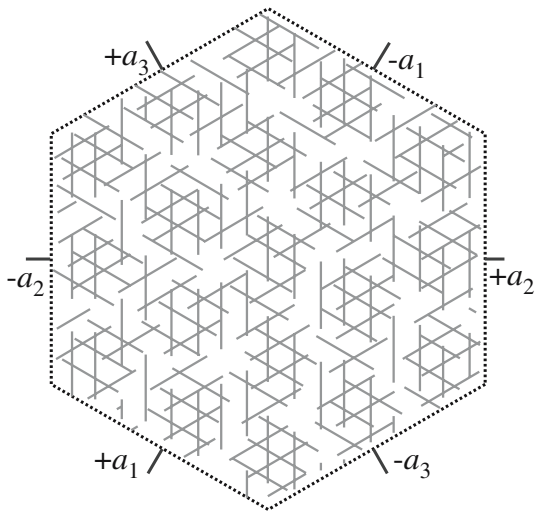


(B)

FIGURE 36.14 Chatoyancy: the scattering of light by aligned fibers or precipitates.



(A)



(B)

FIGURE 36.15 Asterism: the effect of precipitates oriented along several different directions giving rise to the star in star sapphire.

Asterism. This term refers to the star effect that can occur in sapphires, rubies, and garnets. The effect is illustrated for sapphire, where it is often the strongest, in Figure 36.15. In this case, aligned precipitates in the single crystal cause the optical effect. Since sapphire has a 3-fold axis, the precipitates reproduce this symmetry by aligning along particular directions giving the 6-fold star. In black sapphire, the needles are hematite; in essentially all other sapphires they are rutile. Some star sapphires from Thailand contain both hematite and rutile (sometimes called silk because they are so fine) and show 12-fold stars. In star garnets and diopside, the star shows 4-fold symmetry. In garnet the crystals lie at 90° along [001] directions; in diopside they lie at 73° to one another.

Iridescence. The best known form of iridescence is opalescence. The reason opals show different colors when viewed in different directions is that the silica spheres are

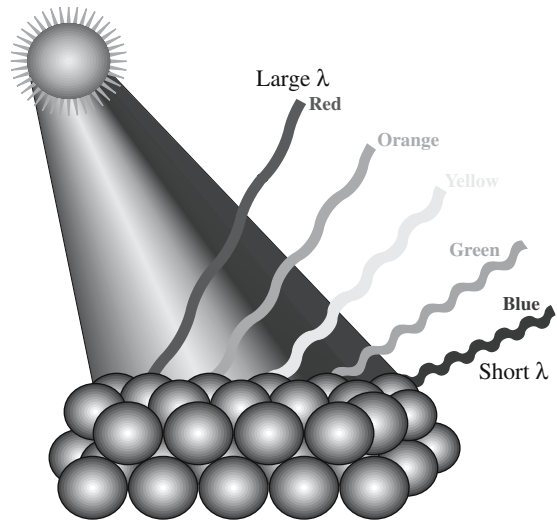


FIGURE 36.16 The origin of opalescence: Bragg scattering of light from a surface of ordered spheres. Best known in opals.

just the right dimensions to diffract light as illustrated in Figure 32.16.

Labradorescence and adularescence (shiller). These are two forms of iridescence caused by planar interference in a transparent mineral. Labradorite is a plagioclase feldspar named after the Labrador Peninsular in Canada; spectrolite is a special feldspar found in Finland. Labradorescence results from the presence of lamellar intergrowths inside the crystal; two phases of slightly different composition separated out as the mineral cooled. The interference occurs when light is reflected from the different interfaces. The color we see (illustrated in Figure 36.17) depends on the effective thickness of the layers and thus on the viewing angle. Moonstone is transparent feldspar that shows this effect. The planar defects in these feldspars are actually lamellar twin boundaries arising from chemical twinning.



FIGURE 36.17 Labradorite causes an iridescence due to scattering by twin planes in the feldspar crystal.

TABLE 36.6 The Classical Mohs' Hardness Scale for Gems

Mohs number	Abs number	Classic mineral	Other materials
1	1	Talc	Pencil lead (graphite)
2	3	Gypsum	Your fingernail (2.2)
3	9	Calcite	Chalk (3), gold (2.5–3.0), dolomite (3.5–4.0), ZnS (3)
4	21	Fluorite	Copper penny (3.2)
5	48	Apatite	Knife blade (5.0), window glass (5.5), strontium titanate (5.5), sodalite (5.5–6.0), hematite (5.5–6.5)
6	72	Orthoclase	Steel file, other feldspars, pumice (6), pyrite (6.5), magnetite (6), porcelain (6–7), anatase (5.5–6)
7	100	Quartz	Streak plate (7.0), zircon (6.5–7.5), olivine (6.5), garnet (6.5–7.5), rutile (6.5)
8	200	Topaz	Spinel (8), YAG (8), ZrO ₂ (8), chrysoberyl (8.5)
9	400	Sapphire	WC (9)
10	1600	Diamond	Scratches everything! B ₄ C ₃ (9–10), SiC (9–10)

36.8 IDENTIFYING MINERALS AND GEMS

Since many gemstones appear quite similar, which is why they can be simulated, it is important to be able to distinguish the real from the synthetic or from the simulant. If you have a scanning electron microscope (SEM) with XEDS available, the latter task is not a problem, but this is usually not the case in the field (or the shop). The basic tests are thermal conductivity, optical properties, and mechanical properties. Using a mechanical test to characterize a material that you do not want to damage is clearly tricky, so the use of hardness measurements is directed more toward minerals than gemstones.

Hardness (Toughness)

Indentation has been discussed in Section 16.3. Although these tests could be used for gemstones, they are not, except as a calibration. The Mohs scratch hardness scale is much more popular since the principle is to test what the stone will scratch, not what will scratch the stone.

The Mohs' hardness test (the word scratch is assumed) is almost a nondestructive test. The hardness of a gemstone is usually referred to as its Mohs' hardness. Since this *hardness* value is determined by a scratch test, it is not actually a *hardness*. The scale has many drawbacks including the fact that it is not linear, it does not necessarily relate to wear resistance, and it damages the specimen so it is not ideal for polished stones.

Table 36.6 gives Mohs' hardness values for the *Gem Scale* and for some other materials as a comparison. (Note that in Chapter 16 we consider the extended version as defined by Ridgeway, but it is not nearly so widely used in the Gem industry.) Table 36.6 also includes a "relative" hardness scale. Remember that minerals are anisotropic, so the Mohs' hardness of kyanite is ~4.5 when scratched parallel to the long axis and ~6.5 when scratched perpendicular to the long axis. Incidentally, this material will not be confused with kaolinite using this test since the latter has a Mohs' hardness of 2–2.5.

An additional problem in using mechanical tests for minerals is that many tend to cleave. Wear (or abrasion) might be a better test but it is more difficult for the gemologist.

Thermal Conductivity

The thermal conductivity of gemstones provides a useful way of identifying the mineral in the field. Table 36.7 lists values used for gemstones. The common assumption is that gemstones are poor conductors of heat. Diamond is actually a much better thermal conductor than Cu. The measurement of thermal conduction of gemstones is particularly attractive as a test because it can be applied to stones that are already mounted, e.g., in a ring. The instrument supplies the heat, and the sink is either the ring or another part of the device. The device shown in Figure 36.18 measures the change in temperature of the tip when it is placed in contact with the gemstone. When testing the poorer thermal conductors, the temperature of the tip is allowed to fall until it reaches a first set value

TABLE 36.7 Thermal Conductivity

Mineral	Thermal conductivity ($Wm^{-1} \text{ } ^\circ C^{-1}$)
Diamond	1000–2600
Synthetic moissanite	200–500
Silver	430
Copper	390
Gold	320
Platinum	70
Corundum	40 ^a
Zircon (high)	30 ^a
YAG	15
GGG	8
Rutile	8 ^a
Quartz	8 ^a
CZ	5
Glass	1

^aMean value between *c* axis and *z* axis directions.



FIGURE 36.18 Pocket-sized instrument for measuring thermal conductivity.

when the subsequent decrease to the next set value is timed; it is much like taking a blood pressure reading.

36.9 CHEMICAL STABILITY (DURABILITY)

Gemstones are usually thought of as being chemically stable. Some are; some are certainly not. Opal contains a significant amount of water; if this water is removed, then the opal will fracture and degrade. Emeralds are slightly different in that they usually already contain many fractures that have been filled with oil or polymer. If this filler is removed, for example by cleaning with a solvent, the fracture may extend. Even though the diamond in an engagement ring is durable, the 18k gold setting holding it in place may not be, especially if it is exposed to chlorine-containing liquids such as in a swimming pool and hot tub.

36.10 DIAMONDS, SAPPHIRES, RUBIES, AND EMERALDS

Why diamond? Yes, it is hard, but it is its optical qualities (and great advertising) that have made it so popular. The refractive index of diamond is 2.42 while rutile (once proposed as a diamond simulant) and moissanite (now being used as such) have refractive indices of 2.6/2.9 and 2.65/2.69, respectively; so it does not have the best optical properties (for internal reflection).

Diamonds can now be synthesized to weigh more than 0.6 g [3 carats (ct)]. This is an art: for the color and clarity. The production of gem quality synthetic diamonds (Section 29.14) results in a deep yellow color. Colored diamonds tend to be more valuable than colorless ones simply because they are more rare. The Dresden Green diamond weighs 40.70 ct and is the largest known green diamond in the world. Natural red, pink, and yellow diamonds can also command prices of near \$1M per ct. The danger is that diamonds can also be artificially colored by irradiating them; diamond was perhaps the first irradiated gem. Blue B-doped diamond is a semiconductor while blue

irradiated diamond is still an insulator. A concentration of 10^{-6} B in diamond gives it a deep blue color as seen in the Hope diamond. A B-doped diamond fluoresces under UV and continues to glow for minutes afterward.

Diamonds are actually mined in large quantities in South Africa and Russia with newer sources in Sierra Leone and northeast of Yellowknife in Canada's Northwest Territories. Natural diamonds are created 150 km beneath the earth's surface and are transported to the

surface by volcanic activity. The Kimberley Pipe is the remains of such volcanic activity. A pipe is a carrot-shaped volcanic neck; there is a cluster of 11 pipes at Kimberley—they are about 1.2 billion years old. The largest kimberlite pipe is now the

Premier Mine at Cullinan, which produces 1.6 million ct annually. The original location of kimberlite is now known as Kimberley's "Big Hole."

Nitrogen causes both synthetic and natural (like the Tiffany Yellow) diamonds to be yellow. A Florida company has up to 200 diamond-making growth chambers, each weighing about 4000 lb (cost ~\$50,000 each). Each chamber can produce eight 3-ct rough stones per month. A little history: a team of five Russian scientists in Novosibirsk, Siberia, managed to create gem-quality diamonds at the relatively low pressure of 60,000 atmospheres in 1989; this avoids the high pressure of the so-called GE process used to make industrial diamond. Carter Clarke, an American entrepreneur, paid \$57,000 in 1996 for a "diamond-growth chamber" during a business trip to Russia; the chamber was the size of a washing machine. He then founded Gemesis.

For some time, mixtures of H_2 and natural gas have been used for chemical vapor deposition (CVD) growth of diamond-like carbon (DLC) films. It is now possible to use this technique to grow diamond seed crystals to produce clear, perfect colorless diamonds. Diamonds grown by the high-pressure methods are invariably doped and thus colored. One company, Apollo, has used the CVD technique to grow 1-ct diamonds.

Examples of famous diamonds are listed in Table 36.8. One obvious feature is that these gemstone were all cut from much larger rough stones. When first extracted from the Premier mine near Pretoria, the *Cullinan* diamond weighed 0.621 kg. It was later cut into nine major gemstones (the largest two being in the list and shown in Figure 36.19) and 96 other stones. The *Hope* diamond, thought to be from the Kollur mine in Golconda, India, was first cut into a triangular $112\frac{3}{16}$ -ct stone. In 1673, it was recut to give a $67\frac{1}{8}$ -ct stone and then presumably cut again to give the current 45.52 ct stone. We say "presumably" because the diamond disappeared for 20 years following looting after the French Revolution in 1792 (the current Hope diamond

DIAMOND MINE
Production began in 2003 in Lac de Gras 300 km north-east of Yellowknife; it may be the richest diamond lode in the world. It has estimated reserves of 30 million tons and yields over 3 ct per metric ton of ore (more than three times the world average). In 2005, 8 million ct were extracted valued at over US\$400 million.

TABLE 36.8 Famous Diamonds

Name	Weight	Notes
Hope	45.52 ct	Blue due to B doping L = 25.60 mm, W = 21.78 mm, D = 12.00 mm In the Smithsonian
Koh-I-Noor (Mountain of Light)	105.60 ct	Originally 186 ct In the Tower of London
Cullinan I (Great Star of Africa)	530.20 ct	Original rough Cullinan diamonds 3106 ct In the Tower of London (10 cm by 6 cm by 5 cm)
Cullinan II (Lesser Star of Africa)	317.40 ct	In the British Imperial crown In the Tower of London
The Regent	140.50 ct	In the Louvre
The Centenary	273.85 ct	Found in 1986 (de Beers Centenary) Rough weight 599 ct In the Tower of London
The Tiffany Yellow	128.51 ct	Found in De Beers mine, Kimberly 1887 Rough weight 287.42 ct Still at Tiffany's New York

could indeed fit inside the old Hope diamond). The *Presidente Vargas* was found in the Rio Santo Antonio in Minas Gerais and weighed 726.6 metric ct (56.2 by 51.0 by 24.4 mm) but was cut into 29 separate stones.

Figure 36.20 shows the different facets produced on natural diamonds; all these shapes just involve {001} and {111} surfaces. Modern diamond faceting does not need to take account of the crystallography because, as a face-centered cubic (fcc) crystal, diamond is structurally quite isotropic.

Sapphire and Ruby

These gemstones are both mainly Al_2O_3 . If the stone is red it is called ruby; if it is any other color it is called

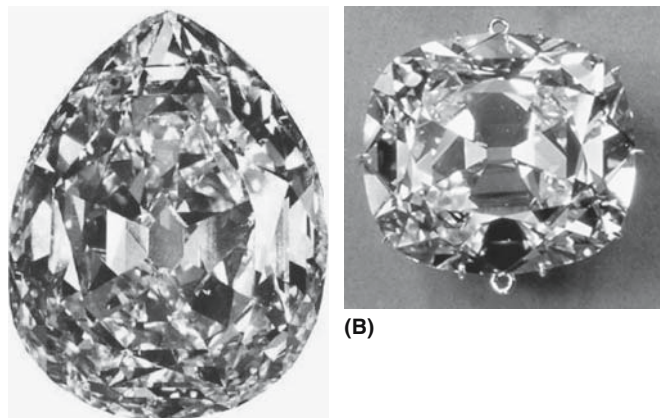


FIGURE 36.19 Two examples of blue diamonds: both were cut from the same Cullinan rough diamond.

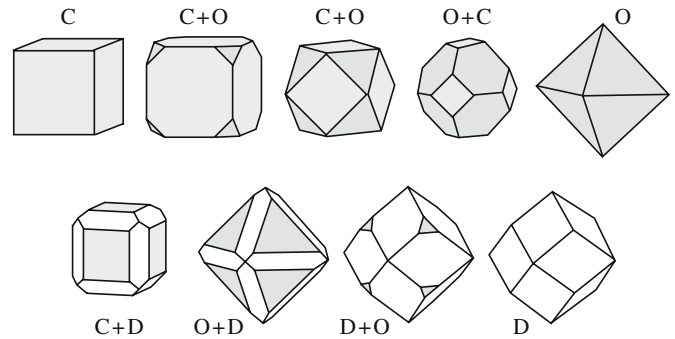


FIGURE 36.20 Different diamond shapes produced by diamonds faceting on three different crystallographic planes while keeping the same symmetry.

sapphire or fancy sapphire. There are many ways to produce the color as summarized in Section 36.6. Ruby is Cr doped while the blue gemstones contain the Fe–Ti complex (see Section 36.7).

Sapphires can be colored by diffusing in dopants. Co gives blue and Be gives yellow. Doping with Be is quite new; the Be diffuses much more quickly than Co and can penetrate the whole crystal so there are no tell-tale effects at the facets. The process involves surrounding the sapphire with chrysoberyl (BeAl_2O_3) powder and heating to $\sim 1300^\circ\text{C}$.

Emerald and Beryls

The mineral is generally referred to as beryl and is found in several forms as summarized in Tables 36.9. Commercially, the mineral beryl is the principal source of Be. Beryl occurs in three forms: emerald, aquamarine, and precious beryl (everything else); this is somewhat analogous to the naming of sapphires. Some precious beryls do have their own names in the gem trade. In the field, gemologists use the Chelsea filter specifically to identify emeralds. The Chelsea filter is a dyed gelatin film designed to transmit the red but absorb the green; through it emeralds appear red. The filter became less useful when synthetic emeralds became common.

The formula is $\text{Be}_3\text{Al}_2\text{Si}_6\text{O}_{18}$ (with up to 1 H_2O); it has $n = 1.595$. The crystal structure is hexagonal and is composed of 6-fold rings of SiO_4 tetrahedra, which make up the Si_6O_{18} unit. It cleaves along both $\{10\bar{1}0\}$ and (0001) faces; fractures on these planes do not need to break Si–O

TABLE 36.9 Beryl ($\text{Be}_3\text{Al}_2\text{Si}_6\text{O}_{18}$)

Name	Color	Dopant
Beryl	Blue	Cr
Emerald	Green	Cr or V
Aquamarine	Blue/light green	Fe
Morganite (rose beryl)	Pink	Mn (also in red beryl)
Heliodor	Gold-yellow	Fe
Goshenite	None	



FIGURE 36.21 An emerald cut in the classical style that minimizes the likelihood of fracture.

bonds. Actually, cleavage is so easy that essentially all natural emeralds contain fractures. The so-called emerald cut shown in Figure 36.21 has the corners removed; it was developed to minimize the likelihood of fracture (while maximizing the size of the stone).

Synthetic emerald can be grown by the flux method or hydrothermally (like synthetic quartz and natural emeralds) as shown in Figure 29.15, and is much more perfect. The largest natural single crystal of gem-quality aquamarine was found in Minas Gerais and weighed 110.5 kg. In one form of aquamarine known as *Maxixe*, the blue is enhanced by irradiation, but the color is not permanent. The coloring of morganite can often be improved by heating the gem above 400°C. The same treatment can change green beryl into blue aquamarine. The likely effect is that the process reduces Fe^{3+} to Fe^{2+} . Not included in Table 36.9 are Co and Ni doping, which produce pink/violet and pale green, respectively.

36.11 OPAL

Natural opal was deposited in fissures in rocks or fossilized (silicified) wood from water-based solutions at relatively low temperatures as illustrated in Figure 36.22. *Precious opal* consists of perfect arrays of identical spheres of SiO_2 as shown in the SEM image in Figure 36.23. The spheres have a radius of ~300 nm so arrays of the spheres look like crystals (3D diffraction gratings) to incident visible light. Thus the light is diffracted (in the actual “reflection” Bragg geometry), which is why we see different colors when viewing the opal from different directions. The spheres can be amorphous or partially crystalline. Not all opal shows these colors since the term opal refers to any material made up of such SiO_2 spheres;



FIGURE 36.22 Natural opal in a vein.

other examples are common opal or fire opal. A key component of opal is the included water, which is typically present in 3–9 wt% but may be as much as 20 wt%. It is a little tricky to polish opal (a fine example is shown in Figure 36.24), partly because you must not remove the water and partly because it is quite soft. Opal thus has much in common with chalcedony, another form of fine-grain quartz.

Opals are synthesized commercially by allowing monosized SiO_2 spheres to slowly settle from a dispersion in the lab. Since the structure is quite open, it is easy to diffuse a dye into the matrix to change the overall color. We can produce inverse opals in a similar way using latex spheres instead of SiO_2 and then various sols such as TiO_2 instead of the dye. When the impregnated polymer is burned out, the inverse opal has potential as a photonic

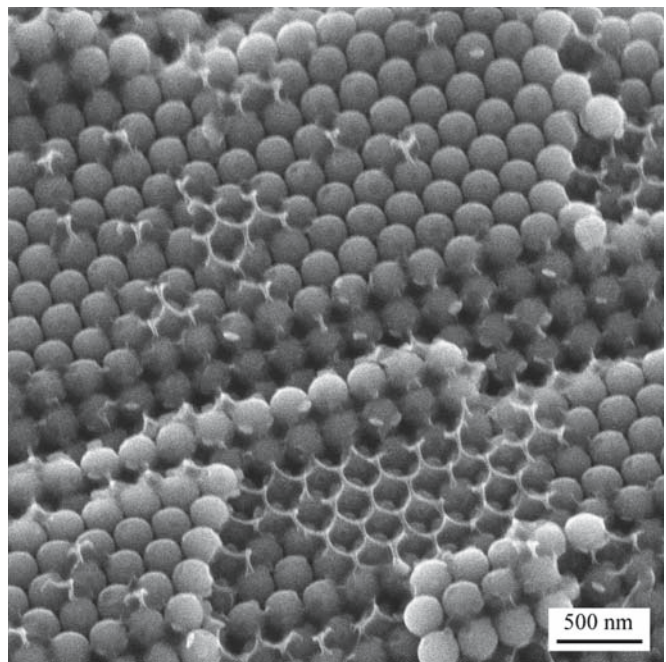


FIGURE 36.23 SEM image of a Gilson opal.

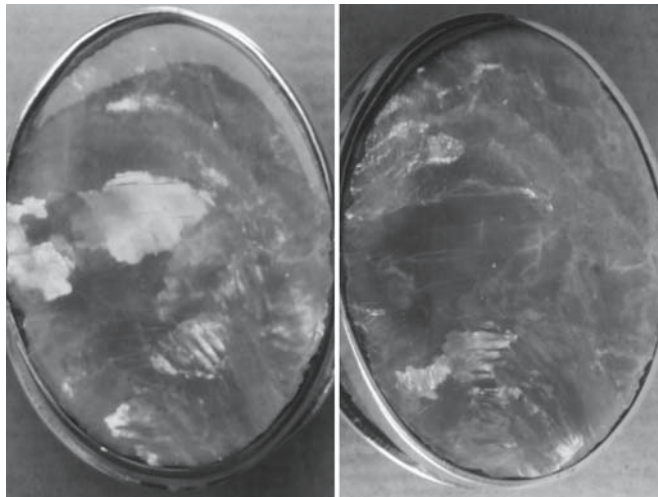


FIGURE 36.24 Polished precious opal.

band-gap material. The last point reminds us that opal was the first photonic material; we are now exploring how we can exploit this natural phenomenon using synthetic materials.

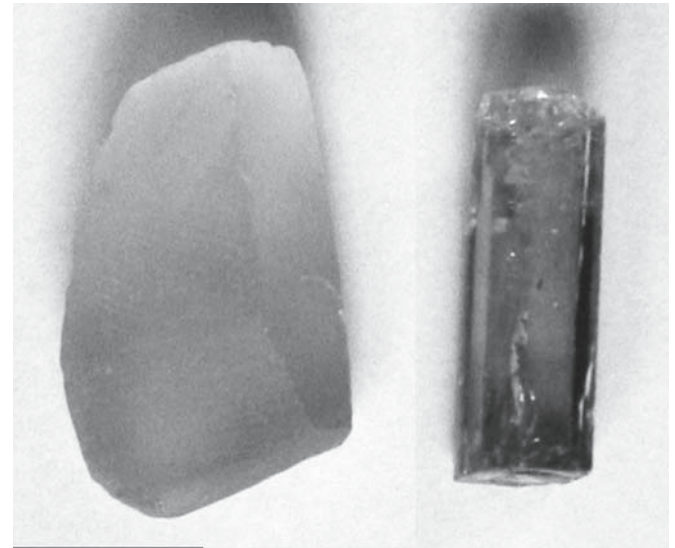
36.12 OTHER GEMS

Quartz crystals are known by several different names. The colorless form is known as rock crystal (see Figure 36.5). Amethyst is single-crystal quartz. The crystals grew naturally by a hydrothermal process and are found as cathedrals or wheels as shown in Figure 36.25. The purple color can be caused by Fe that is in the excited 4+ state due to natural (or artificial) irradiation or by Mn. The Fe concentration is probably in the range of 20–40 ppm. Smoky quartz is gray also due to irradiation, but the dopant is probably Al^{3+} . When heat treated, the stones become yellow-orange-brown and are known as citrine. Rhinestones were originally quartz pebbles collected from the River Rhine. The lesson is that each of these forms of quartz grew by natural hydrothermal processes and were then “treated” by nature (or humans).



FIGURE 36.25 Amethyst crystals from a section of a cathedral: The crystals were initially inside the geode.

Topaz is a silicate with the general formula of $Al_2SiO_4(F_2OH)_3$. It is the hardest silicate, testing at 8 on the Mohs scale. The crystal structure is unusual. It is orthorhombic consisting of chains of AO_6 octahedra linked together with SiO_4 tetrahedra. Cleavage is parallel to the basal plane since there are no Si–O bonds crossing this plane. It is found in a variety of shades of blue and the Imperial Yellow. Figure 36.26 shows several natural single crystals. Color is produced either by high-energy neutron irradiation in a nuclear reactor or in a gamma cell (in Brazil they use ^{60}Co to produce γ -rays) or with a linear accelerator (linac: producing a high-energy electron



(A) (B)



(C)
FIGURE 36.26 Topaz. Examples of irradiated rough, natural imperial topaz and a huge natural single crystal.

TABLE 36.10 Tourmalines

Species	X	Y ₃	Z ₆	T ₆ O ₁₈	V ₃	W	Color
Elbaite	Na	Li _{1.5} Al _{1.5}	Al ₆	Si ₆ O ₁₈	(OH) ₃	(OH)	
Dravite	Na	Mg ₃	Al ₆	Si ₆ O ₁₈	(OH) ₃	(OH)	
Chromdravite	Na	Mg ₃	Al ₆	Si ₆ O ₁₈	(OH) ₃	(OH)	
Schorl	Na	Fe(II) ₃	Al ₆	Si ₆ O ₁₈	(OH) ₃	(OH)	Black
Olenite	Na	Al ₃	Al ₆	Si ₆ O ₁₈	O ₃	F	
Buergerite	Na	Fe(III) ₃	Al ₆	Si ₆ O ₁₈	O ₃	F	
Uvite	Ca	Mg ₃	MgAl ₅	Si ₆ O ₁₈	O ₃	F	
Rossmannite	Ca	LiAl ₂	Al ₆	Si ₆ O ₁₈	(OH) ₃	(OH)	
Foitite	vac	Fe(II) ₂ Al	Al ₆	Si ₆ O ₁₈	(OH) ₃	(OH)	

beam). The stones may be radioactive for some time after processing (a few weeks for the Sky Blue produced by the linac and several months for the London Blue produced with neutrons). One story concerns a gem dealer who was surprised to find that the gems in his pocket were still hot. Gamma radiation can produce both yellow and blue color centers giving a brown color; the yellow can be annealed out by annealing at ~450°C leaving the blue, which lasts a lifetime (but may not be an heirloom).

Tourmaline is another mineral that can show many colors because it can contain different cations, some of which are listed in Table 36.10. This table is quite new and is still being developed. For example, the Y ion in dravite can be replaced by Mn(II) or V(II); Mn doping can be as high as 9 wt% and makes tourmaline pink. Some cations tend to share the Y site, compensating charge. Color variation is especially known for the variant watermelon tourmaline, which is naturally pink in the interior and green on the outside as illustrated in Figure 36.27. As always, we have to be careful since electron irradiation can change yellow-brown tourmaline into pink tourmaline. The terms red tourmaline and blue tourmaline have now replaced the names rubellite and indicolite since these are not distinct minerals. Natural crystals of schorl can be >15 cm long. Tourmaline is an unusual crystal in that it has true 3-fold

symmetry; the space group is *R3m* with *a* = 1.594 nm and *c* = 0.7138 nm, but the actual values of *a* and *c* depend on which cations are present. Commercially, this mineral is a principal source of boron. We mentioned the piezoelectric property earlier; it is strongest along the *c* axis, but quartz is now used more often except in special pressure sensor applications.

Spinel is less common gemstones, but sometimes they are quite famous, even if known by another name; the Black Prince's Ruby (5 cm long) and the Timur Ruby (polished but not faceted, 361 ct) in the English imperial state crown are both spinels. The largest known natural spinel crystal weighed 104 g (520 ct). Although the spinel structure can accommodate wide variations in chemistry, most spinel gemstones are actually naturally doped MgAl₂O₄. One variation is gahnite, the zinc aluminate spinel, ZnAl₂O₄. The best known spinel, magnetite (FeFe₂O₄), is not very attractive as a gemstone. Synthetic spinels can be doped in many colors and have the advantage over synthetic sapphire in that they are more nearly isotropic.

Garnet crystals are one of the older popular gemstones and a special class of mineral (much like spinel). The crystal structure is able to accommodate many different cations, which then produce different colors. All those shown in the box (on the next page) are natural silicates, although several synthetic garnets are now available; synthetic garnets produced for gemstones are usually doped YAG.



FIGURE 36.27 Watermelon tourmaline.

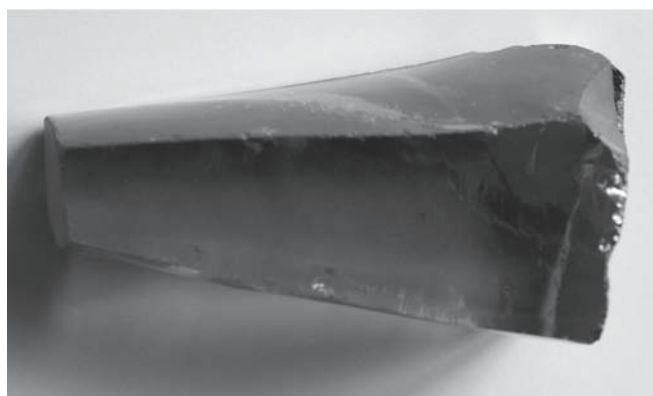


FIGURE 36.28 As grown crystal of RE-doped CZ.

All natural garnets have the general formula $R_3M_2(SiO_4)_3$, where R is Ca, Mg, Fe(II), or Mn and M is Al, Fe(III), or Cr. They form two groups:

- Pyrospites
- Ugrandites

Natural garnets are rarely pure. Natural almandines usually contain Ca, Mg, and Fe^{3+} , so these denote the end-member garnets. We then use whichever name most closely matches the composition we have. There is then a whole extra array of names. Rhodolite lies between pyrope and almandite; tsavorite is a green variation of grossular; demantoid, the most valuable garnet, and the black melanite are andradite garnets. Pyrope is also known as Bohemian garnet and was the favorite red stone in the 1700s and 1800s, but it can look very similar to almandite. Almandite is Dana's name for almandine, which is also known as precious garnet and was probably called alabandine (after the ancient Turkish city of Alabanda) by Pliny, so the two names are used interchangeably.

Cubic zirconia is a special case in that it is ubiquitous as a synthetic gemstone as shown in Figures 36.28 and 36.29. Naturally occurring zirconia is rare and then only as the monoclinic baddeleyite.

Peridot is better known as the mineral olivine. The gemstones usually have a composition close to $(Mg_{0.9}, Fe_{0.1})_2SiO_4$ and have a unique green color. It was mined for 3500 years on the island of Zabargad (St. John's

Island) in the Red Sea near Aswan, Egypt. The largest cut peridot (319 ct) was found on this island.

Alexandrite is a variety of chrysoberyl. It is special because absorption is so different in two directions. When viewed along the different crystallographic axes, its color changes from red to orange-yellow to emerald-green. In daylight the color is green; in artificial light it is red.

Tanzanite is a purple variety of zoisite. Most stones are green when mined and become purple when heat treated. The stone is particularly interesting (valuable) because it is found in only one place, it is quite hard (Mohs 6.5–7), it can be essentially perfect, and it is pleochroic.

SILICATE GARNETS

Pyrospites are named according to the dominant R cation present:

Mg^{2+} : Pyrope $[Mg_3Al_2(SiO_4)_3]$
 Fe^{2+} : Almandine $[Fe_3Al_2(SiO_4)_3]$
 Mn^{2+} : Spessartine $[Mn_3Al_2(SiO_4)_3]$

The M cation in these garnets is Al, usually with Fe^{3+} .

Ugrandites (calcic garnets with R = Ca) are named after the dominant M cation:

Cr^{3+} : Uvarovite $[Ca_3Cr_2(SiO_4)_3]$
 Al^{3+} : Grossular $[Ca_3Al_2(SiO_4)_3]$
 Fe^{3+} : Andradite $[Ca_3Fe_2(SiO_4)_3]$

36.13 MINERALS WITH INCLUSIONS

Inclusions in gemstones are quite common and are often used as an indication that the stone is *natural*. The best-known gems with inclusions are the star stones in which the stone can be sapphire, garnet, etc. Perfect star sapphires can now be synthesized.

Quartz crystals containing a hematite *seed* and the rutile needles are particularly interesting. You will also see hematite needles in quartz. When considering the origin of such structures you should know that the same arrangement of seed and needles occurs without the quartz matrix as shown in Figure 36.30. The name *cat's eye* originally referred to chrysoberyl, which contains inclusions, but the effect is seen in many other gemstones.



FIGURE 36.29 A single-crystal of RE-doped as-grown synthetic CZ. (Diameter = 2.5 cm).



FIGURE 36.30 Rutile growing in hematite. This combination often causes patterns in quartz crystals.

TABLE 36.11 “Treatment” of Gems, Its Effectiveness, and “Publicity”

<i>Treatment</i>	<i>Stable?</i>	<i>Detectable?</i>	<i>Disclosure?</i>
Aquamarine turned from green to blue by heat	Yes	No	No
Zircon heated to turn colorless or blue	Almost all	No, but these colors are very rare in nature	No
Sapphire or ruby heated to remove silk	Yes	Usually	Yes
Sapphire heated to modify or develop a blue color	Yes	Usually	Yes
Topaz turned blue by irradiation	Yes	No	Explained
Topaz or sapphire irradiated to a yellow or brown color	No	No, only fact of fading	Explained
Beryl irradiated: Maxixe-type blue color	No	Yes	Yes
Turquoise or opal impregnated with a colorless stabilizer	Usually	Usually	Yes
Emerald or ruby impregnated with a colorless substance	Variable	Yes	Yes
Beryl or emerald impregnated or coated with color	No	Yes	Yes
Sapphire impurity diffused to produce a surface color or surface asterism	Yes/No	Yes	Yes
Fracture-filled diamond	Yes/No	Yes	Yes

36.14 TREATMENT OF GEMS

Two methods that are widely used to enhance the color of gemstones are irradiation and heating, usually in that sequence. Table 36.11 summarizes some of the heat and irradiation treatments that have been used. The reason for treating (processing) gemstones is invariably to enhance their appearance and thus increase their value. We will review the general features of the different treatments and the science behind them, but refer discussion of the details to the sections on particular materials. All irradiated samples will be heated.

Heating sapphires: Overheating can cause good stones to become so dark that they are not transparent. Most citrine is produced by heating amethyst. This process can also occur naturally.

Irradiation: Topaz is sold as Swiss blue, London blue, etc. In all cases, the material has been irradiated and heated.

Composite stones can be constructed by joining different stones as illustrated in Figure 36.31. One of these methods is essentially equivalent to making a bicrystal with an amorphous (polymer) intergranular layer.

Filling cracks with oil, polymer, or glass is commonplace. The different procedures produce a similar result, the difference being mainly how long it takes until the result degrades. The extreme example of this is the transformation of turquoise chalk shown in Figure 36.32 to something that looks like the *real thing*. In 2004, some highly priced rubies were found to have had internal fractures filled with Pb-containing glass (chosen to match the *n*).

Lasers are used to drill channels into diamonds to remove internal blemishes,

afterward filling the hole with glass having a similar *n*. This is a variation on the technique used to create 3D images inside glass blocks for use as decorations. In either process, a pulsed laser is focused to a small area at the required location in the crystal and pulsed to create an internal fracture (in the glass model) or ablating material (in the gemstone). This process is illustrated in Figure 36.33.

How effective *diffusion* is depends on the rate of diffusion. If the intention is to improve the color of a gemstone, then the color must be uniform throughout the stone. Hence, after diffusion the stone should be equilibrated for a long period to remove the concentration gradient. This equilibration would take too long for the gem trade so the dopant will have a concentration profile peaking at the surface. Dopant is diffused into the cut stone because otherwise the surface region will have a different color when faceted. In the case of Co, which produces a blue color in sapphire, diffusion is slow so that the facets will have a different color from the bulk. The color difference will be particularly obvious at the facet junctions as shown in Figure 36.34.

36.15 THE MINERAL AND GEM TRADE

There are many interesting international aspects to the history of gems. Economies of countries have been based on gem production. Though not usually as bad as precious-metal mines, the effect of gem mines on the environment can be very negative. The Kimberley mine is always associated with “Big Hole,” which by 1914, when work on it stopped, was the largest man-created excavation in the world, having a depth of 215 m, a surface area of ~17 hectares, and a

BLOOD DIAMONDS IN POP CULTURE

Diamonds from Sierra Leone by Kanye West won a 2006 Grammy for Best Rap Song. *Blood Diamond* starring Leonardo DiCaprio and Jennifer Connelly was released by Warner Brothers in late 2006.

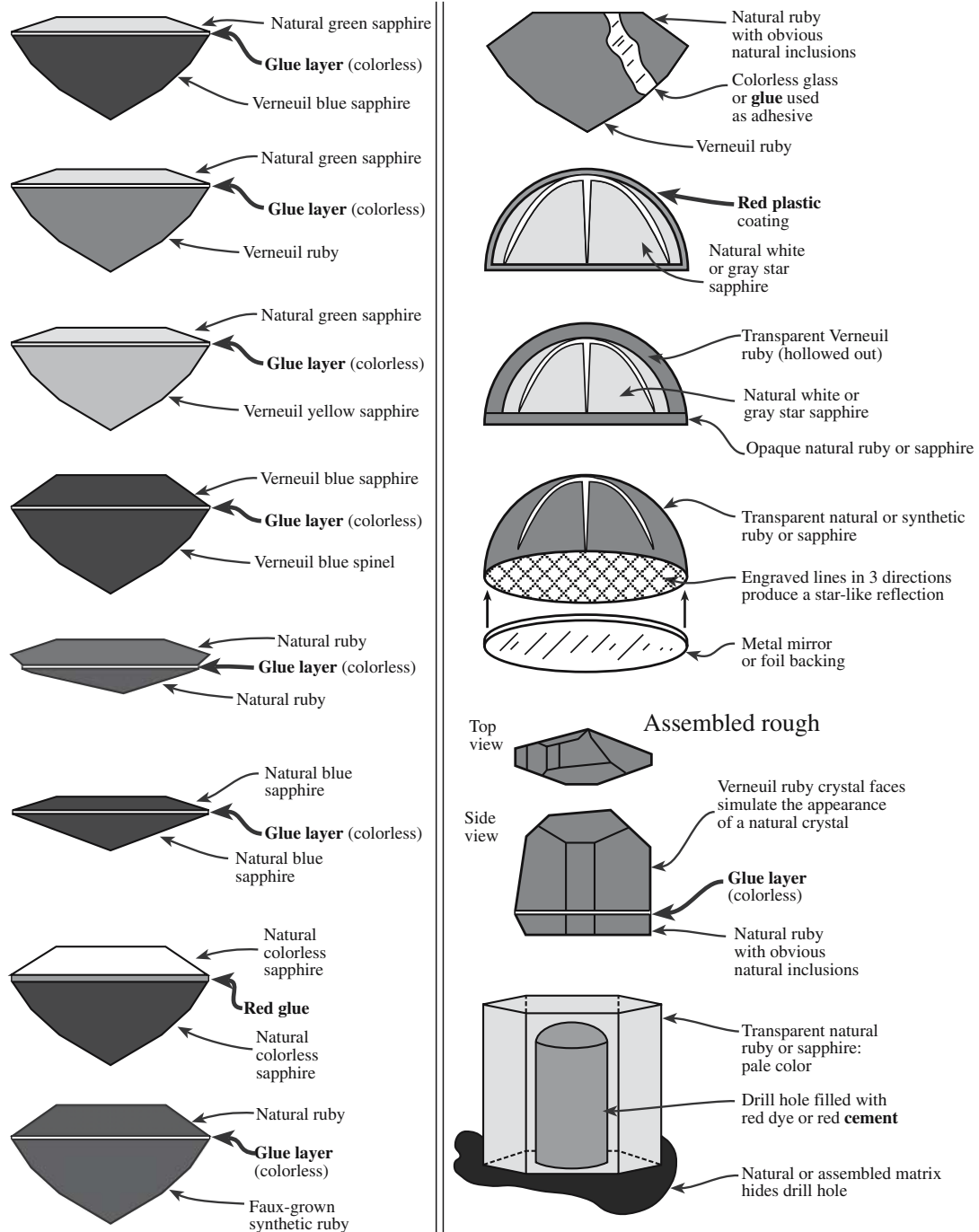


FIGURE 36.31 Different methods of simulating (faking) gemstones by forming composites (bicrystals, etc.).

perimeter of ~1.6km; 22.5 million tons of earth were excavated to produce 2722kg of diamonds. In the 1990s and later, the diamond trade in Sierra Leone became associated with raising funds to fund ongoing wars. The stones were referred to as “blood diamonds” and international organizations tried to minimize the trade in these stones. Now these diamonds account for 0.2% of diamonds sold, down from a peak of 4%.

It is often very difficult to reach the mines in Myanmar (Burma), but historically, Magok is the center of the ruby-

producing region. Many gemstones are exported through Thailand, which is a worldwide center for processing (cutting and polishing) gemstones.

In Brazil, the most important production area for gems and minerals is Minas Gerais. It is a more remote region of Brazil but with a growing industrial presence.

In India, the major source of talc is located in the Dagota district. The talc is prepared by crushing boulders that have been produced in the soapstone mines. Mining is threatening the existence of the Indian tiger (see Section 37.6).



(A)



(B)

FIGURE 36.32 Examples of turquoise before and after processing. Both samples are real turquoise. An old method of infiltration to modify the properties of a material is common for turquoise.

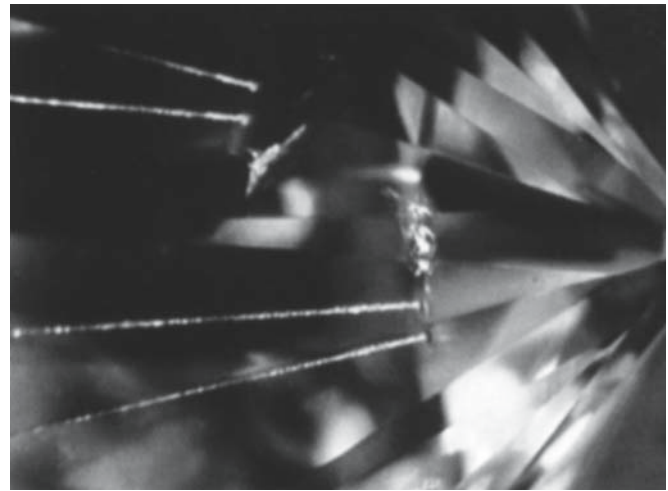


FIGURE 36.33 Laser etching to remove inclusions in a gemstone.

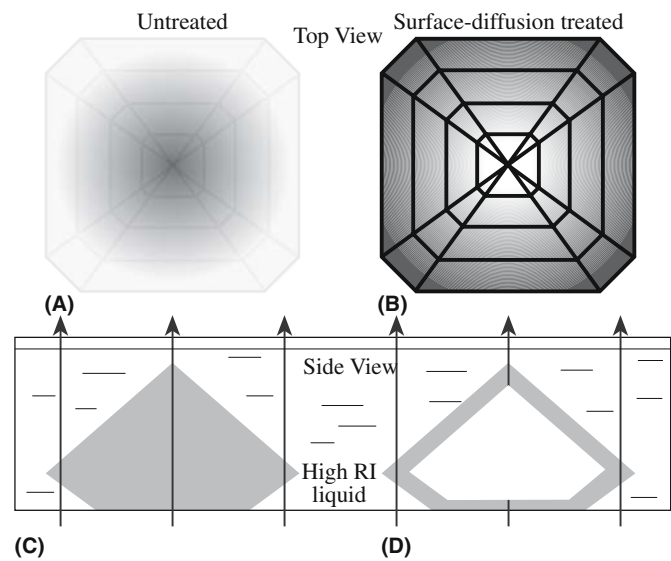


FIGURE 36.34 Diffusion to modify the color of a gemstone.

The history of De Beers and the diamond trade has been covered in several books, so we will not examine it here except to say that it makes for a fascinating story; it surprises some to hear that diamonds are not rare. One aspect of the diamond business is that the stones are very portable and can easily be made unrecognizable. The company De Beers is now based in Amsterdam and Antwerp. A new development is to use a laser to inscribe each diamond with a code number after it has been faceted (another “modification” using

lasers). The diamonds from Canada’s Northwest Territories have a laser-inscribed polar bear and are known as “Polar Bear Diamonds”.

There are, of course, many other uses of gemstones including jewel bearings for watches and other precision machinery, but here we have concentrated on their use in decoration and the science behind the preparation of the gemstone from the rough. There is also a worldwide trade in mineral specimens such as you will see in museums; these specimens can be priced in excess of \$100k.

CHAPTER SUMMARY

The topic of this chapter is unusual in a ceramics textbook. It is an example of real world ceramics where mineralogy, chemistry, physics, materials science, art, and commerce meet.

PEOPLE IN HISTORY

- Cullinan, Sir Thomas, owned the mine where, in 1905, the world's largest diamond was found.
- De Beer, Johannes Nicholas and Diederik Arnoldus, were brothers who owned the farm that became the Kimberley "Big Hole."
- Mohs, Fredrich (1773–1839) introduced the term scratch hardness in 1826. He was born in Gernrode/Harz Germany and studied at the University of Halle and at Freiberg; he later worked in Austria.
- Moissan, Ferdinand Frederic Henri (1852–1907) discovered naturally occurring SiC in 1905 in a meteorite from the Diablo Canyon in Arizona. He developed the electric furnace, which he used to make carbides and to prepare pure metals. He received the Nobel Prize in 1906 for successfully isolating fluorine (1886).
- Winston, Harry (1896–1978) was a key figure in the diamond trade. He opened his business in New York City in 1932 and in 1958 donated the *Hope* diamond to the Smithsonian.

GENERAL REFERENCES

- Hughes, R.W. (1997) *Ruby and Sapphire*, RWH Publishing, Boulder, CO. A great book by the sapphire guru; beautiful illustrations.
- Hurlbut, C.S. and Kammerling, R.C. (1991) *Gemmology*, 2nd edition, John Wiley, New York. The 1991 edition has trigons on the cover.
- Johnsen, O. (2002) *Photographic Guide to the Minerals of the World*, Oxford University Press, Oxford. Another excellent pocket guide.
- Nassau, K. (Ed.) (1998) *Color for Science, Art and Technology*, Elsevier, Amsterdam. A collection of articles describing the origins of color in gemstones.
- Nassau, K. (2001) *The Physics and Chemistry of Color*, 2nd edition, Wiley-Interscience, New York.
- Nassau, K. (1994) *Gemstone Enhancement*, 2nd edition, Butterworth-Heinemann, Oxford. *The book on the topic. Easy reading and fascinating details (see also his books on crystal growth).*
- Read, P.G. (1999) *Gemmology*, 2nd edition, Butterworth-Heinemann, Oxford. This is a classic manageable text at a similar level to this one on ceramics, though aimed at the practicing gemologist.
- Schumann, W. (2006) *Gemstones of the World*, 3rd edition, Sterling Publishing Co., New York. This is *the* pocket book.
- Smith, G.F.H. (1972) *Gemstones*, 14th edition, Chapman & Hall, London. Worth a trip to the library.
- Ward, F. (2003) *Rubies & Sapphires (also Emeralds, Opals, Pearls, Jade, Diamond)*, 4th edition, Gem Book Pub.

SPECIFIC REFERENCES

- Guinel, M.J.-F. and Norton, M.G. (2006) "The origin of asterism in almandine-pyrope garnets from Idaho," *J. Mater. Sci.* **41**, 719. Microscopy study showing origin of the "star" in star garnets and why both 4- and 6-ray stars are possible. Published in the 40th Anniversary issue of *Journal of Materials Science*.
- Muller, H. (1987) *Jet*, Butterworth-Heinemann, Oxford.
- Pritchard, J.B., Ed. (1955) *Ancient Near Eastern Texts Relating to the Old Testament*, Princeton University Press, Princeton, p. 229. Describes the conditions endured by miners during Egyptian times.
- Themelis, T. (1992) *The Heat-Treatment of Ruby and Sapphire*, Gemlab Inc USA.
- Yavuz, F., Gültekin, A.H., and Karakaya, M.Ç. (2002) "CLASTOUR: A computer program for the classification of the minerals of the tourmaline group," *Computers Geosci.* **28**, 1017.

WWW

- <http://atol.ucsd.edu/%7Epflatau/refrtab/index.htm>
- www.Krüss.com
- Makers of gemologist equipment.
- www.diavik.ca
- The Diavik diamond mine in Canada.
- www.debeersgroup.com
- Website for De Beers includes a history of the company.
- www.debeers.com
- Where to buy their diamonds.

WHERE TO SEE GEMSTONES

- Musée du Louvre, Paris.
- www.louvre.fr
- The Smithsonian Institution, Washington, D.C.
- www.minerals.si.edu
- The Tower of London.
- www.toweroflondontour.com/crnjewel.html

EXERCISES

- 36.1 What are the lines in Figure 36.9?
- 36.2 In Figure 36.11 the stones are immersed in a liquid. Why is this liquid chosen? Show that the observations are what you would expect.
- 36.3 What can you deduce regarding the size, shape, and alignment of the particles causing the stars in Figure 36.15?
- 36.4 Explain the phenomenon of labradorescence seen in Figure 36.17.
- 36.5 What is the common flaw found in natural emeralds? Explain your answer from a crystallographic point of view.
- 36.6 If you had a good means for measuring thermal conductivity, would you prefer such a test to Mohs' scratch test? How sensitive would your apparatus need to be? We can use a hand-held tester to distinguish diamond and moissanite. How is this fact connected to the electronics industry?
- 36.7 Why must you be particularly careful when polishing opal? How is opal related to today's electronics industry?
- 36.8 What do the stabilization of turquoise, the treatment of emerald, and ZnO varistors have in common?
- 36.9 Diamond has a high n and is also a very hard material. (a) Are these two features linked? (b) If so, explain why SrTiO₃ has a higher n but is not as hard.
- 36.10 Explain using your knowledge of ceramic processing how you might take turquoise powder and turn it into a gemstone.

Industry and the Environment

CHAPTER PREVIEW

Throughout this book we have highlighted the engineering applications for ceramics. In the final analysis the importance of any material is based on the applications for which it can be used. For example, at the present time high-temperature superconductors (HTSC) are of research interest but are not commercially so important. Because of the unparalleled range of properties shown by ceramics they find application in a vast number of areas. This last chapter looks at the field from an industrial perspective. Because it is impossible to cover every aspect of the multibillion-dollar ceramic industry in one chapter we have chosen to focus on a few topics, mainly through examining case studies. One of the exciting prospects for the industry over the next decade is in nanotechnology. Ceramic nanopowders already represent the largest segment of the nanopowders market and are used for polishing and sunscreens, etc. With the demonstration of the successful growth of ceramic nanowires, nanosprings, and nanotubes, the potential exists for even more applications in critical areas such as hydrogen storage. As we have often done we begin with some history.

37.1 THE BEGINNING OF THE MODERN CERAMICS INDUSTRY

In Chapter 2 we described some of the early history of ceramics and their production. The transition to a large-scale manufacturing industry occurred in Western Europe during the eighteenth century as part of the period that became known as the Industrial Revolution. The great porcelain factories established, and subsidized, by royal patronage at Meissen in Germany and Sèvres in France began to give way to purely commercial products being made in Staffordshire in the north of England. Later the factories at Meissen and Sèvres began to imitate English designs. They were certainly helped in this area by immigrant workers. Emigration was a concern for the ceramics industry more than many others, such as iron production, because it relied on secret processes, such as specific body and glaze compositions. Once these became known a worker would become valuable to a competitor.

The development of the Staffordshire area as the prominent pottery center in England was in large part due to the use of coal as a fuel for the kilns. Coal was abundant in this area as

was, and still is, a source of clay. The proximity of raw materials provided an economic advantage over other rural potteries that were still using a diminishing supply of timber. Staffordshire is a long way from the major metropolitan areas of London, Bristol, and Norwich. Early pictures of

SÈVRES

Royal Commission: The factory at Sèvres was commissioned to make an 800-piece dinner service for Catherine II of Russia. It took 3 years to complete.

Tunstall, one of the six towns that formed the Potteries and in 1910 became absorbed into the city of Stoke-on-Trent, show a town surrounded by hilly countryside. By the mid-eighteenth century there were many separate potteries employing a large number of workers. A petition presented before the British Parliament in 1763 read:

In Burslem [another of the six towns that made up the Potteries] and its neighborhoods (*sic*) are nearly 150 separate potteries for making various kinds of stone and earthenware, which, together, find constant employment and support for nearly 7,000 people.

In the early days of the pottery industry in England, transport of raw materials in and product out was inefficient. The costs of transportation had to be included in the selling price of every article produced. Clearly, quantity production could not be achieved without better transportation.

SIX TOWNS: THE POTTERIES

Tunstall, Burslem, Hanley, Stoke-upon-Trent, Fenton, and Longton

Master potter and entrepreneur Josiah Wedgwood was instrumental in organizing a potters' association to push for the development of improved roads and a canal system. Wedgwood realized that cheaper and more regular transport meant an even flow of production, fewer breakages, lower prices, wider markets, and greater sales. Staffordshire potters lobbied successfully for the development of a canal that would link the rivers Trent and Mersey, which was authorized by an Act of Parliament in May 1766. The project was completed in 1772 at a total cost of £300,000. The completion of the Trent-Mersey Canal ensured that Staffordshire would remain the center of English pottery production. A complex web of railway routes followed and these developments transformed an isolated rural area into a major industrial center.

Wedgwood made contributions in several areas that helped transform the production of pottery into a major industry. He changed the manufacturing process and adopted mechanization that would enable him to increase production while lowering prices; the increased productivity helped to maintain a stable wage for his employees. He had many ideas about sales and marketing of his products and was the first manufacturer to introduce the "satisfaction-guaranteed-or-your-money-back" policy, which is now an extensively used tool for selling.

Wedgwood was an advocate of free trade and a commercial treaty with France was welcomed by many of the ceramic manufacturers as a means of stimulating imports. Industries that had not adapted to new technology, such as the use of steam, feared the competition of imports. Wedgwood wrote on this issue of the treaty with France:

An exchange of the produce of one nation for the manufactures of another are happy circumstances, and bid fair to make the intercourse lasting; but sensible as I am to the interests of trade, manufacturers and commerce, they all give place to a consideration much superior in my mind to them all. I mean the probability that a friendly intercourse with so near and valuable a neighbour (*sic*), may keep us in peace with her—may help to do away with prejudices as foolish as they are deeply rooted, and may totally eradicate that most sottish and wicked idea of our being natural enemies

The production of ceramics became an important and growing export industry. Vast quantities of ceramic ware produced in the Potteries were exported from the major seaports of London, Bristol, Liverpool, and Hull to America, the West Indies, and all over Europe.

Today many of the most famous names associated with the Staffordshire Potteries are still thriving companies, such as Royal Doulton and Spode. A visit to any department store will demonstrate that these companies are still regarded as producing some of the highest quality ceramic

tableware. Wedgwood merged in 1986 with Waterford Crystal forming Waterford Wedgwood plc to become the world's largest tableware company with sales in excess of \$1 billion. As with other industries the ceramic industry has seen much consolidation and acquisition in recent years.

37.2 GROWTH AND GLOBALIZATION

CERAMIC IC PACKAGES

Together with substrates, ceramic packages compete with polymers but are superior in terms of thermal conductivity and hermeticity and are used in high-reliability applications.

Although the UK was a traditional leader in the development of ceramics, there were major changes during the latter half of the twentieth century when Japan became the major

producer of ceramics. Rapid transportation routes meant that manufacturing sites no longer needed to be near mineral resources. For example, Japan has no significant domestic energy supplies but is a major industrialized manufacturing nation. One of the significant changes that led to the growth and dominance of Japan was a shift in its business from traditional low value-added basic ceramics to one that has a large component of high value added. Table 37.1 shows the market for high technology ceramics as it was in 1980. Japanese companies satisfied about half of the \$4.25 billion demand. In some areas they were dominant, producing over 60% of the worldwide market for integrated circuit (IC) packages and almost 80% of the ferrites. The market for IC packages, which is based on alumina, was established largely by U.S. companies, but there are few remaining that sell on the open market.

The rapid growth in the Japanese production of ferrites in the 1970s and 1980s coincided with a decline in this area in the United States and in Europe. The only serious constraint on the expanded production of ferrites in Japan during this period was a shortage of raw material (secondary iron oxide) caused by weak steel production.

TABLE 37.1 The 1980 Market for High Technology Ceramics^a

Product	Japan	World
Ceramic powders	\$130	\$250
Electronic IC packages/substrates	540	880
Capacitors	325	750
Piezoelectrics	295	325
Thermistor/varistors	125	200
Ferrites	380	480
Gas/humidity sensors	5	45
Translucent ceramics	20	45
Cutting tools: carbide, cermet, coated noncarbide	120	1000
Structural ceramics (heat and wear resistant)	120	250
Totals	\$2065	\$4250

^aIn millions of dollars; excluding fibers, nuclear fuels, and spark plugs.

TABLE 37.2 Challenges Facing the Ceramic Industry According to Percentage of Survey Respondants

Environmental standards	39%
Changing markets	33%
Cost of labor	32%
Imports	27%
Health and safety standards	26%
Cost of materials	25%
Quality of labor	20%
Capital for expansion	20%
Quality control	19%
Cost of fuel	19%

Table 37.2 shows some of the challenges that face ceramics companies worldwide. This information was gathered from a survey of over 250 ceramics companies. The major challenges are meeting environmental standards, adapting to changing markets, and labor costs.

The ceramics industry, like many others, can establish production facilities in which labor costs are lower. For example, KEMET Corporation based in Greenville, SC, a manufacturer of tantalum electrolytic and multilayer ceramic chip capacitors, is relocating all manufacturing to lower-cost facilities in Mexico and China.

37.3 TYPES OF MARKET

As we described in Chapter 1, the ceramics industry is generally divided into six distinct markets:

- Glass
- Advanced ceramics
- Whiteware
- Porcelain enamel
- Refractories
- Structural clay

It is in advanced ceramics that many of the exciting developments are occurring. The average annual growth rate of the U. S. advanced ceramics market during the past 5 years was about 8% (now currently \$12 billion). The largest growth segments are electronic ceramics, which includes capacitors, piezoelectrics, and ferrites. In chemical processing and environmental-related applications ceramics are used for automotive catalyst supports and filters that are being increasingly employed to reduce pollutants in response to regulations on both automobile and industrial emissions.

37.4 CASE STUDIES

Again following Chapter 1, the ceramics industry covers a wide range of materials and products. We can generally divide the activities of this industry into three distinct

categories as listed, with examples, in Table 37.3. In this section we describe in more detail one example of each activity and some current industrial trends.

Silicon Nitride Powder

Silicon nitride, Si_3N_4 , is not a naturally occurring mineral. All the Si_3N_4 that we use must be synthesized, usually by one of the following methods (more details are given in Chapter 19):

- Direct nitridation of Si
- Carbothermal reduction of silica in N_2
- Vapor phase reaction of SiCl_4 or silane (SiH_4) with ammonia

The following characteristics of the resulting powder are important to end-users:

- *Particle size and distribution.* Powder compacts containing a few coarse particles produce components with significantly reduced strength and toughness (two of the properties we are often trying to maximize). Milling can be used to reduce particle size but often leads to significantly increased costs and the introduction of unwanted contamination.
- *Surface area.* This affects how easily the powder can be densified during sintering and the final grain size in the sintered component.
- *Purity.* Purity depends on the processing route and wide variations are possible. Oxygen on the surface of the powders can affect densification, however, we need enough to form the liquid phase during sintering.
- *Structure.* A high α - Si_3N_4 content is desirable because this favors the conversion to rodlike interlocking β - Si_3N_4 during subsequent processing into bulk components as illustrated in Figure 37.1.

The cost of Si_3N_4 powders can vary from \$30/kg up to \$150/kg depending on particle size and purity. The high costs of raw material and the subsequent shaping and

TABLE 37.3 Types of Ceramic Industry

Activity	Examples
Ceramic powders	SiC for abrasives Nanosized TiO_2 for sunscreen Bioactive glasses for bone reconstruction Bayer process Al_2O_3 for the production of Al using Hall-Héroult cells
Forming powders into bulk forms	Slip casting of toilet bowls CZ growth of Nd:YAG single crystals AlN sheets by tape casting Glass melting
Fabricating ceramic components	Ceramic chip capacitors Packages for integrated circuits SiC pressure sensors

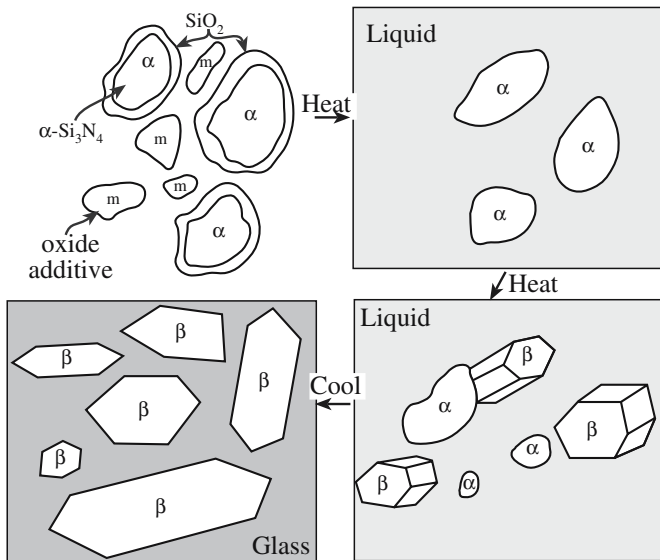


FIGURE 37.1 Schematic showing processing steps in forming Si_3N_4 by liquid phase sintering (LPS). The metal oxide additive (m) would be something like Y_2O_3 and the liquid an oxynitride/silicate.

TABLE 37.4 Summary of Costs for Direct-Nitrided Si_3N_4 Powder

Cost distribution	\$/kg	% of total
By cost element		
Silicon powder	7.49	25.4
Silicon nitride seed powder	1.71	5.8
Capital equipment	0.49	1.7
Direct labor	1.18	4.0
Energy	1.88	6.4
Process materials	16.74	56.8
Total	29.48	100.0
By process step		
Silicon powder	7.49	25.4
Silicon nitride seed powder	1.71	5.8
Direct nitriding	3.30	11.2
Crushing	6.62	29.3
Fine grinding	8.36	28.4
Total	29.48	100.0

forming processes have restricted the use of Si_3N_4 . Table 37.4 shows a summary of a cost analysis performed for direct-nitrided Si_3N_4 powder. Most of the cost of the powder is due to the raw materials and the process materials—namely the milling media. Si_3N_4 milling media is very expensive; it costs about \$150/kg, as compared with alumina or steel media at \$16/kg and \$4/kg, respectively.

Some of the present applications for Si_3N_4 parts

EIA CAPACITOR CODE

The size of MLCCs is “llww”: ll is the length of the capacitor and ww is the width, both in thousandths of an inch (a case where Imperial and U.S. units are still widely used in industry!) *Example*: 0805 means a capacitor of length 0.080 in. (~2 mm) and width 0.050 in. (~1.25 mm).

include cutting tool inserts, bearings and rollers, refractory parts, cam followers in engines blades, vanes in heat engines, and turbocharger rotors. The advantage of using Si_3N_4 for cutting tool inserts should be clear from Figure 37.2. The units are given as SFM, surface feet per minute, which is a measure of the distance covered by a rotating tool (traditionally a saw or lathe now used in wear); the surface foot is a linear foot (3.28 SF = 1 m).

There are several powder manufacturers, primarily in Germany and Japan, producing hundreds of tons of Si_3N_4 . There are currently no U.S. suppliers of Si_3N_4 powder. GTE, Dow Chemical, and Ford Motor Company developed high-quality Si_3N_4 powders between about 1973 and 1995, but none of these companies is a supplier today.

Ceramic Chip Capacitors

We described the structure of a multilayer chip capacitor (MLCC) in Chapter 31. They are used in a large number of products, in particular, personal computers and cell phones. A typical cell phone may contain 400 MLCCs. The goal is to make smaller components with larger capacitances at a lower cost.

Capacitors are extremely price competitive because of their relatively simple structure (see Figure 31.18). The following costs are involved:

- The ceramic dielectric. The ceramic capacitor industry uses more than 10,000 tons of BaTiO_3 -based dielectrics (about 90% of the total produced).
- The metal electrodes are usually precious metal based.
- Labor costs are particularly important in this industry because of the low value-added costs.

Figure 37.3 shows the trend in the size of MLCCs since 1981. The designations used follow the Electronic Industries Association (EIA) guidelines. In the 1980s most MLCCs produced were either 1206 or 0805 (the two largest sizes). By 2000, the 1206 accounted for less than 10% of the market, while 30% of the market was for the 0402: a component with a fraction of the area and using much less material. Since 2000, the very small 0201 has captured an increasingly larger market share.

The use of lower operating voltages in handheld devices and microprocessors has allowed dielectric layer thickness to be reduced; consequently higher layer counts are possible within the same overall device dimensions, as shown in Figure 37.4.

You may recall from Chapter 31 that capacitance, C , is given by

$$C = \kappa \epsilon_0 A/d \quad (31.13)$$

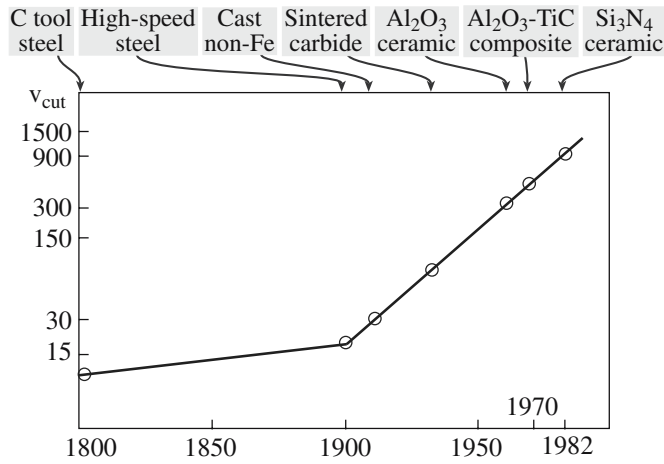


FIGURE 37.2 Improvements in the rate of metal cutting for various cutting-tool inserts.

By reducing d and increasing the number of layers (effectively increasing A) it has been possible to expand the capacitance of MLCCs into the tantalum and aluminum electrolytic capacitor range.

The ability to cast thin layers ($\times 3\mu\text{m}$) requires highly disperse, uniform, fine-grained ceramic powders (100–300nm particle diameter). To achieve these particles sizes extensive milling may be used or the powder can be made by solution methods such as using metal alkoxides as described in Chapter 22.

A major challenge in the MLCC industry has been to replace the precious metal electrodes (usually a Pd–Ag alloy) with base metals such as Ni. The MLCC industry accounts for about 75% of the electronic industries use of palladium.

Nd-Doped YAG Laser Crystals

Yttrium aluminum garnet (YAG) single crystals are the most widely used laser host, with over 100,000 YAG lasers

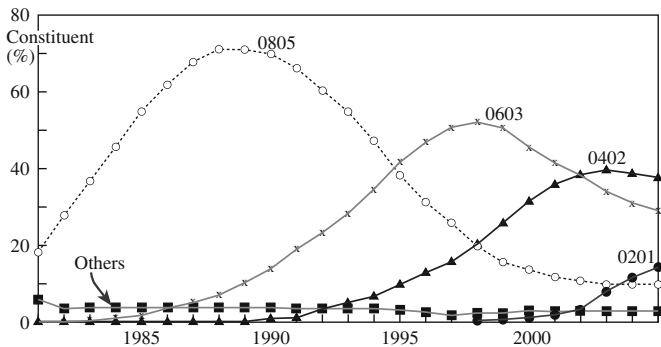


FIGURE 37.3 Multilayer ceramic capacitor-sized trends.

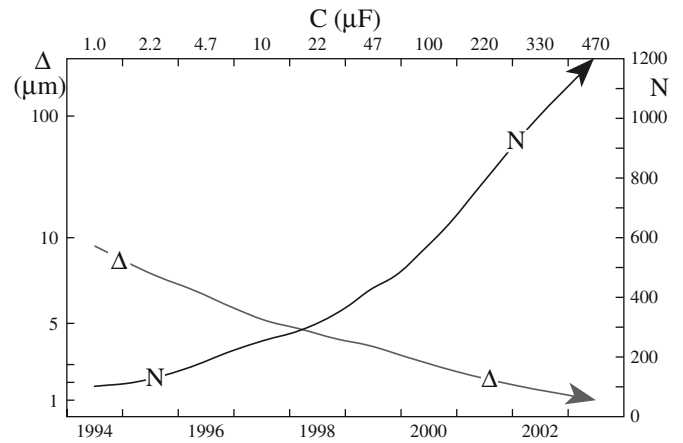


FIGURE 37.4 Trends in number (N) of dielectric layers and thickness (Δ) of the dielectric layer.

worldwide. The Czochralski process, which we described in Chapter 29, is used to grow single crystals of YAG. Typical growth conditions are pull rates of 0.4 mm/h at temperatures nearing 1900°C.

YAG LASERS

The first application for Nd-doped YAG lasers was in laser range finding. Nonmilitary applications include cutting, welding, and drilling of metals for the automobile industry and in medical and dental procedures.

One of the most common dopants is Nd^{3+} , which substitutes for yttrium in the crystal lattice. Commercial Nd-doped YAG is regularly produced with Nd concentrations ranging between 0

and 1.5 substitutional percent (sub%) of yttrium sites; from the chemical formula $\text{Y}_{3-x}(\text{Nd}_x)\text{Al}_5\text{O}_{12}$, the substitutional percent Nd is given by $x/3$. For instance, 1.02 sub% Nd = 0.153 at% Nd. Few crystals beyond 1.5 sub% Nd are available commercially.

The goal for commercial suppliers is to grow highly doped, large-diameter crystals. Increasing the dopant concentration results in a higher absorption coefficient, lower fluorescence lifetime, and greater overall laser efficiency. However, raising the Nd concentration increases the frequency of cracking during growth as we showed in Figure 16.1. If fracture occurs during growth then the process must be halted, which results in significant loss of time as a single boule can take 2 months to grow.

One of the causes of fracture has been shown to be small regions of inhomogeneity in the crystal as shown in the transmission electron micrograph (TEM) image in Figure 37.5. The widely spaced fringes in the image are moiré fringes caused by interference of the electron beam as it passes through two lattices that have different lattice parameters. The particle shown in Figure 37.5 actually has a larger lattice parameter corresponding to a local Nd concentration of 2.768% compared to the matrix, which has an Nd concentration of 1.02% Nd. (There is also a very small misorientation between the particle and the matrix, which also affects the spacing of the moiré fringes.)

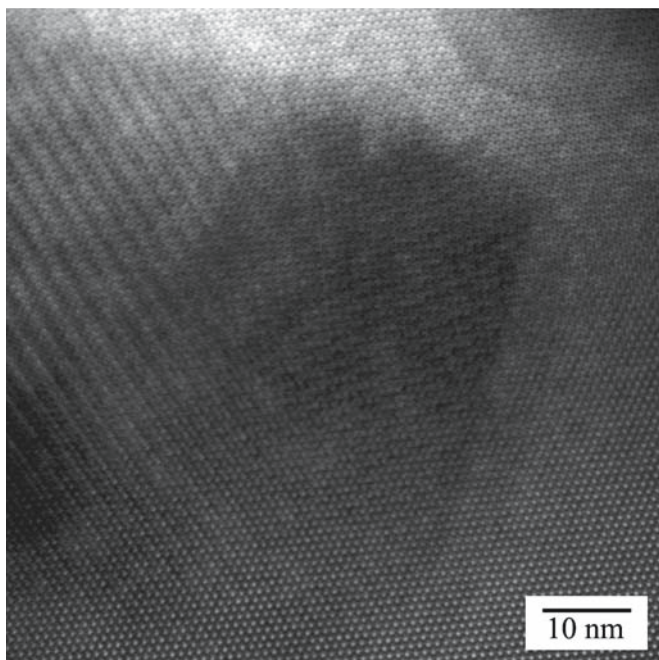


FIGURE 37.5 Moiré fringes spacing ~3nm observed in a high-resolution TEM image of an Nd-rich particle in single-crystal YAG.

More recently there has been interest in using nanopowders to make polycrystalline laser hosts. These would avoid the need to use slow single crystal growth methods. The problem is keeping the grain size small enough during sintering to maintain transparency.

37.5 EMERGING AREAS

The topic of advanced ceramics is exciting as technologies developed in research laboratories and universities become adopted by industry. This market segment shows continued growth offering good employment opportunities for MS&E graduates.

In this section we will describe three emerging areas: ceramic nanopowders, high-temperature superconductors, and ceramic–matrix composites.

Ceramic Nanopowders

Nanotechnology is a “hot” research topic. The field is trendy, popular, and high-tech. Although silica and iron oxide nanoparticles have a commercial history spanning half a century or more it is really only within the past 15–20 years that technologies have been developed for producing ultrapure nanosized powders of a range of ceramics. The

PRECIOUS METAL

In January 2001 Pd prices reached a staggering \$1000 per troy oz. Currently Pd trades for \$330 per troy oz in January 2007.

NANO POWDERS

Nanosized ceramic powders have grain sizes on the order of tens of nanometers or less; conventional ceramic particles typically have grain sizes of several micrometers or more.

global nanoparticle market, which is dominated by ceramics, is now around \$1 billion. Current applications for ceramic nanoparticles are summarized in Table 37.5.

- Electronic, magnetic, and optoelectronic applications account for 70%. The largest single use is slurries of abrasive silica particles (50–70 nm) for chemical/mechanical polishing (CMP).
- Biomedical, pharmaceutical, and cosmetic applications account for 18%. Sunscreens use nanosized powders of TiO₂ or ZnO.
- Energy, catalytic, and structural applications account for the remaining 12%. Uses include catalyst supports (e.g., for low-temperature H₂ production), ceramic membranes, fuel cells, and scratch-resistant coatings.

A recent example of the potential of nanosized ceramic powders in medicine is the demonstration that 5-nm cerium oxide (CeO₂) nanoparticles can prolong the life of brain cells. Usually these cells live for around 25 days in the laboratory, but after a low dose of the nanoparticles they have been shown to survive and function normally for 6 months. The hope is that this approach might one day be used to treat age-related disorders such as Alzheimer’s disease.

It was also found that the treated cells had increased protection against damage from ultraviolet (UV) radiation, as shown in Figure 37.6. The implication is that the

nanoparticles mop up free radicals—reactive molecules that damage cells and are known to be involved in aging and inflammation.

An energy-related application undergoing extensive testing is the use of 10-nm CeO₂ particles as additives to diesel fuel. The CeO₂ nanoparticles catalyze the combustion of the fuel. The claim is that they release oxygen to oxidize carbon monoxide and hydrocarbon gases to carbon dioxide, and also reduce quantities of harmful nitrogen oxides. The result is a cleaner burning fuel that converts more fuel to carbon dioxide, produces less noxious exhaust, and deposits less carbon on the engine walls.

The market for nanosized powders is much smaller than for conventional ceramic powders, but the cost per kilogram is much higher. Despite progress in scaling up production and reducing costs, nanosized powders remain relatively expensive (often 100 times more than conventional ceramic powders).

There are growing concerns about the impact of nanoparticles on human health and the environment.

Inhaling fine quartz particles is known to cause silicosis, a potentially fatal scarring of delicate lung tissue. Fine particles shed from hip and knee replacements as they wear cause

TABLE 37.5 Current and Emerging Applications for Nanosized Powders

<i>Electronic, optoelectronic, magnetic applications</i>	<i>Biomedical, pharmaceutical, cosmetic applications</i>	<i>Energy, catalytic, structural applications</i>
Chemical-mechanical polishing (CMR) supports	Antimicrobials	Automotive catalyst
Electroconductive coatings	Biodetection and labeling	Ceramic membranes
Magnetic fluid seals	Biomagnetic separations	Fuel cells
Magnetic-recording media	Drug delivery	Photocatalysts
Multilayer ceramic capacitors	MRI contrast agents	Propellants
	Orthopedics	Scratch-resistant coatings
	Sunscreens	Structural ceramics
Optical fibers		Thermal spray coatings
Phosphors		
Quantum optical devices		
Solar cells		

inflammation of the surrounding tissues and may result in the implant having to be replaced. Studies in which carbon nanotubes were placed directly into the lungs of mice showed that there was significant damage to the lung tissue. Because many of the potential applications for nanoparticles are in the human body it is important to determine their safety. It is also necessary to evaluate their environmental impact.

High-Temperature Superconductors

One of the benefits of increasing T_c above 77 K is that liquid nitrogen rather than liquid helium can be used as the coolant. Liquid nitrogen is both cheaper and more readily available than liquid helium. You will find the cost of liquid nitrogen described as either less than milk or less than cheap beer! The cost of liquid helium is often likened to fine champagne.

Soon after the discovery of high-temperature superconductors (HTSC) and, in particular, the YBCO compound there were grand predictions that these materials would revolutionize areas such as a high-speed transporta-

tion and power transmission. The applications to date have been a little more modest. Magnetic levitation (maglev) for high-speed transportation has not been achieved with HTSC, but continues to a limited extent with the use of low-temperature materials. The other major application proposed for HTSC was in power transmission. However, due to the high cost and impracticality of cooling miles of superconducting wire, this has happened only with short “test runs.” In May 2001 about 150,000 residents of Copenhagen, Denmark began receiving their electricity through superconducting cables. The superconductor chosen for this application was BSCCO (see Section 7.16) in the form of a tape wrapped around a flexible duct that carries the liquid N_2 . The remainder of the cable consists of thermal and electrical insulation. In November 2001 commercial power was delivered to about 30,000 homes in Detroit, Michigan using a similar approach.

One area in which HTSC is poised to make a significant impact is in filters that improve network performance between wireless (cellular) devices and cell sites. Superconductivity avoids a typical trade-off by filtering out interference from adjacent signal bands without hindering the base station’s ability to pick up weak signals. This market could be a \$10 billion business by 2011.

According to estimates by the European Conectus consortium the worldwide market for HTSC products is projected to grow to about \$5 billion by 2010 and to almost \$40 billion by 2020.

Ceramic–Matrix Composites

Ceramic–matrix composites (CMCs) are being developed to provide an alternative to single-phase ceramic components because of the possibility of designing with higher toughness. The most important CMCs will probably be those with continuous fiber reinforcement. We described some of the processing routes in Chapter 20. Ceramic–matrix composites are at a relatively early stage of development compared to polymer–matrix composites (PMCs) and metal–matrix composites (MMCs) and significant research is needed if they are to meet their full potential. Table 37.6 lists some of the priorities.

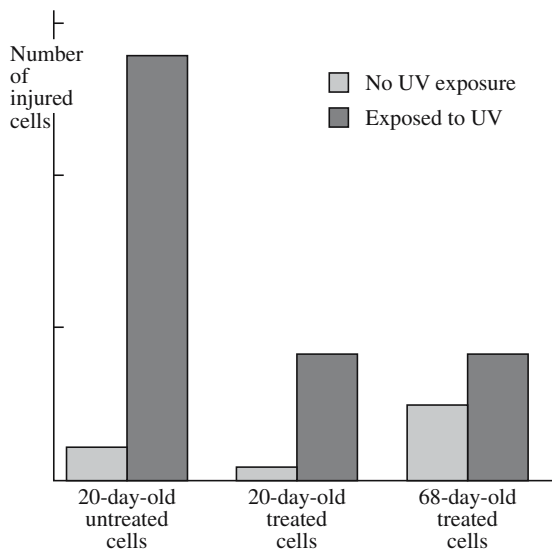


FIGURE 37.6 Effect of nanosized cerium oxide particles on the life of rat neurons.

TABLE 37.6 Priority Needs in CMCs to Address Key Challenges Faced by Ceramic Manufacturers and End Users

Key Challenges for CMCs	Priority needs to address the challenge
Reduce the cost of precursors	Scale-up/cost reduction of fiber manufacturing Lower-cost interface materials and deposition processes
Improve understanding of failure modes	Basic understanding of interactions between CMC constituents and application environments Micro- and macromechanics understanding of interactions of CMC with an applied stress or strain
Increase temperature stability to 1200–1500°C	Higher-temperature fibers, matrix materials, and interface coatings Environmental barrier coatings (EBCs) Active cooling designs
Manufacturing scale-up and cost reduction	Larger furnace design and construction Automation/semiautomation of preform fabrication Low-cost tooling Near-net-shape fabrication Low-cost in-process and postprocess quality assurance

- **Cost:** Nonoxide fibers cost thousands of dollars per kilogram. Oxide fibers, even those that have been commercially available for years, sell for hundreds of dollars per kilogram. The main reason is that production volumes are small. Most fiber-reinforced CMCs utilize a layer between the fiber and matrix to optimize mechanical properties. The methods used for depositing this layer tend to be expensive and difficult to scale up for production.
- **Understanding Failure Modes:** We generally want a weak fiber–matrix interface in CMCs. A propagating crack is deflected around the fibers as shown in Figure 37.7 and does not propagate through the fibers. This

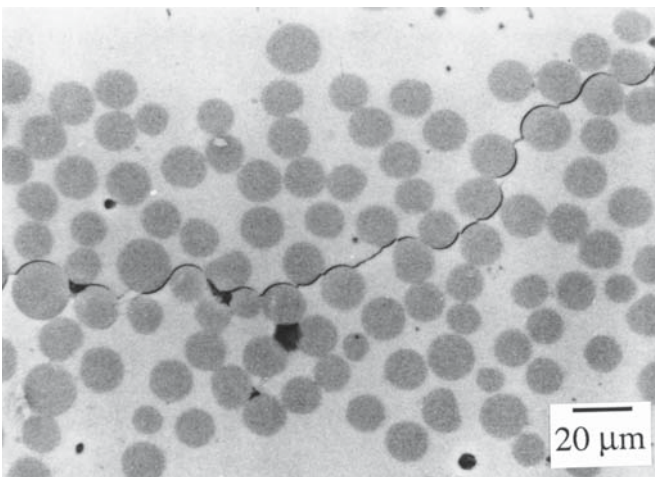


FIGURE 37.7 Crack propagation through a fiber-reinforced composite: SiC fiber in calcium aluminosilicate glass.

situation is opposite to that in PMCs where we often want a strong interface so that the load is transferred to the stronger fibers.

- **Increase Temperature Stability:** Fiber-reinforced CMCs have been demonstrated to survive in the severe environment of a gas turbine engine for 2500 hours at temperatures up to 1200°C. The use of environmental barrier coatings (EBCs) such as oxide layers on SiC appears to help extend durability, but more research is needed to determine whether they present a long-term solution.
- **Scale-up:** The high price of finished components made from fiber-reinforced CMCs is a major limitation. Reducing materials costs and increasing production volume would reduce costs substantially. One of the requirements for large-scale manufacturing of CMCs is the development of quick and inexpensive quality control procedures that can be used during production. The main processing defects are voids, density variations, and cracks. X-ray computed tomography (CT) is a powerful technique for this type of investigation and high-resolution detectors can detect defects and resolve features as small as 5 μm (see Chapter 10). But the technique remains expensive and slow and is not suitable at the present time for in-line process control.

Ceramics as the Enabling Materials

As you have realized from the discussion of capacitors, glass, data storage, etc., ceramic materials are often the critical part of a program or product even if the consumer never sees them.

Sapphire single crystals are grown for use in substrates, as windows, as IR-transparent domes, in jewel bearings, and as the “glass” on your best watch, but there are other applications of these and other single crystals that most of us never see. Large sapphire crystals are being tested for use in the LIGO Fabry-Perot interferometer. The aim of LIGO (laser interferometer gravitational-wave observatory) is to study astrophysical gravitational waves. There are two LIGO sites, one in eastern Washington and one in Louisiana. Sapphire should reduce the thermal noise compared to the fused silica that was initially used. The LIGO requires the crystals to be 35 cm in diameter and 12 cm long and uses 5N-pure alumina powder. The factors studied in assessing the sapphire mirrors for future generations of LIGO include all aspects of the influence of temperature on mechanical properties and the results are compared with the current fused-silica mirrors. In either case, the ceramic is the enabling material and is the topic of very focused research.

37.6 MINING

From the ugliness of an open cast mine, to the health problems of mine workers, to the bitter civil wars fought over mineral resources in Africa, the impact of mining

and our search for raw materials are frequent topics in the news media. Many of the ceramic products we use are produced from natural resources.

For example, the main component of most glasses is SiO_2 , which comes from sand. The main component of traditional ceramic products like tableware and bricks is clay, which is available in different grades and is usually extracted by opencast mining. These raw materials are abundant and widespread.

Talc

A mineral that has caught the attention of environmentalists and conservationists is talc. Talc is used in the production of paper and tiles, and as coatings in the motor industry for dashboards and fenders (bumpers). However, its main use is in beauty products such as eye shadow, lipstick, body lotions, deodorants, and soaps. Talc is produced from soapstone, which occurs in the form of large subsurface boulders. The concern is that some of the finest powder is obtained from soapstone that is the result of illegal mining in India's Jamwa Ramgarh Wildlife Sanctuary and the neighboring Sariska Tiger Reserve 250 km southwest of Delhi. These sites are considered essential to the revival of the Indian tiger. The current population of Indian tigers is about 3000, but they are threatened with extinction because of the loss of habitat and prey caused by the mining activities.

Tantalite

The dielectric in tantalum electrolytic capacitors is tantalum pentoxide (Ta_2O_5), which forms as a thin layer on tantalum as illustrated in Figure 37.8. The benefits of using tantalum capacitors are that they are small, have a

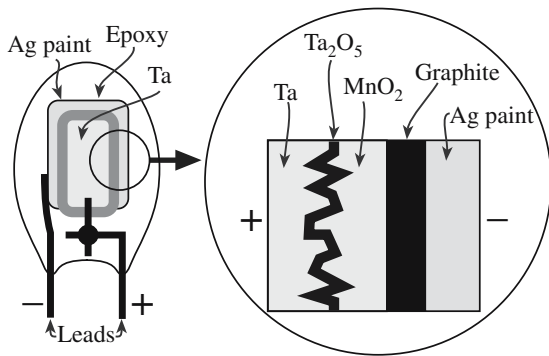


FIGURE 37.8 Schematic diagram of the structure of a solid electrolyte Ta capacitor.

Ta IN CAPACITORS

The major use for Ta is in electrolytic capacitors; it accounts for about 60% of this market. The annual value of all Ta consumed is ~\$200M.

wide operating temperature range (-55°C to 125°C), and are very reliable.

Controversy has arisen recently concerning the source of tantalum: the mineral tantalite, which is found in association with niobium as the ore columbite-tantalite or col-tan. A major supply of col-tan is found in the Kahuzi-Biéga Park in the Democratic Republic of Congo. The park is home to the eastern lowland gorilla, one of the rarest animals in the world. As a result of col-tan mining the gorilla population is being decimated and the billion-dollar export has funded the Congo's civil war.

37.7 RECYCLING

There are three basic reasons given for recycling:

1. Preserve finite resources
2. Protect the environment
3. Save energy

The raw materials used for glass production are abundant and unlike many metal ores are not in any imminent danger of being depleted. But producing glass does involve consumption of large amounts of energy as shown in Table 37.7. (Glass is the lowest on this list because high-purity sources of SiO_2 are readily available.) Table 37.8 shows the total energy involved in producing a 12-oz beverage bottle including factors such as mining and transportation.

consumption of large amounts of energy as shown in Table 37.7. (Glass is the lowest on this list because high-purity sources of SiO_2 are readily available.) Table 37.8 shows the total energy involved in producing a 12-oz beverage bottle including factors such as mining and transportation.

TABLE 37.7 Energy Consumption to Extract 1 ton of Raw Material from Its Ore or Source

Material	Energy (GJ)
Aluminum	238
Plastics	100
Zinc	70
Steel	50
Glass	20

TABLE 37.8 Energy Consumption per Use for a 12-oz Beverage Container

Container	Energy (MJ)
Aluminum can used once	7.4
Glass bottle used once	3.9
Recycled aluminum can	2.7
Recycled glass bottle	2.7
Refillable glass bottle used 10 times	0.6

The energy savings by recycling and reusing glass containers are also shown in Table 37.8.

Glass recycling has been going on for thousands of years; broken glass was reused in antiquity to make new glass objects. This ancient recycling system makes it difficult for archeologists to determine the provenance of a glass object from its chemical composition alone. A structured recycling program for domestic glass waste started in 1975 and was initiated by the glassmaking companies.

In Chapter 26 we described the glass-forming process. The initial step is that the batch, which consists primarily of sand, is melted. The temperature required varies with the composition of the batch, but is typically in the range of 1300–1600°C. Adding crushed recycled glass, called cullet, to the melt promotes melting of the sand permitting the use of reduced furnace temperatures with considerable savings in both raw materials and energy. For example, if a glass batch for beverage container glass contains 25% cullet it requires 5% less energy to melt. Although cullet has been used in ratios ranging from 0 to 100% of the glass, 30–60% cullet is the most effective range. For colored bottles cullet comprises about 50% of the batch.

One difficulty associated with using recycled glass, particularly from consumer recycling, is the necessity to sort the discarded bottles according to color. In the United States over 65% of container glass is clear, 25% is brown or “amber,” and 10% comes in different shades of green and occasional blue and other colors. These percentages do not correspond exactly to the glass contents in domestic waste because of the consumption of imported beverages that come in mostly brown and green bottles. In France, 80% of the glass containers are green. Wine is usually packed in green bottles because it provides better UV protection, but the original reason is that when the wine bottle was invented in England during the seventeenth century it was made of green glass.

Clear glass is the most valuable glass for recycling. Both clear and brown glasses are very sensitive to impurities so they cannot be mixed with each other or with other types of glass. Green glass, however, can accept other glass types without noticeable influence on the color. However, green glass is often the most difficult for the glass manufacturers to use simply because the supply of recycled green glass often exceeds the demand. One application for recycled green glass that is not influenced by color is for fiberglass insulation.

GLASS RECYCLING: FACTS AND FIGURES

More than 40 billion glass containers are produced each year in the United States.

All glass food and beverage containers can be recycled.

Recycling a glass jar saves enough energy to light a 100-W light bulb for 4 hours.

Glass constitutes about 6% of U.S. municipal solid waste.

Approximately 12 million tons of waste glass food and beverage containers are generated each year in the United States.

About 25% of all glass food and beverage containers are recycled in the United States.

The average glass bottle contains over 25% recycled glass.

It is important that container glass is not mixed with other types of glass product such as windows, light bulbs, mirrors, and tableware. These glasses have different compositions as we showed in Chapter 26. Because of problems associated with contamination of recycled glass the use of returnable/refillable glass bottles and containers is increasing. Switching to refillable containers can save up to 56% of the energy consumed, reduce water consumption

by up to 82%, and decrease materials consumption over 10 times for 35 refills.

Currently the cost of recycling far outweighs the value of the recyclables. It may take up to five times the amount of money a recyclable product is worth to collect, process, and transport it to a buyer. As a result, the recycling industry is currently driven by consumer demand, not by profit. Many environmental economists point out that in a “sustainable” economic system (one based on the real costs to the environment resulting from the transportation and production of goods and materials), recycling is financially cost effective. In such a system, the prices of products made from virgin materials would be prohibitive, encouraging manufacturers to use recycled materials instead. However, under such a system, the concept of curbside recycling would become even less cost effective than it is now, due to increasing transportation and energy costs.

Some of the issues that drive the need for recycling in Europe are quite different from those in the United States. One significant difference is population density. Recycling in the Netherlands, which recycles more than 80% of its glass waste, is much more important than in the United States. The population densities are about 372 inhabitants/km² and 27 inhabitants/km², respectively. As the population density increases, the landfilling of waste, particularly industrial waste, becomes more difficult and unacceptable for the nearby population. Landfill space has to compete with the land requirements for expanding suburban developments and in many cases agricultural land as well.

One recycling issue that is important throughout the developed world is what to do with the approximately 300 million TVs and computer monitors that are thrown out each year. The European Union Waste Electrical and Electronic Equipment Directive have banned them from being dumped in landfills because the screens contain PbO added to shield against the X-ray radiation released by the high anode voltage. Table 37.9 shows typical compositions of cathode ray tube (CRT) glasses.

TABLE 37.9 Some Typical Chemical Compositions of CRT Glasses (wt%)

Oxide	Color TV panel	Color PC panel	Color TV funnel	PC funnel
Na ₂ O	8.0–8.6	6.6	6.3–6.8	5.45
K ₂ O	7.0–7.5	7.3	7.8–9.7	8.05
MgO	0.2–1.3	0.33	1.0–1.8	1.5
CaO	0.5–2.5	1.15	1.4–3.8	3.5
SrO	1.5–8.5	8.65	0.15–0.5	0.5
BaO	10–12	1.15	1.0–1.95	3.5
Al ₂ O ₃	2.2–3.2	2.05	3.0–4.0	3.6
ZrO ₂	0.2–1.5	0.95	0.08	0.1
PbO	0.0–0.1	0.05	14.7–22.7	20.25
SiO ₂	60–62	59	52–59	53
CeO ₂	0.25	—	—	—
TiO ₂	0.4	0.6	0.05	0.07
Sb ₂ O ₃	0.25	0.5	0.05	—
As ₂ O ₃	0.02	0.02	0.01	—
Fe ₂ O ₃	0.07	0.12	0.06	—
ZnO	—	0.6	—	0.06

To prevent a growing mountain of TVs one of the plans is to melt down the tubes in a sealed furnace under conditions that would reduce the PbO to Pb. The heavy molten metal would run out of fissures at the base of the furnace, but the molten glass will be retained. The purified glass could then be used for other applications, such as bottles.

The use of recycled glass as an ingredient in concrete is being explored in several locations worldwide.

37.8 IN THE NUCLEAR INDUSTRY

Uranium dioxide (UO₂) has been important as a nuclear fuel since the mid-1950s and is obtained from its major ore, uraninite. After leaching the ore, U₃O₈ is precipitated out. The average price for U₃O₈ is about \$25/kg and the United States used about 24 million kg of U₃O₈ last year. Before use in a nuclear reactor U₃O₈ is converted into UF₆ gas. Then using either diffusion or centrifugal processing, U²³⁵F₆ is separated from U²³⁸F₆. The U²³⁵-enriched gas is reacted to form UO₂ powder, which is pressed into pellets. These pellets are loaded into zirconium alloy tubes making the fuel rods. A 1000-MW reactor will “burn” 25 t of UO₂ per year, and 1 kg of fuel costs about \$900. Thus, a 1000-MW reactor will consume about \$22.5 million of UO₂ annually.

In the United States there are presently about 100 operable nuclear reactors (over 400 worldwide) producing 21% of the country’s electrical power. The number of operable reactors has decreased since it reached its peak in 1990, but there is some interest in reviving the nuclear industry because it is a zero “greenhouse emission” technology and because it does not consume limited resources of fossil fuels.

One of the major problems with increasing nuclear reactor capacity is what to do with the spent fuel. There are two current approaches:

- Reprocessing (adopted by UK, France, Germany, Japan, China, and India)
- Storage (adopted by the United States, Canada, and Sweden)

In Europe, spent fuel is frequently reprocessed, which involves dissolving the fuel elements in nitric acid. Since plutonium is created in the fission process, reprocessed fuel contains both radioactive U and Pu, and is referred to as a mixed oxide (MOX) fuel.

The remaining liquid after Pu and U are removed is high-level waste (HLW), containing about 3% of the spent fuel. It is highly radioactive and continues to generate a lot of heat. This waste must be immobilized and because of the presence of radioisotopes with long half-lives it must be immobilized for tens of thousands of years. Ceramics are key materials in this process.

The following are major requirements for waste immobilization:

- The radioactive elements must become immobilized in the crystal or glass structure.
- The leaching rate of radioactive elements must be low.
- The cost must be acceptable.

The main method of solidifying HLW, not already contained in spent fuel rods, is to “vitrify” it into a borosilicate glass and cast it into stainless steel cans for ultimate burial. Vitrification of civil HLW first took place on an industrial scale in France in 1978. A year’s worth of HLW from a 1000-MW reactor can be stored in about 26 m³.

A second-generation immobilization material, “synroc,” is in development. This synthetic rock, based on mixed titanate phases such as zirconolite, hollandite, or perovskite, incorporates the HLW elements into its crystal structure, yielding excellent chemical stability. Synroc features leach rates more than an order of magnitude lower than borosilicate glass.

Whether the final HLW is vitrified material from reprocessing or entire spent fuel assemblies, it eventually needs to be disposed of safely. This means that it should not require any ongoing management after disposal. While final disposal of HLW will not take place for some years, preparations are being made for sites for long-term disposal. One of these is Yucca Mountain in Nevada.

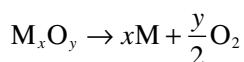
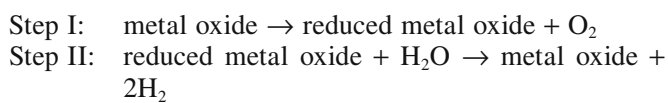
37.9 PRODUCING AND STORING HYDROGEN

Thermochemical Processing

We know it is completely feasible to produce hydrogen using solar energy from the point of view of thermodynamics. The idea is to use thermochemical processing.

The goal is to convert water (in the form of steam) into its components, hydrogen and oxygen, and then to collect the hydrogen for use as a fuel. It is simple! The process is particularly exciting because efficiencies of up to 76% should be achievable, which makes it both commercially and environmentally very attractive.

The principle behind the process is to use solar energy to drive a highly endothermic reaction and then produce hydrogen by a subsequent exothermic reaction. This is known as a *two-step water-splitting cycle*. Solar energy in the form of heat is used to reduce the ceramic (a metal oxide); this reduced metal oxide is then reoxidized by removing the oxygen from water, thus producing hydrogen gas. The reduced (lower valence) metal oxide in step I (thermal reduction) could alternatively be a metal carbide, a metal nitride, or even a metal. The second step (oxidation by water) is known as hydrolysis. The limit for step I would be



If we use FeO in step I, then the temperature must be >1600 K. However, step II is then spontaneous at a temperature of ~1200 K.

Several systems are being explored for this purpose. These include the reduction of ZnO (in some cases enhanced by the presence of C), the reduction of ceria, and the reduction of oxides containing Fe³⁺ (both iron oxide and a range of ferrites).

All that we need to do is to optimize the ceramics and, perhaps the more challenging step, optimize the geometry of the sample to allow repeated cycling (1) without degradation and (2) while allowing easy extraction of the hydrogen. So the usual process is to improve the design (tailor) of both the material (e.g., powder versus multilayer films or foams) and of the reactor itself.

This whole process should remind you of our discussion of phase boundaries (PBs) in Chapter 15 and reactions in Chapter 25. The solar part of this has many similarities to processes that are now being explored for producing lime (the endothermic calcinations of CaCO₃) and other ceramics. Currently we use fossil fuels to produce cement and lime, which account for 5% and 1%, respectively, of the global human-made CO₂ emissions—up to 40% of this is from burning the fossil fuels.

Proton Exchange Membrane Fuel Cells

High purity hydrogen is needed for use in proton exchange membrane (PEM) fuel cells. Hydrogen is currently produced industrially (9Mt per year in the United States) through steam reforming of natural gas. Alternative fossil fuel hydrogen technologies are needed. Coal is a potential

TABLE 37.10 Catalytic Properties of Mo Carbide for Fuel Reforming Applications

<i>Reactivity</i>	<i>Other important catalytic properties</i>
Similar reactivity to Pt in alcohol synthesis, methane dehydrogenation, and hydrocarbon isomerization	High resistance to coking even under stoichiometric fuel reforming conditions
Excellent hydrodesulfurization activity	Shows the potential of being sulfur-tolerant
Promotes the water gas shift (WGS) reaction at low temperatures	High selectivity for hydrocarbon conversions

source of energy for hydrogen production but is more challenging because it is dirty. Abraham Darby I realized the problems with coal in the early eighteenth century, which led to his use of coke (a high purity form of carbon) for smelting iron. This process allowed the expansion of the iron trade.

Catalysts required for reforming of coal into hydrogen must be resistant to poisoning by contaminants. Current catalysts are based on expensive precious metals, mainly platinum. A possible low-cost alternative is molybdenum carbide. Molybdenum carbide is one of the more widely studied carbide systems and has shown useful catalytic properties for fuel reforming applications, which are summarized in Table 37.10.

The stable phase is β-Mo₂C and there are several non-stoichiometric high-temperature phases MoC_{1-x}, with both hexagonal and cubic structures. Nanoparticles of molybdenum carbide seem to be most effective for catalysis because of their large surface areas (up to 200 m²/g). Catalyst nanoparticles about 10 nm in diameter are formed on various supports such as Al₂O₃, ZrO₂, and even carbon nanotubes. It is important to prevent the particles from oxidizing because MoO₂ is inactive for fuel reforming.

Hydrogen Storage

Of all the limitations preventing the achievement of the hydrogen economy the most significant is hydrogen storage. For transportation applications storage requirements are particularly stringent and none of the current approaches comes close to meeting targets. Indeed some of the approaches are actually dangerous. Storing hydrogen on the surface of nanomaterials is an exciting possibility. The idea is again to use the very large surface areas available at the nanoscale. The hydrogen attaches nondissociatively (i.e., as H₂) through weak molecular-surface interactions such as van der Waals forces. Studies have shown that hydrogen will attach to the surface of carbon nanotubes, but the temperatures do not seem to be ideal for transportation needs. Recently, using glasses for hydrogen storage has been proposed and experimentally



FIGURE 37.9 TEM image of silica nanoropes for hydrogen storage (on a lacy C film).

hydrogen has been shown to attach to the surface of two-dimensional silica glass nanostructures (e.g., wires, ropes, and springs) at room temperature and be released at $\sim 100^\circ\text{C}$. Figure 37.9 shows a TEM image of silica nanoropes. The only difference, apart from size, between these nanostructures and “bulk” glass fibers appears to be that the surface is more ionic, which may be important for hydrogen attachment. The nanoropes grow by the vapor–liquid–solid (VLS) mechanism described in Chapter 29. The Au catalyst is the dark particle. The deposition process occurs at temperatures as low as 300°C allowing them to be formed on polymer substrates.

37.10 AS GREEN MATERIALS

Catalytic Converters

Catalytic converters are used in the exhaust system of automobiles and can reduce emissions of carbon monoxide and hydrocarbons by up to 90%. Carbon monoxide can be transformed into carbon dioxide, and unburned hydrocarbons from the fuel get burned on the metal surfaces. Nitric oxide, one of the main contributors to urban smog, will react with carbon monoxide to form carbon dioxide and nitrogen gas. These processes are conducted in catalytic converters.

The first catalytic converters used mainly platinum, but palladium is now the predominant catalyst metal. Sixty percent of the palladium manufactured worldwide is used in catalytic converters. Other uses are as the electrodes in MLCCs and other electronic components, and a small amount is used in jewelry (for example, an alloying element in white gold).

The metal is dispersed as tiny particles on a supporting framework of a porous ceramic. Because of the need for thermal

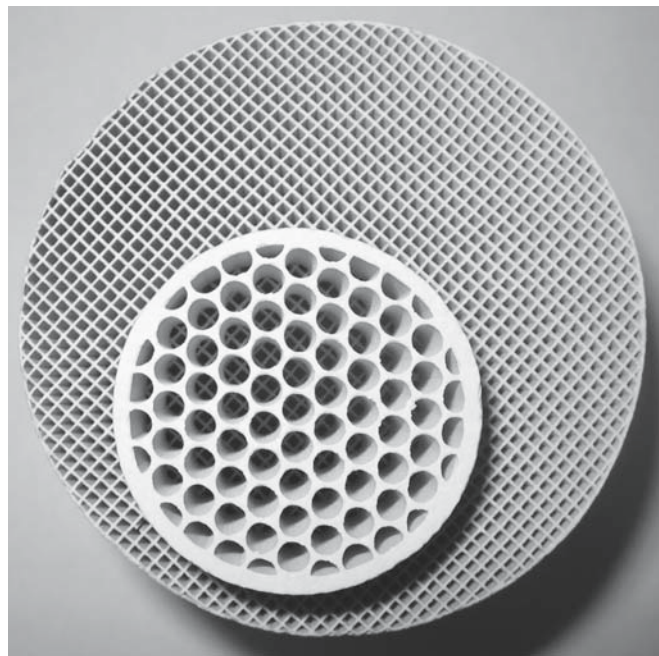


FIGURE 37.10 Looking through two ceramic extruded cordierite honeycomb substrates for catalytic converters.

shock resistance a ceramic with a near-zero coefficient of thermal expansion is required. One such material is cordierite. Figure 37.10 shows an example of a ceramic honeycomb substrate for a catalytic converter. Substrates have been produced with up to 900 cells per square inch and walls of thickness of $50\mu\text{m}$. These complex shapes are produced by extrusion, a process we described in Chapter 23. The ceramic powder is mixed with a hydraulic-setting polyurethane resin. The mix is extruded into a water bath at a rate of about 2 mm/s . The extrusion rate matches the rate at which the resin cures.

Other requirements for the catalyst substrate are

- Low cost
- Thermal-mechanical durability
- Lightweight

Photoelectrochemical Solar Cells

Photoelectrochemical (PEC) solar cells use a hybrid structure consisting of inorganic semiconductors and organic molecules. There are several different geometries. The one shown in Figure 37.11 uses a film of sintered TiO_2 nanoparticles ($10\text{--}30\text{ nm}$) on a conducting glass substrate.

Dye molecules that absorb sunlight are coated onto the TiO_2 particles. The TiO_2 itself does not absorb a significant amount of

CATALYTIC CONVERTERS

These have reduced automobile pollution by more than 1.5 billion tons since 1974.

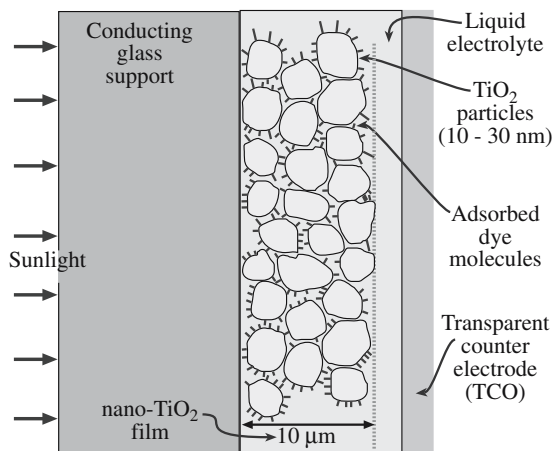


FIGURE 37.11 Schematic of a dye-sensitized nanocrystalline solar cell.

sunlight; it is a wide-band-gap semiconductor ($E_g = 3.0 \text{ eV}$). The dye molecules absorb by electrons moving into excited states. These excited electrons are injected into the TiO_2 , which creates positively charged dye molecules. The incident solar energy has created electron-hole pairs. If these pairs are separated then we have a photovoltaic (or solar) cell. The circuit is completed by a liquid electrolyte and transparent electrode. Despite the high efficiencies of PEC solar cells, the lifetime of the photoelectrode and the high cost have restricted commercialization.

CHAPTER SUMMARY

In this chapter we described some of the industrial aspects of ceramics. Ceramics make money. Unfortunately obtaining the raw materials can have some undesirable environmental and societal impacts. The environmental impact of nanomaterials is an issue that has not yet significantly concerned the ceramics industry because no one knows exactly what that impact is. But as the market for ceramic nanopowders and other nanostructures (such as wires and tubes) increases the environmental concerns will have to be addressed. Many of the “grand challenges” we face as a society, such as energy, the environment, and health care, will require innovative technological solutions. Ceramics can play an important role in these areas, e.g., nuclear waste immobilization, catalytic conversion, and viral nanosensors.

It is important to realize that industry is constantly in a state of flux so numbers reported here can change from year to year. Also this chapter reflects a snapshot of an industry at the beginning of the twenty-first century. In a decade, the relative importance of some of the topics we described may have increased, decreased, or disappeared altogether.

PEOPLE IN HISTORY

Darby, Abraham I (1678–1717) was born in Staffordshire; he patented sand casting in 1708 and invented coke smelting in 1709.

Feynman, Richard (1918–1988). The beginning of research in nanotechnology can be traced back to a visionary talk given by Feynman in 1959 titled “There’s Plenty of Room at the Bottom.” Since then nanotechnology has captured the minds and imaginations of many scientists and engineers. A transcript of his nanotechnology talk can be found at <http://www.zyvex.com/nanotech/feynman.html>. Feynman won the 1965 Nobel Prize in Physics.

Wollaston, William Hyde (1766–1828) was an English scientist who discovered Pd in 1803 and named it after the asteroid Pallas, found in 1802. The mineral wollastonite is named after him.

GENERAL REFERENCES

Tames, R. (1984) *Josiah Wedgwood, An Illustrated Life of Josiah Wedgwood 1730–1795*, Shire Publications Ltd., Aylesbury, Bucks, UK. A brief biography of the man described by British Prime Minister William Gladstone (1868–1874) as “the greatest man who ever, in any age or country, applied himself to the important work of uniting art with industry.”

SPECIFIC REFERENCES

DOE. *Basic Research Needs for Solar Energy*, Report of the Basic Energy Sciences Workshop on Solar Energy Utilization, April 18–21, 2005. Defining the direction for U.S. solar energy research.

Eakins, D.E., Held, M., Norton, M.G., and Bahr, D.F. (2003) “A study of fracture and defects in single crystal YAG,” *J. Cryst. Growth* **267**, 502. This research was funded by a U.S. crystal growth company to help solve a processing problem.

Fletcher, E.A. and Moen, R.L. (1977) “Hydrogen and oxygen from water,” *Science* **197**, 1050.

Fletcher, E.A. (2001) “Solarthermal processing: A review,” *J. Solar Energy Engin.* **123**, 63.

Kennedy, G.B. and Bowen, H.K. (1983) “High tech ceramics in Japan: Current and future markets,” *Am. Ceram. Soc. Bull.*, **62**, 590. Describes the ceramics market in Japan in the 1980s.

WWW

Advanced Ceramics Technology Roadmap—Charting Our Course, December 2000. Sponsored by United States Advanced Ceramic Association and the U.S. Department of Energy. Available on the web at www.ceramics.org/cic/marketresources.asp.

www.kitco.com

Precious metal prices and historical trends.

www.nulifeglass.com

NuLife Glass of Wilmslow in Cheshire. A company that plans to recycle the glass used in TV and computer screens.

www.kemet.com

KEMET Corporation in Greenville, South Carolina is the largest manufacturer of solid tantalum capacitors and the fourth largest manufacturer of MLCCs in the world.

www.conectus.org

The European superconductivity consortium.

Company sites that make some of the products we mention in this chapter:

www.oxonica.com

Oxonica website. You can find out about the status of the nanoparticle fuel efficiency trials.

www.utilities.dteenergy.com

Detroit Edison website.

www.ceramicindustry.com

Ceramic Industry magazine. Also find out about the Giants of Ceramics.

NWT Diamond Industry

www.iti.gov.nt.ca/diamond/production.htm

for details on the Diavikmine.

EXERCISES

- 37.1 In addition to oxygen what other impurities might you expect in Si_3N_4 powder?
- 37.2 Why is the extent of Nd substitution in YAG so small?
- 37.3 What companies make the Pd–Ag metallization used for MLCCs?
- 37.4 Do TiO_2 and ZnO play different roles in sunscreen? Which is the better material for this purpose?
- 37.5 Describe one process used to make CeO_2 nanoparticles.
- 37.6 In the form of a table compare the cost of conventional (micrometer-sized) ceramic powders with the nano-sized equivalents.
- 37.7 How much glass is recycled in your community (or state)?
- 37.8 Compare the costs of recycling to landfilling for various materials.
- 37.9 Why is the BSCCO superconductor the material of choice for superconducting wires?
- 37.10 What is the current world capacity for reprocessing nuclear waste?

Index

A

Abbe, Ernst, 382, 479
absorption, 576, 656
Acheson process, 354, 365
Acheson, Edward Goodrich, 357
adamite, 585
adulescence, 662
agate, 652
AgBr, 182, 186, 200
agglomerates, 364
aggregates, 360
Al₂SiO₅, 77, 84
alabaster, 653
AlAs, 183
alexandrite, 669
alkoxides, 401–6
allotropes, 96
alloys, 3
almandine, 660, 669
almandite garnet, 660
alumina (Al₂O₃), 5, 7, 9, 10, 20, 22, 28, 47, 52, 55, 64, 66, 71, 77, 79, 81, 82, 84, 86, 87, 94, 95, 106, 110, 118, 122, 124, 146, 159, 160, 184, 190, 193, 197, 200, 207, 208, 210, 216, 218, 219, 226, 232, 239, 269, 270, 271, 273, 276, 278, 284, 290, 291, 295, 298, 305, 307, 312, 313, 319, 320, 338, 351, 391, 415, 428, 435–7, 445, 446, 449, 450, 454, 456–8, 463, 466, 543, 548, 585, 589, 596, 628, 635, 639, 640, 649, 651, 655, 665, 686
aluminosilicates, 19, 100, 114, 301
aluminum nitride (AlN), 5, 7, 9, 62, 77, 87, 90, 168, 182, 209, 218, 260, 266, 332, 354, 439, 458, 501, 548, 628
amethyst, 654, 667, 670
anatase, 93, 353
andalusite, 100, 351
anhydrite, 347
anorthite, 264
antiferromagnetism, 606
antiphase boundaries (APB), 168
antireflection coatings (ARC), 577, 580
antisite defect, 182
aquamarine, 665
aragonite, 257, 462
arc-image growth, 511
Arrhenius equation, 47, 321, 543
Arrhenius plot, 47, 48, 195
Arrhenius relationships, 198, 396

Arrhenius, Svante August, 48
arsenic oxide (As₂O₃), 468
Aspdin, Joseph, 22, 30
associated centers, 182
asterism, 662
atomic orbitals, 58, 59, 60, 62, 69
atomic packing factor (APF), 79, 80
atomic structure, 35, 36
atomic-force microscopy (AFM), 154, 161, 162, 176, 177, 219, 236, 237, 240, 263, 278, 301, 435, 436, 571, 610
attrition mill, 362
Auger electron spectroscopy (AES), 174
augite, 109
Avogadro number, 226
azurite, 652

B

backscattered electrons (BSE), 158
Bacon, Roger, 397
baddeleyite, 353
ball milling, 360–1
band gap, 66, 68, 69, 90, 531
band-gap energy, 197, 385
Bardeen, John, 554
Bardeen–Cooper–Schrieffer (BCS) theory, 550–1, 554
barium hexaferrite (BaO.6Fe₂O₃), 5, 438, 608
barium magnetoplumbite, 110
barium titanate (BaTiO₃), 7, 35, 77, 93, 102, 121, 133, 136, 448, 495, 508, 519, 558, 562–65, 567, 571, 573, 597, 631, 678
Barkla, Charles Glover, 36, 37, 48
barrier layer, 453
barriers, 452
basalt, 358
basis, 72
batteries, 544
bauxite, 350, 351, 352, 357, 548
Bayer process, 351, 357
Bayer, Karl Joseph, 357
Be₃Al₂(SiO₃)₆, 519, 652–4, 660, 661, 664, 665
BeAl₂O₄, 127
beam bending, 383
Bednorz, Johannes Georg, 28, 30, 31
Beer-Lambert law, 367, 577
bend test, 297
beneficiation, 345, 347, 348, 349, 351, 352
beryl, 107, 661, 665
beryllia, (BeO), 90, 290, 489, 548
Bessemer converter, 25
binary phase diagram, 121, 122, 126
binder burnout, 421
binder, 412, 413, 482, 489
Binnig, Gerd, 176, 243
bioactive materials, 635, 640
bioceramic composites, 6, 44
bioceramics, 6, 7, 28, 296, 305, 635–42, 646
biomaterials, 635
biomimetics, 648
biotite mica, 353
birefringence, 577
bismuth ruthenate (Bi₂Ru₂O₇), 5, 490
bismuthates, 113
Bitter technique, 610
Bitter, Francis, 616
Blaschka, Leopold, 477
Blaschka, Rudolph, 477
Bloch walls, 609
Bloch, Felix, 616
Blue John, 91
body-centered cubic (bcc), 72, 211
boehmite, 445
Bohr model, 36, 37, 49
Bohr, Neils, 48
Bollmann, Walter, 267
Boltzmann, Ludwig Eduard, 48, 199
Boltzmann's constant, 185, 626
bond strength, 88, 101
bonding, 35, 51, 154, 224, 228, 248
bonding, anodic, 284
bonding, covalent, 3, 4, 53, 58, 64, 66, 100, 208, 283
bonding, hydrogen, 66
bonding, ionic, 53, 64
bonding, metallic, 63, 64
bonding, mixed, 64, 83
bonding, van der Waals, 64, 65
bonds, primary, 51, 63
bonds, secondary, 51, 64, 100
bone china, 20, 422
Born, Max, 69
Born-Haber cycle, 51, 56
Born-Landé equation, 55, 56, 71, 621
Born-Mayer equation, 56
boron carbide (B₄C), 7, 14, 64, 71, 325

boron nitride (BN), 4, 62, 64, 65, 68, 69, 96
boron oxide (B₂O₃), 134, 193, 492
borosilicate glass, 474
Böttger, Johann Friedrich, 20, 30
Bowen's reaction series, 346
Bragg diffraction, 162
Bragg, W.H., 98, 162
Bragg, W.L., 98
Bravais lattice, 72, 73, 88, 101
Bravais, Auguste, 85
brazing, 284
Brewster angle, 658
brick, 4, 5, 6, 7, 142, 146
Bridgman, Percy Williams, 508, 524
Bridgman-Stockbarger method, 508, 509, 515
brittle fracture, 326
brittleness index (BI), 294
brittleness, 4, 294, 309, 325–27
brookite, 93
Brouwer diagrams, 188, 189
Brown, Robert, 424
Brunauer, Stephen, 369, 376
Brunauer–Emmett–Teller (BET) method, 369, 376
bubble memory, 614
buckyballs, 279, 523
buffer layer, 456
bulk diffusion, 457
bulk modulus, 292
Buerger, M.J., 310
Burgers vector, 111, 201, 202, 205, 206, 208, 209, 211, 219, 221, 222, 268, 271, 313
Burgers, Johannes (Jan) Martinus, 202, 221
Burgers, W.G., 221
Burne-Jones, Sir Edward Coley, 479

C
cadmium iodide (CdI₂), 87, 95
cadmium selenide (CdSe), 582
cadmium sulfide (CdS), 241, 387, 582
calcination, 351
calcining, 352
calcite, 72, 74, 85, 86, 103, 347, 462, 578, 585, 596
calcium aluminate cements (CAC), 111
calcium aluminates, 22, 110–111, 176
calcium carbonate (CaCO₃), 72, 86
calcium chloride (CaCl₂), 193, 194, 265
calcium fluoride (CaF₂), 87, 91, 98, 313, 315
calcium magnesium silicate, (CaMgSiO₄), 210
calcium oxide (CaO), 9, 22, 185, 194, 435
calcium phosphate, 20
calcium silicate (CaSiO₄), 22, 119
calcium sulphate, 653
calcium titanate (CaTiO₃), 79, 81, 102
calcium tungstate (CaWO₄), 508
calcium zirconate (CaZrO₃), 100
cancellous bone, 638, 644
capacitance, 565
capacitors, 566–7
capillarity, 230, 231
carbides, 3, 120
carbon nanotubes, 340, 523, 681
carbon, 26, 46
carnelian, 652
Carnot efficiency, 546
Cassius, Andreas, 397
Ca-stabilized cubic zirconia (CSZ), 189
casting, 412, 423
catalysis, 225, 242, 284
catalytic converters, 233, 687
cathodoluminescence, 585
cavitation, 319
cement, 22, 23, 111, 459
center of symmetry, 72
ceramic glass, 393
ceramic implant, 638
ceramic, green, 413, 482
ceramic, single-phase, 429
ceramic-matrix composites (CMC), 4, 5, 7, 22, 111, 297, 335, 341, 359, 373, 374, 375, 376, 378, 446, 496, 508, 681
ceramics, 3–14, 120, 181, 197, 232
ceramics, advanced, 5, 6, 7, 12, 14, 359, 360, 366, 376, 677
ceramics, biomimetic, 233
ceramics, cellular, 232
ceramics, color in, 580–83
ceramics, diamagnetic, 601, 616
ceramics, engineering, 6, 13, 14
ceramics, macroporous, 232
ceramics, magnetic, 598
ceramics, microporous, 232
ceramics, monolithic, 409
ceramics, nitrogen, 27
ceramics, optical, 575
ceramics, paramagnetic, 603
ceramics, polycrystalline, 8, 9, 248, 265
ceramics, porous, 2, 79, 422, 439, 440
ceramics, structural, 291
ceramics, thermal properties, 619
ceramics, tough, 28
ceramics, traditional, 4, 5, 6
ceramics, transparent, 5, 8
ceramming, 474
ceria (cerium oxide) (CeO₂), 173, 184, 339, 433, 655, 680
cesium bromide (CsBr), 88
cesium chloride (CsCl), 55, 56, 71, 77, 78, 81, 87, 88
cesium iodide (CsI), 88
chalcedony, 652
chalcogenides, 92, 95
Champion, Albert, 424
charge distribution, 224
chatoyancy, 661
chemical mechanical polishing (CMP), 339, 655, 680
chemical vapor deposition (CVD), 371, 494, 495–500, 549, 572, 586, 587, 594, 597, 628, 664
chemical vapor infiltration (CVI), 375, 496
chert, 15, 347
chrome ore, 26
chrome oxide (Cr₂O₃), 94, 387, 392
chromium dioxide (CrO₂), 93, 605, 615
chrysoberyl, 127, 661, 669
cinnabar, 652
citrine, 660, 670
Clark, William, 382
Clausius-Clapeyron equation, 122
clay, 4, 6, 7, 15, 19, 20, 22, 109, 120, 349, 357, 365, 413, 419, 438, 548, 677
clay, hard-porcelain, 422
climb dissociation, 211
climb, 213, 216, 217, 317
close-packed lattices, 84
close-packed structure, 79
coatings, 7, 407, 481, 485, 486
coatings, bioceramic, 645
cobalt oxide (CoO), 188, 195
cobaltous oxide, (Co₃O₄), 21, 392
Coble creep, 318, 442
Coble, Robert (Bob) L., 27, 442, 596
coefficient of thermal expansion, 619, 628
Coes, Loring, 98
coincidence-site lattice (CSL) theory, 247, 248, 267
Colburn-Libbey-Owens process, 469
cold isostatic pressing (CIP), 415
colloids, 360, 413
color centers, 190, 581
colossal magnetoresistance (CMR), 605, 606, 615, 616, 617
compliance curves, 301
composites, 3, 4, 5, 7, 376, 496
compression, 297
compressive strength, 5
computed tomography (CT), 157
computer modeling, 199
concentric cylinder (or Couette) viscometer, 405
concrete, 297
conduction band, 532
conductivity, 385, 537
controlled fracture, 339
convergent beam electron diffraction (CBED), 162, 168
Cooper pairs, 530, 551, 553, 554, 603
Cooper, Leon Neil, 554
coordination number (CN), 72, 76–80, 86, 88–90, 95, 99, 100, 101, 107, 112, 115, 116, 184, 200, 226, 562
copper (II) oxide (cupric oxide, CuO), 32, 87, 93, 145, 196, 390, 392
copper carbonate (CuCO₃), 390
cordierite (Mg₂Al₄Si₅O₁₈), 107, 630, 659
core, structure, 208
corrosion resistance, 338
corrosion, 392

- cortical bone, 638, 644
corundum structure, 605
corundum, 52, 94, 312, 351, 581
Couette flow, 405
Couette, Maurice Frédéric Alfred, 410
Coulter counter, 368, 376
Coulter, Wallace H., 376
crack resistance, 330
creep deformation map, 320, 321
creep resistance, 415
creep, 291, 309, 317–9
cristobalite, 100, 105, 106, 351
critical cracks, 331
critical resolved shear stress, 313
critical stress intensity factor, 294
crocidolite, 661
crystal chemistry, 87
crystal growth, 139, 157
crystal growth, hydrothermal, 507
crystal lattice, 71, 83
crystal point groups, 75
crystal structure, 81, 88, 98, 102–3, 106–11, 505
crystal systems, 72, 75
crystal templating, 276
crystallization, primary, 437
cubic zirconia (CZ, ZrO_2), 91, 181, 189, 194, 198, 325, 507, 514, 543, 653, 669
Cullinan, Sir Thomas, 673
cuprite (Cu_2O), 87, 93, 540
Curie law, 604
Curie, Jacques, 573, 617
Curie, Pierre, 573, 617
Curie-Weiss law, 605
Curl, Robert F. Jr, 118
curved interfaces, 461
cyclic fatigue, 332
cymophane, 661
Czochralski process, 191, 296, 508–9, 511–14, 516, 597, 679
Czochralski, Jan, 508, 524
- D**
Dana, James Dwight, 357
Danner, Edward, 382
Darken equation, 453
Davisson, C.J., 37, 48, 49
Davy, Sir Humphrey, 199
de Beer, Diederik Arnoldus, 673
de Beer, Johannes Nicholas, 673
de Broglie, Louis, 49
de Mortillet, Gabriel, 17
Debye frequency, 194
Debye temperature, 620
Debye, Petrus Josephus Wilhelmus, 624, 634
defects, 155, 157
deflocculents, 413, 417
densification, 427, 439
density of states, 67
desintering, 429
devitrite, 281
- dewetting, 231, 243, 247, 260, 261, 266, 453
diamagnetism, 618
diamond, 3–5, 7, 35, 47, 58–62, 66, 69, 71, 96, 125, 136, 325, 354, 521, 652–4, 660, 663–4
diamond-cubic (dc) structure, 90, 209
diatoms, 395
dielectric constant, 103, 558, 619
dielectric strength, 559
dielectrics, 491, 556–60, 577
dielectrics, relaxor, 565
differential interference contrast, 156
differential scanning calorimetry (DSC), 122
differential thermal analysis (DTA), 122, 176, 177
diffraction, 162, 168
diffraction, X-ray, 154, 162
diffusion, 192, 193, 195, 196, 198, 431
diffusion couples, 457
diffusion-controlled reaction, 458
diffusion-induced grain-boundary migration (DIGM), 436
diopside, 109, 662
dip coating, 484, 646
dipoles, 218
dislocation creep, 317
dislocation glide, 310
dislocation velocity, 315
dislocation, screw, 253
dislocations, 201–21, 246, 289, 551, 627
dislocations, core, 207, 209, 220, 221
dislocations, edge, 201–5, 208, 210, 214–7, 219, 222, 223
dislocations, misfit, 451, 454
dislocations, mixed, 202, 205
dislocations, observation of, 206
dislocations, partial, 205, 206, 211
dislocations, screw, 202–5, 215
dispersion, 656
displacement field, 204
displacement-shift-complete lattice (DSCL), 247, 271
dodecacalcium hepta-aluminate, 111
dolomite ($CaCO_3 \cdot MgCO_3$), 25, 26, 146, 347, 352
dopants, 387
doping, 190
drawing process, 469
Drude, Paul Karl Ludwig, 554
dry pressing, 414
Dulong-Petit law, 620
- E**
earthenware, 20, 22
Edison, Thomas, 382
elastic modulus, 289, 294, 301
elasticity, 203
electrical conduction, 3, 4, 6, 8, 9
electrical conductivity, 529, 619, 653
electrical insulators, 546
electrical resistivity, 385
- electroceramics, 27
electron affinity, 42, 44
electron backscattered diffraction (EBSD), 162, 168, 436
electron energy-loss spectroscopy (EELS), 168, 172, 173, 249
electron holes, 196
electron paramagnetic resonance (EPR), 279
electronegativity, 58, 64, 71
electronic defects, 183
electronic thermal conductivity, 626
electro-optic (EO) materials, 590
electro-optics, 592
electrophoresis, 486
electrophoretic deposition, 486, 645
Ellingham diagrams, 120, 121, 283
emerald ($Be_3Al_2(SiO_3)_6$), 519, 652–4, 660, 661, 664, 665
Emmett, Paul, 369, 376
enamel, 390, 392, 474, 580
enameling, 646
energy bands, 51, 66, 69
enstatite, 109
enthalpy of sublimation, 226
entropy charge, 235
environmental SEMs, 159, 241
Eötvös rule, 250
epitaxy, 233, 494
equilibrium, 120
ErAs, 208
etch pits, 208, 253, 228, 316
etching, 226
etch-pit method, 207, 268, 316
ettringite, 23
eutectic temperature, 121, 122, 128
eutectics, 121, 128, 281
evaporation, 500
exaggerated grain growth, 437–38
extrusion, 418
- F**
F centers, 190
face-centered cubic (fcc) lattice, 72, 79, 86, 87–9, 206, 211, 227, 255, 256
facets, 227
Faraday effect, 610
Faraday rotation, 614
fatigue, 325
fayalite, (Fe_2SiO_4), 105, 106, 210
 Fe_2O_3 , 5, 82, 94, 102, 130, 187, 200, 236, 255, 271, 390
 Fe_3C , 3
 Fe_3O_4 , 82, 200
feldspar, 19, 20, 47, 105, 114, 346, 348, 353, 357
 FeO , 82, 84, 86, 130, 187, 195, 390, 472, 686
FeRAMs, 569
Fermi function, 67
Fermi-Dirac function, 532
ferrimagnetism, 598, 606

- ferrites, 101, 266, 362, 598, 612–14
ferroelectric effect, 556
ferroelectric titanates, 27
ferroelectricity, 103, 560
ferromagnetism, 604, 606
FeS₂, 74, 79, 81, 87, 92
Feynman, Richard, 688
fiber elongation, 383, 384
fibers, 359, 363, 370, 372, 373, 375, 376, 400, 407, 408
Fick, Adolf Eugen, 199
Fick's laws, 47, 193, 461
film growth, 233–35, 242
films, 407
fining, 467
flame emission spectroscopy (FES), 370
flame spraying, 646
flame-fusion process, 508, 509
flash glass, 478
flash goggles, 593
flat glass, 468, 472
flaws, 327
flint glass, 382
flint, 15, 22, 325, 347, 380, 653
float glass, 26
float-glass process, 463, 468, 469, 470, 479
floating-zone (FZ) method, 508, 510
flocs, 360
fluorescence, 585, 588
fluorides, 92
fluorite, 91, 585, 660
fluorspar, 91
flux growth, 507, 519
foam glass, 473
foams, 232, 233
focused ion-beam (FIB), 207
formation, 224
forsterite (Mg₂SiO₄), 77, 105, 106, 210
Fourcault process, 469
Fourcault, Emile, 382
Fourier-transform IR (FTIR), 162, 163, 164, 176, 641
fractography, 332
fracture strength, 309, 315
fracture toughness, 294, 300, 307, 330, 335
fracture, 325
fracture, conchoidal, 333, 325
fragility, 380
FRAMs, 569
Frank, Sir Charles, 221
Frank's rule, 203
Frank-Read source, 216, 217, 219, 315
Frenkel defects, 182–4, 186, 187, 200, 619
Frenkel pairs, 191
Frenkel, Jacov Il'ich, 199
Fresnel's equation, 577
Friedel, G., 267
Friedel, J., 267
frit bonding, 490
fuel cells, 28, 544
Fulcher equation, 318
fulgarites, 394
Fuller, Richard Buckminster, 118
fullerenes, 113, 114, 356
furnaces, 139–51
fused deposition modeling (FDM), 420
fused silica, 394
fusing, 350
G
gadolinium gallium garnet (GGG), 614
gahnite, 668
galena, 652
Gallé, Émile, 479
gallium arsenide (GaAs), 77, 87, 89, 90, 183, 211, 236, 269, 502, 508
gallium nitride (GaN), 3, 4, 64, 68, 71, 168, 209, 220, 269, 588
gallium oxide (Ga₂O₃), 94
garnet (Ca₃Al₂(SiO₄)₃), 607, 614
garnets, 84, 107, 252, 347, 519, 654, 660, 662, 668, 669
Gay, D.H., 200
Generalized Utility Lattice Program (GULP), 84, 85
GeO₂, 579
germanium, 67
Germer, Lester Halbert, 37, 48
giant magnetoresistance (GMR), 606, 615, 617
Gibbs adsorption, 251
Gibbs free energy, 45–7, 81, 82, 121, 123, 134, 184, 185, 194, 234, 277, 406, 431, 445, 497
Gibbs phase rule, 121, 124
Gibbs triangle, 128, 130
Gibbs, Josiah Willard, 134
Gibbs-Thompson effect, 461
Gilchrist Percy, 25
Gillinder, William, 25
glass blowing, 24, 463, 470
glass ionomer cements (GIC), 460
glass laser, 388
glass microspheres, 479
glass processing, 463–74
glass, 4–8, 12–14, 24, 25, 48, 82, 100, 116, 117, 120, 133, 139, 181, 325, 408, 433, 259, 264, 270, 278, 677
glass, borate, 394
glass, calcium phosphate (Ca₃(PO₄)₂), 476
glass, ceramic, 380
glass, chalcogenide, 394
glass, coating, 472
glass, coloring, 386
glass, crown, 394
glass, crystallization, 458
glass, defects in, 386
glass, definition of, 379
glass, electrical properties of, 385
glass, flint, 393
glass, halide, 394
glass, heterogeneous, 386
glass, history of, 380
glass, lead, 393
glass, lead-crystal, 25
glass, mechanical properties of, 385
glass, metallic, 380
glass, natural, 394
glass, optical properties of, 385
glass, phosphate, 394
glass, polymer, 380
glass, safety, 297
glass, silicate, 384, 393
glass, structure of, 379, 380, 397
glass, thermal properties of, 385
glass-ceramics, 25, 27, 32, 458, 474, 475, 641
glassmaking, 29
glaze, lead, 20, 22, 32
glaze, tin, 18, 20, 21
glazes, 20, 390, 459, 413, 439, 580, 632
glide bands, 311
glide dissociation, 211
glide plane, 202, 206, 208, 215–7, 312
glide, 216, 317
Glow Discharge Ion Source, 172
goethite, 615
Goldschmidt, Victor Moritz, 85
Gouy method, 604
grain boundaries (GBs), 197, 246, 268, 277, 289, 314, 315, 318, 319, 338, 427, 444, 448, 455, 458, 495, 551, 566, 583, 593
grain boundaries, low-angle, 275, 515, 561
grain boundary, mixed, 246
grain boundary, properties, 265
grain boundary, sliding, 318
grain boundary, tilt, 246
grain boundary, twin, 246
grain boundary, twist, 246
grain growth, 431, 435–37
grain morphology, 246
grain size, 427, 437
grain-boundary diffusion, 457
grain-boundary energy, 249
grain-boundary films, 259
grain-boundary grooves, 262, 263, 267
grain-boundary low-angle tilt, 252
grain-boundary low-energy, 251
grain-boundary migration, 432
grain-boundary pinning, 434
grain-boundary, high-angle, 254, 603
grain-growth inhibitor, 459
granite, 346, 353
granules, 360
graphite, 1, 3, 30, 47, 61, 62, 65, 66, 69, 95, 96, 114, 136, 145, 211, 212, 296, 313, 354–8, 415, 426, 439, 495, 521, 523
graphite, pyrolytic, 646
green body, 428, 429, 439, 440
green machining, 420
Griffith equation, 327
Griffith, Alan Arnold, 325, 327, 339, 340
grinding, 339, 652
grossular, 119

Grove, Sir William Robert, 28, 554
gypsum ($\text{CaSO}_4 \cdot 2\text{H}_2\text{O}$), 32, 347, 350, 450, 653

H

Haber, Fritz, 69
halides, 88
halite, 88, 585
Hall–Heroult cells, 356
Hall–Petch equation, 266, 315
halophytes, 381
Hamada, Shoji, 424
Hamaker constant, 65, 66
Hankel, W.G., 573
hardening, 316
hardness tests, 299, 300
hardness, 292, 294, 299, 301, 307, 338
Hashin and Shtrikman (HS) bounds, 295
Hashin-Shtrikman model, 308
Haüy, René-Just, 85
heat capacity, 619–21
heat transfer, 148
heat-exchange method (HEM), 516
Heisenberg uncertainty principle, 37
Heisenberg, Werner, 49
Helmholtz-Smoluchowski equation, 487
hematite (Fe_2O_3), 82, 94, 276, 339, 345, 361, 446, 615, 652, 656
Hermann-Mauguin notation, 74
Herring, W. Conyers, 323
Hess's law, 56
heterojunctions, 271, 289
hexagonal close-packing (hcp), 79, 87, 94, 95, 209
hibonite, 111
high-alumina cement (HAC), 11, 460
highest occupied molecular orbital (HOMO), 66
high-resolution STEM, 192
high-resolution transmission electron microscopy (HRTEM), 90, 160, 201, 207, 213, 229, 238, 250, 254, 259, 264, 266, 272, 282, 319, 409
high-temperature ceramic superconductors, 6
high-temperature superconductors (HTSC), 4, 7, 12, 27, 112, 113, 269, 495, 529, 551–54, 598, 602, 675, 681
Hockman, George A., 27
holosymmetric point group, 74
Hooke, Robert, 85, 221
Hooke's law, 203, 206, 327
Hoover Dam, 23
hot forging, 434
hot isostatic pressing (HIP), 416, 643, 645
hot pressing, 414, 429, 433
hot-pressed silicon nitride (HPSN), 27
hot-stage XRD, 171
Houghton Sr, Amory, 382
Hume-Rothery rules, 187
Hume-Rothery, William, 134
Hund's rule, 39, 603

Huygens, Christian, 294
hybrid orbitals, 60, 61, 62, 63
hybridization, 51, 60–3, 69, 71
hydrogen storage, 686
hydrothermal method, 517
hydroxyapatite (HA), 7, 635, 642–44

I

illite, 109
ilmenite (FeTiO_3), 94, 102, 345, 353, 565
image, bright-field, 159, 160
image, BSE, 158
image, CT scans, 157
image, dark-field, 156, 159, 160, 273, 310
image, infra-red (IR), 156
image, IR, 217
image, ultraviolet (UV), 156
image, X-ray, 157
imaging, 154, 155
immiscibility, 386
impurities, 270
indentation test, 299
indium oxide (In_2O_3), 94, 158, 453
indium phosphide (InP), 502
induction skull melting (ISM), 514
Inglis equation, 329
Inglis, Sir Charles Edward, 340
injection molding, 419
integrated circuits (IC), 548
interfaces, 87, 155, 224–6, 444, 558
interfacial energies, 231, 232, 270
interferometer, 163
intergranular film (IGF), 270, 280, 318, 319, 323, 541, 583
International Union of Crystallography, 98
interstitials, 182, 183
inverse spinel, 184
inversion axis, 72
invisibility criterion, 207
iolite, 659
ion-beam-assisted deposition (IBAD), 504
ionic conductivity, 197
ionic radius, 57
ionization energy, 36, 42, 44, 53
iridescence, 662
iron oxide (Fe_2O_3), 22, 351
iron, 25, 598
isoelectric point (IEP), 488

J

jadeite, 109
jasper, 15, 652
jeweler's rouge, 339, 655
jog, 206, 214, 215, 216, 223, 239
Jomon, 17
Josephson junction, 266, 554, 603
Josephson, Brian David, 617
Joule, James Prescott, 151

K

Kao, Charles K., 27
kaolin, 19, 20, 348, 349, 350, 357

kaolinite ($\text{Al}_2\text{O}_3 \cdot 2\text{SiO}_2 \cdot 2\text{H}_2\text{O}$), 19, 66, 109, 120, 146, 548
Kawai, Kanjiro, 424
KBr, 309, 310
KCl, 52, 56, 71, 160, 193, 194, 315
Keck, Donald, 27
keramos, 4
Kerr effect, 590, 592, 610
kinetics, 35, 47, 48, 181
Kingery, W. David, 30, 442
kink, 206, 214, 215, 216, 227, 239
Kirchhoff, Gustav Robert, 151
Kirchhoff's law, 141
Kirkendall effect, 449
 KNbO_3 , 102
 KNO_3 , 487
Kröger, Ferdinand Anne, 199
Kröger-Vink notation, 183, 187, 200, 540, 547, 628
Kroto, Sir Harold W., 118
kyanite (Al_2OSiO_4), 72, 77, 100, 350, 663

L

La Farge, John, 397
labradorescence, 662
labradorite feldspar, 660, 662
Lalique, René, 479
Lambert's law, 577
LaMer diagram, 364
laminated glass, 473
lanthanum phosphate (LaPO_4), 112
Lanxide process, 375, 376
lapis lazuli, 652, 660
laser Raman microprobe, 165
lattice energy, 51, 55
lattice misfit, 272, 282, 454
lattice mismatch, 505, 594
lattice parameter, 71, 87, 101, 122, 192, 211, 323
lattice points, 71, 72, 75
lattice spacing, 327
Laue technique, 171
Le Chatelier, Henry, 134
Leach, Bernard Howell, 424
lead iron niobate (PFN), 565
lead iron tungstate (PFW), 565
lead magnesium niobate ($\text{PbMg}_{1/3}\text{Nb}_{2/3}\text{O}_3$ or PMN), 565
lead oxide (PbO), 20, 25
lead ruthenate ($\text{Pb}_2\text{Ru}_2\text{O}_6$), 490
lead titanate (PbTiO_3), 570
lead zirconate (PbZrO_3), 570
lead zirconate titanate (PZT), 7, 27, 400, 570, 572, 624
lead, 22
lead-crystal glass, 382
Lennard-Jones potential, 64
Lenz, Heinrich Friedrich Emil, 617
Libbey-Owens process, 469
Libyan desert glass, 394, 399
ligand field, 580, 660
lime, 22

line defects, 202
 Lipperhey, Hans, 397
 liquid-crystal templating (LCT), 440
 liquid-phase sintering (LPS), 139, 146, 319, 678
 liquidus, 121, 122, 123, 128
 litharge (PbO), 370
 lithium fluoride (LiF), 53, 57, 58, 310, 311, 316
 lithium niobate (LiNbO₃), 516, 565
 lithium, 39
 lithium-alumino-silicates (LAS), 632
 Littleton, Harvey K., 479
 load-displacement curve, 301
 lodestone, 598
 Lomer-Cottrell dislocation, 218
 London, Fritz, 617
 London, Heinz, 617
 long-range order (LRO), 83, 100, 379, 380, 387
 Lord Rayleigh. See Strutt, John William
 Lorentz force, 611
 Lorentz-Lorentz equation, 578
 low-energy electron diffraction (LEED), 174, 236, 238
 low-energy electron microscopy (LEEM), 240
 lowest unoccupied molecular orbital (LUMO), 66
 low-temperature isotropic (LTI) carbon, 646–7
 low-temperature superconductors (LTSC), 551–54
 Lubbers, John, 382
 Lubbock, John, 17
 Lucalox, 27
 luminescence, 588

M

machinable glass-ceramics (MGC), 338
 Madelung constant, 54, 55, 66, 84, 242
 Madelung, Erwin, 69
 maghemite, 102, 615, 616
 magnesite (MgCO₃), 26, 352
 magnesium fluoride (MgF₂), 580
 magnesium hydroxide (Mg(OH)₂), 352
 magnesium oxide (MgO, magnesia), 8, 26, 27, 52, 55, 56, 64, 72, 74, 77, 84, 86–8, 123, 158, 208, 215, 218, 226, 232, 239, 250, 255, 261, 262, 265, 268, 271, 307–10, 313, 314, 316, 319, 323, 326, 330, 340, 352, 432, 435, 436, 446, 452, 504, 547, 585, 630
 magnetic behavior, 619
 magnetic dipole, 599
 magnetic domains, 610
 magnetic ferrites, 27
 magnetic flux density, 601
 magnetic force microscopy (MFM), 610, 611
 magnetic levitation (maglev), 603, 681
 magnetic materials, 598

magnetic moment, 599
 magnetism, 598
 magnetite (Fe₃O₄), 35, 82, 130, 446, 598, 606, 615, 668
 magnetoencephalography (MEG), 603
 magnetoplumbite structure, 607
 magnetoplumbite, 110, 608
 malachite, 660
 manganates, 120, 598, 616
 markers, 452
 MARVIN, 200, 242
 mass spectrometry, 172
 Matthews, John, 267
 Maurer, Robert, 27
 Maxwell, James Clark, 177, 596
 Maxwell's equations, 576, 586
 mayenite, 111
 Megaw, Helen Dick, 118
 Meissner effect, 602, 603, 617
 Meissner, Walter, 617
 melaconite, 93
 Mergules viscometer, 383, 406
 metal oxide semiconductor field effect transistor (MOSFET), 499, 549
 metal oxides, 9, 146
 metal-matrix composites (MMC), 359, 374, 375, 376, 681
 metal-oxide-semiconductor (MOS), 549
 metals, 3–5, 56, 57, 63, 64, 67, 68, 71, 83, 84, 120
 metasilicates, 107
 Mg₂SiO₄, 77, 210
 MgAl₂O₄, 101, 252, 265, 268, 315
 MgCO₃, 26
 MgF₂, 93
 MgFe₂O₄, 511
 MgIn₂O₄, 158, 453
 MgO smoke experiment, 250, 267
 MgSiO₃, 103
 mica, KAl₃Si₃O₁₀(OH)₂, 19, 100, 108, 348, 349, 365, 439, 475, 567, 585
 microdiffractometer, 171
 microelectromechanical systems (MEMS), 7, 27, 407, 410, 411, 485, 556, 572
 microprobe, 449
 microstructure, 3, 5, 8, 154
 Miller indices, 75, 76
 Miller, William Hallows, 85
 Miller–Bravais indices, 75, 76, 94, 95
 milling, 360–1
 mineral formation, 345
 mirror plane, 72
 miscibility gap, 133, 386
 misfit dislocation, 282
 misplaced atoms, 182
 Mn_{0.4}Zn_{0.6}Fe₂O₄, 5
 MnO, 195
 MnO₂, 25, 93, 392
 mobility, particle, 487
 modified chemical-vapor deposition (MCVD) process, 587
 modulus of rupture (MOR), 298, 307

Mohs scratch hardness scale, 294, 663, 667
 Mohs scratch test, 674
 Mohs, Fredrich, 306, 673
 Moissan, Ferdinand Frédéric-Henri, 98, 357, 673
 moissanite, 71, 91, 653, 664
 molar heat capacity, 620
 moldavite, 394
 molding, 423
 molecular dynamic (MD), 82, 84
 molecular orbitals, 58, 59, 66
 molecular-beam epitaxy (MBE), 481, 494, 502
 molten carbonate fuel cell (MCFC), 545
 molybdenite, 95
 molybdenum carbide (Mo₂C), 63, 686
 molybdenum dioxide (MoO₂), 686
 molybdenum disilicide (MoSi₂), 145, 439
 molybdenum sulfide (MoS₂), 62, 65, 87, 95, 96, 211, 296
 molybdenum trioxide (MoO₃), 146
 molybdenum, 146
 monazite, 71, 72, 111, 446
 monticellite, (Ca(Mg,Fe)SiO₄), 106, 210, 458
 montmorillonite, 109, 439
 moonstone, 662
 Morse, Samuel, 152
 Mossbauer analysis, 177
 Mössbauer spectrum, 167
 Mössbauer, Rudolf, 176
 muffle glass, 470
 Müller, Karl Alexander, 28, 30, 31
 Mullins, William W., 267
 mullite, 111, 348, 350, 357, 375, 462, 466
 multilayer chip capacitor (MLCC), 566, 568, 643, 678, 687
 muscovite mica, 346, 349, 357
 Mynon, pit of, 24

N

Na₂O, 117, 134
 Na₂SO₄, 468
 Nabarro, Frank Reginald Nunes, 323
 Nabarro-Herring creep, 318, 323
 Nabarro-Herring source, 217
 NaCl, 52, 53, 54, 55, 56, 57, 58, 71, 74, 77, 78, 81, 87, 88, 89, 183, 190, 197, 198, 208, 209, 214, 215, 226, 265, 310, 313, 468
 nanobioceramics, 647
 nanoceramics, 7, 8, 12
 nanoindentation test, 301
 nanomaterials, 441, 636
 nanoparticles, 228, 241, 242, 250, 273, 360, 365, 376, 409, 441, 616
 nanotubes, 113, 114, 160
 NbN, 63
 Nd₂O₃, 191
 Nd-YAG laser, 589

- near-field scanning optical microscopy (NSOM), 156, 157, 236, 244, 478
- Néel, Louis, 27, 598
- Neri, Antonio, 382
- Nernst-Einstein equations, 198
- neutron activation analysis (NAA), 175
- neutron scattering, 172
- NiAl, 88, 185
- NiFe₂O₄, 184, 271, 275, 511
- NiO, 47, 123, 159, 160, 195, 236, 251, 252, 254, 257, 265, 271, 273, 277, 456
- nitrides, 63, 113, 120
- nitrum, 381
- nodes, 218
- Nomarski, 156
- Norton, Frederick Harwood, 152
- nuclear energy, 26
- nuclear magnetic resonance (NMR), 165, 166, 177, 279, 370
- nucleation, 233, 276
- O**
- obsidian, 15, 358, 379, 380, 394, 653
- Ochsenfeld, Robert, 617
- Oersted, Hans Christian, 599, 617
- Ohm's law, 141
- olivine, 106, 209, 268, 346, 669
- Onnes, Heike Kamerlingh, 554
- opal, 428, 585, 653, 660, 666
- optical fibers, 25, 27, 586–88
- optical transparency, 593
- orbital hybridization, 63
- orbital motion, 599
- ores, 277–80
- orientation, 313
- Orowan equation, 326, 327
- Orowan, Egon, 340
- orthoclase (KAlSi₃O₈), 548
- Orton cones, 150
- Orton Jr., Edward J., 30, 152
- Ostwald ripening, 231, 272, 409, 427, 438
- Ostwald viscometer, 405
- Ostwald, Wilhelm, 410
- outside vapor-phase oxidation (OVPO), 586
- Owens, Michael, 382, 479
- oxides, 87, 88, 92, 93, 120, 228, 236
- oxygen partial pressure (p_{O_2}), 120, 121, 126, 130, 131, 188, 191, 195, 196
- oxynitrides, 120
- P**
- paper clay, 422
- paraelectric, 562, 563
- parallel electron energy-loss spectra (PEELS), 172
- Paris-Erdogan equation, 332
- partial dislocations, 252
- partially stabilized zirconia (PSZ), 28
- particle growth, 276, 454
- particle-induced X-ray emission (PIXE), 169
- particles, 269, 270, 272, 276, 360
- Pascal, Blaise, 397, 505
- paté de verre, 434, 477
- Pauli exclusion principle, 39, 604
- Pauli paramagnetism, 603
- Pauli, Wolfgang, 49
- Pauling, Linus Carl, 49, 71, 76, 77, 79, 85, 86
- Pauling's classification, 45
- Pauling's rules, 71, 76, 82–4, 87, 88, 94, 98, 104, 119, 126, 562
- Pb(Zr_xTi_{1-x})O₃, 7
- PbO, 25, 391, 492, 684
- PbS, 208, 310
- PbTe, 310
- PbTiO₃, 391, 565
- Pearson, 81
- Pechini method, 364, 377
- pegmatites, 353
- Peierls barrier, 216
- Peierls valley, 216, 217, 222
- Peierls, Sir Rudolf Ernst, 222, 625
- Peierls-Nabarro force, 222, 323
- Peierls-Nabarro stress, 313, 315
- periclase (MgO), 26, 88, 352
- peridot, 653, 669
- peridotite, (Mg_{0.9}Fe_{0.1})₂SiO₄, 106
- perovskite structure, 565
- perovskite, 100, 102, 103, 112, 118, 119, 448
- Perrot, Bernard, 382, 397
- P-glass, 499
- phase boundaries (PB), 269–70, 277, 440, 444, 448, 449, 451, 454, 455
- phase diagrams, 120, 121, 386, 570, 516
- phase rule, 47
- phase transformations, 71, 139, 148, 276, 444–45, 447, 459, 619
- phlogopite mica, 109, 357, 475
- phonon (lattice transport), 619
- phonon, 624
- phosphor, 588
- phosphorescence, 585, 588
- phosphorus, 25
- phosphorus-doped glass, 499
- photochromic glass, 474
- photoelectrochemical (PEC) solar cells, 687, 688
- photoelectron spectroscopy (PES), 174
- photosensitive glass, 474
- phyllosilicates, 349
- physical vapor deposition (PVD), 494, 572, 580
- Piccolpasso, Cipriano, 150, 391
- piezoelectric effect, 103, 556
- piezoelectric materials, 507
- piezoelectricity, 71, 84, 569
- pigments, 581
- Pilkington, Sir Alastair, 26, 30, 382
- pillared interlayered clays (PILC), 439
- pinning, 315
- Pittsburgh process, 469
- plagioclase feldspar, 662
- planar defect, 205, 206
- Planck's constant, 624
- plasma spraying, 485, 645
- plaster of Paris (2CaSO₄·H₂O), 24, 653
- plastic deformation, 296, 309, 313, 314, 325
- plastic forming, 412
- plasticity, 299, 309–23, 413
- plasticizer, 413
- platelets, 359, 365
- pleochroism, 658
- Pliny the Elder, 24
- PLZT, 5, 8, 591–94, 597
- pneumoconiosis, 22
- Pockels effect, 590, 592
- point defects, 87, 181, 183, 185, 187, 189, 191, 194, 199, 200, 202, 323, 387
- point groups, 75
- Poiseuille, Jean Louis Marie, 397
- Poisson, Siméon Denis, 306
- Poisson's ratio, 203, 292, 301
- polarizability, 578
- polaron, 533
- pole figure, 171
- polishing, 339
- polymer-matrix composites (PMC), 374, 359, 376, 681
- polymers, 3, 5
- polymorphs, 48, 81, 82, 84, 96, 105, 111, 154
- polytype, 118
- polytypes, 96, 97
- polytypoids, 96
- porcelain enamel, 6, 7, 632, 677
- porcelain, 18–20, 47, 548
- porcelains, feldspathic, 648
- pores, 269, 270, 285, 319
- porosity, 319, 278, 295, 583, 613, 626, 643
- porous coating, 536
- positive temperature coefficient (PTC), 534
- potassium dihydrogen phosphate (KH₂PO₄), (KDP), 27, 157
- pottery, 19–21, 439, 459, 632
- powder compaction, 412
- Powder Diffraction File (PDF), 170
- powders, 359–65, 400, 407
- pozzolana, 22
- precipitate-free zones (PFZ), 274
- precipitation, 363, 448
- pressure enhanced CVD, 572
- primitive cell, 71, 72
- primitive lattice, 72
- proportional limit, 309
- proton exchange membrane (PEM) fuel cells, 686
- pseudo-potential, 84
- pulsed laser deposition (PLD), 453, 503
- pumice, 232, 279, 395
- pyralispites, 669
- pyrite, 92
- pyrochlore (CaNaNb₂O₆F), 565
- pyroelectric effect, 556
- pyroelectricity, 572

pyrolusite, 25
 pyrolytic carbon, 649
 pyrometers, 149
 pyrometric cones, 150
 pyrope garnet, 660
 pyrope, 669
 pyrophanite (MnTiO₃), 345
 pyrophyllite, 65, 521
 pyroxene, 109, 110
 PZT, see lead zirconate titanate 407, 410, 411, 445, 570, 572

Q
 quadruple junctions (QJ), 246, 261–263, 280, 433
 quantum numbers, 35–9, 50
 quartz, (SiO₂), 19, 20, 48, 66, 105, 177, 220, 221, 255, 346–9, 353, 358, 361, 475, 507, 548, 571, 621, 630, 652, 661, 667, 669
 quartz, cryptocrystalline, 15
 quaternary diagrams, 132

R
 Rakuyaki, Chojiro, 397
 Raman spectra, 164
 Raman spectroscopy, 164, 165, 176
 Raman, Sir Chandrasekhara Venkata, 176
 Ramsdell notation, 96, 132
 Raoult's law, 122
 rapid prototyping (RP), 420
 Ravenscroft, George, 30, 382
 Rayleigh scattering, 164, 588
 reaction-barrier layer, 456
 reaction-bonded silicon nitride (RBSN), 27
 reactive bonding, 490
 reactive evaporation (RE), 501
 reactive sputtering, 501
 Read-Shockley formula, 250
 recrystallization, secondary, 437
 recycling, 683
 red lead (Pb₃O₄), 370
 reflection electron microscopy (REM), 239, 240
 reflection high-energy electron diffraction (RHEED), 162, 176, 236, 238
 reflection, 577
 reflectivity, 579
 refraction, 577, 578
 refractive index, 577, 578, 656
 refractories, 4, 6, 7, 14, 25, 120, 358, 466, 467, 621, 677
 Reid, A., 37
 ReO₃, 4
 residual stress measurement, 165
 Reuss model, 295, 308, 310
 Reynolds number, 367, 377
 Reynolds, Osborne, 377
 rhinestones, 667
 rhodolite, 669
 Richard's rule, 621, 623
 Ringer, Sidney, 306

Ringer's solution, 296
 Rochelle salt, 573
 rocks, igneous, 346, 349, 353
 rocks, metamorphic, 346, 349
 rocks, sedimentary, 347
 rocksalt structure, 310, 605
 rocksalt, 88, 126, 183, 265
 Rohl, A.L., 200
 Rohrer, Heinrich, 176, 243
 rotation axis, 72
 ruby laser, 589
 ruby, 507, 510, 575, 652, 653, 654, 660, 662, 665
 Rupert, Prince of Bavaria, 397
 ruthenium dioxide (RuO₂), 490
 Rutherford backscattering spectrometry (RBS), 162, 168, 169, 450
 Rutherford, Ernest, 177
 rutile (TiO₂, titania), 93, 94, 239, 274, 347, 353, 664

S
 safety glass, 473
 sand, 24, 683
 sapphire, 94, 95, 209, 210, 215, 235, 249, 264, 268, 270, 301, 327, 450, 458, 507, 509, 513, 516, 652, 653, 654, 660, 661, 662, 665, 669, 670
 scanned probe microscopy (SPM), 161, 235
 scanning Auger microscopy (SAM), 174
 scanning electron microscopy (SEM)
 image, 389, 395, 595, 666
 scanning electron microscopy (SEM), 23, 235, 237, 239, 241, 262, 278, 279, 366, 449, 455, 501
 scanning tunneling microscopy (STM), 161, 236, 240, 263, 571, 610
 scapolite, 585
 scattering, 162, 171
 scheelite, 585
 Scherrer equation, 369
 Schmalzried, Hermann, 461
 Schmid-Viechnicki method, 516
 Schott, Otto, 382, 479
 Schottky defects, 265, 268, 619
 Schottky formation energy, 194
 Schottky, Walter, 199
 Schrieffer, John Robert, 554
 Schrödinger wave equation, 37
 Schrödinger, Erwin, 49
 Schultz, Peter, 27
 screen-printing, 488
 Seabright, C.A., 596
 secondary electrons (SEs), 158
 secondary ion mass spectrometry (SIMS), 172
 sedimentation, 367
 Seebeck, Thomas Johann, 149, 152
 seeding, 438
 Seger, Hermann A., 30
 Seignette, Pierre, 573
 selected area diffraction (SAD), 162, 168

self-energy, 253
 semiconductor devices, 498
 semiconductors, 3, 4, 12, 67, 68, 83, 89, 90, 91, 92, 93, 183, 192, 208, 226, 255, 270, 537, 632
 shaping, 412, 422, 438, 463
 shear modulus, 203, 292, 301
 shear stress, 313
 Shockley partial dislocations, 206
 short-range order (SRO), 83, 380
 SiAlONs, 113, 118
 Siegbahn, Kai, 98
 Siegbahn, Karl Manne, 98
 Siemens, C.W., 382
 Siemens, F., 382
 sieving, 366, 376
 silane (SiH₄), 677
 silica (SiO₂), 4, 6, 96, 100, 105, 116, 125, 301, 348, 351, 466
 silica glass, 379
 silicates, 100, 101, 104, 105, 107
 silicon carbide (SiC), 4, 5, 7, 62, 64, 66, 68, 71, 89, 96–7, 144–5, 151, 182–3, 211, 220, 269, 282, 296, 308, 322, 327, 354, 364–5, 415, 427, 428, 522
 silicon dioxide (SiO₂), 5, 15, 20, 22, 48, 100, 122, 125, 134, 136, 177, 269, 391, 396, 498, 549, 568, 572, 579, 666, 683
 silicon nitride (Si₃N₄), 5, 7, 27, 113, 259, 260, 262, 266, 296, 303, 304, 354, 355, 364, 376, 415, 498, 568, 572, 677, 678
 silicon oxynitride (Si₂N₂O), 119
 silicon, 157
 sillimanite, 100, 351
 silver bromide (AgBr), 182, 186, 200
 simple-cubic (sc) lattice, 87, 88
 Simpson, Edward, 30
 single-edged notched beam (SENB), 298–9
 single-walled nanotube (SWNT), 114
 sintering, 139, 225, 248, 270, 350, 360, 413, 427–29
 SiO₄, 104, 113
 skull melting process, 514, 515
 Slater-Bethe curve, 604
 slip, 310, 314, 413
 slip bands, 311
 slip casting, 417, 450
 slip planes, 209
 slip systems, 310, 312, 314
 slurry, 412, 413, 482, 492
 Smalley, Robert E., 118
 smectite, 109
 Snell's law, 586
 SnO₂, 5, 93, 391
 Snoeck, J.J., 598
 soda-lime silicate glass, 464
 sodalite, 115
 sodium carbonate (Na₂CO₃), 463
 sodium vapor lamp, 584
 sol-gel process, 363, 359, 364, 371, 377, 400–401, 403–6, 474, 484, 594, 646
 solid casting, 418

- solid freeform fabrication (SFF), 420
solid solutions, 187
solid-oxide fuel cell (SOFC), 28, 32, 181, 545
solid-state laser, 575, 589, 597
solid-state reactions, 444, 445, 449
solid-state sintering, 428
solidus, 123
solubility, 363
solvus lines, 121
space group, 81
spark source mass spectrometry (SSMS), 172
specific heat, 620
spectroscopy, 154, 163
spectroscopy, IR, 163, 164
spectroscopy, Mössbauer, 155, 163–7, 172
spectroscopy, NMR, 165
spectroscopy, Raman, 163, 164
sphalerite (ZnS), 353, 585, 656, 660
spherulites, 281
spin coating, 484
spin, 599
spinel, 101, 102, 106, 110, 118, 127, 161, 162, 182, 211, 213, 218, 227, 228, 239, 253, 254, 255, 256, 258, 268, 274, 311, 450, 454, 456
spinel, 668
splat quenching, 380
Spode, Josiah, 20, 424
spodumene, 109, 110
spray drying, 362
spraying, 485
sputtering, 501, 594, 645
SrO, 242
SrTiO₃, 102, 160, 364, 552, 565
stacking fault (SF), 205, 253
stacking-fault energy (SFE), 206, 211, 212, 218, 253
standard test method, 383
static fatigue, 331
steel, 3, 7, 14, 25
Stefan-Boltzmann constant, 150, 625
Stefan-Boltzmann law, 149
stereolithography (SLA), 420
steric hindrance, 482
Stirling's approximation, 185
stishovite, 93
Stokes law of fluorescence, 585
Stokes scattering, 164
Stokes, Sir George Gabriel, 177, 377
Stokes' law, 367–8, 467, 487
Stookey, S. Donald, 27, 382, 479
strain, 289, 330
strain energy, 204, 206
strain fields, 157, 204
stress birefringence, 579
stress corrosion cracking (SCC), 331
stress intensity factor, 293, 329
stress rupture, 331
stress shielding, 639
stress, 289, 313, 315, 330
stress-probability-time diagrams (SPT), 305
stress-strain curves, 290, 296, 310, 314, 335
structure, 154, 181, 211
structure, antifluorite, 92
Strukturbericht, 81, 85
Strutt, John William (Lord Rayleigh), 177
sublattice, 88
substitutional defects, 183
substrate, 504
superconducting quantum interference devices (SQUIDS), 603
superconductivity, 63, 113, 551, 681
superconductors, 113, 120, 197, 242, 255, 265, 601
superconductors, non-metallic, 552
superplasticity, 322
surface charge, 242
surface diffusion, 228
surface energy, 224, 225, 226, 327, 328
Surface Evolver, 242
surface stress, 225
surface structure, 227
surface tension, 225, 230, 284
surface-enhanced Raman scattering (SERS), 165
surfaces, 224–25
surfactants, 231, 284
symmetry, 71, 72, 74, 75, 82, 84, 85, 86
Syngé, E.H., 244
Système International d'Unités (SI), 10, 11, 12, 124, 347, 383, 600, 619
- T**
talc, 211, 212, 296, 683
tantalite, 683
tantalum nitride (TaN), 490
tantalum pentoxide (Ta₂O₅), 683
tanzanite, 659, 660, 669
tape casting, 481–84, 482, 483, 492, 568
tektites, 394
Teller, Edward, 369, 376
temperature coefficient of resistivity (TCR), 491, 534, 536, 541
temperature stability, 536
tempered glass, 473
tenorite, 93
tensile strength, 297, 328
tensile stress, 579
tensile test, 296
tension, 297
tephroite (Mn₂SiO₄), 106
ternary systems, 128
tetragonal zirconia polycrystals (TZP), 28
thallates, 113
theoretical strength, 327
thermal analysis, 154, 175
thermal barrier coatings (TBC), 269, 446, 461, 621
thermal conduction, 4, 9, 91, 147, 260, 266, 415, 619, 624–28, 653, 663
thermal conduction module (TCM), 438
thermal etching, 219
thermal shock resistance, 633
thermally grown oxide (TGO), 446
thermistors, 541
thermochemical processing, 685
thermocouples, 149
thermodynamic equilibrium, 248
thermodynamics, 35, 45, 47, 48
thermogravimetric analysis (TGA), 176, 177
thermoluminescence, 585
thick-film circuits, 488–92
thin films, 264, 481, 494
thin-film diffractometer, 170
ThO₂, 112, 184, 435
Thomas Sidney Gilchrist, 25
Thompson-Freundlich equation, 461
Thomsen, Christian, 17
Thomson, George Paget, 37, 49, 98
Thomson, Joseph John, 48, 49, 98
Thomson, William (Lord Kelvin), 634
TiC, 63, 208, 315, 354
tiger-eye, 661
tilt boundary, 247, 253, 261, 268, 436
tilt, 254, 268
tin oxide (SnO₂), 145, 652
TiN, 5, 63, 219
TiO, 534
titanates, 93, 362
titania (TiO₂), 87, 93, 95, 161, 315, 353, 351, 391, 487, 687
TiBr, 88
TiCl, 88
tobermorite, 23
Tomimoto, Kenkichi, 424
topaz, 660, 667, 670
Torricelli, Evangelista, 505
total internal reflection (TIR), 586
toughened glass, 473
toughening, 325, 335
tourmaline, 107, 108, 652, 668
Trancrede de Dolomieu, Guy S, 479
transgranular (or cleavage) fracture, 333
transition metal borides, 63
transition metal carbides, 63, 89
transition metal nitrides, 89
transmission electron microscopy (TEM) image, 390, 430, 680, 687
transmission electron microscopy (TEM), 121, 146, 191, 207, 221, 235, 237, 238, 240, 251, 257, 259, 262–4, 274, 278, 366, 369, 370, 380, 436, 449, 454, 455, 457, 501, 537, 611, 655
transparency, 577
triboluminescence, 585
tricalcium phosphate (TCP), 7, 636, 643, 645
tridymite, 48, 105, 111
trinitite, 395
triple junctions (TJ), 246, 261–264, 267, 268, 270, 275, 280, 433, 435
triple points, 439

tsavorite, 660
tungsten carbide (W6C), 3, 356
tungsten oxide (WO₃), 258
tungsten, 146
turbostratic carbons, 647
turquoise, 653
twin boundaries, 247, 255–8, 268, 447, 561
twist boundary, 223, 247–8, 253, 261

U

ugrandites, 669
ultrasonic testing, 301
ultra-violet photoelectron spectroscopy (UPS), 174
unit cell, 71, 76, 83, 112
uraninite, 685
uranium dioxide (urania, UO₂), 26, 87, 92, 184, 194, 227, 277, 279, 685
uvarovite, 660

V

vacancy, 182–3, 185–6, 196, 215, 265, 318
vacancy pairs, 190
Valasek, Joseph, 573
valence, 116, 121
van der Waals bonding, 96, 108, 109
van der Waals forces, 100, 114, 211, 283, 686
van der Waals, Johannes Diderik, 69
van Leeuwenhoek, Anton, 397
van Royen, Willebrod Snell, 596
vapor pressure, 231
vaporization, 231
vapor-liquid-solid (VLS) mechanism, 372, 508, 521, 522
varistor, 540
Venus Flower Basket (Euplectella), 395
vermiculite, 109, 439
Verneuil process, 508, 509, 510
Verneuil, August Victor Louis, 508, 524, 652
viscometer, 384, 405
viscosity, 284, 383, 384, 405, 406, 489
viscous flow, 321
visible light microscopy (VLM), 154, 156, 172, 176, 177, 274, 278, 366, 388, 389, 391, 449, 610
visible light microscopy (VLM), polarized, 156
VO₂, 93
Vogel-Fulcher-Tammann (VFT) equation, 318, 321
voids, 227, 242, 278

Voight model, 294, 308
volatiles, 429
Volterra, Vito, 222
von Fraunhofer, Joseph, 382
Von Hippel, Arthur Robert, 573
von Mises criterion, 314
von Mises, Richard, 323
von Tschirnhaus, Count Ehrenfried Walthers, 20, 30
Vycor process, 386

W

Wagner, Carl, 461
Warren, Bertram Eugene, 397
wavelength dispersive spectrometer (WDS), 172, 173, 653
wear resistance, 338
Wedgwood, Josiah, 20, 21, 24, 31, 424, 676
Wedgwood, Thomas, 199
Weibull distribution function, 302
Weibull modulus, 291, 308
Weibull statistics, 302–5
Weibull, E.H. Waloddi, 306
Weiss, Pierre Ernest, 609, 617
wetting, 231, 243, 247, 284
whiskers, 359, 370, 372, 374, 376, 378
whiteware, 6, 7, 142, 148, 417, 582, 632, 677
wide-band-gap semiconductors, 542
willemite (Zn₂SiO₄), 281, 391, 585
Winston, Harry, 673
Wollaston, William Hyde, 688
wollastonite; CaSiO₃, 391
Wulff plot, 227, 249
Wulff shapes, 242
Wulff, Georgii (Yurii) Viktorovich, 85
Wulffman (NIST), 242
wurtzite structure, 209
wurtzite, 55, 77, 90, 91, 98, 105, 239
wüstite, 82, 130, 187, 188, 446
Wyckoff, Ralph Walter Graystone, 85

X

X-ray backscattering, 483
X-ray computed tomography (CT), 682
X-ray diffraction (XRD), 102, 113, 115, 121, 122, 135, 162, 169, 170–1, 369, 370, 380, 653
X-ray energy dispersive spectroscopy (XEDS), 168, 172, 173, 249, 653
X-ray photoelectron spectroscopy (XPS), 37, 174
X-ray topography, 157

Y

Y₂O₃, 9, 189, 319, 332, 439, 678
Y₃Al₅O₁₂, 5, 589
Y₃Fe₂(FeO₄)₃, 607
Yanagi, Soetsu, 425
YBa₂Cu₃O₇ (YBCO), 4, 5, 28, 32, 93, 100, 112, 118–20, 197, 266, 377, 445, 446, 495, 553, 681
yield strength, 309, 315
yield stress, 315
Young, Thomas, 69, 232, 243, 306
Young's equation, 231
Young's modulus, 51–3, 71, 244, 289–95, 297, 301, 307, 373, 619, 633, 639
Young-Dupré equation, 232
yttrium aluminosilicate (YAS) glasses, 646
yttrium aluminum garnet (YAG), 36, 107, 191, 205, 207, 208, 266, 290, 439, 457, 507, 514, 668, 679, 680
yttrium iron garnet (Y₃Fe₅O₁₂ or YIG), 107, 519, 607, 608, 610
yttrium stabilized zirconia (YSZ), 173, 189, 446, 447
yttrium vanadate (YVO₄), 157
yttrium–aluminum (YA) glass, 386

Z

Zachariasen, William Houlder, 31, 115, 118
Zachariasen's model, 117
Zachariasen's rules, 115
Zeiss, Carl Friedrich, 382, 479
Zeiss, Roderick, 382
zeolite, 227, 233
zeolites, 84, 114, 115, 118, 279, 440
zinc aluminate spinel (ZnAl₂O₄), 668
zinc blende (ZnS), 55, 77–8, 81, 90, 96–8, 105, 211
zinc oxide (ZnO), 7, 64, 90, 188, 191, 195, 196, 200, 254, 266, 353, 519, 539, 541, 686
zincite, 353
zircon, (ZrSiO₄, zirconium dioxide), 100, 146, 281, 347, 353, 358, 392, 507, 582
zirconia (ZrO₂), 7, 28, 122, 144, 145, 189, 194, 198, 276, 295, 336, 446, 507, 447, 501, 635, 639, 640, 655, 686
zirconia-toughened alumina (ZTA), 336, 337
zirconia-toughened ceramics (ZTC), 28
zirconium diboride (ZrB₂), 354, 356
zoisite (Ca₂Al₃(SiO₄)₃(OH)), 659, 669
zone axis, 75
zone refining, 508

Details for Figures and Tables

This list summarizes the sources used for images and the origin of data used in tables and diagrams. Where possible, the original source for each figure is given, but on many occasions the figures have been so widely used in the literature that the original source is not known to us; in these cases, when new diagrams have been created, no citation is given in this list. We will add information regarding original citations to the web site as it becomes available. Images obtained by our students, postdocs or colleagues in collaborative research with the authors but not published elsewhere are denoted here by the author's initials; those obtained by the authors are not attributed further.

Chapter 1

Figure 1.2 Data from Evans, A.G. and Davidge, R.W. (1969) "Strength and fracture of fully-dense polycrystalline MgO", *Phil. Mag.* 20, 373. <http://www.tandf.co.uk/journals>

Figure 1.3 Courtesy of Sandia National Laboratory.

Figure 1.4 McKernan, S., MGN & CBC.

Figure 1.5 Data from Kingery, W.D., Bowen, H.K., and Uhlmann, D.R. (1976) *Introduction to Ceramics* 2nd Ed., p. 1008.

Figure 1.6 Data from Moulson, A.J. and Herbert, J.M. (1990) *Electroceramics*, Chapman and Hall, London, p. 215.

Table 1.3 From the NIST Reference on Constants, Units, and Uncertainty (www.physics.nist.gov).

Table 1.4 From *S.I. and Related Units: Quick-Reference Conversion Factors* (1968), compiled by Dryden, I.G.C, BCURA, Leatherhead, Surrey, UK.

Chapter 2

Figure 2.2 Adapted from Price, T.D. and Feinman, G.M. (2001) *Images of the Past* 3rd Ed., Mayfield, Mountain View, CA.

Figure 2.3 From Hummel, R.E. (1998) *Understanding Materials Science*, Springer, New York, p. 283. Reproduced with permission from Springer. (The figurine is in the Moravske Museum, Brno, Czech Republic.)

Figure 2.4 Adapted from Kingery, W.D. and Vandiver, P.B. (1986) *Ceramic Masterpieces*, The Free Press, New York, p. 19.

Figure 2.7 From Henderson, J. (2000) *The Science and Archeology of Materials*. Routledge, London, p. 199. Reproduced by permission of Taylor and Francis.

Figure 2.8 Courtesy of Paul E. Stutzman.

Figure 2.9 Data from Ashby, M.F. and Jones, D.R.H. (1986) *Engineering Materials 2*, Pergamon Press, Oxford, p. 192.

Figure 2.10 Data from Ashby, M.F. and Jones, D.R.H. (1986) *Engineering Materials 2*, Pergamon Press, Oxford, p. 192.

Figure 2.11 From the *Travels of Sir John Mandeville*, ink and tempera on parchment, Bohemia, circa 1410. The British Library (MS Add. 24189, f.16), London. Reproduced by permission of the British Library.

Table 2.1 Data from Fergusson, J.E. (1982) *Inorganic Chemistry and the Earth*, Pergamon, Oxford, p. 47.

Table 2.2 Data from Wood, N. (1999) *Chinese Glazes*, A&C Black, London.

Table 2.4 Data from Lechtman, H.N. and Hobbs, L.W. (1986) "Roman concrete and the Roman architectural revolution", in: *Ceramics and Civilization III: High-Technology Ceramics—Past, Present, and Future*, edited by W.D. Kingery, The American Ceramics Society, Westerville, OH, p. 95.

Chapter 3

Figure 3.7 Data from Lupis, C.H.P. (1983) *Chemical Thermodynamics of Materials*, Elsevier Science Publishing, New York, p. 35.

Figure 3.8 Data from Schmalzried, H. (1974) *Solid State Reactions*, Academic Press, New York, p. 109.

Table 3.5 Data from Moore, C.E. (1970), *Ionization Potentials and Ionization Limits Derived from the Analysis of Optical Spectra*, NSRDS-NBS 34, National Bureau of Standards, Washington, D.C. Data on the actinides is from Seaborg, G.T. (1968) *Ann. Rev. Nucl. Sci.* 18, 53 and references therein.

Table 3.6 Data from Berry, R.S. (1969) *Chem. Rev.* 69, 533 except: ^aEdlen, B. (1960) *J. Chem. Phys.* 33, 98; ^bBaughan, E.C. (1961) *Trans. Faraday Soc.* 57, 1863; ^cGinsberg, A.P. and Miller, J.M. (1958) *J. Inorg. Nucl. Chem.* 7, 351; ^dPolitzer, P. (1968) *Trans. Faraday Soc.* 64, 2241.

Chapter 4

Figure 4.1a Data from Sproull, R. (1956) *Modern Physics: A Textbook for Engineers*, Wiley, New York, Figure 7-2 on p. 192.

Figure 4.2 Data from Wachtman, Jr., J.B., Tefft, W.E., Lam, Jr., D.G., and Apstein, C.S. (1961) "Exponential Temperature Dependence of Young's modulus for several oxides," *Phys. Rev.*, 122, 1754.

Figure 4.3 Data from Wachtman, Jr. J.B. and Lam, Jr. D.G. (1959) "Young's modulus of refractory materials as function of temperature", *J. Am. Ceram. Soc.* 42, 254.

Figure 4.7 Data from Schoknecht, V.G. (1957) *Z. Naturf.*, 12A, 983.

Figure 4.19 Data from Bader, R.F.W., Keaveny, I., and Cade, P.E. (1967) "Molecular charge distributions and chemical binding: II. First-row diatomic hydrides, AH", *J. Chem. Phys.* 47, 3381.

Figure 4.21 Data from Slater, J.C. (1934) *Phys. Rev.* 45, 794.

Table 4.2 Modified from Van Vlack, L.H. (1964) *Physical Ceramics for Engineers*, Addison Wesley Reading MA (1964) p. 118.

Table 4.3 Data compiled by Huheey, J.E. (1975) *Inorganic Chemistry: Principles of Structure and Reactivity*, Harper & Row, London, p. 62.

Table 4.4 Data compiled by Huheey, J.E. (1975) *Inorganic Chemistry: Principles of Structure and Reactivity*, Harper & Row, London, p. 61.

Table 4.5 Data from (B-H): Johnson, D.A. (1982) *Some Thermodynamic Aspects of Inorganic Chemistry*, Cambridge; (B-L): Morris, D.F.C. (1957) *J. Inorg. Nucl. Chem.* 4, 8.

Table 4.6 Data from Shannon, R.D. (1976) "Revised effective crystal radii and systematic studies of interatomic distances in halides and chalcogenides," *Acta. Cryst.* A32, 751.

Table 4.8 Data compiled by Israelachvili, J.N. (1992) *Intermolecular and Surface Forces*, 2nd Ed., Academic Press, London, p. 186.

Table 4.9 Data compiled by Israelachvili, J.N. (1992) *Intermolecular and Surface Forces*, 2nd Ed., Academic Press, London, p. 190.

Table 4.10 Data from van Vechten, J.A. (1973) *Phys. Rev. B* 7, 1479.

Chapter 5

Figure 5.11 Data from McHale, J.M., Navrotsky, A., and Perrotta, A.J. (1997) "Effects of increased surface area and chemisorbed H₂O on the relative stability of nanocrystalline γ -Al₂O₃ and α -Al₂O₃," *J. Phys. Chem. B* 101, 603.

Chapter 6

Figure 6.2 Data from Galasso, F.S. (1970) *Structure and Properties of Inorganic Solids*, Pergamon, Oxford, p. 113.

Figure 6.5 From Tillman, K., Thust, A., and Urban, K. (2004) "Spherical aberration correction in tandem with exit-plane wave reconstruction: Interlocking tools for the atomic scale imaging of lattice defects in GaAs" *Microsc. Microanal.* 10, 185, with permission from Cambridge University Press.

Figure 6.9 Adapted from Galasso, F.S. (1970) *Structure and Properties of Inorganic Solids*, Pergamon, Oxford, p. 69.

Figure 6.17 Adapted from Parthé, E. (1964) *Crystal Chemistry of Tetrahedral Structures*, Gordon and Breach, New York, p. 16.

Table 6.1 Data from Toth, L.E. (1971) *Transition Metal Carbides and Nitrides*, Academic Press, New York, p. 33.

Chapter 7

Figure 7.16c Reprinted from Iijima, S. (1993) "Growth of carbon nanotubes," *Mater. Sci. Eng. B* 19, 172, Copyright 1993, with permission from Elsevier.

Figure 7.19 Adapted from Zachariasen, W.H. (1932) "The atomic arrangement in glass", *J. Am. Chem. Soc.* 54, 3841.

Figure 7.21 Adapted from Hobbs, L.W. (1995) "Network topology in aperiodic networks" *J. Non-Cryst. Solids* 192 & 193, 79. Copyright 1995, with permission from Elsevier.

Table 7.5 Data compiled by Wenk, H.-R. and Bulakh, A. (2004) *Minerals*, Cambridge University Press, p. 314.

Chapter 8

Figure 8.3 Data from Bergeron, C.G. and Risbud, S.H. (1984) *Introduction to Phase Equilibria in Ceramics*, The American Ceramic Society, Columbus, OH, p. 59.

Figure 8.4 Data from von Wartenberg, H. and Prophet, E. (1932) *Z. Anorg. Allg. Chem.* 208, 379.

Figure 8.5a Data from Lin, P.L., Pelton, A.D., Bale, C. W., and Thomson, W.T. (1980) *CALPHAD: Computer Coupling of Phase Diagrams and Thermochemistry*, Vol. 4, Pergamon New York, p. 47.

Figure 8.5b Data from Dorner, P., Gauckler, L.J., Kreig, H., Lukas, H.L., Petzow, G., and Weiss, J. (1979) *CALPHAD: Computer Coupling of Phase Diagrams and Thermochemistry*, Vol. 3, Pergamon, New York, p. 241.

Figure 8.11 Data from Doman, R.C., Barr, J.B., McNally, R.N., and Alper, A.M. (1963) *J. Am. Ceram. Soc.* 46, 313.

Figure 8.16 Data from Osborn E.F. and Muan, A. (1960) No.3 in *Phase Equilibrium Diagrams of Oxide Systems*, American Ceramic Society, Columbus OH.

Figure 8.18 Data from Morey, G.W. and Bowen, N.L. (1925) *J. Soc. Glass. Technol.* 9, 232, 233.

Figure 8.21 Data from Jack, K.H. (1976) "Sialons and related nitrogen ceramics" *J. Mater. Sci.* 11, 1135.

Figure 8.24 Reprinted from Torres, F.C. and Alarcón, J. (2004) *J. Non-Cryst. Sol.* 347, "Mechanism of crystal-

lization of pyroxene-based glass-ceramic glazes” 45, Copyright 2004, with permission from Elsevier.

Chapter 9

- Figure 9.4** Courtesy of Swindell Dressler.
Figure 9.5 Courtesy of Swindell Dressler.
Figure 9.6 Courtesy of David Demaray and Mike Vinton, University of Washington.
Figure 9.7 Courtesy of Kanthal Corporation.
Figure 9.8 Reprinted from Susnitzky D.W. and Carter, C.B. (1992) “Surface morphology of heat-treated ceramic thin films,” *J. Am. Ceram. Soc.* 75, 2471, with permission from Blackwell Publishing and the American Ceramic Society.
Figure 9.11 Courtesy of Ferro Corporation.
Table 9.1 Data compiled by Atkins, P.W. (1978) *Physical Chemistry*, Oxford University Press, Oxford, p. 107.
Table 9.2 Data compiled by Atkins, P.W. (1978) *Physical Chemistry*, Oxford University Press, Oxford, p. 108.
Table 9.3 Data from Brown, R.L., Everest, D.A., Lewis, J.D., and Williams, A. (1968) “High-temperature processes with special reference to flames and plasmas,” *J. Inst. Fuel.* 41, 433.
Table 9.4 Data compiled by Nassau, K. (1994) *Gemstone Enhancement*, 2nd Ed., Butterworth-Heinemann, Oxford, p. 207.
Table 9.5 Data compiled by Nassau, K. (1994) *Gemstone Enhancement*, 2nd Ed., Butterworth-Heinemann, Oxford, p. 206.
Table 9.6 Data compiled by Nassau, K. (1994) *Gemstone Enhancement*, 2nd Ed., Butterworth-Heinemann, Oxford, p. 205.
Table 9.7 Data compiled by Nassau, K. (1994) *Gemstone Enhancement*, 2nd Ed., Butterworth-Heinemann, Oxford, p. 220, modified with applications from the American Iso-static Presses, Inc. data sheet. ANSI (American National Standards Institute) symbols, except for G, C, and D.
Table 9.8 The pyrometric cone equivalent test is described in ASTM Standard C24-56.

Chapter 10

- Figure 10.1** LeBret, J.B. & MGN.
Figure 10.3 Reprinted from Smolsky, I.L., Voloshin, A.E., Zaitseva, N.P., Rudneva, E.B., and Klapper, H. (1999) “X-ray topographic study of striation formation in layer growth of crystals from solutions,” *Phil. Trans R. Soc. Lond. A.* 357, 2631, with permission from the Royal Society.
Figure 10.4 Reprinted from LeBret, J.B., Norton, M.G. and Bahr, D.F. (2005) “Examination of crystal defects with high-kV X-ray computed tomography,” *Mater. Lett.* 59, 1113. Copyright 2005, with permission from Elsevier.
Figure 10.11 Reprinted with permission from Jia, C.L., Lentzen, M., and Urban, K. (2003) “Atomic resolution

imaging of oxygen in perovskite ceramics”, *Science* 299, 870. Copyright 2003 AAAS.

- Figure 10.12** Reprinted with permission from Han, W. Q., Chang, C.W., and Zettl, A. (2004) “HRTEM image of a BN nanotube partly loaded with a crystal of KI” *Nano Letters* 4, 1355. Copyright 2004 American Chemical Society.
Figure 10.14 Reprinted from Diebold, U. (2003) “The surface science of titanium dioxide” *Surf. Sci. Reports* 48, 53. Copyright 2003, with permission from Elsevier.
Figure 10.18 Reprinted from Richardson, T.J. and Ross, Jr., P.N. (1996) “FTIR spectroscopy of metal oxide insertion electrodes: thermally induced phase transitions in $\text{Li}_x\text{Mn}_2\text{O}_4$ spinels,” *Mater. Res. Bull.* 31, 935, Copyright 1996, with permission from Elsevier.
Figure 10.20 Courtesy of Yahia Djaoued.
Figure 10.21 Data from Simmons, C.J. and El-Bayoumi, O.H., eds (1993) *Experimental Techniques in Glass Science*, The American Ceramic Society, Westerville, OH, p. 88.
Figure 10.22 Data from Simmons, C.J. and El-Bayoumi, O.H., eds (1993) *Experimental Techniques in Glass Science*, The American Ceramic Society, Westerville, OH, p. 91.
Figure 10.24 Source. Data from Simmons, C.J. and El-Bayoumi, O.H., eds (1993) *Experimental Techniques in Glass Science*, The American Ceramic Society, Westerville, OH, pp. 107 and 110.
Figure 10.25 Data from Simmons, C.J. and El-Bayoumi, O.H., eds (1993) *Experimental Techniques in Glass Science*, The American Ceramic Society, Westerville, OH, p. 111.
Figure 10.26 Reprinted from Williams, D.B. and Carter, C.B. (1996) *Transmission Electron Microscopy*, Plenum, New York, with permission from Springer.
Figure 10.27 Reprinted from Farrer, J.K., Carter, C.B., and Ravishankar, N. (2006) “The Effects of Crystallography on Grain Boundary Migration in Alumina” *J. Mater. Sci.*, 41(3), 661–674. Reproduced by permission of Springer.
Figure 10.29 Reprinted from Simpson, Y.K., Colgan, E.G., and Carter, C.B. (1987) “Kinetics of the growth of spinel on alumina using Rutherford backscattering spectroscopy,” *J. Am. Ceram. Soc.* 70, C149. With permission from Blackwell Publishing and the American Ceramic Society.
Figure 10.30 Altay, A. & CBC.
Figure 10.33 Altay, A. & CBC.
Figure 10.34 Gilliss, S.R. & CBC.
Figure 10.35 Data from Haas, T.W., Grant, J.T., and Dooley III, G.J. (1972) “Chemical effects in Auger electron spectroscopy,” *J. Appl. Phys.* 43, 1853.
Figure 10.37 Altay, A. & CBC.
Table 10.5 Data from Raman Spectroscopic Library, Dept. Chemistry, University College London (www.chem.ucl.ac.uk/resources/raman/index.html).

Table 10.6 Data compiled by Banwell, C.N. (1972) *Fundamentals of Molecular Spectroscopy*, 2nd Ed., McGraw-Hill, London p. 328.

Table 10.7 From Smith, D.K. (1986) “Diffraction methods: Introduction,” in: ASM Handbook Volume 10 *Materials Characterization*, ASM International (1986) p. 325.

Table 10.10 Modified after: Bowen, D.K. and Hall, C. R. (1975) *Microscopy of Materials: Modern Imaging Methods Using Electron, X ray and Ion Beams*, Macmillan, London p. 86.

Chapter 11

Figure 11.9 With permission from Voyles, P.M., Chadi, D.J., Citrin, P.H., Muller, D.A., Grazul, J.L., Northrup, P.A., and Gossmann, H.-J.L. (2003) “Evidence for a New Class of Defects in Highly *n*-Doped Si: Donor-Pair-Vacancy-Interstitial Complexes”, *Phys. Rev. Lett.* 91, 125505. Copyright 2003 American Physical Society.

Figure 11.11 Data from Kingery, W.D., Bowen, H.K., and Uhlmann, D.R. (1976) *Introduction to Ceramics*, 2nd Ed., Wiley, New York, p. 237.

Figure 11.12 Data from Kingery, W.D., Bowen, H.K., and Uhlmann, D.R. (1976) *Introduction to Ceramics*, 2nd Ed., Wiley, New York, p. 240.

Figure 11.13 Data from Baumbach, H.H. and Wagner, C. (1933) *Z. Phys. Chem. B* 22, 199.

Figure 11.14 Data from Kingery, W.D., Bowen, H.K., and Uhlmann, D.R. (1976) *Introduction to Ceramics*, 2nd Ed., Wiley, New York, p. 245.

Figure 11.16 Data from Kirk R. and PL Pratt, P.L. (1967) *Proc. Brit. Ceram. Soc.* 9, 215.

Table 11.7 Data from Jeffe, E.R. and Foote, F. (1933) *J. Chem. Phys.*, 1, 29.

Table 11.8 Data compiled by Hayes, W. and Stoneham, A.M. (1985) *Defects and Defect Processes in Nonmetallic Solids*, Wiley, New York, p. 146.

Chapter 12

Figure 12.7 Courtesy of Y. Ikuhara.

Figure 12.9a Reprinted from Dash W.C. (1957) “The observation of dislocations in silicon,” in *Dislocations and Mechanical Properties of Crystals*, Eds Fisher, J.C., Johnston, W.G., Thomson, R. and Vreeland, T. Wiley, New York, pp. 57–68.

Figure 12.9b Eakins, D.E. & MGN.

Figure 12.11c Reprinted from Ray, I.L.F. and Cockayne, D.J.H. (1971) “The dissociation of dislocations in silicon,” *Proc. R. Soc. Lond. A.* 325, 543. With permission from the Royal Society.

Figure 12.13 Reprinted from Nakamura, A., Lagerlöf, K.P.D., Matsunaga, K., Tohma, J., Yamamoto, T. and Ikuhara, Y. (2005) “Control of dislocation configuration in sapphire,” *Acta Mater.* 53, 455. Copyright 2005, with permission from Elsevier.

Figure 12.14 Reprinted from Delavignette, P. and Amelinckx, S. (1962) “Dislocation patterns in graphite,” *J. Nucl. Mater.* 5, 17. Copyright 1962, with permission from Elsevier.

Figure 12.18 Reprinted from Bontinck, W. and Amelinckx, S. (1957) “Observation of helicoidal dislocation lines in fluorite crystals,” *Phil. Mag.* 2, 1. With permission from Taylor and Francis. <http://www.tandf.co.uk/journals>

Figure 12.19 Reprinted from Phillips, D.S., Plekta, B.J., Heuer, A.H., and Mitchell, T.E. (1982) “An improved model of break-up of dislocation dipoles into loops: application to sapphire (α -Al₂O₃),” *Acta Metall.* 30, 491. Copyright 1982, with permission Elsevier.

Figure 12.21 Reprinted from Amelinckx, S. (1964) “The direct observation of dislocations” *Solid State Physics*, Supplement 6, Academic Press, New York pp. 1–487, figure 48, Copyright 1964, with permission from Elsevier.

Figure 12.22 Reprinted from Amelinckx, S. (1964) “The direct observation of dislocations” *Solid State Physics*, Supplement 6, Academic Press, New York pp. 1–487, figure 49, Copyright 1964, with permission from Elsevier.

Figure 12.23a Reprinted from Amelinckx, S. (1964) “The direct observation of dislocations” *Solid State Physics*, Supplement 6, Academic Press, New York pp. 1–487, figure 149a, Copyright 1964, with permission from Elsevier.

Figure 12.24 Reprinted by permission from Macmillan Publishers Ltd: Kodambaka, S., Khare, S.V., Swiech, W., Ohmori, K., Petrov, I., and Greene, J.E. (2004) “Dislocation-driven surface dynamics on solids” *Nature* 429, 49. Copyright 2004.

Figure 12.25 Reprinted from Tanaka, M. and Higashida, K. (2004) “HVEM characterization of crack tip dislocations in silicon crystals,” *J. Electron Microsc.* 53, 353. With permission from Oxford University Press.

Figure 12.27a Reprinted with permission from Gutkin, M.Y., Sheinerman, A.G., Argunova, T.S., Mokhov, E.N., Je, J.H., Hwu, Y., Tsai, W-L., and Margaritondo (2003) “Micropipe evolution in silicon carbide”, *Appl. Phys. Lett.* 83, 2157. Copyright 2003, American Institute of Physics.

Figure 12.27b Reprinted with permission from Qian, W., Rohrer, G., Skowronski, M., Doverspike, K., Rowland, L., and Gaskill, D. (1995) “Open-core screw dislocations in GaN epilayers observed by scanning force microscopy and high-resolution transmission electron microscopy” *Appl. Phys. Lett.* 67, 2284. Copyright 1995, American Institute of Physics.

Figure 12.28 Reprinted from Carter, C.B. and Kohlstedt, D.L. (1981) “Electron irradiation damage in natural quartz grains,” *Phys. Chem. Minerals* 7, 110, with permission from Springer.

Chapter 13

Figure 13.2 Reprinted with permission from Castell, M.R. (2003) “Wulff shape of microscopic voids in UO₂

crystals" *Phys. Rev. B* 68, 235411. Copyright 2003 by the American Physical Society.

Figure 13.4 Reprinted from Yanina, S.V. and Carter, C.B. (2002) "Dislocations at spinel surfaces," *Surf. Sci.*, 511, 133. Copyright 2002, with permission from Elsevier.

Figure 13.5 Reprinted from Heffelfinger, J.R., Bench, M.W., and Carter, C.B. (1995) "On the faceting of ceramic surfaces," *Surf. Sci.* 343, L1161. Copyright 1995, with permission from Elsevier. See also Heffelfinger, J.R. and Carter, C.B. (1997) "Mechanisms of surface faceting and coarsening," *Surf. Sci.* 389, 188.

Figure 13.6(a-c) Reprinted with permission from Frenkel, A.I., Hills, C.W., and Nuzzo, R.G. (2001) "A View from the Inside: Complexity in the Atomic Ordering of Supported Metal Nanoparticles" *J. Phys. Chem. B* 105, 12689. Copyright 2001 American Chemical Society.

Figure 13.6d Ramachandran, D., Basu, J. & CBC.

Figure 13.9 Reprinted from Li, Y., Bando, Y., and Golberg, D. (2004) "Indium-assisted growth of aligned ultra-long silica nanotubes," *Adv. Mater.* 16, 37. With permission from Wiley-VCH Verlag.

Figure 13.11 Kotula, P.G., Michael, J.R., Gilliss, S.R. & CBC.

Figure 13.12 Reprinted from Tuck, C. and Evans, J.R.G. (1999) "Porous ceramics prepared from aqueous foams," *J. Mater. Sci. Lett.* 18, 1003. With permission from Springer.

Figure 13.15 Reprinted from Vaughan, D.J. and Patrick, R.A.D., Eds. (1995) *Mineral Surfaces*, Chapman and Hall, London p. 27. With permission from Springer.

Figure 13.16 Reprinted from Heffelfinger, J.R., Bench, M.W., and Carter, C.B. (1997) "Steps and the structure of the (0001) α -alumina surface," *Surf. Sci.* 370, L168, Copyright 1997 with permission from Elsevier.

Figure 13.16 Yanina, S.V. & CBC. See also Yanina, S. V. and Carter, C.B. (2002) "Terraces and ledges on (001) spinel surfaces," *Surf. Sci. Lett.*, 513, L402.

Figure 13.17 Gilliss, S.R. & CBC.

Figure 13.18 Reprinted from Starke, U., Sloboshanin, S., Tautz, F.S., Seubert, A., and Schaefer, J.A. (2000) "Polarity, morphology and reactivity of epitaxial GaN films on Al₂O₃ (0001)" *Phys. Stat. Sol.* (a) 177, 5. With permission from Wiley-VCH Verlag.

Figure 13.19 Reprinted from Gao, W., Klieb, R., and Altmana, E.I. (2005) "Growth of anatase films on vicinal and flat LaAlO₃ (110) substrates by oxygen plasma assisted molecular beam epitaxy," *Thin Solid Films* 485, 115, Copyright 2005. With permission from Elsevier.

Figure 13.20a Reprinted from Susnitzky D.W. and Carter, C.B. (1992) "Surface morphology of heat-treated ceramic thin films" *J. Am. Ceram. Soc.* 75, 2463. With permission from Blackwell Publishing and the American Ceramic Society.

Figure 13.20b Morrissey, K.J. & CBC.

Figure 13.22 Reprinted from De Cooman, B.C., Kuesters, K.-H., and Carter, C.B. (1985) "Cross-sectional

reflection electron microscopy of III-V compound epilayers," *J. Electron Microsc. Techn.* 2, 533. With permission from Wiley-VCH Verlag.

Figure 13.24 Reprinted from McCarty, K.F. and Bartelt, N.C., "Spatially resolved dynamics of the TiO₂ (110) surface reconstruction," *Surf. Sci.* 540, 157. Copyright 2003, With permission from Elsevier.

Figure 13.25 Ramachandran, D., Basu, J. & CBC.

Figure 13.26(a) Reprinted from *Chem. Phys. Lett.* 394, Wang, Y, Teitel, S., and Dellago, C. "Melting and equilibrium shape of icosahedral gold nanoparticles," 257, Copyright (2004), with permission from Elsevier.

Figure 13.26(b) From Goldstein, A.N., Echer, C.M., and Alivisatos, A.P. (1992) "Melting in semiconductor nanocrystals," *Science*, 256, 1425. Reprinted with permission from AAAS.

Figure 13.27 Reprinted in part with permission from Sayle, D.C. and Watson, G.W. (2002) "Atomistic structures of 25 000-atom oxide nanoparticles supported on an oxide substrate" *J. Phys. Chem. B*, 106, 10793. Copyright 2002 American Chemical Society.

Figure 13.28 Reprinted from Ravishankar, N., Shenoy, V.B., and Carter C.B. (2004) "Electric field singularity assisted nanopatterning," *Adv. Mater.*, 16 76, with permission from Wiley-VCH Verlag.

Table 13.3 Data from Kingery, W.D., Bowen, H.K., and Uhlmann, D.R. (1976) *Introduction to Ceramics*, 2nd Ed., Wiley, New York, p. 210.

Chapter 14

Figure 14.2(a) Data from Chiang, Y-M., Kingery, W.D., and Levinson, L.M. (1982) "Compositional changes adjacent to grain boundaries during electrical degradation of a ZnO varistor," *J. Appl. Phys.* 53, 1765.

Figure 14.2(b) Reprinted from Bouchet, D., Lartigue-Korinek, S., Molins, R., and Thibault, J. (2006) "Yttrium segregation and intergranular defects in alumina" *Phil. Mag.* 86, 1401. With permission from Taylor and Francis. <http://www.tandf.co.uk/journals>

Figure 14.3a Data from Chaudhari, P. and Matthews, J.W. (1971) "Coincidence twist boundaries between crystalline smoke particles," *J. Appl. Phys.* 42, 3063.

Figure 14.3b Nowak, J. & CBC.

Figure 14.4 Data from Morawiec, A. (1999) "Calculation of distribution of grain boundary energy over grain misorientations," *Scripta Mater.* 41, 13.

Figure 14.7 Reprinted from Carter, C.B., Föll, H., Ast, D.G., and Sass, S.L. (1981) "Electron diffraction and microscopy studies of the structure of grain boundaries in silicon," *Phil. Mag. A* 43, 441. With permission from Taylor and Francis. <http://www.tandf.co.uk/journals>

Figure 14.8 Reprinted from Sass, S.L. and Rühle, M. (1984) "The detection of the change in mean inner potential at dislocations in grain-boundaries in NiO," *Phil. Mag.* 49, 759, with permission from Taylor and Francis. <http://www.tandf.co.uk/journals>

Figure 14.9(a) Reprinted from Amelinckx, S. (1958) "Dislocation patterns in potassium chloride," *Acta Metall.* 6, 34, Copyright 1958. With permission from Elsevier.

Figure 14.9(b) Reprinted with permission from Gilman, J.J., Johnston, W.G., and Sears, G.W. (1958) "Dislocation etch pit formation in lithium fluoride," *J. Appl. Phys.* 29, 747. Copyright 1958, American Institute of Physics.

Figure 14.16 Reprinted with permission from Oba, F., Ohta, H., Sato, Y., Hosono, H., Yamamoto, T., and Ikuhara, Y. (2004) "Atomic structure of [0001]-tilt grain boundaries in ZnO: A high-resolution TEM study of fiber-textured thin films," *Phys. Rev. B* 70, 125415. Copyright 2004 by the American Physical Society.

Figure 14.19 Morrissey, K.J. & CBC. See also Morrissey, K.J. and Carter, C.B. (1984) "Faceted grain boundaries in Al_2O_3 ," *J. Am. Ceram. Soc.* 67, 292.

Figure 14.20 Morrissey, K.J. & CBC (as 14.19).

Figure 14.21 Reprinted from Carter, C.B., Elgat, Z., and Shaw, T.M. (1987) "Twin boundaries parallel to the common-{111} plane in spinel," *Phil. Mag.* A55, 1. With permission from Taylor and Francis See also Carter, C.B., Elgat, Z. and Shaw, T.M. (1987) "Lateral twin boundaries in spinel," *Phil. Mag.* A55, 21. <http://www.tandf.co.uk/journals>

Figure 14.22 Kotula, P.G. & CBC.

Figure 14.24 From Moore, M.D., Tilley, R.J.D., and Williams, R.P. (1996) "The systematics of block-structure shift lattices," *Proc. R. Soc. Lond. A* 452, 841. With permission from the Royal Society.

Figure 14.25 Reprinted from Sloan, S., Hutchison, J.L., Tenne, R., Yishay, T.T., and Homyonferà, M. (1999) "Defect and ordered tungsten oxides encapsulated (X 5S and Se) fullerene-related structures," *J. Sol. St. Chem.* 144, 100, Copyright 1999, with permission from Elsevier.

Figure 14.27a Courtesy of Hans-Joachim Kleebe.

Figure 14.27b Reprinted with permission from Shibata, N., Painter, G.S., Satet, R.L., Hoffmann, M.J., Pennycook, S.J., and Becher, P.F. (2005) "Rare-earth adsorption at intergranular interfaces in silicon nitride ceramics: Subnanometer observations and theory," *Phys. Rev. B* 72, 149191R. Copyright 2005 by the American Physical Society.

Figure 14.28 Reprinted from Susnitzky D.W. and Carter, C.B. (1990) "Structure of alumina grain boundaries prepared with and without a thin amorphous intergranular film," *J. Am. Ceram. Soc.* 73, 2485. With permission from Blackwell Publishing and the American Ceramic Society.

Figure 14.29 Reprinted from Ramamurthy, S., Mallamaci, M.P., Zimmerman, C.M., Carter, C.B., Duncombe, P.R., and Shaw, T.M. (1996) "Microstructure of polycrystalline MgO penetrated by a silicate liquid," *JMSA* 2, 113 (reprinted in *Microsc. Microanal.*, 3 suppl. 3). With permission from Cambridge University Press.

Figure 14.30 Mallamaci, M.P. & CBC.

Figure 14.31 Föll, H. & CBC. See also Föll, H., and Carter, C.B. (1979) "Direct TEM determination of intrinsic

and extrinsic stacking-fault energies of silicon," *Phil. Mag.* A40, 497. And Carter, C.B., Föll, H., Ast, D.G., and Sass, S.L. (1981) "Electron diffraction and microscopy studies of the structure of grain boundaries in silicon," *Phil. Mag.* A43, 441. <http://www.tandf.co.uk/journals>

Figure 14.32a Courtesy of David Clarke.

Figure 14.34 Ramamurthy, S. & CBC.

Figure 14.35 See: Simpson, Y.K., Carter, C.B., Morrissey, K.J., Angelini, P., and Bentley, J. (1986) "The identification of thin amorphous films at grain-boundaries in Al_2O_3 ," *J. Mater. Sci.* 21, 2689.

Figure 14.36 Reprinted from Mallamaci, M.P., Bentley, J., and Carter, C.B. (1997) "In-Situ TEM crystallization of silicate-glass films on Al_2O_3 ," *Acta Mater.* 46, 283. Copyright 1997, with permission from Elsevier. See also Mallamaci, M.P. and Carter, C.B. (1999) "Crystallization of pseudo-orthorhombic anorthite on basal sapphire," *J. Am. Ceram. Soc.* 82, 33.

Figure 14.37 Reprinted from McKernan, S., Norton, M.G., and Carter, C.B. (1992) "The 45° grain boundaries in $YBa_2Cu_3O_{7.8}$," *J. Mater. Res.* 7, 1052. With permission from the Materials Research Society.

Chapter 15

Figure 15.2 Rasmussen, Y.K. & CBC.

Figure 15.3 Summerfelt, S.R. & CBC.

Figure 15.4 Anderson, I.M. & CBC.

Figure 15.5 Reprinted from Summerfelt, S.R. and Carter, C.B. (1989) "The movement of the spinel-NiO interface in thin films," *Ultramicroscopy* 30, 150. Copyright 1989, with permission from Elsevier.

Figure 15.6b Guinel, M. & MGN.

Figure 15.7 Reprinted from: Simpson, Y.K. and Carter, C.B. (1990) "Faceting Behavior of Alumina in the Presence of a Glass," *J. Am. Ceram. Soc.* 73 (8), 2391.

Figure 15.8 Summerfelt, S.R. & CBC.

Figure 15.9 Reprinted from Suvaci, E., Oh, K.-S., and Messing, G.L. (2001) "Kinetics of template growth in alumina during the process of templated grain growth (TGG)," *Acta Mater.* 49, 2075. Copyright 2001, with permission from Elsevier.

Figure 15.11 Reprinted with permission from Castell, M.R. (2003) "Wulff shape of microscopic voids in UO_2 crystals," *Phys. Rev. B* 68, 235411. Copyright 2003 by the American Physical Society.

Figure 15.12 Reprinted from Santala, M.K. and Glaeser, A.M. (2006) "Surface-energy-anisotropy-induced orientation effects on Rayleigh instabilities in sapphire," *Surf. Sci.*, 600, 782. Copyright 2006, with permission from Elsevier.

Figure 15.13 Courtesy of Quantachrome Instruments.

Figure 15.14 Blanford, C.F., Stein, A. & CBC.

Figure 15.15 Reprinted with permission from Dhara, S., Pradhan, M., Ghosh, D., and Bhargava, P. (2005) "Nature inspired novel processing routes for ceramic foams," *Adv. Appl. Ceram.* 104, 9. Copyright 2005 Maney Publishing.

Figure 15.14 Riesterer, J.L., Gilliss, S.R. & CBC.
Figure 15.17 Courtesy of Andrew M. Kraynik, from Kraynik, A.M. (2003) “Foam structure: From soap froth to solid foams”, *MRS Bulletin* April 275. By permission of the Materials Research Society. (Redrawn)
Figure 15.18 McKernan, S., Bentley, J. & CBC. See also Bentley, J., McKernan, S., Carter, C.B., and Revcolevschi, A. (1993) “Microanalysis of directionally solidified cobalt oxide-zirconia eutectic,” *Microbeam Analysis* 2, S286.
Figure 15.21 Data from Campbell, I.E. and Sherwood, E.M., eds. (1967) *High-Temperature Materials and Technology*, Wiley, New York, p. 380.
Figure 15.22b From van Helvoort, A.T.J., Knowles, K.M., and Fernie, J.A. (2003) “Characterization of cation depletion in Pyrex during electrostatic bonding,” *J. Electrochem. Soc.*, 150, G624. By permission of ECS—The Electrochemical Society. And from van Helvoort, A.T.J., Knowles, K.M., and Fernie, J.A. (2003) “Nanostructure at electronic bond interfaces,” *J. Am. Ceram. Soc.* 86, 1773. By permission from Blackwell Publishing and the American Ceramic Society.
Figure 15.23 McIlroy, D.N., Nowak, J., MGN and CBC. See also LaLonde, A.D., Norton, M.G., Zhang, D., Gangadean, D., Alkhateeb, A., Padmanabhan, R., and McIlroy, D.N. (2005) “Controlled growth of gold nanoparticles on silica nanowires,” *J. Mater. Res.* 20, 3021.

Chapter 16

Figure 16.1 Eakins, D.E. & MGN.
Figure 16.4a Data from Coble, R.L. (1958) “Effect of microstructure on mechanical properties,” *Ceramic Fabrication Processes*, Wiley, New York, p. 223.
Figure 16.4b Data from Coble, R.L. (1958) “Effect of microstructure on mechanical properties,” *Ceramic Fabrication Processes*, Wiley, New York, p. 217.
Figure 16.5 Data from Wachtman, J.B. (1996) *Mechanical Properties of Ceramics*, Wiley, New York, p. 358.
Figure 16.9 Data from Zeng, J., Tanaka, I., Miyamoto, Y., Yamada, O., and Niihara, K. (1992) “High-temperature strength and cavitation threshold of silicon nitride-silica ceramics,” *J. Am. Ceram. Soc.* 75, 195.
Figure 16.12 Data from Wachtman, J.B. (1996) *Mechanical Properties of Ceramics*, Wiley, New York, p. 362.
Figure 16.17c Courtesy of Dylan Morris.
Figure 16.18 Zagrebelny, A., Lilleodden, E., Gerberich, W.W. and CBC.
Figure 16.23 Data from Sato, S., Taguchi, K., Adachi, R., and Nakatani, M. (1996) “A study of strength characteristics of Si₃N₄ coil springs,” *Fat. Fract. Engng. Mater. Struct.* 19, 529.
Figure 16.25 Data from Barsoum, M.W. (2003) *Fundamentals of Ceramics*, Institute of Physics, Bristol, UK, p. 388.
Table 16.1 Data from ASTM International (www.astm.org).

Table 16.2 Data compiled by Green D.J. (1998) *An Introduction to the Mechanical Properties of Ceramics*, CUP, Cambridge, UK, p. 25.
Table 16.3 Data compiled by Wachtman, J.B. (1996) *Mechanical Properties of Ceramics*, Wiley, New York, p. 25.
Table 16.4 Data compiled by C.A. Harper, Editor-in-Chief (2001) *Handbook of Ceramics, Glasses, and Diamonds*, McGraw-Hill, New York, p. 1.7.
Table 16.5 Modified after Munz, D. and Fett, T. (1999) *Ceramics: Mechanical Properties, Failure Behavior, Materials Selection*, Springer, Berlin, p. 17.
Table 16.6 Data compiled by Rice, R.W. (1970) “The compressive strength of ceramics,” in: *Ceramics in Several Environments*, Vol. 5, Plenum Press, New York, pp. 195–229.
Table 16.10 Data from Ashby, M.F. and Jones, D.R.H. (1986) *Engineering Materials 2: An Introduction to Microstructures, Processing, and Design*, Pergamon Press, Oxford, p. 169.
Table 16.11 Data from Hulbert, S.F. (1993) “The use of alumina and zirconia in surgical implants,” in: *An Introduction to Bioceramics*, edited by L.L. Hench and J. Wilson, World Scientific, Singapore, p. 30.

Chapter 17

Figure 17.1 Data from Gorum, A.E., Parker, E.R., and Pask, J.A. (1958) “Effect of surface conditions on room-temperature ductility of ionic crystals”, *J. Am. Ceram. Soc.* 41, 161.
Figure 17.2 Data from Gilman, J.J. and Johnston, W.G. (1957) in: *Dislocations and Mechanical Properties of Crystals*, Fischer, J.C., Johnston, W.G., Thomson, R., and Vreeland, T., Eds., Wiley, New York.
Figure 17.4a Reprinted with permission from Gilman, J.J. and Johnston, W.G. (1956) “Observations of dislocation glide and climb in lithium fluoride crystals”, *J. Appl. Phys.* 27, 1018. Copyright 1956, American Institute of Physics.
Figure 17.4b Veysseyre, P. and CBC. See also Veysseyre, P. and Carter, C.B. (1988) “Dissociation of dislocations in MgAl₂O₄ spinel deformed at low temperatures,” *Phil. Mag. Lett.* 57, 211. <http://www.tandf.co.uk/journals>
Figure 17.10 Data from Kingery, W.D., Bowen, H.K., and Uhlmann, D.R. (1976) *Introduction to Ceramics*, 2nd Ed., Wiley, New York p. 740.
Figure 17.11 Data from Jiang, B. and Weng, G.J. (2004) “A theory of compressive yield strength of nano-grained ceramics”, *Int. J. Plasticity*, 20, 2007.
Figure 17.12 Data from Evans, A.G. and Pratt, P.L. (1969) “Dislocations in fluorite structure”, *Phil. Mag.* 20, 1213. <http://www.tandf.co.uk/journals>
Figure 17.13 From Gilman, J.J. and Johnston, W.G. (1957) in Fisher, J.G., Johnston, W.G., Thomson, R., and Vreeland, T., Eds. *Dislocations and Mechanical Properties of Crystals* Wiley, New York.

Figure 17.14 Data from Liu, T.S., Stokes, R.J., and Li, C.H. (1964) "Fabrication and plastic behavior of single crystal MgO-NiO and MgO-MnO solid solution alloys", *J. Am. Ceram. Soc.* 47, 276.

Figure 17.18 Data from Wachtman, J.B. (1996) *Mechanical Properties of Ceramics*, Wiley, New York, pp. 329–330.

Figure 17.19 Data from Ashby, M.F. (1972) "First report on deformation-mechanism maps," *Acta Metall.* 20, 887 and Frost, H.J. and Ashby, M.F. (1982) *Deformation-Mechanism Maps: The Plasticity and Creep of Metals and Ceramics*, Pergamon, Oxford.

Figure 17.22 Guinel, M. and MGN. See also Guinel, M.J-F. and Norton, M.G. (2005) "Blowing of silica microforms on silicon carbide," *J. Non-Cryst. Solids* 351, 251.

Table 17.1 Data compiled by Green D.J. (1998) *An Introduction to the Mechanical Properties of Ceramics*, CUP, Cambridge, UK, p. 177.

Table 17.2 Data from Gilman, J.J. and Buerger, J.M. (1930) "Translation-gliding in crystals," *Amer. Mineral.* 15, 45 and 174.

Table 17.4 Modified from Kingery, W.D., Bowen, H.K., and Uhlmann, D.R. (1976) *Introduction to Ceramics*, 2nd Ed., Wiley, New York, p. 714.

Table 17.5 Data compiled by Barrett, C.R., Nix, W.D., and Tetelman, A.S. (1973) *The Principles of Engineering Materials*, Prentice-Hall, Englewood Cliffs, New Jersey, p. 255.

Table 17.6 Data compiled by Green D.J. (1998) *An Introduction to the Mechanical Properties of Ceramics*, CUP, Cambridge, UK, p. 200.

Chapter 18

Figure 18.3 Data from Griffith, A.A. (1920) "The phenomenon of rupture and flow in solids," *Phil. Trans. R. Soc. Lond.*, A221, 163.

Figure 18.6 Data from Griffith, A.A. (1920) "The phenomenon of rupture and flow in solids," *Phil. Trans. R. Soc. Lond.*, A221, 163.

Figure 18.9 Data from Wiederhorn, S. (1967) "Influence of water vapor on crack propagation in soda-lime glass," *J. Am. Ceram. Soc.* 50, 407.

Figure 18.11b Data from Gilbert, C.J., Bloyer, D.R., Barsoum, M.W., El-Raghy, T., Tomsia, A.P., and Ritchie, R.O. (2000) "Fatigue-crack growth and fracture properties of coarse and fine-grained Ti₃SiC₂," *Scripta Mater.* 42, 761.

Figure 18.13a Guinel, M. and MGN.

Figure 18.13b Guinel, M. and MGN.

Figure 18.15 Reprinted from Johnson, J.W. and Holloway, D.G. (1966) "On the shape and size of the fracture zones on glass fracture surfaces," *Phil. Mag.* 14, 731. With permission from Taylor and Francis. <http://www.tandf.co.uk/journals>

Figure 18.16 Reprinted from Eakins, D.E., Held, M., Norton, M.G., and Bahr, D.F. (2004) "A study of fracture

and defects in single crystal YAG", *J. Cryst. Growth*, 267, 502. Copyright 2004, with permission from Elsevier.

Figure 18.18 Reprinted from Bao, Y. and Nicholson, P. S. (2006) "AlPO₄ coating on alumina/mullite fibers as a weak interface in fiber-reinforced oxide composites", *J. Am. Ceram. Soc.* 89, 465. With permission from Blackwell Publishing and the American Ceramic Society.

Figure 18.20 Data from Becher, P. (1991) "Microstructural design of toughened ceramics," *J. Am. Ceram. Soc.* 74, 255.

Figure 18.21 McKernan, S. and CBC.

Figure 18.23 Guinel, M. and MGN.

Figure 18.25 Riesterer, J.L., Gilliss, S.R. & CBC.

Table 18.2 Data compiled by Kelly, A. and MacMillan, N.M. (1986) *Strong Solids*, 3rd Ed., Oxford University Press, Oxford.

Table 18.3 Data from (Al₂O₃): Stokes, R.J. (1972) *The Science of Ceramic Machining and Surface Finishing*, NBS Special Publication 348, U.S. Government Printing Office, Washington, D.C., p. 347. (SiC): Richerson, D.W. (1992) *Modern Ceramic Engineering*, 2nd Ed., Marcel Dekker, New York, p. 170.

Table 18.4 Data compiled by Barsoum, M.W. (2003) *Fundamentals of Ceramics*, Institute of Physics, Bristol, UK, p. 364–365.

Table 18.7 Data compiled by Ziegler, G. and Hüttner, W. (1991) "Engineering properties of carbon-carbon and ceramic-matrix composites, in: *Engineered Materials Handbook, Volume 4 Ceramics and Glasses*, ASM International, p. 838.

Table 18.8 Data from Corning Incorporated (www.corning.com).

Table 18.9 Data compiled by Richerson, D.W. (2006) *Modern Ceramic Engineering* 3rd Ed., Taylor and Francis Boca Raton p. 274.

Table 18.10 Data compiled by Indge, J.H. (1991) in: *ASM Engineered Materials Handbook, Volume 4: Ceramics and Glasses*, ASM International p. 351.

Chapter 19

Figure 19.4 Data from Ernst, W.G. (1969) *Earth Materials*, Prentice-Hall, Englewood Cliffs. p. 38.

Figure 19.5 The reproduction of this image is through the courtesy of Alcoa Inc.

Figure 19.8 Courtesy of Exolon, a Washington Mills Company.

Table 19.1 Data compiled by Mason, B. (1966) *Principles of Geochemistry*, Table 3.4, John Wiley and Sons, New York.

Table 19.2 Data from Gribble, C.D. (1988) *Rutley's Elements of Mineralogy*, 27th Ed., Unwin Hyman, London. p. 119.

Table 19.3 Data compiled by Ernst, W.G. (1969) *Earth Materials*, Prentice-Hall, Englewood Cliffs. p. 10.

Table 19.4 Data from *Mineral Commodity Summaries* (2006) U.S. Department of the Interior, U.S. Geological

Survey, United States Government Printing Office, Washington D.C.

Table 19.5 Data from Annual Minerals Review (1996) *Am. Ceram. Soc. Bull.* 75, 138.

Table 19.7 Data compiled by Lee, W.E. and Rainforth, W.M. (1994) *Ceramic Microstructures: Property Control by Processing*, Chapman and Hall, London. p. 261.

Table 19.8 Data compiled by Lee, W.E. and Rainforth, W.M. (1994) *Ceramic Microstructures: Property Control by Processing*, Chapman and Hall, London. p. 261.

Chapter 20

Figure 20.5 Data from Silberberg, M. (1996) *Chemistry: The Molecular Nature of Matter and Change*, Mosby, Boston, p. 477.

Figure 20.9 Thompson, S., Perrey, C.R., Kortshagen, U. & CBC. Also see: Thompson, S., Perrey, C.R., Carter, C.B., Belich, T.J., Kakalios, J., and Kortshagen, U. (2005) "Experimental investigations into the formation of nanoparticles in a/nc-Si:H thin films," *J. Appl. Phys.* 97, 034310-1.

Figure 20.14 Data from Rahaman, M.N. (1995) *Ceramic Processing and Sintering*, Marcel Dekker, Inc., New York, p. 112.

Figure 20.16 Data from Lowder, R.A. (1993) "Fiber coatings and the mechanical properties of a continuous fiber reinforced SiC matrix composite", in: *Designing Ceramic Interfaces II*. S.D. Peteves (ed.) Comm. of Europ. Communities: Luxembourg pp. 157–72.

Table 20.1 From Rahaman, M.N. (1995) *Ceramic Processing and Sintering*, Marcel Dekker, Inc., NY, p. 40.

Table 20.3 Data compiled by Richerson, D.W. (1992) *Modern Ceramic Engineering*, 2nd Ed., Marcel Dekker, NY, p. 395.

Table 20.4 Data compiled by McColm, I.J. and Clark, N.J. (1988) *Forming, Shaping and Working of High-Performance Ceramics*, Blackie, Glasgow, p. 81.

Table 20.5 Data compiled by Reed, J.S. (1988) *Introduction to the Principles of Ceramic Processing*, John Wiley & Sons, NY, p. 92.

Table 20.8 From Reed, J.S. (1988) *Introduction to the Principles of Ceramic Processing*, John Wiley and Sons, New York, p. 71.

Table 20.9 Data compiled by Chawla, K.K. (1993) *Ceramic Matrix Composites*, Chapman and Hall, London, p. 51.

Chapter 21

Figure 21.2 Copyright the Trustees of The British Museum.

Figure 21.3 Copyright the Trustees of The British Museum.

Figure 21.4a Data from Pfaender, H.G. (1996) *The Schott Guide to Glass*. Chapman & Hall, London, UK, p. 21.

Figure 21.4b Data from Doremus, R.H. (1994) *Glass Science*, 2nd Ed., Wiley, New York, p. 103.

Figure 21.5 Redrawn after schematics on the Edward J. Orton Jr. Ceramic Foundation site (ANS-800 and RSV-1600); see www.ortonceramic.com/instruments (and don't miss the Orton cones video).

Figure 21.6 Data from Moriya, Y., Warrington, D.H., and Douglas, R.W. (1967) *Phys. Chem. Glasses*, 1, 19.

Figure 21.8 Courtesy of Schott Glass.

Figure 21.9 Ravishankar, N. and CBC.

Figure 21.10 Reprinted from Guinel, M. J-F. and Norton, M.G. (2006) "Oxidation of silicon carbide and the formation of silica polymorphs," *J. Mater. Res.* 21, 2550. With permission from the Materials Research Society.

Figure 21.11 Reprinted from Vogel, W. (1971) *Structure and Crystallization of Glasses* The Leipzig Ed., Pergamon Press, Oxford. p. 150.

Figure 21.12 Reprinted from Vogel, W. (1971) *Structure and Crystallization of Glasses* The Leipzig Ed., Pergamon Press, Oxford. p. 176.

Figure 21.13 Reprinted from Vogel, W. (1971) *Structure and Crystallization of Glasses* The Leipzig Ed., Pergamon Press, Oxford. p. 35.

Figure 21.14 Reprinted from Riello, P., Canton, P., Comelato, N., Polizzi, S., Verita, M., Fagherazzi, G., Hofmeister, H., and Hopfe, S. (2001) "Nucleation and crystallization behavior of glass-ceramic materials in the Li₂O-Al₂O₃-SiO₂ system of interest for their transparent properties", *J. Non-Cryst. Sol.* 288, 127. Copyright 2001, with permission from Elsevier.

Figure 21.16 From the ERSF-NL38 newsletter. This plate can be seen in the Museo Regionale della Ceramica di Deruta in Italy. Deruta is a beautiful city, overlooking the Tiber valley, renowned for its ceramic art dating back to the Middle Ages. See: www.museoceramicaderuta.it and www.deruta.net.

Figure 21.19 Riesterer, J.L. & CBC.

Figure 21.20 From Aizenberg, J., Weaver, J.C., Thanawala, M.S., Sundar, V.C., Morse, D.E., and Fratzl, P. (2005) "Skeleton of euplectella sp.: Structural hierarchy from the nanoscale to the macroscale," *Science* 309, 275. Reprinted with permission from AAAS.

Figure 21.21 Data from Zhu, D., Chandra, S., Ray, C.S., Zhou, W., Delbert, E., and Day, D.E. (2003) "Glass transition and fragility of Na₂O-TeO₂ glasses," *J. Non-Cryst. Sol.* 319, 247.

Table 21.6 Data compiled by Tooley, F.V. (1960) *Handbook of Glass Manufacture*, Ogden Publishing Co., New York, NY.

Chapter 22

Figure 22.10 Reprinted from Giuliano Gregori, G., Kleebe, H.-J., Readey, D.W., and Sorarù, G.D. (2006) "Energy-filtered TEM study of Ostwald ripening of Si nanocrystals in a SiOC glass." *J. Am. Ceram. Soc.* 89,

1699. With permission from Blackwell Publishing and the American Ceramic Society.

Table 22.2 Data compiled from Bradley, D.C., Mehrotra, R.C., and Gaur, D.P. (1978) *Metal Alkoxides*, Academic Press, London and Rahaman, M.N. (1995) *Ceramic Processing and Sintering*, Marcel Dekker, New York, p. 211.

Table 22.3 Data from: Gossink, R.G., Coenen, H.A.M., Engelfriet, A.R.C., Verheijke, M.L., and Verplane, J.C. (1975) "Ultrapure SiO₂ and Al₂O₃ for the preparation of low-loss compounds glass," *Mater. Res. Bull.* 10, 35.

Table 22.4 Data from Klein, L.C. (1991) "Sol-gel process," in: *Engineered Materials Handbook Volume 4: Ceramics and Glass*, ASM International.

Table 22.8 Data compiled by Brinker, C.J. and Scherer, G.W. (1990) *Sol-Gel Science: The Physics and Chemistry of Sol-Gel Processing*, Academic Press, Boston, p. 864.

Chapter 23

Figure 23.11a Courtesy of Jim Robison.

Figure 23.11b Courtesy of Michael Sherrill.

Figure 23.15 Data from Mutsuddy, B.C. (1991) "Injection Molding," in: *Engineered Materials Handbook*, Volume 4 Ceramics and Glasses, ASM International, p. 178.

Figure 23.17 Courtesy of Rosette Gault.

Figure 23.18 From Bliss, G. (2001) *Practical Solutions for Potters*. Sterling Pub Co. Inc. New York, p. 103.

Table 23.3 Data compiled by Reed, J.S. (1988) *Introduction to the Principles of Ceramic Processing*, John Wiley, New York, p. 359.

Table 23.4 Data compiled by Richerson D.W. (1992) *Modern Ceramic Engineering*, Marcel Dekker, New York, p. 493.

Table 23.5 Data compiled by Larson, D. (1991) "Green machining," in: *Engineered Materials Handbook, Ceramics and Glasses 4*, ASM International, p. 184.

Chapter 24

Figure 24.2 Courtesy of Saint-Gobain.

Figure 24.3 From Suzuki, K. and Sasaki, M. (2005) "Effects of sintering atmosphere on grain morphology of liquid-phase-sintered SiC with Al₂O₃ additions," *J. Eur. Ceram. Soc.* 25, 1611. Copyright 2005, with permission from Elsevier.

Figure 24.7 Perrey, C.R. & CBC.

Figure 24.10 Data from Kang, S.-J.L. and Jung, Y.-I. (2004) "Sintering kinetics at the final stage of sintering: Model calculation and map construction," *Acta Mater.* 52, 4373.

Figure 24.16 After Burke, J.E.

Figure 24.17 Munoz, N., Gilliss, S.R. & CBC. See also Munoz, N.E., Gilliss, S.R., and Carter, C.B. (2004) "The monitoring of grain-boundary grooves in alumina," *Phil. Mag. Lett.*, 84, 21, <http://www.tandf.co.uk/journals/Munoz>,

N.E., Gilliss, S.R. and Carter, C.B. (2004) "Remnant grooves on alumina surfaces," *Surf. Sci.* 573, 391.

Figure 24.19 Ravishankar, N. & CBC.

Figure 24.20 Farrer, J. & CBC. See also Farrer, J.K., Carter, C.B., and Ravishankar, N. (2006) "The effects of crystallography on grain boundary migration in alumina," *J. Mater. Sci.*, 41, 661.

Figure 24.21 Altay, A. & CBC.

Figure 24.22 Reprinted from Kaysser, W.A., Sprissler, M., Handwerker, C.A., and Blendell, J.E. (1987) "Effect of a liquid phase on the morphology of grain growth in alumina," *J. Am. Ceram. Soc.* 70 339. With permission from Blackwell Publishing and the American Ceramic Society. See also R. D. Monahan, R.D. and Halloran, J.W. (1979) "Single-crystal boundary migration in hot-pressed aluminum oxide," *J. Am. Ceram. Soc.* 62, 564.

Figure 24.24 Altay, A. & CBC.

Figure 24.25 Courtesy of Paolo Colombo.

Figure 24.27 Courtesy of Marc Anglada.

Figure 24.28 From Wakai, F. and Aldinger, F. (2003) "Sintering through surface motion by the difference in mean curvature", *Acta Mater.* 51, 4013. Copyright 2003, with permission from Elsevier.

Chapter 25

Figure 25.1 Reprinted from Hwang, T.J., Hendrick, M. R., Shao, H., Hornis, H.G., and Hunt, A.T. (1998) "Combustion chemical vapor deposition (CCVD) of LaPO₄ monazite and beta-alumina on alumina fibers for ceramic matrix composites," *Mater. Sci. Eng. A*, 244, 91. Copyright 1998, with permission from Elsevier.

Figure 25.2 Moore, L.A. & CBC. See also Tietz, L.A., Carter, C.B., Lathrop, D.K., Russek, S.E., Buhrman, R.A., and Michael, J.R. (1989) "Crystallography of YBa₂Cu₃O_{6+x} thin film-substrate interfaces," *J. Mater. Res.* 4, 1072. Tietz, L.A., De Cooman, B.C., Carter, C.B., Lathrop, D.K., Russek, S.E., and Buhrman, R.A. (1988) "Structure of superconducting thin films of YBa₂Cu₃O_{7-x} grown on SrTiO₃ and cubic zirconia," *J. Electron Microsc. Tech.* 8, 263.

Figure 25.3 Courtesy of David Clarke.

Figure 25.4 Susnitzky D.W. & CBC. See also Susnitzky, D.W., Hertl, W., and Carter, C.B. (1989) "Vanadia-induced transformations in yttria-stabilized zirconia," *Ultramicroscopy* 30, 223.

Figure 25.5 Reprinted from Lee, W.E. and Rainforth, W.M. (1994) *Ceramic Microstructures: Property Control by Processing*, Chapman & Hall, London, p. 912. With permission from Springer.

Figure 25.6 Moore, L.A. & CBC.

Figure 25.7 Ostyn, K.M., Schmalzried, S. & CBC. See also Ostyn, K.M., Carter, C.B., Koehne, M., Falke, H., and Schmalzried, H. (1984) "Internal reactions in oxide solid solutions," *J. Am. Ceram. Soc.* 67, 679.

Figure 25.8 Data from Holt, J.B., Cutler, I.B., and Wadsworth, M.E. (1962) "Rate of thermal dehydration of kaolinite in vacuum." *J. Am. Ceram. Soc.* 45, 133.

Figure 25.9 Rasmussen, Y.K. & CBC. See also Simpson, Y.K. and Carter, C.B. (1986) "A new approach to the study of solid-state reactions," *Phil. Mag.* A53, L1. <http://www.tandf.co.uk/journals>

Figure 25.10 Data from Simpson, Y.K., Colgan, E.G., and Carter, C.B. (1987) "Kinetics of the growth of spinel on alumina using Rutherford backscattering spectroscopy." *J. Am. Ceram. Soc.* 70, C149.

Figure 25.12 After Schmalzried, H. (1981) *Solid State Reactions* p. 106.

Figure 25.13 Data from Pettit, F.S., Randklev, E.H., and Felten, E.J. (1966) "Formation of NiAl_2O_4 by solid state reaction," *J. Am. Ceram. Soc.* 49, 199.

Figure 25.14 Johnson, M.L. & CBC. See also Kotula, P.G., Johnson, M.T., and Carter, C.B. (1998) "Thin-film reactions," *Z. Phys. Chemie* 206 S, 73. Johnson, M.T. and Carter, C.B. (1999) "Movement of Pt markers in MgO during a solid-state reaction," *Phil. Mag. Lett.* 79, 609. <http://www.tandf.co.uk/journals>

Figure 25.15a Data from Chen, W.K. and Peterson, N. L. (1973) "Cation diffusion, semiconductivity and non-stoichiometry in (Co,Ni)O crystals," *J. Phys. Chem. Solids.* 34, 1093.

Figure 25.15b Data from Blank, S.L. and Pask, J.A. (1969) "Diffusion of iron and nickel in magnesium oxide single crystals," *J. Am. Ceram. Soc.* 52, 669.

Figure 25.16 Data from Kingery, W.D., Bowen, H.K., and Uhlmann, D.R. (1976) *Introduction to Ceramics*, 2nd Ed., Wiley, New York, p. 240.

Figure 25.17b,c From Veblin, D.R. and Buseck, P.R. (1981) "Hydrous pyriboles and sheet silicates in pyroxenes and urallites; intergrowth microstructures and reaction mechanisms," *Amer. Mineral.* 66, 1107. With permission from the Mineralogical Society of America.

Figure 25.18 Kotula, P.G. & CBC. See also Kotula, P. G. and Carter, C.B. (1995) "Volume expansion and lattice rotations in solid-state reactions between oxides," *Scripta Met.* 32, 863. Kotula, P.G. and Carter, C.B. (1995) "Nucleation of solid-state reactions between nickel oxide and aluminum oxide," *J. Am. Ceram. Soc.* 78, 248.

Figure 25.19 Kotula, P.G. & CBC. See also Kotula, P. G. and Carter, C.B. (1998) "Kinetics of thin-film reactions of NiO with Al_2O_3 I: (0001) and $\{1\bar{1}20\}$ reaction couples," *J. Am. Ceram. Soc.* 81, 2869. Kotula, P.G. and Carter, C.B. (1998) "Kinetics of thin-film reactions of NiO with Al_2O_3 II: $\{1\bar{1}00\}$ and $\{1\bar{1}02\}$ reaction couples," *J. Am. Ceram. Soc.* 81, 2877.

Figure 25.20 Data from Kotula, P.G. and Carter, C.B. (1998) "Kinetics of thin-film reactions of NiO with Al_2O_3 I: (0001) and $\{1\bar{1}20\}$ reaction couples," *J. Am. Ceram. Soc.* 81, 2869.

Figure 25.21 Heffelfinger and CBC. See also Heffelfinger, J.R. and Carter, C.B. (1994) "Evolution of yttrium aluminum garnet films by solid-state reaction," *Mater. Res. Soc. Symp. Proc.* 317, 553.

Figure 25.22 Susnitzky, D.W. & CBC. See also Susnitzky, D.W. and Carter, C.B. (1986) "The topotactic

growth of β -alumina on α -alumina," *J. Am. Ceram. Soc.* 69, C25.

Figure 25.23 Johnson, M.L. & CBC. See also Johnson, M.T., Schmalzried, H., and Carter, C.B. (1997) "The effect of an applied electric field on a heterogeneous solid-state reaction," *Solid State Ionics* 101–103, 1327. Johnson M.T. and Carter, C.B. (1998) "Thin-film reaction between $\alpha\text{-Fe}_2\text{O}_3$ and (001) MgO," *Microsc. Microanal.* 4, 141. Johnson, M.T., Kotula, P.G., and Carter, C.B. (1999) "Growth of nickel ferrite thin films using pulsed-laser deposition," *J. Cryst. Growth* 206, 299.

Figure 25.24 See (i) Cooper, A.R. and Kingery, W.D. (1964) "Dissolution in ceramic systems: I. Molecular diffusion, natural convection, and forced convection studies of sapphire dissolution in calcium aluminum silicate," *J. Am. Ceram. Soc.* 47, 37. (ii) Samaddar, B.N., Kingery, W.D., and Cooper, A.R. (1964) "Dissolution in ceramic systems: II. Dissolution of alumina, mullite, anorthite, and silica in a calcium-aluminum-silicate slag," *J. Am. Ceram. Soc.* 47, 249. (iii) Oishi, Y., Cooper, A.R., and Kingery, W.D. (1964) "Dissolution in ceramic systems: III. Boundary layer concentration gradients," *J. Am. Ceram. Soc.* 48, 88. (A classic series of papers: all on-line for ACerS members.)

Figure 25.25 After Kingery, W.D., Bowen, H.K., Uhlman, D.R., Kingery, W.D., Bowen, H.K., and Uhlmann, D.R. (1976) *Introduction to Ceramics* 2nd Ed., Wiley, New York, p. 416.

Chapter 26

Figure 26.1 Data from *Ceramic Industry*, August 1993.

Figure 26.2 From Pfaender, H.G. (1996) *Schott Guide to Glass* 2nd Ed., Chapman and Hall, London. p. 39. By permission from Springer.

Figure 26.3 Redrawn after Pfaender, H.G. (1996) *Schott Guide to Glass* 2nd Ed., Chapman and Hall, London. p. 37. By permission from Springer.

Figure 26.4 From Pfaender, H.G. (1996) *Schott Guide to Glass* 2nd Ed., Chapman and Hall, London. p. 38. By permission from Springer.

Figure 26.12 Redraw after Prindle, W.R. (1999) in *Ceramic Innovations* Ed. Wachtman, J.B., *Am. Ceram. Soc.*, Westerville, OH. p. 82.

Table 26.2 Data from Tooley, F.V. (1983) *The Handbook of Glass Manufacture 3rd. Ed. Volumes I*, Ashlee Publishing Co., New York. pp. 28–29.

Table 26.4 Data compiled by Pinckney, L.R. (1991) *Ceramics and Glasses, Engineered Materials Handbook*, Volume 4, ASM International. p. 434.

Chapter 27

Figure 27.3 Courtesy of Richard E. Mistler, Inc., Yardley, PA, USA.

Figure 27.4 Courtesy of Keko Equipment (Slovenia) and Haiku Tech, Inc. (USA).

Figure 27.13 Data from Jang, H.M. and Fuerstenau, D.W. (1986) "The specific adsorption of alkaline-

earth cations at the rutile water interface,” *Coll. Surf.* 21, 238.

Figure 27.18 Data from Hammer, R.B., Powell, D.O., Mukherjee, S., Tummala, R., and Raj, R. (1989) in: *Principles of Electronic Packaging*, Seraphim, D.P., Lasky, R., and Li, C-Y, Eds., McGraw-Hill, New York, p. 296.

Table 27.1 Data from Mistler, R.E., Shanefield, D.J., and Runk, R.B. (1978) in: *Ceramic Processing Before Firing*, Eds. G.Y. Onoda, Jr. and L.L. Hench, Wiley, New York, pp. 411–448.

Table 27.3 Data compiled by Atkins, P.W. (1978) *Physical Chemistry*, Oxford University Press, Oxford, p. 317.

Table 27.4 Data compiled by Patton, T.C. (1979) *Paint Flow and Pigment Dispersion*, Wiley, New York, and Kelly, E.G. and Spottiswood, D.J. (1982) *Introduction to Mineral Processing*, Wiley, New York.

Table 27.6 Data compiled by Walton, B. (1984) in: *Hybrid Microelectronic Technology* (Ed: P.L. Moran) Gordon and Breach, New York. p. 45.

Chapter 28

Figure 28.6 Kotula, P.G. & CBC.

Figure 28.8 Moore, L.A. & CBC. See also Tietz, L.A. and Carter, C.B. (1993) “Structure of the Fe₂O₃-Al₂O₃ (0001) interface,” *Phil. Mag. A* 67, 699. Tietz, L.A. and Carter, C.B. (1993) “Structure of the Fe₂O₃-Al₂O₃ (1012) interface,” *Phil. Mag. A* 67, 729. Tietz, L.A. and Carter, C.B. (1992) “Imaging and diffraction study of continuous α -Fe₂O₃ films on (0001)Al₂O₃,” *J. Am. Ceram. Soc.* 75, 1097. Tietz, L.A., Summerfelt, S.R., and Carter, C.B. (1992) “The effect of substrate orientation on the chemical vapour deposition growth of α -Fe₂O₃ on α -Al₂O₃,” *Phil. Mag. A* 65, 439. <http://www.tandf.co.uk/journals>

Table 28.2 Data compiled by Ohring, M. (1992) *The Materials Science of Thin Films*, Academic Press, Boston, p. 154.

Table 28.3 Data from Veprek, S. (1985) “Plasma-induced and plasma-assisted chemical vapour deposition,” *Thin Solid Films* 130, 135.

Table 28.4 Data compiled by Ohring, M. (1992) *The Materials Science of Thin Films*, Academic Press, Boston, p. 189.

Table 28.5 Data compiled by Ohring, M. (1992) *The Materials Science of Thin Films*, Academic Press, Boston, p. 119.

Chapter 29

Figure 29.9 Redrawn after www.crystalsystems.com/hem.html, an industrial leader in the use of this technique.

Figure 29.10 Data from Brice, J.C. (1986) *Crystal Growth Processes*, Blackie, Glasgow, p. 56.

Figure 29.13 Ramachandran, D., Basu, J., & CBC.

Figure 29.19b Reprinted from Varghese, O.K., Gong, D., Paulose, M., Grimes, C.A., and Dickey, E.D. (2003)

“Crystallization and high-temperature structural stability of titanium oxide nanotube arrays,” *J. Mater. Res.* 18, 156. With permission from the Materials Research Society and Beth Dickey.

Figure 29.19c,d Reprinted from Chen, R.S., Chang, H.M., Huang, Y.S., Tsai, D.S., Chattopadhyay, S., and Chen, K.H. (2004) “Growth and characterization of vertically aligned self-assembled IrO₂ nanotubes on oxide substrates,” *J. Cryst. Growth* 271 105. Copyright 2004, with permission from Elsevier.

Table 29.1 Data compiled by Brice, J.C. (1986) *Crystal Growth Processes*, p. 8.

Table 29.2 Data compiled by Nassau, K. and Nassau, J. (1980) in: *Crystals: Growth, Properties, and Applications*, H.C. Freyhardt, Ed., Springer-Verlag, New York, p. 9.

Table 29.3 Data compiled by Laudise, R.A. (1970) *The Growth of Single Crystals*, Prentice-Hall, Inc, Englewood Cliffs, p. 215.

Table 29.4 Data compiled by Brice, J.C. (1986) *Crystal Growth Processes*, Blackie, Glasgow, p. 130.

Table 29.5 Data compiled by Brice, J.C. (1986) *Crystal Growth Processes*, Blackie, Glasgow, p. 108.

Table 29.6 Data compiled by Hirano, S.-I. (1985) in: *Fine Ceramics*, S. Saito, Ed., Elsevier, New York, pp. 20–23.

Table 29.7 Data compiled by Brice, J.C. (1986) *Crystal Growth Processes*, Blackie, Glasgow, p. 180.

Chapter 30

Figure 30.8 Data from Kingery, W.D., Bowen, H.K., and Uhlmann, D.R. (1976) *Introduction to Ceramics* 2nd Ed., Wiley, New York, p. 867.

Figure 30.9 Data from Moulson, A.J. and Herbert, J.M. (1990) *Electroceramics*, Chapman and Hall, London, p. 129.

Figure 30.10 Data from Kulwicki, B.M. (1991) “Thermistors and related sensors,” in: *Ceramics and Glasses*, Engineered Materials Handbook Vol. 4, ASM International, p. 1148.

Figure 30.13 Data from Baumbach, H.H.V. and Wagner, C. (1933) *Z. Phys. Chem.* B22, 199.

Figure 30.16 Data from Barsoum, M.W. (1996) *Fundamentals of Ceramics*, Institute of Physics, Bristol, p. 208.

Figure 30.17 Data from Gupta, T.K. (1991) “Varistors”, in: *Ceramics and Glasses*, Engineered Materials Handbook Vol. 4, ASM International, p. 1151.

Figure 30.19 Data from Moulson, A.J. and Herbert, J. M. (1990) *Electroceramics*, Chapman and Hall, London, p. 147.

Figure 30.24 Data from Koller, A. (1994) *Structure and Properties of Ceramics*, Elsevier, Amsterdam, p. 474.

Figure 30.25 Data from Duffy, J.A. (1990) *Bonding, Energy Levels and Bands in Inorganic Solids*, Longman Scientific and Technical, Harlow, Essex, UK. p. 138.

Figure 30.26 Data from Kingery, W.D., Bowen, H.K., and Uhlmann, D.R. (1976) *Introduction to Ceramics*, 2nd Ed., Wiley, New York, p. 156.

Table 30.2 Data compiled by Kingery, W.D., Bowen, H.K., and Uhlmann, D.R. (1976) *Introduction to Ceramics*, 2nd Ed., Wiley, New York, p. 853.

Table 30.3 Data compiled by Barsoum, M.W., *Fundamentals of Ceramics*, Institute of Physics, Bristol, p. 43 and Hench, L.L. and West J.K. (1990) *Principles of Electronic Ceramics*, Wiley, New York, p. 91.

Table 30.4 Data compiled by Kingery, W.D., Bowen, H.K., and Uhlmann, D.R. (1976) *Introduction to Ceramics*, 2nd Ed., Wiley, New York, p. 869 and Hench, L.L. and West J.K. (1990) *Principles of Electronic Ceramics*, Wiley, New York, p. 111.

Table 30.6 Data compiled by Moulson, A.J. and Herbert, J.M. (1990) *Electroceramics*, Chapman and Hall, London, p. 141.

Table 30.7 Data compiled by Hench, L.L. and West J.K. (1990) *Principles of Electronic Ceramics*, Wiley, New York, p. 114.

Table 30.8 Data compiled by Hench, L.L. and West J.K. (1990) *Principles of Electronic Ceramics*, Wiley, NY, p. 116.

Table 30.10 Data compiled by Colell, H. and Cook, B. (1999) "Fuel cells—Power for the future" *Education in Chem.*, 36, 123.

Table 30.12 Data compiled by Cyrot, M., and Pavuna, D. (1992) *Introduction to Superconductivity and High-T_c Materials*, World Scientific, Singapore, p. 174.

Table 30.13 Data compiled by Cyrot, M. and Pavuna, D. (1992) *Introduction to Superconductivity and High-T_c Materials*, World Scientific, Singapore, pp. 24 and 38.

Chapter 31

Figure 31.9 Data from Kay, H.F. and Vousden P. (1949) *Phil. Mag.* 40, 1019. <http://www.tandf.co.uk/journals>

Figure 31.10 Data from Moulson, A.J. and Herbert, J. M. (1990) *Electroceramics*, Chapman and Hall, London, p. 76.

Figure 31.14 Data from Merz, W.J. (1949) *Phys. Rev.* 76, 1221.

Figure 31.15 Data from Moulson, A.J. and Herbert, J. M. (1990) *Electroceramics*, Chapman and Hall, London, p. 78.

Figure 31.16 Data from Moulson, A.J. and Herbert, J. M. (1990) *Electroceramics*, Chapman and Hall, London, p. 77.

Figure 31.21 Data from Jaffe, B., Cook, W.R., and Jaffe, H. (1971) *Piezoelectric Ceramics*, Academic Press, London.

Figure 31.22 Courtesy of Ted Charles Norton and the University of Washington Medical Center.

Table 31.4 Data compiled by Walther, G.C. and Hench L.L. (1971) "Dielectric breakdown of Ceramics" in *Physics of Electronic Ceramics*, L.L. Hench and D.B. Dove, eds. Part A, Dekker, New York.

Table 31.6 Data compiled by Yanagida, H., Koumoto, K., and Miyayama, M. (1996) *The Chemistry of Ceramics*, Wiley, New York, p. 213.

Table 31.9 Data from Electronic Industries Association RS-198 (1958), American Standard Requirements for Ceramic Dielectric Capacitors, Classes 1 and 2, American Standards Association, New York.

Table 31.12 Data compiled by Lovell, M.C., Avery, A. J., and Vernon, M.W. (1976) *Physical Properties of Materials*, Van Nostrand Reinhold, New York.

Chapter 32

Figure 32.3 Data from Kingery, W.D., Bowen, H.K., and Uhlmann, D.R. (1976) *Introduction to Ceramics* 2nd Ed., Wiley, New York, p. 647.

Figure 32.5a Data from Kingery, W.D., Bowen, H.K., and Uhlmann, D.R. (1976) *Introduction to Ceramics* 2nd Ed., Wiley, New York, p. 651.

Figure 32.5b Data from Kingery, W.D., Bowen, H.K., and Uhlmann, D.R. (1976) *Introduction to Ceramics* 2nd Ed., Wiley, New York, p. 652.

Figure 32.6 Data from Kingery, W.D., Bowen, H.K., and Uhlmann, D.R. (1976) *Introduction to Ceramics* 2nd Ed., Wiley, New York, p. 653.

Figure 32.16 Modified from Izawa, T. and Sudo, S. (1987) *Optical Fibers: Materials and Fabrication*, KTK, Scientific, Tokyo, Japan.

Figure 32.17 Modified from Izawa, T. and Sudo, S. (1987) *Optical Fibers: Materials and Fabrication*, KTK, Scientific, Tokyo, Japan.

Figure 32.11 Data from Lee, D.W. and Kingery W.D. (1960) "Radiation energy transfer and thermal conductivity of ceramic oxides", *J. Am. Ceram. Soc.* 43, 594.

Figure 32.12 Data from Kingery, W.D., Bowen, H.K., and Uhlmann, D.R. (1976) *Introduction to Ceramics* 2nd Ed., Wiley, New York, p. 657.

Figure 32.28 Aizenberg, J. and Hendler, G. (2004) "Designing efficient microlens arrays: Lessons from nature." *J. Mater. Chem.* 14, 2066. Reproduced by permission of The Royal Society of Chemistry.

Table 32.2 Data compiled by Kingery, W.D., Bowen, H.K., and Uhlmann, D.R. (1976) *Introduction to Ceramics*, 2nd Ed., Wiley, New York, p. 662.

Table 32.4 Data compiled by Bloor, D., Brook, R.J., Flemings, M.C., and Mahajan, S. (1994) editors, *The Encyclopedia of Advanced Materials*, Pergamon Press, Oxford, p. 451.

Table 32.5 Data compiled by Bloor, D., Brook, R.J., Flemings, M.C., and Mahajan, S. (1994) editors, *The Encyclopedia of Advanced Materials*, Pergamon Press, Oxford, p. 452.

Table 32.7 Data compiled by Yanagida, H., Koumoto, K., and Miyayama, M. (1996) *The Chemistry of Ceramics*, Wiley, New York.

Table 32.8 Data compiled by Bloor, D., Brook, R.J., Flemings, M.C., and Mahajan, S. (1994) editors, *The*

Encyclopedia of Advanced Materials, Pergamon Press, Oxford, p. 274.

Table 32.10 Data compiled by Bever, M.B. (1986) editor-in-chief, *Encyclopedia of Materials Science and Engineering*, Pergamon Press, Oxford, p. 2507.

Table 32.11 Data compiled by Bever, M.B. (1986) editor-in-chief, *Encyclopedia of Materials Science and Engineering*, Pergamon Press, Oxford, p. 2507.

Table 32.12 Data compiled by *Engineered Materials Handbook*, Vol. 4, Ceramics and Glasses, ASM International (1991) p. 1129.

Chapter 33

Figure 33.1 Courtesy of Stan Sherer.

Figure 33.6 Data from Standley, K.J. (1962) *Oxide Magnetic Materials*, Clarendon Press, Oxford, p. 89.

Figure 33.15 Adapted from Hench, L.L., and West, J.K. (1990) *Principles of Electronic Ceramics*, Wiley, New York. p. 321.

Figure 33.18 Reprinted from Jakubovics, J.P. (1994) *Magnetism and Magnetic Materials*, 2nd. Ed., The Institute of Materials, London, p. 82. By permission of Maney Publishing.

Figure 33.19 Reprinted with permission from Wolfe, R., Gyorgy, E.M., Lieberman, R.A., Fratello, V.J., Licht, S.J., Deeter, M.N., and Day, G.W. (1992) "High-frequency magnetic-field sensors based on the Faraday-effect in garnet thick-films" *Appl. Phys. Lett.* 60, p. 2048. Copyright 1992, American Institute of Physics.

Figure 33.22a–c Data from Moulson, A.J. and Herbert, J.M. (1990) *Electroceramics*, Chapman & Hall, London, p. 358.

Figure 33.23 Redrawn after Moulson, A.J. and Herbert, J.M. (1990) *Electroceramics*, Chapman & Hall, London, p. 363.

Figure 33.26 Redrawn after Moulson, A.J. and Herbert, J.M. (1990) *Electroceramics*, Chapman & Hall, London, p. 367.

Figure 33.27 After Perez *et al* (cited in Chapter).

Table 33.3 Data from Jakubovics, J.P. (1994) *Magnetism and Magnetic Materials*, 2nd. Ed., The Institute of Materials, London. p. 15.

Table 33.4 Data from *Handbook of Chemistry and Physics*, 61st Ed., CRC Press, Boca Raton, FL.

Table 33.5 Data from *Handbook of Chemistry and Physics*, 61st Ed., CRC Press, Boca Raton, FL.

Table 33.6 Data compiled by Barsoum, M.W. (1997) *Fundamentals of Ceramics*, McGraw-Hill, New York. p. 585.

Table 33.9 Data compiled by *ASM Handbook Vol. 2, Properties and Selection: Nonferrous Alloys and Special-Purpose Materials*, ASM International (1990).

Table 33.10 Data compiled by *Metals Handbook: Properties and Selection: Stainless Steels, Tool Materials and Special Purpose Metals*, Vol. 3, 9th Ed., D. Benjamin, Senior Editor, ASM, 1980.

Chapter 34

Figure 34.1 Data from Kingery, W.D., Bowen, H.K., and Uhlmann, D.R. (1976) *Introduction to Ceramics* 2nd. Ed., Wiley, New York, p. 586.

Figure 34.2 Data from Kingery, W.D., Bowen, H.K., and Uhlmann, D.R. (1976) *Introduction to Ceramics* 2nd. Ed., Wiley, New York, p. 588.

Figure 34.3 Data from Berman, R. (1951) "The Thermal Conductivities of Some Dielectric Solids at Low Temperatures—Experimental", *Proc. R. Soc. Lond A* 208, 90 and Lee, D.W. and Kingery, W.D. (1960) "Radiation Energy Transfer and Thermal Conductivity of Ceramic Oxides", *J. Am. Ceram. Soc.* 43, 594.

Figure 34.4 Data from Kingery, W.D., Bowen, H.K., and Uhlmann, D.R. (1976) *Introduction to Ceramics* 2nd. Ed., Wiley, New York, p. 617.

Figure 34.6 Data from Kingery, W.D., Bowen, H.K., and Uhlmann, D.R. (1976) *Introduction to Ceramics* 2nd. Ed., Wiley, New York, p. 623.

Figure 34.7 Data from Kingery, W.D., Bowen, H.K., and Uhlmann, D.R. (1976) *Introduction to Ceramics* 2nd. Ed., Wiley, New York, p. 620.

Figure 34.11 Data from Van Uitert, L.G., *et al* (1977) *Mater. Res. Bull.* 12, 261.

Figure 34.12 Data from Kingery, W.D., Bowen, H.K., and Uhlmann, D.R. (1976) *Introduction to Ceramics* 2nd. Ed., Wiley, New York, p. 593.

Figure 34.13 Data from Shirane G. and Takeda, A. (1952) *J. Phys. Soc. Japan* 7, 1.

Figure 34.15 Data from Richerson, D.W. (1992) *Modern Ceramic Engineering: Properties, Processing, and Use in Design*, 2nd. Ed., Marcel Dekker, New York, p. 147.

Figure 34.16 Data from Kingery, W.D., Bowen, H.K., and Uhlmann, D.R. (1976) *Introduction to Ceramics* 2nd. Ed., Wiley, New York, p. 597.

Table 34.2 Data compiled by Barsoum, M.W. (1997) *Fundamentals of Ceramics*, McGraw-Hill, New York, p. 97.

Table 34.9 Data compiled by Barsoum, M.W. (1997) *Fundamentals of Ceramics*, McGraw-Hill, p. 103–4.

Table 34.10 Data compiled by Kingery, W.D., Bowden, H.K., and Uhlmann, D.R. (1976) *Introduction to Ceramics* 2nd Ed., Wiley, New York, p. 594.

Chapter 35

Figure 35.1 Data from Hulbert, S.F., Hench, L.L., Forbers, D., and Bowman, L.S. (1982–83) *Ceramurgia Intl.* 8–9, 131.

Figure 35.2 Redrawn after Hench, L.L. and Wilson, J. K. (1993) in: *An Introduction to Bioceramics*, Hench, L. L. and Wilson, J.K. (editors) World Scientific, Singapore, p. 2.

Figure 35.4 Redrawn after Hench, L.L. and Wilson, J. K. (1993) in: *An Introduction to Bioceramics*, Hench, L. L. and Wilson, J.K. (editors) World Scientific, Singapore, p. 13.

Figure 35.6 Reprinted from Richerson, D.W. (2000) *The Magic of Ceramics*, The American Ceramic Society, Westerville, OH, p. 175. By permission of the American Ceramic Society.

Figure 35.7 Data from Bonfield, W., Grynepas, M.D., Tully, A.E., Bowman, J., and Abram, J. (1981) 'Hydroxyapatite Reinforced Polyethylene—A Mechanically Compatible Implant' *Biomaterials* 2, 185.

Figure 35.8 Reprinted from Wang, Q., Huang, W., Wang, D., Darvell, B.W., Day, D.E., and Rahaman, M.N. (2006) "Preparation of hollow hydroxyapatite microspheres," *J Mater. Sci.: Mater. Med.* (2006) 17, 641, with permission from Springer.

Figure 35.9 Courtesy of Medical Carbon Research Institute, LLC the maker of On-X prosthetic heart valves.

Figure 35.10 Reprinted from Dejneka, M.J., Streltsov, A., Pal, S., Frutos, A.G., Powell, C.L., Yost, K., Yuen, P. K., Müller, U., and Lahiri, J. (2003) "Rare earth-doped glass microbarcodes," *PNAS* 100, 389. Copyright 2003 National Academy of Sciences, USA.

Figure 35.12a Redrawn after: Lin, A. and Meyers, M. A. (2005) "Growth and structure in abalone shell," *Mater. Sci. Eng. A* 390 27.

Figure 35.12b Reprinted from Lin, A. and Meyers, M. A. (2005) "Growth and structure in abalone shell," *Mater. Sci. Eng. A* 390 27. Copyright (2005), with permission from Elsevier.

Figure 35.13 Reprinted from Chakrabarti, O., Weisensel, L., and Sieber, H. (2005) "Reactive Melt Infiltration Processing of Biomorphic Si–Mo–C Ceramics from Wood," *J. Am. Ceram. Soc.* 88(7), 1792–1798. With permission from the American Ceramic Society.

Table 35.2 Data compiled by Ravaglioli, A. and Krajewski, A. (1992) *Bioceramics: Materials, Properties, and Application*, Chapman and Hall, London, p. 44.

Table 35.4 Data compiled by Hench, L.L. and Wilson, J. (1993) *An Introduction to Bioceramics*, World Scientific, Singapore, p. 12.

Table 35.5 Data compiled by Hulbert, S.F. (1993) "The Use of Alumina and Zirconia in Surgical Implants" in: *An Introduction to Bioceramics*, Hench, L. L. and Wilson, J.K. (editors) World Scientific, Singapore, p. 26.

Table 35.6 Data compiled by Höland, W. and Vogel, W. (1993) in: *An Introduction to Bioceramics*, Hench, L.L. and Wilson, J.K. (editors) World Scientific, Singapore, p. 126.

Table 35.7 Data compiled by LeGeros, R.Z. and LeGeros, J.P. (1993) in: *An Introduction to Bioceramics*, Hench, L.L. and Wilson, J.K. (editors) World Scientific, Singapore, p. 145.

Chapter 36

Figure 36.1 Courtesy of Richard Hughes. See also his web site www.ruby-sapphire.com.

Figure 36.6a Reprinted from Read, P.G. (1999) *Gem-mology* 2nd Ed., Butterworth-Heinemann, Oxford. With permission from Elsevier.

Figure 36.7 Reprinted from Read, P.G. (1999) *Gem-mology* 2nd Ed., Butterworth-Heinemann, Oxford. With permission from Elsevier.

Figure 36.8a Courtesy of A.Krüss Optronik GmbH, Hamburg, Germany (Karin Leibrock).

Figure 36.8b Redrawn after Read, P.G. (1999) *Gem-mology*. 2nd Ed., Butterworth-Heinemann, Oxford.

Figure 36.9 Adapted from Read, P.G. (1999) *Gem-mology* 2nd Ed., Butterworth-Heinemann, Oxford, plate 10. With permission from Elsevier.

Figure 36.11b Reprinted from Read, P.G. (1999) *Gem-mology* 2nd Ed., Butterworth-Heinemann, Oxford. With permission from Elsevier.

Figure 36.12b Reprinted from Read, P.G. (1999) *Gem-mology* 2nd Ed., Butterworth-Heinemann, Oxford, p. 114. With permission from Elsevier.

Figure 36.19 Courtesy of Ryan Thompson. See also <http://famousdiamonds.tripod.com/cullinandiamonds.html>.

Figure 36.22 Reprinted from Keller, P.C. (1992) *Gem-stones of East Africa* Geoscience Press, Figure 8.1. With permission from Geosciences Press.

Figure 36.23 Riesterer, J.L & CBC.

Figure 36.26 Reprinted from Sofianides, A.S. and Harlow, G.E. (1990) *Gems & Crystals from the American Museum of Natural History*, Simon and Schuster, New York, p. 82. With permission from the American Museum of Natural History. Copyright Van Pelt Photographers/AMNH.

Figure 36.34 Redrawn after the summary table in Hughes, R.W. (1997) *Ruby & Sapphire*, RWH Publishing, Boulder CO.

Figure 36.33 Reprinted from Hurlbut, C.S. and Kammerling, R.C. (1991) *Gemology* 2nd Ed., Wiley, New York. Plate I image 6. With permission from Wiley-VCH Verlag.

Figure 36.34 Redrawn after Hughes, R.W. (1997) *Ruby & Sapphire*, RWH Publishing, Boulder CO.

Table 36.1 Data from Read, P.G. (1999) *Gem-mology*. 2nd Ed., Butterworth-Heinemann, Oxford P27.

Table 36.3 Data compiled by Read, P.G. (1999) *Gem-mology*. 2nd Ed., Butterworth-Heinemann, Oxford p. 219, app G and www.matls.com/search/GetProperty.asp.

Table 36.4 Data compiled by Hurlbut, C.S. and Kammerling, R.C. (1991) *Gem-mology*, 2nd Ed., John Wiley, New York.

Table 36.5 Data compiled by Read, P.G. (1999) *Gem-mology*. 2nd Ed., Butterworth-Heinemann, Oxford, p. 73.

Table 36.7 Data compiled by Read, P.G. (1999) *Gem-mology*. 2nd Ed., Butterworth-Heinemann, Oxford, p. 7.

Table 36.10 Data from Yavuz, F., Gültekin, A.H., and Karakaya, M.Ç. (2002) "CLASTOUR: a computer

program for the classification of the minerals of the tourmaline group”, *Computers and Geosci.* 28, 1017.

Table 36.11 Data compiled by Nassau, K. (1994) *Gemstone Enhancement*, 2nd Ed., Butterworth-Heinemann, Oxford.

Chapter 37

Figure 37.2 Data from Dow Whitney, E. (1976) “New advances in ceramic tooling,” *SME Technical Report, MRR76-15*, Society of Manufacturing Engineers, Dearborn, MI 1976.

Figure 37.3 Data from Reynolds, III, T.G. (2001) “Electronic ceramic materials,” *Am. Ceram. Soc. Bull.* 80, 30.

Figure 37.4 Data from Reynolds, III, T.G. (2001) “Electronic ceramic materials,” *Am. Ceram. Soc. Bull.* 80, 31.

Figure 37.5 Reprinted from Eakins, D.E., Held, M., Norton, M.G., and Bahr, D.F. (2003) “A study of fracture and defects in single crystal YAG,” *J. Cryst. Growth* 267, 502. Copyright 2003, with permission from Elsevier.

Figure 37.6 Data from *New Scientist*, 30 August 2003, p. 16.

Figure 37.7 Reprinted from McKernan S. and Kotula, P.G. (1992) in: Norton, M.G. and Carter, C.B., “Grain and interphase boundaries in ceramics and ceramic composites,” Chapter 4 in *Materials Interfaces: Atomic-level Structure and Properties*, Wolf, D. and Yip, S. Eds., Chapman and Hall, London, p. 186. With permission from Springer.

Figure 37.9 McIlroy, D.N. & MGN. See also Wang, L., Major, D., Paga, P., Zhang, D., Norton, M.G., and McIlroy,

D.N. (2006) “High yield synthesis and lithography of silica-based nanosprings,” *Nanotechnology*, 17, S298.

Figure 37.11 Redrawn from DOE. *Basic Research Needs for Solar Energy*, Report of the Basic Energy Sciences Workshop on Solar Energy Utilization, April 18–21, 2005. Defining the direction for U.S. solar energy research, p. 30.

Table 37.1 Data compiled by Kenney, G.B. and Bowen, H.K. (1983) ‘High tech ceramics in Japan: Current and future markets,’ *Am. Ceram. Soc. Bull.* 62, 590.

Table 37.2 Data from *Ceramic Industry*, August 1993, p. 43.

Table 37.4 Data from Schoenung, J.M. (1991) “Analysis of the economics of silicon nitride powder production,” *Am. Ceram. Soc. Bull.* 70, 114.

Table 37.5 Data from Business Communications Co., Inc. Reprinted in *Am. Ceram. Soc. Bull.*, March 2002, 71, 34.

Table 37.6 Data from *Advanced Ceramics Technology Roadmap—Charting Our Course*. December 2000. Sponsored by United States Advanced Ceramic Association and the U.S. Department of Energy, p. 16.

Table 37.7 Data compiled by Hummel, R.E. (1998) *Understanding Materials Science*, Springer, New York, p. 372.

Table 37.8 Data compiled by Hummel, R.E. (1998) *Understanding Materials Science*, Springer, New York, p. 373.

Table 37.9 Data from Siikamäki, R. and Hupa, L. (2001) “Utilization of EOL CRT-glass as a glaze raw material,” in: *Recycling and Reuse of Glass Cullet*, Dhir, R.K., Limbachiya, M.C., and Dyer, T.D., Eds., Thomas Telford, London, p. 136.